NSTX Upgrade Five Year Plan

for FY2014-2018

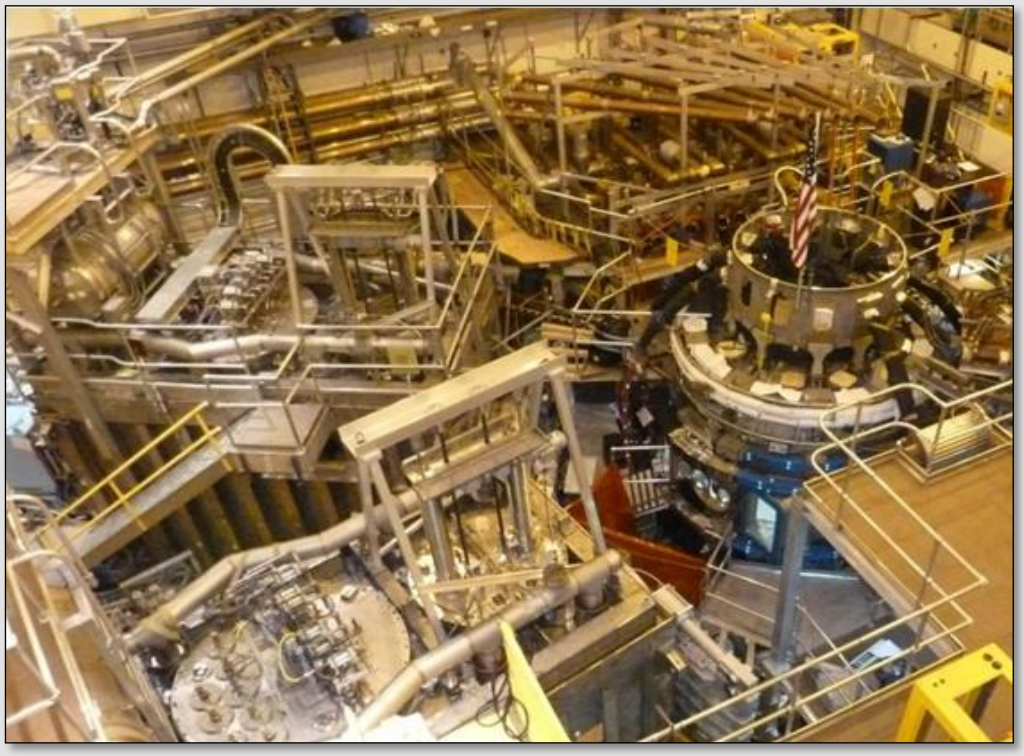

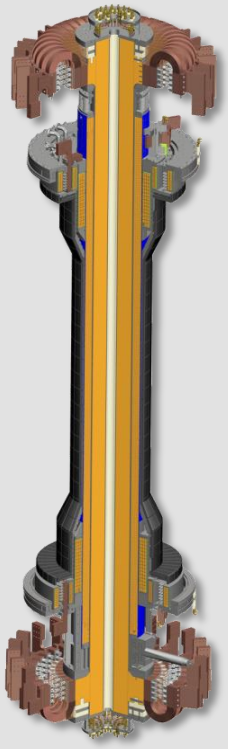

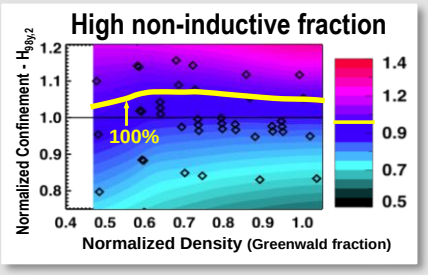

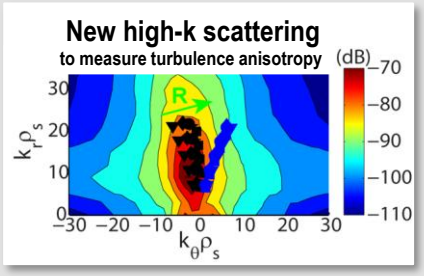

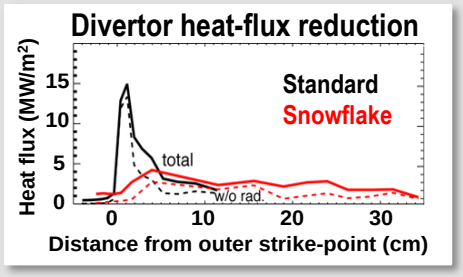

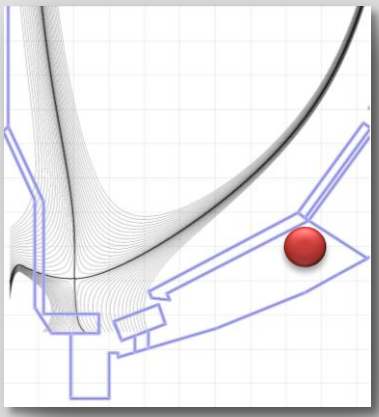

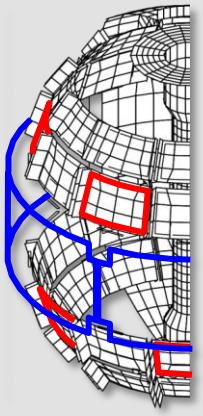

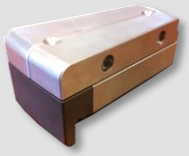

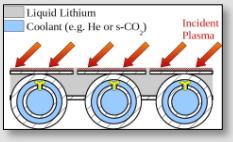

U.S. DEPARTMENT OF ENERGY | Office of Science

PPPL

NSTX-U

Table of Contents

Note: Page numbers below indicate the PDF file page number (not chapter page number).

Executive Summary

The NSTX Upgrade 5 year research plan for FY2014-2018 will make major contributions to narrowing or closing key gaps on the development path towards fusion energy. Underpinning the proposed research program is the upgraded NSTX facility (NSTX-U) which will provide world-leading capabilities in the world fusion program. The mission elements of the NSTX-U research program are: (1) establish the physics basis for the spherical tokamak (ST) as a candidate for a Fusion Nuclear Science Facility (FNSF), (2) understand and develop novel solutions to the plasma-material interface (PMI) challenge, and (3) advance the understanding of toroidal confinement physics for ITER and beyond. Underlying all of these missions is access to a unique plasma physics parameter regime of high normalized pressure combined with reduced inter-particle collision frequency (collisionality) to address fundamental questions about plasma stability and turbulent transport, and greatly extend understanding of toroidal plasma science. *High-priority enhancements for both baseline and incremental budgets are italicized below*.

Establishing the physics basis for a Fusion Nuclear Science Facility (FNSF): An FNSF is arguably the critical major next step in the US fusion program, needed to establish the fusion nuclear science to enable design and construction of a fusion DEMO with acceptable risk. The ST is a potentially attractive candidate for an FNSF, offering the prospect of a compact design with reduced cost and tritium consumption – if the physics extrapolates successfully. NSTX-U will provide access to new physics regimes sufficiently advanced to provide the information for this critical decision on the optimal FNSF configuration. The increased magnetic field and improved beam injection geometry of NSTX-U will enable access to fully non-inductive current sustainment at high current and pressure as required for all steady-state tokamak applications. With the expected results from NSTX-U, the ST may be an attractive candidate for developing fusion component technologies such as blanket modules for thermal conversion and tritium breeding. With access to the highest magnetic field and heating and current drive power of any ST, NSTX-U will be the leading device in the world program to assess the viability of the ST for FNSF applications. The operating range of NSTX-U overlaps or connects to that of an envisioned ST-FNSF in the critical performance metrics of non-inductive bootstrap current, energy confinement enhancement factor, and normalized beta. A key challenge for the ST for the FNSF application is the need for non-inductive plasma formation and current ramp-up. NSTX experimental data has shown that auxiliary heating of helicity-injection start-up plasmas is very likely necessary to bridge the electron temperature gap between start-up (10-50eV) and temperatures projected to be necessary for over-drive ramp-up (0.3-1 keV). *Electron cyclotron heating (ECH) utilizing a 1MW 28GHz gyrotron appears particularly well-suited for heating low-temperature CHI start-up plasmas and is a high-priority facility enhancement for the 5 year period.* NSTX-U start-up and ramp-up data will be used to develop the solenoid-free tokamak/ST design needed for FNSF. If successful, it can also simplify the design of conventional reactors.

Understand and develop novel solutions to the plasma-material interface challenge: The increased heating power and compact geometry of NSTX-U will produce very high exhaust power flux prototypical of fusion reactors, requiring the development of solutions to handle these power levels at the Plasma-Material Interface (PMI). NSTX-U will explore novel solutions to the power exhaust challenge for FNSF and DEMO by testing extreme expansion of the magnetic field lines in a so-called "snowflake" divertor configuration, and by testing liquid metal plasma facing components (PFCs) to mitigate the erosion and melting problems associated with solid materials. The ability to explore very high exhaust power density, high magnetic expansion, and liquid metals in the same device is unique in the world fusion program. The operating range of NSTX-U overlaps or connects to that of an envisioned long-pulse ST-PMI or FNSF facility in the important performance metric of exhaust power flux. A critical enabling capability for accessing reduced collisionality and sustaining non-inductive current drive is control of main-ion and impurity densities. NSTX-U will continue to explore the use of lithium PFC coating techniques for enhanced plasma performance and divertor power and particle handling. In addition to increased lithium coverage, a lithium granular injector will be implemented for ELM pacing at high injection rate to control impurities and to reduce peak ELM heat flux. Presently more research is needed to determine if lithium-based particle pumping will extrapolate to the longer pulse-lengths and higher divertor heat fluxes of FNSF, or even NSTX-U. *In comparison, cryo-pumping is a mature technology and is projected to provide the necessary deuterium pumping capability for both conventional and snowflake divertor configurations in NSTX-U, and is therefore a high-priority facility enhancement for the 5 year period*. Cryo-pumping capability will also enable comparisons to deuterium pumping via lithium coatings, improving understanding of the potential longevity of lithium pumping, and of the impact of lithium on the edge and core plasma. This research will be aided by collaborative laboratory work and theoretical materials science to assess the surface chemistry and physics properties of plasma facing materials used in NSTX-U, and by testing of liquid metal solutions on the Magnum-PSI test stand in the Netherlands by NSTX-U researchers. *With incremental funding, the long-term NSTX-U plan to convert the PFCs from graphite to more FNSF-relevant metal walls would be accelerated, and tests of a flowing liquid metal divertor module would also be accelerated to develop replenishable lithium surfaces. Further, with incremental funding, divertor Thomson Scattering would be implemented to measure kinetic profiles near the divertor target to support power and particle exhaust model validation.*

Contributions to critical ITER physics issues: The unique operating regime of NSTX-U allows it to, in some cases, access directly regimes of interest for ITER that are beyond the reach of higher aspect ratio devices under normal operating conditions. One such area is Energetic Particle physics, where the new heating systems in NSTX-U will provide expanded ability to vary the velocity and spatial distribution of energetic ions in the plasma. These energetic ions can trigger bursting non-linear instabilities that can expel the same ions to the reactor walls. Similar non-linear instabilities may exist in the ITER hybrid and steady-state, reversed shear scenarios.

The requirement for stable plasma operation at high normalized beta combined with 100% non-inductive current drive for long-pulse operation motivates the development of an integrated, physics-based disruption prediction-avoidance-mitigation framework. This framework evolves from the disruption prediction system developed on NSTX, which to date identified 96% of the disruptions with sufficient warning for active mitigation. The framework and real-time control algorithms for this sophisticated system will be transferrable to that being developed for ITER. Planned NSTX-U studies of the density assimilation dependence on the poloidal position of Massive Gas Injection (MGI) for disruption mitigation could also potentially influence the design of the ITER MGI system if results are obtained early enough during NSTX-U operation.

NSTX-U will retain the NSTX set of six mid-plane non-axisymmetric (3D) field control coils which can be independently controlled to enhance plasma stability at high beta, control error fields, apply resonant magnetic perturbations for ELM control, and vary the rotation profile. Analysis for NSTX-U and data from other tokamaks (DIII-D, ASDEX-U, JET, MAST) shows that the addition of off-midplane 3D field coils in NSTX-U would enable much wider variation of the poloidal spectrum and mix of resonant versus non-resonant field components to improve the understanding of error field penetration, tearing mode triggering, resistive wall mode control, and rotation-damping by 3D fields. *To greatly expand the core and edge transport, stability, and rotation profile control in NSTX-U, an off-midplane array of 3D field coils is a high-priority facility enhancement for the 5 year period.* Understanding and controlling such 3D field effects will be critical for avoiding disruptions in both ITER and FNSF. Other specific areas of potentially strong contributions include radiative divertor solutions to the ITER-relevant heat fluxes expected on NSTX-U, and impurity transport using multiple conditioning and PFC scenarios to enable control techniques to be developed in impurity-seeded ITER plasmas.

Develop predictive models for fusion plasmas, supported by theory and challenged with experimental measurement: The low aspect ratio of NSTX-U provides access to physics regimes and phenomena that are important to a moderate aspect ratio tokamak reactor, but less easily observed in the present tokamaks. Thus, NSTX-U can play a special role in the world tokamak program in model validation. Two examples include: (1) energetic particle instabilities where the high value of energetic ion velocity and pressure excite instabilities prototypical of a reactor, and (2) turbulence at high normalized pressure where magnetic fluctuations due to micro-tearing turbulence become significant and drive anomalous electron transport. Supporting electron transport theory validation is an extensive suite of profile diagnostics and a world-leading capability to measure both density turbulence from ion-to-electron gyro-scales, and magnetic fluctuations expected from microtearing modes. Boundary layer physics will be a major component of the NSTX-U program by necessity – the divertor heat fluxes will be comparable to those expected on ITER and FNSF. The strong toroidicity at low aspect ratio is found to have strong leverage in validating the theory governing the scaling of the boundary layer heat flux widths. The research program also includes novel magnetic divertor geometries

such as the snowflake divertor and conventional reactor-relevant metallic PFCs. This major mission will be supported by a theory and modeling program aimed from "atoms to tokamaks," i.e., from atomistic modeling of liquid metals (and solids), by materials scientists, to scrape-off layer modeling with realistic boundaries.

NSTX-U facility and diagnostic capabilities and status, budget, user-base, and next-steps: Since the beginning of operation in FY2000, the NSTX facility has been the most scientifically and technically capable ST in the world fusion program. An upgrade to the NSTX facility was proposed in FY 2009 to provide a timely input for the FNSF construction decision, develop new solutions for the PMI, and better support ITER. The two main elements of the NSTX Upgrade Project are a new and more powerful center-stack and a tangentially-aimed 2nd NBI system. NSTX-U will double the toroidal field from ~0.5 T to 1 T, the plasma current from ~1 MA to 2 MA, the NBI heating and current drive power from ~7MW to 14MW at 90kV, and will greatly increase the plasma pulse length from 1-2 sec to 5-10 seconds. The tangential injection angles of the 2nd NBI enables much higher (~2x) plasma current drive efficiency and current profile control needed for fully non-inductive ramp-up and sustainment. NSTX-U will retain the previous 6 MW of High-Harmonic Fast Wave (HHFW) system for heating and current drive, and the total 20MW NBI and HHFW systems will allow NSTX-U to uniquely produce FNSF/DEMO relevant high divertor heat fluxes. The Upgrade Project is now in the final construction phase, is scheduled for completion in September 2014, and research operations are expected in FY2015.

The NSTX-U user facility has substantial national (245 total, 156 funded by DOE Fusion Energy Sciences (FES) grants) and international (61) researcher participation and supports many early career scientists including 13 post-docs and 33 students. The collaborating institutions will be providing and supporting approximately half of the over 50 state-of-the-art diagnostic systems on NSTX-U. Assuming the DOE-FES funding guidance for FY2014 through FY2018 (based on the FY2012 budget adjusted for inflation), NSTX-U will be able to operate for 15 weeks per year on-average. This funding level will also support the baseline facility enhancements described above. With a 10% increment above the DOE-FES funding guidance, NSTX-U will be able to support 18-20 weeks of plasma operation, and implement the majority of the major facility and diagnostic enhancements delineated in the five year plan including the incremental items described above. With incremental funding, the research budget for both PPPL and collaborators will also be enhanced by 10% to support increased facility operations and capabilities.

If the NSTX-U 5 year plan facility enhancements are implemented and the research goals achieved, the ST will be well-positioned to become a viable candidate for an FNSF, advanced approaches to mitigating FNSF/DEMO-relevant heat fluxes will have been demonstrated (for short durations), and predictive capability for next-step STs, ITER, and DEMO will have been significantly expanded. Further, NSTX-U/PPPL researchers and the wider ST community will be well-positioned to lead or contribute to any future larger-scale FNSF design activities.

Table of Contents for Chapter 1

Chapter 1

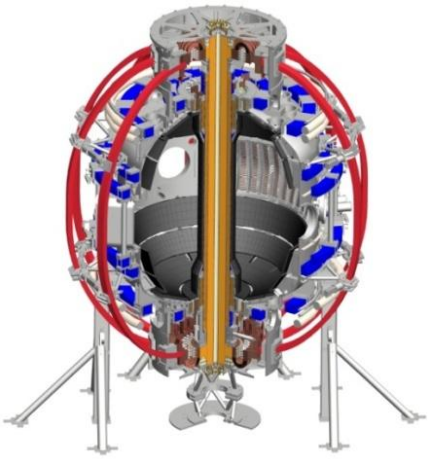

Overview of the NSTX Upgrade Five Year Plan for 2014-2018

1.1 Introduction

Research utilizing the low-aspect-ratio "spherical" tokamak (ST) [1] makes important contributions to the world magnetic fusion program on two fronts. First, the ST configuration is characterized by strong intrinsic plasma shaping and enhanced stabilizing magnetic field line curvature. These unique ST characteristics enable the achievement of a high plasma pressure relative to the applied magnetic field and provide access to an expanded range of plasma parameters and operating regimes relative to the standard aspect ratio tokamak. For example, NSTX [2,3] has accessed a very wide range of dimensionless plasma parameter space with toroidal beta up to 40%, normalized beta up to 7, plasma elongation up to 3, normalized fast-ion speed $v_{fast}/v_{Alfvén}$ up to 5, Alfvén Mach number $M_A = v_{rotation}/v_{Alfvén}$ up to 0.5, and trapped-particle fraction up to 90% at the plasma edge. All of these parameters are well beyond what is accessible in conventional tokamaks, and these parameters approach those achievable in other high-beta alternative concepts. Further, it is also possible and common to overlap with conventional aspect ratio tokamak physics parameters. These characteristics therefore allow ST research to complement and extend standard aspect-ratio tokamak science while providing low-collisionality, long pulse-duration, and well-diagnosed plasmas to address fundamental plasma science issues – including burning plasma physics in ITER [4].

The fundamental scientific goal of ITER is to generate plasmas dominated by alpha particle heating and to understand the dynamics of the thermal and energetic plasma particles under such conditions. The dynamics is potentially non-linear, since a relatively large population of energetic ions originates from fusion reactions (alpha particles), Neutral Beam (NB) injection and injected RF waves may drive Alfvénic instabilities. Of particular concern for ITER are fast-ion-related 'bursting' phenomena that occur on fast time scales, since few control tools are envisioned (possibly dominant ECH heating) for their mitigation or suppression. Thus, energetic particle (EP) research is of high importance to understand the coupled (and predominantly non-linear) dynamics of fast ions and Alfvénic instabilities and eliminate or minimize their potential harm to a reliable exploitation of fusion energy.

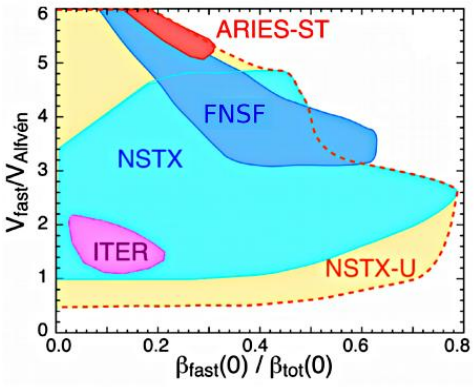

Figure 1.1.1: Ratio of fast ion to Alfvén velocity vs. ratio of fast ion to total pressure for energetic particle research for existing US tokamaks in comparison with expected values for ST-based reactors and for ITER.

The challenge for present tokamaks is to provide the required physics basis to develop and validate theoretical and numerical modeling tools. The parameter regimes accessible in NSTX will be significantly broadened in NSTX-Upgrade/NSTX-U [5] as shown for example in Figure 1.1.1 (and discussed extensively in Chapter 6), with significant overlap with expected energetic particle parameters of future devices such as ITER and ST-FNSF [6]. The capability of spanning a much broader range of parameters for EP physics than conventional tokamaks represents an important advancement for extrapolations from today's experiments to burning plasma regimes.
Second, the reduced aspect ratio and smaller major radius of the ST can provide access to high divertor heat flux which can be exploited to develop plasma-material-interface (PMI) solutions for heat-flux mitigation and particle control [7,8]. Further, the high neutron wall loading potentially accessible in an ST-based Fusion Nuclear Science/Component Test Facility (FNSF/CTF) [6,9,10] could prove attractive for materials and component development for next-step devices. The modular configuration of the ST [9] could also potentially improve accessibility and maintainability in support of high duty factor operation for PMI and FNSF missions. Longer term, the resistive dissipation in the toroidal field of a normally conducting ST power plant [11] or Pilot Plant [12] is generally a disadvantage for electricity production. However, the ST ($A < 2$), combined with $A \approx 3$ conventional aspect ratio tokamaks can strongly inform the physics performance of reduced aspect ratio (A=2-2.6) super-conducting Demo concepts studied in Japan that are projected to minimize device mass, cost, and radioactive waste [13-18]. A range of low-A configurations is shown in Figure 1.1.2. NSTX Upgrade parameters are highlighted in yellow to show that NSTX-U will provide the next factor two in plasma current, magnetic field, and heating power toward an ST-FNSF or Pilot Plant.

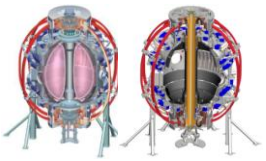

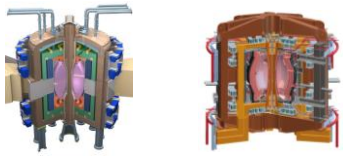

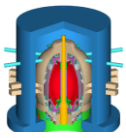

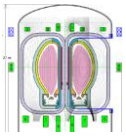

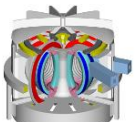

Parameter	NSTX	NSTX Upgrade	Fusion Nuclear Science Facility	Pilot Plant
Major Radius R_0 [m]	0.86	**0.94**	1.3	1.6 – 2.2
Aspect Ratio R_0 / a	≥ 1.3	**≥ 1.5**	≥ 1.5	≥ 1.7
Plasma Current [MA]	1	**2**	4 – 10	11 – 18
Toroidal Field [T]	0.5	**1**	2 – 3	2.4 – 3
Auxiliary Power [MW]	≤ 8	**≤ 19***	22 – 45	50 – 85
P/R [MW/m]	10	**20**	30 – 60	70 – 90
P/S [MW/m^2]	0.2	**0.4**	0.6 – 1.2	0.7 – 0.9
Fusion Gain Q			1 – 2	2 – 10

** Includes 4MW of high-harmonic fast-wave (HHFW) heating power*

Figure 1.1.2: Example low-A tokamak configurations and parameters ranging from NSTX to Power Plants.

The ST configuration also faces many challenges that must be overcome before the ST could be utilized for PMI or FNSF applications [19]. First, both PMI and FNSF applications require very long pulse-lengths (10^3-10^6s), which for STs with small or no solenoid flux implies steady-state operation. To-date, STs (including NSTX) have only sustained non-inductive current-drive fractions of ~65-75% in high-performance H-mode plasmas. Fully non-inductive current drive and sustainment must be demonstrated and the integrated plasma performance assessed before any long-pulse next-step ST can be reliably designed. For the FNSF mission, neutron damage to the centerstack precludes usage of a conventional ohmic solenoid, so non-inductive current start-up and ramp-up are beneficial or required in addition to the requirement for non-inductive sustainment. Further, for the FNSF mission, compact ST-based devices with acceptable auxiliary power are only achievable if the energy confinement time is above the ITER ELMy H-mode scaling. While the ion thermal confinement in ST plasmas is routinely near neoclassical levels in beam-heated H-mode plasmas, thermal electron transport is the dominant power loss channel and remains relatively poorly understood. Long-pulse divertor solutions are also required for an FNSF of any aspect ratio and should be developed in present devices and in either a next-step PMI facility and/or the first phase of FNSF operation. Lastly, the development of radiation-tolerant magnets for normal-conducting TF coils in an ST-FNSF would also be required.

A major goal of the next 5 year plan period (2014-2018) is to address the key physics challenges of the ST identified above while advancing predictive capability for toroidal magnetic confinement more broadly. The primary enabling capability for the next 5 year period of NSTX operation is the major upgrade of NSTX presently scheduled to be completed in 2014.

Figure 1.1.3: (left) Comparison of previous vs. new center-stack of NSTX-U, (right) comparison of present and new 2nd NBI.

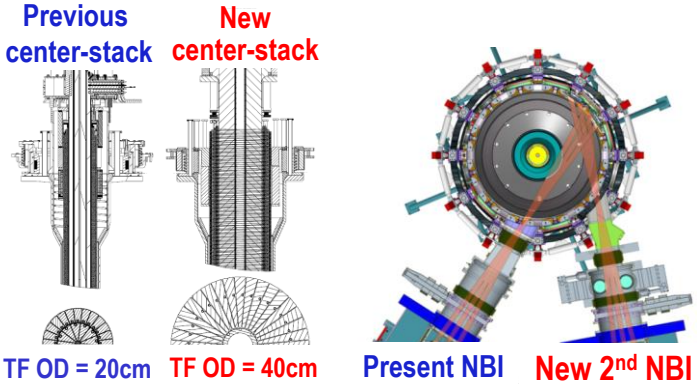

The upgraded NSTX facility (i.e. NSTX Upgrade/NSTX-U) consists of three new major components: (1) a new center-stack capable of doubling the toroidal field, tripling the solenoid flux, and increasing the flat-top duration up to a factor of 5, (2) a second more tangentially injected neutral beam to double the plasma heating and external current drive while also increasing the current drive efficiency and controllability, and (3) structural enhancements to withstand up to a factor of 4 increase in electromagnetic loads enabling a doubling of the plasma current. The new centerstack and 2nd NBI of NSTX-U is shown pictorially in Figure 1.1.3.

The doubling of the toroidal field, plasma current, and NBI heating will provide data critical to the determination of the scaling of thermal confinement as a function of field and current while maintaining access to high β. Expressed in terms of dimensionless parameters, a key physics goal of NSTX-U is to access 3-5 times lower collisionality ν* at similar β and shaping (κ, δ) as NSTX to assess transport, stability, and non-inductive start-up and sustainment at dimensionless parameters much closer to those expected in an ST-based FNSF as shown in Figure 1.1.4. In particular, it is noteworthy that NSTX and MAST have measured a strong (nearly inverse) scaling of normalized confinement with ν*, and if this trend holds at low ν*, high fusion neutron fluences could be achievable in very compact ST-FNSF devices.

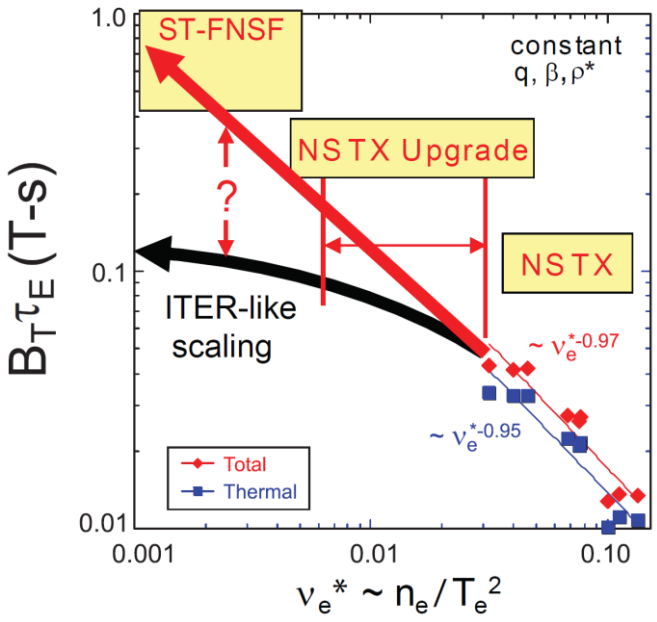

Figure 1.1.4: Product of toroidal field (B_T) and energy confinement time (τ_E) versus ν^*_e for NSTX and projections for NSTX-U and ST-FNSF for ITER H-mode and ST confinement scalings.

Achieving high β_N ~ 5-6 at increased aspect ratio is important not only for accessing the unique physics regime of high β at reduced ν*, but also for assessing the ability to access the required normalized performance of next-step STs as shown in Figure 1.1.5. Beyond extending toroidal plasma predictive capability and establishing the physics basis for possible ST applications, NSTX-U also has a 5 year plan goal of accessing performance levels prototypical of next-steps and approaching Pilot-Plant regimes.

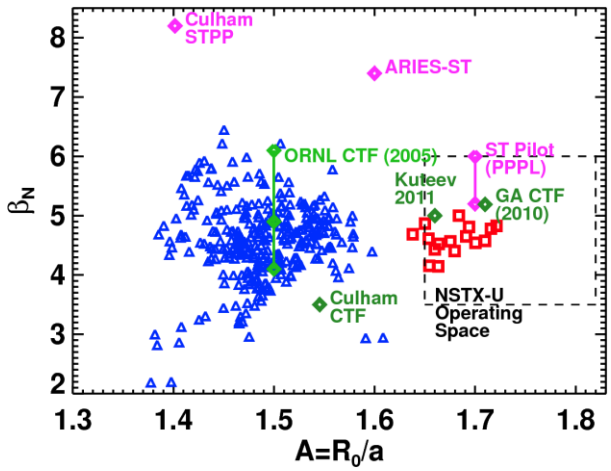

Figure 1.1.5: Achieved β_N vs. aspect ratio A for NSTX (triangles, squares) and values for next-step STs.

Figure 1.1.6 shows that the bootstrap current fractions projected to be accessible in NSTX-U overlap with PMI and FNSF applications and can access the lower-bound levels needed for a Pilot Plant. Similarly, the highest normalized confinement levels (based on extending NSTX values) overlap with the lower ranges needed for PMI, FNSF, and Pilot regimes. The expected high β_N ~ 5-6 is sufficient for PMI and FNSF applications and could also support Pilot Plant requirements. Lastly, the highest levels of normalized heat flux P/S accessible in NSTX-U touch on the lower-bounds expected in PMI, FNSF, and Pilot applications, and are within a factor of 2 of providing prototypical heat fluxes.

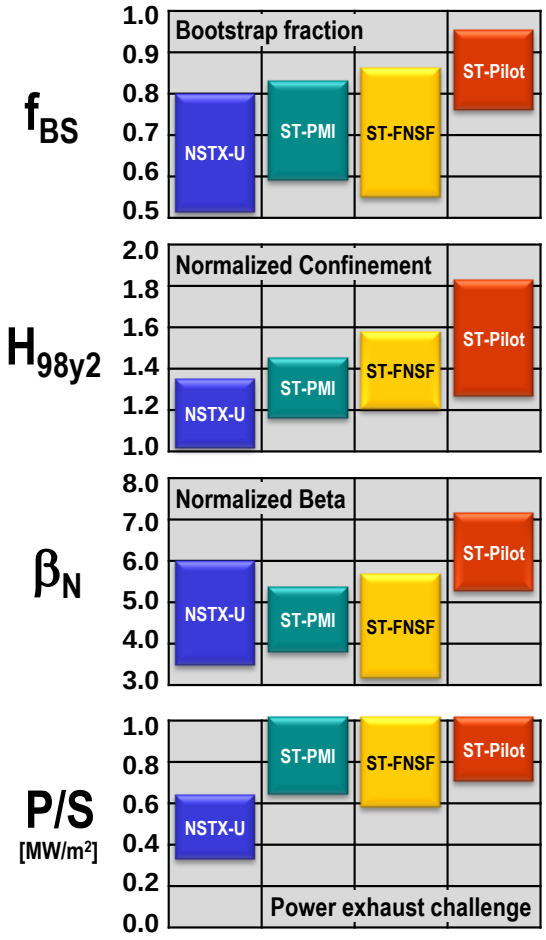

Figure 1.1.6: Normalized parameters projected for NSTX-U compared to possible next-step STs.

Thus, in summary, NSTX-U is expected to inform the achievable performance of all next-step ST options while also contributing strongly to conventional aspect ratio tokamak predictive capability and high-performance scenarios.

1.2 Long-Range Goals and Plans for NSTX Upgrade

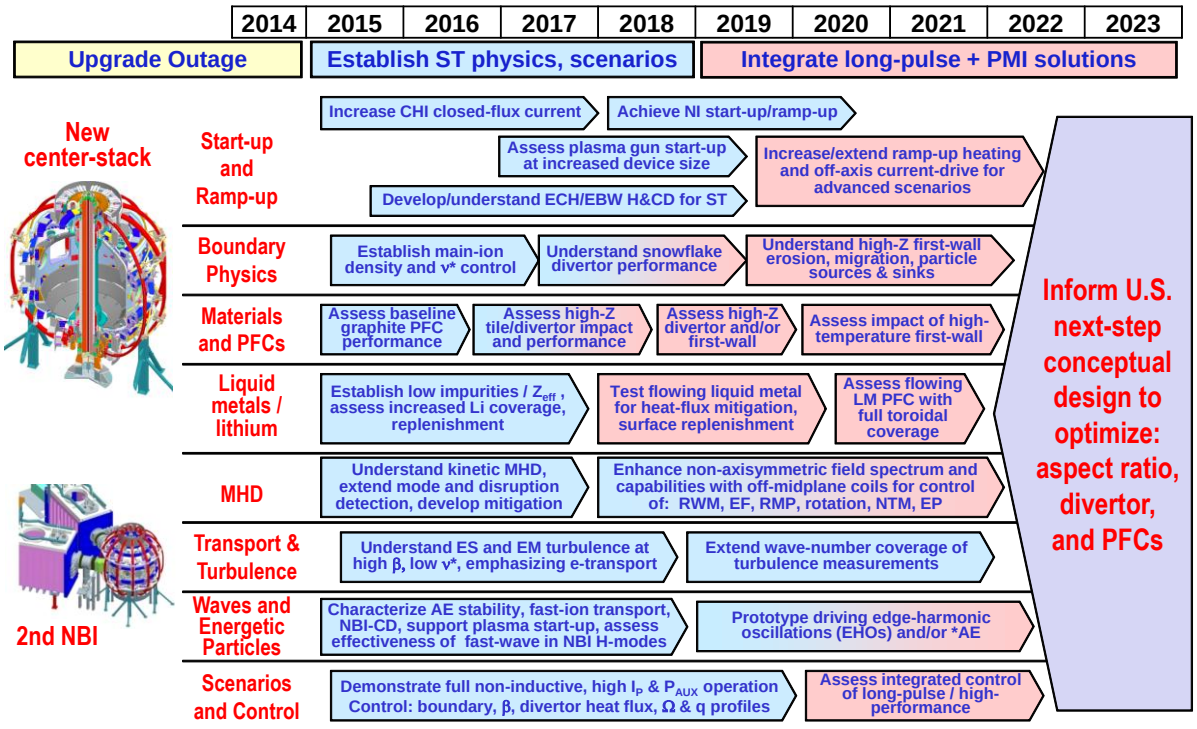

Figure 1.2.1.1: Long-range goals and plans for NSTX-U research in support of PMI research, FNSF, ITER, and DEMO assuming incremental funding of 10% above base funding.

1.2.1 Overview

The NSTX-U research team has developed a comprehensive long-range (10 year) set of goals and plans in support of advancing the ST configuration as a next-step PMI or FNSF facility and to address important scientific and operational issues for ITER and a DEMO. As shown in Figure 1.2.1.1, this long-range plan is divided into 2 phases. The first phase extends from 2014-2018 and emphasizes extending the ST physics basis and demonstrating high-performance operational scenarios including advanced divertor operation. At the end of this first 5 year period, the potential of the ST as a viable next-step candidate can be evaluated by considering NSTX-U (and MAST-U) progress toward achieving non-inductive start-up, ramp-up, and sustainment, reducing high divertor power loads, understanding electron thermal transport, and achieving high plasma [19]. The second phase (2019-2023) consists of further increasing the pulse-length and assessing the viability of integrating high-performance plasma scenarios (100% non-inductive, high β, high confinement) with next-step-relevant long-pulse PMI solutions such as high-Z solid and low-to-mid-Z liquid metal plasma facing components. This second phase of research would strongly contribute to next-step facility design and development independent of whether such a facility was low aspect ratio or conventional aspect ratio.

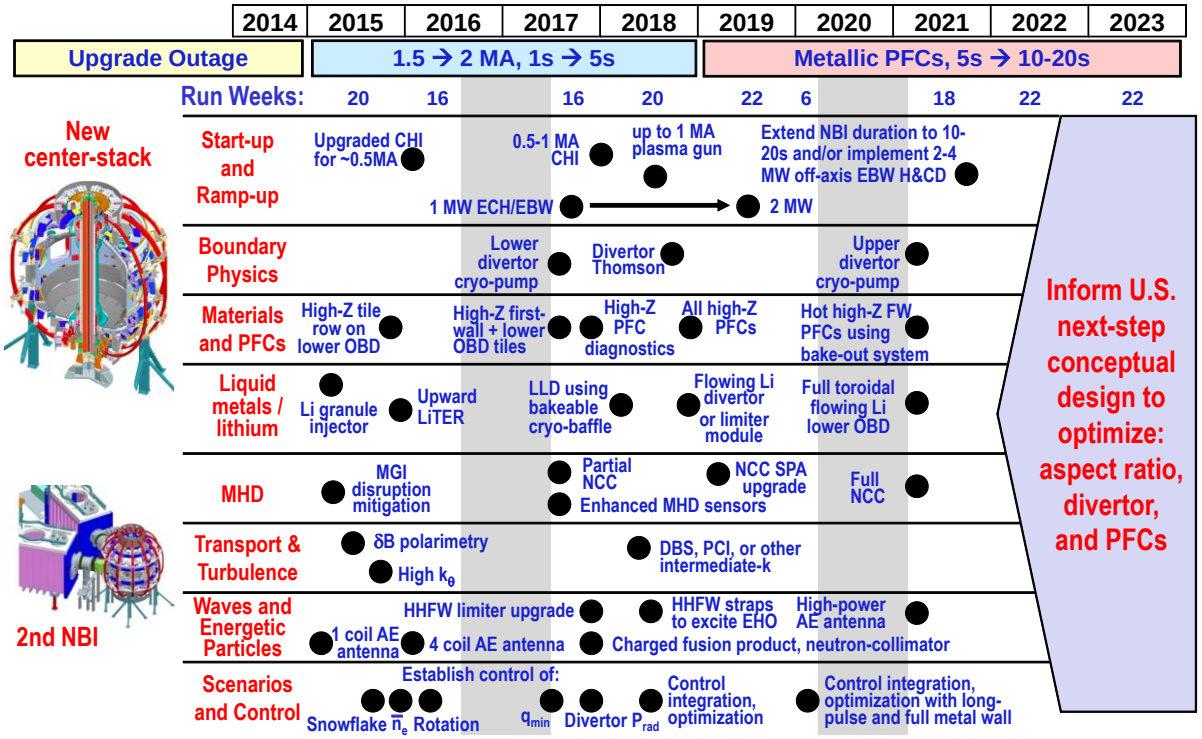

Figure 1.2.1.2: Proposed tools supporting long-range goals and plans from Figure 1.2.1.1 and assuming incremental funding 10% above the base 5 year plan guidance funding level. Vertical grey bars represent ~1 year outage periods utilized to implement major in-vessel upgrades.

Figure 1.2.1.2 shows the tools proposed to support the long-range goals and plans. The plans and tools shown in Figures 1.2.1.1 and 1.2.1.2 would provide a major contribution to the U.S. fusion program in support of developing predictive capability for magnetic fusion and for design of a next-step PMI or FNSF facility. The program and upgrade plan as shown assumes an incremental funding level 10% above base NSTX-U 5 year plan guidance funding. This phased research approach is also feasible at lower funding levels but would require additional time to implement. The plan above also proposes operation for an average of 18 run weeks per operating year which is at or near the highest level achieved over the operating history of NSTX. Additional run-weeks (up to an approximate maximum of 24) could be achieved by reducing both facility upgrades and the duration of associated outage periods.

Plan overviews assuming incremental and lower funding levels are provided in the sections that follow. It should be noted that these plans emphasize new capabilities beyond those already implemented on NSTX, which are expected to also be available on NSTX-U (see Chapter 10 for more details).

1.2.2 High-level Goals for the NSTX-U 5 Year Plan Period

To guide the prioritization of research and facility upgrades for the near-term, five high-level goals have been established for the NSTX-U five year plan period of 2014-2018:

1. Demonstrate stationary 100% non-inductive operation at performance that extrapolates to $\geq 1 MW/m^2$ neutron wall loading in FNSF
2. Access reduced ν^* and high-β combined with the ability to vary q and rotation to dramatically extend ST plasma understanding
3. Develop and understand non-inductive start-up and ramp-up to project to ST-FNSF operation with small or no central solenoid
4. Develop and utilize the high-flux-expansion "snowflake" divertor combined with radiative detachment to mitigate very high heat fluxes
5. Begin to assess high-Z PFCs plus liquid lithium to develop high-duty-factor integrated PMI solutions for SS-PMI and/or FNSF facilities, and beyond

In support of these high-level goals, and expressed in terms of the key scientific issues to be resolved, a cross-cutting set of tools has been identified. These tools are given highest priority in the plan and are included in both the incremental and base 5 year plan budget scenarios. These tools and the issues they help resolve are shown pictorially in Figure 1.2.2.1. These and other tools available to achieve the high-level goals are described for 3 different funding scenarios in the following sections: 1.2.3: Incremental, 1.2.4: base, and 1.2.5: FY2013 Administration levels.

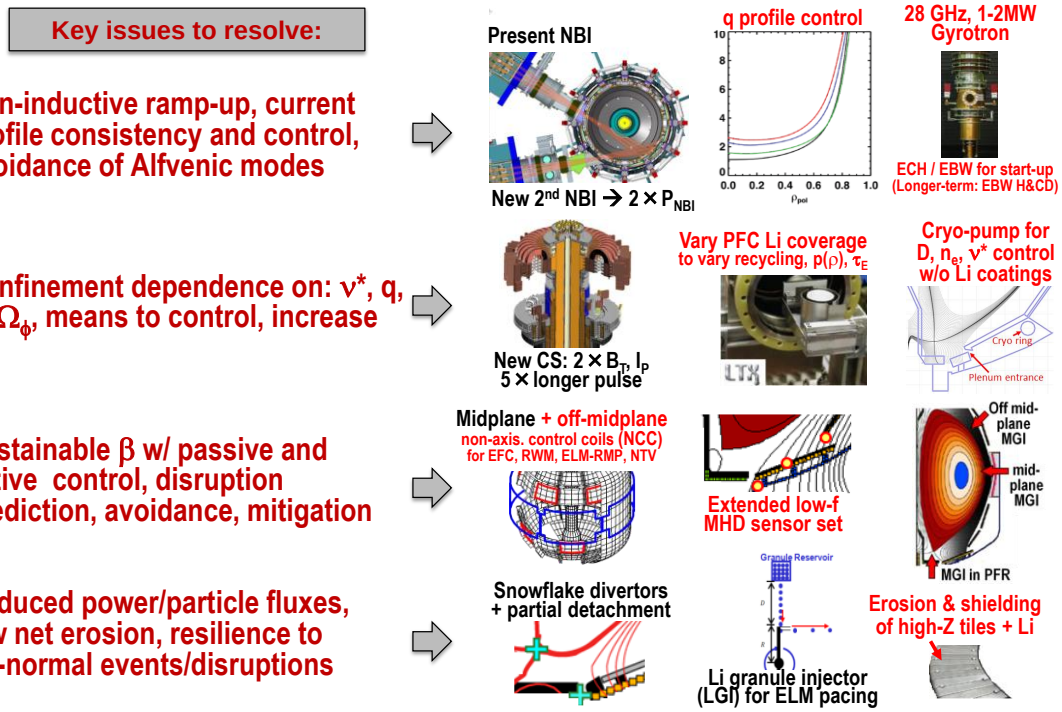

Figure 1.2.2.1: Key scientific issues to be resolved and proposed high-priority research tools in support of the 5 high-level goals. Existing/early tools are labeled in black, new/additional tools are labeled in red.

1.2.3 Goals, Plans, and Tools with Incremental 5 Year Plan Funding

First, to recapitulate, the incremental 5 year funding plan is shown above in Figure 1.2.1.2 in Section 1.2.1. In strong support of the development of non-inductive current formation and ramp-up in the ST, the CHI start-up current will be progressively increased to the 0.5-1 MA range exploiting the higher toroidal field of NSTX-U, plasma guns would be implemented and tested to high current (pending successful development on Pegasus), and 28GHz ECH heating of 1MW (later up to 2MW) implemented to heat CHI and/or high-current (~1MA) plasma gun target plasmas from the 10's of eV range to the 100's of eV range. Increased electron heating of the helicity injection plasma is needed to provide higher electron beta for effective high-harmonic fast-wave (HHFW) absorption (see Chapter 7), and to extend the helicity-injection-formed plasma current decay time from ~1-10ms to ~10-100ms (see Chapter 8) to enable sufficient time to establish gap control for efficient HHFW coupling. Without heating from either ECH or HHFW, NBI heating and current drive will likely not be effective either due to shine-through in the low-density CHI target, and/or because the current drive efficiency is likely too low to provide enough current drive to counteract the rapid decay of the helicity injection plasma (see Chapters 8 and 9). Later in the research program, the same gyrotrons would also be used for high-power EBW coupling, heating, and current drive studies in over-dense plasmas during start-up and in high-performance NBI-heated H-modes to begin to assess EBW as a possible long-term complement to (or eventual alternative to) NBI heating and current-drive (see Chapter 7).

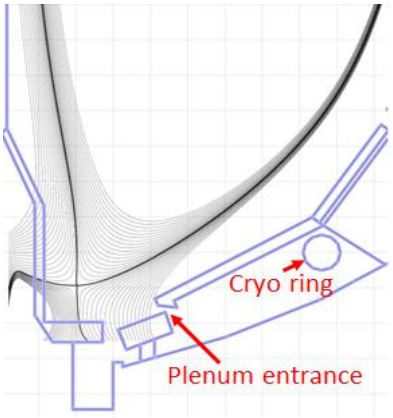

Figure 1.2.3.1: Proposed lower divertor cryo-pump

In boundary physics research, a divertor cyro-pump (see Chapter 4) as shown in Figure 1.2.3.1 would be implemented to provide controllable deuterium pumping without relying on lithium coatings, to compare to lithium-conditioned walls, and to support access to reduced collisionality. Achievement of long-pulse density control to support long-pulse scenario development on NSTX-U is a major motivating factor for the divertor cryo-pump. Further, divertor Thomson scattering would be implemented to measure electron density and temperature near the divertor target plate to support detailed assessments of the validity of leading divertor models for conventional and snowflake divertors for attached and detached conditions. The snowflake divertor and detachment will be systematically developed and utilized to mitigate the high heat fluxes expected for the higher power and current in NSTX-U.

Also in boundary physics research and contingent upon the development of sufficient divertor heat-flux mitigation strategies, the impact and performance of high-Z divertor PFCs (either Mo/TZM or W) would be assessed starting with a single row of high-Z tiles on the lower

outboard divertor combined with nearly complete high-Z first-wall coverage of low heat-flux regions using high-Z coated graphite tiles all to support studies of low-hydrogenic-retention PFCs for next-step facility options. The single rows of high-Z tiles in the outboard divertor regions would provide initial data on the survivability of PFC designs in the high-heat-flux and potentially high-disruption-load regions of the chamber while also providing erosion and melting data (see Chapter 5). The inboard divertor PFCs would remain graphite (until outboard divertor high-Z PFC designs have been proven) to reduce risk of PFC damage in the high-triangularity plasma operation that is expected to be mostly routinely used for NSTX-U (see Chapter 9).

In lithium/liquid metal research, the lithium granule injector (LGI) originally developed for NSTX and successfully tested on EAST for triggering ELMs would be tested on NSTX-U as a means of triggering high-frequency (up to several hundred Hz) ELMs for controlling edge impurities (C and/or Mo/W) for long pulses and for replenishing lithium near the divertor strike-point during a discharge. Further, an upward-pointing lithium evaporation (LiTER) system would be implemented to increase lithium coating coverage and to reduce the exposed graphite PFC surface area to reduce C impurity accumulation in no/small ELM regimes that typically occur with strong lithium wall conditioning.

An important technical detail of the baffle plate of the cryo-pump is that it would be protected using primarily graphite PFCs, and would therefore require bake-out capability to remove water and other impurities following major vents. This bake-out capability also enables controlled (initial) temperature variation of the outboard divertor PFCs and variation of the lithium phase. This control capability will greatly expand studies of vapor shielding of high heat fluxes by lithium (see Chapter 5). Lastly, in support of the long-term goal of developing the understanding and technology of flowing lithium systems capable of providing a replenishable PFC surface either to mitigate erosion and/or high heat flux (through vapor shielding and/or radiation), a prototype flowing lithium module will be developed in the laboratory and implemented and tested in NSTX-U (if technically ready) near the end of the 5 year plan (see Chapter 5).

In MHD research, disruption mitigation tests using massive gas injection (MGI) planned for the NSTX 2011-2012 run campaign will be carried out to assess the fueling/assimilation dependence on poloidal location of injection in support of NSTX-U operation, ITER, and FNSF. The RWM state-space controller developed and utilized for NSTX will be tested and optimized to support long-pulse NSTX-U operation above the no-wall stability limit. Enhanced MHD sensors (divertor RWM δB sensors and possibly shunt tiles for disruption/SOL halo currents) would be implemented to improve disruption and/or ELM evolution understanding and/or enhance non-axisymmetric mode detection and control. A partial set (i.e. 6-12 coils vs. 24 for a full set) of off-midplane non-axisymmetric control coils (NCC) would be installed on the primary passive plates to dramatically expand the spectral flexibility of the 3D field system on NSTX-U in

support of neoclassical toroidal viscosity (NTV) damping research, error field and RWM control, rotation profile control, and RMP ELM control.

In turbulence and transport research, the high-k system used to investigate ETG turbulence on NSTX will be re-configured to better sample the wave-number range of the projected strongest ETG fluctuations and will include high-k_θ measurements. Polarimetry will be implemented to attempt to measure electromagnetic fluctuations from micro-tearing instabilities that non-linear gyrokinetic simulations indicate strongly contribute to electron thermal transport at high β and collisionality. Lastly, Doppler Backscattering (DBS) will be implemented to measure zonal flows and geodesic acoustic modes (GAMs) generated through non-linear turbulence interactions and thought to regulate low-k turbulence levels and which likely influence edge transport barrier (i.e. H-mode) formation.

In Wave Heating and Current Drive research, the high-harmonic fast-wave (HHFW) system will be utilized for heating low-current start-up plasmas from induction and/or helicity injection to support increasing the plasma temperature and duration to provide a target for NBI plus bootstrap current over-drive for non-inductive ramp-up. Further, HHFW acceleration of fast-ions and associated power absorption will be studied at higher toroidal field and correspondingly lower cyclotron harmonic number. The effectiveness of HHFW heating and current drive in high-performance NBI H-modes will be assessed, and if shown to be effective for ~0.5-1s timescales, the antenna limiter will be upgraded. Depending on the HHFW coupling efficiency as a function of antenna-plasma gap, and the fast-ion heating of the limiter from NBI injection, a more robust and/or actively-cooled outboard limiter may be needed to support simultaneous high-power NBI and HHFW for long pulses. Pending assessments of the operational impact of using a reduced number of HHFW straps, several HHFW antenna straps may be utilized for other purposes potentially including excitation/driving of edge harmonic oscillations (EHOs) (observed previously on NSTX) as a possible means of increasing edge particle transport.

In Energetic Particle research, the existing NSTX fast-ion diagnostic suite will be utilized to investigate the fast-ion density and current-drive profiles from the new 2nd NBI and to compare the measurements to theory (i.e. TRANSP/NUBEAM). The prototype antenna planned to be used for measuring Alfvén Eigenmode (AE) damping rates will be utilized on NSTX-U and quickly extended to 4 coil operation. TRANSP and FIDASIM simulations (see Chapter 6) indicate that NBI diagnostic signals could be significantly attenuated at the highest plasma densities anticipated in NSTX-U due to beam ionization over shorter injection distances. If attenuation is problematic and causes low signal-to-noise on fast-ion profile diagnostics, the fast-ion diagnostic set would be extended to include fusion source profile arrays and/or a neutron-collimator. Alfvénic instability excitation and fast-ion redistribution and loss will also be measured as a function of injection radius using the new 2nd NBI and compared to theory.

In advanced scenarios and control research, scenarios with non-inductive current fraction near 100% will be systematically explored, and high-current, partial inductive operation aiming for the facility maximum performance goal of 5 second pulses at I_P=2.0 MA and B_T=1.0T will also be explored as a key means of accessing low collisionality in NSTX-U. Emphasis will be placed on axisymmetric control development including control of the plasma boundary, vertical position, beta, and divertor heat flux control including snowflake divertor and detachment control. Density feedback control will also be developed in support of physics studies and scenario optimization and is expected to be especially important once the divertor cryo-pumping system is operational. Profile control development will be pursued emphasizing core plasma safety factor and rotation control using the 2nd NBI and 3D fields. Disruption detection and slow and fast ramp-down methods will be developed, and MGI tested and utilized as appropriate. Lastly, advanced scenario research will assess the achievable integrated performance of NSTX-U scenarios and then project to next-step ST device design.

1.2.4 Goals, Plans, and Tools with Base 5 year Plan Funding

The long-range goals of the NSTX-U research program assuming base funding are similar to those with incremental funding, but several goals and tools are necessarily delayed or deferred in the base funding case as shown in Figure 1.2.4.1. Highest priority is placed on establishing the ST physics and operational basis for next-step applications, and long-pulse PMI development and several of the more resource-intensive tools are deferred.

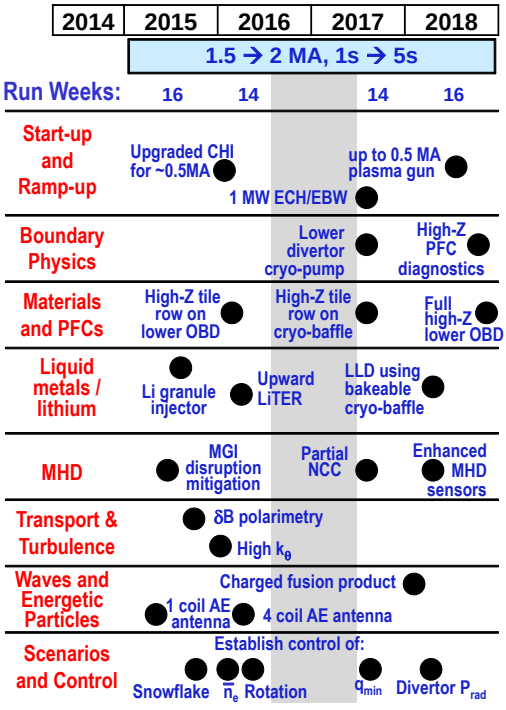

Figure 1.2.4.1: Proposed tools with base funding. Vertical grey bar represents ~1 year outage utilized to implement major in-vessel upgrades.

The development of non-inductive start-up and ramp-up is a unique ST challenge and remains strongly supported in the base plan to assess the viability of the ST as an FNSF. Capabilities for accessing up to 0.5MA of transient CHI are supported, as is up to 1MW of ECH/EBW for ECH heating and pulse-length extension of start-up plasmas for tests of HHFW/NBI heating and current over-drive ramp-up. However, in the base funding scenario, high-current (~1MA) CHI or plasma-gun research cannot be supported. Increased ECH/EBW power (from 1MW to 2MW) would be deferred several additional years.

Access to, and investigation of, reduced collisionality is a major research goal of NSTX-U and impacts nearly all topical science groups. Electron density control has historically been difficult in NSTX with only boron and/or lithium conditioned graphite plasma facing components. In the case of boronized walls, deuterium density pumping is difficult with wall pumping alone but carbon accumulation is acceptable (Z_{eff} ~ 2-3). With strong lithium evaporation, low deuterium density has been sustained, but the lack of ELMs can lead to carbon ion accumulation and Z_{eff} ~ 3-4. ELM triggering by 3D fields has been utilized in NSTX to help control carbon accumulation and achieve stationary electron density, but only near Greenwald fractions in the range of 0.8-1. Improved control of the Li evaporation rate and increased total Li deposition to control both the deuterium pumping and the impurity inventory (via ELM-induced flushing of impurities) may be able to provide sustained and controllable density control in NSTX-U. However, such techniques have not yet been developed for NSTX-U physics studies.

As a result, at the present time, for all funding scenarios, it appears prudent to plan for a divertor cryo-pump to provide a reliable and controllable means of deuterium inventory control with a configuration like that shown in Figure 1.2.3.1. The quantitative rationale for this choice is as follows: Using a definition of normalized collisionality ν^* in which the electron-ion collision frequency is normalized to the electron bounce frequency and assuming fixed geometry, it can be shown that $\nu^* \propto f_{GW}^3 / B_T \beta_N^2$. Here f_{GW} is the line-average electron density normalized to the Greenwald density limit, B_T is the toroidal magnetic field, and β_N is the normalized toroidal beta. Increased toroidal field and maintenance of high β_N are clearly important for accessing reduced collisionality. However, reducing and controlling electron density is especially important since $\nu^* \propto f_{GW}^3$. Thus, assuming naturally occurring or triggered ELMs can provide impurity density control, control of the deuterium via cryo-pumping to control the Greenwald fraction is projected to be an effective means of accessing low ν^*.

Due to resource limitations in the base plan, divertor Thomson scattering would be deferred and the conversion to high-Z PFCs would also be significantly delayed with only the conversion of the lower outboard divertor to high-Z completed by the end of the 5 year plan. The flowing lithium module would not be tested during the 5 year plan period, but usage of the bakeable cryo-baffle as a liquid lithium divertor would be retained in the base plan.

In MHD research, disruption mitigation tests would be carried out and the installation of a partial NCC retained, but improved MHD/RWM sensors would be implemented at a later date and upgrades to the NCC switching power amplifiers (SPA) to provide improved spectral control of the 3D fields would be delayed past the end of the 5 year plan period.

In turbulence and transport research, diagnosis of ETG (high-k) and micro-tearing turbulence (polarimetry) potentially responsible for electron transport are considered vital to establishing a

predictive capability for ST transport and are supported in the base plan. However, DBS and other possible intermediate-k diagnostics (such as PCI) would be deferred.

In wave and energetic particle research, there are insufficient resources to implement a long-pulse HHFW antenna limiter and an EHO excitation antenna in the 5 year plan period. The decision to proceed with either will be based on short-pulse assessments of HHFW heating in H-mode plasmas and on additional data analysis of EHO modes. Energetic particle measurements of the fusion source profile using a charged fusion product diagnostic would be retained in the base plan to support diagnosis of plasmas at high current and density.

Lastly, for advanced scenario development and control, the upgraded center-stack and the 2nd NBI of NSTX-U provide nearly all of the necessary actuator capability for the proposed research, and additional diagnostics and algorithms are either planned to be provided by collaborators and/or are expected to be sufficiently funded in the base program. Thus, the base and incremental plans for advanced scenario and control development are largely the same.

In terms of run-time, the base-plan supports an average of 15 run weeks per operating year which is roughly typical of NSTX operation. Additional run-weeks could be achieved by reducing facility upgrades and associated outage periods.

1.2.5 Goals, Plans, and Tools with Reduced Funding Levels

The near-term deliverables of the NSTX-U program assuming a funding level consistent with the FY2013 Administration Request budget would be significantly delayed and the scope substantially reduced relative to the 5 year plan base budget guidance as shown in Figure 1.2.5.1. Highest priority remains placed on establishing the ST physics and operational basis for next-step applications, but long-pulse PMI development and nearly all major facility upgrades are deferred. In this funding scenario, only 3 years of the 5 year plan have any significant operational time for NSTX-U, and during those 3 years there are only 12 run weeks each year.

As stated previously, the development of non-inductive start-up and ramp-up is a unique ST challenge and must remain supported at some level in any funding scenario. Capabilities for accessing up to 0.5MA of transient CHI are supported, but both the 1MW of ECH/EBW for ECH heating and CHI pulse-length extension are deferred, as is testing of a plasma-gun (at any current level) for non-inductive start-up.

Despite the attractiveness of divertor cryo-pumping for density control, the cost and time needed for design and implementation of cryo-pumps would delay implementation for 1-1.5 run-years relative to the base and incremental funding scenarios. Given the necessary delay in implementing cryo-pumping, means of possibly reducing impurity accumulation (via triggered

ELMs using lithium granule injection) and extending the duration/coverage of lithium pumping of deuterium (via upward evaporation) are the highest priority lithium research activities. High-Z PFC coverage in the divertor region would be reduced to a single row of high-Z tiles.

In MHD research, disruption mitigation tests would be carried out and enhanced MHD sensors would be implemented, but mitigation studies are delayed ~1 year and no NCC coils would be installed during the 5 year plan period.

In turbulence and transport research, diagnosis of ETG and micro-tearing turbulence potentially responsible for electron transport are considered vital to establishing a predictive capability for ST transport and remain supported in all funding scenarios due to modest resource requirements.

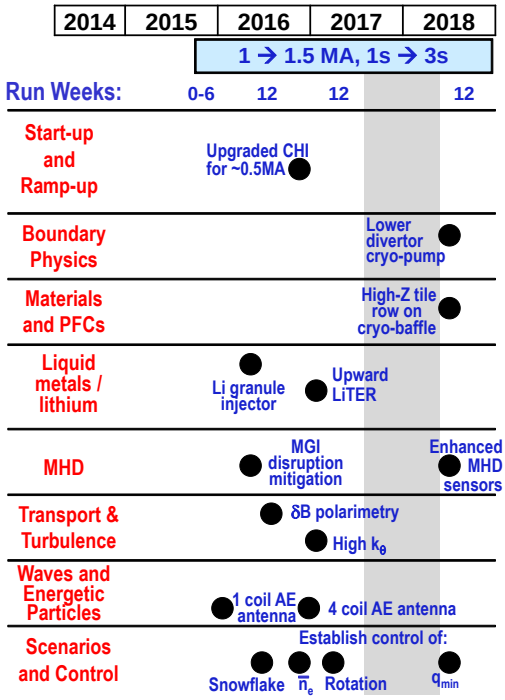

Figure 1.2.5.1: Proposed tools with FY2013 budget. Vertical grey bar represents ~1 year outage period utilized to implement major in-vessel upgrades.

In fast-wave research, there are insufficient resources to implement a long-pulse HHFW antenna limiter or an EHO excitation antenna. Thus, no major upgrades are implemented for HHFW (or ECH/EBW) during the five year period. In energetic particle research the AE antennae are retained since they are relatively inexpensive, but enhanced fast-ion profile diagnostics are deferred which will reduce data fidelity at high plasma density.

Lastly, for advanced scenario development and control, the control algorithm development would be delayed ~1 year and divertor radiation control would not be implemented during the 5 year period, but control development for snowflake, density, rotation, and q profile is retained.

Even with funding for the NSTX-U research program at the FY2013 Presidential budget level, a scientifically compelling and highly productive research program can be achieved. This opportunity is enabled by the substantial investment and capability implicit in the new centerstack and 2nd NBI of the NSTX Upgrade project. Nevertheless, full utilization and exploitation of NSTX-U within the 2014-18 five year plan period is only possible with funding at the 5 year plan base or incremental levels.

1.3 Organization of the Five Year Plan and Team

The NSTX Upgrade research program is organized by topical science area into "Topical Science Groups" (TSGs). Each TSG represents an important area of tokamak/ST research of sufficient importance and specialization that a dedicated group is required to lead research in this area. The TSG leadership structure has one TSG leader, one deputy leader (typically both experimentalists), and in almost all cases a third leader for theory and modeling support of the experiments. The inclusion of theory and modeling in the leadership structure is designed to enhance the scientific coupling between theory and experiment in NSTX-U research. TSG leadership responsibilities/actions include:

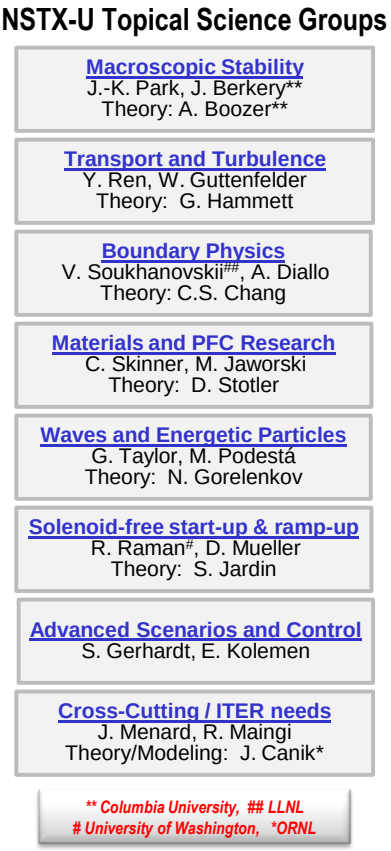

Figure 1.3.1: Topical Science Groups of the NSTX-U research program.

1. Organize, propose, and execute experiments to achieve milestones and address priorities and thrusts
2. Determine and address the highest priority scientific issues within a topical area through group discussion and including the NSTX-U team in TSG meetings
3. Organize the NSTX-U Research Forum guided by (but not limited to) these priorities
4. Define draft scientific and performance milestones utilizing expertise of the TSG
5. Define facility and theory resources required to achieve research goals
6. Aid dissemination of results (help Physics Analysis & Simulation Division)
7. Provide brief summaries of TSG scientific progress at team meetings and other venues
8. Assist and report to the NSTX-U Program and Project directors

The topical science group structure (as of January 2013) is shown in Figure 1.3.1. The NSTX-U five year plan chapters of this document are organized with a very similar structure and were coordinated and/or written in large part by members of the TSG leadership. The only significant differences between the TSG structure and 5 year plan chapter structure are: 1) the Waves and Energetic Particles TSG research is divided into two chapters (Chapter 6: Energetic Particles and Chapter 7: Wave Heating and Current Drive), and 2) cross-cutting activities (such as cryo-pump physics design) and ITER needs and support are incorporated throughout the plan. Lastly, as described further in Chapter 11, NSTX-U collaborators play an essential role in defining and leading the NSTX-U program and strongly contributing to the 5 year plan.

1.4 Summaries of Five Year Plan Research Thrusts

1.4.1 Overview

The NSTX-U 5 year plan is organized into 11 chapters. There are 8 dedicated topical science plan chapters based on the TSG group structure described above. The chapters and corresponding topics are: (1) Overview, (2) Macroscopic Stability, (3) Transport and Turbulence, (4) Boundary Physics, (5) Materials and Plasma-Facing Components, (6) Energetic Particles, (7) Wave Heating and Current Drive, (8) Plasma Formation and Current Ramp-up, (9) Plasma Sustainment: Advanced Scenarios and Control, (10) Facility Capabilities and Upgrades, and (11) Documentation of Collaborator Plans. Each of the 8 topical science areas (Chapters 2 through 9) have identified 2 to 4 research "thrusts" that will be carried out to achieve the high priority research goals identified in Section 1.2.2. Brief summaries of the research thrusts are described below to provide an overview of the research goals of the NSTX-U 5 year plan. More detail on thrust motivation and plans can be found in corresponding chapters of the 5 year plan.

1.4.2 Macroscopic Stability Research Thrusts

1.4.2.1 Sustainment of macroscopic stability

Global MHD instabilities (e.g. kink/ballooning mode, resistive wall mode (RWM), neoclassical tearing mode) are critically important to avoid or control as they lead to plasma disruption, terminating the discharge and leading to large, potentially damaging electromagnetic forces and heat loads on the structure of fusion producing devices. While many targeted performance parameters have been reached in world tokamaks, such plasmas will need to be sustained for far longer pulse lengths in machines such as FNSF, ITER, and DEMO than have been produced to date. Research has therefore changed focus to examine sustained global mode stability over long pulses and to examine profile evolution for routine long pulse operation at high beta and at high non-inductive current fraction. Common to the following studies is the unique physics understanding and control ramifications that come from such operation, and the understanding and prediction of the effect of excursions from this condition due to transient behavior. It is especially important to realize that plasma operation under marginal stability points (set, for example by plasma beta, internal inductance, rotation) is insufficient to ensure disruption-free, continuous operation in either ITER inductive or advanced scenarios due to these transients in plasma profiles. Such transients can rapidly change a stable operational point to an unstable plasma state. Therefore, understanding plasma stability gradients vs. key profiles affecting stability is essential for all operational states in ITER. NSTX-U will provide key capabilities for critical physics understanding based on present research in plasma operation regimes applicable to ITER and future magnetic fusion devices. NSTX-U will be unique in its operation in non-inductively driven plasmas. This major operational regime for NSTX-U, which may require

greater control, provides a unique laboratory to test advanced stability physics. Additionally, NSTX-U will operate in the unique high beta ST operational space, which will allow performance of advanced stability control in an operating space where disruptivity is *not* most probable at the highest β_N, or β_N/l_i. These considerations motivate the following thrust:

Thrust MS-1: Understand and advance passive and active feedback control to sustain macroscopic stability

> *With significantly expanded profile control capabilities (e.g. q, plasma rotation), NSTX-U will allow greater ability to vary these important profiles for investigations of how to prevent plasma disruptions excited by profile excursions. Additionally, profiles theoretically expected to improve stability will be attempted to be sustained at high performance, including fully non-inductive operation. Real-time models to determine favorable profiles for stability will be developed from experimental testing of full theoretical models. Research will focus on the effect of reduced plasma collisionality and energetic particles on the kinetic stabilization of disruptive instabilities, and sustaining stability. Shape and aspect ratio changes, the effect of advanced divertor configurations, and 3D multi-mode spectrum will be assessed. ITER-relevant low plasma rotation regimes will be evaluated. Disruption prevention research will be conducted as a combination of advanced active mode control techniques and active profile control. For example, instability onset leading to global modes growing on a relatively fast timescales (milliseconds) will be actively controlled by an expanded model-based RWM state space controller, while concurrent control of q and plasma rotation profile working on slower timescales (~100ms) will steer the plasma toward stability. Instabilities occurring before plasmas attain full current, and the ability to control largely internal modes will be addressed.*

1.4.2.2 Utilization of non-axisymmetric (3D) magnetic fields

A small non-axisymmetric (3D) field almost always exists in tokamaks, due to imperfect primary magnets and surrounding conductors and machine components. Tokamaks are highly sensitive to 3D fields, which can cause unnecessary transport and instability and even lead to a disruption if not properly compensated. On the other hand, 3D fields can be greatly beneficial if properly controlled, by timely inducing new neoclassical process with non-ambipolar transport and by consequently modifying equilibrium profiles and macroscopic stability, as well known by edge localized mode (ELM) control using resonant magnetic fields and resistive wall mode (RWM) and tearing mode (TM) control using non-resonant magnetic fields. Therefore, it will be critical to achieve the controllability as well as the predictability of these 3D field applications, in order to improve plasma stability and performance in the next-step devices such as FNSF, ST Pilot, and ITER.

There has been substantial progress in understanding of 3D field effects. Research on the n=1 resonant error field correction in NSTX using the ideal perturbed equilibrium code (IPEC) highlighted the importance of plasma response and the developed method has been actively applied to ITER along with the paradigm change in the error field correction. Also, the n=3 non-resonant error field correction was routinely used to maximize the toroidal angular momentum based upon successful validation across experiment and neoclassical toroidal viscosity (NTV) theory. In general, the study of magnetic braking in NSTX using 3D fields demonstrated the importance of NTV physics in tokamaks. Magnetic braking will be an essential tool to control the toroidal rotation and thereby suppress various instabilities in next-step devices. The NTV physics behind it is highly complex depending on regimes and needs further and deeper studies, but nonetheless a number of fundamentals in NTV physics have been theoretically understood, numerically verified, and validated from experiments in various devices including NSTX, DIII-D, and KSTAR. Another well-known effect of 3D fields is the local modification of transport and stability, either by non-ambipolar transport or by stochastic transport with magnetic islands. Although this is demonstrated by RMP ELM suppression in DIII-D, NSTX n=3 applications showed another possible 3D field effect by triggering ELMs rather than mitigating ELMs. All of this evidence points to the utility of 3D fields, but also to complex interactions between 3D fields and tokamak plasmas, and thus substantial research is still required.

NSTX-U will provide a highly relevant environment for 3D field research. Collisionality is one of the most important parameters to govern 3D field physics, and the low collisionality regime relevant for the next-step devices should be carefully and deeply explored. NSTX-U aims for higher temperature and low density operation, which will result in much lower collisionality. Also, the 6 independent switching power amplifiers (SPAs) will give more flexibility in field spectrum. Furthermore, the proposed non-axisymmetric control coil (NCC) will give unprecedented flexibility in 3D field studies, with two rows of coils that can produce static fields up to n=6 and rotating fields up to n=4. The poloidal field spectrum will also be as rich as the ITER RMP coils, if the NCC is combined with the present RWM/EF coil at the midplane and supplied by 6 SPAs. Initial studies show that a 2x6 coil set on the primary passive plates with a toroidal distribution of odd up-down parity is favorable for a range of applications. A possible progression of NCC implementation from a partial set (12 coils) to the full set (24 coils) in NSTX-U is shown in Figure 1.4.2.2-1. These considerations motivate the following thrust:

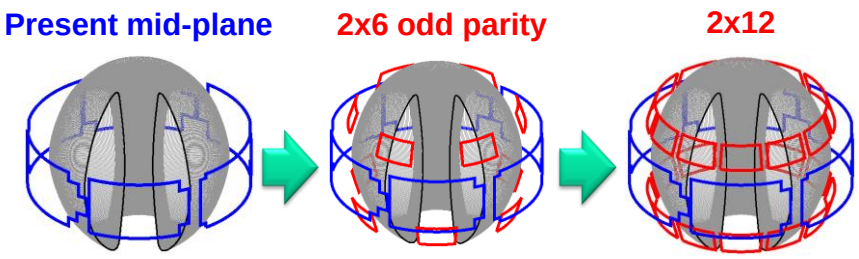

Figure 1.4.2.2-1: Possible progression of NCC coil implementation in NSTX-U.

Thrust MS-2: Understand 3D field effects and provide the physics basis for optimizing stability through equilibrium profile control by 3D fields

Expanded 3D field application capabilities will be utilized to study 3D field effects on resonant error field correction, and to develop the physics basis for control of toroidal rotation through non-resonant magnetic braking while simultaneously applying RWM control and dynamic error field correction. Non-ideal and non-linear island dynamics including neoclassical tearing modes, and the interplay with resonant and non-resonant error fields, will be studied together with strong shaping, high-β, and low collisionality. The NTV physics yielding magnetic alteration of the rotation profile will be systematically studied as a function of plasma collisionality as density control tools are improved during the 5 year plan period. This physics research will be greatly enhanced by the proposed NCC coils. The toroidal rotation profile will also be more widely varied using the 2nd off-axis NBI system. The combination of the new NBI, upgraded independent control of the present midplane coils, and proposed NCC will be utilized to vary and understand toroidal momentum transport for a range of magnetic field spectra and plasma collisionality conditions to develop the physics basis for magnetic rotation profile control to improve and optimize plasma performance.

1.4.2.3 Disruption physics, avoidance, detection, and mitigation

A key issue for ITER and the tokamak/ST line of fusion devices in general is the avoidance and mitigation of disruptions. As a general goal, disruptions must be avoided. The research program in Thrusts MS-1 and MS-2 above as well as in Thrusts ASC-2 and 3 develop many of the necessary tools for disruption avoidance. These tools by themselves, however, are not sufficient to meet the stringent requirements for reliable tokamak/ST operation. For example, disruption "mitigation" techniques is of great importance to ITER, where methods to terminate a discharge without excessive thermal or mechanical loading of the plant are required. These considerations motivate the following thrust:

Thrust MS-3: Study and develop techniques for disruption prediction, avoidance, and mitigation, and understand disruption dynamics and in high-performance ST plasmas

The physics understanding gained in the balance of the macroscopic stability research will be applied to improve disruption prediction and avoidance. Kinetic stability physics models, low frequency resonant field amplification, RWM state-space control models, and expanded sensor input will be used to improve disruption prediction. Real-time implementation of these physical models and measurements will be used for disruption avoidance. The plasma dynamics resulting from the interplay of different stability controllers will be measured and simulated. For instance, resonant field amplification methods will be developed to assess global stability, and may be coupled to the β_N or rotation control algorithms to ensure that the plasma remains in a stable regime. The characteristics and dynamics of NSTX-U disruptions will be measured and modeled – in particular heat loading, the thermal quench, and the generation of halo currents – all to improve the understanding of the impact of disruptions in STs and tokamaks. Techniques for disruption mitigation will be developed and explored. Massive gas injection (MGI) will be explored: the poloidal angle dependence of mitigation efficacy will be examined, and modeling of the gas penetration will be done. A novel electromagnetic particle injector (EPI) will be developed and tested. This technology has the potential to very rapidly deliver large amounts of the material to the plasma.

1.4.3 Transport and Turbulence Research Thrusts

1.4.3.1 Characterize global energy confinement

Future ST devices such as ST-FNSF are expected to operate at significanly higher toroidal field B_T, plasma current I_P, and heating power P_{NBI} than either NSTX or NSTX-U. To help establish the physics basis for future STs, which are generally expected to operate in lower collisionality regimes, it is important to characterize energy confinement over an expanded range of plasma parameters. Determining energy confinement scalings are especially important since compact (i.e. small-major-radius) ST FNSF devices will only be possible if sufficiently high confinement can be obtained. H-mode confinement studies in NSTX have shown that the global energy confinement exhibits a more favorable scaling with collisionality ($B\tau_E \sim 1/\nu^*_e$ – see NSTX data points in Figure 1.1.4) than that from ITER ELMy H-mode ITER98y,2 scaling ($B\tau_E \sim$ independent of ν^*_e – see black "ITER-like scaling" curve in figure 1.1.4). This strong ν^*_e scaling observed in STs unifies disparate engineering scalings between boronization ($\tau_E \sim I_P^{0.4} B_T^{1.0}$) and lithiumization ($\tau_E \sim I_P^{0.8} B_T^{-0.15}$) wall-conditioned plasmas. With a doubling of B_T, I_P and P_{NBI} and beams at different tangency radii, NSTX-U provides an excellent opportunity to assess the core confinement characteristics in regimes more relevant to future STs and to explore the accessibility to lower collisionality. These considerations motivate the following research thrust:

Thrust TT-1: Characterize and validate NSTX H-mode global energy confinement scaling in the lower collisionality regime of NSTX-U

NSTX-U researchers will re-establish and extend energy confinement studies and scaling to lower collisionality with higher B_T, I_P and NBI power ($B_T/I_P \leq 0.8T$ / 1.6MA in FY15 and 1.0T / 2MA in FY16 and beyond) for modest discharge durations (~1-3 seconds). Comparisons of the current and field scaling to the different scalings found on NSTX, which depended on wall conditions (lithiated or not) and different PFC materials, e.g. carbon vs high-Z will be carried out. Confinement will also be characterized in longer duration discharges that approach the magnet engineering limits (~5s flat-top) of NSTX-U and in advanced scenarios (i.e. fully non-inductive discharges) as they are developed. The range of collisionality for assessing global confinement will be extended to lower ν^* by reducing the plasma density using a divertor cryo-pump. These experiments will be coupled with low-k and high-k turbulence diagnosis and gyrokinetic simulations and will provide comprehensive datasets for understanding the mechanisms underlying the observed confinement scalings and also pedestal structure. Parameterizations of the NSTX-U confinement data will be extrapolated to future STs (e.g. FNSF) to assess the implications for ST-FNSF device size and required auxiliary heating power.

1.4.3.2 Identify instabilities responsible for anomalous ST transport

NSTX has made considerable progress in identifying instabilities underlying anomalous transports observed in NSTX. In particular, multiple instabilities have been identified as potential candidates responsible for anomalous electron thermal transport which ultimately limits the confinement performance of future devices and thus is of critical importance. Furthermore, experiment and modeling show that low-k turbulence is likely responsible for observed anomalous momentum and the non-neoclassical contribution to impurity transport whose understanding is important for calculating flow, bootstrap current and density profile etc. in future devices and thus is crucial for predicting and optimizing plasma stability and fusion gain and for achieving scenario sustainment. For example, to achieve the hot-ion scenario, low-k instabilities have to be controlled by ExB shear with optimized flow profile. From both theories and numerical modeling, NSTX has identified a range of the relevant instabilities, which include low-k modes (i.e. ion temperature gradient - ITG, trapped electron mode - TEM, kinetic ballooning mode - KBM, micro-tearing - MT), high-k modes (i.e. electron temperature gradient - ETG), and compressional and global Alfvén eigenmodes (AE), i.e. CAE/GAE. Example micro-instabilities already identified and studied for select NSTX equilibria (and to be extended to lower ν in NSTX-U) are indicated by the colored symbols in Figure 1.4.3.2.1 for different combinations of electron beta and collisionality. The approximate regions of possible mode instability and identity are indicated by the corresponding colored semi-transparent ellipses. Experimental evidence indicates that low-k and high-k modes and AE are all potentially important for electron thermal transport in different scenarios and in different radial regions. Some low-k modes, i.e. ITG/TEM/KBM, are also found to be relevant to momentum and particle/impurity transport. The identification of these candidate NSTX-U instabilities potentially responsible for anomalous transport motivates the following research thrust:

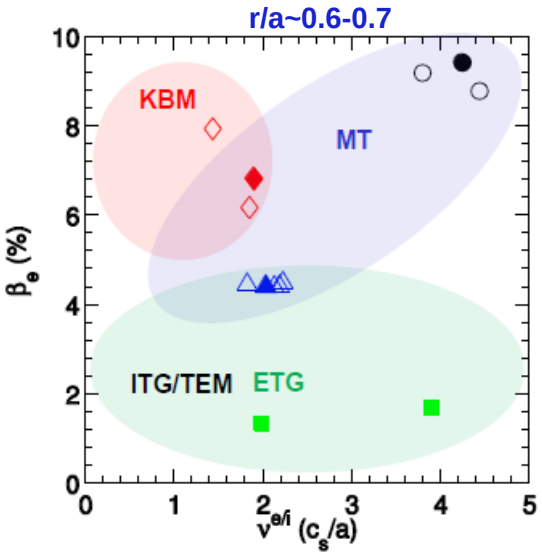

Figure 1.4.3.2.1: Ranges of accessible electron beta and electron-ion collisionality (normalized to sound-wave frequency) in NSTX/NSTX-U, and the micro-instabilities typically found to be unstable.

Thrust TT-2: Identify regime of validity for instabilities responsible for anomalous electron thermal, momentum, and particle/impurity transport in NSTX-U

NSTX researchers will identify isolated regimes for micro-instabilities using theories and reduced/first principle models, experiments for measuring turbulence and transport in these regimes and comparisons between measured transport levels and turbulence characteristics with theoretical and numerical predictions. Experimental parametric dependence will be used for further distinguishing different instabilities. For example, the dependence of micro-tearing and ETG modes on s/q and Z_{eff} are opposite to each other, and this trend can be utilized to identify each mode. The enhanced capabilities of NSTX-U, in particular the increased range of collisionality, doubled heating power from the 2nd NBI, and active flow and current profile modification using the 2nd NBI and 3D coils, will provide a versatile set of experimental control tools for modifying transport and turbulence to achieve the goals of this thrust.

1.4.3.3 Reduced transport models

It would be highly valuable to ITER, FNSF, and other next-steps to develop a physics-based 1D predictive capability of transport for use in integrated modeling that can predict plasma profiles which determine confinement scaling, MHD stability, and current profiles (from bootstrap and NBI/RF driven current) important for studying advanced operating regimes such as steady-state fully non-inductive scenarios. Even without 1D predictive capability, it is useful to have predictions for global (0D) energy confinement times that are used to estimate the required machine size, magnetic field, plasma current and density to achieve prescribed design criteria for future devices (e.g. ST-FNSF or Pilot). The highest priority transport channel to predict in STs is the electron temperature profile since the ion temperature is often expected to be described by neoclassical theory. The next highest priority transport channel to predict are density profiles for electrons, main ions and impurity ions. Perhaps the most challenging prediction is of toroidal flow profiles (momentum transport), which is ultimately critical to have a self-consistent prediction as the corresponding E×B shear strongly influences the drift wave turbulence. These considerations motivate the following research thrust:

Thrust TT-3: Establish and validate reduced transport models (0D and 1D)

NSTX-U researchers will develop and attempt to validate reduced transport models for a range of transport channels (thermal, particle, momentum) that can be used for profile predictions. For validation with experimental core measurements, boundary conditions will first be taken directly from measured profiles, such as near the pedestal top in H-mode plasma. A more complete predictive capability will also be pursued for projecting both 0D and 1D performance and will require a predicted pedestal height and location of each plasma species (and flow for flow profiles). These pedestal values will taken either from empirical pedestal scalings or validated physics-based pedestal models developed in the Boundary Physics TSG.

1.4.4 Boundary Physics Research Thrusts

1.4.4.1 H-mode pedestal structure and stability

For future fusion devices to achieve maximum fusion performance, it is vital to understand, control, and optimize the structure and dynamics of the H-mode edge transport barrier (aka the H-mode pedestal) to maximize the pedestal pressure and to avoid large damaging heat fluxes from edge-localized modes (ELMs). The expanded operating range of NSTX-U with respect to field, current, power, collisionality, and shaping will enable new H-mode transport and stability studies relevant to both spherical and conventional aspect ratio tokamaks. For example, large variations in triangularity and the ability to operate with up-down symmetric conventional or snowflake divertors will enable strong tests of leading models for the H-mode transition such as changes in the ion-orbit loss near the X-point leading to changes in the edge E×B shear and turbulence and transport. As is true for core transport and turbulence, assessing the dependence of edge transport and turbulence on collisionality will be high priority for NSTX-U. As shown in Figure 1.4.4.1.1, NSTX-U is expected to bridge the pedestal collisionality gap between NSTX and FNSF/Pilot Plant regimes. These considerations motivate the following boundary physics research thrust:

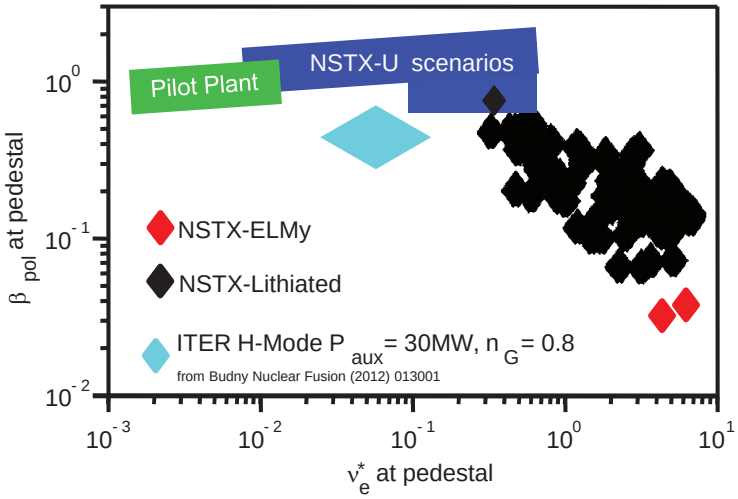

Figure 1.4.4.1.1: Pedestal poloidal beta and collisionality expected to be accessible in NSTX-U.

Thrust BP-1: Assess, optimize, and control pedestal structure, edge transport and stability

NSTX-U researchers will characterize the L-H mode transition thresholds utilizing the extended field, current, and power range of NSTX-U and by measuring turbulence and zonal flow dynamics with beam emission spectroscopy, Doppler backscattering, and gas-puff imaging diagnostics. The maximum achievable pedestal height and variation in pedestal structure will be assessed as a function of increased field, current, and power and also shaping and measured with enhanced spatial and temporal resolution Thomson Scattering. Increased control of pedestal transport and stability will be attempted using such techniques as edge density profile modification with improved fueling control, extended lithium coating coverage, and cryo-pumping. ELM triggering and suppression with 3D fields from mid-plane (existing) and off-midplane NCC (planned) coil-sets and

also triggering with lithium granule injection will be assessed. Enhanced pedestal H-modes (EP H-modes) will be further explored. As high-Z PFCs are introduced, their compatibility with good H-mode pedestal performance will be assessed.

1.4.4.2 Divertor performance

Divertor research on NSTX demonstrated that the ST divertor can present both an opportunity and a challenge for the development of the divertor plasma-material interface (PMI). In future ST-based devices, the inherently compact ST divertor combined with low-collisionality SOL enable a rigorous test of the PMI concepts. In NSTX-U, long-pulse high-power-density plasmas will enable divertor research to address the gaps identified for the ST PMI, namely, high heat and particle flux control at low normalized density, while also addressing all other PMI challenges shared with conventional aspect ratio tokamaks. As shown in Figure 1.4.4.2.1, and circled in blue, NSTX-U will be able access P/R values near ITER and FDF (at ~1MW/m^2 neutron wall loading) values and approximately half the P/R value of ST-FNSF with P/S values comparable to the highest values projected to be achievable in other devices. Recent assessments of the divertor heat flux scaling in NSTX project to peak divertor heat fluxes $\geq$ 20MW/m^2 in the NSTX-U for conventional divertor configurations with flux expansion ~20. Very high flux

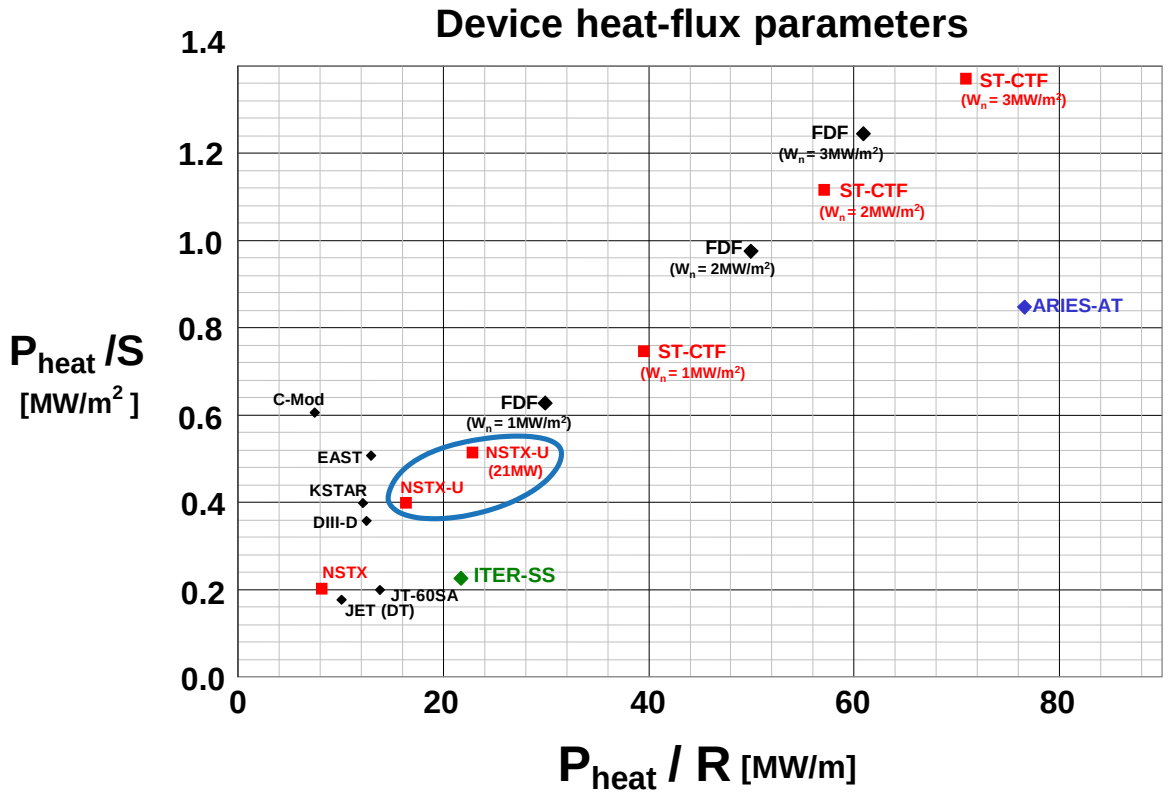

Figure 1.4.4.2.1: Heating power normalized to plasma surface area (P/S) and major radius (P/R) for present and proposed tokamaks.

expansions of ~40-60 have recently been shown to successfully reduce peak heat flux in NSTX, and additional divertor poloidal field coils have been incorporated into the Upgrade design to support high flux expansion "snowflake" divertors and strike point control for high heat flux mitigation. Enhanced divertor radiation using both intrinsic and externally applied divertor impurities have also been shown to achieve partial detachment and factor of 2-3 reduction in peak divertor heat flux in NSTX. The snowflake divertor, partial detachment, and combinations of these heat-flux mitigation techniques are high-priority research areas for NSTX-U.

A key unknown in projecting divertor performance to larger and/or higher-current next-step devices including ITER is an understanding of scrape-off-layer (SOL) transport and the associated heat and particle flux widths which determine the peak fluxes. NSTX-U can shed substantial light on these scalings by extending/increasing the range of field, current, and power for SOL-width studies by up to a factor of two. Divertor cryo-pumps are projected (see Chapter 4, Section 2.3.1) to provide access to deuterium density control for a wide range of normalized density fractions, and characterizing and optimizing the performance of divertor cryo-pumping is a critical goal for NSTX-U research. Lastly, high-Z PFC components will be introduced into the lower divertor surfaces in the base budget plan (with much more extensive coverage in the incremental budget plan), and the impact of plasma-material interactions with these surfaces on boundary physics processes will begin to be assessed. These considerations motivate the following research thrust:

Thrust BP-2: Assess and control divertor heat fluxes

> *NSTX-U researchers will study the investigate SOL heat and particle transport and turbulence and associated flux-widths extending the existing NSTX database to lower ν^*, higher I_P, and P_{SOL}. Measurements will be compared to multi-fluid turbulence and gyro-kinetic models. Novel divertor geometries such as the snowflake divertor will be systematically investigated for power and particle control and magnetic control of divertor configurations will be developed to support standard and snowflake divertor configuration studies. Steady-state and transient heat and particle transport and divertor PFC loads in these configurations configurations will be studied as a function of magnetic balance, magnetic configuration parameters, feedback-controlled impurity seeding rate over a range of SOL powers and widths. Highly-radiating boundary solutions with feedback control will be developed, and divertor detachment operating window and access parameters will be studied. As high-Z PFCs are introduced, their compatibility with the divertor heat exhaust solutions will be assessed.*

1.4.4.3 Particle Exhaust Sustainability

Integrated scenarios on NSTX-U are designed for steady density at 0.5-1 times the Greenwald density limit. To achieve this, a central element of the boundary physics program is the installation of a divertor cryo-pump - a proven technology to control both main ion and impurity density. A key component of the research is to compare lithium pumping and cryo-pumping for density control, while considering the possible synergy of the two methods to contribute to power and particle exhaust solution for NSTX-U and future devices. An integral element to both of these studies is the assessment of impurity sources and transport. These considerations motivate the following research thrust:

Thrust BP-3: Compare the sustainability of particle exhaust via lithium pumping and cryo-pumping, for density, impurity, and Z_{eff} control consistent with integrated scenarios

Experiments will be conducted to validate cryo-pump physics design activities, perform initial density control studies, and assess compatibility with H-mode pedestal and core performance and divertor power exhaust scenarios. Comparisons will be made between lithium conditioning and cryo-pumping for density and impurity control, as well as changes to the edge density profile, which are central to ELM elimination with lithium conditioning. Local recycling coefficients in the upper and lower divertor regions, as well as the wall will be measured. Impurity sources and SOL transport, and the role of ELMs in impurity control will be assessed. As high-Z PFCs are introduced to NSTX-U, their impact on core impurity transport, boron and lithium coatings, and divertor retention and particle control will be assessed.

1.4.5 Materials and PFC Research Thrusts

1.4.5.1 Lithium surface-science

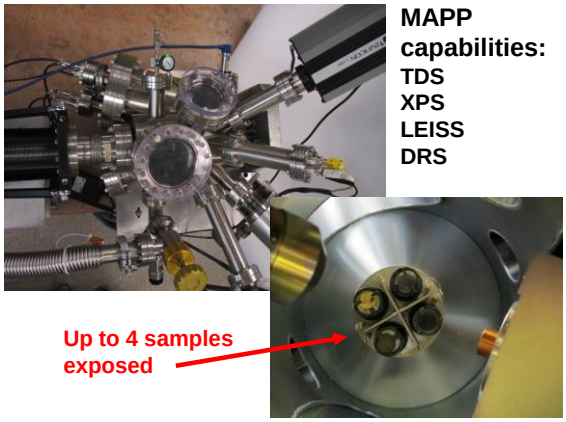

Figure 1.4.5.1.1: MAPP diagnostic capabilities

NSTX has a long history of performance improvement with the usage of lithium wall conditioning. Results from 2008 and 2010 indicate a potential paradox in which confinement improves with small amounts of additional lithium (~1g), but did not improve during the liquid lithium divertor (LLD) campaign in which much larger amounts (~1kg) were used. Further, there are indications that oxygen gettered from vacuum and possibly "scavenged" from the bulk carbon is interacting with the Li and H/D in complex ways. The interactions between lithium, the impurities present in tokamak plasmas, and high-Z PFCs are also relatively unexplored. A key diagnostic capability to be utilized for this research is the Materials Analysis Particle Probe (MAPP) shown in Figure 1.4.5.1.1. New experiments and the utilization of advanced diagnostics are needed to address the aforementioned issues in a systematic way and motivate the following thrust:

Thrust MP-1: Understand lithium surface-science during extended PFC operation

Experiments will be conducted to improve understanding of the role of more complete coverage of the PFCs by evaporated lithium using upward-facing evaporators and/or diffusive evaporation as well as the impact of boronization. The Materials Analysis Particle Probe (MAPP) will be utilized to identify in-situ between-shot chemical states and compositions of the coatings. A boronization campaign in year one will be followed by a controlled Li introduction. The identical total deposited lithium as supplied in 2008 will be applied on both upper and lower divertors. The changes in plasma performance will be compared to the 2008 database. In the second year, a boronization campaign will be eliminated and an identical introduction of lithium as in the previous year will be applied to bare graphite surfaces. These studies will provide a comparison between C+B substrate vs. a C substrate alone in terms of plasma performance. The MAPP diagnostic will be utilized during this year also, and will enable comparisons to surface-science laboratory results including Li-coatings on high-Z metal substrates such as TZM. The uptake of hydrogenic species and the impact of varying levels of impurities (e.g. C, O) on that uptake will be examined in the Li-metal system, and in years 3-5 the surface interactions of Li on high-Z tiles in at least one NSTX-U divertor region will be studied.

1.4.5.2 Material migration and evolution

A key PFC challenge facing long-pulse, high-power devices is the net-reshaping of the PFCs as a result of erosion, migration and redeposition. Charge-exchange to the first-wall scales with the plasma exhaust power normalized the surface area (P/S ratio) of the machine. The value of this parameter is expected to be quite high in NSTX-U with values up to P/S = 0.5MW/m^2 which is approximately half the value of an FNSF or DEMO, albeit with far shorter pulse-length (~5-10s in NSTX-U versus ~10^3-10^7s in FNSF/DEMO) and much lower duty factor (~10^4 shot seconds per year in NSTX-U versus ~10^6 to 2-3×10^7 s/year in FNSF/DEMO). The power exhausted to the divertor also increases particle fluxes in that region, and this is also expected to be a large number in the highest-power discharges projected for NSTX-U. These attributes, combined with longer pulse-lengths expect to be achievable in NSTX-U, can be exploited in experiments to measure the net erosion and re-deposition inside NSTX-U in order to begin to provide a basis for projecting to FNSF. These considerations motivate the following thrust:

Thrust MP-2: Unravel the physics of tokamak-induced material migration and evolution

A combination of quartz-crystal microbalances (QCMs) and marker-tiles will be utilized to provide measurements of shot-to-shot erosion and redeposition in NSTX-U. An upgraded MAPP system with QCM will enable shot-to-shot analysis of not just the quantity of deposited material, but also the composition of that material. The scaling of wall-erosion for typical NSTX-U divertor conditions over a range of P/S values will be used to construct a data-base to estimate/project total wall erosion expected for an FNSF or DEMO. The material transport variations as a function of divertor configuration (e.g. snowflake, detached, vapor-shielded) will also be measured and compared to simulation.

1.4.5.3 Continuous vapor-shielding

Lithium is known to evaporate at significant rates at modest temperatures (T ~ 450C). In experiments on plasma-gun and electron-beam devices (e.g. QSPA or SPRUT), transient vapor-shields have been produced and little damage to the substrate material was observed. Usage of a vapor-layer to protect a solid substrate is analogous to detached divertor operation but utilizes the PFC material itself as the vapor-layer. Such operation has not been demonstrated in steady-state or in the presence of a high-performance tokamak plasma. However, the operation of Li PFCs in the

$$p_u = p_t(1+M_t^2) + p_{Li}$$
$$q_t = \gamma \Gamma^+_{sat} T_e = \gamma n_{es} c_s T_e = \gamma c_s p_t$$

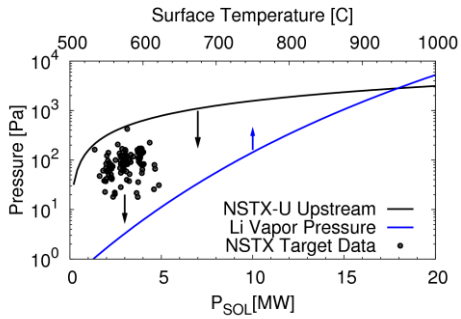

Figure 1.4.5.3.1: (Top) SOL pressure balance and heat flux equations, (bottom) NSTX data and NSTX-U projections indicating possibility of Li vapor pressure providing SOL operation analogous to detachment with application to protecting PFC substrates.

experiments above and results from NSTX in which divertor radiation was observed to increase and divertor peak heat flux decrease with increased lithium indicate vapor shielding may be favorable for reducing divertor heat fluxes. Figure 1.4.5.3.1 shows that NSTX divertor target pressure values (black circles) and projected NSTX-U up-stream SOL plasma pressures (black curve) can be comparable to the projected Li vapor pressure (blue curve) for sufficiently high PFC surface temperature (top abscissa). These projections motivate the following thrust:

Thrust MP-3: Establish the science of continuous vapor-shielding

NSTX-U researchers will begin to establish the scientific basis and experimental demonstration of a continuously vapor-shielded surface in the tokamak environment with application to heat-flux mitigation. Extensive research on the long-pulse linear plasma device Magnum-PSI will be carried out to provide an extrapolable experimental demonstration of such vapor-shielding. These experiments will then be extended to NSTX-U using a lithium-coated high-Z substrate (for transient operation) or a flowing liquid lithium system (for long-pulse operation) with a high-power-density strike-point impinging on the PFC to raise the front-face temperature above the lithium evaporation temperature. MAPP, QCMs, Langmuir probes, and divertor spectroscopy, bolometry, and two-color IR diagnostics will be utilized to provide data for interpreting the results.

1.4.6 Energetic Particle Research Thrusts

1.4.6.1 Develop predictive tools for fast-ion transport

Heating and some non-inductive current drive methods for next step magnetic fusion devices utilize non-thermalized (e.g. fast) ion populations whether as rf-tail ions, energetic neutral beam ions or fusion alphas. Instabilities driven by these fast ions, in particular the Toroidal Alfvén Eigenmodes (TAE), can modify the expected heating or current drive profiles. Projecting which operational regimes will minimize these instabilities, or if necessary, predicting the effect of these modes on the fast ion population, is valuable for designing new devices and planning their operation. These predictions are made through the extrapolation of results obtained in present research devices to larger scale, fusion-grade reactors. The development and benchmarking of numerical codes based on experimental observations from existing experiments is therefore one of the most critical issues in fusion research.

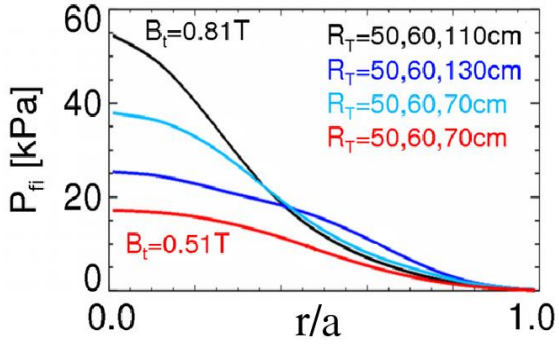

Figure 1.4.6.1.1: Fast-ion pressure as a function of toroidal field strength and NBI tangency radii for various combinations of NBI sources in NSTX-U.

A primary goal for Energetic Particle research on NSTX-U is to develop capabilities that enable reliable and quantitative predictions on properties of, and fast ion response to, unstable modes in future devices such as ITER and FNSF. Variation of $v_{fast}/v_{Alfvén}$ by varying density and field, variation of the fast-ion density and pressure profiles, and variation of the rotation profiles are key NSTX-U capabilities to elucidate fast ion physics. For example, Figure 1.4.6.1.1 shows the wide range of fast-ion pressure peaking (assuming classical slowing down) projected to be accessible using combinations of the original NBI and 2nd more tangential NBI of NSTX-U. Based on results from NSTX and other devices, modes that can induce substantial redistribution and loss of fast ions will be targeted first. These include TAE, RSAE and Energetic-Particle modes (EPMs), as well as higher frequency *AEs (GAE/CAEs) that are responsible for deviations of the neutral beam fast-ion distribution function (F_{nb}) evolution from classical behavior. These considerations motivate the following research thrust:

Thrust EP-1: Develop predictive tools for projections of *AE-induced fast ion transport in FNSF and ITER

*NSTX-U researchers will: (i) study the modes' properties (radial structure, frequency and wavenumber spectrum, stability) and (ii) characterize fast ion transport associated with specific classes of *AEs. In parallel with the experimental research on NSTX-U, the development of numerical and theoretical tools will be pursued to lay the basis for predictive capability. Experimental results will be utilized for extensive code verification and validation, based on the detailed characterization of instabilities and fast-ion distribution available on NSTX-U from the upgraded set of fast ion diagnostics.*

1.4.6.2 Fast-ion Phase-Space Engineering (PSE)

Phase-Space Engineering (PSE) consists of controlled, externally-induced modifications of the fast-ion distribution in order to achieve specific goals such as performance improvement or enhanced stability. Possible applications of PSE include *AE control, stochastic ion heating, alpha-channeling, and stabilization/regulation of sawteeth and other MHD modes (e.g. NTMs). The longer-term PSE objective that requires dedicated research on NSTX-U is the development of schemes for direct *AE control. Experiments will aim at developing tools to control AE activity in NSTX-U and exploit instabilities as an additional actuator to modify, in a controlled way, the evolution of fast ion radial profile and energy spectrum. A parallel line of research is the regulation of electron thermal transport through high-frequency AEs. If successful, PSE will help to control the TAE and other Alfvénic instabilities in a reactor by bypassing the thresholds imposed by thermonuclear instabilities, which is an important (and often under-estimated) issue for devices such as ITER, FNSF and future Pilot plants.

PSE research requires a detailed knowledge of the stability properties of AEs. TAE linear damping rate has been measured on the C-Mod and JET tokamak experiments with the goal of benchmarking codes used to project TAE stability to ITER relevant regimes. Linear damping rates are inferred by exciting stable modes with an antenna and by computing the resonance width from the complex impedance modeling the driven plasma response. Next step Spherical Tokamaks will operate in a different fast ion parameter regime, thus it is necessary to extend the previous benchmarking activity to encompass a broader range of scenarios and different classes of *AE instabilities. For example, the much stronger magnetic shear at the plasma edge (found to be stabilizing in triangularity scans on JET) and the relatively stronger rotational shear, resulting in enhanced continuum interactions, are predicted to affect TAE stability in STs. An example of changes of the TAE radial gap width caused by rotation in NSTX is shown in Figure 1.4.6.2.1

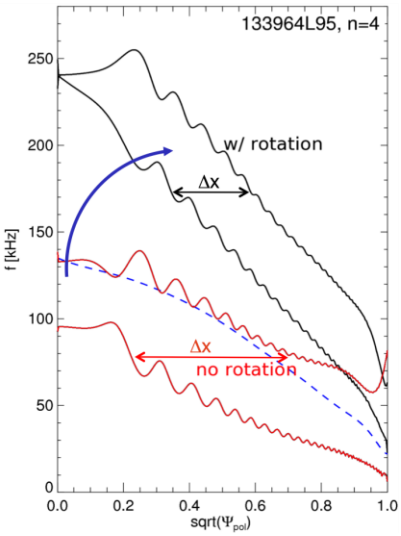

Figure 1.4.6.2.1: NSTX TAE gap modification due to rotation.

Looking beyond the lower frequency TAE modes, higher frequency Alfvénic instabilities are routinely observed in START, MAST, and NSTX NB-heated plasmas. These instabilities clearly have the potential to affect the fast ion distribution, although experimental evidence of the extent of the perturbations is weak at present. Reliance on fast ions to destabilize the natural eigenmodes of Compressional and Global Alfvén waves (CAE and GAE) reveals only a limited subset of the eigenmode spectrum. These considerations motivate the following research thrust:

Thrust EP-2: Assess requirements for fast-ion phase-space engineering techniques

> *Active spectroscopy experiments on NSTX-U, similar to those carried out on JET and C-Mod, will be performed to provide a similar data set of linear TAE damping rates for further benchmarking stability codes at low aspect ratio. This will also help to validate ITER projections by challenging the fundamental understanding of the physics underlying the drive and stability mechanisms of these modes. With incremental funding, the bandwidth of external antennae will be extended to study high frequency modes. The higher frequency of these modes, together with the possibility of cyclotron resonances, may provide an attractive route towards controlled modifications of the non-thermal ion distribution function and possibly lowering the overall fast ion pressure.*

The outcome from PSE research on NSTX-U will be evaluated, possibly in conjunction with results from other devices such as DIII-D, MAST and JET, to assess the feasibility and potential

of PSE schemes on future devices in terms of required power and spectrum, temporal response, time-scales for diagnostics and control. Extrapolations to future devices, such as a ST-based FNSF/Pilot and ITER, will provide information on achievable performance improvement, for instance in the capability of reliable access to the so-called "hot-ion mode" and efficiency of alpha-channeling schemes.

1.4.7 Wave Heating and Current Drive Research Thrusts

1.4.7.1 Fast-wave heating and current-drive for non-inductive start-up and ramp-up

A major goal of the NSTX-U FY2014-18 research program is the development of fully non-inductive discharges. This goal is important for the design and development of an ST-FNSF device and an advanced technology (AT) fusion reactor. It is challenging both scientifically and operationally. The approach on NSTX-U will therefore be to initially develop non-inductive start-up, ramp-up and plasma sustainment scenarios separately, and then later combine these non-inductive scenarios. On NSTX, as shown in Figure 1.4.7.1.1, HHFW heating was successfully used to generate a $T_e(0)$ =2-3keV H-mode plasma with 70% non-inductive current fraction with a total plasma current of ~300 kA. This scenario used an ohmically-initiated L-mode discharge as the target plasma for the HHFW heating and 1.4 MW of HHFW power. These considerations motivate the following research thrust:

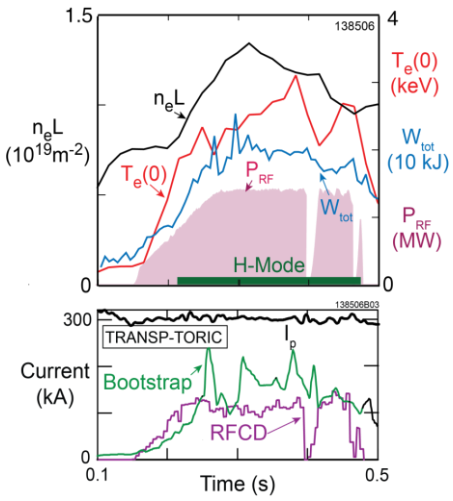

Figure 1.4.7.1.1: HHFW heating and current drive in a low-I_p target plasma.

Thrust RF-1: Develop RF heating and current drive for fully non-inductive plasma current start-up and ramp-up

Experiments in NSTX-U will extend NSTX HHFW H-mode studies by using higher HHFW powers to demonstrate HHFW-driven fully non-inductive plasma current ramp-up to plasma currents significantly higher than 300 kA. Further, high-power HHFW and EC heating (assuming a ~1MW 28GHz gyrotron) will be used to significantly increase the core electron temperature of CHI and plasma-gun-initiated discharges in order to increase the plasma current and extend the non-inductive discharge duration. EBW heating will also be tested as a wave-based means of generating plasma start-up current in NSTX-U using a technique similar to that developed on MAST in which a grooved mirror-polarizer incorporated in a graphite tile on the center stack provides mode conversion from O-mode to X-mode for efficient EBW absorption.

1.4.7.2 Validation and Application of Advanced RF Codes

Advanced RF numerical codes, such as the AORSA-3D full-wave solver with SOL modeling and a realistic antenna model, and the full finite-orbit-width CQL3D Fokker-Planck neoclassical simulation code have previously shown promising capabilities in modeling edge power loss mechanisms and fast-wave interactions with energetic ions in NSTX plasmas. With access to increased toroidal field and reduced cyclotron harmonic number, NSTX-U plasmas will be able to operate significantly closer to the RF parameters of next-step ST plasmas and for ITER. Thus, with sufficient validation, AORSA-3D and CQL3D would be valuable tools for predicting the behavior of the wave fields in the SOL, the plasma edge and the interaction with fast-ions in the bulk plasma in future fusion machines such as ITER and FNSF.

For example, a potentially critical issue for ITER is fast-wave power coupling through the SOL into the core plasma. As shown in Figure 1.4.7.2.1, inclusion of the experimentally-relevant exponentially-decaying SOL density profile projected for NSTX-U can strongly influence fast-wave propagation and surface wave excitation in the plasma edge region. Thus, NSTX-U can play an important role in validating leading models that can be used for modeling ITER ICRF coupling and heating. Considerations such as these motivate the following research thrust:

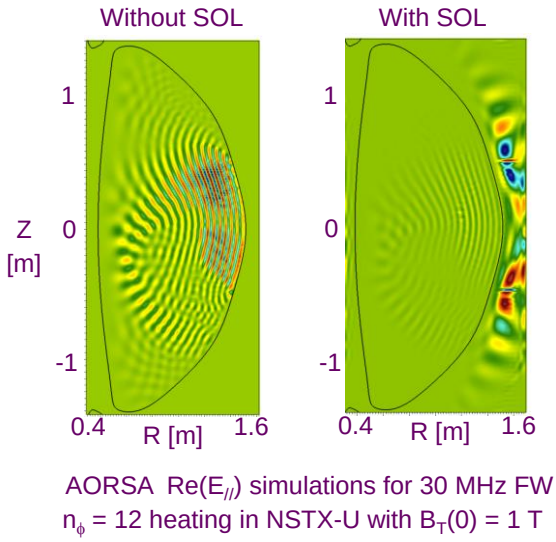

Figure 1.4.7.2.1: AORSA simulations of NSTX-U plasma heating with and without inclusion of SOL density profile

Thrust RF-2: Validate advanced RF codes for NSTX-U to aid prediction of RF performance in FNSF-ST and ITER

Building on measurement and simulation results from NSTX, detailed measurements of the SOL density and temperature profiles, edge fluctuations, RF power flows to the divertor regions, the RF power deposition profile, the RF-driven current profile, and the core fast-ion distribution function will be obtained. These measurements and associated analysis will be systematically compared to modeling results from AORSA-3D and CQL3D. After these advanced RF simulation models have been validated and verified during the first three years of the NSTX-U 5 year plan, they will subsequently be used to predict RF performance in ST-FNSF and for ITER.

1.4.8 Plasma Current Start-up and Ramp-up Research Thrusts

As described in Section 1.1, a major challenge for an ST-based FNSF is the necessity of plasma formation with either small or no central solenoid flux combined with the need for non-inductive current ramp-up using a combination of bootstrap current and NBI and/or RF current overdrive. The goal for NSTX-U non-inductive plasma current formation and ramp-up research for the next 5 years is to first demonstrate current formation and ramp-up independently and then to integrate and optimize start-up and ramp-up to the ~1MA level.

1.4.8.1 Re-establish solenoid-free current start-up, test non-inductive ramp-up

Coaxial helicity injection (CHI) – first demonstrated on the HIT-II ST at the University of Washington and subsequently demonstrated on NSTX – is a promising candidate for non-inductive current initiation. In addition, CHI has the potential to drive edge current during the sustained phase of a discharge for the purpose of controlling the edge current profile to improve plasma stability limits and to optimize the bootstrap current fraction. Experiments on the HIT-II experiment at the University of Washington demonstrated that the method of *transient* CHI (TCHI) could generate high-quality plasma equilibrium in a ST that could be coupled to inductive drive. Since then the transient-CHI method has been successfully applied to NSTX for solenoid-free plasma start-up followed by inductive ramp-up. These coupled discharges have now achieved toroidal currents of 1 MA using significantly less inductive flux than standard inductive discharges in NSTX. These results must be re-established on NSTX-U using new divertor poloidal field coils and other configurational changes, and then extended to higher current (from 200kA to 400kA) to provide plasma current levels compatible with confining NBI fast-ions for subsequent current ramp-up. For current ramp-up, TRANSP simulations indicate that the new 2nd NBI of NSTX-U is predicted to be much better confined at low I_P due to the less perpendicular injection and associated reduction in prompt/bad-orbit loss (see Chapter 8). Thus, substantial experimental tests need to be carried out to characterize and optimize non-inductive current drive in lower-current target plasmas using the 2nd NBI. These considerations motivate the following research thrust to be carried out during first few years of the five year plan period:

Thrust PSR-1: Establish and extend solenoid-free plasma start-up and test NBI ramp-up

> *NSTX-U researchers will re-establish transient CHI discharges utilizing graphite lower divertor tiles, the increased toroidal field capability of NSTX-U, and full Li coating of the lower divertor tiles followed by subsequent lithium conditioning of the upper divertor. The maximum toroidal currents that can be generated with CHI will be assessed by varying and increasing the amount of injector flux, the size of the capacitor bank, and the CHI voltage (up to 2 kV). The upper divertor buffer coils will be used to suppress absorber arcs, and studies of the coupling of the CHI generated plasma to inductive drive will be performed. Researchers will also generate 300-400kA flat-top current inductive*

plasmas and inject the new more tangential beams to assess NBI coupling and current drive efficiency and compare to TSC/TRANSP simulations. NBI coupling to CHI targets will also be assessed and compared to simulation. Combinations of NBI and HHFW heating and current drive will be utilized to heat inductive plasmas and attempt to non-inductively ramp-up the plasma current to the ~0.8-1MA range.

1.4.8.2 Couple CHI plasmas to non-inductive current ramp-up

Previous CHI experiments in HIT-II and NSTX have shown that minimizing impurity radiation is critical to maximizing transient CHI plasma temperature and current decay times and that metallic divertor surfaces can reduce low-Z impurity levels. One and possibly both NSTX-U divertor surfaces are planned to be converted to high-Z PFCs (likely TZM or a W alloy) in order to investigate the performance impact of such PFCs on integrated high-performance plasmas, and such a conversion could also benefit CHI operation. ECH power absorption simulations combined with TSC time-dependent modeling indicate that ~0.5MW of 28GHz ECH heating could significantly increase CHI plasma electron temperatures (from ~10-50eV to 100-500eV) and greatly lengthen the CHI plasma current decay time from tens to a few 100ms. This increase in plasma current duration should be sufficiently large for NBI fast-ions to be confined and slow-down to heat the CHI plasma (see Chapter 8). Increased CHI injector voltage to 3kV (if technically feasible) combined with the higher toroidal field of ~1T of NSTX-U is projected (based on TSC simulations) to generate CHI closed-flux currents of 0.4-0.6MA which would further improve coupling to NBI heating and current ramp-up. As shown in Figure 1.4.8.2.1, TRANSP/TSC simulations indicate that early HHFW heating followed by NBI heating and current drive combined with bootstrap current can in principle increase the plasma current non-inductively from the 0.4-0.5MA level to the 0.8-1MA range. However, these simulations utilized scaled profiles from higher current NSTX experimental plasmas and also ignored possible fast-ion redistribution and/or loss from Alfvénic or other MHD instabilities. Validation of both 2D and 3D simulations of CHI start-up is necessary to provide a reliable basis for extrapolation to an ST-based FNSF. Lastly, the potential for point helicity injection using plasma guns as being developed on the Pegasus toroidal facility (see Chapter 8) makes this technique particularly attractive for an ST-FNSF, and important data on the size and field scaling of gun start-up is needed from NSTX-U to reliably extrapolate to an ST-based FNSF. These considerations motivate the following research thrust:

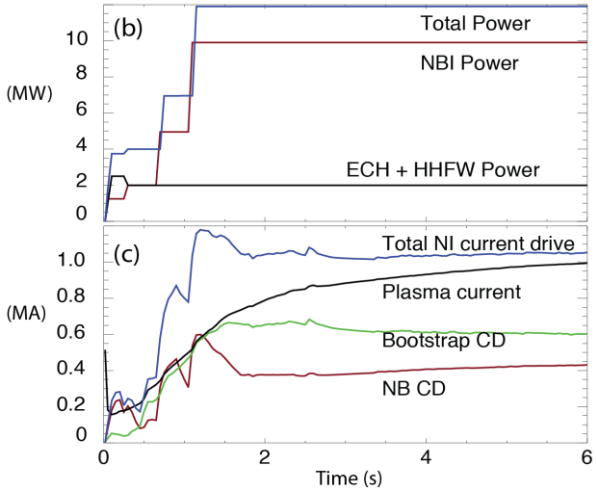

Figure 1.4.8.2.1: TSC simulations of non-inductive ramp-up of an NSTX-U plasma to 0.8-1MA.

Thrust PSR-2: Ramp-up CHI Plasma discharges using NBI and HHFW and Test Plasma Gun Start-up

NSTX-U researchers will maximize the levels of CHI-produced plasma currents using new operational capabilities including 1) metallic divertor plates, 2) 1 MW 28GHz ECH, and 3) 2.5-3 kV CHI capability. All these should allow more injector flux to be injected into the vessel at reduced levels of low-Z impurities. Initial tests of the effectiveness of NBI coupling to a CHI-generated target will be carried out using the best available CHI targets including the expected increase in CHI plasma duration achieved with ECH electron heating, and the NBI coupling and ramp-up of CHI current will be systematically investigated. Detailed comparisons of CHI current drive results to 2D TSC and 3D NIMROD simulations will be carried out to develop a TSC/NIMROD model of CHI for FNSF design studies. If technically ready, plasma gun hardware will be commissioned on NSTX-U and point-source helicity injection (plasma gun) plasma formation will be initially tested and compared to results from Pegasus.

1.4.9 Plasma Sustainment: Scenarios and Control Research Thrusts

1.4.9.1 Scenario development

A critical element of NSTX-U operation will involve developing high performance and/or long-pulse scenarios in support of the NSTX-U scientific research program and for ST development generally. The demonstration of sustainment of high non-inductive fraction (up to 100%) is essential for FNSF applications of the ST. Example projections for 100% non-inductive operation in NSTX-U as a function of normalized density and H-mode confinement multiplier are shown in Figure 1.4.9.1.1. In both figures, the diamond symbols indicate individual TRANSP runs used to generate the contour plots, the red line in the upper plot indicates non-inductive fraction = 1, and the red line in the lower plot indicates q_{min} = 1. Beyond high non-inductive fraction, access to high-current partial-inductive scenarios is necessary to explore the current and collisionality scaling dependence of confinement and stability. These operational goals motivate the following research thrust:

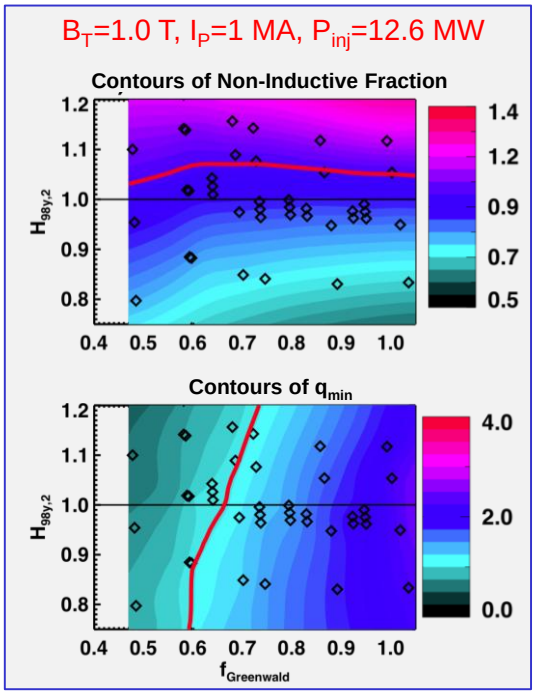

Figure 1.4.9.1.1: TRANSP simulations of non-inductive current fraction and q_{min} vs. normalized confinement and density for NSTX-U

Thrust ASC-1: Development of high non-inductive fraction and high current scenarios

Scenarios with non-inductive current fraction near 100% will be systematically explored. Key questions to be examined include: the impact of the confinement level and profile shapes on the non-inductive current level, the global stability of scenarios with large neutral beam current drive and central fast ion pressures, the optimal density for non-inductive sustainment, and consistency of the non-inductive operating state with divertor integration. Further, NSTX-U researchers will develop high-current, partial inductive operation aiming for the facility maximum performance goal of 5 second pulses at I_P=2.0 MA and B_T=1.0T. These scenarios are the key means of accessing low collisionality in NSTX-U, and the development of lower-density operations is thus critical. It is likely that these high current scenarios will result in the highest divertor peak heat fluxes, so the development of integrated heat flux management solutions is a requirement.

1.4.9.2 Axisymmetric control development

The development of advanced control strategies for achieving and maintaining optimal ST performance is important for NSTX-U operation and for advancing the ST for FNSF applications. Boundary and vertical position control is potentially more challenging for the ST since inboard coils for maintaining the inner gap may not be available and very high elongations are desired to increase the stable plasma beta and bootstrap fraction. Divertor heat flux control is also important – especially for high-current NSTX-U scenarios. NSTX results and collaborative experiments on DIII-D have demonstrated stable single snowflake divertor operation with significant heat flux reduction (see Chapter 4), but control advances will be required in order to control up to four x-points in up/down symmetric snowflake configurations (see Chapter 10). An example snowflake configuration for NSTX-U exhibiting 2 nearby X-points in the lower divertor is shown in Figure 1.4.9.2.1. Developing both core plasma safety factor and rotation control is important for optimizing plasma stability and confinement, and density control will also be a very important tool for varying and optimizing plasma collisionality and NBI current drive. These considerations motivate the following research thrust:

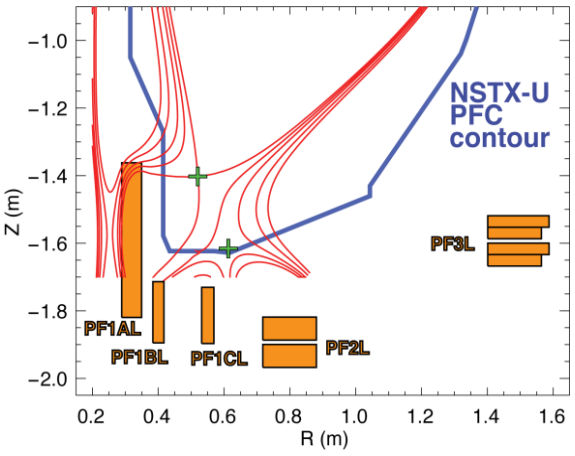

Figure 1.4.9.2.1: Simulated "Snowflake" divertor in NSTX-U showing presence of 2 nearby x-points (green plus signs) in the lower divertor.

Thrust ASC-2: Development of axisymmetric control

NSTX-U researchers will optimize multi-input multi-output boundary shape controllers and improved vertical stability algorithms. This research will also support improved control of the divertor heat flux using the snowflake divertor which uses two or three divertor coils to pull nearly overlapping X-points and has been shown to lead to a significant reduction in the divertor heat flux in NSTX and DIII-D. In particular, NSTX-U researchers will work to develop real-time tracking and closed-loop control of multiple X-points and also divertor radiation using feedback control of impurity gas injection building on earlier success with open-loop detatched divertor experiments in NSTX. Experiments will be conducted to verify TRANSP calculations that show by varying the neutral beam source mix and/or plasma density, the minimum safety factor (qmin) can be controlled. These results will be used to develop simultaneous β_N and q_{min} controllers in NSTX-U. Similarly, the variation of neutral beam torques from the different sources and n=2 and 3 magnetic braking from the RWM/EFC coils will be used to control β_N and the values of toroidal rotation at selected points across the profile. Experiments will also be attempted to examine the feasibility of combined beta, rotation, and q control. Finally, real-time density measurements will be brought to PCS, and improved fuelling actuators will be developed in support of density feedback control.

1.4.9.3 Controlled plasma shut-down

While NSTX-U is designed to withstand the electromagnetic and thermal loads from high current and stored energy disruptions, it is advantageous to minimize the frequency of disruptions associated with the end-of-pulse to minimize any possible risk of machine damage, maximize shot-to-shot reproducibility, and to prototype safe/controlled plasma shut-down techniques for FNSF and for ITER. Example potential complicating factors include rapidly time-varying beta and/or density control needed to avoid operational limits during the ramp-down phase, loss of H-mode due to decreased heating power and/or increased core radiation, and increased internal inductance due to loss of H-mode and/or negative surface voltage possibly leading to vertical instability. These considerations motivate the following research thrust:

Thrust ASC-3: Disruption Avoidance By Controlled Discharge Shutdown

NSTX-U researchers will optimize disruption detection with sufficient time to make a useful intervention during the discharge progression. Real-time inspection of quantities such as coil heating and the solenoid flux evolution will be used to determine when slow ramp-downs are required to avoid exceeding operational limits which might otherwise trigger fault conditions. Multiple real-time diagnostic signals will also be synthesized to form efficient disruption detectors, requiring more rapid ramp-downs. This information

will be used trigger automated rapid ramp-down sequences. It is envisioned that multiple types of ramp-down sequences will be developed, pending the different sources of alarms. A massive gas injection (MGI) sequence will also be included, to take advantage of the MGI system being developed in the MS TSG Thrust MS-3.

1.4.9.4 Scenario optimization for next step devices

A major goal for NSTX-U advanced scenario research is to investigate the achievable integrated performance of NSTX-U scenarios and then assess the potential impact of the observed performance capabilities on next-step ST device design. For example, the plasma shaping and profiles that optimize fully non-inductive operation in NSTX-U will be investigated, and the required shaping and actuator capabilities for a next-step ST will be addressed. These considerations motivate the following research thrust:

Thrust ASC-4: Scenario optimization for next step devices

NSTX-U researchers will study aspects of scenario optimization physics relevant to next-step devices, in ways that may not produce optimized scenarios for NSTX-U. For instance, the simultaneous current and rotation profiles providing optimal performance will be examined. The conditions for classical beam current drive will be explored. Finally, integrated modeling of the thermal energy, toroidal rotation, and current will be pursued, first for validation against NSTX-U results, and then for projection to next-step ST scenarios.

It is noted that while the planned research described above is divided into four separate thrusts for the purpose of organization, there are clearly several interconnections. Examples include:

- The development of high-current long pulse scenarios is captured in thrust #1. However, progress in heat flux mitigation described in Thrust ASC-2 is clearly required to realize these scenarios. This provides a natural linkage between Thrusts ASC-1 and ASC-2.

- The utility of variations in the neutral beam current drive to modify the minimum/central safety factor is a common theme through Thrusts ASC-1, 2, and 4.

- A common analysis tool through the Thrusts ASC-1, 2, and 4 of this research program is the TRANSP code. This tool will, on the one hand, continue to be used to develop experimental plans. On the other hand, experiments will be designed to validate the predictions of the code, revealing areas where its physics treatment is insufficient.

1.4.10 Research Thrust Support of High-Priority 5 Year Plan Goals

The research thrusts described in Sections 1.4.2 through 1.4.9 are supportive of the 5 high priority research goals listed in Section 1.2.2, and the mapping between the high-priority goals and TSG/chapter thrusts is shown in Figure 1.4.10.1. As shown in the figure, all of the thrusts contribute to the achievement of the 5 high-level goals, but the macro-stability (MS), transport and turbulence (TT), boundary physics (BP), and advanced scenarios and control (ASC) thrusts contribute most broadly to the high-priority research goals of the NSTX-U 5 year plan.

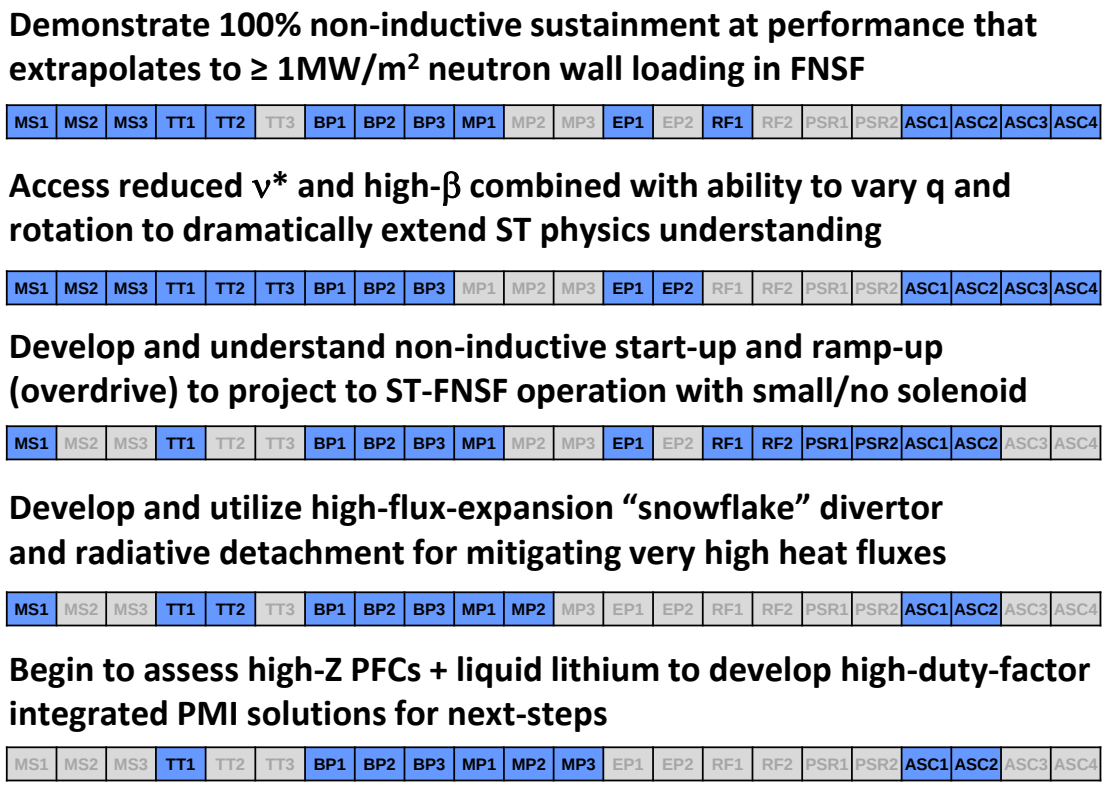

Figure 1.4.10.1: Mapping between the 5 year plan high-priority research goals and the research thrusts.

1.5 Planned NSTX-U Research in Support of ITER

NSTX-U research can support ITER in several different ways. The unique parameter regimes accessible by NSTX/NSTX-U will provide new insight into underlying tokamak physics through direct experiments and associated analysis as well as through theory and code validation. Specifically NSTX-U will be able to explore fundamental toroidal physics issues, use its high toroidicity, shaping and expanded operating space as leverage for theory validation, and develop operational/control hardware, approaches and capabilities. This will help provide the basis for addressing key physics and technology issues for tokamaks at all aspect ratio, including future burning plasma experiments such as ITER.

NSTX-U will contribute to specific High Priority ITER Research and Development needs in all topical science areas. In most cases, these contributions will address longer-term physics and operational scenario development, although in some cases there will be the opportunity for direct contributions to near-term design issues. In the following, we will focus on and detail the more urgent ITER R&D issues where NSTX-U can make the greatest impact. A discussion of additional work and ITPA involvement will follow. These discussions will focus on the high-level aspects of the work; more details are given in the individual chapters of each NSTX-U Topical Science Group.

In the MHD area, NSTX-U is engaged in studies of both Error Field (EF) and Resistive Wall Mode (RWM) physics. These are two critical pieces of the physics that will aid in the development of an integrated framework to provide stable plasma operation, including a physics-based disruption "prediction-avoidance-mitigation" system. Experiments and associated model development are presently focused on developing a self-consistent treatment of both the non-ideal plasma response to the EF coupled to a δf-treatment to determine the associated Neoclassical Toroidal Viscosity through the use of the IPEC and POCA codes. This will provide a general approach that is valid at all aspect ratio for predicting the EF threshold for rotation locking. This work up to now has already revealed the importance of non-resonant components of the EF. It has also identified rotation as a key piece of physics in determining the EF threshold for locked mode growth. IPEC modeling has been used to develop a scaling for this EF threshold which depends more strongly than linear on the plasma rotation, giving better agreement with results from NSTX experiments. Direct contributions to ITER based on this work have already been made; this scaling has been applied to ITER operational scenarios to determine the EF threshold for locked mode growth. In particular, levels of various ITER coil currents have been determined that provide low enough EF for avoiding the growth of locked modes.

The importance of multiple parameters in controlling plasma stability has also been identified in the study of Resistive Wall Modes. As one example, it was found that collisionality, plasma

rotation and kinetic effects of both the thermal and fast ions all factor into determining the plasma stability to RWMs. These effects couple to produce a much more complicated picture of RWM stability than was previously thought, when rotation was the only effect being considered. For instance, the plasma can enter a more stable configuration if its rotation is resonant with either the precession drift or banana motions of the thermal particles. At these resonances, the plasma stability increases with decreasing collisionality. Off resonance, there is no collisionality dependence of the plasma stability. This result, for which experiment and theory agree, is promising for the lower collisionality ITER and ST-FNSF scenarios, and the results framework has been used to map out sample stability space as a function of the β of the alpha-particles and rotation for ITER scenarios.

Both the EF and RWM studies will benefit by the enhanced capabilities in NSTX-U, including the off-axis Neutral Beam (NB) for modification of the fast ion distribution and the current and rotation profile, the state-space controller for active control of low-n modes, and eventual real-time rotation and current profile control. These studies will be aided further by the proposed Non-axisymmetric Control Coil (NCC) system, which can provide an expanded mode spectrum for applied 3-D magnetic fields. RWM research will benefit by the expanded parameter regime in NSTX-U, allowing for a more detailed assessment of the coupled role of collisionality and rotation in determining RWM stability.

A critical element of any disruption mitigation system is the knowledge of when to trigger it in order to limit the deleterious effects of both the thermal and the current quench. To this end, a methodology to predict imminent disruptions was developed. This disruption warning algorithm development proceeded in two steps; first, by using individual sensor- and physics-based signals (neutron emission, loop voltage, plasma motion, RWM growth rates, locked mode growth, plasma inductance, pressure peaking, etc) to predict a disruption, and second by combining these single-signal tests using a simple algorithm. For the latter, a “point score” was assigned to each test, and the total points from 17 such tests were summed at each time slice to determine a aggregate warning level. Different values of this aggregate warning level were chosen, trading off false positives and late warnings. For a carefully chosen warning level threshold, only ~2% of disruptions could not be detected within 10 ms, and only 4% of discharges were false positives (Figure 1.5.1). This methodology will be developed further on NSTX-U and tested on other devices, at higher aspect ratio, as part of an ITPA Joint Experiment/Activity.

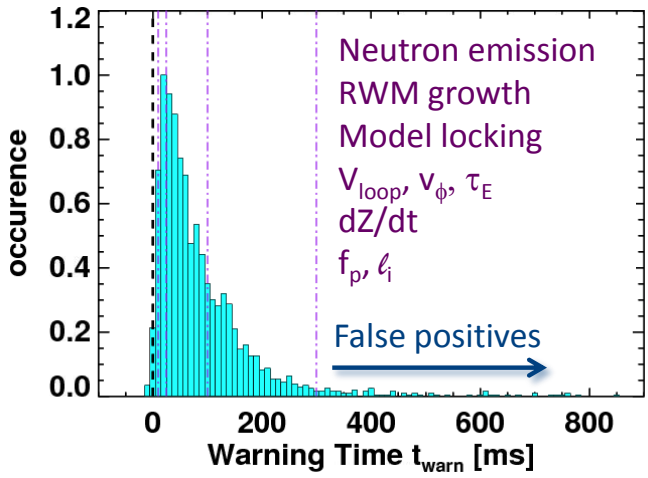

Figure 1.5.1: Results from disruption warning system showing time delay between warning and actual disruption for a chosen-combination of variables and trigger levels. Shown are only some of the variables that were used for this case.

If a disruption is imminent, a Massive Gas Injection system will be used to mitigate the effects of the thermal and current quenches. The system will be implemented in NSTX-U from the start of operation. An important feature of the system will be the ability to inject gas at different poloidal locations (midplane, off-midplane, lower divertor region and private flux regions) to assess the SOL gas penetration and to optimize the amount and type of gas injected. In particular, it is believed that due to the low energy of the plasma in the private flux region, this particular location may give the best penetration. The effect of this localized injection on the radiation profile and related localized heat deposition/melting will also be addressed. These studies will be aided by analysis of the gas penetration physics by such codes as DEGAS-2, and this can lead ultimately to validated predictions for ITER.

An alternative disruption mitigation approach is use of an electromagnetic particle injector (EPI), which uses a rail gun technique for rapid injection of a large amount of particles. This hardware will be proposed by an NSTX-U collaborator during 2013.

The lessons learned from the mode control and disruption studies will be integrated in the longer-term into a framework for physics-based disruption prediction, avoidance and mitigation. This framework is outlined in Fig. 1.5.2. It starts with a set of predictors (measurements) that consist of various plasma equilibrium, profile, and response characteristics. This information is then fed into a set of control algorithms that, using avoidance actuators, steer the plasma towards stable operation in the event that a disruption can be avoided. However, the same set of information is fed into a disruption warning system similar to the one discussed above. If it were deemed from this and other control information that a disruption is unavoidable and imminent, mitigation through early shutdown, MGI or EPI would be initiated. While many of the control algorithms, disruption warning triggers, etc., may be specific to NSTX-U, the general framework and algorithms would be applicable to ITER and ST-FNSF.

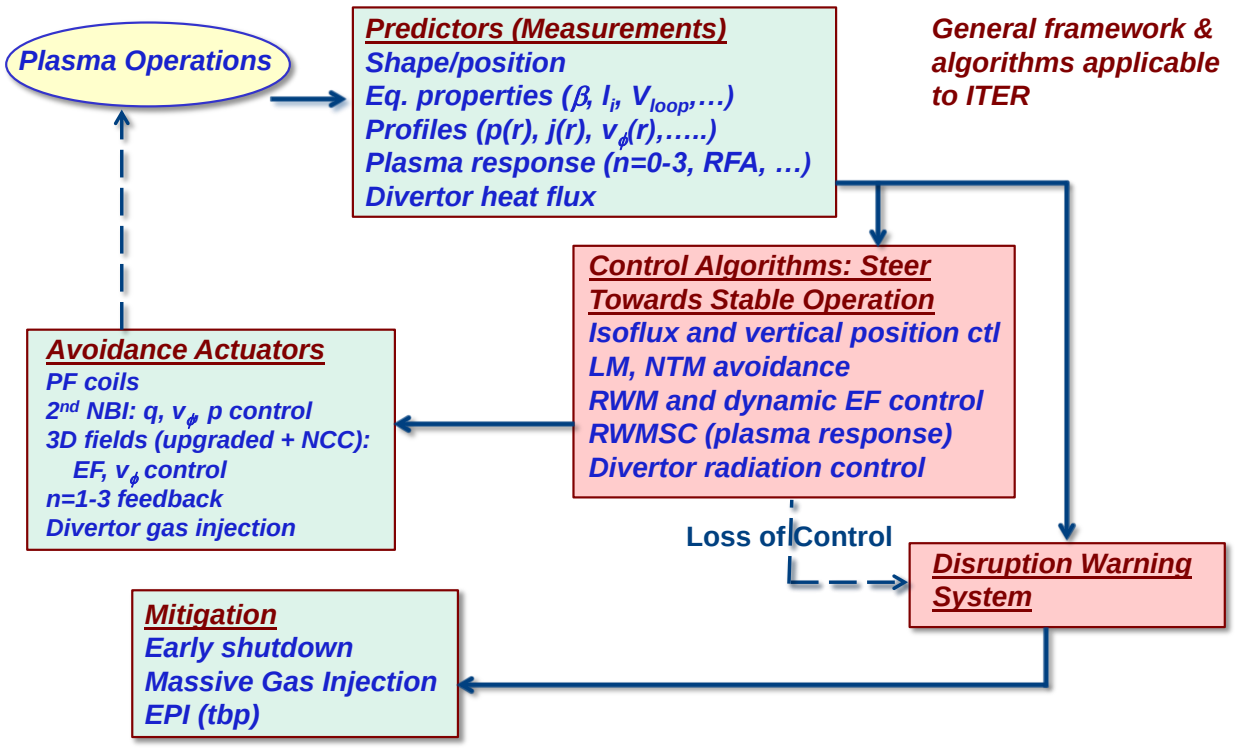

Figure 1.5.2: Framework for integrated, physics-based disruption prediction-avoidance-mitigation system.

ELM-control is one of the highest priority issues for ITER, as well as for present and other future devices such as ST-FNSF, for both limiting high power transient heat loads on the plasma facing components and for mitigating the effects of impurity accumulation. ELM control studies using applied, pulsed 3D fields in NSTX resulted in ELM-pacing, not suppression. By controlling the frequency of the 3D pulses, impurity accumulation and resulting radiated power levels could be controlled, with lower radiation using higher frequency pulses. NSTX-U will be able to use its expanded capability to study further ELM-mitigation with applied 3D fields using the upgraded 3D system plus the NCC. For one, this expanded capability will provide greater range of poloidal mode spectra that can be produced by the applied fields, which may lead to ELM suppression in certain configurations. Second, the applied 3D field NTV profiles can be controlled to some extent, leading to more edge localized perturbations and less core rotation damping. Lower core rotation is known to lead to compromised plasma stability. Finally, higher frequency pulsing of the applied 3D fields will be possible, which, if the trend observed on NSTX continues, can lead to further reductions in impurity accumulation and radiated power from the resulting ELM-pacing. In addition, NSTX-U will explore vertical kicks in its lower collisionality operating space as well as small-ELM and ELM-free regimes (such as Enhanced Pedestal H-mode).

NSTX-U will also be employing a lithium granule injector for developing ELM-pacing scenarios. The injector, which can control speed, size and thus penetration depth of the granules,

has been developed and tested on the EAST tokamak. Each injected granule was found to trigger an ELM with almost 100% success rate. The injector will be installed on NSTX-U for further testing on that platform. This research and development can feed directly into that for a closely-related Be injector, which is of possible interest in both JET and ITER for ELM-pacing.

Key to optimizing ELM control is to understand the transport and stability of the pedestal region. To this end, NSTX research has utilized lithium conditioning to suppress ELMs as a basis for studying the stability and the key microinstabilities that govern the pedestal structure. It was found that it was primarily the change in the density gradient with Li conditioning that changed the microstability properties in the pedestal region and thus determined the stability to ELMs. Micro-tearing, hybrid TEM/KBM and ETG modes were all found to be important in different regions of the pedestal, with micro-tearing important at the top of the pedestal, the hybrid TEM/KBM dominant in the strong gradient region, and the ETG was believed to clamp the temperature gradient near the bottom of the pedestal. As the density profile changed with Li conditioning, so did the absolute location of the modes, although their relative locations (e.g, top, middle, bottom of pedestal) remained the same. A variety of tools on NSTX-U will be used to study the profile and microinstability changes. These include lithium conditioning with both bottom and top facing evaporators, cryo-pump to control the density especially at the edge, and the expanded operating space of NSTX-U, allowing for lower collisionality. A polarimeter to measure magnetic field fluctuations will be implemented early after the beginning of operations, and this will allow for a direct measurement to assess the importance of micro-tearing modes, which may be important for ITER, near the pedestal top [20]. Almost full coverage of the k-spectrum of density fluctuations, from ion scale to electron scale turbulence, will be available from the Beam Emission Spectroscopy and Microwave Scattering diagnostics. This research on NSTX-U will contribute to the determination of whether fueling and/or conditioning techniques will need to be developed on ITER for the purpose of modifying the edge density profile to control ELMs.

NSTX-U will study and mitigate high divertor heat fluxes in long-pulse discharges, with projected high heat flux values of P/R~20 MW/m and P/S~0.4 MW/m^2, which are comparable to the heat fluxes of 25 MW/m and 0.2 MW/m^2 projected for ITER. NSTX has already performed studies and contributed to a multi-machine database examining midplane SOL heat flux widths as a function of poloidal magnetic field. While the NSTX data helped define the strong trend by residing in the transition region between large and small heat flux widths (Fig. 1.5.3), the range of poloidal field was limited. NSTX-U will expand the operating space in both toroidal and poloidal field to validate the SOL width scalings, especially with its operation at lower collisionality, which is more ITER relevant.

Divertor gas puffing was found to reduce the heat flux in the NSTX divertor by causing the divertor plasma to detach and become more highly radiating. In NSTX-U, this technique, which is one of the primary approaches proposed to mitigate heat fluxes in ITER, will be explored further with an aim towards developing closed loop control for producing and sustaining a radiative divertor compatible with high performance, steady-state operation. NSTX-U detachment studies and data can also contribute to model development necessary to improve detachment threshold predictions for existing experiments and also for ITER. The SOL heat flux width scalings discussed above will be studied in this partially detached regime, as will the effects of applied 3D fields. In the longer-term, once rows of high-Z plasma facing components are installed in NSTX-U, the resulting study of mixed material issues will address the ITER high priority issues of metal PFC heat load handling, migration and dust.

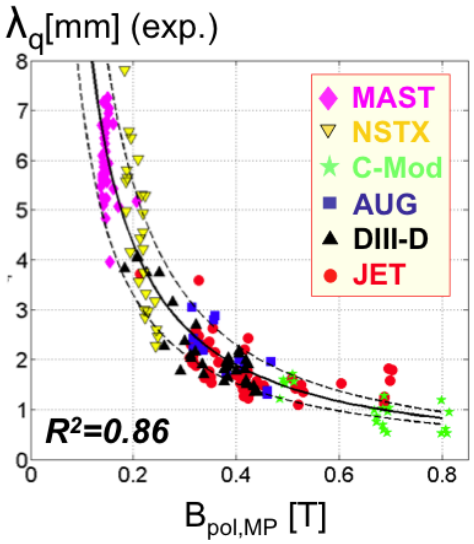

Fig. 1.5.3 Multi-machine study of SOL heat flux widths as a function of poloidal magnetic field, both in the outer midplane.

ITER's interest in studying and understanding impurity transport has clearly heightened over the past several years. This is understandable given that impurity seeding is required for achieving and maintaining good confinement in the metal and ITER-like wall machines ASDEX-U and JET, respectively. Is impurity transport neoclassical, especially near the edge? Will impurities accumulate in the ITER core plasma? These are critical questions for which the answers will help define the requirements for ELM-pacing to control the impurity content. NSTX has engaged in impurity transport studies of both carbon and lithium. MIST and STRAHL modeling results indicate that in plasmas with no lithium conditioning, the carbon density profile structure (i.e., peaking locations) agrees with predictions from neoclassical theory. With lithium conditioning, however, there are large departures from neoclassical, especially near the plasma edge. NSTX-U will be able to study the transport of impurities at lower collisionality. In particular, the near-full k-range of the density turbulence diagnostics will enable an assessment of the roles of neoclassical versus turbulent driven transport. The relative strengths of these two particle transport mechanisms will be assessed and manipulated by control of rotation shear (for suppressing the turbulence) using the second NB and the flexible 3D coil system. Mixed impurity effects will be studied at first with carbon and lithium, and later on high-Z transport will be studied once the rows of high-Z tiles are installed.

An area in which the NSTX-U operational regime will contact directly that of ITER is in Energetic Particles, where the unique NSTX-U unique parameter regime overlaps that of ITER with respect to $v_{fast}/v_{Alfvén}$ and β_{fast}/β_{tot} (Fig. 1.1.1). This contact/overlap will enable linking of the Alfvén Eigenmode (AE) activity and its associated effect on the fast ion population observed in NSTX-U to those expected for ITER with the caveat that the NSTX-U and ITER fast-ion ρ^* will differ. The observed AE activity in NSTX (and that projected for NSTX-U) was strongly non-linear, and such non-linearity may also be present in ITER hybrid and reversed-shear plasmas. This non-linear behavior was reflected by strong avalanches and the associated loss or redistribution of the fast ion distribution resulting from multiple mode overlap, and coupling of AE modes up to ion cyclotron frequencies to lower frequency kink and RWM modes in a predator-prey like relationship. The NSTX-U research on avalanches and non-linear physics is essential for the code validation needed for projecting to ITER. NSTX-U will be uniquely positioned to address this not only because of its operational regime but especially also by its ability to vary the q-profile, known to have a strong effect on non-linear behavior, with the 2nd NB. Furthermore, NSTX-U can study mode stability using its expanded range of toroidal field and the flexibility in the NB system to vary v_{fast} and β_{fast}. An AE antenna will be implemented to study mode stability and excitation, which will be measured by a suite of fast ion diagnostics. Finally, a particular strength of the NSTX-U EP research program will be the code Verification and Validation for both linear and non-linear calculations.

An additional high priority EP issue for ITER is to assess how applied 3D fields affect AE stability and the fast ion distribution. NSTX has laid the groundwork for this with initial studies of applied 3D fields. It was found that the both the mode characteristics and fast ion distribution changed after application (and removal) of these 3D fields on time scales comparable to the fast ion slowing down time. In particular, the changes in the fast ion distribution affected particles close to the higher frequency AE resonances. NSTX-U will bring added capabilities to study this issue, with its flexible neutral beam system to test a variety of injected fast ion distributions and to modify the q-profile, and with the flexible 3D applied field system (including the NCC) to change the mode spectrum of the applied fields and coupling to the fast ion distribution (see Chapter 6).

NSTX-U will be developing and validating heating and current drive scenarios with RF and NB heating, addressing issues of importance to both the ITER ICRF program and the Integrated Operating Scenarios task group. HHFW research includes studying the dependence of coupling on geometry and edge profiles using capabilities such as cryo-pumping and conditioning to change the plasma edge profiles and determine the amount of power that propagates into the core. Related to this is the generation of surface waves, which inhibit the deposition in the plasma core; the ability to vary the toroidal field and density is critical to this study. Wave power

deposited in the SOL near the plasma edge was found to propagate to the divertor region along open field lines, causing higher heat loading of the divertor PFCs. The deposition and transport of wave power will be studied with advanced RF codes, such as TORIC, AORSA and GENRAY, Langmuir probe arrays and IR cameras. Preliminary calculations against NSTX data have already shown that the codes can qualitatively reproduce the topology of the RF power losses through the SOL into the divertor region. These studies will aid in the development of models that can be used to guide operational scenarios in ITER that can optimize the ICRF wave heating and current drive. Related to this development will also be studies of neutral beam and bootstrap current drive in partially and fully inductive NSTX-U discharges, and developing capabilities for controlling the current profile with NB, RF and other discharge evolution techniques. This control capability will be extended to developing robust algorithms for rotation control using, e.g., the off-axis NB and applied 3D fields, this development being important for tailoring target scenarios in both ITER and other future devices.

The areas discussed above represent those in which NSTX-U can most strongly contribute to the ITER R&D Urgent and High Priority issues. NSTX-U can contribute also to other high priority items. In particular, the focus of future research will include measuring the SOL turbulence, including “blobs”, which is believed to control SOL widths. The inferred cross-field transport and parallel flows will be used to validate the theoretical models contained in such codes as BOUT++, SOLT and XGC1. NSTX-U will also be actively developing control technology for heat flux mitigation. Vapor shielding (lithium, in the case of NSTX-U) will be assessed as a possible divertor strategy for mitigating heat fluxes and assessing compatibility with high-performance, steady-state plasmas. Vapor shielding science developed by studying Li in NSTX-U may also be applicable to ITER. More specifically, off-normal events (large ELMs, disruptions) may cause melting of first-wall Be or divertor W, and this melted material may be further/later vaporized in the SOL near the strike-point region of the ITER divertor. Studies of the dependence of H-mode access on plasma species, applied 3-D fields, X-point location and plasma current will be expanded in NSTX-U using the enhanced capability to modify the rotation profile with the 2nd NB, and expanded mode spectrum of the proposed NCC. The focus will also be on assessing achieved confinement with $P \sim P_{LH}$, the role of ion physics, and ultimately on how metal walls affect both the L-H and H-L transitions. The studies will transcend simple global parametric dependence, and will focus on the changes in turbulence and flows leading up to both the L-H and H-L transitions and relating these changes to theory. Other confinement issues important for ITER that will be addressed in NSTX-U include plasma confinement with applied 3-D fields, and the sources and scaling of intrinsic rotation and momentum transport, the latter topic being key for control of both macro- and micro-instabilities. Finally, assessment and development of reduced transport models will be carried out and will be coupled to the continued development of (P)TRANSP as a state-of-the-art integrated predictive transport tool.

1.5.1 International Tokamak Physics Activity (ITPA)

NSTX-U physicists have been participating actively in ITPA activities. NSTX-U has representatives in every ITPA Topical Group, with leadership in many, including past and future Chairs of ITPA groups, leaders of special Working Groups, and spokespersons for many Joint Experiments and Activities. As of January 2013, NSTX-U physicists are participating actively in 24 ITPA Joint Experiments and Activities (Table 1.5.1), many of which address the highest priority ITER R&D needs across all topical science areas. The work NSTX-U physicists is and will be doing towards addressing the high priority ITER R&D needs is described below.

Boundary Physics and PMI

- DSOL-24 Disruption heat loads
- PEP-6 Pedestal Structure and ELM stability in DN
- PEP-19 Basic mechanisms of edge transport with resonant magnetic perturbations
- PEP-27 Pedestal profile evolution following L-H/H-L transition
- PEP-29 Vertical jolts/kicks for ELM triggering and control
- PEP-34 ELM energy losses and their dimensionless scaling

Waves and Energetic Particles

- EP-2 Fast ion losses and Redistribution from Localized AEs
- EP-6 Fast-Ion Losses and associated heat load from edge perturbations

Advanced Scenarios and Control

- IOS-3.2 Define access conditions to get to SS scenario
- IOS-4.1 Access conditions for advanced inductive scenario with ITER-relevant restrictions
- IOS-4.3 Collisionality scaling of confinement in advanced inductive plasmas
- IOS-5.2 Maintaining ICRH Coupling in expected ITER Regime

Macroscopic Stability

- MDC-2 Joint experiments on resistive wall mode physics
- MDC-8 Current drive prevention/stabilization of NTMs
- MDC-15 Disruption database development
- MDC-17 Active disruption avoidance
- MDC-18 Evaluation of Axisymmetric control aspects

Transport and Turbulence

- TC-9 Scaling of intrinsic plasma rotation with no external momentum input
- TC-10 Experimental identification of ITG, TEM and ETG turbulence and comparison w/ codes
- TC-11 He and impurity profiles and transport coefficients
- TC-12 H-mode transport and confinement at low aspect ratio
- TC-15 Dependence of momentum and particle pinch on collisionality
- TC-17 ρ^* scaling of the edge intrinsic torque
- TC-24 Impact of resonant magnetic perturbations on transport and confinement

Table 1.5.1: International Tokamak Physics Activity (ITPA) joint experiments and activities involving participation by NSTX-U researchers as of January 2013.

1.6 Example Contributions to Model Validation

In this short section, we will give several examples of how the NSTX-U program will advance model validation in an effort to develop predictive capabilities across a range of topical areas. The model validation/predictive model development activities focus on specific goals within each group. This work involves active collaborations among experimentalists, theorists and modelers both at PPPL and in the community at large.

1.6.1 Macrostability

Kinetic Resistive Wall Mode (RWM) theory has been a central theme for Verification and Validation (V&V) efforts for NSTX and future NSTX-U plasmas. In particular, including ion kinetic effects has markedly improved the agreement between calculated and measured RWM stability thresholds compared to models for which only rotation effects were taken into account. The kinetic effects include those from both thermal and energetic ions. This work, multi-institutional among PPPL, Univ. Rochester and Culham Laboratory has led to an active Verification exercise among the MISK, MARS-K and HAGIS codes, which are being benchmarked against one another under ITPA auspices. Within this theoretical framework, experiments measuring global RWM stability versus collisionality support the importance of including kinetic effects and provide guidance for NSTX-U operations. In particular, mode stability was measured in NSTX using MHD spectroscopy (active probing of the plasma response to applied MHD perturbations). Theoretical predictions indicated that if the plasma were rotating at frequencies near kinetic drift resonances, the RWM would be strongly stabilized with decreasing collisionality. Off-resonance, collisionality variations would have little effect. The measured plasma response showed precisely those trends, with the n=1 plasma response decreasing with decreasing collisionality for “on resonance” rotation levels, and showing no change “off resonance”. Further work will include improving the physics model by including the phase space anisotropy of the energetic ions. Further, the model is starting to be applied to NSTX-U scenarios, and thus regions of rotation/collisionality space in which the RWM is predicted to be stable are being mapped out. This result can be tested experimentally using the 2^{nd} NBI and both present and future 3D magnetic field coils to modify plasma rotation, and by using lithium and the expanded operating space in NSTX-U to extend the range of accessible collisionality to lower values.

A number of codes are being benchmarked against each other for the calculation of the Neoclassical Toroidal Velocity (NTV) arising from applied magnetic field perturbations. The NTV can be sufficiently large to modify rotation profiles, which in turn can affect both the macro- and micro-stability of the plasma. Consequently, it is important to be able to determine the NTV accurately for predicting plasma performance. The verification study involves six

different codes, IPEC-NTV, MARS-K, MISK, MARS-Q, POCA and FORTEC-3D, and is based on a case with an applied m=3/n=1 field. Kinetic effects are taken into account differently in the above codes, with a bounce-averaged treatment in the first four codes but exact drift orbit calculations in the last two. Because of this and other differences among the codes, their range of applicability has been illuminated by this verification activity. For instance, IPEC-NTV and MARS-Q have found to be good approximations at high aspect ratio, but not at low R/a. POCA and FORTEC-3D, with full drift orbit treatment, were found to be the most appropriate for the low aspect ratio, low collisionality and high rotation frequency regime in NSTX and expected in NSTX-U plasmas. Improvements to enhance the predictive usage of these codes will include incorporation of a self-consistent treatment of the field perturbations and plasma response. The results of the code calculations would then be incorporated into the solution of the momentum balance equation for a prediction of the torque and rotation profiles.

1.6.2 Transport and Turbulence

In the area of thermal plasma transport, NSTX/NSTX-U is addressing three areas of electron transport, which is the dominant energy loss channel in L- and H-mode discharges. For high-k modes, NSTX-U is validating the Electron Temperature Gradient (ETG) electron thermal transport model. ETG modes were seen in a variety of NSTX scenarios using a unique high-k_r scattering system. In particular, ETG modes were found to be important in NBI-heated H-modes near the pedestal, in RF-heated L-modes, and in electron Internal Transport Barrier discharges. Identification of the measured turbulence as ETG modes was supported by both linear and non-linear gyrokinetic calculations, which predicted ETG-driven transport levels that agreed with the experimentally inferred transport levels. Initial TGLF predictions of T_e due to ETG modes in NSTX ITB plasmas, however, showed an over-prediction of electron temperature near the edge of the plasma. In NSTX-U, a new FIR-based high-k_θ scattering system will substantially improve our understanding of the ETG. This new diagnostic will include a 2D k-spectrum measurement, which will allow for the identification of the radial streamers believed to lead to enhanced electron transport. Further validation efforts will focus on using TGLF and the Multi-Mode reduced models as well as further non-linear gyrokinetic calculations using GYRO and GTS to benchmark against each other as well as against experiment. These studies reflect a strong collaborative effort across multiple institutions (PPPL, UC-Davis, Lehigh Univ., Tech-X, GA).

NSTX-U researchers are validating the CAE/GAE-driven electron thermal transport hypothesis. Studies so far have used the ORBIT code to study the stochastic electron transport driven by these modes. Mode amplitudes, the locations of peak mode amplitudes, mode widths, frequencies, and mode numbers are taken from experimental measurements and dispersion equations of these high-frequency modes, and the resulting calculated transport based on these quantities agrees well with the experimentally inferred values in the core of the plasma, where the mode amplitudes are observed to be largest. Future work will move toward a more predictive

calculation using ORBIT and non-linear HYM calculations of the CAE/GAE mode characteristics. This work is also a multi-institutional effort involving PPPL, Johns Hopkins Univ., Univ. of Wisconsin and UCLA.

Finally on the electron transport topic, NSTX-U researchers have performed seminal work in validating the role of micro-tearing modes in driving electron transport in the mid-radius region of NSTX(-U) plasmas. Non-linear gyrokinetic calculations using GYRO have shown that micro-tearing modes in high beta H-mode NSTX plasmas can drive substantial electron transport at levels that match those inferred from experiment, and further, can lead to the same scaling with collisionality that was evident in the NSTX discharges. Global calculations with GTS will be done as soon as electromagnetic effects are implemented in the code, which should be within one year. To further assess the importance of micro-tearing modes in NSTX-U, a polarimetry diagnostic that is capable of measuring magnetic fluctuations driven by micro-tearing modes will be implemented from the start of operation. This diagnostic was designed using predicted micro-tearing mode characteristics from non-linear gyrokinetic calculations that employed a synthetic polarimetry diagnostic. Efforts are also being made to assess the sensitivity of the BES diagnostic to micro-tearing-related density fluctuations to be able to distinguish these modes from electrostatic ITG/TEM turbulence. Again, this is being done in conjunction with the non-linear gyrokinetic calculations using synthetic diagnostics. For the development of reduced models, the theory-based TGLF will be validated and further developed against NSTX-U discharges, and analytic expressions that have been used to predict micro-tearing-driven transport will be improved with better $\delta B/B$ estimates.

1.6.3 Boundary Physics

Several V&V studies have been and are presently being undertaken in the Boundary Physics area. Pedestal widths and structures are being compared to those predicted from kinetic ballooning mode (KBM) calculations at low aspect ratio, with predicted neoclassical effects, and with predicted paleoclassical transport. NSTX data showed pedestal widths to scale more strongly with $\beta_{pol,ped}$ than was observed (and predicted from KBM calculations) for higher aspect ratio, at first-glance drawing this explanation into question for NSTX plasmas. However, KBM calculations specific to NSTX plasmas actually reproduce to a larger extent this stronger scaling, giving reasonable agreement with the NSTX data. XGC0 calculations, on the other hand, show that the predicted neoclassical pedestal width is significantly narrower than that observed experimentally. Paleoclassical transport semi-quantitatively agrees with NSTX pedestal gradients in plasmas both with and without lithium conditioning.

How the snowflake divertor configuration, where the magnetic shear inside the separatrix is higher than that in conventional divertor configurations, may change the pedestal stability due

KBM-peeling modes is presently being investigated. Results from TCV snowflake plasmas are consistent with improved pedestal stability, with increased frequency but reduced size of the Type I ELMs. NSTX plasmas indicate the opposite, however; during snowflake configurations, ELMs that were otherwise stabilized by lithium reappeared, and calculations indicated a reduced stable operating window for peeling-ballooning modes. Also, the overall pedestal stability of DIII-D snowflake discharges did not appear to change. These different experimental results clearly point to the need for future testing of the peeling-ballooning mode theory for these high magnetic shear plasmas. Further, analytic and 3D calculations using the BOUT++ code for snowflake configurations have suggested enhanced turbulence in the X-point region due to ballooning modes, electrostatic flute instabilities and resistive ballooning modes. Edge turbulence will be assessed in NSTX-U plasmas using the Gas Puff Imaging (GPI) diagnostic.

The last example in the Boundary Physics area is validation of the DEGAS-2 neutral transport code against NSTX GPI data. Implementation of a more sophisticated neutral transport calculation in codes such as TRANSP would be a major advance in the study of particle and impurity transport. For this validation exercise, the measured emission from the GPI diagnostic is compared to 3D simulations from DEGAS-2 using a GPI synthetic diagnostic. The DEGAS-2 calculations are constrained by electron density and temperature measurements near the edge as well as reconstructions of the magnetic equilibrium. The GPI data (emission and gas puff) are absolutely calibrated. Preliminary comparisons show good agreement between the two.

1.6.4 Materials and PFCs

New materials simulation techniques are providing an understanding of the behavior of deuterium in lithium-conditioned carbon PFCs. Many plasma codes utilize data from simple models that simulate the behavior of ions incident on materials but neglect the role of chemical interactions within the material (e.g. TRIM, MARLOWE). In contrast, quantum-classical molecular dynamics (QCMD) models simulate the interaction of these incident ions and apply quantum-mechanical calculations to determine the interaction potentials during the simulation. This simulation method has already yielded powerful results explaining the uptake of deuterium in lithium-conditioned, carbon PFCs and the important role of oxygen in this process [21]. In particular the simulations indicate that deuterium is more likely to be chemically bound to oxygen present in the PFC present from reactions with residual gas or other ubiquitous sources in the tokamak. These results have helped understand numerous experimental observations of the surface chemistry of these PFCs [22,23]. In particular, these experimental studies inferred the presence of deuterium by observing shifts in the energy spectra of oxygen atoms in PFC samples; a result that is consistent with those of the simulations, which show preferential oxygen bonding. Tabulated or parameterized results from the code for the uptake or reflection of incident deuterium ions will eventually be coupled to plasma simulation codes, to evolve the plasma alongside the material simulation.

1.6.5 Energetic Particles

One of the overarching aims of NSTX-U is to demonstrate stationary, 100% non-inductive performance that extrapolates to ≥ 1 MW/m^2 neutron wall loading in FNSF. A critical ingredient of this goal is to optimize the neutral beam-driven current profile and magnitude. Current profile studies in NSTX have sometimes exhibited discrepancies between reconstructions assuming classical fast ion physics and profiles based on MSE measurements, with much reduced core currents seen in the measurements. TAE avalanches are observed in these particular discharges, and the discrepancy can be reconciled by applying an impulsive anomalous fast ion diffusivity (AFID) in TRANSP that is both spatially and temporally localized to reflect the effect of the TAE modes have on the fast ion distribution. A proper choice of this fast ion diffusivity brings temporally evolving measured and calculated neutron rates, as well as current profiles, into agreement. The AFID, however, is clearly ad-hoc, and this underscores the need for predictive modeling of avalanche-induced fast ion transport.

Being able to predict this transport involves two steps. The first is the accurate prediction of the TAE mode stability and structure, and the second is the response of the fast ion distribution to these modes. For the first step, a strong theory-experiment collaboration is addressing the Verification and Validation of both linear and non-linear codes for predicting the TAE stability and mode structure. Unstable modes and their properties (mode spectrum, structure and temporal evolution) can be measured using Beam Emission Spectroscopy and reflectometry. On NSTX, these measured mode structures were consistent with those calculated from the linear NOVA-K code. The mode amplitudes calculated by NOVA-K were normalized to match the measured density perturbation, and these normalized modes were then input into the ORBIT guiding center tracking code. The particle losses in the presence of these TAE modes inferred by ORBIT agreed quite well with those inferred from drops in the measured neutron rate during the avalanches, confirming the validity of both the mode structure calculation and the particle tracking. Future work on NSTX-U will involve using SPIRAL, a full-orbit code, as well as ORBIT, and developing fully non-linear models with M3D-K that can predict mode amplitudes as well as structure.

The second phase of developing a predictive capability is the modification of the fast ion distribution in the presence of these modes. To this end, two different approaches are being pursued. The first treats the modifications to the fast ion distribution function and resulting transport that are induced by resonant interactions with AE modes. In this approach the resonant fast ion transport is modeled through use of a “probability function”, based on adiabatic invariants, which reflects kicks in both energy and canonical angular momentum due to AE modes. While the probability function is calculated from models such as ORBIT, it is also based on experimental quantities such as neutron rate and mode amplitude. This reduced model is presently being tested against full ORBIT calculations, and resulting energy distributions show

very good agreement for both co- and counter-phased particles using measured multi-AE mode amplitude spectra (at different n). Once developed, this model will be implemented in the TRANSP code.

The second approach to developing predictive capability for modification of the fast ion distribution in the presence of AE modes uses a quasi-linear relaxation model to determine the radial fast ion profile as a function of time in response to a given set of AE modes. This approach has been developed and tested for DIII-D, and will be extended into the NSTX-U parameter regime. The development approach for NSTX-U is to compute the spectrum of unstable TAE modes (using NOVA) for given NSTX scenarios. NOVA-K will be used to compute the growth and damping rate of these modes, and an unperturbed fast ion distribution function will be computed using TRANSP/NUBEAM. The quasi-linear model will then be applied to find the "relaxed" fast ion distribution function as a function of time, and comparisons to measured FIDA, NPA and neutron measurements will be made to validate this reduced model. Once validated, the model will be implemented in TRANSP.

1.6.6 Wave Heating and Current Drive

A major element of the NSTX-U RF program is the Verification and Validation of simulation codes that not only support the NSTX-U program, but which can also be used to predict heating and current drive in ITER and other fusion devices such as ST-FNSF. Details of this work are described in Sections 7.2 and 7.3, and only two elements will be summarized here.

One of the key issues in predicting the RF power deposition into the plasma is being able to predict direct absorption of RF power by the neutral beam fast ions. To this end, the 2D full wave AORSA code has been coupled to the Monte-Carlo ORBIT-RF codes to perform a self-consistent calculation of the interaction between resonant fast ions and injected HHFW power. Validation of this calculation is being carried out using the computed fast ion distribution into a synthetic diagnostic in the FIDASIM code, which then computes the expected fast ion profile that would be measured by the FIDA diagnostic. While these simulated profiles agreed in a quantitative manner reasonably well with the measured profiles, the computed profiles have a slightly outward shift relative to the measurement. Investigation of the source of this outward shift is underway.

GENRAY is a ray tracing code for HHFW that also contains modules for the determination of the RF current drive. GENRAY has been coupled to CQL3D, a bounce-averaged Fokker-Planck code, for taking into account the fast ion absorption of RF power and thus modifications to the current drive. The computed results, again processed with the synthetic diagnostic in the FIDASIM code, were compared to actual FIDA signals for NB+HHFW cases. Initial comparisons gave poor agreement, with the computed FIDA signals significantly shifted toward

the magnetic axis relative to the measured signals. These calculations, however, tracked only the guiding centers and assumed zero orbit widths. Implementation of the finite orbit width model into the quasi-linear calculation shows a marked improvement in the agreement between measured and calculated profiles. Presently being worked on is a full-finite orbit width model that includes radial transport and a non-thermal bootstrap current contribution.

1.6.7 Plasma Formation and Ramp-up

The final example that will be presented, but which is discussed in much more detail in Chapter 8, is using both 2D and 3D simulation codes to understand non-inductive startup. Development of this capability will allow for projections to ST-FNSF operation with a small or no solenoid. Axisymmetric TSC simulations of CHI-initiated NSTX plasmas show good agreement, with closed flux surfaces forming due to the large electric fields generated by the CHI. However, these 2D calculations may not contain the full MHD physics that forms the basis for the creation of closed flux surfaces. To this end, 3D calculations using the NIMROD code have been initiated.

References

[1] Y.-K.M. Peng and D.J. Strickler Nucl. Fusion **26** (1986) 769
[2] S.M. Kaye, et al., Fusion Technol. **36** (1999) 16
[3] M. Ono, et al., Nucl. Fusion **40** (2000) 557
[4] Editors of "Progress in the ITER Physics Basis", Nucl. Fusion **47** (2007) S1–S17
[5] J.E. Menard, et al., Nucl. Fusion **52** (2012) 083015
[6] Y.-K.M. Peng, et al., Fusion Sci. Technol. **56** (2009) 957
[7] R.J. Goldston, et al., "An Experiment to Tame the Plasma Material Interface" Paper FT/P3-12, presented at 22nd IAEA FEC, Geneva, Switzerland, Oct 13 - Oct 19 (2008)
[8] J.E. Menard, et al., "Physics Design of the NHTX", 34th EPS Conference on Plasma Phys. Warsaw, 2 - 6 July 2007 ECA Vol. 31F, P-1.162 (2007)
[9] Y.-K.M. Peng, J.D. Galambos, and P.C. Shipe Fusion Technol. **21** (1992) 1729
[10] Y.-K.M. Peng, et al., Plasma Phys. Control. Fusion **47** (2005) B263
[11] F. Najmabadi, et al., Fusion Engineering and Design **65** (2003) 143-164
[12] J. E. Menard, et al., Nucl. Fusion **51** (2011) 103014
[13] S. Nishio, et al., http://www-pub.iaea.org/mtcd/publications/pdf/csp_019c/pdf/ftp1_21.pdf
[14] K. Tobita, et al., Journal of Nuclear Materials **329–333** (2004) 1610–1614
[15] T. Nishitani, et al., Fusion Engineering and Design **81** (2006) 1245–1249
[16] K. Tobita, et al., Nucl. Fusion **47** (2007) 892–899
[17] Y. Nagayama, et al., "A Conceptual Design of Super Conducting Spherical Tokamak Reactor", www.sunist.org/shared%20documents/ISTW2011/Nagayama.pdf ISTW2011, NIFS, Japan, Sept. 27-30, 2011
[18] B.G. Hong, et al., Nucl. Fusion **51** (2001) 113013
[19] Report of the FESAC Toroidal Alternates Panel, https://fusion.gat.com/tap/ (2008)
[20] K.L. Wong, et al., "Micro-tearing instability in the ITER pedestal", PPPL-4579 (2010)
[21] Krstic, et al., Phys. Rev. Lett. (2012)
[22] C. N. Taylor, B. Heim, and J. P. Allain, Journal of Applied Physics 109 (2011) 053306.
[23] J. P. Allain, D. L. Rokusek, S. S. Harilal, M. Nieto-Perez, C. H. Skinner, H. Kugel, B. Heim, R. Kaita, and R. Majeski, Journal of Nuclear Materials 390-391 (2009) 942.

Table of Contents for Chapter 2

Chapter 2

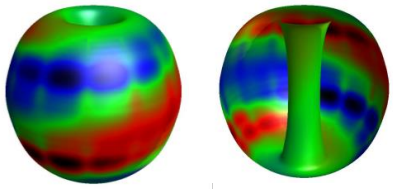

Stability

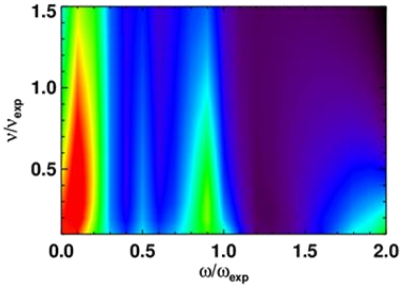

3D Fields

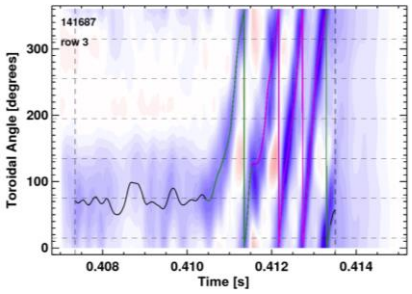

Disruptions

Research Goals and Plans for Macroscopic Stability

2.1 Overview of goals and plans

2.1.1 Overall goal and motivation

The overall goal of macroscopic stability research in NSTX-U is to establish the physics understanding and control capabilities needed to produce sustained stability of high performance ST plasmas in a yet unexplored hotter operational regime at the highest level of current self-sustainment ever routinely produced in such a device. With double the toroidal field, plasma current, and heating power compared to NSTX, the upgraded device will be the most powerful ST in the world, producing the highest stored energy and lowest collisionality ever produced in an ST. Additionally, NSTX-U will provide expanded capability to vary key stability parameters including the plasma rotation and energetic particle density profiles via the unique more tangential injection geometry of the second neutral beam system. This research will provide the predictive physics understanding needed to confidently extrapolate toward the goal of a steady-state Fusion Nuclear Science Facility (ST-FNSF) / Component Test Facility (ST-CTF) [1-3], a pilot plant [4], or DEMO based on the ST [5,6]. As was exploited in NSTX, the unique ST operational space and device geometry of NSTX-U will be leveraged to extend and test physics theories and technological solutions for next-step spherical torus (ST) and tokamak operation, including ITER.

A present urgent need for ITER, as well as for future ST fusion devices planned to operate continuously, is the prediction, avoidance, and mitigation (PAM) of plasma disruptions. Macroscopic stability research on NSTX from its inception has targeted the stabilization of beta-limiting, disruptive instabilities that stop the plasma, or otherwise prevent it from operating at high fusion performance. Passive [7-9] and active [9-11] stabilization studies of global mode stability, and advanced understanding of 3D plasma response [12], including magnetic island dynamics such as neoclassical tearing modes [13], on NSTX provide a firm foundation for the advanced disruption prediction and avoidance research on NSTX-U (Sections 2.2.1, 2.2.3, and 9.2.3). Macrostability research will strongly contribute to a multi-layered control approach toward an ambitious goal of nearly 100% disruption avoidance. The research for NSTX-U will expand to include disruption mitigation as well (Section 2.2.3). NSTX-U will also expand the capability to alter profiles that affect stability. For the better part of a decade, research on NSTX has utilized non-resonant magnetic braking via neoclassical toroidal viscosity (NTV) – an inherent 3D field effect – to finely control the level and profile of plasma rotation to low levels without causing mode locking. Several unanswered questions remain regarding the understanding of this physics and scaling to next-step devices (Section 2.2.2). A significant and unique advancement in the use of NTV will be as an actuator for real-time feedback control of the plasma rotation profile – a unique capability for tokamaks. This research will strongly interconnect with other topical science areas – in particular with Advanced Scenario and Control research (Chapter 9), but also with Transport and Turbulence, Boundary Physics, and Energetic Particle research (Chapters 3, 4, and 6).

2.1.2 Bridging knowledge gaps for ST fusion devices and to support ITER

NSTX-U is designed to address critical stability physics understanding for future STs, and for tokamaks/ITER as stated in Section 2.1.1. Due to its critical need, this physics has been considered in recent DOE reports defining such needs. For example, the report “Research Needs for Magnetic Fusion Energy Sciences” (ReNeW - 2009) [14] defines the key scientific and technical knowledge gaps in magnetic fusion research needed to bridge present systems to devices producing significant fusion power for long (many minutes to weeks) duration. NSTX-U macrostability research will address elements of three of the five ReNeW Themes:

- Theme 1: Burning Plasmas in ITER
- Theme 2: Creating Predictable, High-Performance, Steady-State Plasmas
- Theme 5: Optimizing the Magnetic Configuration

Elements of Themes 2 and 5 will be addressed directly, while elements of Theme 1, for example, "Thrust 2: Control transient events in burning plasmas", will be addressed indirectly. The centerpiece thrust for the spherical tokamak from ReNeW is "Thrust 16: Develop the spherical torus to advance fusion nuclear science". This thrust contains 7 elements, 5 of which address physics needs of next-step ST experiments. Three of these 5 elements are addressed in the macrostability research described in this section, summarized here in sub-bullets:

- ReNeW Thrust 16 Element: *Utilize upgraded facilities to increase plasma temperature and magnetic field to test the understanding of ST confinement and stability at fusion-relevant parameters*
    - Lower collisionality operation of NSTX-U at higher temperature will provide a unique laboratory for the ST to investigate the physics of kinetic resistive wall mode stability at lower ν. It will be determined whether the observed and measured *increase* of mode stability at the highest levels of β_N/l_i in NSTX continues as ν is further reduced, and whether this trend is due to kinetic RWM stability physics.
    - NSTX-U researchers will determine the important dependence of NTV at reduced values of ν^* that is theoretically expected to show an increase in plasma rotation drag, and compare physical models of NTV including fluid models with kinetic effects and particle-in-cell models to determine the most important physics aspects
    - The role of energetic particles on ST plasma macrostability has only begun to be investigated. NSTX-U will provide a greater capability to vary the energetic particle profile via a greater range of B_T, I_p, and NBI injection angles.

- ReNeW Thrust 16 Element: *Implement and understand active and passive control techniques to enable long-pulse disruption-free operation in plasmas with very broad current profiles.*
    - The physics understanding of passive control of low frequency modes will be significantly enhanced by the unique NSTX-U capability of utilizing both NBI and 3D-field (via NTV) actuators to change mode stability by controlling the plasma rotation and equilibrium profiles, including the effect of kinetic RWM stabilizing resonances, and to study and attempt to avoid NTM mode locking conditions.
    - Active control of low frequency modes with toroidal mode number, n = 1 and 2 will be studied in NSTX-U using a combination of upgraded control hardware (available on Day 1), dual-component magnetic field perturbation measurements, and expansion of the present NSTX model-based RWM state space controller (RWMSC) proposed for use in ITER.

- The advantages gained by expanded multi-mode controller capability of the RWMSC will be determined, including enhanced ability to reduce error fields.
- The theoretically computed increase in global eigenmode amplitude in the divertor region at high β_N will be investigated utilizing an expanded RWM sensor set. The prominence of this mode in the full computed multi-mode spectrum and the impact on active mode control will be determined. The impact of snowflake divertor operation on this mode will be assessed.
- Present models will be tested and continued to be developed, and real-time physics criteria will be implemented for use in the NSTX-U disruption avoidance system including simple models of kinetic RWM stability, and the RWM state space controller observer.
- Active, low frequency MHD spectroscopy will be analyzed and developed for real time use to avoid disruptions by altering NBI power and/or rotation/equilibrium profiles, and the importance of multiple modes will be determined.
- Dynamic error field correction will be possible for simultaneous correction of n up to 3 with the present midplane coils.
- The addition of an upgraded non-axisymmetric control coil set (NCC) will significantly expand stability physics research capabilities for dynamic error field correction (n up to 6), RWM control (n up to 4), and NTV physics studies and will be used in rotation profile control, and ELM mitigation/stabilization.

- ReNew Thrust Element: *Employ energetic particle beams, plasma waves, particle control, and core fueling techniques to maintain the current and control the plasma profiles.*
  - The significant impact of fully non-inductive current sustainment on macrostability physics will be determined. This pioneering milestone for NSTX-U is expected to have multi-faceted ramifications on both tearing and ideal instabilities.
  - Improvements to plasma stability enabled by rotation profile control and the RWMSC on plasmas with very low (ITER-relevant) plasma rotation speeds will be determined.
  - NSTX-U researchers will develop reduced NTV models incorporating the most important physical effects possible for real-time use supporting the rotation profile control system.
  - The utility of NBI, and ability and physics of NTV in controlling rotation in plasmas with very low rotation speed will be determined - expanding past NSTX operation in the NTV superbanana plateau regime.

The analysis and use of three-dimensional field (3D) effects in systems that primarily have toroidal symmetry (two-dimensional fields) is considered important, and in many cases essential in present macrostability research. Therefore, research on 3D effects pervades the full NSTX-U macrostability program.

The proposed NSTX-U 5 Year Plan research on macroscopic stability is also highly-aligned with the Department of Energy's vision of US magnetic fusion research. The associate director of DOE's Fusion Energy Sciences Office of Science, Dr. Edmund Synakoswki has defined a program vision incorporating three major components: burning plasma dynamics, long-pulse plasma control science, and fusion materials science. The second element is the major focus of NSTX-U macroscopic stability research for 2014-2018. The research is particularly unique and pioneering in that it plans to move tokamak stability research solidly into a new realm of controlling fully non-inductive plasmas at high beta, with a unique combination of control actuators.

The proposed research is also directly coupled to ITER through the ITPA. Past NSTX research has been communicated bi-annually at each ITPA MHD Stability group meeting for many years. The NSTX-U macrostability group leads the MDC-2 joint experiment / analysis on RWM physics, and co-leads the Working Group 7 effort on aspects of active mode control. The NSTX-U group has also led two elements of the recent ITPA Integrated Plasma Control Working Group study, led by Dr. Joseph Snipes of ITER. The group also contributed with direct calculations for ITER on RWM and error field control associated with this effort. Even through the experimental outage period, the stability research group maintains contributions to five MDCs and two working groups. NSTX-U stability research plans to expand this effort in the coming five year period, especially through the stronger cross-coupling between the NSTX-U macrostability and the advanced scenarios and control topical science groups.

In the following section (2.1.3), an overview is provided of the research goals and plans in macroscopic stability summarized above, now logically subdivided into three separate, but strongly related thrusts. Interconnections between the thrusts are then briefly highlighted. Several experiments proposed for the last NSTX run campaign are appropriate to initiate macrostability research on NSTX-U, and will provide a seamless start to continued experimental research once the upgrade is completed. Finally, the motivation and design of a significant upgrade which will greatly benefit macroscopic stability research – the proposed non-axisymmetric control coil (NCC) - is briefly motivated and discussed in Section 2.1.4, with further detail on the significant physics design analysis performed to date for this system. This upgrade will serve research in several other topical science groups as well, including boundary physics, energetic particle physics, and advanced scenarios and control. Specific uses of the NCC in various physics studies are covered in this chapter, and also in other research thrusts chapters.

2.1.3 Thrusts and goals by topical area

2.1.3.1 Sustainment of macroscopic stability

Macroscopic MHD instabilities (such as the kink/ballooning mode, resistive wall mode (RWM), and tearing modes that lock) are critically important to avoid or control as they lead to plasma disruption, terminating the discharge and leading to large, potentially damaging electromagnetic forces and heat loads on the structure of fusion producing devices.

While many targeted performance parameters have been reached in world tokamaks, such high performance plasmas will need to be sustained for far longer pulse lengths in machines such as FNSF, ITER, and DEMO than have been produced to date. Research has therefore changed focus to examine sustained global mode stability over long pulses and to examine profile evolution for routine long pulse operation at high beta and at high non-inductive current fraction. Common to the following studies is the unique physics understanding and control ramifications that come from such operation, and the understanding and prediction of the effect of excursions from this condition due to transient behavior. It is especially important to realize that plasma operation near but below marginal stability points (set for example by plasma beta, internal inductance, rotation) is insufficient to ensure disruption-free, continuous operation in either ITER inductive or advanced scenarios due to these transients in plasma profiles. Such transients can rapidly change a stable operational point to an unstable plasma state. Therefore, understanding plasma stability gradients vs. key profiles affecting stability is essential for all operational states in ITER or an FNSF.

NSTX-U will provide key capabilities for critical physics understanding based on present research in plasma operation regimes applicable to ITER and future magnetic fusion devices. The NSTX-U plan is unique in its goal to operate 100% non-inductively driven plasmas routinely. This major operational regime for NSTX-U, which may require greater control, provides a unique lab to test advanced stability physics. Additionally, NSTX-U will operate in the unique high beta ST operational space, which will allow performance of advanced stability control in an operating space where disruptivity is *not* most probable at the highest β_N, or β_N/l_i. The research is enabled by independent control of the present midplane RWM coils – a new capability that NSTX-U brings, along with the continued physics development of the present model-based RWM state-space controller for both slow and fast correction of 3D field perturbations with toroidal mode number, n up to 3. The research capability will be significantly expanded in the last two years of the five year period by the planned NCC system (details given

in Section 2.2.1.5 and throughout the chapter), allowing n up to 6, and a broader poloidal spectrum and variability of field helicity. These considerations motivate the following thrust:

Thrust MS-1: Understand and advance passive and active feedback control to sustain macroscopic stability

With significantly expanded profile control capabilities (e.g. q, plasma rotation), NSTX-U will allow greater ability to vary these important profiles for investigations of how to prevent plasma disruptions excited by profile excursions. Additionally, profiles theoretically expected to improve stability will be attempted to be sustained at high performance, including fully non-inductive operation. Real-time models to determine favorable profiles for stability will be developed from experimental testing of full theoretical models. Research will focus on the effect of reduced plasma collisionality and energetic particles on the kinetic stabilization of disruptive instabilities, and sustaining stability. Shape and aspect ratio changes, the effect of advanced divertor configurations, and 3D multi-mode spectrum will be assessed. ITER-relevant low plasma rotation regimes will be evaluated. Disruption prevention research will be conducted as a combination of advanced active mode control techniques and active profile control. For example, instability onset leading to global modes growing on a relatively fast timescales (milliseconds) will be actively controlled by an expanded model-based RWM state space controller, while concurrent control of q and plasma rotation profile working on slower timescales (~100ms) will steer the plasma toward stability. Instabilities occurring before plasmas attain full current, and the ability to control largely internal modes will be addressed.

2.1.3.2 Utilization of non-axisymmetric (3D) magnetic fields

A small non-axisymmetric (3D) field almost always exists in tokamaks, due to imperfect primary magnets and surrounding conductors and machine components. Tokamaks are highly sensitive to 3D fields, which can cause unnecessary transport and instability and even lead to a disruption if not properly compensated [12,15-17]. On the other hand, 3D fields can be greatly beneficial if properly controlled, by using non-ambipolar transport [18] that can modify equilibrium and plasma rotation profiles and therefore macroscopic stability, as well known by edge localized mode (ELM) control using resonant magnetic fields [19,20] and resistive wall mode (RWM) [8,10], and tearing mode (TM) and/or neoclassical tearing mode (NTM) [13,21,22] control using non-resonant magnetic fields. Therefore, it will be critical to achieve the controllability as well as

the predictability of these 3D field applications, in order to improve plasma stability and performance in next-step devices such as FNSF, ST Pilot, and ITER.

There has been substantial progress in understanding 3D field effects. Research on n = 1 resonant error field correction in NSTX using the ideal perturbed equilibrium code (IPEC) (Section 2.4.3) highlighted the importance of ideal plasma response [12,23,24] and the developed method has been actively applied to ITER [25] along with a paradigm change in error field correction. Also, n = 3 non-resonant error field correction has been routinely used to maximize the toroidal angular momentum based upon successful validation across experiments and neoclassical toroidal viscosity (NTV) calculations [18,26]. Based on the improved knowledge on 3D field effects in general, resonant and non-resonant error field effects will be studied together [27-29] in order to provide comprehensive error field correction schemes for the next-step devices. The rotating island dynamics such as neoclassical tearing modes and the interplay with error fields, which are fundamentally 3D effects, will require further extensive research in non-ideal and non-linear regimes [15,30-35]. The strong shaping and high-β in NSTX-U, and with the addition of the NCC, will provide a unique test environment of the island 3D dynamics.

The NTV transport and its magnetic braking on toroidal rotation are well-known effects produced by 3D fields, and the braking can be a useful tool to control the toroidal rotation and thereby suppress various instabilities in NSTX-U. The magnitude of NTV is theoretically expected to change significantly at lower plasma collisionality, so requires further research in this regime. Several NTV physics elements have been theoretically investigated [18,36-51], numerically computed [52-54], and examined in experiments in various devices including NSTX [7,9,55,56], DIII-D [57,58], and KSTAR [59,60]. However, a number of aspects in NTV physics are still not fully resolved and need further study in order to confidently extrapolate understanding to next-step devices. Another outstanding issue regarding 3D fields is their role in local modification of transport and stability, either by non-ambipolar transport such as NTV or by stochastic transport with magnetic islands, which is believed to be the main physics mechanism behind ELM control by resonant magnetic perturbations.

NSTX-U will provide strong capabilities for this research, including unique control of toroidal rotation using both NBI and non-resonant 3D fields, and providing various possibilities of toroidal momentum and rotation profile control in unexplored parametric regimes for NTMs and RWMs. Furthermore, the NCC will give significantly greater flexibility in 3D field studies. The poloidal field spectrum will also be as rich as the ITER RMP coils when the NCC is combined with the present midplane coils. These considerations motivate the following thrust:

Thrust MS-2: Understand 3D field effects and provide the physics basis for optimizing stability through equilibrium profile control by 3D fields

Expanded 3D field application capabilities will be utilized to study 3D field effects on resonant error field correction, and to develop the physics basis for control of toroidal rotation through non-resonant magnetic braking while simultaneously applying RWM control and dynamic error field correction. Non-ideal and non-linear island dynamics including neoclassical tearing modes, and the interplay with resonant and non-resonant error fields, will be studied together with strong shaping, high-β, and low collisionality. The NTV physics yielding magnetic alteration of the rotation profile will be systematically studied as a function of plasma collisionality as density control tools are improved during the 5 year plan period. This physics research will be greatly enhanced by the proposed NCC coils. The toroidal rotation profile will also be more widely varied using the 2nd off-axis NBI system. The combination of the new NBI, upgraded independent control of the present midplane coils, and proposed NCC will be utilized to vary and understand toroidal momentum transport for a range of magnetic field spectra and plasma collisionality conditions to develop the physics basis for magnetic rotation profile control to improve and optimize plasma performance.

2.1.3.3 Disruption physics, prediction, avoidance, and mitigation

A key issue for ITER, and the tokamak/ST line of fusion devices in general, is the avoidance and mitigation of disruptions. As a general goal, disruptions must be avoided. The research program in Thrusts 1 and 2 of this chapter, as well as in Thrusts 2 and 3 of the Advanced Scenarios and Control chapter (Chapter 9), develops the physics understanding and many of the necessary tools for disruption avoidance. These tools by themselves, however, are not sufficient to meet the stringent requirements for reliable tokamak/ST operations. The present thrust describes four additional research tasks for disruption prediction, avoidance, mitigation, and characterization.

The first two elements, described in Sections 2.2.3.1-2.2.3.2, describe the development of techniques for integrated disruption prediction and avoidance. Methods developed in these sections combine various actuators and measurements, in order develop more integrated control of global stability. For instance, resonant field amplification methods will be developed to assess global stability, and will be coupled to the β_N and/or rotation control algorithms with the goal of keeping the plasma in a stable regime. Similarly, the difference between the state-space RWM control observer and measurements will be used to provide an indicator of the onset of disruptions, separate from its use for direct mode control.

The third element, described in Section 2.2.3.3, addresses the topic traditionally known as disruption "mitigation". This topic is also of great importance to ITER, where methods to terminate a discharge without excessive thermal or mechanical loading of the device are required. This research will focus on two technologies for rapidly terminating a tokamak discharge. Massive gas injection (MGI) will be explored: the poloidal angle dependence of mitigation efficacy will be examined, and modeling of the gas penetration with the DEGAS-2 code (Section 2.4.11) will be done. Secondly, a novel electromagnetic particle injector (EPI) will be developed. This technology has the potential to very rapidly deliver large amounts of the material to the plasma, and will be tested on NSTX-U. Note that this topic is complementary to that discussed in ASC Thrust 3, focusing on rapid discharge terminations using traditional inductive ramp-down techniques. NSTX-U is also capable of studying runaway current suppression as described in Section 2.2.3.3.3.

The final element, described in Section 2.2.3.4, focuses on the physics of disruptions themselves. Key topics to be addressed here are the physics of, and heat loading from the thermal quench of a disruption, and generation of halo currents.

Thrust MS-3: Study and develop techniques for disruption prediction, avoidance, and mitigation, and understand disruption dynamics and in high-performance ST plasmas

> *The physics understanding gained in the balance of the macroscopic stability research will be applied to improve disruption prediction and avoidance. Kinetic stability physics models, low frequency resonant field amplification, RWM state-space control models, and expanded sensor input will be used to improve disruption prediction. Real-time implementation of these physical models and measurements will be used for disruption avoidance. The plasma dynamics resulting from the interplay of different stability controllers will be measured and simulated. For instance, resonant field amplification methods will be developed to assess global stability, and may be coupled to the β_N or rotation control algorithms to ensure that the plasma remains in a stable regime. The characteristics and dynamics of NSTX-U disruptions will be measured and modeled – in particular heat loading, the thermal quench, and the generation of halo currents – all to improve the understanding of the impact of disruptions in STs and tokamaks. Techniques for disruption mitigation will be developed and explored. Massive gas injection (MGI) will be explored: the poloidal angle dependence of mitigation efficacy will be examined, and modeling of the gas penetration will be done. A novel electromagnetic particle injector (EPI) will be developed and tested. This technology has the potential to very rapidly deliver large amounts of the material to the plasma.*

2.1.3.4 Thrust and topical science group interconnections

The macroscopic stability research described in this chapter has many interconnections between the stated three thrusts, and also to many of the other topical science group (TSG) research topics in NSTX-U. A summary of several significant elements are:

- Thrust 1 elements that aim to understand the physics of macroscopic mode stability, and the related advanced mode control capabilities, directly serve the disruption prediction and avoidance control elements in Thrust 3
- Thrust 2 elements that aim to control dynamic error fields and understand tearing mode locking directly support disruption avoidance elements of Thrust 3. NTV physics aspects and reduced physics models for real-time use directly support plasma rotation control elements of the Advanced Scenario and Control (ASC) TSG.
- Thrust 3 elements serve the entire NSTX-U Team in producing greater reliability (and eventually, routine capability) of reducing disruptions in the device. These critical capabilities will also have a direct connection to certain tasks as needed, for example, to attempt sustaining Enhanced Pedestal H-mode operation.
- Direct interaction between the Macrostability (MS) and ASC TSGs will occur in all Thrusts, with complementary tasks associated with physical models for plasma rotation control and physical mode stability models used to trigger the disruption warning system.
- Significant interaction between the MS and Boundary TSGs will occur in determining ths impact of snowflake divertor operation on global mode stability, and understanding the physical effects of 3D fields on ELMs.
- The physical effects of energetic particles on macroscopic instabilities found in NSTX will continue to be studied in Thrust 1, coupled to the Energetic Particle TSG.
- The NTV physics and the effects of 3D fields on transport in Thrust 2 interconnects with momentum transport work conducted by the Transport and Turbulence TSG.

2.1.4 Non-axisymmetic control coil (NCC) motivation

The powerful utility of 3D fields has been rapidly appreciated in the tokamak research community, as 3D fields can provide selective channels of transport and thereby allow stability control. The NTV momentum transport by 3D magnetic braking can be well utilized to control and optimize toroidal rotation, and stabilize macroscopic instabilities such as the RWM and NTM, microscopic instabilities such as ITG, TEM, and ETG, and fast ion instabilities such as TAE and GAE by altering the energetic particle population. Also 3D fields can provide particle transport to alter the pedestal and thus modify ELMs, as well known by RMP ELM control.

However, such plasma instabilities are not simple functions of rotation, and NTV itself depends on rotation. RMP ELM control is also not yet well understood and predictable, as essentially all different devices, with different 3D coils, have yielded somewhat different results. In NSTX, 3D fields generated by the existing midplane coils can trigger ELMs, an opposite and nearly unique result compared to other devices. Further extensive studies of 3D fields are therefore necessary, and NSTX-U will provide a unique and important contribution to 3D field physics understanding utilizing its strong 2D shaping and operation in an advanced high-β regime. The results will be greatly enhanced by additional 3D coils added to give greater flexibility in the applied 3D field spectrum that can be coupled to the strong 2D shaping. This motivates the addition of a new non-axisymmetric control coil (NCC).

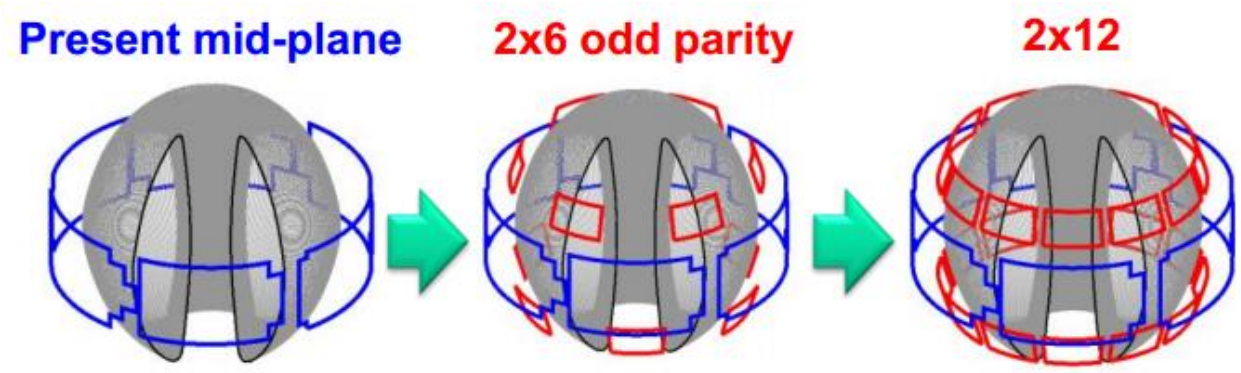

Figure 2.1.4-1. Non-axisymmetric control coil (NCC) (red) proposed for NSTX-U, in a staged installation with partial NCC (2x6-Odd) and full NCC (2x12). The coils shown in blue are the present midplane RWM coils.

The NCC will provide a significant expansion of physics research not only in the Macrostability TSG, by in several physics areas spanning the majority of the NSTX-U topical science areas. The NCC has been proposed as a set of off-midplane coils implemented in a staged approach, with one example illustrated in Figure 2.1.4.1. The NCC, combined with the present midplane coils, can produce a highly flexible 3D field spectrum, comparable to the proposed ITER RMP coils, and. The NCC can significantly increase the RWM β-limit by active control, allows a significant increase in stability physics and disruption control studies (MS, Section 2.2.1), and can increase dominance of non-resonant over resonant field components (MS, Section 2.2.2.1) and NTV variability in the core (MS, Section 2.2.2.5) by an order of magnitude. The NCC will be able to provide edge-resonant field enough to create a stochastic layer, with greater extent than needed for ELM control based on empirical RMP criteria, while decreasing the non-resonant field by an order of magnitude (MS,BP, Section 2.3), and to substantially modify 3D stability and actively control or pace ELMs (BP, Section 4.2.1.3). Also, the improved rotation and rotation-shear control will be very important to perform advanced studies for micro-instabilities such as ITG/TEM/ETG (T&T, Section 3.3.3.1), and momentum transport studies in general (T&T, Section 3.3.3.2). The change of fast-ion transport and stability by 3D fields can be further investigated using the NCC, as such studies started in NSTX using the midplane coils

(EP, Section 6.3.3.1). As is apparent from these applications, the NCC will be a critical tool for NSTX-U research and will largely advance understanding of 3D field physics for tokamaks in general. More details for each subject can be found in the other TSG chapters as indicated above. The main physics design activities of the NCC including quantitative assessment of error field correction, NTV, RMP, and RWM control will be separately described in Section 2.3.

2.2 Research Plans

This section describes the research to be conducted in the macroscopic stability topical science area for the five year period.

Each subsection follows a similar format: First, a description of the research is given, with appropriate motivating work shown which also establishes context, and second, a "Summary of research plans by year" is provided. Note that in these summary subsections, years 1-5 refer to the years of the NSTX-U 5 year plan, with the first year of device operation starting in year 2.

On Day 0 of NSTX-U operation, the device will have significantly upgraded capabilities compared to NSTX, and will also benefit from capabilities that were unable to be utilized in the abbreviated 2010 run. In addition, several significant new control and diagnostic hardware capabilities (described in several sections of this document) will be added during the 5 year period described. Capabilities of special note include a new MGI disruption mitigation system, a partial implementation of a new set of non-axisymmetric field coils, and an extended sensor set for improved low frequency (NTM and RWM) mode characterization. Macrostability research will also help produce, and greatly leverage techniques to control plasma rotation, q, pressure, and $n > 0$ modes. The largest hardware component supporting macrostability research during the 5 year period will be the partial NCC, which is planned to be implemented during an outage between the third and fourth years in the baseline funding scenario.

The timing of research deliverables listed below best utilizes the new capabilities as presently planned. Modification of the availability of these capabilities will logically lead to modification of the deliverables timeline, with completion of tasks shifting to match changes to the hardware and control capability timelines.

2.2.1 Thrust MS-1 – Understand and advance passive and active feedback control to sustain macroscopic stability at low collisionality

2.2.1.1 Macroscopic mode stability at lower collisionality

NSTX-U will provide several important upgraded capabilities to study key dependencies of global mode stability on plasma characteristics. The second neutral beam line with double the available power and will provide the ability to alter the power and momentum deposition profile. This will allow changes to the most basic equilibrium profiles: pressure and q, but it will also, in combination with neoclassical toroidal viscosity (NTV) generated by applied 3D fields, allow significant variation of the plasma rotation profile, which effects both tearing and kink/ballooning/RWM instabilities. Added to these basic variations is another key parameter, the plasma collisionality, ν. Stability is indirectly affected by ν as it changes the steady state rotation profile. But NSTX data has shown that a more direct effect occurs from the influence of ν on kinetic stabilization of global modes. Therefore, it is crucial to create and study the self-consistent, quasi-steady-state equilibrium variations at values of ν not yet attained in the ST. Energetic particle profile and velocity space distribution also influences mode stability, and NSTX-U upgrades will allow variations of this profile as well.

2.2.1.1.1 Assess beta and q limits in NSTX-U shape and off-axis NBI

The upgraded center column of NSTX-U will be approximately double the diameter of the NSTX predecessor. This will increase the plasma aspect ratio and will change the boundary shape. In addition, it is planned that the snowflake divertor [61] configuration will be used in a larger number of plasmas in NSTX-U to handle the high first wall heat loads at high P_{aux}. Such changes to the boundary are expected to affect the ideal stability of the plasma, which will be investigated experimentally. This investigation has already begun, as experimental scenario development in NSTX has already accessed aspect ratios (up to 1.73) and boundary shaping (elongation greater than 2.9) planned for NSTX-U [62] (Figure 2.2.1.1.1-1). The new off-axis neutral beam line will also produce changes to plasma pressure and current profiles that will affect stability. Therefore, a new space of beta and q-profile will be explored to determine the limits on plasma stability. Such studies of the ideal stability are needed as input to studies of the actual marginal stability boundaries that include kinetic stabilization effects.

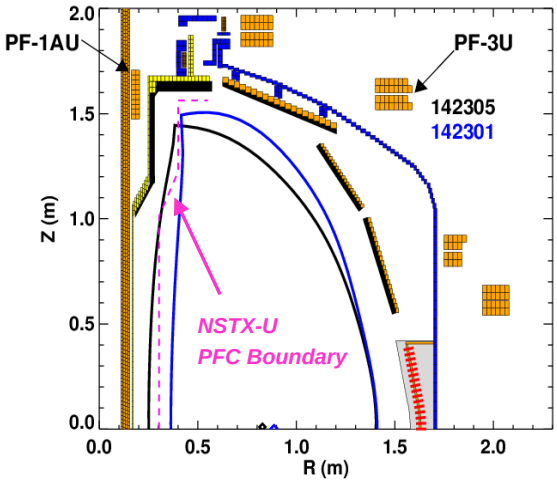

Figure 2.2.1.1.1-1: NSTX plasmas have matched the aspect ratio and elongation planned for NSTX-U.

The three new NBI sources in NSTX-U will inject farther outboard of the magnetic axis at the plasma midplane. This capability can be used to drive off-axis current and therefore raise the core q-profile, which will have a major effect on the macroscopic stability of the plasma, including neoclassical tearing modes (NTMs). Note that NTM physics is discussed mainly in Section 2.2.2.1 of this chapter. Additionally, off-axis NB injection can potentially broaden the plasma rotation profile. This too would have a major impact on stability, particularly RWM stability, and will be fully investigated and compared to theoretical predictions.

2.2.1.1.2 Define favorable combined rotation / kinetic profiles for plasma stability

Time-evolved NSTX-U equilibrium simulations have been created, and these equilibria will be used to best prepare for NSTX-U macroscopic stability experiments. TRANSP calculations are available which provide the full kinetic and energetic particle population information for use by the MISK code (Section 2.4.4) to determine kinetic RWM stability boundaries. These computations will be performed in the years prior to NSTX-U first plasma. In addition to the boundary variations discussed in the prior section, the equilibrium, rotation, and energetic particle profile variations will be considered in this analysis to determine how the kinetic resonances will change in NSTX-U, and therefore how global mode stability will change.

2.2.1.1.3 Test kinetic RWM stability theory in lower collisionality plasmas

Past NSTX research has established a new understanding of resistive wall mode stability by making quantitative correlation between experiments reaching the mode marginal stability point and kinetic RWM stabilization theory [8,9]. This model has important implications for next-step devices operating at reduced collisionality. Early RWM stabilization models relied solely on plasma collisionality as a stabilizing energy dissipation mechanism, yielding reduced stability at reduced collisionality. The present kinetic RWM stabilization theory changes this significantly, yielding a more complex stability picture. As before, stabilizing effects of collisional dissipation are reduced at lower ν, but new stabilizing resonant kinetic effects can be enhanced [63]. Generally, stronger resistive wall mode (RWM) stabilization occurs near broad dissipative kinetic resonances (which depend on the plasma rotation profile) and this stabilization increases with decreasing collisionality, but in stark contrast has almost no dependence on collisionality when the plasma is off-resonance (see Figure 2.2.1.1.3-1). In this figure, ν_{exp} and ω_ϕ^{exp} represent NSTX experimental values in high beta plasmas, and kinetic RWM stability calculations producing the mode growth rate are made using the MISK code [63]. Experiments that utilized n = 1 active MHD spectroscopy [64] diagnosis, which uses n = 1 resonant field amplification to measure

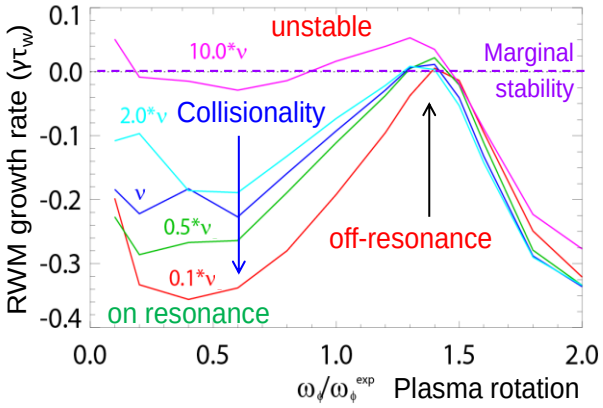

Figure 2.2.1.1.3-1: MISK computed kinetic RWM n = 1 stability vs. collisionality and plasma rotation.

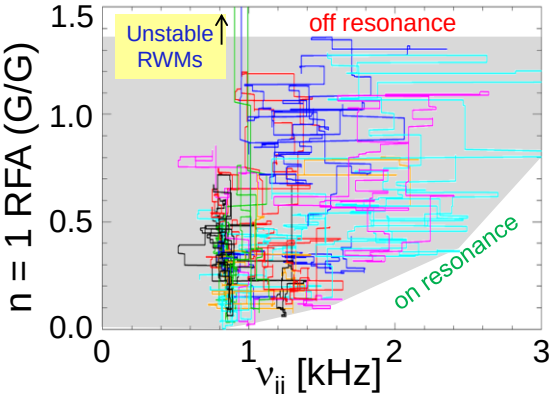

Figure 2.2.1.1.3-2: n = 1 RFA amplitude vs. ν_{ii}, showing a relatively large change at low RFA ("on resonance") vs. almost no change at high RFA.

RWM stability [65], indicate the expected gradient in RWM stability for plasmas with high $5.5 < \beta_N/l_i < 13.5$ (most are above the n = 1 ideal no-wall stability limit) (Figure 2.2.1.1.3-2). The figure shows the trajectory of the RFA amplitude over the entire discharge for 20 shots, over which the ion collisionality, ν_{ii}, is varied by a factor of 3.75. The theoretically expected gradients in kinetic RWM stability are generally reproduced by the upper/lower boundaries of n = 1 RFA amplitude. At high n = 1 RFA amplitude (the upper boundary), the plasma is off-resonance, and there is almost no change in RWM stability (indicated by the n = 1 RFA amplitude) vs. ν_{ii}. At low n = 1 RFA amplitude (the lower boundary), the plasma has greater stabilization by kinetic resonances, and there is a clear increase in RWM stability (decrease in n = 1 RFA amplitude) as ν_{ii} is decreased. Here, ν_{ii} is averaged over $0.55 < \psi_N < 0.75$ of the profile, inside of the pedestal, and ψ_N is the normalized poloidal flux, $(\psi - \psi_0)/(\psi_a - \psi_0)$, where subscript "a" represents the plasma edge, and "0" represents the magnetic axis.

In NSTX-U, it is planned to extend these experimental measurements of mode stability and expectations of kinetic RWM stability theory in experiments ranging to the lowest possible ion collisionality in the device, and also in plasmas having the extra constraint of full non-inductive current drive, which are expected from TRANSP simulations to be constrained to plasma collisionality reduction of a factor of four. Variations of the proximity to stabilizing kinetic resonances (e.g. ion precession drift resonance) will be primarily attained by variation of the plasma rotation profile, by a combination of varying NBI sources at different tangency radii and NTV variation to precisely and reliably produce different rotation speeds and profiles. In early years, the rotation will be changed with open-loop rotation control. Once the rotation feedback system becomes available in later years, closed-loop feedback will be used, using independent and combined variations of NBI and NTV actuators.

Energetic particle effects have also been shown to significantly influence RWM stability. Stabilizing effects of the energetic particle population have been computed, using the MISK code, to play a significant role in the RWM stability of NSTX plasmas [66]. This continues to be an active area of research, as the present EP stability model needs to be tested over a wider range of plasma operation. Extrapolation to ITER Advanced Scenario plasmas shows that the stabilizing effect of alpha particles will be required at expected plasma rotation levels. The greater variations made available by the NSTX-U upgraded NBI system with three additional neutral beam heating sources all aimed at different, and larger tangency radii (farther from the magnetic axis) than the present first three NBI sources, and the larger variation of plasma parameters in NSTX-U will allow greater variation of the EP population, and non-resonant NTV plasma rotation control allows access to very low plasma rotation (applicable to ITER) without mode locking.

2.2.1.1.4 Establish and test approach to marginal stability based on kinetic RWM stability

Previous NSTX research has established the present understanding that a single point rotation measurement is not sufficient as an indicator of RWM stability. Full kinetic RWM calculations with the MISK code [67] capture the necessary physics needed to determine marginal stability. A key goal of the NSTX-U stability research plan is to establish and test the approach to marginal stability both with the more involved kinetic model calculation, and to develop a simpler model that may be used in real-time calculations as input to the NSTX-U disruption warning system.

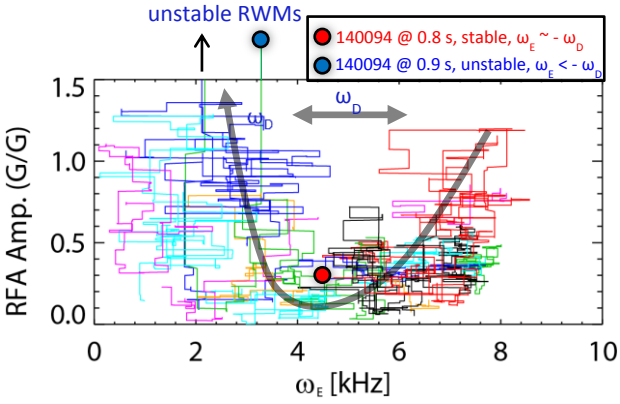

Figure 2.2.1.1.4-1: RFA amplitude vs. an average E×B frequency, ω_E.

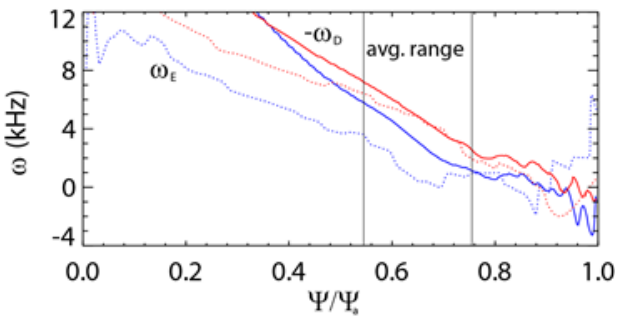

Figure 2.2.1.1.4-2: E×B frequency, ω_E, profiles (dashed) and -ω_D profiles (for ε/T = 2.5 and zero pitch angle), vs. ψ/ψ_a, for NSTX discharge 140094 at 0.8 s (red) and 0.9 s (blue).

An intermediary step in the full MISK calculation that can provide physical insight, and perhaps a calculation than could be approximated in real-time, is to examine the effect of plasma rotation in the context of kinetic resonances between the mode and the particles by examining the E×B

frequency, ω_E, and comparing to the ion precession drift frequency, ω_D. Figure 2.2.1.1.4-1 shows RFA amplitude generated by active MHD spectroscopy measurements plotted against an average ω_E, taken over $0.55 < \psi/\psi_a < 0.75$ of the profile. In Figure 2.2.1.1.4-2 one can see that $-\omega_D$ for hot thermal ions in this ψ range averages roughly 4.5 kHz for discharge 140094 at time 0.8 s (also shown is t = 0.9 s, the time just before this discharge goes unstable). Note that $\omega_E \sim -\omega_D$ at the stable time, and $\omega_E < -\omega_D$ at the unstable time, corresponding to the middle and left sides of Figure 2.2.1.1.4-1, respectively. This can explain the low RFA amplitude in this ω_E range in Figure 2.2.1.1.4-1, with low rotation instability below this, and intermediate rotation marginal stability above. Presumably the RFA would return to lower values at higher ω_E as the mode begins to resonate with the bounce frequency, but this higher level of rotation was not explored in this particular experiment. Similar experiments with MHD spectroscopy in stable plasmas in DIII-D yielded conclusions similarly supportive of kinetic stability theory [68].

This recent NSTX analysis indicates that a simple criterion such as $-\omega_E/\omega_D < K$, where K is a constant, might be used to set a marginal stability condition for NSTX-U in real-time. As this condition is a local condition, further analysis of the present database, and further experiments in the early years of NSTX-U operation will be used to determine how best to implement a criterion such as this for real-time disruption avoidance in later years of the five year research period.

2.2.1.1.5 Investigate early MHD modes

Early MHD modes locking to the wall were a source of low density disruptivity in NSTX. These modes were typically associated with the rational surfaces entering the plasma. Modes at q = 2, 3, and 4 have been observed to lock, with a large degree of variability in the rotation damping dynamics. In NSTX, empirical changes to the fuelling were used to prevent modes from locking. Changes in global parameters due to fuelling changes were quite subtle, but changes to rotation dynamics were profound. A better understanding of mode amplitude and torque dynamics is needed. For example, are there small changes in resistive current evolution, or modification of the early energetic particle modes (EPMs), and is there a measurable quantity to put under feedback control? These questions will be studied in NSTX-U to help improve reliable plasma start-up.

2.2.1.1.6 Summary of research plans by year

Year 1 (2014):

- Begin assessment of theoretically favorable stability conditions, through a combination of existing NSTX data, supplemented by dedicated experiments on DIII-D utilizing low frequency MHD spectroscopy to directly measure stability and creating unstable plasmas, for enhanced kinetic stabilization of global MHD modes. The study will include rotation

profile proximity to stabilizing resonances and energetic particle population variation, for initial experimental scoping studies of the NSTX-U operational space.

- Evaluate simple physics criteria (suitable for real-time use) for the approach to global mode marginal stability based on ideal (e.g. pressure peaking, β_N/l_i) and kinetic stability physics using initial high performance NSTX-U plasmas, emphasizing rotation profile and speed.

Year 2:

- Conduct initial assessment of stability limits on normalized β and q limits at the increased aspect ratio of NSTX-U, with new shaping control and off-axis NBI. Compare to ideal stability limits.
- Utilize off-axis NBI to produce initial investigation determining the effect of pressure, q, and v_ϕ profile variations on RWM and NTM stability.
- Begin investigation of the dependence of global mode stability on reduced collisionality through a combination of dedicated experiments utilizing low frequency MHD spectroscopy to directly measure stability and creating unstable plasmas, and investigating mode-induced disruptions by examining the database in general. Compare experimental results to kinetic stabilization theory. Open-loop rotation control will be the default for these studies, with initial closed-loop control used if available. NBI variations will be conducted with pre-programmed heating, and with β_N feedback.
- Adjust present simplified physics models of RWM marginal stability based on initial high beta, reduced collisionality operation of NSTX-U, appropriate for real-time calculations.

Year 3:

- Theoretically determine improvements to global mode, RWM, and NTM stability expected by the addition of the partial NCC based on improved understanding gained in the first 2 year operation of NSTX-U.
- Test kinetic RWM stability theory expectations, including updated variations of reduced plasma collisionality, based on the more general database of NSTX-U plasmas created during initial device operation.
- Assess modifications of global mode and NTM stability due to expected alteration of q_{min} based on initial device operation, with projections for closed-loop q_{min} control.

Year 4:

- Utilize rotation control to improve RWM/NTM stability: (i) perform closed-loop rotation control studies to alter rotation shear for improved NTM control, and (i) change proximity to stabilizing kinetic resonances for RWM control.

- Validate kinetic RWM stabilization physics at reduced ν^* and varied fast ion populations with closed-loop control of q_{min} in plasmas with non-inductive current fraction approaching, or at 100%.
- Perform initial studies of mode stabilization utilizing improved open-loop plasma rotation profile control afforded by the partial NCC added to the present midplane coil set.
- Initially assess improvements to real-time evaluation of kinetic stabilization model by the addition of initial real-time Thomson scattering results.

Year 5:

- Test kinetic RWM and NTM stabilization models in the lowest ν^* regimes.
- Combine plasma rotation and, q-profile, and, β to demonstrate improved RWM/TM/internal MHD mode stability in 100% non-inductive plasmas, demonstrating very low plasma disruptivity in dedicated experiments.
- Evaluate experimental improvements to real-time kinetic stabilization models through the addition of real-time Thomson scattering.

2.2.1.2 Dual-field component active RWM control and improved mode discrimination at high normalized beta

2.2.1.2.1 Dual-field component active RWM control

Active feedback control of the RWM with the midplane coils was used routinely on NSTX, mostly using poloidal field sensors that discriminated n = 1 mode activity. The control was shown to occur by a combination of limiting mode amplitude and by NTV drag spinning the mode in the presence of the conducting wall at rotation frequency greater than the wall eddy current decay time, leading to strong mode damping [9]. In the last full year of NSTX operation, proportional gain feedback was improved by the addition of radial field sensors and used routinely. Combined radial (24 B_r sensors) and poloidal (23 B_p sensors) field sensor feedback gain and phase were scanned in NSTX experiments to produce significantly reduced n = 1 field and improved stability. The fast (2 - 3 ms) RWM growth was found to be controlled by B_p feedback, while B_r feedback controlled slower n = 1 RFA, which would otherwise cause disruptions once the n = 1 B_r amplitude was sufficiently large (~ 7 – 9 G). Time domain analysis of active control with the VALEN code reproduced the mode dynamics as a function of feedback phase and determined the optimal gain. Modelled feedback evolution agrees with experiment for radial sensor variations examined (Figure 2.2.1.2.1-1), and also shows the optimal gain is still a factor of 2.5 greater than the value used in experiments.

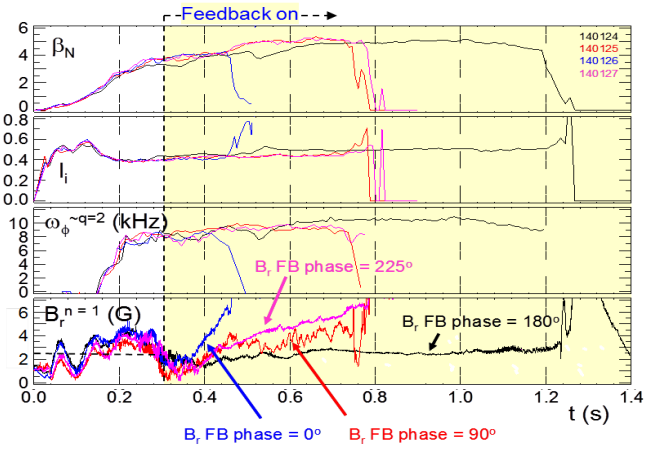

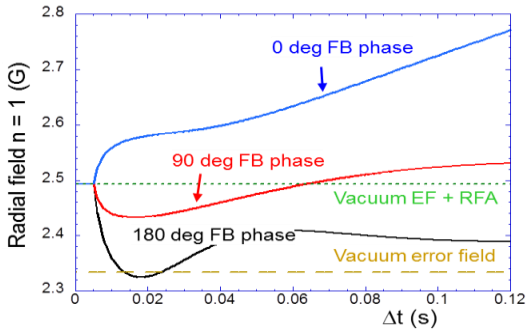

Figure 2.2.1.2.1-1: RWM B_R sensor feeback phase variation with combined radial/poloidal field sensor feedback (a) experiment, (b) theory.

Dual-component active RWM control using proportional gain will be retained on NSTX-U. The system will be improved by adding additional RWM sensors closer to the divertor region. Physics design studies [69] and multi-mode analysis of NSTX (Section 2.2.1.2.2) theoretically show significantly increased mode amplitude in the divertor region at high β_N. This characteristic will be studied using the upgraded sensors, which will be incorporated into the RWM feedback system to further improve mode detection.

2.2.1.2.2 Multi-mode analysis, eigenmode variation at high β_N, and upgraded mode detection

In high β_N plasmas, the influence of multiple RWM eigenfunctions on n = 1 active feedback, including the stable mode spectrum, is a potential cause of β_N fluctuation and loss of control. The multi-mode VALEN code has been applied to NSTX experiments to determine the multi-mode RWM spectrum and characteristics. The perturbed normal field due to induced wall currents shows the influence of the passive conducting plates (Figure 2.2.1.2.2-1a). The computed RWM growth time vs. β_N is in the range observed when such modes are destabilized (Figure 2.2.1.2.2-1b).

The computed spectrum of eigenfunctions comprising the total perturbed field (Figure 2.2.1.2.2-1c) is shown for an unstable mode, and one stabilized by plasma rotation. The RWM multi-mode spectra consist of ideal eigenfunctions computed by the DCON code (Section 2.4.2). These multi-mode components are ordered from lower to higher number, with the lowest number being least stable when each eigenfunction is considered separately in ideal MHD theory. Both spectra show significant amplitude in eigenfunctions up to 10, with the second mode component having the maximum amplitude.

Poloidal cross-sections of the mode components are also shown. Component 1 is ballooning, while component 2, which has dominant amplitude, has maximum perturbation near the lower divertor. There is a significant change in the multi-mode spectrum for the stabilized plasma. In this case, the ballooning component of the perturbation is significantly reduced compared to the component with maximum perturbation in the lower divertor region. The rotationally stabilized multi-mode RWM has a computed rotation frequency of 41 Hz, close to the ~ 30 Hz frequency measured in experiments with both magnetic and kinetic diagnostics (soft X-ray).

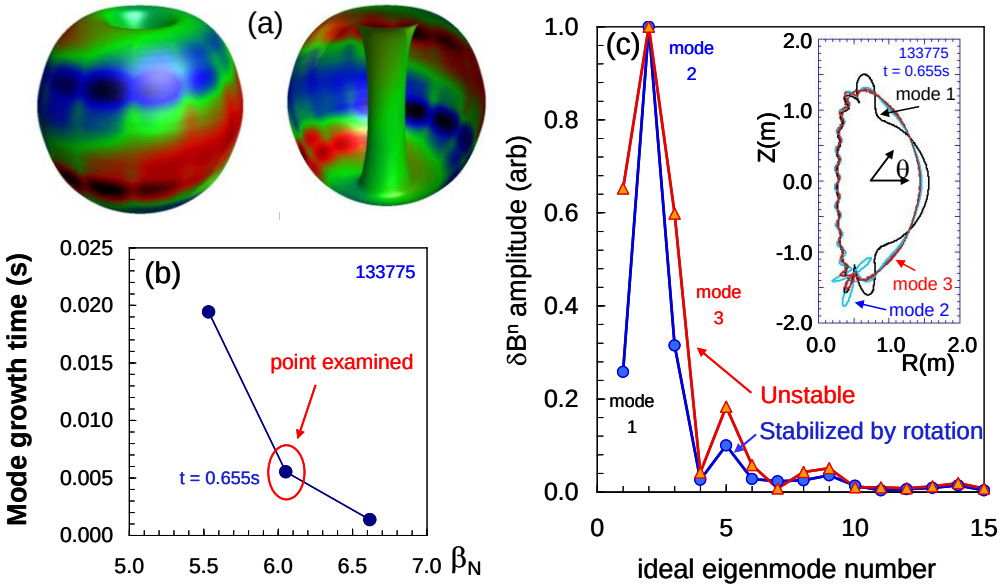

Figure 2.2.1.2.2-1: Multi-mode RWM analysis of high β_N plasmas (a) δB_{normal} from wall currents, (b) growth time vs. β_N, for unstable modes, (c) ideal eigenmode spectrum of multi-mode RWM perturbation showing the spectrum of an unstable mode, and one stabilized by plasma rotation.

Similar calculations for ITER scenario IV plasmas with elevated q_0, β_N = 4, and a modeled blanket conducting structure show multi-mode RWM spectra with up to 6 components of significant amplitude both for unstable n = 1 and n = 2 modes (Figure 2.2.1.2.2-2).

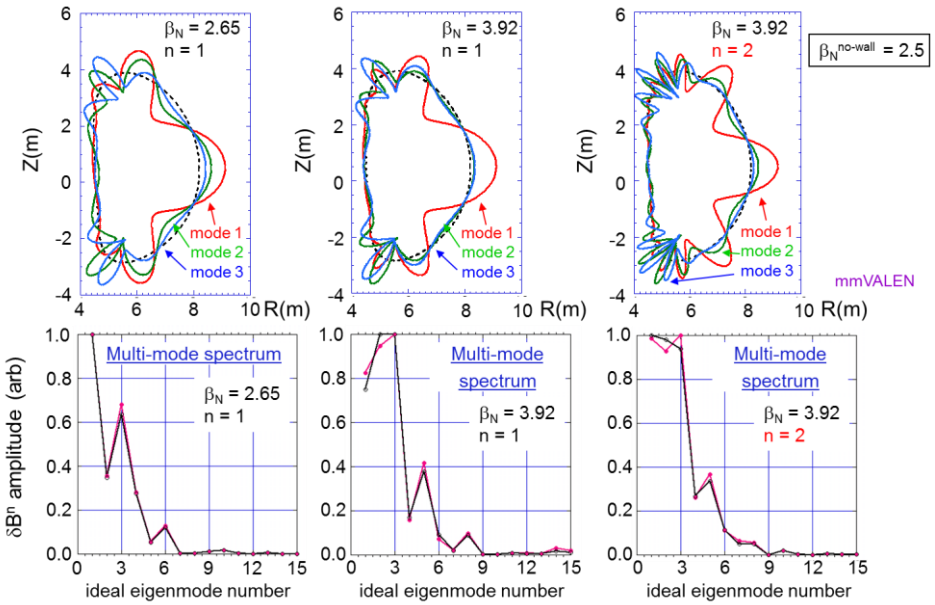

Figure 2.2.1.2.2-2: Multi-mode RWM analysis of ITER advanced scenario discharges, demonstrating a significant eigenmode spectrum in addition to the standard single ideal eigenmode typically assumed in control calculations.

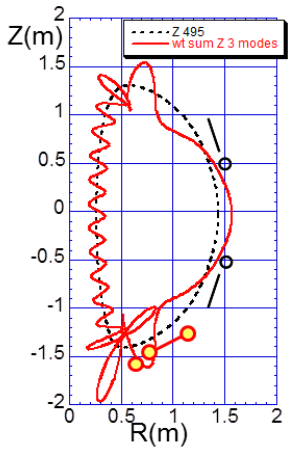

Figure 2.2.1.2.2-3: Weighted sum of three-mode amplitude with present magnetics in black and proposed enhanced magnetics in yellow.

The significant mode amplitude in the divertor region, found both in single and multi-mode studies, motivates the installation of magnetic sensors closer to the divertor region to study the RWM eigenfunction, to compare to expectations of ideal theory, and to directly improve comparisons of the measured mode shape to the real-time RWM state-space controller model (see Section 2.2.1.3.1). Figure 2.2.1.2.2-3 shows the weighted sum of the three modes shown in Figure 2.2.1.2.2-1c as well as the proposed locations of the new sensors, indicating the locations closer to the divertor will improve mode measurement. Figure 2.2.1.2.2-4 shows that a significant change to toroidal phase would be measured by the new sensors due to a significant field line pitch. Note that a relatively long poloidal wavelength still exists (vs. center column region), and the new phase information will help to constrain the RWM state space controller model (Section 2.2.1.3).

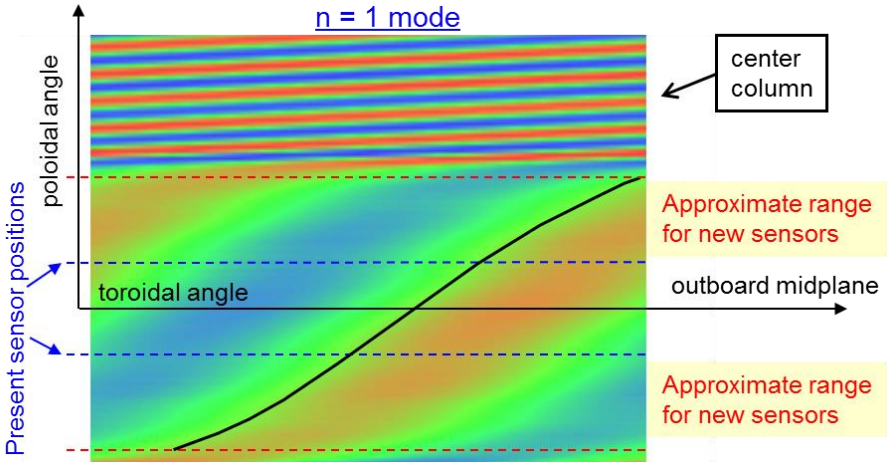

Figure 2.2.1.2.2-4: Mode amplitude vs. toroidal and poloidal angle for an n = 1 mode in NSTX.

Finally, the MARS-K code (Section 2.4.9) will be used to determine the importance of self-consistent alteration of the eigenfunction by kinetic effects and rotation. Additionally, a system of two toroidally displaced, edge and core in-vessel tangential multi-energy soft X-ray arrays (described in detail in Section 10.6.1.3) will be used to measure the mode characteristics.

2.2.1.2.3 Effects of snowflake divertor on RWM stability and eigenfunction

The snowflake divertor configuration is planned to be used extensively in long-pulse, high performance NSTX-U plasmas to handle the high wall heat loads that will be produced by these plasmas. Modifications of the global mode stability due to changes to the edge plasma shaping and eigenfunction modification will be evaluated to determine what ramifications the snowflake will have on stability. In addition, modifications to the RWM control system parameters will be experimentally and theoretically evaluated in the snowflake configuration to determine how the control physics is altered. Changes to the control system will be made to best compensate for any negative ramifications of the configuration.

2.2.1.2.4 Summary of research plans by year

Year 1 (2014):

- Determine theoretically computed optimal feedback parameters for dual component feedback control of projected high beta NSTX-U plasmas.
- Determine multi-mode spectrum for projected high beta NSTX-U plasmas including 3D device geometry.

Year 2:

- Establish dual field component n = 1 active control capability in new NSTX-U operational regime. Compare theoretically expected changes in feedback phase and gain based on NSTX-U plasma shape and aspect ratio to experimental results.
- Examine expanded capabilities allowed by six independent power supplies for the midplane control coils (vs. three in NSTX), including n = 2 pre-programmed error field correction with n = 1 feedback.
- Study and attempt initial control of internal MHD modes that appear at low density during current ramp-up.
- Examine effectiveness of n = 1 active mode control as a function of plasma rotation. Compare theoretically expected changes in optimal n = 1 feedback phase and gain including stabilization effects due to plasma rotation to experimental results.

Year 3:

- Assess global mode stability and control modifications due to more standard use of the snowflake divertor configuration.
- Examine the effect of partial RWM control coil use during n = 1 feedback, examining the impact on the higher-n perturbation spectrum (also supports ITER, JT-60SA).
- Determine effectiveness of n = 1 active control versus operational regime and analyze effectiveness of upgrades including the addition of a poloidally extended sensor set, and multi-mode active control by adding n = 2. Generalize n = 1 control software for $n = 2$ control use and to allow the use of an extended RWM sensor set (available in Year 5).
- Determine theoretically superior partial NCC variations in n = 1 active feedback and update control software to allow actuation of these additional coils for control in Year 4.

Year 4:

- Determine changes to the effectiveness of n = 1 mode control during closed-loop feedback of plasma rotation profile, and q_{min} control in plasmas with non-inductive current fraction approaching, or at 100%.
- Perform initial investigation of dual field component n = 1 active control using the newly-installed partial NCC, including variations feedback phase vs. poloidal angle (varied applied control field helicity with respect to mode helicity).
- Compare n = 2 active feedback control using proportional gain to the NSTX-U model-based RWM state space controller.

Year 5:

- Characterize the poloidal variation of n = 1 – 3 global mode activity using a newly-installed expanded RWM sensor set, including a comparison to the theoretically computed NSTX-U multi-mode spectrum.

- Employ superior multi-mode settings for n = 1 and 2 active control with the partial NCC to demonstrate improved global MHD mode stability in 100% non-inductive plasmas, demonstrating very low plasma disruptivity in dedicated experiments.

2.2.1.3 Model-based RWM state-space controller for active RWM control

A model-based state space controller [70] has been implemented using a state derivative feedback algorithm [71] and incorporating currents due to the unstable RWM eigenfunction and those induced in nearby 3D conducting structure by the applied control field and plasma response. Testing this physics is especially important for ITER [72] and high neutron output devices where greater control coil shielding will be needed. Using a number of states equal or greater than required by Hankel singular value analysis (7 here) provides sufficient 3D conducting structure current detail to match experimental sensors. Open-loop comparisons between sensor measurements and the RWM state space control (RWMSC) model showed agreement with a sufficient number of states and improved agreement when the 3D wall model details (e.g. NBI ports) were added (Figure 2.2.1.3-1). Control was demonstrated to sustain long pulse, high β_N discharges with n = 1 fields applied that normally disrupt the plasma (Figure 2.2.1.3-2). This controller was used for RWM stabilization in long-pulse plasmas (limited by coil heating constraints) reaching β_N = 6.4, and near maximum β_N/l_i = 13.4 (shown in Figure 2.2.1.3-2) [65].

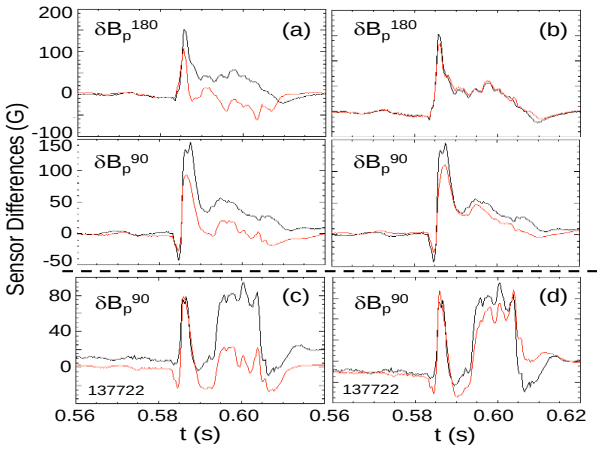

Figure 2.2.1.3-1: Open-loop comparison of RWM sensor subset with RWMSC observer: a) 2 states, b) 7 states, c) without, and d) with the inclusion of the NBI port (7 states).

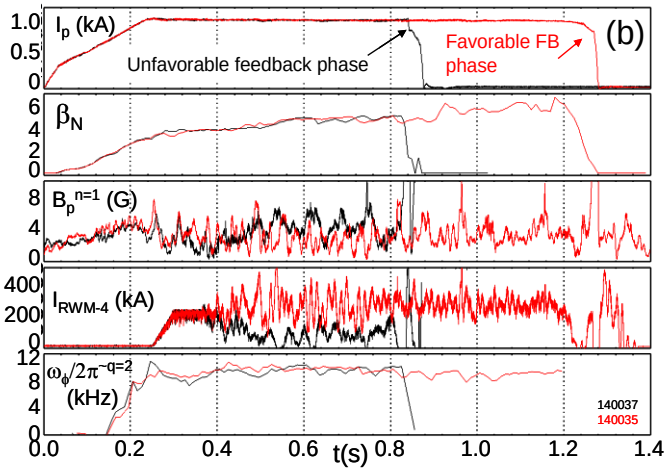

Figure 2.2.1.3-2: Feedback phase variation for RWM state space controller. Favorable feedback phase allowed long pulse plasmas with steady plasma rotation and very high stability parameters $\beta_N > 6.4$, $\beta_N/l_i > 13$.

2.2.1.3.1 Physics model development

The three-dimensional conducting structure (Figure 2.2.1.3.1-1) and plasma response model are defined similarly to detail given in Refs. [10] and [73] and are incorporated in real-time in the RWMSC. NSTX has four rows of 12 copper plates that provide passive stabilization of rotating kink-ballooning modes. Each plate is independently mounted to the stainless steel vacuum vessel with high resistance mounts. The full-order model of this system discretizes magnetic fluxes and currents in the RWM sensors and midplane control coils, and conducting structure along with currents describing the magnetic perturbation of the RWM instability. The geometry of the plasma instability (e.g. see Figures 4 and 6 of Reference [7]) is computed using the DCON code. Magnetic fluxes, Φ, and currents, I, associated with the wall, six control coils, and plasma mode and dissipation (noted by subscripts w, f, p, and d) are determined by equations [24]

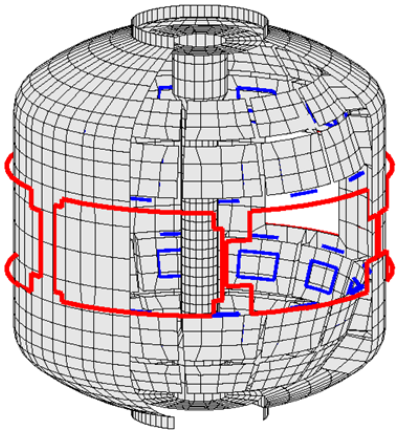

Figure 2.2.1.3.1-1: NSTX 3D conducting structure geometry, including passive stabilizing plates, midplane RWM control coils (red), RWM sensors (blue), and neutral beam (NB) port.

$$\frac{d}{dt}\vec{\Phi}_{w,f,p} + R_{w,f,d}\vec{I}_{w,f,d} = \vec{V}_{w,f,d}$$

with control coil voltage $\vec{V}_f$, and $\vec{V}_w = \vec{V}_d = 0$.

Inductive coupling between elements is defined using computed inductance matrices, L, as

$$\vec{\Phi}_i = L_{iw}\vec{I}_w + L_{if}\vec{I}_f + L_{ip}\vec{I}_d + L_{ip}\vec{I}_p$$

with $i = w,f,p$. The plasma response model alters external field sources through a permeability matrix, P,

$$\vec{\Phi}_p = P(L_{pw}\vec{I}_w + L_{pf}\vec{I}_f + L_{pp}\vec{I}_d) \equiv P\vec{\Phi}_p^{ext}$$

defined for each mode considered as

$$P = -\frac{1}{s^2+\alpha^2}\begin{pmatrix} s & -\alpha \\ \alpha & s \end{pmatrix},$$

where the dimensionless parameters s and α represent the mode instability drive and the differential torque between the plasma and mode [74].

The initial success of the RWMSC on NSTX motivates further expansion of the first implementation and physics model used in the controller. In the initial experiments, the s and α parameters were chosen to represent a mode at marginal stability, but this specification may not

be optimal for control. In NSTX-U, variation of these parameters will be approached in a few ways. The s and α will be varied in experiments, including variation of (s, α) constrained to marginal mode stability, to determine the effect on stability. Also, each of these parameters will be computed theoretically using the MISK code, including the effects of kinetic stabilization, for the high beta target plasma of interest, and compared to experiment. While both s, α are somewhat complex integral quantities of plasma profiles, one can also consider simpler evaluation of these quantities based on plasma parameters (e.g. plasma β_N, and measured mode phase) in real time which would be implemented in the RWMSC in later years of the five year period. Along with plasma stability, the (s, α) strongly affect the plasma response and therefore the total measured perturbed field helicity in the unstable region. This response will be compared directly to the measured mode helicity.

Experimental results to date have only considered a plasma mode that is theoretically predicted to be least stable, and has a single toroidal mode number. The physics model already incorporates the capability of increasing the mode spectrum, which is an important next-step to the controller development and is considered in the next section.

2.2.1.3.2 Active control development, testing, and physics advancements

Although the RWMSC algorithm was written generally for the initial controller, several elements of the control system will be upgraded and expanded, based on both new hardware capabilities and physics advancements. These are briefly summarized below, and addressed individually in the following text. Some of these enhancements will be completed and tested before NSTX-U first plasma, both on offline and real-time implementations:

- independent control of each midplane RWM actuator coil using the new switching power amplifier power supplies
- fully generalize input to allow expanded sensors of any orientation to allow dual component field input
- implement and test n > 1 feedback capability
- implement and test multi-mode spectrum for a given n number

The six midplane coil power supplies, already installed, will be available on Day 0. The plasma control system with the RWMSC will allow full-bandwidth physics applications ranging from open-loop (pre-programmed) error field correction, medium bandwidth ($f << 1/\tau_W$) dynamic error field correction, and high bandwidth ($f \sim 1/\tau_W$) active mode control. The new capability will also allow physics studies of the impact of partial sensor and actuator coil coverage in fulfilling these roles.

In addition to the off-line multi-mode analysis capabilities used on NSTX with the VALEN code (Section 2.4.8), which is directly applicable to NSTX-U, the present model-based RWM state space control system that reached very high values of key stability parameters ($\beta_N > 6.4$, $\beta_N / l_i > 13$) will enable the use of the multi-mode spectrum in real-time global mode control (including 3D mode effects) and 3D detail of the device conducting structure to improve disruption avoidance by improved mode control. Computation of the multi-mode spectrum of NSTX (Section 2.2.1.2.2) has shown that these plasmas exhibit a broader mode spectrum beyond the standard "single-mode" analysis that is typically conducted and that is used in tokamak mode control systems. Operation of NSTX-U plasmas in the high beta operational space accessible by the device will allow testing of the importance of this expanded mode spectrum to further improve active mode control. To support this, the RWMSC will be upgraded to include n > 1 eigenfunctions, and multi-mode capability at constant n number. Use of state space control in a tokamak device was pioneered by NSTX, and these upgrades will take the physics of this control system to unexplored territory. Open-loop testing on existing NSTX data will be possible to test the effectiveness of the added physics before first plasma on NSTX-U.

The addition of the present radial field sensors and the planned magnetic sensor upgrade will also provide additional physics research capabilities for NSTX-U, including the comparison of using radial field sensors alone versus dual-field components in feedback with the RWMSC vessel model included in the calculation. Such testing will be important to determine sensor and actuator needs for future devices, especially where additional shielding of sensors will be needed, such as in ITER.

2.2.1.3.3 Summary of research plans by year

Year 1 (2014):

- Expand RWMSC real-time control software to allow independent actuation of six RWM control coils, and a more general sensor input scheme, for Day 0 plasma operations.
- Implement and perform open-loop tests of n > 1 feedback capability.

Year 2:

- Examine effectiveness of n =1 RWM model-based state space control with independent actuation of six midplane control coils for initial high β_N plasmas in NSTX-U.
- Compare RWMSC modeled sensor signals (controller observer model) with experiment for single mode n = 1 eigenfunction and examine theoretically expected control improvements by adding n = 2 eigenfunctions to the controller.
- Determine optimizations of RWMSC control by varying the amount of plasma rotation-induced stabilization in the controller guided by MISK kinetic stabilization calculations.

- Conduct initial tests on the observer physics model by adding dual-component sensors in RWM feedback, comparing experiment to theory.

Year 3:

- Examine RWMSC multi-mode control with n up to 3 and determine improvements of theory / measurement comparison shown by the controller observer.
- Test optimizations of RWMSC control by varying the amount of plasma rotation-induced stabilization in the controller and compare to MISK kinetic stabilization expectations and experimentally examine effectiveness of the RWMSC as a function of plasma rotation.
- Theoretically determine improvements to the RWMSC by adding the partial NCC (planned for addition to NSTX-U in Year 4) and an extended RWM sensor set (planned for addition to NSTX-U in Year 5).
- Theoretically assess the importance of real-time variation of plasma response parameters in the RWMSC based on experimental studies conducted in Year 2.

Year 4:

- Perform initial investigation RWMSC active control using the newly-installed partial NCC, including variations feedback phase (varied applied control field helicity with respect to mode helicity).
- Determine effectiveness of RWMSC active control during closed-loop feedback of plasma rotation profile, and q_{min} control in plasmas with non-inductive current fraction approaching, or at 100%.
- Examine the effect of varying kinetic RWM stabilization in the RWMSC by varying RWMSC control inputs via multi-phase PCS operation based on real-time β_N calculation

Year 5:

- Test the RWMSC observer physics model by adding a newly-installed expanded RWM sensor set providing improved diagnosis of the mode spectrum in the poloidal direction.
- Examine superior RWMSC settings and multi-mode active control with n up to 3 and the partial NCC to demonstrate improved global MHD mode stability in 100% non-inductive plasmas, demonstrating very low plasma disruptivity in dedicated experiments.

2.2.1.4 Internal kink/ballooning mode control scoping study

The macroscopic mode control research described so far includes activity that yields significant perturbations measurable by external magnetic sensors. However, internal mode activity, which by definition yields small, or immeasurable external magnetic perturbations must also be addressed. Measurement of these modes must be accomplished via non-magnetic means, which

is separately important for mode control systems to be used in future devices with high fusion neutron fluence, such as ITER or FNSF.

Such modes can occur, for example, at the extremes of l_i, or with high pressure peakedness (as can occur, for instance, in a transient H-L back transition). Additionally, coupled m/n=1/1 and 2/1 modes limited many long-pulse scenarios in NSTX. A database of 138 MSE constrained equilibrium reconstructions showed that EPM and ELM triggers cause modes to onset at large values of q_{min}, with rotation shear at q = 2 likely playing a role. There were also "triggerless" modes, that were probably initiated by internal kink or infernal modes as q_{min} approached 1. However, it was also possible to have discharges that have q_{min} just above one for long periods. In NSTX-U, NBCD will be used to understand what the required increment of q_{min} above rational values is to avoid internal/infernal modes.

2.2.1.4.1 Using the RWM state-space observer

An advantage of a model-based controller is that it provides an expectation of how global mode activity will behave in the device as a function of the plasma target. This includes computation of diagnostic measurements in real time. A Kalman filter approach is used to advance the state vector in the presence of noise $\dot{\hat{x}} = (I_r + B_r K_c)^{-1} A\vec{x} + K_o\left(\vec{y}_m - \vec{y}\right)$, where $\vec{y}_m$ is the measured magnetic flux in the RWM sensors, $\vec{y} = C\vec{x} + D\vec{I}_f$, is the controller observer computation of the measurements, I_r is the identity matrix, A and B are the plant and control matrices, and the remaining matrices are the computed controller and observer gain matrices determined by the optimal control algorithm. Subscript "r" is used to denote the reduced order system matrices. It is clear that the second term represents a correction to the plant matrix evolution of the state vector. While typically used to correct the state in active feedback, it can also be used in real time to determine how incorrect the observer is in reproducing the measurements. Therefore, this difference can be used as a criterion of how incorrect the observer is allowed to be in any given sensor, or collection of sensors, and used as input to a disruption warning system. This application can be applied generally, or more specifically as in this instance. In this case, the modeled global mode will have a significant external component, so $\vec{y}_i$ will have significantly larger amplitude than the equivalent sensor measurement.

2.2.1.4.2 Using non-magnetic RWM sensor mode characterization to include sensors in feedback

The multi-energy soft X-ray diagnostic on NSTX was successful in measuring low frequency (less than 500 Hz) mode activity (Figure 2.2.1.4.2-1). Similar, non-magnetic measurement of

global mode activity with multi-energy soft X-rays has been proposed by the Johns-Hopkins group for NSTX-U (see also Section 10.6.1.3). When available, these measurements will be used directly to determine mode amplitude, and in conjunction with the external magnetic sensors to determine the degree to which the mode is internal. Empirical and theoretical criteria can be used to determine and a threshold for these measures, for use as input to the disruption warning system.

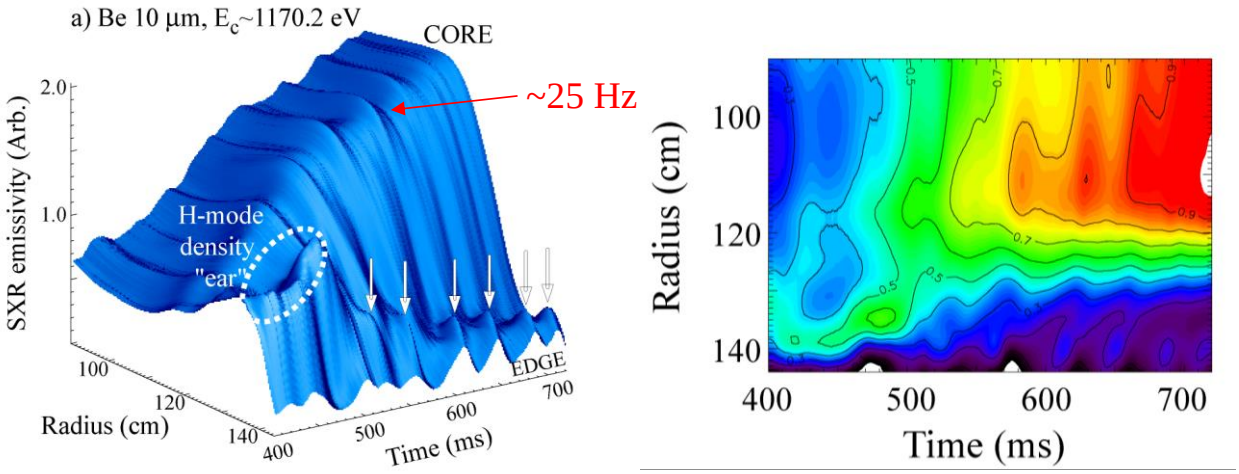

Figure 2.2.1.4.2-1: Low frequency (~ 25Hz) global mode activity measured using multi-energy soft X-ray detectors.

2.2.1.4.3 Summary of research plans by year

Year 2:

- Examine the real-time difference between the n = 1 RWMSC observer and measured RWM poloidal field sensors to evaluate observer physics model and determine thresholds for disruption detection appropriate for use in the NSTX-U disruption warning system.
- Utilize initial NSTX-U ME-SXR and poloidal USXR diagnostics to characterize the RWM eigenfunction by non-magnetic means.

Year 3:

- Examine improvements to disruption detection via the RWMSC based on multi-mode capability of the observer.
- Examine changes to ME-SXR/poloidal USXR measured RWM eigenfunction as a function of plasma rotation.
- Determine the degree of global mode internalization by comparing diagnosis by magnetic and SXR means as a function of proximity to the mode marginal stability point.

- Implement real-time RWMSC observer into disruption warning system.

Year 4:

- Use RWMSC observer in disruption warning system during closed-loop feedback of plasma rotation profile, and q_{min} control in plasmas with non-inductive current fraction approaching, or at 100%.
- Examine time-evolution of global mode internalization using newly-installed, additional toroidally-displaced ME-SXR diagnostic and prepare for real-time input to disruption warning system.

Year 5:

- Determine physics improvements to RWMSC observer for disruption detection and implement to demonstrate reduced disruptivity to internal modes in 100% non-inductive, high β_N plasmas.

2.2.1.5 Use of NCC for mode control and integration of stability control elements

The installation of the NCC will allow studies of NTV physics, and v_φ control with $n \leq 6$. Building off of previous years' research (see Section 2.2.1.1.2), unfavorable rotation profiles can be avoided, and favorable profiles maintained with this capability. Another particularly exciting aspect of this research is the possibility of increasing v_φ via $n > 1$ toroidal propagation with the NCC.

Studies of RWM kinetic stabilization physics can be enhanced by the NCC by exploring such issues as:

1. What are the optimal rotation profiles for RWM kinetic stabilization allowed by adding the NCC field spectra?

2. Can an optimized NCC field spectrum change edge fast ion profiles for RWM stability alteration?

These topics would be explored experimentally and compared to theoretical calculations using the MISK code.

Building upon the experiences of previous years' operation, by the fourth year of NSTX-U operation, a good working understanding of the various feedback and control mechanisms should allow all of them to be used in concert to sustain high performance discharges. Rotation and beta feedback will be used to avoid unfavorable stability conditions while advanced active feedback

systems will be used to control the plasma in the case of excursions from optimal operating regimes. The overall goal is to investigate the combination of v_ϕ-profile, q profile, β-feedback, and active mode control to improve RWM/TM/internal MHD mode stability and to sustain high performance plasmas.

The proposed NCC can be used to demonstrate simultaneous use of actuators sharing multiple control roles. In other words, can the proposed NCC achieve RWM control, ELM control, rotation control, and error field correction simultaneously? Exploring this unique physics coupling in control systems is key for ITER. For example, RWM and NTM stability depend on v_φ, q, n, and T profiles, while v_φ control will depend on NTV (which itself depends on v_φ, q, n, and T profiles). The NCC may improve such control compared to use of the midplane RWM coil alone. A control model must be tested that utilizes the NCC in coupled systems: for v_φ control, β_N control, RWM control (and passive stability), and dynamic error field correction.

The NCC will be extremely useful in the area of RWM active control. Calculations with the VALEN code (Section 2.4.8) indicate that the full option for the NCC coils can provide active RWM control to achieve β_N near the n = 1 ideal wall limit (see Figure 2.2.1.5).

Additionally, the NCC will be used in combination with a model-based RWM state space controller, providing multi-mode RWM control and dynamic error field correction (DEFC). The RWM state-space controller allows far greater flexibility of global mode stabilization physics studies with these coils, with a relatively simple control software upgrade. With the NCC, NSTX-U will be able to demonstrate RWM state space control of ITER-similar coil set.

The NCC can provide quantitative evaluation of the importance of the multi-mode spectrum (n and m) for RWM control and DEFC. The n > 1 mode spectrum has been observed but the importance of control / dynamic correction has never been tested. The performance gained from the added n = 2-3 RWM active control will be evaluated. Also the spectrum will gain helicity, which is important to expand the research.

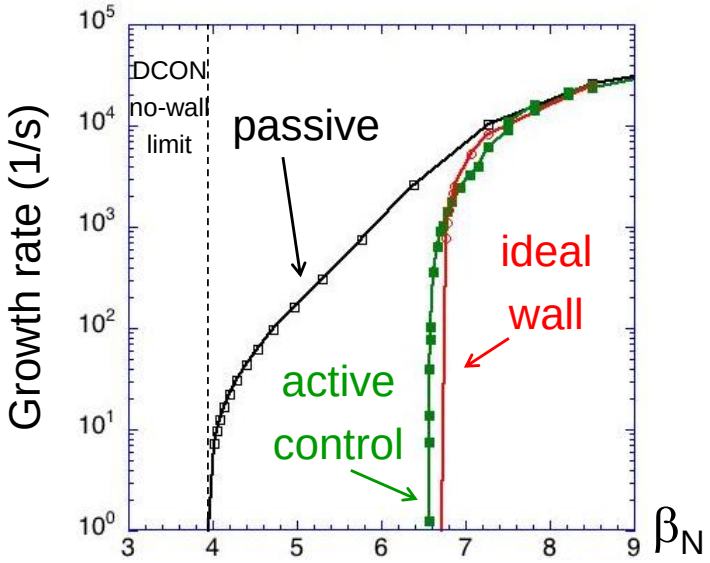

Figure 2.2.1.5: VALEN calculation of RWM active control capability with the full NCC coil set with optimal sensors and optimal gain.

Finally, the NCC will be instrumental in two additional topics of RWM control. First, one can investigate the physics and control of "nonrigid" mode evolution. Second, an important practical topic for ITER is how to prepare to compensate random coil failures in RWM active control. The combination of NSTX-U's RWM state space controller and the flexibility of the NCC allows these issues to be addressed.

2.2.1.5.1 Summary of research plans by year

Year 3:

- Determine improvements to kinetic RWM and NTM stability possible by utilizing expanded capability for non-resonant rotation control by the enhanced 3D field spectrum afforded by the partial NCC, based on theory and the first 2 years of NSTX-U operation.
- Determine improvements to active feedback of n > 0 modes via PID and RWMSC control allowed by the partial NCC, and implement control system changes to test theory in Year 4 device operation.

Year 4:

- Utilize the newly-installed partial NCC to expand plasma rotation profile variation and control, with the goal of improving RWM and NTM stability, with comparison to theory.
- Conduct active n > 0 feedback research using the partial NCC to uniquely address physics for ITER and future STs and tokamaks (e.g. JT-60SA), including (i) mode control with partial toroidal / poloidal coverage of the control coils, (ii) robustness of model based RWM state space control with reduced sensor / control coil availability, (iii) relative importance of midplane vs. off-midplane control coil arrays.
- Determine importance of adding partial NCC capabilities for rotation and mode control in reducing disruptions in high β_N plasmas with non-inductive current fraction approaching, or at 100%.

- Analyze the effect of the partial NCC spectrum on fast ion profiles to determine the effect on RWM stability.

Year 5:

- Utilize the added profile control capabilities allowed by the partial NCC with closed-loop plasma rotation profile control to demonstrate, based on kinetic stabilization theory, reduced disruptivity by actively avoiding global instabilities.
- Employ superior multi-mode physics model settings for n > 0 active control with the partial NCC to demonstrate improved global MHD mode stability in high β_N, 100% non-inductive plasmas scenarios, demonstrating very low plasma disruptivity in dedicated experiments.
- Provide FNSF/Pilot projection on macroscopic stability.

Four years of operation with NSTX-U will culminate in the ability to make projections to next step ST devices, such as FNSF, in the area of macroscopic stability. Specifically, RWM stability as a function of collisionality, rotation, and energetic particle profiles will have been explored and compared to theoretical projections, and experience with advanced active feedback systems operating at the same time as various other control systems (rotation, beta…) will inform schemes for next step devices. Of particular importance to FNSF is whether the integrated controllability is largely changed in fully non-inductive operation.

2.2.2 Thrust MS-2 – Understand 3D field effects and provide physics basis for optimizing stability through equilibrium profile control by 3D fields

2.2.2.1 Error field and tearing mode dynamics

Tokamaks have nested flux surfaces everywhere inside the separatrix and thereby suppress neoclassical transport and provide good confinement. However, flux surfaces can be broken and reconnected to form magnetic islands at the rational surfaces through perturbations unless the plasma is perfectly ideal. Magnetic islands can be more easily formed by external perturbations, can lock to the lab frame by drag due to device error fields, and can also be seeded by internal perturbations and non-linearly grown by changing equilibrium profiles, as called tearing modes.

As mode locking by error fields can be detrimental and lead to a disruption [15,16,17], it is critical to predict the tolerance of the locking of saturated islands and their onset to error fields. This is not a simple task since error fields and plasma responses are intrinsically three dimensional. Recently its understanding has been largely improved, by ideal plasma response calculations, which in fact greatly simplified the view on the interaction between error field and plasmas by finding the dominant field structure [12]. One can call the dominant field affecting the island simply a resonant error field, and the other orthogonal field structure, which can be simply called a non-resonant error field, is predicted to be less influential on the rational surfaces. However, the non-resonant error field can change the island dynamics indirectly through NTV [27,28,29] or possibly directly through non-ideal or non-linear coupling [33]. A number of dedicated experiments will be required to understand the interaction among locking islands, and resonant and non-resonant error fields.

Another important subject is the modification of existing islands, or tearing modes, by error fields. Error fields, or 3D fields in general, can indirectly influence tearing mode dynamics by inducing NTV and thus by altering plasma rotation [13], but also can directly provide the seed island [35,75]. Applied 3D fields can suppress tearing modes by introducing compensating external fields to internal fields arising from the modes. In order to predict tearing mode behaviors under 3D fields, first their own island dynamics without 3D fields must be better understood. The island dynamics can be largely different depending on regimes; whether or not it is linear and more classical [76], or non-linear and neoclassical [77]. The so-called neoclassical tearing mode (NTM) with self-regulating bootstrap currents is itself one of critical issues for the next-step device, as they often limit the achievable β [21,22]. The study of these tearing and neoclassical tearing modes, without and with 3D fields, in NSTX-U, will truly advance the understanding of island dynamics in 3D.

NSTX-U will provide unique environmental elements in this research area, with the low aspect ratio, strong shaping, and high-β. The basic features of resonant and non-resonant error field effects can be well explored with the 6 SPAs, and further comprehensive understanding will be possible when NCC is equipped in later years. The combination of NCC with the 2nd neutral beam will provide various rotation and rotational shear profiles, which are important variables on locking and tearing mode stabilization. The NTM dynamics has never been explored in advanced ST regimes, to which NSTX-U will uniquely contribute. Also, the NSTX-U team can readily use many advanced theoretical and computational tools, such as IPEC and GPEC (Section 2.4.3), MARS-K (Section 2.4.9), and M3D-C[1] (Section 2.4.10), to understand and analyze NSTX-U experiments, and finally to develop predictive capability for locking and tearing modes with 3D fields.

2.2.2.1.1 Error field correction to reduce mode locking

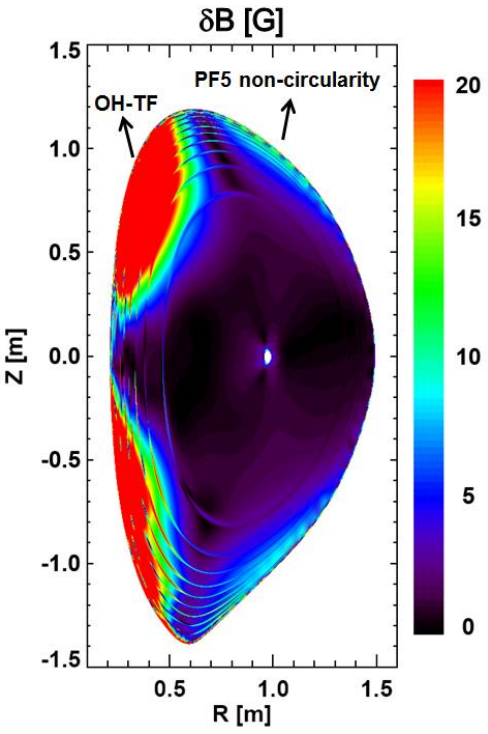

Figure 2.2.2.1.1-1: The perturbed n=1 field strength (calculated by IPEC) due to intrinsic error fields in NSTX.

NSTX-U will be significantly modified in some machine components such as the center-stack and NBI beam ports, and may have different intrinsic error fields. NSTX had two main components of intrinsic errors: (1) n = 1 by OH-TF joint distortion and PF5 non-circularity, as shown in Figure 2.2.2.1.1-1, and also (2) n = 3 by PF5 [23]. The same PF5 coils will be used for NSTX-U and may produce similar error fields, although the coupling to the plasma and the optimal correction against error fields will be different. The OH-TF joint error is not expected to be as substantial as in NSTX, but nevertheless will be investigated since mechanical forces on the center-stack are substantial in ST devices. This investigation will require dedicated effort and time in the first-year NSTX-U operation, since the identification and correction of intrinsic error fields is critical for studies of 3D field physics and for optimal performance.

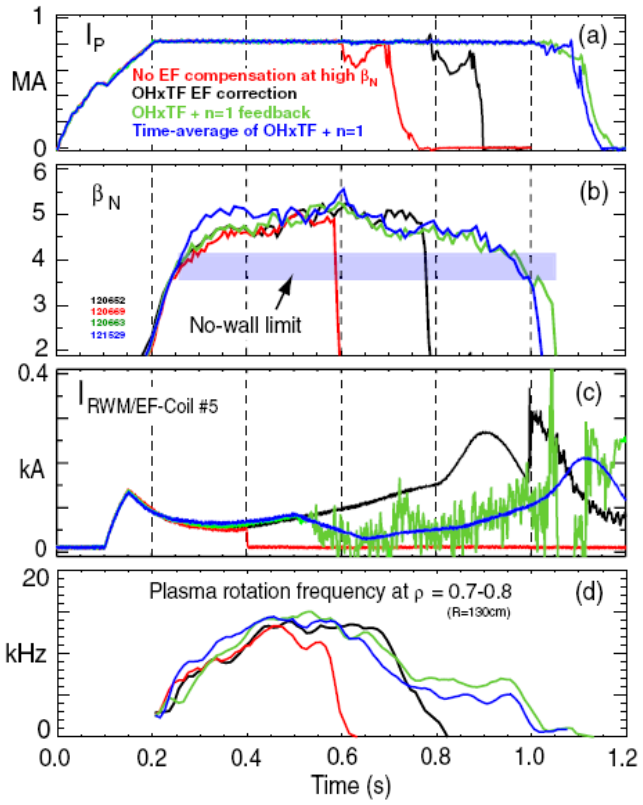

Figure 2.2.2.1.1-2: Various successful error field correction, including the dynamic error field correction in green, which sustained plasma above the no-wall limit and substantial toroidal rotation.

The plan is first to charge the OH, TF, PF coils independently and to measure the vacuum field using magnetic sensors to see the relevance of the previous error field model, such as PF5-triangularity, in NSTX. The model will be revised for NSTX-U as necessary. With updated error field model, IPEC prediction for locking and NTV will be tested with n = 1 ~ 3 compass scan in 4-6 different toroidal phases to optimize static error field correction, which will be important for 3D field physics studies in general. The 6 independent switching power amplifiers (SPAs) will enable n = 2 field rotation for shot to shot, and n = 3 field can also be rotated if the full NCC is installed.

Active mode control and dynamic error field correction are also important especially for high-β since various MHD modes, including the RWM, can arise in typical operation envisioned above ideal no-wall limits. Also the OH-TF error field can be time-dependent and the correction can become more uncertain in high-β due to strong interaction with the plasma. The n = 1 active and dynamic control algorithms were highly successful in NSTX [23] as shown in Figure 2.2.2.1.1-2 and so the plan for the first year is to restore and explore the n = 1 active mode and dynamic error field correction capability in NSTX with the 6 independent SPAs.

The 6 independent SPAs will make any n = 1-3 combination of static and dynamic error field correction possible during operation. Based on the exploratory study for the n = 1 dynamic error field correction in the first year, the optimization of the algorithm will be studied at the interim between experimental campaigns and will be tested in the second year. The optimized n = 1 dynamic correction will be first compared with the pre-programmed static n = 1 error field correction. Next the combination of the dynamic and static correction will be tested with different weighting factors and optimized for the best n = 1 error field correction. The n > 1 dynamic correction will be challenging due to weak plasma response and weak coupling between plasma and magnetic sensors. However, NSTX studies show that n = 2 - 3 RWMs have been

detected [78], and so the possibility for n > 1 dynamic correction will be tested by applying the n = 2 or n = 3 EFC currents to see if the correction algorithm can detect and actuate the proper responses back.

2.2.2.1.2 Study on non-resonant error field effects

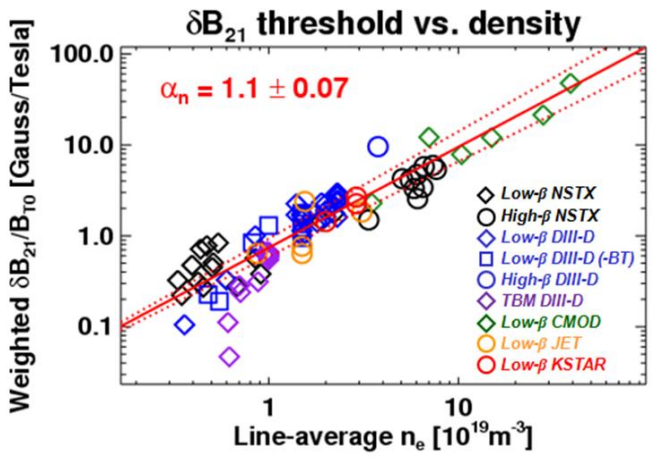

Figure 2.2.2.1.2-1: Error field threshold vs. locking density, constructed using IPEC for five different devices. The coefficient is the power for the density scaling, indicating almost a linear correlation.

Studies of intrinsic error fields have been focused on the resonant component and its compensation to avoid locking. Modeling based on the ideal plasma response has been largely successful across many different devices, including NSTX [12], DIII-D [79], CMOD, JET, and KSTAR, as shown in Figure 2.2.2.1.2-1 The new scaling for error field threshold at locking is still being updated and will be continued with new data and new devices, and will be used to predict the tolerance of error fields in next step devices including ITER.

On the other hand, recent studies with both resonant and non-resonant field applications show that the resonant error field threshold can be significantly altered if the non-resonant error field is substantial. Figure 2.2.2.1.2-2 shows the comparison between the resonant field vs. locking scaling including rotation in NSTX high-β locking experiments [27]. Here the n = 1 resonant field thresholds are significantly lower in the blue cases, due to the additionally applied n = 3 fields that decrease the rotation. The importance of the non-resonant error field correction is clearly demonstrated by recent experiments in DIII-D [28]. In these experiments, the error field was created by external midplane coils (C-coils), and the correction was added with the off-midplane, internal coils (I-coils). The I-coil correction is optimized with conventional compass scans and

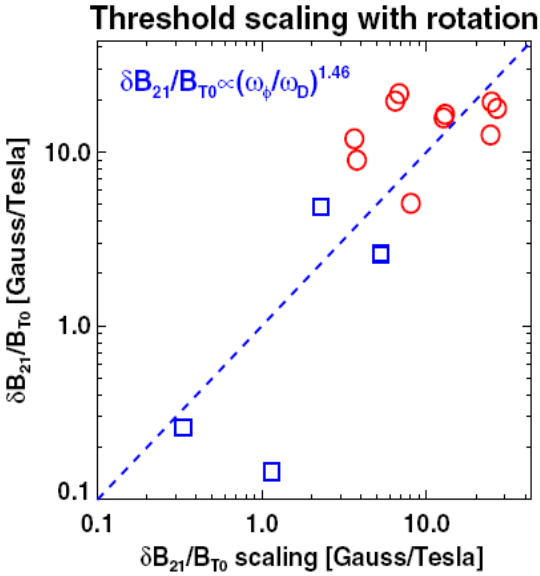

Figure 2.2.2.1.2-2: Comparison between the resonant field (Y) vs. resonant field scaling. Rotation scaling is additionally required for blue points, which included n=3 rotation braking.

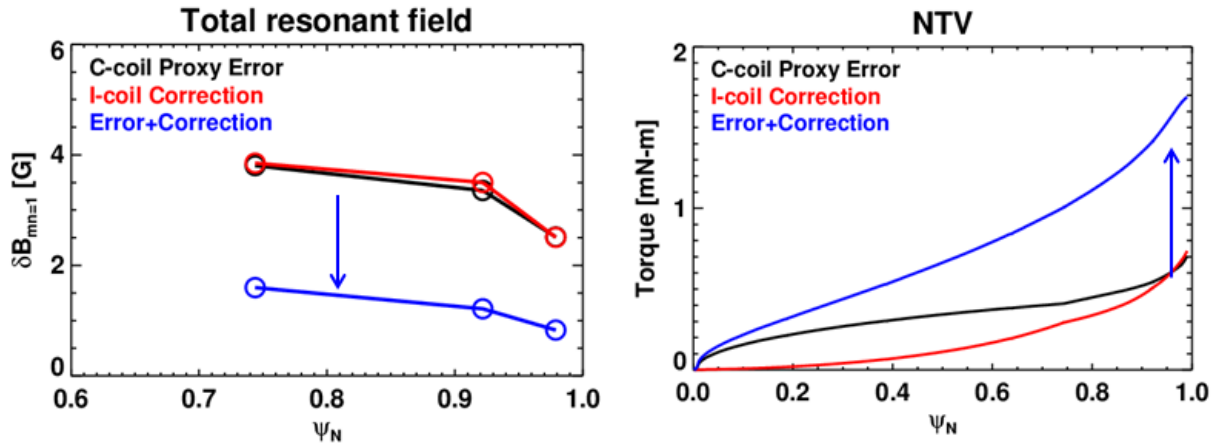

Figure 2.2.2.1.2-3: Total resonant field and NTV in proxy error field experiments in DIII-D. One can see C-coil + I-coil correction reduced the total resonant field, but substantially increased NTV.

this optimization is expected to remove the resonant error field irrespective of the error field sources. However, the optimization for the proxy C-coil error field was not as successful as the intrinsic error field, which may be due to much larger non-resonant components remaining after the correction. Indeed, IPEC and NTV analysis showed that NTV was increased even more than the linear sum of NTV by the C-coil and I-coil fields, while the resonant field was greatly reduced, as shown in Figure 2.2.2.1.2-3. However, although the NTV analysis for the proxy cases shows that the possible resolution may be found in NTV, it is still not clear if the non-resonant component directly influences locking, or indirectly through the NTV rotational damping.

NSTX-U will provide a highly favorable environment to study these non-resonant error field effects, especially when the NCC is installed, but even before then by utilizing the 6 independent midplane RWM coils. In the third year of NSTX-U operation, the study of non-resonant error field effects will be initiated by investigating the n=1 locking threshold by changing n > 1 error fields. The goal is to see if the resonant locking threshold can be modified differently when similar rotation braking is obtained but with different non-resonant fields using n = 2 or n = 3.

The NCC will enable fully systematic investigations of non-resonant and resonant error field effects as a function of plasma rotation. Figure 2.2.2.1.2-4 shows the producible n = 1 resonant field per 1kAt in NSTX-U using different choices of the NCC design; 12U, 2×6-Odd with 6 different phases between upper and lower coils (open red circles) and 2×12 with 12 different phases (filled red circles), compared to the PF5 error field (black) and the midplane field (blue). The resonant fields are the root-mean-square sum of the resonant fields at $\psi_N < 0.85$. The results

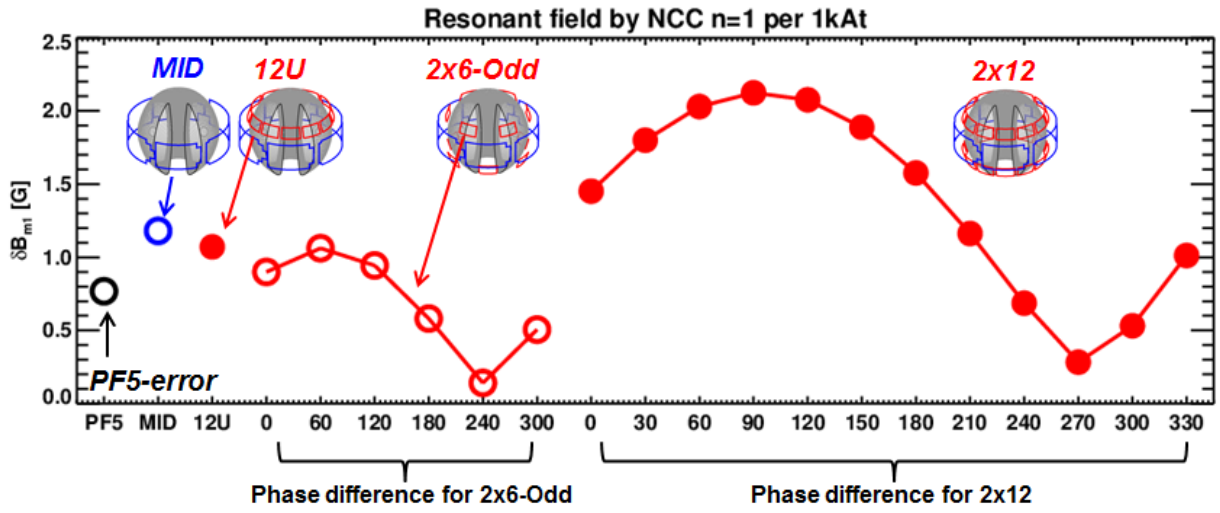

Figure 2.2.2.1.2-4: Resonant fields that can be produced by partial and full NCC coils by 1kAt; 12U, 2x6-Odd with 6 different phases (Open red circles), and 2x12 with 12 different phases (Filled red circles), compared to the present midplane coils (Blue). The resonant field by PF5 coils with 20kA is also shown (Black), which needs to be minimized by error field correction.

show that the proposed NCCs can basically produce a resonant field comparable to the midplane coils, and so they can correct PF5 error fields for example, while at the same time they can provide different poloidal field spectra. This is calculated with the error field figure-of-merit factor (FOM), $F_{N-R} = T_{NTV} \Big/ \sum_{\psi_N<0.85} \delta B_{mn}^2$, which is defined to quantify the ratio of the non-resonant field components to the resonant field components. Neoclassical toroidal viscosity (NTV) torque T_{NTV} was used to represent the physics associated with the non-resonant fields, as well as to give proper weighting on each non-resonant field component. The results are shown in Figure

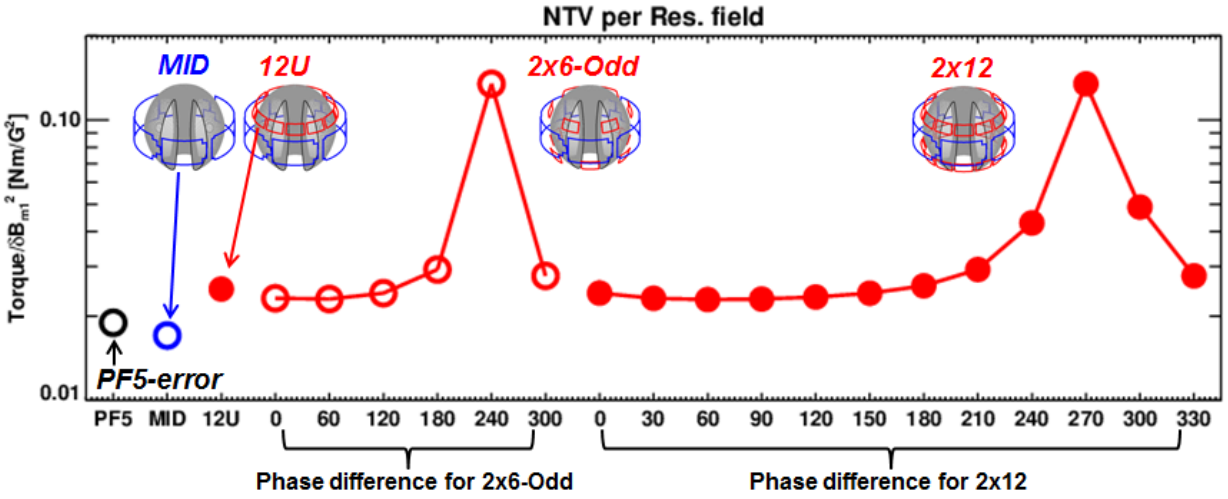

Figure 2.2.2.1.2-5: The NTV per resonant fields for NCCs, which is defined to assess the figure of merit for the error field control. The same labels are used as Figure 2.2.2.1.2-4.

2.2.2.1.2-5, for each NCC configuration. One can see the partial 2x6-odd NCC configuration can give a high FOM as well as variability of the FOM, comparable to the full 2x12 NCC. A high FOM implies that the coils can induce highly non-resonant fields and thus only NTV braking without exciting locking or tearing modes. In contrast, a low FOM means the field is highly resonant, which shows that this particular coil design will allow conclusions regarding the comparison of resonant and non-resonant applied 3D field effects on mode stability and plasma rotation.

Based on the prediction, it will be possible to use the partial NCC configuration to compensate the resonant field produced by the midplane coils, with different ratios of non-resonant vs. resonant field, so that the non-resonant error field effects on locking can be systematically studied. The plasma response, that affects the locking thresholds, will be studied as a function of non-resonant field spectrum and separately as a function of the toroidal rotation. The study will be extended by attempting to produce similar toroidal rotation profiles using different toroidal harmonic perturbations, such as n = 2 or n = 3. This will enable conclusions on whether the non-resonant error field influences the resonant braking directly, or indirectly by toroidal rotation modification.

2.2.2.1.3 Understanding of (neoclassical) tearing mode dynamics in ST

Tearing modes (TMs) and neoclassical tearing modes (NTMs) can be destabilized in the advanced ST regime despite the favorable Glasser [76] and curvature effects [21], by high-β and high bootstrap current fraction in non-inductive operation, and so should be better understood and controlled in NSTX-U. Tearing mode dynamics has some common physics with error field and locking issues, as both are associated with 3D island dynamics. However, different research elements are also required since locking by error fields is external, static, and controllable in ideal and linear regimes, but tearing modes are internal, rotating, and in mostly non-ideal and non-linear regimes. The non-ideal and non-linear nature requires understanding of various second-order physics in the island region including resistivity, viscosity, and two-fluid effects. NSTX-U can provide important regimes with various unique features such as strong shaping and therefore different ion gyro and drift orbits.

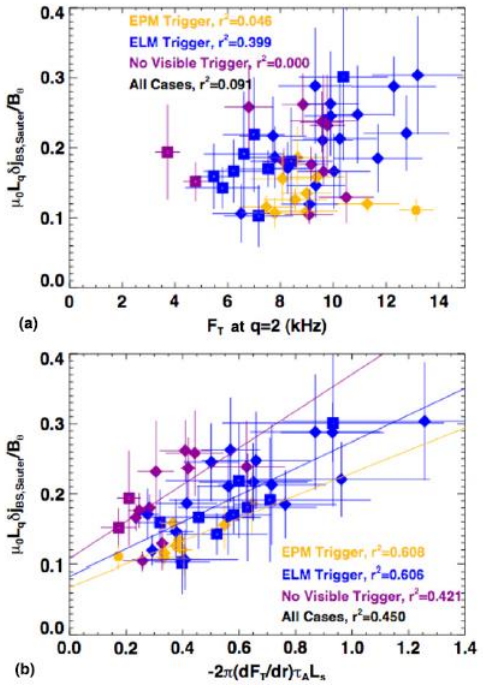

Figure 2.2.2.1.3-1, Onset bootstrap drive at the NTM onset vs. (a) rotation and (b) rotational shear.

The ability of fine rotation control, performed with pre-programmed 3D fields in NSTX, and planned in closed-loop feedback in NSTX-U using NTV, will also be very useful for tearing mode studies. In NSTX, it was shown that rotational shear is a more important variable than the rotation itself in determining NTM onset and stabilizing NTMs [13], as shown in Figure 2.2.2.1.3-1. These correlations between TM/NTM with the rotation profiles will be revised with better separation between the rotation and the rotational shear using the 6 SPAs and three additional NBI sources, and more deeply investigated using NTV braking with NCC in the later years of NSTX-U. The low collisionality and non-inductive operation aimed for NSTX-U can largely modify bootstrap currents, and therefore their effects on NTM stabilization will be extensively studied. Advanced 3D diagnostics such as ME-SXR will also be critical to understand details of island dynamics.

The important dynamics for TM/NTM occur in a narrow island layer, especially at the mode onset, and thus the development of theoretical and numerical understanding of the layer physics is essential to verify and validate TM/NTM physics with available measurements. The development of linear layer calculations with full geometry, such as MARS-K or resistive DCON, will be continued to clearly separate classical effects from neoclassical effects. The layer physics in both codes can be modified to include other non-ideal effects, even non-linearly but coupled to linear treatments for outer-layers. Recent and future theory developments will be used to extend layer calculations [32,33,34]. The fully non-linear codes such as M3D-C1, and particle simulations such as the XGC0 code will also be used to comprehensively understand neoclassical effects, including NTV, on the layer physics. These theoretical and numerical calculations will be tested against experiments, to achieve better predictability and scaling for next-step devices.

2.2.2.1.4 Error field control to stabilize (neoclassical) tearing modes

Tearing modes and neoclassical tearing modes can be modified interactively by both resonant and non-resonant error fields. The non-resonant error field effects are more indirect but better known as the rotation modification by NTV can change TM/NTM stability. Figure 2.2.2.1.4-1 shows the change of the β_N threshold of the NTM onset as a function of rotation, which is varied by non-resonant braking. The trend simply shows the β_N threshold will be decreased if magnetic braking is introduced with non-resonant error fields. However, the interaction can be more complicated if resonant error fields are also applied. Figure 2.2.2.1.4-2 shows the behavior of NTM onset and locking when n = 1 resonant and n = 3 non-resonant

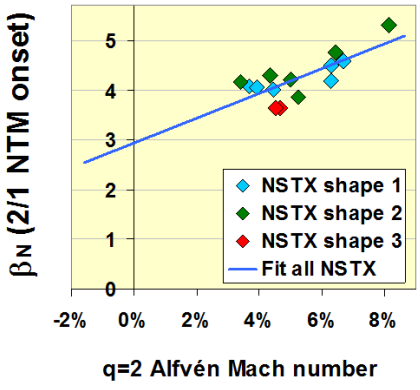

Figure 2.2.2.1.4-1: 2/1 NTM limit as a function of q=2 rotation.

error fields are simultaneously applied. The X-axis is the n = 1 field amplitude, and one can see the rotation (blue vertical lines attached to the data point) is not a strong function of the n = 1 field but the β_N limit (red horizontal lines) is substantially reduced. When the n = 1 field is strong enough, one can see that conventional locking occurred (green data points).

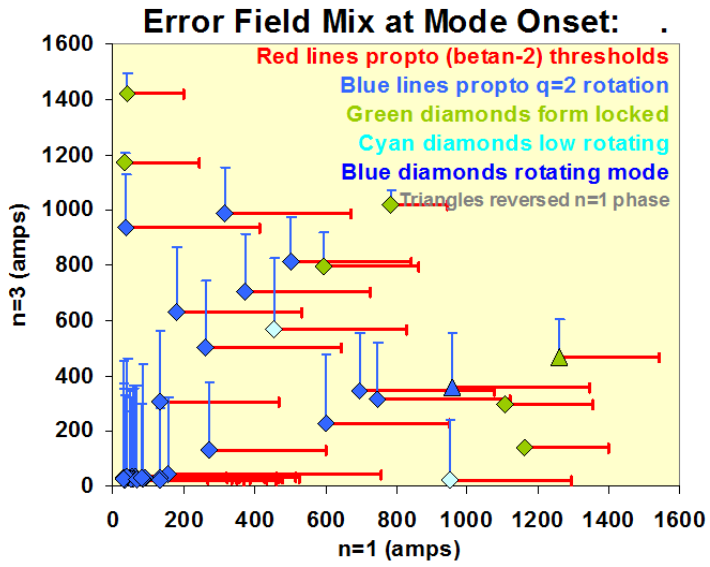

Figure 2.2.2.1.4-2: 2/1 NTM limit as a function of n=1 and n=3 applied fields. Blue points are tearing, green points are locking, blue vertical lines indicate the rotation speed, and red horizontal lines indicate the β_N limit.

There must be a seeding effect by the n = 1 resonant field, and so the research will be continued to improve understanding of the resonant field effect on TM/NTM. This will be started from the third year of NSTX-U operation (Year 4), as the understanding of the intrinsic component of error fields and stable q-profile control is critical for the successful performance of these experiments.

When the partial NCC is available, from the third year of NSTX-U operation (Year 4), the TM/NTM onset by resonant error fields can be fully studied on the two dimensional parametric spaces (β_N,v_ϕ). The rotational shear effect and the direct coupling between non-resonant error fields and tearing modes will be investigated, as the NCC will be able to provide different torque and rotational damping profiles while the same resonant error field is applied. This will allow us to achieve comprehensive understanding of the interaction among locking and tearing islands, and resonant and non-resonant error fields. The detailed dynamics of island onset, suppression, or development, will be attempted using advanced diagnostics such as two toroidally displaced ME-SXR (Section 10.6.1.3), and various real-time measurements planned in NSTX-U.

2.2.2.1.5 Summary of research plans by year

Year 1 (2014):

- Compile resonant error field threshold data from other tokamaks, such as DIII-D, C-MOD, KSTAR, JET, and combine them with NSTX to further support the scaling to ITER.
- Investigate non-resonant error field effects on mode locking based on past NSTX high-beta experiments and DIII-D error field proxy and TBM mock-up experiments.

- Develop numerical codes such as resistive DCON, first to separate linear classical tearing modes from neoclassical tearing modes, and continue to improve layer model.
- Analyze NSTX TM/NTMs in NSTX-U with developed and advanced numerical codes such as resistive DCON, MARS-K, M3D-C1.

Year 2:

- Identify n = 1-3 intrinsic error fields with magnetic sensors, compare to the existing error field model, and update the model as needed.
- Based on the field model and IPEC modeling, optimize the n = 1-3 error field correction using 6 independent SPAs.
- Explore upgraded 3D capabilities of active mode control and dynamic error field correction.
- Investigate the rotation and rotational shear vs. TM/NTM in NSTX-U, compared with NSTX.

Year 3:

- Optimize and combine dynamic error field correction with intrinsic error field correction.
- Initiate the investigation of non-resonant vs. resonant error field effects, by inducing n = 2 and n = 3 fields separately upon the same n = 1 error fields. Vary the rotation profiles using the off-axis NBI with the same 3D field applications, to compare the direct coupling of the non-resonant field components to the resonant fields.
- Investigate the β limit for TM/NTM onsets with varied rotation and rotation-shear.
- Utilize the n = 1 resonant error fields to vary (neoclassical) tearing mode onset.

Year 4:

- Utilize the partial NCC to induce applications of n = 1 non-resonant fields with varied spectra, while the n = 1 resonant field is fixed. Compare the results with the n = 2-3 non-resonant field applications in Year 3 to understand non-resonant and resonant error field effects vs. v_ϕ and the applied field spectra.
- Use the partial NCC and the 2nd NBI beam to study TM/NTM dynamics as a function of (β_N,v_ϕ).
- Investigate the n = 1 non-resonant error field effects on TM/NTM onset and stability, and separate non-linear coupling effects from rotational braking effects.

Year 5:

- Understand error field physics using up-to-date layer theories, and GPEC, M3D-C1, or XGC0 modeling incorporating layer physics across the rational surfaces.
- Understand 3D island dynamics including 3D error fields in tokamaks.

- Develop error field correction predictability for FNSF, ST-Pilot, ITER.
- Develop TM/NTM predictability, including 3D error fields, for FNSF, ST-Pilot, ITER

2.2.2.2 Neoclassical toroidal viscosity at reduced collisionality and applicability to an ST-FNSF and ITER

Neoclassical toroidal viscosity (NTV) [80] is a plasma characteristic resulting from a force created by non-ambipolar particle diffusion. It is an inherently non-axisymmetric (3D) effect, created by intrinsic or applied non-axisymmetric fields, and ideal and resistive MHD instabilities [81,82] which create 3D magnetic field perturbations. The theory of NTV has been developed substantially in the last decade, with extensive work conducted by Shaing, et al., with much work focusing on analytic theory in a variety of collisionality regimes, with smooth connection between these regimes [36-51].

Strong, precise, and controllable neoclassical toroidal viscosity (NTV) effects were observed in NSTX [78,83-85] with direct quantitative comparison to theory of the resultant magnetic torque profile due to applied n = 1 and n = 3 fields, and n = 1 resonant field amplification and resistive wall modes [86]. This extensive study and reliable and reproducible effect has allowed routine open-loop v_φ profile alteration on NSTX. Such rotation control, which is not routinely performed on other devices, places NSTX-U in a position to not only study NTV physics at all levels of plasma rotation, but to also uniquely provide closed-loop plasma rotation control by novel means (e.g. using non-resonant 3D fields to change plasma rotation with feedback) and so allow greater control in studies of the impact of plasma rotation profile on plasma stability. Closed-loop rotation control will be used in the later years of the present NSTX-U five year plan for disruption avoidance and to maintain optimized rotation profiles for plasma stability. This is particularly well-suited for non-resonant NTV rotation control. NSTX has accessed very low plasma velocity (approximately zero over half of the plasma minor radial coordinate, ψ_N) utilizing open-loop plasma control using NTV.

Several aspects of NTV physics are not yet well understood, and this understanding is important for future fusion devices, including an ST-FNSF, and ITER. This physics is summarized in the next several sections, including the potentially important effects of particle resonances, and the nature and scaling of the neoclassical offset velocity – an intrinsic rotation set by NTV. Arguably, the most basic and important dependencies of NTV are on the plasma collisionality and the plasma rotation. For instance, the scaling of NTV in the superbanana plateau (SBP) regime can be very different as NTV is additionally increased when the plasma ExB frequency becomes comparable to the ∇B drift (e.g. when the plasma rotation is sufficiently small). The superbanana plateau regime has been accessed in both NSTX [85] and DIII-D [87]. Similarly,

NTV can be greatly enhanced when the plasma ExB frequency becomes comparable to the bounce motion of trapped particles, called bounce-harmonic (BH) resonances, as predicted by theory [16], shown in simulations [17,18], and may help to explain NSTX [24] and KSTAR [59] results.

NSTX-U provides a significant opportunity to study NTV physics, especially the dependence on collisionality and rotation, for NSTX-U, ST-FNSF and ITER. The dependence of NTV on plasma collisionality is important for NSTX-U, as it is needed to define simple models for the real-time plasma rotation controller. For ITER and FNSF, the strength of NTV needs to be evaluated to understand potential locked mode thresholds for ITER, and the impact of applied 3D fields that will be used for ELM and RWM control. The same applies for an ST-FNSF, except this device is expected to operate at higher plasma rotation. Because of the different expected plasma rotation profiles and speeds, ITER and ST-FNSF are expected to operate with the low torque and rotation, respectively, making the physics understanding in low rotation, e. g. in the superbana plateau regime, of particular importance.

2.2.2.2.1 Comparison of the theoretical dependence on collisionality and rotation to experiment

In the second year of NSTX-U operation, the focus of NTV physics studies will be to understand certain parametric dependencies, especially the dependence on collisionality and rotation. Standard combinations between the n = 3 (or n = 2) applied field, and NBI configurations will be used to test theory with different heating powers and plasma density.

The theoretical dependence of the NTV torque on collisionality and rotation, is given [18] by

$$T_{NTV} \propto \sum_{\ell n m m'} \frac{\nu_{eff}}{(\ell\omega_b - n\omega_{E\times B} - n\omega_B)^2 + \nu_{eff}^2}(\omega - \omega_N)\left[\delta B_m \delta B_{m'} W_{mm'}\right], \quad (1)$$

where ω_b is the bounce frequency, $\omega_{E\times B}$ and ω_B are electric precession and magnetic precession frequency, ν_{eff} is the collisionality, $(\omega - \omega_N)$ is the rotation with neoclassical offset, and the last term contains a quadratic dependence on the variation in the field strength. Depending on the plasma collisionality and the resonances between particle orbits, which are expressed by $\ell\omega_b - n\omega_{E\times B} - n\omega_B$, the NTV torque can vary significantly in theory. Particularly important is how the NTV torque will vary as the collisionality is reduced to levels accessible in NSTX-U. A transition to the superbanana (SBP) regime occurs if the collisionality is sufficiently low and the rotation, or similarly electric precession, is low enough to give $\omega_{E\times B} - \omega_B \approx 0$. Also, in plasmas

with sufficiently fast rotation up to $\ell\omega_b - n\omega_{E\times B} \approx 0$, theory predicts that the NTV can be significantly enhanced by bounce-harmonic (BH) resonances.

The operational regime of NSTX bridging to the lower collisionality of NSTX-U, an ST-FNSF, and ITER takes NTV from Shaing's analysis regimes named the "1/ν" to the "ν – sqrt(ν)" regimes [36,43]. The superbanana plateau regime exists for all three devices at lower collisionality, with $\nu^*_i < 1$. These three regimes have three distinct dependences on plasma collisionality, summarized as follows for ions: the torque due to NTV, $\tau_{NTVi} \propto n_i^{K1} T_i^{K2}$, where K1 = 0, K2 = 5/2 for the "1/ν" regime, K1 = 3/2, K2 = 1/4 for the "ν – sqrt(ν)" regime, and K1 = 1, K2 = 0 for the superbanana plateau regime. Simplified, these scalings show a strong increase in the strength of τ_{NTVi} as the plasma becomes collisionless (here defined as collisionality falls below $\nu_i^* < 1$), then saturates at lower ν. The extended theory states that at sufficiently low ν, τ_{NTVi} will begin to decrease with decreasing ν. Of particular note is that when the superbanana plateau criterion is met, the τ_{NTVi} dependence on ν changes significantly, and increases in magnitude, even though the plasma rotation may be small. This characteristic was found for the SBP regime in NSTX (shown in Figure 2.2.2.2.1-1).

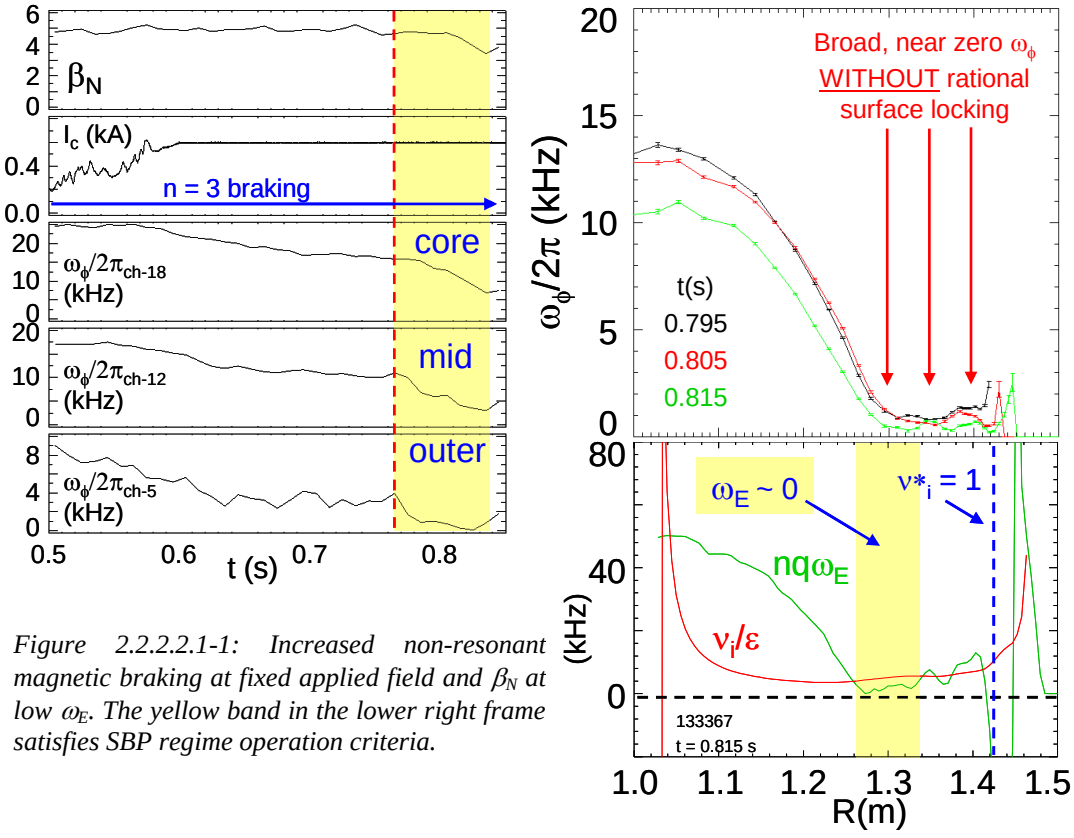

Figure 2.2.2.2.1-1: Increased non-resonant magnetic braking at fixed applied field and β_N at low ω_E. The yellow band in the lower right frame satisfies SBP regime operation criteria.

The dependencies of the NTV torque given by Equation 1 for NSTX plasma parameters, varied over substantial ranges of the plasma collisionality and rotation, are illustrated in Figure 2.2.2.2.1-2.

These theoretical calculations show that NTV torque increases in general when the collisionality decreases, but this fundamental 1/ν behavior becomes more apparent through the rotational resonances. This prediction is qualitatively equivalent to the n = 1 kinetic RWM prediction shown in Figure 2.1.1.3-1, as the kinetic dissipation is the origin of NTV transport in essence [88]. The trend for applied n = 3 magnetic braking is different than the trend for n = 1, as one can see the clear separation between the theoretically computed rotational resonances only for n = 1. This is due to narrower gaps by 1/n between the SBP and BH resonances at higher n. This also implies very different selectivity of the n = 1 and n = 3 NTV torque. With n = 3, the rotation can be decreased until passing the SBP regime at low rotation if the n = 3 field is continuously applied, as found in NSTX [85] (Figure 2.2.2.2.1-1). The calculations also indicate that the 1/ν dependency can be weakened when the collsionality decreases by an order of magnitude.

A simplified expression derivable from Equation 1 for the force on each flux surface due to NTV in the collisionless "1/ν" regime is

$$\left\langle \hat{e}_t \bullet \vec{\nabla} \bullet \overleftrightarrow{\Pi} \right\rangle_{(1/\nu)} = B_t R \left\langle \frac{1}{B_t} \right\rangle \left\langle \frac{1}{R^2} \right\rangle \frac{\lambda_{1i} p_i}{\pi^{3/2} \nu_i} \varepsilon^{3/2} (\omega_\varphi - \omega_N) I_\lambda \quad . \tag{2}$$

This expression scales as $T_i^{(5/2)}$, which is consistent with braking of plasmas with varied T_i in NSTX [89], as well as the plasma inverse aspect ratio, ε, and depends on the neoclassical offset velocity, ω_N. I_λ depends on the spectrum of the 3D field, and other quantities (See Reference [86] for the full definition of other variables). The first key study is the dependence on plasma

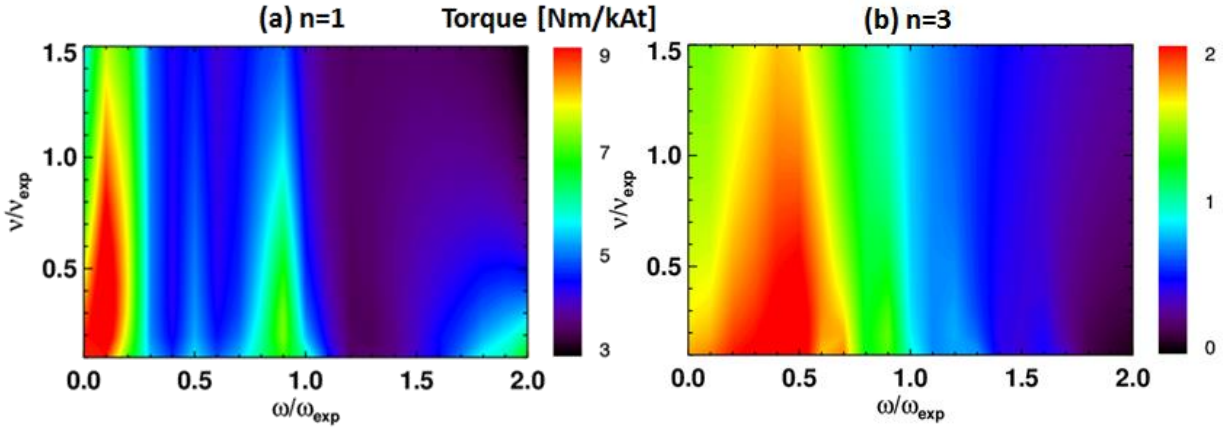

Figure 2.2.2.2.1-2: Analytic NTV calculations for (a) n=1 and (b) n=3 magnetic braking in NSTX, as a function of plasma collisionality and rotation.

collisionality. The collisionality in NSTX-U may be decreased by up to an order of magnitude compared to NSTX. Since the strength of the NTV torque in NSTX was sufficiently large to bring the plasma rotation to near zero on a 100 ms timescale non-resonantly with an applied n = 3 field from the midplane coils, there will clearly be sufficient non-resonant braking in NSTX-U in this regime to quickly access the low rotation regime. The very strong inverse theoretical scaling of τ_{NTVi} with ν will allow a clear test to the present theory, even if collisionality is reduced by a more modest factor of 2 or 3.

Additional elements of NTV theory in connection to plasma collisionality will be explored in the model discussed above. First, the SBP regime at reduced plasma rotation will be able to be accessed similarly as it was in NSTX. The more complex dependencies associated with the various resonances shown in Equation 1 will be examined at the reduced collisionality of NSTX-U. As this regime theoretically has no dependence on T_i, the scaling can be tested experimentally and distinguished from the "1/ν" regime formulation. Second, the theoretically expected saturation of τ_{NTVi} at sufficiently low ν can be examined at the lowest attainable collisionality accessible in NSTX. The lowest plasma collisionality will be accessed once the upward-pointing lithium evaporator system and cryopump are installed.

2.2.2.2.2 Experimental investigation of important theoretical NTV characteristics

Experimental investigations of NTV to date, such as the studies performed on NSTX [83-86], MAST [90], DIII-D [91], and JET [92] have shown general agreement with different aspects of NTV theory, however, the elements have been varied, and are not always consistent among devices. For example, while the neoclassical offset rotation, ω_{NC}, has been observed as significant and consistent with NTV dominated by the ion channel in DIII-D, experiments, results on NSTX show ω_{NC} to be close to zero. In fact, before the NSTX publication of quantitative experimental agreement of the NTV torque profile with theory [86], prior published work at best found qualitative agreement between experiment and theory, and predominantly stated that rotation damping by NTV theory was too weak to explain experiments quantitatively.

The enhanced capabilities of NSTX-U will allow a significantly expanded study of NTV to best leverage and test NTV theory, with the research aiming to unify results across devices. Our collaboration to study NTV on the KSTAR superconducting tokamak will also support this research. As mentioned above, an extensive test of the dependence of NTV on collisionality will be carried out on NSTX-U. Long-pulse aspects, including the evaluation of ω_{NC} will be greatly enhanced by the factor 5 – 10 increase in pulse length of NSTX-U, with analogous comparison with KSTAR long-pulse plasmas. KSTAR also offers the largest aspect ratio difference to NSTX-U, to evaluate the theoretical dependence of NTV on aspect ratio (see equation 2). At

lower collisionality, the effects of the electrons in NTV can be increased, as expected for ITER [93], and this will be examined at the lowest collisionality in NSTX-U. The q-profile is not directly linked to NTV physics, but it can alter the non-axisymmetric variation in the field strength through the plasma response and can result in a strongly modified NTV torque profile. The q-profile will be varied primarily by different combinations of neutral beam current drive (NBCD). Since NBCD will also affect the rotation profile, the rotation and q-profile effects on NTV will be studied together.

The enhanced capability of varying the applied 3D field spectrum utilizing independent control of the midplane RWM coils will allow further testing of the NTV dependence on 3D field configuration on Day 0 of operation. This capability will be significantly enhanced when the partial NCC is installed and operated in Year 4. These additional off-midplane coils will allow applied field spectra that attempt to match or oppose the main plasma field helicity, which will help determine the effects of plasma response and resonant vs. non-resonant damping effects. Further analysis of the expected alteration of NTV by the NCC is given in Section 2.2.2.2.5. All of these aspects will be important for future devices including ITER.

2.2.2.2.3 Comparison of NTV theories and computations

NTV theory continues to be developed and ranges from models formulated in certain asymptotic limits with connection formulae bridging these limits (e.g. the Shaing model), to the solution of the bounce-averaged drift kinetic equation with various collision operators, to particle code simulations. Our present computational toolset spans this range of numerical approaches and includes the NTVTOK code [93], NTV modules included with the IPEC code, and the POCA and FORTEC-3D codes, all of which are described briefly in Section 2.3.

This full range of code capability and analytic models is important for NTV studies in NSTX-U, since the research requires models of varying depth and complexity. For instance, particle simulations (POCA) allow fewer assumptions in the modeling, while analytic

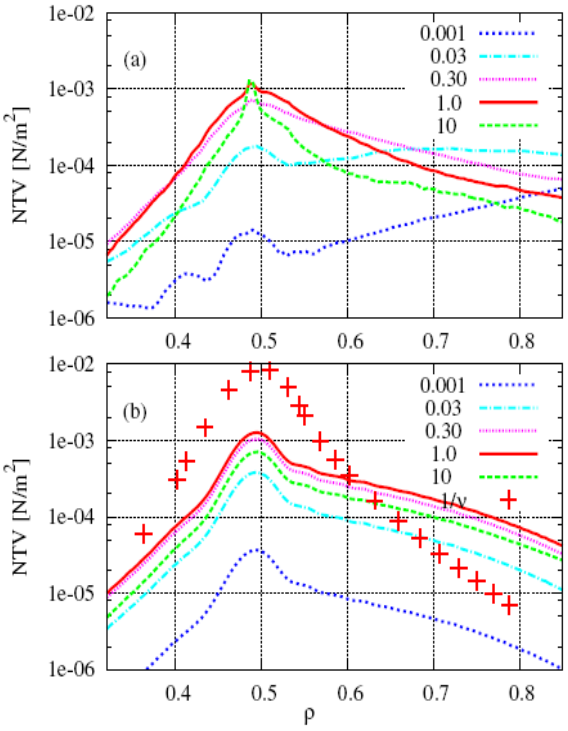

Figure 2.2.2.2.3-1: Comparison between FORTEC-3D (Upper) and analytic NTV (Lower) for different collisionality. One can see good agreements in general, but also a substantial discrepancy in the lowest collisionality.

solutions to the drift kinetic equation allow easier understanding of key scalings for ST-FNSF and ITER. Corrections to analytic models that bridge different operational conditions (e.g. collisionality) can be evaluated by solution of the drift kinetic equation in the various regimes. Factors of 2 to 3 difference between these two types of solutions have been found in the transition regions between the regimes evaluated [93]. Finally, highly simplified models that can be computed in real-time will be needed for use in the plasma rotation control system. These models will be improved as the NSTX-U NTV research develops and updated/tested throughout the five year research period.

In the third year of NSTX-U operation, the study of the NTV dependence on the collisionality will be extended by achieving the lowest density and collisionality regime, which will be directly relevant to future ST applications. The prediction of the analytic theory is a large increase of NTV through the rotational resonances. However, simulations using the global code FORTEC-3D (Section 2.4.12) shows that the analytic NTV may be underestimating the effects of non-resonant field components, as illustrated in Figure 2.2.2.2.3-1. Therefore, NTV validation in the lowest collisionality regimes will be especially important to resolve the different predictions between the numerical and analytic computations.

2.2.2.2.4 Development and testing of models appropriate for closed-loop rotation control

Open-loop rotation control has been routinely conducted on NSTX using non-resonant NTV to alter the rotation profile. This technique has allowed much finer control of the plasma rotation levels than using individual NBI sources, since small changes to the applied 3D field can be made by making small changes to the midplane coil currents. Closed-loop rotation control on NSTX-U will be unique in the world ST and tokamak program, as it will use a combination of NBI source control and NTV via applied 3D field spectra as actuators.

Non-resonant NTV magnetic braking profiles have been experimentally produced for n = 2 and n = 3 applied field configurations in NSTX [84], and results using the n = 1 and n = 3 fields have been quantitatively compared to theory [86]. These results will be used to generate the real-time NTV profile for n = 1, 2, and 3 field “configurations”. Here, the quotes indicate that these configurations are not purely n = 1, 2, and 3, but have higher-n components due to the full 3D configuration of the coils, which are used in the NTV calculations.

Open-loop control of the plasma rotation will be available from the start of NSTX-U operation, utilizing independent control of the 6 midplane coils for the first time. NSTX-U will have greater flexibility to change the toroidal torque than in past NSTX operation, since the 6 independent SPAs will allow the application and switching of n = 1-3 fields simultaneously, and also the 2nd

off-axis NBI system will produce various profiles of injection torques. The experimental quantification of injection torques will be important prior to the NTV study. The total input torques including the intrinsic part and momentum exchanges such as diffusion and convection will be balanced with induced NTV transport, creating the rotational equilibrium.

Closed-loop control, which is expected to start in Year 4, will additionally require a real-time model of the NTV torque profile as a function of applied 3D field current, spectrum, and plasma parameters appropriate to NTV. Real-time 3D coil currents and NTV profiles for closed-loop control for the main n = 2 and 3 non-resonant field configurations will already be available on Day 0. Additional plasma information important to NTV (e.g. plasma rotation speed at several radial positions, real-time evaluation of plasma temperature and density) will be added to the model as they become available in real-time. A real-time toroidal velocity (RTV) measurement system that has been successfully installed in NSTX (and is described in detail in Section 10.6.3.2) will be utilized for rotation feedback control. The neutral beams and 3D fields with the 6 independent SPAs will be used as actuators, to control the input torque and rotation in closed-loop feedback. In this beginning step, the goal is to explore the roughly accessible level of rotation at the center of the plasma and in the pedestal region using NBI. Within the accessible levels of the rotation, the rotation feedback system with RTV and NBIs will be tested to improve RWM/TM stability by altering both rotation and its shear. The ability to control rotation shear will improve during the five years of planned research as additional real-time rotation channels become available.

2.2.2.2.5 NTV theoretical analysis for the NCC physics design

The partial or full NCC coils, available by the third year of NSTX-U operation (Year 4) will provide a more powerful 3D-field actuator for rotation control. This includes the possibility of increasing v_φ via n > 1 toroidal propagation. Figure 2.2.2.2.5-1 shows the integrated NTV torque profiles for the partial and full coil set options, compared to the existing midplane coil. Here $F_{N-N} = T_{NTV}(\psi_N < 0.5) \big/ T_{NTV}(\psi_N < 1)$ is used and a figure-of-merit for NTV is defined as ΔF_{N-N}. The variability can be increased by an order of magnitude with the partial NCCs, ΔF_{N-N}=10~20, and by another order of magnitude with the full NCC, ΔF_{N-N}~200. This means that the NCCs can exert larger torque on the core rather than the edge by 1~2 orders of magnitudes, and thus possibly will produce much stronger rotational shear as well.

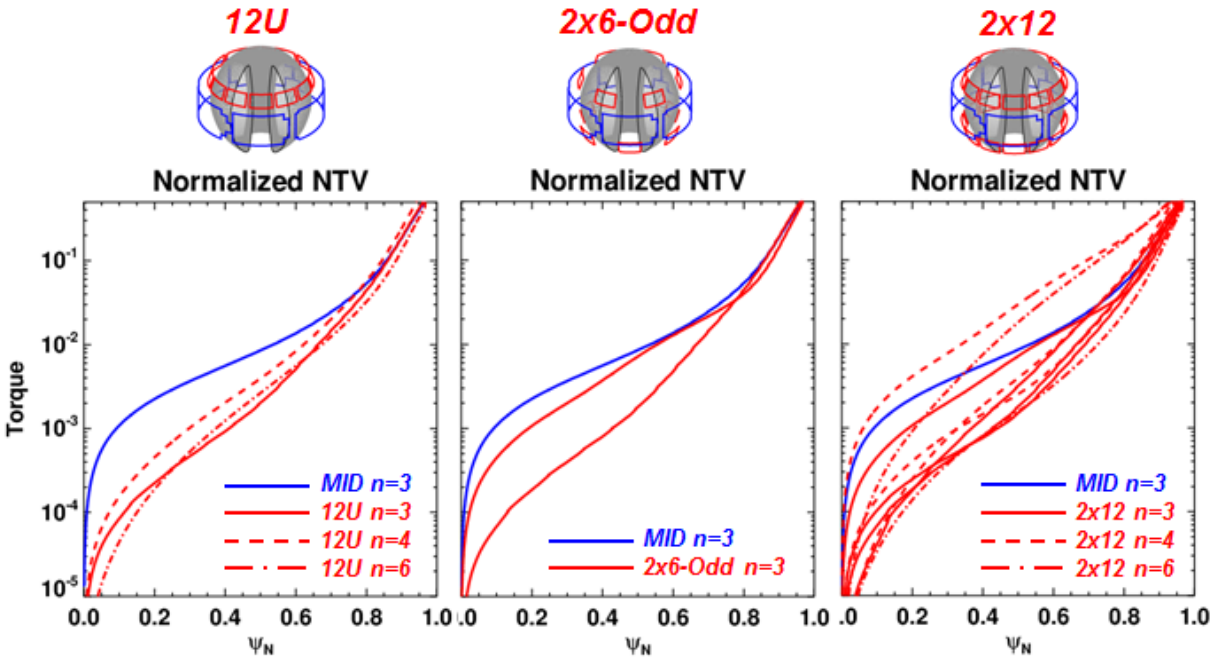

Figure 2.2.2.2.5-1. The torque profiles integrated from the core, for the partial 12U, 2x6-Odd NCC, and for the full 2x12 NCC. One can see that the torque values can be changed in the core by an order of magnitude with the partial NCCs, and by another order of magnitude with the full NCC using high n perturbations.

The variability of the NTV torque profiles will be even greater when the NCC and midplane coils are combined. Examples are shown in Figure 2.2.2.2.5-2, where n = 1 and n = 3 are combined using NCC or midplane coils. The left shows the integrated torque profiles, and the figure on the right shows the damping rates. One easily can see 3~4 orders of magnitude can be produced and can expect that NCC will give indeed unprecedented flexibility of the NTV braking and rotation controllability if truly optimized. Note the examples with the partial NCC, 2x6-Odd configuration, illustrate the powerful n = 1 capability when three rows of coils are used, allowing greater control of the poloidal mode spectra at the outboard side.

The NCC will also allow the expanded investigation of varying rotation in the same q-profile and β, by fully utilizing both NBIs and 3D fields. In particular, the q-profiles and β values favorable to RWM, TM, and internal MHD mode stability will be selected and maintained while the rotation is changed. Next the variation of the q-profiles or β values will be varied while the rotation is held fixed to optimize tradeoffs to improve MHD stability. Rotation (and shear) profile control will be attempted using real-time plasma rotation measurements and improved understanding of the intrinsic torque and NTV braking. This is indeed a research area and capability that will be used by many different topical science groups in NSTX-U, as an optimal rotation profile will be determined to stabilize instabilities from microscopic scale to macroscopic scale and the rotation profile will be controlled using the rotation control system with 3D fields and NBI. Producing and understanding the physics behind optimal and robustly stable rotation profiles will be strongly enabled by the large flexibility of 3D field spectra produced by the NCC. It will enable improved understanding and predictability of the NTV

braking physics and the rotation control capability for the next-step devices such as FNSF, ST-Pilot, and ITER.

Another important issue is whether or not NCC can provide better particle control and also ELM control. As described earlier in Section 2.1.4.1, the 3D field effects on ELMs are not yet fully understood, although various experimental demonstrations have been achieved in different devices. One of the well-known empirical criteria for ELM suppression is the vacuum Chirikov overlap condition for resonant magnetic perturbation (RMP) [19], which partially represents the

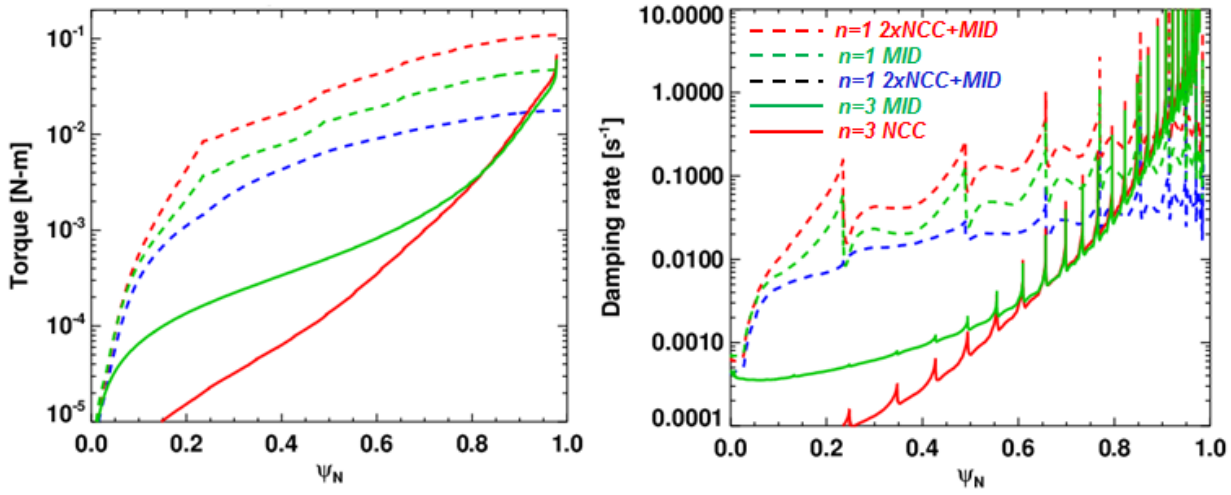

Figure 2.2.2.2.5-2. The torque profiles integrated from the core (on the left) and damping profiles (on the right) when n=1 and n=3 perturbations are used by combining partial NCC (2x6-Odd) and midplane coils. 2xNCC means that the NCC coil currents are twice larger than currents in the midplane coils.

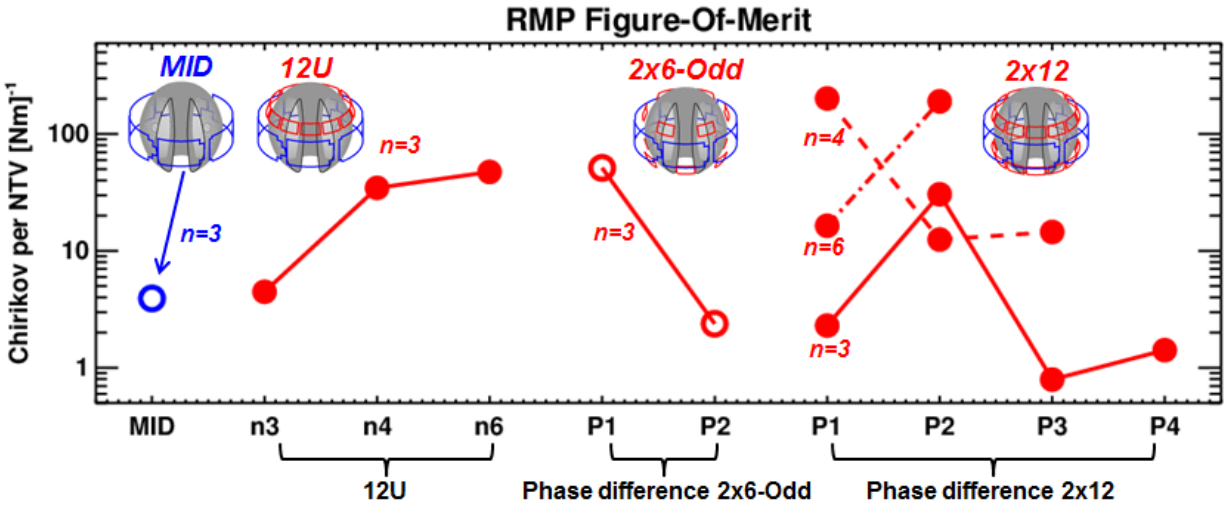

Figure 2.2.2.2.5-3. Comparison for figure-of-merit parameters for ELM control, among existing midplane coils, the two partial NCC options, and the full NCC. (NOTE this figure will be updated consistently with new FOMs.

resonant coupling between 3D fields and rational surfaces in the edge. Another condition is the pitch-alignment condition, and this represents the minimized non-resonant field components other than the edge-resonant components. However, the pitch-alignment condition is qualitative, and a more quantitative condition is needed for actual assessment. The figure-of-merit for RMP ELM control here is defined as $F_{N-C} = (C_{vacuum}, \psi_{N=0.85})^4 / T_{NTV}$, where the numerator is the vacuum Chirikov overlap parameter (with fourth-power to make the FOM independent of field strength), and the denominator represents the non-resonant field components, similarly to the pitch-alignment condition, but quantitatively by NTV strength. The subject of ELM control using 3D fields will be discussed more extensively in Chapter 4, but this FOM assessment related to NTV is shown here in Figure 2.2.2.2.5-3. One can see that this FOM can be increased by an order of magnitude with the partial NCC, and even another order of magnitude when the high n = 4 or 6 is utilized with the full NCC. Although no single criterion, including this FOM parameter, has been found to explain RMP ELM control, this analysis indicates that the NCC will enable significantly expanded testing of RMP ELM control over wide ranges of field spectra to improve the physics understanding of ELM mitigation physics.

2.2.2.2.6 Summary of research plans by year

Year 1 (2014):

- Complete analysis of existing NSTX data from specific experiments investigating NTV. This existing data includes an investigation of NTV vs. plasma collisionality over the range attainable in NSTX, past operation in the superbanana plateau regime, magnetic braking by dominant n = 2 and n = 3 field configurations, and the dependence on plasma rotation speed.
- Update all NTV experimental analysis tools to allow processing suitable for NSTX-U capabilities (e.g. independent control of the midplane coils).
- Continue the design of the NCC with respect to the resonant and non-resonant physics of rotation control.

Year 2:

- Make initial assessment of the dependence of NTV profile and strength as a function of plasma collisionality, and examine the NTV offset rotation utilizing HHFW heated plasmas.
- Prepare an initial simplified real-time model of NTV profile as a function of applied field and available plasma parameters for use in initial tests of the plasma rotation control system (this development carries forward to future years as new real-time diagnostics become available and NTV models improve.)

- Begin verification of the newly developed codes POCA and FORTEC-3D using initial NSTX-U experimental data.
- Investigate NTV effects by intrinsic error fields and find optimal corrections to minimize unexpected rotation braking if needed. Interact with the T&T Topical Science group to best identify intrinsic torque in NSTX-U.
- Investigate NTV physics vs. v_ϕ and q-profile with new NBIs and independent actuator coils.

Year 3:

- Evaluate the neoclassical offset rotation as a function of plasma parameters in long-pulse, steady-state plasmas.
- Determine the experimental dependence of the superbanana plateau NTV on plasma collisionality and compare to theory.
- Utilize real-time model of NTV profile as a function of applied field configuration, strength, and plasma rotation in the plasma rotation control system and evaluate model performance in closed-loop feedback.
- Combine low n perturbations with n = 2, 3 braking and investigate the variability of the rotation and rotation shear profiles using various NBI sources.

Year 4:

- Experimentally determine the dependence of NTV profile and strength as a function of plasma collisionality at the highest ion temperatures, and evaluate the role of electron NTV in this condition.
- Utilize closed-loop rotation control, including initial use of the partial NCC, to produce the broadest and most peaked rotation profiles possible, and high, intermediate, and low rotation levels, comparing offline and real-time rotation models to theory.
- Make initial use of the partial NCC to test theoretical expectations of applied 3D fields as their helicity is varied compared to the equilibrium plasma field helicity.
- Investigate the extended controllability of the rotation using the NCCs. The predicted variability by various phasing between rows will be tested and compared.
- Utilize the NCCs to assess and optimize tradeoffs between v_ϕ, q-profile, β to improve RWM/TM/internal MHD mode stability.

Year 5:

- Examine NTV at the lowest plasma collisionality possible in the device to determine if a saturation of NTV at low collisionality can be found, as expected by theory.
- Demonstrate low rotation profile operation in steady-state with closed-loop rotation control, producing plasma rotation most applicable to ITER and utilizing the partial NCC, with comparison to theory.

- Experimentally determine optimal 3D field spectra, including use of the partial NCC, for minimizing or maximizing NTV vs. applied current and compare to theory.
- Fully utilize and develop the rotation control system to maintain optimized v_ϕ and its profiles for sustained microscopic and macroscopic mode stability.

2.2.3 Thrust MS-3 – Understand disruption dynamics and develop techniques for disruption prediction, avoidance, and mitigation in high-performance ST plasmas

The subsections of this thrust are divided into four main areas for disruption research: prediction, avoidance, mitigation, and characterization.

2.2.3.1 Stability physics for disruption prediction

Next-step STs and steady-state advanced tokamaks both aim to operate continuously at high normalized beta, $\beta_N \equiv 10^8 <\beta_t> aB_0/I_p$, ($\beta_t \equiv 2\mu_0 <p>/B_0^2$) and high non-inductive current fraction. A high bootstrap current fraction yields a broad current profile, corresponding to low plasma internal inductance, l_i. This is favorable for efficient non-inductive operation, but is generally unfavorable for global MHD mode stability, reducing the ideal n = 1 no-wall beta limit, $\beta_N^{\text{no-wall}}$. Past high β_N operation with l_i typically in the range $0.6 < l_i < 0.8$ has an n = 1 $\beta_N^{\text{no-wall}}$ computed by the DCON code (Section 2.4.2) to be 4.2 – 4.4 [7]. Operation at $\beta_N > 7$ and $\beta_N/l_i > 13.5$ has now been demonstrated transiently, with pulse-averaged β_N (averaged over constant plasma current), $<\beta_N>_{\text{pulse}} > 5.5$ in low l_i plasmas in the range $0.4 < l_i < 0.6$ with active n =1 mode control (Figure 2.2.3.1-1). Pulse-averaged values of (l_i, β_N) now intercept the higher l_i portion of the planned operational ranges for ST-CTF and ST Pilot plants. Especially important is that the ideal n = 1 no-wall stability limit is significantly reduced at these low l_i values, so that β_N now exceeds the DCON computed $\beta_N^{\text{no-wall}}$ for equilibrium reconstructions of these plasmas by up to a factor of two. In addition, synthetic variations of the pressure profile for plasmas with $l_i \sim 0.38$ show these equilibria to be at the purely current-driven ideal kink stability limit, as they are computed to be ideal unstable at all values of $\beta_N > 0$. In this operational regime, passive or active kink and resistive wall mode (RWM) stabilization is therefore critical. The disruption probability due to unstable RWMs was reduced from 48% in initial low l_i experiments to 14% with this control, but remarkably, the reduced disruption probability was observed mostly in plasmas at high $\beta_N/l_i > 11$. Disruptions occurred more frequently at intermediate values of β_N/l_i. This agrees with active MHD spectroscopy diagnosis, used to determine the proximity to marginal stability [65] (Figure 2.2.3.1-2). The resonant field amplification (RFA) of an applied 40 Hz co-NBI rotating n =1 seed field shows an increase in RFA to a broad peak near $\beta_N/l_i = 10$. This decrease in RWM stability, shown by the increase in RFA, is expected as β_N increases, and has been as reported for DIII-D [94] and NSTX [7] at lower β_N values. In contrast, and remarkably, RFA is found to decrease at higher values of β_N/l_i in NSTX, indicating increased mode stability (Figure 2.2.3.1-2). This positive result is presently not thought to be a second stability region for the

RWM, but is more likely related to proximity to broad resonances in plasma rotation providing kinetic stabilization of the RWM [8,9]. The result of decreased disruptivity at higher β_N/l_i is also consistent with analysis of the wider NSTX database spanning 2006 – 2010 [95]: no clear increase is found in disruptivity at increased β_N and $l_i < 0.8$.

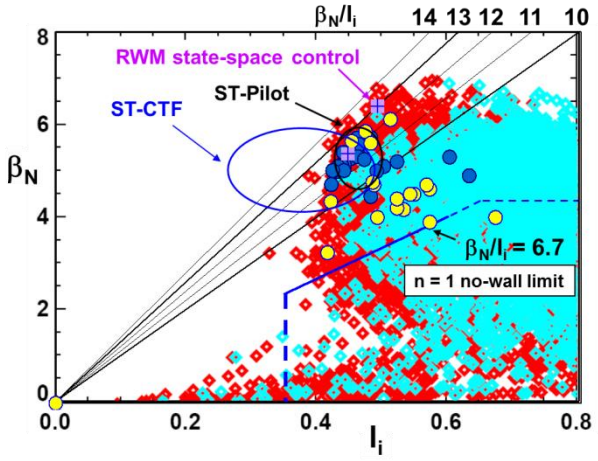

Figure 2.2.3.1-1: High β_N, low l_i operational space. Red/cyan points indicate plasmas with/without n = 1 active RWM control. Blue circles indicate stable long pulse plasmas with active RWM control; yellow indicates disruptions.

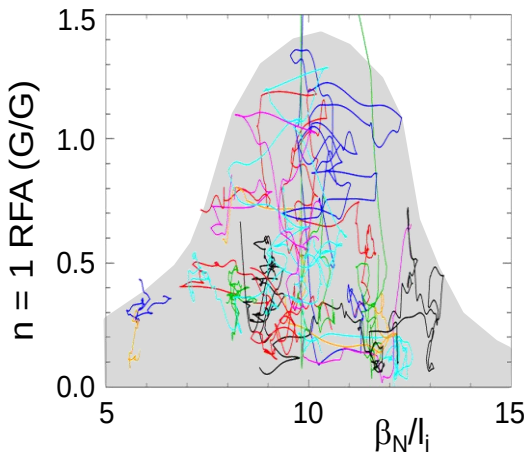

Figure 2.2.3.1-2: n = 1 resonant field amplification during high β discharges using active MHD spectroscopy, indicating improved stability at high β_N/l_i.

2.2.3.1.1 Establish and test approach to marginal stability based on kinetic stabilization for disruption prediction

NSTX research established that global mode stabilization physics is more complex than having a small level of plasma rotation present to ensure stability. Quantitative comparisons of kinetic stabilization theory to experiment [8,9] have shown that unstable bands of rotation can exist at relative high rotation. These bands are defined by the plasma crossing an unstable boundary, rather than a lack of torque balance as can occur for modes (such as tearing modes) that exhibit resonant braking torques. Sections 2.2.1.1.3 and 2.2.1.1.4 discuss and illustrate the physics analysis that motivates a real-time model to predict the proximity to marginal instability. This information can be used in a staged manner to (i) attempt to alter key profiles such as plasma rotation, or NBI heating to move away from a marginal boundary, and (ii) issue a plasma shutdown command if the marginal boundary is very close, or reached.

Simple models will be supplied to the NSTX-U disruption warning system, which will continue to be developed as real-time diagnostics implantation allows. For example, the simple criterion

$|\omega_E - \omega_D| < K$, where K is a constant (see Section 2.2.1.1.4) can be implemented once real-time rotation measurements are available, making very simple approximations for ω_D – even using a fixed ω_D profile based on routine high beta H-mode operation will be enough to start the real-time study. As additional information becomes available (e.g. real-time Thomson scattering, real-time estimates for T_i profile from CHERS), the parameters in the physics model will be known to greater certainty.

2.2.3.1.2 Testing low frequency MHD spectroscopy for active disruption prediction

Low frequency MHD spectroscopy has been used in NSTX and DIII-D to determine global mode stability in stable plasmas, and will be further developed as an important tool for disruption prediction and avoidance in NSTX-U. The striking results of increased stability at increased β_N/l_i shown in Section 2.2.3.1 (Figure 2.2.3.1-2) and dependence of RFA amplitude on collisionality shown in Section 2.2.1.1.3 show how the RFA amplitude correlates well with the complex stability space in NSTX, and is a good detector for the proximity to marginal stability. The present offline analysis is being converted to allow real-time application for disruption prediction.

While the physics of low frequency MHD spectroscopy using single mode RFA amplitude is well known, this technique leaves out at least two important physics aspects that require further research to improve the single mode analysis. First, the single-mode RFA phase carried important information for NSTX plasmas. For example, the transition of the single mode RFA phase from being stationary to rotating in the rest frame of the applied field is a key early warning indicator that the amplification of the applied field is transitioning into a mode. This event is due to the NTV drag of the plasma on the amplified applied field and happens while the plasma is still stable. This event in itself could be used to predict disruption. However, if the mode spins up to sufficiently high rotation frequency, it is strongly damped. Intermediate rotation frequencies are most dangerous and indicate disruption. Second, the multi-mode spectrum of NSTX (Section 2.2.1.2.2) shows that a multi-mode RFA analysis should be used at sufficient β_N. The new capabilities of NSTX-U will allow the application of applied field with different n numbers, and the additional information provided by the upgraded sensors with positions closer to the divertor may provide further mode discrimination.

2.2.3.1.3 Use of RWM state-space controller observer for disruption prediction

The specific use of the RWM state-space controller observer for detecting internal modes was discussed in Section 2.2.1.4.1. This is actually a specific use of the observer, where the correction term $K_o\left(\vec{y}_m - \vec{y}\right)$ becomes large due to $\vec{y}_m$ becoming small. However, this concept can be used more generally, in that sufficiently large $|K_o\left(\vec{y}_m - \vec{y}\right)|$ can be used to predict

disruptions. This difference is already computed in real-time in the RWMSC. It is also important to realize that this difference depends upon how well the physics model reproduces the measurements. If the physics model reproduced the mode dynamics with 100% accuracy at each step, then the observer and measurements would be equal, and the difference would be zero. Therefore, the planned improvement of the physics model in the RWMSC will affect this disruption indicator. The research will begin before the start of NSTX-U by assessing how large this difference becomes before the onset of disruptions in the present NSTX database.

2.2.3.1.4 Summary of research plans by year

Year 1 (2014):

- Evaluate simple physics criteria (suitable for real-time use) for the approach to global mode marginal stability based on ideal (e.g. pressure peaking, β_N/l_i) and kinetic stability physics using initial high performance NSTX-U plasmas, emphasizing rotation profile and speed.
- Initially compare the degree of mismatch between the initial RWMSC observer model and sensor measurements and the occurrence of plasma disruptions from the existing NSTX database to evaluate future use in the disruption warning system.

Year 2:

- Construct an initial MHD spectroscopy database for high performance NSTX-U plasmas to determine the measured variation of global mode stability as a function of key parameters including plasma rotation, energetic particle profile and distribution, q_{min}, and β_N. Determine if results are consistent with past NSTX experimental results.
- Improve simple physics criteria used to determine global mode marginal stability adding energetic particle stabilization and expanding the kinetic stabilization model.
- Determine the applicability of single mode RFA phase information in low frequency MHD spectroscopy measurements to supplement amplification in determining proximity to global mode stability boundaries.
- Improve disruption prediction using the RWMSC observer model and sensor measurements by improving the model and/or sensor mismatch criteria used.

Year 3:

- Determine and implement a real-time evaluation of a simple global mode marginal stability model including important parameters (e.g. plasma rotation speed and profile, q_{min}, T_e, n_e) that will be available in real-time during Years 4-5.
- Determine single mode RFA amplitude and phase criteria that predict disruptions, and evaluate possible improvements afforded by multi-mode RFA.

Year 4:

- Add and use real-time rotation and q_{min} measurements and evaluations for determining global mode marginal stability boundaries, enabling improved evaluation of physics model.
- Examine real-time low frequency MHD spectroscopy in determining global mode stability boundaries for input to stability profile control systems (e.g. rotation, q).

Year 5:

- Add and use real-time Thomson scattering data to improve the simple kinetic stabilization physics criterion used for determining global mode marginal stability boundaries.
- Improve disruption prediction using the RWMSC observer by the addition of the newly-installed expanded RWM sensor set.

2.2.3.2 Stability control for disruption avoidance

Once the physics elements of the disruption prediction are established as discussed in Section 2.2.3.1, the actuators and algorithms to avoid disruption must be defined and implemented. This task will be a joint effort between the Macroscopic Stability and the Advanced Scenarios and Control topical science groups. The elements described here focus on the task elements of the Macroscopic Stability group.

Note that in all examples below, a flag that predicts an approach to an instability boundary can be made to trigger a plasma shutdown, or triggering of the disruption mitigation system, using the NSTX-U disruption warning system. These results are taken as a last resort, based on the most critical disruption prediction flags. The plasma disruption mitigation system is described in Section 2.2.3.3 and plasma shutdown techniques are described in Section 9.2.3.2.

2.2.3.2.1 Rotation and heating control to test kinetic RWM marginal stability, and to maintain r/t stability

Kinetic stabilization of global modes presently has the greatest physics content and understanding in the underlying models. Therefore, the theory guides the relevant actuators. In this case, actuators that affect both the ideal and kinetic stability contributions to δW are relevant, which covers the majority of the real-time actuators planned for the next five year period. For example, once real-time MSE becomes available, it can be matched to the operation of specific NBI sources to change q. The pressure peaking factor is also another basic parameter that affects ideal stability. TRANSP runs provide guidance on NBI deposition, but only NSTX-U operation will determine how the three new NBI sources will specifically alter the pressure

peaking in NSTX-U. Generally, they should broaden the profile, which would provide a more stable profile to global modes. The impact on ELM stability based on these changes will also need to be determined to find optimal profiles in the broadest sense.

The key actuators affecting the kinetic stability will be the rotation control system, and choice of NBI sources. The former itself will use both the NTV from applied non-axisymmetric fields, and the NBI source input to control the plasma rotation with active feedback. Therefore, one input to the real-time rotation control system will be a series of target rotation profiles generated by the kinetic stabilization physics model in real-time. The simple models developed for real-time use (Section 2.2.3.1.1) will output these target profiles. As shown in Section 2.2.1.1.3, these favorable profiles will depend on plasma parameters such as collisionality, and so real-time evaluation of temperature and density will be used in the algorithm as they become available. Since β_N itself has been found to not be a useful indicator of mode stability (higher β_N was *more* stabilizing in NSTX – see Section 2.2.3.1), NBI actuation is planned to be based more on momentum input, energetic particle profile, and pressure peaking alteration than overall input power. However the ability to limit β_N in real-time through total NBI power will be an option in NSTX-U. As shown in this example, some actuators will become overloaded (i.e. asked to perform conflicting action simultaneously). Prioritizing the actuation based on the physics study or stabilization goal in question will be an important aspect of the research.

2.2.3.2.2 Real-time MHD spectroscopy for active disruption avoidance

Real-time low frequency MHD spectroscopy (i.e. RFA amplitude magnitude and phase dynamics) can be used in the simplest ways (e.g. limit β_N) for disruption avoidance. However, this technique has far greater potential for disruption avoidance when used in conjunction with other physics models that predict mode stability in real time. This is state-of-the-art research that will be pioneered in NSTX-U. The plan is to couple the RFA output to the kinetic stabilization (Section 2.2.3.1.2) and RWMSC observer (Section 2.2.3.1.3) models. As each of these models evaluates new criteria for improved stabilization, the real-time low-frequency MHD spectroscopy system can determine whether or not these models are indeed improving stability. This information can be used not only to alter the output of the physics models, but also to catalog a very large database of how successful the physics models are in guiding the control system toward greater stability. This latter aspect will allow a greatly accelerated understanding of what changes in the control lead to improvements in stability well before marginal stability points are approached.

The number of possible variations using this approach is large, so theory will guide the research plan, and experiment will determine how well the approaches actually work. Theory will then be improved if needed until successful approaches are found. One concrete example is the alteration

of the rotation profile. Kinetic stabilization theory will produce real-time rotation profile targets, and the low frequency MHD spectroscopy system will determine in real-time if the change made is superior, or inferior (the change may be inferior simply because the model is approximate and incomplete). Changes to the target rotation profile can then be made solely on the change that is measured from MHD spectroscopy *without* updating the target profile as indicated by kinetic stabilization model. Variations of applied non-resonant 3D fields, NBI momentum input, q profile, and density are four examples of actuators that could be directly guided by real-time MHD spectroscopy.

2.2.3.2.3 RWM state-space controller observer development for RWM avoidance

The RWMSC observer can also guide variations to actuators in a similar fashion to low frequency MHD spectroscopy. For instance, of a set of target rotation profiles from the kinetic stabilization model lead to an increasing difference in $|K_o(\vec{y}_m - \vec{y})|$, perturbations around these profiles can be considered by altering them and observing if $|K_o(\vec{y}_m - \vec{y})|$ decreases. This approach can be used for as long as desired before using a new target rotation profile based on the kinetic stabilization model. Additionally, monitoring the RWMSC observer during disruption avoidance will quickly generate a large database showing how well the difference $|K_o(\vec{y}_m - \vec{y})|$ correlates with favorable stability changes as measured by low frequency MHD spectroscopy. This data can be used to guide improvements to the observer physics model.

2.2.3.2.4 Rotation control to run at ITER-relevant low rotation

Non-resonant NTV braking of the plasma rotation profile has been used in NSTX to produce very low levels of plasma rotation, creating target plasma that are more applicable to rotation conditions expected for ITER. The plasma rotation profile and level alters plasma stability, and so alters demands on the active mode control system, and changes the stability and stability gradients. NSTX-U will provide unique capabilities to study this operational regime for ITER, as it will have an extensive set of actuators and real-time disruption prediction and avoidance tools to study the low rotation plasma state in a tokamak device.

2.2.3.2.5 Coupling of stability and control to ITER and ST-FNSF scenarios

The kinetic stabilization physics model has been used to compute the stability of ITER advanced scenarios, and has drawn important conclusions. Most importantly, present models show that ITER plasmas that are just a few percent over the ideal marginal stability point will be unstable unless a significant alpha particle population is present [66]. As shown in NSTX, even with large plasma rotation, global instability can cause disruptions in ST plasmas. Therefore it is critical that the stability and disruption prediction and avoidance research be conducted in NSTX-U

scenarios that best emulate ST-FNSF operation. Significant development of these stability tools along with the production of the ST-FNSF scenarios are expected synergistically join in the later years of the 5 year period to directly test the physics and control tools in these scenarios, along with scenarios at low rotation to best support ITER.

2.2.3.2.6 Summary of research plans by year

Year 2:

- Perform initial experiments using open-loop plasma rotation, current profile, and energetic particle control to demonstrate the ability to avoid encountering disruptive global mode stability boundaries based on kinetic RWM stabilization models.
- Test stability physics expectations of increased global mode stability at the highest β_N/l_i in NSTX-U plasmas, and compare to positive results found in NSTX, examining potential differences due to aspect ratio.
- Determine physics implications of scenarios that over-constrain 3D field and NBI actuators for simultaneous use in meeting open-loop requests for plasma profile targets for rotation, q, energetic particle population, β_N, and other key parameters in the goal of disruption avoidance.
- Implement and test initial disruption avoidance using the RWMSC observer model in real-time, including open-loop disruption avoidance criteria in low rotation plasmas (most ITER relevant).

Year 3:

- Implement results from a real-time evaluation of the simple global mode marginal stability model into plasma rotation and q profile control systems that will be available in real-time during Years 4-5.
- Implement single mode RFA amplitude and phase as input to profile control systems and disruption warning system.
- Combine physics criteria for disruption avoidance systems (profile control and disruption warning systems) allowing variable prioritization of control to avoid physics request conflicts and to avoid actuator overloading.

Year 4:

- Evaluate and study the stability physics response of real-time rotation and *q* profile control using the simple kinetic stabilization physics criteria and real-time low frequency MHD spectroscopy for avoiding global mode marginal stability boundaries, including initial use of the partial NCC as an actuator for rotation control.

- Test coupling of real-time RFA, simple physics model, and RWMSC observer systems in providing simultaneous actuation of stability profile for avoiding global mode stability boundaries.
- Apply combined disruption avoidance control to high β_N plasmas with non-inductive current fraction approaching, or at 100%.

Year 5:

- Combine disruption avoidance control with simultaneous use of n > 0 active feedback and the partial NCC, determining physics implications of this combination and potential control conflicts.
- Demonstrate improved global MHD mode stability and very low plasma disruptivity in dedicated experiments using ITER-relevant (low rotation), high rotation inductive scenarios, and 100% non-inductive ST-FNSF scenarios.
- Determine the physics and controllability implications of using/omitting upgrades to the combined control systems, including the partial NCC, expanded RWM sensor set, real-time Thomson scattering, and real-time ME-SXR data.

2.2.3.3 Rapid shutdown techniques via mass injection for disruption avoidance

When disruption prediction and avoidance techniques fail, a fast discharge termination method is needed to minimize the deleterious effects of the disruption, particularly the large heat loading from the thermal quench and the generation of large populations of runaway electrons. Massive Gas Injection (MGI) is one approach to addressing this difficult issue for ITER. Research in NSTX-U will compare MGI from different poloidal locations to assess the gas penetration efficiency from each of these locations. NSTX-U researchers have begun modeling gas penetration using the DEGAS-2 code (Section 2.4.11) to quantify the gas penetration past the SOL for NSTX-U. For disruptions in ITER that have short warning times of less than 10ms, the MGI system may not perform satisfactorily. For these extreme cases, for which the ITER disruption mitigation system (DMS) must be designed, more rapid impurity injection systems, such as the Electromagnetic Particle Injector (EPI) planned for NSTX-U might be used.

Note that realtime disruption detection methods are described in Sections 2.2.3.1 and 9.2.3.1. Those methods will be used to trigger these mitigation technologies in NSTX-U to test real-time disruption mitigation.

An important goal of these studies is to assess reductions to the divertor heat loads during an unmitigated vs. mitigated disruption and the radiated power profile during the thermal quench phase. Many of the diagnostics that will be used for these and other measurements (soft X-ray

and VUV measurements, bolometer arrays, Thomson scattering, visible cameras, interferometer, divertor diagnostics including halo current sensors, multi-color IR cameras and divertor thermocouples) are described in Chapter 10 Also, specifically, the instrumented tile diagnostics required for disruption mitigation studies in NSTX-U will be described in Section 2.2.3.4.2. Finally, a description of a dedicated fast diode based XUV radiometer to diagnose impurity dynamics during the disruption mitigation experiments is included in Section 10.6.3.6.

2.2.3.3.1 Massive gas injection experimental development

At present, massive gas injection (MGI) appears to be the most promising method for safely terminating most discharges in ITER [96-100]. MGI involves the rapid injection of large quantities of gas into the tokamak discharge; the quantity of gas is typically several times the inventory of the plasma discharge. Usually some fraction of the injected gas has a high-Z component such as argon or neon. Requirements for the mitigation of disruption effects fall into three categories: (1) Reducing thermal loads on the first wall and the divertor; (2) reducing electromagnetic forces associated with "halo" currents, i.e. currents flowing on open field lines in the plasma scrape-off layer; and (3) suppressing runaway electron (RE) conversion during the current quench phase of the disruption. To accomplish these in ITER, it is projected that about 500 kPa-m^3 of helium with some noble gas fraction will be required.

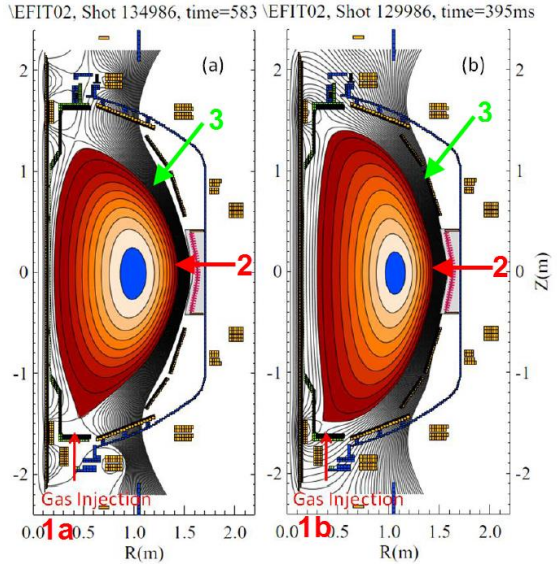

Figure 2.2.3.3.1-1: Shown are the planned Massive Gas Injection locations on NSTX-U. (1a) Private flux region, (2) mid-plane injection, (1b) high field lower SOL region and (3) outer SOL above the mid-plane.

The present understanding of disruption mitigation using massive gas jets is based on work conducted on DIII-D, Alcator C-MOD, ASDEX-U, JET, Tore Supra and other large tokamaks, and is summarized in References [96-100]. Recent experimental results have shown that the cold front from the edge, which has been cooled by an MGI pulse, needs to reach the q = 2 surface for the onset of rapid core cooling to occur. On ITER, it is not known if a simple MGI pulse from multiple locations would be adequate because of its larger minor radius, the increased transit times for the neutral gas, and the larger expected scrape-off-layer (SOL) flows. Insight into ways for reducing the total amount of injected gas and optimizing the injection locations would provide critical help to the design of a suitable system for ITER.

NSTX-U can offer new insight by injecting gas into the private flux and lower x-point regions of divertor discharges to determine if this is a more desirable location for massive gas injection. Injection from this new location has two advantages. First, gas injected directly into the private flux region does not need to penetrate the scrape-off-layer. Second, because the injection location is nearer the high-field side in standard D-shaped cross-sections, the injected gas should be more rapidly transported to the interior as known from high-field side pellet injection [101] and from high-field side gas injection work on NSTX [102]. By comparing massive gas injection from this new location to injection of a similar amount of gas from the outer mid-plane, NSTX-U can improve the knowledge of disruption mitigation physics and thus improve the disruption mitigation system (DMS) design for ITER (provided the NSTX-U results are obtained early in the 5 year plan).

To put the gas penetration issue in perspective, the private flux region in ITER is predicted to have an electron temperature of less than 2eV and an electron density below $2x10^{20}$ m^{-3} [103], and for detached DIII-D plasmas less than 1eV and less than $5x10^{19}m^{-3}$ [104]. The relatively low electron temperature in the private flux region in both ITER and DIII-D is due to active gas puffing in the divertor region to obtain a detached divertor configuration, which is necessary to reduce divertor heat loads. The electron temperature and electron density in the SOL at the mid-plane region of ITER is predicted to be about 100eV and $2x10^{19}m^{-3}$ [105], and for DIII-D less than 20eV and less than $3x10^{18}$ m^{-3} [106]. The parameters for NSTX-U could be expected to similar to those for DIII-D.

These numbers show that plasma parameters in the SOL region for present large tokamaks as well as the projected SOL parameters for ITER are much more challenging for neutral gas penetration compared to the parameters in the private flux region. This is the motivation for proposed experimental work on NSTX-U. These parameters will be used as input in DEGAS-2 simulations to theoretically assess the gas penetration efficiency as a function of SOL and private flux region parameters and will eventually be compared to experimental observations from NSTX-U.

The primary goal of the MGI experiments in NSTX-U is to compare the gas penetration efficiency as gas is injected from the different poloidal locations shown in Figure 2.2.3.3.1-1. These are (1a) the private flux region, (2) the mid-plane region, (1b) high-field side outer SOL region, high-field side inner SOL region and (3) outer SOL region above the mid-plane. A second objective is to determine the uniformity of the radiated power profile. The third objective is to assess the reduction in divertor heat loads and halo currents. The importance of the q = 2 surface proximity to the plasma edge will be studied by gas injection at different times during the discharge as the q = 2 surface evolves. The eventual goal of these studies would be to design a system for NSTX-U that can automatically trigger the MGI system based on input received from

sensor-provided data on an impending disruption. For these up-coming experiments on NSTX-U four ports have been assigned for MGI. The green arrows in Figure 2.2.3.3.1-2 show these MGI port locations.

The gas assimilation efficiency will be measured by obtaining closely spaced (in time) Thomson scattering density profiles just prior to and after the MGI gas begins to interact with the edge plasma but before the thermal quench phase has initiated. EFIT reconstructions would provide the plasma shape and volume. H-alpha detectors would be used to establish the time of contact of the MGI gas with the edge plasma. The time delay between this and the time when the individual MGI valve is triggered would provide the overall system response time for each gas injector. Starting from the time when the MGI gas first makes contact with the edge plasma, the Thomson scattering system would be triggered (at 0.5, 1, 1.5ms) to obtain density profiles before the plasma shape begins to significantly distort or before the Thomson scattering system detectors saturate. Since the Thomson scattering system measures local density this is preferred over the NSTX-U multichord interferometer system as it avoids the issue of profiles obtained using Abel inversion from a few interferometer chords. However, depending on the amount of injected and assimilated gas, both systems will be needed to obtain reasonable estimates for the amount of gas assimilated by the plasma discharge. Measuring this parameter has been challenging in other tokamaks and will prove to be challenging on NSTX-U as well since these diagnostics are not designed for the very high density plasmas that result from assimilation of large quantities of gas.

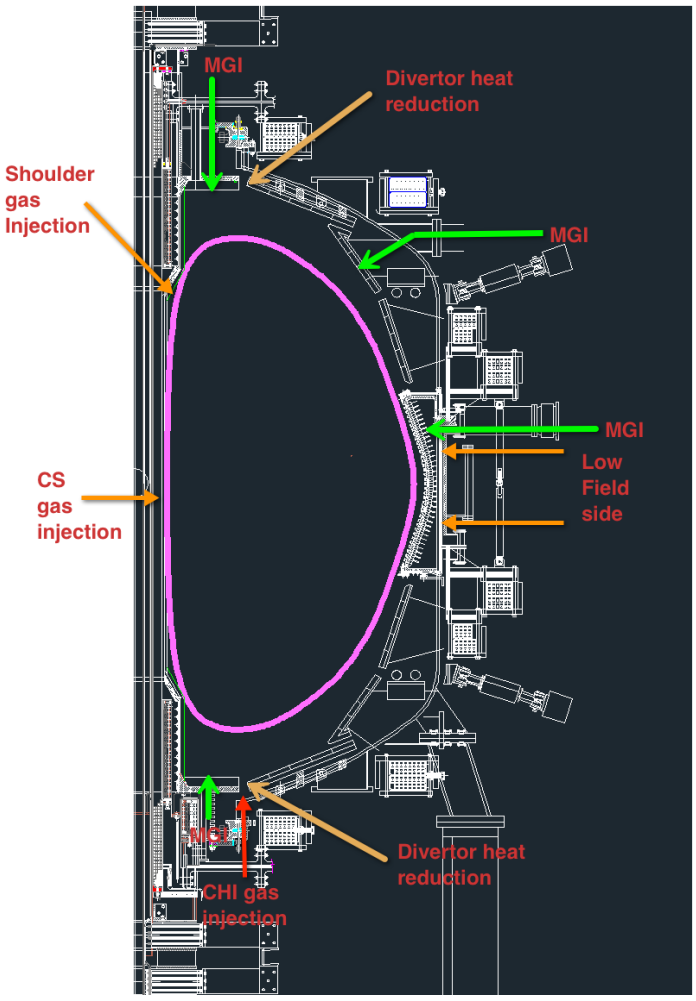

Figure 2.2.3.3.1-2: MGI gas injection locations on NSTX-U are shown by the green arrows.

A concern with localized gas injection for ITER is that the radiation profile could be toroidally localized to a region near the gas injection port. Depending on the plasma parameters, this could lead to localized heat deposition on nearby walls leading to localized melting. Thus measurement of the radiated power profile at three or more toroidal locations is important. This is discussed in detail in a subsequent section, including the need for a new-dedicated diagnostic. Here the NSTX-U multi-chord bolometer array and the multi-chord soft X-ray arrays will be used to obtain the radiated power and soft X-ray emission profiles using an Abel inversion method from a dense array of chords.

The spatial distribution of the divertor heat loads will be measured with two color divertor fast infrared cameras. These were successfully used during the FY2010 NSTX run campaign to measure divertor plate temperatures during the snowflake divertor experiments. These will be complemented with eroding thermocouples that would provide an independent measurement of the divertor plate radial temperature profile at a few toroidal locations. Halo current sensors on the divertor plates will provide data on the extent of halo currents during the different disruption mitigation scenarios and during unmitigated disruptions.

2.2.3.3.2 MGI simulations using the DEGAS-2 code

In support of Massive Gas Injection (MGI) studies on NSTX-U, DEGAS-2 simulations [107,108] are being conducted to better characterize the gas penetration physics and to improve the design of the MGI gas delivery system on NSTX-U.

There are two requirements for successful implementation of MGI in ITER. The first requirement is that an adequate amount of injected gas penetrates past the separatrix. This is related to the physics of neutral gas penetration through an energetic edge plasma region and the SOL. The ratio of the injected gas that couples to the tokamak discharge to the total amount of injected gas is referred to as the gas assimilation or gas penetration efficiency. The second part involves the physics of how the gas that penetrates past the separatrix distributes within the plasma discharge. The dynamics of the gas mixing is responsible for the resulting thermal quench timescales and radiated power profiles. This is referred to as gas dissipation physics inside the separtrix. While much work is in progress to understand the gas dissipation physics, for example through the use of the NIMROD code [109] the more fundamental gas penetration issue is still poorly understood.

A review of the literature [96-99] shows that the amount of gas injected in MGI experiments in present tokamaks varies from 100 $Pa.m^3$ to over 2000 $Pa.m^3$, considerably less than the projections for ITER. The fraction of this gas that penetrates past the separatrix also varies widely, with penetration efficiencies of over 20% being reported for cases that have a short MGI

pulse. To better quantify the amount of gas required in a MGI pulse a DEGAS-2 Monte-Carlo code simulation effort has been initiated to understand the extent of gas penetration through the SOL region and private flux regions. In addition to supporting NSTX-U needs, this simulation effort focuses on studying the fundamental issues of edge penetration to the separatrix, which is needed for predicting gas penetration efficiencies in ITER. This work complements other 3-D MHD modeling (such as with the NIMROD code), initiated by the ITER organization, of the gas dissipation physics inside the separatrix.

Full DEGAS-2 model: For a full detailed simulation of the involved gas penetration physics, both the DEGAS-2 and UEDGE codes are required. The planned simulations will start with plasma parameters from a suitable NSTX-U discharge with neutral beam heating. The computational mesh needed for DEGAS-2 to model the region outside the separatrix region would be generated by the UEDGE code [110,111,112].

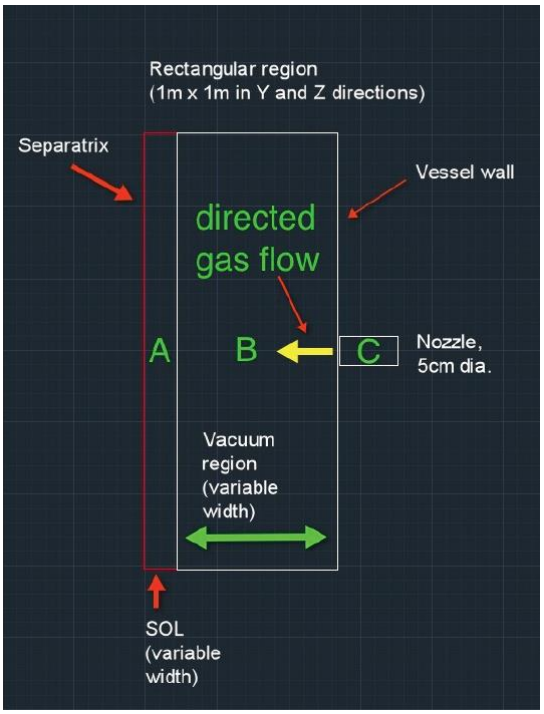

Figure 2.2.3.3.2-1: Simplified rectangular 3-D mode for DEGAS-2 simulations.

As the molecules penetrate the plasma, they would undergo ionization, dissociation, and elastic scattering; resulting molecular ions would undergo ionization, dissociation, or recombination. Any product atoms would then be tracked through the plasma and can undergo ionization and charge exchange. The particle track terminates upon ionization of the atom. Along the particles' paths, the volumetric source of plasma ions is accumulated in each computational zone. The penetration fraction is then the ratio of the volume-integrated sum of those source rates over zones inside the separatrix to the gas puff rate.

Simplified DEGAS-2 model: While we are interested in conducting this full model study during the 5 year period, due to present man-power limitations, we have considerably simplified this model to understand a smaller part of the important gas penetration physics that is relevant to the up-coming NSTX-U MGI experiments. To carry out this simplified study we have used a simple rectangular geometry. In this simplified rectangular geometry, shown in Figure 2.2.3.3.2-1, a 1m x 1m (in the y and z directions) region is used. Region A represents the SOL region and its width and plasma parameters (density and temperature) can be arbitrarily varied. Region B is the space between the SOL outer edge and the vessel wall. This is 20cm in width

and contains no plasma. This width could also be varied to reflect the location of the gas valve with respect to the edge of the SOL. The gas valve, labeled C, is located at the vessel wall.

In this simplified model, the SOL and private flux regions can be modeled by varying the length of the dimension A and the corresponding plasma parameters in region A. Thus depending on the choice of the parameters, region A would represent either the SOL or the private flux region. With the proper choice of the plasma parameters in region A, it should also be possible to obtain estimates for the gas penetration fractions that could be expected in ITER. These simplified DEGAS-2 simulations are planned to be completed before year 2 of NSTX-U operation.

This model will provide a lower bound for the gas penetration efficiency that can then be compared to observed results from DIII-D, C-MOD and other tokamaks. It will also provide guidance for the gas penetration efficiencies for NSTX-U mid-plane and private flux region conditions. Based on the extent of differences between the simplified DEGAS-2 results and experimental observations form present machines as well as from NSTX-U, a full DEGAS-2 simulation could be considered during years 2 to 4 of NSTX-U operations.

These simulations can also be extended to cases where smaller fractions of high-Z gases (neon, argon) are introduced into a carrier He gas to assess the ratio of high-Z to He gas fractions that allow the high-Z component to retain a high velocity. These will be incorporated into the model during years 2 and 3 of NSTX-U operations.

These planned experiments and simulations are expected to contribute to the understanding of important physics questions related to the MGI experiments in support of NSTX-U, ITER and future ST and tokamak based machines. The primary study to be conducted would be to understand the gas penetration efficiency as a function of poloidal gas injection location and variations in plasma parameters, especially at the edge. Supporting DEGAS-2 studies would contribute to quantifying the MGI system requirements aimed at minimizing the gas throughput and maximizing the gas penetration through the separatrix.

2.2.3.3.3 Novel mitigation technologies: electromagnetic particle injector

This section describes our on-going work for developing a new system for safely terminating discharges in ITER and FNSF. The system, referred to as an Electromagnetic Particle Injector (EPI) propels a coaxial projectile, containing particulate matter of various sizes and composition, in a coaxial electromagnetic rail gun, then shatters it in order to inject the smaller sized particles into the tokamak, as shown in Figure 2.2.3.3.3-1. While experiments on NSTX-U would likely shatter the pellet, the system for ITER may choose to inject the capsule intact.

The following observations can be made concerning MGI. First, it is generally agreed that the Massive Gas Injection system is the best understood system for safely terminating discharges in ITER. Second, the time response of this system and the controllability of the amount of gas and impurities injected by this system for variations in the initial plasma current at which a disruption initiates may be inadequate. Third, it may not be possible to fully rely on this system for forced thermal quenches that have less than 10 ms of warning time. Thus, it is generally agreed that other faster acting systems should be tested and developed. The EPI concept was presented at the U.S. Disruption Mitigation Workshop held at General Atomics on March 12-13, 2012. It was noted that this system was more complex as compared to a conventional gas gun, but no technical flaws were identified. It was also suggested that a proto-type should be built and tested before considering it for ITER.

At present the design parameters for such an injector for NSTX-U have been established. We plan to build a proto-type during the second quarter of 2013, and conduct off-line testing during the fourth quarter of 2013.

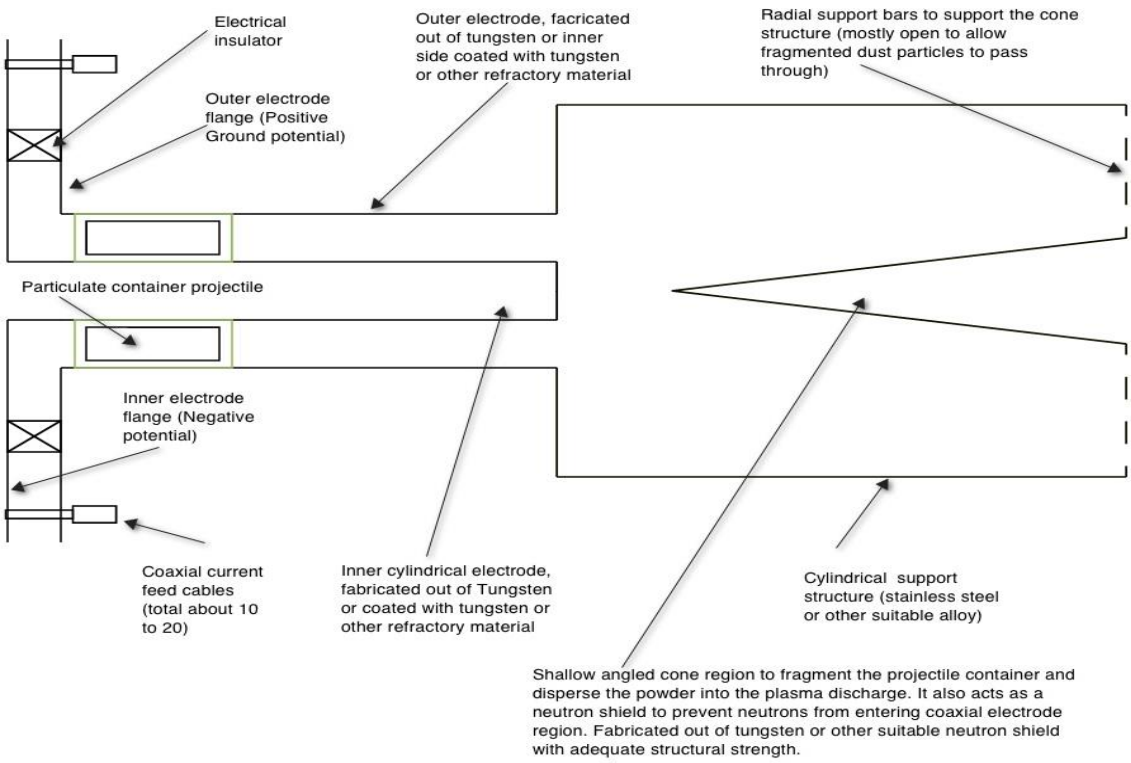

Figure 2.2.3.3.3-1: Electromagnetic Particle Injector (EPI) using a coaxial electromagnetic rail gun.

The proposed system, shown in Figure 2.2.3.3.3-1 and Figure 2.2.3.3.3-2, is now under detailed design. The EPI system has several advantages over other disruption mitigation systems being considered for ITER. These are:

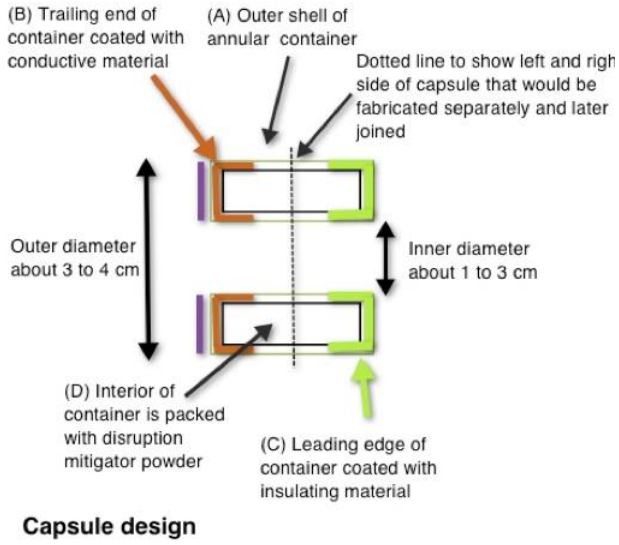

Figure 2.2.3.3.3-2: Shown are the primary elements of the capsule design. The purple ring at the trailing end of the capsule serves two purposes. In an electromagnetic accelerator it is used to increase the inertial strength of the capsule. If the capsule is used in a conventional gas gun it could be fabricated out of a non-conductive material.

- It is capable of delivering a highly tailored mass inventory with:

- A large particle inventory,

- All particles delivered at nearly the same time,

- Particles tailored to contain multiple elements in different fractions and sizes, and

- Particles that are fully ionized only in higher current discharges (to control current quench rates).

- The toroidal structure and conical disperser ensures that:

- For smaller machines, the capsule does not enter the tokamak intact,

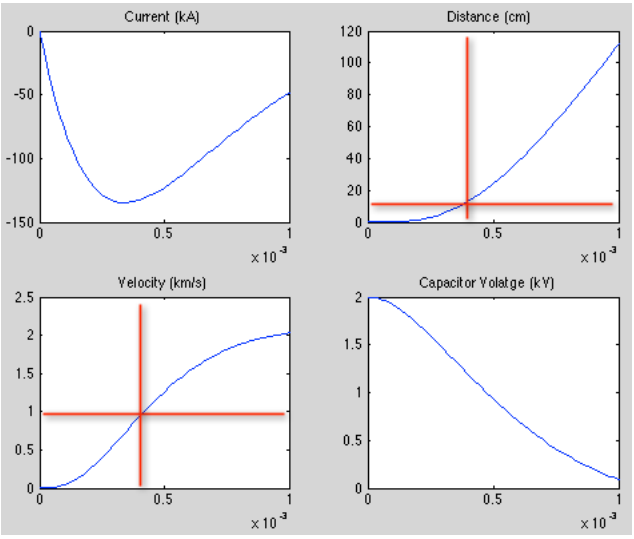

Figure 2.2.3.3.3-3: Accelerator current, capsule velocity, distance traveled by the capsule, and the capacitor bank voltage history all as a function of time after discharge of the capacitor bank.

Figure 2.2.3.3.3-4: The NSTX CHI capacitor bank system is well suited to powering the EPI injector for NSTX-U.

- The capsule will fragment symmetrically and deliver a uniform distribution of particles (or via. tapered final section),

- For larger machines, the capsule can also be injected intact without fragmentation, and

- Particle penetration is not impeded by magnetic fields

- A coaxial rail gun is a fully electromagnetic system with no moving parts, so should have high reliability from long stand-by mode to operate on demand.
- Conventional gas guns will inject gas before capsule and will trigger a pre-mature thermal quench.

Design studies for NSTX-U have now converged on an attractive and viable system. Table 2.2.3.3.3 contains the specifications for the capsule and injector. The capsule volume is about 0.5 to 1.5 cm^3. For present machines, the capsule would be fabricated out of graphite particles compression packed with a bonding agent. The purple ring shown in Figure 2.2.3.3.3-2 would be fabricated out of a layer of conductive graphite. For NSTX-U the capsule would have a mass of about 2-3g and contain enough carbon atoms to equal about 20% of the required impurity atom content for a forced thermal quench in ITER. The inner and outer diameter of the accelerator would be 1 and 2cm respectively. The overall injector length would be 20cm for a final velocity of 1km/s. As shown in Figure 2.2.3.3.3-3 which contains results from rail-gun simulations, by

Capsule Parameters	Injector Parameters
Inner and Outer Radius: 0.5cm and 1cm	Accelerator Length: 0.2 to 1m
Length and Volume: 0.5-1.5cm and 1-3cc	Capacitor bank voltage: 1-2kV
Capsule Mass: 2.8g	Bank Capacitance: 50mF
No. of Carbon atoms: 1.5×10^{23}	Capacitor bank energy: 100kJ
No. of electrons: 9.2×10^{23}	External inductance: 2μH
Electrons in capsule/ITER TQ needs: ~0.2	Accelerator inductance: <1μH

Table 2.2.3.3.3: Capsule and EPI Injector Parameters for NSTX-U

extending the accelerator length to 1m, velocities as high as 2km/s could be achieved. The simulations also show that the velocity of 1km/s is achieved in less than 0.5ms after the discharge of the power supply. In systems such as this, it is the power supply that is the high-cost component. Fortunately, because of CHI research on NSTX, the capacitor bank used for CHI research (shown in Figure 2.2.3.3.3-) is well suited for powering the EPI injector for NSTX-U. The system capacitance is 50mF and it will be operated at 2kV. The RG218 power cables that

feed power into the CHI current bus at the machine would be disconnected and could be connected to the EPI injector bus during disruption mitigation studies.

Given that the high-cost components will be in an operational state during year 1 operations to support the CHI program, what remains is the fabrication and testing of a prototype injector which as mentioned above, will be completed before the start of NSTX-U operations.

2.2.3.3.4 Summary of research plans by year

Year 1 (2014):

- Continue DEGAS-2 modeling of gas penetration physics for NSTX-U.
- Prepare MGI system for operation.

Year 2:

MGI program goals: Test hardware and commission MGI diagnostics

- Using a low triangularity discharge as shown in Figure 2.2.3.3.1-1a, a comparison will be made of massive gas injection (using a combination of deuterium and helium) of gas injected into the lower X-point and private flux region to that from the vessel mid-plane. This is a comparison of locations 1a and 2 in Figure 2.2.3.3.1-1a.
- The shape of the plasma will be varied to make it highly triangular so that the outer strike point rests on the inner divertor plate and at a radius less than the radius of the gas injection port (Figure 2.2.3.3.1-1b). Gas will then be injected into the scrape-off-layer region near the divertor, which is now located in a region of high toroidal field (location 1b in Figure 2.2.3.3.1-1b). This injection location will be compared to mid-plane injection (location 2, in Figure 2.2.3.3.1-1b) to understand the effects of gas penetration through the scrape-off layer that is located in regions of high vs. low toroidal field. The same combination of deuterium and helium will be used for these experiments to compare these results to those for the low triangularity discharges.
- During the first year of NSTX-U operations, much of the MGI studies will use a combination of deuterium and helium primarily to gain experience in conducting these studies on NSTX-U for the first time and to commission the diagnostics that will support MGI studies. Towards the end of Year 2 operations test will be conducted in which neon is introduced as an additional impurity gas in the deuterium/helium gas mix used above to gain experience with the use of high-Z gas and to develop experiments for Year 3 that will begin to use high-Z gasses.

Year 3:

MGI program goals: Increase high-Z gas fraction to satisfy milestone 3a (quantify MGI results from NSTX-U). Systems that were installed, tested and improved during the previous two years

will this year be used to obtain sufficient quantitative results in support of this Milestone, including the following research tasks:

- Based on previous results, a desired fraction of neon (in a combination of deuterium/helium carrier gas) will be used for all subsequent comparison experiments to be conducted this year.
- Compare: (1) the gas transit and system response times, (2) propagation time for the cold front to reach the q = 2 surface, (3) the amount of gas required for initiating a rapid thermal quench and (4) symmetry of the radiated power profile.
- Determine if a cold mantle can be continually maintained around disrupting plasmas by simultaneously injecting gas from three locations (bottom, mid-plane and top. Assess the benefits of multiple injection location for reducing localized radiation thermal loading.
- Replace neon with argon to assess the benefits of each of these gases and to select the gas combination for further experiments.
- Quantify the gas assimilation fraction for variations in the gas injection location and compare to DEGAS-2 modeling results. Assess if a full DEGAS-2 model is required for future work.
- Assess reduction in divertor heat loads and reduction in divertor halo currents for variations in the gas injection location.
- Measure asymmetries in the radiated power profile for variations in the gas injection location and for simultaneous gas injection from multiple locations.

EPI program goals: The primary objective for the EPI system (planned for Year 3) is to assess the EPI injector system's capability to initiate a forced thermal quench in less than 10ms after the system is triggered. This is for assessing its potential to meet ITER needs.

- Conduct an initial commissioning test of EPI injected capsule into energetic NSTX-U plasma so as to obtain sufficient information to assess its potential as a disruption mitigation system for ITER. Parameters of interest would be (1) time when the projectile particles contact the plasma after system trigger time, (2) time for the resulting thermal quench and (3) reliability of the system. For NSTX-U experiments, the system will be designed to inject the capsule at a velocity of 1 km/s. At this velocity, in principle, the particles should reach the NSTX-U core plasma 3-4 ms after the system is triggered. These initial experiments will be used to guide the capsule velocity requirements for ITER and for Year 5 NSTX-U EPI experiments.
- Obtain additional measurements using the EPI system to assess its potential benefits over the MGI system.

Year 4:
Compare MGI and EPI systems in NSTX-U: Characteristics of the thermal and current quench phases for MGI and EPI triggered disruptions will be compared.

- Inject MGI at different times into a discharge in which the q-profile is evolving to understand the importance of the location of the q = 2 surface to the plasma edge.
- Compare the thermal and current quench rates for forced disruptions using MGI and EPI in a high-powered NSTX-U discharge.
- Work with groups using NIMROD, KPRAD, and if possible the EIRENE-SOLPS codes to simulate NSTX-U experimental observations. This is work that will have been initiated during Year 1 of NSTX-U operations.
- Continue to include the NSTX-U MGI and EPI data into the ITER database to contribute to the continued understanding of these systems for ITER, future tokamaks and STs.

Year 5:
Integrate DMS to DM Sensors: Obtain other needed data from the MGI and EPI systems and to test their reliability to trigger on demand using signals provided by disruption detection sensors in NSTX-U.

- Trigger the MGI system based on input from the disruption warning system (see thrust MS-1). Additionally, it will be determined if the DM control system is capable of triggering a specific MGI valve based on the plasma configuration (i.e., downward vs. upward moving disruption).
- Trigger the EPI system based on input from the disruption warning system.

See Section 9.2.3.1 for additional information of the systems for synthesizing NSTX diagnostic data in order to provide pre-disruption triggers to these systems.

2.2.3.4 Disruption physics

The topic of disruption physics captures a number of topics critical for the reliable operation and design of future tokamaks. In general, these include the physics of:

- transport during the thermal quench, and associated power loading of the PFCs,
- the current quench,
- the generation of halo currents,
- the generation of runaway electrons (REs).

Of these topics, the current quench will be studied extensively as part of the mitigation research described in Section 2.2.3.3, and will not be addressed here. Due to the strong shaping and lower toroidal field, disruption RE generation is not expected in NSTX-U (the RE studies in Section 2.2.3.3.3 are proposed to be performed on an RE population generated by low-density Ohmic operation, not disruptions). Hence, the research program described here will focus on the thermal quench and halo current generation.

2.2.3.4.1 Improving understanding of thermal quench physics and transient disruption heat loads

In the chain of disruption consequences, the first event is the thermal quench. The impulsive thermal loading associated with the quench can lead to severe damage to the plasma facing components. The magnitude of this problem can be viewed in Table 2.2.3.4.1, where the thermal quench heat loads are projected using the methodology from Table 5 of Reference [113]. The pre-disruption thermal energy is used for projecting the thermal loads. The divertor area is taken from Reference [113] for ITER, and as $2\pi R_0 \lambda_{mid} f_{exp}$, where λ_{mid} [cm] = max(0.2,1.0/$I_p^{1.6}$) [114] and a flux expansion f_{exp}=30 is assumed for NSTX-U and 60 for the next step STs. Furthermore it is assumed that the SOL expands by a factor of seven during the disruption process, yielding a similar expansion in the wetted area of the divertor. Finally, the time-scale of the heat pulse (τ_{div}) is assumed to be similar to the time-scale of the thermal collapse, and is of order 1 ms. A thermal loading parameter is then estimated as $W/7A_{div}\tau_{div}^{1/2}$.

	ITER	NSTX-U	ST-Pilot	Power Reactor
R [m]	6.2	1	2.2	3.2
I_p [MA]	15	2	19	29
l_{mid} [mm]	*	3.299	2.000	2.000
W [MJ]	350	1.5	282	1100
A_{div} [m]	3.50	0.62	1.66	2.41
t_{TQ} [ms]	0.7	0.5	1	1
Loading [$MJm^2s^{-1/2}$]	540	15	768	2061

Table 2.2.3.4.1: Disruption thermal loading estimated for ITER, NSTX-Upgrade, an ST-Pilot facility, and an ST power reactor.

The results in the table show that for ITER, a thermal load parameter of roughly 540 $MJm^2s^{-1/2}$ is expected, which is much larger than the C or W ablation/melting threshold of 40-60 $MJm^2s^{-1/2}$ [113]. This clearly illustrates why mitigation of the thermal quench is critical for ITER. The NSTX-U disruption thermal loading is significantly smaller than this threshold, and disruption damage to potential metal PFCs is only expected if the PFC temperature is already significantly

elevated. The ST pilot plant, taken from Reference [4] shows thermal loading approximately 30% larger than that projected for ITER. The ST power reactor, whose parameters are loosely based on ARIES-ST, shows thermal loading more than a factor of five greater than ITER and 50 times larger than the melting threshold for tungsten, even with the large divertor area generated by operating at f_{exp}=60 and a further factor of seven increase during the disruption.

The research proposed for this area in the NSTX-U research program is based on examining the assumptions made in constructing this table, and then providing an experimental basis for improving them.

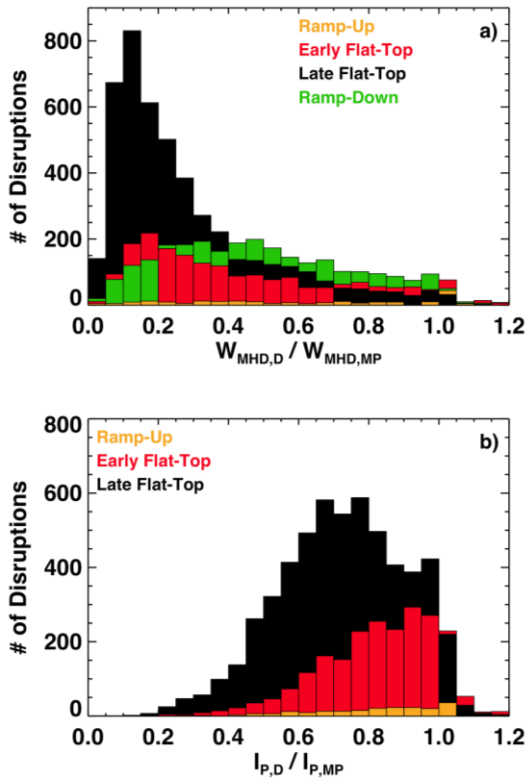

Figure 2.2.3.4.1-2: Histograms of the of a) stored energy, and b) current left at the time of disruption vs. at the time of maximum performance. The data is broken into the current ramp, the period between the start of flat-top (SoFT) and SoFT+250 ms, the later flat-top, and the rampdown. Figure from Reference [95].

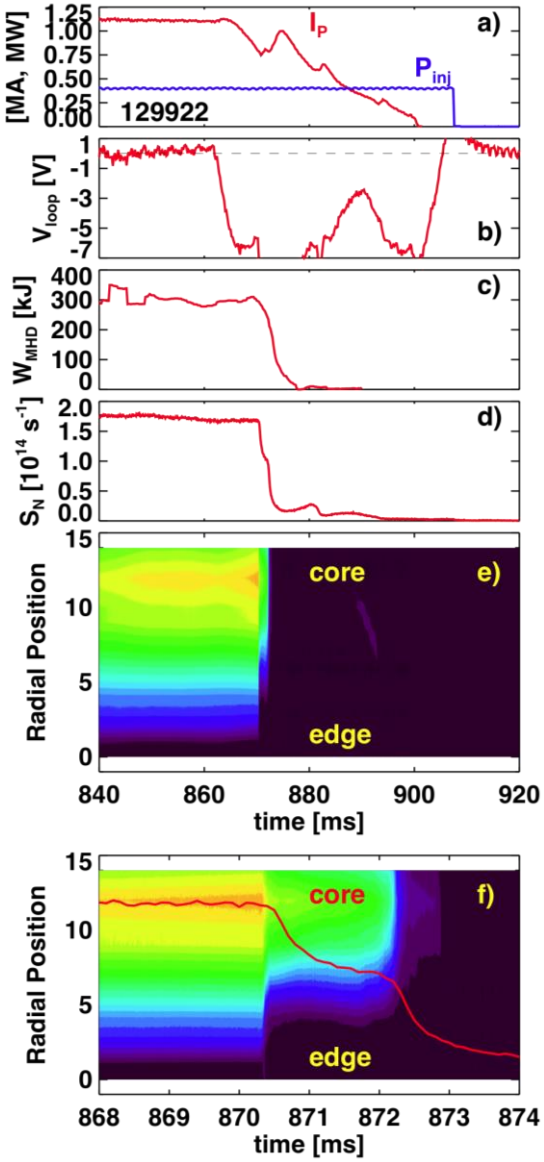

Figure 2.2.3.4.1-1: Time evolution of quantities during a plasma with an extremely rapid thermal quench. Shown are a) the plasma current and injected power, b) the applied loop voltage, c) the stored energy, d) the neutron emission, e) the soft X-ray profile, and f) the neutron and soft X-ray emission zoomed in to the region surrounding the thermal quench. Figure from Reference [95].

This process illuminates the key physics assumptions and processes that must be understood to make improved projections to next step STs.

The first physics assumption in these estimates is that stored energy at the time of the thermal quench is equal to the value during the high performance phase. In fact, as shown in Reference [115] for JET and Figure 2.2.3.4.1-2a for NSTX data [95], there is typically a rather large fractional loss of stored energy during the low confinement phase preceding the thermal quench. For instance, for disruptions in the later flat-top, the most likely case has a stored energy equal to 15-20% of the stored energy at the time of maximum performance. Similarly, Figure 2.2.3.4.1-2b shows that there is typically a loss of plasma current in the phase leading up to the disruption. Both of these effects can help to mitigate the dangerous aspects of the disruption.

Note, however, that there are many examples in Figure 2.2.3.4.1-2a with minimal fractional stored energy loss preceding the disruption. These cases are often among the highest stored energy disruptions in NSTX. An example of such a disruption is shown in Figure 2.2.3.4.1-1, where frames a) through e) share a common time-base, and frame f) zooms in on the soft X-ray emission dynamics during the thermal quench. In this case, the disruption is triggered by a reversal of the loop voltage in Figure 2.2.3.4.1-1b, as the plasma current is ramped down without first reducing the stored energy. The stored energy of 320 kJ at the time of the thermal collapse is quite large by NSTX standards, and shows no substantial reduction in the phase leading up to the thermal quench. In fact, 21 of the 22 largest stored energy disruptions in NSTX were of this variety, where the loop voltage was reversed during the high performance phase. This observation motivates the ramp-down automation tasks described in Section 9.2.3, designed to avoid this occurrence, but also provides a means to generate reproducible disruptions for physics studies, as will be described in the next section.

Research in NSTX-U will continue to examine the typical stored energy losses preceding a disruption. More importantly, it is worth noting that that the levels of energy loss in Figure 2.2.3.4.1-2a are only due to natural plasma processes. Collaborative research between the ASC and MS groups will attempt to actively increase the levels of pre-disruption energy loss by implementing automated soft-stop procedures, as described in Section 9.2.3.2. This will allow a better understanding of the scenarios under which full-energy disruptions are unavoidable.

A second key assumption made in formulating Table 2.2.3.4.1 is that all of the energy present at the time of the thermal quench is conducted to the divertor, and that radiation is not a significant part of the disruption power balance. This assumption will be verified by power balance measurements during disruptions. In particular, a bolometry system will be used to assess the total radiation as a function of time, during both the thermal and current quenches. The fast IR thermography systems and eroding thermocouples will be used to assess the heat conducted to

the PFC surfaces. Measurements of vessel eddy currents will be used to assess the magnetic energy lost to eddy currents. These measurements will be made for both centered major disruptions and vertical displacement event (VDE) disruptions.

The third assumption in Table 2.2.3.4.1 is with regard to the temporal scale of the thermal collapse and the thermal loading. At conventional aspect ratio, a two-stage thermal quench sequence has often been discussed [113], where there is first flattening of the thermal profiles within the q = 2 surface, followed by a complete collapse of the remaining thermal energy. The time-scale of the second collapse is used as a worst-case proxy for the time-scale of the thermal loading in the calculation of Table 2.2.3.4.1, though some measurements from AUG [113] indicate that this may be too conservative.

The largest stored energy disruptions in NSTX are also observed to have a two stage thermal collapse. For instance, the neutral emission trace in Figure 2.2.3.4.1-1d shows a two stage collapse, as does the profile of soft X-ray emissivity in Figure 2.2.3.4.1-1e. The dynamics of this two-stage collapse can be seen most clearly in Figure 2.2.3.4.1-1f, where the neutron and X-ray signals have been expanded around the time of the thermal quench. It is clear that, unlike the conventional aspect ratio case, the first collapse occurs at the edge of the plasma. This collapse takes place over 40-60 ms, followed by a nearly constant phase of 1500 ms duration, and the core thermal energy collapse on a time scale of ~200 ms.

The fast IR thermography and eroding thermocouples will be used in conjunction with the core diagnostics to assess the relative timing between the core thermal collapses and the arrival of heat at the divertor surface. These measurements will be conducted for “hot plasma VDEs”, where there is minimal thermal energy loss preceding the vertical motion, and centered disruptions such as that in Figure 2.2.3.4.1-1, where there is minimal plasma motion preceding or during the thermal quench. The presence of multiple time-scales in the thermal collapse will be documented for the various disruption types, and the levels of thermal loading associated with each time-scale will be documented. The effective duration of the thermal energy pulse will be measured, with a view to determine if various effects such as SOL turbulence or plasma sheath effects [113] result in a temporal spreading of the heat flux compared to the time-scale of the core collapse.

The fourth assumption made in assessing Table 2.2.3.4.1 is that the conducted heat flows along the SOL field in a fashion similar to that during the flat-top phase, but with a factor of seven expansion in the wetted area. Note that significant heat flux is conducted to the inner target during VDEs in DIII-D by poloidal flows and is not fully understood [116]; this effect is potentially more problematic in an ST, given the different divertor areas of the two targets, and must be understood well in order to project for future devices. The IR thermography diagnostics

will be used to assess the spatial extent of the conducted heat flux, to determine the correct area expansion factor for estimating thermal loads. Furthermore, the split between the inner- and outer-divertor legs will be assessed, to determine which locations receive the largest energy loading. As with the time-scale studies, these experiments will be conducted in both hot-plasma VDEs and centered, high-energy disruptions.

The fifth and final assumption involved in Table 2.2.3.4.1 involves the assumption of axisymmetry. The axisymmetry of the heat flux could be violated because of helical distortions of the plasma boundary due to MHD activity, or due to enhanced sheath conduction if thermal electron emission occurs on very hot PFC surfaces [117]. This latter effect could be relevant to cases where the PFC temperatures are already highly elevated when the high-energy disruption occurs, and could be strongly localized. Using the proposed wide-angle IR camera view, NSTX-U researchers will examine the disruption heat fluxes for evidence of strong non-axisymmetry, and quantify those asymmetries if present. The dynamics of those asymmetries will be compared to those for the halo currents, which are the topic of the next section.

2.2.3.4.2 Improving understanding of disruption halo currents

When vertical stability is lost during the disruption process, the plasma typically moves up or down, and comes in contact with the divertors. Large "halo currents" have been observed to flow from the plasma into the divertor structures, through those structures, and then back into the plasma. The part of this current that resides in the structures, when it flows across the magnetic field, can exert damaging forces on those structures.

Much of the early work on "halo currents" focused on the axisymmetric component of those currents, including their inductive coupling to the main plasma current channel [118]; this case corresponds to the currents being driven by a voltage source. More recent work has emphasized the role of halo currents in reducing the otherwise Alfvenic growth of n = 0 and n = 1 instabilities [119,120]; the currents in this case act as if they are driven by a current source. Given incremental funding, halo current research in NSTX-U will attempt to understand the relative importance of these two effects, as well as determine more completely the halo current dynamics in a spherical torus. In particular, the goals for halo current research in NSTX-U are as follows:

- Determine the total halo current fraction in next-step relevant ST conditions.
- Better document the toroidal and poloidal structure of the halo currents, and compare to magnetic measurements of the plasma 3D structure.
- Document the reduction of halo currents with disruption mitigation technologies.

These studies will be made possible by a significant expansion of the halo current measurement systems, as described below.

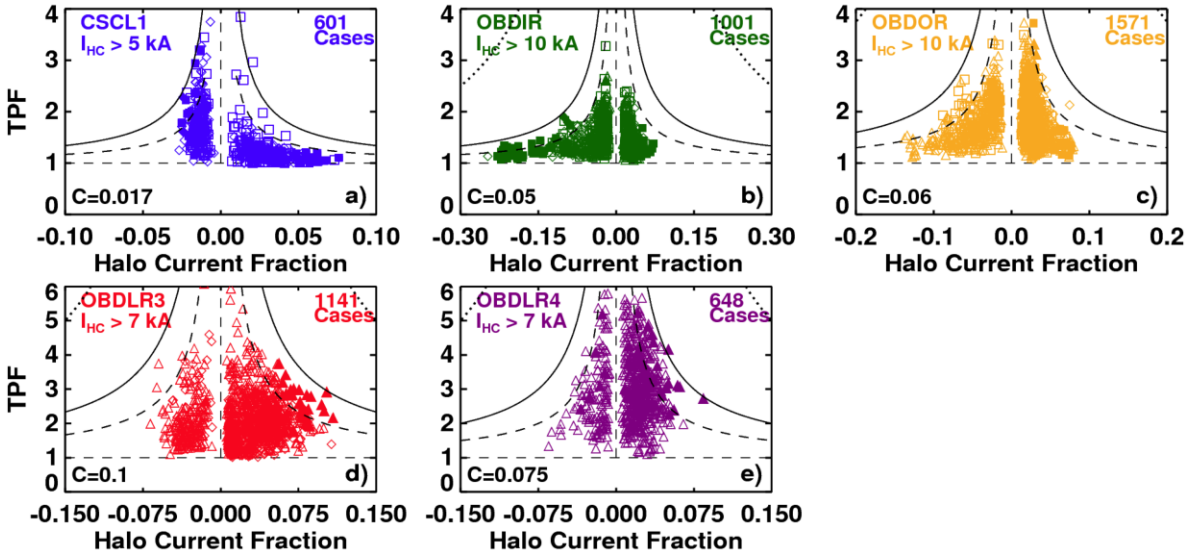

Figure 2.2.3.4.2-1: Halo current fraction vs. toroidal peaking factor, for a series of diagnostics. Frame a) shows data from instrumentation on the center-stack casing, frames b) and c) show data from the lower vessel wall, while frames d) and e) shows data from arrays of tiles located in the outboard divertor. Figure from Reference [122].

NSTX had a significant array of halo current diagnostics: see Reference [121] for a description of the instrumentation, and Refs. [122,123] for example results. However, even with those extensive measurements, it has been impossible to comprehensively measure the total current flowing in the plasma SOL. This can be understood by examining Figure 2.2.3.4.2-1, which shows the halo current fraction vs. toroidal peaking factor for measurements at various positions around the NSTX vessel. The largest halo current fractions are measured at the vessel wall in frames b) and c), where values of up to 25% have been measured. However, this measurement must necessarily underestimate the total halo current, on account of the current which can flow along the copper divertor plates, never entering the vessel wall. Frames d) and e) illustrate the total current flowing into a single row of tiles; both the row 3 and row 4 divertor tiles are illustrated. Unfortunately, the total halo width at the divertor floor can be larger than the poloidal extent of these two tile rows, and the sum of the currents in these two rows thus underestimates the total current.

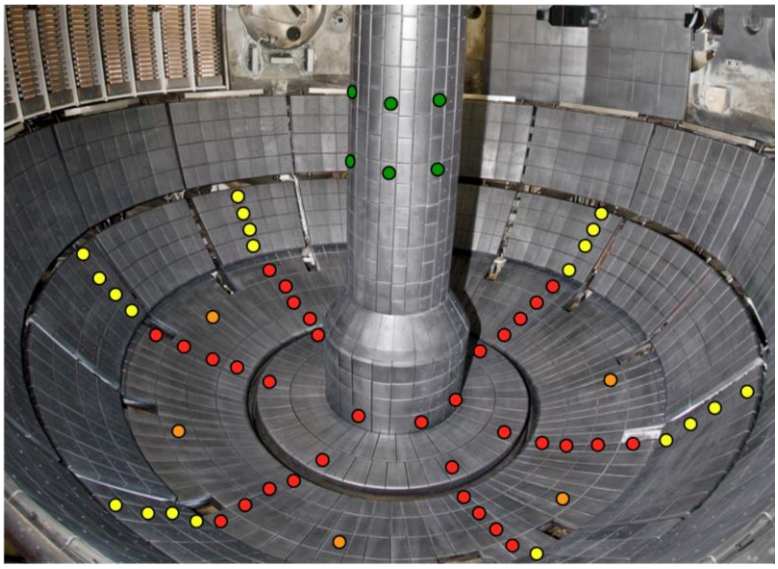

Figure 2.2.3.4.2-2: Proposed expansion of the NSTX-U shunt tile diagnostic set. Each red dot represents a tile which is instrumented with a resistive shunt beneath it. Note that NSTX-U has only a single row of tiles on the inner horizontal target. The colors are explained in the text.

In order to properly measure the total halo current, the shunt tile arrays and other halo current measurements will be significantly expanded. This expansion, indicated conceptually in Figure 2.2.3.4.2-2, will be implemented in a staged way, and if these tiles are eventually replaced by metal PFCs, we will need to reassess our measurement capabilities.

For the ST, the most critical location for halo current loading is possibly the center column, since the toroidal field B_T~1/R is strongest there. Hence, measurements during the first year of operation (Year 2) will focus on diagnosing halo currents at that location, and will utilize an expanded array of sensors on the center column. This includes an array of 12 shunt tiles indicated in green in Figure 2.2.3.4.2-2, as well as a toroidal array of B_T sensors located near the midplane. The shunt tiles will assess the local halo current density in the central region of the center stack, though they may not be sufficiently dense to measure the total current. This measurement will be accomplished using the array of B_T sensors, which act like segments of a partial Rogowski coil and should be able to accurately assess the total vertical current on the center column (though measurements of the peaking factor by this means will be difficult as per the discussion in [121]). These sensors, along with the total and partial Rogowski coils on the upper and lower portions of the center column, should allow a complete inventory of halo currents on the center column.

The next upgrade to the halo current sensor array will involve improved measurements in the outboard divertor, with the goal of significantly improving the toroidal and poloidal resolution. These will include instrumenting all five rows of the outer divertor, as well as the single row of the inner target, with ~6 tiles each; see red circles in Figure 2.2.3.4.2-2 for suggested locations. This toroidal distribution of tiles has proven useful in resolving the approximate toroidal structure of the halo currents in NSTX. Increasing the toroidal coverage in one or two select rows will also be considered, in order to better assess any fine structure in the measurement; the

arrangement in Figure 2.2.3.4.2-2 shows increased toroidal coverage in the third row of divertor tiles as orange circles.

The final upgrade will involve making measurements of the halo currents on the passive plates. While the most common location for the plasma to limit during a VDE is on the divertor floor, plasmas limiting on the secondary passive plates [122] during VDEs were occasionally observed in NSTX. If this type of VDE continues to occur in NSTX-Upgrade, then the tiles on the secondary passive plates will be instrumented in the later years of the five year plan for measurements of currents, as indicated in the yellow circles in Figure 2.2.3.4.2-2. If improvements to the vertical control system described in Section 9.2.2.1.2 eliminate this variety of VDE, then these tiles will not be implemented.

Additional diagnostics will contribute to the understanding of these halo currents. Newly upgraded Langmuir probe diagnostics will facilitate an assessment of the halo electron temperature during the VDE. The new divertor 3D magnetic diagnostics should allow a more precise measurement of the 3D distortions of the configuration during the phase of large currents. These will be used in conjunction with the current measurements to assess the relative phase between the surface distortions and the currents, in order to elucidate the role of the "Hiro current" mechanism [124] in driving these currents. Finally, a divertor Thomson scattering system (incremental) would provide a high-quality measurement of the core and halo temperature density during the VDE.

Using the diagnostic systems described above, it will be possible to measure the total halo current density, at the current entrance and exit points, for a wide range of disrupting plasmas. At a basic level, this diagnostic will provide essential data to project global and local halo current to future ST devices. The scaling of the maximum local and global halo currents with plasma current, toroidal field, and VDE characteristics will be documented. However, beyond this simple parameter, the suggested system will target the following physics issues.

The upgraded halo current sensors will be used to assess the poloidal extent of the halo current channel, known as the halo width. This quantity impacts the total resistance of the halo current path, and thus the current that flows when the halo currents are driven as by a voltage source [117]; this drive term was apparently determined to be dominant in MAST measurements [125]. The width of the halo also impacts the spatial region in the divertor over which the force are applied, and is a key input parameter for many halo current simulation codes. Previous measurements in NSTX have been used to make estimates of the halo width [122], but the present system should resolve it more accurately by providing sufficiently broad poloidal resolution.

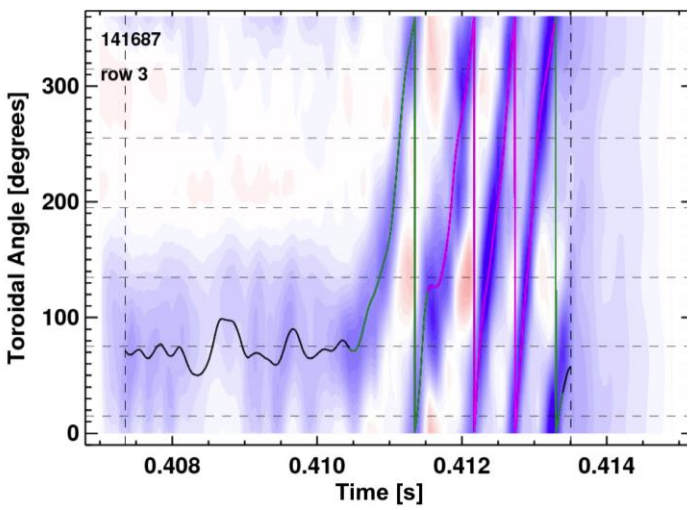

Figure 2.2.3.4.2-3: Evolution of the halo current density as a function of time and toroidal angle but at fixed poloidal angle. Note the strong toroidal rotation of the asymmetry.

NSTX-U studies will also assess the toroidal structure of the halo currents. As shown in Figure 2.2.3.4.2-3, previous measurements using six tiles at a fixed poloidal angle showed that the dominant structure of the halo current tended to be a rotating but toroidally localized lobe [123]. In this particular example, the halo currents flow at largely fixed toroidal angle for ~3 ms, then have a period of ~2.5 ms where they make 4 complete revolutions around the machine. However, previous measurements of the toroidal width of the structure relied on a fitting function that used the intrinsic toroidal rotation of the structure to improve the effective toroidal resolution [123]; the six toroidally distributed tiles were not, in general, sufficient to accurately assess the lobe width using the instantaneous data. This resulted in some uncertainty, especially for cases with little or no toroidal rotation. The system indicated in Figure 2.2.3.4.2-2, if it includes the tiles indicated by the orange circles, should be able to accurately resolve the toroidal structure even in the absence of rotation. Understanding the toroidal structure is critical for determining the potential for severe localization of forces, and can provide key insight into the underlying physics mechanisms generating the currents.

Finally, a key goal of the MGI experiments is to demonstrate a reduction in halo current loading with mitigation. The system described here will be able to comprehensively address this concern, by measuring the total current. With a more sparse measurement set, there is risk that any reduction of current observed with mitigation is simply the result of variations in the VDE dynamics resulting in the location of maximum current moving to a poorly instrumented portion of the divertor.

With regard to the theory of halo currents, there appears to be some consensus that a 3D equilibrium code capable of incorporating the effects of currents in the SOL is required. The development of such a code is beyond the scope of the NSTX-U experimental program. However, should that activity be pursued elsewhere, the NSTX data collected by this diagnostic system would provide a strong constraint on, or test of, those calculations. The research program described above will also produce data for benchmarking simulations of halo currents using extended MHD codes, as described in Reference [126].

If incremental funding is not provided, it is likely that the halo current diagnostics will be significantly more modest, and will be used to provide limited data for the mitigation experiments. The physics research described above would likely not be completed.

2.2.3.4.3 Impact of operating without solenoid induction on disruption physics

NSTX-Upgrade will be able to operate with 100% non-inductive current drive over a range of field, currents, and heating powers; see Chapter 9 or Reference [127] for additional discussion of this operating space. While many scenarios will continue to use the solenoid for I_P feedback control, it is also possible to deliberately disable that feedback loop. This will then duplicate the capabilities envisioned for next-step STs [3,4,5] that do not include an Ohmic solenoid. It is interesting to consider how this modification to the actuator capabilities may modify the disruption characteristics.

Typical H-mode disruptions in NSTX have some precursor modes or event, such as an RWM, locked mode, or H->L transition, that leads to a large drop in stored energy; these are the modes that lead to the large stored energy losses in Figure 2.2.3.4.2-1a. This collapse is typically followed by a 20-100 ms long phase with large loop voltage and, typically, growing vertical instability [95]. The actual thermal and current quenches typically occur only after the solenoid reaches its current limit and begins to ramp down, resulting in a reversal of the loop voltage, or after the plasma is driven into the divertor floor by the uncontrolled vertical motion.

If there were no solenoid induction, the dynamics following the precursor MHD/event would likely be quite different. Rather than responding to the strong inductive edge current drive from the solenoid, the current would begin to decay, though on a time-scale slower than during a true current quench. If the internal inductance were to increase during this process, problems may arise with evolution to unstable current profiles, which could prompt a final disruption. The time available for vertical motion, however, would likely be much less than the cases where induction partially supports the discharge current, and it appears possible that the halo current loading would be reduced in these cases. These various dynamics will be examined in dedicated experiments once 100% non-inductive operations have been established.

2.2.3.4.4 Summary of research plans by year

The timeline for this research is provided below. Note that the halo current research described beyond year 1 will likely require incremental funding, due to the expense of installing the shunt-tile diagnostics.

Year 1 (2014):

- Examine the physics assumptions underlying projections of thermal loading to future devices.

Year 2:

- Investigate halo current loading on the center column, using newly installed center column shunt tiles.

Year 3:

- Upgrade shunt tile diagnostics for complete coverage of the horizontal divertors. Make first assessments of total halo current fraction, toroidal structure, and poloidal width.
- Conduct first experiments on disruption heat loads during VDEs, including studies of spatial extent and timing of the heat deposition.
- Begin assessments of non-axisymmetric heat loading during disruptions, if diagnostic availability permits.

Year 4:

- Extend study of disruption thermal loads to centered major disruptions. Begin efforts to determine the disruption power balance for the various disruption types.
- Complete assessments of halo current scalings using the full field and current capabilities of NSTX-U.
- Conduct experiments examining the impact of fully non-inductive operations, with no loop-voltage feedback, on disruption physics.

Year 5:

- Complete assessments of the disruption power balance for the different disruption types. Complete assessments of 3-D effects in disruptions heat loading
- Utilize upgraded 3D magnetics for comparison of helical distortions and local halo currents.
- Study non-axisymmetric effects on the divertor heat loading.
- Continue support of disruption mitigation experiments by providing data on halo currents and thermal loads. Support halo current and thermal quench modeling activities by providing experimental data.

2.3 Non-axisymmetric control coil (NCC) design and analysis

A non-axisymmetric control coil (NCC) set has been proposed for NSTX-U, to gain understanding of the underlying 3D field physics in many applications in the ST geometry. A more complete overview of the motivation for the NCC was given earlier in Section 2.1.4. In additional, physics design considerations and calculations for the NCC are given in each section describing each of the three Thrusts. In this section, additional design elements are considered, along with a summary of quantitative figures of merit in tabular form, describing the most favorable NCC configurations considered to date.

2.3.1.1 Additional elements of the design motivation

The ST geometry allows the strongest 2D shaping in toroidal confinement, and thus can provide a unique environment to validate 3D field interactions with 2D plasmas. ELM triggering by 3D fields found in NSTX, is a good example illustrating the complexity of 2D shaping itself in 3D field applications. Also, 3D field applications with the snowflake divertor for NSTX-U will help reveal the role of the divertor in ELM applications and the stochastic parallel transport of particles. Non-inductive current drive requires strong bootstrap current with an associated self-consistent q-profile modification, where plasma responses to 3D fields may be very different, but have not yet been explored. Also, it has been shown that the plasma response can become very strong through field amplification at high-β, but amplification effects on resonant and non-resonant interactions between 3D fields and 2D plasmas are not yet fully understood, especially when the high-β is combined with strong bootstrap current in the fully non-inductive scenarios.

The application of 3D fields allows new and selective channels of momentum and particle transport, and thereby can provide rotation, pedestal, and stability control in tokamaks. The modification of the plasma toroidal rotation is a significant capability enabled by 3D field application. Compared to using NBI as the sole actuator, the addition of a 3D field actuator can allow greater and more precise ability to alter plasma rotation and its shear, both of which affect macroscopic and microscopic instabilities in different ways. However, mode stability is not a simple function of rotation or rotational shear, and therefore 3D coils should have sufficient flexibility in the applied field spectrum to finely tune and optimize toroidal rotation and control various instabilities. The particle and ELM control by RMP 3D fields are also complex, as different devices have shown slightly or largely different results on ELM modification. DIII-D has demonstrated complete suppression of ELMs using dominant n = 3 (n is the toroidal harmonic number) RMPs by two off-midplane internal coil sets [128], but in NSTX, n = 2 and 3 fields alone were not successful for ELM suppression and instead showed ELM triggering [19],

although the NSTX midplane n = 3 fields included more non-resonant components than resonant components. The JET tokamak showed that n = 1 fields from external midplane coils can mitigate ELMs by increasing their frequency [129], and the ASDEX-U tokamak showed successful mitigation of ELMs using n = 2 fields by two off-midplane internal coil sets, with the mitigation almost independent of resonant content in the 3D fields [130]. The KSTAR tokamak used three rows of internal coils and showed ELM mitigation and suppression using n = 1 RMPs [131]. Most recently, MAST showed ELM mitigation using n = 6 fields with two off-midplane coil sets [132]. These examples indicate that the present understanding and predictability of the underlying 3D physics are indeed insufficient for low-risk extrapolation to next-step devices.

2.3.1.2 Initial NCC design choices, including partial and full NCC

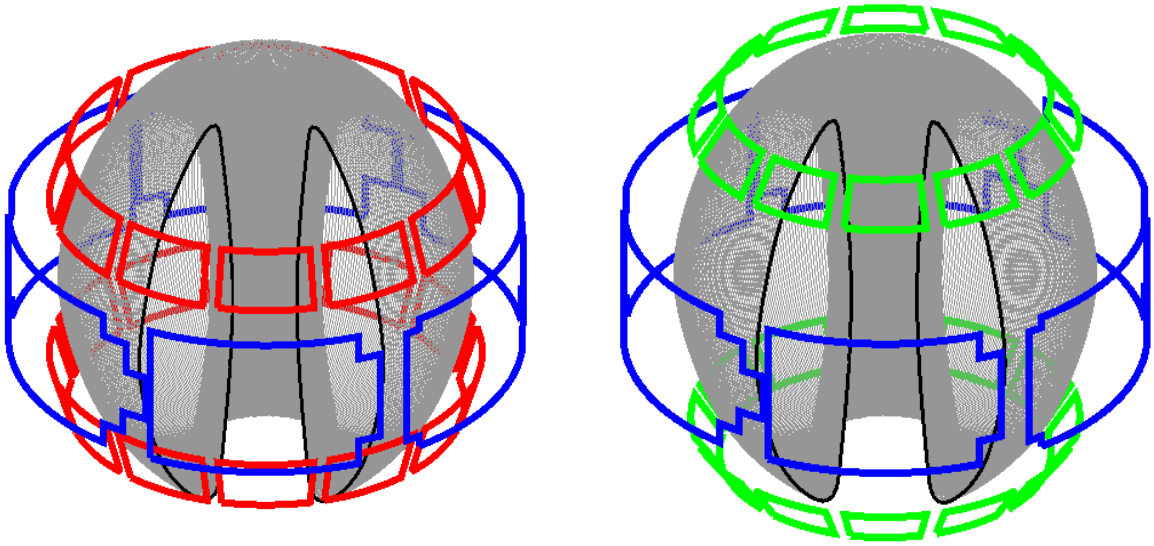

Figure 2.3.1.2-1: The proposed primary (left) and secondary (right) options for the NCC, shown in red (left) and green (right) date back to earlier proposals. Shown in blue are the existing midplane coils.

The physics design of the NCC has been developed over the past few years, and continues to develop as relevant physics understanding in the numerous physics research areas stated above expands. The present designs being considered address these physics topics (see Section 2.1.4) with an aim to maximize research flexibility and effectiveness, given engineering constraints on the coils. Further discussion of the preliminary engineering features of the NCC can be found in Section 10.5.1.2. The present design for the full NCC coil set is planned to have 24 individual coils in total, and our initial NCC design options were correspondingly focused on two sets, called primary and secondary passive plate NCC options, as shown in Figure 2.3.1.2-1 . Both options are two off-midplane rows of 12 coils toroidally, and would be able to generate high toroidal harmonic perturbations up to n = 6, and also up to n = 4 rotating fields. The capability of

3D field rotation is important to enable studies of the toroidal distribution of plasma response using a single toroidal array of diagnostics, such as reflectometry, soft X-ray, or real-time Thomson scattering. Also, these options will add a very different poloidal field spectrum for n = 1-6, compared to the previously limited field spectrum from the midplane coils, and therefore will enable us to better understand, confirm, and extend various unique and interesting physics that has been found in NSTX using only the midplane coil array. However, present physics analyses showed the primary option is superior to the secondary option in many aspects, largely due to its stronger coupling to important plasma modes [12], especially when the coils are operated separately. Therefore, in this section, and also in the remainder of the 5 year plan document, only the primary passive plate NCC option (in the front of the passive plates) will be described to illustrate the NCC utility.

As stated, the total number of the coils in the full NCC will be 24, but for budgetary reasons a staged approach is being considered, with a "partial" NCC set of 12 coils that can be installed in the mid-term of the present five year plan. The NCC design studies, however, will be continued for other full NCC options, including mixed configurations, different coil turns, power supply options, in the next 1~2 years, to achieve the most unique and capable set of 3D coils. The extended NCC design activities will include the most fundamental methods of coil design, based on comprehensive mapping between individual coils and physics advantages. One simple example is to use the coupling matrix $\ddot{C}$ between the 48 coils and the resonant fields at the rational surfaces, which are the critical physics quantities to govern resonant magnetic islands. Once the coupling matrix is developed using available analysis tools, such as the ideal perturbed equilibrium code (IPEC), the singular-value-decomposition (SVD) of the coupling matrix can be used to choose the best coil turns and positions, under constraints such as the total number of coils.

2.3.1.3 Staging of the NCC implementation

As the baseline budget plan does not allow the full implementation of the NCC with independent control of each coil, the performance of partial coil sets have been studied in the present physics design to determine configurations that address as much of the key physics as possible. Presently two partial NCCs options showing the greatest performance and research flexibility: one off-midplane row but with the full set of coils toroidally (named "12"), or two off-midplane rows of 6 coils toroidally (2×6) as shown in Figure 2.3.1.3-1. In these options, the upper and lower arrays are almost identical as NSTX-U plasmas will usually operate near an up-down symmetric configuration. The upper array can be slightly advantageous for the separation of the coils from future enhanced magnetic sensors, which will be largely added in the lower section to detect a higher amplitude of RWM modes near the divertor, and thus "12U", rather than "12L", will be mainly discussed. For the 2×6-coil option, the upper and lower coils can be positioned toroidally

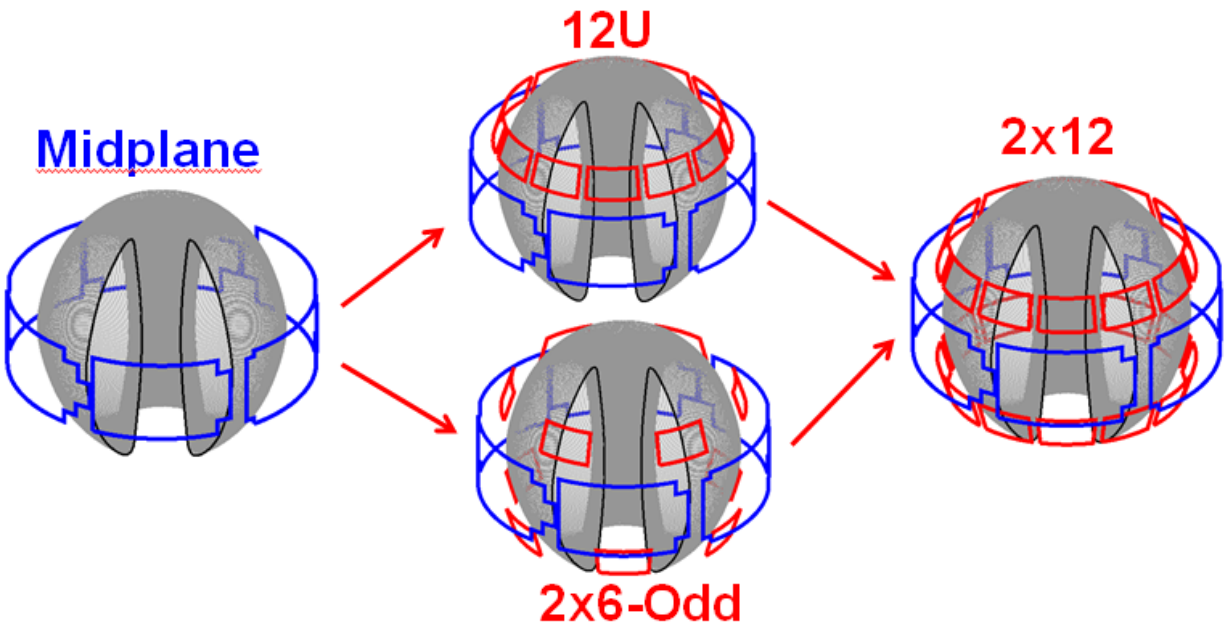

Figure 2.3.1.3-1. Present partial NCCs (12U and 2x6-Odd) and full NCC (2x12), compared to the existing midplane coils. Two partial NCC options will be compared for a staged installation before the full NCC.

in an up-down symmetric (even) or staggering/alternating (odd) configuration. With these options, the goal of design activities is to provide quantified assessment of physics on each as much as possible. As separately described earlier in Sections 2.2.1.5, 2.2.2.1, and 2.2.2.5, present quantitative comparisons of the design choices are based on defined figures-of-merit (FOMs)for each physics element as follows.

- Passive and active RWM control (Section 2.2.1.5):
  The NCC will be extremely useful for both passive and active RWM control. The controllability of toroidal rotation that will be enhanced by NCC will lead us to the best optimization of passive stabilization. Also the NCC will directly add available actuators for expanded physics studies and improve active RWM control. The enhancement of control capability is measured by the RWM FOM, $F_\beta = \beta_{active} / \beta_{no-wall}$, which quantifies the β-gain by the active control, and thus a high F_β value is favorable.

- Error field control (Thrust MS-2):
  Resonant error fields can directly drive mode locking, but non-resonant error fields can also influence locking or tearing, either indirectly by NTV braking of rotation or directly by field coupling. The ratio of the non-resonant error field to the resonant error field is therefore important, which can be quantified by the EF FOM, $F_{N-R} = T_{NTV} / \sum_{\psi_N<0.85} \delta B_{mn}^2$.

Here the non-resonant field effect is measured by the total NTV, and the resonant field effect is measured by the sum of the resonant fields at the rational surfaces, but the rational surfaces $\psi_N > 0.85$ are excluded as they represent the physics outside the pedestal. High F_{N-R} is good to drive the non-resonant field only, but a wide range of ΔF_{N-R} will also be good for related greater range of physics studies.

- Rotation control of NTV braking (Section 2.2.2.5):
  A fundamental motivation for the NCC can be found in rotation control. NSTX-U will uniquely operate in non-inductively driven plasmas and explore the high beta ST operational space. Sustaining this operational regime will require advanced stability control, as for instance disruptivity is not maximized at the highest β_N, or β_N/l_i in such operating space, and therefore will require greater rotation control. The local NTV control capability is measured by the NTV FOM, $F_{N-N} = T_{NTV}(\psi_N < 0.5) \big/ T_{NTV}(\psi_N < 1)$, which quantifies the NTV drive in the core with respect to the total. It is important to have variability of this quantity, and thus it is favorable to have a wide range of ΔF_{N-N}.

- ELM and particle control (Boundary Physics)
  ELM triggering in NSTX using the midplane coils, without clear particle density modification, illustrates the complexity of plasma response to 3D fields and raises concerns on ITER resonant magnetic perturbation (RMP) applications. As this ELM triggering is unique in NSTX, different 3D field applications using NCC in NSTX-U will be extremely beneficial to improve understanding of the mechanism behind ELM modification and particle control by 3D fields. It is not straightforward to quantify the figure of merit for RMP as its understanding is not mature, but the best empirical condition for RMP is the vacuum Chirikov overlap criterion. Also, it may be important to suppress the NTV drive when achieving the condition. This ability is measured by the RMP FOM, $F_{N-C} = (C_{vacuum}, \psi_{N=0.85})^4 \big/ T_{NTV}$,which quantifies the island-overlapping level and thus the degree of stochasticity in a unit NTV strength. The fourth power is needed to make the FOM independent of the applied field strength.

Using the NSTX-U target plasmas and defined FOMs, the up-to-date physics analyses are shown in Table 2.3.1.3, and can be summarized; (1) For the partial NCC options, the 2×6-Odd can provide better variability and gains for active RWM control, error field control, rotation control and ELM control, at most by an order of magnitude for FOMs, compared to existing midplane coils. (2) Full NCC options can provide another order-of-magnitude improvement for FOMs at most, especially for rotation control by high n flexibility, and can provide a significantly

increased capability to study 3D stability. Therefore, presently it has been concluded that the 2×6-Odd option is the best for the partial NCC implementation, and the full NCC will provide further important physics studies if incremental funding resources are available. The final assessment of the coil design will be made based on physics analysis conducted in the next 1~2 years.

Figures of Merit	Favorable values	MID	12U	2x6-Odd	2x12
EF (n=1), $F_{N-R} = \frac{T_{NTV}}{\sum_{\psi_N<0.85} \delta B_{mn}^2}$	High F_{N-R}	0.017	0.025	0.13	0.13
	Wide ΔF_{N-R}	1.00	1.00	5.65	5.65
NTV (n≥3), $F_{N-N} = \frac{T_{NTV}(\psi_N < 0.5)}{T_{NTV}(\psi_N < 1)}$	Wide ΔF_{N-N}	1.00	2.00	3.97	19.6
RMP (n≥3), $F_{N-C} = \frac{T_{NTV}}{(C_{vacuum}, \psi_{N=0.85})^4}$	High F_{N-C}	3.92	47.3	51.3	201.3
	Wide ΔF_{N-C}	1.00	10.5	22.1	252
RWM (n=1), $F_\beta = \frac{\beta_{active}}{\beta_{no-wall}}$	High F_β	1.25	1.54	1.61	1.70

Table 2.3.1.3: NCC performance comparison table, based on defined FOMs. Note here NCCs were used alone without the midplane coils except for the RWM analysis, in which the NCC and the midplane coils were considered.

2.4 Summary of theory and simulation capabilities

Code	*Description*	*Scope*	*Improvements*
DCON	Ideal MHD stability code	Ideal Kink stability analysis with and without the wall up to n=6	Resistive layer physics across rational surfaces (Resistive DCON)
DEGAS-2	Monte Carlo code to compute transport of neutral atoms	Calculation of neutral gas penetration through SOL	Include multiple gas species Use exact NSTX-U SOL conditions from UEDGE
EFIT	Equilibrium reconstruction code	Between-shots equilibrium reconstruction	Higher resolution, auto best level, new diagnostics
FORTEC-3D	Monte-Carlo drift-kinetic physics simulation code	Non-ambipolar transport and NTV physics in general geometry	Continued integration with IPEC and application to NSTX-U
IPEC/GPEC	Ideal and general perturbed equilibrium with 3D fields	Plasma response, locking, and NTV studies with 3D fields	General force balance equation including general jump conditions
M3D-C[1]	Implicit resistive and 2-fluid MHD code	Linear and nonlinear MHD stability	Neoclassical terms, resistive wall being added
MARS-K	Self-consistent kinetic stability calculation	Calculation of RWM stability and plasma response to perturbation	Inclusion of energy dependent collisionality for NTV calculation
MISK	Modifications to ideal stability by kinetic effects	Calculation of resistive wall mode stability	Improved model of energetic particle, anisotropy effects
NTVTOK	Shaing theory NTV computation including ion and electron effects	Calculation for comparison to experiment of NTV in all collisionality regimes	Continued implementation of NTV models, guided by experiment
POCA	δf guiding-center orbit code	Calculation of neoclassical transport, perturbed pressures and NTV	Improved numerical scheme to enhance computation speed
RWMSC	Resistive wall mode state-space controller computations	Generate control matrices for real-time controller, and offline physics studies	Generalization for partial actuator availability, $n > 1$ and multi-mode spectrum
VALEN	Models currents in structures with thin shell finite elements	RWM active feedback simulation, growth rate prediction with 3D walls	Multi-mode effects, study extra time delay in plasma model

Table 2.3: Summary table of the main codes used for theory-experiment comparison on NSTX-U.

2.4.1 EFIT

Accurate equilibrium reconstruction is necessary for experimental analysis as well as input to various other stability codes. In NSTX this capability has been provided automatically between-shots with EFIT [133,134] on two levels: with magnetics only (EFIT01) and with magnetics plus diamagnetic loop plus Thomson electron density and temperature (EFIT02). Additionally, higher levels of reconstruction can be achieved in post-run analysis by including a magnetic field pitch angle constraint from the motional Stark effect (MSE) diagnostic [135] (Section 10.6.1.4). Finally, use of the toroidal plasma rotation (from a charge exchange recombination spectroscopy (CHERS) measurement) is possible. This makes the pressure no longer a flux function, which complicates the reconstruction. Such reconstructions have been successfully generated for NSTX [7].

Plans for EFIT improvements for NSTX-U operation include the following: Higher time and spatial resolution is possible with computer improvements. A scheme for automatically detecting the level of diagnostics available and running up to the highest reconstruction level possible (ie with Thomson, or with Thomson plus MSE, etc…) is planned. Finally, new diagnostics that will be available, such as the motional Stark effect with laser-induced fluorescence (MSE-LIF) diagnostic (Section 10.6.1.5), which has the ability to measure both the magnetic field pitch angle, and the magnitude of the magnetic field, |B| [136], will be incorporated.

Finally, real-time motional Stark effect and Thomson scattering diagnostics are proposed for NSTX-U, and will be incorporated into real-time EFIT reconstructions. These systems are described in detail in Sections 10.6.3.1 and 10.6.3.2.

2.4.2 DCON

Ideal MHD stability is a critical for plasma operation, as the equilibrium states cannot be sustained or need other passive or active stabilizing mechanism if the stability condition is not satisfied. DCON is the fastest stability analysis code by investigating plasma potential energy only, and is also one of the most precise codes with adaptive radial grids. The DCON application to ideal stability will be continued in NSTX-U, and will be extended to higher toroidal harmonic numbers up to n = 6, consistent with the plan for high-n stability studies in NSTX-U.

DCON is an ideal code, but it also has been developed for application to resistive MHD stability analysis. The so-called resistive DCON has been successful for cylindrical geometry, and will be improved and tested for more general toroidal geometry. The resistive DCON code will be very useful to couple and study resistive wall mode and tearing mode physics together in NSTX-U.

2.4.3 IPEC / GPEC

The ideal perturbed equilibrium code (IPEC) has been successfully applied to study the basic feature of plasma responses to small 3D fields in tokamaks. The code utilizes the Euler-Lagrange equation in DCON to solve the ideal force balance and couples solutions to the external 3D field. Various external coils in different devices, NSTX-U, DIII-D, KSTAR, JET, ITER are implemented and IPEC results will be applied to study error field thresholds for locking, plasma response, and neoclassical toroidal viscosity. Recently calculations of neoclassical toroidal viscosity have been implemented into the IPEC code, based on the combined NTV formula without large-aspect-ratio approximation, which will enable us to study NTV more precisely in NSTX-U.

Although the ideal plasma responses are often dominant, non-ideal forces such as NTV torque can modify the 3D equilibrium itself. The general perturbed equilibrium code (GPEC) is under development to incorporate such non-ideal forces in a self-consistent way, as well as more generalized jump conditions across the rational surfaces beyond the ideal constraints. The GPEC code will be highly useful to study plasma responses to 3D fields especially in high-performance plasmas above the no-wall limit and also to investigate the interactions between 3D plasma responses and inner-layer activities when successfully developed.

2.4.4 MISK

The MISK, or Modification to Ideal Stability by Kinetic effects, code [67] calculates the change in potential energy of the plasma due to kinetic effects, δW_K. Along with the fluid δW terms calculated using a marginally stable eigenfunction with the PEST code [137], the dispersion relation or energy principle including kinetic effects is used to predict the growth rate of the resistive wall mode. This approach assumes that kinetic effects do not change the eigenfunction, and that the mode growth rate and frequency are small, so their nonlinear inclusion is unimportant. Cases which are above the ideal no-wall limit, and therefore would be unstable without kinetic effects, are examined. MISK has been used extensively (see Refs. [8,9,68,138,139]) and good agreement between the theory and experimental trends have been found.

MISK will be used in NSTX-U to predict RWM stability dependence on various parameters, such as rotation, the expected reduced collisionality, and the changed energetic particle distribution. Comparisons between experimental results and theoretical expectations will be made.

2.4.5 NTVTOK

The NTVTOK code [93] (NTV computation for TOKamaks) is a code that presently computes the full Shaing model of NTV, including both ions and electrons, across the full collisionality space as theoretically developed over the past decade [36-51], including the superbanana plateau regime. This formulation was used with high success in the initial quantitative comparisons of theory to experiment in NSTX [86] in an initial (unnamed) code, and has been significantly expanded in the NTVTOK incarnation. The code will be used in conjunction with experimental results on NSTX-U to address elements of NTV theory that seem to be disparate among present experimental data, and to test the theory in the important low collisionality regime of NSTX-U. As one example, the theory will be tested to quantitatively determine if NTV begins to decrease at further decreased ν^*, and if so, at what value of ν^* this occurs. The code will be continually developed as needed, to implement additional NTV physics models in the literature, and to correct the theory when experimental results show quantitative disagreement.

2.4.6 POCA

POCA (Particle Orbit Code for Anisotropic pressures) is a newly developed δf particle code to calculate neoclassical transport, perturbed pressures, and NTV in perturbed tokamaks using the δf Monte Carlo method [53]. Every kind of guiding-center motion is tracked by Hamiltonian orbit equations, and the Fokker-Planck equation is solved with a momentum-conserving pitch-angle scattering collision operator. POCA was successfully benchmarked with neoclassical theories, and verified $1/\nu$, $\nu\_\nu^{1/2}$, superbanana plateau regimes, and bounce-harmonic resonances in NTV transport. Good agreement between measured and modeled NTV torques were also obtained with magnetic braking experiments of DIII-D and NSTX [140]. POCA will be extensively used to predict and analyze the non-axisymmetric field effects on neoclassical transport in NSTX-U.

2.4.7 RWMSC

The RWMSC (resistive wall mode state-space controller) code performs the analysis required for both offline physics studies and online real-time RWM state-space control. The code (which continues to expand) presently serves two main roles: (i) it computes the needed input for the real-time controller based on a general implementation optimal control theory and the physics model described earlier, and determines the controller characteristics, most importantly, the controller stability, and (ii) it contains synthetic diagnostics that replicate the expected NSTX-U magnetic sensor measurements, for direct comparison with experiment. The physics model in RWMSC will be continually upgraded both before, and during NSTX-U operation. Simpler

upgrades include the addition of extra sensors, while more sophisticated upgrades include the addition of kinetic measurements to the model.

2.4.8 VALEN

The VALEN code simulates Resistive Wall Mode (RWM) behavior in the presence of 3-D models of conducting structures. The passive growth rate of such an instability is reduced by the interaction of the instability with electrical currents induced in the nearby conducting walls and other structures. The growth rate of the instability can also be altered by additional magnetic fields produced by electrical coils that provide negative feedback. In order to simulate such a problem VALEN models conducting structures, sensor coils, active control coils, power supplies, and a feedback logic in addition to the basic instability.

VALEN will be used in NSTX-U to provide system matrices for the state space controller. Multi-mode VALEN will investigate changes in the plasma mode spectrum due to coils and feedback, plasma wall interaction, and mode to mode interactions.

2.4.9 MARS-K

MARS-F/K (Magnetohydrodynamic resistive spectrum – Fluid/Kinetic code) is a toroidal MHD-kinetic hybrid stability code [141,142] that has been benchmarked with IPEC, MISK and HAGIS codes. The code solves the eigenvalue problem derived from the linearized single-fluid ideal/resistive MHD equations with toroidal flow, self-consistently including the drift kinetic effects in full toroidal geometry. The approach allows the kinetic effects associated with the thermal or energetic particles to consistently modify the mode eigenfunction, which could significantly influence the mode stability and structure in certain circumstances [143,144]. The code simulates a plasma surrounded by a pure vacuum region, includes a set of radially separated, toroidally complete resistive walls and a set of magnetic coils located in the vacuum region. With these features, MARS-F/K has been successfully applied to physical study and support of experiments on various subjects such as MHD instabilities (e.g. resistive wall mode and tearing mode), and plasma response to external fields (e.g. resonant filed amplification and resonant magnetic perturbation).

The MARS-K code has been modified to include the actual collisional frequency with energy dependence and will be used to study perturbed equilibria by including kinetic effects self-consistently. The upgraded MARS-K and the newly developed quasi-linear version MARS-Q will be applied to the calculation of self-consistent kinetic stability and neoclassical toroidal viscosity for NSTX-U plasmas.

2.4.10 M3D-C^1

The M3D-C^1 code [145,146] represents a complete rewrite of the older M3D 3D MHD code. It can be run as resistive MHD or two-fluid MHD, and also can be run as either 2-variable or 4-variable reduced MHD. The code is fully implicit using the split-implicit method and this enables it to take large time steps and run to long time. It uses high-order finite elements in 3 dimensions. These elements force the function and its first derivative to be continuous (C^1-Continuity). This property allows spatial derivatives up to 4th order to be treated when using the Galerkin method. This property is essential for an implicit formulation using the potential/stream function form of the velocity field and magnetic vector potential.

Current emphasis is on modeling sawteeth, snakes, ELMs, the seeding of NTMs, and the effect of rotation on stability, will be applied, as appropriate, to NSTX-U. Future work directly applicable to NSTX-U will be to treat NTMs including neoclassical effects, and to include a resistive wall.

2.4.11 DEGAS-2

DEGAS-2 [107, 108,147] uses Monte Carlo techniques to compute transport of neutral atoms and molecules in the vicinity of material surfaces; general three-dimensional devices can be modeled.

Neutral transport in fusion devices is computed using a Monte Carlo technique in general three-dimensional geometries. DEGAS-2 has been designed as a state-of-the-art code featuring optimized geometry / tracking, dynamic memory allocation, and built-in parallel processing. General methods for handling atomic and surface physics data have been developed to make physics modifications easy. Linear and nonlinear neutral elastic scattering processes have been included. The code is designed to be run in a coupled fashion with fluid plasma codes, as well as in a stand-alone mode. It is intended to be portable with thorough documentation.

DEGAS [148] is the predecessor to DEGAS-2. It uses the pseudo-collision algorithm for scoring, as opposed to the track-length estimator in DEGAS-2. The former works better in a dense plasma; the latter in a vacuum. Unlike DEGAS-2, the surface and atomic physics interactions are hard-wired into the code and are difficult to modify.

DEGAS-2 has been verified against multiple analytic and semi-analytic models. It has been thoroughly compared with original DEGAS and EIRENE, and comprehensively validated against NSTX gas puff imaging experiments.

In NSTX-U, DEGAS-2 will be used extensively for MGI studies, as outlined in detail in Section 2.2.3.3.2.

2.4.12 FORTEC-3D

FORTEC-3D [149-151] is a global Monte-Carlo simulation code, developed to study drift-kinetic physics in fusion devices without any approximation and without any limitation for the geometry. The code can perform the highest level of computations for neoclassical physics, including 3D fields, although the computational cost is quite demanding as it follows 10^7-10^8 particles through the entire region of the plasma. The collision operators are also advanced including energy scattering operator, which may also be important for extremely low collisionality plasmas and non-Maxwellian particles.

The FORTEC-3D code has been extensively benchmarked with other computations and theories. The GAM and basic 3D neoclassical properties have been successfully verified against the GT5D code, which is a gyro-kinetic continuum code in real geometry, for the LHD configuration [118]. Then it has been applied to study non-ambipolar transport in the LHD and in the large-aspect ratio tokamak geometry, and indeed showed almost all essential non-ambipolar transport physics, such as the quadratic δB dependency, $1/\nu$ behavior, superbanana plateau, and neoclassical offset, for the first time by simulation [119]. The actual NTV profiles have been also successfully compared with the combined NTV theory [120], indicating the precision of both methods.

The code is maintained at a different institution, NIFS, but the strong collaboration between PPPL theory and NIFS computation division will be continued. Recently, IPEC inputs were transformed into VMEC-Boozer type data, to enable FORTEC-3D to perform actual NTV calculations in tokamaks. The IPEC coupling to FORTEC-3D will be utilized to investigate NCC capabilities in NSTX-U, by selecting a few limited cases.

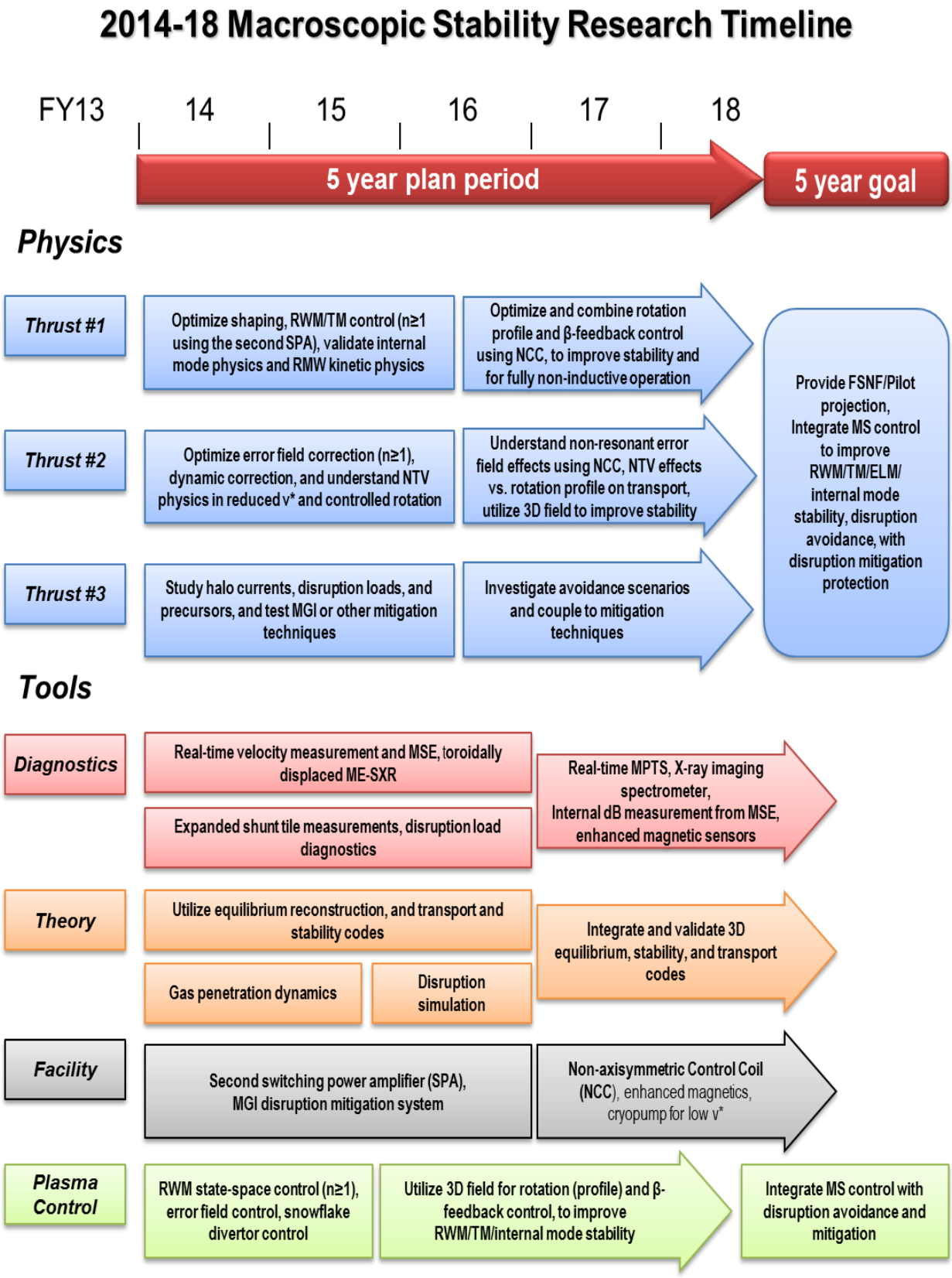
2014-18 Macroscopic Stability Research Timeline
FY13
14
15
16
17
18
5 year plan period
5 year goal
Physics
Thrust #1
Optimize shaping, RWM/TM control (n≥1 using the second SPA), validate internal mode physics and RMW kinetic physics
Optimize and combine rotation profile and β-feedback control using NCC, to improve stability and for fully non-inductive operation
Thrust #2
Optimize error field correction (n≥1), dynamic correction, and understand NTV physics in reduced v* and controlled rotation
Understand non-resonant error field effects using NCC, NTV effects vs. rotation profile on transport, utilize 3D field to improve stability
Thrust #3
Study halo currents, disruption loads, and precursors, and test MGI or other mitigation techniques
Investigate avoidance scenarios and couple to mitigation techniques
Provide FSNF/Pilot projection, Integrate MS control to improve RWM/TM/ELM/ internal mode stability, disruption avoidance, with disruption mitigation protection
Tools
Diagnostics
Real-time velocity measurement and MSE, toroidally displaced ME-SXR
Expanded shunt tile measurements, disruption load diagnostics
Real-time MPTS, X-ray imaging spectrometer, Internal dB measurement from MSE, enhanced magnetic sensors
Theory
Utilize equilibrium reconstruction, and transport and stability codes
Gas penetration dynamics
Disruption simulation
Integrate and validate 3D equilibrium, stability, and transport codes
Facility
Second switching power amplifier (SPA), MGI disruption mitigation system
Non-axisymmetric Control Coil (NCC), enhanced magnetics, cryopump for low v*
Plasma Control
RWM state-space control (n≥1), error field control, snowflake divertor control
Utilize 3D field for rotation (profile) and β-feedback control, to improve RWM/TM/internal mode stability
Integrate MS control with disruption avoidance and mitigation

References

[1] Y.K.-M Peng, et al., Fusion Sci. Technol. **60** (2011) 441.
[2] Y.K.-M Peng, et al., Fusion Sci. Technol. **56** (2009) 957.
[3] Y.K.-M Peng, et al., Plasma Phys. Control. Fusion **47** (2005) B263.
[4] J.E. Menard, et al., Nucl. Fusion **51** (2011) 103014.
[5] F. Najmabadi, et al., Fusion Engineering and Design **65** (2003) 143.
[6] H.R. Wilson, et al., Nucl. Fusion **44** (2004) 917.
[7] S.A. Sabbagh, et al., Nucl. Fusion **46** (2006) 635.
[8] J.W. Berkery, et al., Phys. Rev. Lett. **104** (2010) 035003.
[9] S.A. Sabbagh, et al., Nucl. Fusion **50** (2010) 025020.
[10] S.A. Sabbagh, et al., Phys. Rev. Lett. **97** (2006) 045004.
[11] S.A. Sabbagh, et al., "Resistive Wall Mode Stabilization and Plasma Rotation Damping Considerations for Maintaining High Beta Plasma Discharges in NSTX", *23rd IAEA Fusion Energy Conference*, Daejeon, Republic of Korea, 11-16 October 2010, paper EXS/5-5.
[12] J.-K. Park, et al., Phys. Rev. Lett. **99** (2007) 195003.
[13] S. P. Gerhardt, J. E. Menard, J.-K. Park, et al., Nucl. Fusion **49** (2009) 032003.
[14] R. Hazeltine, et al., "Research Needs for Magnetic Fusion Sciences – Report of the Research Needs Workshop (ReNeW), June 8-12, 2009, USDOE Office of Fusion Energy Sciences."
[15] R. Fitzpatrick and T. C. Hender, Phys. Fluids B 3 (1991) 644.
[16] T. C. Hender, R. Fitzpatrick, A. W. Morris, et al., Nucl. Fusion **32** (1992) 2091.
[17] R. J. La Haye, R. Fitzpatrick, and T. C. Hender, et al., Phys. Fluids **B** 4 (1992) 2098.
[18] J.-K. Park, et al., Phys. Rev. Lett. **102** (2009) 065002.
[19] T.E. Evans et al., Phys. Rev. Lett. **92** (2004) 235003.
[20] J.M. Canik et al., Phys. Rev. Lett. **104** (2010) 045001.
[21] O. Sauter, et al., Phys. Plasmas **4** (1997) 1654.
[22] C. C. Hegna, Phys. Plasmas **6** (1999) 3980.
[23] J.E. Menard, et al., Nucl. Fusion **50** (2010) 045008.
[24] J.-K. Park, et al., Phys. Plasmas. **16** (2009) 056115.
[25] J.E. Menard, et al., ITER Task Agreement #C19TD22FU, "The study of the error fields using Ideal Perturbed Equilibrium Code (IPEC)" (2010).
[26] S.P. Gerhardt, et al., Plasma Phys. Contr. F. **52** (2010) 104003.
[27] J.-K. Park, et al., Nucl. Fusion **52** (2012) 023004.
[28] R. J. Buttery, A. H. Boozer, Y. Q. Liu, J.-K. Park, et. al., Phys. Plasmas **19** (2012) 056111.
[29] A. J. Cole, C. C. Hegna, J. D. Callen, Phys. Rev. Lett. **99** (2007) 065001.
[30] R. Fitzpatrick, Nucl. Fusion **7** (1993) 1049.
[31] R. Fitzpatrick, Phys. Plasmas **8** (2001) 2760.
[32] A. J. Cole and R. Fitzpatrick, Phys. Plasmas **13** (2006) 032503.
[33] R. Fitzpatrick, Phys. Plasmas **17** (2010) 112502.
[34] R. Fitzpatrick, Plasma Phys. Control. Fusion **54** (2012) 094002.
[35] R. J. La Haye, Phys. Plasmas **13** (2006) 055501.
[36] K.C. Shaing, Phys. Plasmas **10** (2003) 1443.

[37] K.C. Shaing, Phys. Plasmas **13** (2006) 052505.
[38] K.C. Shaing, Phys. Plasmas **14** (2007) 049903.
[39] K.C. Shaing, P. Cahyna, M. Becoulet, et al., Phys. Plasmas **15** (2008) 082506.
[40] K.C. Shaing, S.A. Sabbagh, and M. Peng, Phys. Plasmas **14** (2007) 024501.
[41] K.C. Shaing, S.A. Sabbagh, M.S. Chu, et al., Phys. Plasmas **15** (2008) 082505.
[42] K.C. Shaing, Plasma Phys. Control. Fusion **52** (2010) 072001.
[43] K.C. Shaing, S.A. Sabbagh, and M.S. Chu, Plasma Phys. Control. Fusion **51** (2009) 035004.
[44] K.C. Shaing, S.A. Sabbagh, and M.S. Chu, Plasma Phys. Control. Fusion **51** (2009) 055003.
[45] K.C. Shaing, M.S. Chu, and S.A. Sabbagh, Plasma Phys. Control. Fusion **51** (2009) 075015.
[46] K.C. Shaing, J. Seol, Y.W. Sun, et al., Nucl. Fusion **50** (2010) 125008.
[47] K.C. Shaing, S.A. Sabbagh, and M.S. Chu, Nucl. Fusion **50** (2010) 025022.
[48] K C. Shaing, M.S. Chu, and S.A. Sabbagh, Plasma Phys. Control. Fusion **52** (2010) 025005.
[49] K.C. Shaing, M.S. Chu, and S.A. Sabbagh, Nucl. Fusion **50** (2010) 125012.
[50] K.C. Shaing, T.H. Tsai, M.S. Chu, et al., Nucl. Fusion **51** (2011) 073043.
[51] K.C. Shaing, M.S. Chu, C.T. Hsu, et al., Plasma Phys. Control. Fusion **54** (2012) 124033.
[52] S. Satake, J.-K. Park, et al., Phys. Rev. Lett. **107** (2011) 055001.
[53] K. Kim, J.-K. Park, A. H. Boozer, G. Kramer, Phys. Plasmas **19** (2012) 082503.
[54] K. Kim, J.-K. Park, A. H. Boozer, accepted for publication in Phys. Rev. Lett. (2013).
[55] S.A. Sabbagh, et al., Nucl. Fusion **44** (2004) 560.
[56] W. Zhu, S.A. Sabbagh, R. Bell, et al., Phys. Rev. Lett. **96** (2006) 225002.
[57] A. M. Garofalo et al., Phys. Plasmas **16** (2009) 056119.
[58] A. J. Cole et al., Phys. Rev. Lett. **106** (2011) 225002.
[59] S.A. Sabbagh, Y.S. Park, Y.M. Jeon, et al., *"Initial KSTAR Stability and Rotation Alteration Results for High Normalized Beta Plasmas Near or Exceeding the Ideal MHD No-wall Stability Limit"*, 23rd KSTAR conference, Buyeo, South Korea (2013).
[60] J.-K. Park, Y. M. Jeon, the 23rd KSTAR conference, Buyeo, South Korea (2013).
[61] V.A. Soukhanovskii, et al., Nucl. Fusion **51** (2011) 012001.
[62] S.P. Gerhardt, et al., Nucl. Fusion **51** (2011) 073031.
[63] J.W. Berkery, et al., Phys. Rev. Lett. **106** (2011) 075004.
[64] H. Reimerdes, et al., Phys. Rev. Lett. **93** (2004) 135002.
[65] J.W. Berkery, et al., Proc. 24th Int. Conf. on Fusion Energy (San Diego, USA, 2012) (Vienna: IAEA) paper EX/P8-07.
[66] J.W. Berkery, et al., Phys. Plasmas **17** (2010) 082504.
[67] B. Hu, et al., Phys. Plasmas **12** (2005) 057301.
[68] H. Reimerdes, et al., Phys. Rev. Lett. **106** (2011) 215002.
[69] S.A. Sabbagh, et al., Nucl. Fusion **44** (2004) 560.
[70] S.A. Sabbagh, et al., submitted to Phys. Rev. Lett.
[71] T.H.S. Abdelaziz and M. Valasek, Proc 16th IFAC World Congress, Prague (2005).
[72] O. Katsuro-Hopkins, et al., Nucl. Fusion **47** (2007) 1157.
[73] J.M. Bialek et al., Phys. Plasmas **8**, 2170 (2001).
[74] A.H. Boozer, Phys. Plasmas **6**, 3180 (1999).
[75] R. J. Buttery, T. C. Hender, D. F. Howell, et al., Nucl. Fusion **41** (2001) 985.
[76] A. H. Glasser, J. M. Greene, and J. L. Johnson, Phys. Fluids **18** (1975) 875.

[77] H. R. Wilson, J. W. Connor, R. J. Hastie, and C. C. Hegna, Phys. Plasmas **3** (1996) 248.
[78] S.A. Sabbagh, A.C. Sontag, J.M Bialek, et al., Nucl. Fusion **46** (2006) 635.
[79] J.-K. Park, et al., Nucl. Fusion **51** (2011) 023003.
[80] K.C. Shaing, S.P. Hirschman, and J.D. Callen, Phys. Fluids **29** (1986) 521.
[81] K.C. Shaing, *Phys. Rev. Lett.*, **87** (2001) 245003.
[82] K.C. Shaing, T.H. Tsai, M.S. Chu, et al., Nucl. Fusion **51** (2011) 073043.
[83] S.A. Sabbagh, J.M. Bialek, R.E. Bell, et al., Nucl. Fusion **44** (2004) 560.
[84] S.A. Sabbagh, J.W. Berkery, R.E. Bell, et al., Nucl. Fusion **50** (2010) 025020.
[85] S.A. Sabbagh, *et al.*, "Resistive Wall Mode Stabilization and Plasma Rotation Damping Considerations for Maintaining High Beta Plasma Discharges in NSTX", *23rd IAEA Fusion Energy Conference*, Daejeon, Republic of Korea, 11-16 October 2010, paper EXS/5-5.
[86] W. Zhu, S.A. Sabbagh, R. Bell, et al., Phys. Rev. Lett. **96** (2006) 225002.
[87] A. J. Cole, J.D, Callen, W.M. Solomon, et al., Phys. Rev. Lett. **106** (2011) 225002.
[88] J.-K. Park, Phys. Plasmas **18** (2011) 110702
[89] S.A. Sabbagh, J.W. Berkery, R.E. Bell, *et al.*, Nucl. Fusion **50** (2010) 025020.
[90] M.-D. Hua, et al., Plasma Phys. Control. Fusion **52** (2010) 035009.
[91] A.M. Garofalo, et al., Phys. Rev. Lett. **101** (2008) 195005.
[92] Y. Sun, et al., Plasma Phys. Control. Fusion **52** (2010) 105007.
[93] Y. Sun, Y. Liang, K.C. Shaing, et al., Nucl. Fusion **51** (2011) 053015.
[94] H. Reimerdes, et al., Nucl. Fusion **45** (2005) 368.
[95] S.P. Gerhardt, et al., "Disruptions, Disruptivity, and Safer Operating Windows in the High-β Spherical Torus NSTX", submitted to Nuclear Fusion (2012).
[96] D.G. Whyte, et al., J. Nucl. Mater. **363-365** (2007) 1160
[97] G. Pautasso, et al., Plasma Phys. Contr. F. **51** (2009) 124056.
[98] E.M. Hollmann, et al., Phys. Plasmas **17** (2010) 056117.
[99] D.G. Whyte, et al., Fusion Sci. Technol. **48** (2005) 954.
[100] C. Reux, et al., Nucl. Fusion **50** (2010) 095006.
[101] P. Lang et al., Phys. Rev. Lett. **79** (1997) 1487.
[102] R. Maingi et al., Plasma Phys. Contr. F. **46** (2004) A305.
[103] V. Kotov, et al., "Numerical study of the ITER divertor plasma with the B2-EIRENE code package," Bericht des Forschungszentrums Julich, Jul-4257, November (2007)
[104] S.L. Allen, Rev. Sci. Instrum. **68** (1997) 1261.
[105] A.S. Kukushkin, et al., Nucl. Fusion, **47** (2007) 698.
[106] D.L. Rudakov, et al., Nucl. Fusion, **45** (2005) 1589.
[107] D.P. Stotler and C.F.F. Karney, Contrib. Plasm. Phys. **34** (1994) 392.
[108] D.P. Stotler, et al., J. Nucl. Mater., **363-365** (2007) 686.
[109] V.A. Izzo, et al., Phys. Plasmas, **15** (2008) 056109.
[110] T.D. Rognlien, et al., Contrib. Plasm. Phys. **34** (1994) 362.
[111] T.D. Rognlien, et al., J. Nucl. Mater. **266-269** (1999) 654.
[112] D.P. Stotler, et al., Contrib. Plasm. Phys. **50** (2010) 368.
[113] T.C. Hender, et al., Nucl. Fusion **47** (2007) S128.
[114] T.K. Gray, et al., J. Nucl. Mater. **415** (2011) S360.
[115] V. Riccardo, et al., Nucl. Fusion **45** (2005) 1427.

[116] E. Hollmann, private communication.
[117] A.H. Boozer, Phys. Plasmas **19** (2012) 058101.
[118] D.A. Humphreys and A. G. Kellman, Phys. Plasmas **6** (1999) 2742.
[119] L.E. Zakharov, Phys. Plasmas **15** (2008) 062507.
[120] L.E. Zakharov, et al., Phys. Plasmas **19** (2012) 055703.
[121] S.P. Gerhardt, et al., Rev. Sci. Instrum. **82** (2011) 103202.
[122] S.P. Gerhardt, et al., Nucl. Fusion **52** (2012) 063005.
[123] S.P. Gerhardt, et al., Nucl. Fusion **53** (2013) 023005.
[124] L.E. Zakharov, et al., Phys. Plasmas **19** (2012) 055703.
[125] G. Counsell, et al., Plasma. Phys. Contr. F. **49** (2007) 435.
[126] J. Breslau, et al., "MHD Calculation of halo currents and vessel forces in NSTX VDEs", paper PP8.00017, APS-DPP, Providence, RI (2012).
[127] S.P. Gerhardt, et al., Nuclear Fusion **52** (2012) 083020.
[128] T.E. Evans et al., Phys. Rev. Lett. **92** (2004) 235003.
[129] Y. Liang et al., Phys. Rev. Lett. **98** (2007) 265004.
[130] W. Suttrop et al., Phys. Rev. Lett. **106** (2011) 225004.
[131] Y.M. Jeon, J.-K. Park et al, Phys. Rev. Lett. **109** (2012) 035004.
[132] A. Kirk, J. Harrison, Y. Liu et al., Phys. Rev. Lett. **108** (2012) 255003.
[133] L.L. Lao, et al., Fusion Sci. Tech. **48** (2005) 968.
[134] S.A. Sabbagh, et al., Nucl. Fusion **41** (2001) 1601.
[135] F. Levinton, et al., Rev. Sci. Inst. **70** (1999) 810.
[136] E.L. Foley, et al., Rev. Sci. Inst. **79** (2008) 10F521.
[137] R. Grimm, J. Greene, and J. Johnson, "Methods in Computational Physics, Vol. 16," (Academic Press, New York, 1976) Chap. Computation of the Magnetohydrodynamic Spectrum in Axisymmetric Toroidal Confinement Systems, pp. 253-280.
[138] H. Reimerdes, et al., Phys. Rev. Lett. **106** (2011) 215002.
[139] J.W. Berkery, et al., Phys. Plasmas **18** (2011) 072501.
[140] K. Kim, et al., "Study of neoclassical toroidal viscosity in tokamaks with a δf particle code and resonant nature of magnetic braking," Proc. 24th Int. Conf. on Fusion Energy (San Diego, USA, 2012) (Vienna: IAEA) paper TH/P2-27.
[141] Y.Q. Liu, et al., Phys. Plasmas **15** (2008) 112503.
[142] Y.Q. Liu, et al., Plasma Phys. Control. Fusion **52** (2010) 104002.
[143] J.E. Menard, et al. "The role of rotation and kinetic damping in high-beta ST plasma stability", Proc. 39th EPS Conf. 2012, P1.061
[144] Z.R. Wang, et al., Phys. Plasmas **19** (2012) 072518.
[145] N.M. Ferraro, et al., Phys. Plasmas **17** (2010) 102508.
[146] N.M. Ferraro, et al., Phys. Plasmas **19** (2012) 056105.
[147] D.P. Stotler and B. LaBombard, J. Nucl. Mater. **337-339** (2005) 510.
[148] D. Heifetz, et al., J. Comp. Phys. **46** (1982) 309.
[149] S. Satake, R. Kanno, and H. Sugama, Plasma and Fusion Research **3** (2008) S1062.
[150] S. Satake, H. Sugama, R. Kanno, and J.-K. Park, Plasma Phys. Control. Fusion **53** (2011) 054128.
[151] S. Satake, J.-K. Park, H. Sugama, and R. Kanno, Phys. Rev. Lett. **107** (2011) 055001.

Table of Contents for Chapter 3

Chapter 3

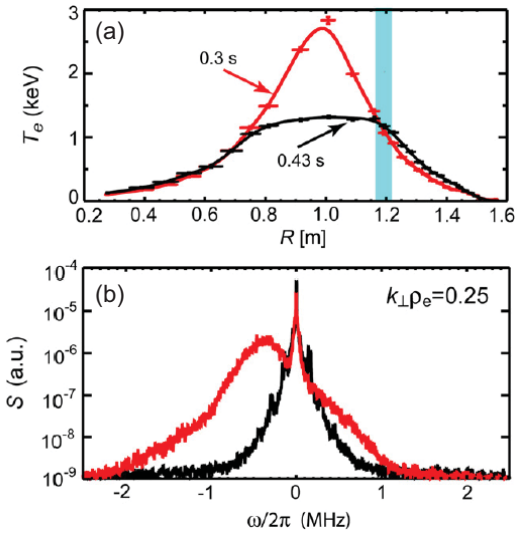

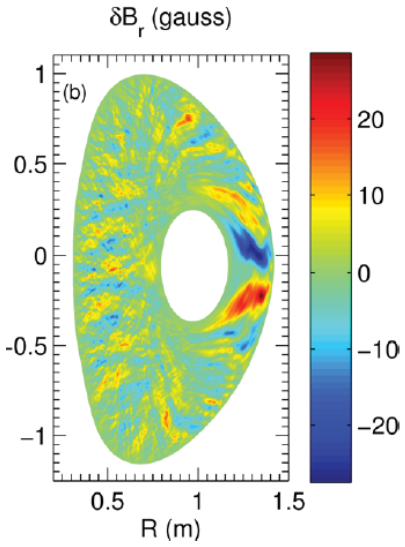

Research Goals and Plans for Transport and Turbulence

3.1 Introduction

The long-term goal of NSTX and NSTX-U transport and turbulence research is to achieve the capability of predicting and optimizing the confinement performance of future fusion devices, e.g. ST-FNSF [1] and ITER. Considerable achievements have been made toward this goal during the operation of NSTX. Built on the success of NSTX, NSTX-U will have much improved capabilities and aims to deliver substantial advances toward the goal. In order to guide the detailed planning of NSTX-U Transport and Turbulence research, three research thrusts are proposed: 1. characterize H-mode global energy confinement scaling in the lower collisionality regime of NSTX-U; 2. identify regime of validity for instabilities responsible for anomalous electron thermal, momentum, and particle/impurity transport in NSTX-U; 3. establish and validate reduced transport models (0D and 1D). The research thrusts and associated research plans will support all of the 5 high-level 5 year plan research goals presented in Chapter 1.

NSTX has distinguished itself as a unique experimental platform for studying transport and turbulence in toroidal confinement devices. The observed neoclassical-level ion thermal transport observed in most NSTX H-mode plasmas is consistent with the suppression of low-k (ion-scale) turbulence resulting from the high beta, low aspect ratio ($\gtrsim$1.3), naturally shaped equilibria of NSTX, and also from the large E×B shear driven by neutral beam injection (NBI), as supported by experiments and modeling [2,3]. On the other hand, the anomalous electron thermal transport determines the confinement properties of NSTX. The NSTX H-mode energy confinement has been shown to have strong inverse dependence on collisionality ($B\tau_E \sim 1/\nu^*_e$) with and without lithium wall coating [4,5], a trend consistent with that on MAST [6]. This strong collisionality dependence is dramatically different from the ITER98y,2 scaling ($B\tau_E \sim$ independent of ν^*_e) [7] and is favorable for next generation STs operating in low collisionality regime. The change in anomalous electron thermal transport is found to be responsible for this.

Several mechanisms have been identified as potential candidates for anomalous electron thermal transport in different operational scenarios at different spatial regions, which are listed in Table 3.1.1. These include ion scale (low k_θ) drift wave instabilities such as ion temperature gradient (ITG) [8], trapped electron mode (TEM) [9], kinetic ballooning mode (KBM) [10], and microtearing (MT) [11]; electron scale (high k_θ) electron temperature gradient (ETG) drift waves [12]; and energetic-particle-driven global and compressional Alfven eigenmodes (GAE and CAE) [13].

Transport Mechanism		**Transport channel affected**			
		ion energy	electron energy	particle/ impurity	momentum
Drift waves	ITG (low k_θ)	×	×	×	×
	TEM (low k_θ)	×	×	×	×
	KBM (low k_θ)	×	×	×	×
	MT (low k_θ)		×		
	ETG (high k_θ)		×		
Neoclassical		×		×	
Energetic particle (GAE/CAE)			×		

Table 3.1.1: Transport mechanisms expected to be important in NSTX and NSTX-U plasmas and the corresponding transport channels affected. The drift wave instabilities include ion temperature gradient (ITG), trapped electron mode (TEM), kinetic ballooning mode (KBM), microtearing (MT), and electron temperature gradient (ETG). The energetic particle instabilities include global Alfven eigenmodes (GAE) and compressional Alfven eigenmodes (CAE).

It can be seen in Table 3.1.1 that in addition to thermal transport, low-k turbulence can influence other transport channels. While neoclassical physics has been shown to capture the gross features of NSTX impurity profiles in many H-mode plasmas, there is evidence of anomalous convective contributions in some discharges [14,15]. Momentum transport is also usually anomalous

despite ion thermal transport in H-mode plasmas being very close to neoclassical levels [2]. These instances of anomalous impurity and momentum transport suggest that some residual level of low-k turbulence may be important even in the presence of relatively large E×B shear.

These theoretical mechanisms often depend distinctly on various plasma parameters which determine when they will be important. One such parameter which NSTX uniquely has the ability to vary over a significant range is the plasma β. For example, as will be discussed later, ETG modes are found to be important in the internal transport barrier (ITB) in low β reversed shear plasmas [16,17], ETG and ITG modes in low β NBI-heated L-mode [3] and H-mode [18] plasmas. On the other hand, microtearing and KBM are important in high β H-mode plasmas [19-21], while GAE/CAE instabilities occur near the magnetic axis of high power NBI H-mode plasmas that exhibit large fast ion beta [13].

In addition to plasma β the various modes also respond differently to changes in collision frequency. All of the ion scale ballooning modes (ITG, TEM, KBM) tend to be stabilized by increasing collisionality, while ETG is insensitive to collisionality and microtearing is often more unstable at higher collisionality. Using these unique parametric dependencies should help clarify the regimes of validity for the different mechanisms responsible for electron thermal transport. This is one of most important transport issues for NSTX and NSTX-U in order to achieve the predictive capability for electron temperature for future ST-FNSF and ITER.

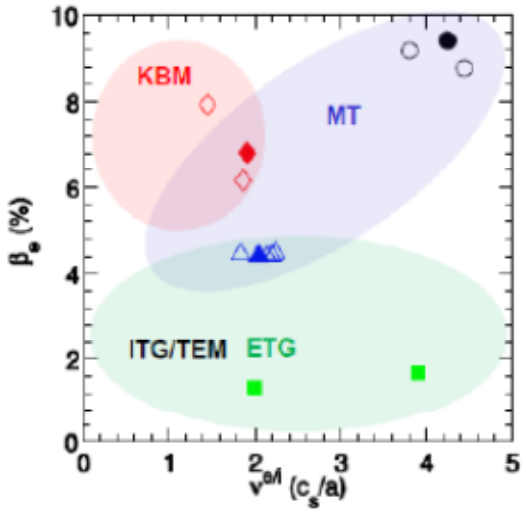

Fig. 3.1.1 Local values of β_e and $\nu^{e/i}$ (r/a=0.6-0.7) for various NSTX H-mode discharges. The colored regions illustrate where various microinstabilities are generally predicted to occur. $\nu^{e/i}$ is the electron-ion collision frequency.

The diversity of drift wave mechanisms and in what instances they are predicted to be unstable is illustrated in Fig. 3.1.1. The symbols indicate values of electron β and collisionality evaluated at

r/a=0.6-0.7 for a number of NSTX discharges while the color shaded regions indicate the dominant unstable mode predicted (using gyrokinetic simulations as will be discussed later in the chapter). Having the ability to access such a broad range of β will allow NSTX-U to study the importance of finite beta electromagnetic effects on transport and confinement which is important for future devices including ITER.

NSTX-U [22] compared to NSTX will have enhanced capabilities that will make it possible to address the above transport issues in parameter regimes more relevant to future devices. The increase in plasma current, toroidal field and heating power is expected to improve confinement, naturally leading to higher temperatures and reduced collisionality. However, the influence of the different mechanisms will themselves vary as discussed above, leading to the inherent limit in confinement improvement and collisionality reduction. The installation of the cryopump during the five year period will provide additional operational flexibility to manipulate collisionality through density control to better isolate its effects on energy confinement and the various transport mechanisms.

In addition to the expanded achievable variation in collisionality, the NCC coils (see Sec. 2.2.2.2.5) will also allow for a broader manipulation of toroidal flow profiles and corresponding E×B shear flow to study its impact on the various transport mechanisms. Although a complex function of collisionality and toroidal flow, the NTV torque applied from the NCC coils is predicted to be nearly as large as that injected from the neutral beams. Furthermore, the radial profile of NTV torque density can be varied with the flexibility of the NCC coils (see Fig. 2.2.2.2.5-2). In addition, the additional neutral beams will inject energy and torque at different tangency radii (Fig. 9.12). Altogether, the flexibility to inject torque and apply flow damping at different locations with different strengths will provide greatly expanded ability to vary flow profile and to test the influence of flow shear suppression on turbulent transport.

Building on the knowledge gained from NSTX, the NSTX-U transport and turbulence research will focus on characterizing/validating H-mode global energy confinement scaling in the lower collisionality regime, identifying the regime of validity of instabilities responsible for anomalous electron thermal, momentum and particle/impurity transport, and also on establishing and validating 0D/1D reduced transport models which are essential to the goal of projecting and optimizing the performance of future devices. In particular, being able to achieve a factor 3-6 decrease in collisionality while at high beta is one of the most important enhancements of NSTX-U compared to NSTX, allowing the access to the upper limit of collisionality of future ST-FNSF. This reduction in collisionality not only provides a unique opportunity to assess the validity of the observed ST confinement scaling on collisionality and to possibly establish a new 0D confinement scaling, but it also provides opportunities to test and improve existing 1D reduced models and to formulate new reduced models in this new regime of NSTX-U and to

extrapolate to future devices. The improvement in accessible parameter regimes also makes it possible to obtain new turbulence measurements and to isolate/determine the regime of validity of the candidate instabilities in driving anomalous transport. The planned enhanced beam emission spectroscopy (BES) diagnostic ([23] and see Sec. 10.6.2.2 and Sec. 11.2.26), a new FIR high-k_θ scattering system ([24] and see Sec. 10.6.2.1 and Sec. 11.2.19), improved reflectometry (see Sec. 10.6.5.2) and polarimetry ([25] and see Sec. 10.6.2.3 and Sec. 11.2.21) diagnostics, coupled with facility enhancements of NSTX-U, will allow new turbulence and steady-state/perturbative transport measurements in a wide range of plasma conditions.

The new experimental opportunities on NSTX-U will couple to turbulence theories and reduced and first principle models in order to identify observed turbulence, to assess its parametric dependence and to identify its operational regime. The new transport and turbulence measurements in the extended parameter region of NSTX-U will naturally challenge existing theories and models and will help extending them to the new regimes and to incorporate new physics, e.g. all aspect ratio, large ExB flow shear, large magnetic shear, fully electromagnetic effects at high beta and multi-scale and global capabilities. For example, comparisons with polarimetry measurements, measured turbulence spreading, e.g. from BES, and coexistence of low-k and high-k turbulence (e.g. from BES and the FIR high-k_θ scattering system) will require electromagnetic effects, global and/or multi-scale capabilities in existing or new numerical codes. This will present a great challenge to computational resources but, on the other hand, will offer new opportunities for validating codes and improving numerical algorithms. Furthermore, as turbulence measurements become more sophisticated in NSTX-U, comparisons with numerical calculations will not be limited to transport levels but will extend to quantitative local/line-integrated multi-field fluctuation levels and fluctuation wavenumber/frequency spectra by utilizing dedicated synthetic diagnostics.

In summary, with the enhanced capabilities of NSTX-U, the planned transport and turbulence research on NSTX-U will be able to address the following important transport questions:
1. Is the ST H-mode global energy confinement scaling still valid in the low collisionality regime achievable by NSTX-U? If not, what is the new scaling in this regime and how does it compare to ITER ELMy H-mode scaling?
2. What is the regime of validity of the instabilities found to be correlated with anomalous electron thermal transport on NSTX? Do predictions from existing first principles simulations and reduced models compare well with experiments with respect to transport levels, multi-field fluctuation level and spectra?
3. Is ion thermal transport still at neoclassical level in NSTX-U H-mode plasmas in the reduced collisionality regime? What are the individual roles of E×B shear and natural shaping of ST in reducing turbulence ion thermal transport?

4. What instabilities are responsible for observed anomalous momentum transport and intrinsic torque/rotation? What is the regime of validity of these instabilities?
5. What are the roles of neoclassical physics and turbulence in driving particle/impurity transport, especially in the reduced collisionality region?

By addressing these questions, NSTX-U will further clarify the validity of the observed H-mode global energy confinement scaling in the lower collisionality regime of NSTX-U, the roles of turbulence in driving anomalous transport, coupled with which development and validation of 0D and 1D reduced models can be carried out. In this five year plan, NSTX-U transport and turbulence research aims to provide predictive capability for core ion and electron temperature profile. Building on the success of this effort, the long-term goal is to deliver a set of tools to predict temperature, plasma flow, particle/impurity profiles with given boundary conditions, e.g. from a plasma edge model of H-mode, and sources and sinks will be delivered for optimizing MHD stability (e.g. pressure and current profile) and fusion gain in order to provide a reliable projection and optimization of confinement performance of future ST-FNSF and ITER.

3.2 Overview of NSTX-U transport and turbulence research plans

Here most relevant operation scenarios and transport issues to future devices are identified and prioritized for the planning of NSTX-U transport and turbulence research, based on which we propose the three research thrusts to guide the detailed planning as presented in subsequent sections. In Sec. 3.2.3, we will briefly summarize the turbulence diagnostic capabilities of NSTX-U to support the validation effort emphasized in Thrusts TT-2 and TT-3.

3.2.1 Most relevant operation scenarios and transport issues

In NSTX-U, we will focus on the transport issues in the most relevant operational scenarios to future devices. Transport and turbulence studies in H-mode, the baseline operational scenario for both ST-FNSF and ITER, will have the priority. In particular, characterization and validation of the ST H-mode global energy confinement scaling in the low collisionality regime will be one of the most important transport studies in the first two years of NSTX-U operation, in particular to assess if the confinement scaling dependence on collisionality remains favorable and will still unify the different engineering scalings found with different wall conditioning, i.e. boronized vs lithiated PFCs. Furthermore, new transport and turbulence measurements, enabled by diagnostics and facility enhancement, and development and validation of reduced/first principle models in H-mode plasmas will also be given priority in NSTX-U. The plan is to measure thoroughly and

document transport and turbulence characteristics of H-mode plasmas of NSTX-U, guided by nonlinear gyrokinetic simulations. These measurements will allow the identification of operational regimes of instabilities underlying anomalous transport and the compilation of a profile database for validation and development of reduced/first principle models. In particular, we would like to emphasize the study of electron anomalous transport and mapping out the regime of applicability of neoclassical ion thermal transport. Both are important for the determination of heating requirement for future devices. For example, understanding the ion thermal transport is important for achieving the hot-ion regime envisioned for FNSF. The dependence of ion thermal transport on plasma shaping, E×B shear and ν^* has to be determined in order to predict the required plasma shaping and flow profile for minimizing ion thermal transport in future devices.

In addition, transport and turbulence measurements in fully non-inductive and partially inductive long pulse plasmas will also be of particular importance due to their relevance to the requirement of long pulse and steady-state operation for ST-FNSF and ITER. These plasmas will have plasma current driven largely by NBI and/or RF and bootstrap current, and it is unclear how global energy confinement scaling would change in fully-relaxed plasmas and plasmas with large non-inductive current fraction, let alone the local transport and plasma turbulence. For example, the reduction or even removal of inductive electric field will significantly reduce/remove the Ware pinch effect, which will certainly enhance the role of turbulence in particle transport and thus affect the evolution of density profile and the bootstrap current. The transport and turbulence research in these scenarios will be coordinated with the scenario development as discussed in Chapter 9. Transport and turbulence research will also be emphasized in other advanced tokamak scenarios, e.g. plasmas with internal transport barrier [26] and enhanced pedestal H-mode identified on NSTX [27]. These advanced scenarios have better performance than normal H-mode plasmas and are candidate operational scenarios for future devices. Understanding their transport properties and underlying turbulence can help the achievement of these scenarios in NSTX-U and extrapolation to future devices.

While transport and turbulence studies on NSTX-U will focus on the above operation scenarios, other scenarios, e.g. RF-heated/NBI-heated L-mode and Ohmic-heated plasmas, will provide additional parameter regimes where operational turbulence could be different from that in H-mode, and thus they provide additional opportunities for testing and validating theories and models against transport and turbulence measurements and facilitate the improvement of existing models and development of new models. In particular, recent studies of NSTX NBI-heated L-mode plasmas [3] show that NSTX-U will be well positioned to address the L-mode transport shortfall found in conventional tokamaks [28].

3.2.2 Research thrusts for NSTX-U transport and turbulence research

As we have shown in previous sections, for NSTX-U, a broad range of transport issues are important in a variety of relevant operation scenarios to future devices. The plans to address these transport issues can be further organized into three overarching research thrusts that will guide our detailed planning in Sec. 3.3.

Thrust TT-1: Characterize H-mode global energy confinement scaling in the lower collisionality regime of NSTX-U

As discussed in Sec. 3.1., the ST H-mode global energy confinement scaling [5] extrapolates to much better confinement performance for future STs, e.g. ST-FNSF, than that from ITER98y,2 scaling [7]. Thus it is of great importance to investigate whether the observed H-mode global energy confinement scaling ($B\tau_E \backsim 1/\nu_e^*$) is valid in the lower collisionality regime of NSTX-U with a factor of 3-6 reduction in ν_e^*, and we particularly propose the first research thrust to addresses this important issue. The plan for this research thrust will closely follow the planned progress in NSTX-U engineering capabilities, e.g. B_T and I_p. By using regression analysis, global energy confinement scaling will be obtained from a large set of NSTX-U H-mode discharges with collisionality varied from the NSTX regime to the lower collisionality regime of NSTX-U and be compared with the existing ST energy confinement scaling. Previous studies in NSTX have shown that the reduction in electron collisionality is mainly induced by the broadening in electron temperature profile which is found to be induced by the increase in toroidal field without lithium wall coating and by the increase of the amount of lithium deposition with lithium wall coating. Studies have also shown that the global energy confinement dependence on collisionality is independent of how collisionality is varied [5], and this conclusion will be further verified by employing both techniques to vary collisionality in NSTX-U. The resulting validated global energy confinement scaling will be used to project the confinement performance of ST-FNSF.

Thrust TT-2: Identify regime of validity for instabilities responsible for anomalous electron thermal, momentum, and particle/impurity transport in NSTX-U

As we have briefly reviewed in Sec. 3.1., NSTX has made considerable progress in identifying possible mechanisms responsible for the anomalous transport observed in NSTX. In particular, multiple instabilities have been identified as potential candidates responsible for anomalous electron thermal transport, which may ultimately limit the confinement performance of future devices and thus is of critical importance. Furthermore, experiment and modeling show that low-k turbulence is likely responsible for observed anomalous momentum and impurity transport whose understanding is important for calculating flow, bootstrap current and density profile in

future devices and thus is crucial for predicting and optimizing plasma stability, fusion gain, and for achieving scenario sustainment. For example, to achieve the hot-ion scenario, low-k instabilities have to be controlled by E×B shear with optimized flow profile.

Having identified many candidates, the second research thrust of NSTX-U transport and turbulence research is to identify the regime of validity for these instabilities. This involves theoretically identifying isolated regimes for the instabilities, experimental measuring turbulence and transport in these regimes, and then comparing the measured transport levels and turbulence characteristics with first principles simulations or other theoretical model predictions. Experimental parametric dependences can be used for further distinguishing different instabilities. For example, in addition to the beta and collisionality dependences discussed above, the dependence of microtearing and ETG modes on s/q and Z_{eff} are opposite to each other [29]. The enhanced capabilities of NSTX-U, i.e. increased range of collisionality (with doubled toroidal field and plasma current), doubled heating power from the 2nd NBI and active flow and current profile modification using the 2nd NBI and external and NCC coils, provides a versatile set of experimental knobs for modifying transport and turbulence which will valuable for achieving the goal of the thrust 2. In the process of achieving the thrust 2, the dependence of transport produced by the above instabilities on collisionality, plasma β and the toroidal angular velocity will be emphasized since these dependences are most relevant for the projection to future ST-FNSF. We also note that the validation of first-principles simulations and turbulence theory against experiments is essential to the achievement of the goal of Thrust 3.

Thrust TT-3: Establish and validate reduced transport models (0D and 1D)

It is important to develop reduced transport modeling capability to predict plasma profiles, which determine confinement scaling, MHD stability, and current profiles (from bootstrap and NBI/RF driven current). The validated transport models can be used in self-consistent integrated modeling scenarios to study and develop advanced operating regimes, such as steady-state fully non-inductive scenarios. Even without fully validated 1D profile predictive capability, it is useful to have 0D confinement predictions validated with observed global (0D) energy confinement scaling trends that can be used to compare with empirical scaling observations when extrapolating to future devices (e.g. ST-FNSF or Pilot).

Thrust 3 will focus on advancing the physics basis of the various instability mechanisms (as elucidated in Thrust 2) and the resulting transport they cause, which will be used to develop and improve predictive transport capability. The bulk of the research will focus on developing reduced transport models that are guided by first principles simulations for the various relevant transport mechanisms (neoclassical, drift wave, energetic particle Alfven eigenmodes). (Note, a summary of the various codes used and their unique capabilities is given in Sec. 3.4.) The highest priority focus is on electron temperature profile as so many mechanisms can potentially

influence it. However, it is also important to predict density and toroidal flow profiles consistently, as they both interact with the underlying transport mechanisms. For validating turbulence theories with experimental core measurements, boundary conditions can be taken directly from measured profiles, such as near the pedestal top in H-modes. However, a truly predictive capability for projecting both 0D and 1D performance will require a predicted pedestal height and location of each plasma species (and flow for flow profiles), which will be coupled with research described in the following chapter on Boundary Physics.

3.2.3 Turbulence Diagnostic Capabilities of NSTX-U

Diagnostics	Measuring quantity	Radial coverage	Radial resolution	k coverage	k resolution
BES	$\tilde{n}_e$, density fluctuation	$r/a \gtrsim 0.1$	2-3 cm (channel spot size)	k_θ $\lesssim 1.5\ cm^{-1}$	$\gtrsim 0.25\ cm^{-1}$
16-channel reflectometer	$\tilde{n}_e$	*Cutoff density $\lesssim 6.9 \times 10^{13}\ cm^{-3}$	*$\gtrsim 0.5\ cm$ (channel spacing)	*$k_r \lesssim 6\ cm^{-1}$	*$\lesssim 0.8\ cm^{-1}$
Polarimeter	$\tilde{B}_r$, radial magnetic field fluctuation	Line-integrated over major radius at midplane	Line-integrated	Line-integrated	Line-integrated
FIR high-k_θ scattering system	$\tilde{n}_e$	$r/a \gtrsim 0.1$	1-5 cm$^+$	$k_\theta \sim 10 - 50\ cm^{-1}$	$\sim 1\ cm^{-1}$

*Table 3.2.1: List of turbulence diagnostics planned for NSTX-U and their measurement capabilities. *Density profile dependent. + Determined by scattering volume and wavenumber.*

In Thrusts TT-2 and TT-3, we emphasized the validation of reduced/first-principle models and turbulence theories against experiments, and this requires simultaneous measurements of multi-scale, i.e. low-k and high-k, and multi-field, e.g. density and magnetic field, fluctuations. Thus multiple diagnostics need to operate simultaneously in operational scenarios of NSTX-U featuring a wide range of plasma parameters. To demonstrate that NSTX-U is well prepared in this regard, the capabilities of turbulence diagnostics planned for NSTX-U are summarized in Table 3.2.1 (more detailed description of these diagnostics can be found in Chapter 10).

As seen in Table 3.2.1, we would like to point out that the radial and wavenumber coverage and resolution of the 16-channel reflectometer will be affected by plasma density profile, e.g.

reduced radial coverage but increased radial wavenumber (k_r) coverage in high performance NSTX-U NBI-heated H-mode plasmas where density is high. The other diagnostics, namely BES [23], polarimeter [25] and the FIR high-k_θ scattering system [24], are less affected by density profile and thus can provide more radial coverage and simultaneous measurements of both low-k and high-k turbulence in high density plasmas. On the other hand, BES requires NBI and thus in RF-heated and Ohmic plasmas, we will rely on the reflectometer, polarimeter and the high-k_θ scattering system to provide multi-scale and multi-field measurements. This is possible since density is usually lower in these scenarios and the reflectometer should be able to provide good radial coverage (but with reduced k_r coverage). Overall, with the combination of planned turbulence diagnostics multi-scale and multi-field turbulence measurements will be possible for NSTX-U operational scenarios. Furthermore, with incremental funding, the implementation of Phase Contrast Imaging (PCI) and Doppler back-scattering diagnostics can be started in FY18. These diagnostics can provide the coverage of the wavenumber gap between BES ($k_\theta \lesssim 1.5\ cm^{-1}$) and the FIR high-$k_\theta$ scattering system ($k_\theta \gtrsim 10\ cm^{-1}$).

3.3 Research plans

Since NSTX-U presently is scheduled to start operation in FY 15, plans for FY 14 will be presented first. In FY 14, data analysis, modeling/simulations, diagnostic preparation and collaboration activities will be the focus, and these activities will provide solid ground for NSTX-U operation in FY15 and beyond. Then the detailed plans for each research thrust are presented: progress will be reviewed, issues will be identified and detailed plans for Year 1, 2 and long term (Year 3-4) of NSTX-U operation. As presently planned, Years 1-4 of operation correspond to FY 15-18.

3.3.1 NSTX-U transport and turbulence research plans for FY14

In FY14, transport and turbulence research activities will focus on the preparation for the initial operation of NSTX-U. One aspect of the preparation is to continue analyzing the existing database of NSTX turbulence and transport data from the BES, a k_r backscattering system [30], a high-k_r microwave scattering system [31], reflectometry and a multi-energy soft x-ray (ME-SXR) diagnostic ([32] and see Sec. 10.6.1.3 and Sec. 11.2.6). The analysis of data and comparisons with gyrokinetic simulations will improve understanding of the relation between turbulence and transport and will also be help us identify possible experiments on NSTX-U. In addition, the data analysis will also help us prepare data analysis tools for NSTX-U, e.g. BES synthetic diagnostics, high-k_μ scattering system scattering volume calculation and a neural network for fast T_e profile analysis using ME-SXR data.

Another important task in FY14 is to prepare turbulence and transport diagnostics for NSTX-U. Integrated bench testing of the FIR high-k_0 scattering system with FIR laser and detectors will be carried out. Sixteen more detecting channels for the BES diagnostic will be installed and calibrated to increase the total number of channels to 48 for use on NSTX-U for the coming run campaigns. A one-channel microwave polarimetry system will be moved from DIII-D (originally from NSTX) to be installed on NSTX-U. Further optimization of the ME-SXR diagnostic design for NSTX-U will also be carried out with the help of an ongoing collaboration with EAST tokamak. Collaboration with FTU tokamak on high-Z impurity transport using an upgraded Transmission Grating Imaging Spectrometer will also occur.

In FY 14, further simulations and modelings for NSTX and NSTX-U will be carried out, e.g. to predict T_e and T_i profiles in a variety of NSTX scenarios with the transport code (P)TRANSP [33] and the transport solver TGYRO [34] and to predict the turbulent transport in NSTX-U (e.g. using the GTS code [35] with kinetic electrons). More details of the planned simulation and modeling activities can be found in the 2014 plans for Thrust TT-3 in Sec. 3.3.4.2.

3.3.2 Thrust TT-1: Characterize H-mode global energy confinement scaling in the lower collisionality regime of NSTX-U

A global energy confinement scaling with strong inverse dependence on collisionality has been established for STs [2,4,6]: $B\tau_E \backsim 1/\nu_e^*$ (see Fig. 3.3.1), while the ITER scaling on collisionality is much weaker: $B\tau_E \backsim \nu_e^{*-0.01}$[7]. The ST confinement scaling leads to an order magnitude of

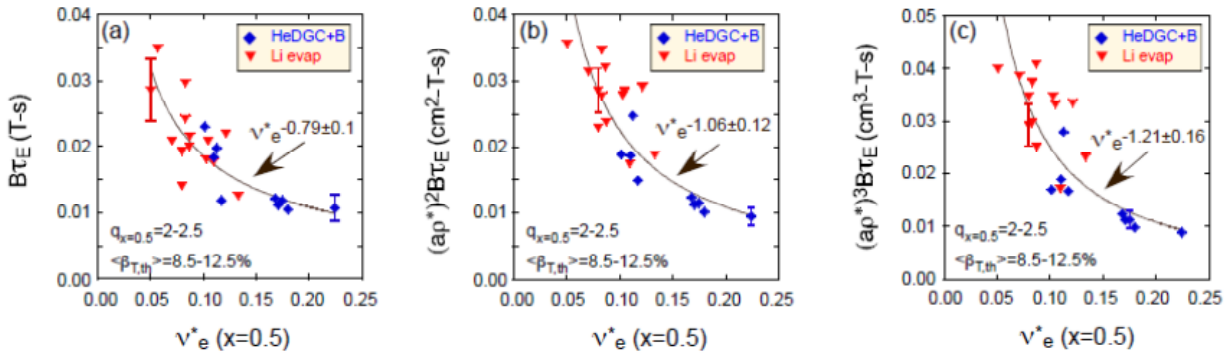

Fig. 3.3.1. Normalized confinement time as a function of collisionality at ρ=0.5 for the ν_e^* scan for assuming (a) $B\tau_E \sim \rho_*^0$, (b) Bohm scaling, $B\tau_E \sim \rho_*^{-2}$ and (3) gyroBohm scaling, $B\tau_E \sim \rho_*^{-3}$. Blue points are from discharges that used HeGDC+B wall conditioning, while red points are from discharges that used Li evap. Discharges from the above scans were constrained to have minimal variation in $q_{r/a=0.5}$ (2-2.5) and $\langle\beta_T\rangle$ (8.5-12.5%). Note that to account for the variation in ρ_*, scalings were also determined assuming either a Bohm ($B\tau_E \sim \rho_*^{-3}$) or gyroBohm ($B\tau_E \sim \rho_*^{-3}$) dependence. Stronger dependence with collisionality, $B\tau_E \sim \nu^*_e{}^{-1.06}$ and $B\tau_E \sim \nu^*_e{}^{-1.21}$, is found for Bohm and gyroBohm scaling assumptions.

improvement in projected performance of ST-FNSF in contrast to that from the ITER scaling as seen in Fig. 1.1.4. Furthermore, as seen in Fig. 3.3.1, this ST global energy confinement scaling is seen to be independent of wall conditioning, either using Helium Glow Discharge Cleaning plus occasional boronization for wall conditioning (HeGDC+B) or between-shot lithium conditioning of the vessel walls through evaporation from two LITERs (LIThium EvapoRators) mounted at the top of the NSTX vessel [5]. This collisionality dependence also unifies the different engineering scaling observed with different wall condition: $\tau_{E,th} \sim Ip^{0.37}B_T^{1.01}$ for HeGDC+B wall conditioning and $\tau_{E,th} \sim Ip^{0.79}B_T^{-0.15}$ for lithium wall conditioning [5] with the latter scaling similar to those in conventional aspect ratio tokamaks, as embodied in the ITER98y,2 scaling [7] with a strong I_p dependence and a weak B_T dependence. This unification implies that collisionality is more fundamental in determining energy confinement and the difference in engineering scalings comes from what engineering parameter collisionality is correlated with. Indeed, it is found that with HeGDC+B wall conditioning, reduction in collisionality is mostly correlated with the increase in B_T and on the other hand, when lithium is used for wall conditioning, reduction in collisionality is correlated well with increase in amount of lithium deposition.

In the research plan for the Thrust TT-1, we are planning to carry out extensive studies of the ST H-mode global energy confinement scaling in the first two years of NSTX-U operations utilizing the full capabilities of NSTX-U to achieve lower collisionality with the different wall conditioning technique, and the emphasis will shift to H-mode confinement scaling in long-pulse and fully non-inductive scenarios in the rest 3 years.

3.3.2.1 Research plans by year for Thrust TT-1

Year 1

The baseline global energy confinement scaling for NSTX-U will be re-established in the first year of operation for comparison with previously observed NSTX scaling (B_T/I_p<0.55 T/1.2 MA). Confinement time scaling will then be extended to higher field strength and plasma current (with operational goals of $B_T/I_P \leq$ 0.8 T/1.6 MA) for modest duration discharges (~1-3 seconds) as these engineering improvements become available. This extension in I_p, B_T (and increased NBI power from day one) will allow us to attain lower ν_e^* to assess the validity the favorable confinement ($B\tau_E \backsim 1/\nu_e^*$) scaling in the lower collisionality regime. Of particular interest will be determining the I_p and B_T scaling and how they compare to the different scalings found on NSTX depending on wall conditioning technique (HeGDC+B vs. lithiated) as discussed above.

Year 2

In the second year of NSTX-U, the confinement time scaling will be extended to the full field strength and plasma current (with operational 1.0 T/2 MA) which, together with increased NBI,

will allow us to attain the lowest ν_e^* values to verify the range over which favorable confinement ($B\tau_E \backsim 1/\nu_e^*$) scaling occurs and whether a roll-over at lowest ν_e^* is found. The expanded empirical confinement scaling will be used to begin projecting 0D performance for relevant next generation STs, e.g. FNSF, Pilot. Select discharges from the expanded confinement database, especially those that have the most complete profile and turbulence diagnostic coverage used for validation studies in Thrust TT-2, will provide the basis for a 1D profile database for testing the development of reduced transport models (Thrust TT-3).

The confinement scaling trends will be separated into both core (W_{core}) and pedestal (W_{ped}) contributions to better understand the relative importance of each in setting the overall I_p, B_T, and ν_* scalings. W_{ped} will be determined from Thomson scattering system with improved edge resolution [36] and CHERS system [37].

Years 3-4

In later years the confinement scaling will be characterized (i) for longer duration discharges that approach the engineering limit (~5 s), (ii) for advanced scenarios, e.g. fully non-inductive discharges, as they are developed (outlined in Sec. 9.2.1), and (iii) for varying PFC wall boundary conditions (sec. 5.3)**.** It will be important to re-confirm the empirical scaling in long-pulse and fully non-inductive advanced scenarios, or if necessary, develop empirical scaling appropriate for refining 0D performance predictions to FNSF or Pilot that are based on the most relevant NSTX-U discharge scenarios.

As steady-state density control using cryopump is implemented in NSTX-U in this time period, we are planning to investigate ρ_* scaling of confinement and transport, which for constant q, β and ν_e^* requires that density vary like $n \sim \rho^{*-2}$. Therefore, to achieve a variation in ρ^* of 1.7 (similar to DIII-D experiments [38]), density will need to be varied by a factor of 3. These ρ^* experiments will help to clarify whether ST confinement scaling follows Bohm or gyroBohm expectations, which influences the inferred strength of the ν_e^* scaling discussed above. It will also test whether turbulence correlation lengths and times follow gyroBohm scaling expected from local drift wave theories. These experiments, coupled with simulations, will provide a more direct measure of the relative importance of non-local effects in STs that should become weaker at smaller ρ^*. If such non-local effects are shown to be important, they will have to be accounted for in associated predictive transport modeling (see Thrust TT-3).

3.3.3 Thrust TT-2: Identify regime of validity for instabilities responsible for anomalous electron thermal, momentum, and particle/impurity transport in NSTX-U

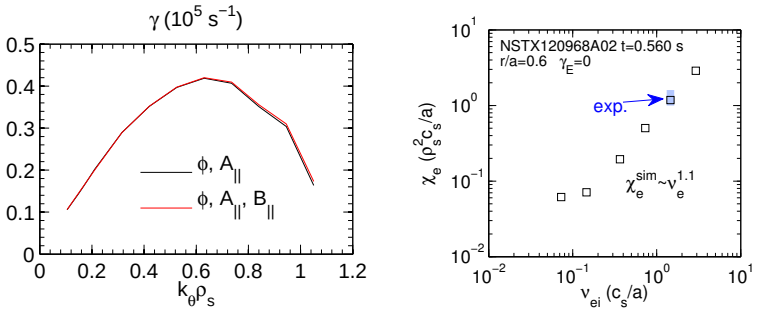

Fig. 3.3.2 (a) Converged linear microtearing growth rate spectra with and without compressional magnetic perturbations ($B_{||}$); (b) Normalized electron thermal diffusivity vs. normalized electron collision frequency (log-log scale). The shaded region shows the experimental values with uncertainties. All calculations are based on an NSTX H-mode plasma using GYRO code (see Sec. 3.4.1.1. for more information about GYRO).

3.3.3.1 Electron Thermal Transport

Electron thermal transport will likely pose the ultimate limit to the confinement performance of future devices. For example, electron heating will be dominant in ITER discharges, and efficient heating of fuel ions by electrons requires good electron thermal confinement. It is well established in NSTX that although ion thermal transport could be reduced to neoclassical level in a variety of operation scenarios [4], electron thermal transport is consistently anomalous. Up to now, a universal mechanism for explaining anomalous electron thermal transport is out of reach, and there is good indication that perhaps there is no unique one. It is likely that anomalous electron thermal transport is driven by different instabilities in different parameter regimes, i.e. in different operation scenarios and radial regions.

A recent breakthrough in understanding anomalous electron thermal transport is the identification of the importance of electromagnetic effects in driving electron thermal transport in outer half of a set of NSTX high beta H-mode plasmas through state-of-art nonlinear gyrokinetic simulations [19,20]. Microtearing modes are shown to be linearly unstable [Fig. 3.3.2(a)] and predicted transport varies with collisionality in a manner consistent with that observed in experiments [Fig. 3.3.2(b)]. It is also shown that experimentally relevant electron thermal transport is driven almost exclusively through the stochastic magnetic field.

Further parametric scans demonstrate that the s/q, Z_{eff}, β and collisionality dependences of microtearing modes are different to those of ETG modes [29], which provides a potential way for distinguishing between them experimentally. Given the strong collisionality dependence of microtearing modes, their importance in the low

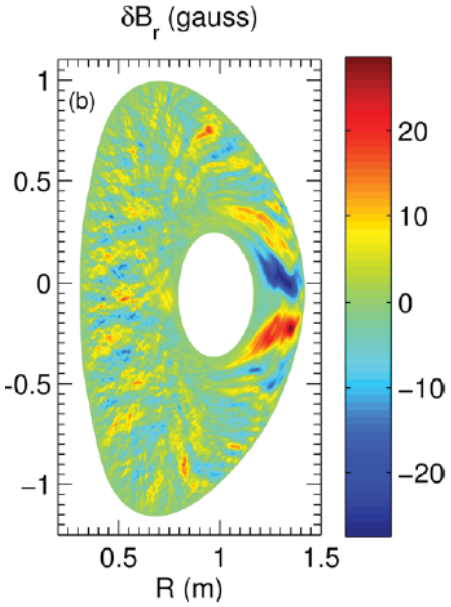

Fig. 3.3.3. δB_r (in Gauss) in a (R,Z) toroidal plane from a nonlinear microtearing simulation of a NSTX H-mode plasma using GYRO code.

collisionality regime of NSTX-U and future devices is unclear. Fortunately, the large scale (n~10) magnetic fluctuations associated with microtearing modes (Fig. 3.3.3) make it possible to measure magnetic fluctuations directly through Faraday rotation effects. A polarimetry diagnostic will be installed on NSTX-U at beginning of its first run campaign (see Table 3.2.1 and more details in Chapter 10) and is shown to be sensitive enough to measure magnetic fluctuations from microtearing modes through a synthetic diagnostic [25,39].

In addition to microtearing modes, other ion scale ballooning instabilities could also play important roles in determining electron thermal transport in high beta H-mode plasmas. It is found that in NSTX low collisionality H-mode plasmas, a microtearing instability is usually subdominant to a ballooning instability [see Fig. 3.3.4 (top)]. The ballooning instability exhibits characetristics very similar to a TEM: driven unstable by electron density and temperature gradients (a/L_n, a/L_{Te}), weakly dependent on ion temperature gradient (a/L_{Ti}), and strongly stabilized by increasing collisionality (ν_{ei}) [see Fig. 3.3.4 (middle)]. However, unlike a traditional electrostatic TEM instability, this mode is extremely sensitive to β_e with the appearance of an effective threshold ($\beta_{e,crit}$~0.8%) similar to that expected for a KBM instability. The fact that the scaling of the growth rates are unified by the MHD alpha parameter [see Fig. 3.3.4 (bottom)], $\alpha_{MHD}=-q^2R\nabla\beta$ [where $\beta=\Sigma(n_sT_s)\cdot 2\mu_0/B^2$], highlights the KBM nature of the instability, so we refer to it as a "hybrid" TEM/KBM [21]. Similar KBM behavior has been

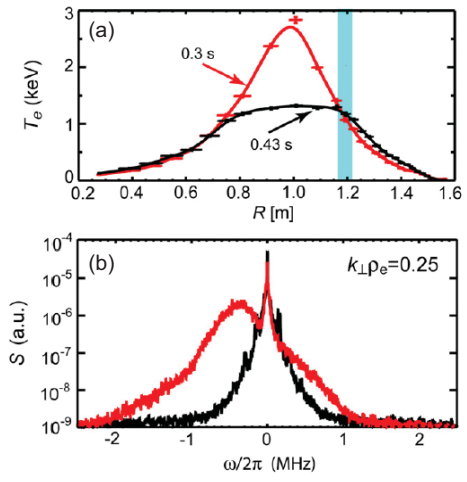

Fig. 3.3.5. Temperature profiles (a) and spectral density of fluctuations (b) at 0.3 (red) and 0.43 s (black). The blue stripe indicates the location of measurement where L_{Te} is 15 cm and 50 cm, respectively. Negative frequencies (b) correspond to wave propagation in the electron diamagnetic direction.

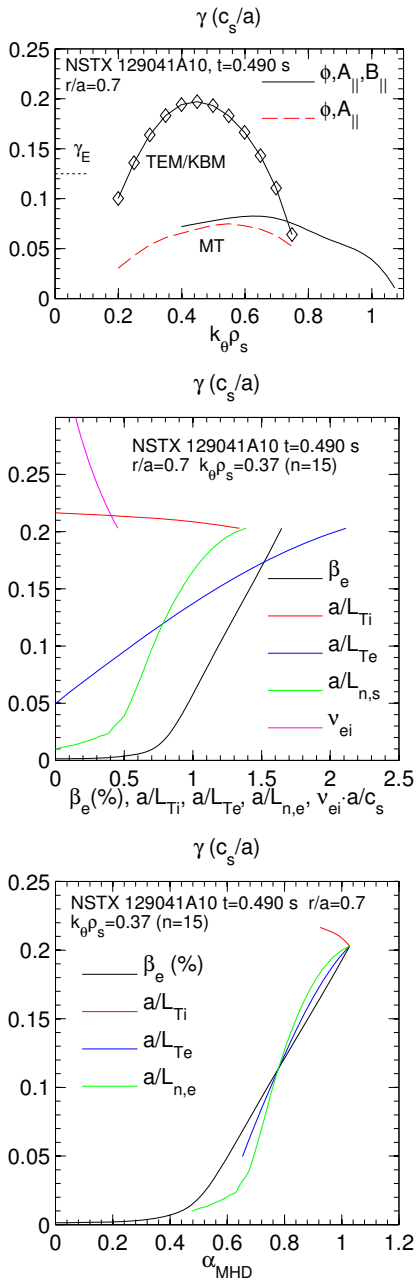

Fig. 3.3.4. (top) Linear spectra of overlapping MT and KBM/TEM instabilities. (middle) Scaling of ballooning mode growth rate with β_e, a/L_{Ti}, a/L_{Te}, a/L_n, ν_{ei}. (Bottom) Ballooning growth rates vs. α_{MHD}.

predicted in GS2 simulations near the top and inside of the pedestal region [40]. Parametric studies in NSTX-U low collisonality H-mode plasmas coupled with gyrokinetic simulations and the BES/polarimetry diagnostics will further clarify the role of these TEM/KBM instabilties in driving electron thermal transport.

Electron-scale turbulence has long been considered as a potential candidate in driving electron thermal transport, i.e. ETG turbulence [41], and its correlation with electron thermal transport has been observed in NSTX. Electron-scale turbulence has been identified in NSTX by using a high-k_r microwave scattering system [31] to measure changes in electron-scale turbulence when the local electron temperature gradient was varied by RF heating in NSTX L-mode plasmas [42]. Figure 3.3.5(a) shows large T_e gradient at the measurement region of high-k scattering system with RF heating (red) and much smaller T_e gradient after RF is turned off (black). In Fig. 3.3.5(b) the appearance of the scattered signal (denoted by the off-center spectral peak shown in red) is correlated with the large T_e gradient. In particular, the appearance of electron-scale turbulence is found to be correlated with the electron temperature gradient exceeding the critical gradient predicted for ETG modes.

Studies of parametric dependences of observed electron-scale turbulence show gross agreement with those of ETG modes. It is observed that ExB shear could stabilize electron scale turbulence when ETG modes are marginally unstable and ExB shearing rate is comparable to ETG growth rate [43]. Suppression of electron-scale turbulence is found in NSTX reversed-shear plasmas with electron internal transport barrier (eITB) and is correlated with large reversed magnetic shear and the formation of eITB [16]. Numerical simulations have shown that the large T_e gradient observed in eITB is shown to be consistent with the reversed-shear-induced nonlinear up-shift of critical T_e gradient for ETG-driven electron thermal transport [17]. Electron-scale turbulence is also found to be stabilized by density gradient, which consistent with increased linear threshold of ETG modes by density gradient, and the observed reduction in electron turbulence is correlated with decrease in electron thermal transport [44] (see Fig. 3.3.6). Nonlinear gyrokinetic ETG simulations reproduce consistent density gradient

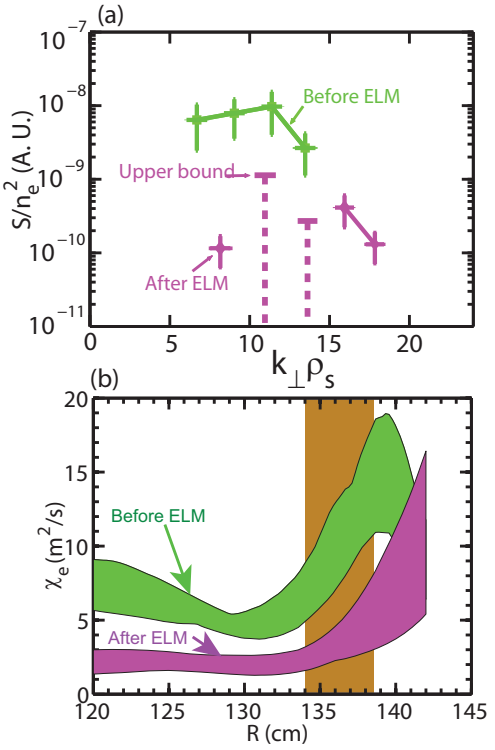

Fig. 3.3.6. An ELM event leads large density gradient in the high-k measurement region [vertical bar shown in (b)] after ELM. (a) The normalized scattered power $k_\perp$ spectra in arbitrary unit before and after ELM; (b) $\hat{A}_e$ radial profiles before and after ELM. $\hat{A}_e$ in the high-k measurement region is reduced after ELM.

dependence on both turbulence and transport [18]. On the other hand, an experimental collisionality scan shows that electron thermal transport and measurement electron-scale turbulence spectral power seem to be anti-correlated, and nonlinear gyrokinetic simulations only show consistent electron heat flux at one location but not across wider radius [18]. Linear stability analysis and nonlinear simulations have shown that ETG mode growth rates and saturation level are sensitive to small profile variations, particularly q and density gradient [18]. It is important to point out that the high-k scattering system used in these experiments could not capture the predicted spectral peak of predicted ETG turbulence, let alone determining the existence of ETG streamers which are predicted to be important for driving electron thermal transport. The new high-k_θ FIR scattering system has been designed to do both [24] (see Table 3.2.1 and Chapter 10 for details).

Alfven eigenmodes (GAE/CAE) are found to be potentially important for electron thermal transport in the core (r/a<0.4) of NSTX high-power NBI H-mode plasmas. This electron thermal transport mechanism is potentially important for ITER since fusion α particles in ITER may drive AE activities and thus could lead to degraded electron thermal confinement. The Alfven eigenmodes are excited by fast particles from NBI due to their super-Alfvenic velocity. In a set of H-mode plasmas, flattening of central electron temperature profile is observed as NBI power is increased from 2 MW to 6 MW with increased AE activity indicated by Mirnov coil measurements [13]. Power balance analysis using TRANSP clearly shows about a factor of 10 increase in electron thermal diffusivity with increased AE activities. A reduced model based on electron drift orbit stochasticity in the presence of multiple core localized AE produces a steep dependence of electron thermal transport on AE amplitude ($\propto \alpha^6$, where α represents the mode amplitude), and experimentally relevant electron thermal transport is predicted by using measured mode amplitude and assumed mode structure using ORBIT code [45] (see section

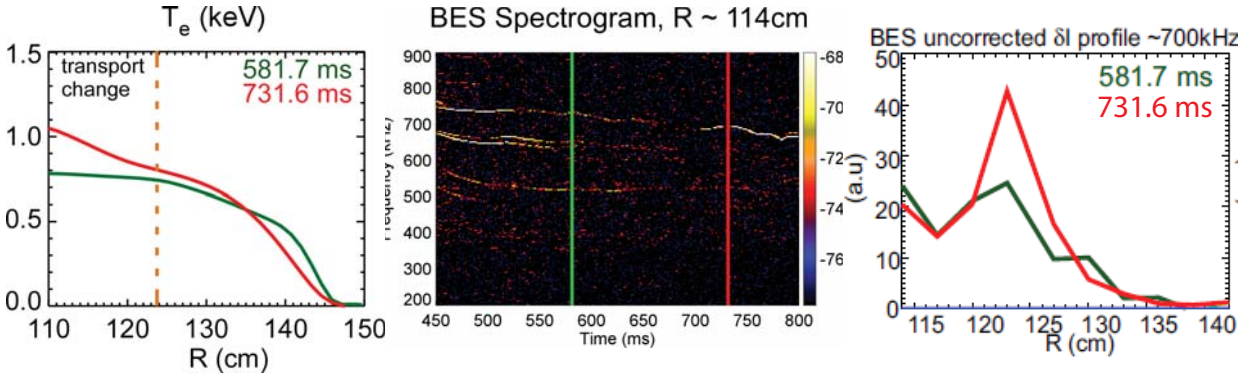

Fig. 3.3.7. (Left) T_e profiles at two time points of interest with different central peaking; (Middle) BES spectrogram at R~114 cm with times of interest denoted by lines with same color codeing in the left panel; (Right) Radial structure of dominant AE frequency at about 700 kHz. Note that the existence of a single dominant mode at t=732 ms (red) shown [see the middle and right panels] corresponds to a peaked T_e profile and a flat central T_e profile corresponds to the existence of multiple modes at t=582 ms (green) shown in the middle panel but with smaller amplitude (see the right panel), which is consistent with ORBIT simulations that multiple AEs are required to generate stochastic electron thermal transport.

3.3.4 for more discussions on reduced model validation and development). Recent measurements from BES diagnostic support that multiple AEs are needed for producing anomalous electron thermal transport (see Fig. 3.3.7). Since a first principle model is not available, experimental investigation of the mode structure and amplitude and their dependence on toroidal field, plasma current and fast particle energy/population has to been carried out to assess the characteristics of these modes in future devices. In parallel, the measured calibrated BES mode structures will be used in future ORBIT simulations to compare predicted electron thermal transport with that from experiments. These experimental studies will also facilitate the development of first-principles and reduced transport models.

In general, NSTX L-mode plasmas (NBI/RF-heated) provide additional parameter regimes where mechanisms for electron thermal transport are different from those in H-mode plasmas and thus provides opportunities for validating theories and models in extended parameter regimes. NSTX L-mode plasmas have suggested additional mechanisms for anomalous electron thermal transport. Experimental observations in a set of NSTX NBI-heated and center-stack-limited L-mode plasmas indicates that ITG modes can drive both electron and ion thermal transport [3]. The increase of the ratio between the ExB shearing rate and the maximum linear growth rate for ITG modes, $\omega_{E\times B}/\gamma_{max}$, is found to be correlated with the reduction in thermal transport in both electron and ion channels, consistent with ExB shear stabilization of ITG turbulence [46,47] (see Fig. 3.3.8, where both the Hahm-Burrell ($\omega_{E\times B,HB}$) [48] and Waltz-Miller ($\omega_{E\times B,WM}$) [49] E×B shearing rates are shown). In particular, ion thermal transport is found to be reduced to 2-3 times of neoclassical level when ExB shear stabilization is large enough. Further nonlinear gyrokinetic studies of NSTX NBI-heated L-mode plasma show that future studies of L-mode plasmas in NSTX-U can contribute to the L-mode transport shortfall found in conventional tokamaks [28].

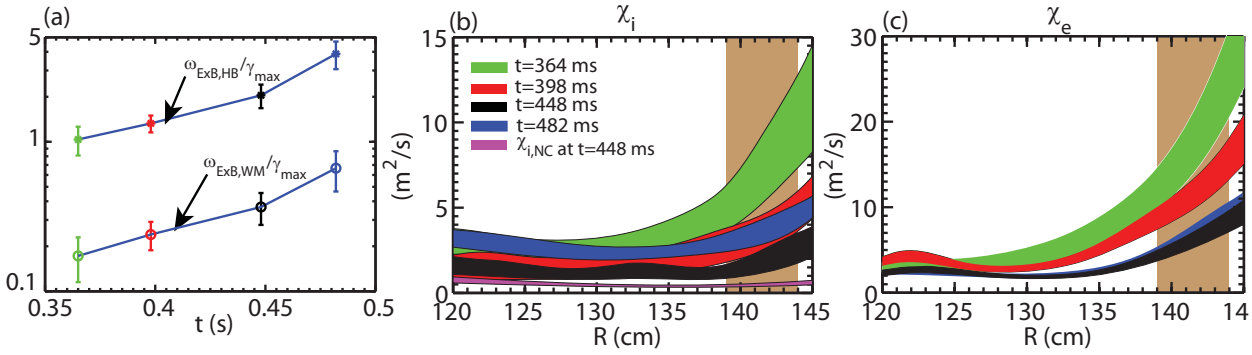

Fig. 3.3.8. (a) The ratio between the ExB shearing rate and the maximum linear growth rate for ITG modes; (b) Radial profiles of ion thermal diffusivity, χ_i, at at the same time points as in (a) and radial profile of neoclassical ion thermal diffusivity at t=448 ms (magenta); (c) Radial profiles of electron thermal diffusivity, χ_e. Note that the width of the colored regions denotes the experimental uncertainty. The width of rectangular shaded region denotes the high-k measurement region. Both χ_i and χ_e in the high-k measurement region continuously decrease from t=364ms to 448 ms as $\boldsymbol{\omega_{E\times B,WM}}$ increases from about 0.2 to 0.4, and the increase of χ_i (and invariance in χ_e) from t=448 ms to 482 ms is correspondent with increased MHD activities.

The above NSTX research on electron thermal transports signifies the importance of identifying the regime of validity of each potential instability, which is required for validating/developing existing/new reduced models.

3.3.3.1.1 Research plans by year for Thrust TT-2: Electron thermal transport

Year 1

The first year of electron thermal transport research is planned according to the timeline for diagnostic and facility upgrades (see the last section of this chapter). Low-k diagnostics (BES, reflectometry and polarimetry) will be installed and will be fully functioning at the beginning of the first NSTX-U run campaign, and the study of electron thermal transport will focus on measurements of low-k turbulence with these diagnostics in H-mode plasmas in the first year of NSTX-U operation. One key physics question is to identify dominant modes in the lower collisionality high beta H-mode plasmas of NSTX-U. Turbulence measurements will be carried out in the experiments addressing Thrust TT-1. Variation in low-k turbulence will be documented as ν_e^* is varied and will be correlated with energy confinement scaling trends. In particular, an assessment will be made on whether density (from BES) or magnetic fluctuations (from polarimetry) correlate better with electron thermal transport. Furthermore, the BES diagnostic is also able to provide zonal flow measurements, which provides an opportunity to study the parametric dependence of zonal flow and its interplay with low-k turbulence. In addition, the unification of engineering scalings with different wall conditions (without and with lithium) by ν_e^* global confinement scaling will be assessed with low-k turbulence measurements. Linear/nonlinear gyrokinetic simulations will be used to identify responsible modes and compare global confinement trend with experiments, and turbulence characteristics will be compared with low-k turbulence measurements (via synthetic diagnostics). Low-k turbulence measurements will also be carried out in microtearing-dominant regimes, e.g. in high β and collisionality H-mode plasmas, with the guidance from gyrokinetic simulations, and change in low-k turbulence will be documented as plasma parameters are varied into and out of the isolated regime, e.g. by lowering collisionality and active q (magnetic shear, $\hat{s}$) and flow profile (E×B shear and parallel velocity shear) variations using the 2nd NBI and existing external 3D coils.

AE (CAE/GAE) mode structures will be measured using calibrated BES/reflectometry with a range of B_T, I_p, collisionality and NBI power in NSTX-U H-mode plasmas, and the measured mode structure and amplitude will be used in ORBIT simulations to assess predicted electron thermal transport in comparison with measured electron thermal transport trends with B_T, I_p, collisionality and NBI power. Polarimetry measurements of line-integrated CAE/GAE magnetic fluctuations will provide a strong constraint on the magnetic fluctuation amplitude inferred from BES/reflectometry density fluctuation measurements.

Year 2

In the second year of NSTX-U, the confinement time scaling will be extended to the full field strength and plasma current attaining even lower ν_e^* values. Similar to the plan of year 1, low-k turbulence changes will be documented as NSTX-U achieves lower ν_e^* (compared to year 1) and will be compared with linear/nonlinear gyrokinetic simulations. The new FIR high-k_θ scattering system will be installed in the first year of NSTX-U operation, and the commissioning the complete system will be carried out in the second year. Preliminary high-k measurements together with low-k turbulence measurements in ETG-dominant regime, e.g. low β and low Z_{eff} H-mode plasmas and L-mode plasmas with eITB, guided by gyrokinetic simulations will be made, and correlation with electron thermal transport will be assessed. In particular the 2nd NBI and external coils will be used to study the dependences of ITBs (both electron and ion ITBs) formation on q, $\hat{s}$ and ExB shear.

A laser-blow off system will become available in FY16 and preliminary experiments of cold pulses propagation from non-recycling impurity injection, coupled with fast T_e measurements from a multi-energy SXR system, will be conducted in both H and L-mode plasmas to study profile stiffness and corresponding change in measured turbulence will be documented. Measurements will be carried out in isolated regimes for low-k modes, e.g. ITG/TEM dominant discharges (in NBI and RF-heated L mode plasmas) with the guidance from gyrokinetic simulations. Active q and flow profile variations using the 2nd NBI and external coils will be used to identify parametric dependence of transport and turbulence. Nonlinear gyrokinetic simulations of these L-mode plasmas will help clarify the L-mode transport shortfall problem in conventional tokamaks [28]. Studies of AE (CAE/GAE) mode will continue with the improved capabilities of NSTX-U. Furthermore, a row of high-Z divertor title will be available in this year, and its effects on electron thermal transport will be investigated.

Years 3-4

The plan for the year 3-4 of electron thermal transport research is made to fully utilize the improved diagnostics and facility upgrades, in particular the high-k scattering system, the laser blow-off system, cryopump for density control and improved reduced/first-principle models and developed synthetic diagnostics, e.g. for the high-k scattering system. The emphasis in years 3-4 is to identify operational regimes of ETG, microtearing and AE (CAE/GAE) modes using the high-k_θ scattering system, the BES, reflectometry and polarimetry measurements with full range of NSTX-U parameters, improved capabilities of varying plasma parameters/profiles [using the 2nd NBI, external coils (and NCC when available) and cryopump] and PFC/divertor condition (different PFC/divertor materials and reduced recycling regime with litihum deposition). Transport and turbulence characteristics dependence on collisionality, plasma β and flow profile will be particularly emphasized. Both steady-state/perturbative transport measurements will be conducted. In particular, cold pulse propagation experiments together with active profile

variation from 2nd NBI and external/NCC coils will allow us to address: 1) the dependences of stiffness of electron thermal transport on q, $\hat{s}$ and ExB shear, 2) the identification of responsible turbulence. The turbulence and transport measurements will be compared with interpretative and predictive gyrokinetic simulations/reduced models and synthetic diagnostics in order to identify the operational turbulence and assess its regime of validity. Identifying responsible turbulence for electron thermal transport in long-pulse and fully non-inductive scenarios will be particularly emphasized in the years 3-4.

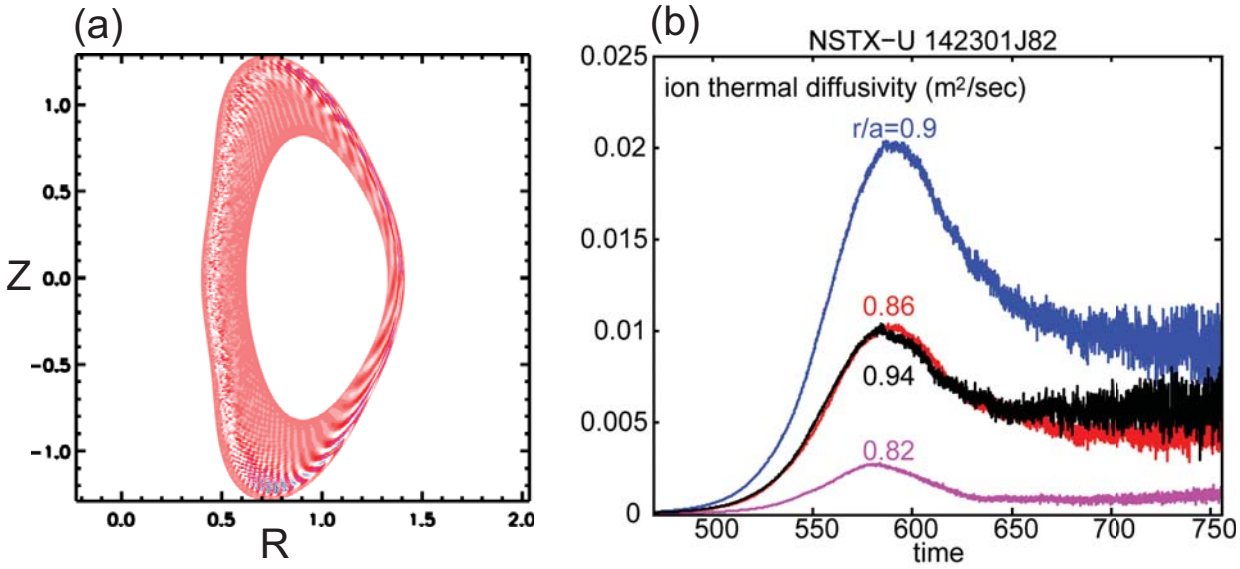

Fig. 3.3.9. Nonlinear gyrokinetic ITG simulation for predicted NSTX-U H-mode plasmas using GTS code. (a) Density fluctuation in (R,Z) plane; (b)Ion thermal diffusivity time evolution at four ITG unstable locations.

3.3.3.2 Ion Thermal Transport

The near-neoclassical level of ion thermal transport in NSTX H-mode plasmas is one of the most important observations made on NSTX [4]. This is consistent with theoretically predicted E×B shear and plasma shaping stabilization of low-k turbulence and has been used to predict ion temperature profiles in NSTX-U scenario development (see Chapter 9 and Ref. [50]). Since neoclassical ion thermal transport will be greatly reduced in NSTX-U and future devices, it is important to determine experimentally in what regime ion thermal transport remains predominantly neoclassical, and its dependence on plasma shaping and E×B shear. This is important since identifying the needed E×B shear and shaping to minimize ion thermal transport in future devices is essential for achieving the envisioned hot-ion regime for ST-FNSF. A numerical prediction of ion thermal transport using GTS gyrokinetic code [35] and predicted NSTX-U H-mode profiles shows negligible turbulent ion thermal transport driven by ITG modes more than 100 times smaller than neoclassical diffusivity ($\chi_{i,neo} \approx 1.6\ m^2/s$ at r/a=0.9) (see Fig. 3.3.9), where flow shear was found to play a small role. However, adiabatic electrons were used

in the simulation, and it is possible that trapped electrons may enhance ITG/TEM/KBM modes to drive more ion thermal transport.

Indeed, collisionality scans in NSTX H-mode plasmas shows an increase in ion thermal diffusivity relative to neoclassical values as collisionality is reduced (see Fig. 3.3.10 and Ref. [5]). As shown in Fig. 3.3.8, ITG modes can play an important role in determining ion thermal transport in NSTX L-mode plasmas, and thus L-mode plasmas provides additional opportunities for turbulence and transport measurements and for validating reduced/first-principle models for ion thermal transport.

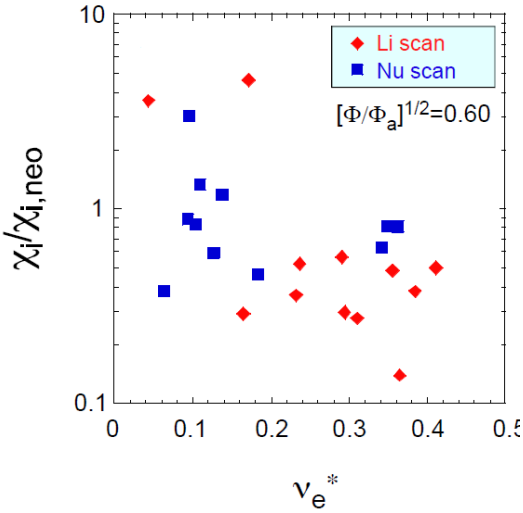

Fig. 3.3.10. Ion thermal diffusivity, χ_i, normalized to the neoclassical ion thermal diffusivity as determined by NCLASS as a function of electron collisionality at ρ=0.6.

3.3.3.2.1 Research plans by year for Thrust TT-2: Ion thermal transport

Year 1

In the first year of NSTX-U operation, χ_i will be determined through power balance analysis in the experiments addressing Thrust TT-1 where lower collisionality H-mode plasmas will be achieved with the extended range of B_T and I_p, and observations will be compared with neoclassical calculations, e.g. using NCLASS[51]/GTC-NEO[52]/NEO[53]. The $\chi_i/\chi_{i,neo}$ as a function of ν_e^* will be evaluated to determine if the trend observed in Fig. 3.3.10 is still valid in the lower ν_e^* H-mode regime of NSTX-U. In addition, to further assess how ion thermal transport is related to low-k turbulence, the 2nd NBI and external coils are to be used to vary q (magnetic shear, $\hat{s}$) and flow profiles (E×B shear and parallel velocity shear) particularly in low collisionality H-mode plasmas where ion thermal transport was found to be more anomalous, and we will determine if observed change in ion thermal diffusivity is correlated with low-k turbulence measurements from BES, reflectometry and polarimetry. Comparison with nonlinear gyrokinetic simulations on both determined transport trend and measured turbulence through synthetic diagnostics will be carried out.

Year 2

The study of $\chi_i/\chi_{i,neo}$ as a function of ν_e^* will continue in the second year of NSTX-U operation as NSTX-U operation is extended to the full field strength and plasma current attaining the lowest ν_e^* values. Combinations of applying the 2nd NBI and external coils will be explored to reduce ion thermal transport to neoclassical level in the lowest ν_e^* regime. Furthermore, ion thermal transport and low-k turbulence will be measured in isolated regimes for ITG/TEM

modes, e.g. in NBI and RF-heated L mode plasmas, with the guidance from gyrokinetic simulations, and modification of q and flow profiles ($\hat{s}$, E×B shear) by the 2nd NBI and external coils will be used to vary the strength of anomalous ion thermal transport and low-k turbulence. In particular, L-mode plasmas with ion ITB will be be used to study the dependences of ion ITB formation on q, $\hat{s}$ and ExB shear. These experimental measurements will be used to validate gyrokinetic codes, and in particular, the L-mode transport shortfall problem [28] will be addressed.

Year 3-4:
In the years 3-4 of NSTX-U operation, we will continue the investigation of the parametric dependence of $\chi_i/\chi_{i,neo,}$ e.g. on β, ρ^*, T_i/T_e and $Z_{eff,}$ expanded beyond B_T, I_p, collisionality, $\hat{s}$ and E×B shear dependences studied in previous years. In particular, the dependence on plasma β will be emphasized. Coordinated with experiments planned to address confinement scaling in fully relaxed and fully non-inductive scenarios, these parametric dependences will also be investigated in these advanced scenarios to form an extensive database. Such a database will allow us to identify relevant low-k turbulence (ITG/TEM/KBM) to ion thermal transport and their operational regime and also provides validations to gyrokinetic codes and reduced models. Again, combinations of applying the 2nd NBI and external 3D coils/NCC will be investigated to reduce ion thermal transport to neoclassical level.

3.3.3.3 Momentum Transport

To project confinement performance of future devices, predicting flow profile is of great importance since E×B shear is known to play an important role in stabilizing low-k turbulence and thus affects both electron and ion thermal transport, e.g. see Fig. 3.3.8. Flow profile projection requires the knowledge of momentum source and transport, e.g. intrinsic torque, diffusivity and pinch. While NBI-heated plasmas have dominant external momentum injection from NBI that can be calculated with reasonable accuracy, the intrinsic torque driven by plasma turbulence is not well understood and its prediction is of particular importance to ITER, which will have small external torque input. In addition to knowing the sources, predictions of momentum diffusivity and pinch are required, and this is particularly important for ST-FNSF where externally input torque by NBI will be the dominant momentum source.

Momentum transport has been studied in both NSTX NBI-heated L and H-mode plasmas and was found to be anomalous in both scenarios (see Fig. 3.3.11 and note that the neoclassical mechanism essentially provides no momentum transport), in contrast to the fact that ion thermal transport is close to neoclassical level in NBI-heated H-mode plasma and is anomalous in NBI-heated L-mode plasmas [2]. The anomalous momentum transport and neoclassical ion thermal transport in NBI-heated H-mode plasmas indicate that some residual low-k turbulence is

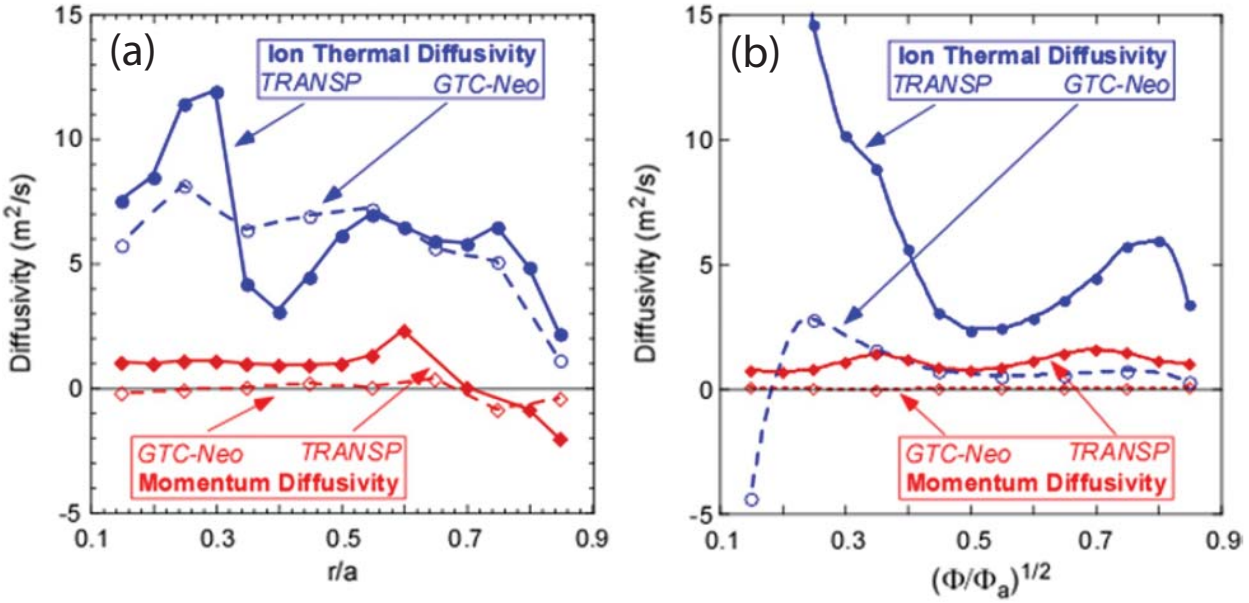

Fig. 3.3.11. Experimentally inferred values of χ_i and χ_ϕ compared with the neoclassical values computed by GTC-NEO for an H-mode (a) and an L-mode (b) plasma.

responsible for observed anomalous momentum transport but produces much smaller anomalous ion thermal transport compared to the neoclassical value. Indeed, perturbative momentum transport experiments using magnetic braking show that the inferred momentum pinch in the outer region of NSTX H-mode plasmas is consistent with that predicted by theoretical models involving low-k ITG turbulence (see Fig. 3.3.12 and Refs. [54], [55]).

Linear analysis has been pursued to calculate quasi-linear Prandtl and momentum pinch numbers (RV_φ/χ_φ) for the peturbative momentum transport experiments reported in Ref. [2]. In many of these discharges microtearing modes dominant the unstable spectra, although there are sub-dominant ballooning modes, at least some of which behave like the hybrid KBM mode. The theoretically calculated Prandtl numbers for the hybrid KBM modes range between Pr<0.2-0.6 over the measurement region (Fig. 3.3.13). However, it may not be meaningful to use the Prandtl number as a figure of merit as the ion thermal transport is near neoclassical levels ($\chi_i \approx \chi_{i,neo}$). The pinch parameters are always rather small or even predict an outward convection of momentum (RV_φ/χ_φ=0-2) which is in contradiction to the experimental analysis (Fig. 3.3.12). While the KBM mode provides a mechanism for momentum transport, there is clearly a lack of understanding

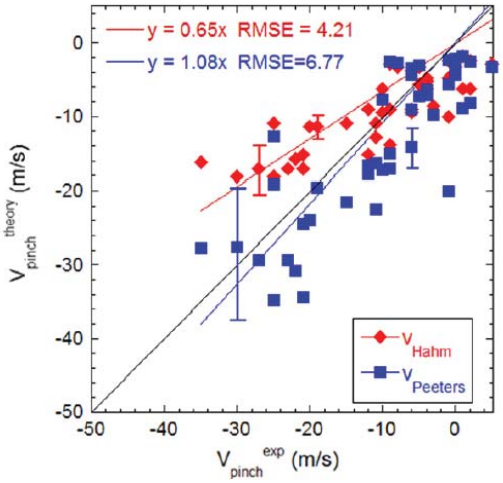

Fig. 3.3.12. V_{pinch} as computed by the Hahm (red) and Peeters (blue) theories versus experimentally inferred values for the outer region of the plasma.

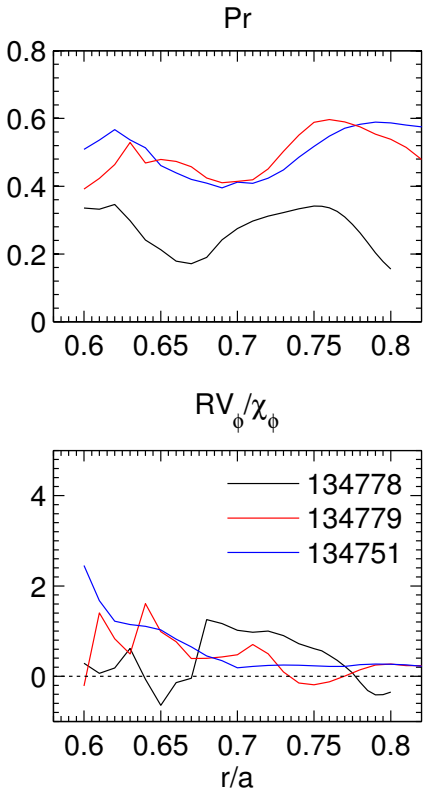

Fig. 3.3.13. Quasilinear Prandtl and pinch parameter (RV_ϕ/χ_ϕ) from hybrid ITG/KBM modes determined from linear GYRO simulations (for three discharges in Fig. 3.3.12).

relating the theoretical predictions with experimental measurements. Nonlinear gyrokinetic simulations are required to assess the Prandtl and Pinch numbers in the nonlinear state.

Intrinsic rotation generation was studied through the L-H transition in NSTX Ohmic plasmas, taking advantage of the zero momentum input and the long momentum transport time scale (~100 ms) compared to L-H transition time (~ 10 ms) [56]. The inferred intrinsic torque was found to correlate best with ion temperature gradient [see Fig. 3.3.14(a)], consistent with a theoretical prediction of residual stress driven by low-k turbulence [57]. Intrinsic torque is also measured in NSTX NBI-heated H-mode plasmas by using NBI torque steps and is found to have some correlations with pedestal pressure gradient [see Fig. 3.3.14(b)]. This result is qualitatively similar to the dependence on pedestal pressure gradient in DIII-D. We note that obtaining long-pulse steady-state plasma would be very beneficial for such a perturbative technique to measure intrinsic torque, and NSTX-U long-pulse scenarios would be ideal. To project intrinsic torque to future devices, the low-k turbulence generating intrinsic torque has to be identified. The research on intrinsic torque will be emphasized on NSTX-U.

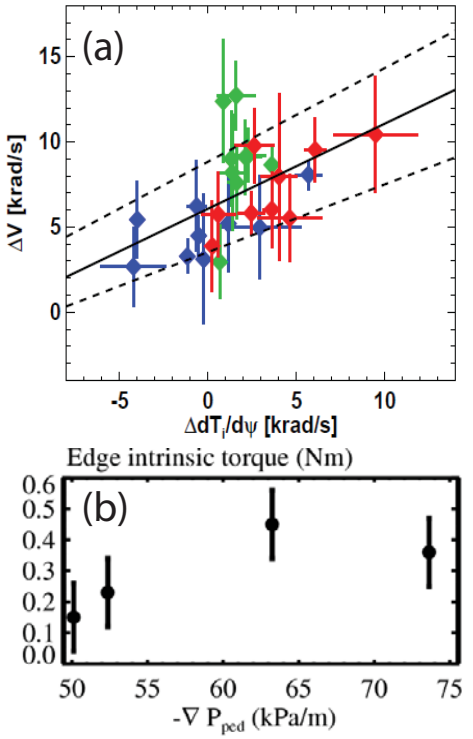

Fig. 3.3.14. (a) Change in intrinsic rotation (proportional to intrinsic torque) as a function of change in ion temperature gradient measured through Ohmic L-H transition (The blue colors for $0.64 < \rho < 0.72$, the green colors for $0.72 < \rho < 0.80$, the red colors for $\rho > 0.80$); (b) Edge intrinsic torque as a function of pedestal pressure gradient in NSTX H-mode plasmas.

The plan on momentum transport is to measure the responsible turbulence for transport and intrinsic torque and identify its regime of validity taking advantage of increased parameter regime of NSTX-U and its diagnostic and facility upgrades.

3.3.3.3.1 Research plans by year for Thrust TT-2: Momentum transport

Year 1

The plan of the first year of NSTX-U operation on momentum transport research will take advantage of the set of low-k turbulence diagnostics, BES, reflectometry and polarimetry, which will be ready at the beginning of first NSTX-U run campaign. Effective χ_φ will be determined through TRANSP analysis together with ion thermal transport in H-mode plasmas achieving lower collisionality with the extended range of B_T and I_p (the experiments addressing Thrust TT-1). Trends in both χ_ϕ and $\chi_i/\chi_{i,neo}$ vs B_T, I_p and collisionality will be studied to identify correlations. Linear gyrokinetic simulations will be used to identify relevant linear instabilities, and inferred momentum transport and low-k turbulence measurements will be compared with nonlinear gyrokinetic simulations. The 2nd NBI and external coils will be used to vary q and flow profiles (E×B shear and parallel velocity shear) to modify underlying turbulence in order to explore the correlation between low-k turbulence and momentum and ion thermal transport. Furthermore, momentum diffusivity, pinch and intrinsic torque will be measured in perturbative momentum transport experiments using NBI and external coil pulses in H-mode plasmas, particularly in microtearing-dominant and ETG-dominant regimes. These studies will be guided by gyrokinetic simulations, and their predicted parametric dependence on q, $\hat{s}$ and flow profiles (E×B shear).

Year 2

The study of effective χ_φ dependence on B_T, I_p and collisionality will be continued in the second year of NSTX-U operation as NSTX-U operation is attaining even lower ν_e^* values with full field strength and plasma current. Perturbative momentum transport experiments will also be carried out in selected H-mode plasmas to determine momentum diffusivity, pinch and intrinsic torque, with a goal of studying their parametric dependence in the expanded parameter range of B_T, I_p and collisionality. Additional perturbative momentum transport experiments will be carried out in isolated regimes for ITG/TEM modes, e.g. in NBI-heated L mode plasmas, guided by gyrokinetic simulations. Validation of gyrokinetic codes against the above experiments will be performed.

Studies of intrinsic rotation will be carried out with passive CHERS in scenarios with negligible external momentum input (e.g. RF-heated and Ohmic plasmas) coupled with low-k turbulence measurements, i.e. reflectometry and polarimetry, and its parametric dependence on B_T, I_p and collisionality will be investigated.

Year 3-4

The long-term goal for momentum transport research is to identify low-k turbulence responsible for anomalous momentum transport and intrinsic torque and its operational regimes coupled with

gyrokinetic simulations. This long term goal will be carried out through investigation of the further parametric dependence of momentum diffusivity, pinch and intrinsic torque, e.g. on β, ν^*, T_i/T_e and Z_{eff}, coupled with low-k turbulence measurements, and it will be facilitated by density control capability from the planned implantation of a cryopump, which will help decouple ρ^* and ν_e^* dependence. Perturbative momentum transport measurements with NBI and external 3D coil/NCC pulses will be the main experimental method to measure momentum diffusivity, pinch and intrinsic torque. Furthermore, the effect of 3D effects (from external 3D coil and NCC) on intrinsic torque will be addressed with the combination of experiments and modeling with global gyrokinetic codes, e.g. GTS and XGC1 [58]. The engineering capabilities of NSTX-U will be exploited to expand achievable plasma parameters. In particular, momentum transport studies in long-pulse and fully non-inductive scenarios will be emphasized in this period. Studies of intrinsic rotation will continue with expansion in parametric dependences and coupling with gyrokinetic simulations.

3.3.3.4 Particle/impurity Transport

Understanding particle/impurity transport is also of great importance to the performance of future devices. Predicting density profile is required to predict bootstrap current which is essential to develop non-inductive long pulse scenarios required for operating all future devices. Understanding the mechanisms underlying impurity transport is important for controlling impurity accumulation in the core of plasma which dilute fuel ions (low-Z impurity) and increase radiation loss (high-Z impurity).

In NSTX, particle transport has been studied by using particle balance analysis. One example is shown in Fig. 3.3.15, where the range of inferred particle fluxes and predicted levels for neoclassical particle transport for the thermal deuterium ions is plotted as function of square root of normalized toroidal flux for an NSTX NBI-heated L-mode plasma. This comparison indicates that the particle flux ranges are comparable to what would be expected from neoclassical transport within r/a~0.6. A greater difference between the two is seen for larger radii, but the experimental determination of particle transport is very uncertain at larger radius due to not knowing the precise source of neutrals from gas puffing. Particle transport of the main plasma species appears to be somewhat decoupled from the energy transport (see Fig. 3.3.8) in that the

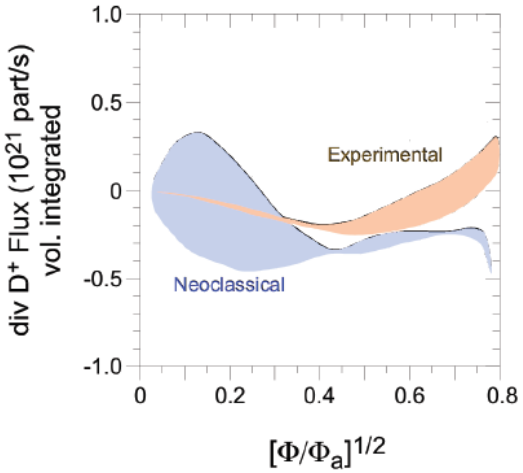

Fig. 3.3.15. Inferred and neoclassical deuterium particle fluxes for L-mode scan

particle transport appears to be consistent with neoclassical estimates in the core (r/a<0.5) of the plasma, while the ion thermal transport for these plasmas is anomalous. Future steady-state particle transport analysis will require better modeling and measurement of edge neutral source (from gas puff and recycling) and neutral penetration into plasma.

In order to understand impurity transport and thus to control impurity content, impurity transport has been emphasized, particularly in ELMy (with boronized PFCs) and ELM-free (with lithiated PFCs) NSTX H-mode plasmas. Carbon is the main impurity in NSTX and CHERS diagnostic provides measurement of its density profile. Carbon transport in NSTX H-mode plasmas is studied with predictive modelings using MIST (an impurity transport code) [59] coupled with NCLASS (a local neoclassical code) [51], where fully predictive MIST runs with time-dependent neoclassical values for both D and v determined from NCLASS are used to derive the full neoclassical prediction of the impurity charges states. In Fig. 3.3.16 the experimental carbon density (n_c) and the n_c evolution as predicted by MIST, assuming neoclassical transport coefficients, are plotted versus radius and time for a discharge with boronized PFCs (ELMy) and a discharge with lithium coatings (ELM-free). The neoclassical prediction for the discharge with boronized PFCs is in reasonable agreement with the experimental profiles. Edge peaking

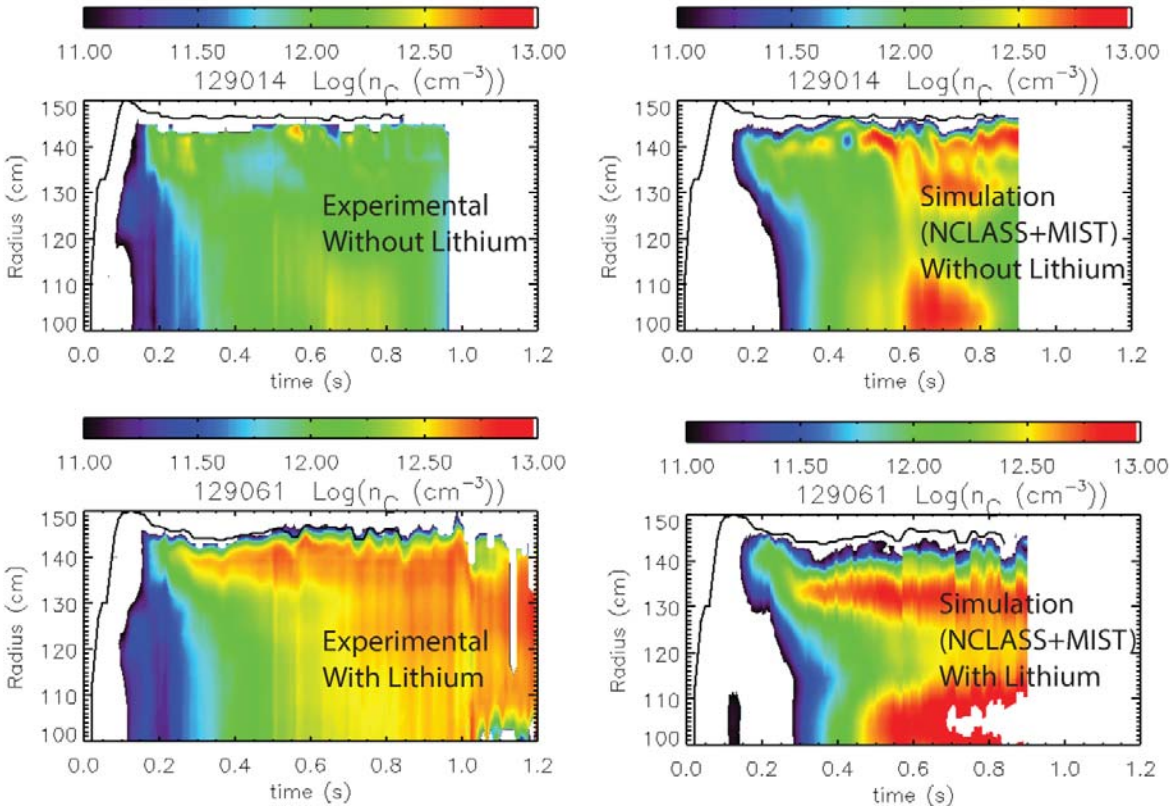

Fig. 3.3.16.. Evolution of the carbon density profile vs time and radius for the experimental measurements in a NSTX H-mode plasma (left panel; boronized discharge- TOP - lithiated discharge - BOTTOM), predictive MIST calculation (right panel; boronized discharge- TOP - lithiated discharge - BOTTOM).

stronger than that observed experimentally can be associated to the impurity flushing effect of ELMs. The neoclassical prediction for the discharge with lithium coatings again shows agreement in the early evolution of the discharge while for later times, when the fuel dilution becomes more important, only qualitative agreement is found. Further analysis shows that an anomalous outward convective component in discharges with lithium conditioning is needed to explain the experimental profiles.

Perturbative trace impurity transport has also been measured with a multi-energy SXR diagnostic in NSTX H-mode plasmas coupled with the STRAHL 1D impurity ion radial transport code [60]. The impurity transport profiles calculated by STRAHL for an I_p = 0.8 MA, B_T = 0.40 T

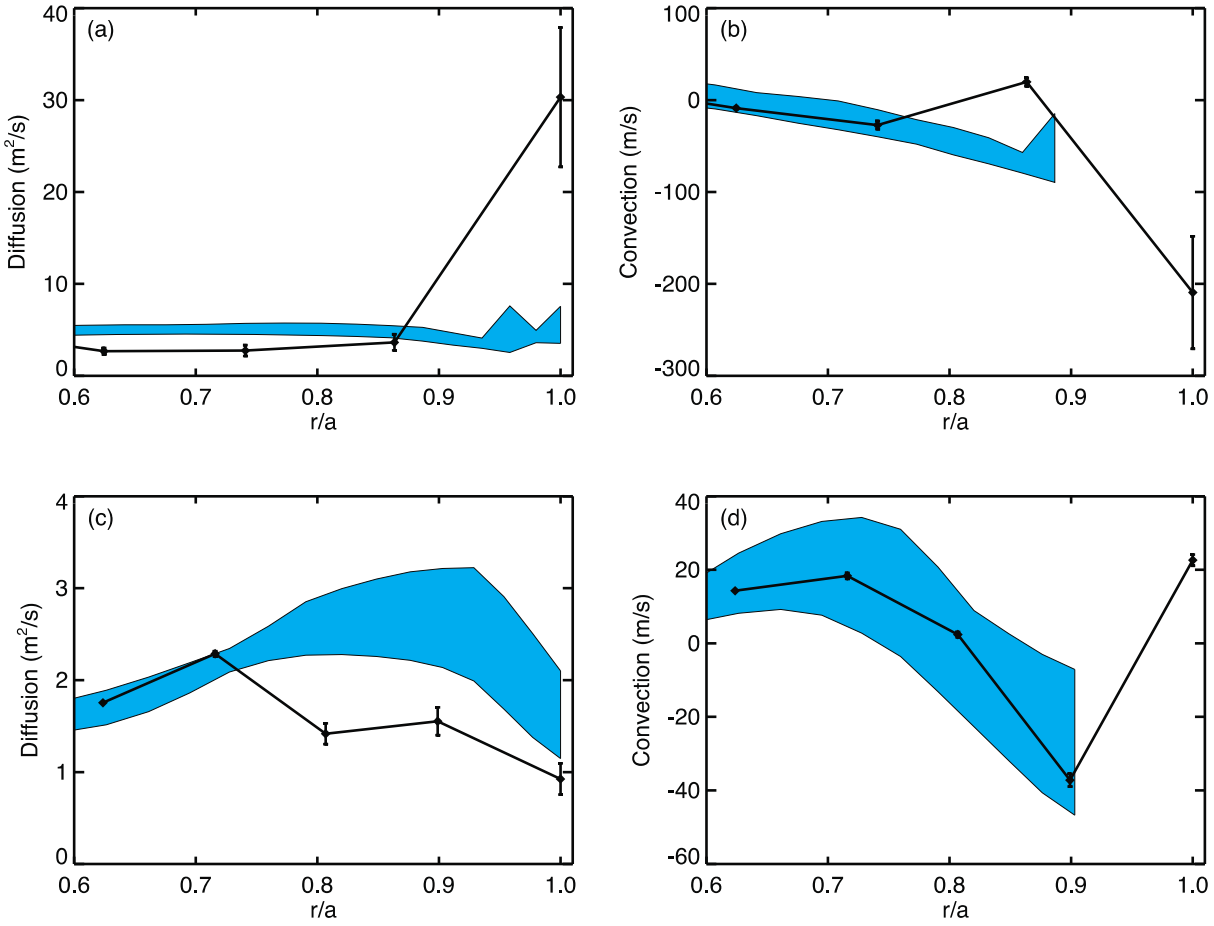

Fig. 3.3.17. The resulting diffusion profile and (b) convection profile from the I_p = 0.8 MA, B_T = 0.40 T discharge. The shaded region represents the results from NCLASS neoclassical transport calculations, covering the variation in the calculations during the time frame of the measurement.. (c) Diffusion profile and (c) convection profile for the I_p = 1.1 MA, B_T = 0.55 T case. The radial knots are defined for fixed values of ρ_{pol} and thus shift radially between the two cases with different q profiles.

discharge and an I_p = 1.1 MA and B_T = 0.55 T discharge together with neoclassical transport calculations (shaded regions) are shown in Fig. 3.3.17. The error bars represent the uncertainty in

the transport profiles due to uncertainty in the ME-SXR and Thomson measurements and in the neoclassical values used to constrain core transport.

The results from the measurements roughly match neoclassical calculations, in agreement with previous results from the core [14,61]. The diffusion coefficients obtained from measurements are within a factor of 2 of neoclassical transport across most of the plasma radius. Deviations from neoclassical diffusion in the edge region, particularly in the far edge of the low-field discharge, are likely due to edge turbulence. The convection profiles also roughly agree with neoclassical values, though NCLASS does not provide reliable convective velocities outside of r/a ~ 0.9. For the two cases shown, the neoclassical convective velocity remains outward far into the core, which is consistent with the hollow neon profile found in the STRAHL simulations at later times. Previous results from core measurements have shown that neon convection near mid-radius can be either inward or outward, depending on the ion temperature and density profiles, and that neon profiles can thus be either peaked or hollow [14, 61]. The conclusion is that inside the pedestal region and under the conditions of these quiescent discharges, plasma turbulence is not sufficient to alter transport from neoclassical levels, consistent with the steady-state impurity transport analysis shown in Fig. 3.3.16.

The above particle and impurity transport results in NSTX H-mode plasmas signify the importance of neoclassical transport in determining both density and impurity profile and also indicates that turbulence-driven anomalous transport can play a role. As we have pointed out, NSTX-U plasmas will have a factor of 3-6 reduction in collisionality and this will significantly reduce neoclassical transport. Thus it is important to determine how important neoclassical mechanism is to particle and impurity transport in the low collisionality regime of NSTX-U and what turbulence and its operational regime in driving anomalous particle and impurity transport. Furthermore, the installation of a laser blow-off system and metal PFC in year 2 (and more metal PFC in subsequent years) will allow us to study high-Z impurity transport in NSTX-U and compare it with neoclassical transport. Results will be compared with those from large aspect ratio tokamaks, e.g. DIII-D. Understanding high-Z impurity transport is important since both ST-FNSF and ITER will have all metal PFC. NSTX-U will have the unique capability to address high-Z impurity transport in low collisionality and high β regime which is relevant to ST-FNSF and ITER.

3.3.3.4.1 Research plans by year for Thrust TT-2: particle/impurity transport

Year 1

In the first year of NSTX-U operation, impurity and particle transport will be studied in H-mode plasmas achieving lower collisionality (and lower neoclassical transport) with the initial extended range of B_T and I_p (similar to experiments addressing Thrust TT-1) in both ELMy (with

boronized PFCs) and ELM-free (with lithiated PFCs) regimes. Impurity diffusivity and pinch will be determined using perturbative methods (trace-impurity with the Multi-energy SXR diagnostics [32]), and carbon and lithium transport will be studied using CHERS measurements coupled with interpretive and predictive modeling using impurity transport codes, e.g. MIST [59] and/or STRAHL [60], and neoclassical codes, e.g. NCLASS [51], GTC-NEO [52] and NEO [53]. Particle transport studies will be carried out through steady-state analysis by TRANSP, coupled with modeling and measurement of edge neutral source (with calibrated D_α measurements from MSE and/or BES diagnostics as a constraint) and neutral penetration into plasma using neutral transport code DEGAS 2 [62]. It is important to determine the trend of impurity and particle transport with respect to neoclassical transport as a function of collisionality and the correlation with low-k turbulence, particularly in lower collisionality H-mode plasmas of NSTX-U that are most relevant to the operation scenario to future machines. Particle and impurity measurements will also be carried out in microtearing-dominant and ETG-dominant H-mode plasmas (guided by gyrokinetic simulations), taking advantage of improved NSTX-U plasma and engineering parameters and the set of low turbulence diagnostics. Impurity transport will be correlated with low-k turbulence measurements with BES, reflectometry and polarimetry coupled with neoclassical calculations and gyrokinetic simulations using synthetic diagnostics. Profile variation capabilities for q and flow profiles using 2nd NBI and external coil will be used to alter neoclassical transport and low-k turbulence, helping to separate neoclassical and turbulent drives underlying impurity transport.

Year 2

In the second year of NSTX-U operation, we will continue impurity and particle transport studies in NSTX-U H-mode plasmas toward even lower ν_e^* values (compared to year 1) with full field strength and plasma current. In particular, a laser blow-off system will be available in this year and will allow us to conduct non-recycling (high-Z) impurity injection, and the installation of metal PFC will also allow the study of high-Z impurity transport with steady-state analysis coupled with impurity transport codes. Impurity and particle transport against neoclassical transport will be assessed in even lower ν_e^* H-mode plasmas achieved in this period, and a combination of applying 2nd NBI and external 3D coils will be utilized to reduce anomalous impurity transport and to modify neoclassical transport in order to control impurity transport. Furthermore, the effect of RF-heating with High Harmonic Fast Wave (HHFW) on high-Z impurity transport will be assessed. Measurements will also be carried out in ITG/TEM-dominant regime, e.g. NBI and RF-heated L-mode plasmas. Particle and impurity transport is expected to be anomalous in such plasmas due to small ExB shear leading to strong low-k turbulence. Again, profile variation capabilities for q and flow profiles using 2nd NBI and external 3D coils will be used to separate neoclassical and turbulent drives underlying particle and impurity transport. Measured particle and impurity transport in above experiments will be correlated with low-k turbulence measurements with BES, reflectometry and polarimetry

coupled with neoclassical calculations and gyrokinetic simulations via synthetic diagnostics to determine the underlying turbulence. Furthermore, as a more robust validation of gyrokinetic codes, simultaneous comparison of thermal, momentum and particle/impurity transport and low-k turbulence measurements with nonlinear gyrokinetic simulations will also be carried out.

Years 3-4

In long term, low-k turbulence responsible for anomalous particle/impurity transport and its operational regime will be identified with low-k turbulence measurements, steady-state/perturbative impurity transport measurements, particularly using the laser blow-off system for non-recycling (high-Z) impurity injection, and measurements will be coupled with neoclassical calculations and gyrokinetic simulations through synthetic diagnostics developed in previous years. The identification will take advantage of the full range of plasma parameters of NSTX-U with parametric dependences expanded to β, ρ^*, T_i/T_e and Z_{eff} etc., which facilitates distinguishing individual instabilities. In particular, particle and impurity transport properties and underlying mechanisms in long-pulse and fully non-inductive scenarios will be emphasized due its relevance to the long pulse and steady-state operation of future devices. It is worth pointing out that in this period of NSTX-U operation, more high-Z (Mo/W) PFCs will be installed and impurity transport studies of Mo/W will receive increased emphasis. In addition, 1 MW ECH/EBW heating will be available in this period and its effect in controlling high-Z impurity accumulation will also be assessed.

3.3.4 Thrust TT-3: Establish and validate reduced transport models (0D and 1D)

During the next five year period substantial emphasis will be placed on using the transport code (P)TRANSP [33] and the transport solver TGYRO [34] incorporating various transport models to predict core plasma profiles in NSTX-U plasmas. As discussed in Section 3.3.3 (Thrust TT-2), there are multiple core transport mechanisms to consider including (i) neoclassical, (ii) drift wave microinstabilities, and (iii) energetic particle instabilities. Neoclassical theory is largely well established for tokamaks, with various models available based on analytic theories [63,64], moment-method approach (NCLASS) and kinetic calculations (GTC-neo; NEO; XGC-0 [65]).

The drift wave microinstabilities (ITG, TEM, ETG, MTM, KBM) are driven by gradients in thermal plasma parameters, which can generally contribute transport in all channels (heat, particle, momentum). Reduced transport models for drift waves are less developed (not as broadly successful at predictions compared to neoclassical theory), although significant advances in theory-based models have been made such as TGLF [66] and the Multi-Mode Model [67]. One goal of this thrust will be to validate the available reduced models with first principles gyrokinetic simulations for parameters relevant for NSTX-U. Semi-empirical or analytic models

based on simulation results will also be considered depending on the success of the available reduced transport models.

The energetic particle driven GAE and CAE modes are driven by phase space gradients in the fast ion distribution function. An important consequence of these modes is that they redistribute fast ions (Chapter 6), although for the purposes of this chapter we are interested predominantly in their effect on electron thermal transport. There have been recent advances for modeling the electron thermal transport due to stochastic particle orbits in the presence of energetic particle driven modes like GAEs and CAEs, assuming a knowledge of the mode spectrum and amplitude (e.g., from measurement). Simulations are required to develop theory based description of mode onset and nonlinear spectra that would provide foundation for a purely theory-based transport model.

The following section will discuss recent results relevant for developing predictive capability for these various mechanisms. Following this are the research plans for the five year period.

3.3.4.1 Recent results

As shown in Sec. 3.3.3.1 ion thermal transport in NSTX H-modes is often well described by neoclassical theory (Figs. 3.3.10, 3.3.11). A validation of the predictive capability of neoclassical theory has been demonstrated for ion thermal transport by using only the Chang-

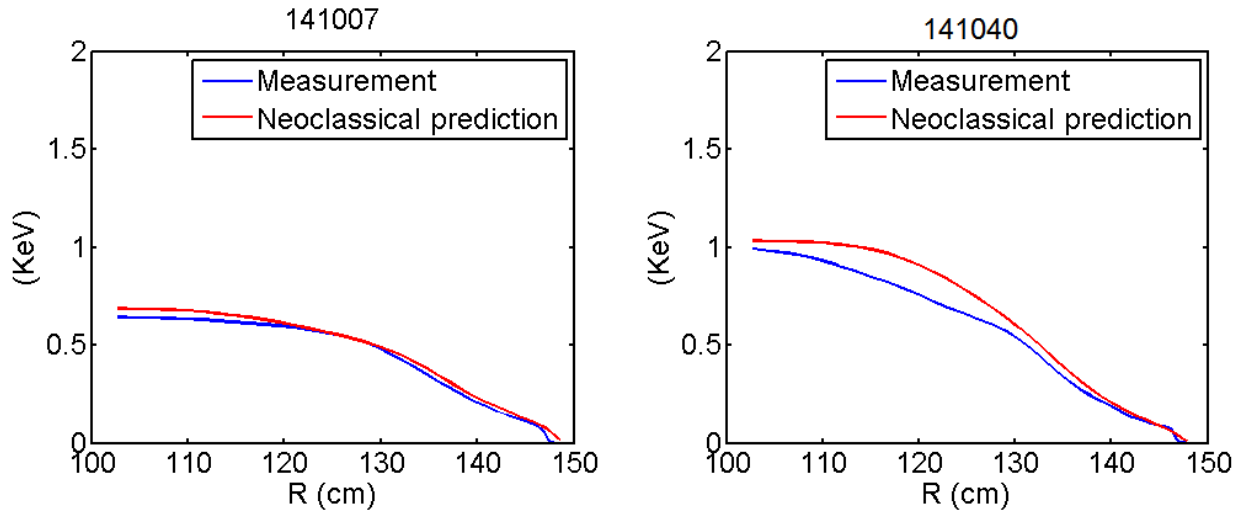

Figure 3.3.18. Prediction of T_i using TRANSP with the Chang-Hinton neoclassical transport model in NSTX H-modes.

Hinton model to predict T_i profiles. This is accomplished in TRANSP using the experimentally inferred heat flux and keeping density and electron temperature fixed to the experimental

profiles. Fig. 3.3.18 shows the neoclassical predictions agree well with the measured T_i profile in two H-mode discharges that are part of a recent ν_* scaling experiment [18]. Similar agreement has been found in other H-mode predictions providing a level of confidence in using neoclassical ion predictions in the NSTX-U scenario studies [22,50]. However, as seen in Fig. 3.3.18, the neoclassical prediction for the lower collisionality NSTX discharge (141040) is already becoming larger than experiment in the inner core suggesting a non-negligible anomalous contribution.

We also note that particle and impurity transport predictions using only neoclassical theory are able to predict carbon profiles shapes in some cases as shown in Sec. 3.3.3.3. One exception occurs at low collisionality with lithium wall conditioning (Fig. 3.3.16). Whether this is due to inadequacy of local neoclassical theory (which can be tested with global codes like GTC-neo) or an unaccounted for anomalous contribution is presently under investigation. Understanding and improving these ion temperature and density profile predictions at low collisionality are of high priority for NSTX-U.

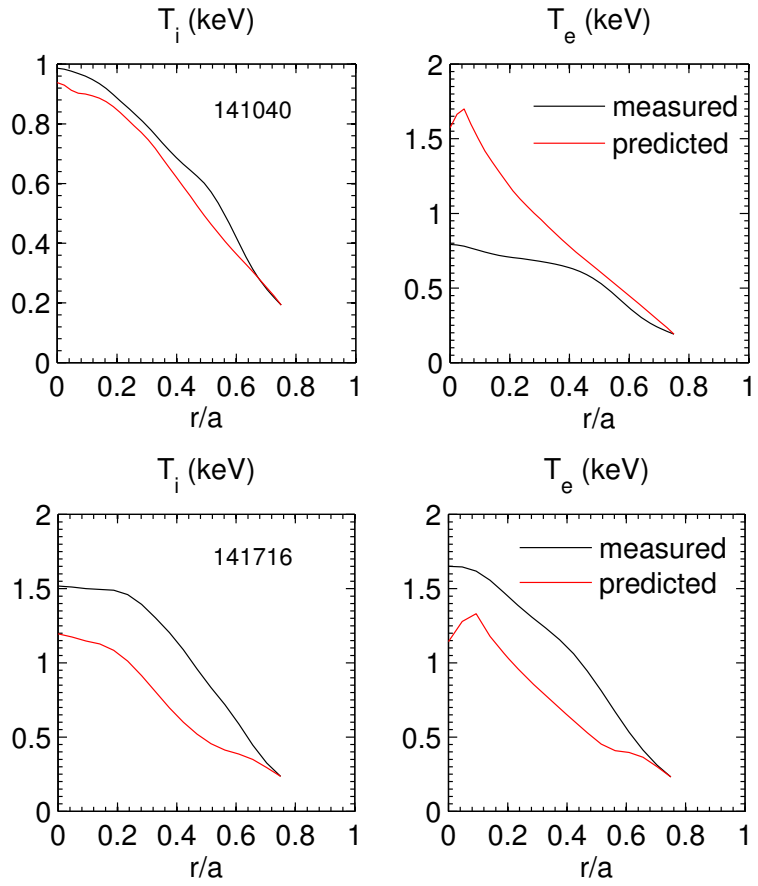

Fig. 3.3.19. Predicted (left) T_i and (right) T_e profiles using TGYRO+TGLF+NEO for (top) low beta NBI H-mode (141040), and (bottom) NBI L-mode.

Predictions of both ion and electron temperature profiles have also begun using the TGYRO transport solver including both neoclassical (NEO) and anomalous drift wave contributions as predicted by TGLF. For a discharge linearly unstable to ETG modes (Fig. 3.3.19, top), there is reasonable agreement in the T_e profile in a narrow region of r/a=0.5-0.7, but the discrepancy becomes quite large inside r/a<0.5. This is likely a result of either a missing transport contribution from energetic particle modes (GAE, CAE), inaccuracy of TGLF for these particular NSTX parameters, or non-local turbulence spreading which is not captured in the local TGLF model. The T_i prediction

remains close to experiment, although in this case is completely fortuitous as the model predicts the ion heat flux is dominated by turbulent modes inconsistent with experimental analysis. For an L-mode dominated by ITG instability (Fig. 3.3.19, bottom), both T_e and T_i are severely underpredicted. These NSTX transport predictions illustrate a number of issues that must be resolved including (i) developing and integrating a model for energetic particle induced electron thermal transport, (ii) improving quantitative accuracy of drift wave models for ST parameters, and (iii) incorporating non-local effects in the models (possibly important for relatively large $\rho^*=\rho/a$ values in NSTX).

As shown in Sec. 3.3.3.1 previous work has uncovered a strong correlation between Global Alfven eigenmode (GAE) activity and core electron transport in the core of high power NBI-heated NSTX H-mode plasmas [13]. Simulations using the ORBIT guiding center code showed that GAE activity can enhance electron transport when a large numbers of modes (> ~15) have sufficient amplitude to overlap and induce stochastic particle orbits [45]. The simulations demonstrate an extremely strong scaling of transport with amplitude (~ a^{3-6}) and showed that the amplitudes measured in the experiment could induce thermal transport that roughly agreed with the experimentally measured values from TRANSP [68].

Further analysis comparing mode frequencies to dispersion equations indicate that the observed modes with frequencies ~400-1000 kHz can actually be a mixture of both GAEs and Compressional Alfven Eigenmodes (CAEs) [69]. Additional simulations using the ORBIT code, modified to include compressional magnetic field perturbations [70], demonstrate transport from CAEs scale similar to GAEs, as illustrated in Fig. 3.3.20. First, a Gaussian radial structure for the CAE modes is chosen to match the experimentally measured mode peak location and width. Frequencies and toroidal and poloidal mode numbers are determined using measurements and theoretical dispersion equations. From these, ORBIT simulations predict a strong scaling of transport with mode amplitude (~ a^{3-4}). The predictions illustrate that CAE & GAE modes

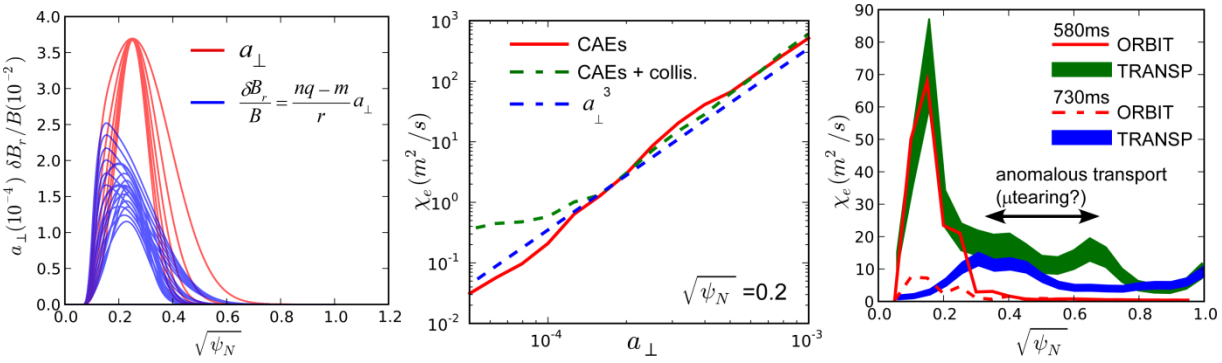

Fig. 3.3.20. (left) CAE model used for ORBIT simulations. (middle) Scaling of simulated CAE-induced electron transport with mode amplitude. (right) Comparison between ORBIT simulated electron transport and TRANSP experimental values.

combined can produce high levels of electron transport (~70 m^2/s) for r/a < 0.2 earlier in this particular discharge. Later in time the number of CAE modes appears to decrease and the corresponding predicted transport is smaller following the experimental trend.

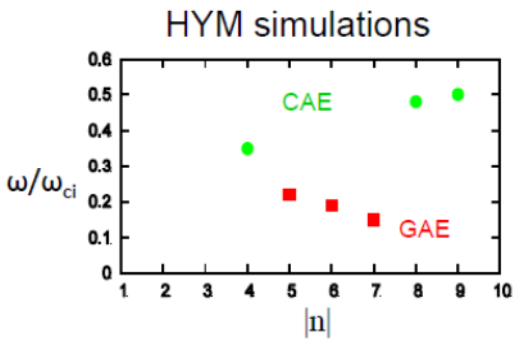

Fig. 3.3.21. Frequency vs. toroidal mode number for most unstable GAE (red) and CAE (green) modes, from HYM simulations for NSTX shot 141398. Frequency is normalized to ion cyclotron frequency at the axis (f_{ci}=2.5MHz).

The consistency between the ORBIT simulations and the TRANSP values for the core electron transport indicates that CAE/GAE modes are a good candidate to explain the high levels of core electron transport and flat electron temperature profiles in high power, NBI-heated, H-mode plasmas on NSTX. However, the predictions rely on measured mode structures and frequencies. Improved predictive capability will require first principles predictions of the unstable mode spectra, structure and nonlinear amplitude. For instance, recent simulations using the Hybrid MHD code (HYM) found that CAEs could in fact be destabilized simultaneously with GAEs (Fig. 3.3.21) in the core plasma region which matches the BES and reflectometer measurements of the radial mode structure. Future work will focus on additional linear and nonlinear simulations of GAE and CAE stability and saturation, and developing and implementing a model for electron thermal transport due to GAE/CAE mode that can be incorporated into transport solvers.

Improving the accuracy of reduced drift wave models requires validating them against first principles gyrokinetic simulations. This is complicated in NSTX plasmas as the high values of beta lead to many microinstability mechanisms (Table 3.1.1, Fig. 3.1.1), each of which exhibit their own unique thresholds and scalings. For accurate predictive capability it will be important to demonstrate that reduced transport models can recover the various microinstabilities and their thresholds and scalings. Such work has recently begun comparing the linear model within TGLF with gyrokinetic simulations. For an L-mode case, TGLF does in fact predict a dominant ITG mode (Fig. 3.3.22, left) with reasonable agreement in real frequencies, but with much larger growth rates. This is likely one reason why the predicted temperatures in Fig. 3.3.19 (bottom) were lower than experiment. For the low beta H-mode, TGLF also predicts ETG modes to be unstable with reasonable agreement in both real frequencies and growth rates (Fig. 3.3.22, right). For a higher beta H-mode, TGLF is also able to predict tearing parity modes over a range of k_θ with a destabilizing dependence on beta, similar to the microtearing modes predicted by GYRO. However, it does not reproduce the correct collisionality scaling. While TGLF can predict some of the appropriate behavior expected from first principles gyrokinetic simulations much more comprehensive validation must be pursued to demonstrate quantitative accuracy over the broad

range of parameters accessible by NSTX-U. Similar comparisons will need to be done for other reduced models such as the Multi-Mode Model.

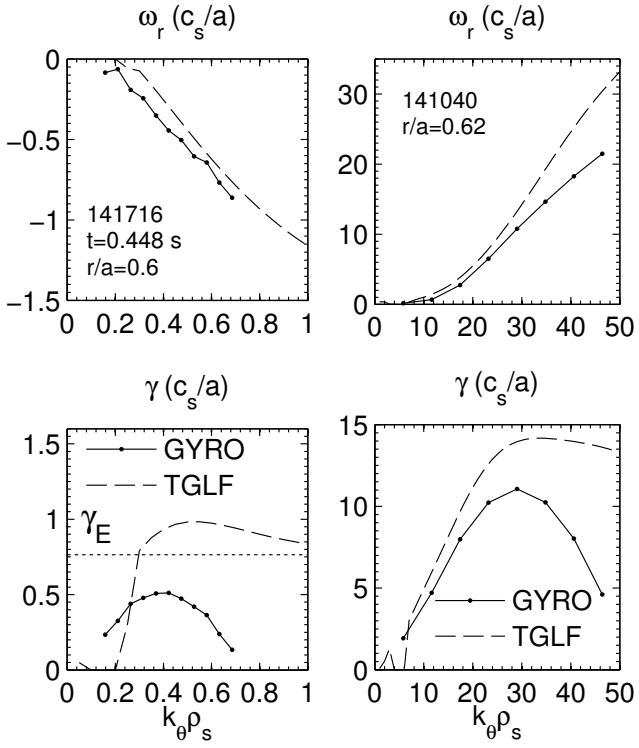

Fig. 3.3.22. (left) Real frequency and growth rates for ITG instability at r/a=0.6 in an NSTX L-mode from both linear gyrokinetics (GYRO, solid) and model (TGLF, dashed). (right) The same for ETG in a low beta NSTX H-mode.

Along with predicting the correct instability mechanisms, reduced transport models ultimately need to predict the correct magnitude of transport and parametric scalings, which can be validated with non-linear gyrokinetic simulations. Recent progress has been made simulating the nonlinear turbulence of each of the above microinstabilities, based directly on NSTX experimental equilibrium and measured profiles. Many of these were discussed already in Thrust TT-2. For example, the predicted microtearing transport (normalized to gyroBohm, $\chi_{GB}=\rho_s^2 c_s/a$) scales almost linearly with increasing electron collisionality, $\chi_{e,sim}/\chi_{GB}\sim(\nu_{ei}\cdot a/c_s)^{1.1}$, roughly consistent with the observed energy confinement time scaling in dedicated dimensionless experimental scans, $\Omega\tau_E\sim\nu^*_e{}^{-0.95}$ [4,5].

The predictions are also sensitive to increases in electron temperature gradient and beta, with transport increasing rapidly above the linear threshold in both β_e and a/L_{Te}. It is also found that experimental levels of E×B shear can significantly suppress the transport. It's important to note that microtearing transport models [71] based on Rechester-Rosenbluth stochastic transport

estimates do not capture these predicted scaling trends. Using a quasi-linear estimate of saturated amplitudes ($\delta B/B \approx \rho_e/L_{Te}$ [72]) the gyroBohm normalized model diffusivity can be written as [71]:

$$\frac{\chi_e^{RR}}{\rho_s^2 c_s / a} = \min\left[1, \frac{1}{\varepsilon^{3/2}\nu_{*e}}\right]\frac{1}{\mu}\frac{qR}{a}\left(\frac{a}{L_{Te}}\right)^2$$

where $\mu=(m_i/m_e)^{1/2}$, $\varepsilon=a/R$, $\nu^*_e = \nu_{ei}\cdot qR/\varepsilon^{3/2}v_{Te}$, and $\min[1,1/\varepsilon^{3/2}\nu^*_e]$ represents the collisionless ($L_c=qR$ for $\lambda_{MFP}>qR$) and collisional ($L_c=\lambda_{MFP}$ for $\lambda_{MFP}<qR$) limits. From this expression we see the model does predict a nonlinear dependence of transport with a/L_{Te} (similar to a stiff dependence). However it does not reproduce the threshold behavior in a/L_{Te} and β_e and if anything predicts a ν_* scaling opposite to that found from the non-linear simulations, illustrating the importance of pursuing the non-linear simulations for developing an accurate predictive transport model.

Recent simulation results have also been obtained for the hybrid TEM/KBM turbulence discussed in Thrust TT-2 (Fig. 3.3.4) [21]. In addition to electron heat flux, these simulations predict significant ion heat, particle, and momentum fluxes with significant contribution from the $B_{\|}$ perturbations (rms $\delta B_{\|}/B \sim 0.08\%$). This TEM/KBM, or overlapping TEM/KBM+MTM turbulence, provides one possible mechanism that could account for both anomalous electron and momentum transport in NSTX [2], and such simulations can eventually be used to validate impurity and momentum transport models for NSTX-U.

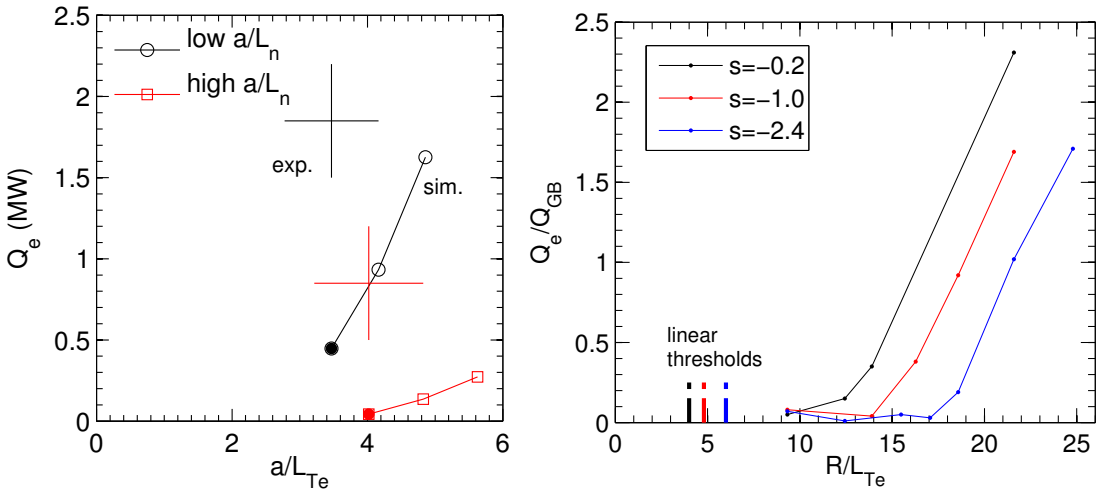

Fig. 3.3.23. (left) Predicted ETG heat fluxes vs. normalized temperature gradient for two different scenarios with significantly different density gradient. (right) Local nonlinear ETG transport vs. R/L_{Te} for varying magnetic shear illustrating the nonlinear upshift in effective threshold gradient.

The nonlinear trends discussed above generally follow linear predictions at least qualitatively, and it is hoped that reduced transport models like TGLF and MMM that are based on quasi-linear transport estimates will be able to capture such features. However, there are often specific non-linear effects that are not so easily captured. For example, nonlinear ETG simulations using dramatically different density gradient (Thrust TT-2, Fig. 3.3.6) show the predicted "stiffness" of ETG transport (i.e. the incremental increase of heat flux for incremental increase in driving gradient) is much smaller with larger density gradient (Fig. 3.3.23, left) [18]. On the other hand, for ETG simulations with strong reverse shear (Sec. 3.3.3.1), the transport stiffness is effectively the same regardless of variation in magnetic shear (Fig. 3.3.23, right) but the nonlinear threshold is varied considerably [17]. Successful transport models must also account for these effects that arise non-linearly.

3.3.4.2 Research plans by year for Thrust TT-3

The highest priority goal of this thrust is to significantly improve predictive capability for both ion and electron temperature profiles, especially the electron temperature as the T_e profile strongly influences confinement scaling, MHD equilibrium (through both resistivity and bootstrap current profiles), and MHD stability through pressure peaking. Towards the end of the five year period we hope to move towards a more integrated predictive capability including particle/impurity and momentum transport, although it is recognized these are often considerably more complex than the thermal channels to accurately model. To accomplish these goals, throughout the five year period we will continuously make and refine predictions with NSTX and NSTX-U data, employing (P)TRANSP and TGYRO, coupled with various transport modules for neoclassical transport, drift wave transport, and energetic particle driven electron thermal transport. As discussed above, we will also emphasize validating the reduced models with first principles simulations.

2014

In the year prior to NSTX-U operations additional effort will be applied to test predictive models for existing NSTX data over a wide range of scenarios, including NBI H-modes, RF discharges and L-modes. This will included more predictive tests of T_e and T_i profiles as discussed above using neoclassical and drift wave transport models. During this year we also intend to perform more validation studies of local neoclassical theory with global codes such as GTC-neo and XGC0.

Although a model for GAE/CAE electron thermal transport will not be available for predictive transport simulations (predicting profiles), modeling development based on ORBIT simulations for predicting electron thermal transport in the presence of GAE/CAE modes will continue. For this period models will predominantly be based on measured or assumed mode structures and

amplitudes to better characterize the sensitivity of predicted χ_e to these parameters. Linear HYM (see Sec. 3.4.1.3 for more about HYM code) simulations of the GAE/CAE stability properties will also continue throughout this year to better understand the threshold scalings of these modes with relevant parameters such as fast ion beta and phase space structures. A first attempt is planned to couple the ORBIT particle following code with HYM CAE/GAE mode calculations to predict core electron thermal transport due to these high-frequency fast ion-driven modes.

In addition, the available drift wave transport models (TGLF, MMM) will also be compared with linear and nonlinear gyrokinetics based directly on NSTX parameters to begin validating the accuracy of these reduced models. For comparison, linear gyrokinetic stability calculations will be pursued not only in the core, but also into the top of the pedestal and down into the sharp-gradient pedestal region, which has already begun [40,73]. This will be investigated using local and global codes to better characterize the influence of profile variations at the larger values of ρ/L in this region. This work will be tightly coupled with the boundary group (Chapter 4, Sec. 4.2.1).

Nonlinear simulations will also be used to calculate the magnitude and parametric scaling of the various turbulence mechanisms. Significant effort will be focused on understanding and demonstrating numerical convergence for the high beta, electromagnetic scenarios (from high performance discharges) as these are challenging computationally but critical to the successful validation of reduced models. In scenarios with multiple unstable modes (such as microtearing plus any of ITG,TEM, or KBM), parameter scans will used to elucidate how mode dominance varies in the nonlinear saturated turbulence, and how dynamics from fundamentally different modes interact and establish not just the magnitude of transport, but also the partition in different transport channels (thermal, particle, momentum). In addition, predictions of the turbulent transport in NSTX-U will be carried out using nonlinear gyrokinetic simulations, e.g. using the GTS code with kinetic electrons.

Year 1-2 of operation

One of the primary goals will be to verify the range over which neoclassical theory successfully predicts ion thermal transport. Predictions of T_i using only neoclassical theory will be performed for various H-mode scenarios to determine if and when discrepancies arise. In the first two years the focus will be on shorter duration discharges that span the full range of I_p, B_T, and P_{NBI}. It may be expected that if ion ballooning mode turbulence becomes more important at lower collisionality, neoclassical predictions will overpredict T_i as suggested by existing NSTX simulations. Throughout the analysis, and especially in regions where discrepancies do arise, the PPPL Theory codes GTC-neo (global) and XGC-0 (global, full-F) will also be used to validate the accuracy of the local neoclassical transport models.

In this period, impurity transport predictions will also be pursued in the same fashion as ion thermal transport for the extended range of NSTX-U operations. As there are uncertainties in the magnitude of the edge sources, only the profile shape will be predicted. The predictions will continue to use impurity transport codes such as MIST and STRAHL coupled with neoclassical models. NEO will be used to investigate the importance of centrifugal effects on the impurity transport as it is unknown how toroidal flow profiles will change for the extended NSTX-U operational space. In scenarios where both T_i and impurity profiles are well described by neoclassical theory, it should be straightforward to simultaneously predict T_i and impurity profiles self-consistently (while holding n_e and T_e fixed) as a first step towards multi-channel transport predictions.

Integrated transport modeling that includes both neoclassical and drift wave turbulent transport contributions (TGLF, MMM, …) will commence for predicting both T_e and T_i profiles based on NSTX-U discharges using boundary conditions chosen from measured profiles near the H-mode pedestal top (or near the edge in L-mode plasmas). The focus in the first two year period will be to identify if and when the predictions work well, particularly in the outer two thirds of the minor radius where drift waves are expected to be most important. Without a model for electron transport from energetic particle modes in the core, T_e predictions are likely to be inadequate. We will characterize when this discrepancy arises in operational space (I_p, B_T, n, P_{NBI}) as well as in radius ($0<r/a<0.5$), and investigate possible correlations with measured energetic particle mode activities (GAE, CAE) to better understand their possible contribution in modifying the core T_e profile. Although predicted core profiles may not be accurate near the magnetic axis, the discrepancy in stored energy should be relatively small due to the small plasma volume in that region ($V\sim r^2$). Therefore it should be reasonable to compare overall energy confinement times with those derived from scaling studies (Sec. 3.3.2.1) to assess whether the physical understanding encapsulated in the neoclassical and drift wave transport models is capable of recovering the favorable ν^*_e confinement scaling observed in NSTX plasmas.

Linear and nonlinear gyrokinetic simulations will be used to continue investigating parametric dependencies of each instability mechanism, each of which is critical for validating reduced transport models. These will be based on discharges in different experimental regimes of interest, including NBI H-modes and L-modes, and RF heated discharges, which will be tightly coupled with the validation work proposed in Thrust TT-2. However the emphasis for this thrust will be on better determining the most important parametric dependencies and quantitative thresholds of each instability mechanism (e.g. β_e and a/L_{Te} for microtearing, a/L_{Te} for ETG, α_{MHD} for the hybrid KBM modes), which can subsequently be used to validate reduced transport models.

Model linear stability predictions from TGLF and MMM will be validated with local linear gyrokinetic simulations, for a wide range of NSTX scenarios, comparing against the scaling and

thresholds of the various instabilities. As TGLF is an eigenvalue solver for gyrofluid equations that fundamentally can represent each mode of interest, it can be also be validated in regimes of overlapping unstable modes such as the TEM/KBM+microtearing discussed above. The quasi-linear fluxes for each transport channel and from each field contribution (φ, $A_{||}$, $B_{||}$) will also be validated with the gyrokinetics as this forms the basis for the TGLF transport model.

The nonlinear gyrokinetic simulations will be used to validate model transport. The initial focus in the first two years will be on thermal transport, especially χ_e, as an overall high priority goal is developing predictive capability for T_e and T_i profiles in NSTX-U over the full range of I_p, B_T, and P_{NBI}. In this period we will also explore developing alternative reduced models specifically for electron thermal transport. This could be as simple as prescribing analytic expressions to capture the most important χ_e dependencies predicted in the nonlinear simulations such as those discussed above for microtearing and ETG. These various contributions could be summed in the spirit of a "multi-mode model" and used in initial integrated transport predictions specifically for the electron temperature profile.

Global nonlinear simulations will be initiated in L-mode plasmas where predominantly electrostatic ITG,TEM instabilities are dominant. These low beta global simulations will allow us to most easily investigate the influence of non-local effects (turbulence spreading, diamagnetic shear, etc…) at the relatively large ρ^* values in NSTX and NSTX-U. If non-local effects are indeed found important, the possible incorporation of heuristic turbulence spreading models [74] will be investigated.

ORBIT simulations will continue using measured GAE/CAE mode structures to predict electron thermal transport, performed for numerous discharge conditions, especially high beta H-modes with different GAE/CAE characteristics (spectra and amplitude). Throughout this two year period it is should be possible to develop a stronger relation between assumed spectrum and amplitude of modes and the resulting stochastic electron thermal transport, and validate with experimental analysis (coupled with Thrust TT-2). In addition, predictions of GAE/CAE stability and mode properties will be continued using the HYM code across a range of operational space (P_{NBI}, n, I_p, B_T) to investigate the sensitivity and scaling of linear spectra with fast ion distribution function. Limited nonlinear HYM simulations will also continue to calculate saturated mode amplitudes which can be eventually be used directly in the ORBIT modeling simulations.

Years 3-4 of operation

In later years of the five year period the focus will shift towards modeling more advanced scenarios that should become achievable in NSTX-U operations. This will included long pulse, non-inductive scenarios (Sec. 9.2) which requires accurate bootstrap current calculations

(sensitive to plasma profiles) for predictive capability. New machine wall/boundary conditions such as different plasma facing components (Sec. 5.3) or installation of a cyropump (Sec. 4.2.3) will both likely influence particle sources and resulting density profiles. These scenarios should offer the best access to a wide range of collisionality and presumably be those best suited for basing extrapolations to next generation designs such as ST-FNSF and are therefore of great interest for validating predictive capability.

To accomplish this will require continued improvements and testing of the various transport modules, including an appropriate χ_e model for GAE/CAE driven transport. Throughout this period it is expected that results from additional linear and nonlinear HYM simulations will better clarify the most important criteria for characterizing GAE/CAE stability and mode structure. This information, coupled with ORBIT simulations, should allow for the development of a theory-based χ_e transport model for GAE/CAE modes. When available such a model will be integrated into the transport solvers and validated with NSTX-U data. The successful development and implementation of an energetic particle model for electron thermal transport is essential to achieve the high priority goal of T_e and T_i profile predictions. As the development of such a model is limited by available NSTX and PPPL Theory personnel, it could possibly be accelerated with incremental funding.

It is likely that the available drift wave models will also require improvements. For example, at present the Muti-Mode Model does not include a prediction of transport from microtearing modes. There are also known areas in the TGLF model that, if modified, will likely improve the agreement for low aspect ratio, high beta ST parameters, including separating curvature and grad-B drift effects (which is important at large equilibrium pressure gradient, and also related to $B_{||}$ dynamics critical to the TEM/KBM modes) and treating the different spatial scales of the eigenfunctions for microtearing modes (extended potential, narrow $A_{||}$). Both of these enhancements are being pursued by General Atomics with whom we will be working and providing feedback throughout this five year period on NSTX-U validation efforts in an attempt to improve the overall accuracy of TGLF for high beta plasmas.

Depending on the success of with T_e and T_i profile predictions, integrated transport simulations can be pursued, simultaneously evolving MHD equilibria with temperature profiles to study long discharge evolution to fully relaxed current profile (validating neoclassical resistivity) as well as ramp-up and ramp-down phases. Boundary conditions will likely be taken from measured edge profiles near the pedestal top. For a truly predictive capability of the entire H-mode profile, either empirical or theory based predictions of the H-mode pedestal parameters will be required, including pedestal temperature height and width for each plasma species. With a lack of predictive pedestal capability we will also test the sensitivity of the core profile predictions to uncertainties in the pedestal parameters.

Beyond establishing accuracy in temperature predictions, additional effort will be given to investigate and better predict particle, impurity and toroidal rotation. All of these profiles are important in determining a self-consistent understanding of the core confinement (e.g. density through instability drive, and q profile via bootstrap current; toroidal flow through stabilization of turbulent transport and macroinstabilities). It is difficult to assess the difficulties that may arise regarding this prediction as momentum transport is one of the least understood. However, we will continue to pursue integrated simulations in an attempt to best clarify strengths and weaknesses in the transport models; e.g., addressing scenarios that are theoretically only unstable to microtearing and/or ETG should lead to virtually no anomalous contribution to momentum or impurity transport. If these scenarios are not explained by neoclassical theory (or possibly energetic particle modes), there is quite likely a deficiency in our understanding of the predicted transport mechanisms. Integrated transport simulations will be used to test the ability of drift wave models and neoclassical theory to predict density (all species) and toroidal flow profiles. Initial simulations could test individual transport channels, for example fixing temperature and flow profiles to predict density. In cases where temperature profiles are successfully predicted, it should be viable to predict densities and temperatures self-consistently.

Transport models will also be validated for particle, impurity and momentum fluxes using available simulations. Both linear and nonlinear simulations can also be used to calculate the predicted scaling of Prandtl (χ_φ/χ_i) and momentum pinch (RV_φ/χ_φ) numbers, although it will likely be necessary to reconsider the relevance of the Prandtl number in scenarios where ion thermal transport is neoclassical ($\chi_i \approx \chi_{i,NC}$). Similar analysis for particle and impurity transport can be pursued analogous to the momentum transport to calculate the relative size of impurity diffusivity and convective fluxes (e.g., V_Z/D_Z). Nonlinear simulations will also be used to address the issue of residual stresses and intrinsic rotation. Such efforts will help elucidate the relative importance of the various mechanisms that may contribute to residual stresses in NSTX-U, e.g. up-down asymmetry [75] or finite ρ^* effects [76] and the ability of transport models to accurately predict these effects.

As PPPL Theory global gyrokinetic codes (GTS, XGC-1) progress to include complete electromagnetic response, global simulations will be pursued to investigate non-local effects in high beta H-modes where different unstable modes can co-exist at similar wavenumbers and the dominant unstable mode can vary depending on minor radius. In particular, XGC-1 fully global simulations that include the H-mode pedestal will allow for investigation of the turbulence interaction between pedestal, top of pedestal, and confinement regions in the larger ρ^* plasmas in STs (in conjunction with the Boundary group, Sec. 4.2.1), and if successful should provide a first principles profile prediction without the need for a reduced transport model.

3.4 Summary timeline for tool development to achieve research goals

3.4.1 Theory and simulation capabilities

3.4.1.1 Gyrokinetic codes

GS2

GS2 [77] is a local "flux-tube" Eulerian gyrokinetic code based on the delta-f formulation, capable of including comprehensive physics: arbitrary numerical MHD equilibria, multiple gyrokinetic species, sophisticated collision operator, fully electromagnetic perturbations (shear and compressional), toroidal flow and flow shear. It is run for rapid linear stability calculations as well as nonlinear simulations. There are many users and good documentation with support available from code developers (Maryland, MIT, Culham).

GYRO

GYRO [78] is similar to GS2 except also has capability for including profile variations (often referred to as global) for studying non-local, finite ρ_* effects which is important for the relatively large $\rho_*=\rho_s/a$ values in NSTX and NSTX-U. It has excellent documentation with prompt support from code developers (General Atomics).

GENE

GENE [79] is similar to GS2 and GYRO. It has recently expanded to perform radially global simulations, as well as poloidally global to address 3D geometry effects e.g. from external coil perturbations. It also has unique numerical algorithms that have been developed to improve performance for the extreme parameters that occur in the pedestal region. It has excellent documentation with support available from code developers (IPP-Garching).

GKW

GKW [80] is similar to GS2, GENE and GYRO. It is presently the only gyrokinetic code to have implemented centrifugal effects for large toroidal flow, allowing for investigation of poloidal asymmetry on particle and impurity transport, as well as influence of poloidally varying density gradient on mode thresholds (such as KBM). There is a growing number of users with much documentation available and available support from code developers (Bayreuth).

GTS

The Gyrokinetic Tokamak Simulation (GTS) [35] code is a full geometry, massively parallel, global delta-f particle-in-cell code developed at PPPL. It can use globally consistent numerical

MHD equilibria reconstructed by MHD codes and employs general magnetic coordinates and a field-line-following mesh. Fully-kinetic electron physics is included in GTS. The real space, global Poisson solver, in principle, retains all toroidal modes from (m/n = 0/0) all the way up to a limit which is set by grid resolution, and therefore retains full-channel nonlinear energy couplings.

Ongoing code development which extends GTS physics capability focuses on:

- Implementation of a new split-weight scheme to achieve a robust, global EM capability critical for high-β, strongly shaped plasmas (e.g., NSTX-U). The new scheme uses fully-kinetic treatment of non-adiabatic electrons with the adiabatic part defined with respect to the total magnetic field $B_0+\delta B$ (including the magnetic perturbation). This unique, physics-based approach is mostly suitable for studying global Alfvenic turbulence and microtearing modes in high-beta fusion plasmas and magnetic reconnections.
- Upgrade of GTS to use equal-arc-length coordinates combined with field-line aligned mesh for improved resolution, efficiency and robustness which are critical for NSTX/U simulations.
- GTS will be extended to treat 3D MHD equilibria, including perturbed tokamak equilibria with islands, so as to simulate 3D effects in burning plasmas, including the NTM dynamics, MHD-turbulence interaction, and particle and heat transport across magnetic island and stochastic magnetic fields.
- The current treatment of energetic particles at GTS will be extended to inclusion of fully nonlinear dynamics.

XGC-1

(See Chapter 4, Sec. 4.3) XGC-1 [58] is a full-F, global PIC code developed at PPPL capable of uniformly treating closed flux surfaces all the way to the magnetic axis, separatrix, and scrape off layer.

3.4.1.2 Neoclassical codes

NCLASS

NCLASS [51] is a well-established, validated, comprehensive neoclassical model which calculates local neoclassical transport properties of a multi-species axisymmetric plasma of arbitrary aspect ratio, geometry and collisionality. NCLASS uses the Hirshmann and Sigmar formulation of neoclassical theory for a multi-species plasma, based on a fluid-moment approximation for the parallel and radial force balance equations to calculate resistivity, bootstrap current, particle and heat transport, rotation and radial electric field. NCLASS can be run as a standalone or as module integrated into TRANSP.

NEO

NEO [53] is a delta-f Eulerian code which provides first-principles based numerical calculations of the neoclassical transport (particle flux, energy flux, bootstrap current, poloidal flows, etc.). NEO solves a hierarchy of equations derived by expanding the drift-kinetic equation in powers of ρ^*, the ratio of the ion gyroradius to the system size. NEO includes the self-consistent coupling of electrons and multiple ion species via complete cross-species collisional coupling, the calculation of the first-order electrostatic potential via coupling with the Poisson equation, general geometry effects, and rapid toroidal rotation effects (including centrifugal effects). NEO has recently been upgraded to include the full linearized Fokker-Planck collision operator. Various reduced collision models are also implemented (Hirshman-Sigmar, zeroth-order Hirshman-Sigmar, and the Connor model) for comparison with analytic theory and testing. NEO has been extensively benchmarked and compared with analytic neoclassical theory.

GTC-NEO

GTC-Neo [52] is a full geometry, delta-f PIC code developed at PPPL to calculate nonlocal neoclassical transport and a self-consistent radial electric field due to the effects of finite orbit size and large plasma profile gradients. Without using any small parameter expansion, GTC-NEO directly solves the drift kinetic equations globally as an initial value problem, from the magnetic axis to the separatrix with appropriate boundary conditions, and with full particle drift orbit dynamics. Moreover, the large scale ambipolar electric field is also consistently calculated by solving the Poisson equation. GTC-NEO will be extended to treat 3D MHD equilibria, including perturbed tokamak equilibria with islands, so as to simulate 3D effects on neoclassical transport, including particle and heat transport across stochastic magnetic fields. The 3D capability of GTC-NEO will be coupled with linear MHD stability calculations, providing an effective approach for including comprehensive, global kinetic effects in MHD stability analyses.

XGC-0

(See Chapter 4, Sec. 4.3) Axisymmetric version of XGC-1, developed at PPPL which ignores turbulence field. It is unique for neoclassical calculation as it allows validation of local codes since it is not restrained by low ρ/L ordering assumption. It also includes neutral particles self-consistently.

3.4.1.3 Energetic particle codes

ORBIT

(see Chapter 6, Sec. 6.4.1) ORBIT [45] is a particle following code used to integrate particle trajectories for estimating stochastic orbit transport from GAEs and CAEs.

HYM
(see Chapter 6, Sec. 6.4.5) HYM [81] is a hybrid-MHD 3D global stability code that can be used to study the excitation of GAE and CAE modes.

3.4.1.4 Transport codes

TRANSP/PTRANSP
TRANSP [33] is a time-dependent, 1 ½-D tool for both interpretive and predictive analysis of tokamak, ST and RFP plasmas. The TRANSP code, first developed at PPPL, has been a centerpiece for transport analysis of the experimental fusion program in the U.S. since the 1970s. All the U.S tokamaks and many outside the U.S. (including JET, MAST, AUG, EAST and KSTAR) are able to analyze the rich set of diagnostic data they obtain by running TRANSP. The synthetic diagnostic capability of TRANSP has allowed it to be used effectively for diagnostic validation. Both the use and development of the TRANSP code is a world-wide effort. Physicists and software engineers from PPPL, Princeton Univ., Lehigh Univ., MIT, ORNL, General Atomics, JET and EAST have been or presently are directly involved in code development, ensuring a validated wide range of code capabilities hat can address a similar wide range of experimental scenarios.

In its interpretive mode, TRANSP converts measurements of temperatures, densities, magnetic fields and flow velocities into inferred energy/particle/momentum transport coefficients which are then suitable for understanding transport trends, comparison to saturated transport levels computed in non-linear gyrokinetic simulations, and other related analyses. This is only possible because so much effort has gone into developing and validating the routines that calculate the detailed heating, momentum, and particle sources from neutral beams, fusion products, RF,

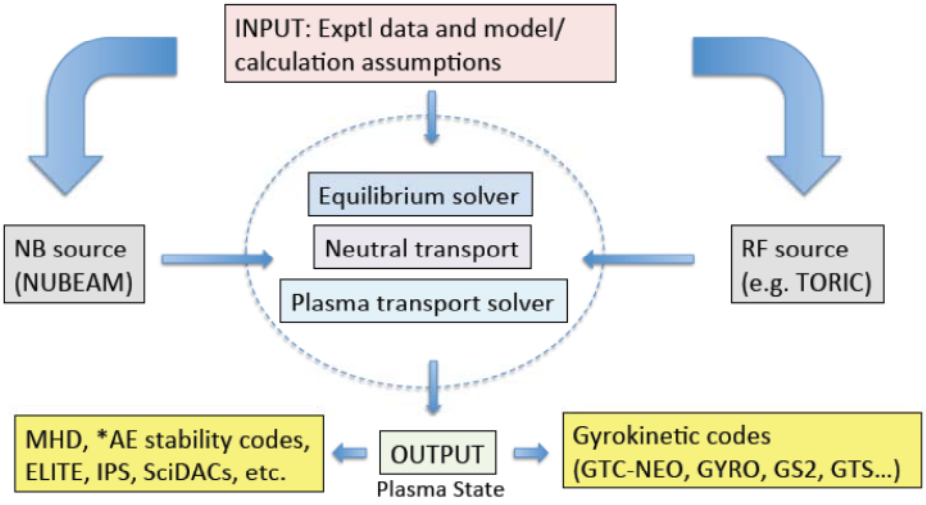

Fig. 3.4.1: Data and calculation flow for TRANSP

Ohmic, and compression. A chart of the data and calculation "flow" of TRANSP is shown in Fig. 3.4.1. Experimental data as well as model/calculation assumptions are fed into both the source modes (e.g., RF and NBI) and the kernel of the transport calculation, which consists of an equilibrium solver, neutral transport model and plasma transport solver.

The use of 0-, 1- and 2-D experimental data is integral to TRANSP. As examples, 0-D data and information include device geometry and NB/RF source configurations, 1-D data include I_p, B_T, diamagnetic flux, V_{loop}, D_a, neutrons, recycling coefficient, outer boundary, etc. as functions of time, and 2-D data include n_e, $T_{e,i}$, n_{imp} or Z_{eff}, P_{heat}, P_{rad}, $v_{f,q}$, B_q/B_T, neutrons, the full equilibrium, etc. as functions of time and space. TRANSP has the flexibility to calculate its own equilibrium internally by solving the poloidal field diffusion and Grad-Shafranov equations, or use a pre-calculated equilibrium from magnetic reconstruction codes such as EFIT. The plasma transport coefficients are then computed using this input and advancing the neutral particle transport equations coupled to the plasma particle, energy and momentum transport equations as functions of time and space. The inferred transport coefficients and fluxes can then be compared to those as calculated from models (simple or sophisticated) to attempt to determine whether the plasma is behaving neoclassically or is governed by turbulent processes, and if the latter to identify the modes driving the transport.

The NB and RF source models in TRANSP are state-of-the-art. NUBEAM [82] uses a 2/3-D Monte-Carlo approach with FLR effects to determine the neutral beam heating and current drive profiles, as well as the fast ion population. Both ad-hoc and, eventually, physics-based 2-D anomalous fast-ion diffusion can be included in this determination. NUBEAM is the most accurate and precise treatment of neutral beam deposition that is integrated into transport codes, and it is used world-wide. TORIC [83] is a full-wave code that addresses deposition of both ICRF and LH waves.

A notable development during this same time period has been the introduction of the Plasma State (PS) software and it subsequent use internal to TRANSP and in other projects. The PS is a netCDF-based file that contains all the physical quantities required to completely define the state of a tokamak plasma at a given time. This includes all variables related to the magnetic equilibrium, heating and current drive sources, and even the fast particle distribution. This well-documented standard interface for exchanging information between plasma physics codes was adopted by the both the SWIM and FACETS projects and It has become the de-facto standard in the U.S. plasma physics community. For example, self-consistent TRANSP output in the form of Plasma State files can easily be input to micro- and macro-stability codes for more fundamental, first-principles, analysis.

While TRANSP could always be run in a predictive mode, over the last several years the TRANSP developers have greatly expanded these predictive capabilities while simultaneously modernizing the code, increasing its modularity, and expanding and standardizing its ability to interface with other codes. It is now possible to develop discharge scenarios in present and future devices by using the predictive capabilities to predict the time evolution of the temperature profiles in a time-evolving, free-boundary magnetic configuration. The predictive code is called "PTRANSP", although it is really the same TRANSP code with certain input variables changed to indicate prediction rather than interpretation. In this mode of operation, the user specifies the thermal conductivity model to use as well as the boundary conditions on the magnetic equilibrium. All the heating, momentum, and particle source routines are identical for the PTRANSP and TRANSP modes of operation.

Developments to enable the full-predictive use of TRANSP over the last few years include (1) the development of a free-boundary equilibrium evolution capability with the correct flux and entropy constraints, and (2) the development of a parallel Newton-based temperature evolution capability that can accurately converge on solutions using modern thermal-conductivity models, among them GLF23, TGLF, and MMM. The free-boundary equilibrium solver, ISOLVER, allows for a self-consistent equilibrium solution that includes realistic constraints on currents in the actual set of poloidal field coils. This free-boundary evolution capability will be extended to incorporate poloidal field circuit equations in a form that can be used to develop algorithms for shape and profile control that can form the basis for actuator control. This capability can be used on present day tokamaks as well as on ITER. The newly implement transport solver, "PT_SOLVER", allows for a multi-zone treatment of the plasma transport, where different models can be used in zones representing the core, the gradient region and the edge. The solver is particularly suited to handle the stiff transport models as reflected in TGLF, GLF23, etc. A large collection of state-or-the-art, as well as older, transport models can be used for the predictive analysis.

Other developments leading to an enhanced fully-predictive capability include: (3) having the NUBEAM package for calculating neutral beam and fusion product heating now running in a parallel processing mode, and (4) the full coupling to the parallel processing version of TORIC for RF heating calculations. These four capabilities, taken together, have combined to make PTRANSP a unique tool for predictive modeling of present and future tokamaks, including ITER. The code's parallel structure and algorithms are well suited to make effective use of modern parallel computing clusters and supercomputers such as exist at PPPL, NERSC and ORNL.

TGYRO

TGYRO [34] is a parallel transport manager with the ability to call multiple instances of GYRO and NEO in order to obtain steady-state temperature and density profiles. It has the capability to include turbulent fluxes from GYRO, TGLF or the simple IFS-PPPL model and neoclassical fluxes from NEO, NCLASS or simpler Hinton-Hazeltine and Chang-Hinton theories.

DEGAS 2

DEGAS 2 [62] is a Monte Carlo code for studying neutral transport in plasmas, with emphasis on fusion applications. DEGAS 2 simulates the transport and behavior of neutral species generated by plasma wall interaction (as well as neutrals sourced externally or by volumetric electron-ion recombination).

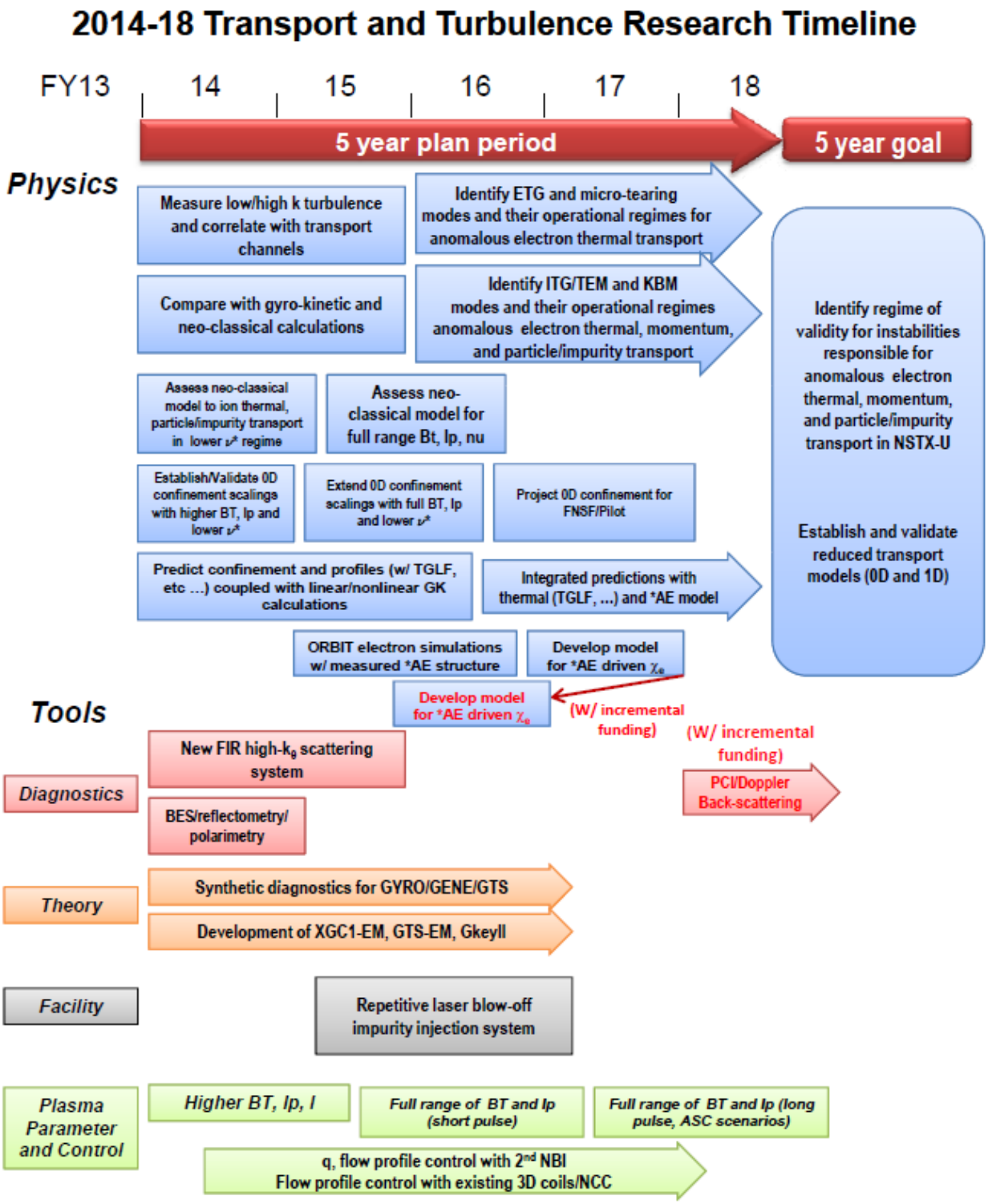
2014-18 Transport and Turbulence Research Timeline
FY13
14
15
16
17
18
5 year plan period
5 year goal
Physics
Measure low/high k turbulence and correlate with transport channels
Identify ETG and micro-tearing modes and their operational regimes for anomalous electron thermal transport
Compare with gyro-kinetic and neo-classical calculations
Identify ITG/TEM and KBM modes and their operational regimes anomalous electron thermal, momentum, and particle/impurity transport
Identify regime of validity for instabilities responsible for anomalous electron thermal, momentum, and particle/impurity transport in NSTX-U
Assess neo-classical model to ion thermal, particle/impurity transport in lower ν* regime
Assess neo-classical model for full range Bt, Ip, nu
Establish/Validate 0D confinement scalings with higher BT, Ip and lower ν*
Extend 0D confinement scalings with full BT, Ip and lower ν*
Project 0D confinement for FNSF/Pilot
Establish and validate reduced transport models (0D and 1D)
Predict confinement and profiles (w/ TGLF, etc ...) coupled with linear/nonlinear GK calculations
Integrated predictions with thermal (TGLF, ...) and *AE model
ORBIT electron simulations w/ measured *AE structure
Develop model for *AE driven χe
Develop model for *AE driven χe
(W/ incremental funding)
(W/ incremental funding)
PCI/Doppler Back-scattering
Tools
Diagnostics
New FIR high-kθ scattering system
BES/reflectometry/ polarimetry
Theory
Synthetic diagnostics for GYRO/GENE/GTS
Development of XGC1-EM, GTS-EM, Gkeyll
Facility
Repetitive laser blow-off impurity injection system
Plasma Parameter and Control
Higher BT, Ip, I
Full range of BT and Ip (short pulse)
Full range of BT and Ip (long pulse, ASC scenarios)
q, flow profile control with 2nd NBI
Flow profile control with existing 3D coils/NCC

References

[1] J. E. Menard et al., Nuclear Fusion **51** (2011) 103014.
[2] S.M. Kaye et al., Nucl. Fusion **49** (2009) 045010.
[3] Y. Ren et al., Proc. 24th Int'l. Atomic Energy Agency Fusion Energy Conference, San Diego, USA, 8-13 October 2012, CD-ROM file EX/P7-02 (IAEA, San Diego, 2012).
[4] S. M. Kaye et al., Nucl. Fusion **47** (2007) 499.
[5] S. M. Kaye et al., Proc. 24th Int'l. Atomic Energy Agency Fusion Energy Conference, San Diego, USA, 8-13 October 2012, CD-ROM file EX/7-1 (IAEA, San Diego, 2012).
[6] M. Valovič et al., Nucl. Fusion **51** (2011) 073045.
[7] ITER Physics Basis, Nucl. Fusion **39** (1999) 2178.
[8] B. Coppi and F. Pegoraro, Nuclear Fusion **17** (1977) 969.
[9] B. Kadomtsev and O. Pogutse, Nuclear Fusion **11** (1971) 67.
[10] C. Bourdelle et al., Phys. Plasmas **10** (2003) 2881.
[11] R. D. Hazeltine and H. R. Strauss, Phys. Rev. Lett. **37** (1976) 102.
[12] Y. C. Lee et al., Physics of Fluids **30** (1987) 1331.
[13] D. Stutman et al., Phys. Rev. Lett. **102** (2009) 115002.
[14] L. Delgado-Aparicio, Nucl. Fusion **47** (2009) 085028.
[15] F. Scotti et al., Proc. 24th Int'l. Atomic Energy Agency Fusion Energy Conference, San Diego, USA, 8-13 October 2012, CD-ROM file EX/P3-34 (IAEA, San Diego, 2012).
[16] H. Y. Yuh et al., Phys. Rev. Lett. **106** (2011) 055003.
[17] J. L. Peterson et al., Phys. Plasmas **19** (2012) 056120.
[18] Y. Ren et al., Phys. Plasmas **19** (2012) 056125.
[19] W. Guttenfelder et al., Phys. Rev. Lett. **106** (2011) 155004.
[20] W. Guttenfelder et al., Phys. Plasmas **19** (2012) 056119.
[21] W. Guttenfelder et al., Proc. 24th Int'l. Atomic Energy Agency Fusion Energy Conference, San Diego, USA, 8-13 October 2012, CD-ROM file TH/6-1 (IAEA, San Diego, 2012).
[22] J.E. Menard et al., Nucl. Fusion **52** (2012) 083015.
[23] D. R. Smith et al., Rev. Sci. Instrum. **83** (2012) 10D502.
[24] R. Barchfeld et al., http://meetings.aps.org/link/BAPS.2012.DPP.PP8.38
[25] J. Zhang et al., Rev. Sci. Instrum. **83** (2012) 10E321.
[26] H. Y. Yuh et al., Phys. Plasmas **16** (2009) 056120.
[27] R. Maingi et al., J. Nucl. Mater. **390-91** (2009) 440-443.
[28] C. Holland et al., Phys. Plasmas **16**, 052301 (2009).
[29] W. Guttenfelder et al., Phys. Plasmas **19** (2012) 022506.
[30] S. Kubota et al., Rev. Sci. Instrum. **77** (2006) 10E926.
[31] D. R. Smith et al., Rev. Sci. Instrum. **79** (2008) 123501.
[32] K. Tritz et al., Rev. Sci. Instrum. **83** (2012) 10E109.
[33] R.J. Hawryluk, "An empirical approach to tokamak transport", in Physics of Plasmas Close to Thermonuclear Conditions: Proceedings Course (Varenna 1979) **vol. 1**, page 19, CEC, Brussels (1980).
[34] J. Candy et al., Phys. Plasmas **16** (2009) 060704.
[35] W.X. Wang et al., Phys. Plasmas **13** (2006) 092505.
[36] B. P. LeBlanc et al., Rev. Sci. Instrum. **83** (2012) 10D527.

[37] R. E. Bell, Rev. Sci. Instrum. **77** (2006) 10E902.
[38] G.R. McKee, Nucl. Fusion **41** (2001) 1235.
[39] J. Zhang, et al., Plasma Phys. Control. Fusion **55** (2013) 045011.
[40] J. Canik et al., Proc. 24th Int'l. Atomic Energy Agency Fusion Energy Conference, San Diego, USA, 8-13 October 2012, CD-ROM file EX/P7-16 (IAEA, San Diego, 2012).
[41] W. Dorland et al., Phys. Rev. Lett. **85** (2000) 5579.
[42] E. Mazzucato et al., Phys. Rev. Lett. **101** (2008) 075001.
[43] D. R. Smith et al., Phys. Rev. Lett. **102**, (2009) 225005.
[44] Y. Ren et al., Phys. Rev. Lett. **106** (2011) 165005.
[45] N.M. Gorelenkov et al., Nucl. Fusion **50** (2010) 084012.
[46] K. H. Burrell, Physics of Plasmas **4** (1997) 1499.
[47] J. E. Kinsey et al., Physics of Plasmas **14** (2007) 102306.
[48] T. S. Hahm and K. H. Burrell, Phys. Plasmas **2** (1995) 1648.
[49] R. E. Waltz and R. L. Miller, Physics of Plasmas **6** (1999) 4265.
[50] S.P. Gerhardt et al., Nucl. Fusion **52** (2012) 083020.
[51] W.A. Houlberg et al., Phys. Plasmas **4** (1997) 9.
[52] W.X. Wang, et al., Computer Phys. Commun. **164** (2004) 178.
[53] E. Belli and J. Candy, Plasma Phys. Control. Fusion **50** (2008) 095010.
[54] A. G. Peeters and C. Angioni, Phys. Plasmas **12** (2005) 0725157.
[55] T. S. Hahm et al., Phys. Plasmas **14** (2007) 072302.
[56] J. K. Park et al., Nuc. Fusion (2013) *in press.*
[57] Y. Kosuga et al., Phys. Plasmas **17** (2010) 102313.
[58] S. Ku, C.S. Chang, and P.H. Diamond, Nuclear Fusion **49** (2009) 115021.
[59] R. Hulse, Nucl. Technol. Fusion **3** (1983) 259.
[60] K. Behringer, Description of impurity code 'STRAHL', Technical Report JET-IR(87)08, JET Joint Undertaking, Oxfordshire: Abingdon (1987).
[61] L. Delgado-Aparicio, et al., Nucl. Fusion **51** (2011) 083047.
[62] D. P. Stotler and C. F. F. Karney, Contrib. Plasma Phys. **34** (1994) 392.
[63] F.L. Hinton and R.D. Hazeltine. Rev. Mod. Phys. **48** (1976) 239.
[64] C.S. Chang and F.L. Hinton. Phys. Fluids **25** (1982) 1493.
[65] G.Y. Park, C.S. Chang, et al, Physics of Plasmas **17** (2010) 102503.
[66] G.M. Staebler, J.E. Kinsey, and R.E. Waltz, Phys. Plasmas **12** (2005) 102508.
[67] T. Rafiq et al., http://meetings.aps.org/link/BAPS.2010.DPP.NP9.2
[68] K. Tritz, et al., "Effects of Global Alfven Eigenmodes on Electron Thermal Transport in NSTX," Invited talk: 52st APS Division of Plasma Physics Meeting, November 8-12, 2010, Chicago, IL
[69] N. A. Crocker et al., Plasma Phys. Control. Fusion **53** (2011) 105001
[70] K. Tritz, et al., http://meetings.aps.org/link/BAPS.2012.DPP.GO6.4
[71] K.L. Wong et al., Phys. Rev. Lett. **99** (2007) 135003.
[72] J.F. Drake et al., Phys. Rev. Lett. **44** (1980) 994.
[73] A. Diallo et al., Proc. 24th Int'l. Atomic Energy Agency Fusion Energy Conference, San Diego, USA, 8-13 October 2012, CD-ROM file EX/P4-04 (IAEA, San Diego, 2012).
[74] R. E. Waltz and J. Candy, Phys. Plasmas **12** (2005) 072303
[75] Y. Camenen et al., Plasma Phys. Control. Fusion **52** (2010) 124037.
[76] A.G. Peeters et al., Nucl. Fusion **51** (2011) 094027.

[77] M. Kotschenreuther et al., Comp. Phys. Comm. **88** (1995) 128.
[78] J. Candy and R. E. Waltz, Phys. Rev. Lett. **91** (2003) 045001.
[79] F. Jenko et al., Phys. Plasmas **7** (2000) 1904.
[80] A.G. Peeters et al., Computer Phys. Commun.**180** (2009) 2650.
[81] E. V. Belova et al., Phys. Plasmas **7** (2000) 4996.
[82] A. Pankin et al., Computer Physics Communications **159** (2004) 157.
[83] M. Brambilla and T. Krücken, Nuclear Fusion **28** (1988) 1813.

Table of Contents for Chapter 4

Chapter 4

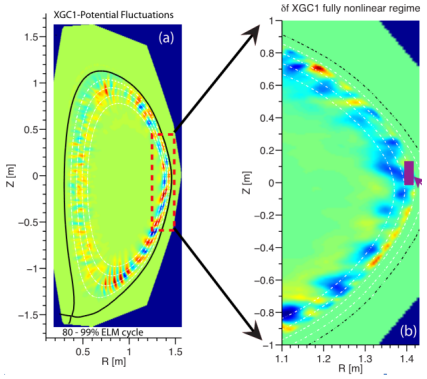

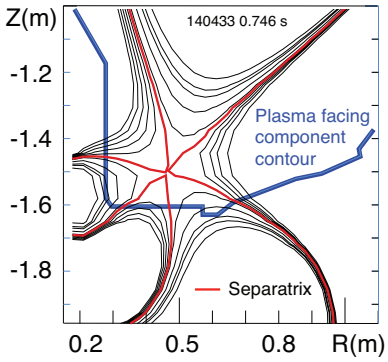

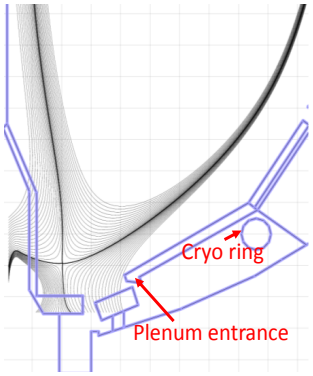

Research Goals and Plans for Boundary Physics

4.1. Overview of goals and plans

Control of the plasma-material interface is a key research area [1, 2, 3] for present and future tokamaks. There are a number of research gaps and required actions needed for ST-FNSF design activities. Indeed recent research in this area has raised concerns about ITER heat exhaust scenarios as well [4, 5, 6].

The NSTX-U will provide a significant advance over the existing STs capabilities to enable world-class, and in certain areas, world-leading boundary physics research. Doubling the I_p and B_t will enable higher confinement, stored energy and H-mode pedestal density and temperature, but will likely also further concentrate heat and particles fluxes on the plasma facing components (PFCs). The increase in the input power is needed to achieve

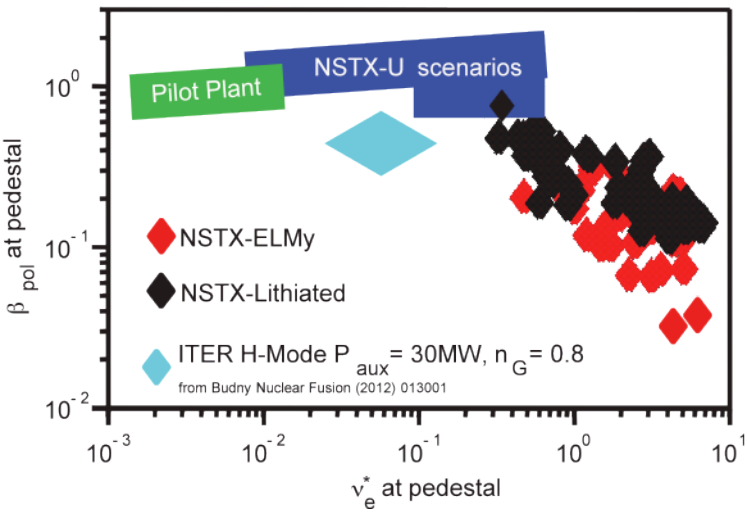

Figure 4.1.1: Pedestal poloidal beta and collisionality expected to be accessible in NSTX-U.

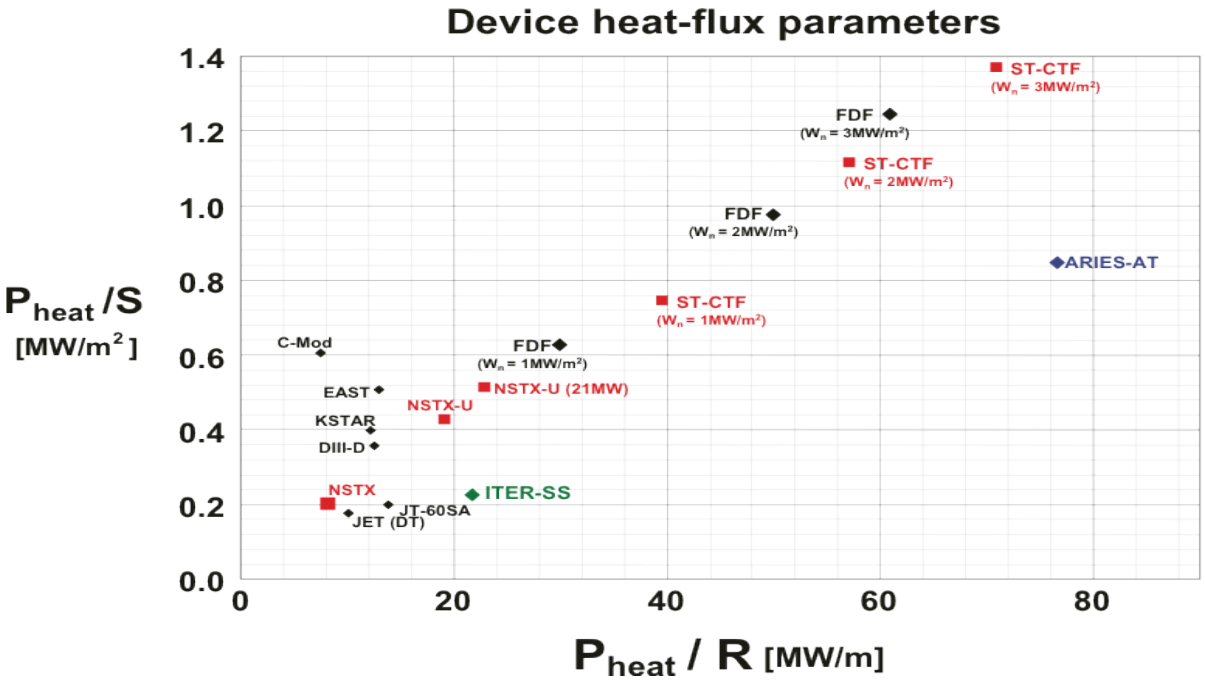

Figure 4.1.2: Heating power normalized to plasma surface area (P/S) and major radius (P/R) for present and proposed tokamaks.

low ν^* at higher I_p and B_t. Figure 4.1.1 shows the expected range in pedestal ν^* and pedestal β_{pol} in NSTX, and the projected range for NSTX-U, ITER, and a Pilot Plant.

Coupled with the ~ 5x extension of pulse length, the augmented heating power will increase the magnitude of the required energy removal from the PFCs between discharges. Two measures of divertor loading are given by P_{heat}/R and P_{heat}/S, where R and S are the major radius and surface area of the device respectively. Figure 4.1.2 shows that capability projected for NSTX-U in these parameters will meet or exceed the capabilities of existing fusion facilities.

In developing an integrated solution that insures successful power and particle control compatible with an attractive core plasma, a mix of innovative and proven conventional technologies will be deployed.

With these considerations in mind, the Boundary Physics goals over the next five years on NSTX-U include several main aspects:

- Support the central mission of NSTX-U, i.e., reduced ν^* fully non-inductive high-β steady-state core H-mode operation development, enabled in part by active particle control via cryo-pumping and lithium PFCs; this bullet encapsulates contributions of boundary physics to the first two overall NSTX-U goals in Chapter 1
- Exploit unique ST and NSTX-U features, e.g., low edge ν^*, high plasma current, high divertor heat flux and compact design, to improve physics understanding of edge heat and

particle transport for validation of novel snowflake and conventional radiative solutions of the plasma-material interface; this bullet connects to the overall NSTX-U goal #4 from Chapter 1

- Control and optimize the H-mode pedestal and edge localized modes (ELMs), as the pedestal represents the key interface between the core physics and divertor physics goals described in the two bullets above; this is necessary to achieve the two goals above with an integrated core-edge solution
- Evaluate the impact of high-Z PFCs on the edge and core plasma, as they are deployed in NSTX-U; this bullet connects to the overall NSTX-U goal #5 from Chapter 1

Below, the three dedicated Thrusts in this part of the program are mapped to these areas, with detailed descriptions given in the next section.

4.1.1 Thrust BP1: Characterize, control, and optimize the H-mode pedestal performance, transport, and stability

Background: H-mode Pedestal and ELM control includes characterization of the L-H transition, pedestal structure, turbulence, and edge stability in ELMy and ELM-free discharges, extending studies done in NSTX to lower ν^*, while making use of new capabilities in NSTX-U. The lower ν^* is expected to affect the pedestal in many ways, e.g. 1) the bootstrap current will be increased; 2) the intermediate collisionality enhancement [144] of bootstrap current relative to the Sauter formulation [145] will decrease; 2) possible re-ordering of which micro-instabilities (micro-tearing vs. hybrid Trapped Electron Mode (TEM)/Kinetic Kallooning Mode (KBM) vs. Electron Temperature Gradient (ETG)) dominate pedestal transport; 3) possible re-ordering of the importance of 2-D particle transport vs. 3-D expected particle transport with application of magnetic perturbations, which could lead to density pump-out in NSTX-U, which was never observed in NSTX H-mode discharges. This thrust also entails pedestal control via the use of ELM pace-making via either pulsed 3-D fields or injected granules or pellets, as well as access to advanced/alternate edge stability regimes, such as the Enhanced Pedestal H-mode and I-mode.

Thrust text: NSTX-U researchers will characterize the L-H mode transition thresholds utilizing the extended field, current, and power range of NSTX-U and by measuring turbulence and zonal flow dynamics with beam emission spectroscopy, Doppler backscattering, and gas-puff imaging diagnostics. The maximum achievable pedestal height and variation in pedestal structure will be assessed as a function of increased field, current, and power and also shaping and measured with enhanced spatial and temporal resolution Thomson Scattering. Increased control of pedestal transport and stability will be attempted using such techniques as edge density profile modification with improved fueling control, extended lithium coating coverage, and cryo-pumping. ELM triggering and suppression with 3D fields from mid-plane (existing) and off-midplane NCC coil-sets and also triggering with lithium granule injection will be assessed.

Enhanced pedestal H-modes (EP H-modes) will be further explored. As high-Z PFCs are introduced, their compatibility with good H-mode pedestal performance will be assessed.

4.1.2 Thrust BP-2: Control divertor heat fluxes with a combination of innovative and proven techniques

Background: Heat flux scaling experiments in NSTX and other devices have identified a strong inverse dependence of the extrapolated midplane heat flux width, λ_q^{mid}, on plasma current [57], with no dependence on B_t or input power. Fortunately the divertor heat flux footprint width was shown to increase with flux expansion [129]. Projections for NSTX-U based on NSTX data indicate a peak heat as high as 40-50 MW/m^2, in low flux expansion, high heating power scenarios (see Chapter 9). Thus heat flux handling will be crucial not only for projection to future devices, but also for achievement of full I_p, full B_t, long pulse NSTX-U plasmas. Validation of novel and conventional solutions for heat exhaust at the high P/R and P/S in NSTX-U includes both high flux expansion 'snowflake' divertor configurations, as well as radiative divertor configurations. Along with the TCV device [81, 82, 83], NSTX pioneered the use of the 'snowflake' configuration, demonstrating control of the heat flux and a strong effect on ELM stability [84]. In addition, radiative divertor operation was successfully demonstrated in highly shaped, high performance NSTX discharges [73], extending a technique demonstrated in higher aspect ratio tokamaks [130]. As shown in Chapter 9, successful high flux expansion configurations and/or radiative dissipation is projected to reduce peak heat flux to acceptable values.

Thrust text: NSTX-U research efforts will investigate the SOL heat and particle transport and turbulence and associated flux-widths extending the existing NSTX database to lower $\nu*$, higher I_P, and P_{SOL}. Measurements will be compared to multi-fluid turbulence and gyro-kinetic models. Novel divertor geometries such as the snowflake divertor will be systematically investigated for power and particle control and magnetic control of divertor configurations will be developed to support standard and snowflake divertor configuration studies. Steady-state and transient heat and particle transport and divertor PFC loads in these configurations will be studied as a function of magnetic balance, magnetic configuration parameters, feedback-controlled impurity seeding rate over a range of SOL powers and widths. Highly-radiating boundary solutions with feedback control will be developed, and divertor detachment operating window and access parameters will be studied. As high-Z PFCs are introduced, their compatibility with the divertor heat exhaust solutions will be assessed.

4.1.3 Thrust BP-3: Compare the sustainability of particle exhaust via lithium pumping and cryo-pumping, for density, impurity, and Z_{eff} control consistent with integrated scenarios

Background: Integrated scenarios on NSTX-U are designed for steady density at 0.5-1 times Greenwald density limit scaling [146]. To achieve this, a central element of the boundary program is installation of a divertor cryo-pump, representing a proven technology to control both main ion and impurity density. A key component of the research is to compare lithium pumping and cryo-pumping for density control, while considering the possible synergy of the two techniques to contribute to the required power and particle exhaust solution for future devices and NSTX-U itself. An integral element to both of these studies is the assessment of impurity sources and transport.

Thrust text: Experiments will be conducted to validate cryo-pump physics design activities, perform initial density control studies, and assess compatibility with H-mode pedestal and core performance and divertor power exhaust scenarios. Comparisons will be made between lithium conditioning and cryo-pumping for density and impurity control, as well as changes to the edge density profile, which are central to ELM elimination with lithium conditioning. Local recycling coefficients in the upper and lower divertor regions, as well as the wall will be measured. Impurity sources and SOL transport, and the role of ELMs in impurity control will be assessed. As high-Z PFCs are introduced to NSTX-U, their impact on core impurity transport, boron and lithium coatings, and divertor retention and particle control will be assessed.

As evident from the texts of the thrusts, the use of lithium touches nearly all areas of boundary physics, and as such represents a valuable tool. From a particle control standpoint, lithium has been shown to control plasma deuterium content; the sustainability of this effect [103], along with its dependence on the increased NSTX-U capabilities, needs to be determined. In addition, the reduced recycling from lithium conditioning has been shown to modify the edge density/pressure profiles and ELM stability, improving H-mode pedestal performance [7, 8, 9]. Finally, lithium affects both the peak heat flux profile and magnitude. At low to intermediate pre-discharge evaporation, the footprint narrows and the peak heat flux increases; at high evaporation rates, the peak heat flux itself is reduced, possibly from evaporative cooling [131]. The detailed studies in NSTX-U, derived from NSTX observations, are laid out primarily in the Materials and PFCs chapter, but specific contributions to the boundary program are described in the individual sections below.

4.2. Research Areas

4.2.1. Thrust BP-1: Characterize, control, and optimize the H-mode pedestal performance, transport, and stability

H-mode access is important for NSTX-U to accomplish its high-performance, non-inductive, long-pulse mission, and it is also a critical issue for future advanced tokamaks, such as ITER.

The H-mode is characterized by a factor-of-two improvement in global energy confinement due to the reduction of radial heat and particle transport across the plasma, but especially in a narrow region near the plasma boundary, referred to as the H-mode pedestal. This allows for a broad core pressure profile leading to improved core plasma magneto-hydrodynamic (MHD) stability, albeit with a large edge pressure gradient and associated bootstrap current that can destabilize edge-localized instabilities termed "ELMs". Access to the H-mode regime requires sufficient plasma heating power such that the power lost through the plasma boundary exceeds a threshold (P_{LH}). The new capabilities of NSTX-U, including an expanded operating range, lower ν^*, expanded spectrum of applied 3D fields, a second neutral beam that will allow for modifying the rotation and current profiles, and a variety of wall conditioning and particle control techniques, will be utilized to study P_{LH}, and improve understanding and control of the H-mode pedestal.

In the following sections, L-H transition research and the ensuing ELM/pedestal dynamics will be described, followed by a discussion of the pedestal transport and stability research and plans. This will be followed by a discussion of tools that have been and will be used to control ELMs through control of the pedestal structure.

4.2.1.1 L-H Transition Physics

a. Power threshold studies

The L-H transition and the subsequent pedestal formation is a multi-scale process, meaning that the important physics spans many orders of magnitude in space and time. Advances in plasma diagnostics and computational resources will allow NSTX-U researchers to examine spatial and temporal phenomena on spatial scales of several cm down to fractions of an ion gyroradius, and on temporal scales from <kHz up to 100 kHz, covering the ranges expected to be important for the L-H transition physics. NSTX-U can contribute to the development of first principles models for the L-H transition in several critical ways, including (1) investigating the impact of X-point geometry (X-point position, up/down magnetic balance, grad-B drift direction) in unique divertor configurations and with independent X-point control at both the top and bottom of the device; (2) decoupling the X-point geometry and divertor recycling effects by leveraging lithium deposition, which is capable of pumping a wide variety of strike point locations, and with the mid-term installation of the lower divertor cryo-pump; (3) studying the impact of 3D fields taking advantage of an expanded spectrum of applied perturbations, with the installation of in-vessel coils in the middle of the Five Year plan; (4) comparing RF and NBI heating; and (5) exploring the effects of aspect ratio by comparing to higher R/a devices, by measuring and assessing the importance of zonal flows, Geodesic Acoustic Modes (GAMs), and turbulence in initiating and sustaining the H-mode. Furthermore, NSTX-U will be able to perform these studies in an expanded operating regime and with more control of density, and rotation and current profiles.

The present L-H power threshold scaling from the ITPA multi-machine database is given by: $P_{LH} = 0.0488\ n_{el}^{0.717}\ B_t^{0.803}\ S^{0.941}$ where the units are P_{LH} [MW], line average electron density n_{el} in 10^{20} m^{-3}, B_t in T, and surface area S in m^2 [132]. Relative to this scaling, both large low R/a devices NSTX and MAST also measured an increasing P_{LH} with I_p [133]. Access to higher I_p and the new measurement capabilities will facilitate unfolding of the underlying physics, which is needed for projection to a low R/a FNSF which will operate at substantially higher I_p than today's devices.

Other dependences to P_{LH} beyond the standard scaling are typically referred to as "hidden parameters"; this is another area in which NSTX made contributions. It was observed on NSTX that P_{LH} decreased as the triangularity decreased (larger X-point radius), as the I_p decreased, as the amount of pre-discharge lithium increased, and the fraction of inboard / outboard neutral fueling increased [10, 11, 12]. Dedicated experiments and subsequent modeling using the full-f kinetic neoclassical XGC0 code[13] indicated that the P_{LH} scaling with R_X and I_p was due, in part, to changes in the edge E × B shear driven by an ion orbit loss hole. The dependence of P_{LH} on the poloidal location of the neutral fueling (inboard, outboard or divertor) was also shown to impact the neutral penetration and fueling efficiency. As the fueling efficiency decreased, the neutral density at the separatrix increased which could lead to more energy loss to charge-exchange and ionization and thus enhanced edge E × B shear that could initiate and sustain the H-mode. Experiments on NSTX also studied the scaling of P_{LH} versus a variety of other plasma parameters, such as toroidal field, electron density, ion species, n=3 field amplitude, X-point balance, grad-B drift direction, wall conditioning and heating balance (ohmic, NBI and RF). These experiments also documented the edge conditions (T, n, v, and their gradients) at the time of the transition.

Because of limitations in control and conditioning capabilities in NSTX, isolating the various effects of geometry and wall conditioning (or recycling) was difficult. The broader range of NSTX-U capabilities to be implemented over the five-year period, however, will enable dedicated studies in which these effects can be isolated. Recycling control will be studied in experiments comparing boronization and lithiumization for wall conditioning, using both downward and upward facing lithium evaporators for increased coverage of the PFCs and for strong pumping on all the divertor legs, and the eventual implementation, in the middle of the Five Year research period, of a cryo-pump situated in the lower divertor.

Application of n=3 3-D fields in NSTX was found to lead to a ~50% increase in P_{LH}. The reason for this is still under study, with e.g. neoclassical and turbulence calculations. It was the case, however, that the limited power supplies in NSTX allowed for only one non-resonant component of the field to be applied for these studies. NSTX-U plans to have six independently controlled radial field coils (NCC) at the outboard midplane, and this will allow for more flexibility in the

mode spectrum of the applied perturbations. Furthermore, midway into the five year research period, a partial set of in-vessel, off-midplane coils will be installed, enabling even more poloidal harmonic flexibility. The coil system will thus provide the tools to study the impact of resonant and non-resonant magnetic field perturbations on the L-mode transport leading up to L-H transition, the L-H transition itself, and the subsequent pedestal growth. Of particular interest is the interaction of flows and turbulence with non-axisymmetric magnetic fields. Another feature of the upgraded and new 3D coil systems is that they will give the capability, in various coil combinations, to vary the edge Neoclassical Toroidal Viscosity (NTV) to enable isolation of 3D effects from rotation effects. Varying the NTV effectively allows for rotation control for a given combination of neutral beam sources. Additional torque variations to control the rotation in the core and mid-plasma region can be provided by a combination of sources from both the original and the new, more tangentially-directed, neutral beams.

b. Turbulence changes

The formation of the edge transport barrier and its correlation with turbulence suppression were investigated in NSTX using a variety of diagnostics, including the ultrafast-swept FMCW reflectometers, gas-puff imaging (GPI) and beam emission spectroscopy (BES). The k_r spectra and radial correlation lengths across the edge region indicate that turbulence across the entire k_r spectrum is suppressed and the correlation length decreases at the time of the transition. This is coupled to an increase in the local electron density gradient, demonstrating a clear correlation between the transport barrier formation and turbulence suppression. This low-k turbulence re-appears during the natural density ramp that precedes the first naturally ELM, and between subsequent ELMs. Oscillatory behavior of the poloidal flow is often observed prior to the transition and resembles limit-cycle oscillations of zonal flows/GAMs near the separatrix, as measured by the GPI diagnostic[14, 15]. These flows were correlated with quiet periods in the edge turbulence preceding the L-H transition[14]; similar oscillations have been seen on ASDEX-Upgrade, TJ-II, DIII-D, EAST, and HL-2A [147] suggesting a common phenomenon. In some cases, however, these zonal flow spectra are broadband and intermittent, rather than coherent with a frequency ~3 kHz.

The enhanced capability of NSTX-U, especially with a broader range of turbulence diagnostics and techniques to vary the ExB shear, will allow a more comprehensive investigation of the turbulence dynamics and evolution from the L-phase into the H-phase. These turbulence diagnostics will measure density fluctuations across the range from ion gyroradius (BES) to electron gyroradius (microwave scattering) scales, and, in addition, a polarimetry diagnostic will be able to measure magnetic field fluctuations in the long wavelength (ion gyroradius scale) regime. The similarities and differences in the L-H transition dependences, dynamics and associated turbulence changes between NSTX-U and higher aspect ratio devices will provide the leverage necessary to test and validate the leading theories of the L-H transition.

4.2.1.2 Pedestal Structure and Edge Localized Mode Physics

The H-mode pedestal formation and evolution following the L-H transition is critical in optimizing fusion performance, both for NSTX-U and future next-step devices such as FNSF. It follows that being able to predict the pedestal structure (heights, widths, gradients) is crucial for determining the parameters in the design of future devices.

Control of the edge pedestal will be necessary in future devices such as ITER, since the observed natural tendency of most H-modes is toward a state with ELMs, that result in periodic edge plasma ejection, and unacceptable PFC erosion when extrapolated to future devices. Since the pedestal performance is strongly correlated with global plasma confinement [148], pedestal control must be done in a way that preserves high pedestal pressures without large ELMs. Furthermore, the edge particle transport must be made sufficiently large that density and impurity levels in the core plasma are controlled—something that does not occur in traditional ELM-free H-modes, which usually suffer from impurity accumulation. An introduction to ELM physics is given here, along with outstanding questions for investigation in NSTX-U.

4.2.1.2.1 Physics of ELMs

ELMs are periodic ejections from the edge plasma[149], thought to be triggered when the edge pressure gradient and/or current density exceed ideal or resistive MHD limits[34]. Violation of the stability criteria leads to the onset of Peeling Ballooning Modes (PBM), in which the instability drive comes from both the pressure gradient and current density [22; 150]. There are often coherent oscillations in magnetic probe signals that precede the ELM crash; these represent the growth of the mode itself. The issues related to ELM research include:

- Identifying common characteristics in the phenomenology of different ELM Types
- Physics of the underlying instabilities
- Transport of ELM heat and particle flux in the SOL, and incident at the divertor and wall

A wide variety of ELMs, driven by different instabilities, have been identified on fusion devices [151; 152]. In NSTX, large Type I ELMs, intermediate Type III ELMs at low and high collisionality, and tiny Type V ELMs appearing in a wide operating space have been observed [31]. The discussion below focuses on the two most common ELM types in NSTX: large Type I and small Type V. Type II ELMs have also been identified, but only in a narrow operating window in edge β and magnetic balance very near double-null configuration [32].

The correlation between violation of PBM stability, which limits the total pedestal height and width, and Type I ELM onset has been established in a large number of devices [25], including

NSTX. Substantial edge stability analysis was done for Type I ELMy discharges in NSTX, particularly in scans with increasing lithium conditioning in which ELMs gradually disappeared[7, 9]. It was generally found that these ELMs correspond to violation of the PBM stability limits, e.g. as shown in Figure 4.2.1. In general, NSTX plasmas tended to be driven more by current driven modes than pressure driven modes [7, 9, 23] owing to the strong stabilization of high-n ballooning modes at low R/a [26]. Only with 'weak' shaping of the plasma, i.e. at low triangularity and elongation, did the ballooning boundary re-appear in stability diagrams [27].

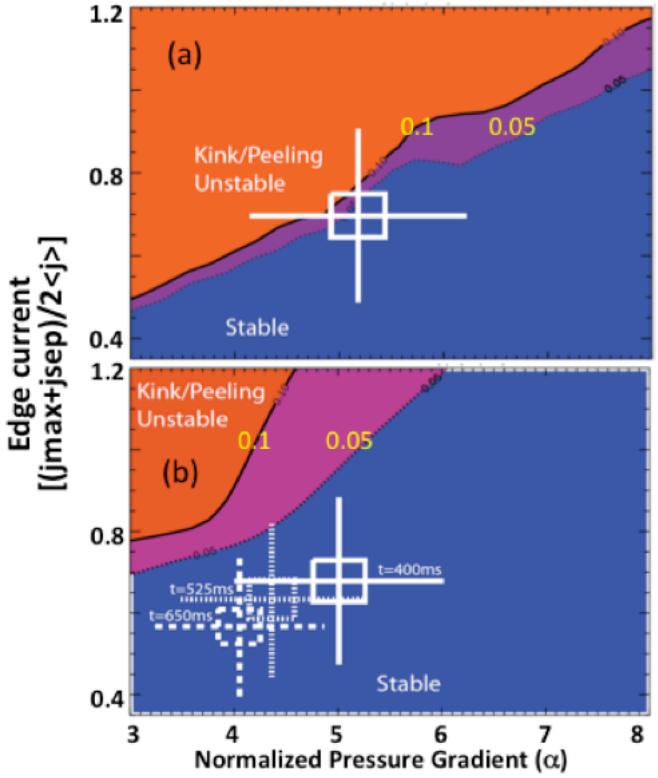

Figure 4.2.1: Comparison of edge stability for (a) Type I ELMy H-mode and (b) lithiated ELM-free H-mode (three time-slices). Contours of the linear growth rate normalized to the diamagnetic drift frequency are plotted, with the purple contour representing the instability transition (given by orange color). The experimental data point and error bars are represented by the white crosses [7].

The use of lithium wall conditioning drastically improved the Type I ELM stability in NSTX, e.g. Figure 4.2.1b [7, 8, 9]. First, a nearly continuous improvement of a number of discharge characteristics, e.g. reduced recycling, ELM frequency, and edge electron transport, with increasing pre-discharge lithium evaporation on graphite PFCs was observed. Profile and stability analysis clarified the mechanism responsible for ELM avoidance and the role of lithium. Lithium coatings reduced recycling and core fueling; thus the density and its gradient near the separatrix were reduced. The T_e gradient near the separatrix was unaffected, possibly due to the exacerbation of ETG modes; hence the pressure gradient and bootstrap current near the separatrix were reduced, leading to stabilization of the PBM thought to be responsible for the NSTX ELMs. It is worth noting that the change of the edge gradients with lithium conditioning was qualitatively reproduced with the paleoclassical transport model [8]. Thus, the enhanced edge stability with lithium coatings was correlated with the reduction of the pressure and its gradient near the separatrix. The key ingredient for ELM avoidance was control of the particle channel *independent* of the thermal channel at the edge: the density profile was continuously manipulated

via the amount of lithium evaporation and resulting recycling control, leading to reduced neutral fueling and relaxed n_e observed gradients.

Figure 4.2.1 also highlights an outstanding question: the linear growth rate of the instability was typically ~ 5-10% of the diamagnetic drift frequency. Normally medium and high-n instabilities with growth rates up to 50% of the drift frequency are computed to be stabilized by the diamagnetic drift. Recently XGC0 was used to directly compute the bootstrap current, to compare with the Sauter formulation. It was found that at intermediate ν^* and low R/a typical of ELMy H-modes in NSTX, the XGC0 bootstrap current was 30-50% higher than Sauter [153], leading to higher ideal growth rates than originally computed[7].

At present, the Type V ELMs appear to have been unique to NSTX operation [33]. These were single or double filament instabilities that propagated in the electron drift direction, and were correlated with operation with boronized walls. With sufficient pre-discharge lithium that raised edge temperatures, Type V ELMs were suppressed, pointing to resistive instabilities. The appeal of this research is easily stated: these ELMs could provide sufficient particle and impurity control with minimal heat flux peaking, if extrapolable to future devices.

ELMs have a strong impact on SOL heat and particle transport, and PFC loading. Calculations have indicated that ELM fluxes are concentrated at the low-field side near the outer midplane [34]. Once in the SOL, part of the ELM flux propagates to the outer target, but substantial flux also reaches the inner target, albeit with a time delay because of the difference in the connection length. As such, there is an observable time delay between when the ELM heat flux reaches the outer target as compared to the inner target; in D_α light on NSTX, this delay was between 0.1 and 1 msec, i.e. ~ the timescale for convective transport at the ion sound speed. The variability in the time scale was correlated with ELM size; the larger the ELM fractional energy loss, the smaller the in-out delay time. Thus, the in-out delay time yields insight to the ELM dynamics and underlying SOL transport physics, which will be the subject of future modeling with BOUT++ and M3D.

A leading concern about ELMs is the high levels of transient heat flux observed at the PFCs [134]. Measurements of the ELM heat flux have been made in a number of devices, including NSTX. While the inter-ELM heat flux reached 15 MW/m^2 in NSTX, transient ELM heat flux peaks up to 100 MW/m^2 were observed [35]. The peak heat flux increases depended on ELM type [135]. Small type V ELMs resulted in $\leq$ 50% transient increase in peak heat flux. During Type III ELMs, the peak heat flux increased by up to 300% relative to the inter-ELM heat flux, and the heat profile width decreased as compared to the inter-ELM width. The peak heat flux was observed to increase by up to 1000% during type I ELMs, with a significant contraction of the profile width. All of the different types of ELMs exhibited a trend of decreasing profile width

with increasing ELM amplitude. Indeed this last observation is in disagreement with measurements on JET, ASDEX-Upgrade, and DIII-D, and is receiving renewed interest through the ITPA toward resolution of this discrepancy. A recent emphasis in NSTX data analysis is the quantification of the degree of toroidal asymmetry of the ELM peak heat fluxes, the first such detailed study reported in the literature. It was found that larger ELMs have a higher degree of toroidal asymmetry, and also higher toroidal peaking factors [136].

While the emphasis of NSTX-U research will be on ELM control, there are several basic physics studies that will help optimize the control techniques:

- Small ELM physics: research will focus on identification of the underlying instabilities for Type V and Type II ELMs. Various observations have led to a hypothesis that Type V ELMs are resistive instabilities originating from the foot of the H-mode pedestal. This will be tested in NSTX-U (if Type V ELMs are observed in operational scenarios), and comparisons will be made with 3-D stability and transport codes, e.g. M3D-C1 [154] and XGC1. If Type II ELMs are observed in NSTX-U, detailed cross-machine comparisons will be made with higher R/a devices, which show a wider operating window for Type II ELMs than observed in NSTX.
- Large ELM stability: edge stability analysis as a function of the Type I ELM cycle will continue in NSTX-U, looking for ELM onset and violation of PBM stability thresholds. The higher aspect ratio of NSTX-U (R/a ~ 1.7, vs. typically 1.4 in NSTX) is expected to lead to a higher instability drive from the pressure gradient term, as compared to the edge current. On the other hand, the lower ν^* will lead to higher bootstrap current, which is de-stabilizing in the first stability regime unless it opens up access to second stability. The higher spatial resolution of the NSTX-U profile diagnostics will facilitate the assembly of the kinetic profiles needed for construction of kinetic equilibria that will be used for evaluation with the ELITE code[22].
- Distribution of ELM heat fluxes on PFCs: research in NSTX focused mainly on ELM heat fluxes to the lower divertor, due to the need for fast IR thermography. In NSTX-U, this research will be expanded to the upper divertor , center stack, and outer wall, as double-null and marginally diverted configurations will be evaluated with an expanded thermography diagnostic set. In particular, the observation of contraction of the heat flux profile with ELM increasing ELM size will be evaluated and compared with other devices, which typically report a 20-50% increase in ELM heat flux footprint for large Type I ELMs. Measurements in NSTX-U will be compared with simulations from XGC0 and XGC1.
- Correlation between ELM heat flux and resulting erosion evaluated with spectroscopy will be initiated.

The role of SOL current (SOLC) in ELM stability will also be investigated. SOLCs are defined as electrical current driven along field lines by thermoelectric potential when the electron temperature is different at the two ends of open field lines in the SOL [50]. These SOLC have been observed to coincide with ELM onsets on NSTX. It has been hypothesized [51, 52] that SOLC provide a key unifying physics element underlying the complete ELM cycle, consisting of triggering, edge thermal collapse, and relaxation, the physics of which remains elusive in spite of the success in creating H-mode discharges free of intrinsic ELMs and in generating ELM-like edge thermal collapses in an otherwise ELM-free discharge. Measurements of the SOLC during ELMs will be made in NSTX-U, and it is anticipated that the study of SOLC current under ELM paced condition will aid in understanding the physics mechanism in the triggering of ELMs. Ultimately manipulation of SOLC will be evaluated as an actuator for ELM control.

4.2.1.2.2 Pedestal Structure

Substantial progress has been made in pedestal physics over the last decade, particularly with development of several pedestal structure models [16, 17]. One leading theory on the physics limits to the pressure profile is the EPED model; this model employs a local pressure gradient limit due to kinetic ballooning modes (KBM), and an overall pedestal height/width limit due to PBM. As described above, violation of PBM stability is thought to destabilize ELMs. While the EPED model compares well with data from high aspect ratio devices, extension of the KBM calculations to low R/a is still in progress, noting recent work in this area from the MAST device [18]. A second pedestal structure model that places limits on the individual density and temperature profiles is the 'paleoclassical' model, in which poloidal magnetic flux diffuses radially and resistively in thin annuli, carrying charged particles [19]. This model reproduces many of the characteristics of the profiles in the steep gradient region near the separatrix. Finally a third pedestal structure model considers the effects of the X-point topology and scrape-off layer on neoclassical (XGC0) and turbulent transport (XGC1), including both recycling and kinetic effects. These pedestal structure models are complemented by interpretive models to determine the cross-field transport needed to reproduce observed profiles (e.g. SOLPS, UEDGE, OEDGE), and stand-along turbulence codes (e.g. BOUT++, SOLT).

In NSTX, comparison of pedestal structure data with the two pieces of the EPED model, namely KBM and PBM, have been promising. These comparisons were made in both ELMy [20] and ELM-free discharges [7, 8, 9]. Figure 4.2.2 shows evolution of the pedestal height, width, and maximum gradient as a function of normalized ELM cycle duration. Panel 4.2.2a shows pressure pedestal height saturation prior to the onset of ELMs in low and intermediate plasma current. At high current (> 1MA), a continuous increase of the pedestal height is clearly observed. Panel 4.2.2b shows that the pedestal width is observed to grow during the ELM cycle. The pedestal pressure gradient, however, is clamped (panel 4.2.2c) within the first 20% of the ELM cycle,

suggestive of a transport process regulating the gradient. Initial characterizations of the fluctuations between ELMs clearly point to the existence of ion-scale turbulence possibly responsible for the transport in the pedestal region [21].

In these ELMy discharges, the pedestal width appeared to scale almost linearly with β_θ^{ped} (see Figure 4.2.3) [20], rather than as $[\beta_\theta^{ped}]^{1/2}$, as observed at higher aspect ratio [22]. The square root dependence at high aspect ratio originates from KBM physics. A preliminary KBM calculation for NSTX indicates a width ~ $(\beta_\theta^{ped})^{0.8}$, i.e. the faster than square root scaling appears to be a low R/a effect [23]. In contrast, MAST found [143] a pedestal width dependence as $[\beta_\theta^{ped}]^{1/2}$; the reason for this apparent discrepancy will be investigated via collaborative studies between NSTX-U and MAST-U, with improved diagnostics on each device. Other theoretical models of the pedestal width are also being evaluated. One such model predicts that Electron Temperature Gradient (ETG) modes are dominant in the pedestal, leading to a near linear scaling of the pedestal width with β^{ped}

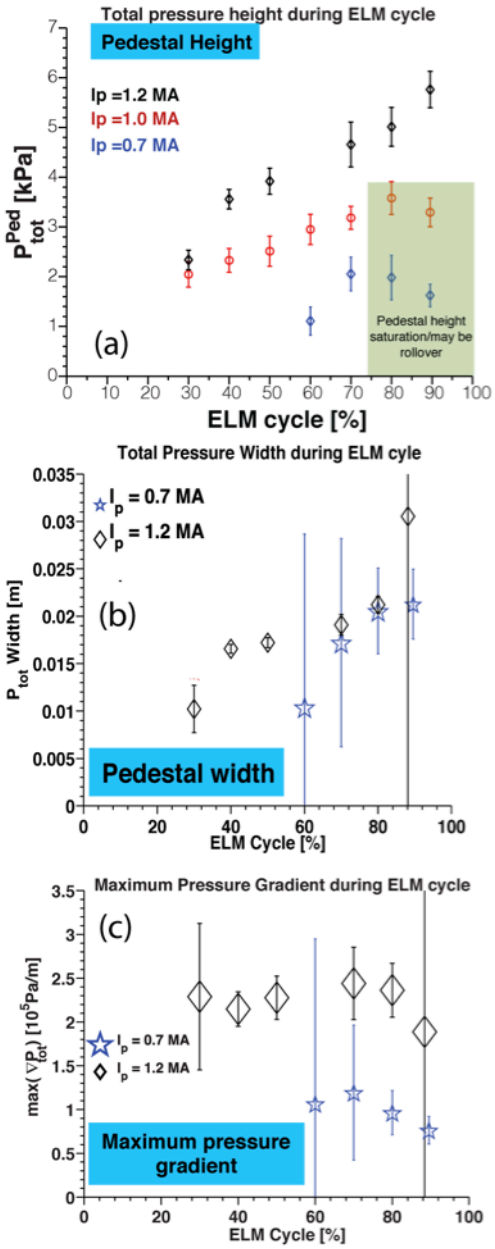

Figure 4.2.2: Shown to bottom the evolution of (a) the pressure pedestal height, (b) the pressure pedestal width, and (c) the pressure maximum gradient.

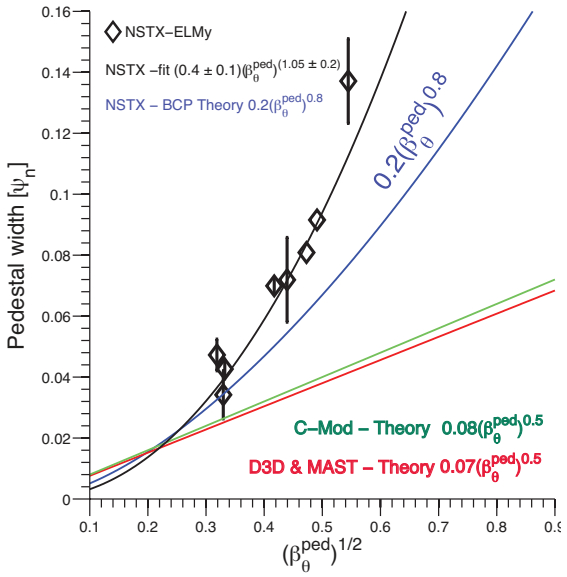

Figure 4.2.3. Pedestal width scaling with predicted width scaling using BCP.

[24].

The use of lithium conditioning radically altered the pedestal structure in NSTX, which was thought to be critical in the observed ELM elimination [7,8,9,44]. The density gradient in the recycling source region from $0.95<\psi_N<1$ was reduced proportionally to the reduction in core fueling from lithium pumping of deuterium at constant cross-field particle transport. However the n_e gradient radially inward of the recycling source region from $0.7<\psi_N<0.95$ was increased relative to the reference discharges, indicating a substantial reduction in cross-field particle transport. This region of improved particle transport correlates with an improved region of electron thermal transport that exhibited much larger T_e and P_e gradients that the reference discharges.

Despite the good progress made in characterization of the NSTX pedestal structure, a number of questions remain from the above studies, requiring new data from NSTX-U. Several of these questions are listed below:

- Given that the near linear scaling of pedestal pressure width on pedestal β_θ^{ped} is close to the dependence from the recent KBM calculation mentioned above, and the pedestal pressure gradient clamped early in the ELM cycle, why was there no evidence of onset KBM or any other modes responsible for transport in NSTX or any other device fluctuation data aligned with the ELM cycle? Note that many devices have reported ion scale turbulence between ELMs [137,21] without conclusive evidence of a stiff onset of instabilities with increasing pressure gradient, as predicted by the KBM calculations.
- Use of lithium conditioning produced very wide H-mode density profiles. What was the origin of the particle transport improvement that resulted in these wider density and pressure profiles?
- Following the lithium studies, to what extent is H-mode pedestal evolution determined by the pressure profile, as opposed to the individual density and temperature profiles?

The extended operating range and new diagnostics capabilities in NSTX-U will help to resolve many of the outstanding questions. During the first two years of this Research plan, the parametric dependences of the pedestal structure will be assessed over the expanded range of B_t, I_p, ν^*, and shaping.

Much of the previous analysis on NSTX required many time slices to create composite density, temperature, and pressure profiles, from which equilibria based on the kinetic profiles were generated, as the starting point for stability and gyrokinetic analysis. This technique, however, requires the assumption that equlibria are unchanging for a particular temporal duration or as a function of the ELM cycle. The improved spatial resolution of the profile measurements, notably Thomson scattering for n_e, T_e, and P_e profiles, will reduce the number of individual profiles

needed to generate a high resolution composite radial profile, and the intrinsic assumptions with the generation of such a profile. Additionally there will be enhanced fluctuation diagnostics in the pedestal region, facilitating the search for pedestal-localized instabilities. These diagnostics include the upgrade of the BES system and the addition of the high-k system with enhanced spatial resolution in the pedestal region.

Following the testing of PBM stability and KBM onset physics, extension and benchmarking of the EPED [25] model in NSTX-U will commence. The predictions of the paleoclassical model will also be tested, as will the predictions of pedestal structure with both XGC0 and XGC1. These studies will be supplemented with continued interpretive modeling of the profiles to infer radial transport coefficients in a variety of operating regimes.

4.2.1.2.3. Pedestal turbulence

It is believed that micro-instabilities and the resulting plasma turbulence are partly or largely responsible for transport in the pedestal region, as is the case in the core plasma. Given the success of the EPED model, the KBM in particular is a leading candidate for limiting the pedestal gradient between ELMs. To improve the physics understanding of pedestal turbulence, efforts have attempted to characterize, both experimentally and through numerical simulations, the instabilities present in the pedestal region.

Edge fluctuation characterization has been performed using reflectometry, which indicates radial correlation lengths of 2-4 cm in the pedestal [21]. These measurements were complemented by dedicated fluctuation studies using the BES system, in which pedestal measurements were made during both ELMy and ELM-free (and MHD quiescent periods) [21, 28]. In the ELM-free regime, for instance, These measurements allowed the parametric scalings among pedestal turbulence

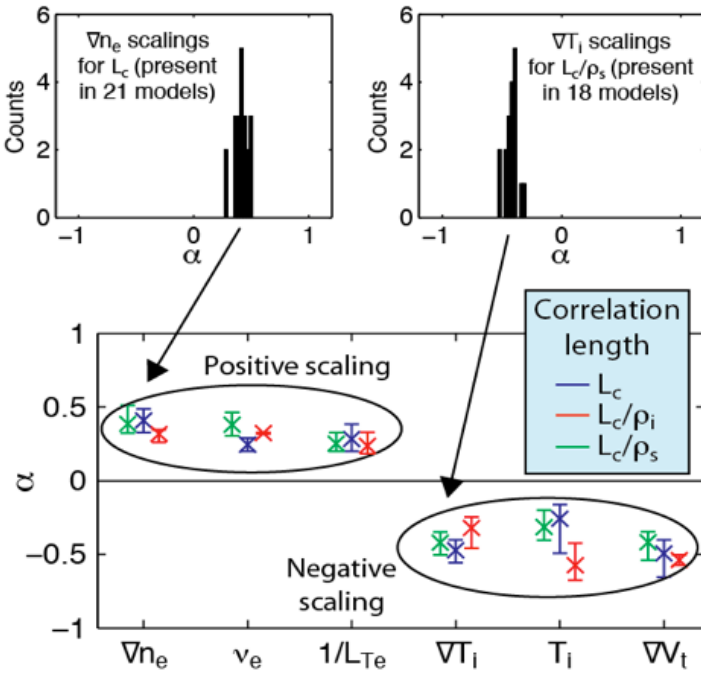

Figure 4.2.4: Regression model aggregation shows poloidal correlation lengths in the pedestal increase at higher density gradient, collisionality, and inverse electron temperature gradient. Similarly, poloidal correlation lengths decrease at higher ion temperature, ion temperature gradient, and toroidal flow shear.

quantities and plasma parameters to be identified [28]. These measurements show broadband fluctuations ($\Delta f \sim 100$ kHz) with poloidal correlation length $L_p \approx 15$ cm and $L_p/\rho_i \approx 10$. Also, poloidal wavenumbers are $k_\theta \rho_i \approx 0.2$ [21, 28] and decorrelation times are inferred to be ~5 a/c_s. The observed low-k dependences indicate that the correlation length increases and the wavenumber decreases at higher ∇n_e, lower ∇T_i, and higher collisionality (see figure 4.2.4). Assuming a relation between turbulence characteristics such as correlation length to be related to linear growth rates, the measured dependences appear to agree most with transport driven by TEM, have some agreement with KBM and micro-tearing mode turbulence, but have the least agreement with T_i gradient turbulence.

A number of gyrokinetic codes have been used to characterize edge microinstability in inter-ELM periods, spanning a broad range in the comprehensiveness of the physics included (i.e, linear vs nonlinear, local vs. global, electrostatic vs. electromagnetic, δf vs. full-f). While it is anticipated that a global, full-f, electromagnetic, nonlinear treatment is ultimately required to accurately simulate pedestal turbulence, such codes are still under active development (culminating in the XGC1 code). In the meantime, reduced physics models are used for studying experimental trends; for example local analysis is useful for indicating the types of modes that are present and how they scale with various instability drives (e.g., density or temperature gradients), even though nonlocal effects are likely to be strong in the pedestal and so will quantitatively affect the results [138].

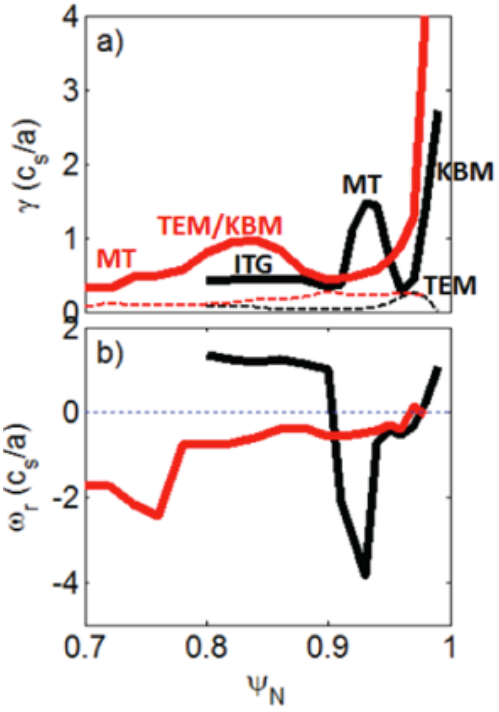

Figure 4.2.5: Profiles of a) growth rate (solid) and ExB shear rate (dashed), and b) real frequency of the most unstable mode without (black) and with (red) lithium.

As an example, a study of the linear gyrokinetic stability of the pedestal was performed using the GS2 code [155]. For a discharge without the application of lithium on the PFCs, these calculations showed that microtearing modes are dominant at the pedestal top (Figure 4.2.5). With lithium applied to the PFCs, the increase in the density gradient in this region stabilized the microtearing modes, and modes with characteristics like those of the TEM becoming dominant with reduced growth rates. In the steep gradient region of the pedestal, ETG modes (not shown) were found to be unstable both without and with lithium, but with higher growth rates and a lower threshold temperature gradient with lithium, suggesting ETG may have played a role in limiting the electron temperature gradient in this region. At mid-pedestal, a hybrid TEM/KBM mode was found to be dominant with and without lithium, with characteristics of both the TEM and KBM [29].

Local gyrokinetic linear simulations have also been performed of a separate set of discharges using the GENE code [156]. A hybrid TEM/KBM mode was identified in the linear GENE simulations[23] during the last 20% of an ELM cycle near the pedestal top, similar to that found within the pedestal using GS2.

Global nonlinear simulations using XGC1 have been performed on inter-ELM periods in these discharges as well, allowing the first comparisons of specific turbulent features between experiment and theory. XGC1 nonlinear global gyrokinetic calculations yielded radial and poloidal correlation lengths of potential fluctuations in the pedestal region that were consistent with those from the measurements of density fluctuations discussed above (figure 4.2.6) [23].

Finally, GEM gyrokinetic simulations [30] of the NSTX pedestal turbulence were performed, based on observed pedestal profiles. The GEM simulations indicate low-k linear growth rates increase at higher ∇n_e and lower ∇T_i, a result consistent with observed correlation length scalings based on BES measurements. In addition, GEM simulations indicate instabilities shift to lower k at higher collisionality, in agreement with observed wavenumber scalings. These dependences indicate, as with inferences from the measurements, low-k turbulence dominated by TEM in this region of these discharges.

Figure 4.2.6: (a) 2D cross-section of the potential fluctuations from XGC1 simulations in the fully nonlinear stage. (b) Zoomed in edge fluctuations indicating the BES and reflectometry measurements region. (c) Evaluations (from simulation) of both radial (4 cm) and poloidal correlation (11 cm) lengths in the edge region showing experimental level radial and poloidal correlation lengths.

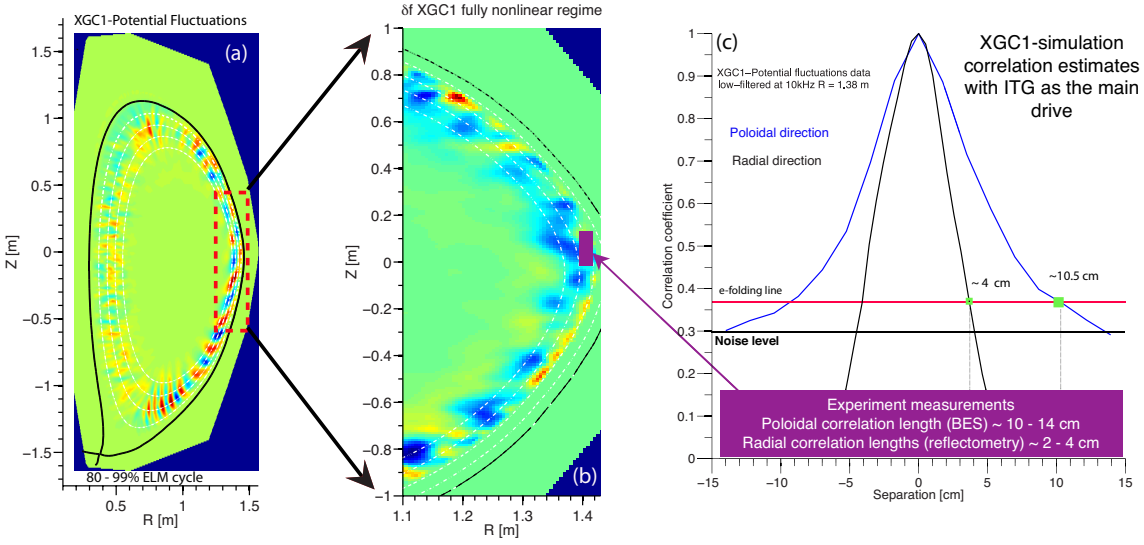

Pedestal turbulence research on NSTX-U will benefit from several diagnostic upgrades. New BES channels will be instrumented, giving expanded 2D spatial coverage of 2 cm by 2 cm in the pedestal region. These will aid advanced analysis techniques, such as velocimetry analysis of

density fluctuations to identify predator-prey relationships between turbulent eddies and flow fluctuations. A high-k_θ microwave scattering diagnostic will also be implemented, and when combined with BES and reflectometry will yield an almost complete range of the k_θ spectrum of fluctuations from ion to electron gyroradius scale lengths. Furthermore, a polarimeter will be installed early in the Five Year research period, allowing diagnosis of magnetic fluctuations as expected due to, e.g., microtearing modes. The pedestal turbulence studies will also be improved by the expanded facility capabilities of NSTX-U. This includes access to a broader range of physics parameters (e.g., ν^*), as well as the ability to probe pedestal turbulence as edge conditions are altered using, e.g., wall conditioning techniques or 3D field application.

Gyrokinetic simulations will be continued in the extended operation range of NSTX-U to identify the micro-instabilities present in the edge region, and to develop a model a predictive model of edge transport. Nonlinear simulations will be a focus of this research, in order to directly compare turbulence characteristics to measurements. Of particular importance in these calculations is proper treatment of the larger physical scale lengths in the ST owing to the low B_t, which may demand global rather than local simulations; this is especially true in the pedestal, where the ion gyroradius is not small relative to characteristic gradient scale lengths. The various codes are being continuously developed to both include more physics and to be able to handle the large spatial ranges required for proper ST simulations; for example, GENE and GYRO are capable of the nonlocal electromagnetic simulations needed for the pedestal, and XGC1 will add full-f capability and inclusion of the separatrix and scrape-off layer to this once electromagnetic effects are fully implemented.

4.2.1.3. Active control of ELMs and pedestal on NSTX

It is well-known that steady operation of ITER hinges on achieving acceptable ELM size. To date the commonly utilized approaches in reducing ELM sizes include the radiating divertor, the magnetic triggering via vertical kicks, pellet pacing, and the external resonant magnetic perturbation fields. In NTSX, lithium conditioning of the PFCs has been observed to eliminate ELMs, albeit with increased impurity accumulation typical of ELM-free H-modes. ELM control will continue to be a high-priority research area in NSTX-U.

4.2.1.3.1. 3D Fields ELM pacing

The use of 3D fields for pedestal control was explored in NSTX experiments. In contrast to RMP ELM suppression experiments at, e.g., DIII-D [36], it was found that the application of 3D fields caused ELMs to be destabilized in NSTX during otherwise ELM-free H-modes [37]. This effect was leveraged to perform ELM-pacing for impurity control during NSTX discharges with strong lithium conditioning [37]. While ELM-triggering by 3D fields was robustly observed, the impact

of 3D fields on the pedestal kinetic profiles was found to vary with discharge conditions. For example, in a discharge at low elongation and without lithium coatings on the PFCs, the 3D field caused the pedestal T_e to increase, while in a high elongation discharge with lithium flat spots were measured in the pedestal n_e and T_e profiles without any increase in T_e [38].

In NSTX-U ELM control using applied 3D fields will be explored using the expanded operational range available as well as upgrades to the 3D coils system. In particular, the lower ν* achievable in NSTX-U will allow contact to be made with $\nu_e^* < 0.2$ ELM-suppression experiments performed on other devices, e.g. DIII-D [39]. Further, it is likely that the transport response will be different at reduced ν_e^* (< 0.12), and a stronger impact on particle transport may be possible [40]. The 3D field system itself will be greatly expanded in NSTX-U, giving a wider spectral range than in NSTX with more flexibility in resonant vs non-resonant field application. This will be facilitated by the implementation of independent power supplies for all six of the existing coils at the start of NSTX-U operations, and the partial installation of the in-vessel NCC coils towards the middle of the Five Year Plan period. The NCC coils will allow for control over the poloidal spectrum of the applied perturbation, which has been shown to be a key ingredient in achieving ELM suppression at DIII-D [41]. These coils may also allow a substantial increase in the ELM frequency to be achieved during pacing via 3D field application. If so, this could allow very small ELMs to be triggered rapidly in order to simultaneously control the ELM size and particle content of the core plasma.

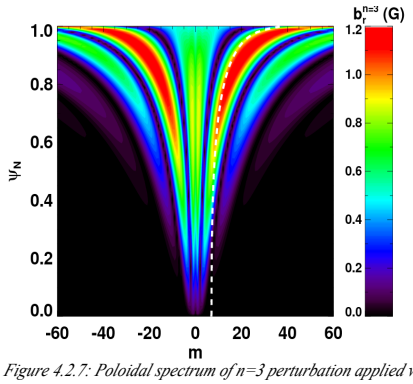

Figure 4.2.7: Poloidal spectrum of n=3 perturbation applied with NCC (dashed white line indicates resonant values)

4.2.1.3.1.1 Projections using the NCC coils

An open question on ELM stability is whether the 3-D fields themselves directly impact ELM stability, or whether the changes to the kinetic profiles can be used in 2-D stability calculations with e.g. ELITE. While 2-D ELITE calculations are consistent with RMPs changing the profiles in a way that improves stability to peeling-ballooning modes [139], very recent analysis suggests that the ELM stability threshold might be reduced by the application of RMPs [140].

The impact of the NCC on ballooning stability has been calculated in order to assess how the new coil set might be expected to alter the pedestal structure and stability. The approach used is described in [38]. First, a 2D equilibrium for NSTX-U was generated with ISOLVER. The pressure and safety factor profile was transferred as input to the 3D equilibrium code VMEC [127], which was then run in free-boundary mode using the same coil currents as in ISOLVER in

order to reproduce the 2D equilibrium. Next, a 3D equilibrium is generated by running VMEC with the same input settings, but with 3D magnetic fields due to the NCC added. The infinite-n ballooning stability of the 3D equilibrium is then analyzed using the COBRA code [128].

The case studied with the NCC applied assumed the full NCC, with two off-midplane arrays of twelve coils each, in an n=3 configuration with even parity (upper and lower coils have the sam toroidal phase). This produces a vacuum perturbation with strong resonant components for the plasma equilibrium under consideration, with much better pitch alignment (Figure 4.2.7) than can be achieved with the midplane coil array alone [37]. Without this field applied, the axisymmetric case is calculated to be stable across the entire plasma radius (Figure 4.2.8, black curves). With the NCC field applied, the VMEC and COBRA calculations indicate a broad region of ballooning instability with 30% of the outer poloidal flux showing positive growth rates (Figure 4.2.8, red curves). For comparison, a case with the midplane RWM coils energized (and not the NCC), again in an n=3 configuration, shows only a narrow edge region (~5% in poloidal flux) that is unstable. This is consistent with the weak impact of the RWM coil set on ballooning stability described in Ref [38]. Similarly a new axisymmetric case, with no 3D fields applied but with the plasma pressure increased by 10%, showed only a small unstable region. Thus, unlike the midplane array [38], the changes to stability caused by the NCC are unlikely to be overwhelmed by small changes in the pressure profile.

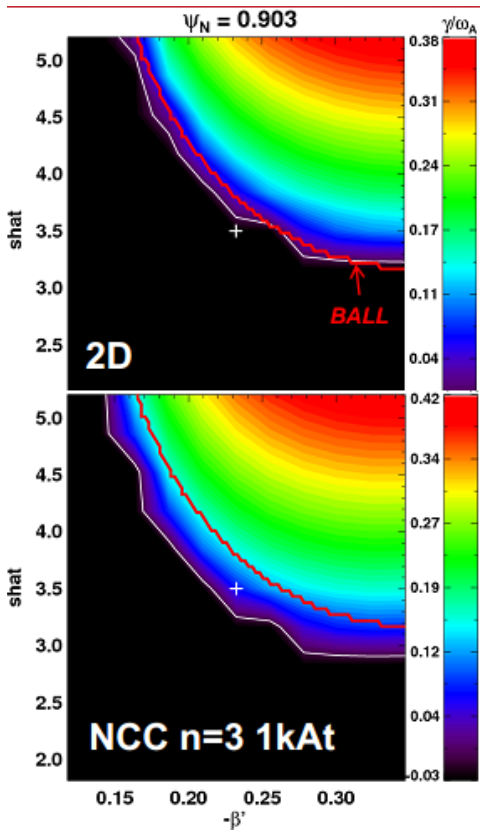

Figure 4.2.9: Ballooning growth rates as a function of pressure gradient (-β') and magnetic shear (shat) for a) axisymmetric case and b) with NCC applied. Red curve indicates axisymmetric BALL calculation of stability boundary.

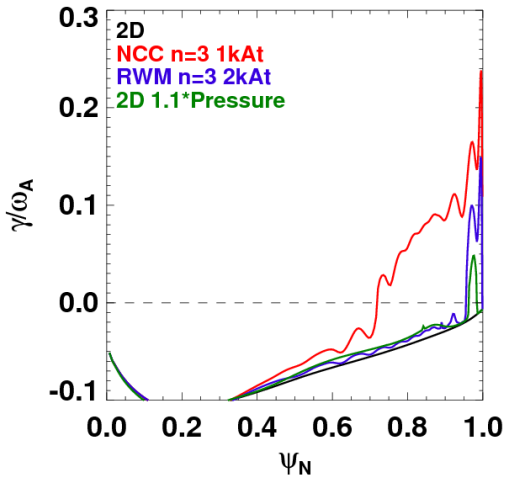

Figure 4.2.8: Ballooning growth rates for nominal axisymmetric case (black), with NCC fields applied (red), with RWM fields (blue), and axisymmetric with 10% pressure increase (green)

To more thoroughly determine the changes to the ballooning stability limits caused by the NCC, large sets of VMEC equilibria were generated with the safety factor and pressure profiles slightly modified near a radius of ψ_N~0.9. This allows the stability to be mapped out as the magnetic shear and pressure gradient are varied, similar to the analysis commonly done for axisymmetric tokamaks. Figure 4.2.9a shows the growth rate contours calculated for this set of VMEC equilibria for the 2D case with no perturbations applied. The red contour line indicates the ballooning boundary as calculated from the BALL code, which assumes axisymmetry and uses the 2D equilibrium calculated by ISOLVER (rather than VMEC). The COBRA-calculated growth rate contours closely match the BALL calculation, confirming that the analysis method used here reproduces calculations based on tokamak codes for the 2D case. Figure 4.2.9b shows the same calculation, but now for the case with 3D fields applied (the red BALL curve is again for the axisymmetric case, and is shown for reference). The unstable region extends to lower values in both pressure gradient and shear, so at that the nominal values at this radius (indicated by the white plus sign) the 3D case causes a transition from stability to instability. These results show that the NCC moves the stability boundary by ~20% in pressure gradient, and ~10% in shear, implying that strong changes in growth rates can be expected if the 2D plasma is relatively near the ballooning boundary to begin with. This has been confirmed through calculations for a set of 2D equilbria with the safety factor and pressure varied, which show that the NCC causes wider regions of instability and higher growth rates the nearer the 2D case is to the ballooning limit to begin with.

Since the H-mode pedestal is typically near stability limits, the NCC is likely to have a strong effect. Although the infinite-n ballooning analysis here does not directly affect ELM stability (which requires finite-n peeling-ballooning calculations), it does at least indicate that a strong 3D effect on stability is possible. Further, since ideal ballooning appears to be a good indicator of KBM onset, it is possible that the NCC may be able to alter KBM stability and hence the inter-ELM pedestal structure. These possibilities will be explored experimentally in NSTX-U (while the full NCC has been considered so far, analysis of the partial NCC available early in NSTX-U operation is underway).

4.2.1.3.2. ELM pacing with Li granules

Another method for controlling ELMs has been to introduce high-speed deuterium pellets into the pedestal [42]. It has been demonstrated that as the pellet frequency increases, the amplitude of the induced ELMs decreases and the heat flux to the divertor is reduced. The maximum injection frequency is 90 Hz for the present deuterium pellet injector on DIII-D. A new device (as shown in figure 4.2.10) utilizing Li granules injected via a rotating impeller was developed at

PPPL and recently installed on the EAST tokamak. At frequencies of 25 Hz, the pellets of ~ 0.7 mm in diameter triggered ELMs with almost 100% efficiency as shown in figure 4.2.11 [43].

A new granular injector is presently being fabricated. It will have four selectable sizes of Li granules and be capable of injecting up to 1000 particles/sec with velocities up to 100 m/s for the full five second discharge duration for NSTX-U. One of the main advantages of using Li granules compared to deuterium pellets is that lithium is redeposited on the wall, and is not an uncontrolled fuel source. A second potential application of the Li granular injector is in continuous wall conditioning for long pulses. The injector is capable of supplying over 100 mg of Li per second into the plasma edge. Li coatings from the LITER evaporators have a finite erosion lifetime; the injector can provide a real-time re-supply of Li for wall conditioning. A second granular injector was provided to RFX for wall conditioning studies and signs of improved performance were seen at the end of their 2012 campaign.

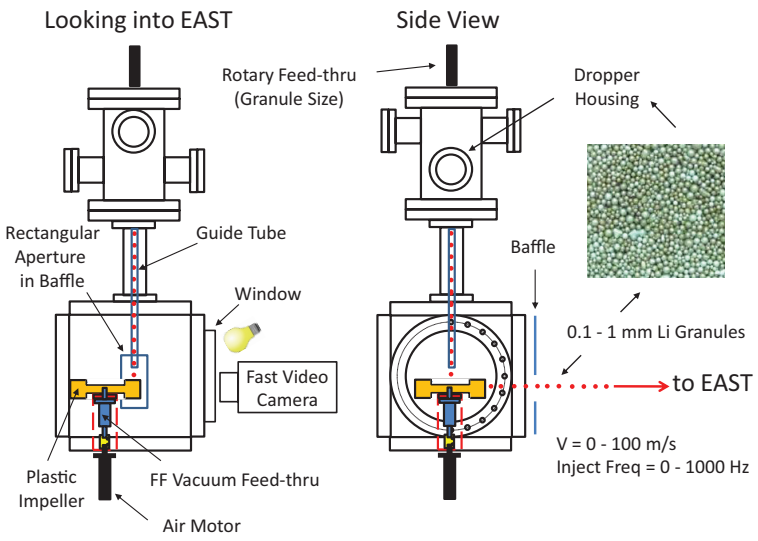

Figure 4.2.10: Two views of the injector hardware used in this work. Pre-sorted spherical Li granules falling through a narrow guide tube were struck by the blade of a rotating plastic impeller. The granules were thus redirected horizontally at higher speeds through a rectangular aperture in a copper baffle and into the midplane of EAST H-mode discharges. Monitoring of the granule/impeller impacts as well as the subsequent granule ablation was accomplished with a fast video camera.

The physics of ELM triggering by pellets has been investigated with the JOREK code [141], and is in good qualitative agreement with observations on DIII-D. Quantitatively the computed pellet size needed to trigger a ballooning mode is several times larger than observations. The excellent diagnosis of edge filaments with visible imaging and the availability of this granule injector will allow NSTX-U to make significant contributions in model validation in this area.

4.2.1.3.3. Lithium Evaporation control of ELMs

As discussed above, lithium conditioning was been shown to reduce edge recycling, suppress ELMs, and improve performance in NSTX [44]. It was observed that the continuous introduction

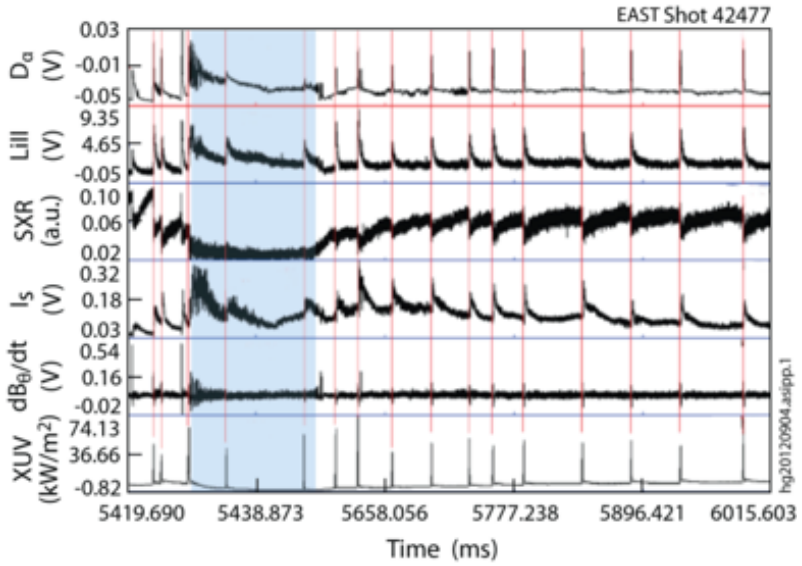

Figure 4.2.11: Shown from top to bottom are signals of divertor Dα, LiII emission, edge soft X-ray emission, divertor ion saturation current, edge Mirnov signal and tangential edge XUV emission. The arrival of injected Li granules is indicated by red vertical lines landmarked to the leading edge of the XUV signal on the bottom. A dithering H to L transition occurs coincident with the injection of the third granule – blue area. After 100 ms, the H-mode returns and a period of 25 Hz ELM pacing driven by the arrival of Li granules at 52 m/s begins.

of lithium coating on the PFCs provides a reduction of the ELM frequency until complete suppression. With increased beam power, B_t, and I_p (all of which are expected to affect ELM stability), NSTX-U will provide a test-bed for the effects of the lithium conditioning on ELM behavior and plasma performance, needed to assess its applicability for next step devices. Finally the effectiveness of more spatially complete lithium conditioning of the PFCs, by implementing an upward facing lithium evaporator (2015) to complement the downward facing evaporators, will be evaluated in NSTX-U.

4.2.1.3.4. ELM pacing using vertical kicks

ELM pacing with vertical kicks had been demonstrated in a number of tokamaks including NSTX [49]. This active ELM control approach has also been demonstrated in ITER-relevant type I ELM regime in ASDEX-U suggesting that this approach may be used for ELM mitigation in ITER. Note, however, that the triggering mechanism is not well understood, and experiments in NSTX-U will be used to improve this physics understanding. With the expanded operational regimes available, NSTX-U will also enable the test of this scheme in scenarios relevant to FNSF.

4.2.1.3.5. Control of ELMs via operational regimes

Two potentially attractive operational scenarios for NSTX-U for controlling ELMS are the Enhanced Pedestal (EP) H-Mode and the I-mode.

The EP H-mode [53, 54] is an attractive regime identified in NSTX experiments, with energy confinement enhancement factors up to $H_{98y2} \sim 1.7$. The EP H-mode usually results from a second confinement transition that occurs following the L-H transition, typically triggered by an ELM (which can itself be triggered using 3-D fields). During the EP H-mode, the pedestal T_e and T_i are significantly (up to nearly a factor of two) higher than in standard H-mode (as shown in figure 4.2.12), while the pedestal density gradient is slightly relaxed. This suggests a separation between the thermal and particle transport channels, and the observed increase in particle transport is promising for achieving stationary densities during EP H-mode. The focus of EP H-mode research in NSTX-U will be on developing techniques to obtain and sustain the EP H-mode. EP H-mode phases that occur shortly after I_p flat-top often terminate in a disruption. To avoid this, β_N feedback control will be used to reduce the power during the EP H-mode. Lithium conditioning will also be used to avoid ELMs during the EP H-mode phase (when an ELM occurs during EP H-mode, the plasma transitions back to a standard H-mode). The application of 3-D fields during EP H-mode will be explored, as it may be necessary to further increase particle transport during EP H-mode to achieve fully stationary conditions.

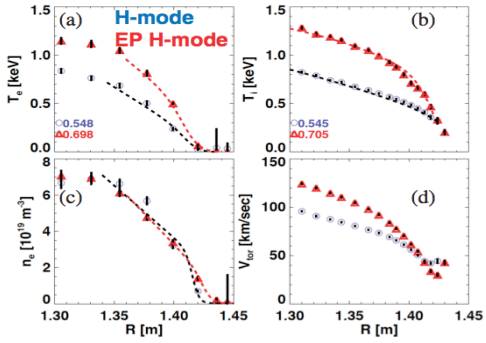

Figure 4.2.12: Profile comparison between Enhanced Pedestal H-mode and H-mode.

The I-mode is also characterized by the presence of an edge thermal transport barrier and the absence of an edge particle transport barrier. The I-mode operational regime is distinct L, H-mode, or EP H-mode and was first observed on ASDEX-Upgrade, and then studied in-depth in the Alcator C-Mod [55]. This regime allows for high confinement and high pressure but without ELMs and without impurity accumulation. While the I-mode regime is an attractive scenario, it has not yet been observed on low aspect ratio tokamaks, such as NSTX or MAST. If such a mode can be obtained, its access conditions and dynamics will be assessed to determine its relevance for both achieving the overarching programmatic goals of NSTX-U and as a possible mode of operation for FNSF.

4.2.1.3.6. External control of particle using EHO Antenna (incremental funding)

It would be highly desirable if particle transport in the pedestal could be externally controlled, perhaps in a finer manner than by driving rapid ELMs. It may be instructive to note that the

ELM-free operation attained in NSTX bears some similarity to the Quiescent H-mode (QH) seen on DIII-D [45] and reproduced on AUG [46], in that ELMs are suppressed in all three cases, in part by operating in a low-recycling regime. A difference, however, is that the electron density and impurity content saturate rapidly in DIII-D and AUG, rather than rising continuously, as in NSTX. The saturation is attributed in DIII-D [47] to the presence of Edge Harmonic Oscillations, EHOs, which appear to increase the particle transport in the pedestal.

In ELM-free lithiated discharges in NSTX, EHOs have recently been observed [48], most clearly in cases with small low-n core MHD activity. These modes are at lower frequency than those observed on DIII-D and AUG, but exhibit a similar harmonic structure. The amplitude of the EHOs on NSTX was less than observed on DIII-D, and at these levels they did not appear to redcue particle confinement on NSTX. The possibility of driving these modes using audio-frequency currents in the NSTX High Harmonic Fast Wave antenna system has been investigated. If successful, this could allow a very attractive new operational regime satisfying the needs for simultaneous avoidance of large ELMs and sufficient particle transport to maintain high-purity, stationary plasma conditions

4.2.1.4. Summary of Research Plans by Year

Years 1-3 (Year 1: 2014):

- Assess the L-H threshold power dependence over expanded parameter range, particularly at higher I_p, including also the effects of geometry and recycling
- Measure the ion and electron turbulence leading up to the L-H transition, and in standard vs. snowflake configurations to compare with predator-prey models and other models of the transition
- Characterize the ELMy regimes in NSTX-U operating scenarios, including access to standard Type I and small ELM regimes, and evaluate the applicability of the EPED model to describe pedestal evolution
- Measure the H-mode pedestal structure (heights, widths, gradients) and pedestal turbulence over the expanded range of both engineering (e.g., I_p, B_t) and dimensionless parameters, in standard and snowflake divertor configurations (see thrust BP-2, section 4.2.2); of special interest are higher I_p (impacting ballooning stability) and lower ν_e^* (affecting micro-stability drive)
- Compare enhanced pedestal turbulence measurements with gyrokinetic calculations
- Assess edge stability of large and small ELM regimes via peeling-ballooning calculations, evaluating if lower ν_e^* causes the computed bootstrap current via Sauter formulation to be in better agreement with XGC0 formulation
- Evaluate the role of resistive MHD in small ELM regimes by comparing data with calculations from BOUT++ and M3D

- Assess the impact of lithium wall conditioning on modifying the edge density profile and ELM stability, in two regimes: where ETG is expected to clamp the T_e profile, and where it is not; assess the efficacy of diamagnetic stabilization in stabilizing peeling/ballooning modes
- Re-establish parameter regime for observation of EHO on NSTX-U, and complete diagnostic studies on their properties
- Investigate the access to EP H-mode, I-mode operational regimes
- Utilize the LGI for ELM control, and initiate collaboration to investigate the physics of the ELM triggering via the JOREK code
- Evaluate the utility of vertical jogs for ELM pacing
- Determine if the midplane coils can be used to alter ELM stability and pace ELMs, and evaluate the peeling-ballooning stability of the triggered ELMs
- *Incremental: begin to design and construct power supplies to drive EHOs*

Year 4-5:

- Compare effect of cyro-pumping (see thrust BP-3, section 4.2.3) on pedestal structure and turbulence with lithium and boron coated PFCs
- Evaluate the impact of high-Z PFCs on the pedestal performance
- Evaluate the compatibility of high-Z PFCs with ELM control tools developed in the first years of the Plan
- Evaluate the ability to control edge particle transport and ELM stability with the NCC coils, and compare with 3-D ballooning calculations
- Combine the new particle control tools (cryo-pump and LGI) to trigger ELMs on demand while maintaining the pedestal structure for maximum fusion performance
- *Incremental: Demonstrate EHO drive and make preliminary measurements of the effects of driven EHOs on pedestal and SOL transport*

4.2.2 Thrust BP-2: Control divertor heat fluxes with a combination of innovative and proven techniques

The discussion of this thrust is broken into two subsections below: edge/SOL transport and turbulence that likely set the upstream heat flux channel, and innovative and conventional methods to control the divertor heat fluxes.

4.2.2.1 Edge/SOL physics

Edge and SOL plasma physics is important since it determines edge gas fueling efficiency and pumping, impurity screening (the influx and redeposition of impurities), and the performance of

RF heating systems. The basic processes that determine the edge and SOL parameters in present and future tokamak-like devices, however, are not yet well understood. The present section, therefore, focuses on fundamental plasma physics issues of the edge and SOL which will be important for *all* operation modes or divertor configurations of NSTX-U, or for any future tokamak-like device including ITER and/or an FNSF. The goal of the research in this section is to obtain a better fundamental understanding of the edge/SOL plasma and to use this understanding to improve and develop new techniques to control edge heat and particle flows.

4.2.2.1.1. Plasma transport and flows in the edge/SOL

Understanding of the inter-ELM heat transport in the tokamak SOL is critical for projecting divertor conditions in ITER and ST-FNSF. In 2010, the US community investigated SOL thermal transport and scaling via a national Joint Research Target (JRT) on SOL thermal transport. In this work, the three large US facilities, C-Mod, DIII-D, and NSTX, collaborated to develop common datasets and analysis techniques on divertor heat flux profiles over a wide range of collisionality ν*, beta β, parallel heat flux $q_{||}$, peak heat flux, and divertor geometry. In particular, the width of the divertor heat flux footprint λ_q^{div} is a critical parameter in projecting the peak divertor heat flux: at constant exhaust power, λ_q^{div} and the peak divertor heat flux q_{peak}^{div} are inversely related [4]. In low-medium recycling conditions, the divertor heat flux channel λ_q^{div} can be related to the midplane heat flux width in the SOL, λ_q^{mid} or simply λ_q, approximately through flux expansion[56,57]. Individual studies and regression analysis of the joint dataset showed λ_q decreasing ~ $1/I_p$, with an additional notable dependence on minor radius. Very importantly, there was little or no consistent major radius R, B_t, or heating/loss power dependence. This result was affirmed when the U.S. dataset was combined with European data through the ITPA. Because of the a/I_p dependence, it was more appropriate to compare λ_q^{mid} across devices using the poloidal magnetic field at the outer midplane, $B_{pol,\ MP}$. As shown in figure 4.2.13, the scaling of the inter-ELM λ_q^{mid}, under attached divertor conditions is given approximately by [157]:

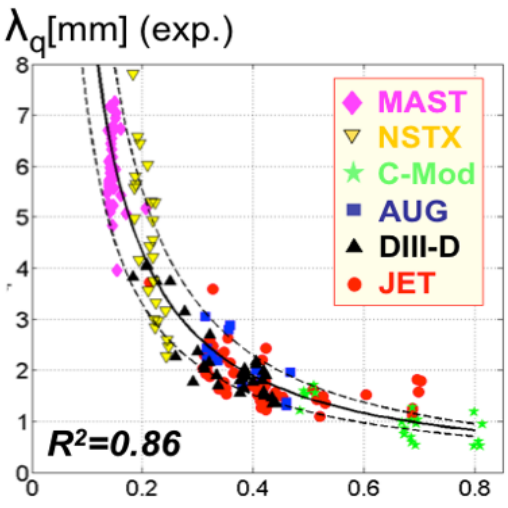

Figure 4.2.13: Multi-machine scaling of the scrape-off-layer width at midplane.

$$\lambda_q^{mid}(mm) = (0.63 \pm 0.08) \times B_{pol,MP}^{-1.19}$$

The projection for ITER under these conditions would be λ_q^{mid} ~ 1mm, which is 70-80% less than the present design assumption. Radiative divertor operation, i.e. near partial detachment, will be necessary for ITER and FNSF, where dissipation of large $q_{||}$ will be required for successful operation and protection of PFCs. Thus new ITPA studies are beginning to address how these dependences change with higher recycling and radiation. Upon commencement of operation, NSTX-U will contribute to these studies, and also attempt to resolve the relatively large variability in spherical tokamak data (i.e. MAST and NSTX in figure 4.2.13) with respect to the scalings.

Additionally in NSTX research, it was found that lithium wall coatings decreased λ_q^{mid} [57] and softened the $1/I_p$ dependence, for which the underlying physics was not determined. These measurements were enabled with a novel two-color IR thermography system [158]. Some basic physics questions that will be addressed by NSTX-U research are:

(a) what dimensionless parameters determine the SOL width in NSTX-U?
(b) what physics mechanisms are responsible for the SOL width scaling?

A neoclassical drift-based transport model, in which cross-field drifts across the separatrix are balanced against near sonic parallel flows in the SOL, was derived, predicting a λ_q^{mid} ~ the ion poloidal gyro-radius. Electron turbulent transport is assumed to allow heat flux from the core to fill the SOL, which drains the heat with Spitzer parallel conduction. The λ_q^{mid} prediction from this model ~ $(a/R)\rho_{pol}$, and is in remarkably good agreement with experiment, as shown in figure 4.2.14 [5, 58].

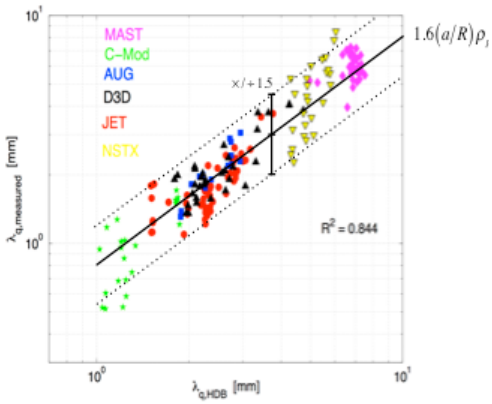

Figure 4.2.14: Comparison of experimental data with heuristic drift-based model.

The derivation of the model is heuristic, and therefore requires stronger theoretical and computational justification, which will be pursued with the XGC suite of codes. Key experimental measurements to test the physics underpinning the theory include the flow speeds at the midplane and divertor, as well as possible dependences of λ_q^{mid} on plasma geometric features, such as triangularity and the direction of the ∇B drift. These will be determined computationally, for comparison with new experiments in NSTX-U.

In general, the SOL width is assumed to be set by interplay of radial transport via plasma turbulence and/or neoclassical drifts, and parallel transport on the open field lines. A typical modeling approach is to simulate the SOL plasma with 2-D transport codes that assume enhanced turbulence-induced radial transport to fit experimental plasma profiles. On the other

hand, plasma turbulence simulations indicate that turbulent fluxes of the required magnitude arise from instabilities driven by radial plasma gradients themselves. Since the profiles and turbulence are strongly coupled, a self-consistent calculation requires coupling of simulations for turbulence and profile evolution. Such self-consistent calculations can be performed using e.g., the turbulence codes BOUT++ and XGC1, coupled in some manner to fluid codes like UEDGE or SOLPS.

4.2.2.1.2. Edge impurity transport

The planned studies of SOL/divertor impurity transport are necessary for a validated numerical model, and will have a direct impact on the impurity-seeded radiative divertor program and PFC plans. The edge/SOL plasma is affected by neutral fueling and by impurity sources at the divertor/first wall, thus, making it a complex multi-species, multi-physics problem. Impurities originating from the PFCs due to ion and energetic neutral sputtering, or introduced externally as a seeded gas, recycle at the divertor and wall, with a small fraction penetrating into the confined plasma. Material migration studies are discussed in Chapter 5; here, SOL transport and screening are discussed.

In the main chamber SOL, the near and far SOL zones are dominated by turbulent, often highly convective, cross-field transport. In the divertor chamber, where parallel gradients develop, the impurity retention and impurity pumping efficiency are determined by the classical transport parallel to the magnetic field as well as classical and neoclassical drifts. New NSTX-U capabilities, namely, a range of ν^*, and long pulse, together with a mixed-material environment that includes low-Z (Li, B, C) and higher Z (e.g., Ne, Ar, Mo) impurities, would enable a comprehensive experimental program of impurity migration and transport studies. In particular, the research program in the initial years will focus on lithium and carbon transport, with increasing emphasis on high-Z transport as high-Z PFCs are introduced.

The experiments will be supported by multi-fluid and gyro-kinetic model development and validation. The multi-fluid codes SOLPS and UEDGE will be used for edge transport and plasma-surface interaction (PSI) modeling. The main questions that the fluid modeling can address are (1) comparison of the measured and modeled impurity source strength evolution, shedding light on the erosion processes; (2) parallel and radial SOL transport and plasma fluxes in reduced recycling regimes with lithium coatings. Numerical modeling of impurity transport in NSTX-U edge plasma using the edge plasma fluid turbulence code BOUT++ will also be done. Multiple fluids can be incorporated in BOUT++ plasma model for representing ions with different charge states. This multi-fluid approach will be sufficient for capturing important physics relevant to impurity ion transport, e.g., inward transport by plasma “holes” in the edge. The BOUT++ modeling can be compared with turbulence-resolving diagnostics (e.g., BES, GPI,

fast cameras) and turbulence-averaged impurity profiles measured by filtered cameras and spectrometers. The most comprehensive code available for these comparisons will most likely be XGC1, which should have 3-D geometry, kinetic neoclassical orbit effects, neutral and impurity models, atomic radiation, and an edge/SOL turbulence model. This code can be used to study the interactions between various physics effects, which are coupled, e.g. through the radial and parallel electric fields, which cannot easily be measured directly. In addition, other specialized codes will probably be useful to help interpret the experimental results; e.g., codes which calculate edge neoclassical transport (NEO) [59], edge MHD (M3D) [60], and edge RF coupling (AORSA-2D) [61].

4.2.2.1.3. The 3-D structure of edge/SOL turbulence

The tokamak edge/SOL is a highly turbulent plasma with up to order unity fluctuation amplitudes. A basic understanding of the edge and SOL must include an understanding of the structure of its turbulence, and how this structure changes with externally controllable variables, e.g. B_t, I_p, NBI or RF power, magnetic configuration. The 3-D turbulence structure can be extremely well diagnosed on NSTX-U because of its excellent access for instrumentation, and shaping flexibility to optimize diagnosis. Turbulence and its 3D structure could have a critical influence on the plasma transport and flows in the edge/SOL to be discussed in the next subsection.

The 3-D structure effects on edge/SOL turbulence are particularly important in spherical tokamaks because of the extreme magnetic shaping and flux expansion ratio, and field-line sear in the edge region. For example, a circular magnetic flux tube in the outer midplane SOL of NSTX is "squeezed" into a very thin ribbon by the time it reaches the X-point region, and finally maps into a toroidally-elongated and very thin radial strip by the time it intersects the divertor plate (see Fig. 4.2.15). Thus a circular blob-filament formed at the outer midplane may be inhibited from reaching the divertor plate if its flux tube becomes thinner than an ion gyroradius near the X-point, which could affect both the parallel and cross-field transport effects of the turbulence. The theory of 3-D edge/SOL turbulence is presently under active development using analytic models [62, 63, 64] and computation simulations such as BOUT++[65] and XGC1 [66].

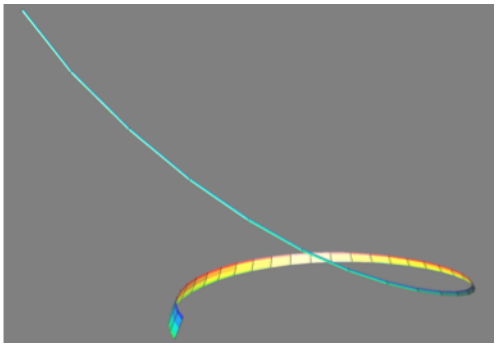

Figure 4.2.15: 3-D visualization of a magnetic flux tube in the SOL of NSTX. A circular tube at the outer midplane (upper left) becomes shaped like a ribbon near the divertor region (bottom).

Some basic physics questions on 3-D edge turbulence physics which can be answered by comparisons with experimental results on NSTX-U are:

(a) where do plasma blobs form and how do they move along/across B field lines?

(b) how does the divertor magnetic geometry affect

the edge turbulence structure?
(c) how do 3-D edge fields (e.g. RF, magnetic) affect the turbulence structure?
(d) how does atomic physics affect the edge turbulence structure?

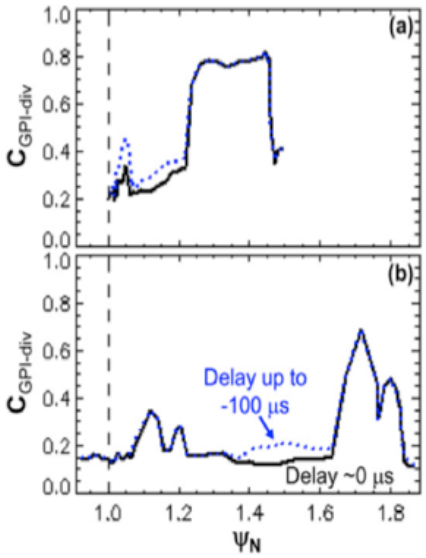

Figure 4.2.16: Cross-correlation between SOL turbulence seen by GPI at the outer midplane and the divertor plate imaging of Li I light in NSTX [15]. The correlationwas up to 0.8 for both low (a) and high (b) X-point locations.

Note that measurements of the 3-D structure of the turbulence will not allow us to *directly* explain or predict the edge/SOL parameters of present or future devices, since the transport effects of turbulence are a complex function of the fluctuations in density, temperature, and electric fields, which can not be directly measured everywhere. However, the 3-D structure of the turbulence can be compared with the turbulence simulation codes, which then can be used to explain and predict the edge/SOL transport (see also Sec. 4.2.3.3 below). This has already been done at the 2-D level in NSTX using data from the midplane GPI diagnostic and the 2-D edge/SOL turbulence simulation code SOLT [67].

The first activity in this area is to re-establish, and modestly upgrade, the edge/SOL turbulence diagnostics that were previously implemented in NSTX, specifically (a) microwave reflectometry/Doppler backscattering [68], (b) GPI [69], (c) BES [28], (d) divertor Langmuir probes [70], and (e) a divertor fast visible camera [15]. The results of these diagnostics should be compared with each other where they overlap in spatial coverage, e.g. (a), (b), and (c) at the outer midplane and (d), (e) at the divertor plate. An initial picture of the 3-D structure of the edge/SOL turbulence can be obtained early in NSTX-U by comparing the outer midplane and divertor plate results. A start in this direction was already taken by comparing the GPI midplane and divertor imaging measurements [6], which showed a high correlation in the SOL (Fig. 4.2.16).

An outcome of this research program should be a theoretical model for edge/SOL turbulence which has been validated by NSTX-U data. This model can then be applied to predict the SOL parameters and SOL heat/particle width at the divertor plates of future devices such as ITER or FNSF.

Incremental items: this area would benefit from a more complete set of diagnostics to diagnose the 3-D structures. For example, additional GPI views using relatively simple gas manifolds and in-vessel fiber optic bundles can be implemented. Furthermore, divertor probes in the top and

bottom divertor plates can be implemented to examine long-range cross-correlations. Finally a second BES system viewing the second NBI is highly desirable.

4.2.2.2. Divertor physics

Divertor research on NSTX demonstrated that the ST divertor can present both an opportunity and a challenge for the development of the boundary interface [71, 72, 73]. In future ST-based devices, the inherently compact ST divertor that limits volumetric losses, combined with low-collisionality SOL, may result in a sheath-limited divertor operating regime. This regime is characterized by small parallel temperature gradients and results in high divertor heat flux and electron temperature, and puts the divertor concepts to a rigorous test. In NSTX-U, long pulse high power density plasmas will enable divertor research to address the gaps identified for the ST boundary interface, namely, high heat and particle flux control at low normalized density, while also addressing many other boundary physics challenges common to tokamaks [2]. Operation at high divertor loading, e.g. high P/R and P/S as shown in Fig. 4.1.2, will allow NSTX-U to make world-leading contributions because the divertor solutions will be needed for NSTX-U scenarios full power and I_p scenarios. In this section a research program for the NSTX-U divertor heat and particle control is presented.

The present plan for initial NSTX-U divertor PFCs includes passively cooled copper backing plates with 2.5 cm thick graphite tiles. A gradual introduction of high-Z PFCs and lithium deposition methods is planned. Handling high heat fluxes and simultaneously addressing material erosion issues and density control will involve both improved PFCs, and advanced magnetic configurations and radiative solutions. The aim is to develop a boundary interface that can reduce high parallel and perpendicular heat fluxes, from the predicted 400 and 40-50 MW/m^2, respectively, to manageable levels, while maintaining high-pressure pedestal and good core confinement [74].

4.2.2.2.1. Connection to SOL and divertor models and improved diagnostics for model validation.

The goal of NSTX-U divertor research is to characterize heat, ion and impurity fluxes at low ν^* and compare them to edge transport and PSI models to enable predictive understanding of divertor physics for future STs. In the initial years, experiments will focus on comparison of heat flux and neutral/impurity profiles and plasma parameters with model predictions, as functions of power, density/collisionality, and grad-B drift direction.

Closely coupled with the experimental SOL and divertor activities will be predictive and interpretive transport modeling efforts. When SOL collisionalities ν^*_e, ν^*_i are sufficiently high

(10-100), as is the case in the SOL of many present-day tokamaks, a multi-fluid Braginskii transport model can be used, with kinetic corrections for heat diffusivities $\chi_{e,i}$ at the lower end of ν^*. High-performance plasma regimes of future ST-based devices will require lower ν^* than present day devices, thus emphasizing the role of convective heat transport, kinetic transport corrections, and the ion transport channel. Therefore, understanding the SOL and divertor power balance even at a basic level, i.e. how much heat is carried through the SOL to divertor targets through electron and ion channels via conduction and convection, how much power is radiated, would be important for characterizing a particular divertor configuration.

A number of analytic and numerical models will be used to assess heat and particle transport in NSTX-U experiments. Despite their inherent simplicity, analytic models, e.g., extended two-point SOL models [75] or the five-point core-coupled SOL model [76] can often provide physics insights into SOL heat transport, and will be used as a first step in data interpretation. The 2-D plasma transport models, e.g., UEDGE or SOLPS based on multi-fluid Braginskii equations and coupled with neutral transport and PSI models, will be used for more rigorous heat and particle transport analyses. With sufficient constraints provided by the proposed and available profile measurements, parallel and radial transport, impurity migration, and low-recycling regimes can be studied. If warranted by the experimental data and theory developments, the 3-D fluid turbulence code BOUT++ will be used for transport simulations. Radial transport coefficients from the BOUT++ code could be used in UEDGE to enable simulation using cross-field transport based on first principles [77]. Finally, 3-D drift-kinetic XGC0 and gyro-kinetic XGC1 codes will be used to compare with observed experimental trends

Incremental budget item: While the basic suite of edge and divertor diagnostics in NSTX-U, as described in Chapter 10, is extensive and enables numerical code benchmarking and transport studies, a particularly high-priority upgrade is mentioned here, presently included in the incremental budget - a multi-point divertor Thomson scattering system for divertor T_e and n_e measurements. These measurements would be highly beneficial for numerical model validation, e.g. for understanding the pressure/temperature balance between midplane, x-point, and target regions. The divertor Thomson scattering system measurements would also provide critical data for the planned studies of ELM and inter-ELM divertor transport, SOL width scaling, role of X-point heat transport, PSI, divertor impurity transport and spectroscopically-inferred material erosion rates. The data would be also be crucial for the radiative detachment model validation and snowflake divertor transport properties, including the X-point β_p measurements as described below. Initial planning and layout of the divertor Thomson scattering system for NSTX-U demonstrated the feasibility of the laser beam and light collection geometry attractive for high flux expansion magnetic configuration studies.

4.2.2.2.2. Heat flux mitigation in NSTX-U and projections for ST-FNSF

Candidate techniques for steady-state mitigation of divertor heat and particle loads in future fusion plasma devices must be capable of reducing particle fluxes to the levels of acceptable divertor plate material erosion rates and heat fluxes down to $q < 10$ MW/m^2, a limit imposed by the present day divertor material and cooling technology constraints. The techniques must also be compatible with high-performance high-confinement (H-mode) core plasma, high-pressure pedestal, particle control methods, and ELM mitigation techniques. At present, candidate mitigation strategies for ITER and next step fusion devices (e.g., DEMO) include both the passive techniques, such as divertor geometry and magnetic balance, and active techniques, such as radiative mantles, radiative divertors, field ergodization and strike point sweeping [77, 74]. Developed ITER plasma scenarios are based on the radiative divertor: it is planned that both inner and outer strike points will be partially detached immediately after the current ramp up phase and throughout the duration of each discharge. Based on NSTX experiments and modeling, it is planned to focus on two heat flux mitigation strategies in NSTX-U: (1) high radiated power fraction plasmas, including radiative mantles and radiative (detached) divertors, and (2) advanced divertor magnetic configurations.

4.2.2.2.3. Divertor configurations

Advanced divertor geometry configurations take advantage of magnetic modifications of the standard X-point divertor to enhance the geometry effects aimed at reducing parallel and perpendicular (deposited) steady-state and transient heat flux. These effects include poloidal magnetic flux expansion (plasma wetted area), an extended connection length, multiple divertor separatrix branches for power sharing, and increased divertor volume available for volumetric losses. The geometries considered for NSTX-U are the snowflake divertor [79] and the X-divertor [80]; limited work may also be possible on the Super-X divertor [159].

The snowflake (SF) divertor was proposed by Ryutov in 2007 [79] and many of the predicted magnetic and geometry properties have been confirmed in experiments in TCV [81, 82, 83], NSTX [84, 85, 86], and DIII-D. The NSTX experiments, in

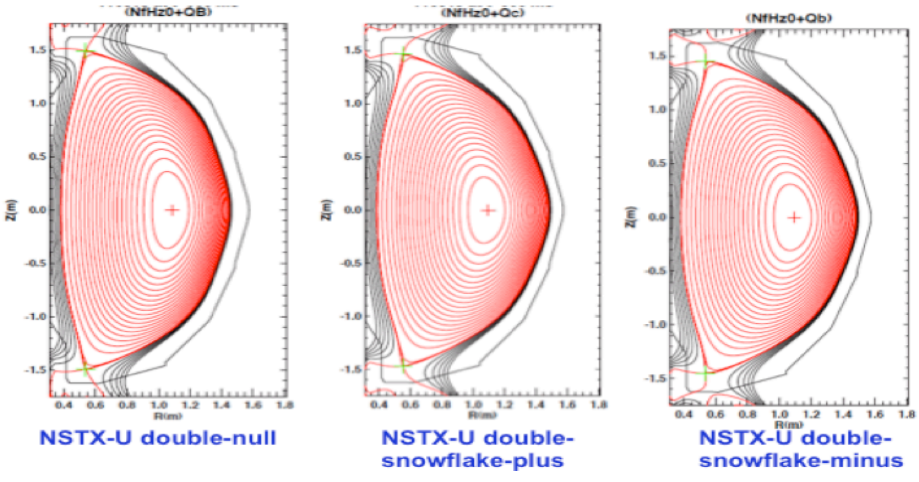

Figure 4.2.17. Examples of modeled plasma equilibria with snowflake divertor

particular, demonstrated a significant inter-ELM and ELM peak divertor heat flux reduction, reduction of core impurities, and impact on pedestal MHD stability, compatibility with H-mode confinement characterized by acceptable H-mode factors. The SF divertor configuration is considered a leading heat flux mitigation technique for NSTX-U. In NSTX-U, two up-down symmetric sets of four divertor coils will be used to test SF divertors for handling the projected steady-state peak divertor heat fluxes of 20-30 MW/m^2 with $I_p \leq 2$ MA, $P_{NBI} \leq 12$ MW, with pulse length ~ few sec. Magnetic equilibria with SF configurations have been successfully modeled using the ISOLVER Grad-Shafranov equilibrium solver (Fig. 4.2.17) and showed that a robust SF control can be maintained even when time-dependent electromagnetic effects are included. 2-D multi-fluid transport models of the SF configuration have been developed for NSTX-U using the UEDGE code [87]. The modeling projections for the NSTX-U SF divertor geometry are favorable and show large reductions in divertor T_e, T_i, as well as peak divertor heat fluxes due to the geometric and radiation effects, both with 4% of carbon impurity and with neon or argon seeding. The modeling results are summarized in Figures 4.2.18 and 4.2.19. SF divertor solutions high radiation fraction and P_{SOL} up to 12 MW were obtained, with q_{peak} reduced from ~15 MW/m^2 (standard) to 0.5-3 MW/m^2 (SF). The compatibility of cryo-pumping and SF power exhaust were also assessed via simulating a reduced neutral albedo at the cryo-pump duct location (particle exhaust projections are described in the next thrust BP-3, section 4.2.3). It was found that cryo-pumping would reduce divertor density and radiation, resulting in reduced volumetric power and momentum losses. Nonetheless, the heat flux reduction due to SF geometry would still make the SF an attractive heat flux mitigation scenario.

NSTX-U experimental studies of the SF divertor will focus on three areas:

- Development of magnetic configuration control
- Core and pedestal properties
- SOL and divertor transport and radiation between and during ELMs

The focus in the magnetic configuration control and scenario development area in the initial years will be at development of SF configurations and their integration with plasmas of various shaping parameters. Initially only three divertor coils (PF1A, PF1C, and PF2L) will be available for SF control, with an additional divertor poloidal field coil PF1B available in later years if necessary. Equilibria will be developed with variants of SF configurations, including up-down symmetric SF configurations. The modeling will aim to develop understanding of possible configurations, trends and clarify dynamic magnetic flux effects.

In the area of core and pedestal studies in the SF configuration, NSTX-U facility and diagnostic capabilities will enable several novel research directions. The SF configuration is characterized by a larger extent of low B_p region. The associated enhanced magnetic shear just inside the separatrix (w.r.t. standard X-point divertor) may have several important consequences for

boundary physics: (a) The additional local X-point and additional shear may reduce the P_{LH}, as observed in operation in an up/down double-null configuration [142]; (b) energy confinement might increase; (c) pedestal MHD stability of ideal and resistive modes would be affected, in that the increased shear would generally improve edge stability in the first stability regime; and (d) interaction with 3-D perturbations and the modified X-point region would increase prompt ion losses and drive higher E_r [88].

Figure 4.2.18: Projections of snowflake divertor parameters to NSTX-U from UEDGE model. Shown are, for the standard and the snowflake divertors: (a) UEDGE high-resolution numerical meshes with the cryo-pump duct entrance shown in blue; (b) peak divertor heat fluxes and electron temperatures as functions of SOL power; (c) Inner and outer divertor heat flux profiles for the 12 MW input power case; and (d) peak divertor heat fluxes and electron temperatures as functions of recycling coefficient.

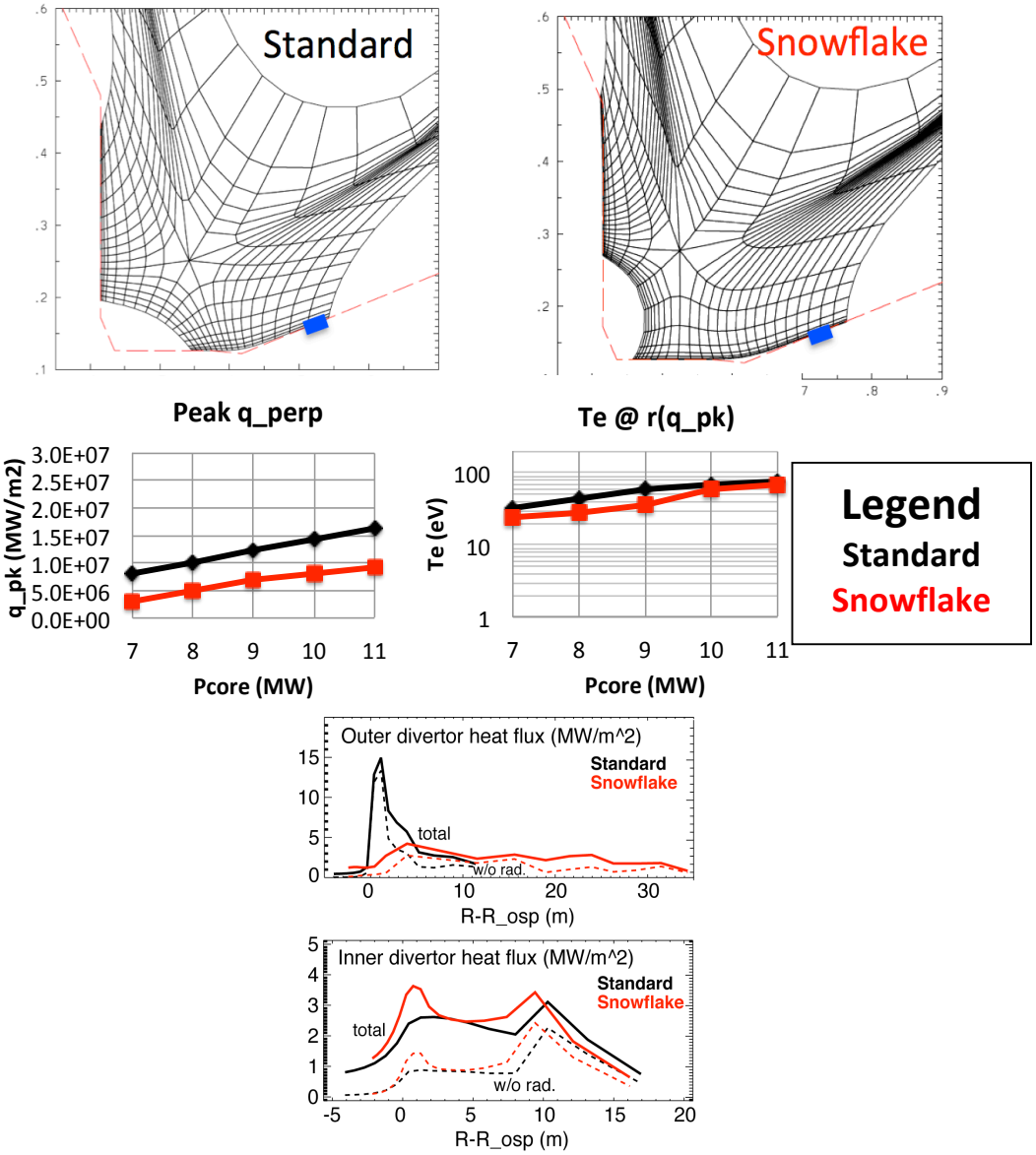

In the SOL and divertor area, the goal is to obtain experiment-based understanding of SF geometry on particle and heat fluxes, so that predictive modeling of the SF configuration for ST-FNSF can be performed. The research will be focused on the comparison of the experimental SF database enabled by the enhanced NSTX-U facility capabilities (e.g. wide range of plasma currents, heat fluxes, different ELM regimes) and multi-fluid models using the codes UEDGE, SOLPS and BOUT++. These comparisons will enable analysis of geometry effects, radiation, ion and impurity transport and turbulence in the SF configurations between and during ELMs [89].

In addition to SF divertor studies and control improvements, evaluation and prototyping of other divertor concepts is envisioned on NSTX-U. These will include the standard up-down symmetric double-null divertor studies and divertor configuration developments. The new divertor coil capabilities may enable experiments with other high flux expansion divertor configurations, e.g., the X-divertor [84, 90]. Pending the outcome of on-going equilibria modeling efforts with the ISOLVER code, experiments presently envisioned for initial NSTX-U years can provide initial tests of stability and heat flux mitigation of these configurations. Collaboration with other facilities, e.g., the spherical tokamak MAST (UK), are also envisioned, particularly toward evaluation of the Super-X divertor configuration.

4.2.2.2.4. Heat flux mitigation based on highly-radiative scenarios

A leading technique for divertor heat load reduction and control via radiated power loss includes increasing impurity radiation fraction to the levels compatible with high-confinement core and pedestal characteristics. The standard operating scenario of the ITER divertor is an impurity-seeded radiative divertor with partially detached inner and outer strike points. In this regime, charge exchange, radiation, and volume recombination are all significant loss channels that bring down peak heat flux. Codes reproduce elements of these processes semi-quantitatively, but do not reproduce the dynamics leading to detachment, e.g. the observation that the inner divertor routinely detaches before the outer, nor do they reproduce the measured SOL flow patterns. Several radiative techniques will be studied in NSTX-U with an aim to improve understanding of divertor detachment process, and develop and demonstrate highly radiative H-mode solutions for ST-FNSF. These techniques will involve radiative boundaries (mantles), radiative divertors with impurity seeding, and lithium vapor-shielding techniques.

In the first two years, basic characterization of these techniques is envisioned, so that further physics-based optimization can be accomplished in later years. These techniques are applicable to steady-state heat flux mitigation, so their compatibility with ELM control or avoidance should also be demonstrated.

Radiative power dissipation at the edge of confined H-mode plasmas (i.e. in the main chamber outside of the divertor) has been demonstrated in several tokamaks, however, its control and scaling have not been studied in detail [91, 92, 93]. High edge radiation fraction scenarios must be compatible with high-pressure pedestal and low core Z_{eff}, therefore, a transport barrier for impurities appears to be a necessary part of these solutions. In initial years of NSTX-U, experiments are envisioned with neon and argon core seeding to provide initial data for evaluation of the concept for ST-FNSF, and further optimization for NSTX-U conditions.

Radiative divertors use deuterium and/or seeded impurities to reduce divertor particle and heat fluxes through volumetric momentum and energy dissipative processes - the ion-neutral elastic and inelastic collisions, recombination and radiative cooling [78, 74]. In NSTX radiative divertor experiments with D_2 and CD_4 seeding, a significant reduction of divertor heat flux from peak values of 4–10 MW/m^2 to 0.5–2 MW/m^2, simultaneously with good core H-mode confinement, has been demonstrated in 1.0–1.3 s discharges [72, 73]. These experiments demonstrated that partial divertor detachment was obtainable in a compact divertor of a high power density ST even with carbon radiation. It is clear, however, that in order to dissipate SOL powers in excess of 5-10 MW in NSTX-U, higher Z impurities (e.g., nitrogen, neon or argon) will be required. Initial multi-fluid edge transport models have been developed for NSTX-U projections with the UEDGE code [87]. The models showed that peak divertor heat flux reduction via partial detachment can be achieved in both the standard and the SF divertor configurations (easier with the latter) in NSTX-U with neon or argon seeding (e.g. Figure 4.2.19). Planned experiments in this area will be critical for further concept development and model validation for ST-based devices that operate at low core and edge ν_e*.

In initial years, experiments will use open-loop impurity seeding in the divertor. The seeding impurity gas is selected based on operational and atomic physics (radiated power at low T_e) considerations. The seeding gas options will include D_2, CD_4, and Ar in the next five years with graphite and partial high-Z PFCs conditioned via lithium and boron coatings. N_2 is excluded at this stage due to its chemical reactivity with lithium coatings and its absorptivity in graphite. Multi-fluid models will be used for the analysis of power balance and impurity transport in the radiative divertor experiments.

These experiments will set the stage for the radiative divertor feedback control development that would take place in later years. For steady-state high-performance operation, steady-state radiative divertor conditions must be sustained. This can be accomplished by feedback through controlling the rate of injection of the deuterium or impurity gas, using a divertor parameter as a control quantity. The partial divertor detachment was characterized [72,73] in NSTX using a number of divertor plasma measurements: divertor plate surface temperature (heat flux), radiated power using bolometry and impurity emission spectroscopy, neutral gas pressure measurements,

ion flux using Langmuir probes, and divertor recombination using UV or NIR spectroscopy. Based on those NSTX experiments, the control diagnostic signals considered for NSTX-U include divertor radiated power, neutral pressure, spectroscopic deuterium recombination signatures, infrared thermography of PFC surfaces, and thermoelectric scrape-off layer current, as well as spectroscopic "security" monitoring of possible confinement or pedestal degradation

Figure 4.2.19. Projections of radiative divertor solutions for the standard and s=snowflake divertor geometries in NSTX-U from UEDGE model. Shown are divertor peak heat fluxes and radiated powers in the core and divertor as functions of impurity fraction, with neon seeding (a) and argon seeding (b).

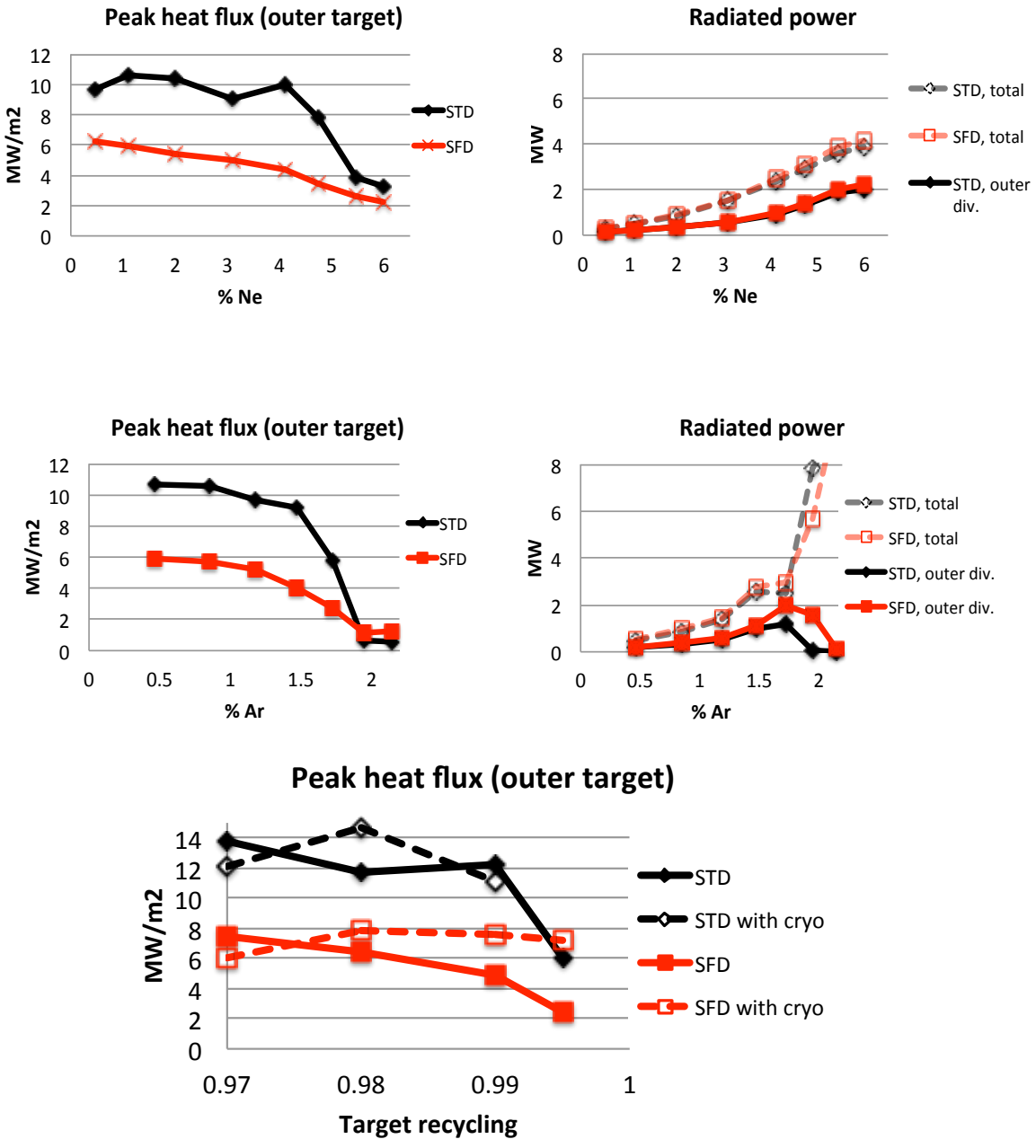

[94].

A prerequisite for radiative divertor feedback control is the cryo-pump that would control the gas inventory. The control aspects of the feedback are described in Chapter 9. The ultimate goal of the radiative divertor feedback control development is a demonstration of a controlled peak divertor heat flux for a long pulse discharge with high performance metrics.

4.2.2.3. Summary of Research Plans by Year

Years 1-3 (Year 1:2014):

- SOL widths, particle/impurity transport, and turbulence
    - Determine scaling of SOL width vs. appropriate local dimensionless parameters, develop measurement of the parallel SOL flows, and compare with expected neoclassical flows
    - Measure seeded impurity screening in radiative divertor experiments
    - Measure lithium, boron, carbon SOL and divertor profiles and assess transport coefficients
    - Measure the edge turbulence with microwave reflectometry/Doppler backscattering, GPI, BES, divertor Langmuir probes, and a divertor fast visible camera
    - Compare turbulence measurements where they overlap in spatial coverage, as in previous studies which showed a high correlation of turbulence in the SOL; compare with simulations with the BOUT++, SOLT, and XGC1 codes
    - *Incremental: perform molybdenum and tungsten injection and screening experiments with a laser blow-off system*

- Snowflake divertor
    - Develop and test X-point tracking algorithms based on real-time magnetics, and real-time multiple X-point control techniques in PCS
    - Develop and test up-down symmetric SF configurations, SF formation and disintegration
    - Evaluate effect of SF on L-H power threshold, edge turbulence and stability, SOL power balance and divertor heat flux, n_e and T_e trends, including detachment onset and characteristics at different n_e/n_G; enhance radiated power with gas seeding (D_2, CD_4, Ne, Ar)

- Divertor studies and radiative divertor feedback control development
    - Evaluate divertor heat and particle transport as a function of magnetic balance; this will be enabled by new two-color IR thermography of the upper divertor

- Perform initial radiative divertor studies: measure power balance and operational space (power, density) of the radiative divertor, radiation and recombination spatial distributions, PFC erosion, neutral and impurity retention and compression, MARFE formation and stability
- Combine radiative divertor with ELM control techniques to keep core impurity concentrations low, if needed

Years 4-5:

- SOL widths, particle/impurity transport, and turbulence
  - Compare data from NSTX-U with theoretical models/mechanisms (e.g. classical collisional neoclassical phenomena, large-scale convective cells, electromagnetic turbulence, MHD activity) for edge/SOL cross-field transport and parallel flow
  - Clarify the 3-D edge/SOL turbulence structure *vs.* edge plasma parameters, magnetic divertor geometry, and the presence of 3-D perturbations of various types, e.g. RMP coils, HHFW heating, NBI injection; add GPI views looking down onto the divertor
  - Continue benchmarking of turbulence models and simulation codes, e.g. BOUT++, XGC1, and SOLT
  - *Incremental: install a more complete 3-D array of edge/SOL turbulence diagnostics at various poloidal and toroidal angles in NSTX-U e.g., (a) additional GPI views using relatively simple gas manifolds and in-vessel fiber optic bundles, (b) divertor probes at top and bottom divertor plates to look at their cross-correlation, and (c) a second BES system viewing the second NBI.*

- Snowflake divertor
  - Combine SF configurations with pedestal control scenarios and tools, e.g., the EP H-mode, RMP of various spectra (n=2,3,4) aiming to optimize pedestal structure, transport and stability.
  - Develop long-pulse discharge scenarios with SF divertor configurations using a full set of all four divertor coils for improved magnetic control, and combine with cryo-pumping
  - Develop experiment-based model projections for future ST-based devices, such as ST-FNSF, and compare with studies in conventional aspect ratio tokamaks (DIII-D, TCV).

- Divertor studies and radiative divertor feedback control development
  - Implement radiative divertor feedback control
  - Demonstrate long-pulse H-mode scenario with feedback-controlled impurity seeding and cryo-pumping

- *Incremental: implement divertor Thomson Scattering to provide critical data for model validation for SF and radiative divertor studies*

4.2.3. Thrust BP3: Compare the sustainability of particle exhaust via lithium pumping and cryo-pumping, for density, impurity, and Z_{eff} control consistent with integrated scenarios

Integrated scenarios on NSTX-U are designed for steady density at 0.5-1 times the Greenwald density limit scaling, and Greenwald fractions as low as 0.35 would be very beneficial to accessing ν^* an order of magnitude lower than NSTX for transport and stability research. To achieve such levels of density control, a central element of the boundary program includes installation of a divertor cryo-pump, representing a proven technology to control both main ion and impurity density. A key component of the research is to compare lithium pumping and cryo-pumping for density control and impurity control. An integral element to both of these studies is the assessment of impurity sources and transport.

Below, the physics design of an in-vessel cryo-pump is described in the first section, as this represents a new, central element of the five-year plan. That is followed by a discussion on the sustainability of pumping via lithium evaporation; liquid lithium PFCs appear only in the incremental budget in this plan and are discussed in the Materials and PFC Chapter. Finally the spectroscopic studies of recycling and impurity sources and transport are described.

4.2.3.1. Cryo-pumping

a. Background

Although the application of lithium coatings on the lower divertor has been shown to be successful in controlling the deuterium inventory of the core plasma in NSTX (see Chapter 9), these plasmas suffer from strong impurity accumulation, leading to a ramping electron density (due to carbon) as well as radiated power. This is attributed to the elimination of ELMs that occurs with large lithium deposition; without the corresponding impurity flushing, the ELM-free regime is commonly observed to be transient with strong particle accumulation. Due to this difficulty in achieving stationary conditions with lithium coatings alone, a cryo-pumping system is being designed for NSTX-U to provide active particle exhaust. The expectation is that this would be used either without lithium, in which case ELMy scenarios can be expected as typical in boronized NSTX scenartios, or with a reduced and optimized lithium deposition amount chosen so that (ideally small and rapid) ELMs remain. This should avoid the impurity accumulation problems of the ELM-free H-mode, and would be more similar to the ELMy H-modes in conventional aspect ratio tokamaks where cryo-pumps are a proven technology for achieving density control.

In addition to facilitating 'particle control' in the sense of avoiding a density that increases throughout the discharge, the cryo-pump will be a critical piece of active control using feedback to maintain the density at desired values. This will be an important capability allowing many physics studies, for example in exploring the role of ν^* in core energy transport. The cryo-pump will provide the particle exhaust needed in conjunction with fueling techniques in order to actively control the plasma density.

b. Physics design

The general layout of the proposed cryo-pumping system is similar to the pump on the lower divertor of DIII-D [95]. As illustrated in Figure 4.2.20, the entrance to the pumping plenum is located on the SOL side of the outer separatrix strike point. The geometry of the plenum entrance (the position of the entrance, along with the height and length of the duct leading to the plenum) has been optimized based on a semi-analytic model for the plenum pressure [95, 96], which was previously developed for the DIII-D pumping system. This model is based on first-flight neutral transport through the divertor plasma (including neutral losses due to ionization) into the plenum entrance, and uses this along with analytic expressions for the pressure in the plenum given the duct geometry and pumping speed. These expressions have been extended as part of the NSTX-U cryo-pump design effort to account for finite duct length at the plenum entrance [97] and the analytic duct conductances as well as plenum pressures has been verified by comparison to calculations using the neutral transport code EIRENE [98].

The analytic pumping model has been used in conjunction with projections of the divertor plasma parameters in order to optimize the height h_{ent} and length g_{ent} of the duct leading into the pumping plenum. Further, an optimization has also been performed to determine the major radius at which the plenum entrance should be placed. This was accomplished using realistic NSTX-U equilibria generated with ISOLVER. Eight equilibria were used, four standard and four snowflake divertors, with the outer strike point position varied from R_{OSP}~0.5 to R_{OSP}~0.7 m in each configuration. To project the divertor heat flux profile, an exponential profile was assumed with a falloff length given by recent NSTX experiments that measured the SOL heat flux

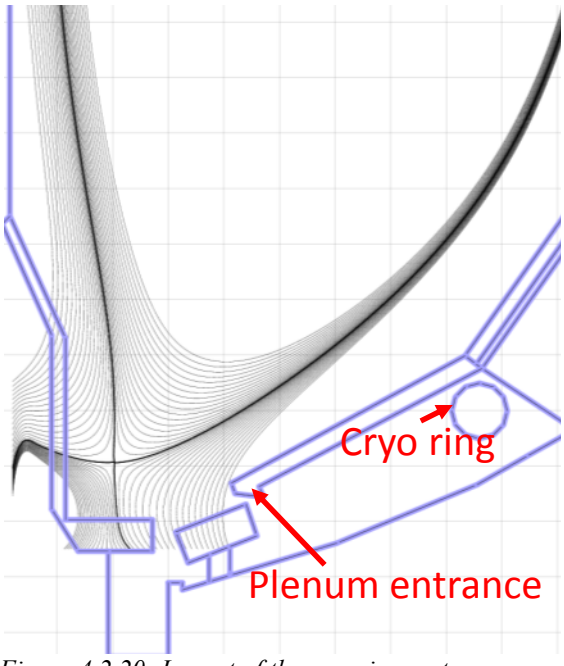

Figure 4.2.20: Layout of the pumping system

width under a variety of conditions.

To assess the effectiveness of the pump, the accessible Greenwald fraction range with the cryo-pump has been estimated. This was accomplished by scanning the divertor T_e in the analytic pumping model and calculating the plenum pressure at each value, then for the T_e at which the pumped flux equals the beam input a two-point model [99] (calibrated to OEDGE modeling and NSTX experiments) was used to estimate the midplane separatrix density. The Greenwald fraction f_G was then calculated assuming the line-averaged density is three time higher than that at the separatrix (based on typical values from NSTX). The resulting f_G is shown in Figure 4.2.21 as a function of separatrix strike point position (which is varies across the set of various equilibria studied) and plasma current (which affects both n_G and λ_q). For the standard divertor configuration (panel a), the achievable f_G is relatively insensitive to plasma current, while the plasma can be pumped down to lower densities if the strike point is moved closer to the plenum entrance (this is similar to the DIII-D experience[96]).

These calculations indicate that the pump should be capable of reducing the plasma density to quite low values, down to f_G<0.4 if R_{OSP} is located very near the pump. However, high R_{OSP} configuration have reduced flux expansion, and so at high plasma current (where the SOL is narrowest) it will not likely be possible to move the strike point very near the pump without exceeding the heat flux limit of ~10 MW/m^2 in the standard divertor configuration (the shaded region of the figure shows the region where this limit is exceeded). The snowflake divertor has a significant advantage in this respect, in that the higher flux expansion allows the strike point to be moved closer to the pump without exceeding heat flux limits, so that it should allow operation at higher I_p with good pumping. Further, the snowflake also shows stronger pumping even with the strike point far from the plenum entrance: for R_{OSP}=0.5m, the snowflake can be pumped down to f_G~0.6 compared to f_G~0.8 in

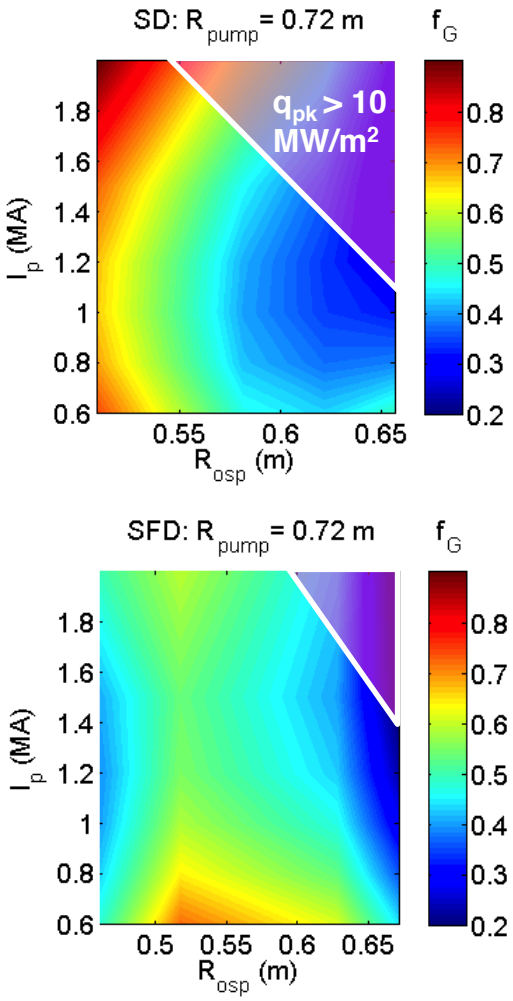

Figure 4.2.21: Estimated Greenwald fraction assuming only neutral beam particle input and cryo-pumping in a) standard and b) snowflake configurations

the standard configuration. While somewhat counterintuitive, the improved pumping in the snowflake is due to the higher flux expansion: with pumping performed in the far SOL as is done here, increasing the flux expansion increases the plasma flux near the pump, which is conducive to higher plenum pressures.

The pumping optimization approach used here is based on a first-flight neutral model, which is expected to be adequate in attached regimes, but to break down in detached divertor cases where charge exchange collisions and diffusive neutral transport are strong. Recently, the analytic model has been checked by comparison to 2D plasma-neutrals modeling with the SOLPS code [REF], which has a much more rigorous neutral transport model that is appropriate in radiative/detached divertor regimes. These calculations showed that in the attached regime (T_e^{div} > ~ 2eV), the semi-analytic model is sufficient to predict the plenum pressure (for given plasma parameters). In detached regimes (T_e^{div} > 2 eV), the semi-analytic model under-predicts the pressure compared to SOLPS calculations by a factor of 2-3 [97]. These calculations confirm the expectations (based on DIII-D experience) that the analytic model predicts lower pressures than are achieved in detached regimes. Therefore, the use of the semi-analytic model in performing the pumping optimization is conservative, and it can be expected that in detached divertor scenarios the pumping will be even stronger than predicted using these simple estimates.

4.2.3.2. Sustainability of pumping with lithium

Lithium evaporation has been shown to reduce the density ramp rate in the subsequent discharge [7] but substantial amounts of lithium lead to ELM-free operation, with temporally rising electron density and impurity accumulation [100, 101, 102]. The ion inventory can be maintained at a constant or slightly declining level.

Interpretive analysis of discharges with variable lithium conditioning, and hence variable ELM frequency, was done with the SOLPS code to determine if the divertor pumping capacity from lithium was changing with time [8]. It was found that the divertor recycling coefficient R decreased with increasing lithium pre-discharge lithium deposition to a minimum value of R ~ 0.85-0.9, and that this low recycling was maintained for the duration of ~ one sec long discharges [103]. Indeed the divertor recycling as represented by D_α baseline level in those discharges was flat or declining with time. In other words, the time constant for saturating the applied lithium with deuterium bombardment was well over one second.

This conclusion was also corroborated by observations following a large evaporation (50-60 g) of lithium into NSTX; following that evaporation, approximately 100 H-mode discharges were achieved with no additional wall conditioning between discharges (although the discharge reproducibility was not nearly as good as when smaller amounts of lithium were evaporated

between discharges). A similar large evaporation was accomplished on the EAST device [104] in which scientists from NSTX participated. In that study, an e-folding time for evolution of the divertor recycling was ~ 20 sec. These observations provide confidence that lithium wall conditioning would last for the design 5-10 sec pulse length in NSTX-U, but assessment of the duration must be done on NSTX-U, and compared with liquid lithium PFC results.

4.2.3.3. Local recycling, impurity generation and transport studies

An understanding of lithium effects on ion pumping, SOL transport and impurity erosion is emerging from the analysis of spectroscopic data from NSTX experiments [94]. On NSTX-U, this research will be expanded into two main PSI aspects: density and impurity control with lithium and boron coated graphite and high-Z PFCs; it includes the studies of recycling, material erosion and SOL impurity transport.

The methodologies previously applied on NSTX for recycling and impurity influx measurements will be further improved on NSTX-U. The main diagnostics to be used are a new Material Analysis Particle Probe (MAPP) [160], divertor Langmuir probes, and spectroscopy. In particular, (1) ultraviolet and visible spectroscopic measurements of hydrogenic neutrals and neutral or ionized impurity atoms will be used for quantitative influx and source measurements using the S/XB atomic factor method; multi-channel spectrometers or cameras with narrow-bandpass interference filters will be used for these measurements. (2) Impurity emission profiles in combination with local plasma temperature and densities will be used for impurity radial and parallel transport studies aided by interpretive modeling; again, cameras and multi-channel spectrometers will be used for the measurements. (3) Extreme ultraviolet impurity emission in the core plasmas, also in combination with local plasma temperature and densities, will be used for impurity transport and accumulation studies; extreme ultraviolet spectrometers are planned for these measurements.

Because the ion fluxes vary by orders of magnitude from the strike point region to the outer wall, different parts of the wall saturate with deuterium at different times. Estimates of local ion recycling coefficients will be inferred from ratios of the recycled flux (inferred from deuterium Balmer line intensity) to the incident ion flux (inferred from Langmuir probe I_{sat}) with proper inclusion of calibration, atomic and geometry factors. Short (~10 ms) intense deuterium pulse injections from the supersonic gas injector (SGI) will be used to characterize pumping by divertor lithium coatings by measuring the divertor density and D_α pump-out times. These experiments will enable characterization both the baseline (lower divertor) or increased area (lower and upper divertor) lithium pumping rates and lifetimes.

In the area of impurity production, the main questions that are to be addressed are (i) accurate accounting of impurity sources for transport studies; (ii) Gross and net erosion fluxes as function

of lithium amount, coverage, and longevity. In the initial years, experiments will be dedicated to lithium and carbon measurements, and as high-Z PFCs are introduced, studies will focus on high-Z erosion and influx measurements. In the area of carbon sources, divertor and midplane C I, C II, CIII, C IV and CD emission profiles will be measured and compared with edge fluid, turbulence and neoclassical edge impurity transport model predictions. The presence of lithium can affect SOL and divertor plasma conditions, change turbulence characteristics, and change parallel forces (e.g., the ion-impurity viscous force and the ion temperature gradient force) that act on divertor impurity ions and regulate divertor retention. This is a critical question for the lithium coating applications, as high Z_{eff} due to carbon was previously observed in NSTX lithium H-mode discharges. In the area of lithium sources, Li I and Li II emission spatial distributions will be measured. Lithium coating lifetime and source strength are dependent on several factors: (1) Lithium erosion process differs from other species in that lithium, being an alkali element, is sputtered as ions (33 %) and neutrals (66 %); (2) because of a low ionization potential and short mean free ionization path, a large fraction of sputtered lithium atoms is re-deposited; (3) because of a low melting temperature (180 C) lithium can melt in the strike point region; (4) lithium erosion rate increases with temperature. In NSTX experiments, the low-level divertor lithium source partially explained very low lithium concentrations in the core plasmas. In the area of high-Z erosion and transport, studies will be initially focused on the basic characterization of high-Z sputtering and transport to the core as a function of boron and lithium coatings, ion and impurity sputtering fluxes, seeded divertor operation, and main plasma heating (e.g., NBI vs HHFW). As the high-Z coverage area is increased, research will be extended to characterize two- and three dimensional erosion distributions (that will also include divertor vs main wall), as well as gross and net erosion fluxes. The ultimate goal of these studies is to understand the PSI with high-Z lithium coated PFCs under seeded or high-flux expansion divertor operations.

4.2.3.4. Summary of Research Plans by Year

Year 1 (2014)

- Complete cryo-pump physics design: a) Better establish how much headroom the system gives for pumping beyond the neutral beam input, on which the present design is based; b) Continue calculations in high density partly detached regime with additional gas input with fluid codes

Years 2-3

- Perform cryo-pump engineering design and install pump, based on the finalized physics design from projected divertor plasma parameters
- Validate cryo-pump physics design calculations which assumed SOL profiles of divertor parameters from NSTX projections, by comparing with initial measurements in NSTX-U
- Assess ability of lithium conditioning to provide density and impurity control for high power, long pulse NSTX-U discharges, using a combination of the downward

evaporators in the first year of operation, combined with upward-facing evaporator(s) in the second year of operation
- Assess lithium coating lifetimes and interaction with ion fluxes in divertor strike point, near-SOL and far-SOL regions with spectroscopy
- Extend local hydrogenic recycling and particle balance measurements to the upper and lower divertor areas, and main wall, including comparisons of boronized and lithium-coated graphite plasma-facing components

Years 4-5
- Characterize performance of pump to compare with design calculations, and also with perform with lithium conditioning
- Assess pump performance with metallic PFCs, as those are introduced into NSTX-U
- Develop scenarios use the cryo-pump for deuterium control while maintaining ELMs for impurity flushing, similar to conventional tokamak operating scenarios; this will inform the use of the cryo-pump in density control schemes described in Chapter 9

4.3 Summary of Theory and Simulation capabilities

4.3.1. XGC Total-f Gyrokinetic Particle Code

XGC1 is a nonlinear gyrokinetic particle-in-cell code for kinetic ions, electrons, and neutrals in realistic diverted tokamak magnetic geometry. Coulomb collisions conserve particle, momentum, and energy, with the option of linearized or fully nonlinear operators. The main difference between XGC1 and the other US gyrokinetic codes is that XGC1 is a total-f code while the others are delta-f codes. In a total-f code, the background plasma profiles, electric field, and rotation evolve self-consistently with external heat source, heat sink, turbulence and transport; while in a delta-f code, the turbulence and transport is evaluated from an assumed fixed plasma background. Neoclassical physics is automatically included in a total-f gyrokinetic code while it is not in a delta-f gyrokinetic code. As a result, the plasma and transport profiles settle to a self-organized state in XGC1, similarly to experimental situation, consistently with externally applied heat source and edge loss. On the other hand, in a delta-f code, transport fluxes vary sensitively to the assumed plasma profile. XGC1 can also be operated in delta-f mode for diagnostics purposes. Spatial simulation domain of XGC1 is usually the whole tokamak volume: from the magnetic axis to the material wall, across the magnetic separatrix surface. In order to reduce the computing time requirement, physics research emphasis is given to the pedestal/SOC region by allowing a more refined grid in that region. An inner radial boundary can be specified in an edge only simulation. However, it is found that the artificial boundary condition distorts the edge turbulence solution. Most of the past study by XGC1 has been performed for the study of nonlinear ITG turbulence and neoclassical physics with adiabatic electrons. Recent studies

include the wall-recycled Monte Carlo neutral particles with charge exchange and ionization physics, and non-adiabatic kinetic electrons in electrostatic turbulence mode. Transition physics from ITG to TEM has been cross-verified with other codes in delta-f simulation mode. XGC1 is under verification for electromagnetic turbulence. Impurity particles with wall sputtering coefficient are being added. Interaction of 3D RMP physics with plasma turbulence will be studied in the near future. All of these processes and effects: turbulence, neoclassical, neutral, impurity, and wall interaction physics, are simulated self-consistently.

4.3.2. XGC0 total-f Axisymmetric Particle Code

XGC0 is the axisymmetric version of XGC1, which ignores turbulence. Instead, turbulent transport is incorporated in the neoclassical Lagrangian particle motion as a radial random walk process. Since XGC0 does not have toroidal grids and uses a much smaller number of poloidal grid points, simulation speed is about 100X faster. Simulations of kinetic plasma profile evolution, pedestal buildup and divertor heat load accumulation are performed usually within a day on a local cluster or on a moderate size HPC, depending upon the physics. For this reason, XGC0 is more popular to experimental users than XGC1 is. Currently, XGC0 contains kinetic ions, kinetic electrons, Monte Carlo neutral particles with ionization and charge exchange cross-sections, multispecies impurities with radiative power loss, logical wall-sheath, heat source, and momentum source. A particle, momentum, and energy conserving Coulomb collision operator is used in linearized and fully nonlinear modes. 3D RMP penetration into plasma is studied with the added perturbed magnetic field solver to the existing electrostatic solver. The gyrokinetic neoclassical effect and the poloidal electrostic potential variation solver are under addition in XGC0. In the future, XGC0 and XGC1 will be combined in subgrid time-integration technique for experimental time-scale simulation of gyrokinetic turbulence, neoclassical and other important physics. XGC0 is coupled to M3D code for pedestal-ELM cycle study.

4.3.3. DEGAS - described in Macrostability Chapter 2

4.3.4 BOUT++

A three-dimensional realistic tokamak geometry edge electromagnetic turbulence and MHD code that solves Braginskii-like fluid equations for ion density, parallel ion and electron velocities, separate electron and ion temperatures, vorticity equation for electrostatic potential, and vector potential A|| equation [147].

4.3.5. The UEDGE code

UEDGE is an edge multi-fluid transport code that simulates plasma, neutral and photon transport in the tokamak SOL and divertor region. The code is based on the solution of the Braginskii-like

fluid equations for ion density, parallel velocity, separate electron and ion temperatures, vorticity equation, neutral density, and neutral parallel velocity [105, 106, 107, 108]. The computational mesh is based on the magnetic equilibrium obtained from MHD equilibrium codes. The plasma transport is classical along the magnetic field with the addition of flux limits for kinetic corrections. The transport across the magnetic field is described by ad-hoc diffusion and convection coefficients. UEDGE also includes the option to model classical cross-magnetic-field drifts associated with E **x** B and gradient-**B**/curvature drifts. Impurity species are treated either in a fixed fraction approximation, or by following the separate charge-state ions. The sputtering of divertor and wall materials as an impurity source is included via physical and chemical yield functions. For neutral species, a fluid model is used, with particle and energy flux limiters determined by thermal streaming values based on a comparison with more detailed Monte-Carlo neutral simulations. Direct coupling to a Monte-Carlo neutral transport code DEGAS 2 is also implemented. The basic UEDGE models have been used extensively to model edge plasma characteristics in a number of existing tokamaks, e.g. DIII-D [109], NSTX [110,111], Alcator C-Mod [112] and JT60-U [113] as well as ITER [114] and some ARIES designs [110].

4.3.6. The SOLT code

The Scrape-Off-Layer Turbulence (SOLT) code [115] is a fluid code that models turbulence in a two-dimensional plane perpendicular to the magnetic field B at the outboard midplane of the torus. SOLT implements classical parallel physics using closure relations [116] for the midplane parallel current and parallel fluxes of particles and energy for collisional regimes ranging from sheath-connected to conduction limited. The SOLT code can describe arbitrarily strong nonlinear plasma dynamics ($\delta n/n \sim 1$), including blob-filaments [116, 118], and the physics model supports interchange-type curvature-driven modes, sheath and Kelvin-Helmholtz (KH) instabilities, and drift waves. Past versions have assumed cold ions; current development work [119] is implementing finite ion pressure including the relevant ion gyroviscous terms, and additionally removes the commonly used but hard-to-justify Boussinesq approximation. For comparison with experimental gas puff imaging data, SOLT employs a synthetic GPI diagnostic to simulate both He and D gas puffs. Recent applications of SOLT have included the study of zonal flow oscillations [120], the effect of parallel currents on turbulence [121], SOL heat flux widths [117, 122, 123], a SOLT quasi-coherent mode [121], and the impact of edge topology and profiles on the generation of flows [124].

4.3.7. The SOLPS suite of codes

The SOLPS suite of codes solve a set of 2-D equations for the coupled plasma and neutral transport[125]. The plasma is treated with a 2-D fluid approximation using the B2.5 code [126] with transport parallel to the magnetic field governed by classical Braginskii-type equations

(with corrections for kinetic effects) and cross-field transport given by user-specified "anomalous" transport coefficients. Neutral transport is calculated by the EIRENE Monte Carlo code[98], a the code has the ability to treat multiple impurity species.

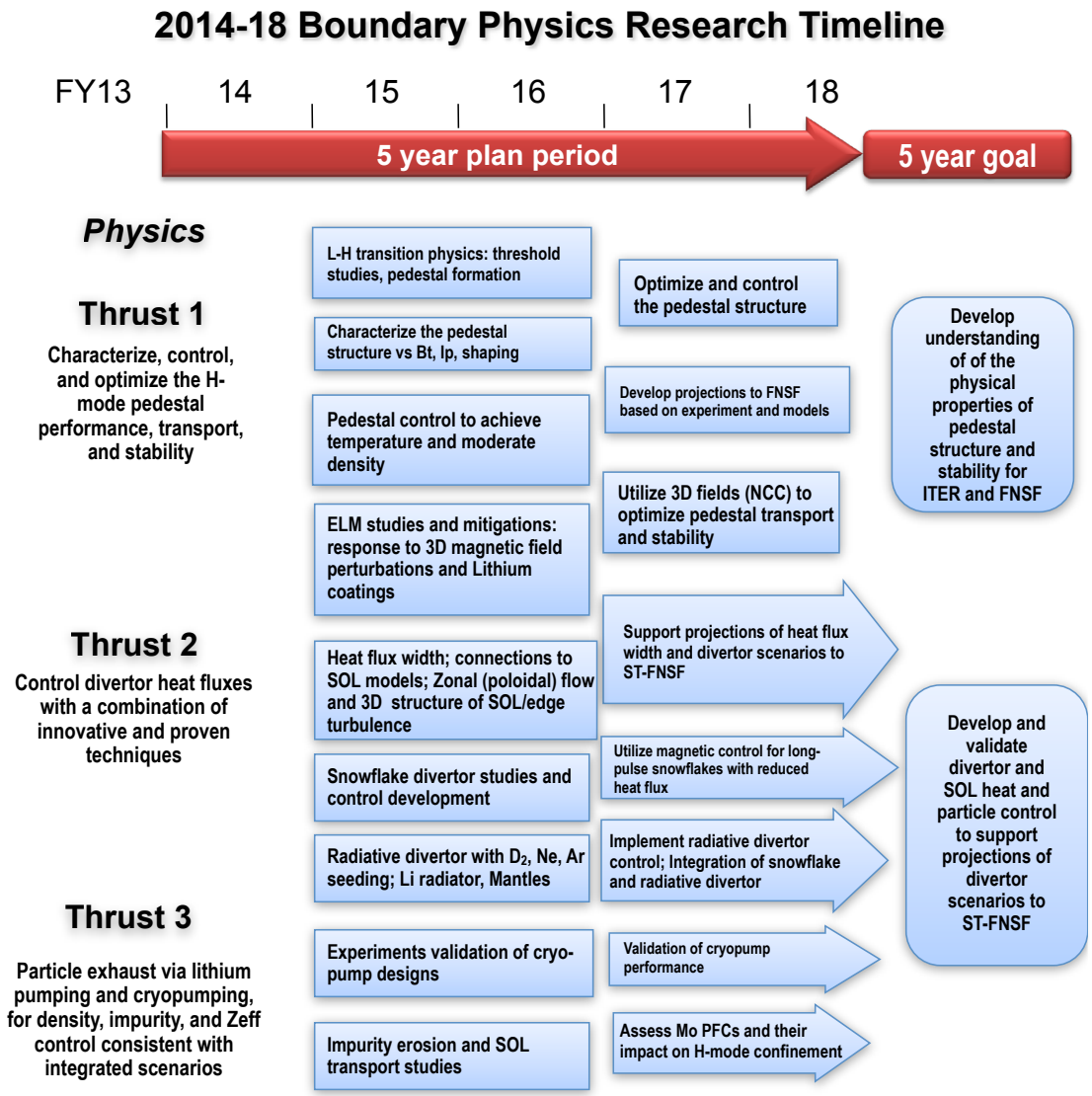

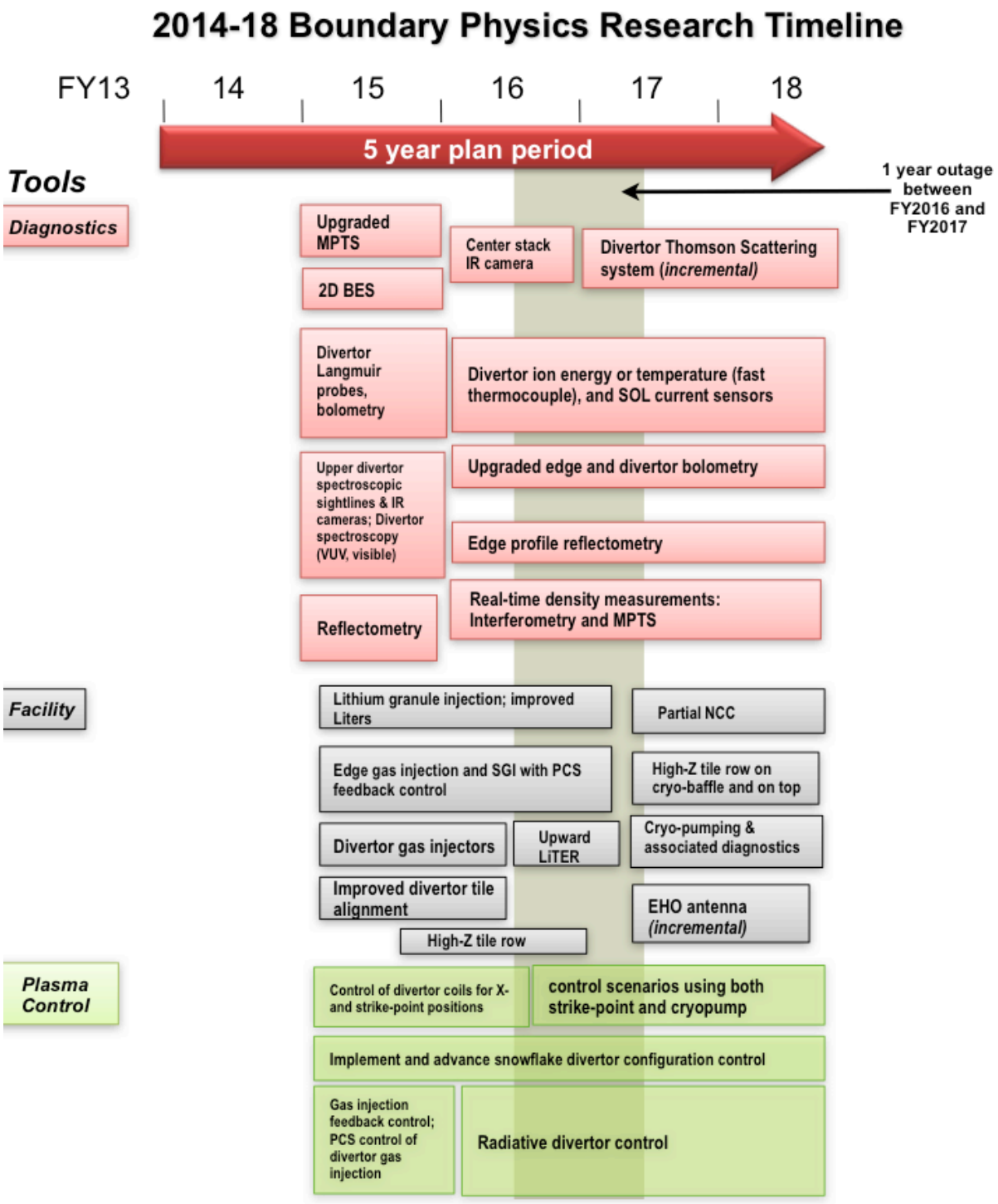
2014-18 Boundary Physics Research Timeline
FY13
14
15
16
17
18
5 year plan period
1 year outage between FY2016 and FY2017
Tools
Diagnostics
Upgraded MPTS
Center stack IR camera
Divertor Thomson Scattering system (incremental)
2D BES
Divertor Langmuir probes, bolometry
Divertor ion energy or temperature (fast thermocouple), and SOL current sensors
Upper divertor spectroscopic sightlines & IR cameras; Divertor spectroscopy (VUV, visible)
Upgraded edge and divertor bolometry
Edge profile reflectometry
Reflectometry
Real-time density measurements: Interferometry and MPTS
Facility
Lithium granule injection; improved Liters
Partial NCC
Edge gas injection and SGI with PCS feedback control
High-Z tile row on cryo-baffle and on top
Divertor gas injectors
Upward LiTER
Cryo-pumping & associated diagnostics
Improved divertor tile alignment
EHO antenna (incremental)
High-Z tile row
Plasma Control
Control of divertor coils for X- and strike-point positions
control scenarios using both strike-point and cryopump
Implement and advance snowflake divertor configuration control
Gas injection feedback control; PCS control of divertor gas injection
Radiative divertor control

References

[1] "Priorities, Gaps, and Opportunities: Towards a Long Range Strategic Plan for Magnetic Fusion Energy, FESAC Greenwald Panel Report, 2007.
[2] "Research Needs (ReNeW) for Magnetic Fusion Energy Science", June 9-13, 2009.
[3] "Report of the FESAC Subcommittee on the Priorities of the Magnetic Fusion Energy Science Program", Rosner Panel, 2013.
[4] Eich, T., *et al.,* Physical Review Letters 107 (2011) 215001.
[5] Goldston, R., Nuclear Fusion 52 (2012) 013009.
[6] Makowski, M. A., *et al.*, Physics of Plasmas 19 (2012) 056122.
[7] Maingi, R., *et al.*, Physical Review Letters 103 (2009) 075001.
[8] Canik, J. M., *et al.*, Physics of Plasmas 18 (2011) 056118.
[9] Boyle, D. P., *et al.*, Plasma Physics and Controlled Fusion 53 (2011) 105011.
[10] Maingi, R., *et al.*, Nuclear Fusion 50 (2010) 064010.
[11] Kaye, S., *et al.*, Nuclear Fusion 51 (2011) 113019.
[12] Battaglia, D., *et al.*, Submitted to Nuclear Fusion, 2013.
[13] Chang, C., *et al.*, Phys. of Plasmas 11 (2004) 2469.
[14] Zweben, S., *et al.*, Physics of Plasmas 17 (2010) 102502.
[15] Maqueda, R., *et al.*, Nuclear Fusion 50 (2010) 075002.
[16] Snyder, P. B., *et al.*, Phys. Plasmas 16 (2009) 056118.
[17] Callen, J. D., Phys. of Plasmas 12 (2005) 092512.
[18] Dickinson, D., *et al.*, Phys. Rev. Lett. 108 (2012) 135002.
[19] Callen, J. D., Canik, J. M., and Smith, S. P., Phys. Rev. Lett. 108 (2012) 245003.
[20] Diallo, A., et al., Nuclear Fusion 51 (2011) 103031.
[21] Diallo, A., *et al.*, Physics of Plasmas 20 (2013) 012505.
[22] Snyder, P. B., *et al.*, Phys. of Plasmas 9 (2002) 2037.
[23] Diallo, A., *et al.*, Submitted to Nucl. Fusion, 2013.
[24] Kaw. P. *et al.*, Submitted to Nucl. Fusion, 2013.
[25] Snyder, P., *et al.*, Nuclear Fusion 51 (2011) 103016.
[26] Snyder, P. B., *et al.*, Plasma Phys. Control. Fusion (46) A131.
[27] Sontag, A., *et al.*, Nuclear Fusion 51 (2011) 103022.
[28] Smith, D., *et al.*, Accepted to Phys. Plasma, 2013.
[29] Canik, J.M., *et al.*, Submitted to Nucl. Fusion 2013.
[30] Chen, Y. and Parker, S., J. Comput. Phys. 220 (2007) 839.
[31] Maingi, R., *et al.*, Nucl. Fusion 45 (2005) 1066.
[32] Maingi, R., *et al.,* Nuclear Fusion 51 (2011) 063036.
[33] Maingi, R., *et al.*, Nucl. Fusion 45 (2005) 264.
[34] Connor, J. W., *et al.*, Phys. of Plasmas 5 (1998) 2687.
[35] Ahn, J.-W., *et al.*, Review of Scientific Instruments 81 (2010) 023501.
[36] Evans, T., *et al.*, Phys. Rev. Lett. 92 (2004) 235001.
[37] Canik, J., *et al.*, Nuclear Fusion 50 (2010) 034012.
[38] Canik, J., *et al.*, Nuclear Fusion 52 (2012) 054004.
[39] Evans, T., *et al.*, Nuclear Fusion 48 (2008) 024002.
[40] Unterberg, E., *et al.*, J. Nucl. Mat. 390 (2009) 486.

[41] Fenstermacher, M., *et al.*, Nuclear Fusion 48 (2008) 122001.
[42] Baylor, L., *et al.*, Submitted to Nucl. Fusion 2013.
[43] Mansfield, D., *et al.*, Submitted to Nucl. Fusion 2013.
[44] Maingi, R., *et al.*, Nuclear Fusion 52 (2012) 083001.
[45] Greenfield, C., *et al.*, Phys. Rev. Lett. 86 (2001) 4544.
[46] Suttrop, W., *et al.*, Plasma Physics and Controlled Fusion 46 (2004) A151.
[47] Burrell, K. H., *et al.*, Physics of Plasmas 12 (2005) 056121.
[48] Park, J.-K., *et al.*, To be published in Nucl. Fusion 2013.
[49] Gerhardt, S., *et al.*, Nuclear Fusion 50 (2010) 064015.
[50] Takahashi, H., *et al.*, Nuclear Fusion 44 (2004) 1075.
[51] Takahashi, H., *et al.*, Phys. Rev. Lett. 100 (2008) 205001.
[52] Evans, T., *et al.*, J. Nucl. Mat. 390 (2009) 789.
[53] Maingi, R., *et al.*, Phys. Rev. Lett. 105 (2010) 135004.
[54] Maingi, R., *et al.*, J. Nucl. Mat. 390 (2009) 440.
[55] Whyte, D. *et al.*, Nucl. Fusion 50 (2010) 105005.
[56] Maingi, R., *et al.*, NSTX Report on FES Joint Research Milestone 2010 and PPPL report 4700, 2011.
[57] Gray, T., *et al.*, J. Nucl. Mater. 415 (2011) S360.
[58] Goldston, R., *et al.*, To be published in J. Nucl. Mat. 2013, 2013.
[59] Belli, E. A. and Candy, J., Plasma Physics and Controlled Fusion 54 (2012) 015015.
[60] Sugiyama, L. E. and Strauss, H. R., Physics of Plasmas 17 (2010) 062505.
[61] Green, D., *et al.*, Phys. Rev. Lett. 107 (2011) 145001.
[62] Angus, J., *et al.*, Phys. Rev. Lett. 108 (2012) 215002.
[63] Mosetto, A., *et al.*, Phys. of Plasmas 19 (2012) 112013.
[64] Baver, D., *et al.*, Computer Physics Comm. 182 (2011) 1610.
[65] Angus, J., *et al.*, Contrib. Plasma Phys. 52 (2012) 348.
[66] Ku, S., Chang, C., and Diamond, P., Nuclear Fusion 49 (2009) 115021.
[67] Myra, J. *et al.*, Phys. Plasmas 18 (2011).
[68] Kubota, S., *et al.*, Rev. Sci. Instrum. 81 (2010) 10D917.
[69] Cao, B., *et al.*, Plasma Phys. Control. Fusion 54 (2012) 112001.
[70] Jaworski, M., *et al.*, Fusion Eng. Des. 87 (2012) 1711.
[71] Soukhanovskii, V. A., *et al.*, J. Nucl. Mater. 337-339 (2005) 475.
[72] Soukhanovskii, V., *et al.*, Phys. Plasmas 16 (2009) 022501.
[73] Soukhanovskii, V., *et al.*, Nucl. Fusion 49 (2009) 095025.
[74] Loarte, A., *et al.*, Nucl. Fusion 47 (2007) S203.
[75] Stangeby, P. C., The plasma boundary of Magnetic Fusion Devices, IoP, Bristol, 2000.
[76] Goswami, R., *et al.*, Physics of Plasmas 8 (2001) 857.
[77] Rognlien, *et al.*, Contrib. Plasma Phys. 44 (2004) 188.
[78] ITER physics expert group on divertor, on divertor modelling, database, and editors, I. P. B., Nucl. Fusion 39 (1999) 2391.
[79] Ryutov, D., Phys. Plasmas 14 (2007) 64502.
[80] Kotschenreuther, M., *et al.*, Phys. Plasmas 14 (2007) 72502.
[81] Piras, F., *et al.*, Plasma Phys. Control. Fusion 51 (2009) 055009.
[82] Piras, F., *et al.*, Plasma Phys. Control. Fusion 52 (2010) 124010.
[83] Piras, F., *et al.*, Phys. Rev. Lett. 105 (2010) 155003.

[84] Soukhanovskii, V., *et al.*, Nucl. Fusion 51 (2011) 012001.
[85] Soukhanovskii, V., *et al.*, J. Nucl. Mater. 415 (2011) S365.
[86] Soukhanovskii, *et al.*, Phys. Plasmas 19 (2012) 082504.
[87] Rognlien, T. D., *et al.*, J. Nucl. Mater. 196-198 (1992) 347.
[88] Ryutov, D. and Umansky, M., Phys. Plasmas 17 (2010) 014501.
[89] Ryutov, D. D., *et al.*, Plasma Physics and Controlled Fusion 54 (2012).
[90] Valanju, P., *et al.*, Phys. Plasmas 16 (2009) 056110.
[91] Mandrekas, J. and Stacey, W.M., J., Nucl. Fusion 35 (1995) 843.
[92] Yamada, I., *et al.*, Plasma Fusion Res. 5 (2010) S2033.
[93] Matthews, G., *et al.*, J. Nucl. Mater. 241-243 (1997) 450.
[94] Soukhanovskii, V., *et al.*, Rev. Sci. Instrum. 83 (2012) 10; Scotti F. *et al.*, Rev. Sci. Instrum. 83, 10E532 (2012)
[95] Maingi, R., *et al.*, Nucl. Fusion 39 (1999) 1187.
[96] Maingi, R., *et al.*, Nuc. Fusion 44 (2004) 909.
[97] Canik, J., *et al.*, APS-DPP 2012, 2012.
[98] Reiter, D., *et al.*, Fusion Sci. Tech. 47 (2005) 172.
[99] Stangeby, P., The Plasma Boundary of Magnetic Fusion Devices, Bristol: Institute of Physics Publishing, 2000.
[100] Kugel, H., *et al.*, Journal of Nuclear Materials 390-391 (2009) 1000.
[101] Mansfield, D., *et al.*, Journal of Nuclear Materials 390-391 (2009) 764.
[102] Bell, M. G., *et al.*, Plasma Physics and Controlled Fusion 51 (2009) 124054.
[103] Boyle, D., Submitted PSI 2013.
[104] Guo, D*., et al.*, Submitted to Science, 2013.
[105] Rognlien T.D. and Rensink M.E., Fusion Eng. Design 60 (2002) 497.
[106] Rognlien T.D., Rensink M.E. and Smith G.R. 2000, User Manual for the UEDGE edge-plasma transport code, Lawrence Livermore National Lab Report UCRL-ID-137121.
[107] Rognlien T.D., *et al.*, J. Nucl. Mater. 363–365 (2007) 658.
[108] Braginskii S.I. 1965 Transport processes in a plasma Reviews of Plasma Physics vol 1 ed M.A. Leontovich (New York: Consultants Bureau) p 205.
[109] Porter G.D., *et al.*, Fusion Sci. Technol. 48 (2005) 1127.
[110] Rensink, M.E., *et al.,* J. Nucl. Mater. 290–293 (2001) 706.
[111] Smirnov R.D. *et al.*, Contrib. Plasma Phys. 50 (2010) 299.
[112] Pigarov A.Yu., et al., J. Nucl. Mater. 363–365 (2007) 643.
[113] Takenaga H., *et al.,* Nucl. Fusion 45 (2010) 1618
[114] Rognlien T.D., *et al.,* J. Nucl. Mater. 363–365 (2007) 658
[115] D. A. Russell, J. R. Myra and D. A. D'Ippolito Phys. Plasmas 16, 122304 (2009).
[116] Krasheninnikov S.I., D. A. D'Ippolito and J. R. Myra, J. Plasma Phys. 74, 679 (2008).
[117] Myra, J.R., *et al*., Phys. Plasmas 18, 012305 (2011).
[118] D'Ippolito, D.A., J.R. Myra and S. J. Zweben, Phys. Plasmas 18, 060501 (2011).
[119] Russell D.A., D.A. D'Ippolito and J.R. Myra, 54th APS/DPP Meeting, Providence, Rhode Island, October 29 - November 2, 2012, paper BP8-159.
[120] Sechrest Y., *et al*., Phys. Plasmas 18, 012502 (2011).

[121] D'Ippolito D.A., et al., Phys. Plasmas 19, 102301 (2012).
[122] Russell, D.A., *et al*., Phys. Plasmas 19, 082311 (2012).
[123] Myra, D.A., *et al*., Plasma Physics and Controlled Fusion 54, 055008 (2012).
[124] Myra J.R., *et al*., 24th IAEA Fusion Energy Conference, San Diego, USA, October 8 - 13, 2012, paper IAEA-CN-197/TH/P4-23
[125] Schneider R., *et al.,* Contrib. Plasma Phys. 46, 3 (2006).
[126] Braams B.J., Contrib. Plasma Phys. 36, 276 (1996).
[127] Hirshman S.P., *et al.*, Comput. Phys. Commun. 43 (1986) 143.
[128] Sanchez R., *et al.,* Comput. Phys. Commun. 135 (2001) 82.
[129] Gray T.K. *et al.*, J. Nucl. Mater. 415 (2011) S360; V. Soukhanovskii *et al.*, 36th EPS 2009 Proceedings, paper 2.178.
[130] Petrie T. W. *et al.*, Nucl. Fusion 37 (1997) 321, and references therein.
[131] Gray T.K., *et al.* J. Nucl. Mater. 2013 at press.
[132] Martin Y., *et al.*, J. Conf. Phys. Series 123 (2008) 012033.
[133] Bush C.E., *et al.*, Phys. Plasmas 10 (2003) 1755.
[134] Loarte A. *et al.*, Phys. Scripta T128 (2007) 222.
[135] Gan K.F. *et al.*, PPCF 2013 submitted.
[136] Ahn J.W *et al.*, J. Nucl. Mater. 2013 at press.
[137] Yan Z. *et al.*, Phys. Rev. Lett., 107 (2011) 055004.
[138] Guttenfelder W. *et al.*, Nucl. Fusion (2013) submitted.
[139] Snyder P.B., *et al.* Nucl Fusion 47 (2007) 961.
[140] Nazikian R., Private Comm, 2013.
[141] Huysmans G.T.A. *et al.*, PPCF 51 (2009) 124012.
[142] Dudson B. *et al.,* Computer Physics Communications 180 (2009), 1467.
[143] Kirk A *et al* 2009 Plasma Phys. Control. Fusion 51 065016.
[144] Koh S. *et al.*, Phys. Plasmas 19 (2012) 072505.
[145] Sauter O. *et al.*, Phys. Plasmas 6 (1999) 2834.
[146] Greenwald M. *et al.*, Nucl. Fusion 28 (1988) 2199.
[147] Conway G.D. *et al.,* Phys. Rev. Lett. 106 (2011) 065001; Schmitz L. *et al.*, Phys. Rev. Lett. 108 (2011) 155002.
[148] Osborne T.H. *et al.*, Plasma Phys. Cont. Fusion 49 (1998) 845.
[149] Zohm H. *et al.*, Plasma. Phys. Cont. Fusion 38 (1996) 845.
[150] Wilson H.R. *et al.*, Phys. Plasmas 9 (2002) 1277.
[151] Wilson H.R. *et al.*, Plasma. Phys. Cont. Fusion 48 (2006) A71.
[152] Oyama N. *et al.*, *et al.*, Plasma. Phys. Cont. Fusion 48 (2006) A171.
[153] Chang C.S. *et al.*, submitted to Nucl. Fusion 2013.
[154] Ferraro N.M. *et al.*, Phys. Plasmas 17 (2010) 102508.
[155] Kotschenreuther M. *et al.*, Comp. Phys. Comm. 88 (1995) 128.
[156] Jenko F. *et al.*, Phys. Plasmas 7 (2000) 1904.
[157] Eich T. *et al.*, Nucl. Fusion 2013 submitted.

[158] McClean A.G. *et al.*, Rev. Sci. Instrum. 83, 053706 (2012).
[159] Valanju P. *et al.*, Phys. Plasmas 16 (2009) 056110.
[160] Taylor C.N. *et al.*, Rev. Sci. Instrum. 83 (2012) 10D703

Table of Contents for Chapter 5

Chapter 5

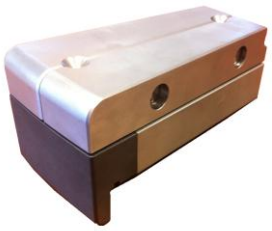

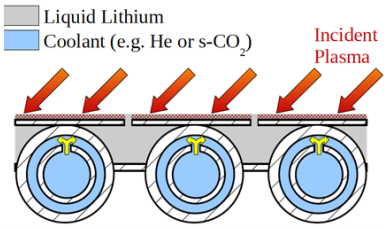

Research Goals and Plans for Materials and Plasma-Facing Components

5.1 Introduction

As described in other chapters of this 5 year plan, substantial progress has been made in producing and controlling stable high-performance ST plasmas with energy confinement at or near levels needed for a next-step facility such as a fusion nuclear science facility (FNSF) [*c.f.* Chapter 1]. A major remaining challenge for NSTX-U and other magnetic fusion devices generally is to extend high-performance plasmas for very long durations, and to integrate this high performance with plasma facing components (PFCs) that can withstand very high heat and particle fluxes while maintaining structural integrity with minimal retention of fusion fuel in a harsh nuclear environment. The present frontrunner material considered in reactor studies to have the best hope of meeting these substantial challenges consists of PFCs composed of a solid refractory metal, typically tungsten or its alloys [1]. As recent reports point out, there are significant uncertainties as to whether tungsten will, ultimately, extrapolate to an economically viable fusion reactor. Several failure modes exist that will force regular component replacement due to erosive fluxes as well as replacement in the case of significant transient events that would cause melting (e.g. disruptions or large ELMs). Given the critical nature of the PFC materials question to the fusion enterprise on a whole, it is prudent to consider, and provide clear comparisons with, alternative technologies when looking at the challenges associated with FNSF and DEMO [2].

An alternative to solid PFCs are those composed of liquid metals (LM PFCs). The most commonly considered metals for this purpose are lithium, tin and gallium. The most intriguing

potential for a LM PFC is that of self-healing which would eliminate both net erosion effects (extending component lifetimes against this damage mechanism) and the effects of transient disruptions as liquid surfaces will simply return to equilibrium positions after an event. These traits are shared by all of the liquid metals. While potential is great, however, LM PFCs raise new issues for both the science and technology associated with this innovative option.

The NSTX-U device [3] will provide unique opportunities for research on both solid and liquid PFCs. With a major radius of only 0.93m and maximum heating power of 19.2MW, NSTX-U will have one of the largest P/R ratios in the world as well as a significant P/S ratio (where P is the heating power, R is the major radius and S is the surface area of the last-closed flux surface). Table 5.1 shows a comparison of NSTX-U projected maximum parameters and those from other machines worldwide in the recent multi-machine heat-flux width database [4] as well as projections to an FNSF based on the ST-Pilot and an ST-DEMO [5] (only maximum heating power for the NSTX-U is provided at this time until more accurate assessments of radiated power fraction are available). High-power density devices present two challenges, the first obviously being reduction of exhaust power to acceptable levels. The second challenge is the ability to handle steady erosive fluxes caused by plasma-material interactions within the vessel.

Table 5.1: Multi-machine comparison of size and various power-exhaust metrics. ST-Pilot and ST-DEMO pulse lengths given in terms of discharge-seconds per year.

Machine	R_0 [m]	$P_{SOL}(P_{AUX})$ [MW]	P/R [MW/m]	P/S [MW/m^2]	τ_{pulse} [s]
NSTX*	0.86	6.8	8	0.2	1
NSTX-U*	**0.93**	**19**	**21**	**0.6**	**5**
JET†	2.95	12 (35)	4.1 (12)	0.03 (0.2)	20
DIII-D†	1.74	5 (20)	2.9 (11)	0.1 (0.4)	6
AUG†	1.65	5 (27)	3 (16)	0.1 (0.6)	10
CMOD†	0.7	3 (6)	4 (9)	0.4 (0.7)	2
MAST†	0.87	5 (7.5)	6 (9)	0.2 (0.25)	1
ITER†	6.2	100	16	0.15	400
ST-Pilot‡	**2.2**	**190**	**86**	**0.7**	6×10^6
ST-DEMO‡	**3.2**	**520**	**161**	**0.9**	∞

* J.E. Menard, *et al.*, Nucl. Fusion **52** (2012) 083015.
† Th. Eich, *et al.*, "Scaling of the tokamak near scrape-off layer H-mode power width and implications for ITER", ITPA-Div/SOL group ITR 1/1, San Diego, October, 2012.
‡ J.E. Menard, *et al.*, Nucl. Fusion **51** (2011) 103014.

These issues are being addressed in the NSTX-U program via multiple routes. In the Boundary Physics plan in Chapter 4, advanced divertor magnetic configurations (e.g. snowflake) and radiative power exhaust are being examined for heat-flux mitigation. In the Materials and PFCs Topical Science Group (M&P TSG), the concept of the continuously vapor-shielded PFC is being examined to reduce power incident on the divertor target itself. In the case of eliminating or controlling erosion and material transport, the long-range concept of liquid-metal PFCs is being pursued in NSTX-U. This work will begin the assessment of high-Z metal PFCs versus liquid lithium PFCs through a systematic conversion of the NSTX-U. This comparison will provide important data informing the use of either technology in future devices. High-Z materials, which are important to study in their own right, are also ultimately needed to provide a fusion-relevant solid substrate to support flowing liquid metals.

Current plans are to begin operations with carbon PFCs in NSTX-U and gradually transition to high-Z PFCs with increasing emphasis on the liquid-metal PFC option (see research timelines at end of this chapter). This transition presents unique research opportunities for both solid- and liquid-PFC research. Over the next 5-years the M&P TSG will undertake three thrusts: (1) Understand lithium surface-science for long-pulse PFCs, (2) Unravel the physics of tokamak-induced material migration and evolution and (3) Establish the science of continuously vapor-shielded plasma-facing components.

Significant progress in liquid-metal technology is required before a flowing-liquid metal module can be implemented in NSTX-U. Ongoing work in understanding the science of liquid metal surfaces and in developing these PFCs will be described. In the incremental budget scenario, such a fully-flowing liquid metal module might be installed in the NSTX-U by the end of the 5-year period. Further, in the incremental budget scenario, a substantial fraction of the first-wall (in low heat-flux regions) will be coated with high-Z materials to accelerate assessments of the ability to integrate high-performance ST plasmas with a high-Z first-wall. Significant progress can still be made in understanding the physics associated with such PFCs even in the baseline budget plan.

Three research thrusts for the NSTX-U Materials and Plasma-Facing Components group are proposed for this 5 year plan with the following thrust titles: Understand Lithium Surface Science for Long-Pulse PMI and PFCs, Unravel the Physics of Tokamak-Induced Material Migration and Evolution, and Establish the Science of Continuous Vapor Shielding The motivation and research strategy for each thrust are provided in Section 5.2 of this document. The solid and liquid plasma-facing component research and development required to implement the staged NSTX-U upgrade is provided in Section 5.3. Finally, supporting theory and modeling tools are described in Section 5.4.

5.2 Research Plans

5.2.1 Thrust MP-1: Understand lithium surface-science for long-pulse PFCs

Lithium research to date on the NSTX has focused on the usage of this material as a wall-condioning tool. This work has demonstrated increases in discharge performance and is also key contributions toward understanding how the wall-conditioning is affecting the PFCs. However, there remain key questions, particularly in the area of what role impurities in the lithium (e.g. boron, oxygen and carbon) affect the coating performance, and how this performance will change when lithium is applied to a high-Z substrate. The purpose of this thrust is to improve the understanding of this wall conditioning method and what other variables may be impacting performance through a combination of tokamak experimental studies and surface-science laboratory studies. These considerations motivate the following research thrust:

> **Thrust MP-1:** *Experiments will be conducted to improve understanding of the role of more complete coverage of the PFCs by evaporated lithium using upward-facing evaporators and/or diffusive evaporation as well as the impact of boronization. A boronization campaign in year one will be followed by a controlled Li introduction. The Materials Analysis Particle Probe (MAPP) will be utilized to identify in-situ between-shot chemical states and compositions of the coatings. The total deposited lithium as supplied in 2008 will be applied on both upper and lower divertors. The changes in plasma performance will be compared to the 2008 database. In the second year, a boronization campaign will be eliminated and an identical introduction of lithium as in the previous year will be applied to bare graphite surfaces. These studies will provide a comparison between C+B substrate vs. a C substrate alone in terms of plasma performance. The MAPP diagnostic will be utilized during this year also, and will enable comparisons to surface-science laboratory results including Li-coatings on high-Z metal substrates such as TZM. The uptake of hydrogenic species and the impact of varying levels of impurities (e.g. C, O) on that uptake will be examined in the Li-metal system, and in years 3-5 the surface interactions of Li on high-Z tiles in at least one NSTX-U divertor region will be studied.*

This section will describe recent developments in the surface characteristics of lithium coatings as well as recent analysis of the effect of lithium wall conditioning on global energy confinement in NSTX. The question of surface purity is highlighted, however, in additional results examining the Liquid Lithium Divertor experiments which did not demonstrate large changes in global energy confinement. The section ends with a description of the detailed research plans expected

to be undertaken in the baseline funding scenario as well as the results expected by the end of the 5-year plan.

The efficacy of lithium PFCs in improving plasma performance was demonstrated on TFTR, CDX-U, T-11M, and other devices prior to lithium evaporation on carbon PFCs in NSTX [12]. On NSTX, there was a concern that the intercalation of the lithium into the carbon would affect its effectiveness as a PFC coating [13]. Instead, NSTX plasmas with lithium-coated PFCs showed higher energy confinement, ELM suppression, and other examples of plasma improvement over discharges with carbon PFCs alone [14]. The research strategy employed here is to understand the changes in surface composition and chemistry at the microscopic scale and link that to overall machine performance. In addition to on-site and collaborator surface-science laboratories, the Material-Analysis and Particle Probe (MAPP) is also a key tool for linking the in-vessel conditions with those that can be studied in a controlled laboratory setting. This diagnostic essentially allows us to identify what changes are occurring when lithium "conditions" the surface of the PFCs and how the plasma interactions change this surface.

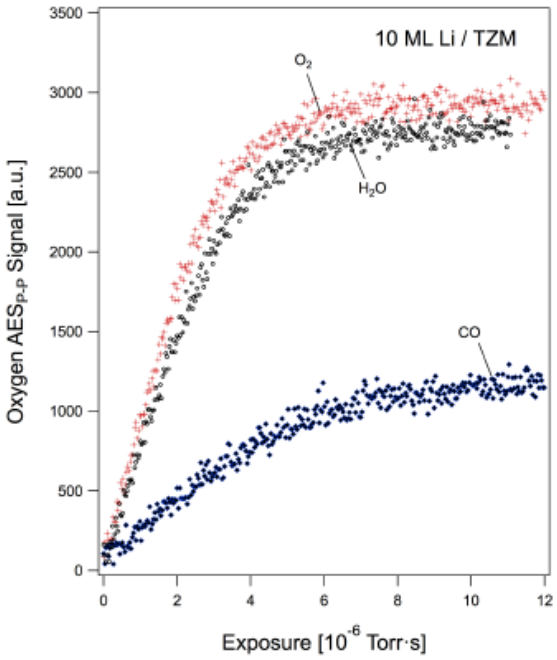

Figure 5.1: Auger electron signal shows that Li film oxidizes in 100s at 1x10^{-7} Torr of water vapor. If Li film is not replenished between shots in NSTX, the plasma will see a mixed material, not a pure Li coating[6].

To take advantage of the benefits of lithium or other liquid metals plasma facing components (PFCs) and provide a design basis for next-step PFCs, it is important to develop a database of measurements on the behavior of lithium / liquid metal surfaces in response to the conditions found at the PFCs within the tokamak. Many of the key processes are amenable to investigation in laboratory experiments where the full range of modern surface analysis equipment may be brought to bear on investigating the atomic-scale details of the chemical composition of solid and liquid liquid metal surfaces and their interactions with plasma constituents and residual gases in well characterized conditions. The results will advance the scientific understanding of plasma-lithium surface interactions, aid the development of liquid metal plasma facing components with superior performance for long-pulse discharges, and provide the pathway to advanced PFCs for FNSF.

Two new laboratories for materials characterization and surface chemistry experiments have been established at PPPL (see also chapter 10, section 10.5.2.9). These contain four distinct surface analysis instruments that interrogate and image surfaces in multiple and complementary ways with ions, electrons and x-rays in controlled UHV conditions. One instrument has applied Auger electron spectroscopy to demonstrate that lithium surfaces react on short time-scales with residual gases such as water and oxygen (Fig. 5.1, [6]). At a partial pressure of water similar that in NSTX, a monolayer of oxide forms on a lithium surface in a time shorter than the inter-discharge time of 600s, thus the NSTX plasma interacts with lithium oxide and not metallic lithium. This work also showed how the surface composition in future flowing Li-PFC systems will depend on residual vacuum pressure and Li flow rate.

Joining surface-science tools and modeling with plasma-facing components has already yielded unexpected findings and increased the understanding of lithium wall conditioning in NSTX. Detailed surface analysis of PFC samples removed from NSTX after run periods indicated that lithium did indeed alter the morphology of the carbon surfaces, but in a way that improved its ability to retain deuterium [15]. Quantum-classical molecular dynamic (QCMD) simulations showed how the interaction of the lithium with the carbon created brought oxygen to the surface, and made it a key factor in binding deuterium [16]. These computational studies were guided, in part, by previous analysis of PFC samples, it is, however, advantageous to study these surface in vacuo to avoid any possibility of contamination by atmospheric gases.

The MAPP [17] is a novel surface analysis capability that will contribute to the study of in-situ NSTX PFC materials. MAPP has the ability to expose samples to NSTX plasmas, and withdraw them immediately after a discharge for in-vacuo surface analysis in an attached chamber with multiple diagnostics. This in-vacuo analysis capability is important as lithium surfaces are highly reactive to air. The MAPP system is able to apply thermal desorption spectroscopy (TDS), x-ray photoelectron spectroscopy (XPS) and low-energy ion scattering spectroscopy (LEISS) to samples immediately following exposure to tokamak discharges. The system is described in more detail in Chapter 10 (Section 10.6.4.1) and Chapter 11 (Section 11.2.17).

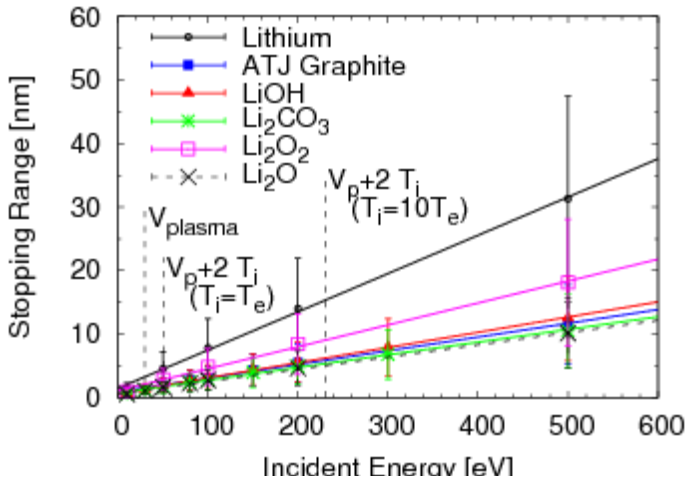

Figure 5.2: Stopping ranges of deuterium ions in pure lithium or a mixed-material surface as a function of incident energy [8].

Surface science studies in the laboratory have already indicated that lithium surfaces react on short time-scales with residual gases such as water and oxygen. Referring again to Figure 5.1, measurements were made of oxygen uptake using Auger-Electron Spectroscopy [6]. A typical inter-discharge base pressure inside the NSTX vacuum vessel is about 10^{-7} Torr. At partial pressures similar to this of oxygen or water, a monolayer of oxide would be expected to form on the lithium surface in about 100-200s. This time is already comparable to the inter-discharge time of 600s. The existence of the mixed-material surface leads to obvious questions in relating results in NSTX with previously published studies in linear machines, such as PISCES-B, where removal of contaminants was performed before studies of deuterium uptake [7]. Given the short time-scales involved, this provides a clear example of how MAPP will provide a link between in-vessel conditions with those reproduced in the laboratory setting. With a combination of XPS, DTS and LEISS, MAPP will be able to characterize the surface of the PFC before and after discharges. These characterizations will provide key metrics that will enable other surface-science laboratories to mimic the in-vessel conditions.

Plasma interactions with contaminated and uncontaminated surfaces are expected to be sensitive to the first 10 nanometers of material. Simple TRIM estimates of implantation depth are shown in Fig. 5.2. This small amount of lithium available for interaction must be considered with observations that the improvement in confinement during lithium deposition experiments improves with increasing deposition quantities. Figure 5.3 shows the deposited lithium in the NSTX vessel during a dedicated experiment in the 2008 run campaign; no lithium was injected before this experiment in 2008. The approximate surface area for deposition is $2m^2$ on the lower divertor floor.

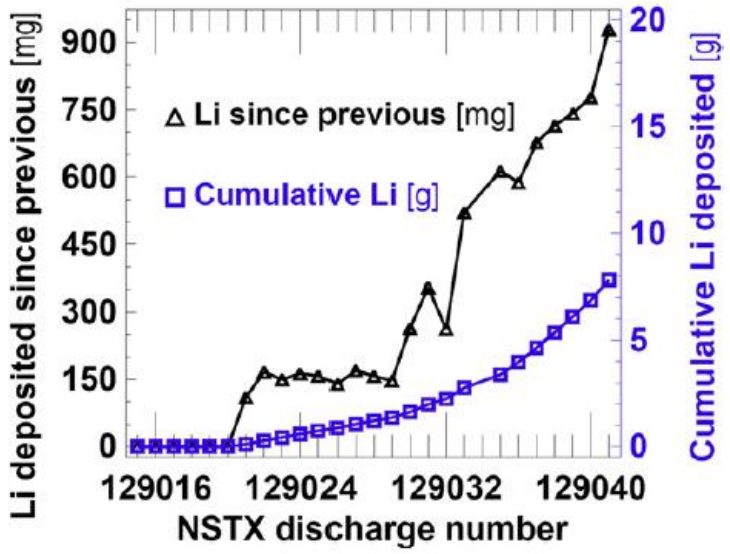

Figure 5.3: Lithium deposition during the systematic introduction of lithium during the FY 2008 run campaign[9].

With this areal coverage, every milligram of deposited lithium results translates to about 1nm of depth on the lower PFCs. That is, the initial deposition of a little more than 100 mg should provide a nominal 100nm of lithium on average in the lower divertor – well in excess of the implantation depth. Despite these estimates, it was found that the discharge performance continuously improves with increasing quantities of lithium. Figure 5.4 shows the evolution of plasma performance as a function of the pre-discharge lithium deposition quantity.

It can be seen that during this scan, panel 4(d) shows a nearly continuous improvement in the confinement factor from an H97-L factor of ~1.6 as much as 3 with increasing amounts of lithium.

The role of gettered oxygen from residual gases vs oxygen migrating to the surface from the graphite substrate remain open questions, as does the role of plasma-induced redistribution of lithium during operations. This highlights the importance of a multi-pronged approach to understanding the lithium surface-science and it's relation to global tokamak discharge performance.

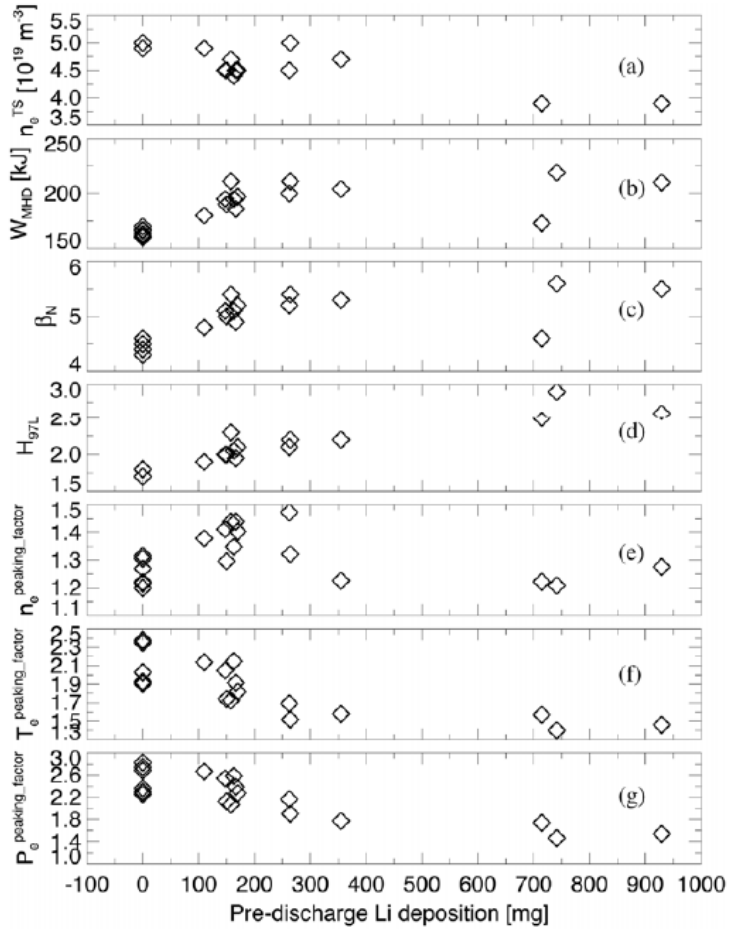

Figure 5.4: Evolution of plasma parameters and profile peaking during the systematic scan shown in Fig. 5.2.1.3. Panel (d) shows the H-factor for confinement relative to the ITER97-L scaling at the time of the peak stored energy. All discharges were operated with 4MW injected NBI except for the final three with the highest Li evaporation which had P_{NBI}=2, 3, 3 MW respectively [9].

The results shown in ref. [8] can be contrasted with those obtained with the liquid lithium divertor (LLD) experiments of FY2010 (see [18] for a description of NSTX operations with the LLD). In this run campaign, no boronization was performed, but operations began after an initial deposition of 15g of lithium onto the lower divertor of NSTX. Discharges on the LLD showed remarkable similarity throughout the run-year, despite the increasing accumulation of in-vessel lithium. Experiments in FY 2010 did not, however, include a dedicated scan of lithium deposition rate (analogous to pre-discharge lithium in fig. 5.3) and this motivates additional studies during this 5-year plan period. An investigation of the relative emission of impurities from the divertor region is shown in Figure 5.5. In this figure the top three panels show the relative emission as a function of strike-point radius during experiments diverted in the vicinity of the LLD. The transition between the graphite tiles and LLD occurs at 0.65m (graphite is inside of

0.65m radius). The emission from the divertor is measured with wide-area divertor filter-scopes for each of the lines listed. Ion saturation current is measured with Langmuir probes, and only those probes calculated to be in the near-SOL of the outer-divertor is reported ($1.00<\Psi_N<1.005$). One can account for variances in exhaust power by normalizing the emission signals with P_{LCFS}, shown in the bottom panel. This quantity is calculated as follows:

$$P_{LCFS} = P_{\Omega} + P_{NBI} - \frac{\mathrm{d}W}{\mathrm{d}t} \quad (1)$$

where P_{Ω} is the ohmic heating power, P_{NBI} is the input neutral beam power and W is the stored energy of the discharge. For comparison, a mean heat flux calculated with Langmuir probes, q_{LP},

$$q_{LP} = \gamma \Gamma^{+}_{SAT} T_e \quad (2)$$

can be calculated using:

where γ is the sheath heat transmission coefficient (here assumed to be 7.5), J_{SAT} is the saturation current density and T_e is the derived electron temperature from the probe I-V characteristic. One can see that the heat flux derived with the Langmuir probes is roughly proportional to the power entering the SOL. A further point indicated by the same proportionality with saturation current is that the electron temperature derived by the Langmuir probes using the classical interpretation[11] is nearly constant over this range of input powers also indicating that only subtle changes are occurring in the vicinity of the strike-point. One can see in the third panel that the relative emission is unaltered by the strike-point location suggesting that the substrate material (i.e. graphite or LLD) makes no difference in the relative

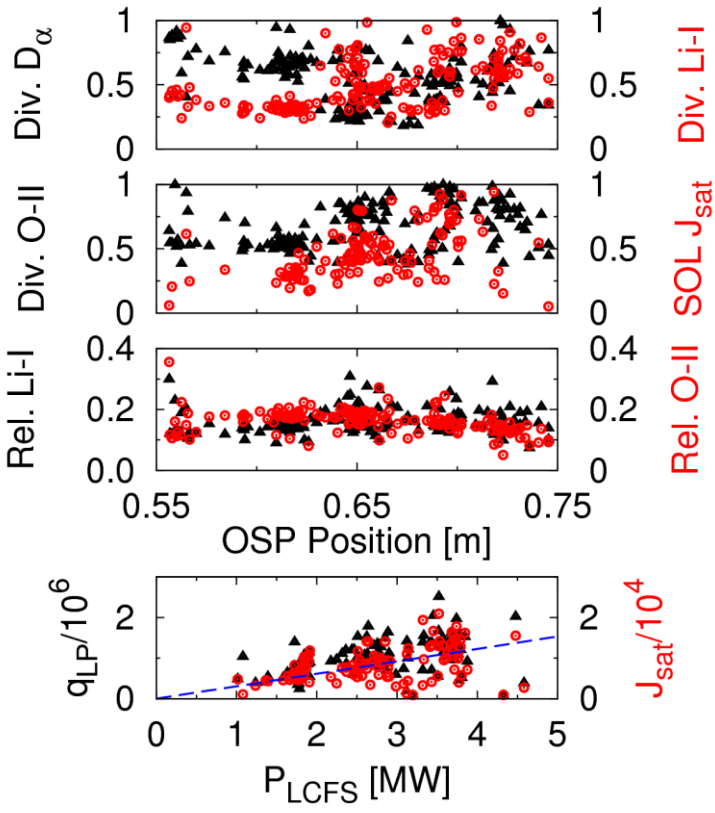

Figure 5.5: Relative emission of hydrogen (D-alpha) and impurities (Li and O) from the divertor of NSTX during LLD experiments. The LLD inboard edge is located at 0.65m. Incident particle flux is proportaionl to exhaust power (bottom panel) and can be used to normalize the emission data. Strong variation between graphite (ROSP<0.65m) and the LLD is not observed [10].

quantity of lithium or oxygen emitting in the divertor of NSTX during these experiments. This is consistent with the shallow-interaction depths expected from TRIM modeling and the rapid oxidation of lithium with the typical NSTX base pressure and leak rate.

Further evidence for the shallow interaction ranges determining the plasma performance is obtained from examining the overall discharge performance for the plasmas operated in FY2010. This is shown in Fig. 5.6 that collects data from the LLD experiments conducted throughout the entire run-year. As can be seen, a total of about 900g of lithium was deposited onto the PFCs in the machine, yet discharges from the beginning of the year showed similar performance as those at the end of the year with H97L~2 throughout[10]. As mentioned above, no dedicated experiment varying deposition *rate* was performed in FY2010 but is motivated by the contrasting performance noted above.

These two apparently contrasting data sets from FY2008 and FY2010 point to not only the need to explore the role of deposition rate, but also the underlying chemical state (i.e. any role of boronization) in determining the impact of lithium wall conditioning on overall plasma performance. Improved divertor diagnostics, such as more extensive Langmuir probe coverage, the MAPP system and improved coverage of the in-vessel PFCs by spectroscopic instruments will provide the base set of measurements to complement standard core diagnostics such as MPTS as well as magnetics. A key operational tool to aid in these experiments will be a new, upward-facing evaporator system, to be deployed in the first two years of

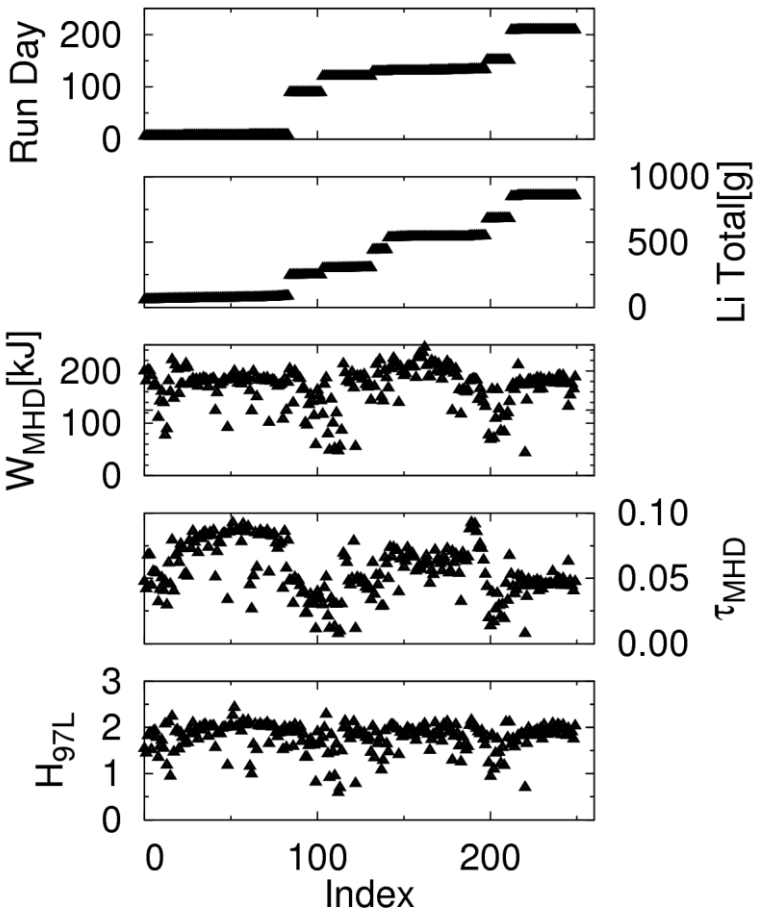

Figure 5.6: Selected entries from the LLD experimental database. Data indicates that normalized confinement was largely independent of the total quantity of lithium deposited in the machine[10] (though no systematic study of deposition rate was conducted). Dishcarges in this data set had input powers that varied from 2-4MW NBI, though yielded similar H-factors.

NSTX-U operations. As will be shown in section 5.2.2, significant fluxes of neutral hydrogen are expected on first-wall elements whereas LITER and LLD experiments focused on application of lithium to the lower divertor. Experiments in diffusive evaporation as well as with upward-facing evaporation system will enable studies on the effect of increasing the areal coverage by lithium. This is important to keep in mind when comparing boronization with lithiumization due to the fact that NSTX is traditionally boronized using a diffuse glow discharge that would cover nearly 100% of the PFCs whereas evaporated lithium with the existing LITER set is focused on the lower divertor alone.

The achievement of particle control with the use of lithium coatings has long been a goal for the NSTX program. The most recent data indicate that the surfaces are complex and evolving throughout the run campaign. While exploration of very low recycling ($R<0.5$) conditions remains a goal, it may not be possible to perform these experiments without more aggressive control of the lithium surfaces in the machine (existing analysis indicates PFC recycling has been reduced to about 0.9 in the NSTX, see chapter 4). This can be achieved with a fully flowing system and/or better vacuum conditions in addition to more complete removal of carbon contaminants. Therefore, in the first few years of NSTX-U operation, the transition toward including these elements will be studied as NSTX-U progresses to a state where another experimental campaign addressing the low-recycling state can be attempted.

5.2.1.1 Research Plans by Year for Thrust MP-1

Year 1 (2014) of the 5-year plan is ongoing before any NSTX-U tokamak experiments can be conducted. During this time, diagnostic check-outs will be conducted to ensure that key systems are ready at the start of discharges in year 2. Exposures of high-Z substrates on the LTX will be conducted with subsequent analysis. This will provide information to dedicated laboratory experiments both at PPPL and offsite on the interactions of lithium coatings on high-Z substrates in the presence of tokamak-relevant vacuum conditions.

- Additional analysis of NSTX discharges with the aid of interpretative and fluid models (e.g. similar to results shown in figure 5.9) will be conducted to identify key locations for QCMs, witness plates and marker tiles for use in NSTX-U. In the context of thrust 1, expected particle fluxes onto the MAPP diagnostic will be modeled for comparisons of experiments conducted in the following years.

- In the on-site surface science laboratories, the oxidation of thin Li films on single crystal Mo substrates, and compare to our previous measurements on TZM surfaces to elucidate the effects of grain boundaries and other non-uniformities in the oxidation of tokamak relevant

materials. We will expose Li-coated Mo with deuterium atoms and ions from a new ECR plasma ion/atom/hybrid source and measure D_2, D^0, D^+ uptake using temperature programmed desorption (TPD). Measurements before and after surface contamination with residual gases will illuminate the role of O in D uptake on solid and liquid lithium-coated substrates. We will study surface conditioning before initial loading with liquid metal to simulate recovery from surface oxidation, resolidification and maintenance vents.

- NSTX-U researchers will investigate surface wetting of Li films on Mo, TZM, stainless steel, and carbon films vs. temperature and oxide contamination using scanning Auger microscopy. Materials characterizations and UHV experiments will be performed to support the interpretation of results from MAPP and Magnum-PSI.

Year 2 - NSTX-U operation is expected to begin with all graphite PFCs with lithium evaporation and boronization. A boronization campaign will provide a baseline operating scenario from which to compare additional PFC and conditioning techniques. The MAPP diagnostic is expected to be available as well as QCMs, witness plates, target Langmuir probes, and standard spectroscopic diagnostics of the divertor plasmas.

- MAPP will be used to identify the basic state of the PFCs before the addition of lithium. For instance, MAPP can be used to measure the uptake of hydrogen due to both deuterium ions and neutrals derived from interpretative modeling creating an important validation for modeling efforts.
- Diffusive evaporation will be used to increase the areal coverage of the NSTX PFCs (in the event of incremental funding and subject to availability, an upward evaporation system will be used as well). With this capability, an injection amount identical to that used in the 2008 lithium introduction can be performed, except utilizing upper and lower coatings. This will identify the effect of increased lithium coverage on discharge performance as measured by thermal energy confinement time, impurity production and accumulation (via Z_{eff} of the plasma) and control of edge pressures.
- An important data set will be obtained by creating medium-to-low triangularity discharges that place the outboard divertor on the future location of the high-Z PFCs.

Year 3 - The introduction of high-Z PFCs will provide the opportunity to examine how this modest addition affects overall discharge performance.

- Comparisons of discharge performance with standard high-triangularity discharges vs. those diverting directly onto the PFCs will be made.
- Variances in deuterium uptake of lithium coatings on graphite vs. high-Z substrates identified in LTX exposures and offline experiments will be examined in the tokamak context. This will establish whether significant departures in lithium coating behavior are to be expected as an increasing amount of the NSTX-U PFCs are converted to high-Z. We expect to begin operations with no boronization and transition directly to lithium evaporations to perform the

specific experiment looking for any synergistic effect that may exist between boron and lithium.

Years 4 and 5 - NSTX-U will provide a comparison of particle control via lithium coatings vs. control with boronized walls and a cryo-pump. We expect to have at least an empirical understanding of deuterium uptake by lithium coatings and the associated changes in neutrals throughout the machine.

- Models of the surface uptake of hydrogenic species will be compared with hydrogenic control with the cryo-pump.
- In addition, examination of lithium coating performance at elevated temperatures will be examined with the heated cryo-plenum. This will inform on the impact of high-temperature lithium PFCs not directly under the divertor, but producing a flux impinging the SOL itself.

Throughout the 5-year plan, while MAPP provides in-situ measurements, simultaneous work in surface-science laboratories will make detailed measurements for comparison. These are also expected to focus on lithium-coatings on high-Z, metal substrates such as TZM-type molybdenum. The uptake of hydrogenic species and the impact of varying levels of impurities (e.g. C, O) on that uptake will be examined in the Li-metal system. This will provide information on whether such coatings can be expected to provide an absorbing surface once NSTX-U PFCs are upgraded to high-Z.

Years 3-5 will continue these initial studies of uptake and the impact on plasma performance an increasing amount of the NSTX-U PFCs are converted to high-Z. As the PMI processes create a mixed material on the PFC surface, this will likely impact the uptake of hydrogen and possibly impact machine performance. A combination of in-situ (i.e. MAPP) and ex-situ surface-science tools will be brought to bear to understand the basic physical processes occurring as the PFC surface is bombarded with plasma. A useful experiment will be to repeat the introduction of lithium performed in year 2 (i.e. begin operation without any low-Z coating). This would provide a measure of high-Z influx into the core plasma as a result of the staged implementation. In addition to studies of deuterium uptake, wetting studies on molybdenum and tungsten substrates of lithium, tin and gallium will be conducted in controlled laboratory settings to inform on the choice of liquid metal PFC for NSTX-U and conceptual design activities for the FNSF.

5.2.1.2 Baseline Deliverables for Thrust MP-1

1. Experimental determination of the role of areal coverage and boron+lithium chemistry on global discharge performance (e.g. energy confinement time)
2. Experimental comparison of lithium wall-pumped discharges vs. cryo-pumped discharges to examine the role large-area changes in PFC chemistry vs. localed pumping in the NSTX-U divertor. This includes the examination of deuterium uptake on clean and oxidized lithium-coated high-Z substrates over a range of temperatures.
3. Detailed characterization of PFC evolution during tokamak operations using the MAPP diagnostic system and coordinated laboratory studies.
4. Wetting studies of candidate liquid metal (lithium, tin and gallium) to examine the role of substrate and liquid impurities on wetting and film-rupture (i.e. exposure of the substrate).

5.2.1.3 Incremental Funding Research Plans and Deliverables

Increased resources will permit a more aggressive upgrade of the NSTX-U PFCs to a high-Z surface to eliminate the effects of lithium intercalation into the substrate material (see section 5.2.2.1 for more on lithium conditioning lifetimes and the impact of intercalation). This will also permit study of lithium coatings on a more reactor-relevant, metallic substrate. A closer integration of surface-science laboratories and tokamak sample exposures would be accomplished (e.g. improved surface preparation techniques to mimic in-vessel components and/or improved sample transfer capabilities).

5.2.2 Thrust MP-2: Unravel the physics of tokamak-induced material migration and evolution

Erosive fluxes are expected on first-wall components, thus limiting their lifetime, and the high power densities achievable on NSTX-U make it particularly well suited to examining issues of wall erosion. The edge plasma of fusion devices continuously interacts with a neutral population at the edge [5]. This creates a charge-exchange flux of high-energy neutrals that will impinge and sputter the first-wall. Recent papers have pointed out that wall erosion could result in thousands of kilograms per year of circulating material in a power reactor [19]. The eventual fate of the eroded wall material is unknown at this point and requires further study. This material has been conjectured to redeposit in the divertor region, where decades of effort have focused on creating a cool, non-eroding plasma [19]. NSTX-U research to be carried out to better understand material erosion is summarized in the following thrust:

Thrust MP-2: *A combination of quartz-crystal microbalances (QCMs), witness samples and marker-tiles will be utilized to provide measurements of shot-to-shot erosion and redeposition in NSTX-U. An upgraded MAPP system with QCM will enable shot-to-shot analysis of not just the quantity of deposited material, but also the composition of that material. The scaling of wall-erosion for typical NSTX-U divertor conditions over a range of P/S values will be used to construct a data-base to estimate/project total wall erosion expected for an FNSF or DEMO. The material transport variations as a function of divertor configuration (e.g. snowflake, detached, vapor-shielded) will also be measured and compared to simulation.*

In this section the erosive flux is estimated for an FNSF scenario based on the ST-pilot plant [5] to illustrate the magnitude of the material migration problem that must be solved. The proposed tools for measuring these processes are quartz-microbalances (QMBs), marker tiles and witness plate systems. An NSTX discharge is analyzed using the OEDGE/DIVIMP code suite to demonstrate the type of modeling that can be validated with improved diagnostic coverage in the upgrade. Erosion in the divertor region region, however, remains important for NSTX-U and for any future liquid metal PFCs. Collaboration with the Dutch Institute for Fundamental Energy Research (DIFFER) on the Magnum-PSI experimental device will provide an early opportunity to examine low-Z coating erosion from carbon and high-Z substrates ahead of operations in NSTX-U. This work helps inform on the lifetime of a given wall-conditioning technique (related to thrust 1) as well as the ability of NSTX-U to examine high-erosion divertor configurations as will be described in thrust 3. Finally, the baseline research plan will be presented alongside the deliverables expected at the end of the 5-year plan.

The ST-pilot plant is a 2.2m major radius machine with an aspect ratio of 1.7. The machine is designed for engineering Q ~ 1. The total fusion alpha heating and auxiliary heating power is about 250MW, and the duty-factor of the machine is assumed to be 0.3 (i.e. ~10^7 s/yr). Using the same assumptions of charge-exchange power as Stangeby,[19] the total erosion of the first-wall components would result in 1800 kg/yr (cf. Stangeby's reactor scenario calculates 8000 kg/yr). While this results in ~0.4 mm/yr of erosion from all the walls (assuming it is uniformly distributed), the consequence of redeposition in the divertor area is severe. Using flux-expansion numbers from Ref. [19], the area ratio of the first wall to the divertor is ~ 50. This results in a growth rate of ~17 mm/yr (assuming uniform redeposition in the divertor). It is difficult to predict how such thick layers will alter the PMI in the divertor. Given that this effect is configuration independent, it is clear that serious challenges face the extrapolation of any solid-material PFCs to a reactor scenario.

In principle, a plasma-facing liquid surface returns to its equilibrium position after being disturbed by transient events, i.e. it is a self-healing material surface. Similarly, for surfaces undergoing net erosion or deposition, a ready solution is available by the supply or removal of additional liquid from the PFC surfaces[20].

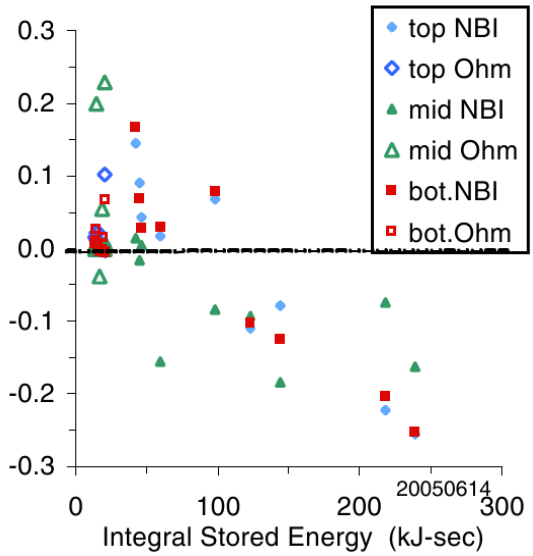

Figure 5.7: Change in mass (μg/cm^2) from 1 min. before a discharge to 1 min. before the next discharge plotted vs. the integral of stored energy and time. The legend denotes the location of the QMB (top, middle or bottom of the machine) and whether NBI or solely ohmic heating was used[21].

At full power, NSTX-U should provide about 15MW heating power to interact with approximately 30m^2, yielding a P/S ratio (in MW/m^2) ~ 0.5, whereas an FNSF pilot plant based on either an advanced tokamak or spherical torus would have a P/S ~ 1 [19]. Using estimates derived from [19], one could expect approximately 2.5nm of carbon to be eroded from first-wall components per NSTX-U discharge, i.e. within the measurement capabilities of QMB diagnostics with a sensitivity down to 0.7nm[21]. Erosion measurements have already been made in NSTX and are shown in Fig. 5.7 [21]. These indicate that the walls are already in a state of net erosion for NBI heated discharges (~5MW) that are sustained for about 1s (average stored energy is about 200kJ for these discharges). By providing multiple measurement locations with QMBs and other surface material diagnostics such as the MAPP system [22], we therefore expect NSTX-U to provide a suitable experimental platform for the study of wall erosion and the resultant deposited material. While carbon is expected to have limited utility as a reactor-relevant material, identifying material migration processes active in the tokamak edge will provide baseline information on the material transport processes assumed in [19], and how these estimates will impact a solid-wall option for FNSF. QMBs are not appropriate for use in high-heat flux regions of the machine, such as in the divertor. In these areas, marker tiles will be utilized to provide campaign-integrated measurements of the net erosion. Additional campaign-integrated measurements in the first-wall region will be made with witness-plate samples.

The equations used to generate estimates of first-wall erosion only provide order-of-magnitude estimates for an entire fusion device. If, however, erosion exhibits poloidal variation, then PFCs throughout the machine could be optimized to account for this and arrive at uniform component lifetimes. The type of analysis that can be carried out, and will be validated in the upgrade will now be demonstrated to provide an examination of just this type of poloidal non-uniformity.

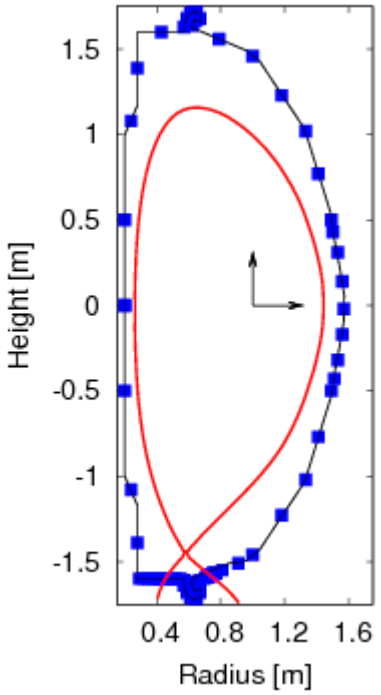

Figure 5.8: OEDGE model geometry for determining mean wall fluxes. Red outline shows separatrix location. Black lines indicate wall geometry. Blue points indicate sampling locations for obtaining an average wall flux measurement. Arrows indicate point of origin from which the poloidal angle (see fig. 5.9) is defined.

OEDGE/DIVIMP analysis is now possible in NSTX with the use of Langmuir probe measurements to reconstruct background plasma profiles[24] from which it is possible to model erosion of the plasma-facing components due to the combined effects of ionic and neutral bombardment. These models are constrained by measurements at the target plates and self-consistently solve the plasma-fluid equations including the hydrogenic neutral transport (see section VI: Theory and Modeling). The discharge modeled was conducted during the LLD campaign and had an 800kA discharge current with 4MW neutral beam heating. Two point modeling indicated a separatrix temperature of about 60eV. Divertor target density was found to be 3-5x$10^{20}$$m^{-3}$ with a strike-point temperature of 3-5eV. Using OEDGE/DIVIMP, it is possible to extract the neutral particle fluxes throughout the machine as a function of location. Figure 5.8 shows the machine layout and Fig. 5.9 shows the corresponding neutral hydrogen flux and average energy at each location. The impinging neutrals originate from target recycling and charge-exchange processes at the plasma edge.

The mean energy on the outer wall elements ranges from 40-90eV which is already in the range where iron sputtering is expected (threshold energy of 44eV [27]) and at the threshold for molybdenum sputtering (threshold energy of 90eV [27]). As these are average incident energies there will be particles exceeding these mean values indicating that even in NSTX discharges, one could have expected molybdenum elements on the wall to be subjected to non-zero sputter yields. If one considers physical sputtering by the incident particles only (neglect chemical erosion), erosive yields of the outer first-wall elements are in the 1-5x10^{18} #/m^2/s range. This would result in mass loss of 0.002-0.01 ug/cm^2/s from ATJ graphite surfaces, equivalently 1.2-5.9 nm/s erosion rates. With a 5s discharge one would measure 6-30nm erosion – well above the detection limit of 0.7nm. This type of modeling and analysis can be validated in NSTX-U with the use of the expanded plasma and erosion diagnostic coverage.

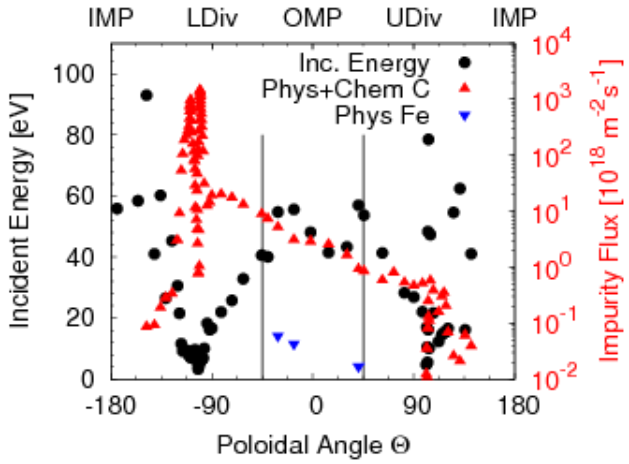

Figure 5.9: Neutral hydrogenic flux to wall elements derived by OEDGE interpretative modeling. Poloidal angle is defined from the plasma center indicated in figure 5.8. High flux at about -135 to -90 degrees is the lower inner and outer divertors. The out-board wall elements are found between 270 and 90 degrees and have incident energies of 40-90eV. Neutral flux to wall elements is the result of recycling and charge-exchange processes. Discharge simulated is 800kA, 4MW NBI heated discharge with a separatrix temperature of 60eV. Peak divertor density is 3-5x10^{20}m^{-3} with a temperature of about 5eV at the strike point (see ref. [24] for discharge parameters).

In the case of liquid metal walls, such transport processes will also occur. The key difference with liquids is the ability to replace lost material and remove excess quantities. The transport of material remains a critical issue for liquids, however, as any liquid metal PFC concept must demonstrate control of the liquid metal inventory to avoid in-vessel buildups. This transport of the liquid metal is particularly critical for the viability of lithium to any future device utilizing tritium. Due to the affinity of lithium to retain hydrogenic species, lithium that transports to remote locations in the machine will become a potential location for tritium retention inside the vacuum vessels.

Before examining whole-machine transport, it is important to assess absolute and net yields from the PFCs. This is typically done in ion-beam facilities [25] and linear plasma devices [26]. While plasma-devices are more relevant simulators than ion-beam facilities, the densities where these tests occur are often much lower than expected in a divertor (10^{18}-10^{19} vs. 10^{20}-10^{21} m^{-3}). In high-density divertor plasmas, ionization mean-free paths are expected to become comparable to the magnetic pre-sheath scale length and strong, local redeposition is expected. Simulations from Brooks, et al., indicated that redeposition fractions very close to 1.0 for tin or lithium can be expected in conventional divertor plasmas (30eV, 3x10^{20} m^{-3}) [29].

Newly-commissioned plasma devices are available to study this local material transport. The Magnum-PSI device is capable of producing high density, low temperature plasmas, similar to those expected in future power divertors [30]. Figure 5.10 shows a fast-camera image taken on the Magnum-PSI experimental device during experiments with lithium coatings. Figure 5.11 below is a quasi-2D simulation of lithium emission calculated using ADAS emission coefficients and experimental plasma profiles obtained on Magnum-PSI. Synthetic diagnostics based on these simulations show qualitative agreement in emission profiles and should be useful for validating local transport models for lithium, hydrogen and other impurities. Quantitative comparison indicates, however, that transport models based on ionization alone are not sufficient to reproduce the observed emission profiles. This makes Magnum-PSI experiments a unique testbed for examining recombination and charge-exchange effects in the expected low-temperature, high-density plasmas of future tokamak reactors.

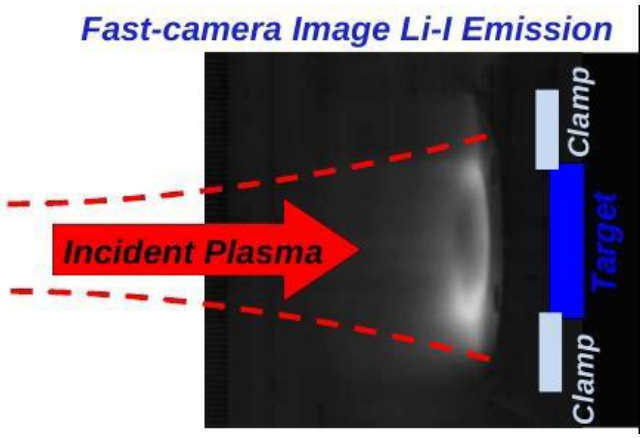

Figure 5.10: Fast camera image of Li-I (671nm) during experiments in the Magnum-PSI experimental device. Clamp and target designations are offset of the actual locations in the image for clarity.

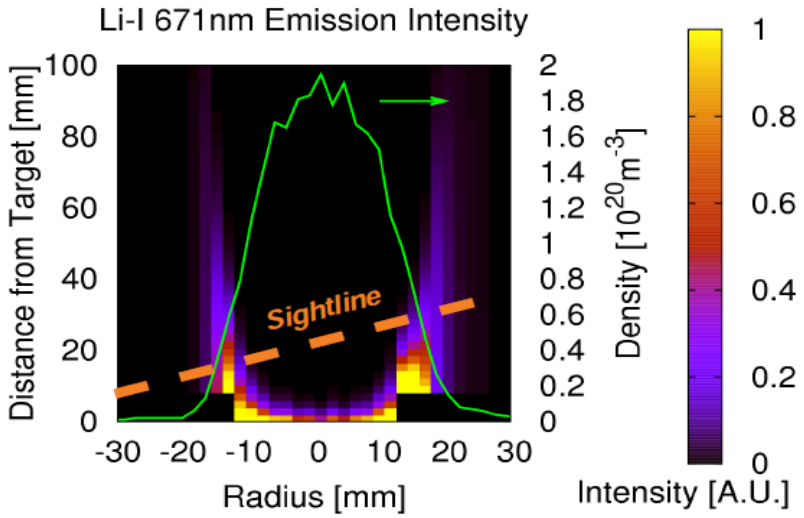

Figure 5.11: Simulated emission of Li-I (671nm) using quasi-2D transport models and experimental density and temperature profiles in Magnum-PSI. Synthetic diagnostics indicate a double-peaked emission structure qualitatively similar to the observed emission shown in figure 5.10.

Table 5.2 provides a comparison of various operational and plasma parameters comparing Magnum-PSI with NSTX discharges during heavy lithium conditioning with plasmas incident on the liquid lithium divertor [23, 24]. The comparison indicates that plasma produced in Magnum-PSI provide similar densities and temperatures as found immediately adjacent to the divertor target plates. The similarity in plasmas near the target indicates that studies of local material transport, and the interpretation of diagnostic signals in these dense divertor plasmas, will be able to inform on experiments in NSTX-U.

Table 5.2: Comparison of Magnum-PSI operational and plasma parameters with those found in NSTX (expected with NSTX-U). Plasma electron temperature, density and parallel particle flux are similar between the two machines as is the expected neutral pressure (≈1–3 [Pa]). The Magnum-PSI device targets can also be tilted with respect to the incident magnetic field to reproduce grazing incidence magnetic field effects near the target.

Parameter	Magnum-PSI	NSTX discharges with heavy lithium (Liquid Lithium Divertor)
Power	60[kW]	4[MW] NBI (15[MW] NSTX-U)
Pressure (source)[kPa]	10	N/A
Pressure target[Pa]	< 3	0.1–1[†]
T_e target[eV]	0.1–10	1–15
N_e target[m^{-3}]	10^{20}–10^{21}	5×10^{20} at strike point
T_i target[eV]	0.1–10	Unknown
Ion flux target [$m^{-2}s^{-1}$]	10^{24}–10^{25} (Normal inc.)	2×10^{23} at strike-point (≈ 3–5°)
Power flux [MWm^{-2}]	10	2–5 (≈ 3–5°)
Magnetic Field[B]	1.9 max.	0.6 (1 NSTX-U)
Beam diameter[cm]	10–15	≈4 FWHM med. triangularity
Pulse length[s]	12–110	1 (5–10 NSTX-U)
Bias [V]	$-100 < V_{target} < 0$	$-20 < V_{floating} < 20$

[†] Calculated using OEDGE interpretative modeling.

Experiments have already been conducted on Magnum-PSI and are undergoing analysis (shown in fig. 5.11). A lithium evaporator was used to deposit lithium onto sample of ATJ graphite, molybdenum (TZM alloy) and pure tungsten. In one experimental run, 100nm (50mg/m^2) of lithium was deposited onto the TZM sample and subsequently exposed to repeated, 5s discharges in Magnum-PSI. The central discharge temperature and density were varied for the experiments over a range of 0.7-2.7x10^{20} m^{-3} and 0.55-1.6 eV with the target biased 20V to simulate a typical bombardment energy expected in the NSTX divertor. By the end of eight 5s discharges (i. e., 40s of total plasma bombardment), lithium was still observed at the center of the samples. TRIM estimates of the sputter yield for a 20eV ion indicate a total yield of 0.0048, only 1/3 of which is sputtered as a neutral.[25]. A gross accumulated erosion over the 40s of bombardment can be estimated at 520mg/m^2, whereas only 50mg/m^2 were deposited.

One method of generating an estimate on the net erosion is to assume that if an additional (ninth) discharge had been performed, no lithium would have been observed. In other words, let us assume that by the end of the 40s all the lithium had been eroded, i. e., a worst-case estimate of the net erosion. In this case, a redeposition fraction for lithium on TZM, obtained from the relation N = (1-R)*G where N is the net erosion, G is the gross and R is the redeposition, is found to be ~0.9, integrated over a number of discharges with densities similar to those found in the NSTX divertor. Such long coating lifetimes on TZM indicate that lithium conditioning in the divertor of NSTX-U with a high-Z substrate could conceivably remain protected by the low-Z coating for a full 5-10s discharge despite large amounts of gross erosion.

Local redeposition has a profound effect on the amount of time a thin coating will remain in one location of the discharge due to the mitigation of the gross erosion rate. Lithium is known to have an increasing sputter yield above the melt temperature as well as a significant fraction of sputtering as ions [26, 28]. With the reported yields in references [26] and [28], estimates for the total yield of lithium neutrals due to evaporation and sputtering as a function of surface temperature. Figure 5.12 provides this estimate of neutral lithium yield for a given surface temperature with an incident deuterium ion flux from a plasma with density $5x10^{20}m^{-3}$ and temperature of 3eV with magnetic field lines incident at 3 degrees w.r.t. the plane of the target(parameters consistent with LLD divertor plasma conditions [24]). Based on these erosion yields the lifetime of a coating can be estimated as follows:

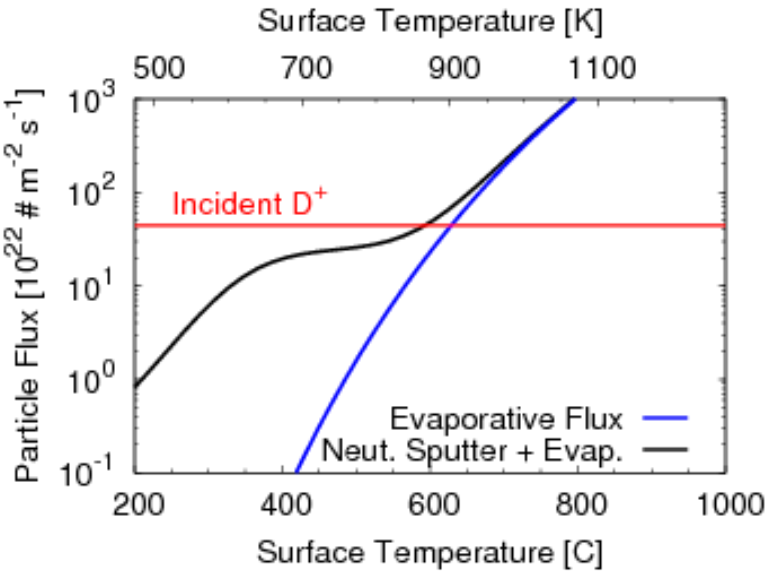

Figure 5.12: Particle fluxes as a function of surface temperature. The neutral lithium particle yield(black) is shown as a function of temperature when exposed to a plasma with density $5x10^{20}m^{-3}$ and temperature of 3eV at 3 degrees angle of incidence. 60% sputtering as ions assumed and removed from the yield curve[25]. Temperature enhanced sputter yield of the lithium is consistent with results reported in [26] and [28], though those studies consisted of low-flux plasmas or ion beams and extended to an upper temperature of 420 and 500C for [26] and [28] respectively. Two transitions can be observed in the figure: one beginning just above the lithium melt temperature that exhibits the temperature-enhanced sputter yield and the second occurring above 550C where evaporative flux begins dominating the total yield.

$$\tau = \frac{J_0 - J_{min}}{\Gamma_{gross}(1 - R_{redep})} \quad (3)$$

where J_0 and J_{min} are an initial and minimum areal number density of atoms, G_{gross} is the gross erosion rate and R_{redep} is the redeposition fraction.

Figure 5.13 shows the expected lifetime of a lithium coating as a function of surface temperature for conditions shown in Figure 5.12. Boron is not reported as having any temperature dependence of sputter yield and the estimated lifetime of an equivalent number-density coating under similar plasma conditions are 2, 22 and 220s for redeposition fractions of 0, 0.9, and 0.99 respectively. In any case should the redeposition fraction actually reach unity as calculated in [29], the coating lifetime tends to infinity. The existence of additional mass-loss terms, such as diffusion of the coating into the substrate material (as is the case with lithium on carbon) will reduce the coating lifetime.

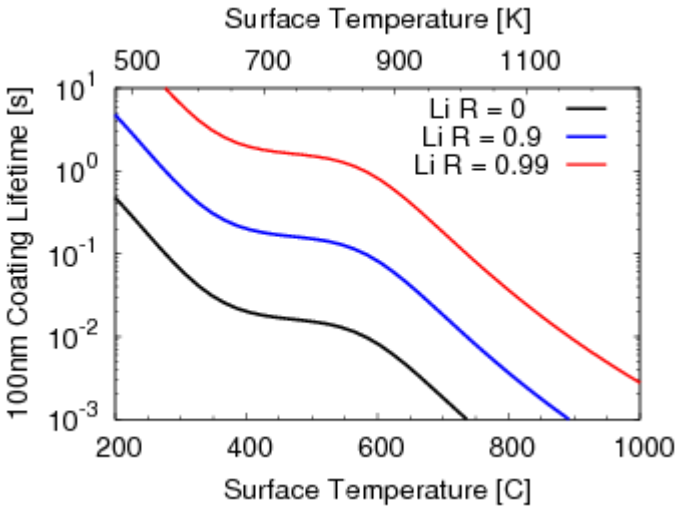

Figure 5.13: Lifetime of a lithium coating on a high-Z (i.e. non-intercalating) substrate for a range of surface temperatures and different assumed values of re-deposition fraction, R. The initial coating thickness is equivalent to 100nm (~50 mg/m^2) and is roughly equivalent to a typical NSTX lithium deposition of 100mg into the vessel. The minimum thickness for this calculation is taken to be 10nm (5mg/m^2).

Once initial studies of lithium depositions on carbon and molybdenum substrates have been carried out on Magnum-PSI, comparisons with results on NSTX-U will be conducted. Again, improved diagnostic coverage is expected in the form of improved Langmuir probe coverage of the upper and lower divertors, as well as more extensive spectroscopic coverage of the in-vessel components to aid in interpretation of local transport of material at the strike-points. More extensive QDM coverage, as well as the MAPP system will enable measurements of global transport. QDMs are not appropriate for use in high-heat flux areas such as the divertor plasma itself. In these locations, marker tiles will be fabricated and used to provide campaign-integrated measurements of thickness changes. Material transport codes such as DIVIMP [19] can then be used to begin linking local and global transport throughout the machine making use of plasma reconstructions based on measured plasma parameters.

With a staged implementation of PFCs, the material migration studies can be conducted with boronized carbon, lithiated carbon, bare high-Z substrate materials (e.g. TZM) and lithiated high-Z substrate materials. With the MAPP XPS capability, the composition of deposited films will be identifiable, potentially, on a shot-by-shot basis. With improved QDM coverage, first-wall erosion and redeposition can be characterized on a shot-by-shot basis. As the estimated first-wall erosion due to charge-exchange neutrals is closely tied with the machine P/S ratio, NSTX-U will be uniquely suited to study first-wall erosive fluxes (c.f. Table 5.1, ref. [19]).

5.2.2.1 Research Plans by Year for Thrust MP-2

Year 1 (2014) of this thrust presents strong overlap with the research plan in thrust 1.

- NSTX discharges will be modeled to determine optimal locations for key material erosion diagnostics such as the QCMs, witness plate samples and marker tiles. Expected fluxes to the MAPP location will be modeled in preparation for the following run years.
- While the above modeling and preparatory studies are occurring, additional experiments will be conducted on the Magnum-PSI device at FOM-DIFFER on lithium and boron coatings. In these experiments gross and net erosion (i.e. measurement of redeposition fraction) of high-temperature lithium PFCs will be measured for comparison to the estimates shown in figure 5.12.
- The effect of intercalation on coating lifetimes on graphite substrates will also be determined experimentally. In addition, the evolution of the film composition due to varying redeposition fractions will be studied to determine if in-situ cleaning by the plasma is a possible method of reducing film contamination (initial experiments already indicate reductions in oxygen content by 1-2s of plasma exposure in Magnum-PSI).
- Experiments at oblique incidence in Magnum-PSI will be conducted to validate models of redeposition at the relevant divertor magnetic configurations.

There is particular ITER relevance in the studies of mixed-material compositional evolution. At present, NSTX-U research create models of the lithium-oxygen-carbon system. A general approach to compositional evolution is being taken, however, such that provided sufficient atomic physics data, it should be possible to predict the evolution of beryllium-tungsten mixed materials under divertor or first-wall relevant plasmas in ITER.

Years 2 – This is the first full year of NSTX-U high-performance plasma operation and NSTX-U researchers will implement the full suite of standard divertor diagnostics such as target Langmuir probes and divertor spectroscopy as well as material migration diagnostics such as QCMs, witness plates and marker tiles.

- QCMs will be used to provide a shot-by-shot measure of mass gain/loss at the crystal location. Marker tiles will provide campaign-integrated measures of erosion/redeposition in locations where QCMs are not suitable (e.g. high-heat flux regions). Similar marker systems can be exposed with the MAPP system for shot-by-shot comparison of these complementary diagnostic systems.
- Using the standard divertor diagnostics, background plasma models will be constructed using any number of modeling tools (e.g. OEDGE, UEDGE, SOLPS are all run by NSTX team members at present).
- With this background plasma, material erosion and transport will also be modeled and compared to measurements (e.g. the fluid codes themselves have some capabilities to do this and additional tools can be brought to bear such as WBC-REDEP and DIVIMP as shown in figure 5.9). By the end of the second year a set of measurements of net erosion/deposition from various locations in the machine is expected to be available for comparison against the above codes. This would provide the base data set with all-carbon PFCs and lithium coatings.

An important question to assess with this system is the origin of carbon entering the NSTX-U core plasma. As indicated in the particle-control section of chapter 4, density rise is due, in large part, to carbon accumulation in the machine. However, recent analysis [60] indicates carbon yields are reduced by a factor of 3 in the divertor. What has not been clearly established is the relative importance of wall sources to the core impurity content. By measuring erosion from the first-wall components, a direct measure of the potential impurity source is measured. Combined with the aforementioned modeling capabilities, a clearer picture of the whole-machine impurity sources will be developed.

Years 2 and 3

- Wall erosion scalings will be established in the ST geometry as a function of input power, pulse length, edge neutral pressure. These scalings will determine the validity of estimates extrapolating wall erosion to long-pulse devices such as those given in section 5.2.2. Again, this topic has particular ITER relevance as NSTX-U will be conducting experiments to directly measure wall erosion due to charge-exchange and far-SOL particle fluxes. These will provide validation of plasma edge and impurity transport models such as OEDGE/DIVIMP.
- Coating lifetimes of boron and lithium that were examined and modeled in Magnum-PSI will

be measured in NSTX-U through the use of conventional plasma spectroscopy and marker tiles. This will provide validation of the material evolution models in the tokamak geometry. Coatings that erode and expose the high-Z substrate will provide the ability to measure discharge performance with the high-Z substrate in the near-SOL plasma as well as in the far-SOL.

- MAPP will be used to provide a means of measuring both total mass deposited (via the QCM) as well as the composition of the material (via XPS) to validate material mixing and transport models developed on Magnum-PSI.

Years 4-5 will concentrate on the impact of vapor-shielding on discharge performance and alterations in material migration. Of critical importance with the presence of lithium PFCs is the control of the invessel lithium inventory as it is expected to contain a significant amount of fusion fuels (in the case of a reactor, tritium). The question is particularly important to address in the vapor-shielded regime where large gross-erosion rates are expected near the strike-point due to a combination of sputtering and evaporation. Measurements of the changes in whole-machine mass deposition during experiments on vapor-shielded PFCs will be made to address this issue and identify locations where recollection of eroded and transported material would be ideal. In addition, the maximum temperature of first-wall elements with lithium coatings is another unknown. With the heated cryo-plenum, the impact of evaporating lithium into the SOL will be assessed (i.e. far from the strike-point region where redeposition is expected to be high). This will begin to determine the compatibility of high-temperature, lithiated, high-Z PFCs with good core performance.

5.2.2.2 Baseline Deliverables for Thrust MP-2

1. Characterization of gross erosion rates for high-temperature (>500C) lithium PFCs and redeposition fractions in typical divertor plasmas.
2. Characterization and modeling of net erosion/redeposition of the first-wall and divertor PFCs in the ST geometry.
3. Determination of the key parameters controlling erosive fluxes to the first-walls of the machine.

5.2.2.3 Incremental Funding Research Plans and Deliverables

In the case of incremental funding, we plan to increase the diagnostic coverage of first-wall elements to include more Langmuir probes and spectroscopic coverage as well as the possibility of neutral hydrogen sensors (both molecular and atomic). These diagnostics will provide improved examination of fluxes to and from the first-wall elements to provide a more complete picture of the processes controlling erosion at the edge.

5.2.3 Thrust MP-3: Establish the science of continuous vapor-shielding

Lithium has a significant evaporation rate at modest temperatures, such that early computational work on lithium PFCs indicated a temperature limit might exist at 350C[31]. Experiments at FTU, however, have demonstrated stable operation with a liquid lithium limiter up to 550C[32]. At these temperatures, a strong evaporation into the local plasma is observed simultaneously with reductions in limiter heat fluxes. This indicates a potentially attractive operating regime where strong local evaporation could lead to a continuously vapor-shielded PFC. Transient vapor shielding has been suspected to play a role in the prevention of PFC substrate damage during exposures to ELM-like transient discharges in the QSPA plasma gun [33]. An experimental determination of the ultimate temperature limits for a liquid lithium PFC in the diverted configuration as well as whether such a novel divertor configuration exists would help resolve these question. These considerations motivate the following research thrust:

> **Thrust MP-3:** *NSTX-U researchers will begin to establish the scientific basis and experimental demonstration of a continuously vapor-shielded surface in the tokamak environment with application to heat-flux mitigation. Extensive research on the long-pulse linear plasma device Magnum-PSI will be carried out to provide an extrapolable experimental demonstration of such vapor-shielding. These experiments will then be extended to NSTX-U using a lithium-coated high-Z substrate (for transient operation) or a flowing liquid lithium system (for long-pulse operation) with a high-power-density strike-point impinging on the PFC to raise the front-face temperature above the lithium evaporation temperature. MAPP, QCMs, Langmuir probes, and divertor spectroscopy, bolometry, and two-color IR diagnostics will be utilized to provide data for interpreting the results specifically examining the roles of lithium impurity radiation and vapor pressure-induced momentum loss on mitigating the incident heat flux.*

In this section, the expected temperature regimes of divertor PFCs in NSTX-U are shown to reach high temperatures – beyond those for which lithium erosion data exist at present (see thrust 2 above). For such high erosion rates, at least two possible methods exist to mitigate the PFC heat flux: plasma pressure reduction and plasma radiation, both of which will be described. The feasibility of examining vapor shielding in the baseline funding scenario (i.e. without flowing systems) will be discussed. As in previous sections, the baseline research plan will then be described followed by the deliverables expected from the 5-year plan.

As the generation of a lithium vapor shield depends on the generation of elevated substrate temperatures, it is necessary to estimate the temperature rise expected with the potential high-Z

substrate materials being considered for NSTX-U. If one assumes that the high-Z substrate is thick enough to make use of the semi-infinite solution, then the temperature inside the material as a function of position and time, T(x,t), is given as:

$$T(x,t) = T_{initial} + \frac{2q_0\sqrt{\alpha t/\pi}}{k}\exp\left(-\frac{x^2}{4\alpha t}\right) - \frac{q_0 x}{k}\mathrm{erfc}\left(\frac{x}{\sqrt{4\alpha t}}\right) \qquad (4)$$

where $T_{initial}$ is the initial temperature, q_0 is the incident heat flux, alpha is the thermal diffusivity and k is the thermal conductivity. The surface temperature exhibits a simple $t^{(1/2)}$ growth and is shown in Fig. 5.14 for a number of candidate materials, TZM-type molybdenum, tungsten and copper exposed to a 10MW/m^2 incident heat flux. The inclusion of copper is made in case an LLD-like substrate [18] should be used, i.e., a copper substrate with thin layers of stainless steel and molybdenum on top. In this case, the long-pulse thermal response of the PFC is dominated by the copper [34]. Without considering the metallurgical implications of these high temperatures (see section IV below), one can see that in all cases, the surface temperature of the PFC reaches as much as 800C in 5s under a 10MW/m^2 constant heat flux. As shown in Fig. 5.12 above, these temperatures are sufficient to equal and even exceed typical divertor main-ion particle fluxes observed in NSTX. Despite these high temperatures, with redeposition fractions greater than 0.9 Fig. 5.13 shows experiments can be conducted for reasonable lengths of time at elevated temperatures without resorting to extreme deposition quantities.

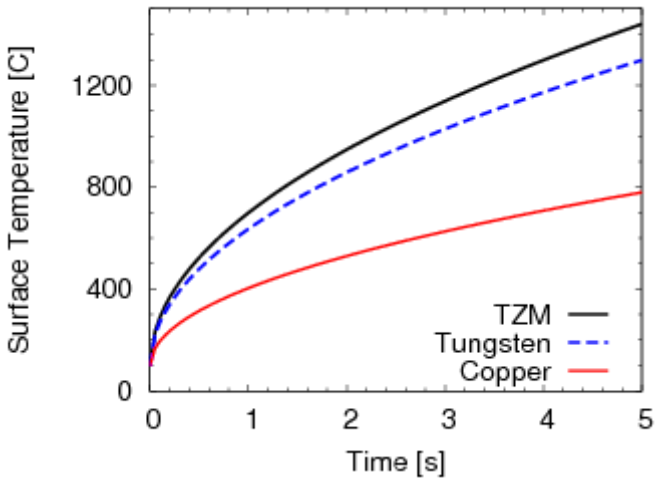

Figure 5.14: Surface temperature as a function of time for a constant 10 MW/m^2 heat flux for a number of candidate substrate materials, TZM-type molybdenum, tungsten and copper.

Given that elevated temperatures and coating lifetimes at these temperatures will be available in the NSTX-U, it is now necessary to consider what may set the ultimate lithium surface temperature in a tokamak divertor. One might consider a first limit on the surface temperature to arise from pressure-balance in a given scrape-off layer flux-tube. One way to estimate upstream pressure in the SOL as a function of input power is given in ref. [35] as:

$$P_{SOL} = 4\pi^2 R_0 a \kappa^{1/2} \frac{\chi_\perp}{\lambda_T} n_u T_u = 4\pi^2 R_0 a \kappa^{1/2} \frac{\chi_\perp}{\lambda_T} p_u \qquad (5)$$

where $p_u=n_uT_u$ is the upstream pressure, P_{SOL} is the power entering the scrape-off layer, R_0, a and κ are the machine major radius, minor radius and elongation respectively, χ_{perp} is the cross-field diffusivity at midplane and λ_T is the electron temperature gradient at the separatrix. χ_{perp} is typically estimated as approximately $2m^2/s$. λ_T can be related to the heat-flux width as $\lambda_T = 7/2\ \lambda_q$ in the limit that classical electron conduction dominates heat transport in the SOL. Using these typical values as well as the expected 3mm scrape-off layer width in NSTX-U as well as the machine geometry[3], one can create an estimate for the upstream pressure as a function of input power into the SOL. This is shown in Fig. 5.15. For comparison, Langmuir probe data taken during the FY2010 run campaign provides a measure of target pressure as a function of power entering the SOL. Also shown is the expected vapor pressure of a liquid lithium surface over a range of temperatures relevant to this study (500-1000C). As can be seen from the figure, very high temperatures of the lithium surface are required to approach the expected upstream pressures in NSTX-U high-power discharges.

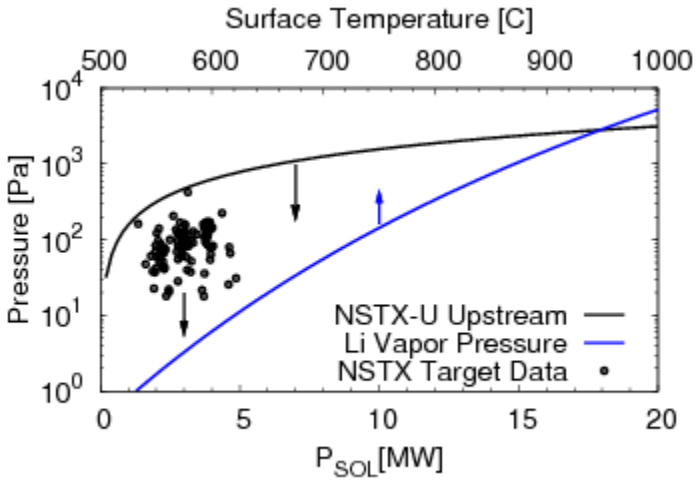

Figure 5.15: Comparison of pressures in considering vapor-shielded PFCs. NSTX-U upstream pressure estimate from equation 5 and NSTX divertor pressures as functions of power entering the SOL. The total lithium vapor pressure as a function of surface temperature is also shown for comparison. This figure indicates that even for NSTX discharges, lithium vapor pressure at surface temperatures of 750-800C would not exceed the divertor plasma pressure as measured by Langmuir probes at the target plate.

The figure informs on several aspects of the continuous vapor shielded regime. First, heat flux to the target due to the plasma charged particles as stated earlier can be rewritten:

$$q_t = \gamma \Gamma^+_{sat} T_e = \gamma n_{es} c_s T_e = \gamma c_s p_t; \quad p_t \propto \frac{P_{SOL}}{S_{plasma}} \qquad (6)$$

This shows that the heat flux impinging a target is directly proportional to the plasma pressure at the target. The total pressure in a given volume is the sum of all the partial pressures. In a strongly evaporating regime, then, the lithium vapor pressure may begin to significantly reduce the incident plasma pressure and provide a momentum sink.

Table 5.3: Comparison of non-equilibrium radiation powers of lithium in the traditional SOL radiation regime *vs.* a vapor-shielded plasma. Calculations assume 10% impurity fraction of lithium.

Case	$N_e[\mathrm{m}^{-3}]$	$T_e[\mathrm{eV}]$	$L_{char}[\mathrm{m}]$	$\tau[\mathrm{s}]$	$L_Z[\mathrm{Wm}^3]$	$P_{R,Z}[\mathrm{Wm}^{-3}\mathrm{s}^{-1}]$
SOL	5×10^{19}	50	15	4×10^{-4}	1×10^{-32}	2.5×10^{6}
Vapor-shield	5×10^{20}	3	1×10^{-3}	1×10^{-7}	1×10^{-31}	2.5×10^{9}

While the vapor pressure itself may provide a momentum loss term to reduce incident power on a target plate, lithium radiation is also expected to provide significant cooling. Figure 5.16 shows the estimated radiative loss function for lithium including transport effects (transport time tau). As can be seen in the figure, for short time-scales, lithium radiation can increase 5 orders of magnitude above the coronal equilibrium amount. Table 5.3 compares some transport time estimates comparing whole-SOL radiation to that expected in a vapor-shielded PFC. The key distinction is in scale lengths of a vapor-shielded PFC vs. the entire SOL flux-tube connection length. A vapor cloud of lithium is expected to extend scale-lengths of order the ionization mean-free path into the plasma. This is typically of order 1mm in a $10^{20}m^{-3}$ target plasma [36]. The specific radiated power is calculated as:

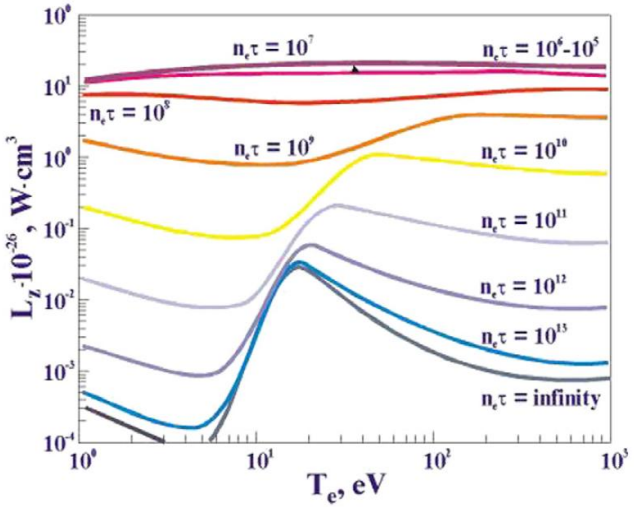

Figure 5.16: Radiative loss function (L_Z) for lithium in coronal ($n\tau$ = infinity) equilibrium and with transport effects included (finite $n\tau$) [37].

$$P_{r,z} = n_e n_z L_Z \qquad (7)$$

where N_e is the electron density, N_z is the impurity density present in the plasma and L_z is the radiative loss function. This indicates the potential effectiveness of a dense plasma near the target to dissipate incident power in a novel divertor configuration. A key question regarding the results shown in figure 5.16 is how increased radiation is achieved at low electron temperatures (below 10eV). At low temperatures (below 10eV), radiation from singly ionized lithium will be difficult to achieve due to the very high ionization potential for the Li^{+2} state (75eV). Identification of power-loss mechanisms in low temperature plasmas (such as found in Magnum-PSI) and those found in the NSTX-U SOL will therefore provide insights into the radiative processes that will dissipate power in the lithium vapor cloud.

Although the radiative power is significant, several unknowns remain. The description used to evaluate the radiative power with the simple loss-function, L_z, is a simplification of the actual transport effects. Recent results have highlighted the importance of accounting for the strong density dependence found in lithium collisional-radiative models [38] and such considerations are not immediately apparent in results shown in ref. [37].

Modeling codes have been in development for a number of years describing vapor shielding in general for several years (e.g. [39]). Close experimental validation in a divertor-relevant plasma has not yet been accomplished. In addition, previous computational studies have focused on transient loading of PFCs. A primary aim of the present work will be to provide high-quality data from linear test-stand experiments as well as the tokamak itself in the steady-state vapor-shielded case to validate existing and new models.

In high-density divertor plasmas, ionization mean-free paths are expected to become comparable to the magnetic pre-sheath scale length and strong, local redeposition is expected. Simulations from Brooks, et al., indicated that redeposition fractions very close to 1 for tin or lithium can be expected in conventional divertor plasmas (30eV, $3x10^{20}$ m^{-3})[40]. This suggests that despite strong gross-erosion rates that might be expected in high-temperature lithium PFCs due to sputtering and evaporation processes, the net impurity ingress into the SOL will be substantially reduced by local redeposition. Such redeposition would also alleviate the amount of material a flowing system would have to source to the PFC surface. This allows initial studies even with limited inventories typical of LITER evaporations onto high-Z substrates relevant to examining the physics of high-temperature, vapor-producing PFC surfaces.

The production of substrate material into the plasma at the target plate ties this research thrust with the study of whole-machine transport described elsewhere in the five-year plan. In this particular topical area, however, more emphasis is placed on local transport near the PFC target, as this is where vapor shielding effects have previously been observed. It is therefore important to assess absolute and net yields from the PFCs. As multiple effects could be occurring simultaneously in a region that is difficult to diagnose, it will be important to obtain as much data as possible prior to attempting this divertor configuration on NSTX-U to ensure operational limits of the underlying substrates are not exceeded. Experiments conducted on linear plasma devices can provide this initial information. Experiments will be focused on demonstrating the concept of a vapor-shielded target, but also assess any impact on core-plasma performance. It is not unreasonable to expect that this divertor configuration could also alter the global transport of material throughout the machine. This would also be re-assessed, though with the benefit of the previous milestone on whole-machine transport in traditional divertor configurations.

5.2.3.1 Research Plans by Year for Thrust MP-3

Due to lithium intercalation into graphite, deposited layers quickly disappear, whereas layers deposited on molybdenum have demonstrate long life-times under similar plasma conditions. As intercalation is expected to occur at an even faster rate at elevated temperatures, experiments in NSTX-U on the vapor-shielded target will only be conducted after the high-Z, tile upgrade in year 3 of the 5-year plan. Before this, however, experiments will be conducted on the Magnum-PSI linear plasma device at FOM-DIFFER.

Years 1-2 (2014-2015)

- Experiments will be conducted on Magnum-PSI with a substrate temperature that varies from 300-800C during plasma bombardment. Both graphite and high-Z metal substrates will be tested and this plan is closely aligned with thrust 2. In these experiments, the local transport of lithium from the surface will be measured to determine the net erosion at the target which would help inform on available "pulse-length" under similar conditions in NSTX-U. These experiments will also provide important information on diagnostic methods and interpretations in this novel plasma regime (i.e. large spatial gradients, high-density, non-minority impurity fractions). Initial estimates of coating lifetime will be validated and refined before conducting experiments in NSTX-U on the high-Z PFCs. A key aspect of this work is the application of conventional diagnostic methods (such as filtered camera diagnostics and target Langmuir probes) to an unconventional divertor regime. This helps ensure that clear comparisons between conventional high-Z PFCs and vapor-shielded targets can be made.

Year 3 - high-Z tiles are expected to be installed into NSTX-U.

- The temperature response of these tiles to the NSTX-U heat fluxes without lithium and with lithium will be examined during this year. Namely, power density will be incrementally increased to validate the engineering design of these components, and develop operating scenarios that minimize the risk of damage under high-power densities.
- Initial demonstration of vapor shielding will be obtained by observing whether strong reductions in the incident heat flux are observed once the high-Z PFCs are coated with lithium. Specific measurements of plasma pressure will be made with divertor Langmuir probes. Surface temperature and heat flux will be measured with IR thermography. Thermocouples embedded in the PFCs will provide measures of integrated energy deposition. In the case of fast, eroding thermocouples, these diagnostics provide an additional measure of surface temperature.
- Divertor bolometry will be used to determine the total amount of radiated power from the near-target plasma. Traditional optical spectroscopy will indicate the amount of lithium and other impurities present in the plasma. If x-ray spectroscopy is available, then identification

of Li-II and Li-III emission will be possible (though Li-II is identifiable with 548nm emission). These diagnostics will all be applied to identify the existence of a vapor-shielding regime.

In years 4-5 we will begin to test the limits of vapor-shielding for reducing incident heat-flux and providing a protective buffer between the target and the plasma. These tests will focus on establishing the operating space of the vapor-shielded regime and compatibility with good core performance. In addition to experimental studies, expanded modeling is expected to occur to extend new and existing fluid models to this high-density, high-impurity fraction regime.

In the event that a full-funding scenario should be applied, we expect to be able to implement a fully-flowing liquid metal module for installation in the NSTX-U vacuum vessel, assuming laboratory testing indicates the technology is sufficiently advanced to do so. In this case, the liquid system would provide continuous replenishment to the surface and long-pulse testing of the vapor-shielded target could be conducted even with reduced redeposition rates. Initial tests with the device under plasma bombardment will also determine whether a flowing system is, in fact, able to maintain an equilibrium impurity concentration of the surface in contact with the plasma.

5.2.3.2 Baseline Deliverables for Thrust MP-3

1. Determination of existence of continuous vapor-shielding regime in the NSTX-U divertor.
2. Determine roles of pressure and radiation as means of reducing incident heat loads to the PFC surface.
3. Determine required flow rates and replenishment of liquid lithium for demonstration of continuous vapor-shielding for long-pulse.

5.2.3.3 Incremental Funding Research Plans and Deliverables

In the incremental funding scenario a fully flowing, liquid lithium divertor module is planned. With this module, it will be possible to extend the amount of time the target sustains vapor-shielding well beyond the pulse-length estimates shown in Figure 5.13. In this plan, then, long-pulse demonstration of the concept will be possible. In addition, efforts would be made to increase the diagnostics in the divertor, in particular, a spatially-resolved, spectrally-resolved instrument could provide key insight into the radiating species and could strongly constrain codes attempting to describe this new divertor regime.

5.3 Plasma-Facing Component Research & Development

In order to clearly identify the effects of changing the PFCs and base materials present within NSTX-U, it is planned for a staged upgrade over the next 5-years. Such a plan requires coordination over the entire 5-year plan and depends on the creation of a base set of diagnostics early in the plan as well as a set of reference discharge scenarios. By returning to the reference data sets, modifications to machine performance as a result of incremental changes to the wall and divertor PFCs will be examined in detail.

Figure 5.17 shows the upgrade scenario proposed for the base budget case. Operations begin in 2015 with carbon divertor and wall PFCs. As indicated in the research plans above, reference plasmas will be established in this first year and compared to subsequent years. The first of these modifications will be the introduction of a high-Z divertor target in 2016 (the technological choice for this PFC is discussed in the section below).

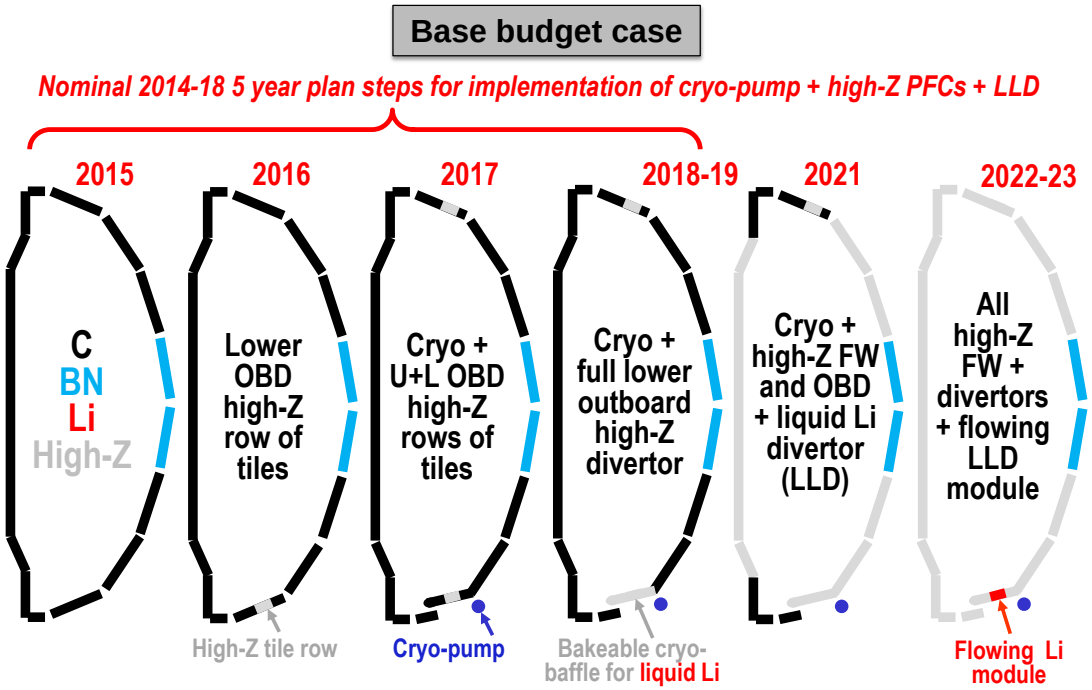

Figure 5.17: Implementation schedule for cryo-pump, high-Z plasma-facing components, and flowing liquid lithium divertor module with base budget funding.

As indicated above, this year will begin operations without a boronization campaign to establish the effect of the boron on the lithium-carbon chemistry (see thrust 1 description above). This also allows for erosion studies to be carried out on the bare high-Z tiles prior to lithium evaporations. This staging also allows a comparison between a high-Z divertor target and the

previous carbon target (in low triangularity discharges) before the divertor geometry is altered for the cryo-pump upgrade. The first immediate benefit to the Materials and PFCs research plan is to provide a non-intercalating substrate enabling high-temperature lithium to be studied with a lifetime limited only be erosion and redeposition as opposed to the additional effects of graphite intercalation.

The cryo-pump upgrade represents a substantial outage period and is planned for the 2016-2017 break. During this this, the high-Z target set that was previously installed on the lower divertor will be moved to the upper divertor while a similar row of high-Z targets is installed on the cryo-pump plenum. This upgrade allows low-triangularity, double-null discharges to divert on high-Z simultaneously. It will also allow impurity studies to be made comparing the effect of a high-Z source localized near the divertor (i.e. 2016 in lower-single null) and the addition of a high-Z source localized on the first-wall (i.e. 2017 in lower-single null).

In the 2018-2019 time period, a full, high-Z cryo-pump plenum is planned. This plenum will be heatable to support bake-out as well as experimental studies. This upgrade will provide data on the effect of increased high-Z divertor coverage and enable experiments on changing the pre-discharge PFC temperature. For example, it may be beneficial to operations to liquefy lithium coatings very soon after a discharge begins. By pre-heating the cryo-baffle to (say) 150C the temperature difference is reduced leading to a faster transition to nominally liquid lithium surface temperatures. Such a strategy was suggested by LLD experiments in the 2010 run campaign but could not be re-examined before the beginning of the upgrade.

In the second 5-year plan, a conversion of the first-wall components will be accomplished by 2021. By retaining graphite PFCs in the divertors but completely converting the walls of NSTX-U to high-Z, the complementary experiment to the LLD can be performed. That is, the LLD sought to address the question of how performance changes when $1m^2$ of the divertor is converted to a high-Z substrate with lithium coatings. By converting the walls, we can ask what effect changing the other ~90% of the PFCs will have on discharge performance. This strategy also maximizes the time available to complete scenario development including heat-flux mitigation schemes such as radiative divertors, snowflake configurations, vapor shielding or combinations of the above. By 2022-2023, the NSTX-U will be converted to a full, high-Z machine.

In addition to the high-Z PFC conversion, a fully-flowing liquid lithium module will be tested by 2022-2023. A number of technical challenges must be addressed before implementation of such a device in a tokamak and are described below. This device will enable long-pulse operation in the continuously vapor-shielded regime. It will also enable demonstration of Li-surface purity control by continuously replacing the surfaces that getter residual vacuum gases with fresh Li.

The baseline budget case can be accelerated in the event that incremental funding is made available as shown in Fig. 5.18. In this budget case FY2016 remains identical to the baseline budget scenario. The long outage to install the cryo-pump is utilized to upgrade the wall to high-Z PFCs. This effectively advances the NSTX-U PFC upgrade program 4 years. This funding would further impact the development and testing of a flowing liquid lithium divertor module to be installed early in the next 5-year plan followed by a full toroidal flowing lithium divertor in 2021.

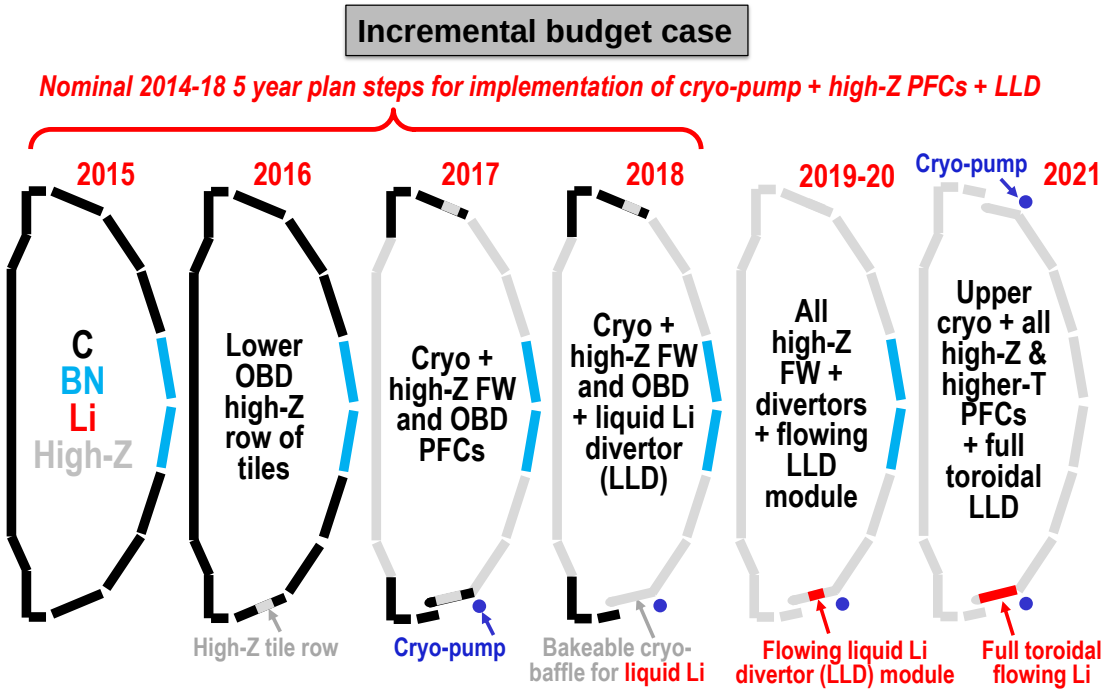

Figure 5.18: Implementation schedule for cryo-pump, high-Z plasma-facing components, and flowing liquid lithium divertor module if incremental budget is funded.

The remainder of this section describes the research program on PFC technology to support the NSTX-U PFC upgrade plan.

5.3.1 Staged Solid PFC Upgrades

Research on an appropriate high-Z target PFC will be conducted in the time leading up to the first outage. Tungsten and molybdenum are both considered candidate materials, though tungsten is preferred due to its relevance to FNSF and potentially, future reactors. Molybdenum is considered an option due to at least two attractive features: 1) a lower sputter threshold will create a larger "signal-to-noise" ratio for material migration studies, 2) molybdenum components are more easily fabricated than tungsten. (Of course, during operation, a higher erosive yield

may prove a liability if core contamination cannot be addressed, but this is a potential problem for any high-Z PFC in a confinement device.) Both materials are compatible over a wide temperature range with all liquid metals currently considered for fusion experiments: Li, Ga, Sn and alloy combinations of these metals.

Several technological options exist for deploying high-Z PFCs within a tokamak experiment. These include application of a thin, high-Z layer on a copper substrate – essentially duplicating the FY2010 Liquid Lithium Divertor module. The next option is to utilize a single high-Z bulk tile – another option developed for the NSTX divertor immediately prior to the upgrade outage (though never tested under plasma operation). A third option is to utilize thin-film coatings of the high-Z on top of existing graphite tiles which is identical to the approach taken by ASDEX-Upgrade [41]. Finally, high-Z structures can be constructed in a lamellae shape as done on C-Mod [42] and JET [43]. Physical processes related to the thermo-mechanical performance of each of these options have already lead to a preference for a lamellae structure in the divertor and thin-film coatings for first-wall PFCs. The following provides a brief description of these considerations.

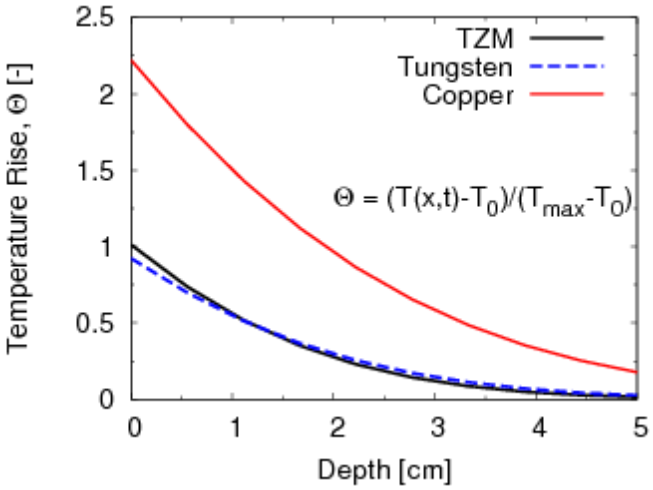

Figure 5.19: Non-dimensional temperature rise as a function of depth into a PFC material at 5s discharge time with 10MW/m^2 incident heat flux. Maximum temperature is defined as the recrystallization temperature of the metal ($T_{recryst}$ ~0.5 T_{melt}).

The first considerations are the temperature limits of the material from a metallurgical perspective. The internal temperature profile given in eq. 4 above is shown as a function of depth into the material at 5s of discharge time in Fig. 5.19. In this figure, the temperature rise is non-dimensionalized with the initial and maximum temperatures allowed by the material itself. This maximum temperature is taken as the recrystallization temperature of the material for which representative values are 1425, 1400 and 400 C for TZM-type molybdenum, pure tungsten and copper respectively. The initial temperature is set to 100C. As can be seen in the figure, both TZM and tungsten would be expected to reach the maximum temperature in 5s under constant heat flux whereas copper exceeds the allowed temperature rise by more than a factor of 2. This essentially eliminates the LLD-like construction from consideration for 5s pulses at 10MW/m^2 incident heat flux (though for lower heat flux regions, or reduced pulse lengths it may still be considered).

The next criterion will be the ability of the material to withstand thermo-mechanical stresses that arise due to large temperature variances between the surface and the back-face of the material. For example, the molybdenum tiles designed for NSTX FY11-12 run campaign could only withstand 2 MW/m^2 average surface heating for 1s before thermo-mechanical strains exceeded allowable margins. This is clearly unacceptable for NSTX-U and would need to be improved. In other machines using high-Z divertor targets such as CMOD[42] or JET[43], the bulk metal is fabricated into lamellae. By segmenting the bulk metal, thermal-mechanical stresses can be alleviated for a given depth of material. The material depth is determined by the desired thermal capacity of the PFC. For instance, in the case of TZM and W shown in figure 5.19, the implied depth of each lamella would be at least 5cm for the semi-infinite thermal solution to be a valid estimator.

It is also possible to create PFCs qualified for operation in the divertor with the use of high-Z coatings on graphite tiles as shown in the ASDEX-Upgrade device[41]. In this scheme the coefficient of thermal expansion must be closely matched between substrate graphite and the high-Z coating. Indeed, ASDEX-Upgrade made use of a specially formulated graphite for this purpose. This does not, however, completely eliminate stresses which can still arise in differentially-heated objects. The adhesion of the surface coating to the substrate is process dependent and several had to be investigated by the ASDEX group before the current design was settled upon. Even in this event, excessive heat fluxes can lead to failure of the coating and exposure of the underlying graphite. In regions of reduced heat flux, however, these thermo-mechanical considerations become less severe and it may be possible to use relatively simple coating technologies to convert the existing graphite tiles.

These last considerations lead to favoring a bulk-W, lamellae design for the divertor target and high-Z coatings of first-wall PFCs where surface heat-fluxes are less of a concern. Prior to implementation, further research on these two options will be conducted in the form of prototype fabrication and testing at suitable heat-flux facilities.

5.3.2 Liquid-Metal Plasma-Facing Component Research and Development

In years previous, the usage of liquid lithium for particle control has been emphasized based on the results observed on TFTR, CDX-U and NSTX with the reduction of lithium as well as the measurements of deuterium retention in PISCES-B. As discussed in section 5.2.1, the vacuum conditions as well as shot-timing used in NSTX (and expected in NSTX-U) create a complicated surface and introduce significant technical challenges to obtaining a “pure” lithium PFC surface

where the recycling coefficient might be expected to remain below 0.5. This motivates examination of a fully-flowing liquid PFC to reduce the residence time of the liquid in contact with the background vacuum conditions as well as a means of removing the gettered materials. In addition to this long-standing scientific goal of studying the low-recycling plasma regime, liquid metals generally offer several advantages over solids as discussed in the introduction. These include the elimination of permanent reshaping of substrate PFCs under plasma bombardment and separation of PMI problems from neutron irradiation problems. As indicated in Figure 13, the amount of time available for high-temperature PFC experiments will be paced by the redeposition fraction. Providing a flowing system to replace the lost material will enable extension of high-temperature regimes to long-pulse operation.

In order to examine these potential benefits in a tokamak device, significant development is required, but must be accomplished in the next 5-10 years if experimental data is to be available to inform on a liquid-metal option for an FNSF.

Progress in understanding liquid metal PFCs has already been accomplished with the Liquid Lithium Divertor in NSTX. Experiments with the NSTX LLD campaign has resulted in several important results related to the implementation of liquid metal PFCs[44]. First, the LLD confirmed the result on limiter machines that liquid lithium provides a protective layer over a high-Z metal substrate. Next, the LLD demonstrated a stable liquid metal using a porous substrate for the first time in a diverted tokamak. In addition to the liquid metal stability, the overall construction of a porous metal substrate was able to successfully operate the entire run year without evidence of damage during post-mortem analysis.

Proceeding from this work, internal development of a liquid metal loop facility is ongoing at PPPL for the demonstration of basic flow control and candidate LM PFCs in NSTX-relevant vacuum conditions. The laboratory tests will inform on whether the basic concept of using flow to control the gettered impurities is feasible. The facility will also demonstrate the basic operation of LM-PFCs so that a transition to NSTX-U will be made as smoothly as possible. Due to the inherent needs of LM-PFCs of the type being development, integral active cooling will be demonstrated in the offline facilities as well.

Alongside development of the loop facility, additional tests on Magnum-PSI will be carried out using pre-loaded liquid metal target samples. These will contain an integrated reservoir of liquid metal to examine issues related to porous-MHD and surface stability in the Magnum-PSI, magnetized plasma environment. They will also enable studies at very high temperatures (e.g. >600C) to explore the continuous vapor-shielding regime and how it extends to long-pulse operation.

In the incremental budget scenario, we plan to demonstrate sufficient technological progress to warrant a fully-flowing, liquid metal divertor module in NSTX-U by the FY2019 (2022 in the baseline scenario). This ambitious goal will provide an experimental divertor target to demonstrate the linkage between all three physics thrusts in this TSG. That is, surface contamination processes studied in the lithium surface-science will inform on the expected surface composition, uptake of deuterium and/or other impurities such as oxygen, and any impact these have on the resulting plasma interactions. The module will provide a temperature-controllable system for examining variations in whole-machine transport that might occur in a transition from low temperature liquid lithium PFCs to high-temperature surfaces. Finally, at high-temperature, long-pulse continuous vapor shielding phenomena could be studied with such a module. This cap-stone project would provide the technical basis for a whole-divertor upgrade to a flowing liquid metal PFC in the next 5-year plan for NSTX-U and strongly inform on the liquid metal option for FNSF.

5.4 Theory and Modeling

The theory and modeling required in support of the three research thrusts overlaps with that of the Boundary Physics TSG in that understanding plasma-material interactions (PMI) and their impact on the core plasma requires a characterization of the incident plasma, as well as an ability to predict the transport of the products of PMI. We will describe below the anticipated role of those codes in M&PTSG research, but refer the reader to the BPTSG chapter for more detailed descriptions.

The codes and models to be described here can be divided into three types:
Materials and atomic physics. These are first principles, or nearly so, descriptions of physics at the smallest relevant scales, femtometers to nanometers.
Surface chemistry and evolution. These codes combine analytic and theoretical descriptions of the material and its state with empirical models where a more fundamental understanding is lacking. This is a relatively new category of tokamak modeling.
Global transport and surface evolution. These codes attempt a comprehensive description of the tokamak environment, including both the material surface and the plasma.

5.4.1 Materials & Atomic Physics

5.4.1.1 Monte Carlo Plasma-Surface Interaction Simulations

Codes like TRIM [45] and comparable variants VF-TRIM (U-Illinois) and SRIM (www.srim.org) rely on the fact that for energies above a few eV, the interaction of an incident

ion or neutral can be described theoretically in terms of multiple binary collisions between the incident particle ("projectile") and atoms in the material surface ("target"). Given a comprehensive characterization of the chemical and structural composition of the material, a Monte Carlo procedure for simulating the resulting chain of collisions can be carried out. The end result of a statistical sampling of such calculations is a set of probabilities for absorption or backscattering of the particle and sputtering of target atoms. Distributions of the outgoing energy and velocity vectors for the backscattered and sputtered particles are also accumulated. All of these outputs are functions of the incident particle's energy and angle relative to the surface normal.

TRIM has long been, and continues to be, a "workhorse" code for simulating PMI because it can produce comprehensive and kinetic characterizations of these processes. The first and most obvious limitation is that it can be applied only to a known and constant material state. In contrast, material surfaces in operating tokamaks are steadily evolving and poorly characterized. A second related limitation is that in attempting to model realistic surfaces, adjustable parameters, such as the surface binding energy, must be estimated or guessed. Finally, the binary collision assumption is known to break down for incident energies of a few eV or less when the incident particle interacts with multiple target atoms.

5.4.1.2 Molecular Dynamics Codes

Such regimes are the realm of molecular dynamics codes. They attempt a closer to first principles characterization of the same problem. In a molecular dynamics (MD) code, the atoms of a three-dimensional portion of the surface are explicitly simulated, with their mutual interactions and the interactions with the incident particles described by a specified interatomic potential. In quantum MD, these potentials are computed "on the fly" by solving Schroedinger's Equation for the relevant electrons in the atoms. Because of the computationally intensive nature of MD codes, the time and space scales that can be simulated are extremely small (femtoseconds to picoseconds; length scales smaller than nanomoeters). Like the TRIM-type codes, one needs to know the surface composition of the material to simulate the PMI. The other principal limitation of MD codes is that accurate potentials are known only for a few, relatively simple systems.

The potential for using MD codes to obtain an improved understanding of the behavior of lithium in NSTX (and other devices) has been already demonstrated by Krstic et al. [46] (Sec. III-1), and we anticipate similar contributions in the future to the "Lithium Surface Science" thrust.

5.4.1.3 Atomic Data and Analysis Structure Database

The Atomic Data and Analysis Structure (ADAS) [47] is now the principle resource for atomic

physics data used (and supported by) the fusion community. ADAS is first a database of fundamental atomic physics cross sections contributed by physicists from around the world. ADAS is second a collection of numerical tools for massaging and assembling those data into a form useful by both fusion experimentalists and modelers. The particular quantities of interest for the M&PTSG (in all three thrusts) are effective rates for ionization, recombination, and line radiation emission of the relevant impurities (neutral and ionized), Li, O, B, C, etc. These "effective" rates are obtained by invoking the assumption (usually valid) that the electronic excited states of ions and atoms equilibrate amongst each other much more rapidly than they do with the ground electronic state. The resulting "collisional radiative" (CR) model allows for the (extremely important at high densities) effects of the excited states to be condensed into effective rates for the ground state species.

ADAS has CR rates for all of the atomic species of interest to the M&PTSG, although with varying degrees of accuracy. The bulk of the fundamental cross sections in the CR model must be computed by sophisticated, and expensive to run, atomic physics codes. As these practitioners work their way up the periodic table, better cross sections are obtained. Presently, such data (and CR models) are available for hydrogen and lithium; carbon, oxygen, and boron model rates rely on older data. The assumptions of the CR model itself are another source of uncertainty. Particularly in the "continuous vapor shielding" regime, these uncertainties may translate into large uncertainties in simulations replicating this operating regime [48]. For this reason, experimental and theoretical work is planned to validate aspects of the CR model for lithium.

5.4.1.4 Surface Chemistry and Evolution Modeling

Developing a truly predictive plasma transport capability will require comparably realistic models of particle and heat transport in the plasma facing materials. Heretofore, plasma transport codes (those in the next section) utilized characterizations of materials and plasma-material interactions, via TRIM or MD codes, that typically assumed pristine, idealized materials. In this Five Year Plan, NSTX-U modeling efforts will begin moving beyond these simplistic models toward ones that allow the material surface to evolve in response to plasma fluxes.

The two codes listed below are being considered for this purpose. However, concerns with usability or suitability for the NSTX-U application may lead to the development of new, but similar, tools.

5.4.1.4.1 WallPSI (UCSD)

The WallPSI code [49] solves transport equations for particles and heat in the material surfaces. As such, it provides a realistic characterization of all processes affecting the hydrogen content of

the surface, including recycling and retention. Impurity erosion processes, including physical sputtering, chemical sputtering, evaporation, and radiation enhanced sublimation are all included with physically realistic models.

WallPSI was developed as part of the FACETS project [50] and was designed to be coupled to plasma transport codes (namely, UEDGE), but it can also be run in a stand-alone mode. For example, [51] describes stand-alone applications to simulate PISCES materials experiments. Analogous applications of interest to NSTX-U could be made in simulating experiments on the Magnum PSI linear device or on smaller lab experiments being carried out in connection with the NSTX-U program.

5.4.1.4.2 WallDyn (IPP-Garching)

The WallDYN code [52] provides a consistent, global solution to the impurity erosion-redeposition problem for a given plasma condition. The principal input is a matrix of transport probabilities describing the likelihood that an impurity eroded from one particular location in the vessel will be transported to a second location. The elements of this matrix are computed with an impurity transport code, say, DIVIMP using that same plasma condition. The basic version of WallDYN uses relatively simple characterizations of the material surfaces, although the most recent version [53] allows the thickness of the surface layer to evolve in time and deposited species to diffuse into the material.

Considerable evidence exists for impurity migration occurring via many small erosion and redeposition steps. The global and consistent solution obtained with the matrix approach used by WallDYN captures this behavior in an effective and efficient way. Since material migration represents one of the three M&P thrusts, a tool like WallDYN would be useful in interpreting the corresponding NSTX-U experiments.

5.4.1.5 Global Transport and Evolution Simulations

Because these codes provide a characterization of the effects of changes in a plasma facing surface on the plasma conditions elsewhere, they will likely prove useful in all three M&P research thrusts.

5.4.1.5.1 SOLPS (IPP-Garching) and UEDGE (LLNL)

The workhorse tools for interpretive and predictive plasma transport simulation the last decade or more have been the 2-D edge and scrape-off layer fluid plasma simulation codes, UEDGE [54] and B2 [55]. Both codes can utilize either a built-in fluid model for neutral transport or couple to a comprehensive, Monte Carlo kinetic neutral transport code, such as EIRENE (FZJ)[56] (used with B2; the coupled system is known as SOLPS [57]) or DEGAS 2 [58]

(usually run with UEDGE in a non-iterative, post-processing mode). UEDGE and SOLPS are described in more detail in the Boundary Physics (chapter 4); DEGAS 2 (PPPL) is described in the MHD chapter (chapter 2).

The fluid plasma transport codes self-consistently solve equations for the density, parallel velocity, and temperature of all ion species, as well as the electron temperature. This capability will allow us to interpret experiments on impurity behavior and, as was discussed in Sec. 5.2.3, provide insight into how a viable continuous vapor shielding regime of operation might be established.

The characterization of particle sources and sinks at material surfaces in these codes resides within the neutral transport models. In the case of the built-in models, the level of detail and realism in these characterizations is limited. The Monte Carlo neutral transport codes provide a great deal more flexibility and very sophisticated models. Presently, the bulk of the data used to describe plasma-material interactions come from TRIM (or equivalent) and / or empirical expressions. We anticipate augmenting these models with data or fits obtained from more detailed and realistic MD simulations.

5.4.1.5.2 XGC-DEGAS2 (PPPL)

Limitations in the ability of fluid plasma-Monte Carlo neutral codes to reproduce aspects of tokamak scrape-off layer and divertor phenomena are well known. A common theme in virtually all of these assessments is that missing kinetic effects, particularly those associated with electrons in the scrape-off layer, are blamed. The XGC codes (chapter 4) will provide a closer to first principles model that will incorporate the missing kinetic effects and, presumably, more faithfully replicate experimental observations. Just as with the fluid plasma transport code, the XGC codes are being coupled to DEGAS 2 to allow detailed PMI models to be incorporated into the simulations.

5.4.1.5.3 OEDGE/DIVIMP (UTIAS)

An alternative approach to simulating scrape-off layer and divertor plasmas is a purely interpretive one. The OEDGE [59] code exploits the fact that our understanding of neutral and parallel plasma transport is vastly superior to that of anomalous, turbulence driven perpendicular transport. At the core of OEDGE is the Onion Skin Model (OSM) which integrates fluid plasma transport equations along individual SOL flux surfaces, starting from the divertor target and extending up to the main chamber, e.g., midplane. The initial plasma densities and temperatures at the divertor target are provided by measurements there, e.g., embedded Langmuir probes. Likewise, the results at the end points of the integration are to be compared with measurements made there, e.g., by a fast scanning probe.

By performing this integration on a set of adjacent flux surfaces, a full 2-D characterization of the SOL and divertor plasma can be compiled. This, in turn, can be used as the background for Monte Carlo neutral (the EIRENE code) and impurity (DIVIMP) transport codes. In addition to providing corresponding sources and sinks that can be fed back into OSM, analogous to the coupling in conventional fluid plasma-Monte Carlo neutral transport codes, the neutral and impurity codes also simulate relevant diagnostic signals, the data from which can be used to further constrain the calculations. The coupling and constraining process can then be iterated until a consistent solution is obtained.

OEDGE would be applied to the research thrusts described in this chapter in a manner similar to that used with the other codes described above.

5.4.1.6 1-D Modeling of Mixed-Material Films

For the "Material Migration" thrust (Sec. 5.2.2), a simpler, local approach to modeling the erosion and redeposition process is planned that can be developed and validated on the linear plasma device Magnum-PSI and then applied to NSTX-U. A particle balance equation for a thin film on the material surface is solved, incorporating contributions from redeposition, sputtering, evaporation, and diffusion. The redeposition term is computed via a semi-analytic, 1-D model characterization of neutral transport from the surface, ionization, and return to the surface. The ionization rates are obtained from the ADAS database. The associated photon emission rates can be compared with diagnostic measurements to infer the overall magnitude of the surface erosion. The surface sputtering rate can be computed using TRIM (or equivalent); direct experimental measurements will also be done. Evaporation rates (e.g., for Li) are well known. The diffusion of film atoms into the substrate is characterized with an empirically determined diffusion coefficient.

References

[1] “Materials science and technology research opportunities now and in the ITER era: a focused vision on compelling fusion nuclear science challenges” FESAC report, February 2012.
[2] F. Romanelli, et al., “A roadmap to the realization of fusion energy” presented at the 1st IAEA DEMO Programme Workshop, Los Angeles, 15-18 Oct. 2018.
[3] J.E. Menard, et al., Nucl. Fusion 52 (2012) 083015.
[4] Th. Eich, et al., “Scaling of the tokamak near scrape-off layer H-mode power width and implications for ITER”, ITPA-Div/Sol group ITR 1/1, San Diego, October, 2012.
[5] J.E. Menard, et al., Nucl. Fusion 51 (2011) 103014.
[6] A. Capece, et al., “The effects of contamination by residual gases in NSTX on D uptake and retention in Li films”, presented at the 54th APS-DPP meeting, Providence, RI, October, 2012; C.H. Skinner, et al., “Plasma Facing Surface Composition during NSTX Li Experiments”, J. Nucl. Mater. (2013) Accepted for publication.
[7] M.J. Baldwin, et al., Nucl. Fusion. 42 (2002) 1318.
[8] R. Kaita, et al., “Comparison of H-Mode Plasmas Diverted to Solid and Liquid Lithium Surfaces” J. Nucl. Mater. (2013) Accepted for publication.
[9] R. Maingi, et al., Nucl. Fusion 52 (2012) 083001.
[10] M.A. Jaworski, et al., “Liquid Lithium Divertor Characteristics and Plasma-Material Interactions in NSTX High-Performance Plasmas”, 24th IAEA Fusion Energy Conference, EX/P5-31, San Diego, October, 2012.
[11] M.A. Jaworski, et al., Fusion Engineering and Design 87 (2012) 1711-1718.
[12] M. Ono et al., Nucl. Fusion 52 (2012) 037001 and references therein.
[13] N. Itou et al., J. Nucl. Mater., 290-293 (2001) 281.
[14] H. Kugel et al., Phys. Plasmas 15, 056118 (2008).
[15] “Surface chemistry analysis of lithium conditioned NSTX graphite tiles correlated to plasma performance” C. N. Taylor, K.E. Luitjohan, B. Heim, L. Kollar, J.P. Allain, C.H. Skinner, H.W. Kugel, R. Kaita, A.L. Roquemore, R. Maingi submitted to Fusion Engineering and Design October 2012.
[16] “Deuterium Uptake in Magnetic Fusion Devices with Lithium Conditioned Carbon Walls” P S Krstic et al., submitted to Phys. Rev. Lett., (2012).
[17] C. N. Taylor et al., Rev. Sci. Instrum. 83 (2012) 10D703.
[18] H.W. Kugel, et al., Fusion. Eng. Des. 87 (2012) 1724-1731.
[19] P.C. Stangeby, J. Nucl. Mater. 415 (2011) S278-S283.
[20] S. Mirnov, S.V., Lazarev, V.B., J. Nucl. Mater., (2011) in press.
[21] C.H. Skinner, et al., J. Nucl. Mater. 363-365 (2007) 247-251.
[22] C. N. Taylor et al., Rev. Sci. Instrum. 83 (2012) 10D703.
[23] M.A. Jaworski, et al., Fusion. Eng. Des. 87 (2012) 1711-1718.

[24] M.A. Jaworski, et al., J. Nucl. Mater. (2013) in press.
[25] J.P. Allain and D.N. Ruzic, Nucl. Fusion, 42 (2002) 202-210.
[26] R.P. Doerner, et al., J. Nucl. Mater. 290-293 (2001) 166-172.
[27] P.C. Stangeby, "Plasma Boundary of Magnetic Fusion Devices" Institute of Physics Press, 2000.
[28] J.P. Allain, M.D. Coventry and D.N. Ruzic, J. Nucl. Mater. 313-316 (2007) 641-645..
[29] J.N. Brooks, et al., J. Nucl. Mater. 290-293 (2001) 185-190.
[30] G. De Temmerman, et al., Nucl. Fusion 51 (2001) 073008.
[31] T. D. Rognlien and M. E. Rensink J. Nucl. Mater., 290-293 (2001) 312.
[32] M.L. Apicella, et al., Plasma Phys. Control. Fusion 54 (2012) 035001.
[33] Evtikhin, V.A., et al., J. Nucl. Mater., 307-311, (2002) 1664-1669.
[34] T. Abrams, et al., J. Nucl. Mater. (2013) in press.
[35] C.S. Pitcher, P.C. Stangeby, Plasma Phys. Control. Fusion 39 (1997) 779.
[36] ADAS Database
[37] S. Mirnov, et al., Plasma Phys. Control. Fusion 48 (2006) 821.
[38] S. Loch, et al., Phys. Rev. E, 69 (2004) 066405.
[39] A. Hassanein and I. Konkashbaev, J. Nucl. Mater. 290-293 (2001) 1074-1078.
[40] J.N. Brooks, et al., J. Nucl. Mater. 290-293 (2001) 185-190.
[41] R. Neu, et al., Physica Scripta **T138** (2009) 014038.
[42] T. Willard, R. Vieira and S. Pierson, "Lamellae tungsten tile design transient thermal/ electromagnetic stress analysis" MIT PSFC internal report, Cambridge, MA, June 8, 2006.
[43] Ph. Mertens, et al., "Conceptual design for a bulk tungsten divertor tile in JET" Technical report EFDA-JET-CP(06)04-02, Sept. 2006.
[44] M.A. Jaworski, et al., "Liquid lithium divertor characteristics and plasma-material interactions in NSTX high-performance plasmas", submitted to Nucl. Fusion.
[45] W. Eckstein and D.B. Heifetz, J. Nucl. Mater. 145-147 (1987) 332.
[46] P. Krstic et al., Phys. Rev. Lett **110** (2013) 105001
[47] H. P. Summers (2004) The ADAS User Manual, version 2.6 http://www.adas.ac.uk
[48] T. Rognlien and M. Rensink, J. Nucl. Materials **290-293** (2001) 312
[49] A. *Pigarov* and S. Krasheninnikov, J. Nucl. Materials **390-391** (2009) 192
[50] J. R. Cary et al., J. Phys.: Conf. Ser. **125** (2008) 012040
[51] A. Pigarov et al., Cont. Plasma Phys. **52** (2012) DOI: 10.1002/ctpp.201210035
[52] K. Schmid et al., J. Nucl. Mat. **415** (2011) 284
[53] K. Schmid, EFDA TF-PWI Joint Working Session, Tervaniemi, Finland, February 2-6, 2013
[54] T. Rognlien et al., J. Nucl. Mater. **196–198** (1992) 347
[55] Braams B. J., "Computational studies in tokamak equilibrium and transport", Ph.D Thesis, Rijksuniversitet Utrecht (1986)
[56] D. Reiter et al., J. Nucl. Mater. **196–198** (1992) 241

[57] R. Schneider et al., J. Nucl. Mater. **196–198** (1992) 810
[58] D. Stotler and C. F. F. Karney, Plasma Phys. **34** (1994) 392
[59] P. Stangeby et al., Proc. 28th European Phys. Soc. Conf. Plasma Phys. Cont. Fusion, Madeira, Portugal, June 18–22, 2001
[60] F. Scotti, "Impurity sources and transport modification due to lithium wall conditioning in NSTX", 54th American Physical Society Division of Plasma Physics meeting, Providence, RI, October, 2012.

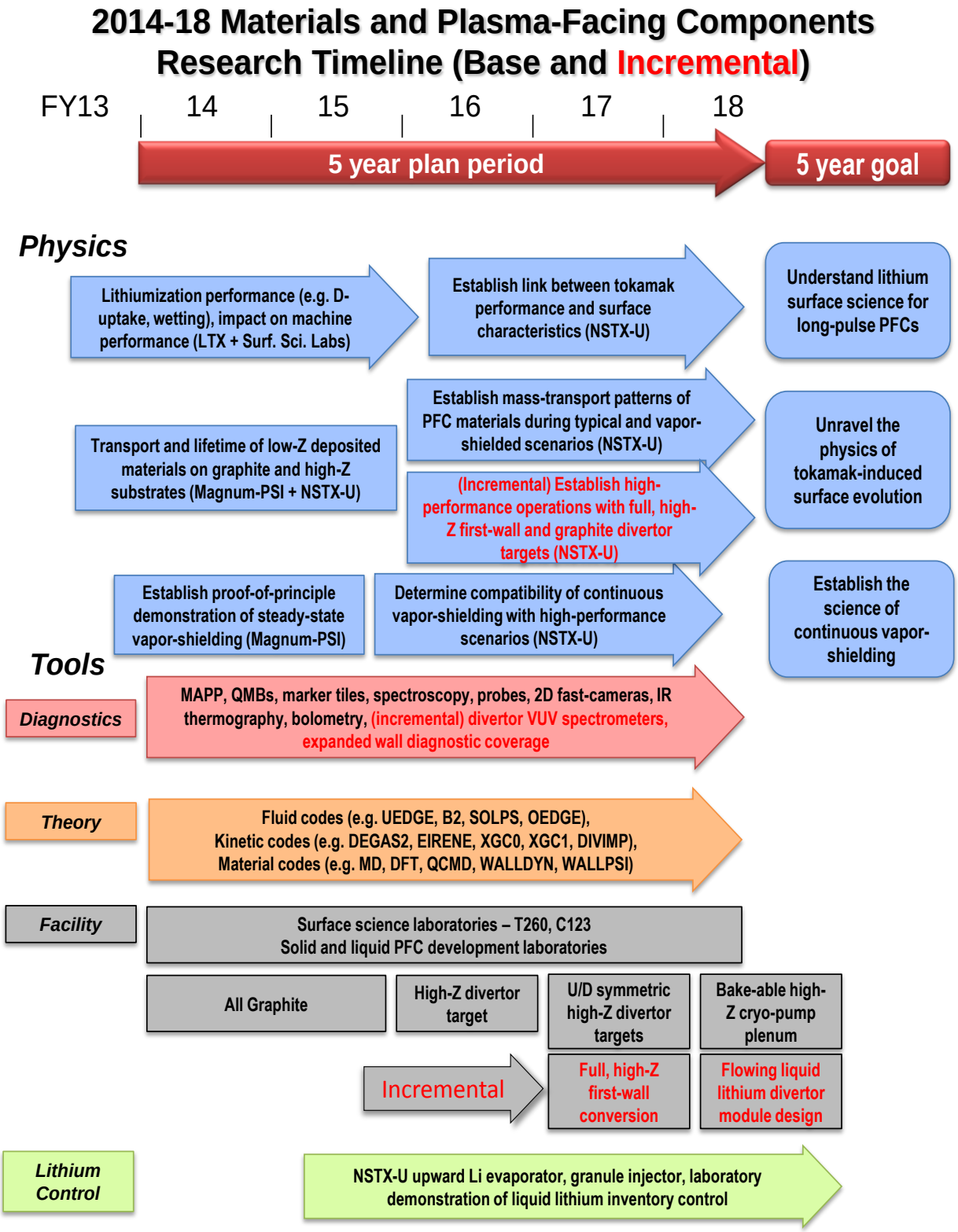
2014-18 Materials and Plasma-Facing Components Research Timeline (Base and Incremental)
FY13
14
15
16
17
18
5 year plan period
5 year goal
Physics
Lithiumization performance (e.g. D-uptake, wetting), impact on machine performance (LTX + Surf. Sci. Labs)
Establish link between tokamak performance and surface characteristics (NSTX-U)
Understand lithium surface science for long-pulse PFCs
Transport and lifetime of low-Z deposited materials on graphite and high-Z substrates (Magnum-PSI + NSTX-U)
Establish mass-transport patterns of PFC materials during typical and vapor-shielded scenarios (NSTX-U)
(Incremental) Establish high-performance operations with full, high-Z first-wall and graphite divertor targets (NSTX-U)
Unravel the physics of tokamak-induced surface evolution
Establish proof-of-principle demonstration of steady-state vapor-shielding (Magnum-PSI)
Determine compatibility of continuous vapor-shielding with high-performance scenarios (NSTX-U)
Establish the science of continuous vapor-shielding
Tools
Diagnostics
MAPP, QMBs, marker tiles, spectroscopy, probes, 2D fast-cameras, IR thermography, bolometry, (incremental) divertor VUV spectrometers, expanded wall diagnostic coverage
Theory
Fluid codes (e.g. UEDGE, B2, SOLPS, OEDGE),
Kinetic codes (e.g. DEGAS2, EIRENE, XGC0, XGC1, DIVIMP),
Material codes (e.g. MD, DFT, QCMD, WALLDYN, WALLPSI)
Facility
Surface science laboratories – T260, C123
Solid and liquid PFC development laboratories
All Graphite
High-Z divertor target
U/D symmetric high-Z divertor targets
Bake-able high-Z cryo-pump plenum
Incremental
Full, high-Z first-wall conversion
Flowing liquid lithium divertor module design
Lithium Control
NSTX-U upward Li evaporator, granule injector, laboratory demonstration of liquid lithium inventory control

Table of Contents for Chapter 6

Chapter 6

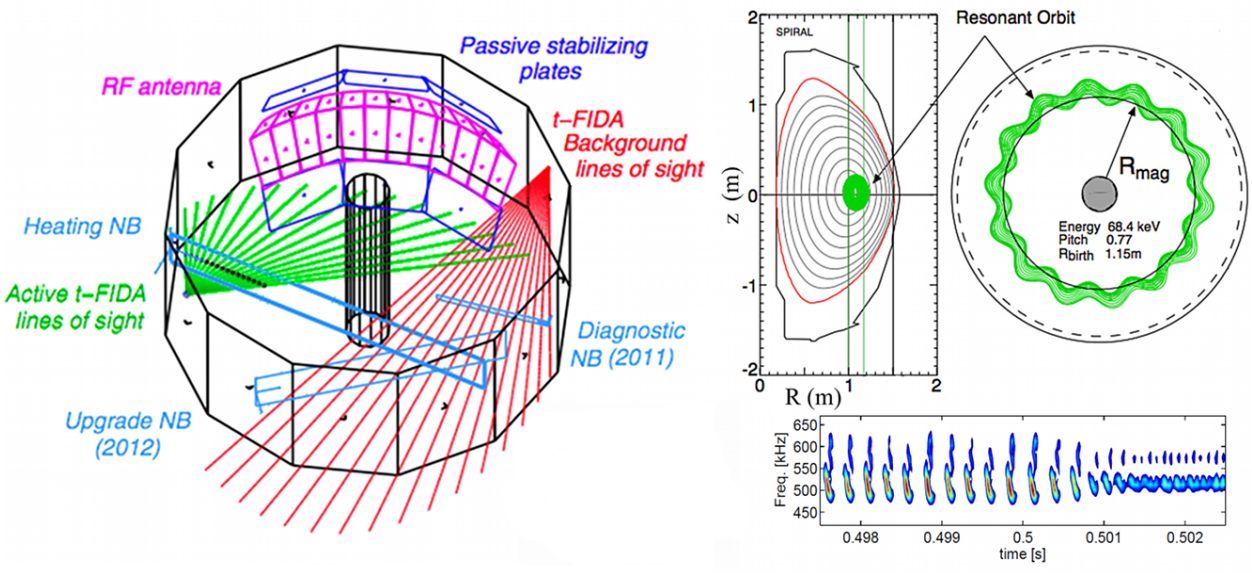

Research goals and plans for Energetic Particle Research

6.1 Introduction

The fundamental scientific goal of ITER is to generate plasmas dominated by self-heating and to understand the dynamics of the thermal and energetic plasma particles under such conditions. The relatively large population of energetic ions originates in fusion devices from fusion reactions (alpha particles), Neutral Beam (NB) injection and injected rf waves [1]. The resulting fast ion pressure can destabilize Alfvén Eigenmodes (AEs) and other fast ion driven instabilities (e.g. fishbones) that, in turn, affect the fast ion distribution through enhanced transport in space and energy [2][3]. This may cause unpredictable variations in the NB-driven current profile [4], loss of macroscopic stability [5] and degraded performance.

Of particular concern are fast ion related 'explosive' phenomena that occur on fast time scales, since no fast control tools are available (or envisioned) for their mitigation or suppression. Energetic Particle (EP) research is of paramount importance to understand the coupled and predominantly non-linear dynamics of fast ions and fast ion related instabilities, and eliminate or minimize their potential harm to a reliable exploitation of fusion energy. The challenge for present tokamaks is to provide the required physical basis to enable the development, verification and validation of predictive theoretical and numerical tools. NSTX-U will encompass an even broader parameter space than NSTX [6]. For instance, relevant NSTX-U parameter regimes for Energetic Particle research will more closely approach those expected for future devices such as ITER and a ST-FNSF, as shown in Fig. 6.1.1. The capability of spanning a much broader range of parameters for EP physics than conventional tokamaks represents an important advancement for extrapolations from today's experiments to burning plasma regimes, with significant contributions to the development of 100% non-inductive, steady-state scenarios and of NBI current ramp up schemes.

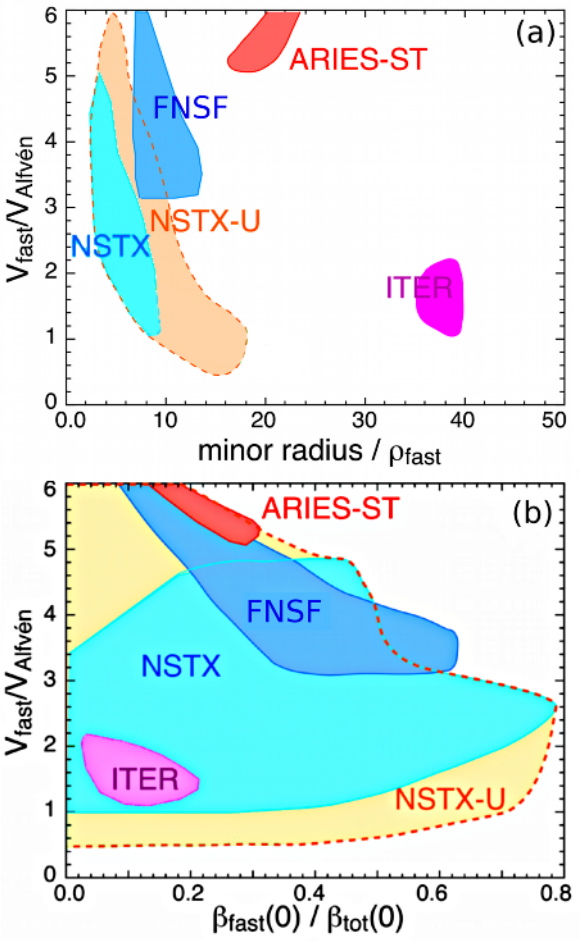

Figure 6.1.1: Representative parameters for Energetic Particles research for NSTX and NSTX-U in comparison with values for a ST-based FNSF and for ITER. (a) Ratio of fast ion to Alfvén velocity vs. inverse of the normalized fast ion Larmor radius. (b) Ratio of fast ion to Alfvén velocity vs. ratio of fast ion to total pressure. Fast ion parameters v_{fast} and ρ_{fast} are calculated at the NB injection energy.

EP research in the initial 5 years of NSTX-U operations will focus on two high-level goals that will directly contribute to developing predictive capability for FNSF, ITER and future devices. Firstly, experiments in the upgraded machine will aim at extensive validation of both linear and non-linear numerical codes and models, taking advantage of the upgraded NSTX-U diagnostic tools for stringent theory/experiment comparisons. This will enable projections of fast ion transport and AE dynamics from present experiments to scenarios relevant for FNSF, ITER and a ST-based Pilot device and provide guidance for further improvements in the design of future reactors.

Secondly, tools and techniques to affect AE and fast ion dynamics through selective excitation/suppression of fast ion-driven instabilities will be assessed. This requires a detailed knowledge of AE drive and damping mechanisms and of the fast ion response to different instabilities. Upgraded diagnostics (e.g. reflectometer arrays [7], beam-emission spectroscopy [8], fast-ion D-alpha spectrometers [9][10], neutral particle analyzers [11][12], and fusion product profile arrays [13]) are being developed to provide detailed measurements of the mode dynamics and of the properties of confined fast ions. The possibility of exploiting instabilities to optimize the NB-driven current profile or enhance the energy transfer from NB ions to thermal ions in a controlled way [14] will be explored. Development of schemes to regulate the electron thermal transport through high-frequency modes [15] will be also pursued. Neutral beam and rf injection are the primary actuators, possibly complemented by coils to induced magnetic perturbations at the plasma edge. For a more refined mode control, a dedicated *AE antenna system will be developed. The latter will be utilized to characterize the *AE stability properties and, pending upgrades of the driving amplifier to >10 kW power levels, to attempt excitation/stabilization of specific modes.

In the past years, NSTX experiments have considerably broadened and enriched the fusion science with respect to EP physics. Research on NSTX-U will further expand the knowledge acquired on NSTX of phenomena that are potentially harmful to ITER and burning plasmas, building upon a unique combination of broad and flexible parameter regime, excellent fast ion diagnostic suite and strong theoretical involvement.

The relatively low field and high current on NSTX, coupled with NB injection at energies up to 90 keV, implies a ratio of beam ion to Alfvén velocity in excess of 2, which is directly relevant for the regimes expected in ITER and FNSF, see Fig. 6.1.1. This, along with the large ratio of fast ion to total pressure, resulted in a broad spectrum of beam-driven instabilities (kinks, fishbones, Energetic Particle Modes and AEs in the sub-ion-cyclotron range of frequency). Therefore, virtually all NB-heated discharges in NSTX provided useful data on the modes' stability and non-linear physics (such as saturation amplitude and mode coupling). As an example, Toroidal Alfvén Eigenmodes (TAE) were found to develop non-linearly [16], as characterized by frequent, rapid bursts (*avalanches*) that resulted in redistribution and loss of fast ions [17][18][15]. There is compelling experimental evidence that TAE avalanches also cause a prompt redistribution of NB-driven current [4], see Fig. 6.1.2. Simulations with TRANSP using a *ad-hoc* time-dependent fast ion diffusivity to simulate enhanced redistribution at TAE bursts were able to reproduce the experimental neutron rate and current profile evolution. However, more recent simulations of fast ion redistribution using a combination of the NOVA/ORBIT codes indicate that the effect of TAEs on fast ions is more complicated than a simple enhancement of radial diffusion. In the presence of multiple modes characterized by different helicity, fast ions can be redistributed in energy as well as space, resulting in more complex

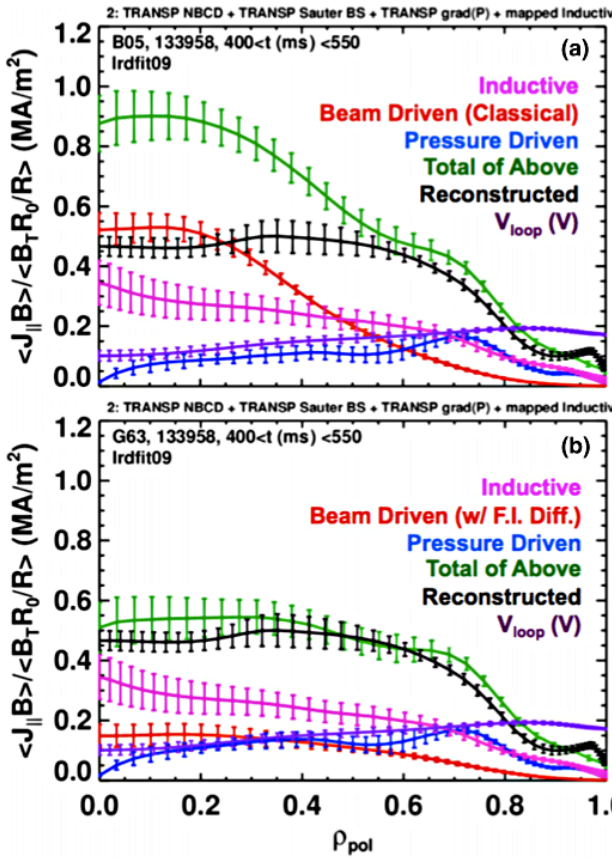

Figure 6.1.2: TRANSP calculations of the different terms contributing to the total plasma current on NSTX in the presence of TAE avalanches. Reconstructions are performed assuming (a) classical and (b) anomalous fast ion diffusion. (From Ref. [4]).

effects on NB-driven current. Research on NSTX-U, facilitated by the enhanced flexibility in NB injection geometries, will serve as guidance to incorporate our improved understanding of fast ion distribution modifications by TAEs into the TRANSP code for improved simulations of beam heating and current drive in the presence of AE instabilities. Moreover, this topic is of great relevance to address Thrusts ASC-1, ASC-2 and SFSU-2 of the FY14-18 NSTX-U 5-year plan on non-inductive scenario development and non-inductive current ramp up (cf. Secs. 9.1.2.1, 9.1.2.4 and 8.3.2).

Besides the characterization of known instabilities such as the Toroidal Alfvén Eigenmode [19][20][21], the investigation of new instabilities and new aspects of AE physics [22][23][24][25][26], as well as associated fast ion transport will be extended to the new regimes achievable in NSTX-U. For example, a broad spectrum of Global and Compressional Alfvén eigenmodes (GAE/CAE) was typically observed in NSTX at frequencies comparable to the ion-cyclotron frequency. Experimental evidence suggests that these modes redistributed fast ions and, possibly, affected electron thermal transport [23]. Progress has been made in simulating and understanding the complicated Doppler-shifted cyclotron resonance drive for counter-propagating CAE and GAE modes [25]. It seems plausible that the relatively low ratio of the cyclotron frequency to the transit frequency in NSTX facilitates this type of resonance drive. The higher field of NSTX-U will enable a thorough assessment of this hypothesis.

Another important area of research in NSTX-U will be the exploration of the possible coupling between different AE instabilities, which can further complicate the non-linear mode dynamic and its effect on the fast ion population. Transient destabilization of otherwise (linearly) stable modes through non-linear coupling [16] has been observed on NSTX. The non-linear saturation level of Alfvénic instabilities can also be affected by non-linear coupling. More generally, experiments on NSTX have indicated [19][21][25] non-linear coupling among TAEs,

GAE/CAEs and low-frequency MHD activity (kinks or tearing modes). The broad spectrum of Alfvénic activity on NSTX can potentially lead to direct interactions, through wave-wave coupling, as well as through indirect ones mediated by modifications of the fast ion distribution. In turn, the latter affects stability and saturation of energetic particle driven modes.

Section 6.2 presents an overview of the two major research thrusts on Energetic Particle research, including a summary of the research needed to support these thrusts. The research plans are described in detail in Section 6.3. Plans are divided into two periods, namely years 1-2 and years 3-5 of the 5-year plan. Summary timelines for each period are provided at the end of each Section. The planned theory/modeling capabilities and NSTX-U facility upgrades are described in Sections 6.4 and 6.5. A description of the main diagnostics that are relevant for EP studies is provided in Chapter 10 (see Section 10.6). Section 6.6 provides a summary timeline for the research goals and tools that are required for the Energetic Particles 5-year program on NSTX-U.

6.2 Overview of goals and plans

6.2.1 Research Thrust EP-1: Develop predictive tools for projections of *AE-induced fast ion transport in FNSF and ITER

Heating and some non-inductive current drive methods for next step magnetic fusion devices utilize non-thermalized (*e.g.* fast) ion populations whether as rf-tail ions, energetic neutral beam ions or fusion alphas. Instabilities driven by these fast ions, in particular Toroidal Alfvén Eigenmodes, can modify the expected heating and current drive profiles. Projecting which operational regimes will minimize these instabilities, or if necessary, predicting the effect of these modes on the fast ion population, is valuable for designing new devices and planning their operation (see also Chapter 9, Sec. 9.2.4). These predictions are made through the extrapolation of results obtained in present research devices to larger scale, fusion-grade reactors. The development and benchmarking of numerical codes based on experimental observations from existing experiments is therefore one of the most critical issues in fusion research.

A primary goal for the next 5 years of Energetic Particle research on NSTX-U is to develop capabilities that enable reliable and *quantitative* predictions on properties of, and fast ion response to, unstable modes in future devices such as ITER and FNSF. Good progress has been made in recent years in developing and validating tools to compute fast ion transport caused by a

given set of instabilities. However, self-consistent and reliable predictions of the modes' properties and of the modes' regime at saturation (e.g. stationary vs. bursting dynamics) still require extensive work from both experimentalists and theory/codes developers. Based on results from NSTX and other devices, modes that can induce substantial redistribution and loss of fast ions will be targeted first. These include TAEs, Reverse-Shear AEs (RSAEs) and Energetic-Particle modes (EPMs), as well as higher frequency *AEs (GAE/CAEs) that are responsible for deviations of the F_{nb} evolution from classical behavior.

This first thrust will be approached from two complementary directions, i.e. (i) study of the modes' properties (radial structure, frequency and wavenumber spectrum, stability) and (ii) characterization of the fast ion transport associated with specific classes of *AEs. In parallel with the experimental research on NSTX-U, the development of numerical and theoretical tools is required to lay the basis for predictive capability. Experimental results will be utilized for extensive code verification and validation, based on the detailed characterization of instabilities and fast ion distribution available on NSTX-U from the upgraded set of fast ion diagnostics.

6.2.2 Research Thrust EP-2: Assess requirements for *fast-ion phase-space engineering* techniques

So-called Phase-Space Engineering (PSE) consists in controlled, externally-induced modifications of the fast ion distribution in order to achieve specific goals such as performance improvement or enhanced stability. PSE is being discussed over several years (including its application to NSTX scenarios) as a potential technique for *AE control, stochastic ion heating [27], alpha-channeling [28][29][14] and stabilization/regulation of sawtooth [30] and other MHD modes (e.g. NTMs), among other possibilities. More specifically, the longer-term PSE objective that requires dedicated research on NSTX-U is the development of schemes for direct *AE control. Experiments will aim at developing tools to *control* AE activity in NSTX-U and *exploit* instabilities as an additional actuator to modify, in a controlled way, the evolution of fast ion radial profile and energy spectrum. A parallel line of research is the regulation of electron thermal transport through high-frequency AEs.

The development of PSE methods on NSTX-U is foreseen to assess these issues. The proposed PSE plan takes advantage of a unique combination of tools that can alter the fast ion distribution (hence the *AE stability), such as NB sources with different tangency radii, the High-Harmonic Fast Wave (HHFW) rf heating system and additional coils to induced controlled magnetic perturbations. The latter include a set of Magnetic Perturbations (MP) coils, a new set of non-axisymmetric control coils (NCC) proposed for the FY14-18 period and a newly developed *AE

antenna system operating at higher frequency (f>>1 kHz). Pending incremental resources and based on the capability of the *AE antenna to detect modes, further progress in exploring *AE control schemes will be achieved through an upgrade of the *AE detection system. The upgrade would enable the real-time detection of marginally stable (via excitation from the *AE antenna) and unstable modes, thus providing the required information to the Plasma Control System (PCS) to implement active control schemes during a discharge, for instance by utilizing different NB injection parameters, MP/NCC coils, rf injection or the *AE antenna itself.
If successful, PSE will help NSTX-U (and PPPL) to maintain a leadership position in the EP physics within the fusion community, both nationally and internationally. It will also help to control the TAE and other Alfvénic instabilities in a reactor by bypassing the thresholds imposed by thermonuclear instabilities, which is an important (and often under-estimated) issue for devices such as ITER, FNSF and future Pilot plants.

Detailed knowledge of the stability properties of AEs, including damping and drive mechanisms, is of paramount importance for PSE research (and EP studies, in general) in order to assess which modes can be more effectively affected by external means. Although theoretical understanding has made good progress in the past years to understand and model specific damping mechanisms for AEs in conventional aspect ratio devices, the applicability of those models to STs is still debated and requires more detailed comparison between theory and experiments. Active spectroscopy experiments planned for NSTX-U, similar to those previously carried out on JET, C-Mod and (more recently) MAST, will provide direct information of linear *AE damping rates for further benchmarking of stability codes at low aspect ratio. This would also help to validate ITER/FNSF projections by challenging our fundamental understanding of the physics underlying the drive and stability mechanisms of AE modes.

In the lower portion of the *AE frequency range, TAE linear damping rates have been measured on the C-Mod and JET tokamak experiments [31] with the goal of benchmarking codes used to project TAE stability to ITER relevant regimes. Linear damping rates are inferred by exciting stable modes with an antenna and by computing the resonance width from the complex impedance modeling the driven plasma response [32]. Next step Spherical Tokamaks will operate in a different fast ion parameter regime, which also implies different properties of potentially unstable modes such as their radial structure. It is therefore necessary to extend the previous benchmarking activity to encompass a broader range of scenarios and different classes of *AE instabilities. For example, the much stronger magnetic shear at the plasma edge (found to be stabilizing in triangularity scans on JET) and the relatively stronger rotational shear, resulting in enhanced continuum interactions, are predicted to affect TAE stability in STs.

Looking beyond the lower frequency TAE modes, higher frequency Alfvénic instabilities are routinely observed in START [33], MAST [34][35] and NSTX [25][36][37] NB-heated plasmas.

These instabilities clearly have the potential to affect the fast ion distribution, although direct experimental evidence of the extent of the perturbations is weak at present. Reliance on fast ions to destabilize the natural eigenmodes of Compressional and Global Alfvén waves (CAE and GAE) reveals only a limited subset of the eigenmode spectrum. Extending the bandwidth of external antennae to study these modes will provide valuable information in the development of our theoretical understanding of these instabilities. Ultimately, the higher frequency of GAE/CAE modes, together with the possibility of cyclotron resonances, may provide an attractive route towards controlled modifications of the non-thermal ion distribution function and its dynamic [28]. The latter scheme would enable a more efficient transfer (or *channeling*) of fast ion energy to the thermal ions. Because the transfer is mediated by instabilities, it happens on time-scales much faster than the typical slowing-down time, thus lowering the overall fast ion pressure. At constant total pressure (e.g. limited by macroscopic stability considerations), this implies that a reactor could achieve a larger thermal ion pressure via an increase of the ion temperature, which is indeed beneficial to enhance the thermonuclear fusion reactivity.

The outcome from PSE research on NSTX-U will be evaluated, possibly in conjunction with results from other devices such as DIII-D, MAST and JET, to assess the feasibility and potential of PSE schemes on future devices. The assessment will be done in terms of efficiency of the different systems (e.g. NB vs. rf or other coils/antenna types), required power and - for rf/*AE antennae and MP/NCC coils - excited spectrum, temporal response, time-scales for diagnostics and control. Extrapolations to future devices, such as a ST-based FNSF/Pilot and ITER, will provide information on achievable performance improvement, for instance through the implementation of alpha-channeling schemes.

6.2.3 Research needed to enable EP Research Thrusts

6.2.3.1 Investigate *AE dynamics and associated fast ion transport mechanisms

Although many aspects of the dynamics of Alfvénic instabilities are known from today's experiments, extrapolations to future burning plasma scenarios require an even deeper understanding of instability drive and damping mechanisms. Even assuming that present stability codes can predict the spectrum of unstable modes for a given set of experimental parameters, the complex mode dynamics observed in the experiments is still hardly recovered. For example, the mechanisms that cause the development of a TAE bursting/chirping regime are still debated, and so are the exact causes of TAE avalanches. In particular, non-linear effects need to be understood

to predict mode saturation level and the effects of disparate classes of modes, including their possible coupling, on fast ion redistribution and transport.

Validation of linear theories on mode stability is required before approaching the non-linear physics aspects. This is especially true for spherical tori such as NSTX-U, for which the large plasma beta, the large rotation, the small aspect ratio and the large gradients in the equilibrium profiles (including the magnetic field and the safety factor profile) clearly pose a challenge for theories and numerical codes. Development of MHD spectroscopy tools, such as a dedicated *AE antenna system, is planned to measure the damping rate of *AEs and provide the data required for a detailed theory/experiment comparison.

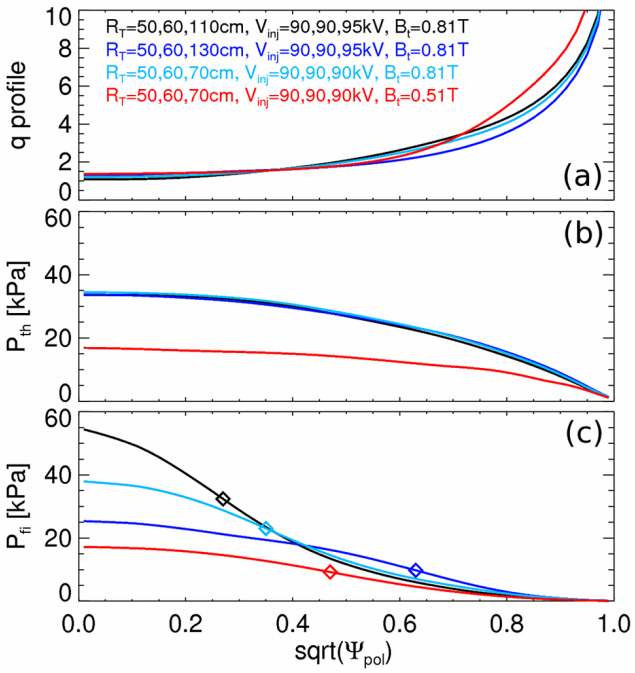

*Figure 6.2.1: Examples of profiles corresponding to different NB injection schemes utilizing sources with different tangency radius. The reference profiles, corresponding to a NSTX H-mode discharge with B_t=0.5 T, are shown in red for comparison. Shown are (a) q-profile, (b) thermal plasma pressure and (c) fast ion pressure. Diamonds indicate the radius of steepest fast ion pressure gradient, where *AE drive is expected to be stronger. Profiles are calculated by TRANSP.*

Ultimately, non-linear mode dynamics will dominate EP physics in burning plasmas, because of its role in affecting mode saturation amplitudes and the mode regime (e.g. stationary vs. bursting mode activity). Saturation mechanisms and non-linear physics (e.g. mode-mode coupling, coupling and interactions between different classes of MHD instabilities) will be investigated in NSTX-U as a function of plasma and NB/rf heating parameters. The latter have large influence on the fast ion distribution function. Future reactors will operate with distribution functions that are considerably different than in today's devices, for instance because of the additional presence of alpha particles from fusion reactions. Therefore, the dependence of stability and saturation of *AEs on the fast ion distribution function will be studied in detail, and the results compared with code predictions to validate our understanding of the drive mechanisms for various distributions. Because of its relevance and broad scope, it is anticipated that this line of research will encompass multiple Topical Science Groups, including Energetic Particle, Macroscopic Stability and Advanced Scenarios & Control groups.

The enhanced flexibility of NSTX-U in terms of NB injection geometry provides a powerful tool to vary F_{nb} in a systematic way, as shown in Fig. 6.2.1. NB injection energy and power scans are

also possible, in order to vary the ratio of fast ion to Alfvén velocity and of relative fast ion beta. The dependence of resonant drive for the different *AEs on those parameters will be investigated, along with the effects of the q-profile on the mode's location and stability. The higher toroidal field of NSTX-U is another important parameter to understand the scaling of unstable spectrum and mode stability toward high-field devices such as a ST-based FNSF and ITER.

Existing (or upgraded) and new diagnostics will be utilized to gather the required information for a meaningful and accurate comparison. The new "tangential" FIDA and fusion product profile systems, along with an upgraded ssNPA and the existing NPA and neutron rate counters, will provide complementary measurements of different phase space portions of the fast ion distribution. Upgraded reflectometer and BES arrays will be available to measure the mode structure. Mirnov coils will provide mode frequency evolution and mode number information.

6.2.3.2 Compare experimental results with theory & numerical codes

Verification & Validation of numerical codes are fundamental steps to enable predictive capabilities. Theory-experiment comparisons on EP-related topics are planned in order of complexity for NSTX-U scenarios. Initial comparison with predictions from numerical codes will be performed in terms of radial structure and frequency of the observed (unstable) modes. Then, the comparison will be extended to the mode dynamics, including saturation level and quasi-stationary vs. bursting regime. The final step will be the full simulation of non-linear *AE mode physics, including for example multi-mode scenarios and mode-mode coupling phenomena. The ultimate goal is to develop and validate self-consistent (non-linear) models to predict how *AEs affect the fast ion population for the complex F_{nb} in a fusion plasma and, in turn, how the modified fast ion distribution affect the *AE dynamics. This is a critical R&D issue for ITER, which can be addressed on NSTX-U based on the great flexibility in NB injection parameters, complemented by rf injection, to explore a broad range of fast ion distributions.

A detailed knowledge of the fast ion distribution function is required for accurate theory-experiment comparison. Good progress has been made in experiments to cover extended regions of phase space, for instance by using different viewing geometries for the same spatial region or comparing results from diagnostics with complementary phase space selectivity. Similarly, a realistic model for F_{nb} is needed in simulation codes to capture the *nuances* of wave-particle interaction in phase space. In fact, whereas a simple slowing-down distribution may be suitable to represent the distribution of fusion-born alphas, it appears as an over-simplification for fast ions originating from NB injection with specific values of pitch and energy. The picture is

further complicated by the fact that the injected energy spectrum for a specific NB system typically includes at least three energy components, whose relative fraction depends (among other parameters defining the NB working point) on the injection energy. Codes that are designed to predict the full, non-linear mode dynamics (e.g. M3D-K and HYM) will therefore be upgraded to include a realistic description for F_{nb}, such as the one computed by the NUBEAM [38] module in TRANSP [39].

Another important feature for numerical codes that aim at modeling the non-linear aspects of F_{nb} evolution is the inclusion of source and sink terms. Linear stability can be studied by following the initial mode's growth for a short time, typically of the order of a few milliseconds or less, over which classical mechanisms (scattering, slowing-down) have little effect on the fast ion distribution. As the modes grow in amplitude and, possibly, saturate in a non-linear phase, the mutual interaction between instabilities and fast ions becomes important. Mode-induced fast ion transport (in both configuration and phase space) competes then with restoring sources (NBI injection) and other transport mechanisms (radial diffusion, scattering and slowing-down), which makes the details of source and sink terms relevant to reproduce the experimental observations.

A number of numerical codes are already being used to simulate NSTX scenarios and their use will be naturally extended to NSTX-U discharges. In particular, a summary of the main capabilities and planned improvements for the numerical tools directly developed (or under development) by NSTX-U researchers and collaborators is provided in Section 6.4 and summarized in Table 6.4.1 at the end of this Chapter. Besides NB injection, HHFW injection is also known to induce modifications of the fast ion distribution [40][41]. Plans and numerical tools that will be available for HHFW research on NSTX-U are described in detail in Chapter 7.

In addition to the codes directly available at PPPL, NSTX-U results will be available for comparison with simulations performed by other groups, both nationally and internationally. For example, initial comparisons between NSTX data on chirping TAE modes and predictions from the gyrokinetic code GTC have started and will be further pursued once NSTX-U begins operations. Other gyrokinetic codes (e.g. GYRO and GEM) will also be considered for Verification & Validation, based on the unique *AE regimes attainable on NSTX-U and STs in general.

6.2.3.3 Develop reduced physics-based models for *AE-induced fast ion transport

Dedicated ("first-principles") codes for comprehensive simulations of MHD instabilities and fast ion dynamics are indispensable tools for EP research. However, their use is somewhat limited in terms of potential users and routine application to a large number of discharges. Energetic Particle research in the next 5 years is required to fill in the gap between dedicated codes and

general, multi-purpose transport simulation codes such as TRANSP [39]. This will make available more detailed information on modifications of F_{nb} by MHD that, in turn, can be used to infer MHD effects on background plasma and fast particles. For instance, more accurate and reliable calculations of NB-driven current would be possible, as required for scenario development and predictions in devices with large NB current drive and central fast ion pressure (cf. Chapter 9, Secs. 9.1.2.1 and 9.1.2.4). Extended comparison of TRANSP analysis and simulations with experimental results will be also enabled by the combination of improved F_{nb} measurements and simulations for a broad range of experimental conditions. To accomplish this goal, knowledge of the transport mechanisms must be translated into *reduced* models that are suitable for inclusion in TRANSP but - at the same time - retain the essential physics of fast ion transport.

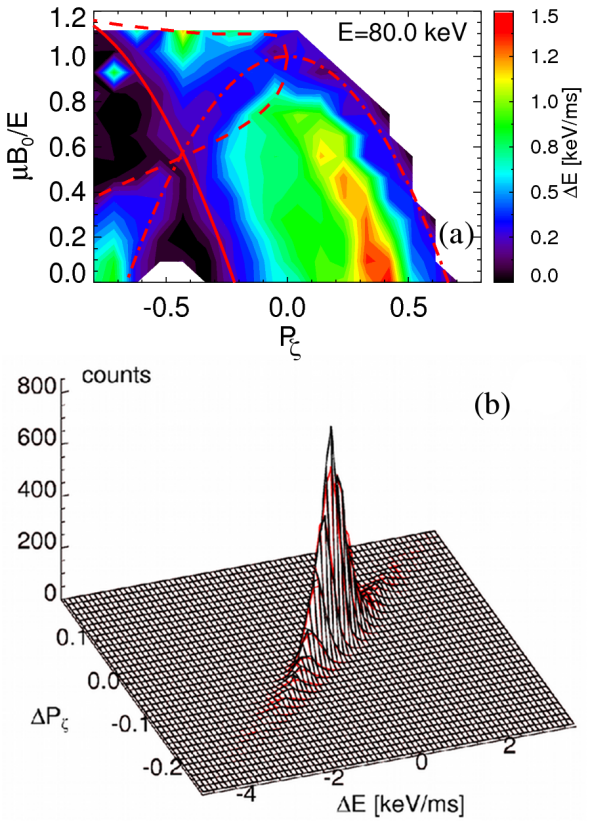

Figure 6.2.2: (a) ORBIT calculations of the average energy step caused by 4 TAE modes after 1 ms for fast ions with initial energy of 80 keV. Red lines show the different domains in phase space. (b) Example of probability distribution for correlated steps in energy and canonical toroidal momentum for E=80 keV, P_ζ~0.5 and pitch ~0.2.

Several fast ion transport models are already implemented in the NUBEAM module of TRANSP. However - as of today - a main limitation is the over-simplified description of *resonant* and *stochastic* transport mechanisms that affect fast ion dynamics primarily in phase space, as opposed to configuration space. New models are therefore required to complement the diffusive/convective radial transport models that are already available. To understand the importance of phase space dynamics in regulating macroscopic fast ion transport and redistribution, it suffices to observe that *AE modes with comparable spatial localization and amplitude, but different frequency and/or polarization, can have very different effects on fast ions. Whereas high-frequency CAE/GAE modes can induce energy and pitch variations with relatively small radial transport, lower frequency TAEs (and EPMs) are much more effective in causing radial redistribution and, eventually, loss from the main plasma. These differences are not correctly captured by standard radial diffusion, as they mostly arise from the details of resonant wave-particle interactions in phase space. Moreover, the same type of interaction set

constraints between phase space variables like energy and canonical angular momentum that are lost in the radial diffusive models.

Two approaches to develop reduced fast ion transport models are currently being pursued by NSTX-U researchers, cf. Secs. 6.4.7 and 6.4.8. A first approach is based on results from combined modeling of fast ion response to a given set of *AE modes or other low frequency MHD modes (kinks, NTMs) through the NOVA-K and ORBIT codes [24]. The initial development is focusing on TAEs and TAE avalanches, but the model is general enough to treat various classes of instabilities. From ORBIT simulations, a probability distribution function, $p(\Delta E, \Delta P_\zeta, \Delta\mu)$, is derived for the expected "kicks" in phase space variables over a certain time as a function of mode amplitude, see example in Fig. 6.2.2. (Variables are energy E, canonical angular momentum P_ζ and pitch μ). This information will be used in NUBEAM/TRANSP to advance the fast ion distribution at each simulation step. (Note that other codes, for example SPIRAL, can also be used to generate $p(\Delta E, \Delta P_\zeta, \Delta\mu)$). In its initial formulation, the model will be suitable for simulations of real discharges, for which information on mode properties (frequency, radial structure, amplitude evolution) is available. More work is required to *predict* the F_{nb} evolution for future devices. Research on NSTX-U will permit to consolidate our understanding of *AE behavior under different plasma conditions, especially at higher magnetic field and with different NB injection geometries.

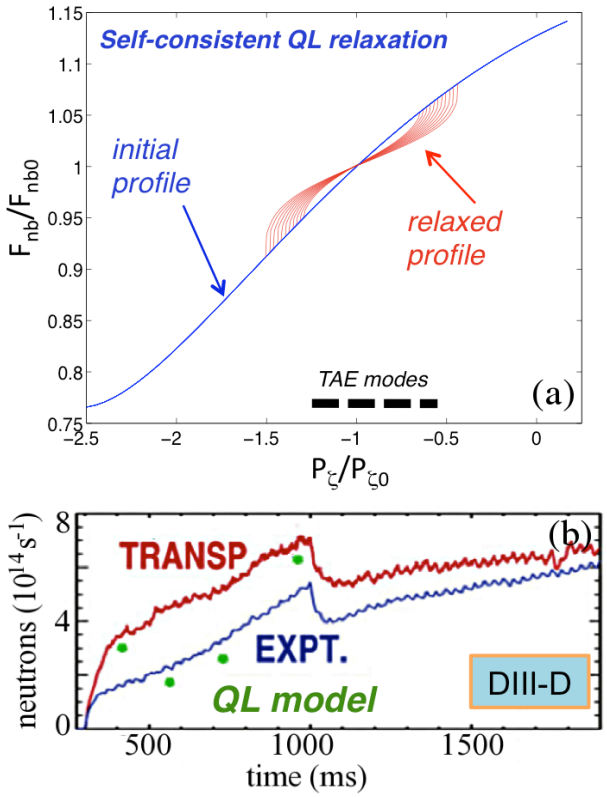

Figure 6.2.3: (a) Schematic of quasi-linear relaxation process showing partial flattening of Fnb in the presence of TAE modes. (b) Initial comparison of neutron rate from the QL model with DIII-D data and TRANSP predictions. (Adapted from Ref. [42]).

A second approach is based on recent improvements of the so-called "quasi-linear" (QL) model to incorporate the effects of resonance line broadening and multi-mode scenarios [42]. The QL theory models the effect of TAE modes on the fast ion distribution by retaining second order perturbations in Vlasov's equation to compute the relaxed F_{nb} radial profile. The model is self-consistent, in that the mode amplitude evolves at the instantaneous linear rate derived from the distribution function itself (Fig. 6.2.3). The model is presently being tested on DIII-D scenarios and extended to ITER predictions. After the validation phase, it will be tested against NSTX

scenarios with TAE-induced fast ion transport and then to predicted NSTX-U scenarios. Its implementation in NUBEAM/TRANSP is foreseen for general use.

6.2.3.4 Assess modifications of *AE dynamics using externally-controllable *actuators*

Future reactors will operate with a mix of additional heating schemes, including NB and rf injection, whose effects combine with those from fusion reactions (i.e. the generation of alpha particles) to define the actual F_{nb}. Our present understanding of the relationship between the expected F_{nb} and possibly deleterious *AE instabilities must progress by including the new scenarios that will be achievable on NSTX-U. Moreover, EP research needs to develop schemes to affect the instabilities and reduce their impact on the successful exploitation of fusion reactors. This long-term goal requires accurate measurements of plasma profiles, of the evolution of F_{nb} and of the instabilities, along with improved theories and modeling of their mutual interactions.

Establishing the link between plasma equilibrium profiles (e.g. q-profile), NB injection parameters (geometry, injection energy) and *AE activity is the first priority and will already provide indications on possible NB injection schemes that minimize (or suppress) *AE activity. An example of NSTX-U profiles predicted by TRANSP for different choice of NB injection geometry is illustrated in Fig. 6.2.1(c), showing the broad range of variations in fast ion pressure for comparable NSTX-U thermal pressure profiles that will be achievable for a similar q-profile.

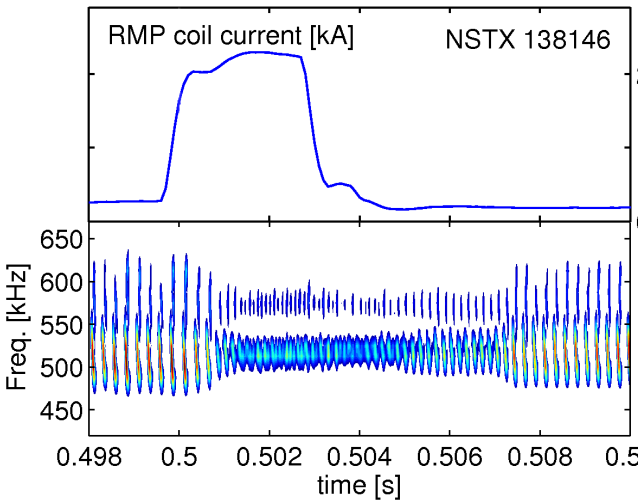

Figure 6.2.4: Modification of GAE dynamic on NSTX through pulses of Magnetic Perturbations with n=3. (Adapted from Ref. [44]).

Scenarios with combined NB and rf injection will then be studied. Based on NSTX experiments, F_{nb} modifications by HHFW injection include both direct acceleration of fast ions and more subtle redistribution in phase space. For example, early NSTX experiments have shown some evidence of modified behavior of "Angelfish" modes (i.e. high-frequency *AEs in the CAE/GAE range of frequency) during HHFW injection [43]. A few examples of HHFW affecting TAE/RSAE stability in NB-heated plasmas have been occasionally collected from NSTX experiments [21]. The new scenarios of NSTX-U require new experiments in the next 5-year

period for further studies of the instability's response to combined NB and HHFW injection, as described in Sec. 6.3.3.4 and Chapter 7, Sec. 7.1.3.1.

A third tool that will be available on NSTX-U is represented by the set of external mid-plane error-field correction and resistive wall mode coils that can be used to apply magnetic perturbations (MP) with a range of toroidal mode numbers (see Chapter 2 for more details). Modification of the behavior of GAE modes from bursting to more stationary has been observed on NSTX during short (2-6 ms), static MP pulses with $n=3$ configuration [44], see Fig. 6.2.4. Initial analysis indicates that the modification in mode activity is caused by a perturbation of the fast ion orbits that resonate with GAEs. Research on NSTX-U will explore this avenue in more detail, exploiting the enhanced flexibility of the MP power supplies control to vary the spectrum and the amplitude of the excited perturbation. The installation after FY16 of *internal and off-midplane* Non-axisymmetric Control Coils (NCC) represents a further, important improvement to study *AE response to applied 3D fields.

Besides the exploitation of NB/rf injection and of MP coils, the development of more refined PSE techniques is envisioned. Two main tasks are foreseen in the 5-year time period FY14-18. The first task is the development, optimization and installation of the required hardware (e.g. an *AE antenna system with frequency and wave-number scanning capabilities). A system comprising up to 4 modules, whose design is based on the prototype antenna that was installed in-vessel for the FY12 Run, will be tested during the first year of NSTX-U operations. Because of the low-power amplifier (~1-5 kW) initially available to drive the antenna, only small perturbations with $\delta B/B \leq 10^{-5}$ will be excited at the plasma edge. Therefore, this prototype system will mainly be used for *AE stability measurements and to provide damping rate data to challenge present theories on *AE damping mechanisms in STs.

Based on the available resources, upgrades/improvements will be implemented in the following years. Improvements of the *AE antenna modules design will be considered to optimize the coupling to *AEs with specific polarization. The diagnostics associated with the antenna system will be upgraded to enable real-time detection of the modes driven by the antenna, and using that information to implement a closed-loop control of the antenna frequency during a discharge. Finally, a high-power amplifier capable of delivering up to 100 kW of power will be used as driver for the *AE antenna modules. Pending the completion of these upgrades, the second task is the experimental assessment of *AE control schemes, that include single-mode entrainment and regulation, multi-mode synchronization/control via three-wave coupling mediated by the external perturbation, and mock-up of so-called *alpha-channeling* processes with fast ions from neutral beam injection (NBI).

6.3 Research Plans

6.3.1 Research Plans for Thrust EP-1: Year 1-2

6.3.1.1 Compare classical TRANSP predictions to experiments for 1st+2nd NB line

One of the major new features on NSTX-U is the addition of a second NB line with more tangential injection than the line already available on NSTX. The first task for EP-related research is to compare experimental results to standard numerical tools that model NBI, namely the NUBEAM module in TRANSP, which is a pre-requisite for all subsequent studies of fast ion confinement in the presence of MHD and other instabilities. Conditions with quiescent MHD activity during NB injection will be explored to assess the consistency of (classical) calculations of fast ion confinement and slowing down processes obtained through NUBEAM with measurements. The comparison will be conducted in terms of direct measurements (e.g. of fast ion distribution function, neutron rate and prompt fast ion losses) as well as derived quantities such as NB-driven current profile. Different NB injection geometries, from more perpendicular to more tangential, will be investigated. Similar to earlier experiments on NSTX that confirmed the validity of classical predictions for beam ion confinement and slowing-down models [45] for "diluted" fast ion populations, scans of plasma current and toroidal field will be performed. For this study, conditions for which MHD activity is minimized or absent will be initially used. For instance, well-established techniques based on the neutron rate evolution following short pulses (*blips*) of NB power [45][46] are envisioned (see example in Fig. 6.3.1).

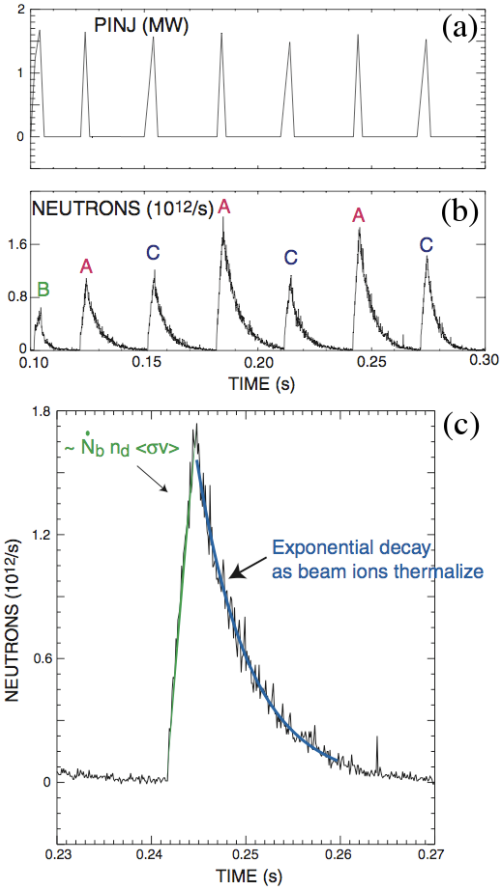

Figure 6.3.1: Example of fast ion confinement study utilizing (a) short NB blips and (b) neutron rate measurements. (c) Data on characteristic rise/decay times are then compared with TRANSP predictions to assess the validity of classical fast ion confinement. (From Ref. [45]).

In addition to EP-related research, the characterization of fast ion properties from NB injection has a broader scope in the NSTX-U research program. In particular, it is also crucial for research on non-inductive scenarios and current ramp-up, cf. Chapters 8 and 9.

In collaboration with the ASC group, the assessment of conditions for classical vs. anomalous fast ion behavior and NB current drive will be extended to high-performance H-mode discharges that are relevant for scenario development and projections to future STs (Thrusts ASC-1 and ASC-4). Scans of plasma current (0.6-1.5MA) and NB power (up to ~12MW) are planned for discharges near the full 1T toroidal field after Year 2 of NSTX-U operation. NB injection voltage will be varied from its maximum value of 100 kV, required to maximize the NB-driven current level, to the 80 kV level required for long pulse duration >5 s. Finally, the possibility of exploiting anomalous fast ion diffusion for scenario optimization, for example to sustain an elevated q_{min} (see details in Sec. 9.2.4), will be explored in later years (Year 3-4).

The EP group will also contribute to the development of non-inductive current ramp-up schemes (Thrust SFSU-2) led by the Solenoid-Free Plasma Start-Up (SFSU) and the WH&CD groups. The goal is to ramp up a 300-400 kA plasma with zero loop voltage up to the 1 MA current level by using a combination of NB-driven and bootstrap current (Sec. 8.6.4). The EP group will focus on the study of fast ion behavior during the ramp up process and on the comparison with TRANSP/NUBEAM predictions. Experiments will indicate the minimum required current that can be ramped up by NB-CD for B_t=0.8-1 T, as well as the optimum NB injection geometry and the requirements on fast ion confinement, for example as a function of toroidal field.

In addition to supporting EP research, scenario development and non-inductive current ramp-up studies, this study will also provide information on more specific issues that are relevant for modeling and interpretation of experimental data. For instance, conservation of magnetic moment of fast ions is debated in spherical tokamaks [47][48] because of the large fast ion gyro-radius compared to the typical scale-length of the background magnetic field. The flexibility of NSTX-U to operate with toroidal field in the range 0.35-1 T provides an excellent opportunity to explore a broad range of conditions in terms of ratio between gyro-radius and gradient scale-length. Conservation of magnetic moment can thus be assessed and quantified through comparison with predictions from the ORBIT and SPIRAL codes, and the most suited codes identified for future studies.

Measurements will exploit the upgraded suite of fast ion diagnostics that will be available on NSTX-U, a summary of which is given in Chapter 10, Section 10.6. Two Fast-ion D-alpha (FIDA, see Fig. 6.3.2) systems [49][50] and an upgraded solid-state Neutral Particle Analyzer (ssNPA) array [51] will provide fast ion radial profile and its temporal evolution with 5 cm, 10 ms spatial and temporal resolution. After the first year of NSTX-U operation, spectral

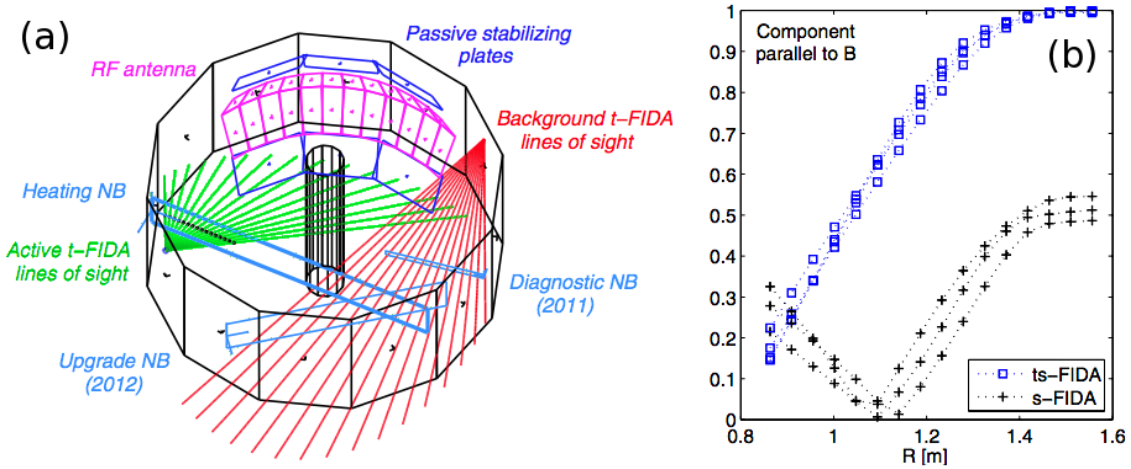

Figure 6.3.2: (a) Layout of the new tangential FIDA system. (b) Expected component parallel to the magnetic field for the tangential (ts-FIDA) and vertical (s-FIDA) FIDA systems. A value of 1 (0) on the y axis corresponds to a parallel (perpendicular) view. (From Ref. [50]).

information from the FIDA systems will be complemented by more accurate energy spectra at one fixed location from the re-located E||B Neutral Particle Analyzer (NPA) [52].

A novel charged fusion products array [53] will complement FIDA and ssNPA data after Year 2 (FY15) by providing space-resolved information, in addition to the volume-integrated data from neutron counters. Pending incremental funding, the latter will eventually be complemented by a set of 2-4 collimated neutron detectors in Years 4-5. It should be noted that fusion products and neutron diagnostics do not rely on charge-exchange, as is the case for FIDA and neutral particle analyzers. Therefore, they maintain good performance even at the high densities ($>10^{20}$ m^{-3}) characterizing some of the projected NSTX-U regimes.

Internal measurements from the diagnostics mentioned above will be compared to energy and pitch resolved measurements from a scintillator-based Fast Loss Ion Probe (sFLIP) that measures fast ions lost to the outer vessel wall at mid-plane [54]. The combination of data from both confined and lost fast ions will give a detailed picture of fast ion dynamics as a function of NB injection parameters and plasma discharge conditions. This information can then be compared with predictions from numerical simulation codes to assess the consistency of measurements with models based on classical fast ion dynamics.

6.3.1.2 Characterize *AE activity driven by more tangential 2nd NBI and associated fast ion transport

Starting from the characterization of reference scenarios with quiescent MHD activity, previous research on *AE physics will resume by investigating *AE activity for the broader operating

space of NSTX-U. A nearly twofold increase in toroidal field, from 0.4-0.45 T for typical NSTX plasmas up to ~0.8 T, is anticipated for the first year of NSTX-U operations. Based on the maximization of wave-particle interaction for values $k_\perp \rho_{fi} \sim 1$ ($k_\perp \sim nq/a$ is the poloidal wave vector, $\rho_{fi} \sim v_f/\omega_{ci}$ the fast ion gyro-radius, a the minor radius and v_f the fast ion velocity), an up-shift of the wave-number spectrum roughly proportional to B_t is expected [55]. However, other considerations about improved confinement of both thermal and fast ion species, along with F_{nb} modifications caused by the 2nd NB line, may affect drive and damping of *AEs in more subtle ways. A detailed characterization of *AE modes over their entire spectral range (from 10's of kHz up to the ion cyclotron frequency) is therefore required, see Sec. 6.3.1.3.

Characterization of *AE and other MHD instabilities will proceed in parallel with the study of their effects on fast ion transport. Fast ion profile diagnostics (FIDA, ssNPA and fusion product array) are used to infer macroscopic modifications of the radial fast ion profile caused by the modes. Broadening and flattening of the profile will be correlated with change in the NB-driven current profile. The resulting change in macroscopic stability for low-frequency MHD modes (kinks, NTMs) is also investigated, in collaboration with the Macro-Stability Topical Science Group.

The possibly different effects on fast ions with different energy and pitch (e.g. passing vs. trapped particles) are inferred from diagnostics with complementary sensitivity in phase space, such as the perpendicular and tangential FIDA systems (Fig. 6.3.2). More precise information on energy and pitch evolution is available from the E//B NPA diagnostic, whose excellent energy resolution is required to investigate subtle changes in F_{nb} induced by instabilities.

6.3.1.3 Compare measured *AE properties to predictions performed in FY12-14

In order to develop a predictive capability for the effects of fast ion driven modes on the plasma, validation of theory is critical. A key ingredient of this is the measurement of mode structure and amplitude. NSTX-U will feature multiple diagnostics with complementary capabilities for measuring the structure and amplitude of fast ion driven modes. For instance, UW Madison's multi-channel Beam Emission Spectroscopy (BES) system [8] will feature 48 channels in the FY14/FY15 time-frame and then later be expanded to 56 channels, which is a significant improvement over the 16 channels that were available on NSTX. The BES system will be capable of density fluctuation measurements over a vertically (ΔZ > ~20 cm) and radially (r/a > 0.1) distributed matrix of locations. In addition to density fluctuations, it will permit time-delay estimation of poloidal flow velocity fluctuations from poloidally-distributed measurements of the density fluctuations.

NSTX-U will also feature UCLA's 16 channel array of fixed-frequency reflectometers [7] and a radial chord polarimeter, both of which will be operational by FY15. The reflectometer array, with operating frequencies spread over 30–75 GHz, will probe density fluctuations at cutoff locations corresponding to equilibrium densities in the range 1.1–6.9x10^{19} m^{-3}. The polarimeter will provide internal measurements of magnetic fluctuation amplitude. Each of these diagnostics will individually prove valuable in pursuit of validation of theory. However, the greatest value will be derived through integration of the diagnostics to obtain a much more comprehensive picture of mode structure. One benefit is the greater spatial coverage and higher spatial sampling enabled by differences in measurement localization of the various systems. Another important benefit is that the different measured quantities (e.g. density, poloidal flow and magnetic fluctuations) offer substantially independent and complementary measurements of the mode's property, which significantly strengthen the comparison with theory when simultaneously available. For instance, density fluctuations associated with shear AEs (i.e. TAEs or GAEs) are primarily a product of displacement of the equilibrium density gradient by radial ExB flow fluctuations (neglecting compressional terms). Thus, combination of density with poloidal flow fluctuation measurements would allow full determination of the perpendicular electric field fluctuation, in the approximation of negligible compressional contribution to density fluctuations. Integration of measurements from multiple diagnostics is a central goal for the next 5-year period.

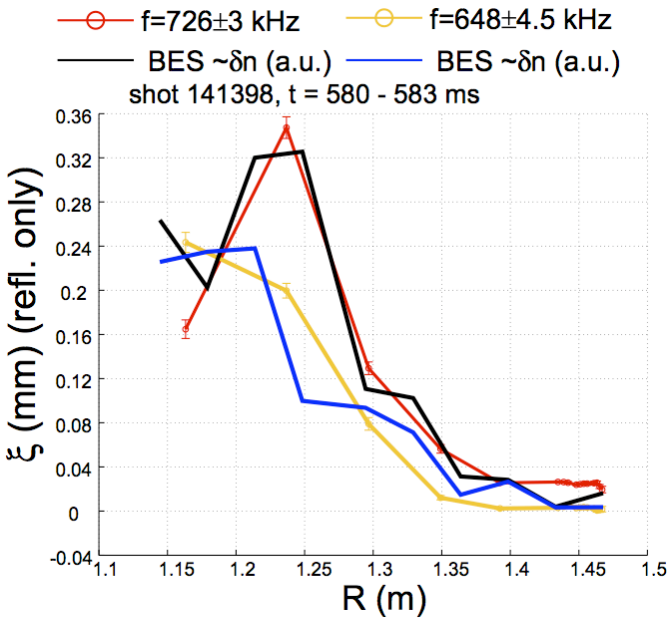

Figure 6.3.3: Comparison of BES and reflectometer measurements of high frequency Alfvén eigenmode structure. (Figure courtesy of K. Tritz, Johns Hopkins University, see Ref. [56]).

Existing reflectometry and BES data from NSTX in 2010 offer the opportunity to begin this effort in preparation for *AE modes investigation in NSTX-U plasma. Figure 6.3.3 illustrates an example of high frequency Compressional Alfvén eigenmode measured simultaneously using BES and the reflectometer array [56]. These measurements were obtained in a high power, beam-heated H-mode plasma similar to those in which high frequency AE activity is observed to correlate with enhanced core electron thermal transport [23].

Mode structure measurements in NSTX via the reflectometer array have produced a variety of results that motivate follow-up in NSTX-U using the full, integrated capabilities of BES, reflectometry and polarimetry. One such result is the measurement of TAE radial structure, including both amplitude and phase (Fig. 6.3.4). The measurements show a radial phase variation that is not consistent with expectation from ideal MHD, a theory that has been notably successful in predicting TAE structure in other cases [57][58]. Preliminary comparison with M3D-K simulations, however, has yielded reasonable agreement between the measured and predicted radial profile of mode amplitude and phase [58]. A key element of the M3D-K simulation that is missing from ideal MHD theory is the kinetic treatment of the fast ion population. One important question arising from these results is what are the limits of ideal MHD theory in predicting the TAE structure. A goal in the development of a predictive capability is the construction of reduced models for prediction of fast-ion transport. An ideal MHD code such as NOVA-K, which is less computationally intensive than M3D-K, would prove a valuable component of such a model if its limits were well understood. NSTX-U will offer the opportunity, even in its first years of operation, to validate codes such as NOVA-K and M3D-K in a new parameter regime, while retaining the ability to connect to NSTX results.

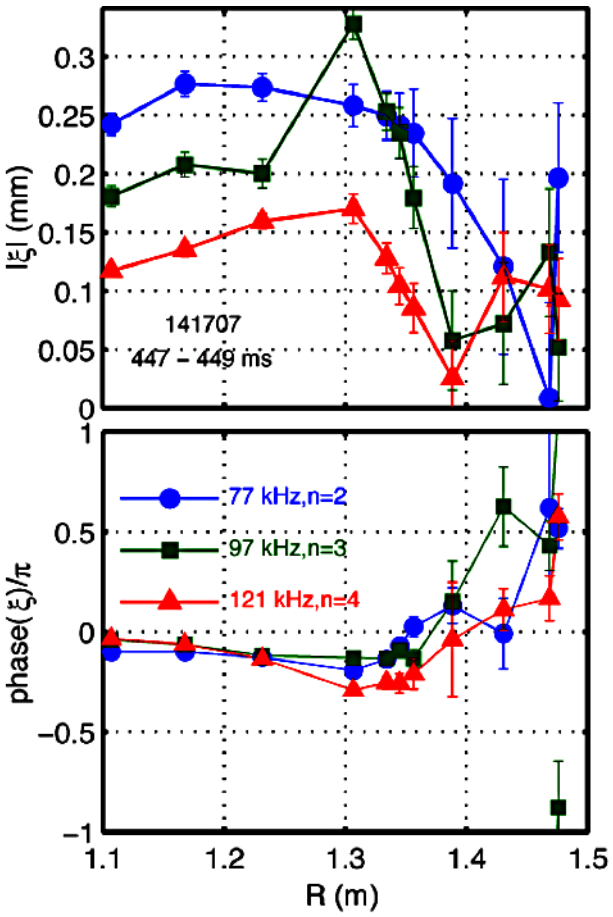

Figure 6.3.4: (a) Amplitude and (b) phase of effective displacement of toroidicity-induced Alfvén eigenmodes measured via the UCLA reflectometer array (cf. Ref. [7]).

6.3.1.4 Study effects of GAE/CAE modes on thermal plasma

The study initiated on NSTX of the effect of GAE/CAE modes on the thermal plasma via the modification of the electron thermal heat conductivity is an important topic to continue on NSTX-U. The study will be carried on in collaboration with the Turbulence and Transport Topical Science Group, see Sec. 3.3.3.1 in Chapter 3.

Two mutually exclusive mechanisms have been proposed to explain the GAE/CAE-induced electron transport. The first mechanism invokes GAE mode conversion to local kinetic Alfvén waves (KAWs) in the region near the edge [59], whereas the second mechanism is based on the magnetic field line stochastization due to multiple GAE instabilities [60]. The two proposed mechanisms were the subject of experimental studies on NSTX and have to be verified with the wealth of diagnostics that are available on NSTX-U.

Detailed analysis of the measured Alfvén wave spectrum is foreseen to exclude one of the proposed physical mechanisms in favor of the other. In recent years, an improved characterization of GAEs and CAEs became available [7]. Along with measurements of the modes' polarization, analysis of data from Mirnov coils and reflectometers, coupled to measurements of plasma profile evolution, are used to differentiate between the two classes of modes. These improvements motivate a dedicated effort on NSTX-U to separate the effects of CAEs from those of GAE modes. As the initial studies on electron thermal transport were based primarily on GAE modes [23], it is important to improve the analysis to account for the Compressional modes as well. One particular change required to use the ORBIT code as it was done for GAEs [60] is the incorporation of the perpendicular component ($A_\perp$) of the vector potential of the perturbation. This is an immediate problem to solve in the near term.

6.3.1.5 Extend *AE simulations to full NSTX-U parameter space

By the end of the initial 2 years of NSTX-U operation, numerical simulations of *AE instabilities and *AE-induced transport will be extended to scenarios with full 1 T toroidal field and 2 MA current that will be achievable in Year 3-5. Predictions will be made for the expected spectrum of unstable *AEs and for their effects on the fast ion distribution. This will provide a reference to guide further experimental studies, as well as an opportunity to assess the maturity of the codes.

For a more direct comparison between experiments and codes, an interface to import F_{nb} data directly from the NUBEAM code will be developed. The goal is to retain all the main features of the beam ion distribution function as calculated by NUBEAM, without introducing further assumptions on the fast ion relaxation and slowing down processes. This interface will first be tested with the M3D-K code. In the present version of the code, an analytic equilibrium distribution function is used with a slowing-down distribution in velocity and an anisotropic distribution in pitch. However, this simple analytic distribution cannot usually describe the full details of a realistic distribution from NUBEAM, which has a complicated 3D structure in phase space. Thus, we plan to use a numerical distribution obtained from the NUBEAM distribution after removal of the inherent MonteCarlo noise. This is necessary to accurately model the excitation and nonlinear evolution of fast ion driven AEs in NSTX and NSTX-U. The

implementation of the same interface in other codes (for instance, NOVA-K and HYM) will be then considered for a more consistent treatment of F_{nb} among different numerical codes.

M3D-K will be applied to investigate the nonlinear evolution of multiple beam-driven Alfvén modes and fast ion transport. We also plan to investigate fast ion effects on global MHD modes such as non-resonant kink modes and the Resistive Wall Mode. The ultimate goal is to predict fast ion transport and effects of fast ion instabilities on the plasma confinement.

The present implementation of the HYM free-boundary equilibrium solver will be improved by adding fixed-plasma-shape capability for equilibrium fits that can better reproduce the experimental profiles. Options for including a more realistic fast ion distribution function, as discussed above for the M3D-K code, will also be developed. Based on the previous work, the study of the excitation mechanisms of GAE and CAE modes will be extended to NSTX-U regimes with higher B_t. This requires the development of numerical diagnostics to identify and characterize the location of resonant particles in phase-space. The upgraded HYM code will be then used to study the self-consistent effects of the sub-cyclotron modes on fast ion distribution function in NSTX-U. Comparisons will be done in terms of the experimentally observable mode properties (such as frequency, mode number, radial structure) and of the variation of mode stability measured under different conditions. The latter include scans of NB tangency radius and injection energy to vary the pitch and energy distribution of F_{nb} in a systematic way.

6.3.2 Research Plans for Thrust EP-1: Year 3-5

6.3.2.1 Extend *AE studies to non-linear and multi-mode physics

Although improving our understanding of linear stability of *AEs (with particular attention to ST configurations) is a necessary first step, investigations of the full non-linear mode dynamics is nevertheless the most important goal. Experiments in Year 3-5 will be aimed at unraveling the mechanisms that determine the coupling between multiple modes, either of the same type (e.g. multi-mode TAE avalanches) or of different types (e.g. TAE coupling to low-frequency MHD modes).

Once the coupling mechanisms are identified, their effect on the saturation level of *AE instabilities will be investigated. In fact, non-linear physics is known to alter linear predictions for the mode saturation level, which may become independent of the linear growth rate [61].

6.3.2.2 Compare numerical and theoretical simulations to data on mode dynamics, mode-induced fast ion transport

As the focus is shifted from linear to non-linear aspects of *AE dynamics, the range of applicability of different models will be established. Predictions of mode stability obtained from the M3D-K and HYM codes will be compared to experimental data and to predictions from linear codes such as NOVA-K to assess the accuracy and the limits of applicability of simple theories as opposed to more self-consistent, non-linear models. The code Verification & Validation effort will also include comparisons with the measured amount of fast ion transport, with emphasis in Year 3-5 on the higher B_t and I_p scenarios.

Further improvements of the HYM code are planned for Year 3-5 to include the effects of finite equilibrium electric field due to bulk plasma rotation and Hall term in the equilibrium model. In order to fully exploit the capability of the code to simulate non-linear phenomena on long time-scales (several growth-rate periods), particle sources and sinks will be added. Numerical diagnostics will finally be included to investigate the effects of GAE and CAE modes on the electron thermal transport

Agreement between codes and experiments will be quantified on the basis of mode dynamics and fast ion response at different levels, based on the level of accuracy that the simulation tools are required to provide. Whereas simpler theories are – at most – expected to provide information on the expected *AE spectrum and qualitative radial structure, more complete numerical tools should also yield the saturation level of the instabilities and any possible mode-mode coupling and other non-linear phenomena. The latter typically involve fast ion redistribution in energy and pitch even in the absence of macroscopic radial transport or loss. The suite of fast ion diagnostics available on NSTX-U can indeed provide the experimental data required for a thorough comparison between theory and experiment.

6.3.2.3 Extend simulations of *AE-induced fast ion transport to FNSF/Pilot

The ultimate goal of *AE stability studies and Verification and Validation of numerical tools is the ability to predict if (and what) *AEs will be potentially unstable in future reactors. If incremental funding is available during the 5 year period considered herein, typical scenarios for FNSF will be identified by Year 5 and *AE stability investigated. Based on the expected unstable spectrum, predictions of fast ion redistribution and loss will be then performed. Simulations will start from steady-state regimes (i.e. during the current flat-top phase) for which background plasma parameters are rather constant in time, thus simplifying the task. Once a

reliable predictive capability is demonstrated, e.g. on the basis of previous agreement between the outcome from the codes and real experiments, simulations will be extended to the even more challenging transient phase of current ramp-up on FNSF. During this phase, the large variations of q-profile and ratio between thermal and fast ion pressure are expected to cause transitions between regimes dominated by different instabilities. The inherently transient mode behavior needs to be characterized, so that specific control schemes can be developed to limit or suppress the appearance of deleterious *AEs.

Predictions for FNSF scenarios performed in Year 5 will also serve as a guide for the optimization of its design. For instance, simulations may suggest an *optimum* NBI configuration that would ensure flexibility in *AE control while providing the required NB-driven current and additional heating. Moreover, design of rf systems may also benefit from EP-related simulations once a deeper understanding of the synergy between NB ions and injected rf waves is achieved. Finally, additional tools may be envisaged (or required) for *AE control in fusion reactors, that is the main focus of Thrust #2 detailed in the next Sections.

6.3.2.4 Summary of research plans by year for Thrust EP-1

Assume a Baseline Funding scenario (*Baseline+10% Incremental scenario in italics*).

Year 1 (2014):

- Improve CX analysis tools in TRANSP for better accuracy in the interpretation of data based on charge-exchange processes (e.g. NPA/ssNPA, FIDA).
- Develop and assess reduced models for *AE-induced fast ion transport. Include reduced models in TRANSP/NUBEAM for improved modeling of NB-heated plasmas, for example to include anomalous fast ion transport driven by resonant *AEs and its effects on NB-driven current profile.
- Improve F_{nb}, rotation description in numerical codes.

Year 2:

- Compare classical TRANSP/NUBEAM predictions with experiments for 1^{st} + 2^{nd} NB line in collaboration with WH&CD, ASC and SFSU groups to establish a baseline for future EP, scenario development and current ramp-up studies.
- Characterize *AE activity driven by more tangential 2^{nd} NB line. Study response of *AE stability to different NB injection geometries for discharge optimization.
- Perform theory/experiment comparison on TAE properties for Verification & Validation of improved codes for *AE stability and associated fast ion transport.

- Extend predictions to full NSTX-U parameter space in preparation for the full 1 T, 2 MA operations in Years 3-5.

Year 3:

- Characterize TAE-induced F_{nb} modifications. Characterize *AE regimes leading to fast ion redistribution (in both space and energy/velocity) or loss.
- Extend TAE studies to non-linear, multi-mode physics for the higher toroidal field and current of NSTX-U.
- Perform theory/experiment comparison on GAE/CAE modes properties.
- Study GAE/CAE effects on electron thermal transport.

Year 4/5:

- Extend characterization of *AE-induced F_{nb} modifications to higher-frequency *AEs to assess the role of high-frequency *AEs in fast ion redistribution.
- Assess theory/experiment comparison on mode dynamics.
- Extend multi-mode *AE studies to higher-frequency *AEs. Study coupling between different classes of instabilities through modifications of F_{nb}.
- Extend *AE simulations to FNSF/Pilot (steady-state); assess implications of *AE and fast ion studies for FNSF/Pilot optimization.
- *Extend *AE simulations to FNSF/Pilot (ramp-up phase). Assess implications of *AEs for current ramp-up with NB in future STs.*

6.3.3 Research Plans for Thrust EP-2: Year 1-2

6.3.3.1 Assess requirements for *fast ion phase-space engineering*

The results on *AE stability and fast ion response achieved during the next 5-year period form the basis for the development of active tools to affect F_{nb} through selective excitation or suppression of specific classes of *AE modes. Experiments will be conducted to assess whether an efficient control of F_{nb} and fast ion driven instabilities can be achieved through the combination of (and synergy between) several techniques.

Neutral beam injection is the primary tool to vary the q-profile, that is one of the most important parameters affecting the stability of *AEs. For instance, maintaining a reversed-shear configuration during current ramp-up phase may favor strong RSAE activity that can redistribute fast ions radially, thus enhancing NB-driven current diffusion to achieve a broader current profile (and improved MHD stability) at early times in the discharge. Similarly, off-axis NB injection during the flat-top phase may be required to sustain the central value of q well above $q_0=1$ and suppress or reduce the occurrence of low-frequency MHD (kinks and fishbones). Another important parameter is the NB injection voltage, which sets the ratio of fast ion to Alfvén velocity. The latter value is expected to play an important role in the particular saturation regime of instabilities such as TAEs, for instance to reduce the avalanching behavior of the modes and to minimize fast ion losses. The efficacy of different NB injection schemes to affect *AE stability and fast ion profile will be assessed as a function of toroidal field, plasma current, confinement mode (L- vs. H-mode).

Besides NB injection, the use of HHFW injection to control *AEs and affect F_{nb} will be investigated. Experiments will be performed to separate the direct effect of rf waves that modify fast ion phase space from indirect effects on *AE stability through variations of the background (thermal) plasma parameters. This requires accurate measurements of F_{nb}, coupled to advanced numerical codes to unfold the effects of HHFW injection on various drive and damping mechanisms. Scans of the HHFW phasing are planned to vary the amount of power coupled to thermal electrons and to fast ions. Similarly, scenarios with different NB injection voltage will be explored to map regions of fast ion phase space that are mostly affected by HHFW.

Existing Magnetic Perturbations external coils, with improved control over the excited spectrum through an additional set of Switching Power Amplifiers (SPAs), will also be used to affect the dynamics of high-frequency *AEs. Further enhancements are expected from a (partial) set of Non-axisymmetric Control Coils (NCC) after FY16. Initial analysis from NSTX data indicates

that pulses of static MP perturbations can indeed modify the drive for GAEs by altering the fast ion distribution, as shown in Fig. 6.2.4. Research on NSTX-U will proceed by investigating the dependence of F_{nb} modifications, and the resulting mode dynamics, on amplitude and spectrum of the magnetic perturbation induced by the 3D field coils. Experimental data on variation of the fast ion profile caused by the applied fields will be compared to results from the SPIRAL code with perturbed magnetic field calculated through the IPEC code.

A more sophisticated control of *AE modes can be achieved by dedicated antenna systems. The first goal for Years 1-2 is to design a *AE antenna system such that the coupling with modes peaking in the core plasma is maximized. A broad range of frequency, spanning from the TAE range (10-200 kHz) up to the GAE/CAE range (~2 MHz), is required to cover the entire range of interest for *AE studies. The antenna design proposed for NSTX-U will have a specific polarization, which would allow the propagation of the power throughout the plasma. For example, one possibility is to excite the Compressional AEs via the excitation of such oscillations near the edge of the plasma. It seems reasonable to expect that the most helpful tools for design and optimization of the system are codes used in the ICRH studies. These capabilities will be developed in the planning and development phases of PSE techniques.

Depending on the availability of incremental funding, the *AE antenna system will be upgraded throughout Years 3-5 to improve the selectivity in the injected frequency and mode number spectrum. The antenna control system will also be improved from the initial pre-programmed mode of operation to a closed-loop control that can track specific modes during the discharge, for example based on measurements from Mirnov coils. The ultimate goal of this research is to assess the requirements for efficient coupling to *AEs over the entire frequency range from TAEs to high-frequency GAE/CAEs. Coupling efficiency will be evaluated in terms of tangible effects on the mode's characteristics (e.g. reduced amplitude/suppression or variations of induced fast ion redistribution and loss). The main figure of merit is the required purity of injected spectrum and amount of coupled power to induce measurable effects.

Based on these experiments, projections to future devices will be performed to assess whether the *AE control techniques developed on NSTX-U are a viable and promising tool that should be further pursued.

6.3.3.2 Test *AE antenna system

A prototype *AE antenna was installed on NSTX in 2011, but never operated. It consists of a single 5-turn coil obtained from a polyamide-insulated 10 AWG copper wire (see Fig. 6.3.6). The 10 AWG copper conductor is stiff enough to be self-supporting. No significant heating is expected at the projected current levels in the low power phase of the experiments.

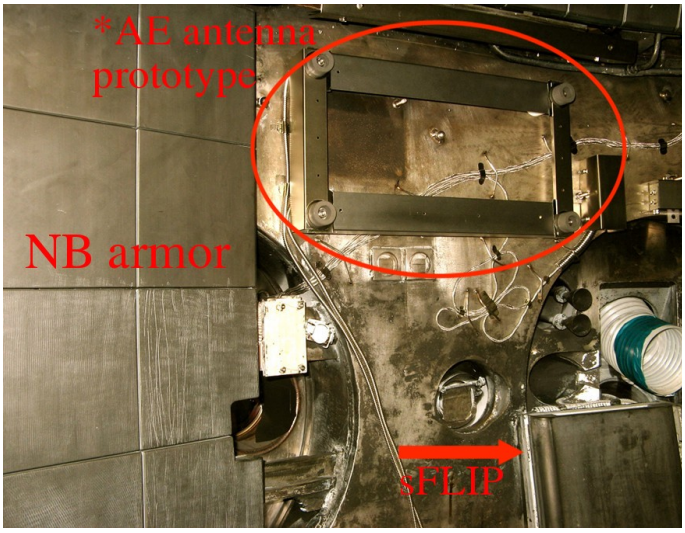

*Figure 6.3.6: Prototype *AE antenna as installed in-vessel prior to the FY-12 Run. The antenna consisted of a 5-turn coil installed above the mid-plane, next to the NB armor (left) and above the sFLIP diagnostic (bottom right).*

The prototype module was intended as the first step to test the efficiency of coupling to different classes of *AEs. However, being a single element, it cannot provide selectivity and flexibility in terms of excited spectrum of toroidal mode numbers. The main limitation for a practical utilization of a single *AE antenna as an *active* tool for MHD spectroscopy is that the rf power is diluted over the entire mode number spectrum, thus increasing considerably the power requirements for damping rate measurements of single modes. To overcome this limitation and proceed more aggressively with the active *AE spectroscopy project, a set of 4 modules, based on the original prototype design, is being developed for NSTX-U. Suitable locations have been identified at bays F-G. The four modules will be installed in pairs, both above and below the midplane, in regions not occupied by (or potentially useful for) other diagnostics. The small toroidal separation of the modules will enable a greatly improved control of the excited spectrum over the single-module prototype for mode numbers up to *n=9-10*, as required for CAE studies.

For the initial operation, the antenna modules will be driven through a broad bandwidth linear amplifier built by Amplifier Research Corp. The amplifier bandwidth extends from 10 kHz up to 100's of MHz. Nominal output power is 1kW CW into a 50 Ohm resistive load. Operations of the amplifier at up to 5 kW are possible in pulsed mode, with a pulse length effectively comparable to the NSTX-U discharge duration. The output power of 1 kW into 50 ohms translates into ≈220V, 4.5A rms. This is a linear amplifier, so a programmable function generator will be used as the source driver for pre-programmed frequency sweeps, with the possibility of implementing more advanced feedback control schemes in later years. The 1-5 kW power level is comparable to what has been used in other MHD spectroscopy experiments. Upgrades to higher power RF systems will be considered after Year 2, based on the available resources (see below).

Improvements to the antenna design will be considered during Years 2-5 to optimize the coupling to TAE and CAE modes. In parallel, the coupling network and control hardware and

software will be developed. There are several potential avenues by which to improve the antenna performance. The addition of more modules in the antenna array will improve both coupling to the modes and selectivity in the excited (toroidal) mode number spectrum. If the heat loading of the existing antenna design by thermal plasma and beam ions appears modest, moving the antenna closer to the plasma surface will likely improve coupling. Finally, a sub-set of coils oriented in the poloidal/toroidal direction might be preferable to the present radial, picture-frame coils. The extent of the antenna will, of course, be constrained by requirements of other internal diagnostics and hardware.

Along with the *AE antenna improvements, an upgrade of the existing set of magnetic pick-up coils will be considered. Pending incremental resources and the success of the *AE antenna, the upgraded coil system will enable real-time detection of unstable (or potentially unstable) *AEs during a discharge. The resulting information on *AE stability and dynamics can then be used to implement a feed-back loop on the *AE antenna to track modes in real time. In addition, it would enable the implementation of *AE control schemes through the Plasma Control System (PCS) by using NBI, MP/NCC coils or rf injection in response to the *AE mode activity for discharge optimization.

6.3.3.3 Compare measured *AE damping rates with models & theory

In the course of the initial *AE antenna operations, it will be natural to exploit any data acquired on *AE damping rate to develop the needed analysis codes, and to identify the necessary experimental conditions. It is envisioned that the initial years of experimentation will be at relatively low power, of the order of ~1 kW, similar to the power level used in experiments on the C-Mod and MAST devices.

Emphasis in Year 3 will be on designing experiments to measure *linear* TAE damping rates under as broad a range of conditions as possible, in order to establish a connection with previous work on C-Mod and JET. It is anticipated that these studies will be complicated in NB-heated NSTX-U plasmas by the fairly ubiquitous presence of unstable *AEs. Thus, initial physics studies will probably concentrate on Ohmic and HHFW-heated plasmas. This will be followed by measurements in beam-heated plasmas using low voltage beams and high plasma density to reduce the fast ion beta. Linear stability can then be measured as a function of NB power to separate fast ion drive from linear damping. Comparison between the measured rates and the outcome of numerical codes is planned. For the lower frequency TAE modes, damping rates will be computed via the NOVA-K and M3D-K codes. Comparison between the predictions from both linear and non-linear codes with experimental values will provide a further cross-validation

between codes. The HYM code will be used for the analysis of high-frequency GAE/CAE modes and comparison with experimental results.

While the highest priority in Years 2-3 will be to develop the capability to study stability properties of TAE modes, experimental time will be devoted to assess the antenna and coupling network performance at frequencies up to 2 MHz, as will eventually be needed for Global and Compressional Alfvén Eigenmode studies. Most likely, this will require modifications of the matching network between the amplifier and the antenna.

6.3.3.4 Characterize scenarios with combined NBI+HHFW

HHFW heating accelerates NBI fast-ions [62][63], altering the fast ion distribution, the spectrum of *AE activity, the fast-ion transport and consequently the NB-driven current profile. While the dominant fast-wave heating mechanisms in NSTX were found to be Transit Time Magnetic Pumping damping on electrons and fast ion damping at high cyclotron harmonics, at the mid-harmonic range expected at the highest toroidal fields in NSTX-U the power partitioning may change.

Initial simulations with advanced rf codes (AORSA, TORIC, METS, GENRAY and CQL3D) indicate that significantly more thermal deuterium damping, in addition to increased NBI fast ion damping, may occur in NSTX-U (see Chapter 7 and references therein). Experiments during the first two years of NSTX-U operation will employ the existing 12-strap HHFW antenna to study the effect of fast-wave heating on F_{nb}, the spectrum of *AE activity and fast-ion transport. Results from these experiments, conducted in collaboration with the Wave Heating and CD group (cf. Chapter 7, Sec. 7.1.3.1), will be used to validate the predictions of rf and energetic particle simulations.

6.3.4 Research plans for Thrust EP-2: Year 3-5

6.3.4.1 Optimize *AE antenna for efficient coupling to *AE modes

After the initial two years of NSTX-U operations, several straps of the HHFW antenna may be disconnected from the 30 MHz rf sources to allow for the installation of an upgraded *AE antenna (see Chapter 7, Section 7.2.1.4 for more details). If removal of (up to) four HHFW antenna straps is found to be acceptable, experiments during Years 4-5 will employ the reduced-strap HHFW antenna for fast-wave heating and an upgraded *AE antenna system for EP studies.

The availability of more in-vessel space would provide more flexibility for the optimization of the layout of the antenna modules to achieve optimum coupling efficiency to modes with a specific toroidal mode number.

Based on the available NSTX-U budget for Year 5, upgrades of the rf amplifier driving the antenna and of the mode detection/antenna control systems will be considered. Higher power operations (>10 kW) would be possible by utilizing rf oscillators instead of the linear amplifier envisaged for Years 1-2, at the expenses of flexibility in the range of excited frequencies. A 100-kW system is available at PPPL, although development work is required to tune the frequency range down to the 1-2 MHz frequencies at which CAE/GAE modes are expected. Such higher-power system would be especially important for assessing the ability to drive modes at sufficiently large amplitudes, so that they can induce measurable effects on the fast ion distribution and, possibly, on the thermal plasma (electrons), see next Section. A coherent detection system is also foreseen to detect and track the mode frequency in real time during a discharge. This implies improvements to the existing Mirnov coils set to reduce the direct coupling to the antenna and improve the signal-to-noise for the detection of *AE modes that are coherent with the antenna excitation. The ability to track modes in real time would enable the implementation of a feedback loop in the antenna driver, in order to maintain good coupling with a specific mode. (*A priori*, that is clearly not guaranteed by operating the system with open loop, i.e. pre-programmed, frequency settings).

6.3.4.2 Measure stability of high-*f* *AEs; assess capability of & requirements for mode excitation

In Years 4-5 there will be increased focus on the higher frequency Alfvén instabilities. The initial goal will be to map the spectrum of natural CAE/GAE eigenmodes. Then, the linear damping rates of the stable modes will be measured with different combinations of neutral beams, including scans of NB injection energy and tangency radius to alter the fast ion distribution. Extensive comparison with numerical codes such as HYM is foreseen.

Low power (≈1 kW) *AE antenna experiments will provide important information on antenna coupling and natural damping rate for each of the eigenmodes. This information will be used to determine the potential benefits of higher power experiments aimed at driving the modes to substantial amplitude. Multiple antenna modules are required to improve the antenna selectivity and focus the rf power over a narrow range of the toroidal mode number spectrum, especially for *AEs with intermediate to high mode numbers, $n>5$. An upgraded *AE antenna system is therefore needed, making this area of research subject to the available budget for Years 3-5.

Stability properties of high-frequency *AEs are also very important in the area of *AE effects on thermal plasma. If the natural eigenmode damping rates are small, there is the possibility of driving them to amplitudes where stochastic heating of thermal ions occurs [27]. This gives an attractive option to spherical tokamaks of direct rf wave heating of the thermal ion population. Conversely, for strongly damped eigenmodes, the rf wave heating will be partitioned between thermal electrons and thermal ions and may still be of interest, if adequate coupling can be obtained through antennae of reasonably compact size.

6.3.4.3 Summary of research plans by year for Thrust EP-2

Assume a Baseline Funding scenario (*Baseline+10% Incremental scenario in italics*).

Year 2 (2015):

- Assess requirements for phase-space engineering using NBI as actuator.
- Test prototype *AE antenna system. Assess antenna performance in terms of coupling to lower frequency *AEs (TAEs, RSAEs).
- Investigate scenarios with combined NBI+HHFW to characterize rf-induced modifications of F_{nb} and implications for efficient rf heating during NB injection.

Year 3:

- Compare TAE damping rates measured via *AE antenna with theory to validate models for *AE damping in ST geometry.
- Based on the results from Years 1-2, assess requirements for phase-space engineering using NBI, HHFW and magnetic coils as actuators. Explore the possibility of controlling *AE modes and resulting F_{nb} modifications to affect NB-driven current and q-profile.

Year 4/5:

- Extend *AE damping rate measurements through *AE antenna to higher-frequency *AEs to validate CAE/GAE stability models and numerical codes.
- Optimize AE antenna for efficient coupling to *AEs. Improve spectrum selectivity to couple to specific modes.
- Assess capability of, and requirements for, mode excitation. Determine power level and spectral requirements to excite *AEs to sufficient amplitude for detectable variations of F_{nb}.
- *Implement and test high-power *AE excitation system*.

6.4 Summary of Theory and Simulation capabilities

Code	*Description*	*Scope*	*Improvements*
ORBIT	Gyro-center particle following code.	Infer fast ion response to given set of modes.	Improved methods for resonance identification.
SPIRAL	Full-orbit particle following code.	Infer fast ion response to given set of modes.	
NOVA-K	Ideal MHD; linear.	Compute eigenfunctions, stability for *AEs.	Improved F_{nb} model. Improved treatment of finite plasma rotation.
M3D-K	Hybrid model; self-consistent, non-linear.	Infer mode dynamics (low-f *AEs, kinks) and fast ion response.	Improved F_{nb} model.
HYM	Hybrid model; self-consistent, non-linear.	Infer mode dynamics (high-f *AEs) and fast ion response.	Improved F_{nb} model. Include sources and sinks.
F_{nb} inversion code	Package for analysis of experimental data.	Infer F_{nb} from a set of measurements.	Under development. Adapt to NSTX-U.
QL model	Reduced model for quasi-linear relaxation of $F_{nb.}$	Compute relaxed $F_{nb}(r)$ in the presence of *AE modes.	Under test. To be included in TRANSP/NUBEAM and validated against NSTX/NSTX-U data.
Resonant fast ion transport model	Reduced model for resonant/stochastic AE-induced fast ion transport.	Advance F_{nb} in NUBEAM under the effects of resonant *AE modes.	Under development. To be included in TRANSP/NUBEAM and validated against NSTX/NSTX-U data.

Table 6.4.1: Summary table of the codes directly developed (or under development) by NSTX-U researchers and collaborators for Energetic Particles related theory-experiment comparison on NSTX-U.

6.4.1 ORBIT

ORBIT [64] is a particle-following code based on the Hamiltonian formulation for the particle guiding center motion in the presence of axisymmetric perturbations. The code has been widely used to simulate the fast ion response to MHD instabilities [65][66] (mostly RSAEs and TAEs) in various magnetic configurations, from tokamaks (including NSTX) to reverse-field pinches. A novel, efficient technique has being developed to identify stochastic regions based on the relative phase between pairs of particles with nearby orbits in phase space coordinates. This technique will be used to identify resonances and characterize magnetic field stochastic regions for *AE modes observed on NSTX-U. More generally, ORBIT provides a consolidated framework to

investigate fast ion loss and redistribution in the presence of TAEs, including the transport scaling as a function of mode amplitude, mode structure and frequency.

The ORBIT code is also used to investigate thermal electron response to high-frequency GAE/CAE modes [60]. Future improvements are mainly based on the accuracy of the mode structure and amplitude used in the simulations. Previous works utilized theoretical mode structures and amplitudes consistent with measurements of magnetic and density fluctuations from Mirnov coils and interferometers. Based on the improved measurements achieved through reflectometry [7], the experimental mode structure can be used [67] to improve the overall mode description in ORBIT for CAE and GAE instabilities. Future work also includes comparisons between thermal electron transport predictions from the ORBIT and HYM codes.

6.4.2 SPIRAL

The SPIRAL code [68] is a full particle-orbit following code recently developed at PPPL for the interpretation and simulation of fast ion dynamics in toroidal plasmas. All gyro-orbit effects are retained, so that the code can also be used to study fast ion interaction with instabilities and externally launched waves with frequency near or above the ion cyclotron frequency. Effects of finite gyro-radius may be particularly important in devices such as NSTX and NSTX-U, in which the combination of small aspect ratio and relatively low toroidal field results in large fast ion orbits compared to the typical scale-lengths of variation of plasma profiles and magnetic field.

The fast ion motion in the presence of general electromagnetic fields is inferred by solving the Lorentz equation. Slowing down and pitch angle scattering are also included. The initial fast ion distribution can be either imported from other codes (e.g. TRANSP/NUBEAM) or defined internally. Initial benchmark and applications of the SPIRAL code are summarized in Ref. [68].

6.4.3 NOVA-K and PEST

The family of NOVA codes [69] has been successfully used and validated in recent years and is now able to comprehensively compute the stability of TAE-like modes in tokamaks. It is capable of using input plasma parameters in the post-processor fashion from TRANSP simulations. The code has been successfully applied to different tokamaks, such as NSTX, DIII-D, C-MOD and ITER for TAE stability predictions. Typically, the kinetic post-processor NOVA-K can compute the mode stability for experiments with relatively small rotation. Rotation enters in the dispersion

relation and stability calculation as a Doppler shift term, and it can therefore modify both the TAE mode structure and its stability (including damping and drive terms).

For low aspect ratio plasmas with large NB input torque such as NSTX and NSTX-U, Doppler shift corrections are of the order of, or larger than, the typical mode frequencies in the plasma frame. (This applies to TAE mode calculations as well as for the internal kink modes). Under these conditions, rotation cannot be considered a small correction and it must be treated more consistently. Improvements of the NOVA code are planned to include a more consistent model for plasma rotation at all levels, from eigenmode structure calculations to damping/drive calculations. Doppler shift corrections based on rotation profiles that are already included in the ideal MHD part (NOVA) will be extended and incorporated in the kinetic part (NOVA-K). A more self-consistent approach is presently implemented in the NOVA-KN code, which already is in working conditions in the MHD approximation. The NOVA-K EP has rotation included for the growth rate calculations, but need better interface with TRANSP profiles.

A separate activity on NOVA-K improvement, which is important for the growth rate calculations, includes the generalization of the model for the distribution function. This becomes especially important for the NSTX-U, which will have a second NBI line and a large variety of possible injection geometries. Improvements will allow the user to import realistic distributions, for example obtained through TRANSP. The more accurate treatment of F_{nb} developed for NOVA-K will then be implemented in the newly developed code NOVA-KN.

In addition to the NOVA code, the ideal MHD code PEST is also available. Possible improvements include a better interface with other codes, e.g. to import profiles from TRANSP, similarly to what is now available for NOVA. One advantage of this improvement would be to allow the user to use the same equilibrium for the different codes. This work was started but did not progress well enough to become available for common use and production runs.

6.4.4 M3D-K

M3D-K is a global nonlinear kinetic-MHD hybrid code [70][71]. In the model, the thermal plasma is treated as single fluid and the energetic particles are described using the drift-kinetic or gyrokinetic equation. The kinetic effects of energetic particles are coupled to the MHD equations via the stress tensor term in the momentum equation. The model is non-perturbative so can be also used to treat strongly driven modes, such as Energetic Particle Modes (EPMs). The code uses numerical tokamak equilibria as initial conditions with capability of treating strong shape and small aspect ratio together with finite plasma rotation. The code has been used successfully to simulate energetic particle stabilization of internal kink mode and excitation and saturation of

fishbone [71], the nonlinear saturation of fast ion-driven TAE with source and sink [72][73], the fast ion stabilization of tearing modes [74], the beam ion excitation of TAE modes in NSTX plasmas [58], the beam-driven Alfven eigenmodes in DIII-D [75], and the fast ion transport due to the non-resonant kink mode in NSTX [76].

6.4.5 HYM

The Hybrid and MHD simulation code HYM is a 3D, non-linear global stability code that includes fully kinetic ion description. It employs a *delta-f* particle simulation method to reduce numerical noise and a full-ion-orbit description of supra-thermal ions in toroidal geometry, as required to study wave-particle interaction in the presence of instabilities in the ion-cyclotron frequency range.

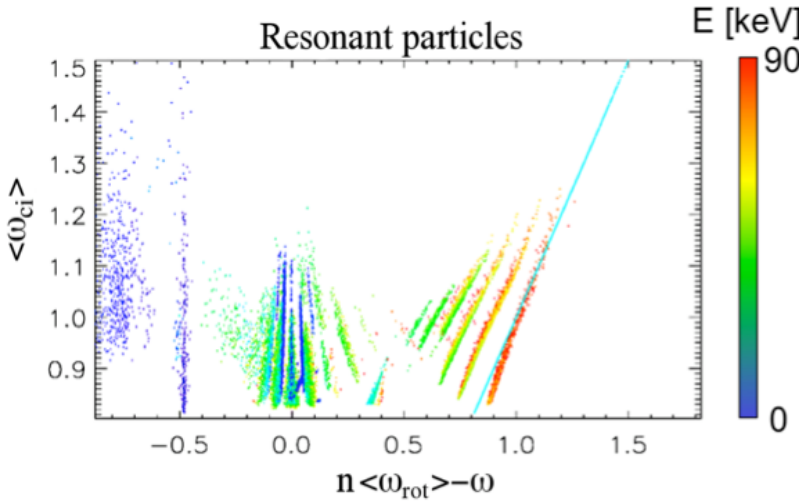

Figure 6.4.1: Resonant particles shown with orbit-averaged cyclotron and toroidal rotation frequencies, normalized to the ion cyclotron frequency at the axis, ω_{ci0} (f_{ci}=2.48 MHz). Results from HYM simulations of the n=8 co-rotating CAE mode (NSTX shot #141398), with $\omega=0.48\omega_{ci0}$, $\gamma=0.004\omega_{ci0}$. Particle color corresponds to different energies from E=0 (purple) to E=90 keV (red), see color bar.

HYM is utilized to study the excitation of GAE modes and co- and counter-rotating CAE modes on NSTX [77][78]. For example, a specific H-mode NSTX discharge, featuring all the high frequency mode activity commonly observed on NSTX, has been analyzed in detail (Figure 6.4.1). In agreement with experimental observations, co- and counter rotating CAE modes are found unstable for low toroidal mode numbers (n=4), whereas lower-frequency counter-rotating GAEs are unstable for intermediate toroidal mode numbers (n=5-7), and co-rotating CAEs are unstable for even higher toroidal mode numbers (n=8,9). The presence of two separate groups of resonant particles, corresponding to regular and Doppler-shifted cyclotron resonances, has been discovered for high-n co-rotating CAEs (cf. Fig. 6.4.1).

In addition to studying F_{nb} modifications caused by sub-ω_{ci} modes, a drift-kinetic description of the thermal electrons has been implemented in HYM to investigate the effect of those modes on thermal electron transport. Evidence of enhanced thermal transport has been already reported from NSTX, and it will be the subject of future experiments on NSTX-U as a candidate mechanism for the regulation of electron temperature profile.

6.4.6 F_{nb} inversion code for interpretation of fast ion data

The fast-ion distribution function F_{nb} is a complicated function of velocity, space, and time. A common choice of independent variables to describe F_{nb} is the energy E and pitch $v_{\|}/v$ in velocity space and the major radius R and elevation z in configuration space. Typically, the distribution function has a non-trivial dependence on all four variables. Because the functional dependencies are complicated, no single diagnostic provides enough information to determine F_{nb} accurately. The sensitivity of a particular fast-ion diagnostic to these variables is described by a *weight function* [79], W (see Fig. 6.4.2). The signal S measured by a diagnostic is the product of W with the distribution function F_{nb}, i.e. $S=\int W*F_{nb}$, where the integral is over all phase-space variables. (In statistical terms, this integral is a kind of "marginalization"; in instrumentation language, the weight function is a type of instrument function.)

Presently, forward-modeling codes exist that predict diagnostic signals S for a given F_{nb}. For example, TRANSP uses the distribution function calculated by NUBEAM to predict the neutron rate. TRANSP also has a module that predicts NPA data. The FIDASIM code [80] predicts FIDA, NPA, and beam emission signals. The code can accept as input distribution functions produced by NUBEAM, CQL3D, SPIRAL and ORBIT. Presently, the production version of FIDASIM is written in IDL. However, in collaboration with ASDEX-Upgrade (AUG), a much faster FORTRAN version has been written and is currently being tested.

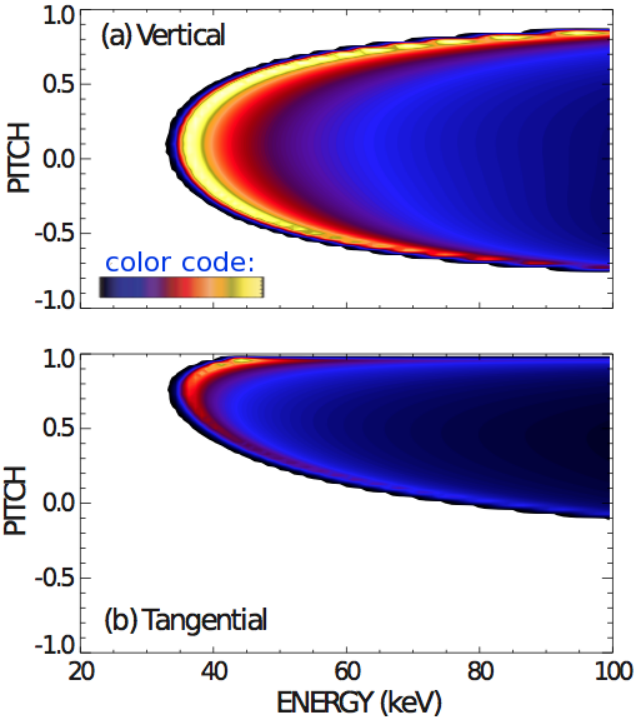

Figure 6.4.2: Example of calculated response function for (a) the vertical and (b) the new tangential FIDA systems for R=1.2 m and at measured energy E_l=35 keV. The color scale, shown in panel (a), is normalized to the maximum value. (From Ref. [10]).

Although forward modeling is useful, it has limitations. In particular, cases exist when *all* available theoretical predictions disagree with the data. For these cases, it is highly desirable to infer the distribution function directly from the data to provide guidance to theory. Another urgent need is better quantification of errors in the comparison between theory and experiment.

Recent progress in understanding the nature

of weight functions [81], together with advances in computer power and the development of extensive sets of fast-ion diagnostics, have made it feasible to develop techniques to infer F_{nb} directly from the data [82]. The planned approach is based on Bayesian techniques. An international team involving scientists from NSTX-U, Danish Technical University, DIII-D, ASDEX-Upgrade, and MAST is involved. In Bayesian terminology, the *likelihood functions* for the various diagnostics utilize diagnostic weight functions. Diagnostics with markedly different sensitivities in phase space are essential for a well-constrained inversion. The combination of complementary fusion product, FIDA, and NPA diagnostics provide the needed data. Initially, these new techniques will be developed and applied to facilities with extensive fast-ion measurements (probably DIII-D and AUG). As fast-ion data become available, the analysis framework will be extended to NSTX-U. During subsequent NSTX-U operation, the inversion capability will be refined and extended as new instruments become reliable.

It is anticipated that the Bayesian inversion code will provide the most accurate and detailed analysis of the data. However, for control-room guidance and data mining, reduced models that sacrifice some accuracy for computational efficiency are needed. Tools of this sort will also be developed by our international development team and adapted for use at NSTX-U.

6.4.7 Quasi-linear model of AE-induced fast ion profile relaxation

The Quasi-Linear (QL) model has been recently validated on DIII-D tokamak plasmas [83]. Several other AE- unstable tokamak scenarios were analyzed using this model [84][85]. The QL model is ready to be used in the regimes of planned NSTX-U operation. In fact, the predicted NSTX-U scenarios are closer than NSTX plasmas to the required conditions for the QL model to be applicable.

The QL procedure can be readily utilized in TRANSP simulations as its integral part. There are two ways the model can be applied. The first case is when the growth and damping rate of the unstable modes can be computed using analytic expressions. This version seems to be more applicable for the burning plasma conditions. Its employment in the integrated codes could be corrected by scaling parameters, similarly to the H-factor parameter in confinement studies. The second case is more suitable for machines with smaller size. A hybrid version is used, in which the NOVA code is first utilized for an initial calculation of the mode drive and damping rate terms, followed by a calculation of the relaxed fast ion profile that leads to a vanishing net growth rate. This method predicts the value of the critical gradient of fast ions. In this case, the initial NOVA analysis requires additional effort and is more time consuming. However, this procedure is especially important for validation purposes and to develop the required database for the “H-factor like” corrections that are then used for the analytic computation of growth rates.

Figure 6.4.3 illustrates an example of QL model applied to ITER scenarios. Here not only the thresholds are predicted for TAEs to be excited but the losses also follow from this model. (It should be noted that additional corrections for the H-like factor might cause a shift of the instability boundary, depending on its value).

Although the full distribution function is not evolved self-consistently by the QL model, the relaxation of the EP profiles could be implemented in codes like TRANSP to change particles' weighting in the calculations. It makes sense to introduce the H-factor like parameter for the QL model to be used in the comparison with experiments.

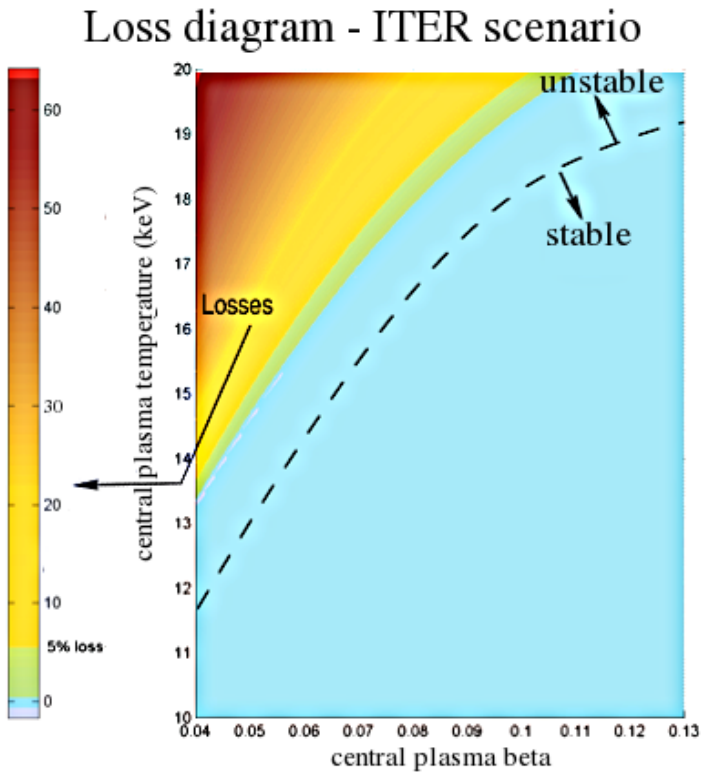

Figure 6.4.3: Example of quasi-linear model predictions of TAE stability for nominal ITER scenarios. On the abscissa is the central value of the plasma beta and on the ordinate is the central plasma temperature. TAE stability regions are indicated, along with the amount of losses expected in the presence of unstable modes.

6.4.8 Resonant fast ion transport model for TRANSP

The NUBEAM module implemented in TRANSP already contains different implementations for specifying anomalous fast ion transport coefficients. However, those models do not contain explicitly any details on the resonant interaction (and resulting transport in phase space) between instabilities and fast ions. In fact, the resonance condition implies that only narrow regions in phase space are strongly affected by the modes, whereas adjacent regions are possibly not affected.

The following features will be included in a new fast ion transport model to mimic the resonant interaction between fast ions and instabilities:

- Characterize particles based on their orbit topology, e.g. in terms of magnetic moment μ, energy E and canonical toroidal angular momentum P_ζ, instead of real-space coordinates such as radius, poloidal/toroidal angles.
- Model transport as steps (or kicks) in phase space, e.g. kicks in energy associated with the resonant interaction. Make no *a priori* assumption on the resulting radial transport, which should naturally follow from the particle dynamics in phase space (namely, from variations of the toroidal angular momentum P_ζ).
- Calculate variations of E and P_ζ consistently. Based on the guiding center Hamiltonian formulation of the particle's motion in the presence of a mode with toroidal mode number n and frequency $\omega = 2\pi f$, one obtains the relationship $\omega P_\zeta - nE = constant$. This implies that, for a single mode, variations in E and P_ζ for particles satisfying are related through $\Delta P_\zeta / \Delta E = n/\omega$, which sets a constraint for the allowed trajectories in the (P_ζ, E, μ) space. In reality, and if more than one mode is present, ΔE and ΔP_ζ can depart from the ideal linear relation between ΔP_ζ and ΔE.
- Derive transport coefficients from consistent simulations or theory, plus comparison with experimental data (whenever possible).
- The model must be suitable for inclusion in the NUBEAM module. In this regard, a Monte Carlo framework is the best approach.

In the proposed approach, the problem is split into two parts: (i) derive a set of transport coefficients in some given form, and (ii) use those coefficients in NUBEAM for the actual computation of fast ion evolution. By doing so, the NUBEAM part of the problem can be developed independently of the different models (or theories) used to infer the transport coefficients. To specify the transport coefficients, the new model introduces the probability distribution function $p(\Delta E, \Delta P_\zeta, \Delta\mu)$ that a particle, whose orbit is characterized by the tern of constant of motions (P_ζ, E, μ), experiences a change over a time δt in energy and canonical toroidal angular momentum of magnitude ΔE and ΔP_ζ (and, possibly, of magnetic moment: $\Delta\mu$) in the presence of a mode with a given amplitude.

In the present plans, the model will first be used to analyze cases for which information on mode structure and amplitude is available, e.g. from reflectometer and Mirnov coils data. To use the model for predictions for future scenarios, some assumptions for the mode behavior have to be made. One possibility is to identify a set of candidate (unstable) modes, for instance through linear stability analysis with NOVA-K. Then, a series of runs with different assumptions on the mode amplitude (e.g. low-amplitude saturation with quasi-stationary modes, weakly busting modes, strong avalanches) may then provide indications on the possible effects on fast ion transport, NB-driven current redistribution and plasma rotation.

6.4.9 Improved 3D 'halo neutrals' model in TRANSP

Existing analysis tools will be improved to extract the required information from the experimental data and enable more reliable projections to future scenarios. For example, the TRANSP code contains a NPA/ssNPA simulation package that has been applied to model charge-exchange neutral particle flux measurements. However, the contribution of 'halo neutrals', surrounding the NB footprint, to the charge exchange flux is not included in the simulation. The existing TRANSP code does not yet treat halo neutrals properly. The effect of halos would be to nearly double the simulated charge exchange flux, thus enabling extension of projected measurements to higher plasma density. An upgrade of TRANSP to provide correct treatment of halo neutrals is nearing completion and will be available for the beginning of NSTX-U operations.

As an example of the present TRANSP capabilities to simulate CX-based diagnostics, discharge scenarios from NSTX-U performance studies [4] are used to assess the viability of NPA measurements for the high-density regimes ($n>10^{20}$ m^{-3}) expected on NSTX-U. NPA simulations were performed for scenarios with 6 NB sources at E_b=90 and 110 keV for low and high n_e cases. An example is shown in Figure 6.3.5 for E_b=90 keV, chosen because this energy enables the simulation to be normalized to existing NPA data from NSTX. The result from this comparison is that quality NPA measurements can be envisioned for NSTX-U, since the calculated flux is above the NPA measurement threshold (shown by the shaded bar). The capability of E||B NPA measurements for even higher performance NSTX-U scenarios with I_p=2 MA, B_T=1 T, E_b=110 keV, P_b=17.4 MW, $n_{e,0}$=2.2x10^{20} m^{-3} (e.g. NSTX-U TRANSP run 142301K54) cannot be adequately addressed until the upgraded halo neutral model is available.

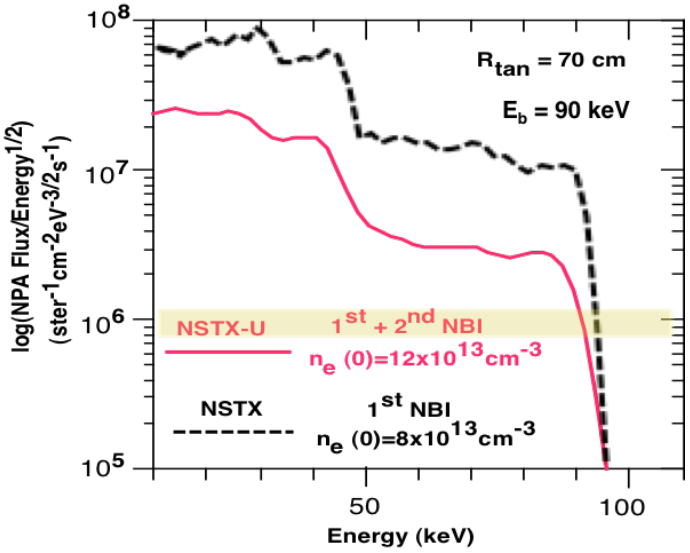

Figure 6.3.5: Comparison of E||B NPA flux calculated by TRANSP for a NSTX discharge with 3 NB sources (black curve: I_p = 1 MA, B_T = 0.5 T, P_b = 6 MW) with a "baseline-142301D48" NSTX-U scenario with all 6 NB sources (red curve: I_p = 1 MA, B_T = 1 T, P_b = 12 MW). The shaded bar depicts the flux threshold for quality NPA measurements above the background noise.

6.5 Summary of other facility capabilities, including plasma control

The Energetic Particle Research plans on NSTX-U will greatly benefit from the improved device capabilities enabled by the second NB line and by the new center-stack. The expanded range of some of the EP-relevant plasma parameters with respect to NSTX has already been discussed in the Introduction of this Chapter, cf. Fig. 6.1.1. In addition, the second NB line will provide enhanced flexibility in terms of NB injection parameters. Although injection energy and flux of the accelerated neutrals from each source will be essentially the same as on NSTX, the different tangency radii of the new sources will translate in an improved capability of manipulating the fast ion distribution and investigate its effects on *AE stability and associated fast ion transport.

The enhancements of both external and internal coils to induced magnetic perturbation will enable studies of fast ion and *AE response to 3D fields, which is an active area of research for ITER and future devices.

The planned improvements to the NSTX-U Plasma Control System also represent an opportunity to target specific issues of *AE physics. For instance, rotation and rotation profile control is essential for an extensive study of rotation effects on the structure of the Alfvén gaps and the resulting *AE stability. Similarly, a better control of the evolution of the safety factor and of the density (keeping other plasma parameters constant) will translate in detailed single-parameter scans that enable (and simplify) the thorough comparison between experiment and theory.

The importance of a dedicated *AE antenna system for EP research on NSTX-U has been already discussed in detail in the previous Sections and is not further discussed here.

6.6 Energetic Particle Research Timeline

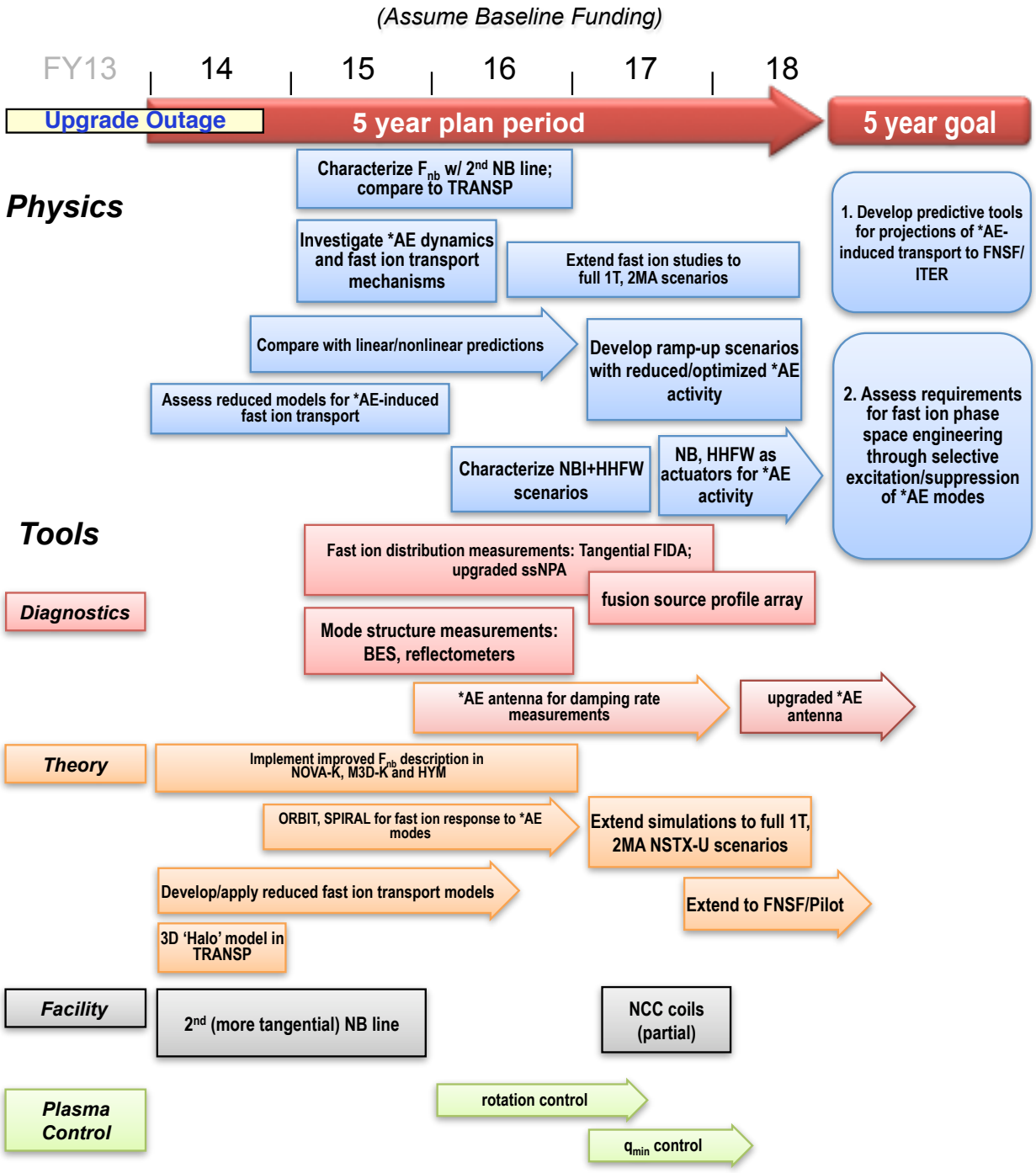

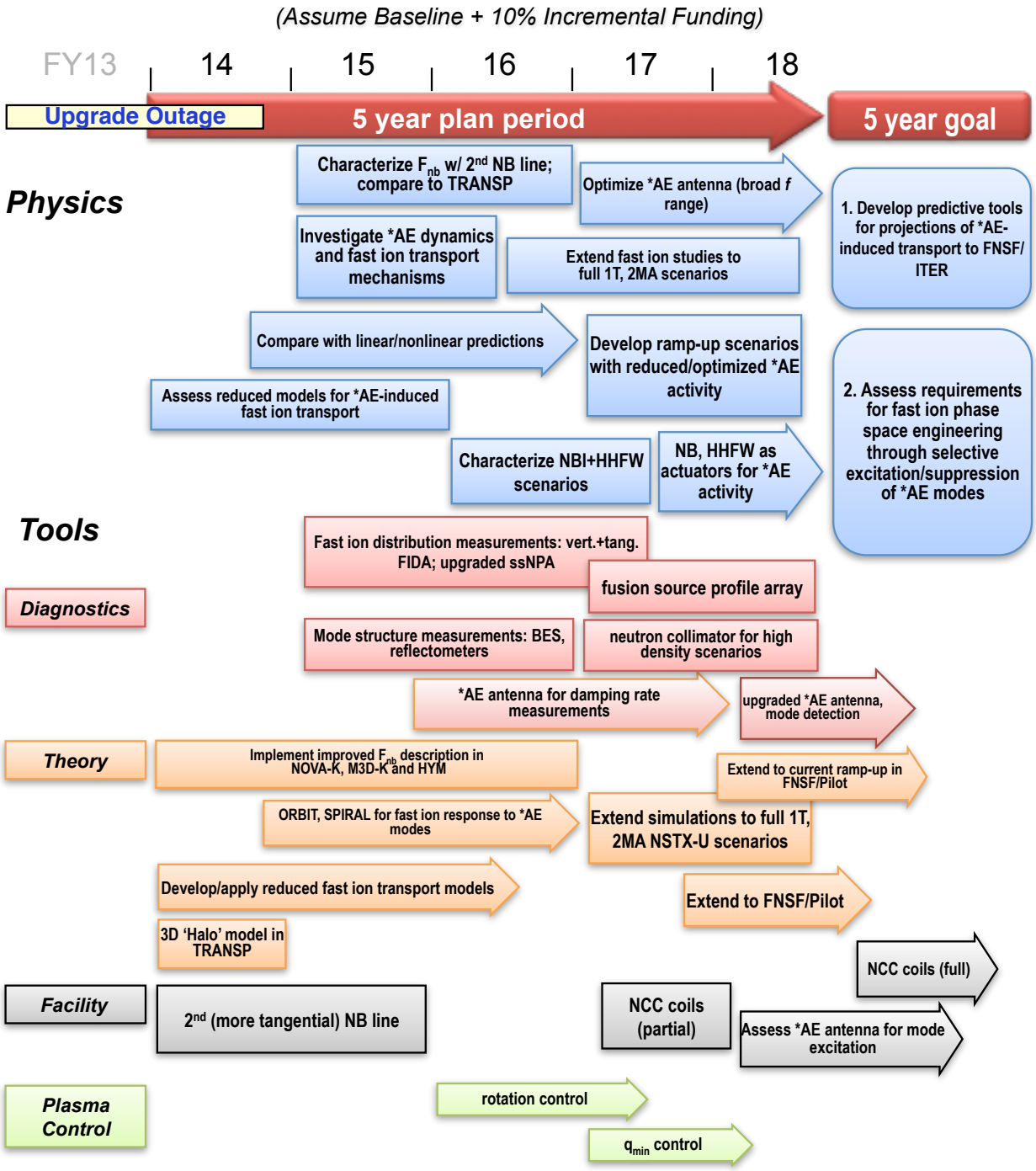
(Assume Baseline + 10% Incremental Funding)
FY13
14
15
16
17
18
Upgrade Outage
5 year plan period
5 year goal
Physics
Characterize F_nb w/ 2nd NB line; compare to TRANSP
Optimize *AE antenna (broad f range)
Investigate *AE dynamics and fast ion transport mechanisms
Extend fast ion studies to full 1T, 2MA scenarios
1. Develop predictive tools for projections of *AE-induced transport to FNSF/ ITER
Compare with linear/nonlinear predictions
Develop ramp-up scenarios with reduced/optimized *AE activity
Assess reduced models for *AE-induced fast ion transport
Characterize NBI+HHFW scenarios
NB, HHFW as actuators for *AE activity
2. Assess requirements for fast ion phase space engineering through selective excitation/suppression of *AE modes
Tools
Diagnostics
Fast ion distribution measurements: vert.+tang. FIDA; upgraded ssNPA
fusion source profile array
Mode structure measurements: BES, reflectometers
neutron collimator for high density scenarios
*AE antenna for damping rate measurements
upgraded *AE antenna, mode detection
Theory
Implement improved F_nb description in NOVA-K, M3D-K and HYM
Extend to current ramp-up in FNSF/Pilot
ORBIT, SPIRAL for fast ion response to *AE modes
Extend simulations to full 1T, 2MA NSTX-U scenarios
Develop/apply reduced fast ion transport models
Extend to FNSF/Pilot
3D 'Halo' model in TRANSP
NCC coils (full)
Facility
2nd (more tangential) NB line
NCC coils (partial)
Assess *AE antenna for mode excitation
Plasma Control
rotation control
q_min control

References

[1] A. Fasoli, et al., Nucl. Fusion **47** S264-S284 (2007)
[2] N. N. Gorelenkov, et al., Nucl. Fusion **43** 594 (2003)
[3] N. N. Gorelenkov, et al., Nucl. Fusion **45** 226 (2005)
[4] S. P. Gerhardt, et al., Nucl. Fusion **51** 033004 (2011)
[5] J. W. Berkery, et al., Phys. Plasmas **17** 082504 (2011)
[6] M. Ono, et al., Nucl. Fusion **40** 557 (2000); J. E. Menard, et al., Nucl. Fusion **52** 083015 (2012)
[7] N. A. Crocker, et al., Plasma Phys. Control. Fusion **53** 105001 (2011)
[8] D. R. Smith, et al., Rev. Sci. Instrum. **83** 10D502 (2012)
[9] M. Podestà, et al., Rev. Sci. Instrum. **79** 10E521 (2008)
[10] A. Bortolon, et al., Rev. Sci. Instrum. **81** 10D728 (2010)
[11] D. Liu, et al., Rev. Sci. Instrum. **77** 10F113 (2006)
[12] S. S. Medley, et al., Rev. Sci. Instrum. **75** 3625 (2004)
[13] W. U. Boeglin, et al., Rev. Sci. Instrum. **81** 10D301 (2010)
[14] N. J. Fisch, Nucl. Fusion **40** 1095 (2000)
[15] D. S. Darrow, et al., Nucl. Fusion **53** 013009 (2013)
[16] M. Podestà, et al., Nucl. Fusion **52** 094001 (2012)
[17] E. D. Fredrickson, et al., Phys. Plasmas **13** 056109 (2006)
[18] M. Podestà, et al., Phys. Plasmas **16** 056104 (2009)
[19] N. A. Crocker, et al., Phys. Rev. Lett. **97** 045002 (2006)
[20] M. Podestà, et al., Phys. Plasmas **17** 122501 (2010)
[21] M. Podestà, et al., Nucl. Fusion **51** 063035 (2011)
[22] N. N. Gorelenkov, et al., Phys. of Plasmas **16** 056107 (2009)
[23] D. Stutman, et al., Phys. Rev. Lett. **102** 115002 (2009)
[24] E. D. Fredrickson, et al., Phys. Plasmas **16** 122505 (2009)
[25] E. D. Fredrickson, et al., Nucl. Fusion **52** 043001 (2012)
[26] S. S. Medley, et al., Nucl. Fusion **52** 013014 (2012)
[27] D. A. Gates et al., Phys. Rev. Lett. **87** 205003 (2001)
[28] N. J. Fisch et al., Nucl. Fusion **34** 1541 (1994)
[29] N. J. Fisch et al., Nucl. Fusion **35** 1753 (1995)
[30] J. P. Graves et al., Nature Communications **3** 624 (2012)
[31] A. Fasoli et al., Plasma Phys. Control. Fusion **52** 075015 (2010)
[32] A. Fasoli et al., Phys. Rev. Lett. **75** 645 (1995)
[33] K. McClements et al., Plasma Phys. Control. Fusion **41** 661 (1999)
[34] M. P. Gryaznevich et al., Nucl. Fusion **46** S942 (2006)
[35] M. P. Gryaznevich et al., Nucl. Fusion **48** 084003 (2008)
[36] E. D. Fredrickson et al., Phys. Rev. Lett. **87** 145001 (2001)
[37] E. D. Fredrickson et al., Phys. Plasmas **11** 3653 (2004)
[38] A. Pankin et al., Computer Physics Communication **59** 157 (2004)
[39] see the TRANSP web-site: http://w3.pppl.gov/transp/
[40] D. Liu et al., Plasma Phys. Control. Fusion **52** 025006 (2010)
[41] M. Choi et al., Phys. Plasmas **17** 056102 (2010)

[42] K. Ghantous et al., Phys. Plasmas **19** 092511 (2012); K. Ghantous, US Transport Task Force Workshop, Annapolis MA (April, 2012)
[43] W. W. Heidbrink et al., Plasma Phys. Control. Fusion **48** 1347 (2006)
[44] A. Bortolon et al., Phys. Rev. Lett. (2013, submitted)
[45] W. W. Heidbrink et al., Nucl. Fusion **43** 883 (2003)
[46] W. W. Heidbrink et al., Nucl. Fusion **28** 1897 (1988)
[47] V. A. Yavorskij et al., Nucl. Fusion **42** 1210 (2002)
[48] Yu. V. Yakovenko et al., Proc. of 29th EPS Conf. on Controlled Fusion and Plasma Physics, ECA Vol. 26B, paper O5.09 (Montreaux, CH 2002)
[49] M. Podestà et al., Rev. Sci. Instrum. **79** 10E521 (2008)
[50] A. Bortolon et al., Rev. Sci. Instrum. **81** 10D728 (2010)
[51] D. Liu et al., Rev. Sci. Instrum. **77** 10F113 (2006)
[52] S. S. Medley et al., Rev. Sci. Instrum. **79** 011101 (2008)
[53] W. U. Boeglin et al., Rev. Sci. Instrum. **81**, 10D301 (2010)
[54] D. S. Darrow, Rev. Sci. Instrum. **79**, 023502 (2008)
[55] M. Podestà et al., Proceedings of the 54th Annual Meeting of the APS Division of Plasma Physics, contribution PP8.23 (Providence, Rhode Island 2012); Phys. Plasmas (2013, submitted)
[56] K. Tritz, Bull. Am. Phys. Soc. 55 BAPS.2010.DPP.PI2.2 http://Meetings.aps.org/link/BAPS.2010.DPP.PI2.2
[57] M. A. Van Zeeland et al., Phys. Rev. Lett. **97** 135001 (2006)
[58] G. Y. Fu et al., Joint US-EU Transport Taskforce Workshop TTF 2011, San Diego, California (April 6-9, 2011). http://ttf2011.pppl.gov/
[59] Ya. I. Kolesnichenko et al., PRL **104** 075001 (2010)
[60] N. N. Gorelenkov et al., Nucl Fusion **50** 084012 (2010)
[61] H. S. Zhang et al., Phys. Rev. Lett. **109** 025001 (2012)
[62] A. L. Rosenberg et al., Phys. Plasmas **11** 2441 (2004)
[63] D. Liu et al., Plasma Phys. Control. Fusion **52** 025006 (2010)
[64] R. B. White et al., Phys. Fluids **27** 2455 (1984)
[65] R. B. White, Commun. Nonlinear Sci. Numer. Simulat. **17** 2200 (2012)
[66] R. B. White, Plasma Phys. Control. Fusion **53** 085018 (2011)
[67] K. Tritz et al., Proceedings of the 54th Annual Meeting of the APS Division of Plasma Physics, contribution G06.4 (Providence, Rhode Island 2012)
[68] G. J. Kramer et al., "Description of the full particle orbit following SPIRAL code for simulating fast-ion experiments in tokamaks", PPPL report no. 4788 (2012); Plasma Phys. Control. Fusion **55** 025013 (2013)
[69] C. Z. Cheng, Phys. Reports **211** 1 (1992)
[70] W. Park et al., Phys. Plasmas **6** 1796 (1999)
[71] G. Y. Fu et al., Phys. Plasmas **13** 052517 (2006)
[72] J. Lang et al., Phys. Plasmas **17** 042309 (2010)
[73] J. Lang et al., Phys. Plasmas **18** 055902 (2011)
[74] H. S. Cai et al., Phys. Plasmas **19** 072506 (2012)
[75] G.Y. Fu, Proceedings of the 54th Annual Meeting of the APS Division of Plasma Physics, contribution JI2.3 (Providence, Rhode Island 2012)
[76] F. Wang et al., "Simulation of Non-resonant Internal kink mode with Toroidal Rotation in NSTX"**,** International Sherwood Fusion Theory Conference (Atlanta, Georgia, 2012)

[77] E. V. Belova, Proceedings of the 52th Annual Meeting of the APS Division of Plasma Physics, contribution TI2.3 (Chicago, IL 2010)
[78] E. V. Belova et al., Proceedings of the 24th IAEA-FEC Meeting, paper TH/P6-16 (San Diego, CA 2012)
[79] W. W. Heidbrink et al., Plasma Phys. Control. Fusion **49** 1457 (2007)
[80] W. W. Heidbrink, Rev. Sci. Instrum. **81** 10D727 (2010); W.W. Heidbrink et al., Comm. in Comp. Phys. **10** 716 (2011)
[81] M. Salewski et al., Nucl. Fusion **51** 083014 (2011)
[82] M. Salewski et al., Nucl. Fusion **52** 103008 (2012)
[83] K. Ghantous et al., Phys. Plasmas **19** 092511 (2012)
[84] H. Berk et al., Proceedings of the 24th IAEA-FEC Meting, paper TH/4-1 (San Diego, CA 2012)
[85] N. N. Gorelenkov, Proceedings of the 54th Annual Meeting of the APS Division of Plasma Physics, contribution U07.5 (Providence, Rhode Island 2012); K. Ghantous et al., "1.5D Quasilinear model for Alpha particle-TAE interaction in ARIES ACT-I", PPPL report no. 4850 (2013);

Table of Contents for Chapter 7

Chapter 7

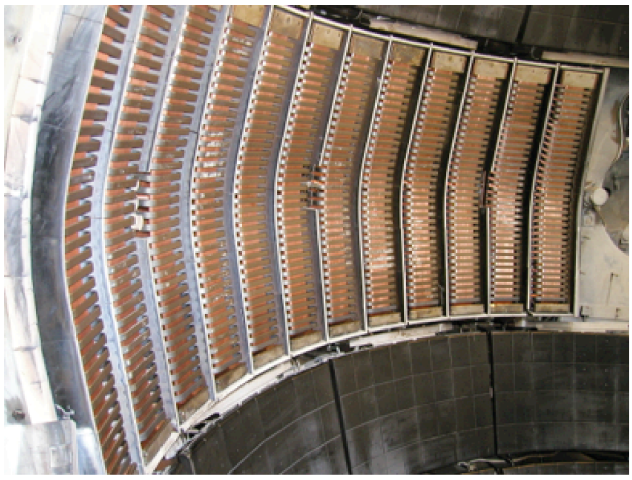

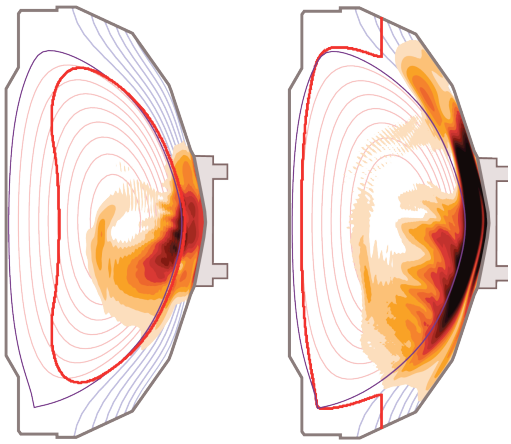

Research Goals and Plans for Wave Heating and Current Drive

7.1 Overview of Goals and Plans

7.1.1 Introduction

Radiofrequency (RF) heating and current drive in both the ion and electron gyro-frequency regimes provide important tools that support the development of burning plasma science. Twenty megawatts of Ion-Cyclotron Range of Frequency (ICRF) heating are currently planned for the International Thermonuclear Experimental Reactor (ITER). Furthermore, Fusion Nuclear Science Facility (FNSF) designs based on the spherical torus (ST) do not have a central solenoid to drive the plasma current so the plasma needs to be initiated, ramped-up and sustained fully non-inductively. Fast wave (FW) power can, in principle, effectively ramp-up the plasma current through bulk plasma heating and bootstrap current enhancement in an FNSF ST device, even at low plasma currents where neutral beam current drive maybe ineffective due to poor fast-ion confinement. FW power is also a good candidate for on-axis non-inductive current generation in other future burning plasma devices. An FNSF ST device will operate in a plasma regime where the local electron plasma frequency can far exceed the electron cyclotron frequency. This "overdense" plasma regime precludes the use of conventional electron cyclotron heating (ECH) and electron cyclotron current drive (ECCD) to assist fully non-inductive plasma current ramp-

up and to suppress deleterious off-axis neoclassical tearing mode activity. In the overdense plasma regime electron Bernstein waves (EBWs) can provide efficient local electron heating and current drive with efficiencies that are better than the ECCD efficiencies achieved in "underdense" tokamak plasmas, and EBWs can efficiently drive current far from the magnetic axis [1, 2]. Note that in this chapter "Year 1" refers to the period covered by FY2014 and so on. There are two RF research thrusts for the period FY2014-18 that support high-level NSTX-U long-term goals noted in Chapter 1; high-level goal #1, to demonstrate stationary 100% non-inductive operation at performance levels that extrapolate to $\geq$ 1 MW/m^2 neutron loading in FNSF, is supported by thrust RF-1 (section 7.1.2.1), and high-level goal #3, to develop and understand non-inductive start-up/ramp-up in order to project to an FNSF ST, is supported by both thrusts RF-1 and RF-2 (section 7.1.2.2).

The FW antenna in NSTX-U will be essentially the same as the antenna used on NSTX, consisting of an array of twelve vertical current elements, or straps, driven by six 30-MHz transmitters. Figure 7.1.1 shows a photograph of the FW antenna viewed from inside the NSTX vacuum vessel. In front of each strap is a Faraday shield. The coupled power typically ranges from 1 to 4 MW, with up to 6 MW possible. The antenna extends toroidally 90 degrees around the vacuum vessel mid-plane. This is a flexible antenna system that is able to launch toroidally balanced ("heating phasing") or directed ("current drive phasing") wave spectra characterized by absolute values of parallel wavenumber, $k_{\parallel}$, between 3 and 18 m^{-1}, by adjusting the phase between adjacent antenna straps [3].

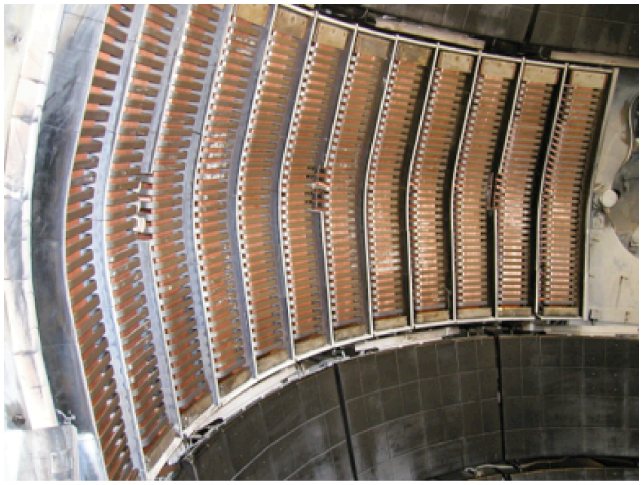

Figure 7.1.1: Photograph of the FW antenna in NSTX.

Traditional challenges for ICRF heating include achieving sufficiently high coupling from the antenna to the plasma in the good confinement region while simultaneously avoiding deleterious effects such as impurity release or overheating of plasma-facing components in the edge regions outside of the last closed flux surface (LCFS). A new loss mechanism was identified during high-harmonic FW (HHFW) experiments in NSTX: a major loss of RF power was sometimes observed to occur along open field lines passing in front of the antenna over the width of the scrape-off layer (SOL) [4-8]. In such cases, the heating efficiency was related to the location of the critical electron density (n_{ec}) for the onset of perpendicular FW propagation which is

proportional to $k_{\parallel}^2$ x B/ω, where B is the local magnetic field, and ω is the angular frequency of the wave. For 30 MHz FW heating of a discharge with $B_T(0)$ = 0.45 T, at $k_{\parallel}$ = 8 m^{-1} n_{ec} is ~ 0.5 x 10^{18} m^{-3} and at $k_{\parallel}$ = 13 m^{-1} n_{ec} is ~ 1.6 x 10^{18} m^{-3}. It is hypothesized that surface waves are being excited outside the radius where n_{ec} is located [4,5]. This hypothesis is supported by the observation that the flow of FW power is aligned along magnetic field lines that pass in front of the antenna throughout the radial width of the SOL [9]. If true, this suggests that this loss mechanism, distinct from the well-studied losses occurring directly at the antenna components, is common to various degrees in other ICRF heating systems. On NSTX-U, the increased magnetic field strength will enable greater exploration of the effects of the location of n_{ec}, while more detailed diagnostic measurements will confirm whether or not strong RF fields are present in the SOL. Further, SOL density control tools such as lithium coatings and divertor cryo-pumping will also influence the location of n_{ec}. These results will determine the validity of advanced numerical simulations of the RF power deposition in the SOL [10]. Fully understanding the underlying mechanisms behind this loss is critical for optimizing FW performance, and in particular for high-power, long-pulse ICRF heating in ITER.

Another issue of importance to ITER that can be addressed on NSTX-U is the assessment of the interaction of FWs with energetic ions generated by neutral beam injection (NBI). Results from NSTX-U experiments that heat neutral-beam-fuelled plasmas with FW power will be used to validate state-of-the-art RF simulation codes, that can in turn be used to predict the FW interaction with fast-ions in ITER, and other burning plasma devices. Since the toroidal field on NSTX-U can be operated at up to twice the level achieved on NSTX FW experiments in NSTX-U can be performed at lower ion cyclotron harmonics than was possible in NSTX. The lower harmonic ICRF heating in this medium-harmonic fast wave (MHFW) regime is expected to have less direct RF electron heating and significantly increased wave field interaction with ions, both thermal and NBI-generated fast-ions. Consequently at full field the FW system on NSTX-U will generate non-inductive current almost entirely via the bootstrap current that results from bulk plasma heating, rather than by a combination of bootstrap current and direct RF current drive. Due to the expense of using helium-3, ITER is considering FW heating of hydrogen for the “low-activation” phase, instead of using hydrogen discharges with a helium-3 minority. If this strategy is pursued on ITER the MHFW deuterium heating experiments on NSTX-U can provide important experimental data that is directly relevant to FW heating during the ITER “low-activation” phase.

FW experiments in NSTX have demonstrated that as little as 1.4 MW of FW power can generate and sustain an H-mode discharge with a plasma current of 300 kA and a non-inductive plasma current fraction of 0.7 – 1 [11]. FW experiments planned for NSTX-U will use much higher RF power and are predicted to demonstrate fully non-inductive plasma current ramp-up via bootstrap current overdrive. The results from NSTX-U FW experiments will be compared to predictions

from advanced RF numerical simulations. If the validity of the advanced RF codes can be validated for the NSTX-U FW experiments they will then be used to predict the FW performance in ITER and other burning plasma devices, such as a plasma-material-interface facility, FNSF and a Pilot Plant.

Non-inductive plasma start-up research will also benefit from the installation of a 1 MW 28 GHz EC/EBW heating system during the Year 3-4 timeframe. An upgraded version of this heating system, which has higher ($\geq$ 2 MW) 28 GHz power and a steerable launcher, may later be used for off-axis EBW heating and current drive during the plasma current flat-top. An advanced microwave EBW imaging diagnostic will be deployed on NSTX-U in Year 2-3 to assess the EBW coupling efficiency in various NSTX-U plasma regimes. These emission measurements will provide important data that will guide the design of a multi-megawatt off-axis EBW heating and current drive system. To enable EBW heating the RF power is launched from external mirrors or waveguide arrays and is coupled to EBWs inside the overdense plasma via mode conversion in the SOL. EBW emission experiments on NSTX clearly demonstrated that the EBW mode conversion efficiency is significantly improved in the H-mode regime by using lithium wall conditioning to mitigate RF power losses in the SOL that occur as a result of collisions near the EBW mode conversion layer [12,13]. The EBW coupling efficiency increased from 10% to 60% when lithium conditioning was applied, and simulations predicted an increase from 30% to 80% due to the change in collisionality in the SOL. In NSTX-U at the higher toroidal field the electron temperature in the SOL will probably be higher than on NSTX so it is expected that the collisional EBW damping will be lower than on NSTX and the EBW coupling efficiency correspondingly higher. During the NSTX-U EBW emission experiments, lithium wall conditioning will be used to enhance the EBW mode conversion efficiency, and this will contribute to the experimental validation of advanced RF simulation codes that will be used to predict EBW heating performance in NSTX-U and future fusion research facilities. Longer-term, the effects of cryo-pumping on the SOL density and EBW emission, heating, and current drive will also be measured.

The remaining sub-sections of section 7.1 of this chapter provide an overview of the two major wave heating and current drive research thrusts and the research needed to support these thrusts. Section 7.2 presents detailed research plans. Section 7.3 reviews the timeline for tools that are needed to support the wave heating and current drive research plan; including theory and modeling requirements, plasma diagnostics, and NSTX-U facility upgrades. Schematic diagrams of the research and supporting tool implementation timelines are included at the end of this chapter. Research plans are presented for a baseline NSTX-U budget scenario and a scenario with a 10% incremental increase above the baseline budget.

7.1.2 Research Thrusts

As mentioned early, the 5-year plan for wave heating and current drive research on NSTX-U has two long-term research thrusts that are part of a long-range plan to support ITER, FNSF-ST, and other burning plasma research facilities. This section presents an overview of these research thrusts and some of the key research needed to support them.

7.1.2.1 Thrust RF-1: Develop of RF/EC Heating for Non-Inductive Plasma Current Start-Up and Ramp-Up

A major goal of the NSTX-U FY2014-18 research program is the development of fully non-inductive discharges that extrapolate to the neutron wall loading in FNSF, namely ≥ 1 MW/m^2. This goal is important for the design and development of future fusion research facilities. It is challenging both scientifically and operationally. The approach on NSTX-U will therefore be to initially develop non-inductive start-up, ramp-up and plasma sustainment scenarios separately, and then later combine these non-inductive scenarios. FW heating was successfully used in NSTX to generate a > 70% non-inductive H-mode discharge with a plasma current of ~ 300 kA, using an inductively-initiated L-mode discharge as the target plasma for 1.4 MW of FW heating [11]. Three quarters of the non-inductive current in these NSTX experiments was bootstrap current and the remaining non-inductive current was generated directly by FW power. Modeling and experiments in NSTX-U will extend these FW H-mode studies by using much higher FW powers to demonstrate fully non-inductive plasma current ramp-up to plasma currents ~500 kA. Coaxial Helicity Injection (CHI) was used for non-inductive start-up in NSTX, in NSTX-U high-power EC heating will be used to significantly increase the core electron temperature of CHI discharges in order to increase the plasma current and extend the non-inductive discharge duration to allow coupling of FW and NBI power. EBW heating will also be used to initiate plasma start-up in NSTX-U using a technique being developed on MAST [14]. More details of the NSTX-U non-inductive plasma formation and current ramp-up research plan are provided later in section 7.2.2 of this chapter and in chapter 8.

7.1.2.2 Thrust RF-2: Validate Advanced RF Codes for NSTX-U and Predict RF Performance in Future Devices

NSTX-U will operate with toroidal magnetic fields up to 1 T, nearly twice the value used during the experiments on NSTX. While the dominant RF heating mechanisms in the HHFW regime in NSTX were direct electron heating, via Landau damping and Transit Time Magnetic Pumping, and NBI fast-ion acceleration, in the MHFW regime in NSTX-U the power partitioning is expected to change. Simulations of NSTX-U discharges with the AORSA [15], TORIC [16] and GENRAY [17] numerical codes predict significantly more thermal deuterium damping in the

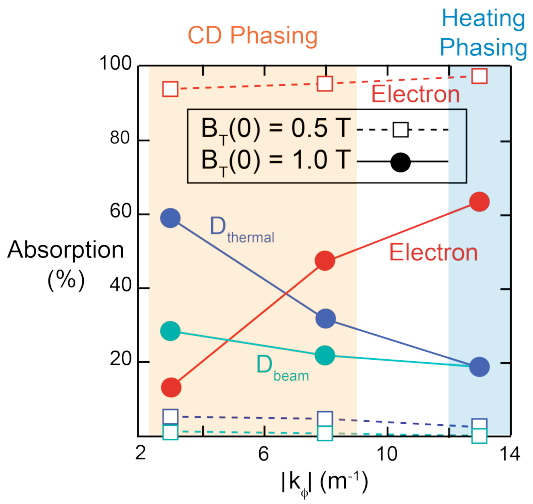

Figure 7.1.2: 30 MHz absorption versus launched wavenumber ($k_{\|}$) calculated by AORSA for a $B_T(0)$ = 1 T, and *a $B_T(0)$ = 0.5 T NSTX-U NBI + FW deuterium H-mode discharge with $n_e(0)$ = 1.09x10^{14} cm^{-3}, $T_e(0)$ = 1.22 keV, $T_i(0)$ = 2.86 keV. Strong RF absorption by thermal deuterium is predicted at the higher $B_T(0)$, especially at the smaller $k_{\|}$ used for CD. Absorption by deuterium is predominantly at the fifth ion cyclotron harmonic. Plasma parameters obtained from TRANSP run 142301G90 at 7 s.*

higher magnetic fields in NSTX-U [Fig. 7.1.2]. The lower electron beta at the higher magnetic fields in NSTX-U will result in less direct electron absorption and as a result more FW power will accelerate NBI fast-ions and thermal ions than it did in NSTX, particularly when long-wavelength, "current drive", antenna phasings are used. It is important to assess the heating and direct current drive capability of the FW system over a wide range of launched wavenumbers, toroidal magnetic fields, and electron densities in NSTX-U, and compare the experimental results to predictions by advanced RF numerical codes. These codes include the AORSA-3D full-wave solver [10] with SOL modeling and a realistic antenna model, and the full finite-orbit-width CQL3D Fokker-Planck neoclassical simulation code [18, 19]. These and other RF codes will be valuable tools for predicting the behavior of the wave fields in the SOL, the plasma edge, and the interaction with fast-ions in the bulk plasma in future burning plasma devices, including ITER. However the RF codes need to be validated against experimental data on present devices, such as NSTX-U. Accurate validation will require detailed measurements in the SOL, including edge fluctuations, RF power flows to the divertor regions, the RF power deposition profile and the current density profile. After these advanced RF simulation models have been validated during the first three years of this plan they will be used to predict RF performance in future burning plasma devices. More details of the advanced RF code validation plans are provided in section 7.2.3, and details of the RF codes are presented in section 7.3.1.

7.1.3 Research Needed to Enable Thrusts

7.1.3.1 Assess FW Interaction with Fast-Ions, and Develop Capability to Heat High-Power NBI H-Mode Plasmas with FW

A significant increase in neutron rate, and an enhancement and broadening of the fast-ion profile were measured in NBI-fuelled plasmas in NSTX when FW heating was applied [7]. These

observations indicated a strong interaction between FWs and NBI fast-ions. At the axial toroidal fields used on NSTX ($B_T(0) \leq 0.55$ T) there was often a significant loss of FW-accelerated NBI fast-ions from the plasma. Lithium conditioning enabled the first observation of significant FW central heating during NSTX NBI-fuelled deuterium H-mode plasmas, but when the NBI beam power was increased from 2 to 4 MW there was a noticeable increase in heating of the limiter surrounding the FW antenna, resulting from NBI fast-ion bombardment. A more robust limiter may be installed to protect the FW antenna from this fast-ion heating during Year 4 of the incremental plan. This upgraded limiter would provide better compatibility with the higher NBI powers available on NSTX-U. The need for a FW limiter upgrade will be assessed in Year 2-3. At the higher magnetic fields in NSTX-U the fast-ion interactions with the antenna should be reduced since the Larmor radius (and banana width at higher plasma current) will be smaller. Also the effect of the higher magnetic fields on the FW interaction with NBI fast-ions will be assessed on NSTX-U. During these experiments the FW interaction with NBI fast-ions generated by the new larger tangency radius neutral beam sources will be compared to the interaction with fast ions from the original neutral beam.

7.1.3.2 Mitigation of FW Power Losses in the Scrape Off Layer

FW heating and current-drive efficiencies on NSTX were significantly decreased by interactions of the FW power with the plasma in the SOL [4-8]. These SOL interactions result in RF power flowing from the antenna to the lower and upper divertor regions, where bright spirals are produced [Fig. 7.1.3]. The location of the spirals in the divertor regions is consistent with the hypothesis that FW power flows through the SOL to the divertor regions along magnetic field lines that pass in front of the antenna [9]. These results are important for benchmarking advanced RF codes, and for predicting the amount of FW power coupled to the SOL [10]. Fully understanding and mitigating the underlying mechanisms behind this power loss in NSTX-U is critical for optimizing FW performance in general. $B_T(0)$ and plasma current (I_p) in NSTX-U will be up to twice as high as in NSTX, which has several implications for FW coupling and heating efficiency in NSTX-U; higher B_T in NSTX-U moves the n_{ec} towards or inside the LCFS, reducing surface wave losses. The SOL width may shrink

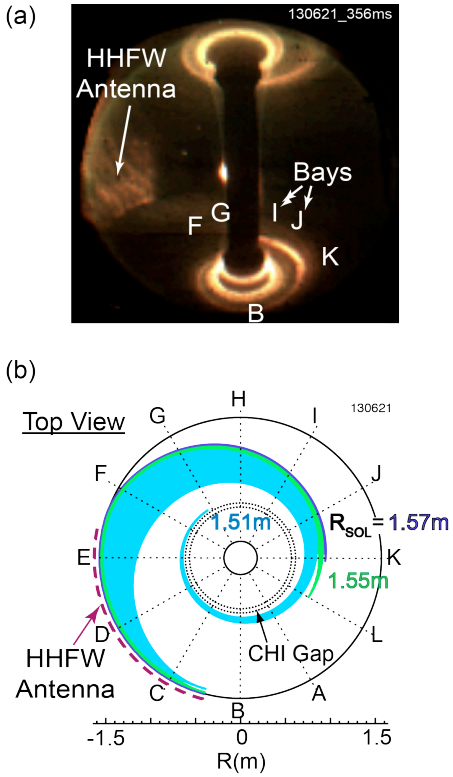

Figure 7.1.3: (a) Visible camera image of FW power flow to the divertor regions in NSTX during a $B_T(0)$ = 1 T H-mode discharge with 1.4 MW of FW power and 2 MW of NBI power (shot 130621 at 356 ms). (b) SPIRAL modeling of SOL field lines from FW antenna to the divertor for the same discharge and time as (a).

at higher I_p, reducing surface wave losses. Also, the higher electron density during high-power NBI in NSTX-U may increase the SOL density moving n_{ec} outside the LCFS and closer to the wall, and possibly increasing surface wave losses. So experiments in Year 2-3 to understand and mitigate FW power loss in the SOL will involve modifying the SOL density profile with gas puffing, lithium conditioning, and by varying I_p and $B_T(0)$ to move n_{ec}. When the cryo-pump becomes available in Year 4 it can also be used to change the location of n_{ec}. Additional IR cameras and RF probes on NSTX-U will allow a better characterization of the FW power flow to the divertor and its toroidal heat deposition.

7.1.3.3 Model and Implement an EC/EBW Heating System

With baseline funding a 28 GHz 1 MW EC/EBW heating system will be installed in Year 4. Initially this system will provide electron heating during non-inductive plasma start-up, later it will be used for off-axis EBW heating and current drive. The CQL3D Fokker-Planck code [18, 19] applied to electrons has enabled calculation of EBW absorption and current drive in the NSTX tokamak. Similar scoping work and analysis will be carried out for NSTX-U for start-up heating scenarios and for off-axis heating and current drive during the plasma current flat top.

7.1.3.4 Develop Advanced Codes that Accurately Model RF Waves in NSTX-U

While significant progress has recently been made developing numerical codes that can accurately model RF power flows and deposition in the core, edge and SOL, currently advanced RF codes, such as the AORSA full-wave code [15], lack accurate antenna geometry. Also slow-wave propagation in the SOL is not accurately modeled due to resolution constraints and because the SOL density profiles used have been approximate due to the lack of SOL measurements. During Year 1-2 the SciDAC Center for Simulation of Wave-Particle Interactions (CSWPI) has milestones to add these more accurate, high-resolution antenna and SOL modeling capabilities to AORSA and the full-wave TORIC solver [16]. As these modeling enhancements become available they will be employed to support FW studies on NSTX-U.

7.2 Research Plans for FW/EC Heating

This section presents the plans for wave heating and current drive research. Section 7.2.1 covers FW research that supports both RF thrusts, section 7.2.2 covers research for thrust RF-1 and section 7.2.3 covers research for thrust RF-2. Sections 7.2.1.5, 7.2.2.6 and 7.2.3.3 contain bulleted, year-by-year summaries for these research plans. Note FY2014 is “Year 1” in the plans.

7.2.1 FW Research Supporting Thrusts

7.2.1.1 Assess Performance of 12-Strap, Double-Feed FW Antenna and Compatibility with NBI H-Mode Discharges

In April 2009, prior to bakeout of NSTX and the beginning of the 2009 experimental campaign, the single-feed, end-grounded FW antenna straps were replaced with double-feed, center-grounded straps to reduce RF electric fields in the vicinity of the Faraday shield for a given strap current. However, the installation of the transmission lines was not completed until July 2009, by which time approximately 300 g of lithium had been deposited in the machine, much of it on the antenna itself. After several days of plasma conditioning reliable high power operation (~ 4 MW) was obtained towards the end of the 2009 campaign, but the double-feed antenna performance was never evaluated during NBI H-mode discharges without prior lithium conditioning, or at least with minimal lithium conditioning [20]. For the 2010 experimental campaign some operational changes were made to accommodate the Liquid Lithium Divertor (LLD) that further degraded the FW antenna performance; there was no boronization of the machine, no glow discharge cleaning between plasma discharges, and increased lithium evaporation rates (typically a factor of two higher than during the 2009 campaign). Furthermore the LLD was prefilled before plasma operation. Consequently the maximum arc-free FW power coupled to the plasma in 2010 was less than 2 MW. For all these reasons the performance of the 12-strap, double-feed FW antenna configuration and its compatibility with NBI H-mode discharges will be assessed for a range of NBI powers during years 2-3 of the 5-year plan.

7.2.1.2 Evaluate, Study and Mitigate RF Power Flows in the SOL and to the Divertors in the H-Mode Regime

It is important to both evaluate the FW power flows through the SOL to the divertor regions in NSTX-U [9], and to explore strategies that can mitigate these power flows (eg. by using lithium conditioning and gas puffing to change the SOL density, and by adjusting the outer gap and plasma shape). The Langmuir probe sets in the divertor tiles will be augmented to include some that have direct RF detection capability. RF probes in the tiles above and below the antenna will be installed prior to the start of NSTX-U operations. These probes will allow the measurement of the relative strengths of the RF fields propagating in both directions (co and counter) along the magnetic field lines. A new wide-angle infra-red (IR) camera viewing the lower divertor and a fast IR camera with a narrower view of the upper divertor will be installed prior to the start of NSTX-U operations. These are in addition to the two existing IR cameras viewing the divertors. Both the new IR cameras are funded in the baseline budget. RF probes in the divertor tiles will directly measure RF power deposition and Langmuir probes will allow the FW field strength to be measured in the vicinity of the RF-produced spiral deposition region. RF magnetic field

strength and RF-induced currents in the vicinity of the RF-produced spirals will also be measured. Probes in the floor and ceiling of NSTX-U will measure the directionality of wave excitation and separate direct propagation effects from standing wave effects. Measurements from the four IR cameras and the RF probes will permit a more complete quantitative assessment of RF power flow patterns across the mid-plane SOL and in the divertor regions in order to validate advanced RF codes. The detailed evaluation of the RF power flows in the SOL will be performed in years 2-3 of the 5-year plan. The effect of the cryo-pump and 3-D fields on RF power flows in the SOL will be assessed in Years 4-5.

7.2.1.3 Study FW Interaction with NBI Fast-Ions

Experiments that combined FW and NBI heating in NSTX showed a competition between two dominant absorption mechanisms in the plasma, namely direct electron heating (via Landau damping and transit-time magnetic pumping) and wave-field acceleration of NBI generated fast-ions. While it was possible to achieve good FW electron heating in Ohmic NSTX target plasmas, this was not necessarily the case when NBI power was also applied. TORIC [16] calculations, based on experimental magnetic and kinetic measurements, revealed that a large fraction (~ 50%) of the power absorbed within the LCFS can be deposited on the fast-ions, at the expense of direct electron heating. This fast-ion heating was undesirable in part because these RF-accelerated particles were poorly confined in NSTX [21], and because it limited the RF power available for current drive by reducing the power transferred to the electrons. An implementation of TORIC into the TRANSP [22] analysis software was used to compute realistic time dependent FW power deposition in NSTX plasmas. It was found that the portion of FW power going to the fast-ions decreased with time as these particles were progressively thermalized [23] consistent with the observed time evolution of the neutron production rate during the FW heating pulse.

NSTX-U will expand the operational range of FW heating to lower ion cyclotron harmonics. In particular, the higher maximum magnetic field will move n_{ec} towards the LCFS and hence reduce losses originating in the SOL that were previously observed in NSTX [9]. Moreover the larger plasma current will better confine the RF-accelerated ions. It is also expected that thermal-ion heating by FWs will become appreciable at the higher magnetic field in NSTX-U. In addition to indirect observations mentioned above, the fast-ion D-alpha (FIDA) [24] diagnostic will provide time and spatially resolved information about the fast-ion density and acceleration, enabling a better understanding of the physics of the FW heating in the presence of NBI. These experiments will be conducted in collaboration with the NSTX-U Energetic Particles group to study the effect of FW heating on the spectrum of Alfvén eigenmode (*AE) activity and fast-ion transport (see section 6.3.3.4). Experimental studies of the FW interaction with NBI fast-ions will be performed in years 2-4 of the 5-year plan.

7.2.1.4 Simulate/Mockup Reduced-Strap FW Antenna

The baseline 5-year plan for the FW antenna is to reduce the number of current straps used for FW heating from 12 to 8 to make room available for antennas that will excite *AE modes and/or use some of the FW antenna straps to excite edge harmonic oscillations (EHOs) after Year 5 in the incremental plan. Before implementing any changes to the number of antenna straps experiments will evaluate the performance of the 12-strap FW antenna when it is configured with only eight active straps. These mocked up reduced-strap experiments will be performed in Year 5.

7.2.1.5 Summary of Research Plan by Year for FW Research Supporting Thrusts

Assuming a Baseline Funding Scenario (*Baseline + 10% incremental scenario in italics*)

Year 1 (FY2014):

- Complete simulation of FW heating during non-inductive I_p ramp-up and the I_p flat top.

Year 2:

- Assess performance of 12-strap, double-feed, FW antenna and its compatibility with NBI H-mode $B_T(0) \leq 0.8$ T discharges. Experiments will be performed with 2-3 MW of FW coupled power in a boronized machine, with the minimum lithium conditioning needed to achieve good FW coupling. Both heating and current drive antenna phasings will be used during these experiments. $B_T(0)$ will be scanned from 0.5 to 0.8 T. The amount of lithium conditioning will be increased to assess the performance of the FW antenna and the plasma heating efficiency.
- Evaluate, study and mitigate RF power flows in the SOL and to the divertor regions in the H-mode regime in $B_T(0) \leq 0.8$ T discharges. Experiments will be performed with 2-3 MW of FW coupled power and 2-4 MW of NBI power in a boronized machine with minimal lithium conditioning. $B_T(0)$ will be scanned from 0.5 to 0.8 T. Both heating and current drive antenna phasings will be used during these studies. Once the SOL RF power flows have been well characterized with RF probes, IR cameras etc., lithium conditioning, gas puffs and outer gap scans will be introduced in an attempt to mitigate the SOL RF power flows to the divertor regions.
- Study FW interaction with NBI fast-ions in $B_T(0) \leq 0.8$ T discharges. $B_T(0)$ will be increased from 0.5 to 0.8 T. The antenna phase will scanned at each level of $B_T(0)$ and a

comparison will be made between the interaction with fast-ions from the original beam lines and the new more tangential beam lines.

Year 3:

- Assess performance of 12-strap, double-feed, FW antenna and compatibility with NBI H-mode $B_T(0) \leq 1$ T discharges. Experiments will be performed with 3-5 MW of FW coupled power in a boronized machine, with the minimum lithium conditioning needed to achieve good FW coupling. Both heating and current drive antenna phasings will be used during these experiments. $B_T(0)$ will be scanned up to 1.0 T. The amount of lithium conditioning will be increased to assess the performance of the FW antenna and the plasma heating efficiency.
- Evaluate, study and mitigate RF power flows in the SOL and to the divertor regions in the H-mode regime in $B_T(0) \leq 1$ T discharges. Experiments will be performed with 3-4 MW of FW coupled power and 2-4 MW of NBI power in a boronized machine with minimal lithium conditioning. $B_T(0)$ will be scanned up to 1.0 T. Both heating and current drive antenna phasings [3] will be used during these studies.
- Continue to study FW interaction with NBI fast-ions in $B_T(0) \leq 0.8$ T discharges.
- *Study FW interaction with NBI fast-ions in $B_T(0) \leq 1$ T discharges. (see Year 4 for more details)*

Year 4:

- Study FW interaction with NBI fast-ions in $B_T(0) \leq 1$ T discharges. The antenna phase will scanned at each level of $B_T(0)$ and a comparison will be made between the interaction with fast-ions from the original beam lines and the new more tangential beam lines.
- *Assess the effect of cryo-pumping and 3-D fields on FW coupling. The cryo-pump and 3-D fields may help to mitigate RF losses in the SOL by lowering the SOL density.*
- *Reduced-strap FW antenna mockup experiments. (see Year 5 for more details)*

Year 5:

- Assess the effect of cryo-pumping and 3-D fields on FW coupling. The cryo-pump and 3-D fields may help to mitigate RF losses in the SOL by lowering the SOL density.
- Reduced-strap FW antenna mockup experiments. These experiments will test heating and current drive antenna phasing during the plasma current flat top of FW-only H-mode discharges, H-mode discharges that combine FW and NBI heating, and for FW-assisted non-inductive plasma current ramp-up. Before these experiments are conducted,

numerical simulations will be performed to determine the coupled spectra of modes for a range of antenna phasings and the resulting RF power deposition and current drive profiles in various NSTX-U target discharges.

7.2.2 Thrust RF-1: Develop RF/EC Heating for Non-Inductive Plasma Current Start-Up and Ramp-Up

This research thrust supports the research goals of the NSTX-U Solenoid Free Plasma Start-Up Topical Science Group (SFPS TSG), whose research plans and goals are discussed in detail in Chapter 8. Here we review experimental plans for non-inductive plasma current ramp-up and start-up that utilize FW, EC and EBW heating and current drive that support experiments also discussed in sections 8.6.3, 8.6.4 and 8.7.5.

7.2.2.1 Fully Non-Inductive FW H-Mode, and Non-Inductive Plasma Current Ramp-up with FW Power

In 2010 1.4 MW of $k_{\parallel}$ = -8 m^{-1} FW power (current drive antenna phasing) was coupled into an I_p = 300 kA, $B_T(0)$ = 0.55 T Ohmic target plasmas (XP-1009) generating a sustained H-mode and achieving a non-inductive current fraction, f_{NI} = 0.7 – 1.1. This result was the consequence of better plasma control, the improved RF coupling due to lithium conditioning, and the positive feedback between a high $T_e(0)$ ~ 3 keV, and a relatively high RF current drive efficiency ~ 0.1 MA/MW. However, lithium compound dust in the antenna played a major role in limiting the arc-free FW power to ~ 1.4 MW. While lithium conditioning has been found to be

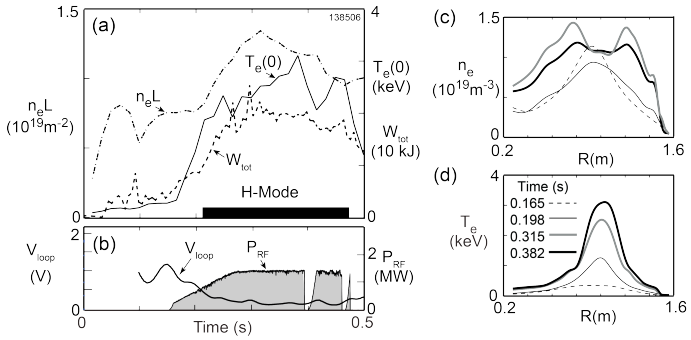

Figure 7.2.1: Time evolution of an I_p = 300 kA FW-generated H-mode plasma (shot 138506) that maintained good FW coupling to the core during the H-mode phase. (a) Line integrated density (n_eL), central electron temperature ($T_e(0)$) and total plasma stored energy (W_{tot}) versus time. (b) The time evolution of the measured loop voltage (V_{loop}) and RF power. (c) Electron density and (d) electron temperature versus major radius at four times during shot 138506; 0.165 s, (dashed line), 0.282 s (thin solid black line), 0.298 s (thick solid grey line) and 0.382 s (thick solid black line).

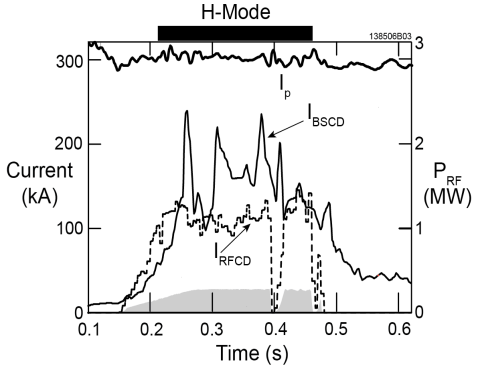

Figure 7.2.2: I_p (thick solid line), I_{BS} (thin solid line) and I_{FWCD} (dashed line) calculated by TRANSP-TORIC for shot 138506, and the RF power (Gray shading) plotted versus time.

generally beneficial for improving FW coupling in NSTX in the past [7], two vacuum leaks produced the dust after extensive lithium conditioning. Another issue with the experiments in 2010 was that NBI source A was not available to provide the heating neutral beam blips necessary for documenting the evolution of $q(R)$ and T_i. Figure 7.2.1 summarizes the results for the best discharge from XP-1009, shot 138506. An H-mode was generated soon after turn-on of the FW power that had good on-axis electron heating. Figure 7.2.2 shows TRANSP-TORIC modeling results for shot 138506, assuming 100% of the FW power is coupled to the discharge. The coupling efficiency was actually ~ 60% during this discharge, so only ~ 25% of the non-inductive current was driven directly by FW power, the rest is bootstrap current, which fluctuated by about 50% due to changes in the off-axis electron pressure. A more stable electron pressure profile is needed to control the magnitude of the non-inductive current. Fully non-inductive FW H-mode experiments will be performed in Years 2-3 of the 5-year plan.

7.2.2.2 Assess Impact of FW Heating on NBI Current Ramp-up

TSC simulations predict that starting from a 400 kA inductive target, bootstrap current overdrive and neutral beam current drive can ramp-up the plasma current to 1 MA in about 3 seconds. In these simulations, an initial 400 kA low-inductance discharge is heated using 4 MW of FW power. The H-mode is initiated at about 150 ms. The NBI power is programmed to increase with the plasma current. The FW power is turned off in the simulations at 900 ms to limit the NBI fast-ion interaction with the antenna. A combination of NBI and FW heating will be used to non-inductively ramp-up the plasma current from 300-400 kA to 0.8-1 MA during Years 3-4 of the 5-year plan. These experiments will assess the impact of adding FW heating to the NBI heated current ramp-up.

7.2.2.3 EC Heating of CHI Plasma

CHI-only target plasmas have $T_e(0) < 10$ eV and pulse lengths that are only 20-40 ms. EC heating at the megawatt-level will significantly increase $T_e(0)$ and the current persistence time. GENRAY [17] modeling of a NSTX CHI plasma with $B_T(0) \sim 0.5$ T (shot 148072) predicts ~25% first-pass absorption of 28 GHz X-mode EC power (see section 8.9.3). With baseline NSTX-U funding a megawatt-level, 28 GHz EC heating system is planned for installation on NSTX-U by Year 4. When the 28 GHz heating system has been commissioned into low density inductive plasmas and becomes available for experiments it will be used to heat CHI target plasmas.

7.2.2.4 Non-Inductive Start-Up with EBW Heating

EC heating cannot be used to heat start-up plasmas once the plasma density exceeds the critical density for EC wave propagation. In this so-called “overdense” regime EBW heating can be used

but it requires a mode conversion process to couple the electromagnetic wave launched from the antenna to the EBW inside the overdense plasma. Once the 28 GHz heating system becomes available on NSTX-U a double mode conversion scheme that has been used successfully in MAST [14] will be used for EBW start-up. Experiments on MAST have so far generated 30 kA of plasma current with about 50 kW of EBW power. EBW start-up experiments in NSTX-U will allow the power scaling of this technique to be tested for EBW power levels above 500 kW. EBW start-up may allow more time to control the plasma position and discharge evolution than CHI start-up. The EBW start-up scheme used on MAST utilizes a grooved graphite mirror polarizer tile on the center column to reflect the launched O-mode power and convert it to X-mode power that then undergoes a subsequent 100% X-mode to EBW mode conversion at the upper hybrid resonance located near the plasma core. In this mode conversion scheme the excited EBW mode is totally absorbed. This coupling scheme avoids the complication of converting to the RF power to EBWs near the plasma edge but it can only be used when the second harmonic is underdense. Under baseline funding EBW start-up experiments will be started in Year 5, with incremental funding they will start in Year 4.

7.2.2.5 EBW Heating in NBI H-Mode Discharges

In conventional tokamaks local off-axis ECH and ECCD have become important tools for suppressing deleterious neoclassical tearing modes (NTMs). Because NSTX-U NBI H-mode plasmas operate well inside the overdense regime it is not possible to employ ECH or ECCD to suppress NTMs. Therefore the long-term plan for NSTX-U is to install a multi-megawatt, long-pulse 28 GHz EBW heating system that can heat and drive current off-axis. This system will use a steerable mirror launcher that can couple power to the plasma via ordinary-mode (O-mode) to slow X-mode to EBW (O-X-B) double-mode conversion. It will be capable of launching 2-4 MW of 28 GHz power for up to

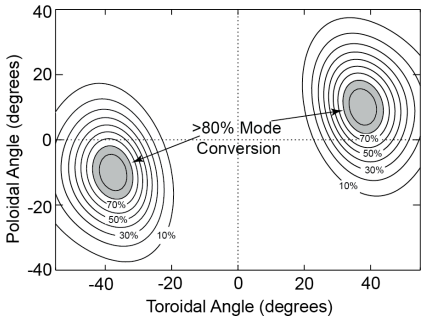

Figure 7.2.4: O-X-B mode conversion efficiency versus poloidal and toroidal angle for NSTX-U TRANSP run 142301V11 at 11.875 s. GENRAY-ADJ modeling was performed assuming a launched $n_{//} = \pm 0.7$, corresponding to alignment of the mirror launcher with the indicated regions of maximum mode conversion.

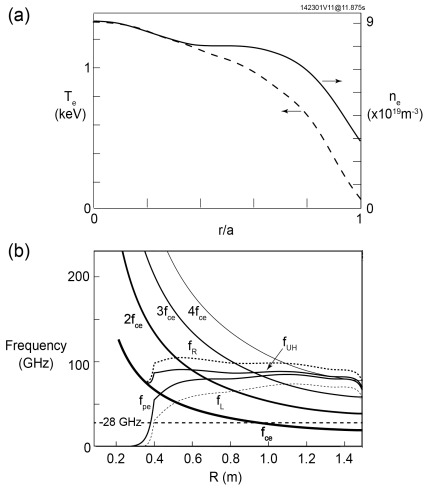

Figure 7.2.3: (a) Profiles of electron temperature (dashed line) and electron density (solid line) used for modeling EBW heating and current drive, and (b) electron cyclotron resonances and cutoffs for NSTX-U TRANSP run 142301V11 at 11.875 s.

5 s, will heat electrons locally off-axis, and will also efficiently drive current off-axis via Ohkawa current drive (see ref. [1, 2] and references therein).

GENRAY ray tracing [17] and CQL3D Fokker-Planck modeling [18, 19] has been performed for EBW heating in a 1.1 MA advance scenario NSTX-U H-mode plasma with 6 MW of NBI heating, an axial toroidal field of 1 T (TRANSP run 142301V11 at 11.875 s). The density and temperature profiles used for the modeling are shown in Fig. 7.2.3(a). The electron cyclotron resonances and cutoffs for this plasma are shown in Fig. 7.2.3(b). 28 GHz EBWs are resonant with f_{ce} at $R \sim 0.95$ m, close to the magnetic axis. The O-X-B conversion efficiency was calculated as a function of poloidal and toroidal angle and the results are summarized in Fig. 7.2.4. The maximum O-X-B mode conversion efficiency was obtained for a poloidal angle of ± 10 degrees and a toroidal angle of ± 38 degrees, corresponding to $n_{//} = \pm 0.7$.

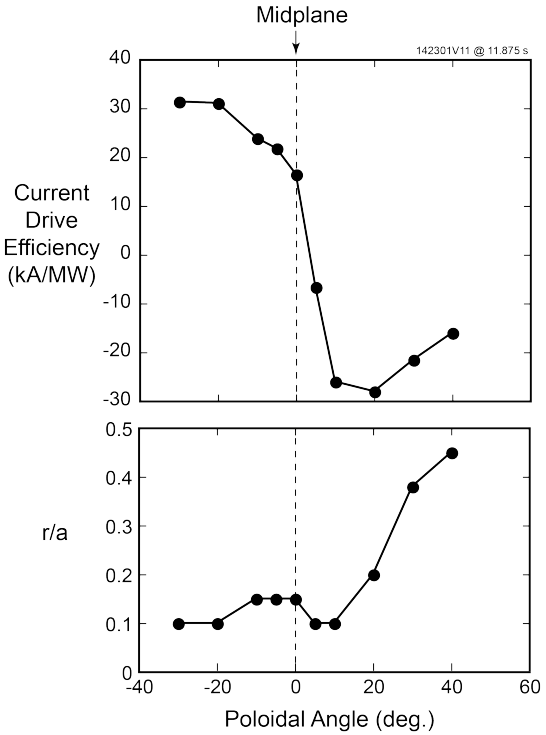

Figure 7.2.5: (a) EBW current drive efficiency versus poloidal angle of the mirror launcher. Negative angles correspond to the launcher being below the midplane and negative current drive efficiency is counter current drive. (b) Normalized minor radius where the peak driven current density is generated.

Modeling of the EBW heating and current drive assumed a launched $n_{//} = \pm 0.7$. The EBW rays were launched at the LCFS and the vertical location of the launched rays was scanned above and below the midplane. Figure 7.2.5 summarizes the CQL3D current drive modeling results for 1 MW of EBW power. The maximum current drive efficiency is 30 kA/MW. When the launching mirror is 30 degrees below the midplane the current is driven in the co-current direction near the magnetic axis. When the launching mirror is 10 degrees or more above the midplane the current is driven in the counter current direction. As the mirror is moved even further above the midplane the EBW-driven current peaks further off axis. Launching the EBW power more than 30 degrees above the midplane resulted in large Doppler shifts, so that the EBW power was absorbed well off axis and the EBW power deposition profile became very broad.

The multi-megawatt O-X-B heating system will not be implemented during the period of this 5-year plan, even with 10% incremental funding. However, the antenna of the 1 MW, 28 GHz EC heating system discussed earlier can be modified to allow a test of O-X-B heating during the flat top of NSTX-U NBI H-mode discharges in Year 5.

7.2.2.6 Summary of Research Plan by Year for Thrust RF-1

Assuming a Baseline Funding Scenario (*Baseline + 10% incremental scenario in italics*)

Year 1 (FY2014):

- Complete simulation of 28 GHz heating system for non-inductive startup and complete conceptual system design.
- Continue simulation of 28 GHz EBW heating and current drive in NSTX-U advanced scenarios and begin conceptual design for O-X-B heating system.

Year 2:

- Generate a sustained fully non-inductive 300-500 kA H-mode discharge with FW power using an inductively generated target discharge.
- EBW emission data acquired to assess O-X-B coupling efficiency (see section 7.3.2).

Year 3:

- Non-inductively ramp I_p in a FW-only H-mode discharge from 300 to 500 kA. These experiments will benefit from current density measurements with the new motional Stark effect laser-induced fluorescence (MSE-LIF) diagnostic (see section 10.6.1.5) which uses a low-power, non-perturbing diagnostic neutral beam rather than the heating beam used by the conventional MSE collisionally-induced fluorescence, (MSE-CIF) diagnostic.
- Assess of the impact of FW heating on NBI current ramp-up. A combination of NBI and FW heating will be to non-inductively ramp-up the plasma current from 300-400 kA to 0.8-1 MA. These experiments will assess the impact of adding FW heating to the NBI heated current ramp-up. These experiments will be continued in Year 4.
- Continue acquiring EBW emission data to assess O-X-B coupling efficiency (see section 7.3.2).

Year 4:

- Continue to assess of the impact of FW heating on NBI current ramp-up.

Year 5:

- 28 GHz EC heating of a CHI plasma. Target conditions will be adjusted for maximum 28 GHz single pass absorption. Core heating with X-mode second harmonic EC heating at $B_T(0) \sim 0.5$ T and O-mode fundamental EC heating at $B_T(0) \sim 1$ T will be studied. TSC simulations predict 0.6 MW of second harmonic 28 GHz EC heating will increase $T_e(0)$ of the CHI target plasma from ~ 5 eV to ~ 400 eV in 20 ms. If reproducible EC-heated

CHI target plasmas can be generated with $T_e(0) \geq 100$ eV they will be heated with FW power to non-inductively ramp the plasma current.

- Non-inductive start-up with EBW heating. The grooved graphite mirror polarizer on the center stack that is needed for these experiments will be installed in NSTX-U during the Year 3-4 machine outage.
- Test 28 GHz EBW heating via O-X-B coupling with a fixed horn antenna. EBW emission data acquired in Year 2-3, together with numerical simulations for specific discharge scenarios, will be used to adjust the launch direction of the 28 GHz horn used for EC heating, so that it efficiently couples to EBWs in the plasma. Experiments would initially attempt core electron heating, because it is easier to detect. If these on-axis heating experiments prove successful, experiments would be extended to off-axis heating, and possibly current drive, if sufficient power can be coupled to the plasma. These experiments would provide valuable experimental data to verify predictions of numerical simulations of EBW heating by advanced RF codes.

7.2.3 Thrust RF-2: Validate Advanced RF Codes for NSTX-U and Predict RF Performance in Future Devices

7.2.3.1 Validate Advanced RF Codes that Include SOL, Realistic Antenna Geometry, Accurate Modeling of Fast-Ion Interaction and the Effect of Edge Fluctuations

An extensive suite of advanced RF simulation codes directly supports the RF experimental research program on NSTX-U, and the existing domestic plasma fusion research program in general. These codes are, and will be, used to predict RF heating and current drive performance in ITER and other fusion devices. A major NSTX-U RF research program goal is therefore to advance the development of these RF theory and simulation tools by experimentally testing their predictions for NSTX-U RF-heated plasmas. Many of these advanced RF numerical codes are currently being upgraded to include detailed models of the SOL and plasma edge region near the LCFS, including edge fluctuations that can scatter RF power, and in the case of AORSA-3D [10] a high-resolution model of the FW antenna. For modeling FW heating, inclusion of the SOL and edge enables the simulation of RF excited normal modes that may contribute to parasitic loss of injected RF power. To complement these upgrades to the advanced RF codes the diagnostics on NSTX-U will be improved to better measure RF fields and power flows, near the antenna, in the SOL and on the divertor plates. Also the edge and SOL reflectometer is being upgraded to operate over a larger frequency range in order to measure the density profile at the higher toroidal fields where NSTX-U will operate. In addition the reflectometer's data acquisition system is being upgraded to acquire more data at a higher rate than was possible on NSTX.

Several numerical codes have now been developed and upgraded to more accurately model the FW interaction with ions in discharges heated by a combination of FW and NBI power. These codes will be invaluable for predicting ICRF heating and current drive in ITER discharges. There will be several enhancements to NSTX-U diagnostics that can measure changes in the fast-ion distribution due to FW ion acceleration that will allow these code predictions of fast-ion behavior to be tested. Upgrades to the multi-point Thomson scattering and MSE diagnostics will also provide improved measurements of RF power deposition and the current density profile that can be compared to the predictions from numerical simulations.

During the period of this five-year plan, detailed diagnostic data from the new and upgraded diagnostic suite on NSTX-U will have been acquired during FW-only H-mode discharges and FW-heated NBI H-modes discharges. Also the advanced RF codes will have undergone significant upgrades to more realistically simulate both RF losses in the SOL and FW interaction with ions inside the LCFS. It will therefore be possible to conduct a detailed validation of these more realistic RF simulations.

7.2.3.2 Use of Advanced RF Codes to Predict RF Performance in ITER and Future Fusion Devices

The advanced RF numerical codes will be upgraded and modified in response to their validation against NSTX-U experimental data for a wide range of plasma regimes, including RF heating during plasma current start-up, ramp-up, and during NBI H-mode discharges. Once the codes have been shown to accurately simulate NSTX-U discharges in these regimes they will be used to predict RF performance in ITER and future fusion devices.

7.2.3.3 Summary of Research Plan by Year for Thrust RF-2

Assuming a Baseline Funding Scenario (*Baseline + 10% incremental scenario in italics*)

Year 1 (FY2014):

- Upgrade advance RF codes to include SOL, realistic antenna geometry, accurate modeling of fast-ion interactions and effect of edge fluctuations.

Year 2-3:

- Detailed validation of advanced RF codes that include accurate SOL and antenna modeling using data from the upgraded diagnostic suite on NSTX-U for H-mode scenarios that employ FW heating and current drive.

Year 4-5:

- Use advanced RF codes to predict RF performance in ITER and future fusion devices.

7.3 Timelines for Tool Development Needed to Achieve Research Goals

7.3.1 Theory and Simulation Capabilities

As a national facility, the development of RF theory and simulation capabilities on NSTX-U involves a collaborative effort between the PPPL NSTX-U physicists and their counterparts in the Alcator C-Mod and DIII-D programs, as well as significant support from the USDOE CSWPI. The funding support includes direct support from the NSTX-U project, individual grants and contracts from USDOE to various institutions such as the PSFC-MIT and CompX, as well as support through the RF-SciDAC Center. Understanding the underlying physics of the RF heating, current drive, interactions with fast-ion populations, and the coupling of power to the plasma and translating that understanding into validated simulation codes that include physics details over a wide range of parameters is a common need for all of these programs. In the following sections details of specific RF numerical simulation codes that support the NSTX-U 5-year wave heating and current drive research plan are discussed.

7.3.1.1 AORSA Full-Wave Code

In its present form, the All Orders Spectral Algorithm (AORSA) full-wave tool [15] lacks a high-fidelity, geometry-accurate antenna model, any slow-wave propagation in the SOL (due to

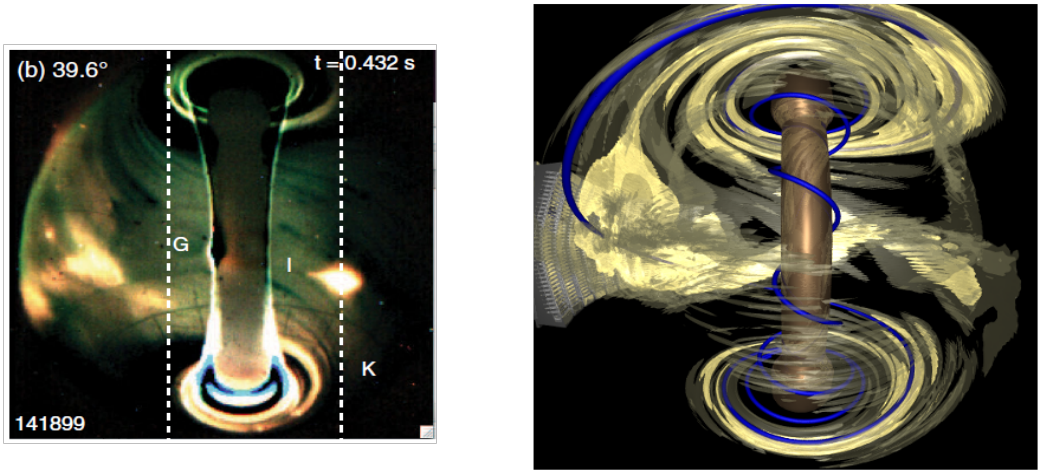

Figure 7.3.1: The left panel shows a visible light image indicating the edge RF power flow following magnetic field lines from the antenna to the divertor during an FW-heated NBI H-mode discharge in NSTX. The right panel shows the AORSA-3D simulation results for the electric wave field magnitude for this case.

resolution constraints), and is typically run with SOL density profiles that are simplified and/or approximate due to the lack of available constraining observations. During the first two years of the 5-year plan these capabilities will be added to AORSA. The impact of any edge localized RF excited normal modes that contribute to parasitic loss of RF power will then be evaluated. Although preliminary work in this area suggests that the Poynting flux associated with FW excited RF normal modes of the SOL is not correlated with that observed in the optical camera images obtained on NSTX during FW heating of NBI H-mode discharges (Fig. 7.1.3(a) and Fig. 7.3.1), a further study will be conducted to examine tracer particles in the FW electric wave-fields calculated by AORSA-3D to investigate if there is a field-aligned particle flux that is accelerated either by the SOL RF normal modes, or the near field of the FW antenna. Normal modes localized near the LCFS have been seen in AORSA results for negative toroidal mode numbers [25], and these modes do exhibit field-aligned Poynting flux, but at the LCFS, not in the SOL as seen in NSTX (c.f., Fig. 7.1.3(a) and Fig. 7.3.1). Long-range plans are to couple AORSA to a high-fidelity antenna model (e.g., VORPAL [26]) that includes a self-consistent RF sheath with AORSA-3D. Such a coupling will provide an electric wave-field solution suitable for examining stochastic heating that may be another possible cause for the observed field-aligned power flow.

EBW heating schemes depend on mode conversion, either via tunneling between the fast X-mode and the EBW (X-B) or via double mode conversion from the O-mode to slow X-mode to the EBW (O-X-B). As such assessing these heating schemes requires some estimate of how much power is converted from the launched mode, to the EBW mode. These conversion efficiencies are typically estimated using 0-D expressions that ignore any effects due to density fluctuations and turbulence in the edge and SOL plasma. However, according to [27] an observed 30% variation in transmission/emission efficiency is probably due to density fluctuations in the plasma edge. AORSA-1D will be used to map the transmission/emission coefficients for the k-space spectrum of a launched wave for arbitrary density profiles, e.g., turbulent density data from a transport simulation. These results will be compared with the standard transmission formulas used in ray tracing calculations (c.f. ref [28] and references therein). The aim will be to predict any degradation in heating efficiency associated with density fluctuations.

7.3.1.2 TORIC full Wave Code, with SOL Model

The present edge model in the TORIC solver [16] consists of a SOL that extends out to a Faraday screen and beyond that is a current strap in vacuum. A conducting wall is placed in the back of the current strap. The locations of the current strap, Faraday screen, and conducting wall correspond to conforming flux surfaces and their locations can be specified arbitrarily. Similarly, the density profile and width of the SOL are also arbitrary. The caveats are that the magnetic

equilibrium in the vacuum region is taken to be closed flux surfaces and the SOL width is imposed using the region just inside the LCFS so that the effective minor radius of the plasma is reduced slightly. Initially this simplified SOL model in TORIC will be used to perform simulations with the Faraday screen removed and the current strap placed right at the edge of the plasma SOL, with a vacuum region extending from the outside edge of the current strap to the conducting wall. Surface wave excitation will then be studied in a manner similar to what has been done with the AORSA solver, whereby 3-D field reconstructions are done by calculating the 2-D (ψ, θ) electric field solutions with TORIC for each toroidal mode of the antenna and then superposing these solutions. Over the longer term the plan is to take advantage of work being carried out with TORIC in the CSWPI where the core solver will be combined with an edge model such as the VORPAL code [28], which allows realistic treatment of the 3-D solid geometry of the ICRF antenna structure and vacuum vessel. This coupling will be done either through standard admittance matrix techniques or through more direct methods that rely on finding regions of overlap between the boundary and core solutions.

7.3.1.3 GENRAY Ray Tracing and TORBEAM Beam Tracing Codes

GENRAY is a ray tracing code based on the geometrical optics approximation for the calculation of electromagnetic wave propagation and absorption in tokamak plasma geometry [17]. While the beam tracing code TORBEAM [29], which is based on the paraxial WKB approximation, takes into account diffraction effects in the RF beam propagation. GENRAY includes a current drive calculation, ADJ [30] that uses an adjoint approach based on the Coulomb Fokker-Planck collisional operator and the relativistic quasilinear flux. GENRAY has been generalized recently to include a 2-D model for the SOL [31] and the effects of scattering induced by edge density fluctuations in the lower hybrid frequency regime [32]. Following the approach in [33], this scattering model utilizes a wave kinetic equation, which is solved by a Monte-Carlo technique. An extension of this scattering model for the FW regime will be implemented in GENRAY in order to evaluate the possible role of scattering in NSTX-U plasmas. GENRAY will also be generalized for the EBW/EC frequency regime in order to evaluate the importance of scattering in NSTX-U plasmas, taking into account several important features already present in the GENRAY code, such as the calculation of the critical angle for EBW O-X-B mode conversion (which depends strongly on the edge density gradient) and the estimate of the reduced coupling if waves are launched away from the optimum angle for O-X-B coupling. An accurate validation of GENRAY and TORBEAM for NSTX-U plasmas will be performed. Such numerical analysis will be also used to predict RF heating performance in future fusion devices.

7.3.1.4 CQL3D Fokker-Planck Code

The CQL3D bounce-averaged Fokker-Planck finite-difference code [18, 19] has been used successfully for modeling the NBI and FW heating in NSTX, particularly including the quasi-

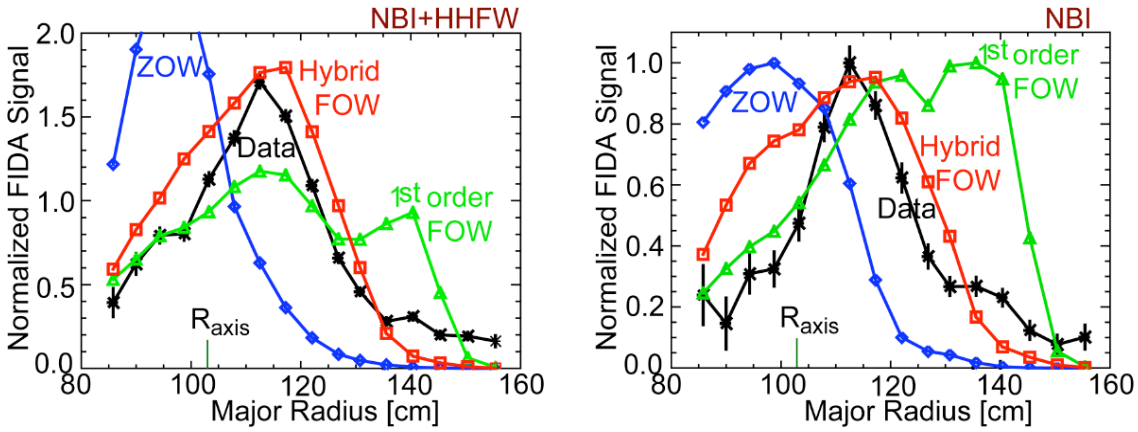

Figure 7.3.2. Experimental FIDA diagnostic fast-ion radial profiles compared to the original zero-orbit-width (ZOW) results from CQL3D, the 1st order finite-orbit-width (FOW) results, and the much more accurate hybrid-FOW results. Calculated FIDA results are normalized to the NBI experimental data. The same normalization is used for the NBI+FW modeling, after reducing FW nominal input power by 35% to account for RF edge losses.

linear RF wave-interaction [34-36]. Along with the GENRAY ray tracing code model for FW, a strong interaction with the NBI ions is obtained [34]. Finite-orbit-width (FOW) effects have recently been implemented in the code [37], computing the bounce-averaged Fokker-Planck terms along guiding-center ion orbits. Two different versions are being developed: (1) A Hybrid-FOW model in which partial FOW capabilities are implemented, namely in the formation of the NBI source, the RF quasi-linear diffusion operator, the particle diagnostics, and the loss cone. There is no neoclassical radial transport in this version. The main advantage of this version of the code is that it is as fast as the original zero-orbit-width (ZOW) version. Initial applications show a marked improvement in the description of diagnostic signals in NSTX, as shown in Fig 7.3.2 [37].

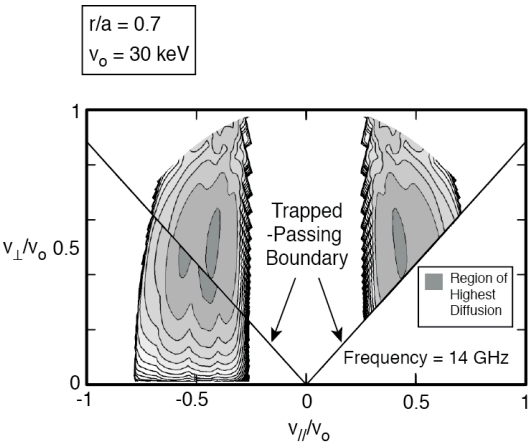

Figure 7.3.3: Contours indicating the strength of the quasi-linear diffusion operator due to the RF [u^2D_{uu}] versus the perpendicular and parallel velocity, normalized to v_o = 30 keV, at the peak of the EBW power deposition profile located at r/a = 0.7 for 1 MW of 14 GHz power launched into the β = 42% NSTX plasma. The quasi-linear diffusion peaks near the trapped-passing boundary. (From ref. [1])

(2) A full-FOW neoclassical model including radial transport and non-thermal bootstrap current is currently under development. An intermediate first order orbit shift model was also developed for application to NSTX, but the fast-ion orbits were too large for this approximation, as shown in Fig. 7.3.2.

Recently the FW quasi-linear coefficients calculated by the AORSA full-wave code [38] have been coupled to CQL3D. Additional wave-particle physics will be included with the Diffusion Coefficient (DC) code, as described in the following section 7.3.1.5.

The CQL3D code applied to electrons has enabled calculation of EBW absorption and current drive in the NSTX tokamak [1, 39]. Figure 7.3.3 shows the strength of the quasi-linear diffusion operator across the trapped-passing boundary due to RF in an NSTX discharge with EBW heating (from ref. [1]). Similar scoping work and analysis will be carried out for NTSX-U [40]. EBW ray tracing from GENRAY provides the data necessary for CQL3D to calculate the RF quasi-linear coefficients. Iteration between EBW absorption giving the EBW electric field strength, and the solution of the Fokker-Planck equation for the non-thermal electron distributions on which the absorption depends, provides self-consistent distributions and absorption profiles. Current drive is calculated from the non-thermal distributions. Off-axis current drive efficiencies were obtained [1] which are about twice that calculated and measured for ECCD near the axis in the DIII-D tokamak. This was determined to be largely due to Ohkawa current drive [41] resulting from a property of EBWs that gives enhanced quasi-linear velocity diffusion near the trapped-passing boundary, rather than the more usual Fisch-Boozer current drive [42].

7.3.1.5 Diffusion Coefficient (DC) Code

The DC code calculates “exact” full-wave RF diffusion coefficients by numerically integrating

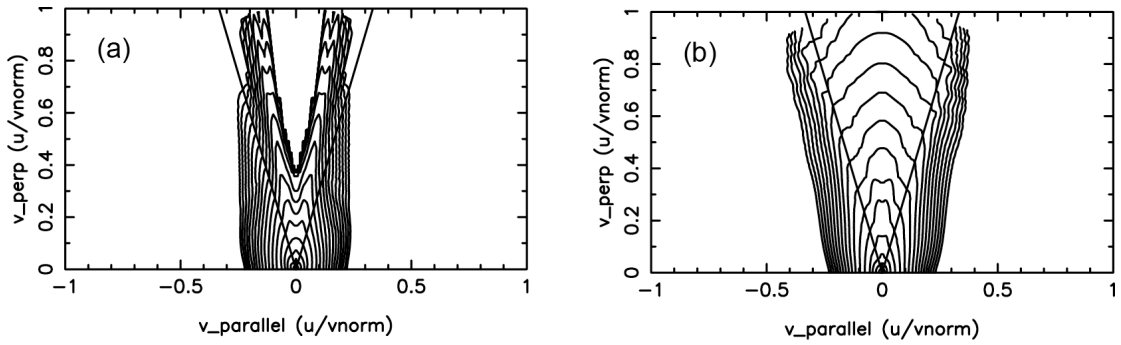

Figure 7.3.4: Contours of minority H+ ion distributions at rho/a=0.143 for 10 msec after beginning of the ICRF simulations. (a) Results from AORSA quasi-linear coefficients, and (b) from the Lorentz-orbit based DC diffusion coefficients. Velocity normalization corresponds to 5 MeV. Contour levels are chosen to be equal spaced for the initial Maxwellian distribution.

the Lorentz force equation for the gyro-orbits of ions in computational equilibria derived from magnetic field data plus the AORSA [15] or TORIC [16] full-wave electromagnetic fields. This provides a means for examining the impact of FOW, finite Larmor radius, correlation and nonlinear effects on ICRF ion diffusion. The particles are launched from mid-plane points in the tokamak, initially equal spaced in gyro-phase (with constant gyro-radius) about the given gyro-centers and also equal spaced in toroidal length along a given RF mode wavelength, and averages the resulting square of the velocity changes after one (or more) poloidal circuits, to obtain the ICRF bounce-averaged, gyro-phase and wave-phase averaged diffusion tensor. This is carried out for a 3-D array ($u_{||}$, $u_{\perp}$, R) of initial conditions, giving the six independent RF diffusion coefficients in 3-D constant-of-motion space. The method follows the formalism of Refs. [43, 44]. FW heating in NSTX-U will allow examination of the effects of wave-induced radial pinch and diffusive transport, in addition to harmonic overlap and correlation effects on velocity space diffusion. Figure 7.3.4 compares the calculated ion distribution function in a Alcator C-Mod ICRF heating simulation using (a) diffusion coefficients obtained from AORSA [15] using quasi-linear theory, and (b) velocity space diffusion coefficients from Lorentz-orbit DC calculations. The resulting heating profiles were close in both cases, but the differences in the tail distributions can strongly affect relevant tail ion diagnostics.

7.3.1.6 AORSA/ORBIT-RF Full-Wave/Monte-Carlo Code

The 5-D finite-orbit Monte-Carlo code ORBIT-RF [45] coupled with the 2-D linear full wave

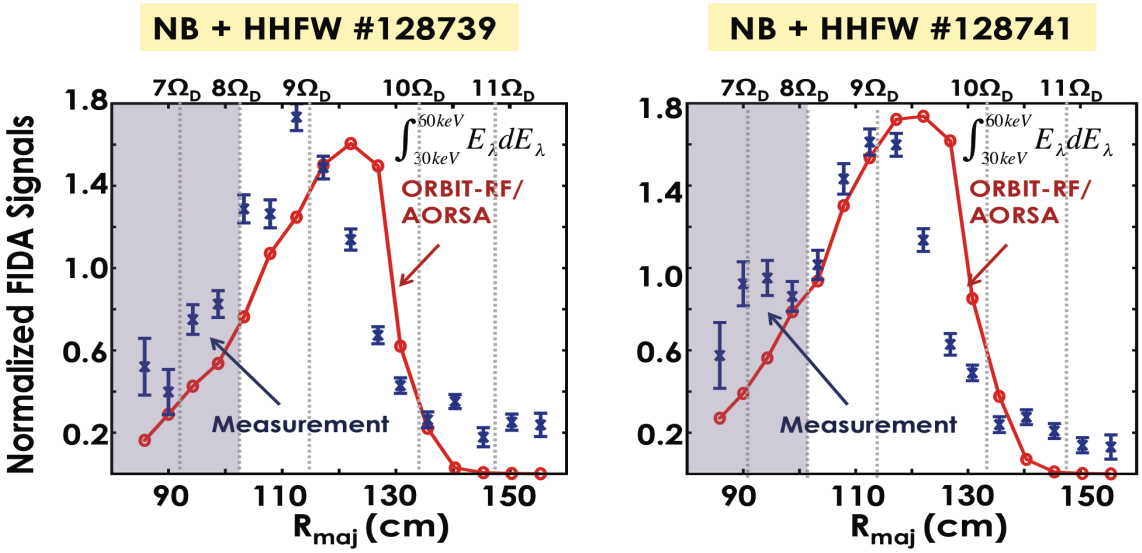

Figure 7.3.5: Comparison of enhanced synthetic FIDA signals from ORBIT-RF/AORSA (solid red lines) and the measured FIDA signal (blue points with error bars) for the two NSTX FW + NBI discharges (a) #128739 and (b) #128741. The beam injection power is 1 MW with a full energy of 65 keV.. 1 MW FW power is launched into the plasma at a frequency of 30 MHz.

code AORSA [46] is a comprehensive numerical model that can perform a fully self-consistent calculation of resonant interactions of injected beam ions with either a single FW or multiple FWs in the plasma. To validate the ORBIT-RF/AORSA simulation suite FIDA experimental fast-ion data were simulated for NSTX discharges heated by a combination of FW and NBI power. Computed beam ion distributions without and with 30 MHz FW were passed to the synthetic diagnostic simulation code FIDASIM [47]. Synthetic FIDA signals were computed for the two cases. For a more quantitative comparison of beam ion populations accelerated by FW, the enhancement was computed by taking the ratio of FIDA signals with and without FW (that is with NBI alone) in both the measurements and the simulations. In Fig. 7.3.5, computed enhancements are compared with measured enhancements for the two FW-NBI discharges (shots 128739 and 128741). Here, the beam ion energy was integrated in the energy range from 30 keV to 60 keV for comparison. ORBIT-RF/AORSA quantitatively reproduced the FIDA measurements for the two NSTX FW plus NBI discharges. However ORBIT-RF/AORSA computed slightly enhanced outboard radial shifts compared to the measurements.

For the initial 2 years of NSTX-U 5-year plan, ORBIT-RF/AORSA will be used to simulate a wide range of FW-NBI experiments to understand the conditions under which fast-ions are effectively accelerated by FW. ORBIT-RF is currently being coupled with TORIC. In addition to benchmarking ORBIT-RF/TORIC with ORBIT-RF/AORSA, both approaches will be tested against experimental data to ascertain the fidelity of each approach. For years 3-5 the two suites, ORBIT-RF/AORSA and ORBIT-RF/TORIC, will be compared with predictions from CQL3D/AORSA, CQL3D/TORIC and SPIRAL/TORIC (see section 7.3.1.7) which model the wave-particle interaction with a different formulation.

7.3.1.7 SPIRAL Using Fields from TORIC

The full Lorentz-orbit following code SPIRAL [48] has been modified to use the FW fields as calculated by the TORIC code. Ensembles of energetic ions can now be followed in the SPIRAL code in the presence of FW wave fields as calculated by the TORIC code. As a result the full interaction between the gyro-motion of the particles and the RF fields is included without any approximations. In the current version of TORIC a Maxwellian fast-ion distribution is assumed which is a poor approximation for the beam-ion slowing down distributions present in NSTX and NSTX-U. Work is under way to include non-Maxwellian distributions in TORIC and once implemented, an iterative method between TORIC and SPIRAL will be used to accurately calculate the interaction between the beam-ions and the FW power, and to compare these results with various measurements of the fast-ions, including confined and lost ion signals, and neutron signals.

7.3.1.8 Upgrade of NUBEAM with an RF Operator for FW

The presence of a fast-ion population in a discharge has a significant impact on FW power absorption. Several quasi-linear code couplings exist to account for both the non-Maxwellian fast-ion distributions, and to capture the self-consistency required between the launched FWs and the plasma ion distribution. This self-consistency typically involves a full-wave RF solver, and an update to the plasma distribution with an RF operator, usually a continuum Fokker-Planck or particle-based Monte-Carlo code. Of the available update codes, NUBEAM has the most comprehensive content in its physics operator, with the exception of an accurate RF operator. Recently PPPL and ORNL have restarted work to complete the inclusion of an RF operator in NUBEAM and the TRANSP framework [49].

In Year 1-2, following the completion of the RF operator in NUBEAM, the goal will be to accurately determine the power partitioning to the beam ion population, and contrast this with that seen using an assumed Maxwellian beam of equivalent temperature as is often done [50]. The impact of any finite-ion-orbit effects will also be examined by comparing coupled AORSA-NUBEAM quasi-linear self-consistent simulation results with experimental observations from the FIDA diagnostic.

7.3.2 Diagnostics and Other Facility Upgrades Supporting Wave Heating and Current Drive Research

This section provides a brief summary of some of the diagnostics systems and facility upgrades that will directly support the wave heating and current drive program on NSTX-U. More information regarding the status and plans for the RF heating and current drive systems and diagnostics systems on NSTX-U can be found in Sections 10.4 and 10.6, respectively.

The two IR cameras on NSTX proved to be invaluable in establishing that the “hot” RF produced spiral deposition patterns were caused by RF power flow along the magnetic field lines from the SOL in front of the antenna to the divertor floor/ceiling [9, 51, 52]. Two additional IR cameras will be installed on NSTX-U allowing a better characterization of this power flow and the toroidal heat deposition. The probe sets in divertor tiles will be augmented to include probes that have direct RF detection capability. Langmuir probes will provide measurements of the RF voltage across the probe sheath and allow the FW field strength at the “hot” RF-produced spiral deposition zones [51, 52] to be measured. RF loop probes will provide measurements of RF magnetic field strength and RF-induced currents in the vicinity of the RF-produced spirals. Probes in both the floor and ceiling will help to determine the directionality of wave excitation and separate direct propagation effects from standing wave effects. Magnetic and Langmuir RF probes installed in the tiles above and below the antenna will allow the measurement of the relative strengths of the RF fields propagating in both directions along the magnetic field lines.

The experimental characterization of FW effects on fast-ions from NB injection in NSTX-U requires accurate measurements of the fast-ion radial profile to identify the regions that mostly contribute to the wave-particle interaction process. In addition, information on the fast-ion response to RF waves in terms of energy and pitch will be needed to discern the behavior of different classes of particles, for example passing or trapped particles. Several diagnostics will provide complementary information on fast-ion interaction with FW power in NSTX-U. Two FIDA systems [53] will provide time, space and energy resolved measurements of the fast-ion distribution; a vertical FIDA system [54] more sensitive to trapped or barely co-going particles and a tangential FIDA system [24] that measures co-passing fast-ions. FIDA measurements will be complemented by an upgraded solid-state Neutral Particle Analyzer [55] array (ssNPA) that measures trapped fast-ions. Additional measurements that are helpful to study fast-ion interactions with FW will be provided by neutron rate counters, a new charged fusion product profile diagnostic [56] (CFPD) that is currently being tested on MAST and may possibly be available on NSTX-U, and a scintillator-based Fast Lost Ion probe [57] (sFLIP).

An upgraded 10-40 GHz reflectometer will provide measurements of plasma electron density profiles in front of the FW antenna array. These profiles will be utilized for RF coupling studies, including the assessment of antenna modifications and the effectiveness of lithium conditioning, gas puffing, and cryo-pumping to modify the SOL density and to mitigate FW losses in the SOL. The reflectometer will also be used to monitor power losses due to PDI, and for the measurement of localized electron density fluctuations in front of the FW antenna.

On NSTX-U there will be a new MSE-LIF diagnostic [58, 59] to measure the current density profile that requires only a low-power, 30-40 kV, 30 mA diagnostic beam blips, in addition to the “conventional” MSE-CIF diagnostic previously used on NSTX [60] that requires a high-power heating beam. Because the MSE-LIF diagnostic uses a non-perturbing, low-power diagnostic neutral beam it is much better suited to measuring the plasma current density profile in plasmas that have no high-power NBI heating; for example during RF-driven, non-inductive plasma current ramp-up experiments.

A 28 GHz, megawatt power level, EC/EBW heating system is planned for installation on NSTX-U. Assuming a baseline NSTX-U budget this system will be become operational in Year 4. Initially this system will provide electron heating during non-inductive plasma start-up, later it will be used for off-axis EBW heating and current drive. The EC/EBW heating system will use a 28 GHz, 1 MW gyrotron originally developed for EC heating in the GAMMA-10 tandem mirror [61]. The gyrotron will be powered by a modified TFTR NBI power supply that will be capable of powering several megawatt-level gyrotrons. The plasma start-up system will use an HE-II low-loss corrugated waveguide and fixed horn antenna.

The York Plasma Institute at the University of York in the United Kingdom has proposed a collaboration with NSTX-U that involves the installation of a Synthetic Aperture Microwave Imaging diagnostic (SAMI) [62] in Years 2-3. Amongst other things, the SAMI diagnostic will measure the B-X-O mode conversion efficiency and determine where the conversion efficiency is a maximum and how stable the angular mode conversion window is with respect to fluctuations in the edge and/or core. These EBW mode conversion measurements will provide valuable data for designing an off-axis EBW heating & current drive system for NSTX-U in Year 4 and for initial tests of O-X-B heating used the fixed horn antenna in Year 5.

References

[1] G. Taylor et al., Phys. Plasmas **11** (2004) 4733-4739.
[2] J. Urban et. al., Nucl. Fusion **51** (2011) 083050.
[3] J. R. Wilson et al., Phys. Plasmas, **10** (2003) 1733-1738.
[4] J. C. Hosea et al., Phys. Plasmas **15** (2008) 056104.
[5] C. K. Phillips et al., Nucl. Fusion **49** (2009) 075015.
[6] J. C. Hosea et al., AIP Conf Proceedings **1187** (2009) 105-112.
[7] G. Taylor et al., Phys. Plasmas **17** (2010) 056114.
[8] J. C. Hosea et al., AIP Conf. Proceedings **1406** (2011) 333-336.
[9] R. J. Perkins et al., Phys. Rev. Lett. **109** (2012) 045001.
[10] D. L. Green et al., Phys. Rev. Lett. **107** (2011) 145001.
[11] G. Taylor et al., Phys. Plasmas **19** (2012) 042501.
[12] S. J. Diem et al., Phys. Rev. Lett. **103** (2009) 015002.
[13] S. J. Diem et al., Nucl. Fusion **49** (2009) 095027.
[14] V. F. Shevchenko et al., Nucl. Fusion **50** (2010) 022004.
[15] E. F. Jaeger et al., Nucl. Fusion **46** (2006) S397-S408.
[16] M. Brambilla, Plasma Phys. and Cont. Fus. **44** (2002) 2423-2443.
[17] A. P. Smirnov and R. W. Harvey, Bull. Am. Phys. Soc. **40** (1995) 1837. http://www.compxco.com/genray.html
[18] R. W. Harvey and M.G. McCoy, The CQL3D Code, *Proc. IAEA TCM on Advances in Simulation and Modeling of Thermonuclear Plasmas*, pp. 489-526, Montreal, (1992), USDOC/NTIS No. DE93002962; http://www.compxco.com/cql3d.html .
[19] R. W. Harvey et al., Proc. 38th EPS Conf. on Plasma Phys. (Strasbourg, France 2011) paper P4.017 http://www-fusion-magnetique.cea.fr/eps2011/ .
[20] P. M. Ryan et al, AIP Conf. Proc. **1406** (2011) 101-104.
[21] B. P. LeBlanc et al., IAEA, Daejeon, Republic of Korea (2010), paper EXW/P7-12.
[22] TRANSP group, PPPL, http://w3.pppl.gov/transp/
[23] B. P. LeBlanc et al., AIP Conf. Proc. **1187** (2009) 117-120.
[24] A. Bortolon et al., Rev. Sci. Instrum. **81** (2010) 10D728.
[25] D. L. Green et al., AIP Conf. Proc. **1406** (2011) 337-340.
[26] D. Smithe, et al., "*Self-consistent modeling of the tokamak RF antennas, edge plasma, and sheath voltages*", APS-DPP, (2012) Paper TP8.00070.
[27] G. Taylor et al., Phys. of Plasmas **12** (2005) 052511.
[28] A.K. Ram and S.D. Schultz, Phys. Plasmas **7** (2000) 4084-4094.
[29] E. Poli et al., Comput. Phys. Commun. **136** (2001) 90-104.
[30] A. P. Smirnov et al., Proc 15th Workshop on ECE and ECRH (World Scientific 2009) pp. 301-306
[31] G. M. Wallace et al. Phys. Plasmas **17** (2010) 082508.

[32] N. Bertelli et al.,*"The Effects of the Scattering by Edge Plasma Density Fluctuations on Lower Hybrid Wave Propagation"* submitted to Plasma Phys. Control. Fusion (2012).
[33] P. T. Bonoli and E. Ott., Phys. Fluids **25** (1982) 359-375.
[34] A. L. Rosenberg et al., Phys. Plasmas **11** (2004) 2441-2452.
[35] D. Liu et al., Plasma Phys. Cont. Fus. **52** (2010) 025006.
[36] R. W. Harvey et al., "Temporal Dynamics of NSTX NBI+FW Discharges using CQL3D-Hybrid-FOW" Bull. Am. Phys. Soc. 57 (2012) Paper PP8.00020.
[37] Yu.V. Petrov and R.W. Harvey, *"Finite Orbit Width Features in the CQL3D Code"*, paper TH/P6-02, IAEA FEC, San Diego, CA (2012).
[38] E. F. Jaeger, et al., Phys. Plasmas **15** (2008) 072513.
[39] R. W. Harvey and G. Taylor, Phys. of Plasmas **12** (2005) 052509.
[40] G. Taylor et al., Proc. 17th Workshop on ECE and ECRH, EPJ Web of Conferences **32** (2012) 02014 http://www.epj-conferences.org/
[41] T. Ohkawa, National Technical Information Service Report No. PB2000-108008, (1976) [T. Ohkawa, General Atomics Report No. GA-A13847 (1976) (unpublished).]
[42] N. J. Fisch and A. Boozer, Phys. Rev. Lett. **45** (1980) 720-722.
[43] A. Kaufman, Phys. Fluids **15** (1972) 1063-1069.
[44] L-G. Eriksson and P. Helander, Phys. Plasmas **1**,(1994) 308-314.
[45] M. Choi et al., Phys. Plasmas **16** (2009) 052513.
[46] D. L. Green et al., AIP Conf. Proc., **1187** (2009) 569-576.
[47] W. W. Heidbrink et al., Comp. Physics **10** (2011) 716-741.
[48] G. J. Kramer, et al., Plasma Phys. Cont. Fus. **55** (2013) 025013
[49] B. H. Park et al., "*Status of RF heating model in NUBEAM*", APS-DPP (2012) Paper JP8.00122.
[50] R. I. Pinsker, et al., Nucl. Fusion **46** (2006) S416-S424.
[51] R. J. Perkins et al., Proc. 39th EPS Conf. on Plasma Physics 36F (Stockholm, Sweden 2012) paper P-1.011
[52] R. J. Perkins et al., Proc. 24th IAEA Fusion Energy Conference (San Diego, California 2012) paper EX/P5-40
[53] W. W. Heidbrink, Rev. Sci. Instrum. **81** (2010) 10D727.
[54] M. Podestà et al., Rev. Sci. Instrum. **79** (2008) 10E521.
[55] D. Liu et al., Rev. Sci. Instrum. **77** (2006) 10F113.
[56] W. U. Boeglin et al., Rev. Sci. Instrum. **81** (2010) 10D301.
[57] D. S. Darrow, Rev. Sci. Instrum. **79** (2008) 023502.
[58] E. L. Foley and F. M. Levinton, Rev. Sci. Instrum. **77** (2006) 10F311.
[59] E. L. Foley and F. M. Levinton, *J. Phys. Conf. Ser.* **227** (2010) 012007.
[60] F. M. Levinton and H. Yuh, Rev. Sci. Instrum. **79** (2008) 10F522.
[61] T. Kariya et al, J. Infrared, Millimetre and Terahertz Waves **32** (2011) 295-310.
[62] S. Freethy et al., Proc. 38th EPS Conference on Plasma Physics (Strasbourg, France, 2011) paper P2.050 http://ocs.ciemat.es/EPS2011PAP/html/

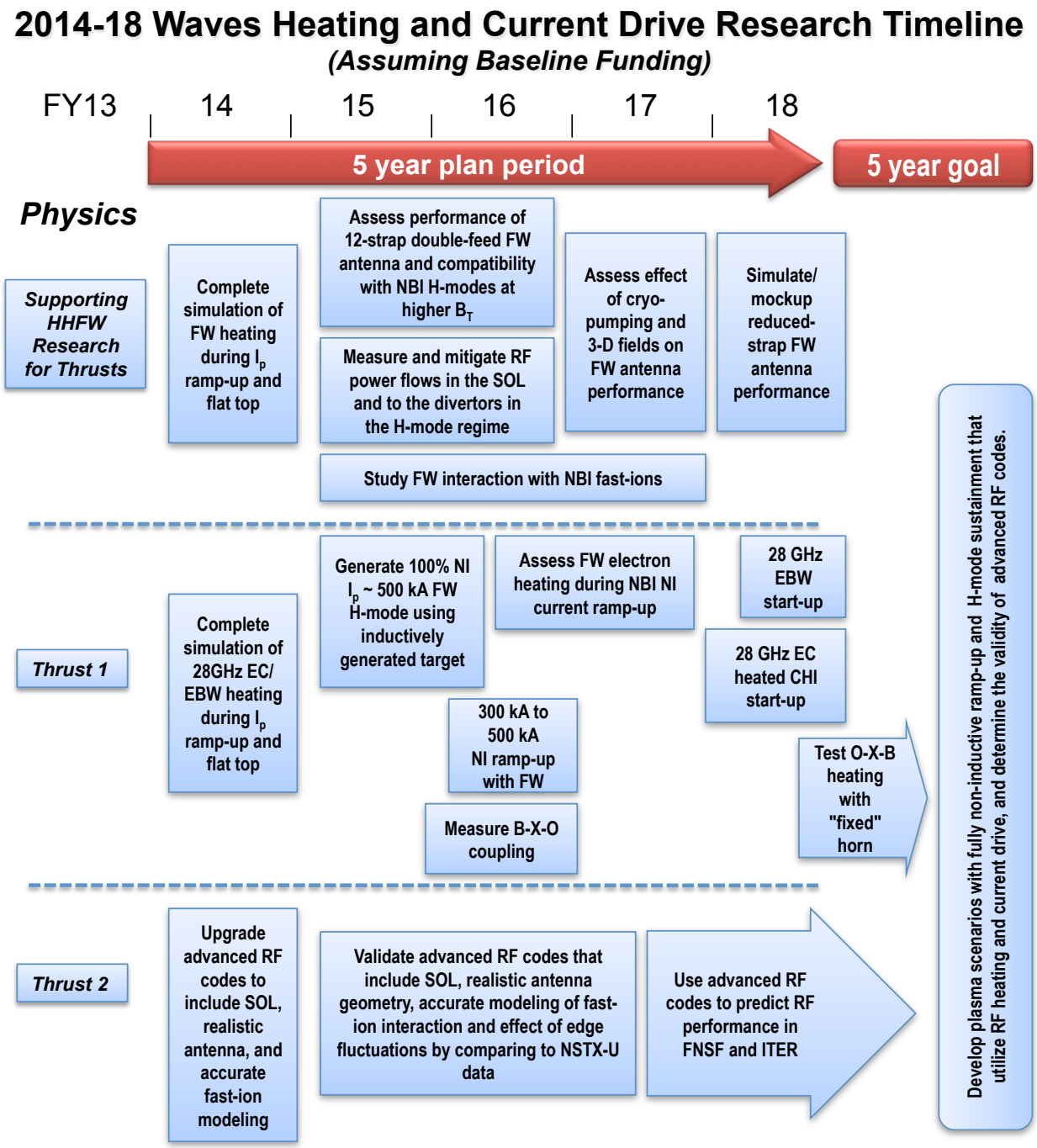
2014-18 Waves Heating and Current Drive Research Timeline
(Assuming Baseline Funding)
FY13
14
15
16
17
18
5 year plan period
5 year goal
Physics
Supporting HHFW Research for Thrusts
Complete simulation of FW heating during I_p ramp-up and flat top
Assess performance of 12-strap double-feed FW antenna and compatibility with NBI H-modes at higher B_T
Measure and mitigate RF power flows in the SOL and to the divertors in the H-mode regime
Assess effect of cryo-pumping and 3-D fields on FW antenna performance
Simulate/ mockup reduced-strap FW antenna performance
Study FW interaction with NBI fast-ions
Thrust 1
Complete simulation of 28GHz EC/ EBW heating during I_p ramp-up and flat top
Generate 100% NI I_p ~ 500 kA FW H-mode using inductively generated target
Assess FW electron heating during NBI NI current ramp-up
28 GHz EBW start-up
28 GHz EC heated CHI start-up
300 kA to 500 kA NI ramp-up with FW
Measure B-X-O coupling
Test O-X-B heating with "fixed" horn
Thrust 2
Upgrade advanced RF codes to include SOL, realistic antenna, and accurate fast-ion modeling
Validate advanced RF codes that include SOL, realistic antenna geometry, accurate modeling of fast-ion interaction and effect of edge fluctuations by comparing to NSTX-U data
Use advanced RF codes to predict RF performance in FNSF and ITER
Develop plasma scenarios with fully non-inductive ramp-up and H-mode sustainment that utilize RF heating and current drive, and determine the validity of advanced RF codes.

2014-18 Waves Heating and Current Drive Research Timeline

(Assuming Baseline Funding)

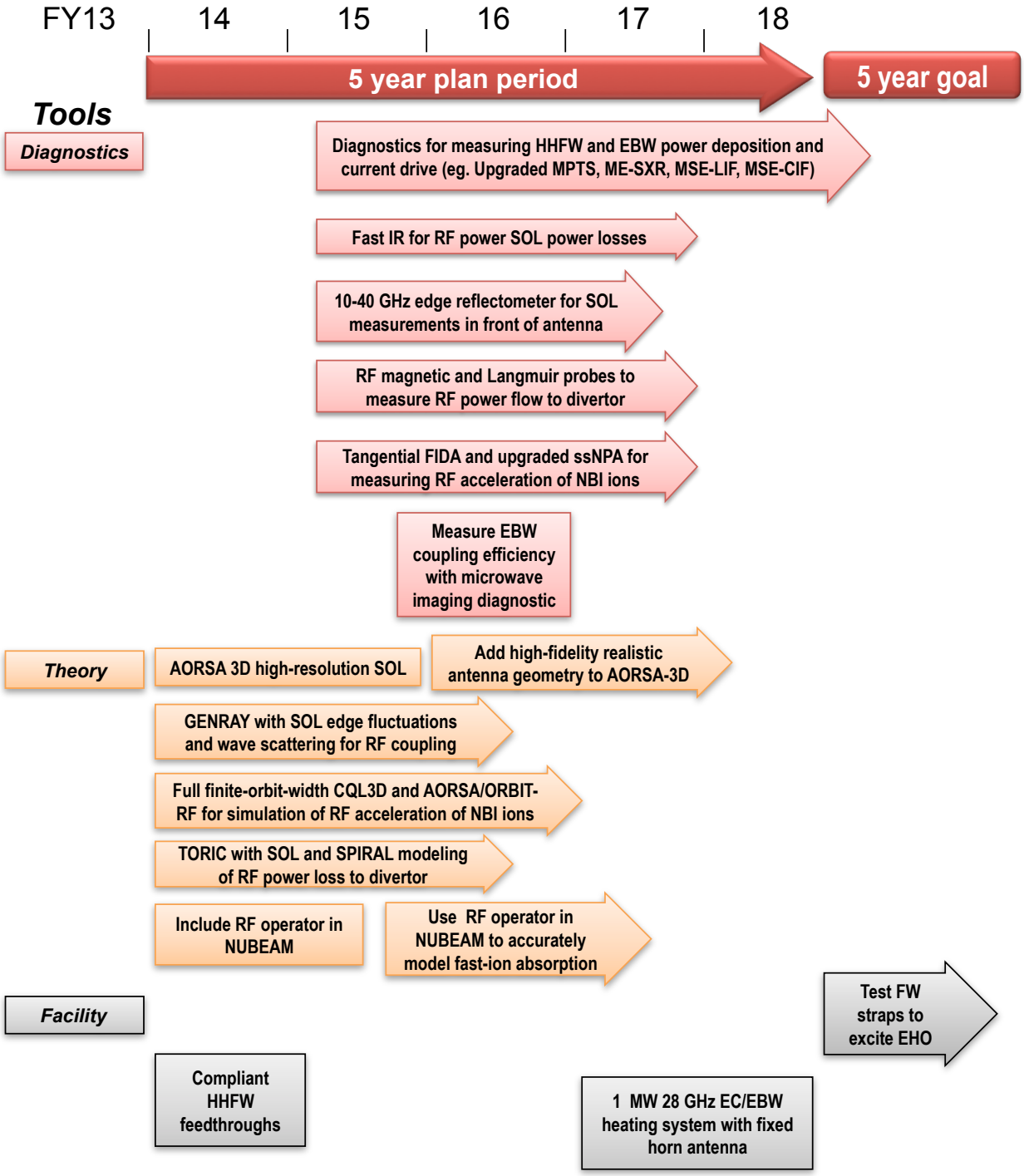

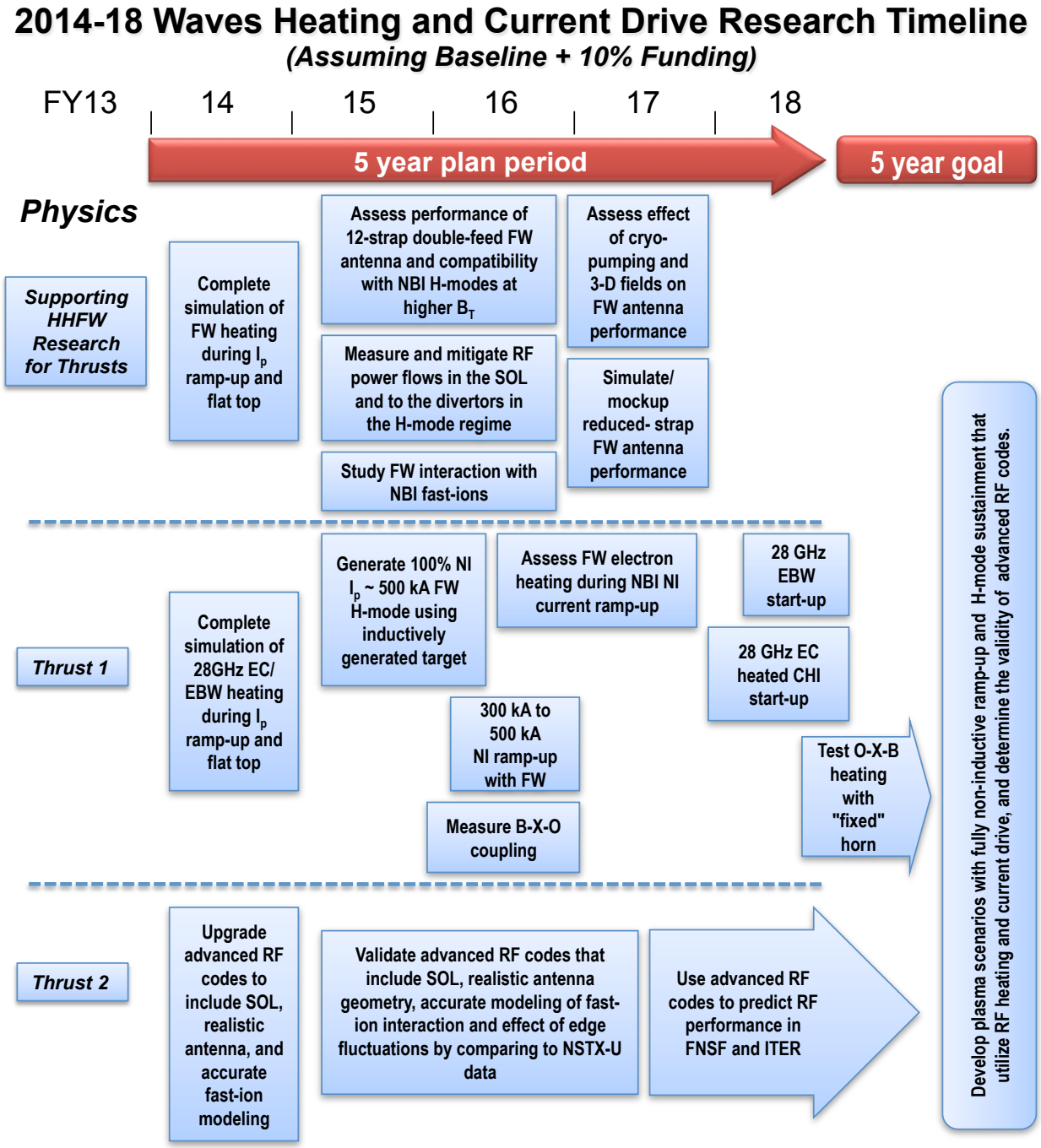
2014-18 Waves Heating and Current Drive Research Timeline
(Assuming Baseline + 10% Funding)
FY13
14
15
16
17
18
5 year plan period
5 year goal
Physics
Supporting HHFW Research for Thrusts
Complete simulation of FW heating during I_p ramp-up and flat top
Assess performance of 12-strap double-feed FW antenna and compatibility with NBI H-modes at higher B_T
Assess effect of cryo-pumping and 3-D fields on FW antenna performance
Measure and mitigate RF power flows in the SOL and to the divertors in the H-mode regime
Simulate/ mockup reduced- strap FW antenna performance
Study FW interaction with NBI fast-ions
Thrust 1
Complete simulation of 28GHz EC/ EBW heating during I_p ramp-up and flat top
Generate 100% NI I_p ~ 500 kA FW H-mode using inductively generated target
Assess FW electron heating during NBI NI current ramp-up
28 GHz EBW start-up
28 GHz EC heated CHI start-up
300 kA to 500 kA NI ramp-up with FW
Measure B-X-O coupling
Test O-X-B heating with "fixed" horn
Thrust 2
Upgrade advanced RF codes to include SOL, realistic antenna, and accurate fast-ion modeling
Validate advanced RF codes that include SOL, realistic antenna geometry, accurate modeling of fast-ion interaction and effect of edge fluctuations by comparing to NSTX-U data
Use advanced RF codes to predict RF performance in FNSF and ITER
Develop plasma scenarios with fully non-inductive ramp-up and H-mode sustainment that utilize RF heating and current drive, and determine the validity of advanced RF codes.

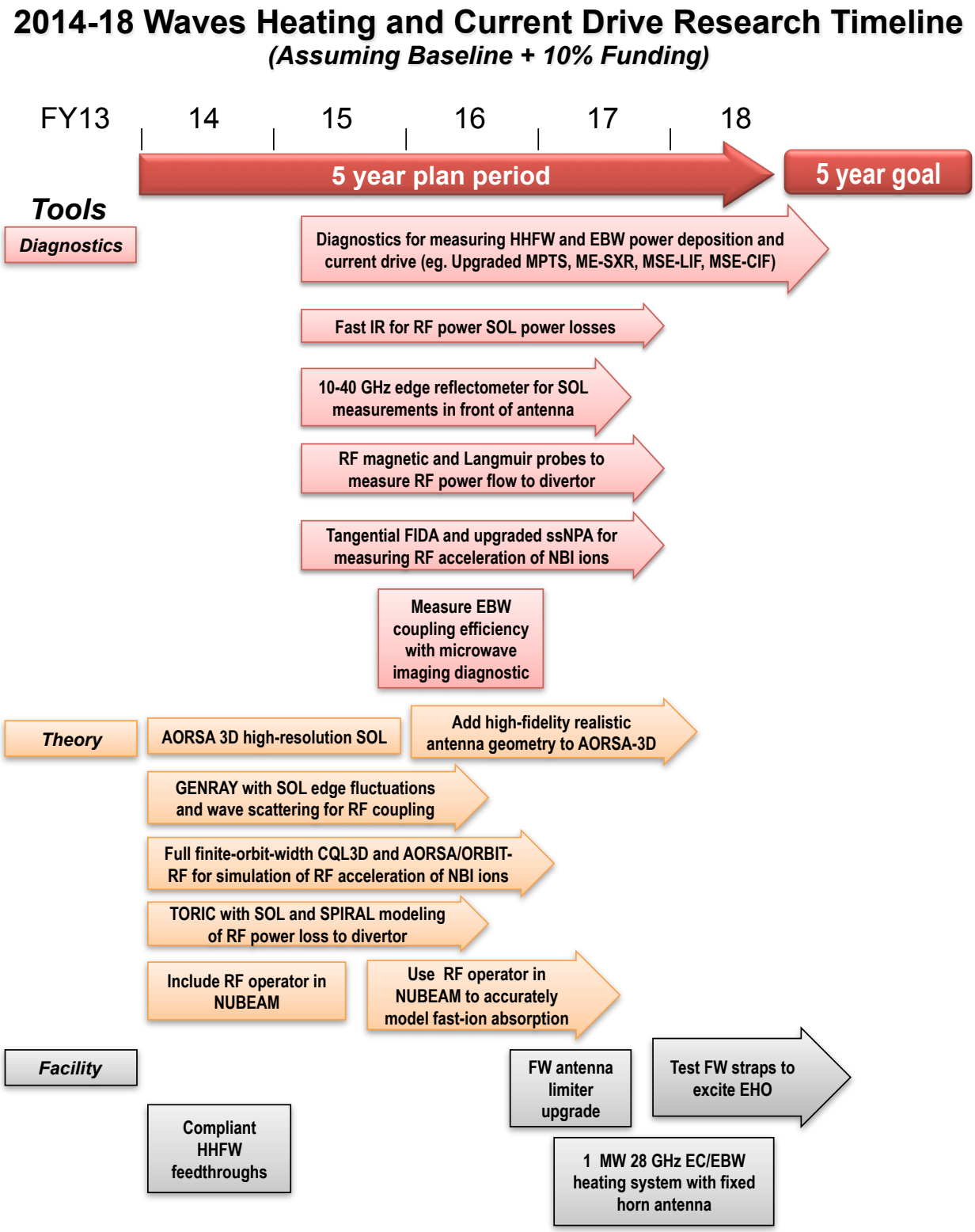
2014-18 Waves Heating and Current Drive Research Timeline
(Assuming Baseline + 10% Funding)
FY13
14
15
16
17
18
5 year plan period
5 year goal
Tools
Diagnostics
Diagnostics for measuring HHFW and EBW power deposition and current drive (eg. Upgraded MPTS, ME-SXR, MSE-LIF, MSE-CIF)
Fast IR for RF power SOL power losses
10-40 GHz edge reflectometer for SOL measurements in front of antenna
RF magnetic and Langmuir probes to measure RF power flow to divertor
Tangential FIDA and upgraded ssNPA for measuring RF acceleration of NBI ions
Measure EBW coupling efficiency with microwave imaging diagnostic
Theory
AORSA 3D high-resolution SOL
Add high-fidelity realistic antenna geometry to AORSA-3D
GENRAY with SOL edge fluctuations and wave scattering for RF coupling
Full finite-orbit-width CQL3D and AORSA/ORBIT-RF for simulation of RF acceleration of NBI ions
TORIC with SOL and SPIRAL modeling of RF power loss to divertor
Include RF operator in NUBEAM
Use RF operator in NUBEAM to accurately model fast-ion absorption
Facility
FW antenna limiter upgrade
Test FW straps to excite EHO
Compliant HHFW feedthroughs
1 MW 28 GHz EC/EBW heating system with fixed horn antenna

Table of Contents for Chapter 8

Chapter 8

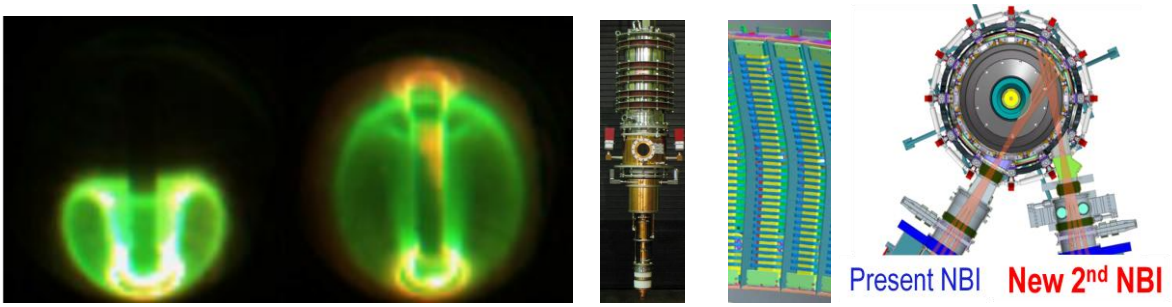

Research Goals and Plans for Plasma Formation and Current Ramp-up

8.1 Introduction

The spherical torus/tokamak (ST) configuration, due to its compact geometry and reduced surface area to volume ratio, is potentially advantageous as a Fusion Nuclear Science Facility/Component Test Facility (FNSF/CTF) by providing high neutron wall loading for nuclear component testing and development in a device significantly smaller than a full-scale reactor. However, in order to achieve low aspect ratio, the thickness of the neutron shielding of the normally conducting central magnets must be minimized, and the insulation of a conventional multi-turn solenoid will be severely degraded in the harsh nuclear environment of an FNSF. Thus, it is anticipated that future nuclear-capable STs will have little or no central solenoid capability, and that non-inductive start-up, ramp-up, and sustainment of an ST-based FNSF plasma will be required. In light of the importance of this issue, this chapter and plan is dedicated to addressing the NSTX-U 5 year plan high-level goal #3 noted in Chapter 1 to: "Develop and understand non-inductive start-up and ramp-up to project to ST-FNSF operation with small or no central solenoid."

It is important to note that conventional aspect ratio tokamaks will also require non-inductive sustainment for steady-state operation, so non-inductive start-up and ramp-up is a unique ST requirement, while sustainment is a broader tokamak/ST requirement. Further, the development of techniques to minimize or eliminate central solenoid action could also be beneficial for enabling reduced aspect ratio and/or reduced-sized superconducting electricity-producing fusion power plants [1] with reduced device mass and reduced radioactive waste production.

Given the scientific and operational challenges of non-solenoidal plasma formation and sustainment, the problem is best solved by dividing it into parts and addressing issues individually while ensuring that the pieces are ultimately compatible and can be integrated. This division of the non-inductive start-up, ramp-up, and sustainment in NSTX-U is shown schematically in Figure 8.1.

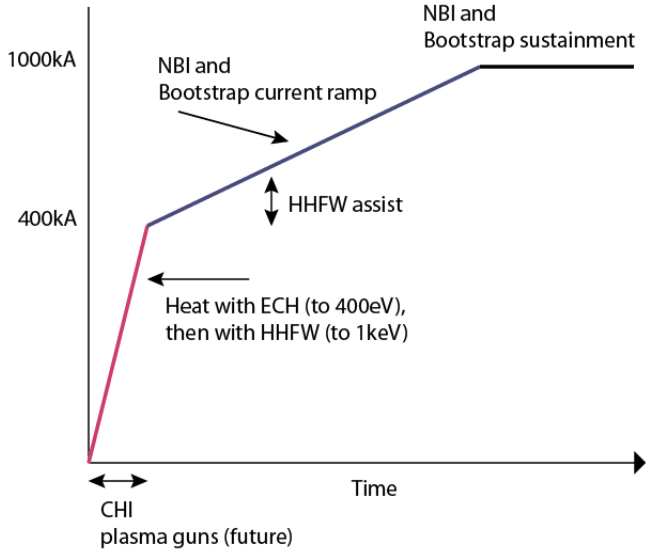

Figure 8.1: Division of plasma formation and sustainment problem into 3 distinct phases as function of time and plasma current: (1) plasma start-up, (2) initial heating and over-drive ramp-up of start-up plasma, primarily using neutral beam and bootstrap current drive and (3) sustainment of the formed plasma using neutral beam and bootstrap current drive.

Coaxial Helicity Injection (CHI), which has been the plasma start-up technique tested most on NSTX (described in Section 8.3.1) will begin operations during the first year of NSTX-U Operations (FY 2015). Plasma guns, also referred to as Point Source Helicity Injection (PSHI) (see also Section 8.3.1), is currently being developed at Pegasus at the University of Wisconsin and may undergo first tests on NSTX-U later during the 5 year plan period. These systems will be used to generate the initial seed current without reliance on the central solenoid.

A key issue for both CHI and PSHI start-up methods is that the total energy input used to form the plasma is limited in both magnitude and duration. Such plasmas are very sensitive to impurities and radiation, and while the plasma current can be high (hundreds of kA), the electron temperatures are generally low (10's of eV in the plasma core), and thus the plasma current can decay very rapidly on a 1-10 ms time-scale. This low temperature does not appear to be associated with MHD instabilities or lack of closed flux surfaces, as CHI target plasmas have been coupled to induction and subsequent H-mode transitions, can have low impurity content, and can provide significant inductive flux savings. Thus, auxiliary electron heating of the plasma to raise the central electron temperature to the 100 eV range (or higher) would be highly beneficial, as this would both reduce the current decay rate and increase the efficiency of auxiliary current drive systems used to ramp up the plasma current. Electron cyclotron heating (ECH) of a low density CHI target plasma appears very favorable for this electron heating application as described in Chapter 7, and is proposed to be used during plasma startup to significantly increase the electron temperature near the magnetic axis during CHI and plasma gun start-up. Electron Bernstein Wave (EBW) heating and current start-up has also been successfully used on MAST [2], but relative to ECH is not as well developed, and will also be tested in NSTX-U as described in Chapter 7.

High-harmonic fast-wave (HHFW) heating (also described in Chapter 7) has been used in NSTX to successfully heat a low-current (300 kA) discharge to $T_e(0) > 1$ keV in less than 40 ms [3] and generated over 70% of the plasma current non-inductively, via bootstrap current and direct fast-wave current drive, in these discharges. However, HHFW heating requires sufficient electron beta to provide sufficient first-pass absorption to heat the plasma efficiently. For typical low-current start-up plasma densities, this corresponds to electron temperatures in the ~100 to few hundred eV range. Thus, additional initial electron heating of CHI plasmas (for example via ECH) is also very likely required for HHFW heating to be effective. Further, the current drive efficiency of NBI at very low temperature is very likely too low to overcome the rapid inductive current decay of an un-heated CHI plasma. Thus, auxiliary electron heating of a CHI target plasma is also very likely required to couple to NBI current ramp-up. For these reasons, additional electron heating of start-up plasmas via 1 MW 28GHz ECH is a high priority in the NSTX-U five year plan, and heating efficiency calculations of this ECH system are shown in Section 8.5.3.

With respect to NBI current ramp-up, on NSTX, neutral beam injection (NBI) power was only well absorbed in discharges with plasma currents above approximately 600-700 kA. Further, the beams are/were not optimally aligned (are too perpendicular) for maximizing current drive efficiency, so NBI current ramp-up of the plasma current was tested to only a very limited extent in NSTX.

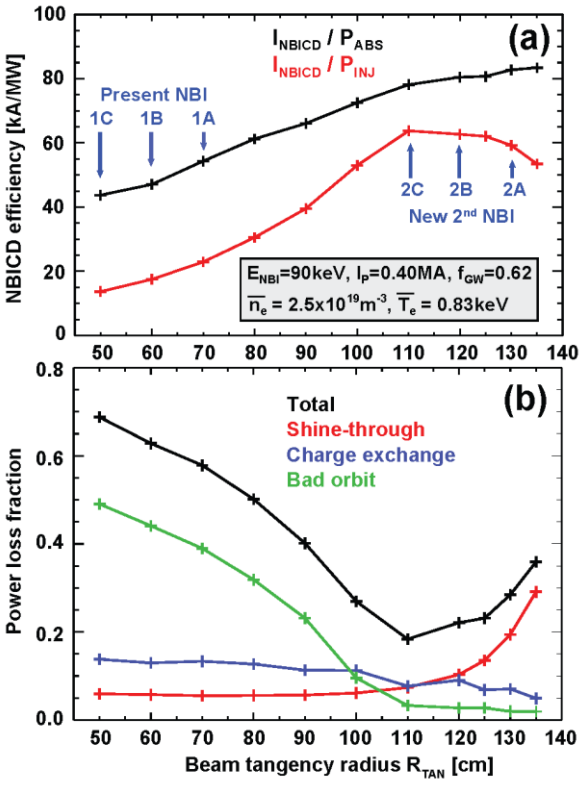

Figure 8.2: (a) NBI current drive efficiency (kA/MW) and (b) power loss fractions (total, shine-through, charge exchange, and bad orbit) as a function of beam tangency radius R_{TAN} for an A = 1.65, I_P = 0.40 MA, B_T = 0.9 T NSTX Upgrade target plasma with a 7.4 cm outer gap.

On NSTX-U, the three additional sources included in the new second NBI system of the Upgrade are aimed more tangentially and are substantially more efficient at driving current at lower plasma current. As shown in Figure 8.2 for a simulated 400 kA, n_e = 2-3×10^{19} m^{-3} and T_e = 0.8-1 keV target plasma, the new NSTX-U NBI sources (R_{TAN} = 110, 120, 130 cm) have acceptable shine-through (< 20%) and much lower bad orbit loss (< 5%) compared to the present (original NSTX) NBI sources, and 3 times higher overall current drive efficiency.

Figure 8.2 also shows that 6MW of 2nd NBI would provide 300-400 kA of current drive, and when combined with the bootstrap current of the same plasma equilibrium (also 300-400 kA) would produce current overdrive for non-inductive ramp-up. Thus, Figure 8.2 provides an initial estimate of the target plasma conditions required for efficient NBI coupling and current ramp-up of a low-current target plasma. Further, this calculation also shows that plasma temperatures in the ~1 keV range are needed for efficient NBI current drive, and this explains why initial fast-wave heating is required. Importantly, additional TRANSP simulations predict that the second more tangential NBI system on NSTX-U may be able to efficiently couple to discharges at even lower plasma currents as small as 300 kA, as described in Section 8.5.1. As will be shown later, the CHI current start-up capability in NSTX-U is expected to be at least 400 kA, providing adequate margin for NBI coupling to a CHI-generated target provided the electron temperature (and density via gas fueling) of the target plasma can be raised using wave heating such as ECH/EBW combined with HHFW. Thus, the major upgrades in NSTX-U (higher toroidal field, 2nd NBI system, and 1 MW ECH/EBW) combined with CHI generated seed current and high-harmonic fast wave heating which were already demonstrated on NSTX, appear to make possible fully non-inductive current formation and ramp-up scenarios to plasma currents up to 1 MA appear possible in NSTX-U.

To establish the predictive capability for plasma start-up in FNSF, NSTX-U research will assess the maximum levels of current that can be generated using CHI and PSHI methods. The properties of these plasmas, including plasma inductance, resistivity, electron temperature and density will be measured and compared to parameters from other machines on which they were previously developed. For CHI these are NSTX, HIT-II and possibly the HIST and QUEST STs in Japan. For PSHI this is the Pegasus experiment. These, in combination with numerical modeling, will provide scaling relations for projecting to a FNSF. These parameters will then determine the level of ECH power required to increase the electron temperature to the levels needed for direct coupling to NBI, and the required levels of NBI power needed to ramp the current to the full sustainment levels.

Numerical modeling of the full non-inductive current start-up and ramp-up will rely heavily on TSC simulations coupled to TRANSP/NUBEAM and RF codes. In addition, 3-D MHD modeling of CHI start-up and PSHI targets will be studied using the NIMROD and possibly the M3D codes to understand in detail the current formation mechanism. Then these codes will be used to understand the external control parameters (eg, operating voltage, injected flux, injector flux shaping and requirements on Z_{eff} and external heating sources) that are needed to increase the magnitude of the generated non-inductive current. Finally, the coupling of neutral beam ions to these types of plasmas will be studied both to learn the requirements on the seed current discharge properties (eg. current profile, current magnitude, electron density, temperature, Z_{eff} and the neutral beam parameters including energy, power and injection angle) that will allow the beams to more efficiently couple to the seed current targets, and for ramping these seed currents to the levels required for current sustainment.

8.2 Overview of Research Thrusts and Plans

8.2.1 Overview of Research Thrusts

The plasma formation and current ramp-up topical science group has two research thrusts. These thrusts are staged sequentially during the 5 year plan. The first thrust aims to re-establish and extend solenoid-free current start-up using coaxial helicity injection and also to test non-inductive current ramp-up using NBI plus bootstrap current overdrive – both during the first several years of NSTX-U operation. The second thrust builds on anticipated results of the first thrust, and utilizes new ECH capabilities (and PSHI if technically ready) to couple helicity-injection start-up plasmas to non-inductive current ramp-up to attempt completely solenoid-free start-up and ramp-up of an ST plasma. The thrust text is provided immediately below, background and motivation for the research plans are briefly summarized below in Section 8.2.2, and year-by-year plans are provided in Section 8.2.3. Additional technical information on start-up and ramp-up are provided in later sections of this chapter. The two research thrusts for plasma start-up and ramp-up are summarized as follows:

Thrust PSR-1: Establish and extend solenoid-free plasma start-up and test NBI ramp-up

NSTX-U researchers will re-establish transient CHI discharges utilizing graphite lower divertor tiles, the increased toroidal field capability of NSTX-U, and full Li coating of the lower divertor tiles followed by subsequent lithium conditioning of the upper divertor. The maximum toroidal currents that can be generated with CHI will be assessed by varying and increasing the amount of injector flux, the size of the capacitor bank, and the CHI voltage (up to 2 kV). The upper divertor buffer coils will be used to suppress absorber arcs, and studies of the coupling of the CHI generated plasma to inductive drive will be performed. Researchers will also generate 300-400 kA flat-top current inductive plasmas and inject the new more tangential beams to assess NBI coupling and current drive efficiency and compare to TSC/TRANSP simulations. NBI coupling to CHI targets will also be assessed and compared to simulation. Combinations of NBI and HHFW heating and current drive will be utilized to heat inductive plasmas and attempt to non-inductively ramp-up the plasma current to the ~0.8-1 MA range.

Thrust PSR-2: Ramp-up CHI Plasma discharges using NBI and HHFW and Test Plasma Gun Start-up

NSTX-U researchers will maximize the levels of CHI-produced plasma currents using new operational capabilities including 1) metallic divertor plates, 2) 1 MW 28 GHz ECH,

and 3) 2.5-3 kV CHI capability. All these should allow more injector flux to be injected into the vessel at reduced levels of low-Z impurities. Initial tests of the effectiveness of NBI coupling to a CHI-generated target will be carried out using the best available CHI targets including the expected increase in CHI plasma duration achieved with ECH electron heating, and the NBI coupling and ramp-up of CHI current will be systematically investigated. Detailed comparisons of CHI current drive results to 2D TSC and 3D NIMROD simulations will be carried out to develop a TSC/NIMROD model of CHI for FNSF design studies. If technically ready, plasma gun hardware will be commissioned on NSTX-U and point-source helicity injection (plasma gun) plasma formation will be initially tested and compared to results from Pegasus.

8.2.2 Overview of Research Plans

8.2.2.1 Solenoid-free current start-up

Three plasma start-up methods that do not rely on the central solenoid and have already shown current start-up capability on NSTX, HIT-II, Pegasus and MAST will be investigated on NSTX-U. This Chapter covers plasma start-up using CHI and PSHI. EBW start-up is described in Chapter 7.

The first method is *transient* CHI (TCHI), first demonstrated on the HIT-II ST at the University of Washington [4] and subsequently demonstrated on NSTX as well [5]. CHI is a promising candidate for non-inductive current initiation and has, in addition, the potential to drive edge current [6] during the sustained phase of a discharge for the purpose of controlling the edge current profile to improve plasma stability limits and to optimize the bootstrap current fraction. Other possible benefits include inducing edge plasma rotation for transport barrier sustainment and controlling edge SOL flows for divertor physics studies.

CHI was originally developed as part of spheromak research [7 8] and has now been used on several spheromak experiments including on the SSPX [9], CTX [10] and RACE devices [11]. Groups in US and Japan have used the method for reconnection merging research [12] and for spherical torus plasma formation [13].

CHI research on NSTX initially used the method of *driven* or *steady-state* CHI for plasma current generation [14]. Although substantial toroidal currents were generated using the steady-state approach [15], it was found that these discharges could not be successfully ramped up in current when induction was applied. Supporting experiments on the HIT-II experiment at the University of Washington demonstrated that the method of TCHI could generate high-quality plasma equilibrium in a ST that could be coupled to inductive drive [16]. Since then the TCHI method has been successfully applied to NSTX for solenoid-free plasma start-up followed by inductive ramp-up [17]. These coupled discharges have now achieved toroidal currents >1 MA using significantly less inductive flux than standard inductive discharges in NSTX.

The second method is PSHI and was first demonstrated on the Pegasus ST at the University of Wisconsin. The first version of the Pegasus PSHI system consisted of one plasma gun mounted near the lower divertor region and an anode mounted near the upper divertor region, both near the machine center stack [18]. The plasma gun consisted of a gas-injected washer stack (channel length of 2 cm) that supported an arc discharge between a cathode cup and an anode washer with an outer diameter of 2 cm [19 20]. The gun could produce large current densities (≤ 0.6 kA/cm^2) with low impurity production as long as the extracted current was less than the arc current (≤ 2 kA). Under this condition, the bulk of the injected current is extracted from the plasma arc discharge rather than from electrode surfaces.

For each discharge, external coils create an initial vacuum magnetic field such that helical field lines connect the aperture of each gun to the anode. Plasma ejected from the gun follows the vacuum field, forming helical plasma filaments. The number of toroidal transits each filament completes between the gun and anode is the geometric windup factor of the field line. At sufficiently high-injected currents, the flux surfaces rapidly heal to quiescent plasma equilibrium.

In later work, the gun's location was moved to larger radii, closer to the mid-plane of the outer vessel and similar results were obtained [21]. In these new experiments up to three small plasma guns were mounted 13—27 cm below the outboard midplane and a single anode was mounted 20 cm above the outboard midplane at the same toroidal location. In recent work, the Pegasus group has found that driving current using electrodes results in similar results [22]. Thus the present plan is to continue to develop PSHI at Pegasus to increase the level of current that can be driven during the electrode phase of the discharge (from the present ~75 kA to ~200 kA) and then during later years of the 5 year plan, if technically ready, to install and generate significant levels of start-up current in NSTX-U. These are described in Section 8.3.1.4.

8.2.2.2 Non-inductive current ramp-up

As described in the introduction, the current ramp-up requirements depend on a number of factors including both the target seed plasma parameters (including radiation losses, transport and MHD stability) as well as the tools available for current ramp-up. An ST-based FNSF is expected to rely largely on neutral beam current drive for current ramp-up. To develop a good understanding of the needs for current ramp-up, NSTX-U will study current ramp-up using a number of different seed current plasmas. These will include both inductively generated discharges as well as non-inductively generated seed current plasmas. The experimental current ramp-up requirements for these discharges that will differ in the initial current profile, density profile and temperature profile, will be compared to TRANSP simulations to develop a good understanding of both the seed current target requirements as well as the requirements on the current ramp-up systems.

Inductively generated seed current plasmas with varying current profiles will be used first to study current ramp-up using both neutral beams and HHFW. Of the three non-inductive start-up scenarios to be tested on NSTX-U (CHI, EBW and Plasma Gun start-up), only CHI will be ready

early during the present 5 year plan for a test of full non-inductive start-up and current ramp-up. The remaining two systems will be used for ramp-up studies when either has established plasma currents in the 200-400 kA ranges on NSTX-U.

8.2.2.3 Linking non-inductive current start-up to ramp-up

The first objective of any new plasma start-up method is to show that current generated by the new system is compatible with conventional inductive operation. Experiments on NSTX and HIT-II demonstrated successful coupling of CHI-initiated discharges to inductive ramp-up with significant central solenoid flux savings to reach given plasma current. CHI is incorporated into the NSTX-U design and is projected to generate over 400 kA of start-up current in NSTX-U. Similarly, the Pegasus experiment has demonstrated coupling of PSHI plasmas to induction from the central solenoid. These results show that the confinement properties of these new start-up methods are good and compatible with the conventional plasma start-up method used in all tokamaks since the inception of the tokamak concept.

CHI (and PSHI, after a suitable design of the PSHI system for NSTX-U is completed and initial current start-up up the few hundred kA established on NSTX-U), and ECH/EBW and fast-wave heating (after 200-400 kA currents are generated on NSTX-U), would be well positioned for the second and final test of the concepts, that of directly coupling to a non-inductive current ramp-up system and demonstrating that the currents could be non-inductively increased to levels required for sustained operation. Such a demonstration requires two conditions to be met: 1) The magnitude of the generated current and the plasma parameters should be adequate for coupling to the non-inductive current ramp-up system, and 2) the availability of a capable non-inductive current ramp-up system. As described in Sections 8.1 and 8.2, CHI on NSTX-U is capable of generating the required current targets needed to meet condition 1). NSTX-U will be equipped with a new ECH gyrotron, the existing HHFW system, and a new second more tangential neutral beam system that is particularly well suited for efficiently coupling to and driving current in low plasma current targets. This satisfies condition 2).

An important objective of NSTX-U is to demonstrate full non-inductive start-up and ramp-up using at least one non-inductively generated seed plasma to show that this is indeed possible, and these objectives motivate the research thrusts described above.

8.2.3 Summary of Research Plans by Year

In this Chapter, the following terminology is used in reference to Years. 'Year 1' by itself means Year 1 of the NSTX 5 year plan. 'Year 1 of NSTX-U Operations' means Year 2 of the NSTX 5 year plan, because NSTX-U will begin operations in FY 2015.

The current ramp-up studies on NSTX-U will explore two specific scenarios. These are:

(1) Bootstrap current drive: This first scenario will use discharges in which the initial plasma density is typical of the densities that exist in standard inductive discharges. These discharges will rely on HHFW for heating and driving fast wave current and also rely on bootstrap current to ramp the plasma current up. Neutral beams will also be used to provide additional current drive. This is similar to the scenarios previously studied in NSTX 300kA discharges, but these new discharges would benefit from both the increased toroidal field and higher coupled HHFW power. This scenario is also directly applicable to Advanced Tokamak scenarios.

(2) Neutral beam current drive: The second scenario will rely on discharges with densities lower than the ECH cut-off density. These will rely on initial heating by ECH and HHFW to increase the electron temperature. Neutral beams will be injected into these plasmas, and they will rely on the longer slowing down time of the neutral beam ions in the low density targets to ramp the current up. NBI current drive would be the primary component. They will also benefit from additional current drive from fast wave current drive and bootstrap current drive.

Much of the supporting work for developing these scenarios will be conducted during FY2013 and FY2014

Year 1

TSC Simulations: Develop CHI start-up scenarios for NSTX-U using TSC to support Year 2 objectives.

TRANSP Simulations: Assess NBI coupling to low current plasmas with varying internal inductance, electron temperature and electron density in support of Year 2 and Year 3 objectives.

TSC/TRANSP/GENRAY: Develop current ramp-up scenarios in support of Year 2 to Year 4 objectives. This involves simulations in which the plasma inductance, density and temperature are varied so that conditions for both bootstrap current and neutral beam driven current drive are understood.

NIMROD Simulations: Develop a model for transient CHI start-up in NSTX and begin to extend the model to the NSTX-U vessel geometry.

Year 2 (First Year of NSTX-U Operations - 2015):

Plasma start-up: Establish transient CHI discharges using graphite lower divertor tiles, using up to 0.8 T capability of NSTX-U, and full Li coating of the lower divertor tiles. Using the 2 kV capability of the CHI capacitor bank, assess maximum toroidal currents that can be generated by increasing the amount of injector flux and the size of the capacitor bank. Use the upper divertor buffer coils to suppress arcs.

CHI Coupling to induction: Couple the CHI generated plasma to inductive drive to show compatibility with inductive operation. Use a solenoid with zero pre-charge.

Ramp-up of an inductive plasma target using NBI: Generate 300 – 400 kA low density inductive plasma, with and without HHFW heating, and inject NBI from the new tangential beam system and assess NBI coupling efficiency and compare to TSC/TRANSP simulations. Based on an assessment of these results, using an inductively initiated plasma, hold the solenoid current constant and inject NBI sources. HHFW may be used to heat this plasma.

Year 3:

Plasma start-up: Improve the magnitude of the closed flux CHI produced current by using Li coating of the upper divertor to further reduce the influx of low-Z impurities. The objective is to improve on the results from the previous year and to obtain 400 kA of closed flux plasma current that is suitable for meeting the needs for satisfying Thrust 2 during Years 4-5. Compare to and improve the NIMROD simulations.

CHI Coupling to induction -1: Extending on the work from the previous year establish the flux savings that can be realized using the above plasma start-up target and with zero pre-charge in the central solenoid.

CHI Coupling to induction -2: Conduct an initial test of coupling CHI to induction using 10 – 20% solenoid pre-charge. The goal is to use some solenoid flux to increase the magnitude of the plasma current generated by CHI, but by ramping the current in the solenoid to zero, so that it can be maintained at zero during sustained non-inductive operation at this higher current level.

Assess CHI coupling to NBI: In CHI discharges that are weakly driven by induction, so as to slow down the decay of the CHI current, increase the magnitude of the neutral beam

driven toroidal current. Compare these results to TRANSP simulations to assess the neutral beam power deposition profile and neutral beam current drive.

Ramp-up an inductive plasma target using HHFW: Using a higher density 300 – 400 kA inductive plasma, ramp the current using bootstrap current over drive and increase the magnitude of the non-inductively driven current fraction. The emphasis here will be to ramp the initial current using HHFW with NBI added later during the current ramp. Use these results to improve the TSC/TRANSP/GENRAY model.

Edge current drive: To a pre-formed lower single null discharge, apply a current pulse using the CHI capacitor bank and measure the presence of any edge driven current and the resulting changes to the edge current profile.

Year 4:

ECH heating of CHI discharge: Heat a CHI iniated plasma using ECH, to demonstrate heating and a longer current decay time and provide a better target for NBI.

Plasma start-up: Maximize the levels of CHI produced plasma currents using the new capabilities that will be available during Year 4. These are (1) metal divertor plates, (2) 1 MW ECH, and (3) 2.5-3 kV CHI capability. All these should allow more injector flux to be injected into the vessel at reduced levels of low-Z impurities. If results are available from QUEST, compare with QUEST results to understand any differences between the two machines.

Couple CHI to NBI: Using the best available CHI targets, conduct an initial test of the effectiveness of NBI coupling to a CHI generated target. Results obtained with ramp-up of inductively generated plasmas (during Years 2 and 3) will determine the level of effort devoted to ramping up purely CHI generated discharges vs. additional experiments that continue to investigate NBI ramp-up of inductively generated discharges.

Couple CHI to induction: Couple to induction using the maximum possible solenoid pre-charge CHI allows. This would be dictated by the maximum amount of the central solenoid fringing fields that are compatible with CHI discharges. Ramp the solenoid current to zero, maintain the solenoid at near zero current, and test establishment of a >600 kA high temperature plasma target for use by other TSGs for sustained non-inductive operation.

Ramp-up an inductive plasma target using HHFW and NBI: Extending on the work from the previous year, discharges with both low and high internal inductance will be used as seed current targets. Extend the plasma current at which current ramp-up is initiated to lower values to assess the minimum required poloidal flux for successful current ramp-

up. Then, establish inductive plasmas with this level of poloidal flux by reducing the pre-charge on the solenoid to determine the amount of pre-charge needed to generate plasmas with the minimum required poloidal flux.

Edge current drive: Based on Year 3 results, to a pre-formed lower single null target, apply a current pulse using the DC power supplies to extend the magnitude and duration of the edge current pulse, and measure changes to the edge current profile, edge current penetration to the interior and changes to the plasma MHD stability limits and plasma transport. Use the non axis-symmetric coils to impose fluctuations to study imposed-dynamo current drive [23].

Year 5:

Plasma start-up: Maximize the levels of CHI produced plasma currents now also using the new divertor cryo pump. Validate NIMROD simulations on CHI plasma start-up using NSTX-U results and begin to develop a NIMROD model for FNSF. Compare results obtained from NSTX with other recent results from QUEST. Of the more than 300 mWb of injector flux that is available in NSTX-U determine the maximum levels that are usable and use these results for CHI design studies for a FNSF. Use these results to improve the TSC model for FNSF.

Couple CHI to NBI: Using the best available CHI targets, ramp a CHI started discharge to 0.6-1 MA using a combination of NBI/HHFW and bootstrap current over drive. Use experimental results to improve the NBI current drive model in NIMROD simulations. Validate the full TSC model (including coupling to TRANSP, NUBEAM and GENRAY) using current ramp-up results from NSTX-U.

Test plasma gun start-up: If technically ready, commission the new plasma gun hardware and test establishment of a PSHI plasma formation in NSTX-U and compare with results from Pegasus.

8.3 Research Plan

In this section we list the research plan for the five-year period. This also serves as a quick overview of the research to be conducted within the solenoid-free plasma start-up and current ramp-up topical science group. The subsequent sections provide details for the proposed work and are arranged as follows.

Section 8.3.1 introduces the reader to the transient TCHI and PSHI systems, including a brief summary of relevant previous experimental results. Section 8.3.2 describes the research plan and

detailed breakdown of the work for first two years of NSTX-U operations, which complete the task requirements for Thrust PSR-1 on current start-up and testing NBI ramp-up. Here Sections 8.3.2.1 to 8.3.2.4 describe the work to be conducted in a general manner, including supporting results from previous work. Section 8.3.3 describes the research plan and detailed breakdown of the work for Years 4 and 5 of the NSTX-U 5 Year Plan, which complete the task requirements for Thrust PSR-2 on linking current start-up and NBI ramp-up and testing point-source helicity injection. Similarly, sections 8.3.3.1 to 8.3.3.6 describe the work to be conducted in a general manner, including supporting results from previous work.

8.3.1 Overview of Helicity Injection Start-up

The primary objective of these new current start-up methods is to generate an initial seed current at a magnitude sufficient enough for directly coupling to the second more tangential neutral beam system on NSTX-U so that the current could be ramped up to the 1 MA level, which is the projected current magnitude for sustained 100% non-inductive operation in NSTX-U. To meet the requirements for coupling to neutral beams, these discharges are required to satisfy certain key confinement parameters. The first requirement is that the plasma current should be above 300 kA so that the neutral beam ions couple to these discharges. The second requirements is that the electron temperature should be sufficiently high for two reasons: 1) The higher electron temperature is required to provide the seed current discharges a sufficiently long L/R current decay time so that the neutral beam ions have sufficient time to slowdown in these discharges and drive current, and 2) the neutral beam current drive efficiency scales as the ratio of electron temperature to electron density. A third requirement is that the initial discharges should have a low electron density to ensure 2) and because it allows an efficient electron heating system such as ECH to be used as an auxiliary heating system to rapidly boost the electron temperature of these discharges to satisfy the electron temperature requirement. For NSTX-U, at a toroidal field of 1 T and for the planned 28 GHz ECH system the cut-off density for O-Mode propagation is an electron density of 5×10^{18} m^{-3}. CHI discharges on NSTX have routinely demonstrated the achievement of high-current discharges at densities of $\leq 4 \times 10^{18}$ m^{-3}.

8.3.1.1 Implementation of Transient CHI (TCHI) in NSTX-U

CHI will be implemented in NSTX-U by driving current along field lines that connect the inner and outer lower divertor plates, as shown in Figure 8.3 In NSTX-U the inner vessel and lower inner divertor plates will be the cathode while the outer divertor plates and vessel will be the anode. The configuration is very similar to that used in NSTX as described in NSTX CHI publications.

Prior to initiating a TCHI discharge the toroidal field coils and the lower divertor coils will be energized. The lower divertor coils are used to produce magnetic flux linking the lower inner and outer divertor plates, which are electrically isolated by toroidal insulators at the top and bottom

of the vacuum vessel. A programmed amount of gas will be injected into the vacuum chamber in the region below the divertor plates and voltage would be applied between these plates, as on NSTX. This will ionize the gas and produce current flowing along magnetic field lines connecting the plates. In NSTX-U initially a 5 to 100 mF capacitor bank charged up to 2 kV will provide this current, called the injector current.

The resulting current will initially flow along helical magnetic field lines connecting the lower divertor plates. The large ratio of the applied toroidal field to the poloidal field will cause the current in the plasma to develop a strong toroidal component, the beginning of the desired toroidal plasma current generation. If the injector current exceeds a threshold value, known as the bubble burst condition, the resulting ΔB_{tor}^2, ($J_{pol} \times B_{tor}$), stress across the current layer will exceed the field-line tension of the injector flux causing the helicity and plasma in the lower divertor region to expand into the main torus chamber. When the injected current is then rapidly decreased, magnetic reconnection will occur near the injection electrodes, with the toroidal plasma current forming closed flux surfaces. Figure 8.3 has a cartoon of TCHI formation in NSTX. The fast camera images in the same figure show that the TCHI discharge is fully formed about 2.5 ms after the capacitor bank is discharged.

What is note worthy is that TCHI in NSTX-U will have numerous improvements over NSTX, to be discussed in more detail in later sections, but briefly summarized here.

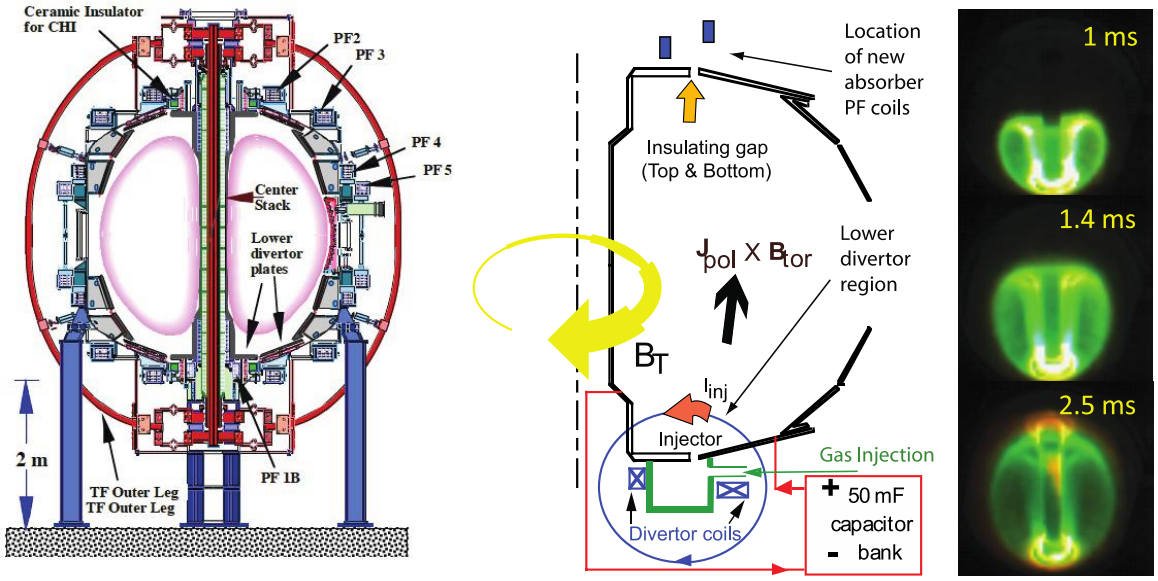

Figure 8.3: Shown are (left) drawing of the NSTX machine, (middle) cartoon of CHI start-up and (right) fast camera images of an evolving CHI discharge in NSTX 1ms, 1.4ms and 2.5ms after discharge of the CHI capacitor bank.

- The injector coil location on NSTX-U allows much better shaping of the initial injector flux because it is much closer to the gap between the divertor plates.

- The injector flux capability of the injector coils, which directly translates to the TCHI plasma current generation capability, is more than 2.5 times that in NSTX.
- The maximum toroidal field in NSTX-U will be 1 T, compared to 0.55 T on NSTX. Because of the increased toroidal flux, the current multiplication factor will proportionally increase. The current multiplication factor is defined as the ratio of the CHI generated plasma current to the injected current.
- NSTX-U is planned to be equipped with a 1 MW, 28 GHz ECH system. This will rapidly boost the electron temperature of TCHI discharges.
- The absorber coils used for absorber arc suppression on NSTX-U are also better positioned and have more than two times the current slew rates that in NSTX.
- NSTX-U will have capability for full divertor Li coating, which will further reduce the influx of low-Z impurities.
- NSTX-U will have the capability for coating the upper divertor with Li. This will reduce the influx of impurities during the occurrence of an absorber arc.
- NSTX-U will be equipped with a second more tangential neutral beam system, which is far superior to the capability on NSTX for driving current. We project, from simulations, that this should be capable of directly ramping the current produced by a TCHI discharge to the levels required for steady-state sustainment on NSTX-U.

8.3.1.2 Implications of NSTX TCHI results to NSTX-U

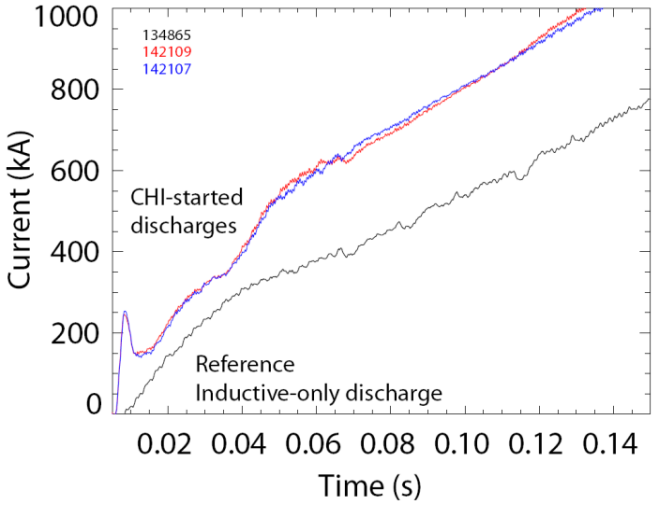

Figure 8.4: Shown are the plasma currents for two discharges initiated using CHI startup and ramped up using the central solenoid (142109 and 142107). The black trace (134865) is for a reference inductive only discharge from the NSTX 10-year database that remained in L-mode and ramped up to 1 MA in the shortest possible time. Note that at 130 ms, the CHI started discharges have ramped up to 1 MA whereas the inductive discharge that has used the same amount of inductive flux has ramped to a lower value of 700 kA.

Figure 8.4 shows two CHI started discharges that were coupled to induction. The third discharge is an inductive-only case that is a non-CHI discharge from the NSTX database (assembled over 10 years of operation) that reached 1 MA in a shorter time than other L-mode discharges. For the CHI initiated discharge at 132 ms, a total of 258 mWb of central solenoid flux was required to ramp the discharge to 1 MA. The non-CHI discharges at this time only get to about 0.7 MA and do not reach 1 MA until 180 ms, by which time 396 mWb of central solenoid flux had been consumed. Thus, the L-mode discharges from the NSTX data base

require at least 50% more inductive flux than discharges assisted by CHI. The inductive-only discharge on NSTX that consumed the least amount of solenoid flux to reach 1 MA, among all the discharges in the NSTX data base, transitioned to an H-mode. That discharge required 340 mWb to reach 1 MA, which is still significantly higher than the CHI started discharges.

In Figure 8.5, we show other parameters for discharges started with and without CHI [24]. The CHI assisted discharges have much lower plasma internal inductance and their line-integrated electron density is about one half that of the standard NSTX discharges. As a result of the lower inductance, the CHI started discharges also have a higher plasma elongation for a similar programming of the NSTX shaping coils. The CHI assisted discharge 142140 has a higher electron density than discharges 140872 and 140875, starting from 80 ms, due to increased gas puffing.

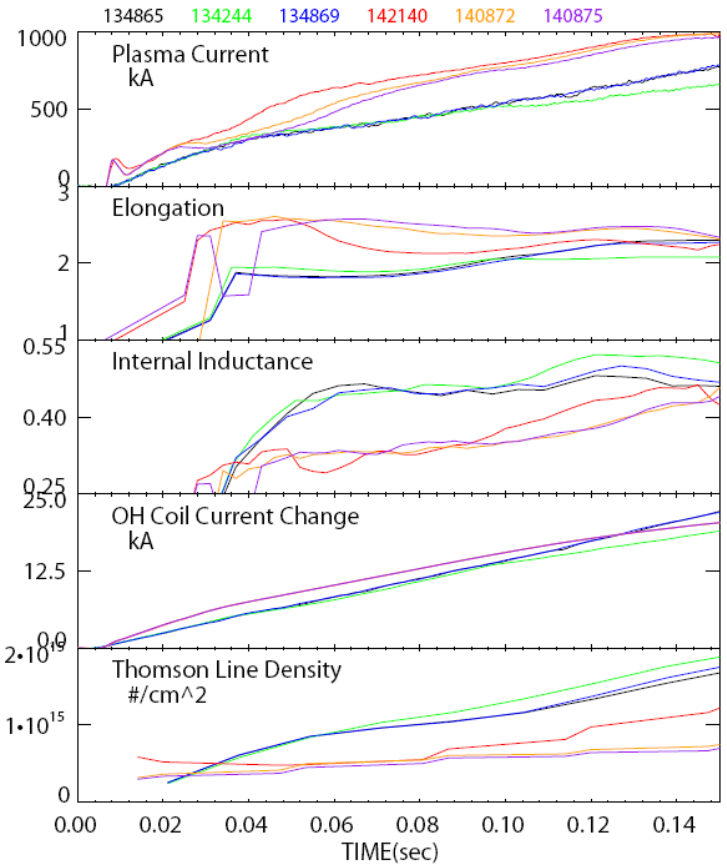

Figure 8.5: Shown are from top to bottom, time traces for the plasma current, plasma elongation, normalized plasma internal inductance, current change in the central solenoid and the electron line density from a Thomson scattering diagnostic. The traces are for three discharges initiated using CHI startup (142140, 140872 and 140875) and three reference inductive-only discharges from the NSTX 10 year database that ramped to 1 MA in the shortest possible time.

We note from the traces showing the difference in the flux change produced by the central solenoid that initially the CHI started discharges consume more inductive flux. For the CHI started discharges the initial loop voltage is about 3 V for 20 ms while the plasma current is about 200 kA, which results in a modest input power of 600 kW. In future devices auxiliary heating power of this magnitude for about 20 ms, such as from Electron Cyclotron Heating, should be able to boost the electron temperature and reduce plasma resistivity. However, past this initial time, the loop voltage consumed by the CHI discharge drops below the level in the non-CHI discharge. At about 120 ms, the inductive flux used by both discharges becomes equal. Beyond 120 ms, the flux usage by the CHI discharge drops rapidly because the CHI discharge uses a unipolar central solenoid swing with a maximum

available flux of 330 mWb. The non-CHI discharges use a bipolar swing and so have twice as much flux available (660 mWb). At 150 ms, the loop voltage for the CHI started discharges becomes too low to sustain these 1 MA plasmas. The drop in the applied loop voltage is also the reason for the gradual increase in the internal inductance after 120 ms.

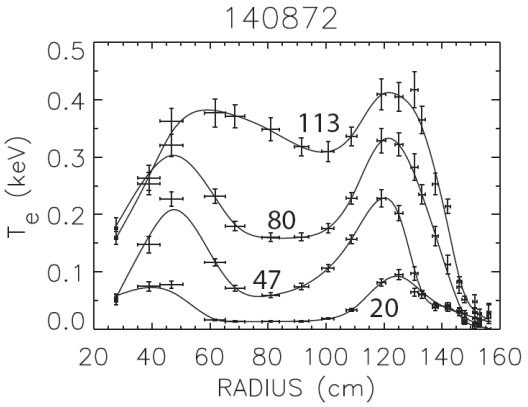

Figure 8.6: T_e profiles at t = 20, 47, 80 and 113 ms for a CHI started discharge that was inductively ramped up. The initial hollow T_e profile is retained during the current ramp.

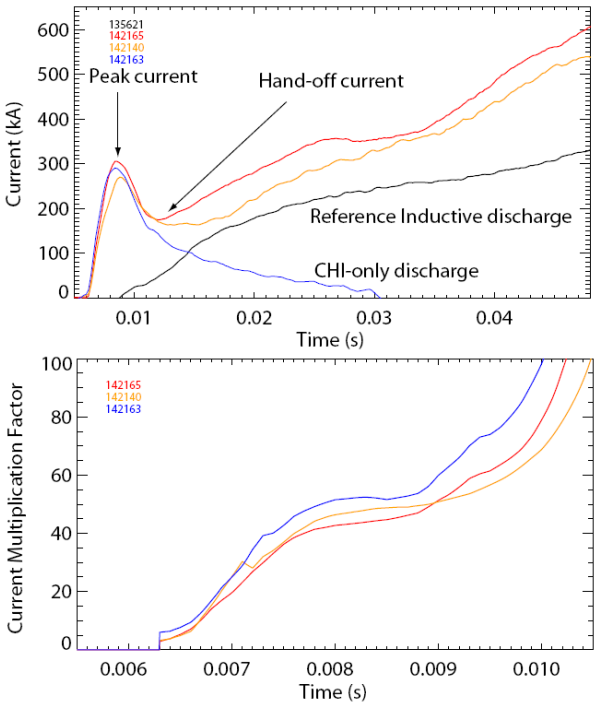

Figure 8.7: Top – Plasma current traces for a CHI-only discharge (142163), CHI started discharges that were ramped up using induction (142165 and 142140) and for a reference inductive-only discharge that had the same inductive loop voltage programming as the CHI discharges that were ramped up using induction. Note that the initial peak startup currents are 300 kA and when ramped using induction, the CHI started discharge ramps up to over 600 kA whereas the inductive-only discharge reaches about 300 kA. Bottom – shown are the current multiplication factors for the three CHI-started discharges.

Operational experience has shown that for the standard inductive startup in NSTX, both the higher plasma density and the slower current ramp rates of the discharges in Figure 8.5 are required to avoid MHD instability during the current ramp. The CHI started discharges seem immune to this, however, although the reasons for this are not known at this time. It could be related to the hollow electron temperature profile, shown in Figure 8.6, that is characteristic of CHI startup [25]. Initially CHI drives all current in the edge region of the plasma. After flux closure it could then be expected that most of the current would still flow at the edge until current relaxation causes the edge current to diffuse to the interior. This initially hollow current profile should result in a higher edge temperature and relatively cooler plasma center. This is indeed seen in the CHI started discharges as shown in Figure 8.6. This hollow electron temperature profile persists during the subsequent inductive ramp, which causes more of the current to flow in the outer region resulting in lower inductance plasma. The lower inductance is favorable for achieving high elongation of the plasma cross-section as the plasma current is then

closer to the equilibrium control coils. That CHI started discharges naturally provide this plasma configuration is a desirable feature for developing advanced scenarios.

Another beneficial aspect of the CHI started discharges is their lower electron density. Because the energetic neutral-beam ions take a longer time to slow down in lower density discharges, the neutral beam current drive fraction increases. Low-density targets are thus a requirement for ramping up an initial current to higher current levels with NBI. In this scenario, NSTX-U will rely on reduced density to increase the neutral beam current drive fraction during the initial current ramp-up phase [26].

Figure 8.7 shows a representative CHI-only discharge (142163) that attained a peak current of 0.3 MA and two similar discharges (142140, 142165) with induction also applied. The fourth discharge (135621) is an inductive-only discharge that used the same loop voltage programming as discharge 142165. By about 45 ms, the CHI started discharge reaches a current about 0.3 MA more than the reference inductive-only discharge. The initial energy stored in the capacitor bank was 29 kJ resulting in a current generation efficiency of over 10 Amps/Joule. The current multiplication factor defined as the ratio of the plasma current to the injector current is over 50.

8.3.1.3 Increased TCHI current start-up capability in NSTX-U

CHI started discharges that have induction applied, both on HIT-II and on NSTX generally show a drop in plasma current before the current eventually begins to ramp-up. The lowest current during the current ramp is referred to as the hand-off current, as shown in Figure 8.7. The magnitude of this drop can be as small as 10% but generally it is about 30%. There are two reasons for this. The first reason is due to the plasma resistivity. Reducing the impurities further would reduce the plasma resistivity through decreasing the Z_{eff} and reducing the radiated power that decreases the electron temperature. Auxiliary heating could also overcome the effects of any residual low-Z impurities.

The second reason for the current drop is a change in plasma inductance as the initially hollow, and therefore low inductance, current profile naturally relaxes. This current profile relaxation is simply resistive diffusion of current. The ratio of the initial peak current to the hand-off current provides an estimate of the initial inductance of the CHI started plasma at the time of peak startup current. Soon after coupling to induction the normalized plasma internal inductance of about 0.35 as computed by the EFIT code for these discharges is maintained through most of the inductive ramp, until the loop voltage becomes too small to sustain the plasma current. The poloidal flux corresponding to this plasma inductance is given as,

$$\psi_p = I_p R_p l_i \mu_0 / 2 \qquad (1)$$

Substituting l_i = 0.35 and I_p = 165 kA, and the EFIT computed value of the plasma major radius R_p = 0.87, Eq. 1 gives ψ_p = 31.5 mWb. In the absence of flux amplification this is the amount of poloidal injector flux that must be injected into NSTX. Assuming that there is no poloidal flux

decay due to resistive loss, the initial plasma internal inductance at the peak toroidal current of 270 kA is then 0.21 for these discharges.

We can now calculate the current multiplication factor using two different methods. In the first method, we use the poloidal flux calculated by Eq. 1. In the second method we use the experimentally measured plasma and the injector currents.

The plasma enclosed toroidal flux for NSTX at 0.55 T is 2.68 Wb. From Eq. 1 the calculated poloidal flux is 31.5 mWb. The current multiplication factor calculated as the ratio of the toroidal to poloidal flux,

$$CM = \phi_T/\psi_p \qquad (2)$$

is 85, which is roughly consistent with the measured current multiplication in NSTX, which is in the range of 50 to 100.

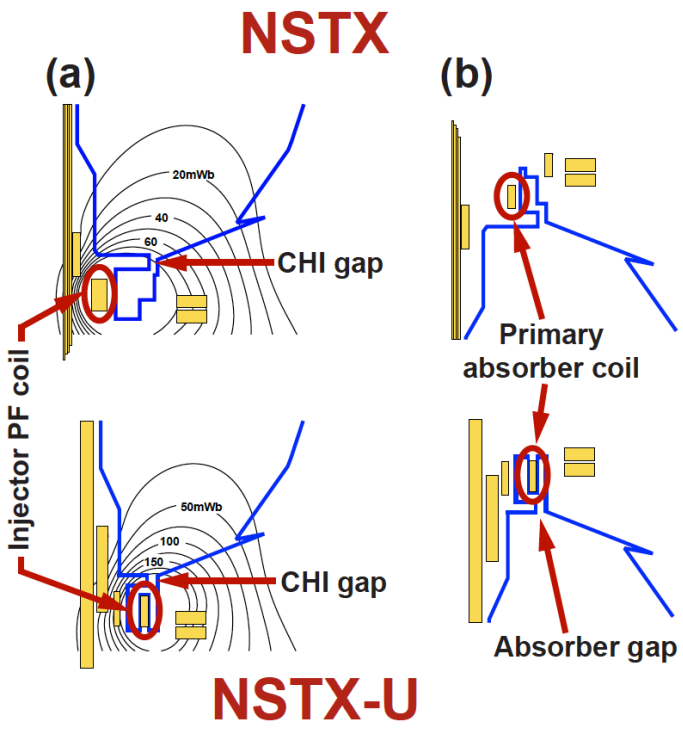

Figure 8.8: Shown are the locations for the injector and absorber PF coils on NSTX (Top) and for NSTX-U (Lower figures). Note that on NSTX-U there are two injector coils. Use of both coils would increase the injector flux to over 300 mWb.

The experimentally measured current multiplication is calculated as the ratio of the plasma current to injector current as:

$$CM_{Exp} = I_p/I_{inj} \qquad (3)$$

For discharge 142140, this current multiplication factor is about 60. A likely reason for the higher current multiplication factor that is obtained from the poloidal flux calculation using plasma inductance is that between the time of peak plasma current and the hand-off current some of the injected poloidal flux has decayed away. These calculations also assume that there is no dynamo activity that generates additional poloidal flux. If there is flux amplification, then the poloidal flux calculated using Eq. 1 would exceed the injector flux calculated using experimental poloidal flux loop measurements. Flux amplification would result in the generation of more toroidal current than can be accounted for by the amount of injected flux.

The injected poloidal flux based on external magnetic measurements varies between 30 and 50 mWb depending on the calculation method. The higher value is the difference in measured

poloidal flux between poloidal flux loops located on the outer edge of the inner divertor plates at the top and bottom of the machine. This provides an upper bound. The lower value is the difference in poloidal flux between poloidal flux loops located at the inner and outer edges of the outer divertor plate, which provides a lower bound. The range of experimental flux measurements is consistent with the poloidal flux calculation using plasma parameters in Eq. 1.

Parameters	**NSTX**	**NSTX-U**
R(m)	0.86	0.93
a(m)	0.68	0.62
B_0(T)	0.55	1.0
Toroidal Flux (Wb)	2.68	3.78
Normalized internal inductance, *l*i	0.35	0.35
Full non-inductive sustainment current, Max Ip (MA)	0.7	1
Poloidal Flux for Max Ip (mWb)	132	206
Required Injector Flux for 50% Max Ip (mWb)	66	103
Current Multiplication factor	41	37
Peak current multiplication	53	48
Peak startup current (kA)	450	650
Injector current	**8.6**	**13.6**
Maximum available Injector Flux (mWb)	63-80	220-340
Max startup current potential (kA)	~400	~1 MA
Required injector current For Max current potential (kA)	10	27*

*Table 1: CHI startup parameters in NSTX and NSTX-U (*HIT-II routinely operated with 30kA injector current without impurity issues)*

Using these equations we can now calculate the projected values of the current multiplication factor and the toroidal current CHI could generate in the NSTX-U. The device parameters and the calculated values are listed in Table 1.

First we assume that CHI will be capable of generating discharges with a normalized internal plasma inductance of about 0.35, as on NSTX, which is a reasonable assumption. The planned level for fully non-inductively sustained plasma currents in NSTX-U is 1 MA. For these conditions, Eq. 1 results in an enclosed poloidal flux of 206 mWb. Because in NSTX, the EFIT calculated value of the plasma major radius is very close to the machine major radius of 0.86, we have here assumed that R_p for NSTX-U in Eq. 1 is equal to 0.93.

For CHI plasma startup at a current level of about 500 kA the enclosed poloidal flux in NSTX-U is reduced to 103 mWb. For this condition, using Eq. 2, we can calculate the current multiplication factor in NSTX-U to be equal to 37. Based on the hand-off current magnitude of 500 kA and this value of current multiplication the required injector current, calculated using Eq. 3, is 13.6 kA. Because of an initial lower inductance, the peak CHI produced toroidal current could be expected to be higher than the hand-off current by about 30%, as described before. The peak toroidal current and the current multiplication factor could be expected to be 650 kA and 48 respectively. TRANSP analysis suggests that the second more tangential neutral beam system on NSTX-U may be capable of coupling to discharges with a plasma current as small as 300 kA. Based on results from NSTX and projection to NSTX-U, CHI should be able to generate currents well above this level.

Based on vacuum field calculations for NSTX and NSTX-U, we note that the available injector flux for NSTX-U is considerably more than the enclosed poloidal flux in a 1 MA NSTX-U discharge. This significantly improved current generation potential in NSTX-U is due to the much-improved design of the CHI injector flux coil, which is positioned much closer to the CHI insulating gap. Note from Figure 8.8 that the injector coil in NSTX is much farther away from the insulating gap, resulting in a much smaller amount of the flux generated by this coil that usefully connects the inner and outer divertor plates. The much larger range for the injector flux in NSTX-U is due to the provision of two injector coils. The lower limit on the injector flux assumes that only one of these coils (the primary coil) would be used and the flux is calculated using the second method described above. The upper bound on the injector flux uses both injector coils and the injector flux is calculated using the first method.

Although the injector flux capability in NSTX-U is large, the amount of useful injector flux defined as the amount of flux that can be injected with acceptable amounts of low-Z impurities may be determined by electrode conditions. This is because a larger value of injector flux requires a higher level of injector current [27] and the higher current densities on electrode surfaces would increase the amount of impurity influx. Present NSTX experiments that have a graphite inner divertor electrode have been able to achieve injector current as large as 10 kA and these discharges when coupled to induction have successfully ramped to 1 MA. So this could be assumed to be a lower injector current bound on NSTX-U. Because the toroidal field on NSTX-U is nearly twice that in NSTX, the same value of injector current can inject nearly twice the injector flux in NSTX-U. This should result in a lower bound on CHI produced toroidal current in NSTX-U on the order of 0.5 MA. If the injector current can be increased without creating additional impurity influx, CHI-generated toroidal currents in excess of 1 MA are theoretically possible in NSTX-U. With better electrode surfaces, HIT-II TCHI discharges routinely operated with injector currents of 30 kA without impurity issues [28]. NSTX-U plans to implement metal divertor plates. This in combination with more complete coverage of Lithium on divertor surfaces and ECH capability should allow NSTX-U to operate at injector currents well above the 10 kA achieved on NSTX.

8.3.1.4 Point source helicity injection (PSHI) plasma start-up

Local helicity injection is a non-solenoidal current drive technique, similar in concept to CHI, except that the injector is relatively compact and can be located anywhere at the plasma boundary. Current is driven on open field lines at the tokamak edge, injecting both power and magnetic helicity, and over time MHD activity incorporates this increased magnetic helicity as an increase in the toroidal plasma current. Experimental studies in Pegasus have demonstrated the formation and growth of more than 170 kA of plasma current, using only 4 kA of driving open-field-line current [29]. This technique appears to be scalable to a device of the scale of the NSTX-U, and the conceptual design of a 1 MA startup system for NSTX-U is presently under development in an external collaboration with the Pegasus team. This collaborative activity encompasses the materials and technology in any deployed NSTX-U injector, a deeper

understanding of the physical processes that guide the injector design, pre-deployment conditioning and testing of the NSTX-U injector and associated power systems, and development of realistic operating scenarios for helicity injection startup to the 1 MA level on NSTX-U. The system is currently being developed at Pegasus and it is envisioned that the full design would be completed during the first two years of the NSTX-U 5 year plan. The system may be ready for installation in NSTX-U during Year 4, with tests up to the 0.5 MA conducted during Year 5.

8.3.1.5 PSHI Results from Pegasus

Past studies of compact helicity injection in Pegasus used an array of compact active PSHI guns to form an axisymmetric but turbulent plasma equilibrium. Substantial ramps in the outboard poloidal field coil currents provided both inductive current drive and radial force balance as the toroidal plasma current increased. MHD activity and the induction have been shown capable of driving up to 170 kA of toroidal plasma current, using only 4 kA of bias current on open field lines. Detailed analysis shows that the vast majority of the current drive in these scenarios is actually from the induction, especially during the high-current phase of the plasma evolution [30]. Although induction-driven scenarios are an effective demonstration of this non-solenoidal startup technique, the strong reliance on induction presents significant limitations. Note, the quantity of Volt-seconds available to induction is limited, which may prevent the technique from successfully driving high-current startup plasmas in the presence of strong dissipation (e.g., high impurity content). Also, the strong outer poloidal field (PF) ramp greatly complicates the radial position control problem, as the dominant drive for the plasma current is also the vertical field. For these reasons, efforts have been recently directed at the development of hardware and operating scenarios in which the helicity injection current drive dominates over any inductive effects from changes in the vertical field. Proof-of-principle demonstration discharges, in which the helicity injection is providing nearly all of the current drive, have been formed and sustained in the Pegasus tokamak, and further development is ongoing.

In terms of the technological development, major strides were made in the past year at the Pegasus facility in developing a viable large-area electrode assembly integrated with one to three active plasma gun current injectors. After tests with both graphite and Mo electrodes, the Mo structure was found to best handle the high heat load and high extracted current density required for an injector.

A local scraper limiter concept was successfully tested to control the density in the injector vicinity and reduce plasma interactions with the injector hardware in the scrape off region. Electrode geometry was developed which both insulates the injector in front of a boron-nitride (BN) insulator assembly and reduces excessive plasma interactions with the BN hardware. This assembly showed reduced impurity generation, to almost negligible levels in the bulk tokamak plasma.

Studies on Pegasus over the past two years have shown that the impedance of the edge current sources is very sensitive to the gas-fueling rate through the plasma gun injectors. It appears that a fast-varying gas flow rate and different flow rates for the passive electrode and active gun sources will be required to optimize the helicity injection rate. To that end, an integrated single-gun, extended electrode injector assembly with a fast piezo-electric gas feed has been designed and installed in Pegasus for testing. It includes the material and geometry advances noted above. Together, this integrated assembly provides a first generation conceptual design for a possible injector assembly that may be deployable to NSTX-U.

Finally, a test electrode assembly has been installed in the divertor plate region of Pegasus to provide initial tests for optimizing the tradeoffs between increased helicity injection in the high-field region near the centerstack and some poloidal induction current drive available from injection in the low-field side outer plasma region. Results from these tests will be integrated with the modeling to suggest optimal geometries for deployment on NSTX-U.

New power systems are under development for the helicity injection systems on Pegasus, and these will provide prototype tests of concepts for power systems on NSTX-U. A new single-quadrant H-bridge assembly has been developed for the bias voltage power supply, which drives the current into the plasma chamber. This system has the advantage of high-voltage (~ 2 kV) and high current (~14 kA) with a single solid-state switch assembly. It promises higher reliability and more robust fault protection than the 4-quad assemblies used earlier in Pegasus. This system will be tested in helicity drive operations in the next year on Pegasus. Incremental improvements in the safety features of the plasma gun arc systems have also been deployed, and should be transferable to the eventual NSTX-U design concepts.

8.3.1.6 Proposed PSHI hardware and access for NSTX-U

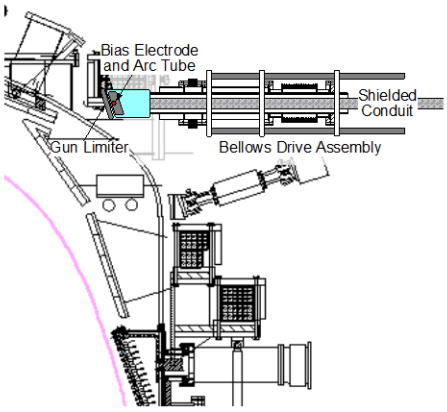

Figure 8.9: NSTX/NSTX-U cutaway, with pre-conceptual injector.

The conceptual design for the NSTX-U PSHI is presently under development, and will be finished in FY2014. What follows is based on a particular pre-conceptual design for the startup system, and is broadly consistent with the developing parameters and features of the final conceptual design.

Figure 8.9 shows a partial cutaway of the NSTX-U vessel with the pre-conceptual injector structure superimposed, to illustrate the scale and location for any eventual compact injector. Machine access would be through a large (8-inch diameter or larger) off-midplane port on the outboard side. The injector will be designed to be fully retractable, using a bellows drive for vacuum integrity, and will be kept outside the NSTX-U vessel and behind a gate valve (in a "garage" region) when

not in use. The plasma-facing portion of the injector will incorporate a limiter structure, an active plasma gun (the arc tube), and a passive electrode. The electrode will be shaped, as much as possible within the footprint of the port, to maximize the Taylor limit [31] while keeping an adequate cross-section for the corresponding current drive. The umbilical cables, tubing, and diagnostic lines from the injector to the power supplies and control system will be kept in a shielded conduit, both to isolate the diagnostic lines from external noise sources and to mitigate the electrostatic noise associated with high-power switching of the injector H-bridge bias supply. Deuterium gas for the active plasma gun is supplied through flexible tubing, with most fueling during the electrode-drive phase supplied through the usual NSTX-U fueling valves.

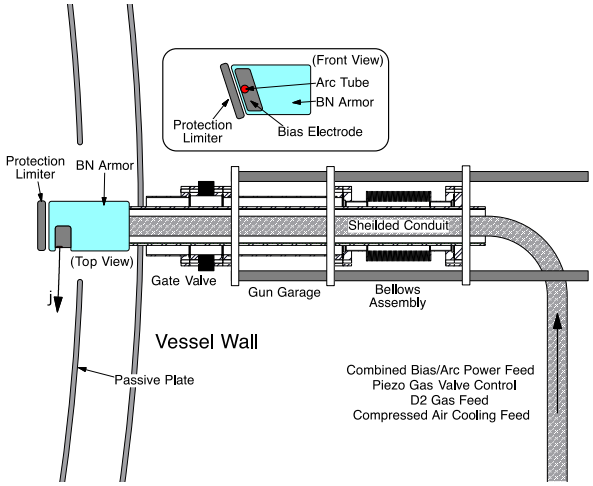

Figure 8.10: Detailed view of pre-conceptual design.

Figure 8.10 shows a more detailed top-down view of the proposed injector, with explicit detail of the gate valve, injector "garage", bellows structure, and the umbilical cables and tubing. The injector is shown inserted between two passive plates, though those details are dependent on the exact port that is made available on NSTX-U for these studies. A more detailed insert shows the elements of the pre-conceptual injector, including the limiter, the arc tube surrounded by an electrode, and an insulating surface behind the electrode to prevent arcing back along the field lines. The present design uses boron nitride as both the insulating surface and the plasma-facing armor for the sides of the injector. The final conceptual design may well use molybdenum or tungsten armor around and behind the injector, in order to shield the boron nitride from plasma impact.

The power supplies and control system can be relatively compact, depending upon the total stored energy that will be necessary for driving the bias during the high-current startup scenario. A simple pulse-forming network will provide the arc discharge in the active plasma source, with a crowbar switch on the outputs to the arc tube. The bias power supply will be based on the technology used on Pegasus, with an array of reduced H-bridge supplies providing the required current and voltage. The arc supply, bias bridges, deuterium gas supply, and control systems will perhaps occupy the volume of an office desk. The total stored energy for the bias supply, necessary for a high-current startup scenario, remains to be determined.

8.3.2 Thrust 1 Research Plans (Years 1 to 3): Establish and Extend Solenoid-free Plasma Start-up and Test NBI Ramp-up

The goals for TCHI plasma start-up will be to first establish plasma start-up in the new vessel configuration, test the capabilities of the CHI hardware such as the new injector and absorber coils, relying on increased Li coverage capability and to ramp a CHI plasma using induction. In other experiments 300-400 kA inductively generated plasma will be ramped-up in current using HHFW and neutral beams. In support of this work, simulations using TSC, TRANSP, GENRAY and NIMROD codes will be conducted during Year 1, as outlined in Section 8.2.3, and discussed further in Section 8.5.

In the area of plasma gun start-up, development work will continue at the Pegasus facility as described in Section 8.3.1 aimed at finalizing the hardware specifications for implementing the PSHI capability on NSTX-U after the system is ready.

8.3.2.1 Use graphite divertor plates with full Li coverage, improved absorber PF coils

During the first two years of NSTX-U operations, NSTX-U will be configured for operation with graphite divertor plates. Initial discharge development on NSTX-U will therefore use the graphite divertor plates as the CHI electrodes. This has the benefit of touching base with previous results from NSTX and assessing in more detail the benefits of full Li coverage and the resulting increases in injector current that can realized on NSTX-U. This also then allows for comparison of the results with full metallic divertor plates during years 4-5.

Significant progress was possible as a result of dedicated efforts to reduce the influx of low-Z impurities in NSTX using methods such as divertor surface conditioning using long-pulse CHI discharges, absorber arc suppression using absorber poloidal field coils and through the use of Li evaporative coatings. This allowed the CHI plasma temperature in NSTX, for the first time, to reach 50 eV in parts of the CHI discharge. This was a significant step as these improvements allowed record levels of start-up currents, up to 300 kA, to also be generated by CHI in NSTX that were then successfully coupled to induction with the realization of central solenoid flux savings.

In CHI terminology the lower part of the vessel from which poloidal flux is injected is called the injector region. The opposite end of the machine is referred to as the absorber region, because the E x B drift is away from the injector region and into the absorber region. During CHI operation if the expanding CHI plasma makes adequate contact with the absorber end of the machine, then it is possible for the injected current to flow along the vessel and bridge the insulator gap at the absorber end of the machine. This is a condition to be minimized, as it can introduce low-Z impurities in to the plasma.

An example of the dramatic benefits of reducing low-Z impurities in a CHI discharge is illustrated in Figure 8.11. Both discharges in this Figure benefitted from similar level of Li conditioning. One of the discharges benefitted from the use of absorber coil, shown in Figure

8.8. Energizing this coil generates a local magnetic buffer field. This has the consequence that this buffer field holds the expanding CHI discharge back from contacting the upper divertor plates. Discharge 135622, which has no current in the absorber buffer field coils, shows no coupling to induction for otherwise identical conditions. An examination of the injector current trace shows the characteristic spike at 9 ms, indicative of the occurrence of an absorber arc. The occurrence of the absorber arc is also seen as a bright ring around the top of the center column in the fast camera image at 8.5 ms. On the other hand, the discharge 135616, with buffer field applied, does not have the absorber arc and the CHI-produced discharge couples well to induction and ramps up to 800 kA. Note that both discharges show nearly identical fast camera images just prior to the occurrence of the arc at 7.5 ms. At 20 ms, the discharge with the absorber arc shrinks in size and is still radiating in the visible spectrum whereas the discharge with no arc, because of its higher temperature is no longer radiating in the visible spectrum.

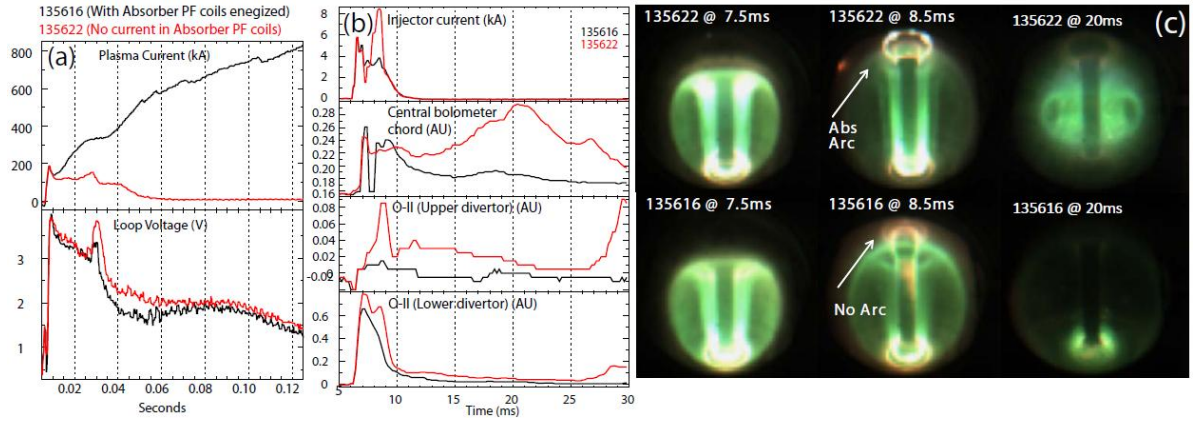

Figure 8.11: Shown are (a) the plasma current and pre-programmed loop voltage for two discharges. Discharge 135622 is a reference discharge in which the absorber PF coils were not energized. In discharge 135616 the absorber PF coils provided a buffer flux to the expanding CHI discharge. Also shown are (b) the injector current, signal from a central chord bolometer, the upper and lower divertor O-II signals. (c) The right column contains fish-eye camera images just prior to, during and after the absorber arc for both discharges.

Traces for the oxygen line radiation signatures show that although the lower divertor oxygen levels are nearly the same for both cases (due to similar levels of Li conditioning), a dramatic increase in the upper divertor oxygen signal is seen when the absorber arc occurs. The central chord bolometer signal also shows significantly elevated levels of radiated power well after the absorber arc has ceased, indicating the presence of increased amounts of low-Z impurities, as is also apparent in the upper divertor oxygen signal.

An added benefit of reducing the low-Z impurities has been that for the first time in NSTX, the electron temperature in the CHI discharges remains above 20 eV (reaching 50 eV in parts of the discharge) as the size of the capacitor bank is increased. Now the additional capacitor bank energy is contributing to heating the plasma, rather than being lost as impurity line radiation, as was the case in previous experiments on NSTX. We have seen this behavior on the HIT-II experiment as well that show that the highest plasma currents are produced immediately after

titanium wall conditioning is used. Thus on NSTX-U further controlling the low-Z impurity influx should allow the plasma electron temperature to increase and also contribute to increasing the magnitude of the initial start-up current. Such future discharges could also be expected to have longer L/R current decay times.

8.3.2.2 Test benefits of (partial) upper metal divertor and Li during absorber arcs

It was noted in the previous section that contact of the evolving CHI discharge with the upper divertor plates resulted in an influx of impurities (Oxygen) that subsequently degraded the performance of the CHI discharge. In addition to the absorber buffer field coils, another method for controlling low-Z impurities, which has not been used thus far, is to use lithium conditioning of the upper divertor plates. It is seen from Figure 8.11 that that soon after the CHI plasma contacts the upper divertor the O-II signal from the upper divertor increases and the discharge subsequently runs into a radiation issue. One of the reasons for this could be because NSTX is routinely operated in a lower single null configuration or a double null that is biased towards the lower divertor. During the final two years of NSTX operations, NSTX did not have significant dedicated experiments in the upper single null configuration. Thus the upper divertor never gets adequately used and has more surface impurities. Thus it is conceivable that if plasma contacts the upper divertor, surface contaminants would enter the discharge. Also, the usual Li evaporative coatings on NSTX direct a plume of Li towards the lower divertor surfaces and none of this Li coats the upper divertor. So in addition to not being conditioned by plasma discharges the upper divertor also does not benefit from Li coatings.

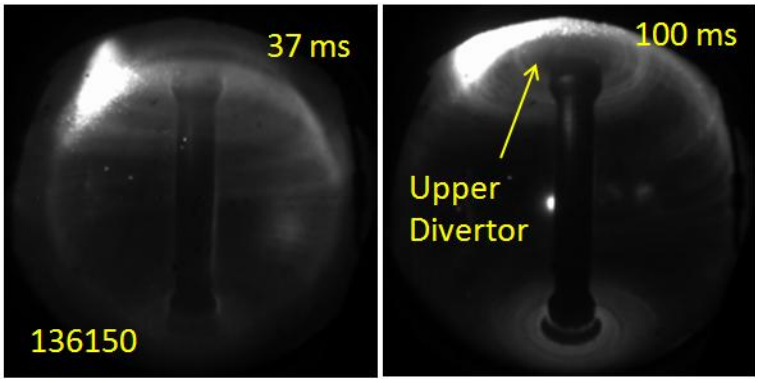

Figure 8.12: The image on the left shows Li powder being dropped on to the top of a NSTX discharge. The image on the right shows the ionized powder being transported towards the upper divertor.

An observation in past experiments that used the Lithium Dropper system [32] was that, when the Li powder was dropped on to a weakly upper biased double null discharge (produced during the FY09 reversed B_T campaign) the ionized Li is transported towards the upper divertor region and presumably coats the upper divertor. A visible camera image of this is shown in Figure 8.12. Thus, if a few of these discharges are run prior to a CHI discharge, then, in the event that the top of a CHI discharge contacts the upper divertor, possibly less oxygen and other surface contaminants, would enter the discharge. While this could be tried on NSTX-U, NSTX-U will have the benefit a Li evaporator dedicated for conditioning the upper divertor. Thus, on NSTX-U, with Li conditioning of the upper divertor the CHI discharges could in principle be driven harder to allow increased absorber arcing to occur, but without the influx of significant oxygen influx.

8.3.2.3 Initially couple to induction, then assess coupling to NBI and HHFW

A good way to quickly assess the quality of discharges produced using a new start-up method is to couple it to induction using the central solenoid. Coupling to induction is a first step to assess if the confinement properties are adequate for eventual coupling to neutral beams. The goals on NSTX-U will be to initially couple to a central solenoid that has zero pre-charge, for a direct comparison to results obtained on NSTX. The extent of central solenoid flux savings flux will be measured. The electron densities and temperatures and their profiles during current ramp will be measured as a function of current ramp-rates with and without the presence of neutral beams and HHFW heating. In other experiments, some pre-charge will be introduced into the central solenoid to determine the minimum pre-charge that is needed to ramp a CHI started discharge to the 0.6-1 MA range. This would be of considerable benefit to other experiments on NSTX-U aimed at sustained non-inductive operation in the 0.6 to 1 MA range of currents as the central solenoid current could be maintained at zero after the sustainment current levels are achieved.

The next step will be to gradually reduce the loop voltage and improve the neutral beam injection parameters (based on TSC and TRANSP simulations coupled to experimental measurements) to understand the requirements for full sustainment with neutral beams during years 4 to 5. The electron temperature, especially during the first 50 ms after initiation of a CHI discharge will be particularly important for full sustainment by beams, and the 28 GHz ECH capability will not be available until Year 4 of the NSTX-U 5 year plan. In support of this goal, the temperature and density requirements of the CHI target will be studied using HHFW heating and the best-developed wall conditioning methods to increase the intrinsic CHI discharge temperature by reducing low-Z impurities to the extent possible.

8.3.2.4 Assess ramp-up of a 400 kA inductive target with NBI and HHFW

In support of Year 4-5 goals to fully ramp a 400 kA CHI target to the 1 MA levels, data will be gathered during the first two to three years in which a the CHI discharge will be experimentally simulated by using a 300-400 kA inductively generated target. In such discharges the solenoid current will be held constant and neutral beams and HHFW injected into the decaying target to determine the plasma parameters that are required for full non-inductive ramp-up. Targets with both low and high internal inductance will be used, furthermore Te will be varied to improve our understanding of the sensitivity to both current and electron temperature profiles. Changing the initial inductive current ramp rates supplemented by early heating by HHFW and NBI will generate discharges with variations in internal inductance and electron temperature. We are at present studying the NBI coupling efficiencies (using TRANSP) in these simulated targets that have been generated by TSC.

TSC simulations, such as the one shown in Figure 8.13 suggest that starting from a 400 kA inductive target, the combination of bootstrap current overdrive plus neutral beam current drive could ramp the current to 1 MA in about 3 s. In these simulations, an initial 400 kA low-inductance discharge is heated using 4 MW of HHFW power. The H-mode is initiated at 150 ms and the HHFW power is turned off at 0.9 s. The neutral beam power is programmed to increase with the plasma current. Starting from 1.5 s, a Greenwald density fraction of 0.5 and electron temperature of 1.7 keV is maintained until 5 s. The energy confinement time is maintained at about 30 ms, consistent with NSTX experimental results.

These simulations give confidence that full non-inductive current ramp-up should be possible in NSTX-U. It is also necessary to cross check the simulation results with experimental measurements to improve the model of electron transport, neutral beam absorption and current drive fractions. This would be an important part of the experimental program during Years 1 and 2 of NSTX-U operations.

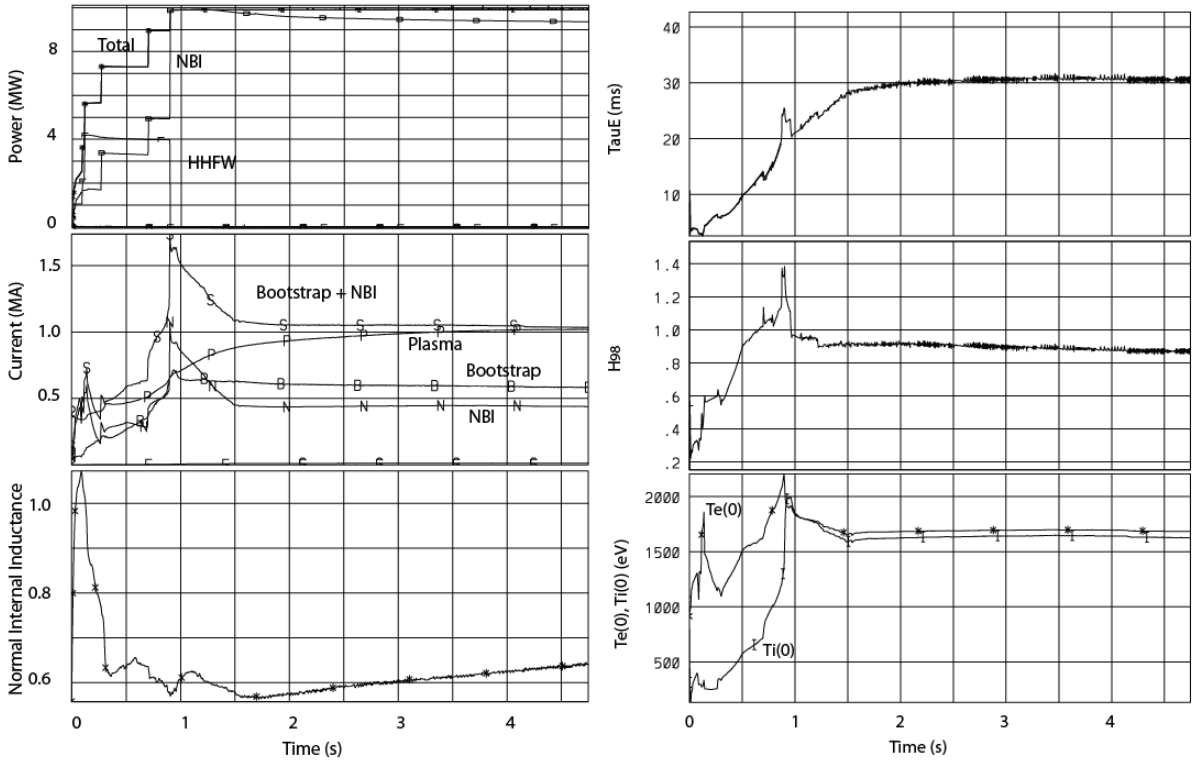

Figure 8.13: TSC simulations in which a 400 kA discharge is ramped up using bootstrap current and neutral beam current overdrive.

8.3.3 Thrust 2 Research Plans (Years 4 to 5): Ramp-up CHI Plasma discharges using NBI and HHFW and Test Plasma Gun Start-up

8.3.3.1 Establish CHI discharges using metal divertor plate electrodes

Another method to increase the electron temperature in electrode based plasma start-up methods is to use refractory metal electrodes, rather than carbon electrodes. This is because metals do not radiate strongly until the electron temperature exceeds 100 eV. Because the TCHI start-up is a pulsed method, with the electrode current driven phase lasting for less than 3 ms, any metals (even if sputtered into the discharge) should be lost in a few particle confinement times. The electrode-based spheromak experiments that generated high electron temperature plasmas (> 400 eV) used metal electrodes. During Years 4 to 5, it is planned that high-Z tiles would replace the lower divertor graphite tiles. We will run reference discharges from the Year 3 to determine the improvements to the CHI electron temperature, peak plasma current and reduction in impurities and the required CHI operating voltages that results from the use of metal electrodes.

8.3.3.2 Assess benefits and compare to QUEST results (if available)

We are currently engaged in a CHI systems design for the QUEST ST in Japan. The QUEST CHI electrode would likely use tungsten plasma spray coating on a stainless-steel substrate. In addition, QUEST will have access to a 0.5 MW ECH system. If the CHI hardware is installed on QUEST before 2015, transient TCHI results should be available from QUEST during the 2016 to 2018 time frame. These results will be compared to results obtained on NSTX-U with graphite and metal electrodes. These results from QUEST would help NSTX-U CHI research and provide additional information related to the electrode designs for a ST FNSF.

8.3.3.3 Assess benefits of lithium deposition in the upper divertor region

During the actively driven portion of a CHI discharge the E X B drift is away from the injector region and into the absorber region. As a result, over time, the neutral pressure can build up in the absorber region. This increase in gas and plasma density in the absorber region is a condition that is favorable for the generation of absorber arcs. This issue is much more pronounced during steady-state CHI during which the neutral pressure could build up to high levels. For steady-state CHI, active pumping may be required in the absorber region to keep the neutral pressure low and to deplete the region of charge carriers so as to reduce the incidence of absorber arcs. During TCHI this is much less of an issue for the following reasons. First, the neutral gas transit time is about a meter per ms. The distance between the injector and absorber regions in NSTX-U is about 4 m. So it takes approximately 4 ms for the gas injected in the injector to reach the absorber region. The actively driven CHI pulse duration is a strong function of the operating voltage. At the 1.7 kV that was used in NSTX, the active portion of the CHI pulse length was 3 ms. Thus during the 3 ms period, most of the energy from the capacitor bank is depleted before much of the injected gas reaches the absorber. So, the arcs should be mostly governed by the time taken by the leading edge of the CHI discharge to reach the absorber region. Absorber arcs generated in this manner could be suppressed through the use of a buffer flux as previously

described. Nevertheless, on these time scales some gas will get into the absorber region, and so active pumping in this region will only help. Active pumping in the absorber region may also provide more flexibility in the amount of injected gas or in the CHI operating voltage. The planned installation of an upward-pointing lithium evaporator would allow testing of the benefits of operating CHI with reduced neutral pressure in the absorber region that may result due to stronger deuterium pumping in the upper divertor region.

8.3.3.4 Maximize current start-up

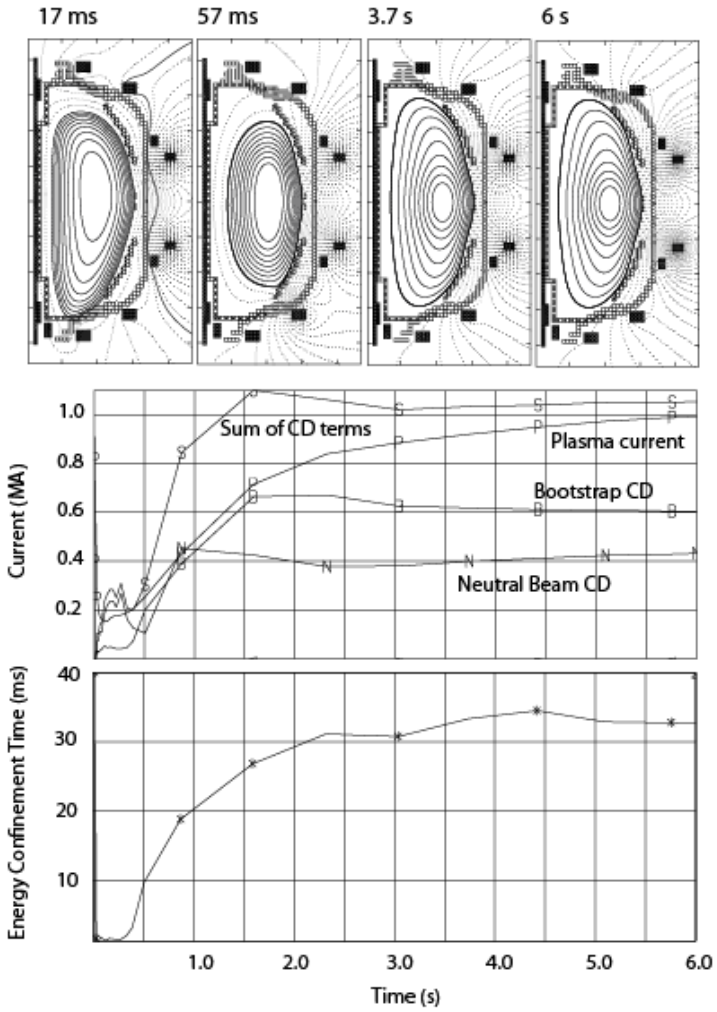

Figure 8.14: Shown are TSC results from a full discharge simulation that involves plasma start-up using CHI and current ramp-up using NBI and bootstrap current overdrive. Top frame: Shown are the poloidal flux contours at 17 ms, during the end of the CHI-phase, at 30 ms during the coupling phase and at 3 and 6 seconds during the current ramp-up phase. Middle frame: The different components of current drive. N: Neutral beam, B: Bootstrap, P: Plasma current and S: Sum of current drive terms. Bottom frame: The energy confinement time calculated with respect to input power.

During Years 2 and 3, we will have established CHI start-up and demonstrated coupling to induction. These experiments will have used graphite divertor tiles and 2 kV CHI operational capability. During Years 4 and 5 new CHI enhancing capabilities will become available. These will be used to maximize the CHI current start-up potential in NSTX-U.

First, discharges will be generated during Year 4 using metal divertor plates as described above to further reduce low-Z impurities and to increase both the electron temperature and the plasma current magnitude.

Second, higher capacitor bank voltage capability of up to 3 kV will be used to reduce the CHI pulse length and to increase the magnitude of injected poloidal flux to further increase the plasma current. To increase the injected flux at a given toroidal field, the bubble burst criterion requires that the injector current be increased. Increasing the injector current at low voltage

requires a longer injector pulse length that increases the amount of electrode generated impurities as well as increasing the possibility of absorber arcs. During TCHI, reducing the CHI pulse length during the actively driven portion is only possible by increasing the operational voltage. At the higher voltage, which would now require a bank with smaller capacitance (but more total stored energy), the higher injector currents could be achieved at shorter pulse lengths. This would both reduce the impurities injected from the injector and minimize the severity of absorber arcs. Voltage control is a very powerful knob for CHI start-up. During the FY09 and 10 CHI campaigns, NSTX-U essentially always used the maximum available voltage of 1.7 kV as a reduction to this voltage reduced CHI performance levels. This CHI voltage capability will be increased for the first time in NSTX-U, to 2 kV during Years 1 and 2 of NSTX-U operations and up to 3 kV during Years 3 and 4 of NSTX-U operations. This new capability should allow NSTX-U to use more of the available injector flux to explore the maximum levels of start-up currents possible in NSTX-U. Experimental assessment of these limits will directly influence the CHI system design for FNSF.

During this period the secondary CHI injector coil will also become operational. This would increase the CHI injector flux capability from about 220 to 340 mWb. As previously mentioned, the CHI generated plasma current scales proportional to the injector flux.

8.3.3.5 Heat CHI target using 1 MW ECH, then HHFW for coupling to NBI

TSC simulations of NSTX TCHI discharges have successfully demonstrated current persistence [33], which is the toroidal current persisting after the injector current has been reduced to zero. The generation of closed flux is the result of an effective (positive) toroidal loop voltage induced by the changing poloidal flux on the open field lines as the injector current is reduced to zero. Reference [33] also shows that CHI scaling with toroidal field is favorable for larger machines so that peak plasma currents in excess of 600 kA could be generated in NSTX-U. The higher toroidal field allows more poloidal flux to be produced in the plasma at the same level of injector current.

We have now conducted the first simulations of a fully non-inductive start-up with CHI and subsequent non-inductive current ramp-up using neutral beams in support of planned experiments on NSTX-U (Figure 8.14). The CHI discharge is initiated by TSC as described in Reference [33], and a 400 kA closed-flux target is generated. The first step involves current driven by the external injector circuit on purely open field lines. This causes the injected poloidal injector flux to fill the vessel. Then, the applied CHI voltage is rapidly reduced. This results in a rapid decrease in the injector current. As a result, the injected poloidal flux begins to reduce in magnitude. The time-changing poloidal flux induces a positive loop voltage within the plasma, which causes the generation of closed field lines carrying toroidal current.

At the onset of flux closure a second step in the simulation is initiated. This continuously solves for the plasma boundary, including locating the divertor X-point and begins solving the flux

surface averaged transport equations. This phase begins 17 ms after the CHI discharge is first initiated.

For these simulations, the initial electron temperature for the CHI discharge is 100 eV. This is a reasonable starting value based on other simulations that show that 1 MW of 28 GHz RF heating power could rapidly increase the electron temperature of a CHI-like discharge to over 100 eV. The initial electron density is assumed to be 3×10^{18} m^{-3}, similar to the densities obtained during CHI start-up in NSTX as shown in Figure 8.5. In the simulation, the initial plasma internal inductance is also below 0.5, consistent with that calculated by EFIT for the CHI discharge in NSTX shown in Figure 8.5.

At 17 ms, horizontal position control is implemented and at 40 ms vertical position control is used to vertically center the highly up/down asymmetric CHI plasma. The electron transport is adjusted to keep the energy confinement time at about 30 ms, consistent with energy confinement times in neutral beam heated NSTX discharges. During the low density phase of the discharge the RF power is increased to 2.5 MW. This is assumed to be from a combination of 0.5 MW absorbed ECH power and 2 MW of absorbed HHFW power. After that 2 MW of HHFW power is retained in these simulations. Neutral beams are added in increments to keep the current overdrive at acceptable levels, as TSC is not capable of handling the formation of current "holes" where the toroidal current density drops to zero or to very low values. After the current has built up to sufficient levels, both the density and neutral beam power are ramped-up. Figure 8.14 shows the results from this first evolving discharge, which at 6 s reaches 1 MA of plasma current.

8.3.3.6 Test plasma gun start-up on NSTX-U

During the first two years, work in progress at the Pegasus facility will focus on competing the detailed systems design for NSTX-U. During the next three-year period, the work will focus on the construction and deployment of this startup system. The complete startup system (injector hardware, control system, and power supplies) could be deployed at NSTX-U as early as Year 3 or 4. Then, initial shakedown experiments could be conducted during Year 4 or 5.

Initial experiments using the compact helicity injection system at NSTX-U will be guided by operating scenarios developed in the computational activities of the previous years, and will establish the necessary elements of a successful high-current startup. Using an active plasma source to form a tokamak-like state in the presence of the passive plates, transition of the drive from the active gun source to the passive electrode, buildup of the plasma current due to helicity injection drive, and demonstration of the plasma position control through the current buildup phase must all be experimentally demonstrated on NSTX-U before attempting a high-current startup. Optimistically, by the end of Year 5, initial experiments using the newly deployed compact helicity injection system may have demonstrated these features and the NSTX-U team may be poised to attempt a full-power 1 MA startup in the following year.

8.4 Diagnostics

8.4.1 General NSTX-U diagnostics

Standard NSTX diagnostics used for plasma operations on NSTX have been used to diagnose CHI discharges on NSTX and will continue to be used to support CHI discharges on NSTX-U. These systems are described in Chapter 10 of the 5 year plan document.

As in previous years, discharges established using CHI will be diagnosed using the multi-point Thomson scattering diagnostic to obtain electron temperature and density profiles as a function time. The multiple laser beams are triggered in close temporal proximity to each other to measure radial profiles or temperature and density during the current decay phase of a CHI discharge. The far infrared tangential interferometer/polarimeter (FIReTIP), will be used in conjunction with the Thomson scattering diagnostic to provide continuous line-integrated density measurements.

Visible and VUV spectroscopy will be used during control room operations to improve discharges so as to minimize the influx of low-Z impurities. These have been quite helpful in the past for assessing vessel impurity levels and for qualitatively assessing impurity levels in CHI discharges.

The fast camera diagnostic has also been very effective for quickly determining the shape of the evolving discharge and for controlling the discharge during the pre-programmed coil current phase. The Plasma TV system provides a fisheye view of the entire NSTX plasma from a re-entrant port located on Bay B midplane. A Vision Research Miro 2 color camera is used. The camera has a 10 bit depth and has a full frame acquisition speed of 1.24 k frames per second (fps) @ 640x480 pixels. The resolution typically used varies between 448x448 pixels and 176x176 pixels (the latter being more commonly used in CHI experiments). These resolutions correspond respectively to a maximum frame rate of 1.8 kfps and 10 kfps. Qualitative information about the radiating species can be obtained from the color of the emission. Two wide-angle lower divertor views (Bay E and Bay J) will be available in the same configuration as in 2010, providing a full toroidal coverage of the lower divertor [34]. In the 2010 configuration a Vision Research Phantom 7.3 and a Vision Research Phantom 710 were used with 12 and 14 bit depth resolutions. The Phantom 7.3 has a maximum full frame acquisition speed of 6.8 kfps (800x600 pixels) while the Phantom 710 has a maximum full frame acquisition speed of 7.5 kfps (1280x800 pixels). The typical resolutions are of 256x208 pixels (Phantom 710) and 224 x 184 (Phantom 7.3), which correspond to maximum acquisition speeds of respectively 100 kHz and 60 kHz and resolutions of about 0.8 cm/pixel. Reducing the field of view acquisition speeds up to 200 kHz were achieved in the same configuration. These cameras are equipped with remotely controlled filter wheels.

The multi-energy SXR array with, eventually, two toroidally displaced sets of views has a frequency response <100 kHz. Spatial resolution varies from ~1 cm at the outboard midplane

(130<R<150 cm) to ~3 cm in the core region (90<R<140 cm). Faster measurements with up to ~500 kHz bandwidth will be available from a system of two poloidal SXR arrays. Each array contains 16 channels viewing poloidally through two variably selected filters, with 2-3 cm resolution. The system can also be operated in the bolometer mode to obtain total radiated power profiles. Additional descriptions of these systems are provided in Chapter 10.

New for NSTX-U will be a Motional Stark Effect with Laser-Induced Fluorescence (MSE-LIF) diagnostic. Comparing to the MSE diagnostic on NSTX, MSE-LIF does not rely on heating beams and has its own dedicated diagnostic neutral beam with beam energy of 30-40 keV. Different from conventional MSE, which depends on emission from collisionally induced fluorescence, MSE-LIF uses laser to induce fluorescence and thus leads to stronger emission. Beam voltage is swept across spectrum and spectral peak separations can be measured, from which magnetic field magnitude can be obtained, and additional polarization measurement provides pitch angle information. Preliminary measurements from beam-into-gas shots on NSTX show a sensitivity of 5-10 gauss for the field amplitude measurement. MSE LIF will be used to measure the magnetic field line pitch angle, which will be used to measure q profile in CHI discharges. The time response of the system is 10 ms, which should be sufficient for longer pulse, higher-current CHI start-up discharges expected in NSTX-U. The spatial resolution is 2-3 cm. These measurements will be used to further improve CHI start-up simulation capability using the NIMROD and TSC codes.

8.4.2 CHI specific diagnostics

CHI Voltage monitors: During CHI operations, the voltage of the inner and outer vessel with respect to ground is individually measured. On NSTX, the voltage was measured using a resistive-divider network that was connected to the vessel near the bottom of the machine (near the injector region). The electrical signals were then converted to optical signals using a fast fiber optic transmitter/receiver system and then recorded on a remote digitizer known as a handyscope. The handyscope was floated with respect to NSTX ground. Because much of the long-distance signal transmission was over a fiber optic network, the system avoided electrical noise pick-up including ground loops and so had a high system bandwidth of more than 100 kHz and was digitized at sample rates of 1 MHz. For NSTX-U, this system will be retained and an additional duplicate system installed to measure the voltage on the upper part of the vessel as well. In addition to these we will digitize the signal from a separate voltage divider network without the use of a fiber optic network using conventional digitizers. This back-up system will be functional for all NSTX-U discharges and will have a much slower bandwidth of 10 kHz.

CHI current monitors: The CHI injector current is measured at the CHI capacitor bank location using a Pearson current transducer mounted on the CHI current feed to the vessel. This system will be retained for NSTX-U operations. In addition, we plan to install additional current transducers near the CHI connections to the NSTX-U vessel. There will be a total of four

additional current sensors composed of a Pearson current transducer and a Direct Current Current Transducer (DCCT) on each of the input and return current legs to the machine. These would be located on the machine side of what is known as the McBride switch. The McBride switch functions to either short the inner and outer vessel components or allow them to be individually biasable. The purpose of the new current monitors would be to further improve the resolution of the current measurements during CHI as well as to provide current measurements across the vessel components during normal NSTX-U operations to measure divertor halo currents and thermoelectric currents during standard inductive operation.

New set of inner vessel magnetics: During NSTX CHI operations, especially during discharges in which a long pulse edge current was driven using the CHI DC power supplies, it was observed that the inner vessel magnetics were prone to EMI noise pickup. This was largely due to inadequate shielding of the sensors mounted inside the inner vessel casing. For NSTX-U we will have an array of sensors that will be specially shielded for EMI using a braid that fully surrounds the return current leads. Because of space limitations inside the center stack casing this was not possible on NSTX. For NSTX-U, the number of such specially shielded sensors is reduced to provide adequate space for the braid inside the center stack casing.

Additional flux loops and Mirnov coils on lower and upper divertor: To improve the measurement of the CHI injector flux and in support of NIMROD simulations, two additional Mirnov coils and an additional polodal flux loop will be added to each of the upper and lower divertor plates on NSTX-U.

Electrode diagnostics: NSTX-U will have a Langmuir probe array at one toroidal location on the lower outer divertor plate. The sensors will provide information on the radial changes to the ion saturation current and the floating potential and will be useful for localizing the region where the CHI injector current flows. In addition to these sensors, a dual color, fast infrared camera will be used to measure the plate temperature during CHI operations. A third diagnostic is a fast visible camera that can be used either as a visible camera or as a filtered camera to view light emissions from lithium or carbon lines. All three of these diagnostics will be used to determine the radial extent of the CHI injector current. This information will be used to improve simulations using the NIMROD code.

8.5 Theory and Simulation capabilities

8.5.1 2D equilibrium evolution simulations

TSC is a time-dependent, free-boundary, predictive equilibrium and transport code [35 36]. It has previously been used for development of both discharge scenarios and plasma control systems. It solves fully dynamic MHD/Maxwell’s equations coupled to transport and circuit equations. The device hardware, coil and electrical power supply characteristics are provided as input. It models the evolution of free-boundary axisymmetric toroidal plasma on the resistive and energy

confinement time scales. The plasma equilibrium and field evolution equations are solved on a two-dimensional Cartesian grid. Boundary conditions between plasma/vacuum/conductors are based on poloidal flux and tangential electric field being continuous across interfaces. The circuit equations are solved for all the poloidal field coil systems with the effects of induced currents in passive conductors included. Currents flowing in the plasma on open field lines are included, and the toroidally symmetric part of this "halo current" is computed. For modeling CHI in NSTX, the vacuum vessel is specified as a conducting structure with poloidal breaks at the top and bottom across which an electric potential difference is applied from which TSC calculates the injector current using a model for the resistivity of the "halo" plasma. This circuit, however, contains a sheath resistance at each electrode, which is difficult to model.

Shown in Figure 8.15 is the simulation of an early NSTX TCHI discharge that successfully demonstrated current persistence, a condition when the CHI produced toroidal current persisted after the injector current had been reduced to zero. We used the same poloidal field (PF) coil currents as were used in NSTX Shot 118340 [5]. Due to the difficulty in computing the actual plasma resistance including the plasma-vessel sheath resistance in this case, we did not attempt to use the experimentally measured voltage, but rather applied a voltage V across the lower vessel gap and adjusted this value V to give approximate agreement with the measured toroidal current. About 60 kA of toroidal current is generated soon after the current peak, and as in the experiment, at the time of peak toroidal current, the injector current is similar to the experimental value. The poloidal flux plots show the plasma evolves in much the same way as observed experimentally from fast camera images.

In these simulations the injector voltage is varied by a controller to obtain the required injector current. This is similar to what is done experimentally. The injector current is the parameter that needs to be controlled. For example, experimentally, for identical injector flux conditions in the same machine a different value of the voltage may be required to produce the same injector current since the magnitude of the injector current depends on the resistivity of the plasma and the edge sheath conditions. These depend on many things that are difficult to predict such as the conditioning of the machine, the presence of impurities, and the possible presence of auxiliary heating. Experimentally, if we are unable to get the injector current needed to inject a given amount of poloidal injector flux, then we simply increase the voltage to a level that is required to obtain the needed injector current.

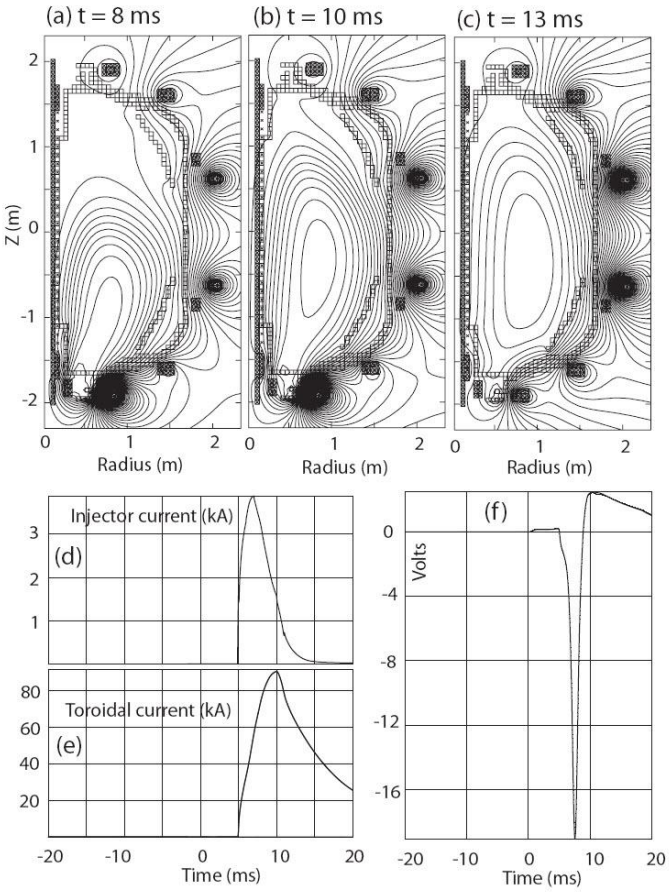

Figure 8.15: Simulation of a 60 kA NSTX TCHI discharge (shown in Reference 33) with the TSC code. For these simulations, the coil currents used in the experiment were used as input parameters. The CHI voltage is applied at 5 ms. Shown are (a-c) poloidal flux contours, (d) the injector current, (e) the plasma current and (f) the induced loop voltage at Z = -0.3 m along the inner vessel during the growth and decay of the CHI plasma discharge.

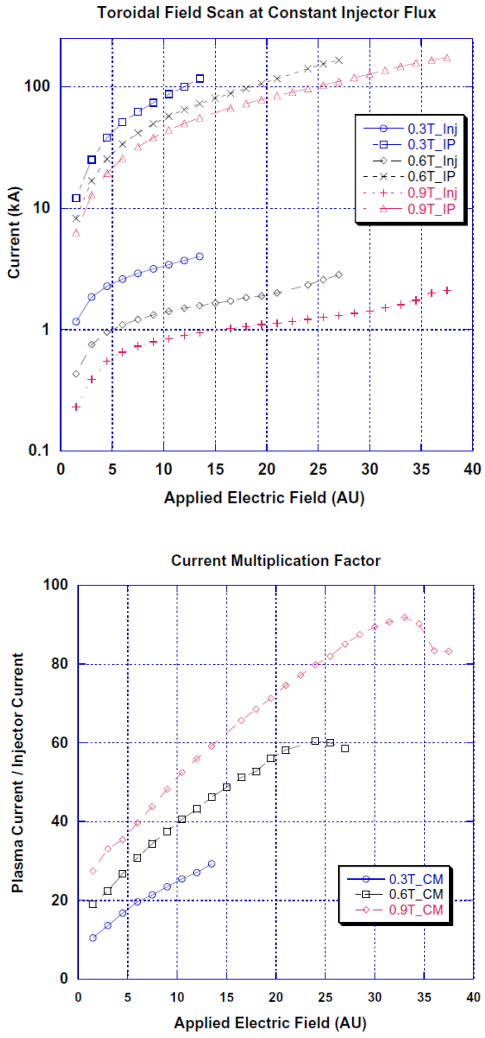

Figure 8.16: The top frame shows the injector current (lower traces) and the CHI produced toroidal current (top traces) as the injector voltage is increased. The lower frame is the ratio of the toroidal current to the injector current and represents the attained current multiplication factor.

Generation of closed flux in TSC is as a result of an effective toroidal loop voltage induced by the CHI ejected poloidal flux that decreases as the injector current is reduced to zero, as shown in Figure 8.15f. These are described in more detail in Reference [33].

Shown in Figure 8.16 is the result of several TSC runs in which the injector flux was maintained constant and the toroidal field was increased. Simulations were run at 0.3, 0.6 and 0.9 T. For each of these cases the applied electric field across the CHI injector gap was sequentially increased until the discharge filled the vessel and began to interact with the absorber region. In the upper plot shown in Figure 8.16, the three lower traces correspond to the injector current and the three upper traces correspond to the CHI produced toroidal current. The injector current

shows an initial change in slope as the voltage is increased. The inflexion point of this trace is related to the bubble burst current. Thus as the toroidal field is increased, less injector current is required to satisfy the bubble burst current while a higher voltage is needed to get to same injector current as for the lower toroidal field case. This indicates that at 1 T, a slightly higher voltage capability may be required on NSTX-U, but probably less than a factor of 2. Additional analysis is needed to establish the voltage requirements for NSTX-U.

The lower frame of Figure 8.16 shows the attained current multiplication for the three toroidal field cases and it shows the multiplication to significantly increase with toroidal field. The maximum current multiplication seen in these discharges is similar to the values achieved experimentally, which varies from 60 to nearly 100 for some discharges. These results for the simulations, are consistent with the earlier simple model developed by Jarboe [27], which states that the minimum injector current to meet the bubble burst condition is given as, $I_{inj} = 2\Psi_{inj}^2/(\mu_0^2 d^2 I_{TF})$ where I_{TF} is the current in the toroidal field coil and d is the width of injector flux "footprint" on the electrodes.

Given the resolution of the data points near the inflection point, the inflection point for the 0.9 T case occurs at about 0.65 kA, around 0.95 kA for the 0.6 T case and around 1.85 kA for the 0.3 T case. Because the injector flux magnitude and the flux footprint width are not varied in these simulations, the $1/B_T$ scaling is seen in these TSC simulations. It is seen that the discharge with the highest value of toroidal field does indeed require less injector current. As the toroidal field is increased, the injector impedance increases. This is a consequence of the longer field line length, which now requires more voltage to drive a similar magnitude current. Thus for these three cases, as the toroidal field is increased, the injector voltage also needs to be increased to be able to drive an adequate amount of injector current.

Results from Ref. [27] also show that the attained current multiplication factor should vary as the ratio of the toroidal flux in the vessel to the injected poloidal flux (the gun flux). This trend is also seen in the TSC simulations. An examination of the highest current multiplication factor attained for the three toroidal field cases shows that after the discharge fully fills the vessel, a condition that is reached at close to the highest value of the applied electric field for each of the cases, the 0.3 T case has a current multiplication factor of about 29, it is 59 for the 0.6 T case and 90 for the 0.9 T case, again reflecting the effect of the toroidal field scaling. Thus, machines that have a higher toroidal field or a larger physical plasma volume would have higher values of the current multiplication factor in achieving a given plasmas current. The higher multiplication with size has also been observed experimentally. The smaller HIT-II machine typically saw current multiplication factors of 6, whereas NSTX, which has ten times more toroidal flux than HIT-II typically, sees a current multiplication factor of about 60.

Plans for TSC simulations: The non-inductive plasma start-up and current ramp-up program on NSTX-U will make extensive use of TSC simulations coupled to TRANSP/NUBEAM and RF codes (such as GENRAY) to adequately understand non-inductive current ramp-up requirements for NSTX-U and an ST FNSF. TSC will be used to simulate the scenario and will provide experimental-like conditions to TRANSP/NUBEAM, which will be used to calculate the heating a nd current drive profiles that are given back to TSC for re-calculation of the scenario. Alternatively, the SWIM framework will also be used, with TSC calling directly NUBEAM and GENRAY. An example of a TRANSP simulation for a 300 kA plasma discharge in NSTX is shown in Figure 8.17. On NSTX-U there are a total of 6 individual beam sources, each at a different tangency radius. The absorbed and loss power in MW for the traces in Figure 8.17 are for an injection power of 2 MW for each source. The simulations are for each individual source at injection energy of 65 or 80 keV.

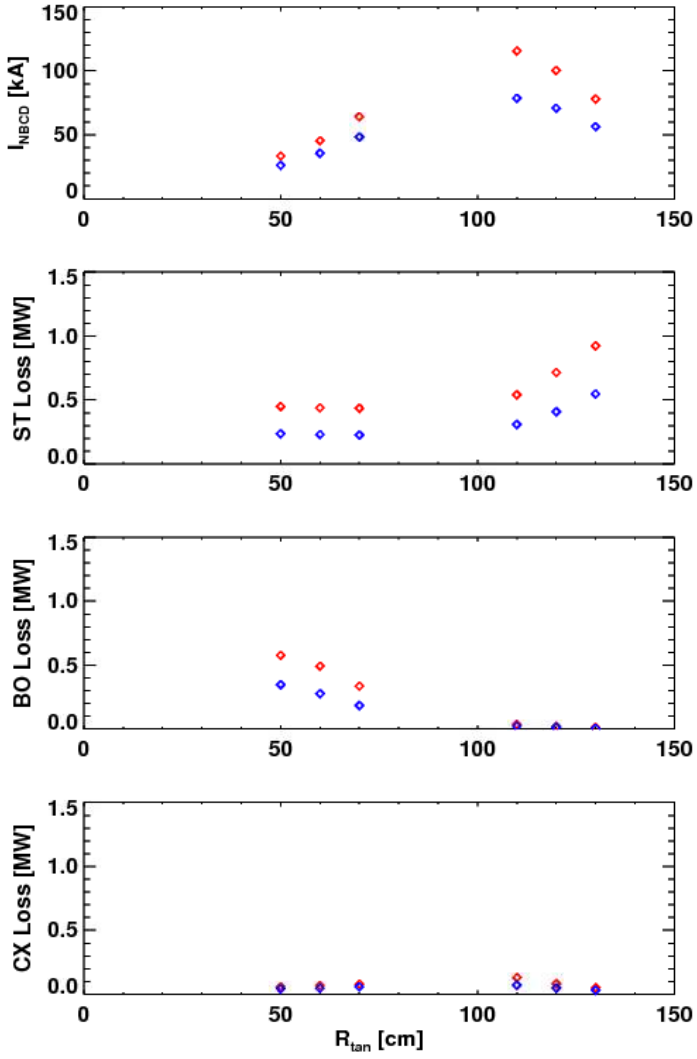

Figure 8.17: TRANSP simulations of NBI coupling efficiency for a 300 kA discharge at a density of ~1.3E19 /m^3. Red is for 80 keV NBI energy and blue is for 65 keV injection energy. The power each source is 2MW. Shown from top to bottom are the NB driven current, the shine through loss, the bad orbit loss and charge exchange loss power all as function of beam tangency radius.

Figure 8.17 shows that the absorbed current drive efficiency increases from about 40 kA to about 120 kA, a factor of 3 increase, as the tangency radius is increased from that of the least tangential source (RTAN = 50 cm) of the present NBI with the least tangential radius (RTAN = 110 cm) of the new 2nd NBI. Even for the new sources at 120 and 130 cm the NB current drive efficiency is significantly higher than for the present sources that have a tangency radius of 70 cm or less. The NBI power loss is also a function of tangency radius, and Figure 8.17 shows that for small RTAN, the more perpendicular injection increases the number of particles that are promptly lost (i.e. bad orbits).

Figure 8.17 also shows that large R_{TAN} can lead to increased power losses due to increased shine-through. This is caused by the decrease in NBI path-length intersecting the plasma when RTAN is large, and this results in decreased beam ionization and absorption. However, for the source with a tangency radius of 110 cm, it is about the same as that for the present NBI sources. The charge exchange losses for all sources are small. Overall, the current drive efficiency for injected power is at least 50-100% higher for the new 2nd NBI compared to the present NBI.

Before the start of NSTX-U operations we will have developed a TSC geometry of the NSTX-U vessel and used it to simulate initial CHI plasma start-up. These early simulations are needed for planning the initial CHI start-up experiments to be conducted during Year 1 of NSTX-U operations. TSC will be used to assess the favorable B_T and injector flux scalings indicated by the NSTX CHI experiments and by NSTX TSC simulations. These will be compared to and improved after CHI discharges are established and improved during Years 1 and 2 of NSTX-U operations.

Starting from 2013 and extending into Years 1 and 2 of NSTX-U operations, we will use TSC coupled to TRANSP/NUBEAM and RF codes to adequately understand the initial seed plasma parameter requirements for current ramp-up to the full 1 MA sustainment levels planned for in NSTX-U. Of particular interest are the importance of Z_{eff}, electron density levels and ramp rates, electron temperature and density profiles, the transport models used, electron and ion thermal diffusivities and the plasma shape. Much of this work will be carried out in parallel with experiments on NSTX-U so that a realistic TSC/TRANSP model of non-inductive current ramp-up will be developed. To develop this model, we will initially rely on TRANSP/NUBEAM simulations of representative discharges that have profiles and plasma parameters similar to the type of discharges developed on NSTX, but also extending the range of parameters to adequately cover the CHI target parameters anticipated in NSTX-U.

During Years 2 to 4 the TSC model being developed for inductive discharges will be used to model neutral beam coupling to CHI discharges that would now be available.

During Years 4 and 5 we will adapt the TSC models that have been validated with NSTX-U experimental results to simulate non-inductive current start-up and non-inductive current ramp-up in a ST FNSF device. We will also begin to implement the CHI start-up scenarios directly in TRANSP, after the TRANSP free-boundary predictive capability matures to a level where its use becomes routine for NSTX-U inductively generated discharges.

8.5.2 3D resistive MHD simulations – NIMROD, M3D

The present understanding of transient CHI start-up implies that much of the scaling and projections to larger machines could be carried out using 2D simulations with the TSC code. The primary goal of NIMROD simulations is to understand the impact and role of any possible 3D physics mechanisms in transient CHI plasma formation. NIMROD studies will investigate the

role of additional 3D physics to see if the 2D calculation is valid, especially as the plasma current is increased. The primary parameters of interest are the injector and plasma current ramp-up time histories, effect of voltage programming, the poloidal flux evolution and the electron temperature and current profiles during the initial 1 to 10 ms of the plasma formation phase.

The NIMROD code (Non-Ideal Magnetohydrodynamics with Rotation, http://nimrodteam.org) solves linear and nonlinear plasma models including magnetohydrodynamics, two-fluid systems, and kinetic extensions as 2D and 3D initial-value problems. The spatial representation features a 2D plane of nodal spectral finite elements for geometric flexibility and accuracy in the extremely anisotropic conditions that characterize magnetized plasmas, [37] and the third direction is assumed to be periodic (cylindrical/toroidal or straight) and uses the finite Fourier series spectral method. The temporal advance staggers flow velocity from other fields. Implicit methods are used when advancing the physical fields in time to avoid numerical stability limits that are associated with wave and flow propagation in the multiscale problems of interest. [38] Kinetic extensions include a simulation-particle-based method for drift and large-orbit effects from a minority species of hot ions. [39] In addition, important nonlocal effects from free-streaming particles are modeled with integral closures that evaluate the drift-kinetic equation for parallel heat flow and stress. [40]

The goals with 3D resistive MHD simulations are two fold. First is to better understand the CHI dynamics during the initial 3 to 10 ms of a CHI discharge and second to model neutral beam coupling and current drive in CHI generated plasmas.

The initial objective is to produce large volume open flux that fills the entire vessel and then test flux closure. Turning off the injector voltage to determine conditions under which closed flux is generated will test flux closure. Initially these simulations may be conducted using pre-programmed coil currents; Then, by using coil currents from a NSTX experimental discharge. Vessel eddy currents may be ignored during these initial runs. After this, we will include the vessel eddy current effects by using the time changing boundary flux generated by the LRDFIT code.

Beyond this, other physics capabilities will be added to determine limiting factors, i.e. the impact of adding electron temperature and density evolution. Simulations at this stage, that correctly reproduce the primary parameters noted above, should be suitable for studying the effects of adding n=1 and higher order modes. We will now vary parameters and understand mechanisms that lead to closed flux generation and control parameters that maximize closed flux generation. These are: Injector gap width, injector current ramp rates, voltage programming history, changes to required voltage for static and time varying injector flux, resistivity of the plasma in the injector, resistivity of the bulk CHI plasma (based on Te ~ 10eV, 20eV, 50eV, 100eV), bulk CHI plasma density and the effect of oxygen impurities in the discharge.

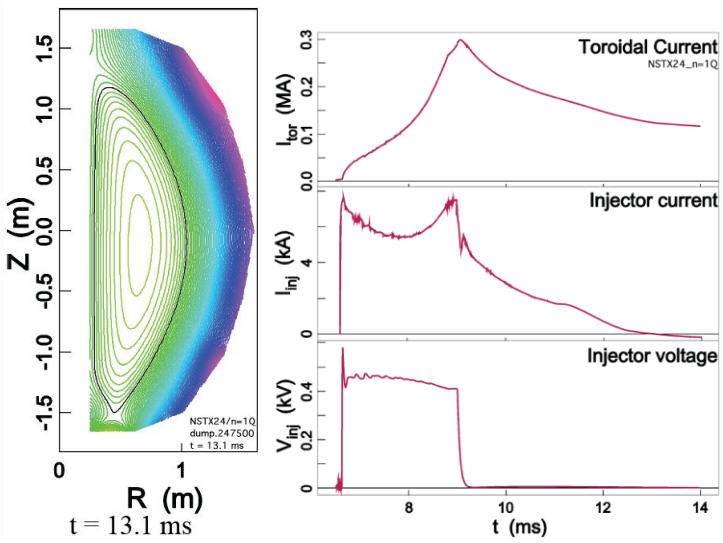

Figure 8.18: Flux surface closure for a simulation of a 4-cm wide injection slot. (a) "Fast" closure within 50 μs after rapidly reducing the injection voltage. The flux plot is for t = 13.1 ms (b) Injector voltage and current; Toroidal current for (a).

Part way through these studies, the code would be modified to study NBI coupling to CHI generated targets to understand the required CHI parameters and NBI parameters that improve NBI current drive.

Resistive MHD simulations using the NIMROD code are at present being used to model CHI start-up in NSTX; to improve understanding of the physics of injection, flux-surface closure, and current drive for CHI plasmas; and to extend these results to NSTX-U. During FY12/13 the NSTX model was improved by comparison with experiment and exploration of simulation parameters. Flux surface closure following the helicity-injection pulse has been observed in recent simulations, as shown in Figure 8.18, and is being understood. Critical to the closure has been a narrow 4-cm wide injection slot as used in the experiment and a rapid, monotonic voltage reduction at the end of injection. An X-point forms above the injection slot resulting in a separatrix surrounding a closed flux region. These results were obtained in an axisymmetric simulation indicating that resistive effects are important. A narrow current foot-print along the bottom boundary of NSTX (due to the narrow injection slot) may be needed for the reconnection generating this closure. The enclosed volume and toroidal current decay slowly following closure, although faster than experimental results. Ongoing, near-term research is directed to obtaining a larger volume of closed surfaces, to demonstrating improved quantitative comparison with experiment, and to determine the optimum conditions for closure.

Neutral-beam current drive is planned for building significant plasma starting from a NSTX-U start-up plasma generated by CHI. Nimrod will be used to simulate neutral-beam injection in NSTX-U.

Because NIMROD evolves time-dependent equations for the spatial distributions of number density, flow velocity, temperature, and magnetic field, effects of neutral beams in NSTX-U will be modeled as source densities in these equations. Source densities have been used in other NIMROD applications. For example, Ref. [41] describes resistive-MHD modeling which includes effects from ECCD that is targeted to reduce magnetic islands in tokamaks. The magnetic-field evolution in these simulations includes an effective electric-field source density in Ohm's law that represents an average force density from the RF on the electrons. This source

density is spatially localized in the poloidal plane and has nonzero curl to induce magnetic field and current density. In these simulations, the source density represents the RF effects in an ad hoc manner. More recent work by Jenkins [41] also couples wave propagation and deposition that are based on the wave electric field and quasilinear diffusion coefficient computed by the GENRAY code. The source density in these integrated simulations is localized toroidally and poloidally. Modeling of DC current injection from miniature plasma guns in the Pegasus ST uses similar source densities in NIMROD simulations. Results described in Ref. [42] have been computed with a source density in the magnetic-field equation and a source density in the temperature evolution to model the heat supplied by the plasma guns. Here, the source densities are spatially localized in the poloidal and toroidal directions.

Incorporating the effects of neutral beams in startup transients in NSTX-U can be addressed similarly to the ECCD and current injection modeling described above. Local source densities based on transport computations can be included in the advances to magnetic field, temperature, and momentum density. Each may be handled in one of two ways that are analogous to constant voltage and constant current sources in electrical circuits. Simply specifying a source-density magnitude adds energy, but the time-asymptotic effect will depend on transport. As an alternative, one may specify the source as a target value and a relaxation rate. A momentum source density, for example, would be $mn\nu(\mathbf{x})(\mathbf{V}_b - \mathbf{V})$ in this approach, where $\nu(x)$ is a relaxation-rate function that is local to the beam deposition region, V is the flow velocity, and V_b is the specified asymptotic flow-velocity. Note that this second form can act as a sink if other dynamics tend to accelerate flow in the direction of the applied force density.

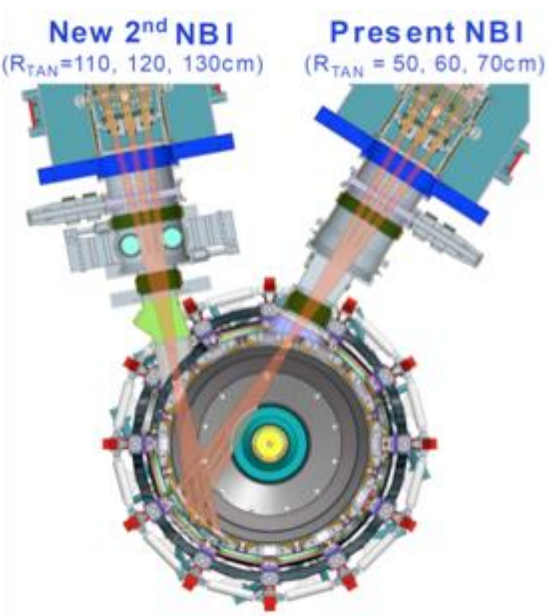

Figure 8.19. Neutral beam injection into NSTX-U. The total power available from the two beams will be 10 MW at 80 kV, 5s to 14 MW at 95 keV. Each beam system has three individual sources at different tangency radius.

NSTX-U will have two neutral beams with energy of 65-95keV. The beam geometry is shown in Figure 8.19. TRANSP calculations have shown that the second more tangential beam is well suited for driving current and will be the primary system (in addition to bootstrap current drive) for ramping the current generated by a CHI target. In support of incorporating the neutral beam model for NSTX-U CHI discharge within NIMROD, we plan to initially use standard inductive discharge parameters from NSTX discharges and then to arbitrarily vary the electron density, electron temperature and plasma current in these simulated plasmas and to compare the Nimrod results to those obtained from TRANSP simulations. After

satisfactory agreement between both codes we will switch to using the NIMROD NBI model on simulated NSTX-U CHI discharges.

The M3D-C code [43, 44] represents a complete rewrite of the older M3D 3D MHD code. It can be run as resistive MHD or two-fluid MHD, and also can be run as either 2-variable or 4-variable reduced MHD. The code is fully implicit using the split-implicit method and this enables it to take large time steps and run to long time. It uses high-order finite elements in 3 dimensions. These elements force the function and its first derivative to be continuous. This property allows spatial derivatives up to 4th order to be treated when using the Galerkin method. This property is essential for an implicit formulation using the potential/stream function form of the velocity field and magnetic vector potential. Initially we will rely on the NIMROD code for much of the 3D CHI simulations but will also consider using M3D based on future needs.

8.5.3 GENRAY-ADJ for EC/EBW Heating and Current Drive

The GENRAY [45] ray tracing numerical code, and the ADJ [46] Fokker-Planck numerical simulation are used to model electron cyclotron (EC) and electron Bernstein wave (EBW) heating and current drive during plasma start-up and plasma current ramp-up. An example of GENRAY-ADJ simulation results for second harmonic 28 GHz X-mode EC heating in a NSTX CHI start-up plasma with an axial toroidal field, $B_T(0)$ = 0.5 T (shot 148072) is presented below. Figure 8.20(a) shows the electron density and temperature profiles that were used for the GENRAY-ADJ modeling. As shown in Figure 8.20(b), 28 GHz microwave power is resonant with the second harmonic EC resonance ($2f_{ce}$) at a major radius (R) of 0.9 m. The right hand cutoff (f_R) is just below 28 GHz at R = 0.9 m.

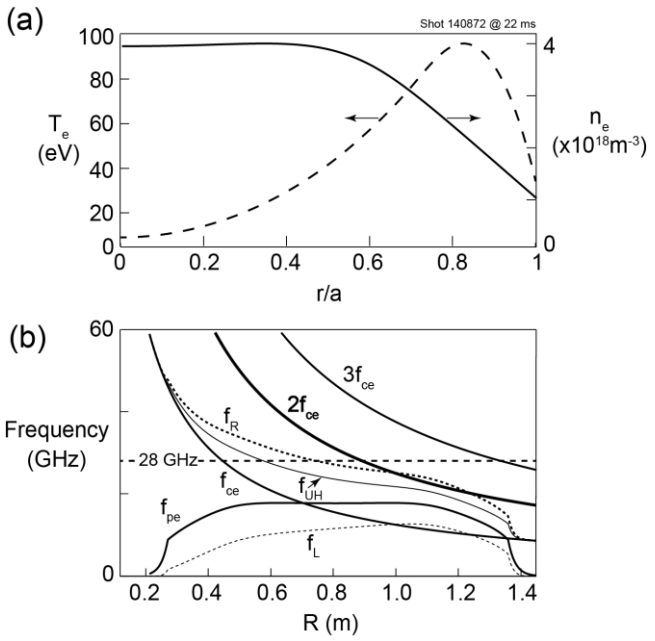

Figure 8.20(a) Electron density (solid line) and temperature (dashed line) profiles used for the GENRAY-ADJ ECH modeling, derived from multi-point Thomson scattering data acquired at 20 ms during NSTX CHI shot 148072. (b) Electron cyclotron resonances and cutoffs on the midplane of shot 148072 calculated using magnetic equilibrium data at 22 ms and the density profile data of Figure 8.18(a).

In a series of simulations the EC antenna orientation was adjusted for maximum first pass absorption. Figure 8.21 shows the ray trajectories calculated by GENRAY when the antenna was oriented for maximum first pass absorption. The power deposition profile is relatively narrow and located

at a normalized minor radius, r/a ~ 0.17 on the low field side of the magnetic axis (Figure 8.21(c)).

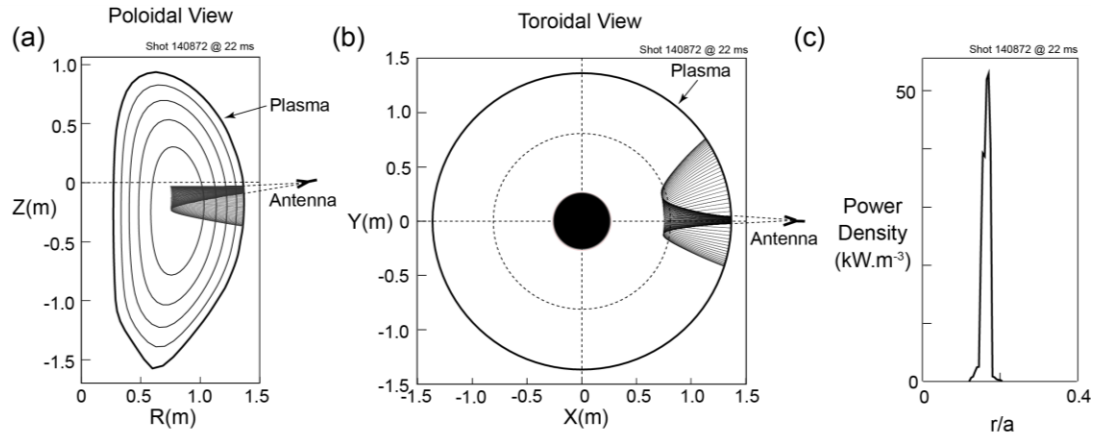

Figure 8.21: Ray trajectories calculated by GENRAY plotted in (a) the poloidal and (b) the toroidal midplane for the case with maximum first pass absorption of 28 GHz ECRH at 20 ms during NSTX CHI shot 148072, with the antenna pointing 5 degrees down and 1 degree right of the normal to the ECRH port. (c) First pass power deposition profile versus normalized minor radius (r/a) calculated by GENRAY for 1 MW of 28 GHz.

Figure 8.22(a) shows the dependence of the first pass absorption on toroidal launch angle. The peak first pass absorption reaches 27% with the antenna pointing 1 degree from normal to the plasma surface, and falls to 10-15% as the toroidal angle is increased from 3 to 8 degrees. The

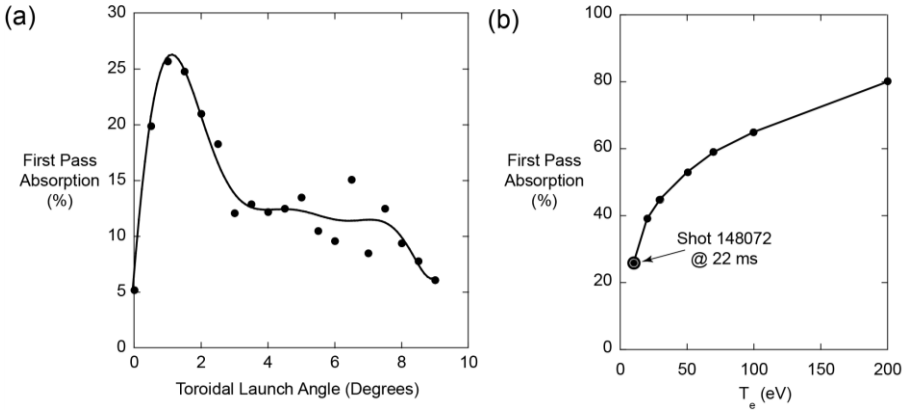

Figure 8.22: (a) First pass absorption fraction plotted versus the toroidal angle between the antenna axis and the normal to the plasma surface when the antenna is pointing 5 degrees down, and (b) the dependence of first pass absorption on electron temperature when the antenna is pointing with a toroidal angle of 1 degree to the normal to the plasma surface and 5 degrees down.

actual absorption will probably be enhanced significantly by wall reflections. As the core electron temperature rises as a result of the EC heating the first pass absorption increases, reaching about 60-80% when the central temperature is 100-200 eV (Fig 8.22(b)).

GENRAY simulation results shown in Figs. 8.21 and 8.22 were produced by launching the rays at the last closed flux surface rather than from the EC antenna. GENRAY has been upgraded to include a scrap-off layer (SOL) model and edge fluctuations. This will be particularly important for modelling EBW heating. More details of the SOL and fluctuation upgrade to GENRAY are presented in section 7.3.1.3 of the 5-year plan.

8.6 Summary

An important objective of NSTX-U is to demonstrate full non-inductive start-up and ramp-up using at least one non-inductively generated seed plasma. A second parallel objective is to understand current-ramp physics and the requirements for current ramp-up in a ST-FNSF. At present, CHI research on NSTX has made sufficient progress to provide confidence that, with the new capabilities available on NSTX-U, CHI targets could achieve this objective within the present 5 year time frame. EBW and Plasma gun generated targets will also be used as they become available. In support of these important goals, during the first two to three years, we will be conducting NBI plus bootstrap current overdrive ramp-up studies on inductively generated targets that have varying current and temperature profiles. Experimental results obtained from these studies, and later with ramp-up of CHI initiated plasmas, will be compared to TSC/TRANSP simulations to improve our models for current ramp-up requirements for an ST-FNSF. This work is also of considerable importance to AT plasma operation in tokamaks.

CHI research on NSTX-U will benefit from numerous new upgrades that are needed for a demonstration of full non-inductive current start-up and non-inductive current ramp-up to the 1 MA current sustainment levels. These are (1) higher toroidal field, (2) higher injector flux, (3) improved absorber coils, (4) ECH system, (5) tangential neutral beam system, (6) improved Li coating coverage, (7) higher CHI voltage capability, and (8) metallic divertor plates. These are briefly described below. These upgrades to NSTX-U are described in Chapter 10. Chapter 10.5.3 specifically discusses upgrades related to Start-up and Ramp-up.

Higher toroidal field: As previously discussed, the current multiplication factor in CHI discharges increases with the magnitude of the toroidal field. This means that for a doubling of the toroidal flux twice as much injector flux can be injected at the same value of the injector current. The toroidal field in NSTX-U will be 1 T, approximately twice that in NSTX. This in combination with the other upgrades described below will allow NSTX-U to generate much higher (more than 2x) levels of plasma current than what was possible on NSTX.

Higher injector flux: In TCHI discharges, the magnitude of the CHI generated plasma current is directly proportional to the injected poloidal flux. As previously noted (Figure 8.8), improved positioning of the divertor coils on NSTX-U allows the injector flux in NSTX-U to increase to 220-340 mWb. This is an increase of 2.75 to 4.25 times that in NSTX. On NSTX using 40 mWb of injector flux 200 kA of closed flux current was generated. Thus NSTX-U has very high

injector flux capability. With improved divertor plates and higher CHI voltage capability, NSTX-U in principle has the capability to generate all of the current needed at the 100% non-inductive sustainment levels (see Table 1). The initial goals, however, are to modestly double the closed flux current achieved on NSTX, which should be much easier to accomplish.

Improved absorber coils: As the CHI discharge grows in elongation, it can contact the upper divertor and bridge the upper divertor gap generating a condition known as an absorber arc. NSTX relied on two specially installed coils in the upper divertor region. Known as absorber flux coils, these generate a buffer magnetic flux in the upper divertor region that transiently delay the contact of the CHI plasma with the upper divertor until the CHI capacitor bank voltage has dropped to a sufficiently low level, so that even in the event of plasma contact an absorber arc could not be generated or it would be sufficient weak to have any detrimental effect on the CHI discharges. On NSTX-U, because of improved positioning of the upper divertor coils, (Figure 8.8) it is not only better positioned than the dedicated absorber coils on NSTX, but also has more than twice the current slew rates of the coils used on NSTX. These coils should therefore be more effective for absorber arc control.

ECH system: As previously described, direct coupling of a CHI discharge to current drive using NBI requires a plasma temperature on the order of several hindered eV. To meet this need an electron cyclotron heating system is most suited. The CHI plasma electron density is below the cut-off density for 28 GHz ECH propagation. The details of the proposed ECH system are described in Chapters 7 and 10.4.2.

Tangential Neutral Beam System: As previously discussed, a major objective of NSTX-U is the demonstration of full non-inductive current start-up and current ramp-up. This will be achieved primarily using the second more tangential neutral beam that NSTX-U will have. This system is described in Chapter 10.3.2, and the sustainment capabilities of this system are described in Chapter 9.

Improved Li coverage: NSTX CHI discharges routinely relied on Li evaporative coatings on the lower divertor tiles to reduce the influx of oxygen impurities. However, during final weeks of CHI discharge improvements on NSTX, the lower divertor tiles were only partly coated with Li as only one of the lower divertor Li evaporator was functional. NXTX-U CHI discharges will benefit from dual Li evaporators to coat the lower divertor tiles more completely. This is expected to further reduce the oxygen influx into the CHI discharge. In addition, NSTX-U will also have a Li evaporator to coat the upper divertor tiles. This should be particularly helpful during absorber arcs, as Li instead of oxygen will be primary species injected into the CHI plasma. Because of both these systems the resulting CHI discharges could be expected to have a higher intrinsic electron temperature and a higher plasma current magnitude. The Li evaporator system is described under Section 10.5.2.5

Higher CHI voltage capability: Results from the HIT-II experiment show that by optimizing the injector voltage, injector flux and toroidal field, the extent of closed flux current can be

increased. To increase the closed flux current more injector flux is needed. To reduce the injector current at higher levels of injector flux, the toroidal field needs to be increased. At higher toroidal field, the injector voltage needs to be increased.

On NSTX, such an optimization was not possible as during the final three years of NSTX operations the capacitor bank was essentially operated at its highest voltage of 1.7 kV, as reducing the voltage reduced the achievable plasma current. The present voltage snubbing system on the CHI system (the Metal Oxide Varistors) begins to significantly conduct at a voltage of 1.7 kV. In order to extend the voltage to the full 2 kV that the CHI capacitor bank system is capable of, new MOVs with a higher voltage rating are required. The higher voltage also allows the injector current pulse width to be reduced. Shorter pulse width CHI discharges would have less impurity influx from the injector and from the absorber. Thus CHI voltage, which is a very powerful control variable, has not been exercised on NSTX. NSTX-U itself is being designed for 4kV CHI capability, which is a factor of two higher than the 2kV capability of NSTX. On NSTX-U a staged approach will be used to increase the CHI capacitor bank voltage to at least 2.5 kV, and possibly as high as 3 kV.

The present CHI power supply consists of up to ten capacitors, each 5 mF in capacitance. Any number of these can be connected in parallel and discharged. During Years 1 and 2 of NSTX-U operations, the voltage capability of the MOVs will be increased so that the CHI capacitor bank can be operated at the full 2 kV level it was designed for. The staged capability that allows a smaller portion of the capacitor bank to be discharged at different times will be used. The maximum bank size will be 50 mF at 2 kV and it will have the capability for three staged operations (i.e., the bank can be broken into three parts and each part can be individually triggered).

Based on the results from these experiments, during Year 3, new upgrades will be implemented. First, the capacitor bank voltage will be increased to 3 kV. Simultaneously the MOVs will be upgraded to handle the higher voltage. The staged capability will be increased to four stages.

Metallic divertor plates: During plasma start-up, whether it is inductive or CHI start-up, low-Z impurities need to be reduced in magnitude. At the low electron temperature of start-up plasmas, impurities such as carbon and oxygen can radiate heavily and keep the plasma temperature from increasing. During plasma start-up using an electrode discharge process such as CHI it is preferable to have metallic electrodes, as metallic impurities do no radiated heavily until the electron temperature generally exceeds about 100 eV. All spheromak experiments that generated high electron temperature plasma (over 100 eV) relied on metallic electrodes. During Year 3 of NSTX-U operations, NSTX-U plans to replace the graphite divertor plates with tiles fabricated out of refractory element. This upgrade is described in Section 10.5.2.6. These, in addition to the other upgrades mentioned above should work synergistically and help to significantly increase the intrinsic CHI plasma electron temperature and current magnitude.

In summary, the successful demonstration on NSTX of CHI start-up, and subsequent ramp-up to 1 MA when induction applied in combination with the major upgrades in NSTX-U (higher toroidal field, 2nd NBI system for additional power and more tangential injection, and a 1 MW ECH system) combined with density reduction that is possible with CHI generated seed current plasmas, NSTX-U is well positioned for a demonstration of full non-inductive current start-up and ramp-up to 1MA in support of a FNSF.

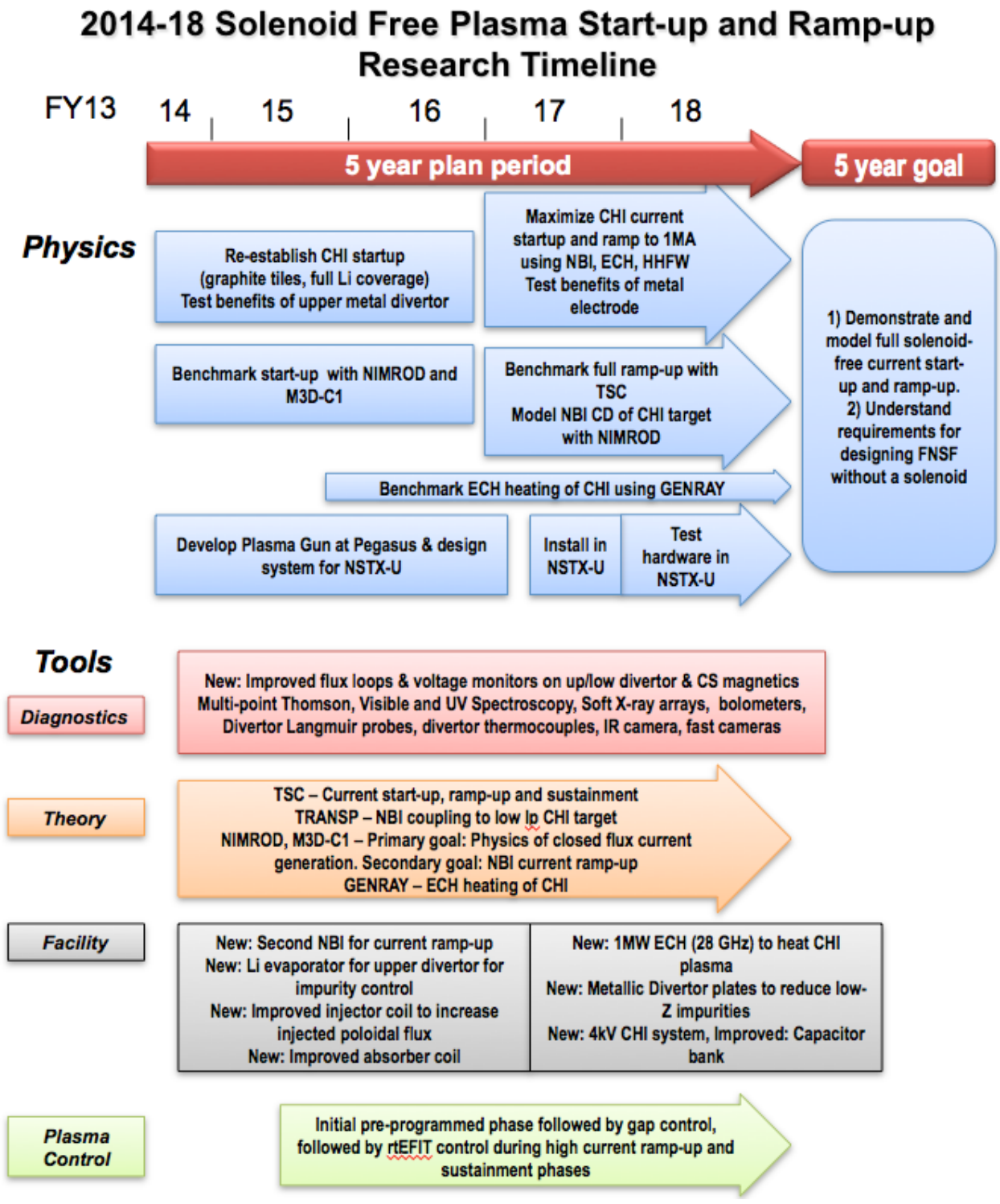
2014-18 Solenoid Free Plasma Start-up and Ramp-up Research Timeline
FY13
14
15
16
17
18
5 year plan period
5 year goal
Physics
Re-establish CHI startup (graphite tiles, full Li coverage) Test benefits of upper metal divertor
Maximize CHI current startup and ramp to 1MA using NBI, ECH, HHFW Test benefits of metal electrode
Benchmark start-up with NIMROD and M3D-C1
Benchmark full ramp-up with TSC Model NBI CD of CHI target with NIMROD
Benchmark ECH heating of CHI using GENRAY
Develop Plasma Gun at Pegasus & design system for NSTX-U
Install in NSTX-U
Test hardware in NSTX-U
1) Demonstrate and model full solenoid-free current start-up and ramp-up. 2) Understand requirements for designing FNSF without a solenoid
Tools
Diagnostics
New: Improved flux loops & voltage monitors on up/low divertor & CS magnetics Multi-point Thomson, Visible and UV Spectroscopy, Soft X-ray arrays, bolometers, Divertor Langmuir probes, divertor thermocouples, IR camera, fast cameras
Theory
TSC – Current start-up, ramp-up and sustainment
TRANSP – NBI coupling to low Ip CHI target
NIMROD, M3D-C1 – Primary goal: Physics of closed flux current generation. Secondary goal: NBI current ramp-up
GENRAY – ECH heating of CHI
Facility
New: Second NBI for current ramp-up
New: Li evaporator for upper divertor for impurity control
New: Improved injector coil to increase injected poloidal flux
New: Improved absorber coil
New: 1MW ECH (28 GHz) to heat CHI plasma
New: Metallic Divertor plates to reduce low-Z impurities
New: 4kV CHI system, Improved: Capacitor bank
Plasma Control
Initial pre-programmed phase followed by gap control, followed by rtEFIT control during high current ramp-up and sustainment phases

References

[1] See references 13-18 in Chapter 1
[2] V.F. Shevchenko et al., Nucl. Fusion **50** (2010) 022004
[3] G. Taylor et al., Phys. of Plasmas **19** (2012) 045001
[4] R. Raman, T.R. Jarboe, B.A. Nelson, et al., Phys. Rev. Lett., **90**, 075005 (2003)
[5] R. Raman, B.A. Nelson, M.G. Bell, et al., Phys. Rev. Lett., **97**, 175002 (2006)
[6] D. Mueller, B.A. Nelson, W.T. Hamp, et al., Phys. Plasmas, **12** (7) 070702 (2005)
[7] T.R. Jarboe, Plasma Phys. Control. Fusion **36**, 945 (1994)
[8] C.W. Barnes, T.R. Jarboe, et al., Phys. Fluids **B 2**, 1871 (1990)
[9] H.S. McLean, et al., Phys. Rev. Lett. **88**, 125004 (2002)
[10] C.W. Barnes, J.C. Fernandez, I. Henins, et al., Phys. Fluids **29**, 3415 (1986)
[11] J.H. Hammer et al., Phys. Fluids B **3**, 2236 (1991)
[12] Y. Ono et al., Phys. Rev. Lett. **76**, 3328 (1996)
[13] M. Nagata et al., Phys. Plasmas **10**, 2932 (2003)
[14] R. Raman, T.R. Jarboe, D. Mueller et al., Plasma Phys. Control. Fusion **43**, 305 (2001)
[15] R. Raman, T.R. Jarboe, D. Mueller, et al., Nucl. Fusion **41**, 1081 (2001)
[16] R. Raman, T. R. Jarboe, W.T. Hamp, Physics of Plasmas, **14**, 022504 (2007)
[17] R. Raman, D. Mueller, B.A. Nelson, Phys. Rev. Lett., **104**, 095003 (2010)
[18] N.W. Eidietis, R.J. Fonck, G.D. Garstka, et al., J. Fusion Energy, 26, 43 (2007) doi: 10.1007/s10894-006-9072-z
[19] G. Fiksel, A. F. Almagri, D. Craig, et al., Plasma Sources Sci. Technol. **5**, 78 (1996).
[20] D. Den Hartog, D. Craig, G. Fiksel, and J. Sarff, Plasma Sources Sci. Technol. **6**, 492 (1997)
[21] D.J. Bataglia, M.W. Bongard, R.J. Fonck, et al., Phys. Rev. Letter **102**, 225003 (2009)
[22] A.J. Redd, et al., APS DPP (2012) **PP8 24**, Providence, Rhode island
[23] T.R. Jarboe, B.S. Victor, B.A. Nelson, et al., Nuclear Fusion **52**, 083017 (2012)
[24] R. Raman, D. Mueller, T.R. Jarboe, et al., Physics of Plasmas **18**, 092504 (2011)
[25] B.A. Nelson, T.R. Jarboe, D. Mueller, R. Raman, et al., Nuclear Fusion **51**, 063008 (2011)
[26] J.E. Menard, et al. Nuclear Fusion **52**, (2012) 083051
[27] T.R. Jarboe, Fusion Tech. **15**, 7 (1989)
[28] R. Raman, T.R. Jarboe, R.G. O'Neill, et al., Nuclear Fusion - Letter, **45**, L15-L19 (2005)
[29] A.J. Redd, et al., APS DPP (2011) **B04 14**, Salt Lake City, Utah
[30] R.J. Fonck, et al., APS DPP (2012) **GO6 10**, Providence, Rhode Island
[31] J.B. Taylor, Reviews of Modern Physics **58**, 741 (1986)
[32] H. W. Kugel, et al., Physics of Plasmas **15**, 056118 (2008)
[33] R. Raman, S.C. Jardin, J. Menard, et al., Nuclear Fusion **51**, 113018 (2011)
[34] F. Scotti et al., Rev. Sci. Instrum. **83**, 10E532 (2012)
[35] S.C. Jardin, C.E. Kessel, N. Pomphrey, Nucl. Fusion, **34**, 8, (1994)
[36] S.C. Jardin, M.G. Bell, N. Pomphrey, Nucl. Fusion, **33**, 371 (1993)
[37] C. R. Sovinec, A. H. Glasser, T. A. Gianakon, et al. J. Comput. Phys **195**, 355 (2004)
[38] C. R. Sovinec, D. D. Schnack, A. Y. Pankin, et al., J. Physics: Conference Series **16**, 25 (IoP, London, 2005)
[39] C. C. Kim, C. R. Sovinec, S. E. Parker, and the NIMROD Team, Computer Physics

Communications **164**, 448 (2004)
[40] E. D. Held, J. D. Callen, C. C. Hegna, et al., Phys. Plasma **11**, 2419 (2004)
[41] T. G. Jenkins, S. E. Kruger, C. C. Hegna, et al., Physics of Plasmas **17**, 12502 (2010)
[42] J. B. O'Bryan, C. R. Sovinec, and T. M Bird, Physics of Plasmas **19**, 080701 (2012)
[43] N. M. Ferraro, et al., Phys. Plasmas **17** (2010) 102508
[44] N. M. Ferraro, et al., Phys. Plasmas **19** (2012) 056105
[45] A. P. Smirnov and R.W. Harvey, Bull. Am. Phys. Soc. **40**, 1837 (1995)
[46] A. P. Smirnov, et al., Proc. 15th Workshop on ECE and ECRH, (World Scientific, 2009), p. 301

Table of Contents for Chapter 9

Chapter 9

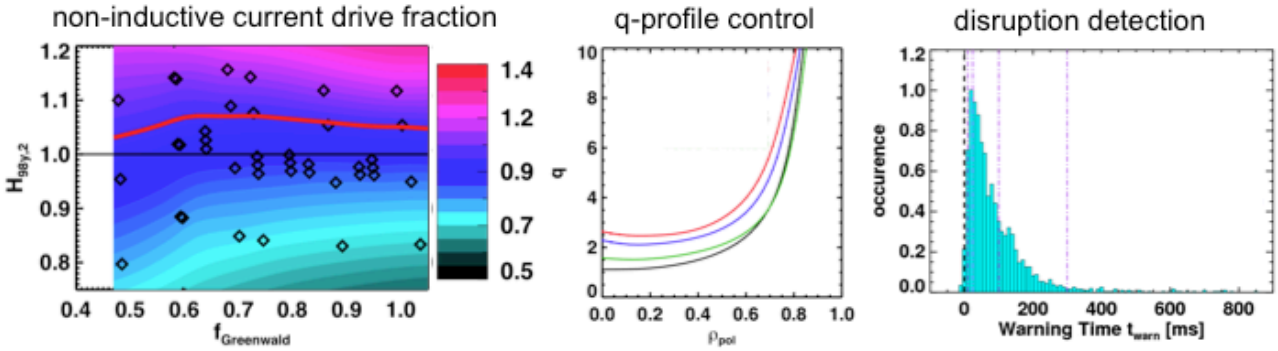

Research Goals and Plans for Plasma Sustainment: Advanced Scenarios and Control

9. 1 Overview

9.1.1 Introduction

As described in Chapter #1, the ST has been suggested for use as the fusion core of Fusion Nuclear Science Facilities (FNSFs) [1-3] and Component Test Facilities (CTFs) [4], pilot power plants [5], and even full-scale power reactors [6,7]. While there is a range of operating points suggested for these next step spherical torus devices, they have many features in common.

As shown in Fig. 9.1a), these next-step STs generally operate with β_N>4, exceeding the no-wall n=1 kink stability limit and requiring optimization of the passive and active stability. The values of boundary elongation, illustrated in Fig. 9.1b), are typically quite high, generally exceeding 2.5. These high values of β_N and elongation contribute to a large fraction of the required current being driven by the bootstrap effect. These devices generally rely on neutral beam current drive (NBCD) to supplement the bootstrap current, in order to maintain 100% non-inductive current drive. They all have potentially very high power loading of the divertor, and so heat flux mitigation strategies are required. Finally, they all must have a much lower rate of unmitigated disruptions than achieved in current low and high aspect ratio tokamaks, in order to avoid plant damage and the loss of valuable discharge time.

Scenario development research in NSTX made considerable progress toward achieving these goals [8], as evidenced by the TRANSP analysis of NSTX data in Fig. 9.1. The data points are averages of durations longer than τ_E during stationary periods of high-performance discharges. Fig. 9.1a) demonstrates that values of β_N in excess of 6 have been achieved for substantial durations, with values above 4 quite common. Elongations up to 2.9 were similarly achieved. However, the evolution of the current, rotation, and density profiles during the discharge typically resulted in deviations from the optimal conditions, often leading to disruption. Furthermore, the maximum non-inductive fraction ever achieved in NSTX was 65-70% [8-10].

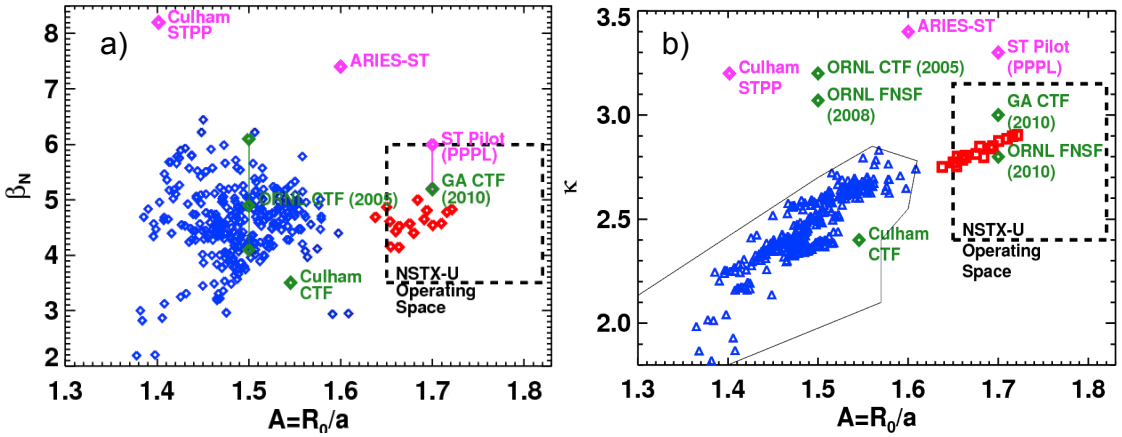

Fig. 9.1) Comparison of the NSTX operating space to the proposed steady state solutions for fusion nuclear science facilities, component test facilities, and power generating facilities. NSTX data from a dedicated higher aspect ratio experiment is shown in red, while the remainder of an NSTX high-performance database is shown in blue.

Based on the NSTX experience and R&D needs for next step devices, the following overarching questions guide the scenario and control research plans in NSTX-U [11]:

- What are the optimal current and rotation profiles for achieving a 100% non-inductive state?
- What are the optimal control strategies for maintaining those profiles?
- Under what conditions can neutral beam current drive be understood using neoclassical theory alone?
- Can the divertor heat flux be controlled in a fashion consistent with a high-performance plasma core?
- How can impending disruptions be detected, and what are the optimal discharge termination responses?
- How can NSTX-U results be used to project to next-step STs?

In order to make progress on these important problems, research in the Advanced Scenarios and Control (ASC) topical science group will be divided into four thrusts. The first thrust will focus on scenario development and optimization using the NSTX-U actuators; this thrust will demonstrate 100% non-inductive operating points as well as develop high-current partial-inductive scenarios for the use by other topical science groups. The second thrust will focus on axisymmetric control development, including profile and divertor control. The third thrust will focus on the controlled termination of high-β_N ST discharges, including disruption detection and intervention. The fourth thrust will examine critical issues related to scenario development for next-step STs, including regimes of classical beam current drive and transport modeling. As described in Section 9.1.2, these thrusts are entirely supportive of the five high-level goals for the NSTX-U research program defined in Section 1.2.2.

Finally, note that while these research goals are framed in terms of next-step ST needs, the physics and technology issues are very relevant to the problems facing ITER. An incomplete list overlapping research tasks includes:

- ITER will rely on off-axis neutral beam current drive in its advanced scenarios, and so improving the understanding of NBCD, including the range of validity of neoclassical treatments and its use as a control actuator, is critical.
- ITER will rely on profile control to maintain a stable operating scenario. The development of robust algorithms for that control is thus critical.
- ITER modeling has and will continue to rely on reduced transport models for predicting scenario characteristics. Benchmarking these models on the widest possible range of scenarios, including STs, increases the confidence in those predictions.
- ITER will need to radiate a large fraction of the power that crosses into the SOL, in order to avoid damage to the divertor places. Closed loop radiative divertor control research in NSTX-U can aid in developing the appropriate control for ITER.
- ITER will need to trigger its disruption mitigation systems based on realtime diagnostics, and this research can aid in developing the appropriate trigger algorithms.

9.1.2 Overview of Research Thrusts

9.1.2.1 Thrust ASC-1: Scenario Development

This thrust will focus on developing the highest-performance scenarios possible in NSTX-U. Broadly speaking, there are two types of optimization to be considered in this research thrust: 100 % non-inductive current drive and high current partial inductive.

The first optimization aims at 100% non-inductive current drive scenarios at the largest possible currents. Key questions to be examined are the impact of plasma transport and the resulting

profile shapes on the non-inductive current level, the global stability of these scenarios with large neutral beam current drive and central fast ion pressures, the optimal density for non-inductive sustainment, and consistency of the non-inductive operating state with divertor integration. The research of this first optimization activity provides the basis for achieving the highest priority research goal #1 of the 5 year plan in Chapter 1: Demonstrate stationary 100% non-inductive operation at performance that extrapolates to ≥ 1MW/m2 neutron wall loading in FNSF.

The second optimization task will develop high-current, partial inductive operation, pushing toward the facility goal of 5 second pulses at I_P=2.0 MA and B_T=1.0T. These scenarios are the key means of accessing low collisionality in NSTX-U, and the development of lower-density operations is thus critical. Additionally, it is likely that these scenarios will result in severe divertor thermal loading, and so the development of integrated heat flux management solutions is a requirement.

Overall, this thrust supports all five of the high-level NSTX-U goals described in Section 1.2.2, and will be described in detail in section 9.2.1.

9.1.2.2 Thrust ASC-2: Axisymmetric Control Development

This thrust will focus on developing the control strategies for achieving and maintaining optimal ST scenarios. Maintaining the plasma boundary shape and vertical position may be the most basic tokamak control requirement, and NSTX-U research will optimize multi-input multi-output boundary shape controllers and improved vertical stability algorithms. This is a critical issue for the ST, where inboard coils for maintaining the inner gap may not be available and very high elongations are desired.

In addition to the boundary shape, control of the divertor heat flux is critical. The snowflake divertor [12,13], which uses two or three divertor coils to pull nearly overlapping X-points, has been shown to lead to a significant reduction in the divertor heat flux in NSTX [14,15] and DIII-D [16]. NSTX-U researchers will work to develop realtime tracking of multiple X-points. This information will be used to develop closed-loop control of the 1st and 2nd X-point locations, and this control will be incorporated into advanced scenarios. Furthermore, direct control of the divertor radiation using feedback control of impurity gas injection will be developed, based on earlier success with open-loop detached divertor experiments [17,18].

The safety factor and rotation profile shapes play a key role in determining the global transport and stability levels. TRANSP calculations show that by varying the neutral beam source mix and/or plasma density, the minimum safety factor (q_{min}) can be controlled; experiments will be conducted to verify this prediction. These results will be used to develop simultaneous β_N and

q_{min} controllers in NSTX. Similarly, the variation of neutral beam torques from the different sources and n=2 & 3 magnetic braking from the RWM coils will be used to control β_N and the values of toroidal rotation at selected points across the profile. Finally, experiments will attempt to examine the feasibility of combined control, for instance, simultaneous β_N, q_{min}, & $F_{T,0}$ control (here, $F_{T,0}$ represents the central rotation frequency).

Finally, it will be important to develop means to control the particle inventory. Realtime density measurements will be brought to the plasma control system (PCS), and improved fueling actuators will be developed. When added to the pumping produced by lithium coatings or a cryo-pump, these tools will provide a means of generating a controlled density evolution in NSTX-U.

This thrust also supports all five of the high-level NSTX-U goals described in Section 1.2.2, and will be described in detail in section 9.2.2.

9.1.2.3 Thrust ASC-3: Disruption Avoidance By Controlled Discharge Shutdown

All tokamak discharges must end, either in controlled rampdown or in disruption. The purpose of this thrust is to optimize disruption detection with sufficient time to make a meaningful intervention. Realtime inspection of quantities like the coil heating and the solenoid flux evolution will be used to determine when slow rampdowns will be required. Multiple realtime diagnostic signals will be synthesized to form efficient disruption detectors, requiring more rapid rampdowns.

This information will be used to trigger automated rapid rampdown sequences. It is envisioned that multiple types of rampdown sequences will be developed, pending the different sources of alarms. A massive gas injection (MGI) sequence will also be included, to take advantage of the MGI system being developed in the MS TSG as described in Chapter 2.

This thrust supports the first two high-level NSTX-U goals described in Section 1.2.2, and will be described in detail in section 9.2.3.

9.1.2.4 Thrust ASC-4: Scenario Optimization for Next Step Devices

As noted above, Thrusts 1-3 aim to optimize the discharges given the facility constraints of NSTX-U. Thrust 4 will study aspects of scenario optimization physics relevant to next-step devices, in ways that may not produce optimized scenarios for NSTX-U. For instance, the simultaneous current and rotation profiles providing optimal performance will be examined. The conditions for classical beam current drive will be explored. Finally, integrated modeling of the

thermal energy, toroidal rotation, and current will be pursued, first for validation against NSTX-U results, and then for projection to next-step ST scenarios.

This thrust supports the first two high-level NSTX-U goals described in Section 1.2.2, and will be described in detail in section 9.2.4.

9.1.2.5 Thrust Connections to Research Described in Other Chapters

The thrusts in this chapter are not only related to each other, but also both build on and support the research described in other chapters. A non-exhaustive list of examples include:

- This research is directly coupled to macrostability thrust MS-3 on disruption dynamics, detection, mitigation and avoidance. In particular, the massive gas injection research described there will utilize the disruption detector research described in thrust ASC-3, while techniques developed in that ASC thrust will provide the trigger for MGI.
- Research in Transport and Turbulence thrusts TT-1 on global confinement scaling and TT-3 on reduced transport models will contribute directly to understanding the optimal profiles for advanced scenario plasmas, as described in thrust ASC-4
- Progress in understanding the physics underlying the scaling and control of the divertor heat flux in Boundary Physics thrust BP-2 will be critical in executing thrusts ASC-1 and ASC-2.
- The understanding of neutral beam current drive required to execute thrusts ASC-1, -2 and -4 will build on knowledge developed in thrust EP-1, dedicated to understanding *AE induced fast ion transport.
- The H-mode scenarios and control algorithms described in thrusts ASC-1 and ASC-2 may benefit from the use of HHFW heating, as described in Section 7.2.1.
- The knowledge of neutral beam current drive derived from the studies described in thrusts ASC-2 and ASC-4 will assist in the non-inductive ramp-up research described in the Solenoid-Free Start-Up thrusts.

9.2 Research Plans

9.2.1 Thrust 1: Scenario Development of NSTX-U

As implied by the name of the chapter, the development of high-performance operating scenarios for NSTX-U is a key goal of this research effort. These scenarios are important in their own right, but also as “laboratories” for physics studies in other topical science areas. This section describes plans for developing these scenarios, focusing on 100% non-inductive scenarios first, followed by high-current partial inductive scenarios.

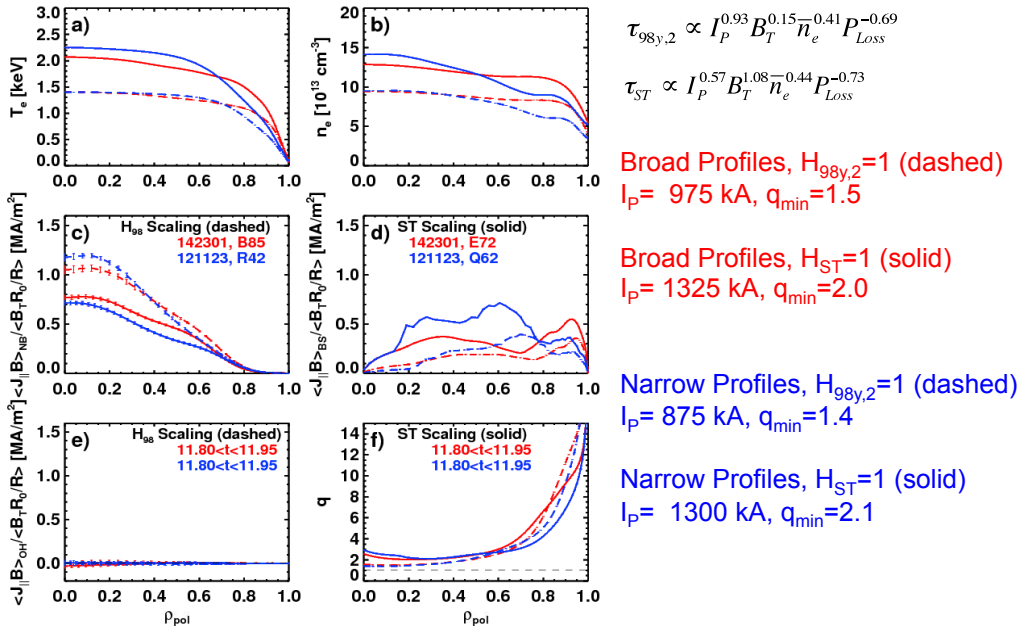

Fig. 9.2: Profiles of a) the electron temperature, b) the electron density, c) the neutral beam driven current, d) the bootstrap current, e) the loop voltage, and f) the safety factor. The colors correspond to different thermal profile shapes, while the line-style indicates the confinement level (dashed for H_{98}=1, and solid for H_{ST}=1).

9.2.1.1: 100 % Non-Inductive Scenarios

9.2.1.1.1: Research Description

Before addressing the development path for 100% non-inductive scenarios, it is useful to consider some of the key variables impacting these scenarios [19]. To begin with, the impact of the confinement level and profile shapes is shown with the simulations in Fig. 9.2. Fig. 9.2a) shows four electron temperature profiles, while Fig. 9.2b) shows four electron density profiles; the parameters defining these profiles will be defined below. The toroidal field is B_T=1.0 T for all these calculations, with an injected power of 12.6 MW from all six sources operating at 90 kV. The elongation is κ=2.8 in these cases, with high boundary triangularity, a condition known to maximize the core performance in NSTX [20,21]. The Greenwald fraction is 0.7 in all cases, with Z_{eff}=2. The plasma current has been chosen to yield a fully non-inductive operating point in all cases, and has been allowed to fully relax.

The two red curves correspond to broad density and temperature profiles, while the two blue curves come from discharges with more peaked profiles; these two profile sets bound the range of thermal pressure profile peaking observed in NSTX. The solid lines correspond to the assumption of an ST specific scaling expression for the thermal energy confinement [22] $\tau_{ST} = I_P^{0.57} B_T^{1.08} \bar{n}_e^{0.44} P_{Loss}^{-0.73}$, while the dashed lines correspond to the ITER-98$_{y,2}$ scaling expression: $\tau_{98(y,2)} = I_P^{0.93} B_T^{0.15} \bar{n}_e^{0.41} P_{Loss}^{-0.69} R_0^{1.97} \varepsilon^{0.58} \kappa^{0.78}$. It is anticipated that, in lieu of any validated thermal and particle transport models, these two profile and global confinement assumptions will bracket the operational point for this field, current, and power

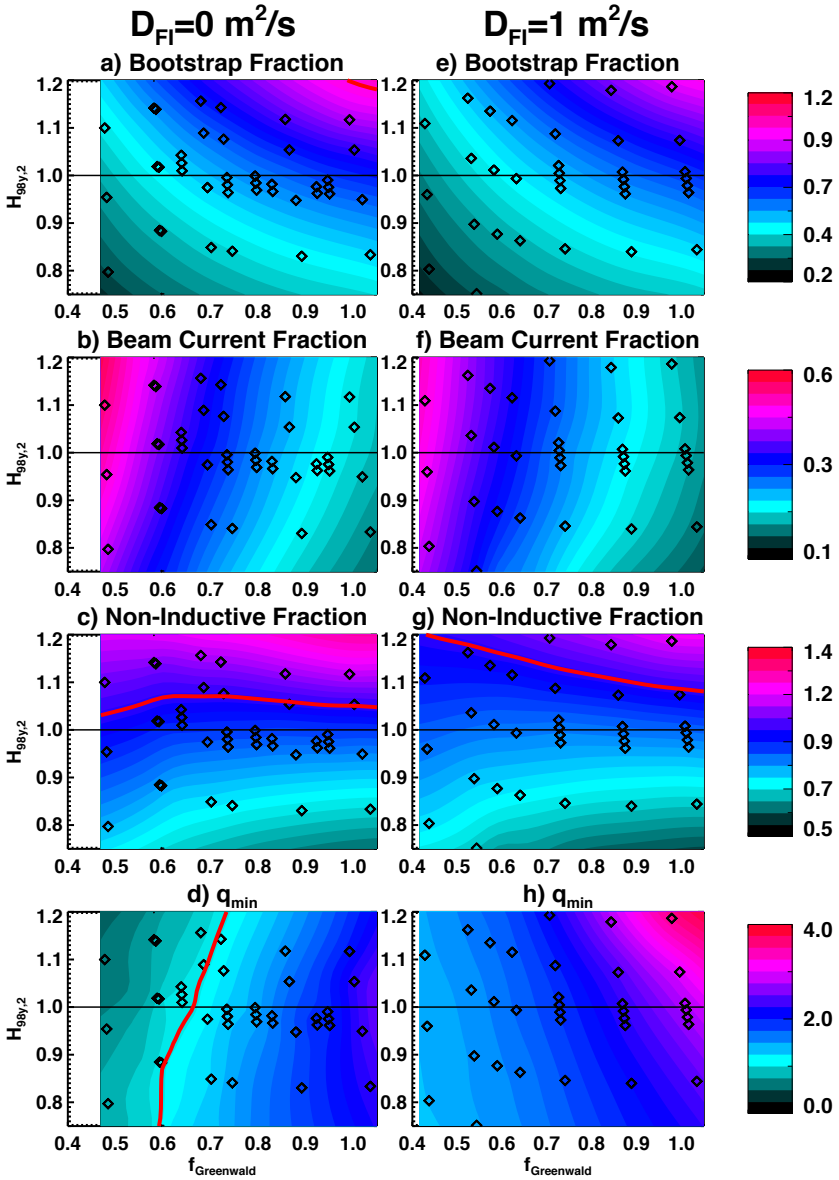

Fig. 9.3) Contours of bootstrap fraction, beam current drive fraction, non-inductive fraction, and q_{min}, as a function of the confinement multiplier and density. The left column is for classical beam physics, while the right column invokes a small level of fast-ion diffusion. The points are the underlying TRANSP simulations from which the contours are interpolated, and the red curves correspond to a non-inductive fraction of 1 or q_{min}=1.

With this background, a large number of trends can be observed in this figure. The most critical is that the non-inductive current level, for this toroidal field, boundary shape, injected power, and Greenwald fraction, is in the vicinity of 900-1000 kA for ITER-98 scaling, but ~1300 kA for the case with the ST specific thermal confinement scaling. This large difference is due to the different B_T scaling of confinement in the two expressions, with the strong B_T dependence of the ST scaling law having a strong impact. As a consequence of both the stronger B_T scaling and the increased non-

inductive level of plasma current, the central electron temperature for the H_{ST}=1 case is in the vicinity of 2.0-2.2 keV, while it does not exceed 1.5 keV for the case with ITER-98$_{y,2}$ scaling. Finally, the central safety factors are above 2 and have some reversed shear for the cases with ST thermal confinement scaling, while the ITER confinement scaling leads to the result of $q_{min}=q_0\sim1.5$. Hence, the difference between these two confinement scaling expressions, a critical question for projecting next-step ST operating points, should be quite visible when the non-inductive operating point is determined in NSTX-U.

A second variable key to determining the non-inductive operating point is the plasma density. Fig 9.3 shows how key parameters vary as a function of density and confinement level for a scenario with P_{inj}=12.6 MW, I_P=1.0 MA, B_T=1.0 T, and Z_{eff}=2. Consider the left column for now, where the calculations assume that the fast ion slowing down is classical.

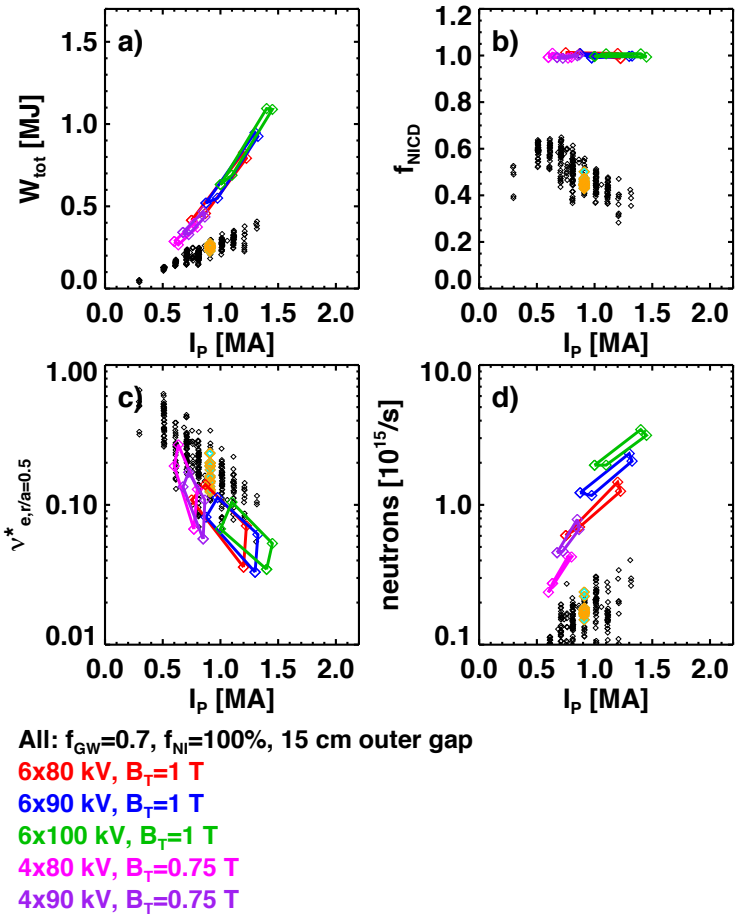

Fig. 9.4: Plots of a) the stored energy, b) the non-inductive current fraction, c) the mid-radius collisionality, and d) the neutron emission, as a function of the plasma current, for NSTX data and projected NSTX-U scenarios.

Fig 9.3a) shows the bootstrap fraction as a function of confinement and density; the bootstrap current increases with both confinement at fixed density, and with density at fixed confinement multiplier. The beam current drive fraction in frame 9.3b) increases with confinement, but decreases strongly with increasing density.

When these results are summed (along with the small contribution from Pfirsch-Schlueter and diamagnetic currents), the resulting non-inductive fraction is shown in Fig. 9.3c). Interestingly, the non-inductive fraction is largely independent of f_{GW} in this region of parameters space, and 100% non-inductive operations is achieved at $H_{98y,2}\approx1.04$.

The central safety factor, however, is a strong function of density in

this configuration. Beneath f_{GW}~0.6, the central safety factor tends to fall beneath unity, a situation guaranteed to result in disruptive core n=1 kink/tearing modes [9,23-27]. This is due to the strong neutral beam current drive at lower density, which tends to be peaked on the magnetic axis, as indicated in Fig. 9.2c). At higher densities, the NBCD is reduced, while the off-axis peaked bootstrap current contributes to an elevated central safety factor. Furthermore (not shown), the strong central peaking of the fast ion pressure at lower density results in the configuration becoming n=1 MHD unstable. Hence, it will likely be critical to avoid too-low a density in these scenarios; the caveat to this statement is shown in the right-hand column of Fig. 9.3, where a small level of fast ion diffusivity has been added to the simulation. These simulations with fast ion density included will be discussed in greater detail in Section 9.2.4.2.

Additional information about fully non-inductive scenarios in NSTX-U is given in Fig. 9.4. This figure shows the basic NSTX database in black points, and data from the dedicated high-A experiments in NSTX as orange points. Each of the colored shapes corresponds to a family of scenario simulations with the same toroidal field strength, boundary shape, and heating power; the four corners of each shape corresponding to the two confinement assumptions and the narrow and broad thermal profiles, as discussed in the context of Fig. 9.2. This figure will guide the description of the research plan given below.

B_T [T]	P_{inj} [MW]	Heating Pulse Duration [s]	I_P Range [kA]	τ_{CR} [s]
0.75	6.8	5.0	$600<I_P<800$	$0.3<\tau_{CR}<0.4$
0.75	8.4	3.0	$675<I_P<850$	$0.3<\tau_{CR}<0.45$
1.0	10.2	5.0	$750<I_P<1200$	$0.35<\tau_{CR}<0.75$
1.0	12.6	3.0	$875<I_P<1300$	$0.4<\tau_{CR}<0.8$
1.0	15.6	1.5	$1000<I_P<1450$	$0.4<\tau_{CR}<0.85$

Table 9.1: Selected parameters for 100% non-inductive scenarios at f_{GW}=0.7 in NSTX-U. See Table 2 and Appendix 1 of Ref. [19] for additional information.

As described in Section 10.7, the toroidal field for the first year of NSTX-U operations will be ≤ 0.8 T. The associated operating points for different heating powers are shown in Fig. 9.4 in magenta and purple, and in the first two rows of Table 9.1. The TRANSP simulations project the non-inductive currents to be in the range of $600 < I_P$ [kA] < 800. The goal for the first year operations (2nd year of the plan) will be to demonstrate these operating points for short periods, for instance, a few τ_E. In the second year of operations, research will attempt to extend these scenarios at 0.75 T to a few τ_{CR}.

In the second year of operation, shorter pulses at B_T=1.0 T will be available, and it is envisioned that from the third year on, full-field (B_T=1.0 T) operation will be allowed with full 5 second

flat-top durations. The details of these scenarios are illustrated in the red, blue, and green curves of Fig. 9.4, and the lower three rows of Table 9.1. It can be seen that these scenarios project to higher stored energy and larger neutron emission than any scenarios achieved in NSTX; the collisionality of these scenarios, which are not designed to reduce this parameter, is comparable to the lowest achieved in NSTX. Some run-time will be dedicated to develop short-duration 100% non-inductive scenarios at B_T=1.0 T in the 2nd operations year, using 90-100 kV beams to increase the current level. These 100 % non-inductive scenarios at 1.0T will be extended to the full 5-second flat-top in the later years, using 80 kV beams.

Lack of particle control is a potential barrier to completing these plans for long-pulse fully non-inductive operations; this will be addressed in the following way. The divertor cryo-pump does not come online until the third year of NSTX-U operations. During the period before the pump is installed, both boronization and lithium technologies will be explored to facilitate density and impurity control. For instance, it is possible that ELMs triggered by the lithium granule injector can be used to reduce the impurity accumulation. Alternatively, ELM pacing by 3-D fields can be explored. Additional discussion of these particle control techniques will be given in section 9.2.1.2 and 9.2.2.4, as well as in the boundary physics chapter.

During the final two years of the research program, additional attention will be given to integrating the 100% non-inductive operating point with other discharge goals. One goal will be to maximize the non-inductive current level at 1.0 T and high β_N. These studies will benefit from stability and profile optimization studies to be conducted in collaboration with the Macro Stability (MS) group. Another such integration step will be to add advanced-geometry or radiating divertors to the configurations; these scenarios may not require active heat flux mitigation, but testing their compatibility with those mitigation techniques will have value. Experiments will also begin to integrate the high-performance non-inductive flat-top scenarios with non-inductive current ramp-up research. This integration will be described in section 9.2.1.4.

9.2.1.1.2: Research Plans by Year

The plans and goals for this research topic can be summarized as:

Year 1 of operations (2015):

- Develop very high non-inductive fraction discharges at 600< I_P [kA]<800 at B_T=0.75, for a few τ_E.

Year 2 of operations (2016):

- Extend the duration of the very high non-inductive fraction at B_T=0.75 T to a τ_{CR} or longer.

- Utilize higher toroidal fields up to B_T=1.0 T to achieve 100% non-inductive at higher I_P levels for short pulse.

Year 3-4 of operations (2017-2018):

- Extend the duration of fully non-inductive currents to the full five second beam heating pulse, including optimization of particle control with the cryo-pump.
- Integrate 100% non-inductive scenarios with advanced divertor solutions.
- Integrate 100% non-inductive scenarios with non-inductive ramp-ups.

9.2.1.2: Long-Pulse Partial Inductive Operations

9.2.1.2.1: Research Description

In addition to the 100% non-inductive goal described in the previous section, the NSTX-U program has a goal of achieving long pulse with controlled density and higher current, up to I_P=2.0 MA. Scientific motivations for this scenario goal include:

- Testing the I_P scaling of core transport and the SOL width.
- Accessing low collisionality for core transport and global stability studies.
- Testing long-pulse disruption avoidance for many current redistribution times.

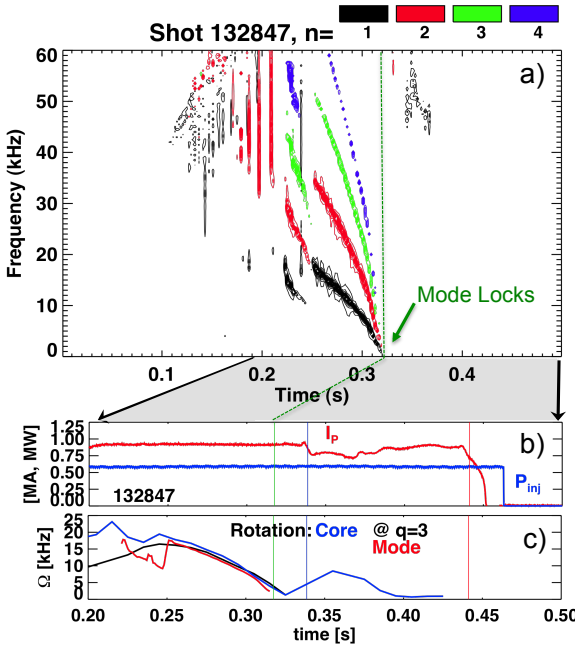

Fig. 9.5: Example dynamics of a discharge with incorrect early fueling. Shown are a) a spectrogram decomposed by toroidal mode number, b) the plasma current and heating power, and c) the core, q=3 surface, and mode rotation frequencies.

Accessing low collisionality is most easily done at lower density, since the normalized collisionality scales as $\nu^* \propto \frac{f_{GW}^3}{B_T \beta_N^2}$ at fixed β_N and toroidal field (it is assumed here that sufficient heating power is available to heat to the β-limit at any Greenwald fraction). β_N is limited by transport and/or global stability, and B_T is limited to 1.0 T in NSTX-U. Thus, reducing f_{GW} is the best means to reduce the collisionality. However, achieving sustained low density in NSTX has proven to be quite difficult, for two reasons:

- the requirement to provide strong fueling during the early phase of the discharge,
- the continued rise of the electron

density during the H-mode phase.

These two issues will be discussed below.

When insufficient fueling is provided at the beginning of the discharge, a wide variety of disruptive MHD activity has been observed to occur. A single example of this activity is shown in Fig. 9.5, where the MHD activity associated with an incorrectly fuelled discharge is illustrated [27]. In this case, a large n=1 mode strikes at t~0.24, and rapidly spins down to zero frequency. The disruption follows rapidly after the mode locks to the wall. Disruptions of this type are typically eliminated by increasing the fueling, often from the high-field side gas injector. This fueling modification does not prevent the early MHD modes from developing, but rather prevents them from spinning down to zero frequency; their frequency tends to saturate at 5-15 kHz in these non-disruptive cases, while their amplitude decays over a period of ~100-200 ms [27].

Experiments will explore a number of options for eliminating these and other disruptive MHD modes from discharges with reduced fueling during the first two years of NSTX-U operations. One hypothesis is that the extra gas fueling cools the plasma edge, resulting in more rapid current penetration and avoidance of the most unstable current profiles. The present fast ramps in NSTX were designed to provide the longest possible I_P flat-top for the rather modest flux capabilities of that solenoid. Given the larger flux of the NSTX-U solenoid, most scenarios are projected to tolerate greater flux consumption during the I_P ramp. Hence, the impact of ramping the plasma current more slowly will be examined. The gas fueling and I_P ramp rate will be scanned, to determine the optimal combination for achieving stable flat-top configurations at reduced density. The feedback-control of the line-average density described in section 9.2.2.4, when available, will be very beneficial for this study.

Beyond the I_P ramp rate, other means of achieving reduced density at the end of the ramp-up phase will be explored. Given that modes locking to the vessel wall precede many of these disruptions, experiments will investigate whether new error-field correction strategies in the early part of the discharge can improve the discharges. The dominant source of n=1 error-field in NSTX was from the tilting of the toroidal field coil due to interaction with stray field from the OH solenoid connections [28]. These OH connections have been i) moved from the top of the coil in NSTX to the bottom of the coil in NSTX-U, and ii) replaced with a coaxial design with smaller stray fields [11]. It is anticipated that these two changes will dramatically reduce error fields during the startup phase, but a new error field assessment must be performed as described in Chapter 2. Experiments will also examine whether use of more tangential neutral beam sources can result in greater rotation of the plasma, potentially preventing modes from locking to the wall.

Regardless of whether the density at the start of flat-top was f_{GW}=0.2 or f_{GW}=0.6, NSTX discharges tended to have a ramping electron density evolution. In ELMy H-mode with boron coatings of the plasma facing components, this increasing density was due to the accumulation of deuterium in the plasma. In ELM-free conditions with lithium-coated PFCs, the ramping electron density was typically due to the accumulation of carbon; as described in section 9.2.2.4, the deuterium inventory was often well controlled in those discharges. Research in the first years of NSTX-U will, in conjunction with the boundary physics and M&P research plans described in Chapters 4 and 5, attempt to stop the density rise by the following means:

- In cases with boronized PFCs, natural ELMs will be used to provide impurity control. The deuterium supplied to the plasma will be minimized via careful optimization of the plasma startup phase.

- In ELM-free lithium-conditioned discharges, the lithium granule injector will be used to attempt both lithium replenishment and ELM pacing. It is anticipated that this combination will provide both the good confinement of lithium-conditioned H-modes and the impurity transport of an ELMy regime.

- If this method fails, then experiments will be conducted to optimize magnetic ELM pacing with non-axisymmetric fields [29], for control of the impurity inventory in lithium-conditioned H-modes. In this case, the key task will be to maintain the desired impurity flushing properties without inducing large rotation damping or MHD modes.

- There is evidence that regimes with modest lithium conditioning may provide some confinement improvement without eliminating ELMs. Research will explore these regimes, with the goal of determining whether some small amount of lithium conditioning can provide deuterium pumping while not suppressing ELMs.

- ELM pacing with vertical jogs [30] may be used in advanced scenarios if the previous methods fail.

- Most NSTX H-mode discharges used fueling from a high field side (HFS) gas value to induce H-mode. This gas was injected down a long tube, and continued to flow into the plasma long after the H-mode transition. NSTX-U research will attempt to replace this fueling with that from injectors with more rapid time-response, namely the center-stack “shoulder” injector, and outboard supersonic gas injectors. See section 9.2.2.4 for more information on these fueling studies.

It is anticipated that the cryo-pump will be available between the 2nd and 3rd years of operations. Once this pump is installed and commissioned, it will, as described in the boundary physics chapter 4, be used to investigate density control in these higher current NSTX-U scenarios. See section 4.2.3 for additional information on the physics design of the cryo-pump system.

In addition to achieving density control, a second critical requirement will be to incorporate feedback controlled heat flux mitigation strategies into high-current and high-power scenarios. It is anticipated that this work will begin in the third year of the research program. The magnitude of the issue can be seen from Table 9.2, which describes the peak heat flux and time for the tile surface to reach T_{max}=1200°C, as a function of heating power, plasma current, and flux expansion. The temperature limit of 1200°C was selected here, as radiation induced sublimation has been observed above this temperature [31]. Additionally, the horizontal target tiles have been qualified for an average heat flux of 5 MW/m^2 for five seconds, with the limit being due to internal thermal stresses. In evaluating the tile heating for NSTX-U scenarios, the following assumptions have been made: the midplane scrape-off layer heat flux scales as $\lambda[mm] = 9.2 I_P^{-1.6}$, the peak heat flux scales as $Q_{Pk} = \frac{P_{loss} f_{div}}{2\pi R_{OSP} \lambda_q f_{\exp}}$, and that the time dependence of the surface temperature varies as $T_{surf} = 90 Q_{avg} \sqrt{t}$ [32], with $Q_{avg} = Q_{Pk}\left(1 - e^{-1}\right)$. Here, f_{div} is the fraction of the input power reaching each divertor, with f_{div}=0.4 implying that 80% of the input power enters the SOL, and that it is split evenly between the upper and lower divertors with no radiation in the divertor itself. f_{exp} is the flux expansion at the outer strikepoint, with values of 15 typical for standard divertors in NSTX-Upgrade.

				f_{exp}=15, f_{div}=0.4, T_{max}=1200 C		f_{exp}=60, f_{div}=0.4, T_{max}=1200 C or f_{exp}=15, f_{div}=0.1, T_{max}=1200 C	
Case	I_P (MA)	P_{inj} (MW)	Heating Pulse Duration [s]	Q_{PK} [MW/m^2]	Time to T_{max} [s]	Q_{Pk} [MW/m^2]	Time to T_{max} [s]
1	0.75	10.2	5.0	6.0	12.6	1.5	200
2	1.2	5.1	10	6.3	11.2	1.6	180
3	1.5	10.2	5.0	18	1.4	4.5	21
4	1.5	15.6	1.5	27	0.6	6.9	9.4
5	2.0	10.2	5.0	28.5	0.5	7.1	8.7
6	2.0	15.6	1.5	43.6	0.25	10.9	3.7

Table 9.2: Peak heat fluxes and time for tile surface temperature to reach 1200 C, as a function of plasma current, heating power, and flux expansion. P_{inj}=10.2 MW corresponds to six beam injecting at 80 kV, while 15.6 MW corresponds to six beams injecting at 100 kV. More information on these scenarios can be found in Ref. [19].

Case 1 in the table shows the expected tile heating at I_P=0.75 MA and P_{inj}=10.2 MW, parameters which should be typical of 100% non-inductive operation for 5 second pulses. For these discharge parameters with f_{exp}=15 and f_{div}=0.4, tile heating and thermal stresses will limit the pulse to between 4 and 5 seconds. However, modest increases in the divertor radiation or flux expansion will remedy this problem. Comparatively low input power scenarios at B_T=0.75 T have also been identified that can potentially run for 10 s; case 2 of the table shows that these will require some modest reduction in the heat flux compared to the base parameters. However, the lowest collisionalities are expected for I_P>=1.5 MA, for which scenarios are listed in the final four rows of the table. With f_{div}=0.4 and f_{exp}=15, rapid tile surface overheating and thermal stress accumulations is expected to occur within the duration of the heating pulse for either heating power considered. Note that some expressions for the SOL width scaling have a weaker dependence on I_P than what is used here, with exponents in the range of -1.3 to -1.2. Using this exponent certainly lengthens the time to T_{max} in table 9.2, but does not move it beyond the duration of the heating pulse in cases 3 through 6.

NSTX research has identified two means of mitigating this problem, and these are indicated in the final two columns of Table 9.2. The first is to increase the flux expansion dramatically, using the snowflake divertor. Candidate snowflake divertors in NSTX-Upgrade have flux expansions of 60 to 80; a conservative value of 60 is chosen for the table. The second mitigation strategy is to radiate the power in the divertor volume, before it can reach the divertor surface. This is captured in the above table by reducing f_{div} to 0.1. It can be seen that either of these techniques can reduce the peak heat flux such that the tile heating is not an issue for the duration of the heating pulse in all scenarios but one: the I_P=2.0 MW, P_{inj}=10.2

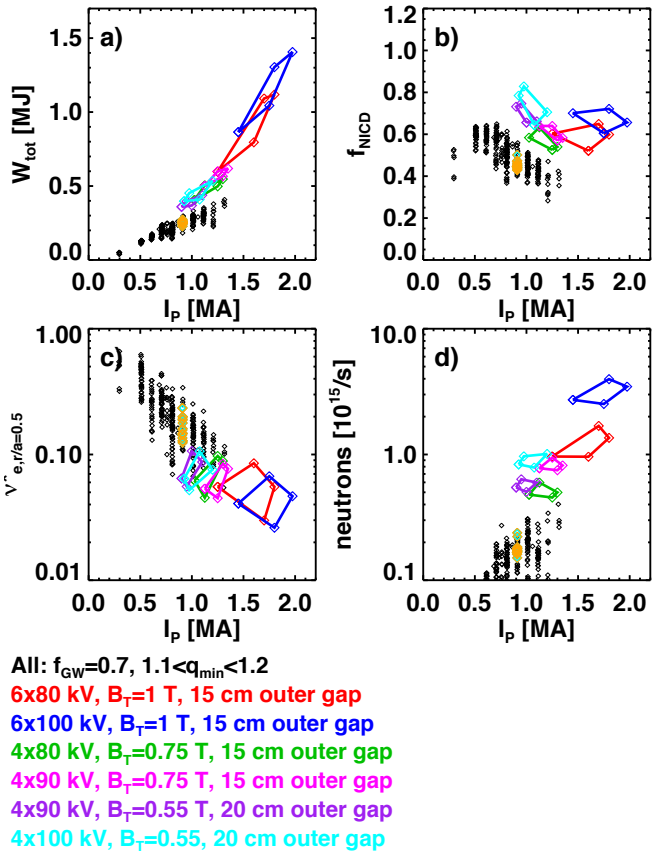

Fig. 9.6: Performance characteristics of NSTX-U scenarios that are predicted to relax to q_{min}>1.1. All NSTX-U simulations are for fully relaxed profiles, and have f_{GW}=0.7.

MW case will likely require a combination of both flux expansion and increased divertor radiation to achieve the desired pulse length with acceptable heat fluxes. Research in NSTX has shown that this exact combination of effects is common when a snowflake divertor is formed in NSTX [14,15].

The details of the NSTX-U strategy for heat flux mitigation are described in the Boundary Physics (BP) Research chapter, and section 9.2.2 of this chapter. Briefly, the development of the physics basis for these two control techniques will be part of the BP research program. ASC research on magnetic control of the snowflake divertor will begin in the first year of the research program, with a goal of providing a "standard" control algorithm by the end of the 2nd year. Development of the measurements and actuators for radiative divertor control will occur in the first two years of research in the BP TSG, and closed loop control experiments will begin in the 3rd or 4th year of the research program.

With this background, the plan for developing long-pulse partial-inductive scenarios is as follows. As discussed in Section 10.7, he first year of NSTX operations is projected to have toroidal fields limited to B_T~0.75T. Under the constraint that the relaxed q_{min} should be greater than 1.1, scenarios with this toroidal field are predicted to be limited to $1.0 < I_P$ [MA]< 1.3 at P_{inj}=6.8 MW, and $1.1 < I_P$ [MA]< 1.35 at P_{inj}=8.4 MW, where the range depends on the confinement assumptions used. Fig. 9.6 shows that these fully relaxed scenarios, indicated in magenta and green, should be able to exceed both the neutron emission and stored energy achieved transiently in NSTX. These relaxed $q_{min}>1$ scenarios at B_T=0.75 T are also not expected to present a thermal challenge to the divertor. The q-profile evolution in these discharges will be used to validate, or drive improvements in, the TRANSP simulations of NSTX-U scenarios.

Experiments will also increase the current towards the 1.5 MA administrative limit planned for the first year, anticipating that this will likely result in q_{min} falling beneath unity. The current redistribution time for these scenarios is expected in to be in the range of 0.5 seconds, so discharges of duration ~$3\tau_{CR}$=1.5 s will be attempted. This time is comparable to the maximum allowed duration due to tile heating in cases 2 & 3 of Table #1, and should allow an early experimental assessment of the thermal heat loading under real divertor conditions.

It is anticipated that full B_T=1.0 T operation with reduced field duration will be allowed in the 2nd year of operations. For relaxed $q_{min}>1.1$ with B_T=1.0 T, TRANSP simulations predict the current levels in Table 9.3 as a function of heating power and Greenwald fraction, with the range again determined by confinement variations. Two of the f_{GW}=0.7 operating points from this table are illustrated in blue and red in Fig. 9.6. These scenarios are anticipated to achieve stored energies in excess of 1 MJ, with neutron flux up to 10 times greater than achieved in NSTX. Experimental time will be spent in the second year accessing these relaxed $q_{min}>1$ scenarios at

B_T=1.0 T. However, the final column of the table shows that the without heat flux mitigation, these scenarios will be limited to short pulse. If snowflake divertors, either pre-programmed or in closed-loop control, are available, they will be used to extend the pulse length. Additionally, the rather high density in these scenarios, chosen to assist in elevating q_{min}, may help raise the divertor radiation fraction and reduce f_{div} compared to the assumption in Table 9.3. Research in the second year will also attempt to extent the B_T=0.75 T scenarios to the full 5 second duration of the heating pulse.

P_{inj} [MW]	Heating Pulse Duration [s]	f_{GW}	Plasma Current Range [MA]	τ_{CR} [s]	Time to T_{max}=1200 C, for middle of I_P range [s]
10.2	5.0	0.7	$1.3<I_P<1.8$	0.45-0.8	1.2
10.2	5.0	1.0	$1.5<I_P<2.0$	0.4-0.7	0.8
12.6	3.0	0.7	$1.4<I_P<1.9$	0.5-0.85	0.65
15.6	1.5	0.7	$1.5<I_P<2.0$	0.6-0.9	0.35

Table 9.3: Current levels and other parameters for relaxed q_{min}>1.1 operations in NSTX-U, for B_T=1.0 T. The tile temperature calculation is based on f_{div}=0.4 and f_{exp}=15.

Experiments will also begin to explore higher-current and lower density scenarios at B_T=1.0 T that may relax to q_{min}<1.1, but have properties favorable for physics exploration. These include short pulse scenarios at I_P up to 2.0 MA. These scenarios will allow a first exploration of transport, global stability, and divertor physics at high-field and current. Monitoring of IR cameras and divertor thermocouples will be used to avoid excessive divertor heating.

The pace of high-current long-pulse development in the latter years will likely be determined by progress in heat flux and particle control. If divertor heating presents the most significant problem, closed loop control of the snowflake divertor may be given additional emphasis, allowing it to be used in scenarios more quickly. If particle control presents the most serious problem, then the ELM pacing and lithium explorations described in the bulleted list at the beginning of this section will receive highest priority. When the cryo-pump is brought on line between the 2nd and 3rd year of operations, it will immediately be used to assist in regulating the density. The ultimate goal for this development will be to form B_T=1.0 T, I_P=2.0 MA discharges that are sustained for 5.0 seconds.

9.2.1.2.2: Research Plans by Year

The time-scale for development of high-current, partial inductive scenarios is summarized as follows:

Year 1 of operations (2015):

- Begin studies of current ramp-up optimization with reduced fueling, including required error field reduction studies.
- Develop short pulses scenarios at B_T=0.75 T and I_P up to 1.5 MA, for studying confinement and divertor physics.
- Extend the discharge durations at B_T=0.75 T and I_P~1.1 MA to the full 5 second pulse duration, using both boron and lithium PFC conditioning.

Year 2 of operations (2016):

- Develop short-pulse scenarios at B_T=1.0 T and I_P up to 2.0 MA, for studying confinement and divertor physics.
- Extend the pulse length at B_T=1.0 T and I_P~1.5 MA to the limits provided by power handling consideration.

Year 3-4 of operations (2017-2018):

- Begin the integration of divertor control techniques, in order to extend the pulse length (see Section 9.2.2.2)
- Establish maximum pulse duration at B_T=1.0T, I_P=2.0 MA, using full complement of current drive and heat flux reduction tools.

9.2.1.3: RF Heating for Advanced Scenarios

As described in Chapter 7 of this 5 year plan, there is a dedicated development effort for coupling high-harmonic fast wave (HHFW) heating and current drive power to NBI heated H-mode plasmas. The goals of that research are to maximize the heating power coupled to the thermal core plasma, and increase the efficiency of core HHFW current drive. Key issues to be resolved include i) reducing the loss of HHFW power in the SOL [33], and ii) reducing the coupling of HHFW power to energetic fast ions [34] (see Sections 7.2.1.2 and 7.2.1.3). ASC researchers will assist in this development, for instance, with control of the antenna-plasma gap regulation or use of density control techniques.

Pending progress in improving coupling, ASC research will dedicate time to couple HHFW heating and current drive into high-performance scenarios, with two goals: increasing the electron temperature for higher non-inductive fraction, and heating and current drive as part of closed-loop profile control. Ref. [19] showed explicitly the benefits of increasing the electron temperature in these scenarios: the bootstrap current is increased by the simple increase in β_P, while the NBCD is increased through lengthening the fast ion slowing down time. These benefits must be weighed against two potential drawbacks of incorporating HHFW to these scenarios. First, the smaller outer gaps favorable for HHFW coupling result in a decrease in the elongation, which causes the large R_{tan} sources from the new beamline to drive their current closer to the magnetic axis. Secondly, the lower densities that may be required to avoid wave propagation in

the SOL [33] may be incompatible with maintaining elevated q_{min} in relaxed profiles or with reducing the divertor heat fluxes. Ultimately, only experimental exploration can determine if the benefits of additional electron heating can overcome these potential issues. Use of HHFW in control loops will be discussed below.

Finally, under incremental funding, the system for EBW heating and current drive may be available for advanced scenario applications in the later phase of the research program. While the primary use of this system is for heating start-up plasmas to increase their coupling to NB and HHFW heating and current drive (see Chapters 7 and 8 for details), it is also possible that this system could provide substantial heating and current drive during the flat top. Current drive efficiencies of 30-60 kA/MW are predicted, which with an ~70% conversion efficiency, indicate that 20-40 kA could be driven with 1 MW of power. Pending the results of dedicated experiments in the wave heating group described in Section 7.2.2.5, exploration will begin for scenarios that incorporate this tool, likely focusing an EBW heating in the during the present research program.

9.2.1.4: Coupling to Non-Inductive Startup and Ramp-Up

As described in Chapter 8, the Solenoid Free Start Up (SFSU) topical science group is researching methods to form and ramp-up the ST plasma current without use of the Ohmic solenoid. This consideration is motivated by the engineering constraint that a full-size solenoid coil capable of ramping the plasma current to full value may be unavailable in next-step STs. Methods under consideration for ST startup in NSTX-U include coaxial helicity injection and plasma gun startup. The subsequent plasma current ramp-up is envisioned to be accomplished by a combination of ECH, HHFW heating, and neutral beam heating and current drive.

This SFSU research on non-inductive ramp-up has many parallels to that described earlier in this section, and ASC researchers will be involved in this development. Particular areas where ASC will contribute include:

- Boundary control at low current, and in the presence of transients, can be challenging. ASC activities will support control of the plasma boundary during non-inductive ramp-up.
- Controlling the density evolution during the current ramp will be critical for controlling the current and pressure profile evolution. The density control tools developed by ASC and BP TSGs will thus be important.
- The modeling of neutral beam current ramp-up has many similarities to modeling the flat-top scenarios, and the ASC and SFSU groups will continue to work together on these modeling tasks. See further discussion in section 9.2.4.3.

The ASC and SFSU research programs will be joined in the later years of this research program. In particular, fully non-inductive flat-top scenarios will be developed for coupling to non-inductive ramp-up, while the ramp-up scenarios will be tailored for coupling to the flat-top. Dedicated experiments will then be conducted to produce discharges with little or no solenoid induction used from breakdown through the end of flat-top as described in Thrust 2 of Chapter 8.

9.2.1.5: Impact of High-Z PFC Conversion on Scenario Development

As described in section 5.3, the base program places high-Z materials in the outboard divertors (see Figure 5.3.1). These locations have been chosen so that the high heat flux regions for high triangularity plasmas remain graphite. Hence, the high-Z upgrades envisioned in the base program should have minimal impact on the scenario development described here.

With incremental funding, the high-Z coverage would be increased more rapidly. In particular, the tiles on the center stack and passive plates would be converted to high-Z materials, as well as the full lower outer divertor and a portion of the upper outer divertor. However, the inner divertor horizontal and vertical divertor targets would remain graphite through this 5 year research program, mitigating some of the risk to high performance scenario development. Under this incremental research program, the development of radiative divertor control (9.2.2.3.2) will be made a high priority for those additional resources. Furthermore, it may be necessary to accelerate the research in safe discharge shutdown techniques. Finally, the use of HHFW in these scenarios may become a higher priority, if it is demonstrated to be a useful tool for controlling the core high-Z impurity content.

9.2.2 Thrust 2: Axisymmetric Control Development

9.2.2.1: Overview of Control Development

As described in 9.1.2.2, axisymmetric control is a critical topic reaching across all areas of tokamak operations and physics. In this section, research on measurements, control loops, and actuators enabling closed loop control are described. NSTX-U research in this area will focus on four broad area: boundary and position control, divertor heat flux control, control of the safety factor and rotation profiles, and particle inventory control.

These control tasks will be executed through the NSTX implementation [35, 36] of the General Atomics Plasma Control System (PCS) [37,38]. At present, the gas injection systems, TF, PF, OH, and RWM coils, and neutral beams [39] are all available to this system as actuators. Present input data include the coil currents, vessel pressure, and extensive magnetic measurements. The

inclusion of additional diagnostic data allowing the execution of the research plan is described below.

For reference, the four sub-topics in Thrust 2 are as follows:

- Advanced boundary and position control (Section 9.2.2.2).
- Control of the divertor magnetic geometry and radiation (Section 9.2.2.3).
- Control of the current and rotation profiles (Section 9.2.2.4).
- Control of the plasma fueling and density (Section 9.2.2.5).

Control of n>0 MHD modes, as manifest in techniques such as resistive wall mode control or error field correction, are described in Chapter 2.

9.2.2.2: Advanced Boundary and Position Control

Control of the plasma boundary is critical for maintaining the high-performance plasma state. Slow boundary control is required in order to maintain high boundary elongation and prevent any of the plasma-wall gaps from becoming too small; note that this problem may be more severe in an ST, where there will likely not be any inboard PF coils to control the inner gap. Fast control is required to stabilize the n=0 vertical mode. This section describes NSTX-U research plans in the area of boundary and position control.

9.2.2.2.1: Realtime Equilibrium Reconstruction and Boundary Control

In order to begin physics operations in NSTX-U, the realtime Grad-Shafranov solver rtEFIT [40] will be upgraded for the new geometry and PF coils of the device. Following that, a reoptimization/retuning of the shape control algorithm is necessary for reliable plasma operations. The boundary control task will produce a Single-Input-Single-Output (SISO) shape controller that connects each of the PF coils to a single, mostly independent, control task such as the outer-gap control, strike point radius control, etc. This development time, as part of device commissioning will restore the ISOFLUX gap control capabilities [40,41] that were used routinely in NSTX. Furthermore, retuning of the strike-point and X-point controllers will be done as necessary, using the relay-feedback control techniques developed for NSTX [42,43].

The underlying tool for boundary control in NSTX-U is realtime equilibrium reconstruction. The previous real time EFIT reconstructions in NSTX used 33x33 grid spacing. The accuracy of this reconstruction is insufficient for many of the tasks in NSTX-U such as snowflake divertor calculations. The primary reason for the course grid has been the computational load on the real-time computers. However, with the upgrade to the computer hardware and software described in Section 10.3.3.4, NSTX-U will have substantially greater realtime computing power, allowing higher resolution 65x65 grid reconstructions to be tested and implemented for NSTX-U.

A second improvement to the rtEFIT reconstructions will be made via improvements to the constraint set. In NSTX, only magnetic measurements were used to reconstruct the plasma state; this will be the initial state when operations resume in NSTX-U. Research during the 5-year period will include the development of real-time kinetic measurements, such as MSE and MPTS. When such measurements become available, including them as constraints to the rtEFIT reconstruction will be high priority. For instance, the rtMSE diagnostic will provide a strong constraint on the q-profile, for use in q-profile control development described in Section 9.2.2.4.1. This diagnostic will also provide a strong constraint on the magnetic axis location, helping to constrain β_N via knowledge of the Shafranov shift. The realtime MPTS data can also help resolve the Shafranov shift correctly, as well as help resolve the plasma outer boundary more accurately. The planned availability of real-time MSE is late in the first year of operations, or possibly during the second year, and work on rtEFIT reconstruction with MSE will start as soon as that data is available. Real-time MPTS may be available during the final years of the 5 year plan, and will be used as either part of an isotherm or loose isobar constraint [44].

SISO boundary control will be used for initial NSTX-U operations, based on its comparatively fast implementation time and proven capability in the base NSTX scenario operations. However, this approach may not be sufficient to reach the full operation capabilities of NSTX-U. For instance, due to the small radius of the center columns, NSTX-U and future ST devices will not have PF coils on the inner wall to specifically control the inner gap. This can result in uncontrolled inner gap motion when other shape parameters are modified or the plasma profiles change. Furthermore, the new snowflake divertor will need a new complex control for the divertor region PF coils in both upper and lower divertor regions (see Section 9.2.2.3.1) which will interact with the control processes for the other PF coils. If these or similar phenomenon result in operational problems, ASC researchers will begin a program in multi-input, multi-output shape control development. In this case, this task involves coupling the voltage requests for the PF coils to more distant shape control points. For instance, the coils that control the divertor geometry will also be tasked with some control of the inner gap. The control code exists for this in the present ISOFLUX shape control, but has not been exercised. Relay-feedback optimization will be used to develop the optimal control gains.

As the facility develops, continued development of shape control algorithms will likely be required. For instance, the NSTX-U plan calls for a cyro-pump to be installed after the second year of operation. The pumping provided by this system is extremely sensitive to the strike point location, and special strike-point control development may be required. Furthermore, the PF-2 coil may be upgraded to bipolar capability. This would open up additional possibilities for control of the bottom gap in high-triangularity and elongation scenarios, and development tasks to exploit this capability would be executed.

9.2.2.2.2: Vertical Position Control

Vertical position control may restrict the operating space available to the NSTX-U physics program. An example of this can be seen if Fig. 9.7, taken from the high-A and κ experiment conducted during the short 2011 run campaign; one of the discharges is typical of NSTX at κ~2.5 and A=1.45, while the other pushes κ towards 2.9 and the aspect ratio to 1.7. In the high-A cases, transient increases in l_i resulted in the control system reducing the PF-3 currents, in an effort to maintain the plasma elongation. As the PF-3 coil currents become smaller, the stabilizing field index was reduced, eventually leading to a vertical displacement event and disruption. Reducing the requested elongation would have resulted in an increase in the PF-3 current, and restoration of vertical stability.

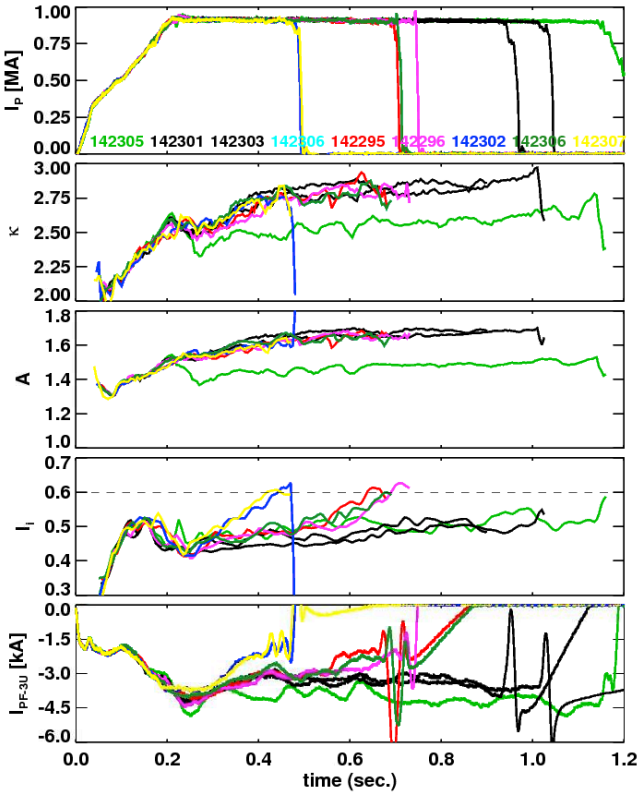

Fig 9.7: Loss of vertical position control when the internal inductance reached a threshold value in higher aspect ratio discharges.

While operation with bad field curvature will never be feasible and certain portions of κ-l_i space will not be accessible, this result underscores the importance of optimizing the active vertical stability control. The following steps have been implemented to potentially improve the vertical position control of NSTX-U plasmas:

- Added additional poloidal flux loops to the vertical position observer. This should provide a more accurate and less noisy measurement of the plasma position and velocity for use in feedback control.
- Added PCS code to use the n=0 radial field from the RWM coils for feedback control of the vertical position. The field from these coils is significantly smaller than from the large PF-3 coils, but this system has the advantage of a more rapid power supply response, with less conducting structure between the coils and the plasma.
- Improved the digital communication links between the realtime computer and the large radial field coils (the PF-3s). This will result in a reduction in the latency of the position control.

- Moved the PCS code for vertical position control to a new PCS "category". This will allow more rapid addition of new vertical control algorithms, and will provide the capability to easily add additional PF coils to the vertical control loop should that prove desirable.

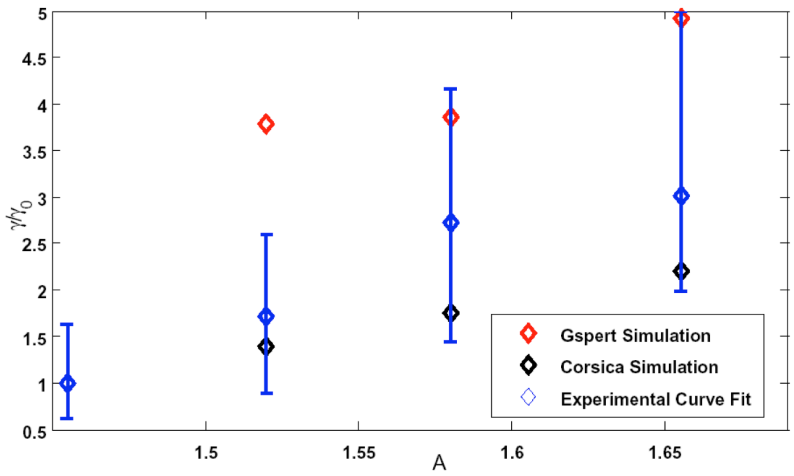

Fig 9.8. Change in γ versus A for Corsica and Gspert simulations, and experimental data (#141639-141642)

It is expected that the improvements noted above will improve control of the vertical stability with the regular constant coefficient Proportional-Derivative (PD) control scheme, as has been used in NSTX and other many major tokamaks such as DIII-D, JET and EAST [45]. However, a plan has been formulated to improve the vertical control algorithm in case the PD control proves inadequate. There are usually two sources of poor vertical control performance. The first is the actuator (PF coil) saturation, while the second is measurement noise, potentially due to effects such as ELMs and n=1 RWM/locked-mode pickup. If the main issue is assessed to be actuator saturation, a higher-level control implementation such as an anti-windup scheme will increase the control stability by avoiding reaching the voltage/current limits of the coils. An example of anti-windup vertical position control for a tokamak is shown in [46]. Similarly, if the main control issue is measurement noise, a more sophisticated algorithm that is robust to noise, such as a non-linear adaptive optimum control, will be developed [47].

Finally, the infrastructure for real-time vertical stability calculations will be included in the PCS during the later years of the research program. This will enable real-time adjustment to the vertical stability control during the shot. One potential method for attaining this information is to measure vertical growth rates perturbatively using relay-feedback algorithms (see for example [48] and reference within). In this method, the vertical control is modified for a short amount of time. The control response induces the system to oscillate at its unique frequency and amplitude, which can be used to find the vertical stability of the system.

Alternatively, the vertical stability can be computed using stability codes. Fig. 9.8 compares numerical simulations to experimental data from aspect ratio scans, where the vertical position

control was frozen and the plasma allowed to drift [49]. The n=0 growth rates were calculated with Gspert [50], a non-rigid plasma response model based on the linearized Grad-Shafranov equation, and CORSICA [51], a free-boundary equilibrium and transport code. The simulations are in reasonable agreement with the experimental results. Thus, the simulation results, if available in realtime, could be used as a proxy for measurements of the vertical stability.

Research in the later years of the plan will assess whether a real-time version of Gspert code should be included in the PCS, or whether a perturbative-like stability analysis will be required. This information would be used to change the vertical position control law, or trigger a loss of control alarm (see Section 9.2.3.1.3).

9.2.2.2.3: Research Plans by Year

The time-scale for these boundary and vertical position control activities are summarized as follows:

Year 1 of operations (2015):

- Retune the PD vertical control algorithm with improved measurement and actuator capabilities. Assess the vertical stability.
- Restore the SISO boundary and strike point control capabilities in NSTX-U.
- Begin implementation of the higher resolution (65 x 65) version of rtEFIT.
- Begin implementation of the real-time MSE constrained version of rtEFIT.

In the case that the vertical control is not satisfactory, make improvements during years 1 and 2:

- Assess the conditions under which the vertical control system fails. Model the vertical motion of the plasma and disturbances such as ELMs.
- If the main issue is the actuator saturation: Implement a new anti-windup vertical control algorithm.
- If the main issue is disturbances in the measurements: Implement a new noise filter for the vertical motion observer that takes into account ELMs and other disturbances.

Years 2 of operations (2016):

- Test and implement higher resolution (65 x 65) version of rtEFIT.
- Based on diagnostic availability, implement and test the real-time MSE constrained version of rtEFIT.
- Assess strike-point control capabilities and make necessary improvements in anticipation of cryo-pump operation.

Years 3-4 of operations (2017-2018):

- Implement real-time vertical stability calculations for improved vertical feedback and loss of control detection.
- Test and implement improved rtEFIT using additional non-magnetic measurements as constraints (for instance, realtime MPTS)
- If it appears necessary, begin the implementation of MIMO shape control.

9.2.2.3: Closed Loop Control of Divertor Magnetic Geometry and Radiation

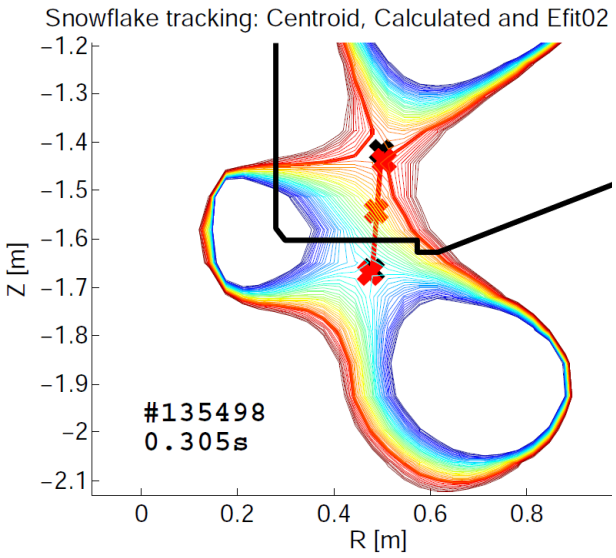

Fig. 9.9. Snowflake tracking for NSTX: Red crosses are the algorithm computed snowflake centroid and the X-points; Black crosses are the calculated real X-points.

As noted in the context of table 9.2, the heat flux in NSTX-U is projected to be quite large, easily exceeding 10 MW/m^2 if it is not actively mitigated. The unregulated heating of the divertor surface will rapidly result in the surface temperature exceeding the 1200° C sublimation limit of carbon. This section describes the NSTX-U strategies for closed loop control of divertor heat fluxes: magnetic control of the snowflake divertor, and feedback control of the divertor radiation via gas puffing

9.2.2.3.1: Snowflake Divertor Control

The snowflake divertor (SFD) is formed when a second divertor coil is used to introduce an additional X-point in the vicinity of the "primary" X-point; see discussion in section 4.2.2. The SFD has resulted in very large divertor poloidal flux expansions, which as a geometric effect directly reduces the heat flux. Interestingly, NSTX divertor heat fluxes have been reduced even beyond that expected from geometric effect, due to inducement of outer-strikepoint detachment with the SFD [14]. Hence, the SFD is a key tool for reducing the divertor heat flux. However, magnetic control of the SFD, required to maintain the geometry against changes in plasma profiles or the current in the other poloidal field coils, has not yet been attempted.

The implementation of SFD control in NSTX-U will utilize two steps:

- Realtime tracking of simultaneous X-point will be implemented, in collaboration with GA and LLNL.
- Additional terms will be added to the divertor coil feedback loops, to do snowflake divertor control.

The realtime tracking of multiple X-points will be accomplished with an algorithm that uses a local expansion of the Grad-Shafranov equation [52,53].

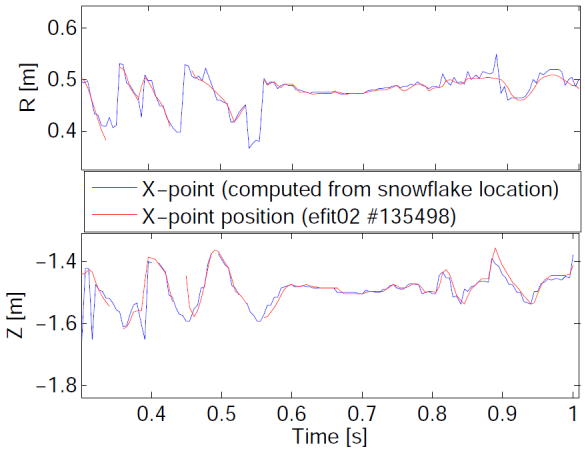

Fig. 9.10: Comparison of the X-point position computed from the tracking algorithm and the EFIT02 calculations.

$$(R+x)\frac{\partial}{\partial x}\left(\frac{1}{R+x}\frac{\partial \Psi}{\partial x}\right)+\frac{\partial^2 \Psi}{\partial z^2}=0$$

Keeping the 3rd order terms allows the dual magnetic nulls to be found given the values of the poloidal flux at three given sample points. Note that this is a one-step algorithm, which does not require any iteration. An offline version of this algorithm has been implemented and tested against the EFIT calculations as shown in Fig. 9.9. The algorithm is able to find the snowflake centroid and approximate X-point locations with good accuracy. Tracking results for the algorithm for a full shot is shown in Fig.9.10. The algorithm robustly finds the X-points at every time point without computational instabilities, which is required for essential real-time computation. A PCS version of this code will be implemented using the equilibrium reconstructions from rtEFIT to provide the poloidal flux map.

Once the X-point locations have been determined, they must be used for feedback control: this will be accomplished within the existing NSTX implementation [41] of the ISOFLUX shape control algorithm [40] as follows. The code that computed the PF coil voltages will be upgraded to contain a new term, listed second in the standard formula for the coil voltage request:

$$V_{PF} = M_{mat} PID(E_{seg}) + X_{mat} PID(E_{snow})$$

Here PID is the standard proportional, integral, and derivative error operator. E_{seg} is a column vector that contains the segment flux errors as computed by rtEFIT, while M_{mat} is a matrix which maps the elements of PID(E_{seg}) to the various coil voltage requests; both of these presently exist in the ISOFLUX control algorithm. E_{snow} is a new column vector of SFD related geometric quantities. These could include the radius and height of the primary X-point, the distance between the primary and secondary X-points, and the angle of the line connecting these X-

points. The matrix X_{mat} maps the result of the PID operator on the SFD errors to the PF coil voltage requests. In this way, closed loop control of the SFD can be completed.

The parameters to be used in these feedback loops will be determined in two steps. First, free-boundary equilibrium codes like ISOLVER will be used to determine initial guesses for the proportional control gains. Then relay-feedback techniques, as implemented for single X-point divertor control and described in Ref. [43], will be used to tune the gains for optimal control fidelity.

It is anticipated that SFD control development will begin in the first year of NSTX-U operations, with realtime tracking of the X-points and modifications to the ISOFLUX control algorithm taking place. The upper and lower PF-1A, PF-1C, and PF-2 coils will be used for control in this initial development. More advanced tuning of the algorithm will be completed in the second year of operations. A key issue to be addressed in this development is the maintenance of the up-down magnetic balance (dr_{sep}) in the presence of 4-X-points, so that the 50% power splitting between the upper and lower divertors is maintained. Experiments will also examine the maintenance of the SFD during the OH flux swing. Some calculations [11] suggest that the PF-1B coil will be necessary for precise SFD control over the full range of OH coil currents, and a decision on the powering of this coil will be made after this campaign. Final control development, including possible tuning with the additional PF-1B coils, will be complete in the third year, and use of this control in scenario development will begin at that time.

9.2.2.3.2: Radiative Divertor Control

Beyond active control of the divertor geometry, scenario and control research will assess direct control of divertor radiation via feedback control of impurity gas injections. This effort, in conjunction with the Boundary Physics (BP) research group, will be completed in two steps.

During the first two year of operations, a focused effort will be made in the BP group to determine the best realtime measurements for actuating the impurity gas flow. As described in Ref. [54], measurement options that have been identified include:

- Radiated power measurements, for instance, using AXUV diodes.
- The divertor neutral pressure, measured, for instance, by Penning gauges.
- Recombination radiation from Balmer or Paschen series deuterium lines, measured by an imaging EUV spectrometer.
- Surface temperature measurements from infrared thermography.
- Thermoelectric SOL currents.

These options will be examined for sensitivity, reliability, and ease of implementation in realtime, and dedicated efforts to bring the signals into the PCS will begin in the 2nd and 3rd years.

Simultaneously, control of appropriate gas injectors by PCS will be implemented. It is envisioned that at least two upper and two lower divertor gas injectors will be utilized, at first for open loop experiments in the BP TSG.

These development tasks can be brought together by the fourth year of NSTX-U operations. Initial closed loop control experiments will then be executed. A first step will be simple PID control, for instance, with the voltage on the gas injectors given by V=PID(E), with E the error between the reference and measured diagnostic signal. Steady-state control of the divertor radiation and reduction of the divertor heat flux should be demonstrated, for discharges much longer than the current relaxation time, and without degradation of the H-mode pedestal. If needed, and time permitting, realtime monitors of the pedestal performance will then be used to regulate the feedback, in order to prevent over-fueling of the radiating gas.

9.2.2.3.3: Research Plans By Year

The time-scale for these divertor control activities under the base program is summarized below. Under incremental funding, the radiative divertor control experiments can be accelerated by at least a year.

Year 1 of operations (2015):

- Implement realtime X-point tracking and modifications to the shape controller to allow dual X-point control. Make first attempts at snowflake divertor control.

Year 2 of operations (2016):

- Begin development of realtime heat flux or divertor radiation diagnostics.
- Optimize closed-loop control of the snowflake divertor.

Year 3-4 of operations (2017-2018):

- Finish development of realtime heat flux and radiated power diagnostics, and begin development of radiative divertor control.
- Use close-loop control of the snowflake divertor in high-current, high-power, long-pulse scenarios.

Under incremental funding, high priority would be given to accelerating the radiative divertor control development. In particular, realtime measurements associated with this control would be brought into PCS earlier in the research period, and the additional run time would allow this research to be initiated more quickly. This choice of priority supports the plan to convert most of

first wall, and a fraction of the divertors, to high-Z metal by the end of the 5 year plan period given incremental funding.

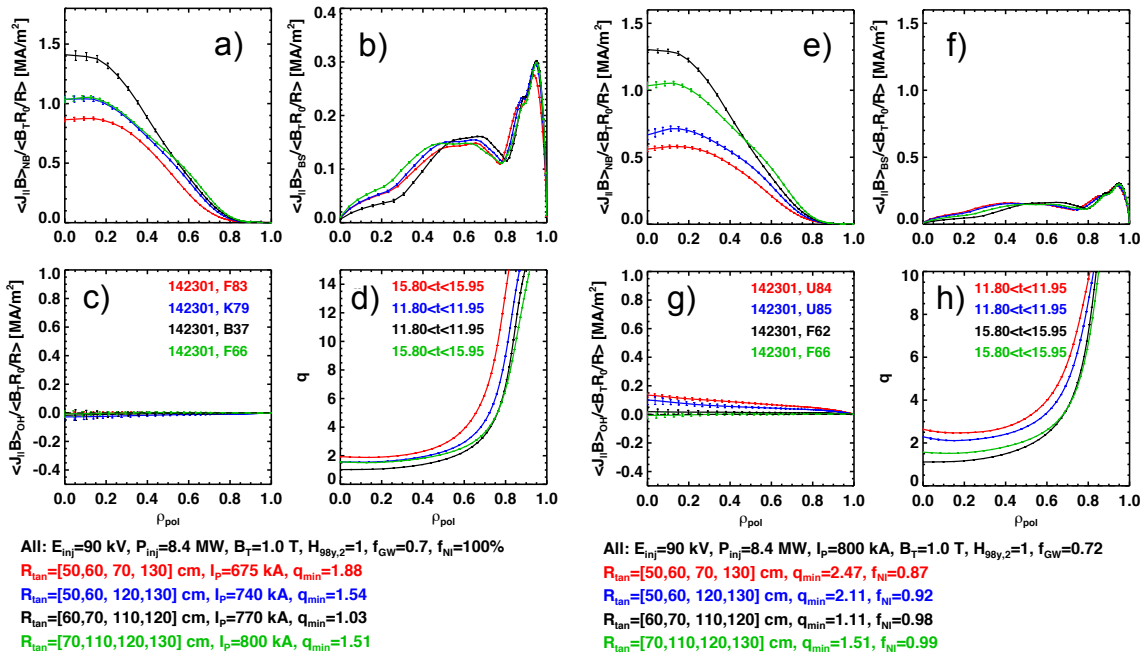

Fig. 9.11: Control of the safety factor profiles (frames d) and h)) by varying the choice of neutral beam sources. The four frames at the left are calculations at constant non-inductive fraction of 100%, while those at the right are at constant current of 800 kA.

9.2.2.4: Profile Control

The shape of the rotation and safety factor profiles can have a profound impact on the performance of the discharge. For instance, increasing the central safety factor can improve the stability of n=1 internal kink/tearing modes, but can also result in an increase in thermal transport. The correct toroidal rotation profile can result in stabilization of the resistive wall mode, while toroidal rotation shear can improve the stability of m/n=2/1 neoclassical magnetic islands. Toroidal rotation is also believed to modify the turbulent transport level through its impact on ExB shear. Hence, controlling these two profiles is critical for optimizing tokamak and ST scenarios.

9.2.2.4.1: Safety-Factor Profile Control

With regard to the safety factor profile, NSTX-U will have a number of important actuators. The impact of the plasma density on q_{min} in scenarios with large non-inductive fractions was already discussed in conjunction with Fig. 9.3, where it was shown that raising the density results in an increase in q_{min}. As shown in Ref. [19], increasing the outer plasma-wall gap increases the

elongation and the effective tangency radius of the neutral beam relative to the magnetic axis, resulting in an increase in the minimum safety factor. However, changes to the outer gap and plasma boundary shape will impact many other features of the discharge. Hence, it is important to consider a third key actuator on q_{min}: the neutral beam source selection.

Fig. 9.11 shows TRANSP calculations of the impact of variations in the beam source selection on the safety factor profile. The set of four plots on the left is done under the constraint of fixed non-inductive fraction of 100%, while the set of four plots on the right has a constant plasma current of 800 kA. The plasma is heated by four 90kV neutral beams in all cases, with a toroidal field of B_T=1.0 T and Greenwald fraction of f_{GW}=0.7. All profiles are fully relaxed, and classical beam physics is assumed.

The left hand plots show that fully relaxed q_{min} can vary between 1.0 and 1.9, and the plasma current can vary from 675 kA to 800 kA, with 100 % non-inductive current drive. The lowest-current, highest-q_{min} case uses the original three NSTX beam sources, with their lower current drive efficiency, as well as the single largest R_{tan} source of the new beamline. This combination of sources results in a slightly less peaked NBCD profile, and less overall NBCD. The lowest-q_{min} case, on the other hand, uses the four sources which produce the most central NBCD: the smaller R_{tan} sources from the new beamline and the larger R_{tan} sources from the old beamline. The highest non-inductive current level comes when using R_{tan}=[70,110,120,130] cm sources, which have the highest current drive efficiency

The right hand set of four plots show a relaxed q_{min} varying between 1.1 and 2.5, for fixed I_P = 800 kA, as the non-inductive fraction varies between 87% and 100%. Once again, the lowest q_{min} comes from using the R_{tan}=[60,70,110,120] cm beams, the first two of which are from the old beamline and the last two of which are from the new beamline, while the highest q_{min} occurs with the R_{tan}=[50,60,70,130] cm sources. The highest non-inductive current fraction comes again when using R_{tan}=[70,110,120,130] cm sources.

Initial experiments on q-control will utilize feed-forward programming to verify that the predicted variations in q_{min} will indeed occur. Experiments in the first year of operations will focus on the cases with fixed plasma current, as in Figs. 9.11e)-h). The relaxed current profiles with different beams injecting will be measured, and then compared to the predictions from classical models such as are in TRANSP; these comparisons will use the measured thermal profiles, so that transport variations can be removed from the studies. The experiments will be conducted at lower densities, where the effects of the different sources may be more profound that in Fig. 9.11, and a higher densities, where the effect may be smaller. As the non-inductive scenarios are better developed in the second and third operational years, the calculations in the left frame documenting q_{min} variations in 100% non-inductive scenarios will be experimentally

tested. These experiments will also provide data for assessing the role of *AE activity on fast ion physics, as described in Sections 9.2.4.2.

In parallel with these actuator validation/development activities, the development of current profile controllers will begin. Two parallel efforts will be required to make these efforts successful: implementation of realtime q-profile measurements, and development of appropriate control algorithms.

The realtime measurements of the q-profile will be implemented as part of the NSTX collaboration with Nova Photonics. Up to 18 channels of pitch-angle data will be available in realtime, spanning from the small-radius side of the magnetic axis to the outboard midplane SOL. It is presently envisioned that the processing of the pitch angle data, requiring very rapid acquisition, will be done on dedicated computers, and only processed pitch angle and status bits provided to the plasma control system. These pitch angle measurements will be used to constrain the rtEFIT reconstructions, providing an accurate realtime measurement of the safety factor profile. It is anticipated that this system will be developed during the 1st year of NSTX-U operations, with calibrated realtime pitch angle data available to PCS during the 2nd year. See section 10.6.3.2 for additional information on this diagnostic system.

The measurements and actuators are connected by control algorithms. These profile control algorithms are under active development and experiments are being conducted on the DIII-D tokamak. One of the aims of this DIII-D participation is to gain insight into the best possible NSTX-U profile control implementation. Based on this experience, the planned profile control for NSTX-U is based on gray box control, which relies on physics based model with experimentally obtained coefficients. These models are simplified and experimentally fitted coefficients are used to develop plasma profile control algorithms. Lehigh University collaborators have already designed and tested some q profile controls based on physics model [55,56]. The evolution of the current profile can be written from Faraday's law as [57]

$$\frac{\partial \psi}{\partial t} = \left(\frac{< \vec{E} \cdot \vec{B} >}{< R^{-2} > f} \right),$$

where f (R, Z) = RB_φ(R, Z) in the cylindrical coordinates, (R, φ, Z). This expression is then expanded to

$$\frac{\partial \psi}{\partial t} = f_1(\hat{\rho}) u_1(t) \frac{1}{\hat{\rho}} \frac{\partial}{\partial \hat{\rho}} \left(\hat{\rho} f_4(\hat{\rho}) \frac{\partial \psi}{\partial \hat{\rho}} \right) + f_2(\hat{\rho}) u_2(t)$$

using experimental obtained data $f_1(\hat{\rho})$, $f_2(\hat{\rho})$ and $f_4(\hat{\rho})$ to obtain a nonlinear diffusion equation with the forcing terms $u_1(t)$ and $u_2(t)$ which are the functions of the control actuators

such as NB and HHFW. In order to find an optimal control, the cost function, which is the sum of the error in iota and control effort,

$$J = \frac{1}{2}\int_0^1 \alpha(\hat{\rho})(\iota^*(\hat{\rho}) - \iota(\hat{\rho},T))^2 d\hat{\rho} + \frac{1}{2}\sum_{i=1}^{3}\gamma_i \int_0^T u_i^2(t)dt$$

is minimized. Extremum-seeking [55] and nonlinear-programming [56] algorithms have been considered for the numerical solution of this optimal minimization problem. Similar gray box control designs will be implemented at NSTX-U PCS for profile control. Note that initial "tuning" of these controllers will be done with TRANSP simulations of the type described above. The controllers can then be refined based on actual experimental data.

Assuming that pitch angle data from rtMSE-constrained rtEFITs are available in the 3rd year of operations, first attempts at combined q_{min} and β_N control will be done. The neutral beams, and potentially the loop voltage, will be the sole actuators for these first studies. Here, the β_N component of the control is likely a loose constraint, needed to prevent the input beam power from becoming too large or too small, both of which will lead to disruption. This combined q_{min} and β_N control will be refined in subsequent years, until it can be a reliable control tool for NSTX-U.

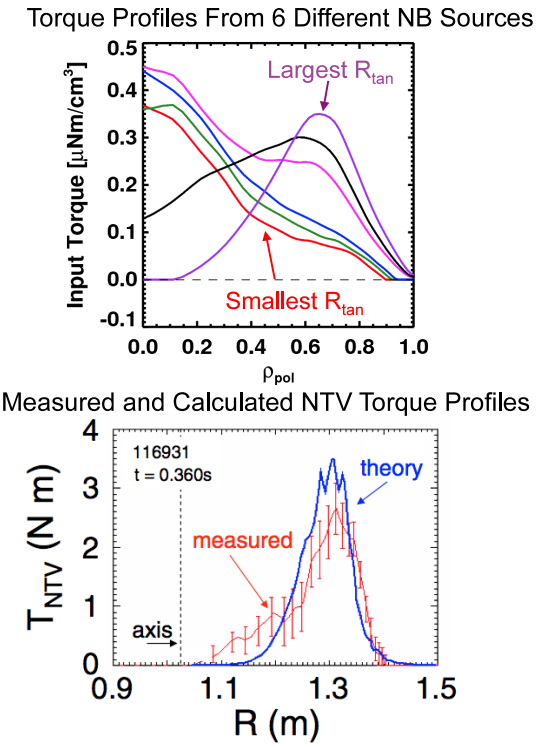

Fig. 9.12: Torque profiles from a) the six NSTX-U neutral beams, and b) applied 3D fields from NTV

In the later years of the plan, additional goals and actuators will be included. For instance, if viable schemes for HHFW heating of H-mode plasmas are developed, then the HHFW system will be included in the control loop. This will allow a heating system with no current drive, increasing the flexibility of the controllers. Research in those later years will also assess the ability to control additional points on the q-profile, instead of q_{min} alone.

The schedule for the implementation of current profile control is indicated in Section 9.2.2.4.4.

9.2.2.4.2: Rotation Profile Control

As noted in the introductory paragraph to this section, the second profile of interest for control is the rotation profile. In this case, the two actuators under consideration are the neutral beams and 3D fields.

Fig. 9.12a) shows the torque profiles for the six NSTX-U neutral beam sources. The innermost three sources, corresponding to the original NSTX beamline, produce centrally peaked torque profiles, and are not expected to have profoundly different impact on the plasma rotation beyond the different scale factors on the profiles; this was indeed the operational experience in NSTX. However, the three new sources have profoundly different torque profiles. The R_{tan}=110 cm waveform remains centrally peaked, but with a "bump" near the mid-radius. The R_{tan}=120 and 130 cm sources are peaked off axis, with the largest R_{tan} source providing minimal on-axis torque.

The second actuator for use in rotation profile control is NTV (neoclassical toroidal viscosity) magnetic braking [58-60] using the EFC/RWM coils. Experiments have shown that the torque profile from the 3D fields tends to be peaked at about the mid-radius, since the torque is proportional to $T_i^{5/2}$ (increasing inwards) and δB^2 (increasing outwards). Numerous experiments have demonstrated that magnetic braking can provide excellent open-loop control of the rotation magnitude [60,61], and it is anticipated it will be an excellent braking actuator in closed loop as well.

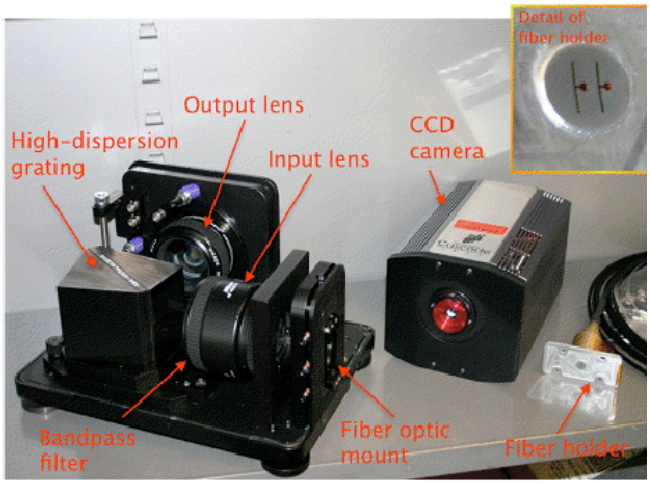

Fig. 9.13 Camera hardware associated with the RTV diagnostic.

As with q_{min} control, once the actuators have been understood, the technical steps required to implement closed loop control include the development of realtime diagnostics and the implementation of control algorithms.

With regard to realtime velocity diagnostics, the RTV system shown in Fig. 9.13 has been designed and implemented [62]. This system utilizes two cameras, each of which monitors two radial locations in the plasma. The four measurements capture the rotation in the plasma core, the plasma edge, and two intermediate locations. These locations were selected to enable an optimal resolution of the rotation profile, given the constraint that only spare fibers from the offline

toroidal CHERS system were available for use. Non-linear fitting routines are used in realtime to compute line shifts, and readout and line fitting from test light sources has been demonstrated at 1 kHz. It is anticipated that this system will be commissioned in the 1st year of NSTX-U operation, for use in control during the 2nd year.

Initial work on the development of model-based rotation control algorithms has been completed [63]. In this work, a reduced toroidal angular plasma momentum equation was obtained by examining the NSTX experimental data, as processed by the TRANSP code. The angular velocity of the plasma, ω, can be described dynamically by the flux surface average of the one-dimensional toroidal momentum equation:

$$\sum_i n_i m_i \left\langle R^2 \right\rangle \frac{\partial \omega}{\partial t} = \left(\frac{\partial V}{\partial \rho} \right)^{-1} \frac{\partial}{\partial \rho} \left[\frac{\partial V}{\partial \rho} \sum_i n_i m_i \chi_\phi \left\langle R^2 (\nabla \rho)^2 \right\rangle \frac{\partial \omega}{\partial \rho} \right] + T_{\mathrm{NBI}} + T_{\mathrm{NTV}}$$

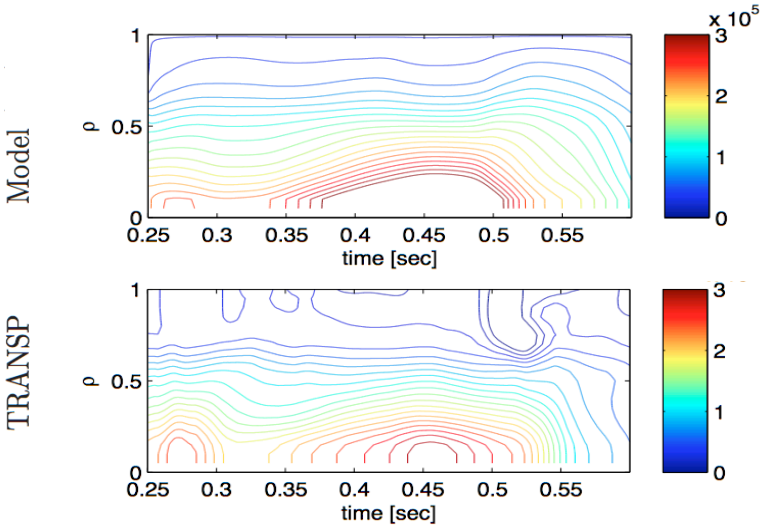

Fig. 9.14: Contour plots showing a comparison of that rotational frequency ω [rad/sec] from the simplified model and TRANSP data for shot 128020.

In this exercise, the torque from neutral beams was modeled as a Gaussian spatial distribution with a first order time constant in the temporal domain and the NTV torque was modeled as a linear function of rotation with a modified Gamma function in the spatial distribution with a first order time constant in temporal domain. The simplified rotation evolution model was validated with the NSTX experimental data as shown in Fig. 9.14, using the experimental χ_ϕ profile data. The qualitative behavior of the rotation is captured with this model and indicates that the actuator models are sufficient for model development.

Based on the actuator and the rotation evolution models new algorithms to control the rotation profile were developed. A time-dependent LQR (Linear Quadratic Regulator) control algorithm was designed using the Neutral Beams and the 3D coils as actuators. Fig. 9.15 shows a simulation of the normalized rotation profile under this control when a broad 10% average increase in rotation profile is requested. It is predicted that with the new control, regulation of the

rotation profile within the fully controllable phase space capabilities of the actuators will be possible.

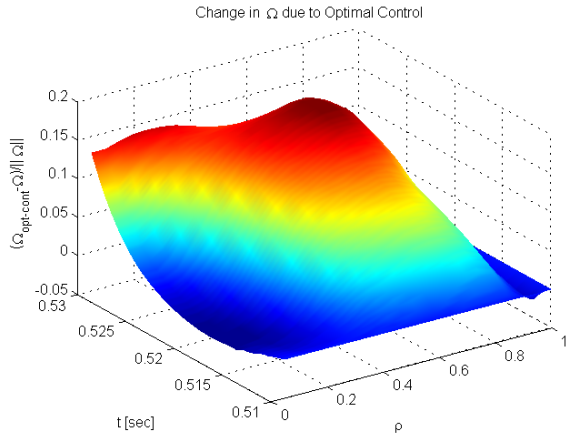

Fig. 9.15: Simulation of the normalized rotational frequency profile change of the plasma under the LQR control.

Assuming that realtime camera data is available in the 2nd year of NSTX-U operations, rotation control development will begin at that time. Work in the 2nd year will begin with combined $F_{T,0}$ and β_N control, using the NBs and 3D fields as actuators (here $F_{T,0}$ denotes the central rotation frequency). Work in the third and fourth years will extend the control to additional spatial points, for instance, the mid-radius, and potentially a point near the edge of the plasma. Furthermore, research with the MS group will begin, where rotation control is used as a component in integrated disruption avoidance studies (See section 2.2.3.1 for additional information on those studies). If schemes with reliable HHFW heating in H-mode can be identified, then HHFW will be used to provide heating without torque input in these control loops.

Finally, while q_{min} and F_T control will be implemented as somewhat separate research lines initially, the long-term goal of the research is to use them simultaneously. In the latter years of the proposal, combined control of the rotation profile, q_{min}, and β_N will be assessed and implemented if it appears feasible. Reliable schemes for HHFW heating will likely be a very beneficial for these control scenarios, in order to provide heating without torque or direct current drive.

9.2.2.4.3: Collaborations in Profile Control

Recently, PPPL has been expanding collaborations within the control engineering community. Princeton University Mechanical and Aerospace Department collaboration under the leadership of Prof. Clarence Rowley have been working on the producing reduced order models specifically useful for model-based control development. This collaboration already produced valuable solutions in strike point and boundary control. Longer-term plans are to develop integrated controllers, which can address multiple objectives (e.g., vertical mode stabilization, strike point control, shape control, and rotation control) within a single control design.

The new collaboration with Lehigh University under the leadership of Prof. Eugenio Schuster began in 2013. The aim of this work will be to study and understand the current profile dynamics

for NSTX-U, to develop current profile control algorithms that enable the efficient and optimal use of the actuators using modern model-based control approaches, and in this way to further the scientific mission of the NSTX-U. The main task of this collaboration is the development of validated reduced control-oriented dynamic models of the NSTX-U plasma current profile evolution, the diagnostic measurements, and the effect of the actuators on the plasma. Then, with these models, the collaborators will development real-time current-profile control algorithms based on the developed control-oriented dynamic models. These control algorithms will be tested and tuned using TRANSP simulations.

9.2.2.4.4: Research Plans by Year

The time-scale for these profile control activities under the base budget is as follows. Note that because the primary actuators (the neutral beams, 3D field coils) are already in the baseline plan, the rtV_ϕ diagnostic is already well along in development, and the rtMSE system is a funded collaborator diagnostic, it appears that the primary benefit of incremental funding is increased run-time, allowing the development to be completed more rapidly.

Year proceeding operations (2014):

- Do initial control designs with Princeton University and Lehigh collaborators.
- Do test stand development of the realtime MSE diagnostic.

Year 1 of operations (2015):

- Perform initial validation of q_{min} control via changes in the beam sources in partial inductive scenarios.
- Implement realtime MSE and V_ϕ diagnostics. Incorporate MSE measurements into rtEFIT.

Year 2 of operations (2016):

- Begin development of combined β_N and $F_{T,0}$ control
- Finish validation of q_{min} control via beam source selection in partial inductive scenarios, and begin validation in 100% non-inductive scenarios.

Year 3-4 of operations (2017-2018):

- Begin joint research with the MS group on integrated disruption avoidance, using rotation control as an actuator.
- Add additional spatial points to the rotation controller, for instance control of the central and edge rotation in addition to β_N.
- Begin development of combined β_N and q_{min} control, expanding to additional points on the profile as appears feasible.
- If feasible, incorporate HHFW into the profile control algorithm, for improved decoupling between heating and momentum or torque actuators.

9.2.2.5: Deuterium Inventory Control

The phrase “density control” has been used elsewhere in this plan to indicate the achievement of non-evolving plasma density, typically via the pumping provided by a new cryo-pump. This section, however, addresses closed loop control of the deuterium inventory in terms of the measurements, actuators, and control loops, to be developed in collaboration with the BP TSG as described in Chapter 4. When impurity control techniques, such as ELM pacing or the development of small-ELM regimes, are implemented, this deuterium control will facilitate control of the total plasma density. As described in section 9.2.1.2, achieving this control is critical for the development of low-collisionality operating regimes in NSTX-U.

9.2.2.5.1: Realtime Density Measurements

NSTX-U has two options for realtime density measurements. The first is a single chord FIR interferometer channel provided by UC-Davis collaborators as a new implementation of the FIReTIP diagnostic [64]. This chord is presently envisioned to be oriented toroidally, passing near the magnetic axis. Note that a conceptual design for density control using this diagnostic has already been developed and published [65]. If this diagnostic should not be available, the backup plan will be to use a realtime implementation of the Thomson scattering diagnostic (MPTS [66]). This has the advantage of better resolution of the full profile, especially at small major radius where the plasma resides during startup. However, the time resolution of the MPTS system (16.7 ms with two lasers, and 11.1 ms with a third laser upgrade) is significantly less than that of the FIReTIP system, which has sub-millisecond time resolution. Note that, as discussed in sections 9.2.2.1.1, realtime MPTS would accrue other benefits to PCS and NSTX operations in general, for instance, improved assessment of the pressure peaking factor and outer-gap if used as a constraint in rtEFIT. See chapter 10 for additional information on these diagnostics.

9.2.2.5.2: Conventional Gas Injectors

With regard to fueling actuators, initial operations in NSTX-U will use fueling from dedicated injectors on the low- and high-field sides of the machine. The low-field injectors are traditional piezo-electric injectors, and are generally used for the pre-fill and early ramp-up phase. They have characteristic opening/shut-off times of 5 ms. However, these injectors suffer from the well-known short-comings of low fueling efficiency due to the opacity of the SOL to injected neutrals, and loading of in-vessel surfaces with hydrogenic fuel.

H-mode access is generally provided by injection of gas from the high-field side [67], via a long tube running under the graphite tiles to the inboard midplane; the characteristics shut-off times of these valves are 10s of ms. Compared to the implementation in NSTX, this fueling line will be 2 times larger in diameter in NSTX-U. Furthermore, NSTX-U will not only have injectors at the

midplane and CS top (the "shoulder injector"), but also a high-field side injector half-way between the midplane and top. These changes will facilitate density control by allowing these tubes to pump out more quickly during the discharge.

Finally, two other "conventional" gas injection systems will be used on NSTX-U. A divertor gas injection system will be available, composed of two piezoelectric valves in the lower and in the upper divertor with orifices located in bull-nose tiles at the CHI gap. This system is primarily designed for radiative divertor studies, but could also be used for fueling studies. A massive gas injection (MGI) system for disruption mitigation studies will also be implemented. See section 2.2.3.3 for more information on this system.

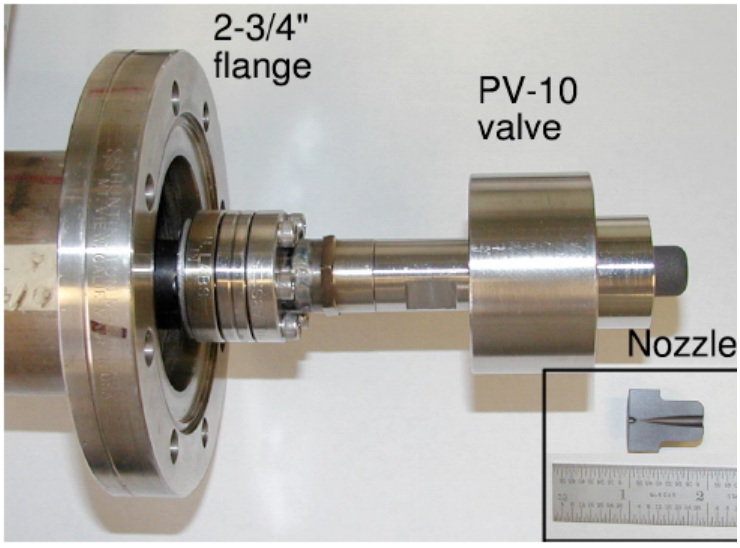

Fig. 9.16: Photograph of the SGI nozzle. The stainless steel parts are covered in a CFC shroud.

9.2.2.5.3: Supersonic Gas Injectors

The long time response of the high-field side fueling system and the low fueling efficiency of the low-field side injectors motivate the inclusion of advanced fueling systems in NSTX-U. In particular, it is desirable to minimize the amount of gas that enters the torus but does not fuel the main plasma. To this end, a supersonic gas injector (SGI) has been developed for fueling and diagnostic applications on NSTX and NSTX-U [68]. It is comprised of a graphite converging-diverging Laval nozzle and a commercial piezoelectric gas valve mounted on a movable probe on low field side midplane port. The SGI flow rate is up to 4 x 10^{21} particles/s, comparable to conventional NSTX gas injectors. The nozzle operates in a pulsed regime at room temperature with a reservoir gas pressure up to 0.33 MPa. The deuterium jet Mach number of about 4, and the divergence half-angle of 5^{o} - 25^{o}, have been measured in laboratory experiments simulating NSTX environment. Fueling efficiencies in the range 0.1 - 0.3 has been obtained from the plasma electron inventory analysis, compared to values of 0.02-0.1 using conventional injectors. This system will be integrated with the NSTX-U plasma control system, allowing it to be used for feedback applications

It is planned to develop routine use of SGI, in support of plasma operations on NSTX-U. In initial years, H-mode fueling scenarios with SGI fueling will be developed. A primary benefit of the SGI is a precise control of injected gas inventory. The SGI will support H-mode density limit

and pedestal studies, as well as perturbative transport experiments. In later years, it is planned to integrate the SGI in a feedback-control loop for active density control with PCS.

If, in the latter years of the research program, it appears that greater flexibility in fueling would be beneficial, the use of a cryogenic SGI (also known as a molecular beam/cluster injector) will be considered. Fueling efficiencies in the range of 30-60% have been observed with this technology on HL-2A [69]. Recent fueling experiments in LTX [70] indicate that cryogenic SGI can maintain high fueling efficiency even when placed far from the last closed magnetic surface; conventional SGI systems must have the nozzle near the plasma to maintain high efficiency. The increased gap between the nozzle and the plasma may prove advantageous as the total input power and pulse durations are increased. The need for such injectors, and any plans for implementation, will be assessed in conjunction with researchers from LTX, where such systems have already been developed.

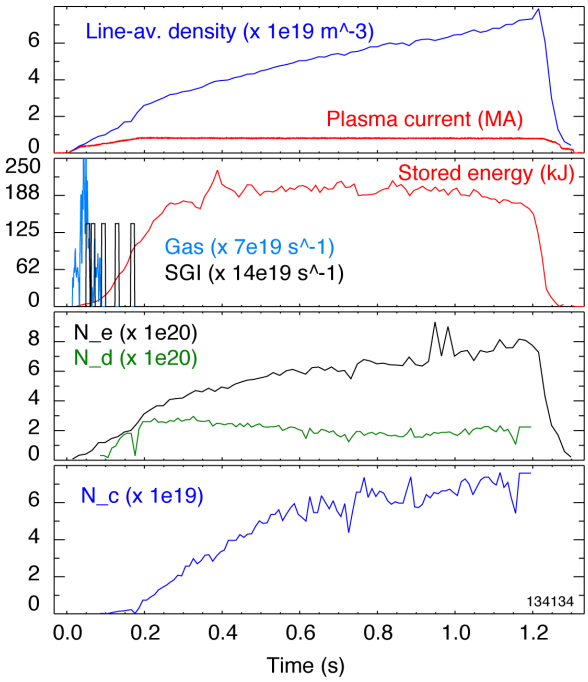

Fig.9.17: Example of deuterium inventory control using SGI and lithium pumping in a high-performance NSTX discharge. Shown from top to bottom are the line average density and the plasma current, the stored energy and gas fueling, the electron and deuteron inventories, and the carbon inventory.

9.2.2.5.4: Pumping Schemes

For deuterium pumping, NSTX-U will initially rely on lithium coatings. Note that as shown in Fig. 9.17, the combinations of actuators (low-field side fueling from the super-sonic gas injector, lithium pumping) available in the early phase of NSTX-U operation has already proven capable of producing a controlled deuterium inventory; it is the impurity accumulation that contributes to the rising electron inventory. Similar results have also been attained using traditional gas injection only. The cryo-pump will be installed between the 2nd and third years of operations, and is projected to provide sufficient deuterium pumping to meet the scenario development needs of NSTX-U. As described in Section 9.2.1.2 and the Boundary Physics chapter, various lithium coating systems and ELM pacing technologies will be used to control the impurity content in these scenarios.

9.2.2.5.5: Deuterium Inventory Control Plans

Density control experiments before the cryo-pump is installed will concentrate on the early phase of the discharge, using a PID-type controller to regulate the density. SGI will be used as the feedback actuator, and attempts will be made to develop reliable H-mode scenarios with minimal or no high-field side fueling. It is anticipated that this will facilitate improved early discharge reliability and the avoidance of early mode locking as in Fig. 9.5. This control development will be started as soon as either of the realtime density measurements are available, which may be as early as the first year in the case of the interferometer measurement.

Later experiments will use the cryo-pump to regulate the deuterium inventory. These experiments will first place the outer strikepoint in the vicinity of the cryo-pump entrance, and use the fueling feedback to control the density; both L-mode and H-mode density control will be assessed. Later experiments may, if necessary, incorporate the outer strike-point position in the density control loop, allowing the degree of pumping to be actively controlled. If successful, these combined fueling and pumping control schemes will be incorporated into the 100% non-inductive and high-current partial inductive scenarios described in section 9.2.1.

9.2.2.5.6: Research Plans by Year

The timeline for these efforts is as follows.

Year proceeding operations (2014):

- Implement PCS control of SGI.

Year 1 of operations (2015):

- Establish H-mode schemes with SGI and minimal high field side fueling.

Year 2 of operations (2016):

- Begin density feedback control development with realtime density measurements provided by interferometry (if available).

Years 3-4 of operations (2017-2018):

- Examine molecular cluster injector for advanced fueling applications.
- If interferometry is not available, then begin density feedback studies using realtime MPTS.
- Optimize combinations of cryo-pump and feedback controlled fueling to produce controlled density throughout the discharge.

9.2.3 Thrust 3: Disruption Avoidance By Emergency Stop Development

The three other thrusts in this chapter, and the research in the solenoid-free start-up group (Chapter 8), address key questions regarding plasma sustainment. However, the discharge is only complete when the stored energy and plasma current have been returned to zero. Developing the means to reliably compete this task is the subject of this section. This research program is divided into two complementary topics: detection of the need to terminate the discharge, and the actual rampdown sequencing.

This research complements the disruption avoidance techniques being developed in the MS TSG (Chapter 2), which aim to:

- develop MHD control techniques to avoid the need to terminate the discharge before the programmed rampdown, and
- develop the physics understanding of disruption mitigation techniques such as massive gas injection (MGI), and provide that technology as a potential actuator for disruption mitigation in NSTX-U if that is desired.

9.2.3.1 Realtime Determination of Need for Discharge Termination

The first step in this research sequence is to develop the necessary control system capability to determine when a discharge needs to be ramped down. Some of the necessary triggering events come from direct plasma diagnostic indicators of imminent disruption, while others are related to observation of infrastructure signals. These will be described in the following two sub-sections.

9.2.3.1.1: Engineering Indicators

In the first two years of the research program, NSTX PCS development will include the capability to automatically ramp-down the discharge based on certain non-disruptive indicators, in the hope of preventing the plasma from ever entering a disruptive state. The implementation of these indicators will include the following:

- The discharge will be ramped down before the solenoid coil reaches its current or force limit, based on extrapolation of the current waveform using the present loop voltage.
- The discharge will be ramped down if any coil systems are approaching their heating limit.

- The discharge will be ramped down if the value of χ^2 from rtEFIT is too high for a significant duration, indicating that the equilibrium reconstructions from which the shape control is derived are cannot be trusted.
- The physics operator will be able to initiate a rampdown with a single PCS waveform.

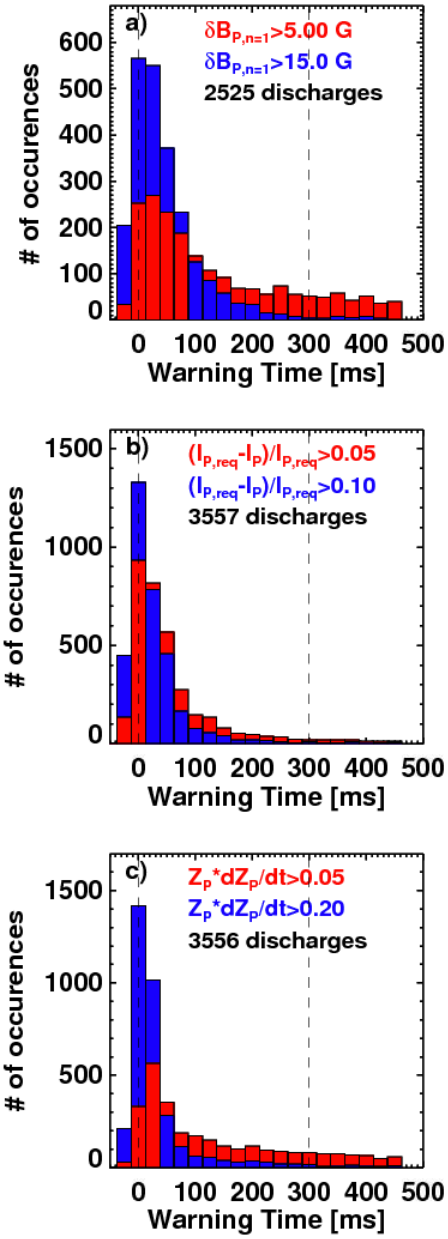

Fig 9.18: Histograms of warning times provided by threshold tests on a) the n=1 B_P amplitude, b) the plasma current deviation, and c) a measure of the vertical motion of the plasma column.

9.2.3.1.2: Data-Based Disruption Indicators

In the first two years of the research phase, ASC researchers and the MS stability group will also begin the implementation of realtime disruption detection algorithm. The initial realtime implementation will utilize the three signals in Fig. 9.18: the n=1 RWM amplitude, the plasma current deviation, and a vertical motion indicator. These diagnostics have the advantage of being already implemented in PCS, so that their output can be used for this disruption purpose immediately. The output of this disruption detector will likely be used to trigger a "fast-rampdown" of the plasma current and stored energy. Note that the data mentioned in this section are described in more detail in Ref. [71].

Fig. 9.18 shows histograms of the time between when one of these signals crosses a given threshold value and when the current quench occurs; this time is called the "warning time". Considering the n=1 B_P sensors in frame a), it can be seen that setting a threshold of 5G results in an unacceptable fraction of false positives, defined as cases where the threshold is crossed more than 300 ms before the current quench occurs. On the other hand, a threshold of 15 G results in elimination of most false positives, albeit with a significant increase in the number of late warnings. Frame b) shows a similar plot, where the quantity under consideration $\left(I_{P,req} - I_P\right)/I_{P,req}$ captures the extent to which the plasma current is less than the request; there is often a 10-30% loss

of plasma current in the phase preceding a disruption, which can be used for disruption detection. In this case, it is clear that a plasma current loss of more than 10% of the request is a good predictor of disruption. Finally frame c) shows disruption detection based on the quantity $Z_P \cdot dZ_P/dt$. This quantity has the benefit of being large when the plasma is above the midplane and moving upward rapidly, or below the midplane and moving downward rapidly. A threshold of 0.05 m^2/s results in detection with a large fraction of false positives, while increasing the threshold to 0.2 results in a reasonable disruption detector.

While the previously mentioned tests can provide a solid basis for disruption detection early in the research program, it will likely be necessary to add additional tests if the goal is to detect all disruptions with a minimal number of false positives. To this end, additional diagnostic indicators have been examined, to determine what signals should be brought in to the system in realtime.

Examples of three additional indicators are shown in Fig. 9.19, Frame a) shows an example where the ratio of measured to modeled neutron emission is used as an indicator, based on the observation that there are often large fast-particle losses due to MHD modes [72] in the phase proceeding a disruption. The neutron emission is predicted using a simple slowing down models, using n_e, T_e, and Z_{eff} measurements as input. This figure shows that the having the neutron emission drop beneath 50% of the model prediction is a good indicator of imminent disruptions. Fig. 9.19b) shows that having the core rotation drop beneath ~3.5 kHz is a good indicator of disruption; both RWMs or n=1 core/kink modes that lock to the wall contribute to these statistics. Finally, disruptions are often preceded by a rapid reduction of particle confinement, manifest as a drop in the line density. Fig. 9.19c) shows that dn_e/dt beneath $\sim -3\times10^{14}$ $1/cm^2s$ is a good indicator of imminent disruptions. These diagnostics required to implement these tests in realtime (realtime rotation, realtime Thomson scattering), are not presently available at NSTX. However, a realtime rotation diagnostic is likely to be available from the 2nd year of the research program, and a realtime Thomson scattering diagnostic may also be implemented in later years.

In order to use these many disruption indicators, it will be necessary to combine the information from the various tests. This has often been done via a neural networks (see Ref. [73] and references therein). However, NSTX researchers have explored an alternative scheme [71]. In this scheme, a series of ~15 threshold tests as defined above are evaluated at each time-slice. For each of the ~15 tests, various "point" totals are assigned to various threshold values. For instance, 1 point might be assigned for the B_P n=1 signal exceeding 5 G, 2 points for it exceeding 10 G, and 3 points for exceeding 15 G; similar assignments of point values to various thresholds have been made for all the tests. At each time step, all of the threshold tests are evaluated and the points from all tests are summed to make the aggregate point total. When this aggregate point total exceeds a given value, a disruption warning is declared.

An example distribution of warning times from these compound detection algorithms is given in Fig. 9.20, for an aggregate point total of 9 required for disruption. With this formulation, ~2.5% of disruptions have the warning declared "late", defined here as after the time 10 ms before the current quench. Approximately 3.4% of disruptions have "false positives", where the warning is more than 300 ms before the current quench. The remainder of disruptions (94%), have the disruption warning declared within 10 ms of the current quench, but not more than 300 ms before.

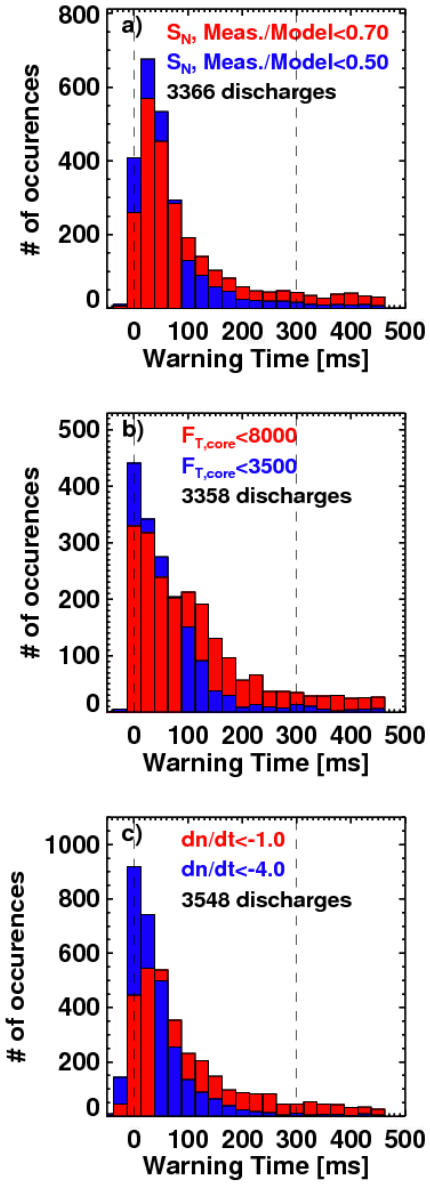

Fig. 9.19: Disruption warning time histograms, using as diagnostic indicators a) the ratio of measured to modeled neutron rate, b) the core rotation frequency, and c) the time derivative of the line-density.

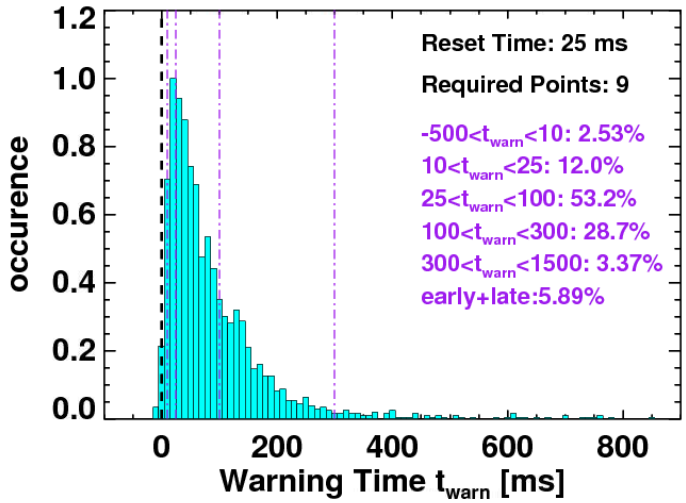

Fig 9.20: Histogram of disruption warning times using the compound disruption warning algorithm.

It is interesting to consider the sources of those false positives and missed warnings. A large fraction of the false positives are due to rotating MHD mode that slow the plasma rotation, and sometimes even lock to the wall. These are generally disruptive events, with alarms being generated due to the slowed rotation and large mode amplitudes, but the plasma does on rare occasion survive, reheat, and continue on with the discharge. The missed-warnings are dominated by rapidly growing ideal and resistive wall modes. Hence, improved control and early detection of these modes will be critical for avoiding unmitigated disruption

Future research will further establish which of the diagnostics beyond those in Fig. 9.18 & 9.19 are most important for improving the detection fidelity. These will then be translated into requirements for additional realtime diagnostics to be implemented in the later phase of the research period. These new diagnostics will be incorporated into a disruption detection algorithm, either similar to that described here, or new algorithms determined through further research.

9.2.3.1.3: Physics-Based Disruption Indicators

The methods above utilize a rather simple interpretation of the in-vessel RWM sensors for mode detection: a simple Fourier analysis is utilized to determine the n=1 distortion amplitude and phase, and a series of threshold on the distortion amplitude is defined. While this procedure generally works well, it does result in some fraction of missed disruptions. Fortuitously, as described in section 2.2.1.3, research in the macro-stability group has resulted in a state-space RWM controller [74], which can be used for disruption detection applications in addition to the feedback control role (described in more detail in section 2.2.3.1.3).

The state space controller uses a physics model for the resistive wall mode eigenfunction and plasma response, as well as a model for the 3-dimensional conducting structures in NSTX. The controller is being expanded for NSTX-U to allow independent control of the midplane RWM coil set, as well as multiple RWM eigenfunctions. The real-time computation of a model for the expected field measured by the RWM sensors (the "observer") allows the controller to determine when the differences between the modeled and measured signals are sufficiently large that feedback is no longer likely to stabilize the modes. When this occurs, a "Loss of Control" alarm will be declared, resulting in the appropriate rapid shut-down or MGI mitigation.

Similarly, the description in 9.2.3.1.2 relies on detection of plasma motion for assessing vertical stability. However, more first-principle measures of loss of vertical control will be assessed, based on the calculations described in section 9.2.2.2.2. For instance, realtime calculations of the field index will be assessed as an indicator of approaching the limits of vertical control. More sophisticated realtime evaluations of the growth rate will also be examined, for instance, with a c-language implementation of the Gspert code or relay feedback measurements. These measures will be used to determine when the limits of vertical control have been approached, and shut-down of the plasma is required.

9.2.3.2: Soft- and Hard-Stop Sequence Development

Once it is determined that the plasma discharge must be terminated, a complicated sequence of events, using multiple actuators, must be initiated. Clearly, the plasma current must be ramped down. Additionally, the heating power should be reduced sufficiently fast to reduce the plasma

energy content, but not so fast as to trigger rapid back-transitions and disruptions. The plasma shaping should be reduced, in order to prevent vertical instabilities if the internal inductance rises. It may be desirable to increase the gas fueling as well.

To begin this development, a PCS algorithm containing the rampdown initiating capabilities of 9.2.3.1 will be implemented. It appears that the tests in 9.2.3.1.1 will be used to trigger a transition to a "slow rampdown" sequence, while the disruption tests in 9.2.3.1.2 will trigger a transition to a "fast rampdown" sequence. The tests in section 9.2.3.1.3 may trigger either of these sequences. The software for developing these alarms will likely be based on the "alarm" category presently in use at DIII-D, but with modifications to increase its generality. This new alarm category will do the evaluations noted above, and at the appropriate time, issues "phase sequence changes" to the PCS code controlling the various relevant actuators (beams, PF coils, OH coil, etc.) This in turn will initiate the appropriate sequence of actions for each of these actuators.

In the first years of NSTX-U research, the basic parameters of the two rampdown sequences will be established. For the slow-rampdown sequence, which presumes that the health of the plasma is good at the start of the rampdown, a stored energy rampdown and de-shaping step will likely start the rampdown sequence. This will be followed by a reduction of the plasma current. Of course, the detection of a disruption during this phase can lead to a transition to the fast rampdown sequence.

In the fast rampdown sequence, the plasma health has already degraded to the point where a disruption is considered imminent. The timing intricacies of the "slow rampdown" sequence will likely be avoided, with deshaping and energy and current rampdowns beginning immediately. Efforts during the first years will demonstrate under what circumstances this method works. For instance, experiments will indicate circumstances when the fast rampdown sequence will bring the current down smoothly, compared to cases where the initiation of the rampdown accelerates the disruption. Those latter cases will eventually become a third branch in the rampdown scheme, trigger a mitigation method such as massive gas injection (MGI).

There is an effort in the MS group to develop massive gas injection for rapid discharge shutdown; this research program is described in thrust MS-3. As that system matures, it will be brought into this shutdown scheme as an additional branch, where MGI can be triggered based on information from the disruption detection algorithms. Note that triggering MGI while the neutral beams are injecting will not be allowed, as the increased neutral pressure can result in enhanced beam reionization in the drift duct and localized damage to the duct or vessel. With the PCS, the beams will be turned off before the MGI is triggered, preventing this potential problem.

This would allow closed-loop MGI testing, and possibly even inclusion of MGI as a routine on-line system if that is found to be desirable.

9.2.3.3: Research Plans By Year

The time-scale for these automated ramp-down experiments under the baseline budget scenario is presented in the following list. Under incremental funding, this research plan could be significantly accelerated by the additional run-time and improved realtime diagnostics (real-time MPTS earlier, real-time rotating MHD signals, realtime bolometry).

Year 1 of operations (2015):

- Implement the formulation for declaring "alarms" in PCS. These alarms will be useful for soft-stop automations, as well as general event handling in PCS.
- Implement simple algorithms to detect the need for discharge shut-down.

Year 2 of operations (2016):

- Begin development of slow- and fast- rampdown sequence

Year 3-4 of operations (2017-2018):

- Improve disruption detection schemes, including additional realtime diagnostics.
- Complete development of ramp-down sequences, and assess circumstances when these rampdown methods are insufficiently fast to interdict the disruption.
- Use the disruption detection algorithm to trigger MGI.
- Assess and implement realtime measures of vertical stability.

9.2.4 Thrust 4: Exploration of Scenario Physics of Next Step STs

Thrusts 1 through 3 described above are designed around the extensive capabilities of the NSTX-Upgrade facility. For instance, Thrust #1 attempts to optimize scenarios in NSTX-U, Thrust #2 develops control strategies with the NSTX-U actuators, and Thrust #3 develops strategies for ramping down or otherwise terminating NSTX-U discharges. However, there will be scenario research for next-step STs that is not captured in these thrusts, for instance, research exploring the basic physics leading to advanced scenarios. These research elements are captured in this fourth research thrust.

9.2.4.1: Optimal Profiles for High-β_N Steady State

9.2.4.1.1: Research Description

As described in the introduction to Section 9.2.2.3, there may be conflicting demands in determining the optimal current and rotation profiles. For instance, elevating q_{min} may be good for core stability, but deleterious for confinement. Increasing the rotation is generally beneficial,

but the optimal details of the profile shape, including the effects on tearing modes, RWMs, and micro-turbulence, remains a question for research. Both q-shear and rotation at the edge may impact the pedestal parameters. Focused experiments in the BP, MS and T&T TSGs will address each of these issues in detail, though often in lower-performance scenarios designed to improve diagnostic access or ease modeling. However, it remains a task for the ASC TSG to integrate these results.

Experiments in the later phase of the research period will address this question of optimal profiles, building on results from the first years in the following sense. The focused physics experiments in the other TSGs will give clear indication of the optimal profiles for any single goal, for instance, transport reduction or core n=1 mode stability. The control development described in Section 9.2.3.2 will additionally provide a first look at some of the underlying physics. For instance, the q_{min} control experiments will provide first data on how confinement and stability varies with q_{min}, while the rotation control experiments will provide data on how rotation impacts those two quantities.

Previously developed high-performance scenarios, likely with near-100% non-inductive current drive and strong boundary shaping, will be used for dedicated experiments. Controlled scans of the core or edge rotation with approximately fixed safety factor, and core and edge safety factor with approximately fixed rotation, will be conducted, at various values of β_N. It is likely that the non-inductive fraction or even the current level will vary in these cases, which is an acceptable compromise given realistic actuator constraints. The turbulence characteristics, global confinement, and global stability will be documented, the latter potentially via resonant field amplification (RFA) measurements [74,75] The outcome will be an improved experimental understanding of what profiles lead to simultaneously high-confinement and high β-limits. These experiments will also provide an excellent set of benchmarking discharges for the integrated modeling described in section 9.2.4.3.

This chapter is largely written in the context of standard H-mode scenarios, which provided the basis for nearly all NSTX experimental operations and the modeling described previously in this chapter. However, there may be other beneficial regimes of operation, as partially described in the boundary physics chapter, section 4.2.2. These include I-mode [76,77], regimes with internal transport barriers [78,79], and the "Enhanced Pedestal H-mode" (EPH) [80]. The last of these (EPH) is likely the most attractive for future ST development, as, in contrast to the first two, it tends to reduce the pressure peaking factor. If it appears practical, these regimes will be examined from the standpoint of developing integrated long-pulse scenarios.

9.2.4.1.2: Research Plans by Year

The research program in the area of profile optimization will have dedicated experiments weighted towards the later years, and be executed in conjunction with the T&T, BP, and MS topical science groups.

Years 1 and 2 of operations (2015-2016):

- Examine data collected from the q_{min} control experiments (at fixed I_P) to understand the confinement dependencies on q_{min}.

Years 3-4 of operations (2017-2018):

- Augment data from previous scans to complete scans of rotation, q_{min}, and q_{95}. Use data to determine optimal safety factor for next-step STs.
- Exploit research on alternative pedestal scenarios (EPH, I-mode) to develop scenarios if that research appears creditable.

9.2.4.2: Range of Validity for Classical Neutral Beam Current Drive Calculations

9.2.4.2.1: Research Description

Many of the calculations discussed above rely on the assumption that the fast ion slowing down, radial transport, and net current are determined by (neo)classical processes. However, this assumption is not always valid in the experiment. For instance, chirping TAEs and fishbone modes are known to provide anomalous transport or slowing down of the fast ions [81], and can modify the current profile [10]. Understanding the regimes in which deviations from classical behavior are observed, and the magnitude of those deviations, are critical for projecting equilibrium scenarios for ST FNSF devices.

Research in the first few years of NSTX-U operations will, in conjunction with the Energetic Particle physics research group, attempt to understand the circumstances where beam current drive is anomalous. To begin with, beam blip experiments with the new and old sources will be conducted to better understand the confinement and prompt loss of the injected fast ions, following the methodologies in Refs. [72,82]. Following this, scans of the relevant parameters (plasma density, beam voltage and tangency radius) will be conducted under the relevant high-performance H-mode discharge conditions; these scans may be accomplished as part of the q_{min} control validation experiments described in section 9.2.2.4.1, in which case they would be augmented with additional required data. The neutral beam current drive and fast ion distribution will be inferred by comparing TRANSP simulations to reconstructions of the current profile,

neutron emissions rates, FIDA signals, and fusion product rates. Any anomalies in the fast ion physics will be correlated with the plasma parameters and observed MHD activity.

Following this phase of physics study, experiments will attempt to exploit any observed non-classical behavior for improved scenarios. An example of such scenario improvement is shown in the right-hand column of Figure 9.3, where the confinement and density dependence of the non-inductive current drive sources are shown for an I_P=1.0 MA, B_T=1.0T, P_{inj}=12.6 MW with a spatially uniform anomalous fast ion diffusivity D_{FI} of 1 m^2/s. This value is roughly consistent with the largest values inferred during MHD quiescent phases in NSTX high-performance discharges [10]. This column of figures should be compared to the left column of the figure, previously discussed in the context of Section 9.2.1.1, which has no imposed fast ion diffusivity.

As might be expected, the fast ion diffusion has essentially no effect on the bootstrap current level in Fig. 9.2e). However, the central beam current drive at low density, on the left of frame f), is reduced when the fast ion diffusivity is imposed. This causes the confinement required for full non-inductive current drive in Fig. 9.2g) to increase at low density, to make up for the lost current drive. Alternatively, at lower density, the non-inductive current level for $H_{98(y,2)}$=1 will be reduced due to the loss of beam current drive.

Countering this negative result, however, is the observation in Fig. 9.2h) that q_{min} is maintained above unity over the entire range of density and confinement. This implies that the low-density limit apparently imposed in Fig 9.2d) by the onset of core n=1 MHD as q_{min} approaches 1 is eliminated in this case. Additionally, Ref [19] shows that the total pressure peaking is reduced in this case with imposed fast ion diffusivity. This has the result of improving the global stability limits, and DCON calculations indicate that, with an ideally conducting wall at the location of the NSTX passive plates, all idea n=1 modes are stable. Hence, at the expense of a reduction in current drive efficiency, a fast ion diffusivity of $1m^2/s$ results in a significant expansion of the stable operating space.

These trends are further emphasized in Fig. 9.21, where parameters of B_T=1.0 T, I_P=1.0 MA, P_{inj}=12.6 MW, f_{GW}=0.7 scenarios are shown as a function of applied fast ion diffusivity; these parameters are those near the center of the space illustrated in Fig. 9.2. As noted above, values of to ~1 m^2/s are consistent with the values inferred from MHD quiescent phases in NSTX while D_{FI}=~4 m^2/s is roughly consistent [19] with that observed in a single discharge with a string of rapid TAE avalanches [10]. It is clear from frame a) that increasing D_{FI} from 0 to 1 m^2/s reduces the central NBCD by almost a factor of 2, and that the increase to D_{fi}=4 m^2/s reduces it by half again. Fig 9.21b) shows the rapid drop in total pressure peaking with non-zero D_{FI}, an effect that tends to taper off above D_{FI}~3 m^2/s. The minimum safety factor also has the largest variation for smaller values of D_{fi}, varying from 1.25 all the way to 2 of the range of D_{FI} shown. The non-

inductive current fraction drops from 91% to 65%. Note that this strong sensitivity of the equilibrium parameters to small values of D_{FI} provides a sensitive test of the fast-ion behavior.

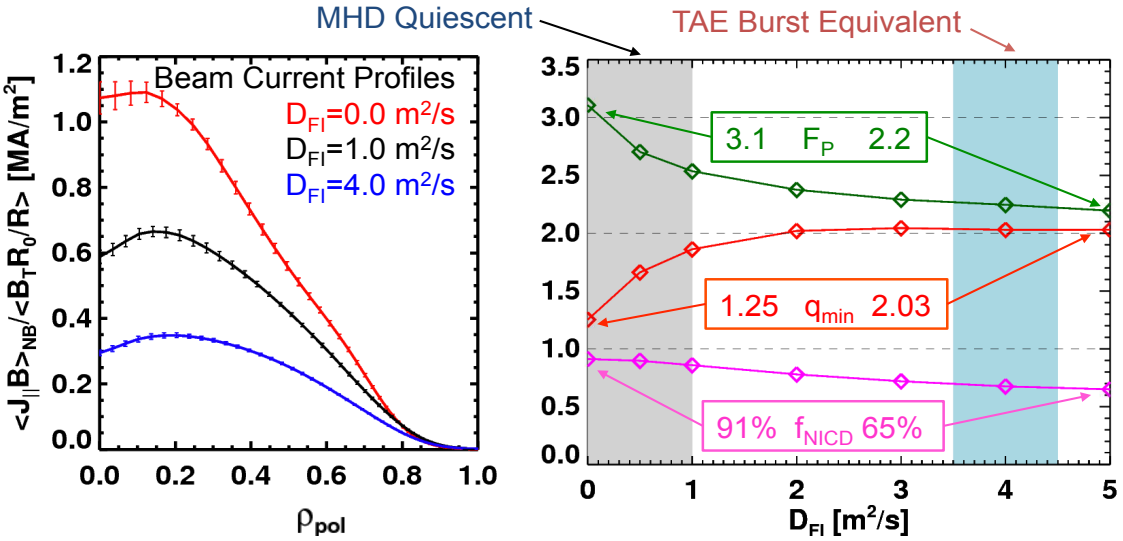

Fig. 9.21: Effect of $D_{FI}\neq 0$ on the NBCD profile (left), and on the pressure peaking (F_P), minimum safety factor, and non-inductive current fraction (right).

Regimes where Alfvénic activity was used to elevate q_{min} have been observed in DIII-D [83,84]. If similar physics can be used for control in NSTX-U, it may allow regimes with both lower density, and higher central heating power. Experiments in the final years will attempt to exploit this physics, in order to expand the high-performance operating space of NSTX-U.

9.2.4.2.2: Research Plans by Year

The research plan in this area, to be conducted in conjunction with the energetic particles research group, is as follows.

Year 1 of operations (2015):

- Make measurements of beam prompt loss and slowing down, for comparisons to TRANSP/NUBEAM calculations, over a range of beam and plasma parameters.
- Make first assessments of non-classical behavior using the q_{min} control experimental data.

Year 2 of operations (2016):

- Continue assessments of non-classical NBCD behavior, over a wide range of parameters.
- Begin comparisons of NSTX-U data to models of fast ion diffusion

Year 3-4 of operations (2017-2018):

- Continue comparisons of NSTX-U fast-ion data to models of fast ion diffusion.

- Develop, if appropriate, discharge scenarios that exploit anomalous fast ion diffusion in order to expand the high-performance operating space of NSTX-U.

9.2.4.3: Exploration and Validation of Integrated Models for FNSF and other Next-Step STs

The current drive simulations presented above are all based on calculations imposing the thermal profiles: the profile shapes are taken from experiment, and then scaled so that desired values of f_{GW} and H_{98} or H_{ST} are achieved. While this approach is useful for scenario development in NSTX & NSTX-U, where reasonable assumptions about the profile shapes and confinement levels can be made based on well documented discharges, it has insufficient predictive power for projecting scenarios for next-step STs. Rather, those projections ultimately require that the profiles of rotation, temperature, and current be modeled simultaneously, with realistic source and transport models.

Joint research between the BP, T&T, SFSU and ASC TSGs towards this end will proceed along converging paths in the proposed research program.

- The Boundary Physics group will work to develop an improved predictive understanding for the pedestal height and width. This will involve both empirical understanding of the pedestal scaling with engineering parameters (I_P, B_T, P_{inj},…), and first-principle model development and validation. This research is described in section 4.2.1.2.

- The Transport and Turbulence group will work to develop an improved predictive understanding of the core momentum and energy transport. This is an extremely complex research task, and involves the following elements. The 0D confinement trends with field current, and power, or alternatively q and υ^* will be examined in the first 2 years of NSTX-U operations; these will enable 0D projections to next-step STs with improved confidence. Next, reduced models such as TGLF will be tested against both non-linear transport simulations for NSTX-U and actual NSTX-U data; both the thermal, particle and momentum transport will be addressed, and the modified retuned if necessary. Simultaneously, electron thermal transport driven by *AE modes will be simulated, and semi-empirical models for the electron thermal transport will be developed, tested, and, if successful, incorporated into integrated predictions. This research is described in Chapter 3.

- As described in this chapter, the ASC research group, in close collaboration with energetic particle researchers, will validate the current drive predictions from codes such

as NUBEAM, and determine regimes where the (neo)classical models of fast ion current drive, slowing down, and radial transport are valid.

- Additionally, researchers will work to further refine the free-boundary equilibrium model in TRANSP. This model has already been used successfully in developing the large database of NSTX-U equilibria [19]. New capabilities include the coupling of the plasma current and PF coils to the resistive, assumed-axisymmetric, vacuum chamber, and control of the plasma boundary and current through voltage control of the PF & OH coils, using simplified power supply models. These capabilities will be especially critical when simulating the ramp-up and ramp-down of the current, a phase with large vacuum vessel currents and rapid shape variations.

Testing of these models will be an interactive process throughout the full 5-year research program. However, the focus on integrated testing of these models on the highest performance discharge scenarios will increase in the later years of the research campaign. For instance, if the core transport models cannot provide sufficient profile prediction, integrated pedestal and current drive calculations can be attempted, with prescribed core profiles. Alternatively, core transport models can be integrated with current drive calculations, using a prescribed pedestal structure. This research is facilitated by the improved multi-region capability in the PT-SOLVER upgrade to PTRANSP. In this way, progress towards integrated scenarios can be achieved even if one research area is not yet mature.

The modeling described in the previous paragraph will proceed in two steps. First, these integrated simulations will be applied to high-performance NSTX-U (and potentially MAST-Upgrade) scenarios, in order to validate the predictions. The targets for simulation will likely come from the most attractive 100% non-inductive scenarios described in section 4.2.1.1, and from the q- and rotation scans described in section 9.2.4.1. It is envisioned that some period of iteration between the integrated models and experiment will be required to improve agreement. This modeling will first focus on the steady, relaxed flat-top phase, and agreement between models and both 0D and 1D parameters will be examined. In parallel, the SFSU TSG, in collaboration with ASC, will be developing models for the plasma current ramp-up. As the two phases of the experimental discharges are brought together (see section 9.2.1.4), the modeling will also be combined.

Next, integrated simulations of next-step ST scenarios will be conducted. While the exact scenarios to be studied have not been identified, it is likely that they will be based on designs such as the PPPL pilot plant [5], PPPL FNSF [85], ORNL FNSF [2], or Culham CTF [4]. Key goals of these simulations will include determining the current drive requirements for achieving

non-inductive ramp-up and sustainment, predicting the pressure and rotation profiles for use in stability calculations, and assessing the fusion power and neutron wall loading for those devices.

9.3 Simulation Tools for Integrated Scenario Research and Control Development

Many codes are used for the development of advanced scenario plasmas and associated control systems. A summary of these codes is provided here:

9.3.1: TRANSP

The TRANSP code [86] is a critical tool for the understanding scenario physics in NSTX-U. It is described in detail in Section 3.4.1.4.

9.3.2: DCON

The DCON code provides rapid analysis of the low-n ideal stability of tokamak plasmas, and is useful for assessing the no-wall and with-wall stability limits. It is described in detail in Section 2.3.2.

9.3.3: TOKSYS

The TokSys is a modeling and simulation environment which allows closed loop simulation of the full Tokamak plasma and shape control system by connecting the plasma model to the Plasma Control System code through a simulation server (the “simserver”). While it is possible to connect different plasma models (e.g. the Corsica DIII-D model is connected to Toksys), TokSys contains its own finite element code to solve a non-rigid plasma response model based on the linearized Grad-Shafranov equation [50]. This model can be used for shape and position control development.

9.3.4: EFIT & LRDFIT:

EFIT [87] and LRDFIT [88] are codes used to construct experimental equilibria, constrained by experimental measurements of the external field and flux, measured pitch angles, and kinetic parameters. The implementation of EFIT for NSTX [89] is described in greater detail in Section 2.3.1.

9.3.5: NUBEAM

The NUBEAM [90] Monte-Carlo code is used to compute the neutral beam heating and current drive parameters for scenario development. It is generally used as a module within TRANSP, as described in Section 3.4.1.4.

9.3.6: Other Codes

Note that HHFW and EBW heating and current drive may become more important to advanced scenario research in the later years of the plan. These schemes have dedicated codes (TORIC, AORSA, GENRAY, CQL3D) that are described at the end of Chapter 7. Similarly, reduced transport models will be tested on high-performance discharges. The codes that manifest these models are discussed at the end of chapter 3.

9.4 Research Timeline

The projected research timeline under base funding is shown below. Under incremental funding, additional run-weeks and staff would allow the research program to be accelerated. Additionally, the more rapid transition to a high-Z first wall will provide more stringent tests of the scenario extrapolability to next-step ST devices.

There are a number of tasks summarized in by the phrase “Run Prep.” in this timeline. These include commissioning tasks done in tandem by the physics and engineering staffs, such as commissioning of the gas injection system, high-speed data links for the control system, and operations magnetic diagnostics, as well as upgrades to the plasma control system to support initial operations.

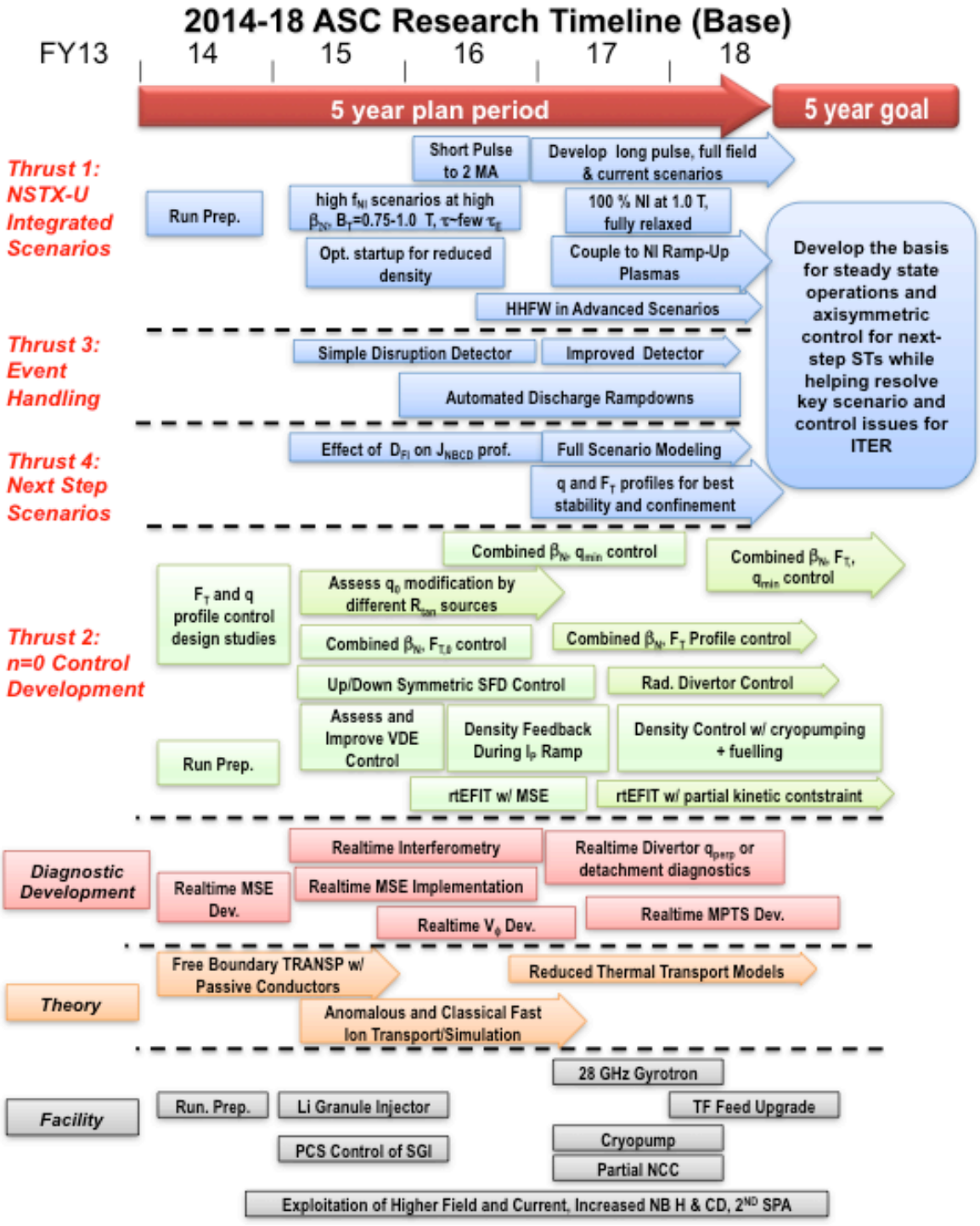
2014-18 ASC Research Timeline (Base)
FY13
14
15
16
17
18
5 year plan period
5 year goal
Thrust 1: NSTX-U Integrated Scenarios
Short Pulse to 2 MA
Develop long pulse, full field & current scenarios
Run Prep.
high f_{NI} scenarios at high β_N, B_T=0.75-1.0 T, τ~few τ_E
100 % NI at 1.0 T, fully relaxed
Opt. startup for reduced density
Couple to NI Ramp-Up Plasmas
HHFW in Advanced Scenarios
Develop the basis for steady state operations and axisymmetric control for next-step STs while helping resolve key scenario and control issues for ITER
Thrust 3: Event Handling
Simple Disruption Detector
Improved Detector
Automated Discharge Rampdowns
Thrust 4: Next Step Scenarios
Effect of D_{FI} on J_{NBCD} prof.
Full Scenario Modeling
q and F_T profiles for best stability and confinement
Thrust 2: n=0 Control Development
Combined β_N, q_{min} control
Combined β_N, $F_{T,}$ q_{min} control
F_T and q profile control design studies
Assess q_0 modification by different R_{sep} sources
Combined β_N, $F_{T,0}$ control
Combined β_N, F_T Profile control
Up/Down Symmetric SFD Control
Rad. Divertor Control
Assess and Improve VDE Control
Density Feedback During I_p Ramp
Density Control w/ cryopumping + fuelling
Run Prep.
rtEFIT w/ MSE
rtEFIT w/ partial kinetic contstraint
Diagnostic Development
Realtime Interferometry
Realtime Divertor q_{perp} or detachment diagnostics
Realtime MSE Dev.
Realtime MSE Implementation
Realtime V_ϕ Dev.
Realtime MPTS Dev.
Theory
Free Boundary TRANSP w/ Passive Conductors
Reduced Thermal Transport Models
Anomalous and Classical Fast Ion Transport/Simulation
Facility
28 GHz Gyrotron
Run. Prep.
Li Granule Injector
TF Feed Upgrade
PCS Control of SGI
Cryopump
Partial NCC
Exploitation of Higher Field and Current, Increased NB H & CD, 2ND SPA

References

[1] Y.-K. M. Peng, et al., Plasma Phys. Control. Fusion **47** (2005) B263.
[2] Y.-K. M. Peng, et al, Fusion Science and Technology **56** (2009) 957.
[3] R.D. Stambaugh, et al., *Candidates for a Fusion Nuclear Science Facility (FDF and ST-CTF),* Paper P2.110, 37th EPS Conference on Plasma Physics, Dublin, Ireland (2010), http://ocs.ciemat.es/EPS2010PAP/pdf/P2.110.pdf.
[4] G.M. Voss, et al., Fusion Eng. and Design **83** (2009) 1648.
[5] J.E. Menard, et al., Nuclear Fusion **51** (2011) 103014.
[6] F. Najmabadi & the ARIES team, Fusion Engineering and Design **65** (2003) 143.
[7] H.R. Wilson, et al., Nuclear Fusion **44** (2004) 917.
[8] S.P. Gerhardt, et al., Nuclear Fusion **51** (2011) 073031.
[9] J.E. Menard, et al., Phys. Rev. Lett **97** (2006) 095002.
[10] S.P. Gerhardt, et al., Nuclear Fusion **51** (2011) 033004.
[11] J.E. Menard, et al., Nuclear Fusion **52** (2012) 083015.
[12] D. Ryutov, Phys. Plasmas **14** (2007) 64502.
[13] D. Ryutov, et al., Phys. Plasmas **15** (2008) 092501.
[14] V.A. Soukhanovskii, et al., Nuclear Fusion **51** (2011) 012001.
[15] V.A. Soukhanovskii, et al, Phys. Plasmas **19** (2012) 082504.
[16] S.L. Allen, et al., *Results From Initial Snowflake Divertor Physics Studies on DIII-D*, IAEA FEC, San Diego, CA (2012).
[17] V.A. Soukhanovskii, et al., Phys. Plasmas **16** (2009) 022501.
[18] V.A. Soukhanovskii, et al., Nuclear Fusion **49** (2009) 095025.
[19] S. P. Gerhardt, et al., Nuclear Fusion **52** (2012) 083020.
[20] D.A. Gates, et al., Phys. Plasmas **13** (2006) 056122.
[21] D.A. Gates, et al., Nuclear Fusion **46** (2006) S22.
[22] S.M. Kaye, et al., Nuclear Fusion **46** (2006) 848.
[23] J.E. Menard, et al., Nuclear Fusion **45** (2005) 539.
[24] I.T. Chapman, et al., Nuclear Fusion **50** (2010) 052002
[25] I. T. Chapman, et al. Nuclear Fusion **51** (2011) 073040.
[26] J. Breslau, et al., Nuclear Fusion **51** (2011) 063027.
[27] S.P. Gerhardt, et al., Nuclear Fusion **53** (2013) 043020.
[28] J.E. Menard, et al. Nuclear Fusion **50** (2010) 045008.
[29] J.M. Canik, et al., Nuclear Fusion **50** (2010) 064016.
[30] S.P. Gerhardt, et al., Nuclear Fusion **50** (2010) 064015.
[31] J. Roth, et al., Journal of Nuclear Materials **122 & 123** (1984) 1447.
[32] See figure on page 8 of NSTX-U engineering calculation NSTXU-CALC-11-03-00, by K. Tresemer.

[33] J. Hosea, et al. Phys. Plasmas **15** (2008) 056104 (2008).
[34] D. Liu, et al., Plasma Phys. Control. Fusion **52** (2010) 025006.
[35] D. Gates, et al., Fusion Engineering and Design **81** (2006) 1911.
[36] D. Mastrovito, et al, Fusion Engineering and Design **85** (2010) 447.
[37] B.G. Penaflor, et al., *A structured architecture for advanced plasma control experiments*, Proc. 19th Symp. On Fusion Technology (Lisbon, Portugal) (16-20 September) p. 965 (1996).
[38] B.G. Penaflor, et al., Fusion Engineering and Design **71** (2004) 47.
[39] S.P. Gerhardt, et al., Fusion Sci. and Tech. **61** (2012) 11.
[40] J.R. Ferron, et al., Nuclear Fusion **38** (1998) 1055.
[41] D.A. Gates, et al., Nuclear Fusion **46** (2006) 17.
[42] E. Kolemen, et al., Nuclear Fusion **50** (2010) 105010.
[43] E. Kolemen, et al., Nuclear Fusion **51** (2011) 113024.
[44] S. A. Sabbagh, et al., Nuclear Fusion **46** (2006) 635.
[45] B. Wu et al., *Plasma vertical position control simulation of EAST Tokamak,* 31st EPS Conference on Plasma Phys. London, 28 June - 2 July 2004 ECA Vol.28G, P-5.131 (2004).
[46] E. Schuster, et al., Automatica **41** (2005) 1173.
[47] L. Scibile and B. Kouvaritakis, IEEE Transactions on Control Systems Technology **9** (2001) 148.
[48] S. Majhi, and D. P. Atherton. "Online tuning of controllers for an unstable FOPDT process." Control Theory and Applications, IEE Proceedings **147** (2000) 421.
[49] E. Kolemen et al., "*Vertical Stability of NSTX and NSTX-U*", 24th IAEA Fusion Energy Conference, October, 2012, # EX/P4-28.
[50] A. Welander et al., *Linear Plasma Response Model Based on the Solution to a Perturbed Grad-Shafranov Equation*, 52nd APS/DPP Meeting, Chicago, Illinois, 8–12 November, 2010).
[51] L. L. Lodestro and L.D. Pearlstein, Phys. Plasmas **1** (1994) 90.
[52] M.A. Makowski & D. Ryutov, "X-Point Tracking Algorithm for the Snowflake Divertor", private communication.
[53] M.V. Umansky et al., "Analysis of geometric variations in high-power tokamak divertors." LLNL Report LLNL-JRNL-410565 (2009).
[54] V.A. Soukhanovskii, et al, Rev. Sci. Instrum. **83** (2012) 10D716.
[55] Y. Ou et al., Plasma Phys. Control. Fusion **50** (2007) 115001.
[56] C. Xu, et al., Transactions on Plasma Science **38** (2010) 163.
[57] J. Blum*, Numerical Simulation and Optimal Control in Plasma Physics*, Gauthier-Villars Series, Wiley, 1989.
[58] W. Zhu, et al., Phys. Rev. Lett. **96** (2006) 225002.
[59] J.-K. Park, et al, Phys. Rev. Lett **102** (2009) 065002.
[60] S.A. Sabbagh et al., Nuclear Fusion **50** (2010) 025020.
[61] A.C. Sontag, et al., Nuclear Fusion **47** (2007) 1005.
[62] M. Podesta and R. Bell, Rev. Sci. Intrum. **83** (2012) 10D903.

[63] K. Taira, et al., *Rotational Control of Plasma in NSTX*, American Physical Society, 51st Annual Meeting of the APS Division of Plasma Physics, November 2-6, 2009, #PP8.078
[64] H. Park, et al., Rev. Sci. Instrum **70** (1999) 710.
[65] J.-W. Juhn, et al. Rev. Sci. Instrum. **81** (2010) 10D540.
[66] B.P. LeBlanc, et al., Rev. Sci. Instrum **83** (2012) 10D527.
[67] R. Maingi, et al., Plasma Phys. Control Fusion **46** (2004) A305.
[68] V. Soukhanovskii, et al., Rev. Sci. Instrum. **75** (2004) 4320.
[69] D.L. Yu, et al., Nuclear Fusion **50** (2010) 035009.
[70] D. Lundberg, "*Fueling Studies on the Lithium Tokamak Experiment*", PhD. Thesis, Princeton University, 2012.
[71] S. P. Gerhardt, et al., "*On the Predictability of Disruptions in the High-β Spherical Torus NSTX*", submitted to Nuclear Fusion (2013).
[72] W.W. Heidbrink, et al, Nuclear Fusion **43** (2003) 883.
[73] T.C. Hender, et al., Nuclear Fusion **47** (2007) S128.
[74] J.W. Berkery, et al., *Global Mode Control and Stabilization for Disruption Avoidance in High-β ST Plasmas*, paper EX/P8-07, IAEA FEC, San Diego, CA (2012).
[75] H. Reimerdes, et al., Nuclear Fusion **13** (2006) 056107.
[76] D. Whyte, et al., Nuclear Fusion **50** (2010) 105005.
[77] A.E. Hubbard, et al., Phys. Plasmas **18** (2011) 080705
[78] H.Y. Yuh, et al., Phys. Rev. Lett **106** (2011) 055003.
[79] H. Yuh, et al., Phys. Plasmas **16** (2009) 056120.
[80] R. Maingi, et al. Phys. Rev. Lett. **105** (2010) 135004.
[81] E.D. Fredrickson, et al., Phys. Plasmas **16** (2009) 122505.
[82] W.W. Heidbrink, et al, Plasma Phys. Control. Fusion **51** (2009) 125001.
[83] K.L. Wong, et al., Phys. Rev. Lett **93** (2004) 085002.
[84] K. L. Wong, et al., Nuclear Fusion **45** (2005) 30.
[85] J.E. Menard, et al., *Progress on Developing the Spherical Tokamak for Fusion Applications,* paper FTP/3-4, IAEA FEC, San Diego, CA (2012).
[86] R. J. Hawryluk, et al., "An Empirical Approach to Tokamak Transport", in Physics of Plasmas Close to Thermonuclear Conditions, ed. by B. Coppi, et al., (CEC, Brussels, 1980), Vol. 1, pp. 19-46.
[87] L. L. Lao, Nuclear Fusion **25** (1985) 1611.
[88] See http://nstx-u.pppl.gov/software/lrdfit.
[89] S.A. Sabbagh, et al., Nucl. Fusion **41** (2001) 1601.
[90] A. Pankin, et al., Comput. Phys. Commun. **159** (2004) 157.

Table of Contents for Chapter 10

Chapter 10

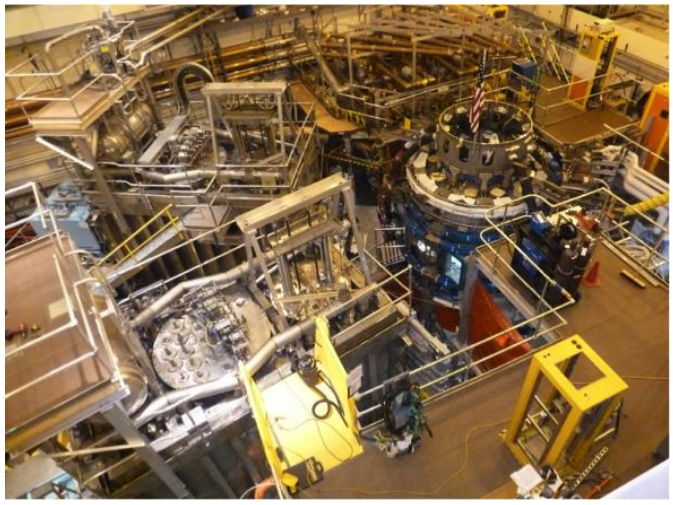

NSTX-U Facility Status and Proposed Upgrades

10.1. Introduction

The National Spherical Torus Experiment Upgrade (NSTX-U) is the world's leading spherical tokamak, combining an exceptionally wide plasma parameter space, a high degree of facility flexibility, and state-of-the-art diagnostic systems. Presently, the NSTX-U is undergoing a major upgrade construction with a new and more powerful center-stack and a tangentially injecting 2nd Neutral Beam Injection (NBI) system. The upgraded NSTX or NSTX-U will double the toroidal field from ~0.5 T to 1 T, the plasma current from ~ 1 MA to 2 MA, the NBI heating and current drive power from ~ 7 MW to 14 MW, and greatly increase the peak field plasma pulse length from 1 sec to 7 sec. The present upgrade construction is scheduled to be completed in the summer of 2014. These upgrades are aimed at achieving fully non-inductively sustained, long-pulse high-performance operation and exploring an expanded plasma parameter space in terms of higher plasma temperature and lower collisionality. The new physics regimes made accessible by these upgrades will significantly reduce the gap, and thus the uncertainty in extrapolating, from the present NSTX to projected next-step ST experiments such as the Fusion Nuclear Science Facility. From the beginning of the NSTX-U operation, it will have the capability of 6 MW High-Harmonic Fast Waves (HHFW) heating and current drive system and the coaxial helicity injection (CHI) with a project start-up current of 400 kA. In addition to advanced plasma shaping capabilities, NSTX is equipped with a set of six non-axisymmetric control coils which can be independently controlled by the Switching Power Amplifier (SPA) sources to enhance plasma stability and is also exploring and developing the use of lithium as a plasma facing material. Additional major facility hardware and diagnostic systems are proposed for the Five Year Plan to

fully take advantage of the NSTX-U facility capabilities as shown in Fig. 10.1. Attracted by its unique capabilities, NSTX-U plans to host a large number of national and international researchers (over 250 annually) with over 55 institutions participating in the research program. Nationally, the team members are from 30 universities, national laboratories, and industries. The collaborating institutions will be providing about half of the NSTX-U diagnostic systems.

10.2. Overview of Facility and Diagnostics

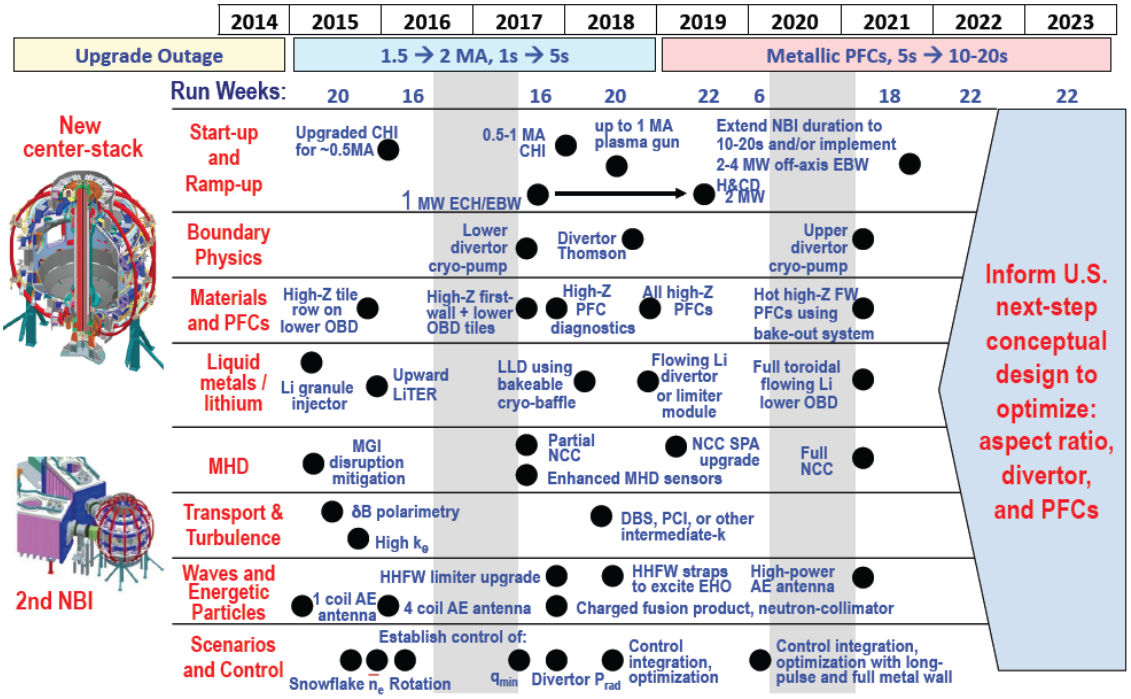

Fig. 10.1 Long-range facility upgrade vision for NSTX-U supporting ITER and FNSF with 5 YP incremental funding.

There are a number of important facility related enhancements which are needed to take full advantage of the NSTX-U device capabilities as shown in Fig. 10.1. In preparation for the NSTX-U operations and for the 2014-18 Five Year Plan, the NSTX-U facility enhancement brainstorming meeting was held on Feb. 7 and 8, 2012. Many innovative ideas were proposed to support and enhance the NSTX-U 5 Year Research Plan. In the start-up area, the CHI capability will be readied with a base capability of 0.3 – 0. 5 MA level. Further CHI upgrade for higher start-up current level for 0.5 – 1.0 MA will be implemented after the initial assessment of the performance of the base CHI system on NSTX-U. The plasma gun start-up being developed by the PEGASUS group will be implemented on NSTX-U at 0.2 – 0.4 MA level start-up capability when it is technically ready.

Further upgrades toward 1 MA start-up current for the plasma gun will be assessed after the initial gun performance on NSTX-U. A MW-class 28 GHz ECH/EBW system will be implemented at high priority to assist the start-up and ramp-up research. With favorable results, the system will be upgraded to 2 MW level to provide off-axis current drive for current profile control. For boundary physics, the divertor cryo-pump will be installed for increased particle pumping at the lower divertor after the initial operation. The divertor Thomson scattering system will be implemented as resources become available. For Materials and PFCs, the moly tiles will first be implemented in the lower divertor. After the initial assessment, the moly tile installation for both upper and lower divertor will be implemented and coverage of the first-wall with high-Z PFCs will be increased. For lithium capability, the baseline is the dual upper (lower aiming) evaporators as in NSTX. A design will be developed for an upper aiming evaporator to cover the upper divertor region. The lithium granular injector for ELM pacing which was successfully demonstrated on EAST will be available for NSTX-U. Various concepts are being considered for liquid lithium divertor system. A flowing liquid lithium loop R&D facility supported by LDRD (laboratory internal funding) is being built at PPPL. If successful, the design will be adapted for NSTX-U. The HT-7 tokamak is also testing liquid lithium PFCs. For MHD research, the massive gas injector disruption mitigation system will be implemented while the resonant field amplification (RFA) / resistive wall mode (RWM) sensors will be enhanced. For a longer term upgrade, the non-axisymmetric control coil (NCC) system is being considered and a conceptual design of NCC is being developed. For Transport and Turbulence research, an upgraded high-k scattering system with significant κ_θ component will be implemented along with a 48 channel BES for low-k turbulence measurements. A microwave polarimeter will be installed for magnetic fluctuation measurements. For high harmonic fast wave (HHFW) research, antenna enhancements are being performed to enable the HHWF feed-thru conductor to

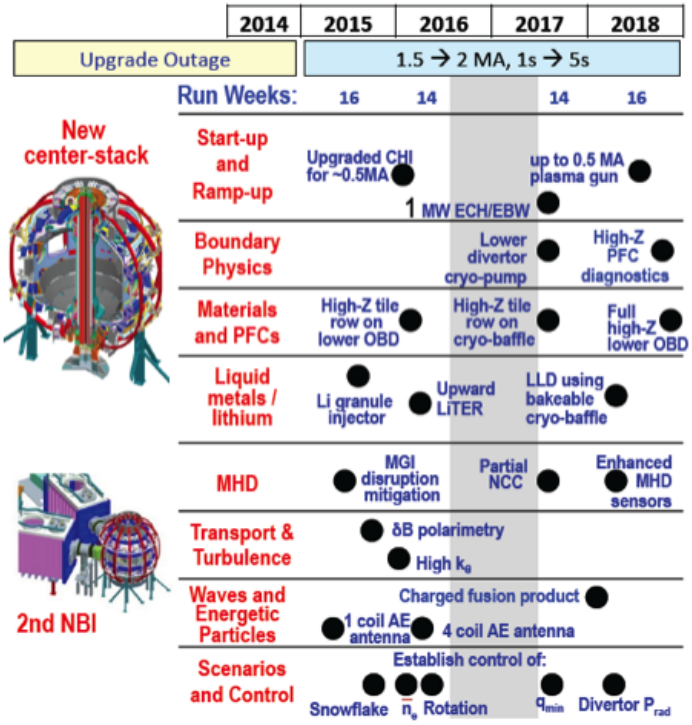

Fig. 10.2 Long-range facility upgrade vision for NSTX-U supporting ITER and FNSF with 5 YP base funding.

handle the higher disruption loads (~ x 4) in NSTX-U. A HHFW poloidal limiter upgrade to handle higher power and longer pulse NBI power is also considered for NSTX-U. Antennas for EHO and *AE excitations will also be considered after initial assessments. For Advanced Scenario and Control area, the real time plasma control system and real time diagnostic systems will be implemented for snowflake, density, rotation, and q-profile control. With the base budget without the increment, the implemental plan will be delayed as shown in Fig. 10.2. Note that several long-range facility upgrades will be delayed beyond FY 2018 in this budget scenario.

10.3. NSTX Upgrade Project Status and Plan

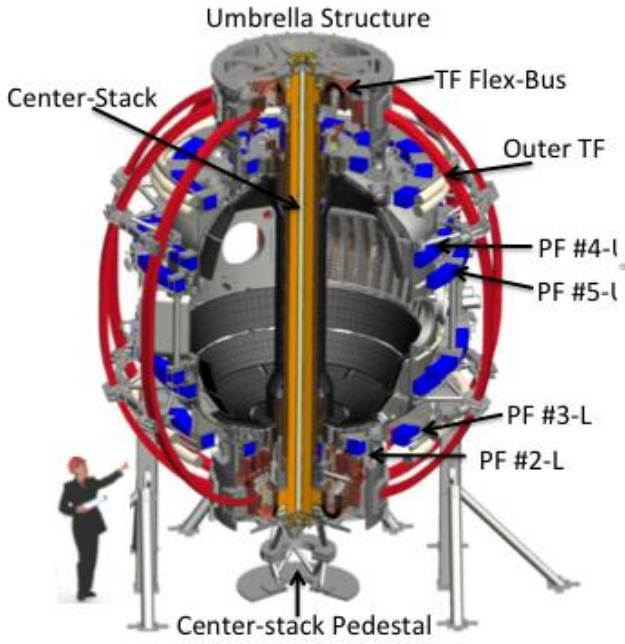

Fig. 10.3 A schematic of the NSTX-U device.

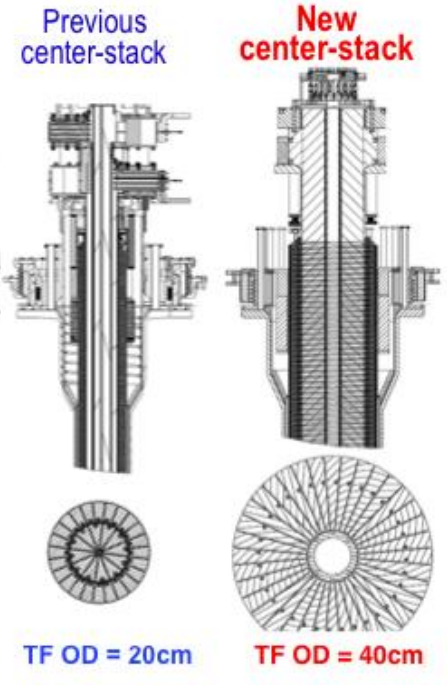

Fig. 10.4. Comparison of the new center-stack for NSTX-U and the previous one for NSTX.

The NSTX facility is presently undergoing a major upgrade with construction of a new and more powerful center-stack and a tangentially injection 2nd Neutral Beam Injection (NBI) system. The upgraded NSTX or NSTX-U will double the toroidal field from ~ 0.5 T to 1 T, the plasma current from ~ 1 MA to 2 MA, the NBI heating and current drive power from ~ 7 MW to 14 MW, and greatly increase the peak field plasma pulse length from 1 sec to 7 sec [1]. Schematics of the NSTX-U device and the new upgrade center-stack cross-section along with the previous one on NSTX are shown in Figs. 10.3 and 10.4. The larger (nearly x 4) TF conductor size enables the doubling of the toroidal field and much more extended pulse length. The larger OH solenoid radius (~ x2) enables ~ x 3 OH flux needed to support higher longer pulse plasma current as shown in Fig. 10.5. The injection geometry of the second NBI along with the existing NBI system on NSTX is shown in Fig. 10.6. The tangential injection angles of the 2nd NBI enables much higher (~ 2x) plasma current drive efficiency and current profile control needed for the fully non-inductive advanced plasma operation. In Fig. 10.7, the general arrangement of the NSTX-U Test Cell is shown with the 2nd NBI.

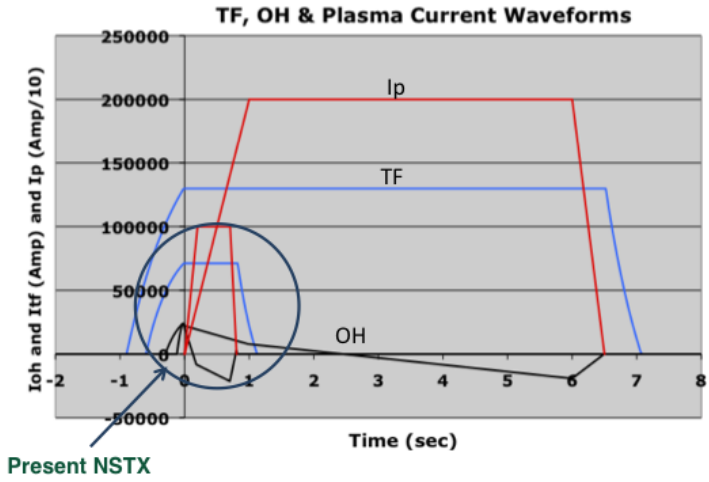

Fig. 10.5. NSTX and NSTX-U TF, OH, & Plasma Current Waveforms.

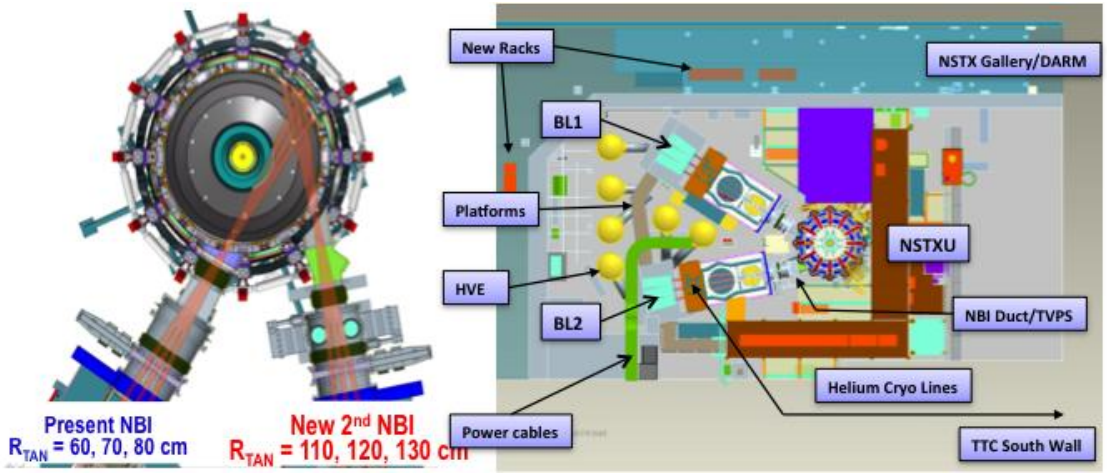

Fig. 10.6. The injection geometry of the new tangential 2nd NBI compared to the present more perpendicular NBI.

Fig. 10.7. NSTX-U Test Cell general arrangement schematic drawing with key 2nd NBI system components.

On February 23, 2009, the CD-0 Mission Need for the NSTX Upgrade Project was approved by the US Department of Energy Office of Science. During FY 2009 the conceptual design of the center-stack and NBI upgrade was carried out which culminated in a successful independent conceptual design review in October 2009. Features of the machine upgrade include; 1. a new toroidal field (TF) inner leg bundle including flags, hubs, and flexible connectors, 2. a new ohmic heating (OH) solenoid, 3. new upper and lower poloidal field (PF) coils PF1A, B, C, 4. new microtherm thermal insulation, 5. a new Center Stack Casing (CSC), 6. new plasma facing components (PFC) associated with CSC including the inboard divertor (IBD), and 7. a second beamline (BL) including the necessary structural, vacuum pumping and BL services. A successful Office of Science (Lehman) CD-2 review was conducted in August 2010 followed by an External Independent Review (EIR) in October 2010 which found the project ready to move forward with final design. DOE granted CD-2 approval in December 2010. A final design was conducted in June 2011 in preparation for a CD-3 (Critical Decision -3) Readiness Review. CD-3 approval was granted in December 2011, [2].

The NSTX upgrade outage started on Oct. 1, 2011, six months earlier than the original schedule due to the TF electrical short that occurred in FY 2011 on NSTX. After a review by a panel of external magnet experts, the lessons learned on the soft solder flux issue which led to the TF failure was incorporated into the NSTX center-stack upgrade manufacturing process to prevent similar failures for NSTX-U. This start of the upgrade outage offered an opportunity to accelerate the NSTX Upgrade Project schedule by up to six months. At the start of the outage, the NSTX diagnostics were carefully removed with proper documentation and were stored or shipped to the collaborating institutions as requested. After properly securing the NSTX facility, the NSTX operations technical staff was shifted to the Upgrade Project tasks as rapidly as possible. The NSTX technical staff also supported the NSTX-U infrastructure refurbishments including fault detector and firing generator for rectifier controls, migration of the plasma control system to modern processors, and reconfiguration of the Multi-Pulse Thomson Scattering (MPTS)

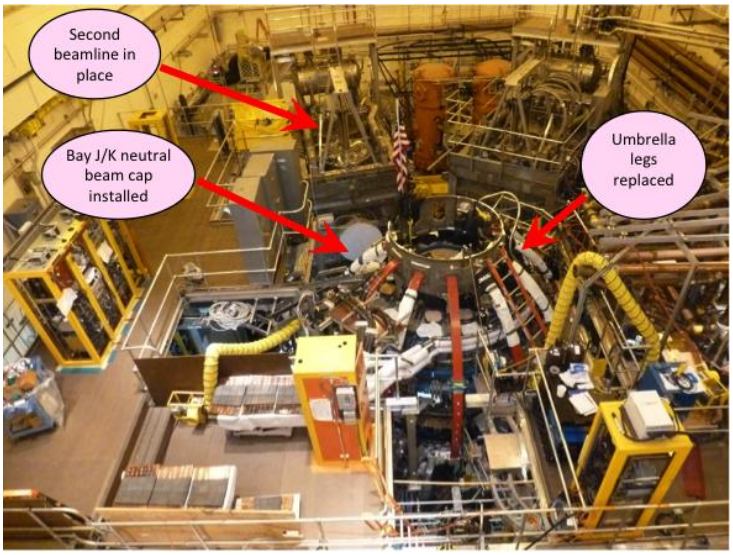

Fig. 10.8. An aerial view of the NSTX-U Test Cell with the 2nd NBI placed in its final position (March 2013).

system. The NSTX technical staff also supported outgoing collaboration activities including lithium granular injectors and droppers on EAST, RFX, and DIII-D. The NSTX Upgrade Project has made excellent progress in FY 2012. The existing center-stack and associated components have been removed from the NSTX device. The Upgrade Project activities ramped up rapidly in all areas and are currently on pace to be completed in the summer of 2014 well ahead of the Sept 2015 CD-4 completion target date. The recent NSTX-U Test Cell aerial view taken in March 2013 is shown in Fig. 10.8. To provide capabilities needed to carry out the NSTX-U scientific research, the NSTX Team identified high priority facility and diagnostic enhancements for post upgrade operations. These include diagnostics provided by NSTX Research Team members from U.S. laboratories other than PPPL. To facilitate the planning process, facility and diagnostic enhancement brainstorming meetings were held and many innovative ideas were proposed. A theory brainstorming meeting was also held, and this motivated discussion on future experimental opportunities and associated facility and diagnostic needs.

10.3.1. New Center Stack Upgrade

The new center-stack part of the NSTX Upgrade Project has multiple elements including the fabrication of the new center-stack (10.3.1.1), the structural enhancements to the device for the ~ 4x increased electromagnetic forces (10.3.1.2), and the associated sub-system enhancements to supported the doubling of the TF current and 5 sec plasma pulse length (10.3.3).

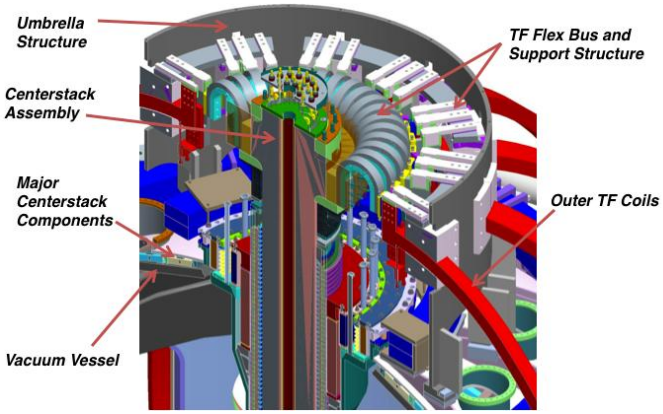

Fig. 10.9. A general arrangement drawing of upper umbrella structure area including the center-stack and TF Flex bus and associated support structure.

10.3.1.1. New Center Stack Fabrication

A general arrangement drawing of the upper umbrella structure area is shown in Fig. 10.9. The new center-stack is connected to the outer TF through 36 U-shaped TF Flex Buses. A more detailed the center-stack drawing is shown in Fig. 10.10 (a). The NSTX Upgrade Project has begun work on the critical path fabrication of the center-stack (CS) components including friction stir welding of lead extensions to the inner TF conductors.

The procurement of critical and long lead items are being carried out including the center stack plasma facing components, inner PF coils, the center-stack casing, and other TF/OH materials. During FY 2011, the design of the center-stack components including the Ohmic heating coil, inner TF bundle, Inner PF coils and the Center-stack casing was completed. The TF flex-bus is an important component to handle the TF current (130 kA) for about 7 sec while the accommodating the vertical growth of inner TF coil conductor of ~ 1cm and the electromagnetic forces. The TF flex-bus as shown in Fig. 10.10 (b) was successfully manufactured using EDM process and tested for 200,000 cycles which is more than three times the pulse cycle requirement. In FY 2012, the center-stack fabrication has started. NSTX technical staff have also set up in-house manufacturing facilities for soldering the TF cooling tubes and manufacturing of the OH and TF coils. A number of purchase orders and contracts have also been issued. These include:

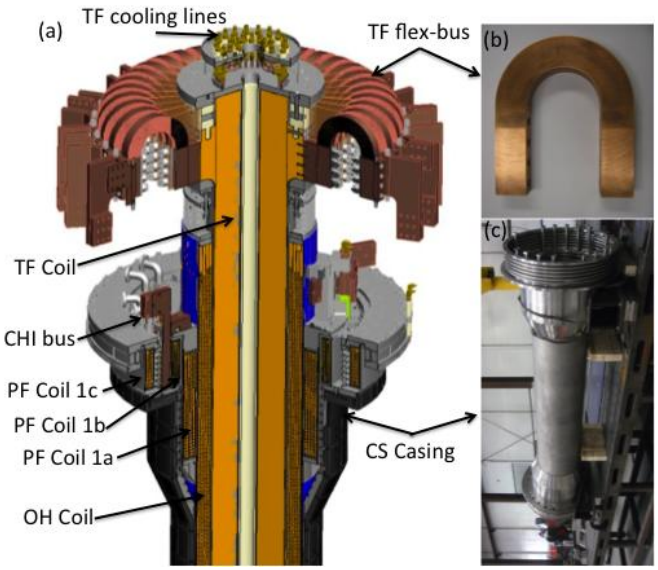

Fig. 10.10. (a) A schematic of the new center-stack and the TF joint area. (b) Fabricated flex-bus. (c) Fabricated center-stack casing.

1) Copper conductor for the Inner TF, OH and Inner PF coils were placed and they have been received. The Inner PF copper has been completed and has been shipped.
2) The machining and Friction-Stir-Welding operations for joining the joint section with the Inner TF conductor was awarded to Major Tool. All of the 36 inner TF conductors needed for making up the full TF bundle

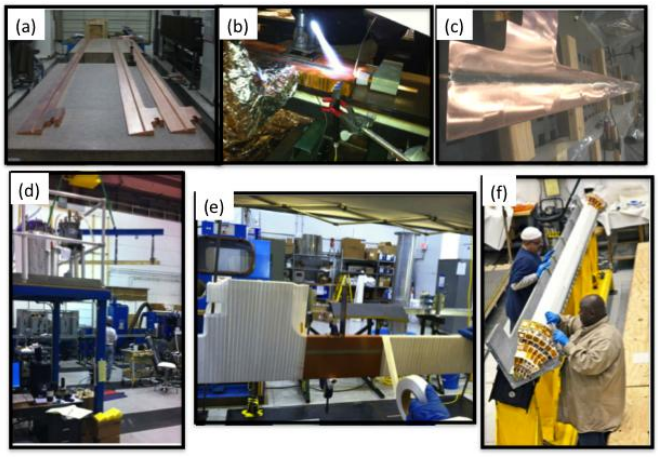

Fig. 10.11. The inner TF bundle manufacturing stages. (a) Machined conductor, (b) Cooling tube being soldered into conductor, (c) Conductor after cooling tube installation and grinding, (d) Conductor being removed from oven after sandblasting and priming, (e) Conductor being wrapped with fiberglass insulation, and (f) Insulated conductor being placed into mold.

were received along with a few spare conductors.

3) The contract for the Inconel Casing was delivered in December 2012 as shown in Fig. 10.10 (c). And
4) Requisition for the Inner PF coils and structure is ready for procurement.

The TF bundle manufacturing stages are shown in Fig. 10.11. During this past year, PPPL has developed the methodology for soldering the cooling tube into the Inner TF conductors without use of the zinc chloride based flux which caused the original TF bundle failure. The soldering operation for a full bundle has been completed. The coil fabrication area has been setup and is fully functional. The inner TF conductors for 3 quadrants have been sandblasted, primed and insulated. The insulated conductors are installed into the quadrant mold for Vacuum Pressure Impregnation (VPI) with CTD-425 (Cyanide-Ester Blend Hybrid) as shown in Fig.10.11. The first quadrant was successfully VPI'd as shown in Fig. 10.12 in early March 2013 and it passed the electrical test. Following the first VPI, the VPI for the balance of quadrants will be performed at a pace of about one quadrant per month. Once the individual Quadrants are VPI'd, the full TF bundle will be VPI'd. Then the winding of the OH coil over the full TF bundle will be performed followed by a VPI of the entire TF-OH center-bundle. In parallel, the completion of the Center-Stack Casing will begin this spring with the welding of the 700 inconel studs for mounting the carbon tiles to the walls. The carbon tiles (PFC) will then be mounted with surface diagnostics to the casing walls. Once the inner poloidal field (PF) coils arrive, they will also be joined to the casing as shown in Fig. 10.10. The completed OH/TF bundle and CS casing will be transported to the NSTX-U for final assembly. Delivery of the completed CS Assembly is scheduled for Spring 2014.

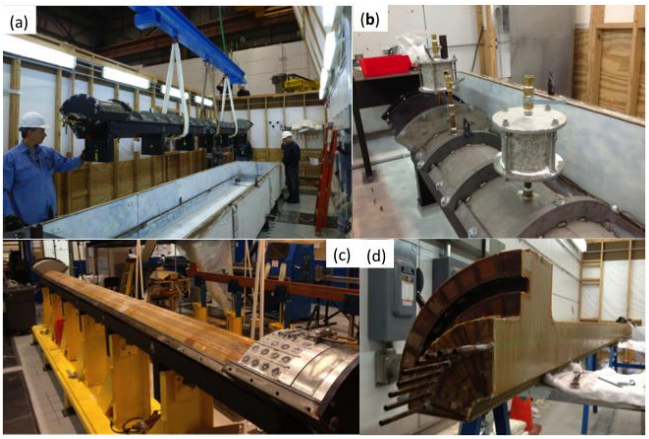

Fig. 10.12. TF Quadrant VPI. (a) TF Quadrant VPI mold lowered into the oven. (b) TF Quadrant VPI mold readied for VPI. (c) and (d) TF Quadrant after VPI.

10.3.1.2. NSTX-U Device Structural Enhancements

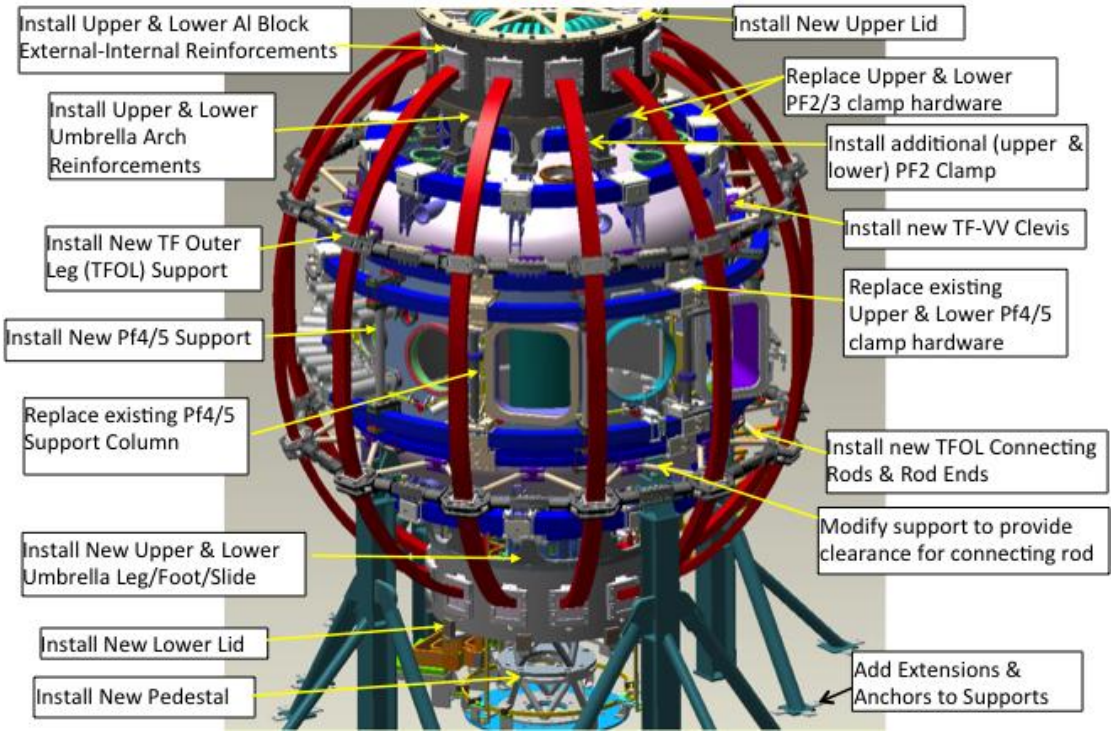

Fig. 10.13. NSTX-U support structural upgrades

I

In order to handle the anticipated 4x greater electromagnetic forces for NSTX-U, the vacuum vessel and associated magnetic field coil support structures must be enhanced accordingly. During FY 2011, the drawing details were completed for the Vacuum Vessel (VV), outer TF coil, PF coil, and passive plates support upgrades. The planned device structural upgrades are illustrated in Fig. 10.13. Procurements were placed for the fabrication of the umbrella structure reinforcements, PF 2/3 support upgrade hardware and PF 4/5 support upgrade hardware. The outer TF leg support upgrades were also fabricated. The TF-VV clevises to better support outer TF legs were welded onto the vessel. The new umbrella legs were installed on the machine.

The vacuum vessel leg attachment connections were modified to clear the clevises. In addition, since the plasma disruption forces are also expected to also increase by a factor of 4, the internal passive plates were reinforced by replacing the stainless steel attachment hardware with Inconel versions. The support structure enhancement activities are on-going. Some photos of the support structure enhancements are shown in Fig. 10. 14.

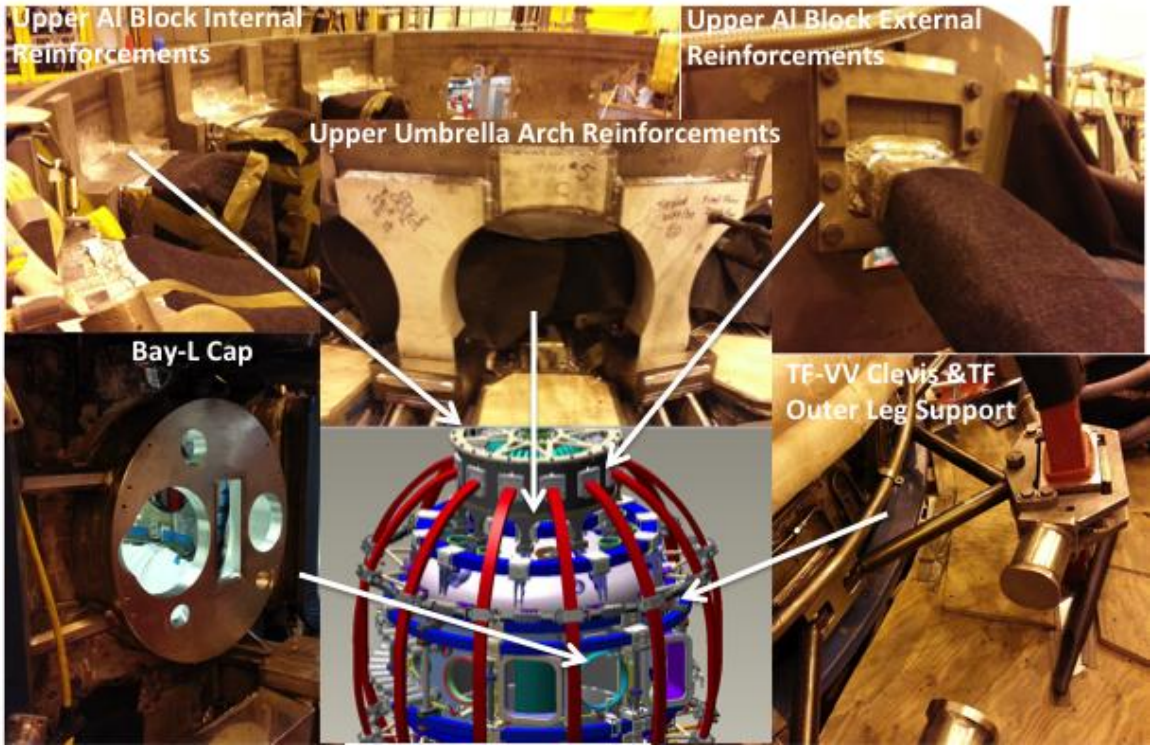

Fig. 10.14. NSTX-U support structural upgrades photos (March 2013).

10.3.2. Second Neutral Beam Injection System Upgrade

The 2nd NBI upgrade scope is to add a complete, functional second beam-line (BL) to NSTX-U at aiming tangency radii of 110, 120 and 130 cm compared to 60, 70, 80 cm for the 1st Present NBI as shown in Fig. 10.6. This task largely utilizes the existing TFTR NBI infrastructure. The 2nd NBI tasks include the TFTR NBI BL tritium decontamination, refurbishments, sources, relocation, services, power and controls, and NTC arrangements, as well as Vacuum Vessel modifications, the NBI and TVPS Duct, and NBI armor. The general drawing of the NSTX-U Test Cell with the 2nd NBI system is shown in Fig. 10.7. Decontamination of a TFTR BL began in 2009 and was deemed complete such that the BL was acceptable for use on NSTX. Refurbishment of the BL includes box, lid and cryopanels, ion dump, 90 inch flange, calorimeter, magnet, and shields, and the source platform and peripherals. Relocation involved a series of steps to make way for the BL from TFTR Test Cell (TTC) to South High Bay into the NSTX-U Test Cell (NTC) as well as the discreet equipment moves. The ion source refurbishment job has been completed and closed. The BL decontamination (decon) was performed in the TTC with full disassembly of TFTR BL4, inspection and refurbishment of components. The decon job was completed and closed. BL relocation began in September 2012. The BL box and lid were moved into the NTC and reassembled as shown in Fig. 10.15. The installation of the support structure and alignment of the BL has been completed as shown in Fig. 10.16. The refurbished 90 inch flange, ion dump, calorimeter, and bending magnet shown in Fig. 10.17 were installed on the BL. The source platform has been fully decontaminated and installed. The latest 2nd NBI view can be seen in the recent (March 2013) test cell aerial view shown in the chapter heading. Relocation also includes moving three High Voltage Enclosures (HVEs) from the TTC Basement into the NTC also. The HVEs have been prepared for removal. The pathways through the areas have been cleared. When the BL components have been removed from the TTC and the floors decontaminated, the HVEs will be brought up to the TTC floor and taken into the NTC. This work is planned for 2nd quarter FY13.

Fig. 10.15. Relocation of the 2nd NBI beam line box. (a) The beam box lifted over the NSTX-U Test Cell. (b) The beam box being lowered into the final position in the NSTX-U Test Cell. (c) The beam box being assembled.

The BL services include water, vacuum, Liquid Nitrogen (LN) and Liquid Helium (LHe) cryogenics, SF6, feedstock gas, and pneumatics. Progress includes the fabrication and installation of the LN manifolds in the NTC up to the BL, fabrication of LHe lines and valve manifolds in the NBI shops. Penetration drilling in the NTC floor for water system piping and in the NTC West wall for LHe cryogenics piping has been completed.

Fig. 10.16. 2nd NBI alignment performed and confirmed.

A water system installation package is in development for a requisition and subcontract planned for later this fiscal year. Power system progress includes the preparation of specification and purchase of all major cabling required to fully connect the N4ABC power systems from the TFTR area to the NTC location via the TFTR Test Cell Basement. The major high voltage cabling triax has been manufactured, delivered and successfully tested on site. A power cable and tray procurement package is being prepared for installation of tray and cable pulls to connect the power supplies. This subcontract will be awarded and cable and tray installed beginning later this FY 2013. The penetrations required in the NTC West wall have been completed for all of the power cabling.

Major progress on controls may be noted. Racks have been installed in the gallery area and populated with chassis electronics to control both BL1 and BL2. The Local Control Centers for N4ABC have been addressed to add NI electronics and LabView software controls. Power supply controls have been updated in the Switchyard, Surge Rooms, Mod/Regs, and Decels. Three Gradient Grid Dividers have been fabricated for the Mod/Regs. Progress continues on LCCs.

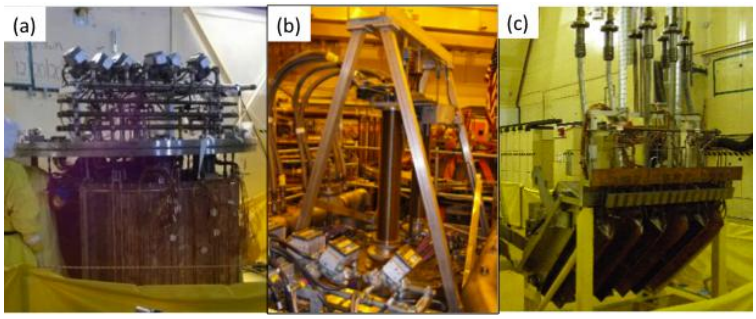

Fig. 10.17. Beam-line component refurbishment. (a) Ion Dump replacement reassembly in progress. (b) Calorimeter upgrade with double bellows – double drive in progress. (c) Bending Magnet ready for installation.

Fabrication of the NBI armor to be located inside the VV is in progress. The carbon tiles have been machined. The backing plates have been fabricated. The assembly and brazing are planned later this month in the shop. Supports have been tack welded in the vessel and will be checked with the backing plates. A Bay H port cover has been for the water and thermocouple feedthroughs. Final welding, assembly, and installation of the NBI armor was completed for January 2013. The Duct and VV modification at Bay JKhas been completed. A new Bay JK "bay window" or cap was required for accommodating the strongly tangential aiming angles. The NBI vacuum vessel modification is shown in Fig. 10.18. The opening for the new caps was cut on the VV and the welding of the new Bay JK and Bay J caps onto the VV has been completed. The rectangular bellows for the NBI duct has been fabricated and leak checked. The major flanges and structures for the duct have been fabricated or are in progress in the shops. Since the original vacuum vessel duct and the torus vacuum pump system (TVPS) located in Bay L were removed, the TVPS was incorporated into the NBI transition duct for NSTX-U as shown in Fig. 10.19. The Torus Vacuum Pump System (TVPS) ducts have been fabricated. All procurements for the duct and TVPS are delivered. The large circular and rectangular bellows have been procured, manufactured, and

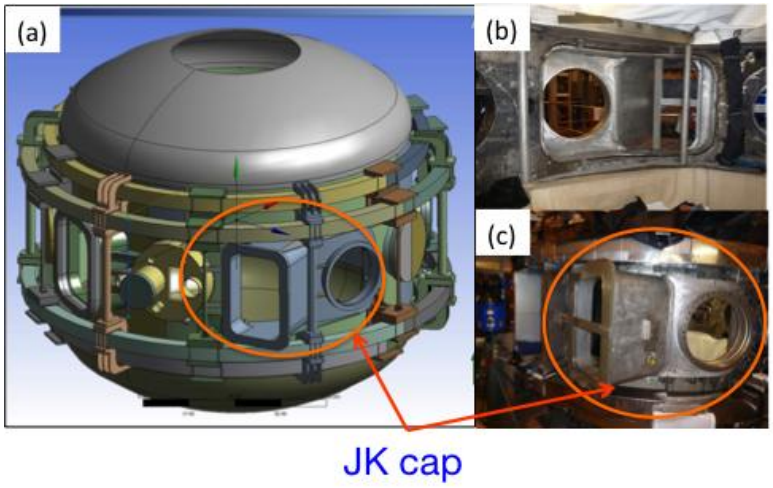

Fig. 10.18. NBI-related vacuum vessel modification (a) Modified vacuum vessel schematic. (b) Bay J-K bay window inside view. (c) Bay J-K bay window external view.

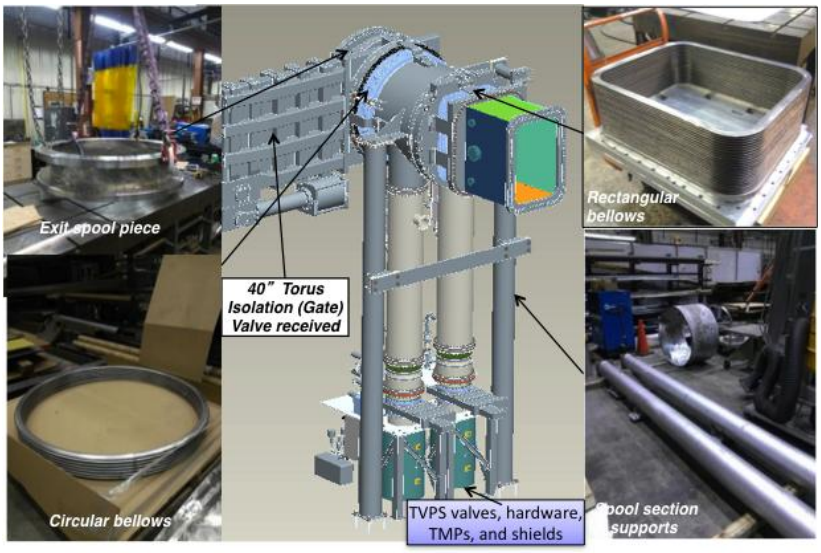

Fig. 10.19. NBI Duct and Torus Vacuum Pumping System (TVPS) components being procured and fabricated.

received. The Torus isolation Valve for the BL has been received. The NTC required extensive rearrangements to create the floor space for the BL. All rearrangements have been completed. New platforms have been installed. The TVPS racks have been moved to the gallery area. Diagnostics were removed and the Bay L pump duct was permanently removed. The BL has been located into its final position so reassembly of the locale is in progress and will continue for the rest of FY13.

With successful completion of the above tasks, preoperational testing of BL systems and N4ABC power and controls will be required to commission subsystems and confirm readiness for operations. This testing will begin in FY14 and flow into startup operations based on project baseline schedules and funding profiles.

10.3.3. NSTX-U Facility Subsystems

The NSTX TF, OH, PF1AU, PF1AL Power Systems are redesigned to meet NSTX Upgrade requirements. Other circuits remain the same. The re-design is done under space constraints of the NSTX power supply facility.

10.3.3.1. TF and OH Power Systems for NSTX Upgrade

NSTX Upgrade requires an increase in the TF field. Thus the TF feed was designed to a rating of 1kV, 129.8kA for 7.45 seconds every 2400 seconds. Also the design is such that the pulse period can be reduced to 1200 seconds in the future by providing additional power cabling in the power loop. The NSTX rating was 1kV, 71.2kA for 1.3 seconds every 300 seconds. To meet the upgrade requirements, four additional branches are added to the existing four branches. The existing four TF Safety Disconnect Switches (SDS) will be continued to be used with two parallel branches through each SDS. Extensive power cabling reconfiguration has been undertaken in the TF wing of Field Coil Power Conversion (FCPC) building. Ninety-six (about 6200 feet) TFTR-era cables are being disconnected, removed, and scrapped. Hundred of cables (about 5800 feet) are to be pulled and installed. Also additional cables from the Transition area to the NSTX test cell are to be provided for TF circuit. So far (as of March, 2013), about 70% of the installation work is completed.

New accurate fiber optic DCCTs (+/-150kA) will be provided to measure the TF current. The PF1A circuit is redesigned without the ripple suppression reactors, which were used with the previous PF1A coils. These ripple reduction reactors (the original PLT TF coils) will now be used in the upgraded OH circuit as the branch DC current limiting reactors (CLR) and the power cabling will be modified as needed. The existing OH power supply

is designed to have the capability of 6kV, +/-24kA and meets the new requirements based on PSCAD analysis.

A Digital Coil Protection (DCP) System is being designed and implemented. Protection system will be upgraded to meet the new requirements. Currently each circuit is protected from over-current, I^2 x t, higher pulse duration, and higher than permitted pulse period. In the new scheme, the forces from a combination of current in coils will also be computed and additional protection accorded. The Hardwired Control System (HCS) is being upgraded with a PLC for the TF wing. A unique TF turn to turn short detection scheme has been designed using a fiber optic DC Current Transducer (DCCT). In this scheme a fiber sensor will be installed towards the top of the machine and will interleave the 12 TF bundles detecting the differential current which will be normally zero. In the event of a fault the DCCT will detect a current and the circuit will be tripped.

10.3.3.2. Rectifier Control System Upgrades

The Transrex AC/DC Convertors of the NSTX Field Coil Power conversion System (FCPC) provide a pulsed power capability of 1800 MVA for 6 seconds every 300 seconds The modular converter concept of 74 identical, electrically isolated 6-pulse "power supply sections" was originally used on TFTR as shown in Fig. 10.20, and then adapted to NSTX which has a more complex topology including anti-parallel and three wire configurations. In order to extend the useful operational life of this system, which has remained largely unchanged since 1984, it is necessary to replace key elements of the FCPC controls. The elements to be redesigned and replaced are the Firing Generators, the Fault Detectors, the electromagnetic relays which provide the interlock logic in the "Hardwired Control System (HCS)", and the HCS to Fault Detector interface.

Fig. 10.20. Photograph of the FCPC facility.

The rationale for this refurbishment is based on the facts that many parts are nearing end-of-life due to age and wear, replacement parts are rare or unavailable, and that

performance can be improved to the NSTX-U requirements using more modern control equipment. Precise control of thyrister firing angles by the FCPC firing generators has always been necessary for NSTX operations, and becomes more critical for the new 8-parallel, 130kA TF system configuration. In addition, the ability to separately control the "A" and "B" sections of each power supply unit allows for more efficient utilization of the 74 available sections. The new Firing Generator (FG) is the highest priority task and, compared to the original FG, will deliver firing pulses with far greater resolution, precision, and repeatability, and can receive and process separate commands to the A and B sections as noted above. The prototype FG has been fully tested in a Transrex rectifier, and production units are being fabricated. The new Fault Detector (FD) provides the same functionality as the existing FD in terms of faults detected, but includes an improved external interface compatible with the present NSTX data acquisition system. The implementation of the new FD is considered a lower priority than the FG, but testing of the FD prototype has been completed in conjunction with the new FG in a Transrex rectifier.

The electromagnetic relay logic in the Hardwired Control System (HCS-Relays) is being replaced with PLC-based interlock logic. This will provide enhanced reliability via the elimination of old electronic devices, and will provide an interface to the NSTX data acquisition system which will indicate the status of all interlock logic criteria. A further improvement to the system involves the implementation of PLC compatible I/O modules to each Transrex power supply, interfacing the new FD, and connecting to the PLC in the HCS control board (HCS-FD). This feature provides a redundancy to the existing HCS fault logic, and includes the ability to see the status of each individual power supply in the loop.

10.3.3.3. Poloidal Field Coil Power Supply Upgrades

The NSTX-U Upgrade will have three PF 1 coils, PF 1A, 1B, and 1C for both upper and lower divertor regions as shown in Fig. 10.21. The new upgraded configuration would allow improved divertor configurational control and up-and-down symmetric configurations. The first-year power supply capabilities of NSTX-Upgrade will yield considerable experimental flexibility. For instance, by powering the PF-1A & Bipolar PF-1C upper and lower supplies,

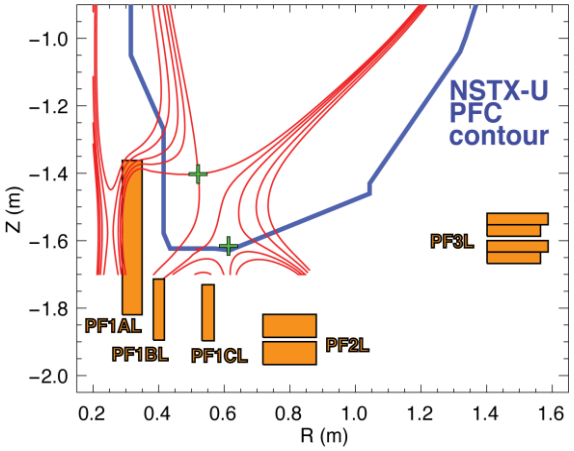

Fig. 10.21. A schematic of lower PF 1A, B, C, 2, & 3 coils in NSTX-U.

it will be possible to generate up-down symmetric snowflake divertors in NSTX-U, a capability that did not exist in NSTX. This upper and lower PF-1A and Bipolar PF1-C capability also facilitate the coaxial helicity injection current start-up research (10.5.3.1). Longer-term, the following potential upgrades to the power supply systems may add considerable new capability: The PF-2 coils, currently configured for unipolar operation, may be upgraded to bipolar operations. This will allow those coils to either create the snowflake divertor or to control the lower plasma-wall gap in the high-triangularity shapes, without changes to the power supply links. The PF-1B coil will not be powered during initial upgrade operations. However, calculations have indicated that this coil may be important for maintaining a steady snowflake divertor through the full OH swing, and that coil will be powered if this deficiency is found to be significant for operations. In future PF5 is also proposed to be upgraded to carry 34kA as compared to the existing level of 24kA.

10.3.3.4. Migrate Plasma Control System to Modern Processors

A substantial upgrade to the NSTX-U plasma control system infrastructure is occurring in parallel with the Upgrade construction activity. A new 32-core control computer has been acquired. This computer, provided by Concurrent Computer Corporation, uses the Red Hawk operating system, a version of Red Hat Enterprise Linux customized for real-time applications and equipped with numerous advanced real-time debugging and testing features. The new computer has four input data streams which, along with upgrades to the digitizers used for acquisition, will allow the sampling rate for real-time data acquisition to be increased from 5 kHz to ~25 kHz. Finally, the TFTR-legacy system for sending commands to the PF & TF coil power supplies has been updated, eliminating one of the slowest sections of the real-time data and control stream. As the date for NSTX-U operation nears, a second real-time computer will be acquired, providing a backup for NSTX-U operations and allowing parallel testing of control code during NSTX-U operations.

10.4. RF Heating and Current Drive Systems

The NSTX RF heating and current drive (CD) systems will consists of the existing 6 MW high harmonic fast wave (HHFW) system [3] and the new ECH/EBW system, which is an important element of the NSTX five year facility upgrade plan. The HHFW system is expected to perform better with higher toroidal field of NSTX-U. After the initial HHFW operation with the NSTX-U plasmas, an upgrade of the HHFW antennas is envisioned to increase the heating power and heating / CD efficiency. The ECH/EBW system is particularly crucial for the non-inductive start-up research where it can be effectively

bridge the temperature gap between the CHI based start-up plasmas which tends to be below 50 eV and the HHFW heating and CD regime which tends to be above ~ 200 eV. It is estimated that about 0.5 to 1 MW to ECH/EBW power would be sufficient to heat the CHI plasmas to ~ 200 eV range. The ECH/EBW system could also provide an efficient off-axis CD needed for advanced ST operations.

10.4.1. HHFW Upgrades

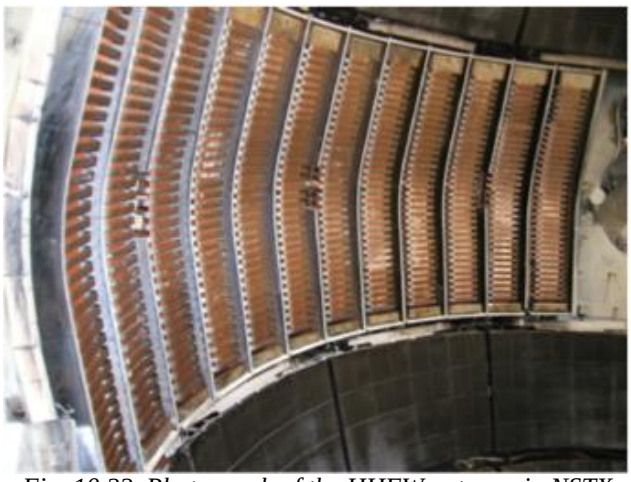

Fig. 10.22. Photograph of the HHFW antenna in NSTX.

In the HHFW area, while the system is basically unchanged, the HHWF feed-thru conductor must be modified to be able to handle the higher disruption loads (~ x 4) in NSTX-U. The HHFW antenna installed in NSTX is shown in Fig. 10.22. To handle those disruption loads, compliant connectors will be designed, tested and installed between the feed-throughs and antenna straps for the NSTX-U operations. A HHFW poloidal limiter upgrade to handle higher power and longer pulse NBI power will also be considered once the power handling requirements are obtained during the initial NSTX-U operation. In order to increase the power from the existing 12-strap HHFW antenna, RF voltage stand-off tests will be conducted on an RF test stand in FY2013-14. These tests will allow the determination of the location of RF-induced arc-prone areas so that those weak areas can be modified to achieve higher voltage stand-off. These tests will also determine if the feed-through geometry needs to be modified to achieve a higher stand-off voltage. During HHFW operations on NSTX lithium compound dust entered the HHFW antenna resulting in significant antenna arcing that limited the maximum arc-free power that could be coupled to the plasma. To mitigate this problem a double Faraday shield will be considered. If budgets permit, the RF source controls will be upgraded on sources 3 and 4 from the existing relay control system to a modern programmable logic controller (PLC) system. The RF source 1 and 2 controls will also be upgraded to a PLC system at lower priority. This should lead to a significant improvement in source reliability.

In order to provide space for the ECH/EBW launcher and antennas that can couple to edge harmonic oscillations (EHO) and/or Alfvén eigenmodes, it is possible that four of the HHFW antenna straps would be eventually removed. With improvements in antenna

voltage stand-off hoped for with the RF test stand and the reduced lithium-induced arcing resulting from installation of the double Faraday shield discussed above, it may be possible to couple sufficient HHFW power with only 8 antenna straps. Before removing the straps the 12-strap antenna will be temporarily configured for 8-strap operation so that 8-strap operation can be evaluated in NSTX-U.

10.4.2. Electron Cyclotron / Electron Bernstein Wave Heating System

A 28 GHz high-power electron cyclotron/electron Bernstein wave (EC/EBW) heating system is planned for installation on NSTX-U. Assuming the baseline (or incremental) budget this system will be installed in 2017-18. Initially this system will provide electron heating during non-inductive plasma start-up, later it will be used for off-axis EBW heating and current drive [4]. EC modeling of a CHI start-up plasma predicts significant first pass absorption even at the relatively low core electron temperatures that were typical of CHI plasmas in NSTX. For EC heating of under-dense start-up plasmas a fixed corrugated horn launcher will launch extraordinary mode (X-mode) 28 GHz power. In order to heat over-dense start-up discharges at 28 GHz a double mode conversion scheme will be employed to excite EBWs in the plasma. The scheme will use a grooved graphite mirror polarizer tile on the center column of NSTX-U to mode convert ordinary mode (O-mode) power incident from the low field side of NSTX-U, into X-mode power. The X-mode power reflected from the polarizer propagates back to the plasma, passes through the EC resonance (ECR) layer and undergoes a subsequent X-mode to EBW mode conversion near the upper hybrid resonance (UHR) layer. Then the excited EBW mode is totally absorbed before it reaches the Doppler-shifted ECR layer.

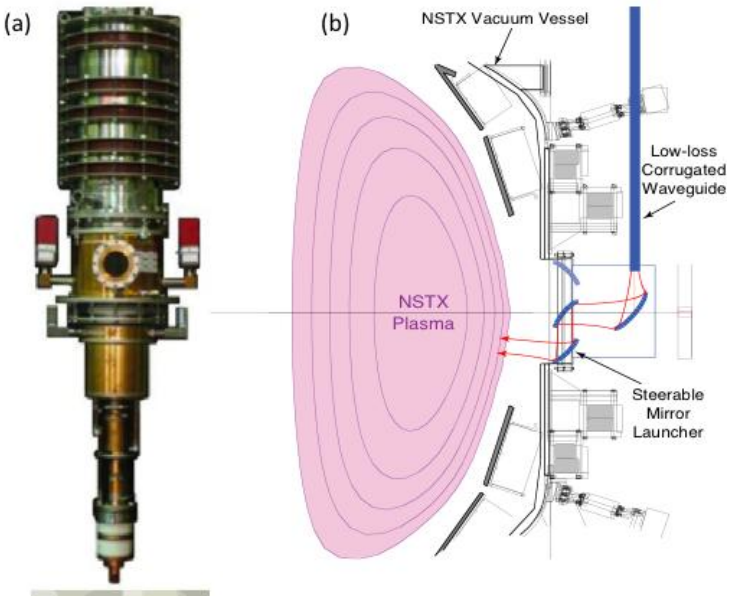

Fig. 10.23. NSTX-U ECH/EBW System. (a) 28 GHz – 1MW gyrotron tube by U. of Tsukuba. (b) A schematic of the NSTX-U ECH/EBW launcher

The EC/EBW heating system will use a 28 GHz gyrotron originally developed for EC heating in the GAMMA10 tandem mirror [5]. The gyrotron as shown in Fig. 10.23(a) has an output power of ~ 1 MW, a pulse length of up to 5 s and uses a $TE_{8,3}$ cavity mode. The gyrotron will be powered by a modified TFTR neutral beam power supply located in the former TFTR test cell located next to NSTX-U. The 28 GHz power will be transmitted to NSTX-U via low-loss, 50 mm diameter, corrugated $HE_{1,1}$ waveguide. Initially the 28 GHz heating system for heating start-up discharges. Later, when the system is used for off-axis EBW heating and current drive studies during the plasma current flattop, and the gyrotron power will be increased to 2-4 MW. A schematic of the ECH/EBW launcher is shown in Fig. 10.23 (b). Coupling to the EBWs in the plasma will be accomplished via O-mode to slow X-mode to EBW (O-X-B) double mode conversion. An actively-cooled, concave steerable mirror launcher will focus the 28 GHz power on the EBW mode conversion layer. To generate EBW current drive, in addition to EBW heating, the focal spot will be poloidally offset from the mid-plane to introduce an up-shift in parallel wave number in the plasma.

10.5 Facility Science Tools

10.5.1. Macro-stability Tools

While NSTX-U is a modification of NSTX, changes to the device conducting structure (e.g. new 2nd NBI port structure), mid-plane RWM control coils, and equilibria require re-computation of n = 1 active RWM control performance using proportional gain, and RWM state space control. The upgrade also adds new capability, such as independent control of the 6 RWM coils. The base NSTX-U 3-D MHD control coils and magnetic sensor are shown in Fig. 10.24 [6]. This new capability, combined with the upgrade of the RWM state space controller will also allow simultaneous n = 1 and n = 2 active control, along with n = 3 dynamic error field correction. Finally, the active control performance of the proposed off-mid-plane non-axisymmetric control coils (NCC) [6] also needs to be evaluated. A significant increase in controllable β_N is expected with the RWM state space control in NSTX-U, as was found for NSTX.

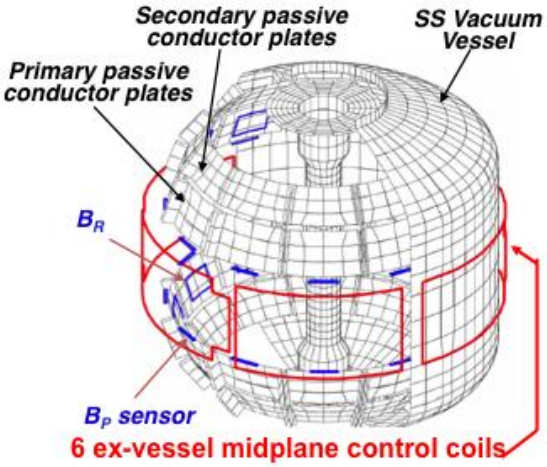

Fig. 10.24. 3-D MHD control coils and magnetic sensors.

10.5.1.1. 2nd Switching Power Amplifier (SPA)

An additional 3-channel Switching Power Amplifier was installed and commissioned in FY2011. With this addition, six SPA channels will allow each of the six non-axisymmetric radial-field perturbation coils (Fig.10.24) on NSTX-U to be powered independently, thereby providing the capability for simultaneous control of the toroidal harmonics, $n = 0 – 3$, of the applied field perturbations. The power testing of the rectifier and DC power link from the FCPC power supply hall was completed in March, 2011. Following pre-operational testing of the system and the incorporation of changes to the NSTX power supply controller to accommodate the additional SPA commands in its output stream, operation of all six SPA channels powering their respective error-field control coils was achieved in July, 2011. The basic software modifications to the higher-level Plasma Control System (PCS) software for operating and controlling the second SPA were then installed and independent programmed control by the PCS of the currents in the six error-field correction coils was demonstrated. This capability should be available for the Day-1 NSTX-U operation.

10.5.1.2. Non-axisymmetric Control Coils

Recent RWM stability calculations have been performed for NSTX-U using an expanded non-axisymmetric coil set similar to one originally proposed for NSTX [6]. The proposed non-axisymmetric control coil (NCC) will enable us to explore such variability and utility of 3D field applications, with much wider and unprecedented flexibility of field spectrum in space. In Fig. 10.25, schematics of possible NCC configurations are shown. The full toroidal NCC array (2 x 12) shown in Fig. 10.25 (a) has 12 coils in the upper and lower primary passive plate positions (see Fig. 10.24) and it is chosen to generate high toroidal harmonic perturbations up to n = 6, and also up to n = 4 rotating fields. Because of limited resources, it might be necessary to implement the NCC system in stages. A reduced coil set NCC (odd 2x6) is shown in Fig. 10.25(b) with 6 coils each instead. While the n number is reduced to up to 3 for the

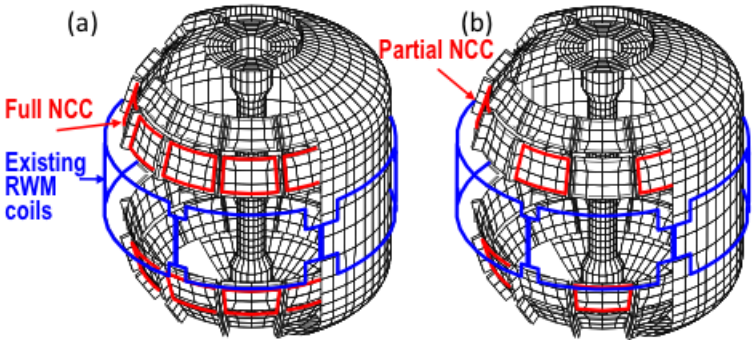

Fig. 10.25. Non-axisymmetric Control Coils shown in red. The existing error field coils are shown in blue. (a) Full NCC Option with 12 x 2 coil arrays. (b) Partial 6 x 2 NCC Option for incremental installations.

reduced set, it can still provide essential NTV, RMP, and EF selectivity with flexibility of field spectrum as synergy with the existing 3-D/EFC system. The implementation of the NSTX-U NCC coils is expected to benefit from the experience gained from the internal control coil system on DIII-D.

10.5.1.3. Disruption Mitigation Systems

A key issue for ITER, and the tokamak/ST line of fusion devices in general, is the avoidance and mitigation of disruptions. Most of the disruptions are expected to be mitigated by massive gas injection (MGI) as described in 10.5.1.3.1 [7]. For some disruptions, the warning time may be less than 10ms. At present there is no suitable disruption mitigation system that can deliver the required impurities to the core plasma on this timescale after an imminent disruption (with a warning time of < 10ms) is detected. For mitigating those specially fast disruption events, an electromagnetic particle injector (EPI) is proposed as described in 10.5.1.3.2.

10.5.1.3.1. Massive Gas Injection

In order to investigate Massive Gas Injection (MGI), the most promising method found thus far for safely terminating discharges in ITER, the University of Washington team installed and commissioned high-capacity gas injectors at two different poloidal locations on NSTX-U. With these, NSTX can offer new data by injecting gas into the private flux and lower x-point regions to determine if this is a more desirable location for massive gas injection. By comparing gas injection from this new location to results obtained from a similar amount of gas injected from the conventional outer mid-plane, NSTX-U can provide additional insight, new data for improving computational simulations, and additional knowledge to understand disruption mitigation physics. For Massive gas injection

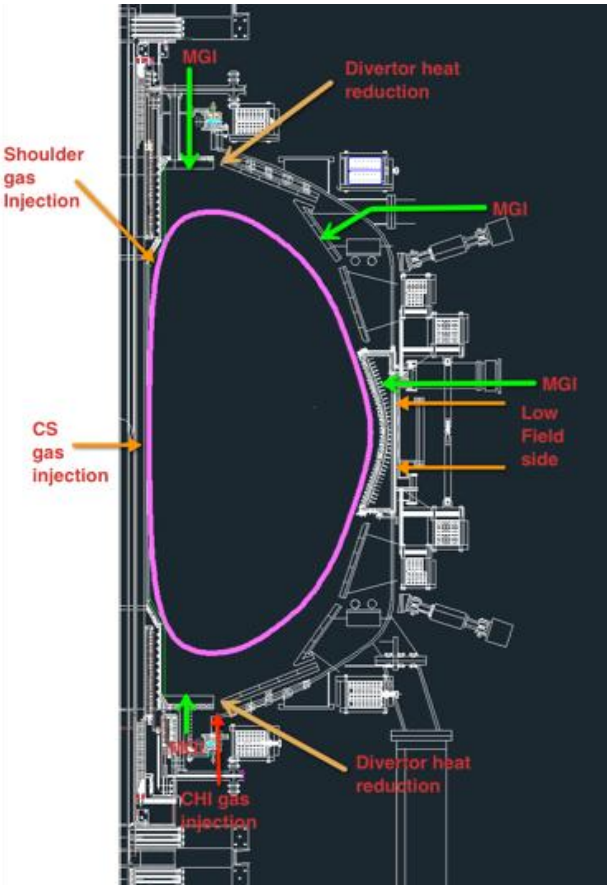

Figure 10.26. A schematic showing the various gas injection locations on NSTX-U.

studies, NSTX-U had the capability for injection from the lower divertor and from the mid-plane. In addition to these two locations, we will increase the poloidal injection locations (over a period of two years) to include a third location from the upper divertor and a fourth location from the upper primary passive plate region, as shown in Fig. 10.26. In addition, work is underway to improve the gas valves to provide faster gas throughput capability and reduced total amount of injected gas. This is based on recent results from DIII-D, C-MOD and ASDEX-U that indicate that only the gas injected within the first ms is efficiently assimilated by the plasma discharge.

10.5.1.3.2. Electromagnetic Particle Injector (EPI)

NSTX-U plans to test a novel mitigation technology referred to as the Electromagnetic Particle Injector (EPI). The system, propels a coaxial projectile, containing particulate matter of various sizes and composition, in a coaxial electromagnetic rail gun, then shatters it in order to inject the smaller sized particles into the tokamak. While experiments on NSTX-U would likely shatter the pellet, the system for ITER may choose to inject the capsule intact. The advantages of this system are that it can respond and deliver the impurity particles to the plasma core in much less than 10ms and that the system is well suited for long stand-by mode operation with high reliability. There are two components to this system. These are the injector itself and the power supply needed to drive the injector. Design studies of an injector for NSTX-U have converged on an attractive design, which results in a simple, compact injector. The injector measures about 12 inches in length and can be mounted on a 6-inch diameter port. The high cost component of the EPI system is the driving power supply, which must deliver about 150 kA of current for 0.5ms. Interestingly, the capacitor power supply used on NSTX-U to drive the CHI system is well suited to drive the EPI injector as well. During EPI system operation the coaxial current feeds that connect to the CHI bus bars will be disconnected from the NSTX-U machine and connected to the EPI injector. The EPI system is described in detail in Section 2.2.2.3.3.

10.5.1.3.3. Compact Toroid Injection

A system based on Compact Toroid Injection (CT) system has the potential for runaway electron suppression. On NSTX-U runaway electrons can be created during inductive start-up by maintaining a low vessel neutral pressure. Steady-state Advanced Tokamak (AT) scenarios and Advanced ST scenarios will rely on optimized density and pressure profiles to maximize the bootstrap current fraction. Under this mode of operation, the fuelling system must deposit small amounts of fuel where it is needed, and as often as needed, so as to compensate for fuel losses, but not to adversely alter the established density and pressure profiles. CT fuelling has the potential to meet these needs, while

simultaneously providing a source of toroidal momentum input. NSTX-U has access to a single pulse CT injection system that could be used for these studies. However, present priorities and budget levels would not allow these to be tested during the present 5 year plan.

10.5.2. Boundary Physics Tools

The base line PFCs for the initial NSTX-U operation is graphite tiles. The vacuum vessel interior with carbon tiles is shown in Fig. 10.27(a). Because of the increased plasma heat loads due to the increased NBI heating power and pulse duration, it was decided to enhance the protection of the CHI Gap. "CHI Gap" is the region between the NSTX-U inner and outer vacuum vessels, above or below the CHI insulators. As indicated in Fig. 10.27, there is a gap in the graphite PFCs in the divertor region, resulting in exposure of the stainless steel and PF 1C to the plasma as shown in Fig. 10.27(b). Also because of the new PF 1C coil, which is placed in the CHI Gap region, an improved protection was deemed necessary. Control room observations showed that when the strike-point was placed in this region, severe contamination of the plasma could occur. This problem was anticipated to be much more severe in NSTX-U, where the horizontal inner target is narrower by a factor of two. Hence, as shown in Fig. 10.27(c), the graphite tiles on both the inner and outer divertors will be extended downwards, coming in close contact to the PF-1C coil casing and stainless steel outer vessel flanges and shielding these components from plasma contact. This narrower and deeper CHI gap will protect the vessel and PF-1C coil from excessive heat flux and protect the plasma from metal contamination, while continuing to provide the capability for CHI operations.

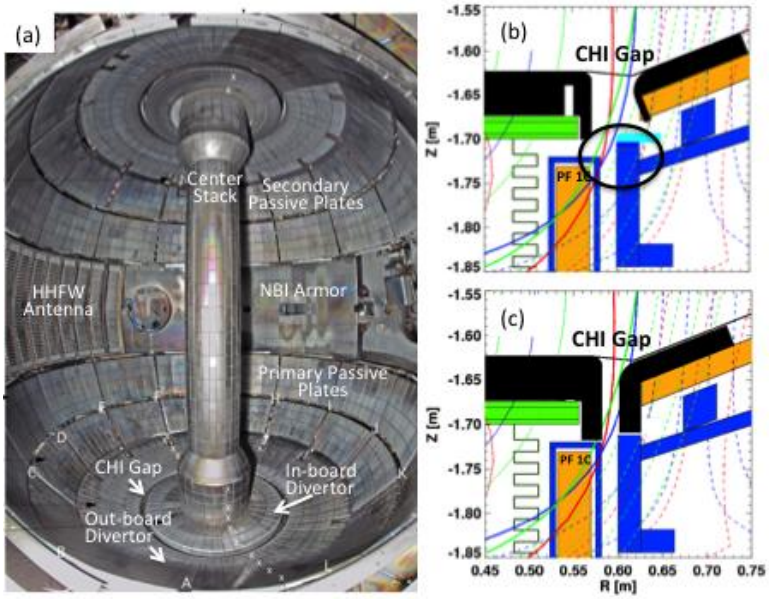

Fig. 10.27. (a) NSTX in-vessel view. (b) CHI gap view with NSTX gap tiles. (c) CHI gap view with new gap tiles for NSTX-U.

10.5.2.1. Divertor Cryo-pump

For boundary physics, a conceptual level design was performed on a closed divertor cryo-pump system as shown in Fig. 10.28(a) [8]. The initial indications are promising for providing divertor pumping for a relatively broad divertor parameter space including the snow-flake configuration. A physics design study of a cryo-pumping system for the NSTX-Upgrade has been performed; the results of the design were presented at the PAC-31 meeting and also at the APS-DPP meeting. A semi-analytic pumping model was used in this effort, and extended to include the effect of finite plenum throat length on achievable neutral pressure. Recent NSTX experiments measuring the scaling of the divertor heat flux profile, as well as measurements of the electron temperature in the far SOL were used in this model to provide a semi-empirical projection of the pumping performance of candidate cryo-pumping geometries, as illustrated in Fig. 10.28 (b). This model was used to optimize the length, height, and radial position of the plenum entrance. Using the optimized entrance parameters, the achievable plasma density has been estimated by assuming a balance between neutral beam fueling and the pumped flux, and combining this with a two-point model for the SOL to relate the upstream and line-averaged density to the divertor density at which this balance is achieved. Pumping in the optimized configuration has been tested over a wide range of plasma position relative to the cryo-pump and flux expansion, and the modeling indicates that low plasma densities ($f_G \sim 0.5$) can be achieved over a broad range of configurations. Notably, the cryo-pump is found to be compatible with the high flux expansion Snowflake divertor, and in fact performs better in this configuration. Due to the improved power handling capability in this configuration, the allowable operating space with simultaneously sufficient pumping and low peak heat flux is larger with a Snowflake divertor. This work has been extended by using 2D plasma-neutrals modeling to evaluate pumping efficiency in radiative/detached regimes (which are not captured by the semi-analytic model used). The NSTX-U divertor cryo-pump engineering design will take place in FY 2014–15 and then component fabrication in FY 2016 and in-vessel installation in an extended outage in FY

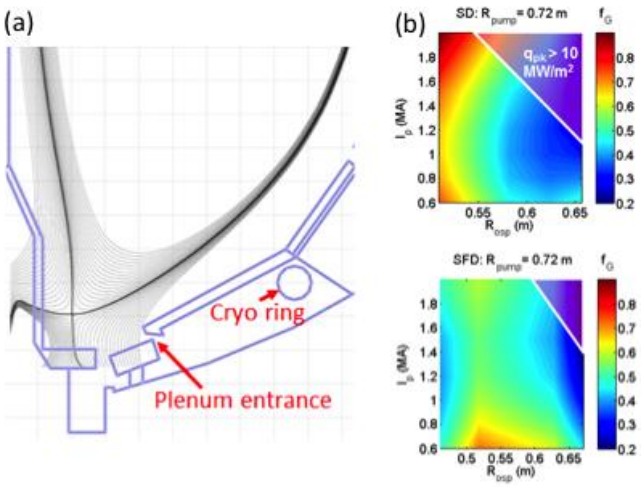

Fig. 10.28. (a) A conceptual design of divertor cryo-pump. (b) Projected density achievable for various R_{OSP} in standard and snowflake divertor configurations

2016 – 2017. The cryo-pump enables NSTX-U to establish density control without lithium coatings.

10.5.2.2. EHO antenna

Edge Harmonic Oscillations (EHOs) have been produced in lithiated NSTX discharges with the Mirnov amplitude of tenths of Gauss vs. ~ 3 Gauss for EHOs on DIII-D. External, adjustable control of edge density and pressure gradients enabled by the enhanced particle transport associated with EHOs of sufficient amplitude would be extremely valuable for NSTX-U, ITER and Demo. Initial calculations for NSTX-U indicate that EHOs may be efficiently driven with audio currents in HHFW antenna, using ½ of the HHFW antenna driven by audio-amplifier system (which was built by PPPL for DIII-D) [9].

10.5.2.3. Fueling Tools

NSTX-U plasma operations will require the capability for gas injection from numerous locations. The gas injection systems on NSTX are not adequate to meet the physics program needs of NSTX-U as improvements are needed in the area of divertor heat flux mitigation, massive gas injection studies, and increased levels of gas injection from high-field side to meet the up to 10s discharge pulses planned for in NSTX-U. These are briefly summarized. Fig. 10.26 provides an overview of the different gas injection systems.

For normal inductive plasma operation, NSTX-U will rely on three mid-plane gas injectors as on NSTX. However, Injectors 2 and 3 are being relocated to bays I and G as their original location on Bay K is now taken up by the second neutral beam port. NSTX relied on two high-field side gas injectors. These were used for H-mode triggering, and the mid-plane injector was routinely used on most of the H-mode discharges. However, because of the short pulses in NSTX and narrow diameter pipe and long length, these could not be used in a controlled manner. These are being upgraded in NSTX-U to include large-diameter pipes so that the flow could be controlled and maintained during the 5-10s discharge pulses planned for in NSTX-U. In addition the system will have the capability for injection from two mid-plane locations and two locations from the region near the PF1A-U coil, as shown in Fig. 10.26. These will be toroidally displaced by 180 degrees. The higher flow-rates from these injectors may be required during Li conditioned operation on NSTX-U as the injectors on NSTX were at some times (such as during the diffusive Li coating experiments) were found to be inadequate to maintain the required electron densities in NSTX.

For CHI start-up, in addition to the existing gas injector on bay K bottom, a Tee will be added at Bay G bottom port, which is the location of lower divertor Penning gauge, and this too used to provide more control and improved toroidal gas injection symmetry.

HeGDC will use one of the mid-plane injectors as on NSTX. For boronization, the system is being significantly modified, by adding a new gas delivery system. In addition to the mid-plane injection, provisions will also be provided for gas injection from both the upper and lower divertor regions from the regions labeled as MGI in Figure 10.26. This is based on recent results from DIII-D that suggests that the divertor plates are much better conditioned with boron if the Tri-Methyl-Boron (TMB) that is included in the He carrier gas is injected from the divertor region.

For divertor heat flux mitigation studies, NSTX relied on a single gas injection location beneath the lower divertor plate on Bay-E. This capability will over a period of two years be expanded to two toroidal locations from the lower divertor and two toroidal locations from the upper divertor.

A supersonic gas injector (SGI) has been developed for fueling and diagnostic applications on NSTX. It is comprised of a graphite converging-diverging Laval nozzle and a commercial piezoelectric gas valve mounted on a movable probe at a low field side mid-plane port location. The SGI flow rate is up to 4 x 10^{21} particles/s, comparable to conventional NSTX gas injectors. The nozzle operates in a pulsed regime at room temperature and a reservoir gas pressure up to 0.33 MPa. The deuterium jet Mach number of about 4, and the divergence half-angle of 5^{o} - 25^{o} have been measured in laboratory experiments simulating NSTX environment. The SGI has been used for fueling of ohmic and 2-4 MW NBI heated L- and H-mode plasmas. Fueling efficiency in the range 0.1 - 0.3 has been obtained from the plasma electron inventory analysis. In NSTX, long-pulse discharge scenarios with controlled ion inventory have been demonstrated via the use SGI fueling and lithium-coatings for ion pumping. It is planned to continue using the SGI routinely in support of plasma operations on NSTX-U. In initial years, H-mode fueling scenarios with SGI fueling will be developed. A primary benefit of the SGI is a precise control of injected gas inventory. The SGI can support H-mode density limit and pedestal studies, as well as perturbative transport experiments. In later years, it is planned to integrate the SGI in a feedback-control loop for active density control with PCS. Another gas fueling method that is envisioned for NSTX-U is a cryogenic supersonic gas injection (also referred to as molecular beam injection). Recent fueling experiments at HL-2A and LTX indicated that molecular clusters obtained via cryogenic gas cooling could penetrate deeper into the plasma due to a much higher neutral density in a cluster jet and smaller ionization cross-sections of molecular clusters, thereby improving fueling efficiency of the supersonic gas injection even further.

10.5.2.4. Lithium Granule Injector for ELM Control

The lithium granular injector for ELM pacing [10] which was successfully demonstrated on EAST will be available for NSTX-U. The NSTX-U lithium granule injector (LGI) for ELM control has been completed in FY 2011 as shown in Fig. 10.29. The LGI system was shipped to the Chinese Academy of Science, institute of Plasma Physics and installed on the EAST Tokamak. The NSTX-U LGI system is capable of injecting horizontally redirected spherical Lithium granules (0.6 mm) at speeds approaching 100 m/s. The dropping rates (pacing frequencies) of 500 Hz have been achieved in the laboratory test. A dropper apparatus allows the granule size to be changed between discharges. After an extended shake-down period, the injector was used to trigger/pace ELMs in EAST H-modes. Using Li granules with diameters of several tenths of a millimeter injected at speeds of several tens of meters per second, ELMs were triggered at high efficiency. Pacing frequencies ranging between 10's to 100's of Hertz were observed. It is anticipated that much higher pacing frequencies can eventually be achieved using similar injector technology. The JET group is interested in the NSTX-U granular injector using beryllium granules for ELM pacing with application to ITER. A similar LGI system was also sent to RFX in Italy and successfully commissioned. An NSTX-U lithium dropper was also shipped to DIII-D for divertor recycling control.

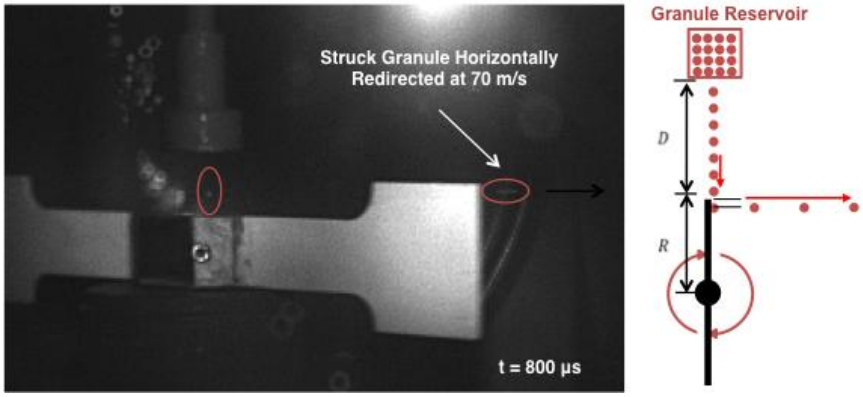

Fig. 10.29. NSTX-U lithium granular injector for ELM pacing.

10.5.2.5. Lithium Evaporator and Upgraded Lithium Coating Systems

With encouraging results in NSTX, the NSTX lithium evaporator (LITER) system as shown in Fig. 10.30(a) is planned for NSTX-U from Day 1 [11]. The LITER system is essentially a temperature controlled stainless steel container filled with liquid lithium (LL), with a nozzle to direct the lithium vapor for coating PFCs at desired locations.

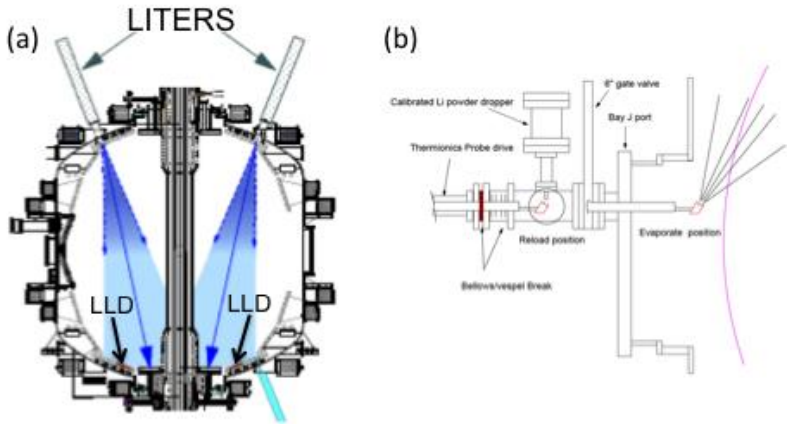

Fig. 10.30. (a) A schematic of the lithium evaporators (LITERs) injecting vapor which condenses on the room-temperature plasma facing components in the lower part of the vacuum chamber, including the lower divertor plates. (b) A schematic of the upward facing lithium evaporator concept.

The nozzle is typically aimed toward the middle of the inner divertor to maximize the lithium deposition on the divertor plates. Two LITERS units were used for better toroidal PFC coverage of lithium on NSTX. The units each have a 90 g lithium capacity. The LITER consists of a main reservoir oven and an output duct to allow insertion in a PFC gap in the upper divertor region. Two heaters were used on each LITER, one heater on the output duct and one heater on the main reservoir. The heater on the main reservoir was typically operated to maintain the LL temperatures of 600–650 °C which enables an adequate lithium evaporation rate, as this rate increases rapidly with temperature. The heater on the output duct was operated about 50–100 °C hotter than the heater on the main reservoir to reduce lithium condensation on the output duct aperture. Typical evaporation rates have been in the range of 1 to 40 mg/min. The lithium evaporation typically takes place between plasma discharges to obtain the desired level of lithium coating on the PFCs, which could be in the range of 30 – 500 nm thick. In NSTX, nearly 1,000 g of lithium was delivered onto the PFCs during the last experimental campaign in FY 2010-2011. For the initial NSTX-U lithium capability, the baseline is the dual upper and lower aiming evaporators and a new Li granular injector on the mid-plane. A design is being developed for an upper aiming evaporator to cover the upper divertor region. An example of a possible system is shown in Fig. 10.30 (b). The mini Li evaporator concept requires a lithium dropper as a source to fill a Li crucible which is then inserted into the edge of NSTX-U well outboard of the SOL, and heated to above 700 °C to cause rapid evaporation of the Li powder. Electron beam heating is the leading candidate for a heat source. Due to the high temperature, all Li is promptly evaporated to the upper vessel. This has advantages of requiring no shutters after evaporation. Since the

evaporator is outside of the plasma volume, the discharge can commence without retracting the evaporator. This reduces the time between the end of the evaporation and the start of the discharge ensuring minimal passivation of the fresh lithium.

10.5.2.6. High-Z Metallic Divertor

While the baseline NSTX-U operation plan is to start with all graphite tiles, in view of the natural progression toward future facilities such as FNSF, it is important to investigate the viability of high-Z metallic divertor on NSTX-U. After making an assessment of all graphite PFC plasma operations, a row of high-Z tiles will be installed on lower OBD (outboard divertor) region as shown in Fig. 10.31. By placing the high-Z divertor PFC at larger major radius on the OBD, the risk to standard high-delta shapes and scenarios is minimized as was the case for the original LLD. The high-Z tile design will be assessed for tolerance to thermal and disruption loads. This plan enables a transition to high-Z PFCs to support PMI/FNSF next-steps. With the OBD high-Z tiles, erosion and migration of high-Z tile materials to be transported into the plasma core can be investigated with and without lithium. Additional high-Z tiles will be installed in conjunction with the installation of the cryo-pump in FY 2016 – 17 long outage. It is envisioned that both upper and lower divertor surfaces will be covered by high-Z material by 2018.

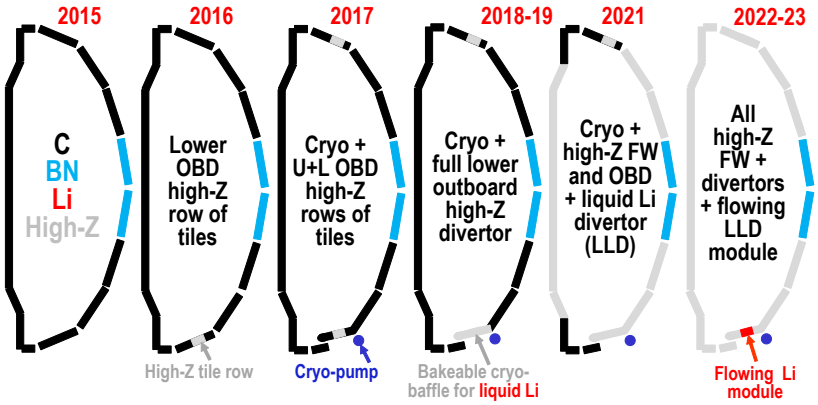

Fig. 10.31. Nominal implementation plan of boundary physics capability including cryo-pump and high-Z PFCs + Liquid Li Divertor module with 5 YP base funding.

10.5.2.7. High-Z Outer and Inner Wall PFCs

As noted above in Section 10.5.2.6, the present NSTX-U PFC strategy is to start with all graphite tiles for Day 1 and progress in stages with rows of high-Z tiles as shown in Fig. 10.31. After assessing the plasma behavior and the high-Z tile performance, the entire NSTX-U PFC will be replaced with high-Z PFCs. One can envision TZM or W (tungsten) lamellae or tiles if workable. For low heat flux regions such as the passive plates and CS off-midplane, one may use W-coated graphite tiles.

10.5.2.8. Flowing Liquid Lithium Divertor/Module

Various concepts are being considered for a liquid lithium divertor system [12]. A flowing liquid lithium loop R&D facility (LDRD funded) is being built at PPPL [Fig. 10.32]. If successful, the design will be adapted for NSTX-U. The HT-7 tokamak is also testing liquid lithium PFCs. Development of flowing liquid lithium PFCs and related technologies is also underway at PPPL supported by the LDRD funding which if successful could be adopted as the NSTX-U liquid lithium divertor. The present efforts focus on a capillary-restrained system that incorporates gaseous cooling. In this conceptual diagram, "T-tubes" are considered for the active cooling scheme with either helium or super critical–CO2 (s-CO2) as the primary coolant. The PFC includes a porous or textured front face, similar to that used on LLD for liquid lithium stability against disruptive loads. Lithium flow channels are located parallel to the cooling channels with discrete ports to allow the liquid metal to wick quickly to the front-face. In addition to size scaling, an examination of the basic cooling fluid is also being carried out. S-CO2 has been identified by many in the fission power industry as having favorable properties in a power cycle over helium. Experimental demonstration of liquid metal PFC concepts is currently underway to complement the design studies described above. These begin with the development of a liquid lithium loop which will provide active pumping into and out of

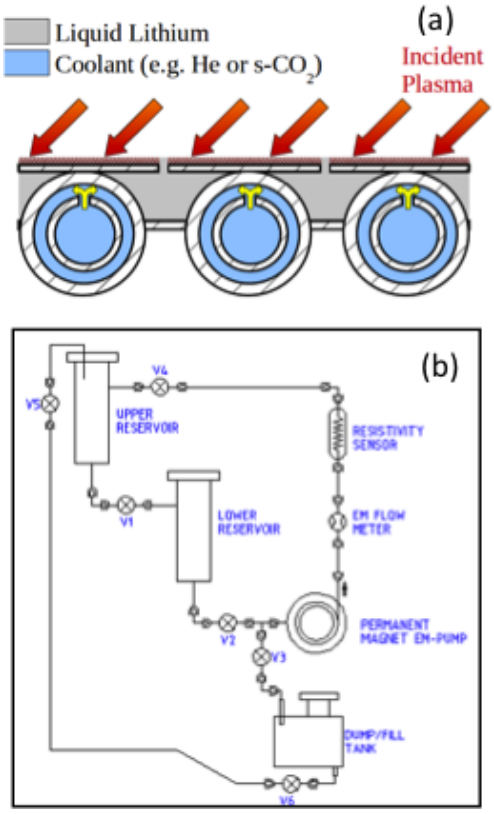

Fig. 10.32. Liquid lithium R&D. (a) A conceptual capillary-based lithium divertor PFC design. (b) A flowing liquid lithium test loop.

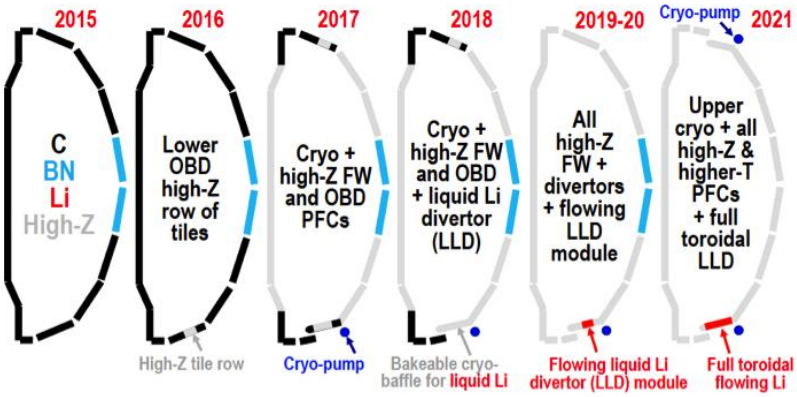

Fig. 10.33. Nominal implementation plan of boundary physics capability including cryo-pump and high-Z PFCs + Liquid Li Divertor module with 5 YP incremental funding.

vacuum chambers. The facility will be utilized for testing of candidate PFC designs to show such things as (1) stable operation and flow in a tokamak-relevant vacuum environment (10^{-7} to 10^{-6} Torr pressures), (2) restart capability after periodic shut-down and gettering of residual gases, (3) maintainability and reliability in addition to safe operation. Future plans include active purification of lithium inventory and upgrades to include integrated tests with s-CO2 cooling systems. The boundary physics capability plan would be modified with the incremental funding as shown in Fig. 10.33.

10.5.2.9. Laboratories for Material Characterization and Surface Chemistry

NSTX-U is collaborating with two new laboratories established at PPPL in collaboration with Princeton University dedicated for materials characterization and surface chemistry experiments. The Surface Science and Technology Laboratory is equipped with three surface analysis systems and an ultrahigh vacuum deposition chamber. Substrates for vapor deposition of metal films can be heated and cooled from 85 – 1500K using liquid nitrogen cooling and resistive and electron-beam heating. These systems have a variety of surface diagnostics, including high resolution electron energy loss spectroscopy (HREELS), which is capable of probing both optical and vibrational excitations over a wide range of 0 - 100 eV with an electron energy resolution of 3 meV, alkali ion-scattering spectroscopy (ALISS), and angle-resolved X-ray photoelectron spectroscopy (XPS). Another instrument has XPS, low energy ion scattering (LEIS), and reflection high-energy electron diffraction (RHEED) capability for thin film growth studies. In this laboratory, the time evolution of the chemical composition of lithium surfaces exposed to typical residual gases found in tokamaks was recently measured. Solid lithium samples and a TZM alloy substrate coated with lithium have been examined using XPS, temperature programmed desorption (TPD), and Auger electron spectroscopy (AES) both in ultrahigh vacuum conditions and after exposure to trace gases. Lithium surfaces near room temperature were oxidized after exposure to 1-2 Langmuirs ($1L=1x10^{-6}$ torr s) of oxygen or water vapor. The oxidation rate by carbon monoxide was four times less. An important result of the measurements for NSTX-U is that lithiated PFC surfaces in tokamaks were found to be oxidized in about 100 s depending on the tokamak vacuum conditions which is much less than a typical time duration between the tokamak plasma shots [12]. A second laboratory, the Surface Imaging and Microanalysis Laboratory, contains a high-performance field emission Auger and multi-technique surface microanalysis instrument with a field emission electron source and lateral resolution of 30 nm for elemental analysis of surfaces of samples on the micro and nano scale.

10.5.3. Start-up and Ramp-up

10.5.3.1. CHI upgrades

A significant new upgrade for CHI is the improved location of both the injector and absorber buffer field coils [13]. In a CHI discharge the maximum plasma current CHI can generate is directly proportional to the magnitude of the injector flux. As shown in Fig. 10.34, the injector coil on NSTX-U is positioned much closer to the CHI gap. This allows more of the flux generated by this coil to connect the inner and outer divertor plates. This increases the theoretical injector flux capability in NSTX-U to over 300 mWb, compared to a maximum of 80 mWb in NSTX. To put this in perspective, a low inductance 1 MA discharge in NSTX-U will contain on the order of 200 to 250 mWb of poloidal flux. To control a condition known as absorber arcs, NSTX relied on two small coils located on top of the machine that were dedicated to providing a buffer field to keep the expanding CHI discharge from contacting the upper divertor plates and generating an absorber arc. On NSTX-U these dedicated coils are not necessary as the main PF1C-U coil that is located closer to the absorber gap more than doubles the current capability and the current slew rates of the absorber buffer field coils used on NSTX. The key parameters for the CHI system for NSTX and NSTX-U are given in Table 10.1.

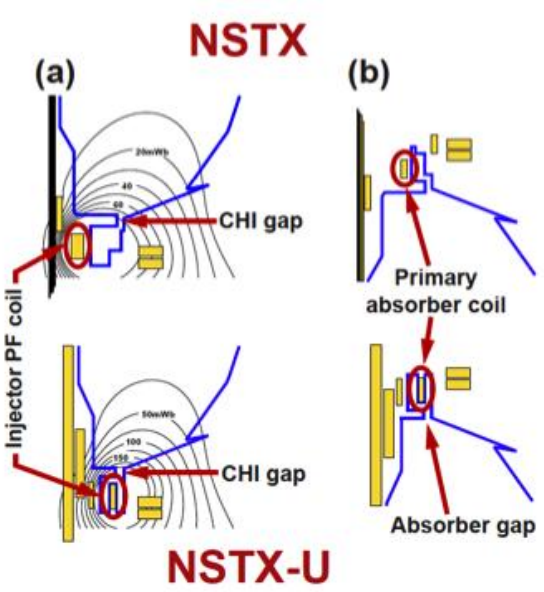

Fig. 34. A schematic of old and new CHI system configuration.

Parameters	NSTX	NSTX-U
R(m)	0.86	0.93
a(m)	0.68	0.62
B_0(T)	0.55	1.0
Toroidal Flux (Wb)	2.68	3.78
Normalized internal inductance, l_i	0.35	0.35
Full non-inductive sustainment current, Max Ip (MA)	0.7	1
Poloidal Flux for Max Ip (mWb)	132	206
Required Injector Flux for 50% Max Ip (mWb)	66	103
Current Multiplication factor	41	37
Peak current multiplication	53	48
Peak startup current (kA)	450	650
Injector current	**8.6**	**13.6**
Maximum available Injector Flux (mWb)	63-80	220-340
Max startup current potential (kA)	~400	~1 MA
Required injector current For Max current potential (kA)	10	27*

Table 10.1. Comparison of the NSTX and NSTX-U CHI system parameters

10.5.3.2. Plasma Gun Start-Up

The conceptual design for the NSTX-U compact helicity injection startup system is presently under development by the University of Wisconsin PEGASUS group [14]. Figure 10.35 shows a top-down view of the proposed injector, with explicit detail of the gate valve, injector "garage", bellows structure, and the umbilical cables and tubing. Machine access would be through a large (8-inch diameter or larger) off-midplane port on the outboard side. The injector is shown inserted between two passive plates, though those details are dependent on the exact port that is made available on NSTX-U for these studies. A more detailed insert shows the elements of the pre-conceptual injector, including the limiter, the arc tube surrounded by an electrode, and an insulating surface behind the electrode to prevent arcing back along the field lines. The present design uses boron nitride as both the insulating surface and the plasma-facing armor for the sides of the injector. The final conceptual design may well use molybdenum or tungsten armor around and behind the injector, in order to shield the boron nitride from plasma impact. The injector will be designed to be fully retractable, using a bellows drive for vacuum integrity, and will be kept outside the NSTX-U vessel and behind a gate valve (in a "garage" region) when not in use. The plasma-facing portion of the injector will incorporate a limiter structure, an active plasma gun (the arc tube), and a passive electrode. The electrode will be shaped, as much as possible within the footprint of the port, to maximize the Taylor limit while keeping an adequate cross-section for the corresponding current drive. The umbilical cables, tubing, and diagnostic lines from the injector to the power supplies and control system will be kept in a shielded conduit, both to isolate the diagnostic lines from external noise sources and to mitigate the electrostatic noise associated with high-power switching of the injector H-bridge bias supply. Deuterium gas for the active plasma gun is supplied through flexible tubing, with most fueling during the electrode-drive phase supplied through the usual NSTX-U fueling valves. The power supplies and control system can be relatively compact, depending upon the total stored energy that will be necessary for driving the bias during the high-current startup scenario. A simple pulse-forming network will provide the arc

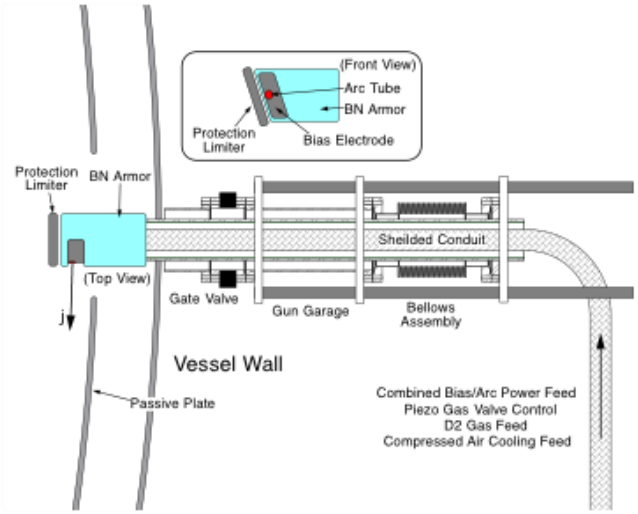

Fig.10.35. Detailed view of pre-conceptual PEGASUS point-source helicity injector gun design.

discharge in the active plasma source, with a crowbar switch on the outputs to the arc tube. The bias power supply will be based on the technology used on the Pegasus Toroidal Experiment, with an array of reduced H-bridge supplies providing the required current and voltage. The arc supply, bias bridges, deuterium gas supply, and control systems will perhaps occupy the volume of an office desk. The total stored energy for the bias supply, necessary for a high-current startup scenario, remains to be determined.

10.6 NSTX-U Diagnostic System Status and Plans

The NSTX-U diagnostic planning meeting was held in July 2011 and also in July 2012. Since the 2012-2016 non-laboratory NSTX-U diagnostic grant recipients were decided in FY 2012, they represent a significant fraction of the planned NSTX-U diagnostic capability. The diagnostics which were operational in FY 2011 are generally expected to be available for the NSTX-U operation unless otherwise noted. A list of the existing diagnostic systems which are expected to be available for NSTX-U within two years of operation is shown in the Table 10.2. We note that at least half of those diagnostic systems have strong collaboration components. We shall describe major diagnostic systems in the following sections.

MHD/Magnetics/Reconstruction
- Magnetics for equilibrium reconstruction
- Halo current detectors
- High-n and high-frequency Mirnov arrays
- Locked-mode detectors
- RWM sensors (n = 1, 2, and 3)

Profile Diagnostics
- MPTS (42 ch, 60 Hz)
- T-CHERS: $T_i(R)$, $V_\phi(r)$, $n_C(R)$, $n_{Li}(R)$, (51 ch)
- P-CHERS: $V_\theta(r)$ (71 ch)
- MSE-CIF (18 ch)
- MSE-LIF (20 ch)
- Midplane tangential bolometer array (16 ch)

Turbulence/Modes Diagnostics
- Tangential microwave high-k scattering
- Beam Emission Spectroscopy (48 ch)
- Microwave Reflectometer,
- Microwave Polarimeter
- Ultra-soft x-ray arrays – multi-color

Energetic Particle Diagnostics
- Fast Ion D_α profile measurement (perp + tang)
- Solid-State neutral particle analyzer
- Fast lost-ion probe (energy/pitch angle resolving)
- Neutron measurements
- Neutral particle analyzer

Edge Divertor Physics
- Gas-puff Imaging (500kHz)
- Langmuir probe array
- Edge Rotation Diagnostics (T_i, V_ϕ, V_{pol})
- 1-D CCD H_α cameras (divertor, midplane)
- 2-D divertor fast visible camera
- Metal foil divertor bolometer
- AXUV-based Divertor Bolometer
- IR cameras (30Hz) (3)
- Fast IR camera (two color)
- Tile temperature thermocouple array
- Divertor fast eroding thermocouple
- Dust detector
- Edge Deposition Monitors
- Scrape-off layer reflectometer
- Edge neutral pressure gauges
- Material Analysis and Particle Probe
- Divertor Imaging Spectrometer

Plasma Monitoring
- FIReTIP interferometer
- Fast visible cameras
- Visible bremsstrahlung radiometer
- Visible and UV survey spectrometers
- VUV transmission grating spectrometer
- Visible filterscopes (hydrogen & impurity lines)
- Wall coupon analysis

Table 10.2. Existing NSTX-U Diagnostic Systems

10.6.1. Profile Diagnostics

10.6.1.1. Multi-Pulse Thompson Scattering System

Twelve additional channels bringing the total number of channels to 42 for the multi-pulse Thomson scattering (MPTS) system were installed and commissioned in FY2011. After acceptance testing, the new polychromators were first assembled and aligned, and then installed in the MPTS room. The optical fiber bundles bringing scattered light from the plasma were then reconfigured to produce the desired spatial distribution of measurement points. The locations of all the MPTS channels were then measured by back-illumination along each fiber of a target plate mounted inside the vacuum vessel. The spectral transmission curve of each polychromator was then measured with a scanning monochromator and the overall calibration was performed *in situ* by employing Rayleigh and Raman scattering of the light from the MPTS laser system by nitrogen and argon introduced into the vacuum vessel. Measurements of the optical transmission of the observation window were also made to establish a baseline for monitoring its evolution through the run. The upgraded MPTS system with 42 total channels was ready for operation in July 2011.

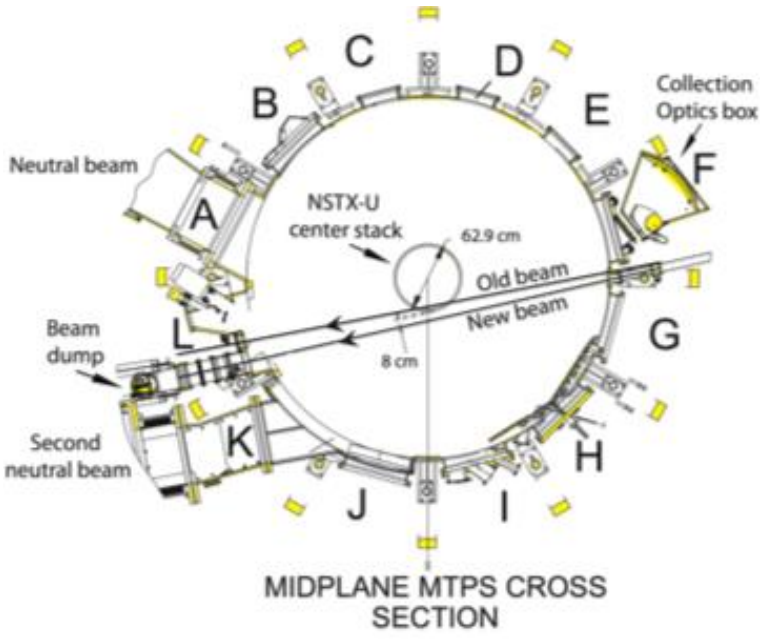

Fig. 10.36. Mid-plane cross section of NSTX-U showing old and new MPTS laser beam paths, relocated laser input port on the vacuum vessel, new beam dump, and scattered light collection optics box.

Modifications to the Multi-Pulse Thomson Scattering (MPTS) diagnostic required for the NSTX Upgrade were designed, and fabrication and procurement of the needed components were started [15]. The larger diameter of the center stack in NSTX-U requires that the MPTS laser beams be re-aimed to avoid striking the center stack, which would cause damage to it as well as an unacceptable level of scattered laser light in the vacuum vessel [Fig. 10.36]. The re-aiming of the laser beams requires several other changes to the MPTS diagnostic configuration: 1) a new laser beam dump must be provided on a new vacuum vessel port structure on the opposite side of the vacuum

vessel (Bay L) from the laser input port; 2) the laser input port on the vacuum vessel must be moved several centimeters on the vacuum vessel and re-aimed to achieve the needed laser beam path; and 3) the MPTS light collection optics must be modified and re-aimed to provide high-resolution imaging of the re-aimed laser beam. This new configuration is shown in Figure DIAG-1. Redesigning the MPTS system to meet these requirements was accomplished and a successful preliminary design review was held. A successful final design review for the modifications to the vacuum vessel was held, and final design reviews for the remaining modifications to the system are planned for early FY2013. The new port structure required for the laser beam dump is located at Bay L and includes ports for several other diagnostics. The reconfigured MPTS diagnostic will be installed prior to NSTX-U first plasma and commissioned in early experimental operation following first plasma.

10.6.1.2. Charge-Exchange Recombination Spectroscopy

10.6.1.2.1. Toroidal and Poloidal CHERS

The NSTX-U charge exchange recombination spectroscopy (CHERS) diagnostic suite measures impurity ion temperature, impurity flow, and impurity density [16]. A schematic of the system is shown in Fig. 10.37. Together, these measurements can be used to determine the radial electric field in the plasma. The CHERS systems[i] on NSTX-U use the n = 8-7 transition of the C^{5+} ion at 529.1 nm to infer the temperature, density, and velocity of the parent ion C^{6+}. Along with the charge exchange emission, intrinsic background emission from C^{5+} ions is also present. Dedicated views that do not intersect the beam are used to measure this background emission. Both

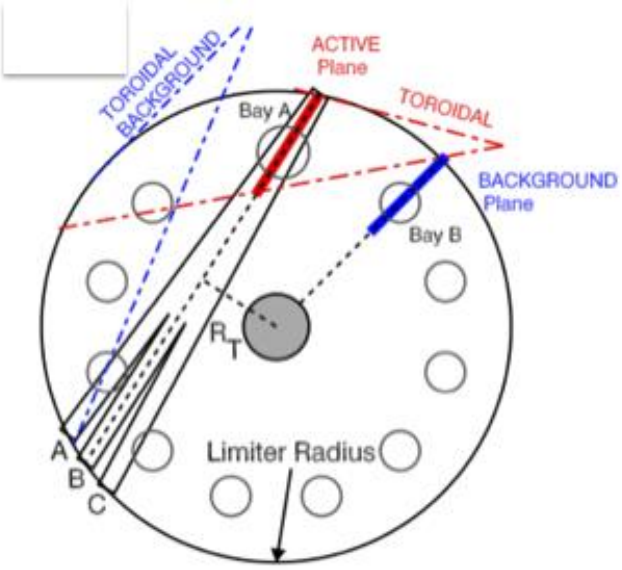

Fig. 10.37. Plan view of NSTX-U midplane showing the locations of the active and background detection planes for the poloidal CHERS views. The active plane shares the same tangency radius (R_T) as the central beam. Also shown are the range of the toroidal CHERS views and the corresponding background views.

poloidal and toroidal viewing CHERS systems are used on NSTX. An absolute photometric calibration is performed allowing accurate carbon density profile measurements. Profile measurements are obtained every 10 ms.

The toroidal viewing system is situated at the plasma midplane. Two sets of sightlines view across the neutral beams and parallel to the neutral beams to provide active measurements and simultaneous independent background measurements. The active view has 51 spatial channels across the midplane, while the background view consists of 39 spatial channels. The radial resolution is variable, about $\Delta r = 0.6$ cm near the edge and increasing to about $\Delta r = 3.0$ cm in the core. With the low magnetic field typical of the spherical torus, the edge resolution is comparable to the gyro radius. The toroidal viewing optics are shared with the Motional Stark Effect (MSE) diagnostic.

The poloidal viewing CHERS has matched symmetric views from above and below the plasma. The upper and lower sightlines are precisely aligned where they intersect at the midplane. The active plane of measurement is aligned with the central neutral beam trajectory. The background emission is measured in a radial plane at a toroidal location about 30° from the neutral beams. Higher resolution is provided in the outer portion of the plasma ($R \geq 120$ cm) with twice as many sightlines. The poloidal viewing system is sufficient to measure line-integrated velocity. To obtain local poloidal measurements, an inversion is performed, which requires information from the toroidal viewing system. The radial resolution after inversion is $\Delta r = 0.6$ cm is the outer range and $\Delta r \leq 1.8$ cm near the plasma center, comparable to the toroidal viewing system.

The NSTX Upgrade introduces an additional set of neutral beam sources (NB2) with larger tangency radii than the original set of neutral beams (NB1). NB2 sources are in the field of view of the CHERS background sightlines, preventing the independent measurement of background emission when they are operated. When only the original neutral beam sources (NB1) are used, the existing analysis techniques can still be used. When any of the new neutral beam sources (NB2) are used, another method must be used for analysis. One possibility is to modulate a neutral beam to provide the background measurement, either NB1 or NB2. However, there may be limitations to the number of modulations allowed during a discharge. The quality and time resolution of the CHERS measurements will be degraded with the operation of the NB2 sources.

10.6.1.2.2. Edge Rotation Diagnostic

This collecting lens for the CHERS background is shared by the toroidal views of an edge Doppler spectrometer (ERD), which measures emission from C^{2+}, He^{+}, Li, and

Li^{+}[18]. The collecting lens for the background poloidal CHERS views at the top of NSTX-U is shared by the ERD system providing poloidal velocity measurements. Seven toroidal channels and six poloidal channels are used. The spatial resolution of the ERD is ~ 3 cm with a time resolution of 10 ms. The radial electric field near the edge can be computed using the torodial and poloidal velocity measurements of C^{2+}or He^{+}. During HHFW operation, the ERD is used to monitor the anisotropic ion heating near the plasma edge.

10.6.1.3. Soft X-ray Diagnostics

A suite of new and upgraded soft X-ray (SXR) to VUV diagnostics based on the multi-energy imaging technique developed in the previous NSTX research will be installed on NSTX-U by the Johns Hopkins group [18-19]. The SXR-VUV diagnostic suite will enable improved measurements of the impurity content and radial transport, of radial and toroidal MHD mode structure and of Te profiles and perturbations in the core, edge and divertor, and in all NSTX-U operating scenarios, from non-inductive start-up and sustainment, to high power beam and RF driven regimes. A layout for the in-vessel, atmospheric re-entrant EDGE and CORE ME (multi-energy)-SXR system, as well as the fast (100Hz) Transmission Grating Imaging Spectrometer is shown in Fig. 10.38.

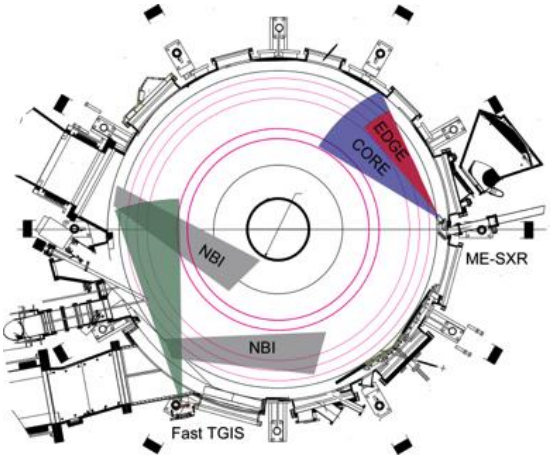

Figure 10.38. Plan view for the in-vessel, atmospheric re-entrant EDGE and CORE ME-SXR system, as well as the fast (100Hz) Transmission Grating Imaging Spectrometer

A system of two toroidally displaced, edge and core in-vessel tangential ME-SXR arrays. This system will simultaneously measure the core and edge plasma emission profiles in up to five energy bands spanning the range from a few eV (bolometry) to several keV, and at two toroidal locations separated by ~90°. Each of the two toroidally displaced tangential arrays will include an edge sub-array covering the region $0.6<r/a<1$ with 1 cm resolution and a core sub-array covering the entire inboard to outboard plasma with ≥3 cm resolution. The time resolution will be ≥10μs. The high spatial resolution combined with energy resolution and extended toroidal coverage will enable the following multiple physics capabilities:

- Impurity and electron thermal perturbative transport measurements from the edge to the core using gas puffs and the repetitive laser blow-off proposed below,

- Fast, high resolution measurements of edge Te profiles (and with external ne constraint also n-z profiles) for ELM studies, for edge code validation, and for improved edge stability analysis,

- Fast, toroidally resolved measurements of edge and core Te, n-z profiles and perturbations for the study of 3D-field effects, RWMs, and disruptions,

- Real-time Te and Zeff measurements for stability prediction and feedback control development, and

- Enhanced sensitivity non-magnetic toroidal mode identification for disruption sensing.

The ME-SXR array diagnostic has been successfully prototyped and tested in our recent NSTX research. For NSTX-U we will develop an *in-vessel* design that will enable implementing the arrays without requiring mid-plane port space, which will be scarce on NSTX-U due the addition of the second neutral beam.

A fast tangential Transmission Grating Imaging Spectrometer (TGIS) This device is an upgrade of the TGIS diagnostic implemented on NSTX and will enable absolute impurity spectra measurements in the XUV range (50-800 Å) with high time resolution (≥5-10 ms) and with high space resolution (≥2 cm). The instrument will have a tangential view of a heating beam, enabling simultaneous diagnostic of low-Z impurities through the beam excited CX emission and of the high-Z impurities through the combined electron and beam excited emission. The upgraded TGIS will enable routine measurements of the radial profile of all impurity fractions in NSTX, from lithium to molybdenum, for an accurate modeling of the ME-SXR profiles from the edge to the core and for an improved impurity monitoring capability in all NSTX-U operating scenarios, including noninductive startup and sustainment.

A repetitive laser blow-off system for multiple injections of non-recycling impurities during the shot - A laser blow-off (LBO) system, which will ablate a thin film of material from a glass slide, injecting a short burst of neutral impurity atoms into NSTX-U plasmas for impurity and electron thermal perturbative transport measurements, will be implemented by the JHU group. A high-powered Nd:YAG 1064 nm laser, with pulse energy ≥ 800 mJ and pulse frequency ≥ 10 Hz, will be utilized. It should be also noted that the same laser and optical configuration, with the addition of in-vessel steerable optics, can be used for laser-induced breakdown spectroscopy (LIBS) of in-vessel PFC components as proposed by Purdue University which would allow in-situ, real-time characterizations of surface impurities, concentrations, and erosion/deposition rates between discharges in NSTX-U

10.6.1.4. Motional Stark Effect – Collisional Induced Fluorescence

With a doubling of the magnetic field as part of the NSTX upgrade the Motional Stark Effect measurement based on Collisionally Induced Fluorescence (MSE-CIF) collection optics can be optimized to increase the throughput [20]. A schematic of the MSE-CIF system is shown in Fig. 10.39. An aperture on the collection optics is used to reduce the geometric broadening. With the higher field this will change the optimal aperture width and polarization fraction for maximizing the signal-to-noise. We will use our numerical models and optical design code to re-optimize the aperture width. To support its Five Year Plan, the NSTX-U team has expressed a desire for more flexibility from the MSE measurement. The neutral beams will only be able to inject for three seconds at 90 kV, or five seconds 80 kV. With the possibility of long NSTX-U discharges, it would be desirable if MSE can switch from viewing one neutral beam to another within a single discharge to provide data over long pulse discharges. Preliminary tests have shown that this can be accomplished with the existing high voltage power supplies on the birefringent filters. We propose adding a high voltage relay bridge that will provide fast tuning during a discharge. The bridge circuit will allow switching both the voltage amplitude and polarity. This will enable the MSE-CIF system to switch between beams with a time delay of less than 200 ms. The MSE-CIF system will starts with 18 sightlines but the real-time capability will be also implemented as described in (10.6.3.2). The MSE-CIF system is upgradable to 40 sightlines budget permitting.

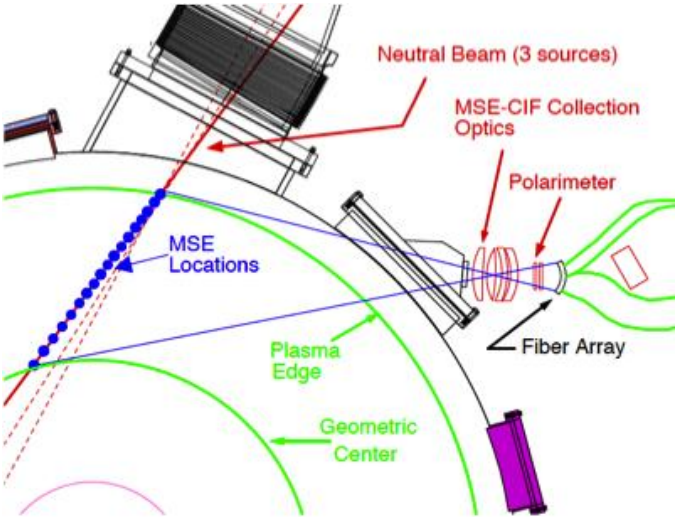

Figure 10.39. MSE-CIF layout on NSTX-U with radial locations indicated by the blue dots along the neutral beam trajectory.

10.6.1.5. Motional Stark Effect – Laser Induced Fluorescence

The Motional Stark Effect measurement based on Laser Induced Fluorescence (MSE-LIF) diagnostic as shown in Fig. 10. 40 will provide measurements of the field line pitch angle profile without requiring injection of the heating neutral beam needed for the present MSE system on NSTX-U which is based on collisionally induced fluorescence (MSE-CIF) [21]. It will therefore provide critical data for measuring RF-driven current in NSTX-U without the competing effect of current driven by the heating neutral beam. Also, direct reconstruction of the total plasma pressure profile should be possible from its

capability to make local measurements of the total magnetic field in the plasma. Combining this measurement with the comprehensive thermal profile measurements already available on NSTX-U, the fast-ion pressure profile can be inferred and compared to prediction to determine the influence of Alfvén Eigenmodes and other MHD activity on fast-ion confinement. Furthermore, the data from the two MSE systems, MSE-CIF and MSE-LIF, can be combined to calculate the radial electric field profile, an important element in plasma transport research. In collaboration with researchers from Nova Photonics Inc., the installation and commissioning of the first three channels of the Motional Stark Effect measurement based on Laser Induced Fluorescence (MSE-LIF) was completed in August 2011. After extensive development and testing in the laboratory, the diagnostic neutral beam, surrounded by a two-layer magnetic shield, was mounted on its stand and connected to the NSTX-U vacuum vessel, its power supplies and other services. After commissioning its control and interlock systems operation of the diagnostic neutral beam was achieved. The development of a high-power, narrow-line laser source for excitation of the injected neutrals was completed and the laser was installed. The viewing optics, filters and detectors for 10 sightlines crossing the neutral beam path were designed, procured and installed. Finally, in September, the magnetic field sensitivity of the MSE-LIF system was tested by injecting the neutral beam into deuterium gas introduced into the NSTX-U vacuum vessel with up to 3mT applied by the poloidal field coils. In this test, the MSE-LIF system was able to distinguish changes of less than 1mT. For NSTX-U Day-1 operation, 20 sightlines of the MSE-LIF system will be available.

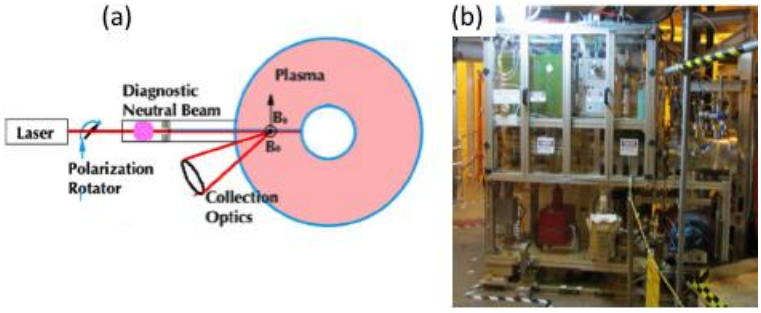

Fig. 10.40. MSE-LIF System: (a) NSTX MSE-LIF system layout schematic, (b)MSE-LIF system installed on NSTX.

10.6.2. Turbulence Diagnostics

For turbulence diagnostics systems, the high-k scattering system detector array presently located at Bay K will have to be relocated to Bay L after the 2nd NBI installation at Bay K [22]. By re-aiming the microwave beam, it is possible to measure both the radial and poloidal components of the high-k turbulence. The existing 280 GHz system will be replaced by a ~600 GHz system. The higher frequency system is designed to improve high-k resolution and SNR. For low-k turbulence, the beam emission spectroscopy (BES) system with a new generation of BES detector has been developed by the University of Wisconsin group. The group is planning to expand the BES system from

28 spatial channels to 48 channels for NSTX-U. A 288 GHz polarimetry system for magnetic fluctuation measurements is presently being tested on DIII-D. For the edge region, the gas puff imaging (GPI) diagnostic will be implemented.

10.6.2.1. High-k Scattering System

The 280 GHz high-k tangential scattering system of NSTX will be replaced by a 604 GHz poloidal scattering system being developed by UC Davis for NSTX-U, thereby considerably enhancing planned turbulence physics studies by providing a measurement of the k_θ-spectrum of both ETG and ITG modes. The probe beam in this case will enter the plasma from a port on Bay G while a tall exit window located on Bay L will be employed to collect the poloidally-scattered beams and image them onto an array of 5-8 waveguide mixers. The reduced wavelength in the poloidal system will result in less refraction and extend the poloidal wavenumber coverage from the current 7 cm^{-1} up to > 40 cm^{-1}. As pointed out earlier, measuring the k-θ spectrum as well as k-r spectrum is crucial for identifying the source of turbulence since the 2D k-spectra driven by different instabilities have difference anisotropies. More importantly, the peak of the 2D k-spectrum has to be measured so that the turbulence amplitude can be experimentally correlated to observed plasma transport. The unique property of this new high-k scattering system is that it uses only one microwave launching system but is able to achieve four scattering configurations, which are sensitive to different regions of the turbulence 2D k-spectrum owing to the large magnetic shear in NSTX-U. The probe beam and two scattering beams for the two toroidal scattering schemes are plotted in Fig. 10.41 (a); here the probe beams are tilted toroidally with respect to the scattered beams for +'ve and –'ve radial scattering. In the poloidal scattering arrangement of Fig. 10.41 (b), the first scheme, plotted in blue, has scattered beams going upward in the positive Z direction (upward scattering) while the other scheme, plotted in red, has scattered beams going downward in the negative Z direction (downward scattering). A total of four scattering schemes is thus possible with different combinations of toroidal and poloidal tilt angles. It is noted that the proposed

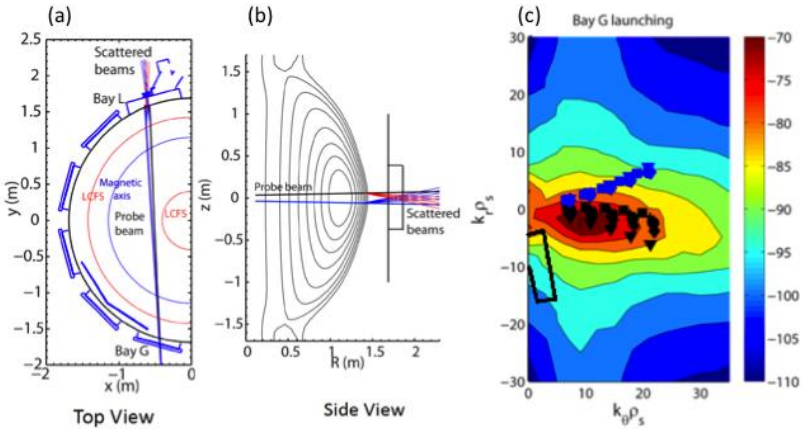

Fig. 10.41. High-k scattering system with two scattering schemes. (a) Schematic of the toroidal cross section of the high-k scattering beam geometry. (b) Poloidal cross sectional view of the beam geometry. (c) Regions in 2D k-r and k-θ space covered by two scattering schemes.

high-k scattering system mainly relies (as did the previous system) on the large magnetic shear in NSTX-U to provide radial localization. The simulation is performed using predicted profiles for a high-performance NSTX-U H-mode plasma. The anisotropy in the 2D k-spectrum of ETG turbulence, i.e. the existence of ETG streamers, can be determined by comparing the k-spectrum measured by the different schemes. Furthermore, a range of kθ and kr can be scanned by varying launching and receiving optics to map a wide range of 2D k-spectrum. An example of the scattering geometries and 2D k-spectrum of turbulence is shown in Fig. 10.41(c).

10.6.2.2. Beam Emission Spectroscopy

The Beam Emission Spectroscopy (BES) diagnostic on NSTX-U, based upon observing the Dα emission of collisionally-excited neutral beam particles, will enable direct spatially-resolved measurements of longer wavelength density fluctuations in the plasma core, providing valuable insights into the suppression of ion turbulence and the attainment of near-neoclassical ion confinement on NSTX-U [23]. The BES diagnostic together with the existing microwave tangential scattering diagnostic (which measures medium to short wavelength turbulence) will provide the most comprehensive turbulence diagnostic set available. The BES diagnostic also enhances measurements of the spatial structure of fast-ion-driven instabilities such as the TAE and BAAE observed on NSTX. BES measurements therefore contribute to several NSTX-U research areas, including turbulence and transport, waves and energetic particles, and boundary physics. Specific scientific applications include investigations of turbulence, turbulent flows, zonal flows, energetic particle modes, and Edge Localized Modes. University of Wisconsin has previously developed an advanced 24-channel Beam Emission Spectroscopy (BES) diagnostic system on NSTX. A schematic of the BES system layout and the collection optics installed inside of the NSTX-U vacuum chamber are shown in Fig. 10.42, respectively. For NSTX-U, an expansion of BES to 48 detection channels will be implemented to improve the scientific productivity of the BES system on NSTX-U. Initial BES measurements on NSTX have identified the general characteristics of long-wavelength turbulence in NSTX plasmas. BES point spread function calculations will be developed to apply BES synthetic diagnostics to simulation results.

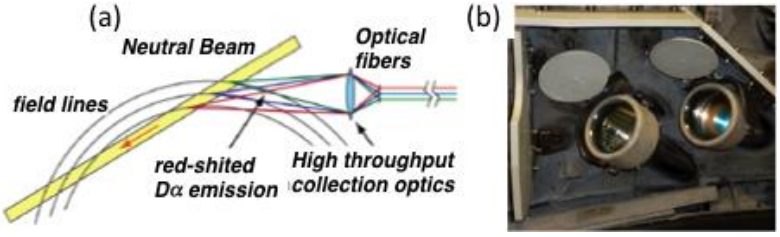

Fig. 10.42. Beam Emission Spectrocopy. (a) A schematic of BES diagnostic system. (b) BES collection optics placed in NSTX-U.

10.6.2.3. Microwave Polarimeter Magnetic Fluctuation Diagnostic

UCLA recently completed development of a sensitive ~300GHz radially-viewing polarimeter to directly measure magnetic field fluctuations in NSTX-U [24]. The polarimeter has been installed on DIII-D in preparation for NSTX-U. DIII-D plasmas are well-suited since operation at magnetic fields (0.5 – 1T) is practical and consistent with NSTX-U. NTM, fast-ion driven mode and microtearing simulations will be utilized to assess feasibility and interpret polarimetry measurement of magnetic fluctuations. Experimental data in conjunction with predicted mode structure will be used to validate simulation codes. It is expected that magnetic fluctuation levels $\tilde{B}$ / B ~ 0.01% will be observable.

10.6.2.4. Gas Puff Imaging Diagnostic

The gas puff imaging (GPI) diagnostic was operated successfully on NSTX from 2000 to 2010, and the existing GPI hardware from 2010 will be reinstalled on NSTX-U at the same location (Bay B) [25]. This diagnostic viewed the 2-D structure of edge turbulence near the outer midplane and provided detailed data on the physics of L-H transitions, zonal flows, blob dynamics, and ELMs. It is planned to add one or more additional GPI views in order to clarify the full 3-D structure of edge turbulence, which is crucial for understanding edge and SOL transport. One of these views would be in the lower divertor region, where interesting turbulent structures have already been seen using (passive) imaging of LiI light. New GPI views at other toroidal and poloidal angles are also desirable to understand the formation process of blobs (which determine the scrape-off layer width) and the structure of zonal flows (which may be important for the L-H transition). In addition, there are interesting interactions between RF waves and the SOL on NSTX which can be studied with GPI at the RF antenna structure. These additional GPI views can be implemented using in-vessel fiber optic bundles and telescopes, as previously done for the GPI diagnostic on C-Mod.

10.6.3. MHD / ASC Diagnostics

For advanced ST operations, it may be necessary to control the pressure and plasma current profiles which would require real time measurements of plasma pressure and current profiles. The JHU group is installing 96 channel edge and core tangential multi-energy-soft-x-ray arrays for fast time scale plasma profile measurements (10.6.1.3). Nova Photonics is implementing real time MSE which can give the real time plasma current profile information in addition to the MSE-CIF (10.6.1.4) and MSE-LIF (10.6.1.5) systems.

10.6.3.1. Magnetics For Equilibrium Reconstruction, Boundary Control, and RWM Suppression

NSTX had a comprehensive set of magnetic diagnostics, including ~ 45 poloidal flux loops, ~ 60 magnetic field sensors for constraining equilibrium reconstruction codes such as EFIT, and 48 in-vessel sensors for measuring and controlling resistive wall modes [26]. These sensor systems will be retained on NSTX-U, but with some significant improvements. In particular, the density of poloidal magnetic field probes flux loops in the divertor region will be increased, in anticipation of improving the magnetic reconstruction of snowflake divertor configurations. Furthermore, a second vertical array of poloidal field sensors will be installed on the center column, increasing the redundancy of these critical measurements. Finally, the density of poloidal magnetic flux loops in the vicinity of the divertor coil mandrels will be increased, allowing better reconstruction of the eddy currents induced in these support structures.

10.6.3.2. Real-Time Velocity Diagnostic

A Real-Time Velocity (RTV) diagnostic was installed on NSTX to measure the plasma toroidal velocity with high temporal resolution [27]. The real-time velocity data will be incorporated into the plasma control system for feedback control of the plasma rotation profile using the NBI systems and non-resonant magnetic braking using the 3-D control coils (10.5.1) as the actuators.

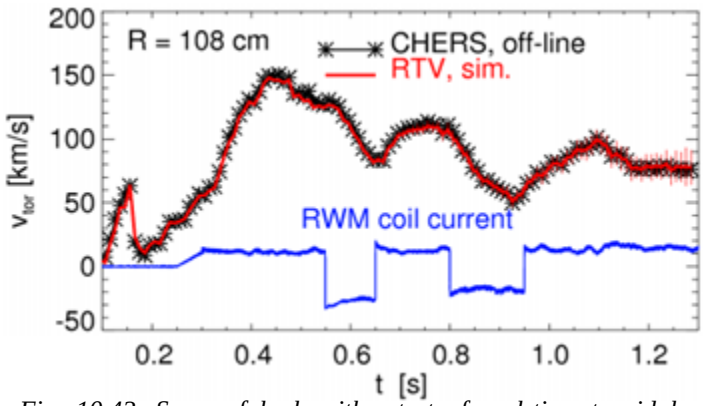

Fig. 10.43. Successful algorithm test of real-time toroidal velocity measurement in NSTX.

The RTV system, based on active charge-exchange recombination spectroscopy (CHERS), can measure at up to six radial locations with a maximum sampling rate of 5 kHz. The RTV system uses two toroidally separated views to distinguish the CVI emission from the region intercepting the heating NB from the background (intrinsic) contribution. The system uses fixed-wavelength spectrometers coupled to fast CCD cameras to provide the high sampling rate needed for real-time control. Acquisition of camera data by a computer and its analysis within a total time interval under 200μs, including the read-out, background subtraction and fitting of multiple Gausian components to the measured line shape, was demonstrated. A scheme for conveying the analyzed data to the NSTX-U plasma control system using its existing data acquisition hardware was developed and tested. The spectrometer wavelength

calibration was established by observing spectral lines close in wavelength to the CVI line from a neon glow discharge run in the NSTX vacuum chamber. A real-time velocity diagnostic, which is integral to macroscopic stability research because of its use in rotation control and disruption detection, has already been installed and successfully tested in NSTX as shown in Fig. 10.43.

10.6.3.3. Real time MSE (rtMSE)

High performance commodity computers have become fast enough to handle the real-time computing requirements needed for rtMSE [28]. We propose to use a fast quad core server running a modified version of the Linux operation system that is used for the NSTX PCS (10.3.3.3). The OS modifications allow for real-time operations and will be coordinated with the computing group on NSTX-U. The digitizer hardware needs to be chosen carefully for compatibility. Equipment from National Instruments and D-Tacq is under consideration. The NI digitizers are more attractive from a hardware perspective, as they are based on the newer PXIe (PXI express) format, which has a very high streaming bandwidth with low latencies. Since MSE derives the pitch angle from a carrier signal at is that National approximately 44 kHz, the digitization rate we currently use is 800 kSamples/s. High density modules suitable for MSE are readily available from NI. However, driver support in Linux needs to be investigated. An encouraging development, NI has begun supporting the PXIe series of digitizers with their MHDDK (Measurement Hardware Driver Development Kit), which allows for custom driver development in Linux at the register level. Another possibility is to use D-Tacq (http://www.d-tacq.com) digitizers, which have already been adapted for use with the custom Linux in question at multiple fusion experiments, including DIII-D, C-Mod, and EAST. In the near term, a suitable digital lock-in will be developed in a language to perform real-time analysis. The MSE pitch angles need to be transmitted to the NSTX-U PCS software. The NSTX-U PCS team will be integrating the rtMSE data into the PCS system via the real-time reconstruction program rtEFIT.

10.6.3.4. Real-Time Multi-Pulse Thomson Scattering (rtMPTS)

The MPTS diagnostic can be modified to supply inputs to the real-time plasma control system (PCS) [29]. An initial step for real-time MPTS (rtMPTS) would be to use existing buffered outputs of the multiplexed raw-data signal as input for a rapid – real-time – calculation of T_e and n_e, for a subset of the existing 42 radial channels. The resulting data would be transferred to PCS in numeric or analog form, as needed. The current two-laser configuration provides a 16.7ms time resolution; the implementation of a third laser would reduce this number to 11.1ms. An advantage of using the buffered outputs mentioned above is that the normal flow of the CAMAC based data acquisition will not be interrupted or compromised, but it comes with an intrinsic latency of 0.4ms.

Using PXI (Peripheral Component Interconnect) electronics or equivalent, one could expect an overall latency of the order of 1ms. The rtMPTS electronics and computer would be located in the polychromator room. A more direct access to the preamplifier outputs would reduce latency at the cost of greater complexity. On the other hand a replacement of the CAMAC data acquisition is clearly needed and at such time attention will be given to the needs of rtMPTS. It might be possible to have all MPTS radial channels available for rtMPTS. In its simplest form rtMPTS could provide two radial channels data: center and edge. But a likely PCS need will be real-time line average density in which case at least ten MPTS radial channels would be needed. In a more advanced scenario, profile information from rtMPTS would be used for real-time equilibrium calculation based on isobaric (p_e) isobaric or isotherm (T_e) isotherm flux surfaces. Such calculation are routinely made in "between shots" analyses, *e.g.* isobaric EFIT02 and isotherm LRDFIT04.

10.6.3.5. Real-Time Density Interferometry

The far infrared tangential interferometer/polarimeter (FIReTIP) has operated reliably in providing line-integrated density measurements on NSTX. Its feasibility for real-time density control has been investigated [30]. Fringe jumps that have been prohibiting the plasma density from use in the direct feedback to actuators have been suppressed. A conceptual design of a density feedback control system including the FIReTIP, control hardware, and software that takes advantage of the NSTX-U plasma control system (PCS) has been developed. It can be used as the basis for a density feedback control system on NSTX-U. A central FIReTIP sightline is to be implemented initially for this a purpose. Fringe jumps in the FIReTIP were well characterized using data obtained with new fast electronics prior to the end of NSTX operations. The algorithms used to suppress the density errors they caused were shown to work properly through comparisons with the Thomson scattering diagnostic. The fringe jump correction algorithm, as well as safety and feedback modules, can be included as part of the PCS effort for NSTX-U.

10.6.3.6. Diagnostics for disruption mitigation experiments

Toakamak disruption mitigation experiments have shown that the dissipation of plasma energy usually consists of two distinct phases: (a) the thermal quench in which plasma loses most of its thermal energy (Δt ~1 ms), and (b) the current quench during which the cold plasma slowly dissipates the stored magnetic energy ($\Delta t \leq 10$ ms). During the thermal quench phase on NSTX, the fast dynamics of the hot plasma ($T_e > 1$keV) can be diagnosed using a collection of soft X-ray (SXR) diagnostics (see 10.6.1.3). The SXR diagnostic suite will be a valuable tool in understanding the role of impurity dynamics during the thermal quench and disruption evolution. Additionally, detailed SXR

measurements of intrinsic impurity concentrations will be used to validate simulation results which can show significant discrepancies in edge plasma densities and impurity levels. ME-SXR measurements on NSTX-U will also provide T_e profile data for the dynamic plasma cooling during a disruption thermal quench, and hence provide quantitative estimates of the large perpendicular heat transport ($\chi_\perp$) [31].

The current quench phase of the tokamak disruption is generally more difficult to diagnose using SXR measurements due to the low electron temperature (~few eV) of the plasma. Therefore, the JHU group plans to develop a novel, fast XUV 2D imaging radiometer which will measure impurity dynamics and spectrally resolved radiated power during the current quench. This diagnostic design is based on previous transmission grating instruments built by the JHU group, with the advanced 2D diode detector providing fast (~10kHz) spatially and spectrally resolved XUV impurity emission measurements (Fig. 10.44) [32]. Like previous TG spectrometers, the fast 2D disruption radiometer uses an imaging slit coupled to a freestanding transmission grating to produce spectrally resolved one dimensional images of the plasma on the 2D diode array detector. The 2D diode detector will measure the impurity line radiation during current quench phase in the XUV range (200-1400Å), with enough SNR to measure the spectra with a rate of ~20 kHz.

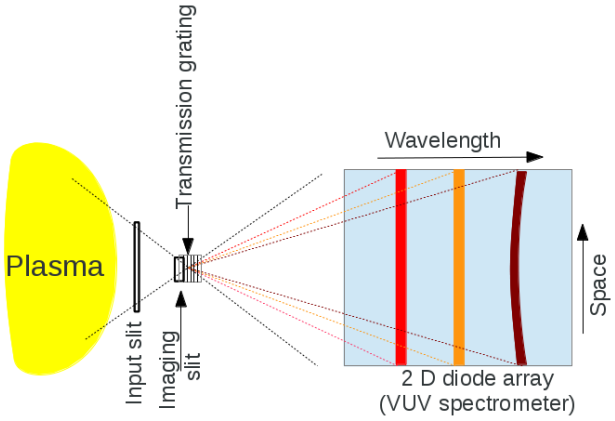

Fig. 10.44. Schematic of TG disruption radiometer.

10.6.4. Boundary Physics Diagnostics

The NSTX/NSTX-U facility has been investing strongly in boundary physics related diagnostics in the past several years. Some of the recently implemented PMI diagnostics which will be available for Day 1 on NSTX-U are shown in Fig. 10.45. There are over 20 PMI and edge plasma diagnostic systems on NSTX-U and additional ones are being readied. They includes Gas-puff Imaging (500kHz), Langmuir probe array [33], Edge Rotation Diagnostics (T_i, V_ϕ, V_{pol}), 1-D CCD H_α cameras (divertor, midplane), 2-D fast visible cameras for divertor and overall plasma imaging [34], Divertor bolometer, IR cameras (30Hz), Fast IR camera (two color), Tile temperature thermocouple array, Divertor fast eroding thermocouple, Dust detector, Quartz Microbalance Deposition Monitors, Scrape-off layer reflectometer, Edge neutral pressure gauges, Material Analysis and Particle Probe, Divertor Imaging Spectrometer, Lyman Alpha (Ly_a) Diode Array, Visible bremsstrahlung radiometer, Visible and UV survey spectrometers, VUV transmission grating spectrometer, Visible filterscopes (hydrogen & impurity lines), and Wall coupon analysis. Major upgraded boundary physics diagnostics are described in more detail below.

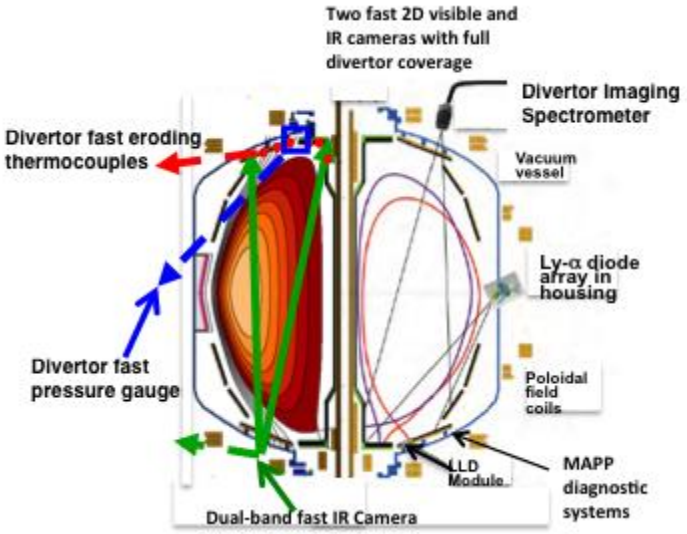

Fig. 10.45. Initial divertor diagnostics for NSTX-U.

10.6.4.1. Material Analysis Particle Probe (MAPP)

A major NSTX-U PMI diagnostic addition is the Material Analysis Particle Probe (MAPP) by Purdue University as shown in Fig. 10.46 (a) [35]. MAPP is an in-vacuo inter-shot diagnostic capable of correlating surface chemistry evolution with plasma response to PMI conditioning. MAPP utilizes multiple surface-science measurement techniques to characterize a sample material exposed to NSTX-U conditions and assess plasma-surface interactions near the divertor strike point. A unique sample head has been designed for MAPP to allow simultaneous exposure of up to four samples to plasma discharges [see Fig. 10.46(b)]. The surface of each sample is positioned (via shims or custom machining) colinear to the top surface of the retaining stems in order to avoid self sputtering.

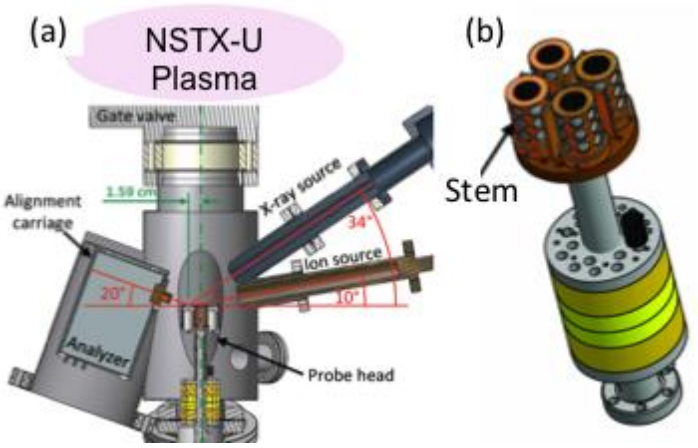

Fig. 10.46. MAPP System (a) Schematic of MAPP system. (b) A schematic of MAPP sample head.

Independently controlled heaters are contained beneath each sample and radiative and conductive cross-talk heating is reduced using perforated sample stems and vertical heat baffle shields. Following plasma exposure, samples are retracted *in-vacuo* into an adjoining chamber, where a variety of analysis techniques are performed during the in-between shot window. Analysis techniques include X-ray photoelectron spectrscopy (XPS) – used to assess the chemical interactions of the top ~10 nm, ion scattering spectroscopy (ISS) – interrogates the top 1-2 monolayers to determine surface chemical composition, and direct recoil spectroscopy (DRS) – uniquely capable of measuring the surface hydrogen content in samples. In addition, thermal desorption spectroscopy (TDS) can be performed at the end of each day in order to measure and quantify bulk deuterium retention.

10.6.4.2. Divertor Spectrometers and Two-Color Fast Infrared Camera

The LLNL collaboration in the divertor diagnostics area on NSTX focused on new and improved measurements for plasma-surface interaction studies with lithium-coated graphite and molybdenum plasma-facing component, as well as divertor impurity and plasma diagnostics. New capabilities included a new vacuum-ultraviolet divertor spectrometer (SPRED) that was brought from LLNL to NSTX-U to monitor carbon and molybdenum emission in the divertor for impurity and power balance studies [36, 10.37]. Another new capability intended to support the NSTX-U lithium program is a new near-infrared spectrometer for divertor molecular and atomic spectroscopy. To provide pilot measurements for radiative divertor control, a new optical Penning discharge chamber is installed in the lower divertor area to provide a way to monitor pressure of deuterium or or gaseous impurities (e.g., argon) that could be injected to increase divertor radiated power. Improvements were also made to other LLNL-supported diagnostics, notably the divertor Lyman-alpha and radiometer array, four one-dimensional filtered CCD arrays, divertor imaging spectrometers, and filterscopes. The goal was to provide routine quantitative emission measurements in the upper and lower divertor areas, as well as the inner outer walls.

Another important divertor diagnostic recently developed is a two-color or dual-band device developed for application to high-speed IR thermography by ORNL [38]. Temperature measurement with two-band infrared imaging has the advantage of being mostly independent of surface emissivity, which may vary significantly for an LLD as compared to that of an all-carbon first wall. In order to take advantage of the high-speed capability of the existing IR camera (1.6-6.2 kHz frame rate), a commercial visible-range optical splitter was extensively modified to operate in the medium wavelength (MWIR) and long wavelength IR (LWIR). This two-band IR adapter utilizes a dichroic beamsplitter which reflects 4-6 micron wavelengths and transmits 7-10 micron wavelength radiation, each with > 95% efficiency and projects each IR channel image side-by-side on the camera's detector. The ORNL boundary physics group has designed and implemented a wide angle, 30 Hz infrared camera system on NSTX in FY 2011. A dual-band adapter was also implemented for variable surface emissivity due to lithium films. This system was designed as part of Princeton University student's first year experimental project. In addition, two eroding thermocouples near the PFC tile surface were installed and instrumented. These thermocouples, which have a design response time ~ 1 ms are intended to be used in the future for feedback control of PFC surface temperature in NSTX-U. Finally a set of 16 new "filterscope" chords were implemented. The gain control and data acquisition is done dynamically via PC. The units are capable of 100 kHz sampling speeds.

A Divertor Imaging Radiometer for spectrally resolved measurements of the radiated power by Johns Hokins will extend the multi-energy concept to divertor diagnostic by performing absolute measurements of the radiated power in tens of spectral bins covering the range from several eV to few hundred eV (VUV to XUV). The radiometer will use dual transmission gratings in conjunction with a direct detection CCD camera and will view the divertor from the outboard side, with vertically spaced lines of sight from the X-point region to the strike-point region. The instrument will have ≥2 cm space resolution and ≥10 ms time resolution. The proposed diagnostic will provide, for the first time in a tokamak, measurements of the spectrally resolved radiated power from the divertor and will enable determination of the radiating impurity type and charge state distribution over the range of temperatures expected for the NSTX-U divertor. This in turn will provide information on the radiating efficiency and transport of *injected* impurities for radiative divertor studies, as well as information on *intrinsic* impurities and associated radiation. In addition, the proposed diagnostic will be used to calibrate and validate the advanced divertor modeling codes used at NSTX-U. We will also study using the radiometer in conjunction with divertor emission modeling for a spectroscopic diagnostic of the electron temperature and cross-field particle transport in the divertor. Even if approximate, such measurements will be useful for the NSTX-U divertor research.

10.6.4.3. Dust Detector and Quartz Crystal Microbalances

Another novel PMI diagnostic is the first real-time detection of surface dust inside a tokamak that was made using an electrostatic dust detector [39]. As shown in Fig. 6(a), a fine grid with 25 μm spacing of interlocking circuit traces was installed in the NSTX-U vessel and biased to 50 V. Impinging dust particles created a temporary short circuit and the resulting current pulse was recorded by counting electronics. Various techniques were used to increase the detector sensitivity by a factor of 10,000 to match NSTX-U dust levels while suppressing electrical pickup. The results were validated by comparison to laboratory measurements, by the null signal from a covered detector that was only sensitive to pickup, and by the dramatic increase in signal when Li particles were introduced for wall conditioning purposes. It should be noted that the real time dust measurement is necessary to safely manage the dust generated in ITER. Dynamic retention of deuterium, lithium deposition, and the stability of thick deposited layers were measured by three quartz crystal microbalances (QMB) deployed in plasma shadowed areas at the upper and lower divertor and outboard midplane. Deposition of 185 $\mu g/cm^2$ over 3 months in 2007 was measured by a QMB at the lower divertor while a QMB on the upper divertor, that was shadowed from the evaporator, received an order of magnitude less deposition. Occasionally strong variations in the QMB frequency of thick lithium films were observed suggesting relaxation of mechanical stress and/or flaking or peeling of the deposited layers.

10.6.4.4. Divertor Thomson Scattering System

Understanding divertor heat and particle transport in the advanced divertor configurations is a necessary first step toward their performance optimization. Also understanding the linkages between the midplane SOL and divertor is very important for ITER and the design of future fusion devices. An effort is underway by the LLNL group to develop a conceptual design of the Divertor Thomson Scattering (DTS) system in NSTX-U [40]. The DTS system would not only support the planned advanced and radiative divertor studies, but would also enable unique physics studies of the lithium coated plasma facing components, ELM transport in the divertor, and many others. In combination with the additional midplane SOL Thomson scattering channels in the SOL, the DTS system would provide unique two-point T_e and n_e profile measurements upstream and downstream of the divertor X-point region that would allow critical tests of SOL heat and particle transport models. Implementation of DTS is a large technical effort that involves various personnel skills, e.g. physics, engineers, technicians, safety engineers, as well as a wide range of work activities: mechanical and optical engineering and design, diagnostic assembly, and facility integration. The latter alone is a large effort which would require designing and fabricating three new ports on the NSTX-U vacuum vessel, their metrology and safety. The LLNL activities in the area of conceptual design are summarized as follows. LLNL personnel have been involved in operation of the DIII-D DTS since the beginning of 2012. Valuable experience has been gained from hands-on maintenance, alignment, and design of upgrades. A beam schematic of a possible divertor Thomson scattering system is shown in Fig. 10.47. LLNL have also identified possible laser beam and collection optics placement and viewing geometries using the NSTX-U center stack and vacuum vessel models.

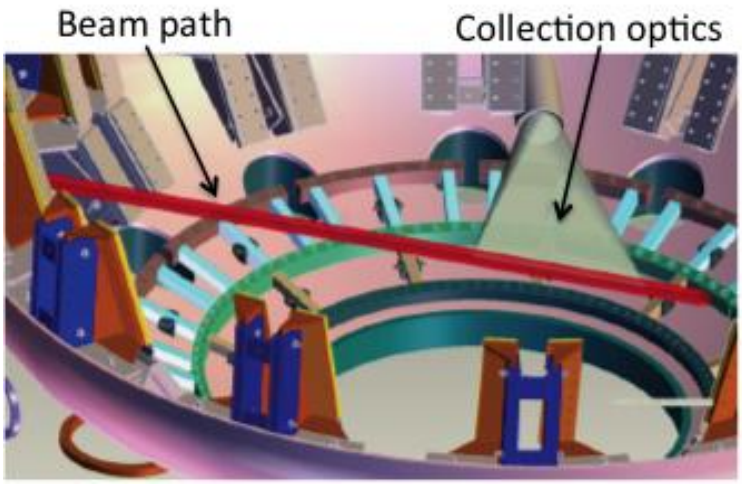

Fig. 10.47. Divertor Thomson Scattering geometry proposed for NSTX-U

10.6.5. Energetic Particle Diagnostics

In the energetic particle (EP) research area, in addition to the perpendicular and newly implemented tangential fast ion D-alpha (FIDA) diagnostics, additional SSNPA (Solid-State Neutral Particle Analyzer) channels will be implemented since the scanning NPA was removed. Additional diagnostics for EP studies on NSTX-U include neutron rate counters, a scintillator-based Fast Lost-Ion Probe (sFLIP), installed on the vessel wall, and a new charged fusion product (CFP) profile diagnostic. The 16 channel reflectometry will be also installed for the energetic particle mode measurements.

10.6.5.1. Energetic Particle Distribution Diagnostics

On NSTX-U the radial fast ion profile is characterized through the FIDA and ssNPA systems. A vertical FIDA system [41] measures fast ions with small pitch, corresponding to trapped or barely passing (co-going) particles. A new tangential FIDA system [42] (Fig. 10.48) measures co-passing fast ions with pitch *~0.4* at the magnetic axis up to *1* at the plasma edge. Both FIDA systems have time resolution of *10* ms, spatial resolution *≈5* cm and energy resolution *≈10* keV. An upgraded solid-state Neutral Particle Analyzer [43] (ssNPA) will provide energy-integrated measurement of trapped fast ions, with a lower energy threshold E_{min}*~20* keV, from 5 radii. The ssNPA system will mainly work in current-mode to get fast time response. The sampling rate is *≈ 1* MHz. Two ssNPA channels will also incorporate pulse-counting mode capability to obtain energy spectra with *~10* keV energy resolution and *~10* ms temporal

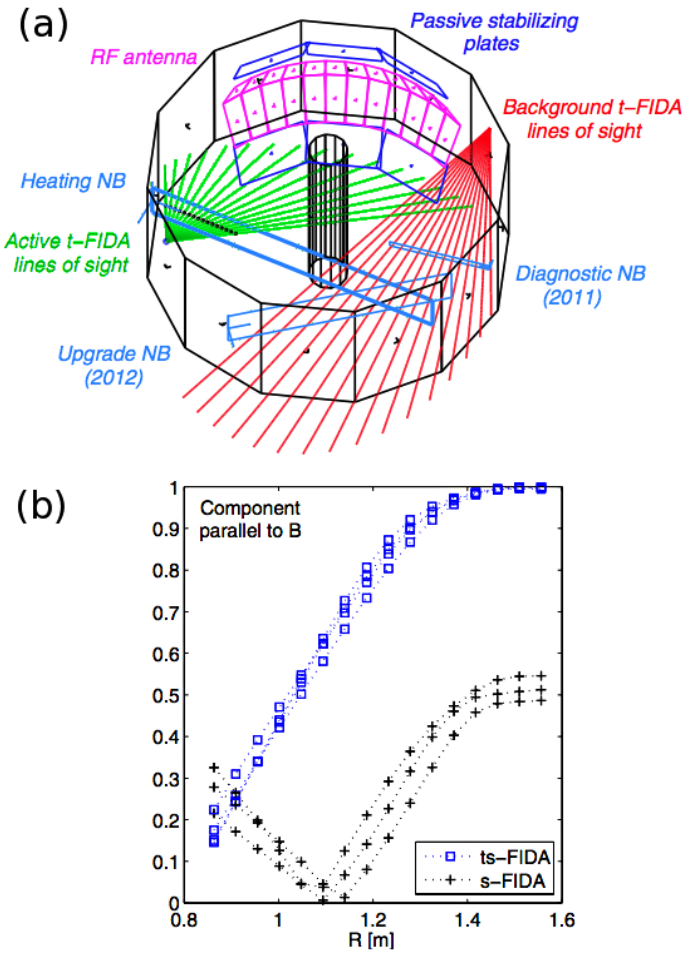

Figure 10.48. (a) Layout of the new tangential FIDA system. (b) Expected component parallel to the magnetic field for the tangential (ts-FIDA) and vertical (s-FIDA) FIDA systems. A value of 1 (0) on the y axis corresponds to a parallel (perpendicular) view.

resolution. The fast-ion distribution function F is a complicated function of energy, pitch angle, space, and time. Successful reconstruction of F requires multiple measurements with a variety of techniques.

In hardware, UC Irvine will concentrate on four active beam measurements: vertical FIDA, tangential FIDA, E||B NPA, and SSNPA. In analysis, we will develop software that uses these and other fast-ion diagnostics to infer the fast-ion distribution function from the data. Inverted distributions will be compared with calculations by theoretical collaborators. The vertical FIDA system is a working diagnostic that has been producing valuable data for several years. Only minor changes to this diagnostic are proposed. The tangential FIDA system is patterned after the vertical FIDA diagnostic. Although it has not collected data during plasma operations, its installation is essentially complete. The SSNPA diagnostic will be displaced from its present location by the new beam-line. A new SSNPA diagnostic will be designed and installed to measure trapped fast ions at several radial locations.

Spectral information from FIDA is complemented by data from a NPA system at a fixed radius. The excellent spectral resolution of the NPA is required for careful validation of NUBEAM predictions. The neutral particle analyzer (NPA) in use on NSTX [42] utilizes a E||B (superimposed parallel electric and magnetic fields) spectrometer developed at PPPL that simultaneously measures the mass-resolved energy spectra of both H and D neutrals with a time resolution of ~0.1 ms, set by signal-to-noise levels. A multi-anode micro-channel plate detector provides 35 energy measurements for each species with an energy dynamic range of $E_{max}/E_{min}=30$. The tunable energy range is $E_H=1–600$ keV, $E_D=1–300$ keV and the energy resolution varies over a range of $\Delta E/E=2–5\%$, moving from high to low energy. Intersection of the E||B NPA sightline with the neutral beam footprint enabled localization of measurements to the plasma core region. The primary applications of the E||B NPA on NSTX have been measurement of fast ion redistribution and/or loss due to wave-particle interactions that are driven by MHD activity and the characterization of fast ion response to HHFW injection.

Additional diagnostics for EP studies on NSTX-U include neutron rate counters, a new charged fusion product (CFP) profile diagnostic and a scintillator-based Fast Lost Ion probe (sFLIP), installed on the vessel wall. Neutron counters are strongly weighted toward the higher-energy portion of the distribution function, with no pitch dependence. For example, an increased count rate during HHFW injection is a straightforward indicator of the formation of tails in the fast ion distribution above the NB injection energy. In addition to the volume-integrated detectors that were already available on NSTX-U, a set of 4 collimated neutron detectors is being considered for installation in

Year 3 (pending incremental funding). These additional measurements can be integrated in the TRANSP code for improved constraints on the simulated neutron rate.

Similarly to neutron counters, the CFP diagnostic would provide direct measurements of the fusion reactivity [45]. Because both protons and tritons are largely unconfined for NSTX-U parameters, fusion products are eventually detected outside the plasma volume. By knowing the magnetic field geometry, their orbit can be tracked back in the plasma. Such orbits are equivalent to curved sightlines for each detector, so that multiple signals can be inverted to infer a radial profile of the high-energy fast ions. A 4-channel CFP prototype will be tested in FY-13 on the MAST device, then a 8-channel (possibly upgraded to 16 channels) system will be ready for installation on NSTX-U in FY-14. Target performance is 1-2 ms temporal resolution for fusion reactivity levels comparable with the NSTX-U values.

A scintillator-based Fast Lost Ion probe (sFLIP) contributes to the NB characterization by providing energy and pitch resolved spectra of lost fast ions, e.g. from prompt losses, as the NB tangency radius is varied. sFLIP is being upgraded with a faster CCD detector capable of frame rates up to 100 kHz [46]. A set of photo-multiplier tubes is also being installed on sFLIP for energy and pitch integrated measurements at rates up to 250 kHz from 6-10 sub-regions of the sFLIP scintillator plate.

10.6.5.2 Energetic-Particle-Induced Mode Diagnostics

A recently-developed, UCLA 16-channel comb quadrature reflectometry system has been utilized on NSTX to study the eigenmode structure of fast-ion driven Alfven as well as other MHD modes [47]. This unique system has also provided a wealth of additional information including investigation of three-wave coupling processes and identification of the potential role of Compressional Alfven Eigenmodes (CAEs) in contributing to core anomalous transport. In order to prepare for higher density operation in NSTX-U it is proposed to expand operation to 100GHz through the installation of 8 additional channels. This upgrade to 24 channels will allow detailed eigenmode structure measurements in high performance NSTX-U plasmas.

Similarly to NSTX, several arrays of high-frequency Mirnov coils will provide routine measurements of the fluctuations spectrum on NSTX-U. Two sets of coils are toroidally displaced to enable the computation of the toroidal mode number of the modes from the phase of the complex spectrum. A reduced set of coils is displaced poloidally to provide information on the poloidal mode structure. The bandwidth of the magnetic fluctuation measurements will be extended on NSTX-U from the present 2-2.5 MHz up to 4 MHz, to

account for the expected frequency up-shift of the modes as the toroidal field is increased.

Another quantity of great relevance for EP studies is the radial structure of *AE modes. Several complementary systems will be available to this end on NSTX-U, including beam emission spectroscopy (BES) arrays, reflectometers, interferometers, polarimeters, and X-ray detectors. A proposal for installing a Doppler back-scattering (DBS) system will be also considered based on the available funds (see below).

The BES system (as described in Sec.10.6.2.2.) will provide low-k density fluctuation measurements near the mid-plane for normalized radii $0.1<r/a<1$. The number of channels will be increased from 32 up to 64 to simultaneously sample a wide region of the plasma. The measurement region will extend poloidally to cover a ~10 cm broad strip along the mid-plane. Further improvements may include a toroidally-displaced set of viewing channels, possibly limited to the edge region, to measure background emission (in the absence of the 2nd NB source) or the toroidal mode number of the instabilities.

Density fluctuations are also derived from a multi-channel reflectometer system. The 16 channels available on NSTX will be complemented by 8 new channels at higher frequency, which will enable fluctuation measurements up to densities ~10^{20} m^{-3}. Line-integrated measurements of density fluctuations will also be available from 3-4 far-infrared interferometer with sampling frequency ~4MHz.

Beside density fluctuations, other quantities such as magnetic field and velocity fluctuations are important for a thorough identification and characterization of the different instabilities. A new radial polarimeter system will provide direct measurement of magnetic fluctuations along the mid-plane. Pending incremental funding for diagnostics development, flow fluctuations will be measured through a millimeter-wave Doppler back-scattering (DBS) system operating in the 80-100 GHz frequency range. This new measurement capability represents an alternative, substantially independent tool for identifying fast-ion modes that would significantly strengthen comparison with theory, expanding previous internal measurements of fast-ion modes previously restricted to perturbed density on NSTX.

Additional information on fluctuations with frequency < 100 kHz will be provided by a multi-energy SXR array with two toroidally displaced sets of views. Spatial resolution varies from ~1cm at the outboard mid-plane ($R>150$ cm) to ~3 cm in the core and inboard mid-plane region ($40<R<140$ cm) (see Fig. 10.38). Faster measurements with up to ~500 MHz bandwidth will be available from a system of two poloidal SXR arrays.

Each array contains 16 channels viewing poloidally through two variable selected filters, with 2-3 cm resolution.

10.6.5.3. Alfven Eigenmode Antenna for AE Stability Measurements

Simple antennae have been used in several machines (JET, C-Mod) to study TAE stability. The linear damping rate can be measured by sweeping the antenna frequency through the mode frequency. It will be useful to extend these studies to low aspect ratio tokamaks (MAST and NSTX). This would also help to validate ITER projections by challenging our fundamental understanding of the physics in the drive and stability of these modes. For low aspect ratio the antenna can also be used to study higher frequency Alfvén modes such as GAE and CAE.

The "MHD active spectroscopy" plan begins with relatively simple antenna design. As operational experience builds up, more ambitious designs will be tried. In years 1&2 several proto-type antenna designs will be evaluated to optimize the coupling to TAE and CAE. The NSTX-U prototype AE antenna system consists of up to 4 compact modules, each of which is a single, 5-turn 'window-frame' coil, similar in principle to those used on JET, C-Mod and MAST. In parallel, the external power supplies for driving the antenna, the coupling networks and control hardware and software will be developed. While the highest priority will be to develop the capability to study TAE, some time will be devoted to evaluating the antenna and coupling network at frequencies up to 2MHz, as will eventually be needed for Global and Compressional Alfvén eigenmode studies.

Pending incremental funding, in Years 3-5 there will be the opportunity for continued improvement of *AE antenna designs and perhaps amplifier upgrades. Additional coils will allow for improved selectivity of the toroidal mode number, as well as improving the coupling of the antenna to the modes. However, particularly in years three and four there will an emphasis on designing experiments to measure TAE linear damping rates under as broad a range of conditions as possible. The low power (≈1kW) experiments will provide important information on antenna coupling and natural damping rates for each of the eigenmodes. This information will be used to determine the potential benefits of higher power experiments. If the natural eigenmode damping rates are small, there is the possibility of driving them to amplitudes where stochastic heating of thermal ions occurs.

10.7. NSTX-U Plasma Operation Start-Up Plan

Making the transition from engineering project management to operations engineering requires certain considerations. For example, sound project management will lead to the successful completion of a system to all of its technical requirements, but may not consider important concerns such as that system's operation in concert with other systems, staging the pre-operational and subsequent integrated system testing, establishing and controlling interrelated subsystem operating limits, maintaining interrelated safety interlock and equipment protection circuitry, maintaining configuration control during repairs/maintenance, proper analysis of hazards before beginning work, training and work authorizations for engineers/operators/technicians, managing personnel access to the various experimental areas, defining expected personnel conduct while in these areas, and managing temporary modifications.

The NSTX-U project has addressed the above considerations with a network of administrative and technical procedures to assign operational roles, coordinate operations-related activities and machine configurations, and maintain a safe work environment. This includes the authorization of allowable operating parameters for a given machine configuration, and the system for the establishment/testing of all coil protection systems for those parameters.

The NSTX-U integrated system testing, commissioning, and start-up will follow the same process as the NSTX initial start-up in 1999, and each subsequent return to operations after an extended outage where machine upgrades were implemented. There are four components to NSTX-U post-construction start-up:

1. Activity Certification Committee (ACC) Review
2. Operational Readiness Assessment (ORA)
3. Completion of sub-system preoperational testing (PTP's)
4. Run start-up procedure (OP-NSTX-02) including integrated system testing (ISTP)

The NSTX-U Activity Certification Committee (ACC), comprised of representatives from PPPL Engineering, Physics, Safety, and the DOE Princeton Area Office (PAO), reviews newly installed sub-systems and collateral devices with regard to personnel, environmental, and machine safety. The ACC will perform physical walk-downs of equipment and document reviews in developing a findings report to be submitted to the PPPL Deputy Director of Operations and the NSTX-U Operations Manager. After submittal of the ACC report and any associated open items, non-compliances or safety concerns, the PAO will conduct an Operational Readiness Assessment (ORA) before the project may move to start-up.

By this time, the sub-system cognizant engineers will have developed and are performing their pre-operational test procedures (PTP's). The NSTX-U Start-Up procedure (OP-NSTX-02) will coordinate and document the completion of the various sub-system PTP's, interlock and equipment protection test procedures, and all safety system checks. OP-NSTX-02 concludes with the NSTX-U Integrated System Test Procedure (ISTP-01) which establishes, tests, and documents the allowable NSTX-U operating parameters. ISTP-01 must be re-performed for any changes in those operating parameters.

The NSTX-U team is formulating the operational plan toward full operational capability for NSTX-U. In Table 10.3, a draft plan is shown based on assessment of physics needs for first year of operations. As shown in the table, the 1st year goal is to operate NSTX-U with the electromagnetic forces (I_pB_T) at halfway between NSTX and NSTX-U limits and 50% of the NSTX-U design-point of heating of any coil. This still allows NSTX to operate at B_T ~ 0.8 T, I_p ~ 1.6 MA, and the maximum flat-top duration of 3.5 s in the first year which is far beyond the achieved NSTX parameters. The device will be inspected and refurbished as needed at the end of the each operating year. For the second year, the toroidal magnetic field will be increased to its full field value of 1 T but keeping the heating of the coil to 75% of the design-point of any coil. This will allow 3 sec discharges at full field and current. The same limits should allow the full 5 sec discharges at B_T ~ 0.8 T, I_p ~ 1.6 MA. The device will be brought to full operational capability in the third year of NSTX-U operation. The proposed NSTX-U research operation weeks are shown in Fig. 10.2 and 10.3 depending on the budget scenarios. The operation weeks are reduced in FY 2016 and 2017 to accommodate the significant outage activities to install major upgrade hardware such as cryo-pump and divertor PFCs as shown in the figures.

	NSTX	Year 1 NSTX-U	Year 2 NSTX-U	Year 3 NSTX-U	Ultimate Goal
I_P [MA]	1.4	1.6	2.0	2.0	2.0
I_PI_P [MA^2]	2.0	2.5	4.0	4.0	4.0
B_T [T]	0.55	0.8	1.0	1.0	1.0
B_TB_T [T^2]	0.3	0.65	1.0	1.0	1.0
I_PB_T [MA*T]	0.61	1.3	2	2.0	2
Allowed I^2t Fraction On Any Coil	1.0	0.5	0.75	1.0	1.0
I_P Flat-Top at max. allowed I^2t, I_P, and B_T [s]	~0.7	~3.5	~3.	5	5

Table 10.3. A draft NSTX-U operational plan toward full operational capability.

References

[1] J. E. Menard, S. Gerhardt, M. Bell , et al., *Nucl. Fusion* **52**, 083015 (2012).
[2] NSTX Upgrade Project Team.
[3] J. Hosea, et al., Phys. Plasmas **15**, 056104 (2008).
[4] G. Taylor et al., US-Japan RF Heating Phys!ics Workshop, Nara, Japan, December 14, 2012.
[5] T. Kariya, et al, J. Infrared, Millimetre and Terahertz Waves **32,** 295-310 (2011).
[6] S. A. Sabbagh, J. Bialek, R.E. Bell, *et al., Nucl. Fusion* 44 (2004) 560.
[7] R. Raman, et al., IEEJ Transactions on Fundamentals and Materials, Vol. **132**, No. 7 pp 468-471 (2012)
[8] J. Canik et al., APS-DPP, PP8.00030 (2012).
[9] J-K Park et al., IAEA FEC, EX P4-33 (2012), Submitted to Nuclear Fusion.
[10] D. K. Mansfield, A. L. Roquemore, H. Schneider, et al., Fusion Eng. and Design **85**, 890 (2010).
[11] H. W. Kugel, et al., Physics of Plasmas 15, 056118 (2008).
[12] C.H. Skinner et al., J. Nucl. Mater. (2013), http://dx.doi.org/10.1016/j.jnucmat.2013.01.136.
[13] R. Raman et al., IAEA FEC, EX P2-10 (2012), Submitted to Nuclear Fusion.
[14] R.J. Fonck, et al., APS DPP (2012) **GO6 10**, Providence, Rhode island.
[15] A. Diallo, B. LeBlanc et al., Rev. Sci. Instrum. **83**, 10D532 (2012); doi: 10.1063/1.4740267
[16] R.E. Bell, R. Feder, Rev. Sci. Instrum. **81**, 10D724 (2010).
[17] T. M. Biewer, R. E. Bell, et al., Rev. Sci. Instrum. **75**, 650 (2004).
[18] K. Tritz, D. J. Clayton, D. Stutman, et al., Rev. Sci. Instrum. **83**, 10E109 (2012).
[19] D. Stutman, M. Finkenthal, et al., Rev. Sci. Instrum. 70, 572 (1999)
[20] F. M. Levinton, H. Yuh, Rev. Sci. Instrum. **79**, 10F522 (2008).
[21] E.L. Foley and F.M. Levinton, Journal of Physics: Conference Series **227**(2010) 012007.
[22] R. Barchfeld, C.W. Domier, et al., APS-DPP PP8.38 (2012)
[23] D. R. Smith, R. J. Fonck, G. R. McKee, and D. S. Thompson, Rev. Sci. Instrum. 83, 10D502 (2012)
[24] J. Zhang, et al., Plasma Phys. Control. Fusion **55** (2013) 045011.
[25] S.J. Zweben et al, Phys. Plasmas **17**, 102502 (2010).
[26] S. P. Gerhardt, et al., NSTX-U Diagnostic Brainstorm Meeting, July 2011.
[27] M. Podesta and R.E. Bell, Rev. Sci. Instrum. **83** (2012) 033505.
[28] F. Levinton, et al., NSTX-U Diagnostic Brainstorm Meeting, July 2011.
[29] Ben LeBlanc et al., NSTX-U Diagnostic Brainstorm Meeting, July 2011.
[30] J.-W. Juhn, K. C. Lee, Rev. Sci. Instrum. **81**, 10D540 (2010)

[31] L F Delgado-Aparicio, D Stutman, K Tritz, et al., Plasma Physics and Controlled Fusion, 49(8):1245, 2007.
[32] D Kumar, M Finkenthal, D Stutman, et al., Plasma Physics and Controlled Fusion, 54(6):065010, 2012.
[33] M.A. Jaworksi et al, Fusion Eng. Design **87** 1711 (2012)
[34] R.J. Maqueda et al, Nucl. Fusion **50**, 075002 (2010)
[35] C.N. Taylor, et al., *Rev. Sci. Instrum.* **83**, 10D703 (2012).
[36] V.A. Soukhanovskii, et al., *Rev. Sci. Instrum.* **81**, 10D723 (2010).
[37] F. Scotti, et al., *Rev. Sci. Instrum.* **83**, 10E532 (2012).
[38] A.G. McLean, *et al. Rev. Sci. Instrum.* **83** 053706 (2012).
[39] C. H. Skinner, et al., *Rev. Sci. Instrum* **81,** 10E102 (2010).
[40] V. Soukhanovskii, et al., NSTX-U Diagnostic Brainstorm Meeting, July 2011
[41] M. Podestà et al., Rev. Sci. Instrum. **79** 10E521 (2008)
[42] A. Bortolon et al., Rev. Sci. Instrum. **81** 10D728 (2010)
[43] D. Liu et al., Rev. Sci. Instrum. **77** 10F113 (2006)
[44] S. S. Medley, et al., Rev. Sci. Instrum. **75** 3625 (2004)
[45] W. U. Boeglin et al., Rev. Sci. Instrum. **81** 10D301 (2010)
[46] D. S. Darrow, Rev. Sci. Instrum. **79**, 023502 (2008)
[47] S. Kubota et al, Rev. Sci. Inst. **81**, 10D917 (2010)

Table of Contents for Chapter 11

Chapter 11

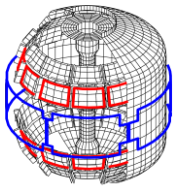
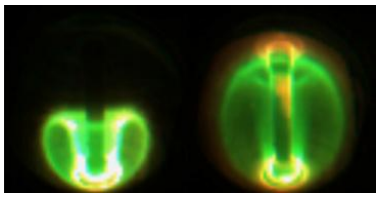
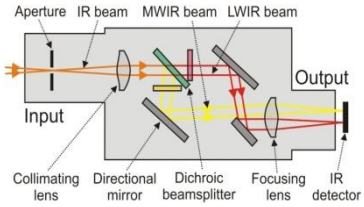

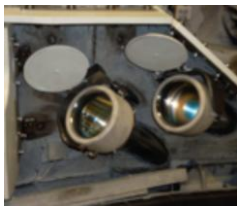

NSTX-U Collaborator Research Plans

11.1 Introduction

Research on NSTX-U is carried out by a National Team of research groups from 24 universities, national laboratories (including PPPL), and private industry, many of which participated in the team building effort since FY1998, obtaining direct collaboration funding from DOE. Approximately 68% of the NSTX-U scientific staff is from these collaborating institutions. The contributions of all collaborating institutions, including foreign cooperation not funded by DOE, have been extensive, as is evident from the overview and plan sections of this 5-year plan. The collaboration plans by U.S. institutions other than PPPL are briefly described in this chapter to provide supporting information to the overall NSTX-U 5-year plan. These plans include activities already funded by DOE for durations up to 4 years, and contain new ideas that extend to FY2018. The out-year collaborative research plans will require timely discussions within the NSTX-U research team before formal proposals are submitted to DOE for peer review and approval. It is expected that during the FY2014-2018 period the research efforts by collaborating institutions will increase at a rate proportional to the rate of NSTX-U research efforts by PPPL. Among the 156 research users of NSTX-U funded by DOE including graduate students and post-doctoral researchers, 106 are from collaborating institutions and 50 are from PPPL. An additional 89 national and 61 international scientists not funded by DOE also collaborate on NSTX via analysis, simulation, and experiments. PPPL engineers and technicians carry out the operation, maintenance, and upgrades of the NSTX facility, and the interface, installation, and maintenance of diagnostics including those provided by the collaborating researchers at an effort level of 107 FTEs. The research and facility operations teams have worked together effectively to enable rapid progress toward the mission of NSTX-U since the beginning of NSTX operation.

11.2 NSTX-U National Collaborator Research Plans

Detailed descriptions of proposed/planned research are provided below organized by institution, research topic, principal investigator, and contributing scientists and students. Multiple listings for the same institution imply research is being carried out on more than one grant and/or topic.

11.2.1 University of Colorado at Boulder

Research Topic: Assessment of Edge Turbulence and Convective Transport through Velocity Field Analysis

Principal Investigator: Tobin Munsat
Participating Graduate Students: Yancey Sechrest
Funded under DOE Grant: DE-FG02-08ER54995

Introduction

This collaboration involves both analysis of data from the NSTX Gas Puff Imaging (GPI) diagnostic and hardware modifications to this diagnostic instrument. The goal of the data-analysis portion of the project is to bring the unique GPI data to bear on the diverse topics of scrape-off layer turbulence and transport, identification of zonal flows and geodesic acoustic modes (GAMs) in the NSTX edge, the relationship between edge poloidal flow and turbulence, relationships between flows and transport bifurcations (including L-H transitions), ELM physics and ELM-related transport including Lithium effects, and divertor and x-point fluctuation studies. Analysis of this type and advanced understanding of the quantities uniquely accessible to GPI are critical to the evaluation the plasma-boundary interface in fusion plasmas, and can have significant impact on next-step devices.

The hardware portion of the project involves a continual evolution of the GPI instrument (as space and budget allow) to address several of the scientific goals of NSTX-U through a suite of edge turbulence studies. Potential modifications include the implementation of multiple cameras and multiple simultaneous views (increased from 1 view currently). The hardware plans are kept as simple as possible, taking advantage of re-entrant windows and external coherent fiber bundles (i.e. avoiding in-vacuum optical hardware), while making use of fast cameras that are already in-hand. The enhanced capability will enable extended measurements of 3-D turbulent structures along common B-field lines, as well as detailed information on the interplay between 3-D resonant magnetic perturbations (RMPs) and turbulence dynamics.

Current research contributions to NSTX Upgrade

Recent studies include the development of the HOP-V velocimetry code, written by the Principal Investigator specifically for use with the NSTX GPI data [1], as well as a series of edge-turbulence studies which have characterized the behavior of coherent structures in the NSTX edge [2-5]. We have collaborated closely with Dr. Stewart Zweben on this work.

Summary of proposed research plan for 2014-18

To address several of the scientific goals of the forthcoming NSTX upgrade, we propose to continue our experiments with the curent Gas-Puff Imaging (GPI) diagnostic for a suite of edge turbulence studies, as well as implement a series of upgrades, as access and budget allow. Critical topics addressed by this diagnostic (in its current and modified form) include scrape-off layer turbulence and transport, identification of zonal flows and geodesic acoustic modes (GAMs) in the NSTX edge, study of the underlying relationship between edge poloidal flow and turbulence, relationships between flows and transport bifurcations (including L-H transitions), ELM physics and ELM-related transport including Lithium effects, and divertor and x-point fluctuation studies. Many of the topics studied for general understanding of edge turbulence and flow will have additional importance when studied in the context of resonant magnetic perturbations (RMPs) in the upgraded NSTX.

While there is not currently budget for an extensive modification of the diagnostic or the NSTX interface, there are several diagnostic enhancements that are possible using existing hardware. Specifically, the current single GPI view can be extended to include a second view from Bay B with only a minor modification of the existing GPI re-entrant port and will enable simultaneous sightlines in opposite directions along the same flux tube. In addition to the second Bay B view, we may have an opportunity to make use of a top-view (Bay E) onto a divertor-region gas manifold, all of which exists or is already under development.

Furthermore, we may be able to implement two additional Phantom v710 cameras, which were purchased by PPPL and are currently in use at C-Mod, if they become available (the additional cameras are perhaps the most costly component of an enhanced GPI system). These relatively minor modifications will enable extended measurements of 3-D turbulent structures (along common B-field lines), as well as detailed information on the interplay between 3-D resonant magnetic perturbations (RMPs) and turbulence dynamics.

The elements of our plan displayed in a timeline are:

Timeline

FY2014:

- Continue analysis of single-view GPI data, emphasizing "blob" transport and interplay with edge turbulence, transport bifurcations, and ELM studies.

FY2015:

- Continue analysis of single-view GPI data, emphasizing "blob" transport and interplay with edge turbulence, transport bifurcations, and ELM studies.

FY2016:

- Implement second Phantom v710 camera at Bay B for dual-view studies.
- Analysis of extended 3-D structures in NSTX edge.

FY2017:

- Implement top-view camera of divertor gas-manifold.
- Analysis of divertor behavior and linkage between divertor and edge structures.

FY2018:

- Continue analysis of combined GPI dataset for boundary turbulence studies.

Contributions to the NSTX-U 2014-18 Five Year Plan:

The plan above was defined in a process carried out over CY2011-12 in coordination with the NSTX-U Research Team. The research defined above contributes to the Boundary Physics chapter of the NSTX-U Five Year Plan and was defined in consultation with Dr. Ahmed Diallo who is deputy leader of the Boundary Physics topical science group.

References

[1] T. Munsat and S.J. Zweben, "Derivation of time-dependent two-dimensional velocity field maps for plasma turbulence studies," *Review of Scientific Instruments* **77**(10) 103501:1-13 (2006).

[2] Y. Sechrest, T. Munsat, D.J. Battaglia, and S.J. Zweben, "Two-Dimensional Characterizaton of ELM Precursors in NSTX," Nucl. Fusion **52** 123009 (2012).

[3] D.A. Russell, J.R. Myra, D.A. D'Ippolito, T.L. Munsat, Y. Sechrest, R.J. Maqueda, D.P. Stotler, S.J. Zweben, and the NSTX Team, "Comparison of scrape-off layer turbulence simulations with experiments using a synthetic gas puff imaging diagnostic," *Physics of Plasmas* **18** 022306 (2011).

[4] Y. Sechrest, T. Munsat, S.J. Zweben, R.J. Maqueda, D. Russell, D.A. D'Ippolito, and J.R. Myra, "Flow and Shear Behavior in the Edge and Scrape-off Layer in NSTX L-Mode Plasmas," *Physics of Plasmas* **18** 012502 (2011).

[5] S.J. Zweben, R.J. Maqueda, R. Hager, K. Hallatschek, S. Kaye, T. Munsat, F.M. Poli, L. Roquemore, Y. Sechrest, and D.P. Stotler, "Quiet Periods in Edge Turbulence Preceding the L-H Transition in NSTX," *Physics of Plasmas* **17** 102502 (2010).

11.2.2 Columbia University

Research Topic: Study of MHD Stability, Active Mode Control, and Disruption Avoidance in NSTX-U

Principal Investigator: Dr. Steven A. Sabbagh
Participating Scientists: Dr. John Berkery, Dr. James Bialek, Dr. Young-Seok Park
Funded under DOE Grant: DE-FG02-99ER54524

Introduction

The overall goal of macroscopic stability research in NSTX-U is to establish the physics understanding and control capabilities needed to produce sustained stability of high performance ST plasmas in a yet unexplored hotter operational regime at the highest level of current self-sustainment ever routinely produced in such a device. Dating back to before the construction of the NSTX device, Columbia University group research has historically aimed toward advancing the goal of sustained high beta, high performance operation in the ST. The presently proposed research plans to logically extend this successful work in the areas of passive global mode stabilization and the prediction of marginal kinetic stability boundaries, active RWM detection, real-time modeling and control, rotation control and related physics of non-resonant neoclassical toroidal viscosity, and to expand our understanding of 3D fields for MHD mode stabilization. Past work had the implicit goal of disruption avoidance. An emphasis for the coming 5 year plan is the application of the physics understanding of the global mode passive and active stabilization physics, and non-resonant rotation alteration for direct prediction of disruptions, and avoidance of disruptions through rotation and q profile control. This research will provide the predictive physics understanding needed to confidently extrapolate toward the goal of a steady-state Fusion Nuclear Science Facility (ST-FNSF) / Component Test Facility (ST-CTF) [1-3], a pilot plant [4], or DEMO based on the ST [5]. As was exploited in NSTX, the unique ST operational space and device geometry of NSTX-U will be leveraged to extend and test physics theories and technological solutions for next-step spherical torus (ST) and tokamak operation, including ITER. To further support ITER, and expand explicit connection between NSTX-U and ITER, Columbia U. group leadership in the ITPA will evolve to improve connection and communication of global mode stabilization and control with the disruption avoidance goals of both devices. Also, in the last five years, the Columbia U. group has expanded international collaboration activities with the South Korean long-pulse superconducting tokamak program and the KSTAR device. This work has been, and continues to be a complementary connection to our primary research on NSTX/NSTX-U. Along with the unique long-pulse, advanced tokamak device capability of KSTAR, the device also offers the largest difference in aspect ratio of large-scale tokamaks in the world, providing the best platform to compare experimental results and test theoretically expected differences due to aspect ratio with NSTX/NSTX-U. A summary of our research plan elements is given below:

Physics Research Elements

- Understand and advance the passive stabilization physics of global modes for disruption prediction and avoidance, focusing on plasmas with reduced collisionality.

- Create and study improved techniques of global mode active feedback control to sustain macroscopic stability, including ITER-relevant low rotation regimes.

- Understand unverified theoretical aspects of neoclassical toroidal viscosity physics (NTV), with direct and unique application of non-resonant NTV for open and closed-loop rotation control.

- Expand the understanding of the application of 3D fields for MHD mode stabilization.

Current research contributions to NSTX-Upgrade and vision for the next five years

The Columbia University group research has contributed to NSTX since the conceptual design of the device. As this research has a long history, we restrict this brief summary to start with the significant milestone reached by the group on NSTX - the first active stabilization of the resistive wall mode (RWM) at low aspect ratio, and at reduced plasma rotation applicable to ITER [6]. This initial work evolved into expanded long-pulse control capability [7], and the most recent successful application of dual-field component (poloidal and radial field) proportional gain feedback of $n = 1$ RWM instability [8]. The Columbia University group was also responsible for the design and implementation of the first model-based real-time RWM state-space controller, first run on long-pulse plasmas with among the highest $\beta_N = 6.4$ and $\beta_N/\ell_i > 13$ operated in the device [8-10]. The group will continue this research in the coming 5 years of NSTX-U, expanding the present system for independent control capability of the actuator coils, addition of new coils, and advancing the physics models used in control, for both off-line and real-time research. This will include an initial study of the control or avoidance of large internal instabilities. During the last 5 years, the group established a new physics paradigm to explain the complex behavior of the observed RWM stability boundary as a function of plasma rotation. A theoretical model of kinetic RWM stabilization physics [11] was tested against specific NSTX experiments [7,12]. The model and coding (the MISK code) continues to be developed, with attention now placed on the effects of fast particles and plasma collisionality [13]. Recent analysis of specific experiments directly measuring the RWM stability of plasmas approaching the marginal stability boundary by low frequency MHD spectroscopy is helping to explain striking experimental results by the group of improvement to RWM stability at the highest values of $\beta_N/\ell_i > 10$ [8,14]. The results appear generally consistent with the present kinetic RWM stabilization physics hypothesis. Critical research in the coming NSTX-U operation will be the testing of this hypothesis at further reduced plasma collisionality. This will include the testing of

highly-simplified stability models that will be used in real-time instability avoidance via rotation profile control. The Columbia U. group began the investigation of plasma rotation alteration via the application of non-resonant 3D fields in the early 2000s, and a multi-year research program of experiments and quantitative theoretical understanding led to the published observation of neoclassical toroidal viscosity [15] (NTV) in NSTX [16]. In 2013, the group plans to continue analysis on data taken in several dedicated experiments run on NSTX, including further analysis of the superbanana plateau regime in NSTX [9]. The Columbia U. group will continue this research in the coming five years of NSTX-U, aiming at quantitative comparison between theory and experiment. Some examples include the comparison of results from several codes including NTVTOK which the Columbia U. group is now testing, and the IPEC (J.K. Park) and POCA (K. Kim) codes, understanding of NTV physics at reduced collisionality, and long-pulse aspects such as the NTV offset rotation, which appears to be quite small in NSTX, and therefore is different from results published on DIII-D. This research will additionally be directly applied toward creating a reduced model of NTV suitable for use in the planned real-time rotation control system for NSTX-U. The Columbia U. group was also responsible for the physics design of the present RWM control coils system on NSTX [17], and continues this effort in the present calculations of RWM control performance (see Chapter 2) of the proposed off-midplane NCC coils, which are included in the base research budget of NSTX-U. These coils will bring significant new capability that will greatly enhance research on NSTX-U for the entire team, as well as for the Columbia U. group. Intriguing results of ELM mitigation attempts in NSTX by a team experiment led by the Columbia U. group are of increased importance when compared to recent ELM mitigation results on KSTAR by the Columbia U. group using $n = 2$ non-resonant applied fields. The comparison of these results may reveal key physics aspects of ELM mitigation due to the significant aspect ratio difference between the devices. A present urgent need for ITER, as well as for future ST fusion devices planned to operate continuously, is the reliable prediction, avoidance, and mitigation (PAM) of plasma disruptions. Macroscopic stability research by the Columbia U. group on NSTX from its inception has targeted the stabilization of beta-limiting, disruptive instabilities that stop the plasma, or otherwise prevent it from operating at high fusion performance. The research described above will directly and substantially contribute to the advanced disruption prediction and avoidance studies and control described in detail in Sections 2.2.1, 2.2.3, and 9.2.3. This research will be addressed in close conjunction between the Macrostability and Advanced Scenario and Control topical science groups. An essential component of all research mentioned above has been the ready availability of accurate, between-shots experimental kinetic equilibrium reconstructions with the NSTX EFIT code [18,19]. The Columbia U. group has provided this capability for NSTX since its inception, and will continue this effort on NSTX-U with upgrades suitable for the new device capabilities.

Summary of proposed research plan for 2014-18

Progress accomplished to date in the study of MHD stability, active mode control, and configuration optimization in NSTX sets the stage for the Columbia U. group to propose a 5 year program of study, leading research in several key areas to support the long-pulse sustainment of high beta plasmas created in the device. The research applies to NSTX-U and the future development path of the ST, and will provide key physics understanding for advanced tokamak operation and future burning plasma devices, including ITER. This plan is well-aligned with the detailed plan presented in the Macroscopic Stability research chapter (Chapter 2) of this document. A summary of specific tasks in our plan displayed in a timeline are:

Timeline

FY2014:

- Expand RWMSC real-time control software to allow independent actuation of six RWM control coils, and a more general sensor input scheme, for Day 0 plasma operations.
- Complete analysis of existing NSTX data from specific experiments investigating NTV. This existing data includes an investigation of NTV vs. plasma collisionality over a broad range attainable in NSTX, past operation in the superbanana plateau regime, and magnetic braking by dominant $n = 2$ and n = 3 field configurations.
- Update all NTV experimental analysis tools to allow processing suitable for NSTX-U capabilities (e.g. independent control of the midplane RWM coils).
- Evaluate simple physics criteria (suitable for real-time use) for the approach to global mode marginal stability based on ideal (e.g. pressure peaking, β_N/l_i) and kinetic stability physics using initial high performance NSTX-U plasmas, emphasizing rotation profile and speed.
- Compare $n = 2$ ELM mitigation results on KSTAR using the midplane in-vessel coil configuration with past NSTX results showing a lack of mitigation with a similar applied field scenario, targeting field pitch and aspect ratio effects as key differences.

FY2015:

- Conduct initial assessment of stability limits on normalized β and plasma rotation, V_ϕ, at the increased aspect ratio of NSTX-U, with new shaping control and off-axis NBI. Compare to ideal and kinetic stability limits using DCON and MISK codes.
- Begin assessment of theoretically favorable stability conditions, through a combination of dedicated experiments utilizing low frequency MHD spectroscopy to directly measure stability and by probing unstable plasmas, for enhanced kinetic stabilization of global MHD modes (including rotation profile proximity to stabilizing, energetic particle profile and distribution, q_{min}, and β_N). Test stability physics expectations of increased global

mode stability at the highest β_N/l_i in NSTX-U plasmas, and compare to positive results found in NSTX, examining potential differences due to aspect ratio.

- Establish dual field component n = 1 active control capability in new NSTX-U operational regime. Compare theoretically expected changes in feedback phase/gain to experiment. Examine expanded capabilities allowed by six independent power supplies for the RWM control coils.
- Examine effectiveness of n =1 RWM model-based state space control with independent actuation of six control coils for initial high β_N plasmas. Compare RWMSC modeled sensor signals (controller observer model) with experiment for a single n = 1 eigenfunction versus adding n = 2 eigenfunctions. Initially compare the degree of mismatch between the RWMSC observer model and sensor measurements, and the occurrence of plasma disruptions for future input to the disruption warning system.
- Determine optimizations of RWMSC control by varying the amount of plasma rotation-induced stabilization in the controller guided by MISK kinetic stabilization calculations.
- Examine the real-time difference between the n = 1 RWMSC observer and measured RWM poloidal field sensors to evaluate the observer physics model and determine thresholds for disruption detection appropriate for use in the NSTX-U disruption warning system.
- Utilize initial NSTX-U ME-SXR and poloidal USXR diagnostics to characterize the RWM eigenfunction by non-magnetic means.
- Make initial assessment of the dependence of NTV profile and strength as a function of plasma collisionality. Conduct initial experiments using combined n = 2 and 3 field configurations versus the separate application of n = 2 and n = 3 fields.
- Prepare an initial simplified real-time model of NTV profile as a function of applied field and available plasma parameters for use in initial plasma rotation control system.
- Evaluate the neoclassical offset rotation as a function of plasma parameters in long-pulse, steady-state plasmas. Examine the NTV offset rotation utilizing HHFW heated plasmas.
- Perform initial experiments using open-loop plasma rotation, current profile, and energetic particle control to demonstrate the ability to avoid encountering disruptive global mode stability boundaries based on kinetic RWM stabilization models.

FY2016:

- Begin investigation of the dependence of global mode stability on reduced collisionality through a combination of dedicated experiments utilizing low frequency MHD spectroscopy to directly measure stability, creating unstable plasmas, and investigating mode-induced disruptions in the general database. Compare experimental results to kinetic stabilization theory. Open-loop rotation control will be the default for these studies, with initial closed-loop control used if available.

- Adjust present simplified physics models of RWM marginal stability based on initial high beta operation of NSTX-U in the first year of operation, and operation at reduced collisionality reached in the second year, appropriate for real-time calculations.
- Theoretically determine improvements to global mode stability expected by adding the partial NCC based on improved understanding gained in the first 2 years of operation.
- Examine effectiveness of $n = 1$ active mode control as a function of plasma rotation. Compare theoretically expected changes in optimal $n = 1$ feedback phase and gain including stabilization effects due to plasma rotation to experimental results. Examine the effect of partial RWM control coil use during $n = 1$ feedback, examining the impact on the higher-n perturbation spectrum (also supports ITER, JT-60SA).
- Assess global mode stability and control modifications during the more standard use of the snowflake divertor configuration.
- Examine RWMSC multi-mode control with n up to 3 and determine improvements of theory / measurement comparison shown by the controller observer. Test optimizations of RWMSC control by varying the plasma rotation-induced stabilization in the controller; compare to experiment and MISK calculations. Examine improvements to disruption detection via the RWMSC based on multi-mode capability of the observer.
- Conduct initial tests on the observer physics model by adding dual-component sensors in RWM feedback, comparing experiment to theory.
- Theoretically assess the importance of real-time variation of plasma response parameters in the RWMSC based on experimental studies conducted in the second year of operation.
- Theoretically determine improvements to the RWMSC by adding the partial NCC (planned for addition to NSTX-U in FY2017) and an extended RWM sensor set (planned for addition to NSTX-U in FY2018).
- Examine changes to ME-SXR/poloidal USXR measured RWM eigenfunction as a function of plasma rotation. Determine the degree of global mode internalization by comparing magnetic and SXR diagnosis as a function of proximity to marginal stability.
- Determine improvements to kinetic RWM stability possible by utilizing expanded capability for non-resonant rotation control by the enhanced 3D field spectrum afforded by the planned partial NCC, based on theory and the first 2 years of NSTX-U operation.
- Determine improvements to active feedback of $n > 0$ modes via PID and RWMSC control allowed by the partial NCC, and implement control system changes to test theory in Year 4 device operation.
- Determine the experimental dependence of the superbanana plateau NTV on plasma collisionality and compare to theory.
- Utilize real-time model of NTV profile as a function of applied field configuration, strength, and plasma rotation in the plasma rotation control system and evaluate model performance in closed-loop feedback.

- Improve simple physics criteria used to determine global mode marginal stability adding energetic particle stabilization and expanding the kinetic stabilization model.
- Determine the applicability of single mode RFA phase information in low frequency MHD spectroscopy measurements to supplement amplification in determining proximity to global mode stability boundaries.
- Improve disruption prediction using the RWMSC observer model and sensor measurements by improving the model and/or sensor mismatch criteria used.
- Implement and test initial disruption avoidance using the real-time RWMSC observer model. Test open-loop disruption avoidance criteria at low rotation (most ITER relevant).
- Implement results from a real-time evaluation of the simple global mode marginal stability model into plasma rotation and q profile control systems that will be available in real-time during FY17-18.
- Implement single mode RFA amplitude and phase as input to profile control systems and disruption warning system.
- Determine physics implications of scenarios that overload 3D field and NBI actuators for simultaneous use in meeting open-loop requests for plasma profile targets for rotation, q, energetic particle population, β_N, and other key parameters for disruption avoidance.
- Combine physics criteria for disruption avoidance systems (profile control and disruption warning systems) allowing variable prioritization of control to avoid physics request conflicts and to avoid actuator overloading.

FY2017:

- Utilize V_ϕ control to improve RWM stability by: (i) performing closed-loop rotation control studies, and (ii) changing proximity to stabilizing kinetic resonances for stability control
- Validate kinetic RWM stabilization physics at reduced v^* and varied fast ion populations with closed-loop q_{min} control in plasmas with non-inductive current fraction approaching, or at 100%; determine changes to the effectiveness of n = 1 PID and RWMSC active mode control during closed-loop feedback of plasma rotation profile and q_{min} control in these plasmas.
- Generalize n = 1 control software for n = 2 control use and to allow the use of a poloidally extended RWM sensor set (available in Year 5) and the partial NCC coils.
- Compare n = 2 active feedback control using proportional gain to the NSTX-U model-based RWM state space controller.
- Examine the effect of varying kinetic RWM stabilization in the RWMSC by varying RWMSC control inputs via multi-phase PCS operation based on real-time β_N calculation.
- Implement real-time RWMSC observer into disruption warning system. Use RWMSC observer in disruption warning system during closed-loop feedback of plasma rotation profile, and q_{min} control with non-inductive current fraction approaching or at 100%.

- Examine time-evolution of global mode internalization using newly-installed, toroidally-displaced ME-SXR diagnostic; prepare for real-time input to disruption warning system.
- Experimentally determine the dependence of NTV profile and strength as a function of plasma collisionality at the highest ion temperatures, and evaluate the expected stronger role of electron NTV in this condition.
- Determine/implement a real-time evaluation of a simple global mode marginal stability model including key parameters (e.g. plasma rotation speed and profile, q_{min}, T_e, n_e) that will be available in real-time during Years 4-5.
- Add/use real-time rotation and q_{min} measurements and evaluations for determining global mode marginal stability boundaries, enabling improved evaluation of physics model.
- Examine real-time low frequency MHD spectroscopy in determining global mode stability boundaries for input to stability profile control systems (e.g. rotation, q). Determine single mode RFA amplitude and phase criteria that predict disruptions, and evaluate possible improvements afforded by multi-mode RFA.
- Evaluate and study the stability physics response of real-time rotation and q profile control using the simple kinetic stabilization physics criteria and real-time low frequency MHD spectroscopy for avoiding global mode marginal stability boundaries, including initial use of the partial NCC as an actuator for rotation control.
- Test coupling of real-time RFA, simple physics model, and RWMSC observer systems in providing simultaneous actuation of stability profile for global mode stability avoidance.
- Perform initial studies of mode stabilization utilizing improved open-loop plasma rotation profile control afforded by the partial NCC added to the present RWM coil set.
- Perform initial investigation of dual field component $n = 1$ active control using the newly-installed partial NCC, including variations of feedback phase vs. poloidal angle.
- Perform initial investigation RWMSC active control using the newly-installed partial NCC, including applied control field helicity with respect to mode helicity.
- Utilize the newly-installed partial NCC to expand plasma rotation profile variation and control, with the goal of improving RWM stability, with comparison to theory.
- Conduct active $n > 0$ feedback research using the partial NCC to uniquely address physics for ITER and future STs and tokamaks (e.g. JT-60SA), including (i) mode control with partial toroidal / poloidal coverage of the control coils, (ii) robustness of model based RWM state space control with reduced sensor / control coil availability, (iii) relative importance of midplane vs. off-midplane control coil arrays.
- Utilize closed-loop rotation control, including initial use of the partial NCC, to produce the broadest and most peaked rotation profiles possible, and high, intermediate, and low rotation levels, comparing offline and real-time rotation models to theory.
- Make initial use of the partial NCC to test theoretical expectations of applied 3D fields as their helicity is varied compared to the equilibrium plasma field helicity.

FY2018:

- Test kinetic RWM stabilization models in the lowest ν* regimes.
- Characterize the poloidal variation of $n = 1 – 3$ global mode activity using a newly-installed expanded RWM sensor set, including a comparison to the theoretically computed NSTX-U multi-mode spectrum.
- Evaluate experimental improvements to real-time kinetic stabilization models through the addition of real-time Thomson scattering results.
- Determine physics improvements to RWMSC observer for disruption detection and implement to demonstrate reduced disruptivity to internal modes in 100% non-inductive, high β_N plasmas. Improve disruption prediction using the RWMSC observer by the addition of the newly-installed expanded RWM sensor set.
- Combine disruption avoidance control with simultaneous use of $n > 0$ active feedback and the partial NCC, determining physics implications and potential control conflicts.
- Experimentally determine optimal 3D field spectra, including use of the partial NCC, for minimizing or maximizing NTV vs. applied current and compare to theory.
- Examine NTV at the lowest plasma collisionality possible in the device to determine if a saturation of NTV at low collisionality can be found, as expected by theory.
- Demonstrate low rotation profile operation using NTV in steady-state with closed-loop rotation control, producing plasma rotation most applicable to ITER and utilizing the partial NCC, with comparison to theory.
- Combine plasma rotation, q-profile, and, β control to demonstrate improved RWM and internal MHD mode stability using ITER-relevant (low rotation), high rotation inductive scenarios, and 100% non-inductive ST-FNSF scenarios, demonstrating very low plasma disruptivity in dedicated experiments.
- Determine the physics and controllability implications of using/omitting upgrades to the combined control systems, including the partial NCC, expanded RWM sensor set, real-time Thomson scattering, and real-time ME-SXR data.
- Test the RWMSC observer physics model by adding a newly-installed expanded RWM sensor set providing improved diagnosis of the mode spectrum in the poloidal direction.
- Examine superior RWMSC settings and multi-mode active control with n up to 3 and the partial NCC to demonstrate improved global MHD mode stability in 100% non-inductive plasmas, demonstrating very low plasma disruptivity in dedicated experiments.
- Utilize the added profile control capabilities allowed by the partial NCC with closed-loop plasma rotation profile control to demonstrate, based on kinetic stabilization theory, reduced disruptivity by actively avoiding global instabilities.

Contributions to the NSTX-U 2014-18 Five Year Plan:

S.A. Sabbagh is responsible for defining the Columbia University group contributions to the NSTX Five Year Plan. J.W. Berkery is the present deputy leader of the Macroscopic Stability topical science group and is responsible for overseeing the Macroscopic Stability chapter (Chapter 2) of the NSTX-U Five Year Plan. The plan above was defined in a process carried out over CY2011-12 in coordination with the NSTX-U Research Team. The research defined above contributes significantly to the Macroscopic Stability research plan, and interfaces with other topical science group research, especially the Advanced Scenarios and Control group.

References

[1] Y.K.-M Peng, et al., Fusion Sci. Technol. **60** (2011) 441.
[2] Y.K.-M Peng, et al., Fusion Sci. Technol. **56** (2009) 957.
[3] Y.K.-M Peng, et al., Plasma Phys. Control. Fusion **47** (2005) B263.
[4] J.E. Menard, et al., Nucl. Fusion **51** (2011) 103014.
[5] H.R. Wilson, et al., Nucl. Fusion **44** (2004) 917.
[6] S.A. Sabbagh, R.E. Bell, J.E. Menard, *et al.*, Phys. Rev. Lett. **97** (2006) 045004.
[7] S.A. Sabbagh, et al., Nucl. Fusion **50** (2010) 025020.
[8] S.A. Sabbagh, et al., "Overview of Physics Results from the National Spherical Torus Experiment", 24th IAEA Fusion Energy Conference, San Diego, CA, USA, 8-13 October 2012, paper OV/3-1; submitted to *Nucl. Fusion*.
[9] S.A. Sabbagh, et al., "Resistive Wall Mode Stabilization and Plasma Rotation Damping Considerations for Maintaining High Beta Plasma Discharges in NSTX", *23rd IAEA Fusion Energy Conference*, Daejeon, Republic of Korea, 11-16 October 2010, paper EXS/5-5.
[10] S.A. Sabbagh, et al., "Model-based global MHD instability control in high beta tokamak plasmas including real-time influence of three-dimensional conducting structure", submitted to Phys. Rev. Letters (2013).
[11] B. Hu, and R. Betti, Phys. Rev. Lett. **93** (2004) 105002.
[12] J.W. Berkery, et al., Phys. Rev. Lett. **104** (2010) 035003.
[13] J.W. Berkery et al., Phys. Rev. Lett. **106** (2011) 075004.
[14] J.W. Berkery, et al., "Global Mode Control and Stabilization for Disruption Avoidance in High-β NSTX Plasmas", 24th IAEA Fusion Energy Conference, San Diego, CA, USA, 8-13 October 2012, paper EX/P8-07.
[15] K.C. Shaing, S.P. Hirschman, and J.D. Callen, Phys. Fluids **29** (1986) 521.
[16] W. Zhu, S.A. Sabbagh, R.E. Bell, et al., Phys. Rev. Lett. 96 (2006) 225002.
[17] S.A. Sabbagh et al., Nucl. Fusion **44** (2004) 560.
[18] S.A. Sabbagh, et al., Nucl. Fusion **41** (2001) 1601.
[19] L.L. Lao, et al., Nucl. Fusion **25** (1985) 1611.

11.2.3 CompX

Research Topic: Collaboration with NSTX in Calculations of Radiofrequency and Neutral Beam Heating and Current Drive Sources

Principal Investigator: R.W. (Bob) Harvey
Participating Scientists: R.W. Harvey, Yuri V. Petrov
Funded under DOE Grant: DE-SC0006614

Introduction

This grant supports development of finite-orbit-width (FOW) capabilities in the CQL3D Fokker-Planck code, and validation, interpretation and prediction of the NSTX-U experimental heating, current drive, and prompt fast ion losses. CQL3D is used in conjunction with the DC Lorentz equation FOW RF diffusion coefficient calculator, the GENRAY ray tracing code, and the ORNL AORSA full wave code. NSTX, and now NSTX-U, are ideal machine for exploration of finite-orbit-width effects on heating, current drive, transport, and NBI particle sources. CompX's code suite provides relatively fast estimates of FW, EC, EBW and NBI heating and current drive. The codes calculate time-dependent velocity distribution functions of ions and electrons throughout the tokamak cross-section, from which many synthetic diagnostic signals are (and others can be) obtained, for validation against experiment.

Current research contributions to NSTX Upgrade

Implementation and validation of finite ion orbit width effects in the bounce averaged Fokker Planck code CQL3D

A sequence of major modifications was made to the ion zero-orbit-width (ZOW) Fokker Planck code CQL3D [1] to include finite-orbit-width (FOW) corrections [2,3,4]. In addition, the effects of evolving the background plasma, and of time-dependent modulated neutral beams, were implemented [5]. Part of the motivation for these modifications came from 2010 comparisons between measured and simulated Fast Ion Diagnostic FIDA by Liu *et al.*[4] of signals resulting from neutral beam injection (NBI) and high harmonic fast wave (HHFW) RF power injected into the NSTX spherical tokamak. A significant radial inward shift of the simulated FIDA signal using the previous zero-orbit-width (ZOW) CQL3D was found compared to the NSTX experimental results [6,7]; however, the comparison between finite-orbit-width the PPPL (FOW) NUBEAM Monte Carlo Fokker-Planck code (NBI only) derived FIDA and experiment was excellent[7]. This [7,8] strongly motivated, and led to, a new program to include FOW effects in the CQL3D finite-difference FP code.

A first order (in banana width over minor radius) FOW correction was initially implemented in CQL3D which gave too large an outward shift [2], presumably due to very fat orbits.. This is shown by the green curves in Figures 1(a) and 1(b). On the other hand, the ZOW CQL3D

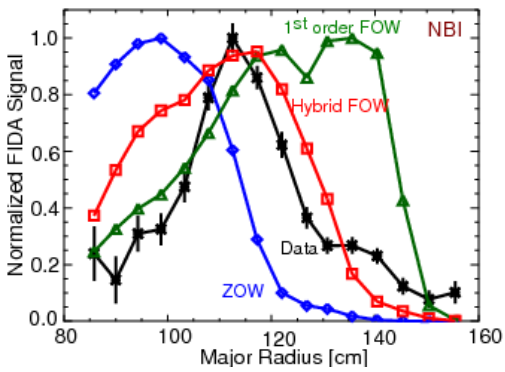

Figure 1(a): Measured and simulated FIDA signals for NBI heating only in NTSX. FIDA data is shown as black curve and symbols, simulated FIDA data for ZOW, 1st order FOW, and Hybrid FOW CQL3D are shown as the blue, green, and red curves and symbols respectively.

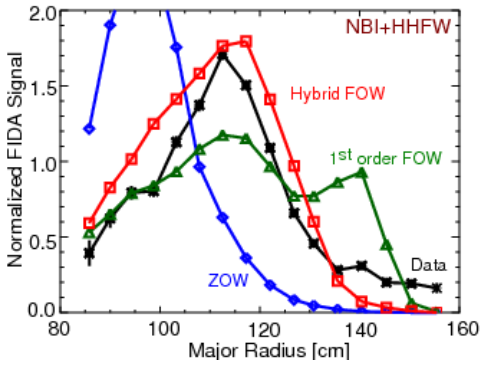

Figure 1(b): Measured and simulated FIDA signals for NBI+HHFW heating in NTSX. FIDA data is shown as black curve and symbols, simulated FIDA data for ZOW, 1st order FOW, and Hybrid FOW CQL3D are shown as the blue, green, and red curves and symbols respectively.

predictions (blue curve) are clearly shifted inwards compared to the experimental FIDA data (black curves) . CQL3D was modified by including full guiding-center orbits in the neutral beam and HHFW quasilinear diffusion calculations [3]. This model gives accurate fast ion losses to the plasma edge, including an added gyro-radius shift from the guiding center orbits. Simulations based on this most recent model (red curves in Fig. 1) were found to produce quite good comparison with experiment.

A new result from the CQL3D NBI+HHFW NSTX calculation is greatly enhanced FI power losses to the chamber wall compared to the NBI phase Losses are 7% of NBI power, and 28%, and increasing, of the HHFW power.

The Hybrid-FOW CQL3D does not currently include neoclassical radial diffusion, but rather calculates the distribution function separately on each flux surface. A full FOW upgrade of CQL3D that is now underway will provide neoclassical radial diffusion. It is a step beyond the usual theory in that there is no assumption of small orbits, and it includes nonthermal effects. The inclusion of the full radial neoclassical diffusion may account for the small calculated FIDA signal (in red curves) compared to the measured FIDA signals in Figure 1(a) and 1(b) at high plasma radius. This work is in progress.

CompX Recent Supporting Activities for GENRAY/CQL3D at PPPL

(1) Gary Taylor was assisted in modeling of ECH for NSTX-U, using updated GENRAY/CQL3D at PPPL[9].
(2) GENRAY ray tracing results were benchmarked against a new paraxial ray tracing code (LHBEAM), and the TORIC-LH code, in work led by Nicola Bertelli at PPPL[10].
(3) CompX assisted Nicola Bertelli at PPPL in using GENRAY, particularly in his addition of a density fluctuation scattering operator for modeling of LHCD in C-Mod. Further modeling in conjunction with CQL3D examined the effects on density fluctuation scattering on calculated C-Mod LH current drive profiles[11].
(4) Gary Taylor was supported in calculations of HHFW CD pertaining to NSTX, using GENRAY/CQL3D [12].

Summary of proposed research plan for 2014-18

CQL3D, DC, GENRAY and AORSA will be validated against NSTX-U and NSTX, and applied to interpretation and prediction of these experiments. The primary near term goals are upgrade and verification of NFREYA in CQL3D, verification against NUBEAM, completion of the finite-orbit-width neoclassical modification of CQL3D, application and comparison of the DC-AORSA RF diffusion coefficient calculation with GENRAY/CQL3D-FOW, and support of HHFW, MHFW, EBW, EC, and NBI code application activities of PPPL NSTX scientists.

Elements of our plan displayed in a timeline are:
(Throughout the period, NSTX scientists are supported in use of CompX codes.)

Timeline:

2014-2015:

- Complete Finite-Orbit-Width CQL3D Modification.
- Upgrade NFREYA cross-sections in CQL3D and verify against NUBEAM.
- Continue DC-AORSA Lorentz orbit RF diffusion calculations.

2015-2016:

- Comparisons/predictions of CQL3D-FOW with NSTX and NSTX-U.
- Continue DC-AORSA Lorentz orbit RF diffusion calculations.

2016-2017:

- Introduction of radial transport, per gyrokinetic codes, into CQL3D.
- Comparison of transport effects with experiment.

2017-2018:

- Comparison of transport effects with experiment.

Contributions to the NSTX-U 2014-18 Five Year Plan:

The plan above was defined in a process carried out over CY2011-12 in coordination with the NSTX-U Research Team. The research defined above contributes to the Wave Heating and Current Drive chapter of the NSTX-U Five Year Plan and was defined in consultation with Dr. Gary Taylor who is leader of the Waves and Energetic Particles topical science group.

References

[1] R. W. Harvey and M. G. McCoy, "The CQL3D Fokker Planck Code", in IAEA Technical Committee Meeting on Advances in Simulation and Modeling of Thermonuclear Plasmas, Montreal, (1992) pgs. 489–526, http://www.compxco.com/cql3d.html.

[2] R. Harvey, Y. Petrov, E. Jaeger, G. Taylor, C. Phillips, "First order finite-orbit-width corrections in CQL3D ion Fokker-Planck modeling of the NSTX HHFW experiment", 38th EPS Conference on Plasma Physics, Strasbourg, France, Vol. 35G, paper P4.017 (2011).

[3] Yu. V. Petrov, R.W. Harvey, "Finite Orbit Width versions of the CQL3D code: Hybrid-FOW and Full-FOW", APS/DPP Meeting, Providence RI, TP8.68, Bull. Amer. Phys Soc. 57, (2012).

[4] Yu. V. Petrov, R. W. Harvey, "Finite Orbit Width Features in the CQL3D Code**",** Proceedings of IAEA FEC 2012**,** San Diego, CA, paper THW/P6-02 (2012).

[5] R.W. Harvey, Yu. V. Petrov, D. Liu, W.W. Heidbrink, G. Taylor, P.T. Bonoli, "Temporal Dynamics of NSTX NBI/HHFW Discharge Using CQL3D-Hybrid-FOW", APS/DPP Meeting, Providence RI, Poster PP8.20, Bull. Amer. Phys Soc. 57, p. 259 (2012).

[6] W. W. Heidbrink, K. H. Burrell, Y. Luo, N. A. Pablant and E. Ruskov, "Hydrogenic fast-ion diagnostic using Balmer-alpha light", Plasma Physics and Controlled Fusion **46**, 1855 (2004).

[7] D. Liu, W.W. Heidbrink, M. Podesta, R.E. Bell, E.D. Fredrickson, S.S. Medley, R.W. Harvey and E. Ruskov, ``Profiles of fast ions that are accelerated by high harmonic fast waves in the National Spherical Torus Experiment", Plasma Phys. Control Fusion 52, 025006 (2010).

[8] M. Choi, D. Green, W. W. Heidbrink, R. Harvey, D. Liu, V. S. Chan, L. A. Berry, E. F. Jaeger, L. L. Lao, R. I. Pinsker, M. Podesta, D. N. Smithe, J. M. Park, P. Bonoli, and RF SciDAC and SWIM Teams, "Iterated finite-orbit Monte Carlo simulations with full-wave fields for modeling tokamak ion cyclotron resonance frequency wave heating experiments", Physics of Plasmas **17,** 056102 (2010).

[9] G. Taylor, R.A. Ellis, R.W. Harvey, J.C. Hosea, and A.P. Smirnov, "ECRH/EBWH SYSTEM FOR NSTX-U", EC-17, Deurne, The Netherlands, May 7-10,2012, Eds. E. Westerhof and P.W.J.M. Nuij, EPJ Web of Conferences 32, 020 14 (2012).

[10] N. Bertelli, O. Maj, E. Poli, R. Harvey, J. C. Wright, P. T. Bonoli, C. K. Phillips, A. P. Smirnov, E. Valeo, and J. R. Wilson, "Paraxial WKB method applied to the lower hybrid wave propagation", accepted for publication in Physics of Plasmas (2012).

[11] N. Bertelli, G. Wallace, P. T. Bonoli, R. W. Harvey, A. P. Smirnov, S. G. Baek, R. R. Parker, C. K. Phillips, E. J. Valeo, J. R. Wilson, J. C. Wright, "The effects of the scattering by edge plasma density fluctuations on lower hybrid wave propagation", accepted for publication in Plasma Phys. and Controlled Fusion (2012).

[12] G. Taylor, J. C. Hosea, C. E. Kessel, B. P. LeBlanc, D. Mueller, C. K. Phillips, E. J. Valeo, J. R. Wilson, P. M. Ryan, P. T. Bonoli, J. C. Wright, and R. W. Harvey, ``High non-inductive fraction H-mode discharges generated by high-harmonic fast wave heating and current drive in the National Spherical Torus Experiment", Physics of Plasmas 19, 042501 (2012).

11.2.4 Florida International University

Research Topic: Fast Fusion Proton Diagnostic
Principal, Co-Principal Investigators: Werner U. Boeglin (PI/PD)
Participating Scientists: Douglass S. Darrow
Participating Post-docs: none
Participating Graduate Students: Ramona Valenzuela Perez
Participating Undergraduates: 3
Funded under DOE Grant: DE-SC0001157

Introduction

The purpose of a charged fusion product detection system is to obtain time-dependent, precise information on the d(d,p)t fusion rate profile in NSTX-U with the goal of determining the neutral beam ion density profile as a function of R, z, and t and to provide new data for a global analysis of fast ion diagnostic data with the aim of extracting the fast ion distribution function.

Besides providing new data on the slowly varying neutral beam radial density profile, this measurement would provide new data on how MHD and other activity in the plasma transport neutral beam ions radially and would allow one to study modes such as toroidal Alfvén eigenmodes (TAEs), neoclassical tearing modes (NTMs), edge localized modes (ELMs), fish-bones/energetic particle modes, and internal reconnection events (IREs). This extensive new data set will be used to test models of neutral beam current drive and the effect of MHD instabilities on the profile of the driven current. In NSTX-U and future spherical tokamaks, neutral beam current drive is relied upon heavily to obtain the necessary current profiles. Designing these new machines therefore requires well-tested current drive models and a thorough understanding of the effects of MHD activities on current drive. The new diagnostic would consist of two arrays of collimated MeV ion detectors arranged in such a way that they measure MeV charged fusion products (CFPs) within well defined bundles of orbits (similar to sight lines) that cross the plasma. The detection system, based on solid state detectors and fast multi-channel digitizers, will be able to handle the expected high particle rates (up to a few MHz) allowing integration times as short as 1 ms, and leading to a time resolution of the same order of magnitude [1].

The same profile information could in principle also be measured with a neutron camera. However, the sheer physical size of a neutron camera together with a lack of space close to the NSTX-U vacuum vessel prevents its implementation without severely affecting the multiplicity of available diagnostics. Conversely the proton detector system is highly compact and hence can be installed with little effect on other diagnostics.

Current research contributions to NSTX Upgrade

Current funding has been used to build a first two-channel prototype system with adjustable detector orientations including the necessary hardware and software for the data acquisition system as well as a 4 channel system with fixed orientations. We are currently carrying out signal noise tests at MAST and plan to install and use the new 4-channel system in MAST in July 2013. A new version of the Lorentz orbit code as been tested and is currently being used for simulation calculations for the upcoming experimental campaign at MAST. Unfortunately due to the NSTX TF coil problem no data could be taken up to now but we are on track to obtain first physics data this July, 2013 at MAST using the 4 channel system. The upcoming MAST experiment offers a unique opportunity to observe simultaneously the same DD reaction rate profiles with both the proton detector array and a neutron camera, two very different methods employing different reaction products. Request for continued funding have not been successful up to now [2].

Summary of proposed research plan for 2014-18

Given the necessary funding and the experience gained by operating the prototype system at MAST we plan to upgrade the system to 16 channels, which would allow for a much more model independent analysis of the emissivity profile [2].

Timeline

2014-2015:

- Take data with prototype array at NSTX-U (contingent on available funding)
- Complete and publish analysis of MAST data
- Obtain funding for upgraded system
- Design full 16 channel system and Procure equipment for full system

2015-2016:

- Pass final design review
- Construction of fixed array completed
- Full data acquisition system ready
- System ready for installation

2016-2017:

- Construction of probe arm array completed
- Installation in the NSTX-U Vessel

2017-2018:

- Data taking with fully instrumented system
- Analysis and presentation of first data

Contributions to the NSTX-U 2014-18 Five Year Plan:

Mario Podesta is the present leader of the Energetic Particles topical science group and is responsible for overseeing the Energetic Particles chapter of the NSTX-U Five Year Plan. The plan above was defined in a process carried out over CY2011-12 in coordination with the NSTX-U Research Team. The research defined above contributes heavily to the plan.

References

[1] Concept of a charged fusion product diagnostic for NSTX, W.U. Boeglin, R. Valenzuela Perez, D.S. Darrow, Rev. Sci. Instrum. 81, 10D301 (2010)).

[2] Construction of a 16 Channel Fast Proton Diagnostic, W. U. Boeglin, Funding Proposal submitted to DOE/Office of Science Program Office: Office of Fusion Energy Sciences, Funding Opportunity Announcement Number: DE-FOA-0000744 (2012)

11.2.5 General Atomics

Research Topic: National Spherical Torus Experiment Research Participation
Principal Investigator: Robert J La Haye
Co-Principal Investigators: Todd E Evans, David A Humphreys and Thomas H Osborne
Participating Researchers: Philip B Snyder, Michael L Walker, Anders Welander and Wen Wu
Funded under DOE Grant: GRANT10701787 (March 1, 2011 – March 1, 2014)

Introduction

General Atomics is principally participating [1] in the NSTX research program in three topical areas: (1) plasma control, (2) H-mode edge pedestal characterization, and (3) boundary physics research focusing on applied resonant magnetic field perturbations.

We are continuing to support the existing plasma control software that has already been provided. In addition, we are implementing the advanced model-based shape control algorithm which has been under development during the previous grant period. These algorithms will be particularly useful for the precise control of the strike point location required by the liquid lithium divertor research program.

General Atomics has supplied data processing tools used for extracting pedestal characteristics from NSTX experimental data. In addition, we have provided edge stability analysis using the ELITE code and pedestal structure analysis under the EPED model. These efforts have contributed to improved understanding of pedestal physics in spherical tokamaks including contributing to an understanding of the effects of Lithum coatings on pedestal characteristics.

The use of magnetic perturbations primarily located in the H-mode edge pedestal region has shown great promise for the stabilization of ELMs. The General Atomics team has extensive experience in this type of research, including the design of the optimized coil set to produce the necessary magnetic fields. We are continuing analysis to understand the existing set of non-axisymmetric coils to study the effect of resonant magnetic perturbations on ELMs in NSTX.

Current research contributions to NSTX Upgrade

Control - Recent progress includes a study of the mid-plane gap controllability and steps toward more accurate predictions of vertical growth rates in NSTX. A key result of the recent model validation process is that the representation of experimental response appears accurate enough to enable reasonable calculation of high order matrix controllers produced using the decoupling

approach or other model-based design method. Work on disruption halo current dynamics is also in the current grant.

H-mode edge physics - An ability to include the fast ion pressure computed with the TRANSP transport code into the MHD equilibrium pressure profile was added which significantly improved the accuracy of the equilibrium fits. A new model for the bootstrap current based on results from the XGC0 code was added to the equilibrium reconstruction tool. A number of improvements were made to the codes to simplify their application including simplification and consolidation of the code run control tables, improved auto-knotting for the spline fits, and improved documentation. Several improvements in the visualization tools for equilibrium reconstruction and profile analysis were made. The equilibrium and profile analysis has been applied to the study of ELM suppression in discharges with lithium conditioning. The XGC0 model predicts a pedestal bootstrap current in NSTX that is 40% larger than the standard Sauter model. ELITE peeling-ballooning stability calculations based on the XGC0 mode indicate a closer agreement between the critical current density for peeling instability and the pedestal conditions just before an ELM.

Resonant Magnetic Field Perturbations - The TRIP3D code has recently been modified to run on a 960 core Tesla GPU computer and is being used to study the open field line properties in NSTX due to 3D fields from an external non-axisymmetric RWM field-error correction coil. The Tesla computer is essential for carrying out these studies since reasonably good quality simulations of divertor footprint distributions require calculations of at least 800,000 field lines.
Stability - Work on the physics of neoclassical tearing modes and the effects of error fields on their stability was ongoing and a continuation of the previous 3 year grant; advantages at low aspect ratio were confirmed of both a relatively larger characteristic small island for NTM stabilization/seeding and the presence of a significant stabilizing curvature effect and published in [2].

Summary of proposed research plan for 2014-18

Control - A strong role will continue to be played in the development of the NSTX plasma control system that is providing capability for production of the quality discharges required for the experimental research program.

H-mode edge physics - General Atomics will continue participation in analysis to improve understanding of the H-mode edge pedestal and edge localized modes in NSTX. Plans include adding the MSE data to the equilibrium reconstruction. We would also like to add the ability to use density profiles from the reflectometer diagnostic as a standard in the profile reconstruction. We will also port IMFIT to NSTX. IMFIT provides a widget-based interface to several high-

level analysis codes including EFIT (MHD equilibrium), ELITE (MHD stability), and TRANSP (transport). IMFIT handles construction of input files for these codes and translation of output from one code to input to another.

Resonant Magnetic Field Perturbations - We are collaborating with the NSTX team in the modeling and design optimization of a new resonant magnetic perturbation (RMP) coil set to be installed in NSTX. As the development of the TRIP3DGPU code continues over the next few years, simulations of the open field line properties from a proposed internal non-axisymmetric perturbation coil on NSTX-U will be carried out and field-error models will be tested. New algorithms have recently been added to the TRIP3DGPU code for modeling field-errors from misaligned poloidal field coils and non-axisymmetric toroidal field coil busbar field-errors. These will be used with NSTX-U equilibria to assess the symmetry of divertor footprints as the field-error spectrum from each source is varied. Once completed, predictions from these divertor footprint simulations will be compared to IR camera data in order to better understand potential sources of intrinsic field-errors in NSTX-U and to help refine the field-error models in the TRIP3DGPU code. In addition, it is anticipated that the conceptual design of a new RMP coil, to be done under the existing grant using the TRIP3D, SURFMN, PROBEG, and TRIP3DGPU codes, will assist in leading to an engineering design, fabrication, and installation with both experimental analysis and modeling participation by GA.

RF Physics, Stability and More - Contributions continuing from the current grant are anticipated that could also include rf physics (antennas), the physics of rotation and NTMs, error fields, resistive wall modes, and MHD stability in general, and extension of axisymmetric modeling to include analysis and design for NSTX-U control needs. This work could also include an NSTX-U simserver for testing of NSTX PCS algorithms in simulation.

A proposal for a further three-year grant renewal is expected on or around October 1, 2014.

References

[1] GACP 20001465 National Spherical Torus Experiment Research Participation, September 28, 2010, General Atomics

[2] R.J. La Haye et al., Phys. Plasmas 19, 062506 (2012)

11.2.6 Johns Hopkins University

Research Topic: Soft X-ray measurements of transport and MHD activity in the core and edge NSTX plasma

Principal, Co-Principal Investigators: Dan Stutman (PI), Kevin Tritz (Co-PI)
Participating Scientists:
Participating Post-docs: Dan Clayton
Participating Graduate Students:
Participating Undergraduates:
Funded under DOE Grant: DE-FG02-99ER5452

Introduction

The Johns Hopkins Plasma Spectroscopy Group will continue to expand its collaborative NSTX research by implementing and operating on NSTX upgrade (NSTX-U) a suite of new and upgraded SXR to VUV diagnostics based on the multi-energy imaging technique developed in our previous research. The diagnostic suite will enable improved measurements of the impurity content and radial transport, of radial and toroidal MHD mode structure and of T_e profiles and perturbations in the core, edge and divertor, and in all NSTX-U operating scenarios, from non-inductive start-up and sustainment, to high power beam and RF driven regimes.

These diagnostics will contribute to multiple NSTX-U research priorities and will also constitute the basis for continuing and expanding the physics studies initiated by our group at NSTX. In addition, the proposed diagnostics will be useful also for the initial and routine operation of the upgraded NSTX (Sec. 10.6.1.3). The proposed implementation tasks include:

i) Set of edge and core tangential ME-SXR arrays
ii) Fast tangential Transmission Grating Imaging Spectrometer (TGIS)
iii) Repetitive laser blow-off system for multiple injections of non-recycling impurities during the shot

If further resources become available, the JHU group proposes the following additional measurements over the course of the NSTX five year plan:

iv) Divertor Imaging Radiometer for spectrally resolved measurements of the radiated power

v) Additional, toroidally displaced set of edge and core tangential ME-SXR arrays
vi) Set of SXR sensors for non-magnetic plasma boundary and position measurement with eventual application to real-time feedback control

Current research contributions to NSTX Upgrade

The ME-SXR diagnostic system is the primary tool for the planned JHU research on NSTX-U. Such a system has provided measurements of the temperature profiles on fast (>10kHz) time scales by using measurements of several filtered soft X-array emission radial profiles to interpolate between Thomson scattering profiles [1,2]. A AXUV diode-based system, which provides higher sensitivity, better dynamic range, and a more compact design, has been tested on NSTX and is the basis for the system planned for NSTX-U, which will have coverage both in the core, and in the edge with higher spatial resolution (Sec. 3.4.2.4). Additionally, a novel first stage A/D electronics design is under development to decrease system costs, increase modularity, and improve the capability for 'in-vessel' installation of the ME-SXR systems.

The main research goals of the fast T_e profile measurements include the investigation of low-f MHD activity and mode structures, ELM profile dynamics, the evolution of the thermal quench during disruptions, and perturbative electron thermal transport measurements. The transport measurements are especially important to probe the response of the typically flat core T_e profile. Given recent work that demonstrates a correlation between Alfven Eigenmode activity in NSTX and high core electron thermal transport (Sec. 3.3.2.2.3) [3,4,5], measurements of perturbative thermal transport using ELMs or LBO-induced cold pulses provide a method of directly comparing measured e^- thermal transport with predictions of AE structure from HYM simulations coupled with ORBIT transport modeling.

In support of this research, two additional tools are under development. The use of Neural Network algorithms to derive electron temperature profiles from ME-SXR measurements has already provide fast T_e profiles with error bars <~10% [6]. Further algorithm development can improve these results by using additional constraints, such as time and space resolved spectroscopy from the JHU Transmission Grating Imaging Spectrometer (TGIS), line integrated density measurements, and other diagnostics (e.g. BES) that may help constrain the neural network reconstructions. Potentially, with enough additional diagnostic constraints, fast measurements of density and impurity concentration profiles may also be extracted from the ME-SXR measurements.

The other important tool that will assist the perturbative thermal transport measurements is the Laser Blow-off (LBO) system. The flexibility in choosing the injected material and the ability to precisely control the timing and amount of injected impurity will provide an excellent tool for initiating a cold pulse at the plasma edge. The propagation of this cold pulse perturbation will probe the electron thermal transport in the NSTX-U core and provide validation comparisons with the predictions from the simulations mentioned previously. Additionally, the LBO will

provide a precision tool for the investigation of impurity transport. The JHU group has previously measured impurity transport using the ME-SXR system and neon gas puffs (Sec. 3.3.1.3) [7], but the flexibility of the LBO system will dramatically improve this capability and provide access to a wide range of impurity transport studies including Z-scaling experiments, a comparison between recycling and non-recycling impurities, and a simultaneous measurement of transport in multiple channels.

The proposed diagnostics requiring additional resources also have significant contributions to research on NSTX-U. One region that could benefit greatly from increased diagnosis is the divertor. The increased power handling in NSTX-U along with the proposed advanced divertor regimes discussed in Sec. 4.2.4 indicate the importance of a thorough characterization of divertor parameters such as radiated power, electron temperature, and impurity concentration, distribution, and transport. The JHU Divertor Imaging Radiometer (DIR) is a variant of the TIGS optimized to provide spatially and spectrally resolved measurements of radiated power for the plasma divertor regime. These measurements are an essential tool that can be coupled with divertor codes and synthetic diagnostic outputs to provide a powerful constraint on the relevant divertor physics. Simulations have already demonstrated the utility of the DIR [8,9], and the JHU group considers this diagnostic to be high priority in the event that further resources become available.

The other proposed diagnostics, the additional toroidally displaced ME-SXR system and ME-SXR sensors, are aimed at improving non-axisymmetric measurements of low-f MHD activity. The two displaced ME-SXR profile systems will provide detailed measurements of asymmetries in the X-ray and T_e profiles, suitable for mode structure measurements of islands, RWMs, ELMs, disruptions, and similar events. The ME-SXR sensors will provide distributed measurements of plasma position and boundary which can be used for real-time feedback of plasma control as well as detection and potential real-time feedback of MHD as described in section 2.2.1.4.2.

Summary of proposed research plan for 2014-18

The JHU research plan will focus first on development and testing of the ME-SXR system, including the advanced electronics featuring onboard A/D and digital data streaming. The final, validated system will be ready for installation and operation by Day 0 operation. An upgraded TGIS with a faster frame rate along with the poloidal USXR system will also be ready for initial plasma ops. Along with the diagnostic development, code development and simulations will focus on improving the neural network T_e profile reconstructions as well as AE-induced core electron thermal transport using a coupling between the HYM and ORBIT numerical codes.

The JHU operational research plan includes using ME-SXR measurements of impurity transport, initially with gas puffing, to compare with previous NSTX results. Upon addition of the LBO system, our group plans more advanced impurity transport experiments along with cold pulse perturbative transport experiments utilizing the full flexibility of the injection system.
Both the divertor research and non-axisymmetric MHD research with the ME-SXR arrays and sensors depend on additional resource availability, and is planned for later in the NSTX-U 5 year run plan.

Timeline

FY14:
- Development and testing of ME-SXR advanced electronics and data acquisition
- Simulations and predictions of AE-induced core e^- transport on NSTX-U using HYM-ORBIT coupled modeling
- Development of advanced Neural Network algorithms for improved measurements of fast T_e, n_e, and impurity concentration profiles
- Use fast measurements of profile with NSTX data for study of ELM induced perturbative e^- transport measurements.

FY15:
- Installation/operation of ME-SXR edge/core systems
- Installation/operation of TG spectrometer
- Initial impurity transport experiments with comparisons to previous NSTX results
- Installation/operation of poloidal USXR system

FY16:
- Installation/operation of Laser Blow-off system
- Advanced impurity transport experiments using repetitive LBO
- Perturbative e^- thermal transport experiments and relationship to core AE activity

FY17:
- Installation of Divertor Imaging Radiometer
- Installation of toroidally displaced ME-SXR edge/core systems
- Measurements of spectrally/spatially resolved radiated divertor power in advanced divertor regimes

FY18:
- Installation of SXR edge sensors

- Measurements of non-axisymmetric MHD/disruptions using fast T_e profile diagnostics
- Development of position/boundary non-magnetic measurements, make available for integration with real-time feedback control system

Contributions to the NSTX-U 2014-18 Five Year Plan:

The plan above was defined in a process carried out over CY2011-12 in coordination with the NSTX-U Research Team. The research defined above contributes heavily to the plan and is represented throughout the chapters on Transport and Turbulence (Chap. 3, impurity transport and AE-induced e^- transport), Macrostability (Chap. 2, MHD measurements, non-magnetic RWM detection and feedback, disruption physics), Solenoid Free Startup (Chap 8, impurity measurements using the TGIS and SXR diagnostics), and Boundary Physics (Chap 4, divertor characterization using the DIR). The broad applicability of the JHU diagnostics and measurements across the range of important physics topics guarantees a tight integration of the JHU research plan and the broader mission of the NSTX-U program.

References

[1] L.F. Delgado-Aparicio, et al., Plasma Phys. Control. Fus., 49, 1245 (2007)
[2] K. Tritz, et al., Rev. Sci. Instrum., 83, 10E511 (2012)
[3] D. Stutman, et al., Phys. Rev. Lett., 102, 115002 (2009)
[4] K. Tritz, et al., "Effects of Global Alfven Eigenmodes on Electron Thermal Transport in NSTX," Invited talk: 52st APS Division of Plasma Physics Meeting, November 8-12, 2010, Chicago, IL
[5] K. Tritz, et al., "Investigation of CAE/GAE-induced electron thermal transport on NSTX," Contributed talk: 54th APS Division of Plasma Physics Meeting, October 30, 2012, Providence,
[6] D.J. Clayton, et al., "Electron temperature profile reconstructions from multi-energy SXR measurements using neural networks," in preparation
[7] D.J. Clayton, et al., Plasma Phys. Control. Fus., 54, 105022 (Oct. 2012)
[8] D. Kumar, et al., Rev. Sci. Instrum., 83, 10E511 (2012)
[9] D. Clayton, et al., Rev. Sci. Instrum., 83, 10D521 (2012)

11.2.7 Lawrence Livermore National Laboratory

Research Topic: CHI Modeling on NSTX-U

Principal Investigator: E. B. Hooper
Participating Scientists: R. Raman (U. Washington), C. R. Sovinec (U. Wisconsin), F. Ebrahimi U. New Hampshire

Funded under DOE Contract: DE-AC52-07NA27344

Introduction

This research contributes to the NSTX Relevant Area of Research V, *Start-up, Ramp-up and Sustainment without Solenoid*. It will continue resistive MHD simulations of plasma startup using Transient Coaxial Helicity Injection (TCHI) using the NIMROD code, with the focus on NSTX-U. Tasks include extending simulations from the present NSTX model to NSTX-U and participating in studies on the transition to using non-inductive current drive. Simulations addressing physics in NSTX will continue to be important for validation of the models used in the code.

Current research contributions to NSTX Upgrade

Current whole-device simulations have resulted in a model of NSTX in NIMROD, including the geometry, boundary conditions for the injection and absorption slots, time-varying boundary conditions for the bias magnetic field including wall eddy currents, and coupling to a power supply for the CHI injection. Simulations using this model produce injected flux bubbles that compare well with photographs and reconstructions from experiment, with the injected current concentrated in a layer at the boundary of the injected flux. Toroidal currents and plasma temperature magnitudes and distributions are similar to experiment. A toroidal n=1 mode has been found but shown to have little effect on the flux injection and plasma evolution. Flux-surface closure is observed in high-resolution axisymmetric simulations when the injection voltage and current drop at the end of injection. Closure for the experimental extractor width (4 cm) occurs when local currents driven by injected plasma flow near the forming X-point drop sufficiently to allow resistive reconnection. Ongoing research includes the optimization of injector parameters to maximize the closed volume and current, which are less than in the experiment.

Summary of proposed research plan for 2014-18

The research in this project will: (a) add additional physics to the simulations, including density evolution and impurity effects. Validation will be done by comparison with NSTX, including plasma behavior following flux-surface closure; (b) construct a model in NIMROD of NSTX-U; (c) run predictive simulations in NSTX-U to support preparations for TCHI experiments, including determining scaling with injection voltage and current, injection-slot dimensions, input density and other parameters; and (d) collaborate in simulations of non-inductive current drive, addressing the transition from the TCHI plasma to neutral-beam current drive. In addition, extension to possible future machines will be explored.

The elements of our plan displayed in a timeline are:

Timeline

2014-2015:
- Continue Ohmic-drive simulations in NSTX to optimize flux surface closure and other parameters. Improvement the modeling of plasma external to the injected flux.
- Develop and exercise a CHI model for NSTX-U. Determine optimization parameters in support of experimental planning.
- Assess neutral beam current drive in NSTX-U and conduct initial current drive simulations.

2015-2016:
- Undertake quantitative comparison with CHI experiments when available.
- Conduct current-drive simulations in NSTX-U.

2016-2017:
- Support experimental planning for NSTX-U.
- Extend simulations to possible future machines.

2017-2018:
- Continue and extend simulations as appropriate.

Contributions to the NSTX-U 2014-18 Five Year Plan:

The research defined above contributes strongly to the solenoid-free start-up and ramp-up chapter of the 5 year plan.

References

[1] R. Raman, T. R. Jarboe, B. A. Nelson,V. A. Izzo, R.G. O'Neill, A. J. Redd, and R. J. Smith, Phys. Rev. Letters **90**, 075005 (2003).

[2] R. Raman, D. Mueller, B. A. Nelson, T. R. Jarboe, S. Gerhardt, H.W. Kugel, B. LeBlanc, R. Maingi, J. Menard, R. Raman, D. Mueller, B. A. Nelson, T. R. Jarboe, S. Gerhardt, H.W. Kugel, B. LeBlanc, R. Maingi, J. Menard, Phys. Rev. Letters **104**, 095993 (2010).

[3] E. B. Hooper, R. Raman, J. E. Menard, and C. R. Sovinec, Bull. Am. Phys. Soc. **55**(15), 44 (2010).

[4] E. B. Hooper, C. R. Sovinec, R. Raman, and J. E. Menard, Bull. Am. Phys. Soc. **56**(12), 254 (2011).

[5] E. B. Hooper, C. R. Sovinec, R. Raman, F. Ebrahimi and J. E. Menard, Flux surface closure in helicity injected startup plasmas for NSTX (in preparation).

11.2.8 Lawrence Livermore National Laboratory

Research Topic: The Plasma-Material Interface Development and Boundary Physics Program support on NSTX-U

Principal Investigator: Vsevolod A. Soukhanovskii
Participating Scientists: P. Beiersdorfer, one LLNL Theory and Modeling scientist
Participating Post-docs: 2
Participating Graduate Students: 1
Participating Undergraduates: none
Funded under DOE Contract DEAC5207NA27344
LLNL-PROP-62511

Introduction

The goal of the present LLNL research effort on NSTX-U is to contribute to the development of physics basis for an integrated boundary interface for ST-FNSF and ITER, by taking advantage of the unique edge and divertor plasma conditions expected in NSTX-U. Our approach is based on four main elements: 1) design and execution of experiments, 2) numerical multi-fluid transport and turbulence modeling, 3) diagnostic development, operation and calibration, 4) NSTX-U Boundary Physics program development. The present research effort is a continuation of a long-term collaboration of LLNL's Fusion Energy Sciences Program on NSTX that included a number of leading contributions, e.g., the first successful divertor heat flux mitigation studies with radiative divertor in a high-power spherical-tokamak [1-3], snowflake divertor configurations studies [4-9], and a major contribution to the lithium research program in the areas of impurity transport and plasma-surface interactions [10-29]. We plan to expand and continue these studies on NSTX-U as described below.

Current research contributions to NSTX Upgrade

The LLNL collaboration in currently contributing to NSTX-U program in data analysis, active experiments on other devices, and diagnostic development for future measurements, as follows:

- Diagnostic development and data analysis on boron and molybdenum erosion at Alcator C-Mod tokamak [30]
- Snowflake divertor configuration control and physics studies at DIII-D [31]
- Radiative divertor with feedback control at DIII-D, and development for NSTX-U [32]
- Modeling of NSTX snowflake divertor and lithium radiation with two-dimensional multi-fluid code UEDGE and projections to NSTX-U [4, 33-35]
- Diagnostic development in preparation for NSTX-U operations

Summary of proposed research plan for 2014-18

The LLNL research collaboration program takes a full advantage of the LLNL Boundary Physics experimental and modeling expertise. The goal of the proposed research is to advance an experiment-based understanding and a predictive modeling capability of the main plasma-material interface elements: the SOL and divertor heat and particle transport and control in innovative divertor configurations, plasma-surface interactions with lithium-coated graphite and molybdenum plasma-facing components, and their impact on core plasma. The planned research program directly addresses highest NSTX-U Research Program priorities and enable the FNSF-relevant boundary interface development. Substantial model development and validation are planned with NSTX and NSTX-U data. The elements of the planned research are:

- In the area of **SOL energy and particle transport and turbulence** studies, we plan edge theory development and turbulence simulations using the BOUT++ code to enable comparisons with NSTX data and first-principle projections of the SOL heat flux width for NSTX-U and ST-FNSF. We also plan to contribute to the NSTX-U cryogenic panel design using the multi-fluid edge transport code UEDGE, by simulating the cryo-pump particle removal effects in high-flux expansion (snowflake) divertor configuration and with impurity seeding.
- In the **snowflake divertor and radiative divertor** areas, we plan to continue our successful multi-year experimental divertor effort. In the snowflake divertor area we plan to study heat and impurity transport, SOL turbulence, as well as pedestal stability and ELM transients, compatibility with high-Z plasma-facing components, and the possible radiation enhancement with lithium. The radiative divertor experiments will study detachment properties and calibrate the detachment control diagnostics for active feedback control of divertor heat flux via impurity gas seeding. Deuterated methane, neon and argon are planned for radiative divertor with lithium-coated graphite plasma-facing components. The developed control solutions of divertor power and particle exhaust will be integrated with **advanced operating scenarios** to support high-performance H-mode plasmas with reduced collisionality.
- In the area of **lithium-based plasma facing components** we plan to continue our multi-year experiment, analysis, modeling and diagnostic efforts to study the multi-faceted effects of lithium-coated graphite plasma-facing components on hydrogenic fuel recycling and pumping, divertor impurity erosion and SOL transport. In this area, we plan to field additional diagnostics to support Li, C, and Mo impurity erosion studies: 1) an intensified camera diagnostics enabling two wavelength two dimensional imaging of impurity emission; and 2) a spectroscopic monitor of the Material Analysis Particle Probe head (a collaboration with Purdue University). The experiments will be supported by UEDGE simulations of SOL impurity transport, lithium radiation effects, and improved erosion models.
- In the area of **multi-scale transport physics**, we plan to extend the studies of low-Z impurity transport and accumulation in ELM-free H-mode plasmas with lithium conditioning to high-Z impurities - molybdenum and tungsten. The impurity density measurement capabilities in this area will be enhanced by three extreme ultraviolet spectrometers that can measure line radiation over a wide spectral band that covers K-shell, L-shell, and M-shell radiation impurity ions such as Li, B, C, O, Ne, Ar, Mo, W. Comparisons to neoclassical models implemented in numerical codes TRANSP, NCLASS and NEO will be made. The medium-Z and high-Z core impurity density measurements

would also be instrumental in divertor impurity compression and impurity penetration factor studies in snowflake and radiative divertor experiments.

- In the **diagnostic** area, we plan to continue supporting the existing edge spectroscopic diagnostics, namely: 1) 30 spectrally filtered detectors (EIES); 2) the LADA divertor radiometer array; 3) the divertor vacuum ultraviolet spectrometer SPRED; 4) Upgraded one-dimensional filtered camera arrays with divertor and midplane views; 5) the ultraviolet-visible-near-infrared spectrometers VIPS and DIMS. The DIMS spectrometer was designed to provide ion temperature measurements using Doppler line broadening, and this capability would be further pursued in NSTX-U.

Timeline

FY2014:

- Continue analysis of boron and molybdenum erosion data from Alcator C-Mod tokamak
- Develop multi-spectral imaging (charge-injection device camera and image splitter) for NSTX-U and prepare for installation
- Develop and install one-dimensional camera array modules on NSTX-U
- Install LLNL-operated diagnostics on NSTX-U (SPRED, LADA, VIPS, DIMS, EIES)
- Install supersonic gas injector
- Construct MonaLisa spectrometer at LLNL and complete photometric calibration
- Develop BOUT++ model and apply to NSTX and NSTX-U geometry. Start comparisons with NSTX heat flux width database.
- Modeling with UEDGE
    - Use the developed snowflake model for cryo-pump studies
    - Start developing impurity-seeded divertor model
    - Start modeling of lithium radiation effects
- Start setting up neoclassical and impurity transport codes for NSTX-U

FY2015:

- Finalize diagnostic and erosion analysis approach based on NSTX and Alcator C-Mod studies
- Develop and install optics for viewing the Material Analysis Particle Probe head
- Install of all three XUV spectrometers on NSTX-U
- Develop projections of heat flux width and impurity transport for NSTX-U using BOUT++
- Modeling with UEDGE
    - Continue modeling of cryo-pumping impact on snowflake and radiative divertors
    - Continue modeling lithium radiation effects
- Continue development of collisional-radiative and transport models in support of impurity transport modeling for NSTX-U geometry
- Snowflake and radiative divertor studies
    - Prepare and execute scoping studies of snowflake divertor configurations
    - Collaborate on snowflake magnetic control development
    - Prepare and execute scoping studies of radiative divertor with deuterium and argon seeding
    - Start comparing initial divertor data with UEDGE models

- Plasma-surface interaction studies and diagnostic development
    - Prepare and execute scoping studies of recycling and impurity influx with boron and lithium coatings on graphite plasma-facing components
    - Support experiments with UEDGE interpretive modeling
- Operate all three extreme ultraviolet spectrometers
- Develop improved K-shell emission models and determine absolute impurity concentrations of K-shell ions in the core of NSTX-U plasmas
- Initiate interpretive analysis of impurity transport with impurity transport codes

FY2016:

- Snowflake and radiative divertor studies
    - Continue experimental studies of snowflake divertor configurations with divertor cryo-pumping and magnetic control
    - Optimize radiative divertor with impurity seeding and start implementing radiative divertor control diagnostics
    - Continue comparing divertor data with UEDGE models
- Plasma-surface interaction studies
    - Prepare and execute scoping studies of recycling and impurity influx with lithium coatings on molybdenum PFCs, if installed
    - Support Material Analysis Particle Probe studies
    - Support experiments with UEDGE interpretive modeling

- Impurity transport
    - Operate all three extreme ultraviolet spectrometers
    - Perform experiments and interpretive analysis of high-Z impurity transport

FY2017-FY2018:

- Execute experiments with snowflake divertor configurations with cryo-pumping and combine with high-performance H-mode scenarios
- Radiative divertor feedback control experiments
- Continue molybdenum core, edge transport and erosion studies
- Characterize divertor lithium radiation in experiments
- Validate UEDGE models with measurements

Contributions to the NSTX-U 2014-18 Five Year Plan:

V. A. Soukhanovskii is the present leader of the Boundary Physics topical science group and is responsible for entire overseeing and parts of the Boundary Physics chapter of the NSTX-U Five Year Plan. He presented the Five Year Plan for pedestal, scrape-off layer and divertor research at the NSTX-U Physics Advisory Committee meeting in February 2013.

References

[1] V. A. Soukhanovskii, R. Maingi, D. A. Gates, J. E. Menard, S. F. Paul, R. Raman, A. L. Roquemore, M. G. Bell, R. E. Bell, J. A. Boedo, C. E. Bush, R. Kaita, H. W. Kugel, B. P. LeBlanc, D. Mueller, and the NSTX Team. "Divertor heat flux mitigation in the National Spherical Torus Experiment", Phys. Plasmas, 16, (2009).

[2] V. A. Soukhanovskii, R. Maingi, D. A. Gates , J. E. Menard, S. F. Paul, R. Raman, A. L. Roquemore, R. E. Bell, C. E. Bush, R. Kaita, H. W. Kugel, B. P. LeBlanc, D. Mueller, "Divertor Heat Flux Mitigation in High-Performance H-mode Plasmas in the National Spherical Torus Experiment", Nuclear Fusion, 49, 095025 (2009).

[3] V. A. Soukhanovskii, R. E. Bell, A. Diallo, S. Gerhardt, R. Kaita, S. Kaye, E. Kolemen, B. P. LeBlanc, R. Maingi, A. McLean, J. E. Menard, D. Mueller, S. F. Paul, M. Podesta, R. Raman, A. L. Roquemore, D. D. Ryutov, F. Scotti, Divertor heat flux mitigation with impurity-seeded standard and snowflake divertors in NSTX, Proceedings of the 39th EPS Conference on Plasma Physics, Stockholm, Sweden, 2012, Paper P5.049

[4] V. A. Soukhanovskii et. al., Snowflake Divertor as Plasma-Material Interface for Future High Power Density Fusion Devices, IAEA FEC 2012, to be submitted to Nucl. Fusion (2013).

[5] V. A. Soukhanovskii, R. E. Bell, A. Diallo, S. Gerhardt, S. Kaye, E. Kolemen, B. P. LeBlanc, A. G. McLean, J. E. Menard, S. F. Paul, M. Podesta, R. Raman, T. D. Rognlien, A. L. Roquemore, D. D. Ryutov, F. Scotti, M. V. Umansky, D. Battaglia, M. G. Bell, D. A. Gates, R. Kaita, R. Maingi, D. Mueller, and S. A. Sabbagh, Phys. Plasmas 19, 082504 (2012)

[6] V. A. Soukhanovskii, R. E. Bell, A. Diallo, S. Gerhardt, S. Kaye, E. Kolemen, B. P. LeBlanc, A. McLean, J. E. Menard, S. F. Paul, M. Podesta, R. Raman, D. D. Ryutov, F. Scotti, R. Kaita, R. Maingi, D. M. Mueller, A. L. Roquemore, H. Reimerdes, G.P. Canal, B. Labit, W. Vijvers, S. Coda, B.P. Duval, T. Morgan, J. Zielinski, G. De Temmerman, B. Tal, Advanced divertor configurations with large flux expansion, J. Nucl. Mater., at press, 2013. http://dx.doi.org/10.1016/j.jnucmat.2013.01.015

[7] Soukhanovskii, VA; Ahn, JW; Bell, RE; Gates, DA; Gerhardt, S; Kaita, R; Kolemen, E; LeBlanc, BP; Maingi, R; Makowski, M; Maqueda, R; McLean, AG; Menard, JE; Mueller, D; Paul, SF; Raman, R; Roquemore, AL; Ryutov, DD; Sabbagh, SA; Scott, HA. "Taming the plasma-material interface with the 'snowflake' divertor in NSTX", Nucl. Fusion, 51, (2011), DOI: 10.1088/0029-5515/51/1/012001.

[8] V.A. Soukhanovskii, J.-W. Ahn, R.E. Bell, D.A. Gates, S. Gerhardt, R. Kaita, E. Kolemen, H.W. Kugel, B.P. LeBlanc, R. Maingi, R. Maqueda, A. McLean, J.E. Menard, D.M. Mueller, S.F. Paul, R. Raman, A.L. Roquemore, D.D. Ryutov, H.A. Scott, "Snowflake" divertor configuration in NSTX, Journal of Nuclear Materials, Volume 415, Pages S365-S368

[9] V. A. Soukhanovskii, J.-W. Ahn, D. Battaglia, R. E. Bell, A. Diallo, S. Gerhardt, R. Kaita, S. Kaye, E. Kolemen, B. P. LeBlanc, R. Maingi, A. McLean, J. E. Menard, D. Mueller, S. F. Paul, M. Podesta, R. Raman, T. D. Rognlien, A. L. Roquemore, D. D. Ryutov, F. Scotti, M. V. Umansky. "The snowflake divertor: a game-changer for magnetic fusion devices?", 38th EPS Conference on Plasma Physics, (Strasbourg, France, 06/27/2011-07/01/2011), Europhys. Conf. Abstr., 35G, p O3.109.

[10] H.W. Kugel, J.P. Allain, M.G. Bell, R.E. Bell, A. Diallo, R. Ellis, S.P. Gerhardt, B. Heim, M.A. Jaworski, R. Kaita, J. Kallman, S. Kaye, B.P. LeBlanc, R. Maingi, A. McLean, J. Menard, D. Mueller, R. Nygren, M. Ono, S.F. Paul, R. Raman, A.L. Roquemore, S.A. Sabbagh, H. Schneider, C.H. Skinner, V.A. Soukhanovskii, C.N. Taylor, J.R. Timberlake, M. Viola, L. Zakharov, NSTX Research Team, NSTX plasma operation with a Liquid Lithium Divertor, Fusion Engineering and Design, **87**, 1724-1731, (2012)

[11] M. Ono, M.G. Bell, R. Kaita, H.W. Kugel, J.-W. Ahn, J.P. Allain, D. Battaglia, R.E. Bell, J.M. Canik, S. Ding, S. Gerhardt, T.K. Gray, W. Guttenfelder, J. Hosea, M.A. Jaworski, J. Kallman, S. Kaye, B.P. LeBlanc, R. Maingi, D.K. Mansfield, A. McLean, J. Menard, D. Muller, B. Nelson, R. Nygren, S. Paul, R. Raman, Y. Ren, P. Ryan, S. Sabbagh, F. Scotti, C. Skinner, V. Soukhanovskii, V. Surla, C.N. Taylor, J. Timberlake,

H.Y. Yuh, L.E. Zakharov, Recent progress of NSTX lithium program and opportunities for magnetic fusion research, Fusion Engineering and Design, **87**, 1770-1776, (2012)

[12] H.W. Kugel, M.G. Bell, J.P. Allain, R.E. Bell, S. Ding, S.P. Gerhardt, M.A. Jaworski, R. Kaita, J. Kallman, S.M. Kaye, B.P. LeBlanc, R. Maingi, R. Majeski, R. Maqueda, D.K. Mansfield, D. Mueller, R. Nygren, S.F. Paul, R. Raman, A.L. Roquemore, S.A. Sabbagh, H. Schneider, C.H. Skinner, V.A. Soukhanovskii, C.N. Taylor, J.R. Timberlake, W.R. Wampler, L.E. Zakharov, S.J. Zweben, the NSTX Research Team, NSTX plasma response to lithium coated divertor, Journal of Nuclear Materials, Volume 415, Pages S400-S404

[13] M. Ono, M.G. Bell, Y. Hirooka, R. Kaita, H.W. Kugel1, G. Mazzitelli, J.E. Menard, S.V. Mirnov, M. Shimada, C.H. Skinner and F.L. Tabares, Conference Report on the 2nd International Symposium on Lithium Applications for Fusion Devices, Nucl. Fusion 52 (2012) 037001 doi:10.1088/0029-5515/52/3/037001, http://isla2011.pppl.gov/

[14] C.H. Skinner, J.P. Allain, W. Blanchard, H.W. Kugel, R. Maingi, L. Roquemore, V. Soukhanovskii, C.N. Taylor, Deuterium retention in NSTX with lithium conditioning, Journal of Nuclear Materials, Volume 415, Pages S773-S776

[15] Soukhanovskii, V.A., Ahn, J.W., Bell, M.G., Bell, R.E., Gates, D.A., Gerhardt, S., Kaita, R., Kolemen, E., Kugel, H.W., LeBlanc, B.P., Maingi, R., Maqueda, R., McLean, A., Menard, J.E., Mueller, D., Paul, S.F., Pigarov, A.Y., Raman, R., Rognlien, T., Roquemore, A.L., Ryutov, D.D., Sabbagh, S.A., and Smirnov, R., Synergy between the Innovative Snowflake Divertor Configuration and Lithium Plasma Facing Component Coatings in NSTX, Paper EXD/P3-32, Proceedings of the 23rd IAEA Fusion Energy Conference, 11-16 October 2010, Daejon, Korea

[16] V. A. Soukhanovskii, "Plasma-Material Interface Development for Future Spherical Tokamak-based Devices in NSTX", The Joint Meeting of 5th IAEA Technical Meeting on Spherical Tori, 16th International Workshop on Spherical Torus and the 2011 US-Japan Workshop on ST Plasma, September 2011, Naka, Japan

[17] V. A. Soukhanovskii, "Recycling, Pumping and Divertor Plasma-Material Interactions with evaporated lithium coatings in NSTX", The 2nd International Symposium on Lithium Applications for Fusion Devices, Princeton, New Jersey, 04/2011, http://isla2011.pppl.gov/

[18] Maingi, R; Kaye, SM; Skinner, CH; Boyle, DP; Canik, JM; Bell, MG; Bell, RE; Gray, TK; Jaworski, MA; Kaita, R; Kugel, HW; LeBlanc, BP; Mansfield, DK; Osborne, TH; Sabbagh, SA; Soukhanovskii, VA. "Continuous Improvement of H-Mode Discharge Performance with Progressively Increasing Lithium Coatings in the National Spherical Torus Experiment", Phys. Rev. Lett., 107, (2011), DOI: 10.1103/PhysRevLett.107.145004.

[19] Canik, JM; Maingi, R; Kubota, S; Ren, Y; Bell, RE; Callen, JD; Guttenfelder, W; Kugel, HW; LeBlanc, BP; Osborne, TH; Soukhanovskii, VA. "Edge transport and turbulence reduction with lithium coated plasma facing components in the National Spherical Torus Experiment (vol 18, 056118, 2011)", Phys. Plasmas, 18, (2011), DOI: 10.1063/1.3641488.

[20] J.M. Canik, R. Maingi, V.A. Soukhanovskii, R.E. Bell, H.W. Kugel, B.P. LeBlanc, T.H. Osborne, Measurements and 2-D modeling of recycling and edge transport in discharges with lithium-coated PFCs in NSTX, Journal of Nuclear Materials, Volume 415, Pages S409-S412

[21] F. Scotti, V.A. Soukhanovskii, R.E. Bell, W. Guttenfelder, S. Kaye, S. Gerhardt, R. Kaita, B.P. Leblanc and the NSTX Team, Study of Neoclassical Core Transport of Intrinsic Impurities in the National Spherical Torus Experiment, Proceedings of the 39th EPS Conference on Plasma Physics, Stockholm, Sweden, 2012, Paper P4.031.

[22] F. Scotti et. al., Modifications of impurity transport and divertor sources with lithium wall conditioning in NSTX, Invited Talk GI2.00005, To be presented at 54th Annual Meeting of the APS Division of Plasma Physics, October 29–November 2 2012; Providence, Rhode Island, To be submitted to Phys. Plasmas (2013)

[23] F. Scotti, V.A. Soukhanovskii, S. Kaye, S. Gerhardt, R. Andre, W. Guttenfelder, R.E. Bell, B.P. Leblanc, R. Kaita, Study of Carbon and Lithium Neoclassical Impurity Transport in ELM-Free H-Mode Discharges in NSTX, IAEA FEC 2012, Submitted to Nucl. Fusion (2013).

[24] F. Scotti, A. L. Roquemore, and V. A. Soukhanovskii, Rev. Sci. Instrum. 83, 10E532, 2012.

[25] Soukhanovskii, VA; Roquemore, AL; Bell, RE; Kaita, R; Kugel, HW. "Spectroscopic diagnostics for liquid lithium divertor studies on National Spherical Torus Experiment", Rev. Sci. Instrum., 81, (2010), DOI: 10.1063/1.3478749.

[26] J. Lepson, P. Beiersdorfer, J. Clementson, M. F. Gu, M. Bitter, L. Roquemore, R. Kaita, P. Cox, A. Safronova, EUV Spectroscopy on NSTX, Journal of Physics B 43, 144018 (2010)

[27] J. K. Lepson, P. Beiersdorfer, J. Clementson, M. Bitter, K. W. Hill, R. Kaita, C. H. Skinner, A. L. Roquemore, and G. Zimmer, High-Resolution Time-Resolved Spectroscopy on NSTX, Review of Scientific Instruments (in press, 2012)

[28] A. S. Safronova, N. D. Ouart, J. K. Lepson, P. Beiersdorfer, B. Stratton, V. Kantsyrev, P. G. Cox, V. Shlyaptseva, K. M. Williamson, X-ray spectroscopy of Cu impurities on NSTX and comparison with Z-pinch plasmas, Review of Scientific Instruments 81, 10E305 (2010)

[29] P. Beiersdorfer, J. K. Lepson, M. Bitter, K. W. Hill, and L. Roquemore, Time-resolved X-Ray and Extreme Ultraviolet Spectrometer for Use on the National Spherical Torus Experiment, Review of Scientific Instruments 79, 10E318 (2008).

[30] A. Tronchin-James, V. A. Soukhanovskii, M. Churchill, B. Lipschultz, D. Miller, M. Reinke, J. Terry, C. Theiler, Intensified imaging of PFC erosion via Mo I emission in C-mod, Poster JP8.00104, 54th Annual Meeting of the APS Division of Plasma Physics, Volume 57, Number 12, October 29–November 2 2012; Providence, Rhode Island. To be submitted to Rev. Sci. Instrum. (2013)

[31] S. L. Allen, V.A. Soukhanovskii, T.H. Osborne, E. Kolemen, J.A. Boedo, N.H. Brooks, M.E. Fenstermacher, R.J. Groebner, D.N. Hill, A.W. Hyatt, C.J. Lasnier, A.W. Leonard, M.A. Makowski, W.H. Meyer, A.G. McLean, T.W. Petrie, D. Ryutov, and J.G. Watkins, Initial Snowflake Divertor Physics Studies on DIII-D, Oral Talk PD-1, IAEA FEC 2012

[32] V. A. Soukhanovskii, S. P. Gerhardt, R. Kaita, A. G. McLean, and R. Raman, Rev. Sci. Instrum. 83, 10D716 (2012)

[33] E. T. Meier, V. A. Soukhanovskii, R. E. Bell, S. Gerhardt, R. Kaita, H. W. Kugel, B. P. LeBlanc, J. E. Menard, S. F. Paul, T. D. Rognlien, F. Scotti, M. V. Umansky, Modeling core impurity reduction via divertor gas injection in NSTX, Proceedings of the 39th EPS Conference on Plasma Physics, Stockholm, Sweden, 2012, Paper P1.002.

[34] E.T. Meier, V.A. Soukhanovskii, A.G. McLean, T.D. Rognlien, D.D. Ryutov, R.E. Bell, A. Diallo, S. Gerhardt, R. Kaita, B.P. LeBlanc, J.E. Menard, M. Podesta, F. Scotti, UEDGE modeling of NSTX and NSTX-U snowflake divertor configurations, Poster PP8.00028, 54th Annual Meeting of the APS Division of Plasma Physics, Volume 57, Number 12, October 29–November 2 2012; Providence, Rhode Island.

[35] T.D. Rognlien, E.T. Meier, V.A. Soukhanovskii, A mechanism for large divertor plasma energy loss via lithium radiation in tokamaks, Poster PP8.00031, 54th Annual Meeting of the APS Division of Plasma Physics, Volume 57, Number 12, October 29–November 2 2012; Providence, Rhode Island.

11.2.9 Lehigh University

Research Topic: Model-Based Current Profile Control Development for NSTX-U
Principal, Co-Principal Investigators: Prof. Eugenio Schuster (PI).
Participating Scientists: N/A
Participating Post-docs: N/A
Participating Graduate Students: 1 PhD Student.
Participating Undergraduates: N/A
Funded under DOE Grant: N/A

Introduction

Setting up a suitable current profile, usually defined in terms of the safety factor q or the rotational transform ι profiles, plays a critical role in the achievement of advanced tokamak scenarios characterized by high confinement and the non-inductive sustainment of the plasma current necessary for steady-state operation. Therefore, while the control of scalar parameters associated with the safety factor q such as q_{min} has been proven critical to mitigate plasma instabilities and improve confinement, the shaping of the entire q profile (q at several points in space) will be necessary to stably maximize the fraction of bootstrap current in advanced scenarios. Therefore, techniques to actively control the evolution of the entire q profile during the discharge are of paramount importance to the success of ITER and their development has recently begun to receive a great deal of attention. The high dimensionality of this problem, along with the strong nonlinear coupling between magnetic and kinetic profiles motivates the use of model-based control synthesis that can accommodate this complexity through embedding the known physics within the design. By capturing the response of the system to the available actuators in a control-oriented model, such control designs can achieve improved performance without the need for extensive trial-and-error tuning. Motivated by this need, the Lehigh University (LU) Plasma Control Group has worked for several years now on the development of control-oriented models for current-profile response and the design of active current-profile controllers based on those models for L-mode and H-mode discharges.

A substantial theoretical and experimental physics effort has been going on for several years to develop predictive models for plasma evolution in toroidal plasmas. The work by the LU Plasma Control Group draws on the result of those efforts but does not supersede it, since the purpose is the conversion of these accepted physics models to a form useful for control synthesis and simulation. It is important to emphasize that these plasma response models are developed only for control design and not for physical understanding, and consequently, the developed model needs only to capture the physics that is relevant for control design. The objective of the control-oriented plasma-response models is two-fold: control synthesis and control simulation. To be

tractable from the point of view of available control techniques, the complexity of models used for the synthesis of controllers usually needs to be lower than that of models used for the performance evaluation of controllers in closed-loop simulations. Therefore, the control-oriented models used for control simulation must be reduced further in complexity before being used for control synthesis. The control-oriented models used for control simulation need however to be much less sophisticated than those powering predictive codes such as PTRANSP, CORSICA or ONETWO, which are used for physics studies. This need is motivated by the fact that a control control-oriented predictive simulation code must be capable of running closed-loop simulations in a matter of minutes, at the most, to be an effective tool for iterative control design. Control-oriented models of the current profile dynamics can be divided into two groups: those created entirely from experimental data and those that are driven by first principles.

The data-driven modeling approach lacks unfortunately the ability of arbitrarily deciding on the level of simplicity, accuracy and validity of the model since it directly produces *linear models based on ordinary differential equations (ODEs)*. As the identified models are linear, they are only valid around the reference plasma state adopted during the system identification experiment. Therefore, the effectiveness of the controllers synthesized based on these models may be limited when the plasma state moves away from the reference state. Moreover, as these models are device-specific, dedicated system identification experiments are needed in each device, and potentially for each control scenario, to develop model-based controllers. A robust, model-based, MIMO, ι-profile and β_N controller has been recently designed and experimentally tested by the LU Plasma Control Group for the flat-top phase of DIII-D H-mode discharges. The design is based on a data-driven, two-timescale, linear, dynamic, plasma-response model that has been identified around a reference profile during the flattop phase. The feedback controller [1] is designed to regulate the system around a target profile, which is assumed to be close to the reference profile around which the model has been identified. The proposed controller represents one of the first profile controllers integrating magnetic and kinetic variables ever implemented and experimentally tested in DIII-D. More experiments are needed to assess the appropriateness of using data-driven linear models for current profile control. While data-driven, control-oriented, linear models may still be useful for the design of local regulators around a reference state in the flat-top phase, being able to control the current profile during the ramp-up and ramp-down phases, being able to regulate the current profile for different scenarios (around different reference states), or being able to drive the current profile from one target profile to another will most likely require adaptive or nonlinear control approaches based on richer dynamic models obtained by first-principles-driven modeling.

First-principles-driven modeling, and subsequent controller design, has the potential of overcoming some of the limitations exhibited by the data-driven approach. Unlike data-driven modeling, first-principles-driven modeling has the potential of producing *nonlinear models*

based on partial differential equations (PDEs). The LU Plasma Control Group advocates for a first-principles-driven approach to model-based control and estimation. The availability of a first-principles-driven PDE model capturing the nonlinear dynamics of the system allows not only for: i- the design of feedback controllers with objectives beyond just regulation around a fixed reference state but also for: ii- the design of optimal feedforward controllers for a systematic model-based approach to scenario planning, iii- the design of state estimators for a reliable real-time reconstruction of the plasma internal profiles based on limited and noisy diagnostics, and iv- the development of fast (potentially real-time), control-oriented, predictive simulation codes for closed-loop performance evaluation of the controllers before experimental implementation. As dictated by the application (control simulation vs control synthesis (see above)) and the design objective, the complexity of the first-principles-driven model can be eventually reduced. It is interesting to note that a first-principles-driven nonlinear PDE model can be reduced all the way to a linear ODE model, similar to that produced by data-driven modeling, by linearization and spatial discretization. However, the first-principles-driven modeling approach provides the freedom of arbitrarily handling the trade-off between the simplicity of the model and both its physics accuracy and its validity range, i.e., provides the freedom of deciding on the level of simplification of the model as a function of the design goal. While first-principles-driven modeling may still need empirical correlations from experimental data to provide closure to the first-principles laws, unlike data-driven modeling, it does not need dedicated experiments to produce a model. Moreover, the empirical laws employed to close the first-principle model (e.g., the magnetic diffusion equation in the case of the current profile response model) are based on physical observations of the plasma response to the control actuators, which are not unique to any one machine. Robust/optimal/backstepping, model-based, MIMO, θ-profile ($\theta=\partial\psi/\partial\rho$) controllers have been recently synthesized and experimentally tested by the LU Plasma Control Group for the ramp-up and flat-top phases of DIII-D L-mode discharges. The first-principles-driven, two-timescale, non-linear, dynamic, plasma-response model proposed in [2] was used to synthesize combined feedforward [3, 4] + feedback [5-7] control schemes to drive the current profile to a desired target profile. The controllers were tested very successfully in both reference-tracking and disturbance-rejection experiments [8-11]. These experiments mark the first time ever a first-principles-driven, model-based, closed-loop, current-profile controller was successfully implemented and tested in a tokamak device. The quality of the experimental results demonstrates the applicability of a first-principles-driven control approach to active, closed-loop, current-profile control.

Current research contributions to NSTX Upgrade

New actuator capabilities planned for the NSTX-U will enable the manipulation and optimization of the current profile in a way that was not possible with the NSTX. In order to study and optimize the Spherical Tokamak (ST) concept for future fusion reactors and to make

use of the new actuator capabilities to their fullest, new control algorithms are needed. These algorithms will synergistically combine diagnostics and actuators to manipulate not only the bulk plasma properties but also the plasma profile to achieve the scientific goals of the NSTX-U. The objective of the work currently carried out by the LU Plasma Control Group on NSTX-U is to study and understand the current profile dynamics for the NSTX-U, to develop current profile control algorithms that enable the efficient and optimal use of the actuators by using modern model-based control approaches, and in this way to further the scientific mission of the NSTX-U.

Summary of proposed research plan for 2014-18

Broadly, the work by the LU Plasma Control Group has five separate components:

1. Development of first-principles-driven, control-oriented, nonlinear, dynamic models of the NSTX-U plasma current profile evolution, the diagnostic measurements and the effect of the actuators on the plasma. The aim of this component of the work is to set the groundwork for the scientific understanding of the current profile response dynamics in the NSTX-U that is necessary for control design.
2. Development of real-time current-profile control algorithms based on the developed control-oriented dynamic models. Testing and tuning of the developed control algorithms in simulations based on PTRANSP.
3. Implementation and validation of the developed control algorithms on the NSTX-U PCS (Plasma Control System).
4. Testing and tuning of the developed control algorithms in experiments on the NSTX-U. The focus of this component of the work is on the development of control tools that will be used routinely by PPPL scientists.
5. Integration of current profile control with other control objectives in NSTX-U.

Scientific publications and presentations on current-profile control-oriented dynamic modeling and modern model-based control synthesis for the NSTX-U and ST in general are also part of the work carried out by the LU Plasma Control Group on NSTX-U.

Timeline

FY2014:

- Continue development of first-principles-driven control-oriented models for the NSTX-U current-profile dynamic response. The LU Plasma Control Group is currently working on determining the critical factors that need to be modeled to capture the relevant dynamics of the feedback system composed by the control logic, the actuators, the plasma current-profile dynamics, and the diagnostics. The PTRANSP simulation code is employed to tailor the first-principles-driven model to the NSTX-U geometry. These models provide the capability of understanding the effect of the control actuators on the NSTX-U current profile dynamics

and will be exploited during control design (synthesis + simulations). First-principles-driven modeling has the potential of retaining the nonlinear dynamics of the plasma in the control-oriented model, which is critical for current profile control as dictated by the experience acquired by the LU Plasma Control Group in recent years.

- Development of real-time current-profile control algorithms for the NSTX-U. The response models that capture the relevant dynamics of the current profile in the NSTX-U will be embedded in the control synthesis. Model-based, feedforward+feedback, control algorithms that can be implemented in the real-time NSTX-U PCS will be developed. Preliminary closed-loop simulations will be carried out based on the developed current-profile nonlinear dynamic models. Promising control algorithms will be further tested in closed-loop simulations based on more sophisticated predictive codes such as PTRANSP.

FY2015:

- Continue development of real-time current-profile control algorithms for the NSTX-U.
- Implementation of the control algorithms on the NSTX-U PCS. The NSTX-U will use a modified version of the General Atomics PCS. The ability to evaluate the closed-loop behavior of the control algorithms based on a simplified response model is available in the PCS through a Simserver simulation. The proposed control algorithms will be implemented in the PCS and linked with a Simserver based on the developed control-oriented current-profile nonlinear dynamic model to debug the PCS implementation.

FY2016:

- Testing and validation of the proposed control algorithms in NSTX-U control experiments. It is anticipated that the experimental results will dictate the need for model refining and control redesign. The physics-based control-oriented model may need adjusting of parameters in order to achieve the required accuracy level. The adjustment of the model-based control algorithm will follow.

FY2017:

- Continue testing, validation and redesign of the current profile controller in the NSTX-U.

FY2018:

- Work towards integration of current profile control with other control objectives.

Contributions to the NSTX-U 2014-18 Five Year Plan:

Prof. Eugenio Schuster is one of the contributors to the Safety-Factor Profile Control task described in Chapter 9 of the NSTX-U Five Year Plan. The research plan above was defined in a process carried out over CY2011-12 in coordination with the NSTX-U Research Team.

References

[1] W. Shi, W. Wehner, J. Barton, M.D. Boyer, E. Schuster, D. Moreau, M.L. Walker, J.R. Ferron, T.C. Luce, D.A. Humphreys, B.G. Penaflor and R.D. Johnson, "System Identification and Robust Control of the Plasma Rotational Transform Profile and Normalized Beta Dynamics for Advanced Tokamak Scenarios in DIII-D," *Nuclear Fusion*, under review.
[2] Y. Ou, T.C. Luce, E. Schuster, J.R. Ferron, M.L. Walker, C. Xu and D.A. Humphreys, "Towards model-based current profile control at DIII-D," *Fusion Engineering and Design* 82 (2007) 1153-1160.
[3] Y. Ou, C. Xu, E. Schuster, T.C. Luce, J.R. Ferron, M.L. Walker and D.A. Humphreys, "Design and Simulation of Extremum-seeking Open-loop Optimal Control of Current Profile in the DIII-D Tokamak," *Plasma Physics and Controlled Fusion*, 50 (2008) 115001.
[4] C. Xu, Y. Ou, J. Dalessio, E. Schuster, T.C. Luce, J.R. Ferron, M.L. Walker and D.A. Humphreys, "Ramp-Up-Phase Current-Profile Control of Tokamak Plasmas via Nonlinear Programming," *IEEE Transactions on Plasma Science*, vol. 38, no 2, pp. 163-173, 2010.
[5] Y. Ou, C. Xu and E. Schuster, "Robust Control Design for the Poloidal Magnetic Flux Profile Evolution in the Presence of Model Uncertainties," *IEEE Transactions on Plasma Science*, vol. 38, no. 3, pp. 375-382, 2010.
[6] Y. Ou, C. Xu, E. Schuster, T.C. Luce, J.R. Ferron, M.L. Walker and D.A. Humphreys, "Optimal Tracking Control of Current Profile in Tokamaks," *IEEE Transactions on Control Systems Technology*, vol. 19, no. 2, pp. 432-441, 2011.
[7] Y. Ou, C. Xu, E. Schuster, T.C. Luce, J.R. Ferron, M.L. Walker and D.A. Humphreys, "Receding-Horizon Optimal Control of the Current Profile Evolution During the Ramp-Up Phase of a Tokamak Discharge," *Control Engineering Practice*, 19 (2011) 2231.
[8] J. Barton, M.D. Boyer, W. Shi, W.P. Wehner, E. Schuster, T.C. Luce, J.R. Ferron, M.L. Walker, D.A. Humphreys, B.G. Penaflor and R.D. Johnson, "First-Principles Model-based Closed-loop Control of the Current Profile Dynamic Evolution on DIII-D," *24th IAEA Fusion Energy Conference*, San Diego, California, USA, October 8-13, 2012.
[9] J. Barton, M.D. Boyer, W. Shi, E. Schuster, T.C. Luce, J.R. Ferron, M.L. Walker, D.A. Humphreys, B.G. Penaflor and R.D. Johnson, "Toroidal Current Profile Control During Low Confinement Mode Plasma Discharges in DIII-D via First-Principles-Driven Model-based Robust Control Synthesis," *Nuclear Fusion* 52 (2012) 123018 (24pp).
[10] M.D. Boyer, J. Barton, E. Schuster, T.C. Luce, J.R. Ferron, M.L. Walker, D.A. Humphreys, B.G. Penaflor and R.D. Johnson, "Backstepping Control of the Toroidal Plasma Current Profile in the DIII-D Tokamak," *IEEE Transactions on Control Systems Technology*, under review.
[11] M.D. Boyer, J. Barton, E. Schuster, T.C. Luce, J.R. Ferron, M.L. Walker, D.A. Humphreys, B.G. Penaflor and R.D. Johnson, "First-Principles-Driven Model-Based Current Profile Control for the DIII- D Tokamak via LQI Optimal Control," *Plasma Physics and Controlled Fusion*, under review.

11.2.10 Lodestar Research Corporation

Research Topic: Edge and Scrape-off-Layer Physics for NSTX-U

Principal, Co-Principal Investigators: James R. Myra (PI), Daniel A. D'Ippolito (Co-I), David A. Russell (Co-I)

Participating Scientists: (separately funded external collaborators) S.J. Zweben (NSTX research contact), J. Boedo, B. Davis, T. Gray, R. Maingi, R.J. Maqueda, D.P. Stotler

Funded under DOE Grant: DE-FG02-02ER54678

Introduction

An improved understanding of edge and scrape-off-layer (SOL) physics is essential to the goals of NSTX-U, future spherical tokamaks, and to ITER. The work carried out under this project will address critical physics associated with boundary plasma turbulence: the origin and propagation of blob-filaments, their interaction with oscillating zonal flows and mean flows, and the resulting scaling of SOL characteristics (such as the heat flux width) with experimental parameters. Plasma exhaust in the form of heat flux impacting the divertor is still one of the most critical issues facing the magnetic fusion program in general, and the spherical torus concept in particular. Radial transport competes with classical parallel transport to determine the radial penetration of plasma into the tokamak SOL, and therefore the area "wetted" by the exhaust power. Furthermore, convective radial transport in the boundary plasma is believed to be mediated by intermittent coherent propagating structures, i.e. blob-filaments, produced by edge turbulence.[1,2] Thus, both the SOL heat flux width and the physics determining it are of primary importance.

Current research contributions to NSTX Upgrade

Ongoing work is focused on two major research areas: basic properties of the SOL plasma, especially the heat flux width, and fundamental physics of blob-filaments and their interaction with zonal and mean flows. In previous work[3,4] we successfully modeled (at factor-of-two or better level accuracy) the scaling of the heat-flux width for four discharges in NSTX. The experimentally observed strong inverse scaling with plasma current, I_p, and a much weaker scaling with exhaust power, P_{sol}, were obtained numerically. These studies provided an experimentally validated base from which further numerical exploration of the SOL width scaling are being carried out using the SOLT (Scrape-Off Layer Turbulence) code.[5] (See the Boundary chapter section on Theory and Simulation Capabilities for a brief description of SOLT.) The new studies have so far revealed an important phenomena: a transition from quasi-diffusive to convective transport in the SOL.[6] At the transition, the transport becomes

intermittent, and the SOL heat flux width is broadened due to increased blob emission. At the resulting larger values of the SOL width, gradient driven diffusion is ineffective and gives way to convective transport. It is expected that this blob-filament-driven transport acts in addition to particle-driven transport described by drift-orbit theory[7], which could set a minimum density width. In a drift-orbit theory, turbulent transport of electron heat in the SOL is still required to obtain the heat flux width.

Closely related to the practical matter of determining scalings of the SOL heat flux width is the underlying fundamental physics that controls the formation and propagation of blob-filaments and their dynamical interactions with mean and zonal flows. In particular, in recent work[8-10] it was shown that strong sheared flows can either trap blobs preventing their ejection or enhance their ejection and radial velocity in the SOL. This work employed both SOLT code simulations and gas-puff-imaging (GPI) data analysis of NSTX discharges using a recently developed blob-tracking algorithm.[11] The simulations reproduced many qualitative and quantitative features of the data including size, scale-length and direction of perpendicular (approximately poloidal) flows, the inferred Reynolds acceleration and residual stress, and poloidal reversal of blob tracks. Mechanisms related to blob motion, SOL currents and radial inhomogeneity were shown to be sufficient to explain the presence or absence of mean and oscillating zonal sheared flows in selected shots.

Summary of proposed research plan for 2014-18

Ongoing and future work will continue in the two key areas of SOL properties (including the heat flux width, and associated scalings) and fundamental questions elucidating blob-filament dynamics. In particular, the behavior of blob-filaments in lithiated discharges is of special interest. Such discharges provide modified edge conditions which are potentially beneficial for plasma performance and of great scientific interest in their own right. Diagnostics of potential interest for this work include gas puff imaging, probes, infrared thermography, Thomson scattering and beam emission spectroscopy.

In addition to studying the effect of lithium, we are working on a version of SOLT that includes the physics of neutrals. It would be interesting to assess whether neutral friction and neutral recycling have a significant effect on SOL turbulence and blob propagation. This would also relate directly to the effect of Li on recycling in NSTX-U.

Depending on the results of these ongoing studies, several ideas for experimental tests may be interesting. These include controlled broadening of the SOL width by increasing blob radial velocities with SOL collisionality as a knob, and blob control using driven *axisymmetric* SOL flows which may provide an alternative to non-axisymmetric biasing [12].

The elements of our plan displayed in a timeline are:

Timeline

2014-2015:

- Carry out detailed comparison studies between the SOLT code and experimental data (GPI and other diagnostics) for discharges with varying degrees of lithium, including studies of blob structure and motion and the resulting SOL properties.

2015-2016:

- Extend previous studies using the SOLT turbulence code to examine the variation of SOL turbulence and the heat flux width with machine (plasma) parameters on NSTX-U.

2016-2017:

- Work with NSTX-U team to design possible critical experiments to further test and/or explore scalings and critical phenomena. Assess the role of neutrals in modifying SOL turbulence and edge confinement.

2017-2018:

- Analyze available additional experimental data from previous years and assess the implications of all the work for future STs and ITER.

Contributions to the NSTX-U 2014-18 Five Year Plan:

Lodestar has contributed to the development of the NSTX-U 2014-18 Five Year Plan through discussions with the NSTX-U team on blob-filament diagnostics, blob and SOL flow control and SOL modeling using the SOLT code. See the Boundary chapter section on Theory and Simulation Capabilities for a brief description of SOLT.

References

[1] S. I. Krasheninnikov, D. A. D'Ippolito and J. R. Myra, J. Plasma Phys. **74**, 679 (2008).

[2] D.A. D'Ippolito, J.R. Myra and S. J. Zweben, Phys. Plasmas **18**, 060501 (2011).

[3] J.R. Myra, D.A. Russell, D.A. D'Ippolito, J-W. Ahn, R. Maingi, R.J. Maqueda, D.P. Lundberg, D.P. Stotler, S.J. Zweben, M. Umansky, J. Nucl. Mat. **415**, S605 (2011).

[4] J. R. Myra, D. A. Russell, D. A. D'Ippolito, J.-W. Ahn, R. Maingi, R. J. Maqueda, D. P. Lundberg, D. P. Stotler, S. J. Zweben, J. Boedo, M. Umansky, and NSTX Team, Phys. Plasmas **18**, 012305 (2011).

[5] D. A. Russell, J. R. Myra and D. A. D'Ippolito Phys. Plasmas **16**, 122304 (2009).

[6] J. R. Myra, D. A. Russell and D. A. D'Ippolito, Plasma Phys. Control. Fusion **54**, 055008 (2012).

[7] R. J. Goldston, Nucl. Fusion **52**, 013009 (2012).

[8] J.R. Myra, W.M. Davis, D.A. D'Ippolito, B. LaBombard, D.A. Russell, J.L. Terry, and S.J. Zweben, 24th IAEA Fusion Energy Conference, San Diego, USA, October 8 - 13, 2012, paper IAEA-CN-197/TH/P4-23.

[9] "Edge Sheared Flows and Blob Dynamics," J. R. Myra, et al., invited talk presented at the Fifth-fourth Annual Meeting of the Division of Plasma Physics, Providence, RI, October 29 - November 2, 2012, paper YI3.00002.

[10] J.R. Myra, W.M. Davis, D.A. D'Ippolito, B. LaBombard, D.A. Russell, J.L. Terry, and S.J. Zweben, submitted to Nucl. Fusion (2012).

[11] W. M. Davis, et al., *54th Annual Meeting of the APS/DPP*, 2012, Providence, RI., paperYP8.00038.

[12] S. J. Zweben, R. J. Maqueda, A. L. Roquemore, C. E. Bush, et al., Plasma Phys. Control. Fusion **51**, 105012 (2009).

11.2.11 Massachusetts Institute of Technology

Research Topic: Full-wave studies of high harmonic heating in NSTX with application to antenna coupling and parasitic fast ion interactions in advanced operating modes

Principal, Co-Principal Investigators: Paul T. Bonoli (PI/PD), John C. Wright (Co-I.)
Participating Scientists: Joel C. Hosea, Stan Kaye, Cynthia K. Phillips (PPPL), L. A. Berry, D. L. Green, and E. F. Jaeger (ORNL)
Participating Post-docs: Nicola Bertelli (PPPL)
Funded under DOE Grant: DE-FG02-99ER54525

Introduction

During the past several years radio-frequency power in the high harmonic fast wave (HHFW) regime was used with increasing success on the National Spherical Torus Experiment (NSTX). Experimental breakthroughs were achieved in understanding how to avoid surface wave excitation by moving the onset density for wave propagation farther into the plasma and away from the antenna array. This resulted in record central electron temperatures of 6.2 keV with core HHFW electron heating in L-mode plasmas and greater than 5 keV electron temperatures in H-mode plasmas with concomitant neutral beam injection (NBI) heating. These successes have underscored the importance of having an accurate predictive capability for HHFW wave propagation, absorption, coupling and current drive in order to optimize the use of HHFW power in the NSTX-U device for plasma heating and bootstrap current generation in plasma startup and ramp-up scenarios and for H-mode sustainment.

Current research contributions to NSTX Upgrade

During FY2012 the MIT effort contributed to the NSTX-U program in three important areas: (a) completed the testing and demonstrated the efficacy of a new parallel TORIC solver that can be invoked directly from TRANSP [1], thus enabling time dependent transport simulations of proposed discharges in NSTX-U with adequate numerical resolution and multiple toroidal modes; (b) assisted in the theoretical and numerical analysis of slow wave mode conversion in NSTX and NSTX-U in the HHFW regime; (c) assisted in the assessment of HHFW damping on thermal and non-thermal ion populations in NSTX-U, which is expected to be important because of the higher toroidal field (B_T ~ 1T). Much of this work was done in close collaboration with C. K. Phillips, E. Valeo, and N. Bertelli at PPPL and E.F. Jaeger and L.A. Berry at ORNL.

Summary of proposed research plan for 2014-18

1. Verification studies of ion cyclotron damping in the HHFW TORIC solver

Recently Dr. C. K. Phillips initiated an effort to simulate HHFW heating in the NSTX-U device using the TORIC and AORSA solvers. Particular emphasis was given in these studies to the predicted damping of

the HH fast wave on the background deuterium and energetic deuterium neutral beam. Initial results from these studies [2] indicate more power absorption by the thermal D ions is seen in NSTX-U than was seen previously in NSTX simulations at similar values of incident parallel wavenumber. This result is not surprising owing to the lower cyclotron harmonics in NSTX-U. However significant differences between TORIC and AORSA on the power absorbed by thermal D and nonthermal beam ions was also found, with TORIC predicting 3-4 times as much absorption on thermal D ions than AORSA, and about 1/3 as much power absorption on energetic deuterium beam ions than AORSA. The working hypothesis thus far is that the AORSA simulations are correct because that code retains all-orders in the ion cyclotron harmonic sum of the conductivity operator. During 2014-2015 we will determine the reasons for this discrepancy and make the required modifications in TORIC if necessary so that its predictions are valid in this regime. This will enable the TORIC in TRANSP code to continue to be used as a useful tool for NSTX-U discharge analysis.

By 2015-2016, work will have been completed on the implementation in TORIC of a non-Maxwellian dielectric tensor valid in the HHFW regime. This work is being led by Dr. N. Bertelli, in collaboration with the SciDAC Center for Wave-Plasma Interactions (CSWPI). This will then make it possible to more accurately assess the interaction of HHFW power in NSTX-U with fast ions from NBI heating.

2. HHFW coupling studies in NSTX-U plasmas

During 2016-2017 we plan to investigate linear HHFW coupling and surface excitation using the standalone TORIC solver. Recently the TORIC code was modified to allow specification of density and temperature profiles for the SOL in an improved manner. Using an exponential step function, the normal generalized parabolic profiles inside the last closed flux surface (LCFS) were modified to include a scrape-off layer of a specified width by multiplying the exponential shape function with the original profile. This is an improvement over the original scrape-off layer model that deformed the profile to make room for the addition of a scrape-off layer within the LCFS. We plan to use this improved SOL model for these coupling studies.

As with the previous SOL model, the new model still extends out to a Faraday screen and beyond that is a current strap in vacuum. A conducting wall is placed in back of the current strap. The locations of the current strap, Faraday screen, and conducting wall correspond to conforming flux surfaces and their locations can be specified arbitrarily. Similarly, the density profile and width of the SOL are also arbitrary. We will perform simulations with the Faraday screen removed and the current strap placed right at the edge of the plasma SOL, with a vacuum region extending from the outside edge of the current strap to the conducting wall. In order to better study the possibility of surface wave excitation it will be necessary to perform 3-D field reconstructions. This will be accomplished by calculating the 2-D (ψ, θ) electric field solution with TORIC for each toroidal mode of the antenna and then superposing these solutions. Additionally each toroidal mode will be weighted by the vacuum power spectrum of the antenna and the partial loading resistance computed by TORIC for each toroidal mode.

These studies will be aimed at understanding qualitatively the experimentally observed dependence of HHFW electron heating in NSTX with toroidal magnetic field, antenna phasing, and SOL density profiles

[3, 4]. These dependencies were successfully simulated [5] using the all-orders full-wave spectral code AORSA with the inclusion of a realistic scrape off-layer in that code and thus the comparison with AORSA and experiment will serve as an important validation of the adequacy of the coupling model in the HHFW TORIC solver. Recall that the density for onset of fast wave propagation scales as $n_{onset} \approx B_\phi \times (k_{//})^2 / \omega$. Plasma parameters, in particular the SOL density profiles from discharges reported in Ref. [2] will be used in the full-wave simulations. The antenna phasing will be fixed at $k_\phi = -8\ m^{-1}$ (current drive phasing) and 3-D field reconstructions will be performed, one at $B_\phi = 4.5$ kG and one at $B_\phi = 5.5$ kG. In each case the radial, poloidal, and toroidal extent of the fields will be investigated with the expectation that at 4.5 kG the wave fields will be confined to the periphery. Because these studies are considered qualitative and scoping in nature we plan to scan the toroidal field beyond 5.5 kG if a clear effect on wave penetration is not seen initially. The next simulation comparison will be a 3-D field reconstruction at 4.5 kG using heating phasing ($k_\phi = 14\ m^{-1}$), where good wave penetration was also seen experimentally. The final simulation study will be to fix (B_ϕ, $k_{//}$, ω) and change the density profile of the SOL from what is expected typically without lithium wall conditioning [3] to what was reported with lithium conditioning [4]. Qualitatively it would be expected that the 3-D field reconstructions using the lower SOL densities characteristic of lithium wall conditioning will exhibit better wave penetration. Again, because of the scoping nature of these simulations we plan to vary the shape and magnitude of the SOL density profile in order to investigate the sensitivity of surface wave excitation to this plasma parameter.

If it is found that the 3-D field reconstructions qualitatively reproduce the conditions for surface wave excitation and its avoidance found in NSTX then this approach would be used in 2017-2018 for assessing the viability of applying HHFW power under a variety of distinctly different edge plasma conditions in NSTX-U; for example L-mode, H-mode, and start-up plasmas. These simulations would be both standalone and time dependent, using 3-D wavefields reproduced from the multi-toroidal mode capability of the parallel TORIC in TRANSP. This work will be carried out in collaboration with Dr. J. Hosea, Dr. C. K. Phillips, and Dr. G. Taylor at PPPL.

Timeline

2014-2015:

- Benchmark ion cyclotron damping at intermediate harmonic number (2-4) against AORSA solver for thermal (Maxwellian) and non-thermal (bi-Maxwellian) ion distributions.
- Resolve differences between TORIC and AORSA solvers.

2015-2016:

- Compare ion cyclotron damping in TORIC solver with new non-Maxwellian dielectric tensor against AORSA solver, using bi-Maxwellian distribution functions.
- Carry out time dependent simulations with TORIC in TRANSP, using effective temperature Maxwellian from NUBEAM to evaluate the non-Maxwellian dielectric tensor in TORIC.

2016-2017:

- Test adequacy of modified TORIC SOL model for reproducing dependency of NSTX coupling results on B_ϕ, k_ϕ, and n_{SOL}.
- Implement modifications to SOL model as needed based on tests.

2017-2018:

- Perform standalone simulations of antenna coupling for NSTX-U configuration using TORIC with benchmarked SOL model.
- Study time dependent coupling of HHFW heating power in start-up and ramping plasmas in NSTX-U discharges using parallel TORIC in TRANSP.

Contributions to the NSTX-U 2014-18 Five Year Plan:

The plan above was defined in a process carried during CY2012, in coordination with the NSTX-U Research Team as they developed their 2014-2018 Five Year Plan document. Specifically this plan contributes to Thrust RF-1: "Develop RF/EC Heating for Non-Inductive Plasma Current Start-Up and Ramp-Up" and to Thrust RF-2: "Validate Advanced RF Codes for NSTX-U and Predict RF Performance in Future Devices", as articulated in Chapter Seven of the NSTX-U Research Plan on Wave Heating and Current Drive.

References

[1] J. P. Lee and J. C. Wright, "A versatile parallel block tri-diagonal solver for spectral codes", to be submitted to Computer Physics Communications (2013).

[2] C. K. Phillips, N. Bertelli, R. Budny, S. Gerhardt, J. C. Hosea, B. LeBlanc, J. Menard, G. Taylor, E. J. Valeo, J. R. Wilson, E. F. Jaeger, P. T. Bonoli, J. C. Wright, R. W. Harvey, L. A. Berry, D. Green, and the NSTX-U and RF SciDAC Teams, "Initial predictive studies of HHFW heating in the NSTX-U device", Bulletin of the American Physical Society **57**, 321 (2012).

[3] J. Hosea, R. E. Bell, B. P. LeBlanc, C. K. Phillips, G. Taylor, E. Valeo, J. R. Wilson, E. F. Jaeger, P. M. Ryan, J. Wilgen, H. Yuh, F. Levinton, S. Sabbagh, K. Tritz, J. Parker, P. T. Bonoli, R. Harvey, and the NSTX Team, "High harmonic fast wave heating efficiency enhancement and current drive at longer wavelength on the National Spherical Torus Experiment"**,** Physics of Plasmas **15**, 056104 (2008).

[4] G. Taylor, R. E. Bell, J. C. Hosea, B. P. LeBlanc, C. K. Phillips, M. Podesta, E. J. Valeo, J.R. Wilson, J-W. Ahn, G. Chen, D. L. Green, E. F. Jaeger, R. Maingi, P. M. Ryan, J. B. Wilgen, W. W. Heidbrink, D. Liu, P. T. Bonoli, T. Brecht, M. Choi, and R. W. Harvey, "Advances in high harmonic fast wave physics in the National Spherical Torus Experiment", Physics of Plasmas **17**, 056114 (2010).

[5] D. L. Green, L. A. Berry, G. Chen, P. M. Ryan, J. M. Canik, and E. F. Jaeger, "Predicting High Harmonic Ion Cyclotron Heating Efficiency in Tokamak Plasmas", The Physical Review Letters **107**, 145001 (2011).

11.2.12 Nova Photonics

Research Topic: The Motional Stark Effect Diagnostic for NSTX
Principal, Co-Principal Investigators: Dr. Fred M. Levinton
Participating Scientists: Dr. Howard Yuh
Participating Post-docs: N/A
Participating Graduate Students: 0
Participating Undergraduates: 0
Funded under DOE Grant: DE-FG02-99ER54520 & DE-FG02-01ER54616

Introduction

The MSE diagnostic addresses several needs of the project as outlined in the "NSTX Program Letter for Research Collaboration Employing Innovative Diagnostics for FY 2012-2015" and "NSTX Research Program Five Year Plan for 2009-2013". The NSTX project goals for FY 2012-2015 are grouped into six scientific topics; Macroscopic Stability, Multi-Scale Transport Physics, Plasma Boundary Interfaces, Energetic Particles, Start-up, Ramp-up, and Sustainment without a Solenoid, and Advanced Operating Scenarios. The need for MSE measurements is listed in all six scientific areas because of its fundamental importance for equilibrium, stability, and transport. As part of our collaboration on NSTX we have designed, fabricated, and installed the MSE-CIF diagnostic system. This includes the collection optics, polarimeter, fiber optic bundles, detectors, and development of a new, high throughput, high resolution, birefringent interference filter (BIF) that has made MSE-CIF measurements at low magnetic fields possible. The development of the birefringent filter for the MSE-CIF diagnostic was key to its success. This filter allows very high throughput with high resolution (FWHM~0.06 nm). We have also completed the data acquisition and control system using LabVIEW and integrated it into the NSTX data system that uses MDS+. Software development is now complete, and analysis of the MSE-CIF data is completed between shots and made available for equilibrium reconstruction for between shot analysis. This has proven extremely valuable in many experimental campaigns where development of the appropriate q-profile was essential to guide the session leader toward the experimental goals. At present the diagnostic is providing calibrated magnetic field pitch angle data from 18 channels with sightlines covering from inboard of the magnetic axis to the plasma edge. The MSE-CIF system has been operating routinely, supporting many experimental proposals (XP's) on NSTX at toroidal fields between 3.0-5.5 kG. During the 2011 run period we installed the new MSE-LIF diagnostic, including the diagnostic neutral beam, laser, and collection optics for 5 sightlines. We completed some initial testing of the system and will resume shakedown when NSTX-U starts up in FY15. The new Motional Stark Effect with Laser-Induced Fluorescence (MSE-LIF) diagnostic will allow radially resolved, high-precision measurements of magnetic field magnitude as well as pitch angle. The installation and use of the

MSE-LIF diagnostic on NSTX will enable new physics studies in several topical areas, including fast ion instabilities from a unique measurement of the non-thermal ion population, rf heating and current drive as well as non-inductive startup and current drive in the absence of heating beams, effects of radial electric fields with the combination of the existing MSE-CIF system and the new MSE-LIF, and a contribution to ITER via a unique opportunity to directly compare the utility of two proposed types of MSE measurement that have been proposed for ITER equilibrium reconstruction. Because the MSE-LIF is based on the use of a diagnostic neutral beam, MSE measurements can be made in the absence of heating beams, which will contribute to studies of HHFW heating and current drive, as well as CHI methods of non-inductive startup and current drive.

Current research contributions to NSTX Upgrade

Working with NSTX-U on rtMSE plans and best way to deliver signals to the NSTX-U PCS.

Summary of proposed research plan for 2014-18

The proposed goals of the collaboration for FY14-18 are;

1. Provide calibrated magnetic field pitch angle profiles for the NSTX project. This involves operation of the diagnostic and routine calibration. We will work closely with the NSTX team on several related diagnostic issues such as equilibrium reconstruction. Install MSE-LIF system with 20 channels.

2. Upgrade the data acquisition and computer system to provide real-time MSE-CIF (rtMSE) data for current profile control utilizing the new neutral beam injectors being installed on NSTX as part of the upgrade.

3. Provide measurements of radially resolved internal magnetic fluctuations.

4. Hardware modifications for NSTX-U compatibility. With a doubling of the magnetic field as part of the NSTX upgrade the MSE-CIF collection optics will be optimized to increase the throughput.

5. Participate in physics planning and the experimental program on NSTX. In addition to supporting experiments by providing MSE data, we have proposed and run experiments on NSTX in the past and plan to continue to do so in the future. We expect to continue studies of the effect of magnetic shear on electron transport, and investigate neutral beam current drive from the new current drive beam that will be installed during the NSTX

upgrade. With the combination of the MSE-CIF and the new MSE-LIF, that is supported under a separate Diagnostic Development Grant from DOE/OFES, we will be able to provide radial electric field (E_r) and pressure profiles.

The elements of our plan displayed in a timeline are:

Timeline

FY2014:
- Development of rtMSE hardware and software.
- Installation of MSE-CIF and MSE-LIF components removed for upgrade.
- Installation of additional fiber, filters, and detectors for the MSE-LIF system.
- Modify optics of the MSE-CIF for higher throughput.

FY2015:
- Operation of MSE-CIF to measure pitch angle and magnetic fluctuations.
- Shakedown of rtMSE.
- Shakedown of MSE-LIF.

FY2016:
- Operation of MSE-CIF to measure pitch angle and magnetic fluctuations.
- Equilibrium reconstruction from MSE-LIF using magnitude of the magnetic field, |B|.

FY2017:
- No Operation for extended outage.
- Additional MSE-LIF channels installed to bring the total to 38.

FY2018:
- MSE-CIF/MSE-LIF operation.
- MSE-CIF/MSE-LIF combination to measure radial E_r profiles.
- rtMSE operation.

References:

[1] F. M. Levinton et al., Phys. Plasmas **14**, 056119 (2007).
[2] F. M. Levinton et al., Rev. Sci. Instrum. **79**, 10F522 (2008).
[3] H. Yuh et al., Phys. Rev. Lett. **106**, 055003-1 (2011).
[4] E. L. Foley and F. M. Levinton, Rev. Sci. Instrum. **77,** 10F311 (2006).

11.2.13 Oak Ridge National Laboratory

Research Topic: Boundary Physics, Heating, and Current Drive Program

Principal, Co-Principal Investigators: J.M. Canik, P.M. Ryan
Participating Scientists: J.-W. Ahn, T. S. Bigelow, J. B. O. Caughman, S. J. Diem, T.K. Gray, D. L. Green, D.L. Hillis, J.D. Lore, A.C. Sontag, J. B. Wilgen
Participating Post-docs: 1
Participating Graduate Students: 0
Participating Undergraduates: 0
Funded under DOE Grant: DE-AC05-00OR22725

Introduction

The ORNL research program is divided into two main thrusts: Boundary Physics and RF Heating. The focus of the Boundary Physics program is on improving the physics basis for projecting and optimizing the edge plasma in fusion devices, including the scrape-off layer and divertor. The particle and power exhaust challenge in STs is enhanced by their compact nature, which results in high fluxes and constraints on the space available for highly shaped PFCs. This motivates the search for novel solutions such as the use of liquid metal PFCs and the application of 3D fields for edge control, both of which are areas of emphasis for the ORNL collaboration. The focus of the RF Heating and Current Drive program is to progress toward fully non-inductive operation and solenoid-free plasma current ramp-up to steady-state high-beta operation. RF power will be used to initiate plasma pre-ionization, ramp up low current coaxial helicity injection (CHI) plasmas to the currents and densities needed for neutral beam application, and to further reduce volt-second consumption for long pulse operation at high beta. The ORNL research program includes the installation and operation of several boundary diagnostics, the design, execution, and analysis of experiments, and modeling and simulation in support of these experiments.

Current research contributions to NSTX Upgrade

ORNL staff leads research in the areas of H-mode pedestal and ELM physics [1-9]. We also contribute to the experimental test of lithium as a divertor PFC [10-15]. Our divertor physics program includes leading research on divertor heat flux scaling and the impact of 3D fields [16-23]. ORNL researchers conduct 2D modeling of ST plasmas, including both of present-day experiments and for projection to future STs such as ST-FNSF, and have also led the physics design of the cryo-pumping system for NSTX Upgrade.

ORNL staff operates several IR cameras, including both fast and slow systems, with the capability of dual-band measurements for extracting the divertor heat flux when lithium coatings are present. We also operate a fast filterscope array, visible spectrometers, and thermocouples for PFC temperature measurements.

ORNL historically provides manpower and support for HHFW system design, equipment operation, and experimental implementation and analysis, as well as theory assistance through rf/plasma modeling. The ORNL reflectometer and other edge diagnostics provide crucial information for the optimization of the power coupling and performance of the HHFW systems. The edge profile data is also used to benchmark the modeling codes in order to better understand and interpret the experimental results.

Summary of proposed research plan for 2014-18

The ORNL Boundary Physics program involves research in three main areas: 1) power and particle exhaust, 2) H-mode pedestal research including the effects of lithium, and 3) the effects of 3D magnetic fields on the edge plasma.

In the area of power and particle exhaust, ORNL researchers will conduct experiments measuring the divertor heat flux, characterizing its width, and documenting its scaling with various machine parameters including plasma current and divertor flux expansion. We will also test the effects of lithium on the heat flux profile, including possible novel scenarios such as a highly radiating regime induced by strong lithium evaporation from the PFC surface. The use of lithium for particle control will be studied, including combining lithium PFC coatings for deuterium control with ELM-triggering for impurity control, and extending these scenarios to the longer pulse durations planned for NSTX-U. In addition, ORNL researchers have led the physics design of a cryo-pumping system to be installed on NSTX-U, and will conduct experiments to test the effectiveness of this more conventional pumping technique.

H-mode pedestal research will also be conducted by ORNL researchers. This includes conducting experiments to document the pedestal characteristics (e.g., height and width) over the widened operating space available in NSTX-U in terms of plasma current, magnetic field, heating power, and collisionality. A further emphasis will be on researching the impact that lithium has on the pedestal structure, including both experiments and simulations using gyrokinetic codes such as GS2 and GENE.

The final ORNL boundary physics research area is on the impact of 3D fields on the edge plasma. This thrust includes characterizing how 3D field application alters the pedestal structure and stability, and scenario development using these effects to improve NSTX-U plasma

performance, for example by expelling impurities and reducing losses due to core radiation. The effect of 3D fields on the divertor plasma is also an area of ORNL research. This includes both the geometric changes to the heat and particle strike patterns on the divertor (so-called strike point splitting), as well as the impact these fields have on detachment onset conditions. This research will be performed through a combination of experiments on NSTX-U and modeling using state-of-the-art tools such a EMC3-EIRENE.

These proposed research elements reflect a continuation of the ORNL contribution to the NSTX boundary physics program. To carry out this research, the following ORNL diagnostics, which were operated on NSTX, are proposed for implementation on NSTX-U:

- Fast framing dual-band infrared camera viewing the lower divertor,
- 32 channel filterscope system for visible light emission,
- 3-4 compact Ocean Optics high throughput visible spectrometers,
- A wide-angle IR camera with dual-band adapter, and
- Fast time response eroding thermocouples for PFC surface temperature.

To this suite of diagnostics, we are proposing to add:

- An upper-viewing fast dual-band IR camera,
- An additional 8-10 fast time response ‘eroding’ thermocouples,
- Neutral pressure gauges in the cryopump plenum region and main chamber, and
- A densely packed diagnostic tile near the plenum entrance for detailed measurement of local divertor plasma properties.

The ORNL RF research program will concentrate on the following areas of activity over the FY 2014-2018 time period:

- Assess HHFW heating and current drive efficiency for the upgraded plasma conditions of NSTX-U. Analyze and perform experiments to optimize HHFW heating and current drive in low-current, low-density, low-temperature, start-up target plasmas.

- Perform experiments, measure RF/edge plasma interactions, and provide data to theoretical models to understand, predict, and control the RF power flow from the antenna to the core plasma, including wave interactions with NBI fast ions and edge plasma losses (parametric decay instabilities, sheath losses, wave scattering, edge ion heating, and power propagation in the scrape off layer).

- Improve the high power capability and reliability of the HHFW system by designing and testing antenna modifications.

- Design and evaluate the overall operation of a HHFW launcher employing a reduced number of array elements, including control, tuning and matching, and protection.

- Provide and operate antenna/edge diagnostics (microwave reflectometer, antenna IR camera) to measure edge conditions and RF/plasma/antenna interactions.

- Model and evaluate ECH/EBW start-up/ramp-up scenarios. Design the power transmission and delivery system for a 1 MW, long pulse system operating at 28 GHz.

The elements of our plan displayed in a timeline are:

Timeline

FY2014:

- Continue analysis of edge microstability without and with lithium coated PFCs in NSTX experiments
- Complete preliminary physics design of cryo-pumping system consistent with engineering design
- Install and commission a slow wide-angle dual-band IR camera for the lower divertor, obtain full (r, ϕ) 2D heat flux profiles
- Install and commission a high-speed dual-band IR camera for the upper divertor along with the implementation of the existing high-speed dual band IR camera for the lower divertor, obtain 2D heat flux profiles with ELM resolution
- Initiate EMC3-Eirene modeling for 2D divertor heat and particle profiles, preliminary comparison with IR measurements with and without 3D fields
- Install and commission eroding thermocouples embedded in divertor tiles for power and magnetic balance control
- The electronics, data acquisition hardware, and waveguide needed to bench-top test the upgraded NSTX-U reflectometer will be purchased in 2013. In 2014 the replacement vacuum flange and launch/receive antennas will be fabricated and the microwave reflectometer system will be tested and installed on NSTX-U.
- Install and test the IR camera for dedicated antenna structure temperature monitoring.
- Begin modeling the fast wave interaction with fast ions at high cyclotron harmonics, using DIII-D/NSTX experimental data and offset Maxwellian ion distributions in AORSA.
- Initiate EC/EBW modeling using GENRAY/CQL3D and perform code comparisons between GENRAY/CQL3D and ARM.

FY2015:

- Document plasma profiles near candidate plenum entrance, and use this data to confirm and finalize cryo design
- Improve IR analysis software to deal with heat flux onto metallic PFC and long pulse
- Effect of 3D fields on divertor heat and particle profiles; parameter dependence on the asymmetry in heat flux and mean heat flux width (stationary and transient)
- Initiate study of 3D effects on divertor detachment, both for heat and particle flux profiles. Begin EMC3-Eirene modeling for 3D effects on detachment
- Continue analysis of how heat flux and the SOL width vary at the higher Ip, Bt and PSOL available in NSTX-U. Scale for a potential ST-FNSF divertor design.
- Perform initial pedestal scaling studies in NSTX-U
- Assess performance of HHFW array with/without lithium.
- Quantify expected improvement of center-grounded vs end-grounded strap configuration.
- Apply operating techniques for power coupling into ELMing H-modes being developed on DIII-D to NSTX-U.

FY2016:

- Continue data taking, analysis of 3-D effects from ELM control experiments
- Conduct study on relationship between pedestal and divertor/SOL plasmas in the presence of 3D field
- Begin to study 3D effects on divertor flux profiles and EMC3-Eirene modeling in the lithium environment
- Assess the effect of increasing lithium deposition on NSTX-U divertor plasmas and SOL thermal transport
- Verify the microwave reflectometer edge profile measurements and test the full quadrature detection of PDI and edge density fluctuations will be tested, under the supervision of a postdoc.
- Complete design and evaluation of a reduced-element antenna array and power transmission system (tuning/matching/decoupling/phase control).
- Compare the HHFW power flow in the edge plasma with AORSA-3D calculations.
- Heating of low current plasmas for full non-inductive H-modes will be investigated and non-inductive current ramp-up will be initiated.

FY2017:

- Conduct experiments testing performance of cryo system and compare to models
- Extended parameter scan (ν^*, q_{95}, β_N) for 3D divertor physics study with lithium, establish relationship with pedestal parameters

- Extend EMC3-Eirene modeling to deal with 3D + detachment + lithium, and comparison with measurement
- Install and commission divertor "smart tile" with eroding thermocouples, ASDEX style pressure gauge and Langmuir probes to help assess the performance of the newly installed cryo-pump
- Provide routine diagnostic operation of the microwave reflectometer and antenna IR camera.
- Simulate reduced-element HHFW array operation with portions of existing array and compare with design code predictions.
- Test low frequency wave excitation with modified HHFW system.
- Make fully self-consistent iterative calculations of wave-particle interactions with AORSA-2D and NUBEAM. Plasma edge wave fields will be investigated with test particle tracing.
- Design an optimized wave launcher for AE or EHO studies.
- Design low loss, high power EC/EBW transmission system and launcher.
- Optimize plasma start-up, ramp-up, and sustainment during NBI H-mode using HHFW.

FY2018:

- Fully implement measurement and modeling capabilities for the full plasma performance for lithiated PFCs
- Comparison with simultaneous modeling of upper and lower divertors with EMC3-Eirene
- Comparison of particle pumping ability of cryo-pumped and lithiated discharges
- Implement reduced-element HHFW array to drive central current in H-mode plasmas.
- ECH will be used with CHI for plasma startup scenarios. Test EBW heating with fixed horn system; use results to finalize optimized launcher design.

Contributions to the NSTX-U 2014-18 Five Year Plan:

Major contributions were made to the Boundary Physics chapter of the NSTX-U Five Year Plan, including sections 4.2.1, 4.2.2, 4.2.4, and 4.2.6, and to the Wave Heating and Current Drive chapter, including sections 7.2.1, 7.2.2, 7.2.3, and 7.3.2. The plan above was defined in a process carried out over CY2011-12 in coordination with the NSTX-U Research Team. The research defined above contributes heavily to the plan.

References

[1] J.M. Canik, R. Maingi, T.E. Evans, R.E.. Bell, S.P. Gerhardt, et. al., "ELM de-stabilization with 3D magnetic fields in NSTX", *Nucl. Fusion* **50** (2010) 034012.
[2] J.M. Canik, R. Maingi, T.E. Evans, R.E.Bell, S. Gerhardt, et. al., "On demand triggering of edge localized modes using external non-axisymmetric magnetic perturbations in toroidal plasmas", *Phys. Rev. Letts.* **104** (2010) 045001.
[3] R. Maingi, S.M. Kaye, and the NSTX team, "Overview of L-H power threshold studies in NSTX", *Nucl. Fusion* **50** (2010) 064010.
[4] J.M. Canik, A.C. Sontag, R. Maingi, R. Bell, D.A. Gates, et. al, "Progress in the development of ELM pace-making with non-axisymmetric magnetic perturbations in NSTX", *Nucl. Fusion* **50** (2010) 064016.
[5] R. Maingi, R.E. Bell, J.M. Canik, S.P. Gerhardt, S.M. Kaye, et. al., "Triggered confinement enhancement and pedestal expansion in high confinement mode discharges in the NSTX", *Phys. Rev. Lett.* **105** (2010) 135004.
[6] R. Maingi, A.E. Hubbard, H. Meyer, J.W. Hughes, A. Kirk, et. al., "Comparison of Small ELM Characteristics and Regimes in Alcator C-Mod, MAST, and NSTX", *Nucl. Fusion* **51** (2011) 063036.
[7] A.C. Sontag, J.M. Canik, R. Maingi, J. Manickam, P.B. Snyder, et. al., "Pedestal characterization and stability of small ELM regimes in NSTX", *Nucl. Fusion* **51** (2011) 103022.
[8] J.M. Canik, S.P. Hirshman, R. Sanchez, R. Maingi, J.-W. Ahn, et. al., "First use of three-dimensional equilibrium, stability, and transport calculations for interpretation of ELM-triggering with magnetic perturbations in NSTX", *Nucl. Fusion* **52** (2012) 054004.
[9] J.D. Lore, J.M Canik, J-W. Ahn, A. Bortolon, E.D. Fredrickson, et. al., "Effect of n=3 fields below the ELM triggering threshold on edge and SOL transport in NSTX", *J. Nucl. Mater.* (2012) submitted.
[10] J.M. Canik, R. Maingi, S. Kubota, Y. Ren, R.E. Bell, et. al., "Edge transport and turbulence reduction with lithium coated plasma facing components in the National Spherical Torus Experiment", *Phys. Plasmas* **18** (2011) 056118.
[11] R. Maingi, S.M. Kaye, C.H. Skinner, D.P. Boyle, J.M. Canik, et. al., "The continuous improvement of H-mode discharge performance with progressively increasing lithium coatings in NSTX", *Phys. Rev. Lett.* **107** (2011) 145004.
[12] J.M. Canik, R. Maingi, V.A. Soukhanovskii, R.E. Bell, H.W. Kugel, et. al., "Measurements and 2-D Modeling of recycling and edge transport in discharges with lithium-coated PFCs in NSTX", *J. Nucl. Mater.* **415** (2011) S409.
[13] A.G. McLean, J-W. Ahn, R. Maingi, T.K. Gray, and A.L. Roquemore, "A dual-band adaptor for infrared imaging," *Rev. Sci. Instrum.* **83** (2012) 053706.

[14] R. Maingi, D.P. Boyle, J.M. Canik, S.M. Kaye, C.H. Skinner, et. al., "The effect of progressively increasing lithium coatings on plasma discharge characteristics, transport, edge profiles, and ELM stability in the NSTX", *Nucl. Fusion* **52** (2012) 083001.
[15] T.K. Gray, A.G. McLean, R. Maingi, J-W. Ahn, J.M. Canik, et. al., "The effects of increasing lithium deposition on the power exhaust in NSTX", *J. Nucl. Mater.* (2012) submitted.
[16] J-W. Ahn, R. Maingi, D.A. Mastrovito, A.L. Roquemore, and the NSTX team, "High speed infrared camera diagnostic for heat flux measurement in NSTX", *Rev. Sci. Instr.* **81** (2010) 023501.
[17] J-W. Ahn, J.M. Canik, V.A. Soukhanovskii, R. Maingi, and D.J. Battaglia, "Modification of divertor heat and particle flux profiles with applied 3D fields in NSTX H-mode plasmas", *Nucl. Fusion* **50** (2010) 045010.
[18] J-W. Ahn, R. Maingi, J.M. Canik, A.G. McLean, J.D. Lore, et. al., "Effect of non-axisymmetric magnetic perturbations on divertor heat and particle fluxes in NSTX", *Phys. Plasmas* **18** (2011) 056108.
[19] T.K. Gray, R. Maingi, J.E. Surany, V.A. Soukhanovskii, J-W. Ahn, and A.G. McLean, "Dependence of divertor heat flux widths on heating power, flux expansion, and plasma current in the NSTX", *J. Nucl. Mater.* **415** (2011) S360.
[20] J-W. Ahn, J.M. Canik, R. Maingi, T.K. Gray, A.G. McLean, et. al., "Characteristics of divertor heat and particle deposition with intrinsic and applied 3-D fields in NSTX H-mode plasmas", *J. Nucl. Mater.* **415** (2011) S918.
[21] J.D. Lore, J.M. Canik, Y. Feng, J.-W. Ahn, R. Maingi, and V. Soukhanovskii, "Implementation of the 3D edge plasma code EMC3-Eirene on NSTX", *Nucl. Fusion* **52** (2012) 054012.
[22] J-W. Ahn, K.F. Gan, F. Scotti, J.D. Lore, R. Maingi, et. al., "Study of non-axisymmetric divertor footprints using 2-D IR and visible cameras and a 3-D heat conduction solver in NSTX", *J. Nucl. Mater.* (2012) submitted.
[23] J-W. Ahn, J.M. Canik, F. Scotti, J.D. Lore, R. Maingi, et. al., "Progress in the experimental investigation of 3-D field effects on the divertor and pedestal plasmas in NSTX", *Plasma Phys. Control. Fusion* (2012) submitted.

11.2.14 Princeton University

Research Topic: Extended MHD Studies of Flow-Driven and Reconnecting Instabilities in Toroidal Plasmas

Principal, Co-Principal Investigators: Fatima Ebrahimi (PI) and A. Bhattacharjee (co-PI)
Participating Post-docs: 1/2 Post-doc
Funded under DOE Grant: DE-SC0007868

Introduction

Reconnecting and flow-driven instabilities are believed to play an important role in fusion plasmas as well as in the nonlinear dynamics of astrophysical settings. Our work aims to study these instabilities and their role in the nonlinear dynamics of the NSTX fusion toroidal device in the framework of MHD. NSTX has achieved high beta regimes (both toroidal and normalized beta) with large toroidal plasma flows (near Alfvenic). As NSTX-U plans to operate in high-beta regimes using non-inductive current-drive techniques and neutral beam injection, plasma flows can be expected to have increasing impact on MHD instabilities, mircoinstabilties and ultimately on plasma transport. Doubling of the toroidal field, plasma current and NBI heating in the NTXS-U would introduce new physics challenges. Numerical modeling of both reconnecting and flow driven instabilities in these new regimes would therefore be essential. Our work aims to study two major physics aspects of NSTX and NSTX-U, 1) physics of coaxial helicity injection as a non-inductive startup current drive technique, 2) the role of rotation and magnetic shear on ideal and non-ideal current-driven instabilities in the linear and nonlinear regimes. The simulations will be performed using the extended MHD codes NIMROD (nimrodteam.org) and M3D-C1.

For steady-state reactor scenarios, inductive ohmic current drive alone is not sufficient. If helicity is created and injected into a plasma configuration, the additional linkage of the magnetic fluxes can sustain the configuration indefinitely against resistive decay. Various techniques of helicity injection can be used for steady-state current drive, edge current drive and non-inductive startup current drive.

Advancing toward non-inductive current drive, a solenoid-free plasma start-up method called transient coaxial helicity injection (CHI) first developed on the small HIT-II device, has been extended to the large NSTX device. [1] Recent CHI experiments in NSTX have demonstrated a closed-flux equilibrium with a peaked CHI-driven current of about 300 kA. In addition, it was shown that the CHI-produced toroidal current well couples to the induction, resulting in an additional total plasma current of 200kA.[1]. CHI experiments will be extended to NSTX-U and will be coupled to NBI for non-inductive startup current drive. We perform nonlinear CHI

simulations in NSTX, which will provide further insight into the viability of CHI as a startup current drive technique and its role in ultimate steady-state operation of fusion reactors.

Slowly evolving reconnecting instabilities may limit the confinement and long time operation of fusion plasmas. They have been demonstrated to be critical in the nonlinear dynamics of many processes in toroidal laboratory plasmas, such as sawtooth oscillations, saturation of internal kink modes and plasma disruption. Toroidal fusion plasmas also rotate in the toroidal and poloidal directions. Experimental observations have demonstrated that rotation and rotation shear can strongly affect reconnecting instabilities as well as plasma transport. Recent experiments in the NSTX have shown correlation between the rotation/magnetic shear and the onset and dynamics of reconnecting events. [2,3] In slab and cylindrical geometries it has been shown that the tearing mode growth rate is increased for small shear flow and the tearing mode becomes stable at larger shear flow. In fact, the ratio of shear flow to magnetic shear determines the stability of the tearing mode.[4] At higher shear, the tearing mode can transition to a Kelvin-Helmholtz instability. The numerical study of these effects in experimentally relevant *toroidal* configurations, and in the nonlinear regimes, is very limited.

Current research contributions to NSTX Upgrade

NSTX geometry and experimentally relevant boundary conditions for CHI operations, including external magnetic fields and coil currents, have been incorporated in NIMROD (by Hooper and Sovinec). NIMROD simulations of CHI with time-dependent boundary fields from an experimental discharge have been performed and reported. [5,6] We have also performed NIMROD simulations of CHI for NSTX with *fixed boundary flux*. The purpose of our simulations is first to explore the possibility of flux closure with constant boundary fields and second to understand the physics of flux closure by isolating different physics models. Our resistive MHD simulations started with fixed boundary fields (including NSTX poloidal coil currents) for a narrow slot of 4 cm, with an injector voltage of 1.77 kV as in the experiment. A large injector current (I_{inj} ~ 12 kA during the flat injected phase) and total toroidal current (I_{tor} ~ 0.28 MA) are generated in this simulation. To understand the physics of flux closure as was observed during the CHI experiments in NSTX, we have isolated different physics models. The finding of our simulations at constant flux are 1) We find that as in the experiment, an X point followed by a fairly large volume of closed-flux surfaces are rapidly formed when the injector voltage (between the two divertor plates) ramps down to zero in the simulations, 2) We also find that unlike the HIT-II simulations at zero beta [7], in the constant flux NSTX simulations, flux closure is only obtained when plasma temperature is evolved by including anisotropic thermal diffusivity, ohmic heating and temperature dependent resistivity. We have started using M3D-C1 to perform simulations of double tearing modes in toroidal geometry.

Summary of proposed research plan for 2014-18

The goals of our simulations are to understand the physics of current relaxation by CHI in relation to transport and mode dynamics, and to perform long term simulations when CHI is coupled to the induction. The nonlinear 3-D simulations are also planned to provide guidance and possible improvement for the present CHI experiments in NSTX-U. We propose to continue the ongoing computational efforts for understanding and reproducing the CHI experiments in NSTX as was explained above. To further investigate and obtain the exact volume size of the closed flux surfaces, which is observed experimentally, we also propose to port the time-dependent boundary conditions from an experimental discharge into the simulations and to compare with the constant flux simulations. Using higher injector voltage and new divertor poloidal coils, CHI experiments in NSTX-U are planned to produce larger CHI-generated current (0.4-0.6MA). It is therefore expected that the CHI-generated current and the volume of the closed flux in NSTX-U is very different from NSTX. To study the stability of CHI-driven current, we therefore propose to perform simulations in NSTX-U geometry and its parameter regimes. We propose to perform long timescale simulations in which the CHI simulations are coupled with induction. This is of great importance since the coupling of CHI with the induction will determine the global and long term behavior of the plasma. Global MHD dynamics and possible reconnecting events such as double tearing observed in the experiment will be investigated. In each step in addition to axisymmteric simulations, we will also study the role of non-axisymmteric modes by including more toroidal modes.

We also propose to perform numerical simulations to study the role of rotation/magnetic shear on reconnecting instabilities in both linear and nonlinear regimes. The proposed simulations will be carried out in the NSTX configuration with experimentally relevant equilibria. In NSTX with high power neutral beam injection, mean flows can play critical roles on the plasma stability. Shear flows can affect ballooning modes and resistive tearing modes. Other important questions are whether large mean flows can cause instability of the continuum spectrum or whether plasma flows by themselves can be the source of free energy or instability. Flow-driven instabilities and local pressure-driven instabilities, Suydam modes, in the presence of shear flows have been studied in cylindrical geometry. [8] It was found that Suydam criterion was significantly modified by the mean flows. It was also found that in the absence of pressure gradient, purely flow-driven modes are unstable at speeds slightly below the critical speed.

As the Alfven Mach number may reach up to 0.5 in the NSTX-U, flows and flow-driven instabilities can have an increasing role on the plasma stability. Preliminary simulations with the MARS-K code predict instability at ½ the rotation of the experimental value in the absence of dissipation.[2] To study flow-driven instabilities in NSTX-U, we propose to preform similar linear stability with M3D-C1 code and compare with the eigenvalue code MARS.

Timeline

2013-2014:

- Continue the ongoing computational efforts for understanding and reproducing experimental closed-flux currents in NSTX. Perform simulations with experimental time-dependent boundary conditions, by using the boundary flux generated by LRDFIT to compare with constant flux simulations. Also include n=1 and higher order modes (in collaboration with B. Hooper and C. Sovinec) with evolving temperature and density. Perform parameter scan to maximize closed flux generation.
- Perform linear simulations of current-driven and flow-driven instabilities using M3D-C1 code with NSTX relevant equilibria. Perform linear simulations of NSTX cases with high rotation (in collaboration with S. Jardin).

FY2015:

- Continue parameter scan for NSTX-U and implement the NSTX-U geometry in NIMROD. Perform nonlinear simulations of CHI coupled to the induction. The physics of this coupling will be investigated and compared with experiment.

- Perform simulations of reconnecting instabilities in NSTX, such as double tearing mode with different equilibria (with magnetic shear) in the presence of shear rotation in the linear regime.

FY2016:

- Continue nonlinear simulations of CHI for NSTX-U with and without coupling to induction.
- Study self-consistent nonlinear generation of shear flows using extended-MHD simulations by including two-fluid physics at different equilibria (with magnetic shear).

2017 -2018 :

- Simulations of CHI coupled to NBI to find parameter regimes to improve NBI current drive.
- Start to couple MHD codes to gyrokinetic codes to investigate transport properties of self-generated MHD flows.

Contributions to the NSTX-U 2014-18 Five Year Plan:

Contributed to Chapter 8 Plasma Current Start-up and Ramp-up Research Thrusts.

References

1. R. Raman, et al. Phys. Rev. Lett., Phys. Rev. Lett., Vol. 104, 095003, 2010.

2. J. Menard, private communications

3. F. M. Levinton, et al. , Physics of Plasmas, 14, 056119, 2007.

4. F. Ebrahimi, V. V. Mirnov, and S. C. Prager, Phys. Plasmas, 15, 055701, 2008.

5. E. B. Hooper, C. R. Sovinec, R. Raman, F. Ebrahimi, and J. E. Menard, Bulletin of the American Physical Society, 57 Nov. 2012.

6. E. B. Hooper, C. R. Sovinec, R. Raman, F. Ebrahimi, and J. E. Menard, to be submitted to PRL.

7. R.A. Bayliss, C.R. Sovinec, and A. J. Redd, Physics of Plasmas, 18, 9, 094502, 2011.

8. A. Bondeson, R. Iacono, and A. Bhattacharjee, Physics of Fluids, 30, 2167, 1987.

11.2.15 Princeton University

Research Topic: Rotation control in NSTX
Principal, Co-Principal Investigators: Clarence W. Rowley (PI), David A. Gates (PI)
Participating Scientists: Stefan Gerhardt
Participating Post-docs: (none)
Participating Graduate Students: Imène Goumiri
Participating Undergraduates: (none)
Funded under DOE Grant: PPPL NSTX grant number

Introduction

The main motivation of our work is model-based control of plasmas in tokamaks. Previous successes include strike point control [2] and shape control [3] in NSTX. These controllers were designed using models tuned to match experimental data; our present plans are to build on these results, and develop control-oriented models directly from simulations. This capability would have a large impact: fewer experiments would be needed to calibrate the models/controllers, and more importantly, one could predict actuator requirements (e.g., amplitude, bandwidth, latency), and any inherent performance limitations for planned/future machines such as ITER.

Ultimately, we wish to develop these control-oriented models from high-fidelity simulations, such as those being developed in P-TRANSP. This is a complex task, however, so for now we are working with simpler model problems.

Current research contributions to NSTX Upgrade

Over the past year, this collaboration supported a graduate student (Imène Goumiri), who studied a two-dimensional model problem, in order to test model-based control strategies. In particular, she worked with the modified Hasegawa-Wakatani model, a PDE in two variables that models edge turbulence in a cold plasma. This model describes the interaction of drift waves and zonal flows: zonal flows are known to inhibit the growth of drift waves, and hence quench plasma turbulence. Our aim was to tap into this interaction, and attempt to stabilize the overall system using feedback.

We successfully obtained a low-dimensional model, and used it to stabilize the drift waves in numerical simulations of the full PDE model. In particular, we considered parameter values for which only one or two modes were unstable, and used a technique called balanced Proper Orthogonal Decomposition to determine a linear model of just a few ODEs (about 10) that closely represents the full dynamics. Actuation was introduced using a modification to the

potential, and we designed a feedback controller using standard tools from optimal control (Linear Quadratic Regulator) to stabilize the linearized model. We then tested this controller on the full nonlinear PDE, and indeed the controller was able to stabilize the drift waves. This work was recently accepted to *Physics of Plasmas*.

Summary of proposed research plan for 2014-18

Building on this success with a model problem, we plan to apply these techniques to rotation control in NSTX. Specifically, we plan to control plasma rotation using neutral beam injection, together with manipulation of neoclassical toroidal viscosity (NTV) using RWM coils. Our starting point is simplified physics (including only diffusive terms in the momentum diffusion equation, for instance neglecting pinch terms), and our aim is to identify diffusion coefficients and other parameters in the model, in order to obtain a highly simplified model that only crudely represents the actual physics, but captures the essential effects of the control parameters (neutral beam injection and NTV) on the rotation and shape. These models can then be used for model-based control design as in our previous work described above.

Our longer-term plans are to continue with model-based control design, applying these techniques to more complex problems, with more realistic physics and boundary conditions. In particular, we plan to leverage recently-developed predictive capabilities in PTRANSP, integrating them with our data-driven model-reduction techniques to develop reduced-order models suitable for control design.

Longer-term plans are to develop integrated controllers, which can address multiple objectives (e.g., vertical mode stabilization, strike point control, shape control, current profile control, and rotation control) within a single control design. Such an integrated controller would have significant advantages over the current piecemeal design, because when controllers are designed separately, they often ``fight" each other, resulting in decreased performance, or even loss of stability. An integrated, model-based control design would allow us to understand the interactions between the different control objectives, and design better controllers to meet these objectives.

Timeline

2014-2015:

- Develop reduced momentum diffusion models based on NSTX data/TRANSP analysis
- Design basic rotation controller based on reduced NSTX model
- Verify reduced model and PTRANSP predictive model against NSTX data

2015-2016:

- Demonstrate control PTRANSP predictive model using basic controllers
- Develop predictive PTRANSP model for NSTX-U
- Develop reduced model of NSTX-U

2016-2017:

- Develop advanced rotation profile controllers for NSTX-U
- Begin implementation of advanced controllers in the NSTX-U PCS

2017-2018:

- Demonstrate control of the rotation profile within the PTRANSP predictive model
- Complete implementation of NSTX-U rotation control
- Begin rotation control experiments

Contributions to the NSTX-U 2014-18 Five Year Plan:

Stefan Gerhardt is the present leader of the Advanced Scenarios and Control (ASC) topical science group and is responsible for overseeing the ASC chapter of the NSTX-U Five Year Plan. The plan above was defined in a process carried out over CY2011-12 in coordination with the NSTX-U Research Team. The research defined above contributes heavily to the plan.

References

[1] I. R. Goumiri, C. W. Rowley, Z. Ma, D. A. Gates, J. A. Krommes, and J. B. Parker. Reduced-order model based feedback control of the modified Hasegawa-Wakatani model. *Physics of Plasmas*, (to appear), 2013.

[2] E. Kolemen, D. A. Gates, C. W. Rowley, N. J. Kasdin, J. Kallman, S. Gerhardt, V. Soukhanovskii, and D. Mueller. Strike point control for the national spherical torus experiment (NSTX). *Nuclear Fusion*, 50(105010), Sept. 2010.

[3] E. Kolemen, D. A. Gates, S. Gerhardt, R. Kaita, H. Kugel, D. Mueller, C. Rowley, and V. Soukhanovskii. Plasma modelling results and shape control improvements for NSTX. *Nuclear Fusion*, 51:113024, 2011.

11.2.16 Purdue University, West Lafayette IN

Research Topic: Impact of Disruptions and ELMs on Liquid Lithium Surfaces in NSTX and Mitigation and Extrapolation to ITER Relevant Conditions

Principal, Co-Principal Investigators: Ahmed Hassanein (PI), Tatyana Sizyuk (Co-PI)
Participating Scientists: Valeryi Sizyuk, Jeff Brooks
Participating Post-docs:
Participating Graduate Students: A. Al-Ajlony
Funded under DOE Grant: DE-FG02-08ER54991

Introduction

Edge plasma evolution plays major role in tokamak plasma confinement and determines/control the High-confinement mode (H-mode) operation. Experiments show the complex character of the edge plasma interaction with tokamak components and as a result the complex self-consistent behavior of plasma in the entire SOL. The edge plasma drift and contact with plasma facing components (PFCs) results in changing of D-T plasma and components material impurities, affects toroidal plasma motion, and redistributes energy load. The integrated models should combine micro- and macro-scale physical processes within the divertor nearby areas and the SOL edge plasma. The energy load emitted from core plasma particles into divertor/wall surface and the resulting heat conduction, melting (solid components), and vaporization of plasma facing materials should be considered in detail in which the MHD vapor expansion and evolution is controlled by the heating of the escaped core particles. Magnetic diffusion, heat conduction, and photon radiation transport should be calculated in fine details in the developed vapor edge plasma. Most recent experimental and theoretical studies of PFCs erosion were performed considering only local areas of tokamak PFCs [1-3]. Composite/mixed materials as plasma facing components (PFCs) in NSTX device add significant challenge to understanding the effects of core plasma particles impact on LLD surface, lifetime, core plasma contamination, hydrogen recycling, and surface material dynamic properties. For example, deuterium recycling from chamber walls in NSTX is determined by recycling conditions at inner divertor with Mo tiles, characterized as high recycling region, and at outer divertor with liquid Li coating on porous Mo substrate (LLD). Theoretical predictions of low deuterium recycling from LLD are based on the low reflection of hydrogen isotopes from Li surface and high diffusion and uptake of deuterium in liquid lithium. However, realistic picture of the reactor environment can significantly change the value of deuterium recycling, obtained theoretically or in the laboratory experiments.

Current research contributions to NSTX Upgrade

In our recent study [4] we simulated the evolution of edge plasma during the normal and disruptive operation of tokamak devices in localized areas of the SOL using our HEIGHTS (High Energy Interaction with General Heterogeneous Target Systems) computer simulation package containing various integrated models [5-7]. We included in our models five main parts: Monte Carlo block of disrupting plasma particles interaction with solid and plasma matter; MHD block of plasma evolution taking into account magnetic field diffusion; heat conduction and vaporization block for plasma facing components; heat conduction block for vapor and plasma; and Monte Carlo radiation transport block. The radiation transport block is based on the optical data calculated by HEIGHTS atomic physics package [8]. Direct expansion of the computational domain to include the entire SOL leads to significant calculations overload and to the problem of multiscale description of the complex various design components. The size of the fusion device is measured in meters, accurate MHD calculations require cell sizes of 100–200 μm, and detail surface erosion simulation requires mesh discretization level of cell size less than 0.5 μm. To avoid the described limitations in edge plasma modeling and to adopt the multiscale approach of the integrated physical and mathematical models, we developed unstructured adaptive mesh approach in computational domain and reconstructed all integrated physical processes in the upgraded numerical methods and computational algorithms of HEIGHTS package. A five-layer quadtree refinement scheme [9] is used for simulation of the entire SOL plasma evolution and the extra refinement (~ 0.5 μm) allowed calculations of subsurface particle implantation, heat deposition, and erosion processes. Using actual NSTX geometry and magnetic field structure we simulated in full 3D the evolution of escaped core plasma particles: starting at core border, gyration and scatterings in SOL, and penetration and deposition into PFCs [10]. The escaped core particles determined the initial energy source and boundary conditions for the edge plasma MHD evolution. The plasma magnetic diffusion, heat conduction, and radiation transport are also considered in the quadtree grid hierarchy (Fig.1). The lithium divertor heat load, divertor surface erosion profile, and potential lithium impurities drift were calculated for the coupled system of the inner and outer divertors interconnected through the SOL. We implemented, verified, and benchmarked our new Monte Carlo kinetic model in our HEIGHTS simulation package to study the spatial profile of ions and electrons energy deposition of the escaped core particles of both inner and outer divertor plate for NSTX and ITER device parameters, magnetic field complex structure, and components geometry [11]. The detailed simulation results of the inner-outer divertor system are currently under preparation now for the comprehensive publications.

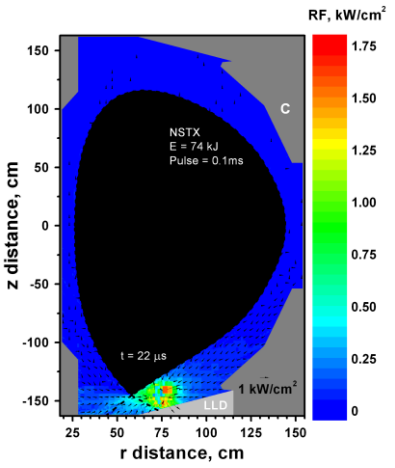

Fig.1. HEIGHTS calculated radiation fluxes for a disrupted energy of 74 kJ

We also enhanced our dynamic Monte Carlo ITMC-DYN package [12,13], combining integrated models for studying the time-dependent dynamic surface evolution at nano/micro layers under impact of plasma particles to address self-consistently all phenomena, specific for NSTX design and conditions. These phenomena include the effect of compounds formation and impurities, the influence of Mo substrate porosity on Li erosion, mixing, deuterium diffusion and desorption, and overall fuel recycling. Using ITMC-DYN we simulated deuterium release from the surface due to reflection, surface molecular recombination, and desorption for various lithium compounds, layers thicknesses, temperatures, and impurities concentrations. Simulation results showed that formed lithium compounds filling porous Mo, such as layers of lithium oxide or hydroxide, will result in deuterium accumulation near the surface due to the reduced diffusion to the bulk, that can slightly increase desorption rate (Fig.2). On the other hand, increase of carbon impurities in edge plasma will lead to carbon accumulation on LLD that will act as barrier to deuterium release from the surface [14].

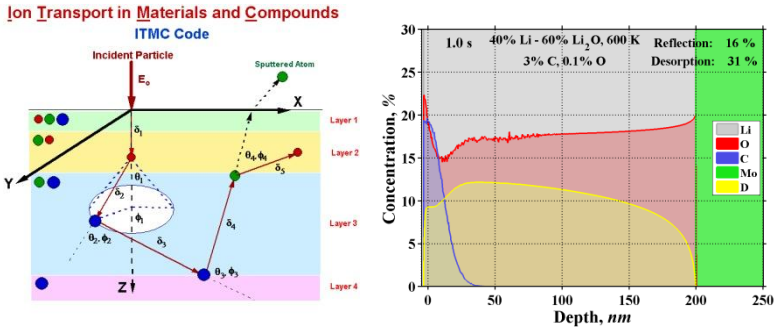

Fig.2. Schematic of ITMC-DYN base model and simulation results: deuterium diffusion and desorption in Li/Li_2O compound at 600 K temperature

Summary of proposed research plan for 2014-18

We developed and benchmarked the initial version of the integrated HEIGHTS package for simulation of the edge plasma evolution in entire SOL area of the actual NSTX device geometry. Our next activity should be focused on three main directions: 1) continue enhancement and improvement of physical and mathematical models, significantly enhance parallel calculation scalability, upgrade of computer package/routines for acceleration of tokamak device simulations; 2) application of package to current NSTX experimental studies of the edge plasma phenomena as interaction with the device components, energy and mass redistribution in SOL including detail radiation losses, study of escaped core particles drift, prediction and optimization of the heat load scenarios of the new NSTX divertor design; 3) investigate different transient mitigation methods and extrapolate to help ITER conditions.

We will further enhance our ITMC-DYN package to simulate plasma facing surfaces evolution in NSTX environment and analyze parameters and conditions, which can determine and optimize deuterium recycling. In such complicated PFC system, as NSTX, with lithium and molybdenum surfaces, with presence of carbon and oxygen, several factors and the interplay of various

processes will influence particles diffusion and surface molecular recombination, surface modification and erosion, impurities distribution, sputtering, and overall plasma performance.

The timetable for our plans is given below:

Timeline

FY2014:

- Continue development/enhancement of new scalable methods and numerical algorithms for simulation of plasma dissipative processes: heat conduction and magnetic diffusion.
- Increasing the multi-scale efficiency of HEIGHTS package simulations, optimization of computational time balance and accuracy of the physical processes involved.
- Integrated simulation of NSTX transient events in current geometry. Investigation of the escaped core particles drift, edge plasma evolution, components heat load, and shielding effects. Calculation of radiation loses. Comparison with available experimental data.
- Models development and simulation of LLD surface evolution during NSTX operation. Development and integration into ITMC-DYN package models for chemical compounds formation to predict surface chemistry and surface composition of LLD as function of surface temperature and chamber plasma edge conditions before, during, and after discharge.

FY2015:

- Continue upgrade the parallel version of HEIGHTS package for the calculation acceleration of multi-scale physical processes during edge plasma evolution in SOL. Development of effective merge procedure of the MHD and under-surface subdomains in multiprocessor calculations.
- Integrated simulation of the NSTX-U device transient events in novel "snowflake" divertor (SFD) configuration. Investigation of the escaped core particles drift, edge plasma initiation, components heat load and shielding effects. Calculation of accurate radiation losses in whole 3D domain. Comparison with available NSTX data.
- Modeling deuterium trapping in lithium and compounds and analyze mechanisms of hydrogen isotopes exchange in PFMs (e.g., initial presence of hydrogen in lithium hydroxide on the surface of LLD) to predict H/H+D ratio in desorption rate from the surface.

FY2016:

- Comparison of simulation results for both divertor configurations: heat load, erosion, contamination drift, and radiation losses. Integrated simulation and optimization of the tokamak overall components geometry.
- Investigation of edge plasma drift during NSTX-U normal operation and contamination of core plasma. Comparison of the calculated plasma parameters with NSTX-U data.
- Benchmarking of modeling results for deuterium retention and desorption with data from NSTX-U device and particle beam experiments. Theoretical prediction of deuterium recombination and diffusion coefficients for pure and contaminated lithium and comparison with experimental results.

FY2017:

- Development of physical and mathematical models for neutral gas injection into the SOL. Enhancement of the MHD, heat conduction, and radiation transport models.
- Upgrade of HEIGHTS package for modeling neutral gas injection optimization and capability.
- Initiate studies of various transient mitigation methods in full NSTX-U geometry.
- Based on predicted surface chemistry and compounds evolution on LLD, benchmarked with experimental results, modeling deuterium interaction with materials in surface layers. Evaluate the effect of impurities and surface composition on hydrogen isotopes molecular recombination and desorption or penetration to the bulk.

FY2018:

- Integrated simulation of the NSTX-U transient events and the neutral gas injection. Investigation of the heat load parameters. Optimization of the neutral gas injection.
- Detail studies of transient mitigation methods and feedback to ITER design.
- Modeling ions / target interaction on the surface of inner divertor (high recycling region), taking into account impurities in edge plasma, dynamic changing of surface composition, diffusion and deuterium recombination from Mo surface and Mo with lithium coating.

Contributions to the NSTX-U 2014-18 Five-Year Plan:

The plan above contributes strong to the research goals established in the Materials and Plasma Facing Components chapter of the 2014-2018 NSTX-U five year plan plan and was defined in a process carried out over CY2011-12 in coordination with the NSTX-U Research Team.

References

[1] V. Sizyuk and A. Hassanein Nucl. Fusion 50 (2010) 115004.
[2] J.W. Coenen et al., Nucl. Fusion 51 (2011) 083008.
[3] A. Kreter et al., J. Nucl. Mater. 390–391 (2009) 38.
[4] V. Sizyuk and A. Hassanein, J. Nucl. Mater. 415 (2011) S881.
[5] V. Sizyuk and A. Hassanein, Nucl. Fusion 49 (2009) 095003.
[6] A. Hassanein, et al., Fusion Eng. Des. 69 (2003) 781.
[7] A.Hassanein, I. Konkashbaev, J. Nucl. Mater. 313-316 (2003) 664.
[8] V. Tolkach, V. Morozov, and A. Hassanein, Development of comprehensive models for opacities and radiation transport for IFE systems, Argonne National Laboratory Report ANL-ET/02-23, Argonne, IL (2002).
[9] W. Lee, A. Borthwick, P. Taylor, J. Comp. Phys. 230 (2011) 4848.
[10] V. Sizyuk and A. Hassanein, J. Nucl. Mater. (2013), in press.
[11] V. Sizyuk and A. Hassanein, Nucl. Fusion (2013), submitted.
[12] A. Hassanein and D. L. Smith, Nucl. Instr. and Meth. B 13, 225 (1986).
[13] T. Sizyuk and A. Hassanein, J. Nucl. Mater. 404, 60-67 (2010).
[14] T. Sizyuk and A. Hassanein, J. Nucl. Mater., accepted for publication (2013).

11.2.17 Purdue University, West Lafayette IN

Research Topic: Deciphering the PMI Surface Chemistry of Lithium-based PFCs

Principal Investigator: Jean Paul Allain
Participating Scientists: Charles Skinner (PPPL), Robert Kaita (PPPL), Predrag Krstic (UTK),
Participating Post-docs: Osman El-Atwani
Participating Graduate Students: Sean Gonderman, Anton Neff, Kara Luitjohan, Brandon Holybee
Participating Undergraduates: Tian Qiu, Dan Klenosky, Stephen Taller,
Funded under DOE Grant: DE-FG02-08ER54990

Introduction

This project leverages previous work by our group under Grant DE-FG02-08ER54990, which elucidated the role surface chemistry plays on D particle pumping in lithiated graphite. This project will *elucidate the role surface chemistry and topology has on the ability for liquid lithium surfaces and lithium-based surfaces on graphite and refractory metal (e.g. W, Mo) substrates to control particle pumping and plasma performance in NSTX-U plasmas*. In addition, this project will provide for controlled *in-situ* characterization of re-deposited mixed materials and the effect on deuterium pumping.

Mixed materials continue to be a dominant environment at the plasma-material interface given the transition in NSTX-U from carbon-based PFCs to full-metal PFCs beyond 2018. Questions addressing how the role of carbon can influence the performance of refractory substrates (e.g. W) in pumping hydrogen and influence performance of thin Li films will be assessed. The work pioneered by our group at Purdue University has already made great strides in understanding what will continue to be the baseline NSTX Upgrade PFCs, mainly: lithium conditioning resulting in thin-film coatings on a variety of substrate materials including graphite and tungsten.

The work proposed in this project effectively complements the surface science work being conducted at Princeton University and at PPPL. In the former case a newly funded project focuses on liquid-metal interface behavior. In the latter, lab experiments are addressing specific questions on lithium-based coatings on refractory metal substrates. Our work focuses on the *dynamic* measurement of an irradiated surface with candidate materials under simulated conditions of the NSTX-U private-flux region and outboard region. None of the groups in either PPPL or PU are addressing the lingering question of the effect surface morphology has on lithium conditioning and *dynamic* hydrogen particle control. Moreover the interplay between surface chemistry (as indicated by the role of oxygen) and nano and micro-scale morphology on

particle pumping is still largely not understood. Our group and this project addresses those questions directly.

In this project, fluence exposures will be extended to those of shots of longer duration expected in NSTX-U. This strategy will address the fundamental question about the ability for lithium conditioning to provide effective particle control over longer time scales as previously studied in NSTX. Further studies will study liquid lithium and its ability to control particle recycling and power handling. These are two aspects critical to NSTX-U's PMI overall research strategy. One important aspect of the controlled *in-situ* work in this project is the development through a growing collaboration of surface response computational simulation codes. This is accomplished with a successful collaboration with Dr. Predrag Krstic and colleagues from the Oak Ridge National Laboratory (ORNL).

Current research contributions to NSTX Upgrade

Currently work under this project has mainly focused on understanding particle pumping in lithiated graphite systems. In particular, our work identified the role of oxygen in the retention of deuterium on lithium-conditions ATJ graphite surfaces by a detailed effort between controlled *in-situ* experiments and advanced atomistic simulations [1]. Simulation results demonstrated that oxygen contributes to the effective pumping of hydrogen but only in the presence of lithium in the ATJ graphite matrix. Moreover, the amount of oxygen is important and it was discovered that the magnitude needed to be comparable to the amount of lithium on the surface. However, the most striking result was that it wasn't until lithiated graphite was irradiated that led to a dramatic increase in surface oxygen content enabling enhanced hydrogen retention. This *dynamic* effect was discovered by running *in-situ* surface characterization of the lithiated graphite irradiated with low-energy deuterium ions as demonstrated in Fig. 1.

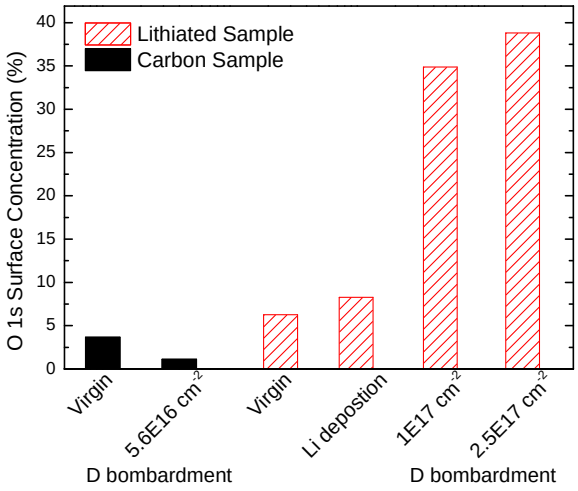

Additional work in this project also included the study of lithium thin-film coatings on porous Mo substrates (the same Plasma Processes, Inc. (PPI, Huntsville, AL) material for the liquid lithium divertor (LLD)). These studies identified surface chemistry behavior of the lithium coatings and on-going work currently is investigating the ability for these coatings to pump hydrogen. Critical questions remain on lithium coating viability and solid-liquid metal transitions influenced by the substrate morphology (e.g Mo porosity).

Summary of proposed research plan for 2014-18

This project proposes to continue addressing critical questions for PFC/PMI strategies in NSTX-U and in particular the planned transition from carbon-based PFCs to metal-based PFCs. There remain questions about how effectively will lithium conditioning influence NSTX-U long pulsed plasmas in the context of particle control (e.g. D uptake) and heat flux mitigation. Given the ability for thin lithium coatings (~ 100-500 nm or depositions of as little as 100 mg Li) to control plasma behavior, a fundamental question that remains unanswered is how long can lithium coatings maintain their hydrogen uptake property given that plasma shots will increase a factor of 5-10X in time. This is nearly an order of magnitude in fluence. Additional questions linger on the amount of lithium needed for effects on plasma behavior (e.g. heat flux mitigation) and whether erosion/redeposition processes could also be playing an important role in providing for "active" hydrogen pumping interfaces to the plasma. More importantly, questions remain on the exact mechanism responsible for such thin lithium coatings deposited on graphite to effect plasma behavior. Furthermore, the use of lithium coatings in a next step device has been questioned due to its feasibility and potential issues with tritium retention. Tritium retention must be assessed; however indications show that annealing up to 500-600 C could remove implanted deuterium and likely similar for tritium. Furthermore, although applying lithium evaporated coatings may not scale to a large-scale reactor alternative delivery methods of lithium to PFC surfaces could be explored by the use of nanostructured materials being developed in Prof. Allain's labs.

One particular example of how *in-situ* experiments by our group using PRIHSM coupled to simulations will address these questions is by examining re-deposited layers on candidate material substrates (e.g. amorphous hydrogenous carbon and W) under He and D irradiation to dynamically measure surface chemistry (e.g. O, H) and deuterium uptake. These questions will address concerns about reliance on lithium coatings to provide particle control in NSTX-U and the need for cryo-pumping in future NSTX-U operations.

NSTX-U will also be addressing the issue of particle heat flux control. Power handling is an important issue for future burning plasma fusion reactors. P/S ratios between 0.5 and 1.0 are attractive experimental scenarios accessed by NSTX-U that can be exploited to study power handling PMI issues. In this context, the strategy to progressively convert from an all-carbon fusion device to an all-metal (e.g. with tungsten) fusion device, opens the door for questions regarding how PFCs will perform under a changing PFC platform. Although the current plan between 2014 and 2018 is to keep NSTX-U as a predominant all-carbon machine, mixed-material scenarios with the introduction of a liquid lithium divertor (LLD) and tungsten outboard upper and lower toroidal sections will certainly have an impact on particle pumping and power

handling PMI strategies. Our proposed work here will examine the implications of these changes in PFCs by studying *dynamically* how candidate systems behave including: 1) lithium coatings with re-deposited hydrogenated carbon surfaces on ATJ-graphite and tungsten, 2) on boronized ATJ graphite and 3) hot lithium films on ATJ graphite, tungsten and Mo substrates. Our work will address particle pumping via measurement of *both* surface chemistry and hydrogen emission from these surfaces utilizing the suite of materials characterization tools in PRIHSM: XPS, TDS, DRS and LEISS. Furthermore, a newly designed technique using energetic hydrogen forward scattering (HFS) will also be utilized.

Two key collaborations will be central to the work proposed: 1) Sandia National Labs with Richard Nygren and Dennis Youchison on correlation of surface emissivity, surface temperature and surface chemistry for measurements of lithium coatings on candidate substrates, and 2) high heat flux exposures on advanced tungsten substrates with lithium coatings in the Pilot-PSI and Magnum-PSI facilities in DIFFER in collaboration with Greg DeTemmerman.

Collaboration with SNLA

PFC surface temperatures in NSTX are routinely measured based on IR thermography. Temperature is measured by converting intensity signals from infrared energy emitted from the PFC surfaces inside a tokamak, such as NSTX. One critical gap is how the emissivity changes with surface chemistry (e.g. impurities, re-deposited material, etc…) and surface roughness (e.g. morphology, phase variation, etc…). The goal of this project is to correlate the surface emissivity of candidate PFCs in NSTX including: ATJ graphite, TZM (molybdenum alloy), and tungsten with and without lithium surface coatings with: 1) surface chemistry and 2) surface roughness. The objective is to conduct systematic studies using IR thermography in the PRIHSM (Particle and Radiation Interaction of Hard and Soft Matter) experimental facility in RSSEL. The hypothesis is that surface chemistry and surface roughness will have an effect on surface emissivity measurements. To achieve this objective and test this hypothesis a number of systematic experiments are envisioned:

1. Determining and calibrating measurement of temperature on the sample surface
    a. Test with local thermocouples temperature gradients from PRIHSM sample e-beam heater to sample surface
    b. Design and integrate a movable temperature finger to map in 2D the temperature field on the sample surface
2. Measurement of surface chemistry of candidate fusion materials
    a. Measure with IR thermography temperatures in range between 25-400 C on candidate materials and correlate with XPS, TDS and LEISS
    b. Correlate IR thermography data with surface roughness

i. For example controls with smooth samples (e.g. HOPG, polished Mo)

3. Measurement of IR thermography and impurities
    a. Expose candidate sample materials to controlled impurities via local doser of impurity source such as H_2O, methane, oxygen and monitor effect on emissivity and surface chemistry (e.g. XPS, TDS, LEISS)

Collaboration with DIFFER

Advanced nano and micro-structured tungsten materials are under development at Purdue University with various collaborators including UC Davis, Oklahoma State University, UCLA and a number of faculty at Purdue. The aim is to process a scalable tungsten material that is both tough and radiation resistant. Spark plasma sintering (SPS) has been the synthesis technique of choice yielding tungsten samples with greater than 98% theoretical density, averaging 500 kg/mm^2 Vickers hardness and stable surface and grain boundary chemistry. The samples nomially have a bimodal microstructure with large grains averaging about 1-2 um and small grains between 100-500 nm [O. El Atwani et al. Materials Science and Engr A, 528 (2011) 5670]. An alternative synthesis route is being also pursued in collaboration with Prof. K. Trumble and Prof. S. Chandrasekar of the School of Materials and Industral Engineering, respectively. This work focuses on using a technique known as large strain extrusion machining (LSEM) can introduce plastic deformation to both surfaces and small chips of tungsten. This approach has led to novel tugnsten nanograin materials with average grain sizes between 50-100 nm.

Another aspect of the tungsten work at Purdue has focused on coupling low-Z coatings on refractory metals including tungsten and molybdenum. Our group has worked on high temperature examination of lithium on micro-porous Mo materials [see: B. Heim, NIMB 269 (2011) 1262]. We have also extensive work on lithiated graphite, which we'd like to extend this work mostly from the PhD effort of Chase Taylor. In our work with thin films and nanopatterning we have evidence that the films can dramatically change the nano-topography. This correlation between the surface composition/chemistry and nanomorphology is being conducted in our *in-situ* PRIHSM device and would be good to extend in our collaboration with FOM-DIFFER.

To date MMG-W and LSEM samples have been irradiated at nominal He and D fluences of order 10^{18} cm^{-2} and temperatures below and above (600 C) the thermal vacancy migration limit for tungsten. Incident particle energies between 50-200 eV have been used for He ions using nominally an RF broad-beam ion source at normal incidence.

One key question in PMI performance of tungsten materials in general is both their resistance to erosion and mechanical property behavior after irradiation. The irradiation-driven surface

nanostructured morphology is also an important issue given the propensity for He to induce bubble formation even at energies below the damage and sputter thresholds (e.g. between 50-200 eV). To elucidate the underlying mechanisms of low-energy irradiation of refractory metal surfaces at Purdue University we have focused on two primary fronts: 1) study of defect dynamics of nano and micro-structured W using TEM techniques before and after irradiation, and 2) study *in-situ* correlation between erosion and morphology evolution from these surfaces and their impact on ion-surface interactions. At Purdue University in the PRIHSM facility we are limited to fluences of 10^{18} cm^{-2} and fluxes of less than 10^{14} $cm^{-2}s^{-1}$. Therefore complementary work is necessary at a high-flux facility such as the Magnum-PSI and Pilot-PSI plasma devices at DIFFER. In addition, lower flux plasmas are also desired to obtain a full spectrum of plasma-surface interactions on advanced tugnsten materials developed at Purdue University. More importantly the interest in the DIFFER facilities are plans for the use of a combined high flux of low-energy ions coupled to transient heat/particle pulse. This is by far the biggest motivator for the collaboration in the context of fusion materials science given no other linear plasma device has such capability as described in a recent paper [De Temmerman et al. Nucl. Fusion 51 (2011) 073008]. There are therefore the following three thrusts of fusion-related work in the Purdue-DIFFER collaboration:

- Irradiation of nanostructured tungsten and molybdenum with and without lithium coatings in ELM simulated experiments coupled to steady-state plasma (Magnum-PSI)
- Flux and fluence-dependent irradiations (across all plasma devices at FOM-DIFFER) of nanostructured W or Mo with/without Li to study damage and surface morphology
- Temperature-dependent effects on H and He sputtering of W and Mo surfaces

The elements of our plan displayed in a timeline are:

Timeline

2014-2015:

- *In-situ* surface characterization of dynamic lithium conditioned ATJ graphite surfaces as a function of deuterium fluence and surface temperature
- Studies with SNLA to correlate surface emissivity of lithium conditioned ATJ graphite and surface properties (chemistry, morphology) to assess effect on IR measurements of surface temperature in NSTX-U
- Studies on advanced nanostructured refractory metal substrates with and without lithium coatings in PRIHSM and Magnum-PSI (DIFFER)

2015-2016:

- Study of re-deposited lithium-treated hydrogenated amorphous graphite coatings under various irradiation conditions (effect on D uptake)
- Study of alternative nanostructured matrices containing lithium for dynamic delivery of lithium coatings to PFC surfaces (coordinated tests with MAPP can be included)

2016-2017:

- Conduct coordinated and support experiments with MAPP-U diagnostic and other surface analysis facilities on lithium coatings on high-Z metals and liquid Li surfaces
- Continue study of alternative nanostructured matrices containing lithium for dynamic delivery of lithium coatings to PFC surfaces

2017-2018:

- Conduct mixed-material studies of C, W and Li and their surface chemistry effect on D uptake properties
- Study of hot lithium coatings on candidate substrates and correlate with NSTX-U MAPP experiments and DIFFER exposures

Contributions to the NSTX-U 2014-18 Five Year Plan:

Dr. Michael Jaworski is the present leader of the Materials and Plasma-Facing Components (M and P) topical science group and is responsible for overseeing the M and P chapter of the NSTX-U Five Year Plan. The plan above was defined in a process carried out over CY2011-12 in coordination with the NSTX-U Research Team. The research defined above contributes heavily to the plan.

References

[1] P.S. Krstic, J.P. Allain, C.N. Taylor, et al. “Deuterium uptake in magnetic fusion devices with lithium conditioned carbon walls,” Phys. Rev. Letters, In Press 2013.

Research Topic: Upgrade of the Materials Analysis Particle Probe (MAPP)

Principal Investigator: Jean Paul Allain
Participating Scientists: Charles Skinner (PPPL), Robert Kaita (PPPL), Predrag Krstic (UTK),
Participating Post-docs: Osman El-Atwani
Participating Graduate Students: Felipe Bedoya, Sean Gonderman, Anton Neff, Eric Yang
Participating Undergraduates: Mitch Ketinley, Miguel Gonzalez, Mohammad El-Atwani
Funded under DOE Grant: DE-FG02-08ER54990

Introduction

The Materials Analysis Particle Probe (MAPP) is the first in-vacuo surface-sensitive inter-shot tokamak diagnostic capable of correlating surface chemistry evolution with plasma response to PMI (plasma-material interface) conditioning. MAPP utilizes multiple surface-science measurement techniques to characterize a sample material exposed to NSTX plasma conditions and assess plasma-surface interactions near the strike point. MAPP will help elucidate the complex surface physics and chemistry correlating PSI behavior at spatial scales of 10 to 100's nm (penetration depth of incident energetic D atoms) to the macro length scales of plasma behavior (e.g. ELMs, confinement, etc…). Due to the harsh conditions in the tokamak edge, surface-sensitive conditions on the order of 10 to 100 nm are rendered impossible. However, ion-induced modification mechanisms at fluxes above 10^{15} $cm^{-2}s^{-1}$ typically have time scales between a few seconds to 10's of minutes (nearly 50-60). Therefore correlations between surface chemistry and physics via surface conditioning are plausible by characterizing these plasma-facing surfaces within the order of a few minutes to 10's of minutes. MAPP includes a manipulator probe to insert a probe head with four samples expose to plasma and in between shots characterize these surfaces. Techniques currently include: Thermal Desorption Spectroscopy (TDS), X-ray Photoelectron Spectroscopy (XPS), Low energy Ion Secondary Scattering (LEISS), and Direct Recoil Spectroscopy (DRS).

Current research contributions to NSTX Upgrade

MAPP-U will allow time-resolved PMI data by tuning plasma shots that vary from 1 second and stepped up to longer pulses (up to 5 seconds for NSTX upgrade), the surface chemistry can be assessed under the context of "long-time" "high-power" operation with ramifications to materials design for future steady-state devices and for the progressive transition of NSTX-U from carbon to an all-metal PFC device. Both strategies would be in principle important to ST-FNSF and ITER. Currently much of the work on MAPP has been its engineering design, testing and integration to the NSTX environment. Due to NSTX shutdown for the upgrade, diagnostics are being improved in MAPP including an upgrade that integrates a QCM system for erosion measurements. Details of the preliminary engineering design and testing can be found in a

recent publication by Taylor et al. [1]. Initial tests have successfully shown measurements of TDS and XPS measuring D uptake in lithiated graphite surfaces. Current development focuses on the use of ion-probe based spectroscopies.

Summary of proposed research plan for 2014-18

MAPP-U will enable the study of advanced materials and their controlled exposure to designed plasma shots to guide materials and component options. For example tests will include nanostructured lowZ/highZ hybrids, nanocomposites, liquid metals and alloys, and any new material configuration being considered. One particular knowledge gap that MAPP addresses is to correlate shot-to-shot PMI behavior to the surface physics and chemistry. Mixed materials and migration via erosion/redeposition processes will become more important as NSTX-U includes more metal-based PFCs (e.g. tungsten, liquid lithium, etc…). The upgrade to MAPP will consist of integrating a quartz crystal microbalance (QCM) system to assess erosion levels and correlate them to surface chemistry. The QCM system in MAPP-U will allow *in-situ* erosion diagnosis, critical to determine re-deposition vs erosion mechanisms and their effect on surface chemistry ultimately influencing hydrogen-recycling properties.

The MAPP-U system will be integrated to NSTX-U and plans for 2014-2018 are to enable deciphering the surface chemistry and materials mixing and migration effects on particle control in NSTX-U plasmas.

The elements of our plan displayed in a timeline are:

Timeline

2014-2015:

- Integrate MAPP-U remote systems with probe assembly linear and rotational actuation
- Verify all interlocks and systems are compliant and under proper procedures for running in new NSTX-U configuration
- Install MAPP-U chamber on TIV along with electronics rack housing all desired equipment

2015-2016:

- Integrate probe assembly and MAPP-U chamber, overlay all interlocks and proper procedures to verify MAPP-U operation does not interfere with NSTX operation and vise versa.

- Preliminary piggy-back experiments to test MAPP-U operations and verify all systems can work on shot to shot basis. Also to measure and assess particle fluxes for various NSTX-U plasma configurations at the outboard location of MAPP.

2016-2017:

- Investigate new novel material substrates for use with lithium coatings and as robust high-Z materials in NSTX-U.
- Elucidate the surface properties of lithiated graphite and the performance this baseline NSTX PFC in the context of NSTX-U advanced plasmas with 4-5 second discharges.
- Measure D pumping from various ATJ graphite morphologies under fluences equivalent to 4-5 second NSTX-U discharges
- Study liquid lithium surfaces in an upgraded MAPP-U holder for liquid-metals
- Initial boron vs lithium conditioning techniques

2017-2018:

- Comparison of local plasma parameters between Lithium and non-lithium wall conditions.
- Study of lithium deposition and passivation as a function of lithium deposition by LITERS and deuterium flux.
- Comparative data relating the chemical functionalities of lithiated graphite interaction with deuterium and lithium wall conditions influence on plasma performance.
- Mixed material studies using MAPP-U

Contributions to the NSTX-U 2014-18 Five Year Plan:

Dr. Michael Jaworski is the present leader of the Materials and Plasma-Facing Components (M and P) topical science group and is responsible for overseeing the M and P chapter of the NSTX-U Five Year Plan. The plan above was defined in a process carried out over CY2011-12 in coordination with the NSTX-U Research Team. The research defined above contributes heavily to the plan.

References

1. C.N. Taylor, B. Heim, S. Gonderman, J.P. Allain, Z. Yang, R. Kaita, A.L. Roquemore, C.H. Skinner, and R.A. Ellis, “Materials Analysis and Particle Probe: A compact diagnostic system for *in-situ* analysis of plasma-facing components (invited)”, Rev. Sci. Instrum. 83 (2012) 10D703.

11.2.18 Sandia National Laboratories

Research Topic: Sandia thermal analysis of NSTX-U Tiles and approaches for gas cooling and flowing lithium

Principal, Co-Principal Investigators: Richard E. Nygren (PI), Dennis Youchison (Co-I.)
Participating Graduate Students: To Be Determined
Funded under DOE Grant: LAB12-03

Introduction

One important parameter related to power handling is the thickness of the relatively thin layer (called the power scrape-off length or λ_q) that carries power out of the plasma and primarily onto the divertor. For a given configuration of a long pulse plasma, the width of this layer determines the peak heat load and therefor the maximum surface temperature of the divertor. Furthermore, λ_q is not easy to manipulate, nor are the processes that set this key parameter well enough understood to support confident predictions of λ_q in future devices such as an FNSF or DEMO. Extracting accurate estimates of λ_q is an important objective in research in all large confinement experiments. The main focus of our proposal relates to this area of power handing.

A second area of focus for this proposal is the initial development of approaches to gas-cooling for some structures in NSTX-U. The critical points are (1) Sandia has extensive expertise in this area, and (2) the goal of going to longer pulse lengths in NSTX-U as well as interest in a component exposure probe or CEP is likely to bring a requirement for active cooling of some structures in NSTX-U. Such gas-cooled structures have relevance to the path of development for an FNSF and DEMO. The necessary staging of the development and deployment of such structures means that, to be included in the next NSTX-U 5-Year Plan, some significant design development must be done during the period of this proposal.

Current research contributions to NSTX Upgrade

The deployment at PPPL of the liquid lithium divertor (LLD) in NSTX and trays of liquid lithium in CDX-U were the first deployments with large area of liquid lithium. Over the last six years with two previous NSTX-Lab Grants, Sandia has collaborated on the development of the LLD and experiments in NSTX. Sandia delivered the four heated plates for the LLD and the control network for the heaters. Figure 1 shows one of the plates after the HIP-brazing operation that joined a 0.3 mm thick stainless

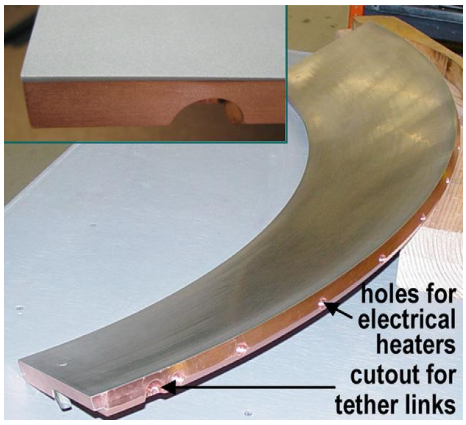

Fig. 1. Copper plate with brazed stainless steel skin for LLD

steel skin the underlying copper plate.[1] Sandia has also performed thermal analysis of the LLD in the interpretation of experiments.

Figures 2 and 3 respectively show the peaked heat load profile used for the thermal analysis and some results. These results were presented at the 2nd International Workshop on Lithium Applications in Fusion[2] and only a brief explanation is given here. The point is that a detailed 3-D thermal analysis is needed to explain the observed behavior. The results here are included in a paper being prepared for publication that compares the thermal performances of graphite and moly tiles and the LLD with a focus on the evolution of the thermal footprint of the strike point in the outer divertor.

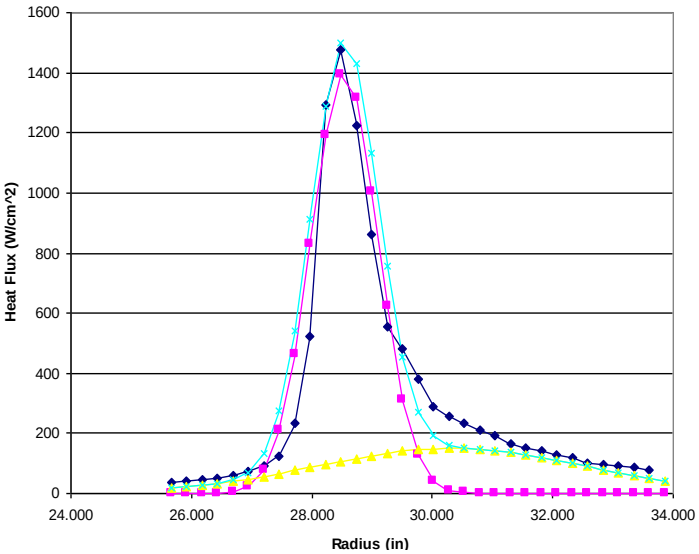

Fig. 2. Heat load profile at the strike point, from data provided by Maingi; broadest profile (crosses) is sum of peak and background (squares and triangles); diamonds shows fit of polynomial series.

The assumption of simple thermal diffusion in a semi-infinite solid with the rise in temperature proportional to the square root of time is inaccurate for the LLD. Copper's high conductivity permits heat to diffuse rapidly both into the heated surface and laterally away from the peak heating.

In the plot on the upper left of Figure 3, by 4800.5 s (0.5 s after the shot starts) heat has reached the back of the Cu plate (bottom of LLD) and the Li surface is over 140° higher than the underlying Cu (top surface). After this time the thermal gradient through the plate is established and the plate does not behave like a semi-infinite solid. The temperature rises more slowly and roughly linearly with time. At the end of the 5-s shot, the Li has risen to 875K from ~650K, the heat load ceases and the temperatures near the top surface drop and those at the bottom increase as the plate attains its average temperature.

Explanations involving broadening of the heat load due to evaporative cooling and lithium in the plasma edge have been proposed to explain the rollover of the temperature curve in the first second of the shot. But another explanation accounts for the observed temperature.

The rise in the temperature of the Li is proportional to the heat load, as can be verified by the plots at the bottom of Figure 3. After 4 s at10 MW/m^2, the rise is 465° and at 5.4 MW/m^2 it is 262°. In each case the rise in temperature divided by the heat load is 46.6 degrees per MW/m^2. So evaporative cooling is not a significant factor. And, lateral conduction of heat is important as the initial peaked heat load diffuses into the LLD. If the loading is changed from a peaked load to a uniform load of 5.4 MW/m^2, so there is no lateral heat conduction, the temperature rises to over 800º.

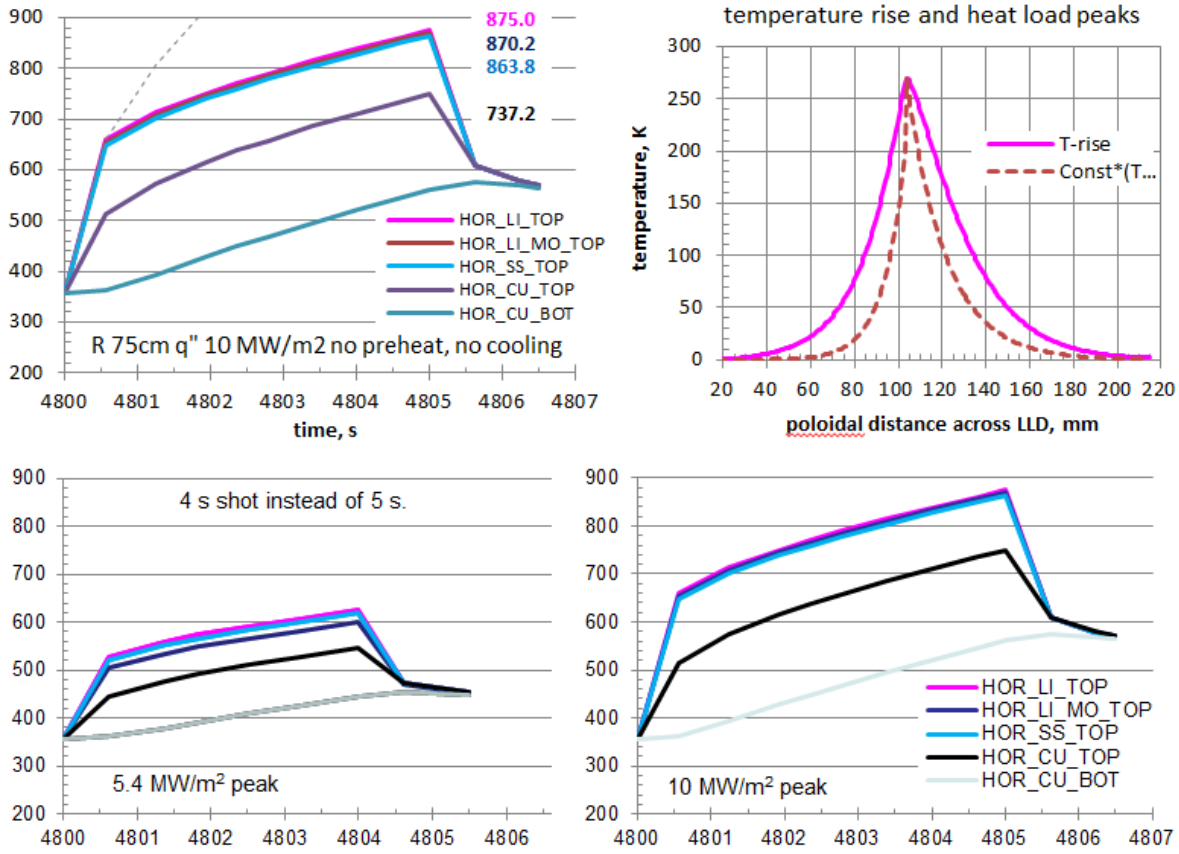

Fig. 3. Plots show temperature versus time on the LLD for the heat fluxes indicated and the following positions: Li plasma facing surface (red), top of porous Mo (black), top of SS skin 0.1 mm below Li surface (blue), top of Cu plate (black), back of Cu plate (gray).

Finally, the plot at the upper right shows the shape of the peak heat load superimposed with a normalized distribution of temperature from the end of the shot, when the peak has broadened by about a factor of two. The temperature rises during the shot, and the peak progressively broadens due to lateral heat conduction in the plate. This broadening is greatest at the end of the shot when the temperatures are highest. This is also the time when the IR data are the most likely to be selected for evaluation.

Continuing work in FY2012-13 includes further thermal analysis comparing the thermal performances of graphite and moly tiles and the LLD with a focus on the evolution of the thermal footprint of the strike point in the outer divertor. We are also completing a collaborative effort with Purdue University to measure the emissivity of liquid lithium surfaces with varying degrees of contamination by C and O.

Summary of proposed research plan for 2014-18

The primary focus of this proposal is (a) 3-D thermal analyses of NSTX-U divertor tiles as the primary deliverable and (b) an improved understanding by the NSTX-U Team working on the plasma edge of heat exhaust in NSTX-U under various conditions. The 3-D analysis is off-site work to be done at Sandia. The interaction to improve understanding includes off-site work to compile, digest and evaluate data from NSTX-U and on-site participation in experiments. The on-site participation includes such activities as monitoring data during shots, engaging in meetings and discussions with other investigators to discuss the conditions and diagnostics for shots, and discussing the implications of accumulated data and planning for various experiments. An example of the latter would be to estimate peak temperatures for hot spot conditions that present limitations on power and shot duration. This effort complements the work proposed by ORNL in their NSTX-U-Lab Grant proposal.

The cases will be of the types listed below. The sequence in this task will depend on results from NSTX-U.

1. Analyses of inboard and outboard tiles (3-4) with fast thermocouples (FTCs) – (a) initial cases to confirm the correlation between the FTC temperature and temperatures at nearby locations on the tile and (b) later cases for clarification of data taken during campaigns.
2. Analyses of misaligned tiles, e.g., hot leading edges – (a) initial cases with step height, angle of incidence of parallel heat flux, nominal power and shot duration as variables, and (b) later cases with iterations to try to match observed tile heating in NSTX-U campaigns.
3. Analyses of tiles with split strike points – (a) initial cases based on observations with 3-D fields and n=1 and n=3 modes and (b) later cases with iterations to try to match observed tile heating during applications of 3-D fields in NSTX-U campaigns.
4. Off-site work will also include effort to collect data, e.g., from IR cameras and FTCs, and to discuss the interpretations with NSTX-U Team members in calls and by e-mail. This element includes the use of NSTX-U data to develop the loads for 1a, b and c above. Typical data will be IR data, FTC data, D_α and probe data, and plots (magnetic reconstructions) that give the angle of incidence of parallel heat flux on the divertor. The heat loads will be developed from extracted data from past shots.

A second focus is participation in component design in two areas: 1) concepts for lithium

surfaces in the NSTX-U divertor (e.g., a future upgrade of an LLD) that provide a lithium reservoir or other system for active regeneration of the lithium surfaces plus a scheme, e.g., gas cooling, for active heat removal; and 2) the development of active heat removal schemes for in-vessel components such as RF launchers and guard limiters and materials probe that receive high heat loads. The roles of Sandia will be (a) to work with PPPL staff and suggest how gas-cooling can be applied to some specific NSTX-U components of interest and how such structures can be fabricated with existing industrial capability and (b) to perform thermal-hydraulic analyses to show the effectiveness of the heat transfer in the applications of interest. The expectation is that some ideas will need to be developed to the point of confidence, perhaps even with plans for some limited testing, during the period of performance of this proposal in support of planning and decisions for the next NSTX-U 5-year Plan.

Collaboration Researcher Questions and Issues:
The primary task of thermal analysis requires access to NSTX-U data that is supported by ORNL, specifically IR cameras, probes and fast thermocouples as noted above. Sandia will work closely with ORNL in requesting and exchanging information. Sandia has spoken with ORNL staff in this regard. They indicated the ORNL proposal would acknowledge possible collaboration with Sandia. The collaboration is also likely to extend into activity related to approaches for future applications of flowing lithium.

PPPL also has several ongoing international collaborations and Sandia is interested in becoming a partner in these collaborations. One is with EAST that involves ORNL. Sandia has also spoken to PPPL about the ORNL connection in this regard as well as Purdue. Another is design work with Korea on a Korean DEMO under the leadership of PPPL for the US effort. The request for this effort is likely to grow and include R&D if Korea launches an intensive program to develop a Korean DEMO. Sandia has also spoken with PPPL about its involvement.

Timeline
The elements of our plan are summarized below by year.

2014-2015:

- Continue thermal analysis of divertor heat load profiles for NSTX shots. Anticipated cases for analysis are: a) strike point on inner divertor near location of FTCs, b) strike point on outer divertor near FTCs, c) preferred snowflake divertor configuration, d) strike point splitting for n=1 3-D ELM suppression fields and possibilities for plasma rotation to enhance view under down-looking IR camera, and e) strike point splitting for n=3 ELM suppression fields and possibilities for plasma rotation to enhance view under down-looking IR camera.
- Develop concepts for gas-cooling of NSTX-U components and study related issues

with machine interfaces, e.g., RF guard armor and machine interfaces for gas-cooling, e.g., N_2 and He systems, feed-through locations and services for RF antennae and MAPP-U, etc. Perform 3-D heat transfer model of preferred application, e.g., gas-cooled frame for BN RF protection tile. Consider development path for deployment of hardware, e.g. detailed design and fabrication of mockup(s) and deployable testing in NSTX-U.

2015-2016:

- Continue thermal analysis of divertor heat load profiles for NSTX shots. Revise work scope based on observations during experimental campaign, e.g., more/different analyses of leading edge problems, issues with MAPP-U, etc.
- Continue development of concepts for gas-cooling of NSTX-U components and study of related issues with machine interfaces.

2016-2017:

- Sandia looks forward to a continuing collaboration with PPPL and the NEXT Team in further thermal analysis of heat loads in the NSTX-U divertor and refinement of gas-cooling concepts, pending additional funding.

Contributions to the NSTX-U 2014-18 Five Year Plan:

Dr. Michael Jaworski is the present leader of the Materials and Plasma-Facing Components topical science group (MP-TSG) and is responsible for overseeing the MP chapter of the NSTX-U Five Year Plan. The plan above was defined in a process carried out over CY2011-12 in coordination with the NSTX-U Research Team and the MP-TSG.

References

[1] R.E. Nygren, G.R. McKee, J. A. Fordham, S.A. Lewis, H. Kugel, R.A. Ellis, et al., Preparation of the Liquid Lithium Divertor Plates for NSTX, 14th Int. conf. on Fusion Reactor Mat., Sapporo, Japan, Sept 7-11, 2009

[2] R.E. Nygren, presentation at workshop, M. Ono, Conf. Rep on the 2nd Int. Symposium on Lithium Applications for Fusion Devices, M. Ono *et al* 2012 *Nucl. Fusion* **52** 037001 doi:10.1088/0029-5515/52/3/037001

11.2.19 University of California, Davis

Research Topic: FIR Density Monitoring, Feedback Control and Fluctuation Diagnostics
Principal, Co-Principal Investigators: N.C. Luhmann, Jr.
Participating Scientists: C.W. Domier
Participating Post-docs: C.M. Muscatello
Participating Graduate Students: R. Barchfeld
Funded under DOE Grant: DE-FG02-99ER54518

Introduction

UC Davis is reconfiguring and upgrading the Far Infrared Tangential Interferometer/ Polarimeter (FIReTIP) and high scattering systems on NSTX for use after the completion of the center stack and 2nd neutral beam injector (NBI) source upgrade now underway. UC Davis will also operate and maintain these systems once they have been installed and commissioned.

The FIReTIP system was previously configured as a 6 chord system operating at 119 μm. The two central chords monitored the NSTX core density while the other chords provided core and edge density fluctuation data. All FIReTIP beams entered through Bay K, with retro reflectors positioned on Bays F, G, H, and I. The previous high-k_r scattering system employed a 280 GHz source to form a beam that was launched via a translatable/rotatable mirror on Bay H to different plasma radii with scattered signals collected over a 20º range. The scattered signals were coupled through a rotatable collection mirror to a set of 5 mixers located outside the Bay K exit window. Each mixer monitored density fluctuations at a different wave-number with a k_r wave-number range up to ±20 cm^{-1}.

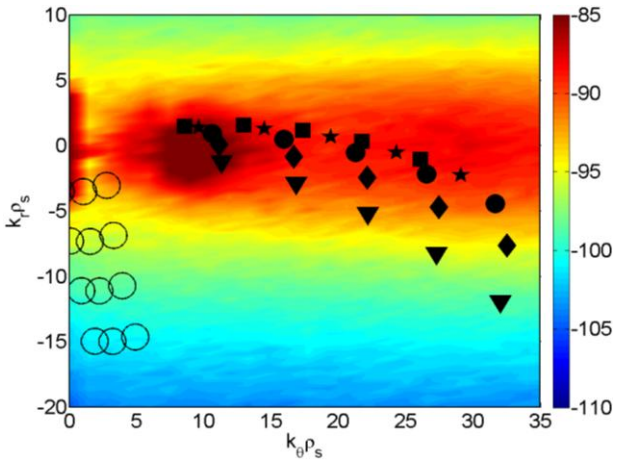

Fig. 1. A simulation by Dr. Y. Ren of PPPL, of ETG turbulence on NSTX overlaid with k-space coverage of the previous (o) and new (●,■,▼,◆,★) high-k scattering systems.

The use of Bay K for a second NBI source has forced the FIReTIP and high-k scattering systems to be dramatically reconfigured. The high-k_r scattering system [1,2] will be transformed into a high-k_θ scattering system employing a vertically extended window on Bay L, with significant changes proposed to both source and receiver hardware coupled with new optics. While the previous system provided primarily radial wavenumber ($k_r\rho_s$) coverage, the new

system additionally provides poloidal wavenumber ($k_\theta \rho_s$) space with coverage very near the estimated spectral peak of the 2D ETG fluctuation k-space (see Fig. 1).

The reconfigured FIReTIP system will comprise 4 chords: two central channels to monitor the NSTX core and provide density feedback data for NSTX, and two to monitor core and edge density fluctuations. The central chords will be incorporated into a density feedback control system for NSTX and provide density calibration data for the Thomson scattering system. Polarimetry data collected on all FIReTIP channels will provide chord-integrated information on NSTX magnetic profile and fluctuations.

Current research contributions to NSTX Upgrade

As part of the NSTX upgrade activities, the FIReTIP lasers (CO_2 and FIR) were returned to UC Davis in Spring 2012 for overhaul and refurbishment. The FIReTIP system employs one high power CO_2 laser and three optically-pumped FIR lasers. The new high-k_θ scattering system will employ an ~600 GHz source (which is double the frequency of the previous high-k_r scattering system) will initially be generated by an optically pumped FIR laser. Thus, the need to refurbish not only the FIReTIP lasers, but also additional CO_2 and FIR lasers is a major effort currently being taken on by students and staff at UC Davis.

The CO_2 and FIR lasers for both FIReTIP and high-k_θ scattering will be placed outside the NSTX test cell, in an area that housed the previous high-k scattering source. Collimated FIR beams for both systems will be transported via low loss waveguides to the NSTX vacuum vessel. The high-k_θ beam will be launched from Bay G, as will the initial two chords of the reconfigured FIReTIP system. Design of the Bay G port cover is nearing completion, with installation planned for June 2013. The high-k_θ scattered beams will exit through a large window [5 inches (wide) by 13.4 inches (high)] on Bay L, whose port cover is already designed. The initial FIReTIP beams will reflect from internal retroreflectors to be mounted on the inside of a large flange on Bay B. The remaining two FIReTIP chords (to be added in future years as NSTX resources permit) will have sight lines stretching from Bay F to Bay K (to monitor core density and magnetic fluctuations) and Bay I to Bay L (to monitor edge density and magnetic fluctuations).

Design of the Bay L receiver optics is underway in collaboration with PPPL personnel under the leadership of Dr. Yang Ren. Both the FIReTIP and high-k_θ scattering systems will be installed and begin operating in FY2015.

Summary of proposed research plan for 2014-18

Hardware

The FIReTIP system will begin operation in FY2015 with two plasma chords. In subsequent years, two additional FIReTIP chords, for a total of 4, will become available. Albeit a reduced number of channels, the new FIReTIP system will nonetheless continue to play a key role for NSTX in providing density feedback stabilization for NSTX and provide density calibration for the Thomson scattering system. The high-k_θ poloidal scattering system will be installed in FY2015 with a 4×1 imaging receiver array, with commissioning to be completed in FY2016. The high-k_θ receiver system will be expanded in later years to 2-D as resources permit.

In the long term, UC Davis is investigating ways to replace the large cumbersome ~600 GHz optically-pumped FIR laser with a compact, higher-power source. UC Davis has entered into a collaboration with Prof. Claudio Paoloni of Lancaster University to investigate the fabrication of an ~600 GHz backward wave oscillator (BWO) capable of delivering > 100 mW. This leverages separately funded work at UC Davis on microfabricated THz vacuum electron beam sources.

Physics

There is no doubt that electron thermal transport will pose the ultimate limit to the confinement performance of future devices. For example, electron heating will be dominant in ITER discharges, and efficient heating of fuel ions by electrons requires good electron thermal confinement. It is shown that experimentally relevant electron thermal transport is driven almost exclusively through stochastic magnetic field. Further parametric scans demonstrate that the s/q, Zeff, β and collisionality dependences of microtearing modes are different to those of ETG modes [3], which provides a potential way for separating them experimentally. Large scale magnetic fluctuations (n~10) associated with microtearing modes make it possible to measure magnetic fluctuations directly through Faraday rotation effects. The FIReTIP system, with its high sensitivity to magnetic fluctuations, will be particularly useful here.

Electron-scale turbulence has long been considered as a potential candidate in driving electron thermal transport, i.e. ETG turbulence [4], and its correlation with electron thermal transport has been observed in NSTX. Electron-scale turbulence was first identified in NSTX with the previous high-k scattering system [5] with local electron temperature gradient varied by RF heating in NSTX L-mode plasmas. However, the relationship between the electron scale turbulence measured by the previous high-k system and electron transport is not fully established, with agreement in certain situations but not in others [6,7]. This is not surprising, since limitations of the previous scattering system (which consisted of five channels measuring five radial wavenumbers with k_θ scannable from 0–7 cm^{-1}) spanned a perpendicular

wavenumber range of $k_\perp \approx 5–25\ cm^{-1}$. The limited coverage of the previous high k_r scattering system failed to sample the spectral peak of the ETG fluctuations (at ~10 cm^{-1}, assuming ρ_s~1) as calculated by the nonlinear GYRO code [8]. The new configuration will span $k_\theta \approx 5–40\ cm^{-1}$, centered at $k_r \sim 0$. Additional benefits include an enhanced signal-to-noise ratio arising from (a) increased incident beam power, (b) increased scattering cross-sections (due to low k_r), and (c) significantly increased radial coverage.

Furthermore, Alfvén eigenmodes are found to be potentially important for electron thermal transport in the core (r/a<0.4) of NSTX high-power neutral-beam injected H-mode plasmas. This electron thermal transport mechanism is potentially important for ITER since fusion α particles (which ITER relies on to heat electrons) may drive AE activities and thus could lead to degraded electron thermal confinement. The Alfvén eigenmodes are excited by fast particles from neutral beam injection due to their super-Alfvénic velocity. In a set of H-mode plasmas, flattening of central electron temperature profile is observed as NBI power is increased from 2 MW to 6 MW with increased AE activity indicated by Mirnov coil measurements [9]. Multi-chord density fluctuation measurements of spatially extended instabilities, such as Alfvén eigenmodes, would support ongoing research of a broad range of transport issues from electron thermal transport to fast-ion transport due to avalanches and other Alfvénic instabilities.

The reconfigured FIReTIP system, with its high sensitivity to edge density fluctuations and its demonstrated realtime capabilities, would help to address many physics demands of NSTX as well as providing density control in support of advanced operating scenarios. The prospect as a real-time density diagnostic for advanced plasma control would complement, for example, measurements of the safety factor profile, temperature and density profiles, divertor heat-flux, radiation, and/or surface temperature measurements.

Timeline

FY2014:

- Mock up the FIReTIP and high-k_θ scattering diagnostics at UC Davis, and characterize these systems using synthetic targets
- Install and operate the FIReTIP system on NSTX

FY2015:

- Commission the reconfigured FIReTIP system
- Work with NSTX personnel to implement a density feedback control system
- Install and operate the high-k_θ scattering system on NSTX, and employ initial plasma data to optimize system performance

- Physics studies will focus on assessing low-k turbulence (e.g. electron thermal transport in ITG/TEM regimes) appropriate for interferometric fluctuation measurements

FY2016:

- Install 3rd FIReTIP sight line
- Commission the (optimized) high-k_θ scattering system
- Physics studies continue to assess low-k turbulence, shifting focus toward high-k turbulence (e.g. ETG regimes) appropriate for newly commissioned scattering diagnostic

FY2017:

- Install 4th FIReTIP sight line
- Expand high-k_θ coverage from 1D to 2D with addition of a second 4-channel mixer array
- Conduct laboratory tests of a new high power (>100 mW) ~600 GHz BWO source
- Extensive testing of turbulence models; develop synthetic fluctuation diagnostics for rigorous testing of high-k/FIReTIP data against models

FY2018:

- Phase-out 600 GHz FIR laser for high-k_θ system in favor of a higher power BWO source for increased signal-to-noise ratios

Contributions to the NSTX-U 2014-18 Five Year Plan:

UC Davis contributed to Section 3.4.2.1 for Turbulence (and Transport) Diagnostics.

References

[1] Y. Ren, *et al.*, *Physics of Plasmas* **19**, 056125 (2012).
[2] S.S. Medley, *et al.*, *Nuclear Fusion* **52**, 103014 (2012).
[3] W. Guttenfelder, *et al.*, *Physics of Plasmas* **19**, 022506 (2012).
[4] W. Dorland, *et al.*, *Physical Review Letters* **85**, 5579 (2000).
[5] D. R. Smith, *et al.*, *Review of Scientific Instruments* **79**, 123501 (2008).
[6] S.M. Kaye, *et al.*, *Physical Review Letters* **98**, 175002 (2007).
[7] S.M. Kaye, *et al.*, *Nuclear Fusion* **47**, 499 (2007).
[8] R.E. *et al.*, *Physics of Plasmas* **9**, 1938 (2002).
[9] D. Stutman, *et al.*, *Physical Review Letters* **102**, 115002 (2009).

11.2.20 University of California, Irvine (UCI)

Research Topic: Active Beam Diagnostics to Measure the Fast-ion Distribution Function in NSTX-U, Beam Ion Studies in NSTX

Principal Investigator: Bill Heidbrink
Participating Scientists: Deyong Liu
Participating Graduate Students: Luke Stagner. *Note: an additional postdoc or Ph.D. student will be recruited once operation commences.*
Participating Undergraduates: 1
Funded under DOE Grants: DE-FG02-06ER54867, DE-FG03-02ER54681

Introduction

UCI joined the NSTX team at the beginning of NSTX operation. A study of beam-ion confinement based on the "beam-blip" technique was published in 2003. Several studies of fast-ion driven instabilities followed. Meanwhile, UC Irvine assumed responsibility for the solid state neutral particle analyzer (SSNPA) diagnostic and Deyong Liu began a Ph.D. project at NSTX. Following the development of the fast-ion D-alpha (FIDA) technique on DIII-D, a FIDA diagnostic for NSTX was proposed and funded. Mario Podesta was the postdoc who developed the NSTX spectroscopic "s-FIDA" and bandpass-filter-based "f-FIDA" instruments, both of which worked very well. For his thesis, Deyong Liu analyzed FIDA measurements of fast ions accelerated by HHFW. More recently, a new postdoc named Alessandro Bortolon completed assembly of new tangentially-viewing FIDA instruments just prior to the shutdown. Bortolon also performed new studies of fast-ion instabilities.

Current research contributions to NSTX Upgrade

Current Irvine personnel on the NSTX-U project are Prof. Heidbrink, Dr. Deyong Liu, and Mr. Luke Stagner. In addition, although he no longer works for UCI, Dr. Alessandro Bortolon is completing papers on projects he performed while an Irvine postdoc.

Deyong Liu is stationed at PPPL and works full time on the NSTX-U project. Under the supervision of Guo-Yong Fu, he is presently spending ~50% of his time on simulations of NSTX data. In particular, he has developed a method to incorporate accurate modeling of the fast-ion distribution function into the M3D-K code. The other half of Liu's effort is devoted to NSTX-U diagnostics. He is presently designing the new SSNPA diagnostic. Our ASDEX-Upgrade collaborator Benedijt Geiger has improved our synthetic diagnostic code FIDASIM; Liu is responsible for porting and testing FIDASIM for NSTX-U use.

Heidbrink and Bortolon are concentrating on completion of Bortolon's physics papers. A draft submission for *Physical Review Letters* on "Mitigation of Alfven activity in a tokamak by externally applied static 3D fields" was recently completed. Another paper will be based on Bortolon's invited talk at the 2012 APS-DPP conference on the synergy between AEs and kink modes. Earlier work presented at the IAEA Technical Meeting on Energetic Particles will also be published.

For his Ph.D. thesis, Luke Stagner is developing Bayesian techniques to infer the fast-ion distribution function. This project is in collaboration with Mirko Salewski of the Danish Technical University. The project is jointly supported by DIII-D and NSTX-U, as it is anticipated that Stagner's algorithms will be employed on both devices.

Summary of proposed research plan for 2014-18

In hardware, UCI will concentrate on four active beam measurements: vertical FIDA, tangential FIDA, SSNPA, and E||B NPA. The vertical FIDA system [1] is a working diagnostic that has been producing valuable data for several years. The tangential FIDA system [2] is patterned after the vertical FIDA diagnostic. Although it has not collected data during plasma operations, the diagnostic is essentially complete. The SSNPA diagnostic [3] was displaced from its former location by the new beamline. A new SSNPA diagnostic is being designed that will measure trapped fast ions at several radial locations. In addition, we will collaborate with Princeton personnel on operation of the E||B NPA if and when it is reinstalled.

Software to interpret the fast-ion data is another area of responsibility. FIDASIM [4] is a forward-modeling synthetic-diagnostic code that models active FIDA and NPA signals. Improvements to this code that allow it to run an order of magnitude faster will be implemented. A new code that models passive FIDA signals [5] (i.e., signals produced by collisions with edge neutrals rather than injected neutrals) is under development. In addition to these forward-modeling efforts, direct reconstruction of the fast-ion distribution function F from the fast-ion data is desirable. This is the topic of Luke Stagner's Ph.D. thesis. Through our collaboration with Salewski, initial progress in this area has already been achieved [6]. We will also develop a reduced model for the expected signals produced by classical fast-ion populations. This rapid, reduced model will be used to guide experiments in the control room and also for mining extensive datasets.

In experiments, we expect to contribute to validation experiments for the second neutral beamline; these will likely be similar to experiments Heidbrink performed at DIII-D [7]. New FIDA measurements of the interaction of fast ions with fast waves [8] (at intermediate cyclotron

harmonics) are also anticipated. In later years, we plan to concentrate on studies of fast-ion driven instabilities.

In analysis, Liu will continue to work closely with Princeton theorists to simulate NSTX-U experimental conditions. Once the machine is operating, a new postdoc or Ph.D student will be recruited who will assume some of Liu's diagnostic or analysis responsibilities.

The elements of our plan displayed in a timeline are:

Timeline

FY2014:
- FIDA calibrations
- SSNPA electronics
- Complete NSTX fast-ion instability papers
- Test fast-ion inversion code on best available data from NSTX, DIII-D, and other devices

FY2015:
- Operate and maintain FIDA and SSNPA diagnostics
- Deploy reduced model during operations
- Validation experiments for 2nd neutral beamline
- First fast-wave measurements of beam-ion acceleration

FY2016:
- Operate and maintain FIDA and SSNPA diagnostics
- Publish paper on beam validation experiments
- Dedicated beam-ion acceleration by fast waves experiment
- New study of an interesting fast-ion instability

FY2017:
- Operate and maintain FIDA and SSNPA diagnostics
- Publish paper on FIDA fast-wave acceleration observations
- Fast-ion instability studies

FY2018:
- Operate and maintain FIDA and SSNPA diagnostics
- Fast-ion instability studies

Contributions to the NSTX-U 2014-18 Five Year Plan:

UCI contributed material to chapters 6 and 7 of the Five Year Plan, particularly these sections:

- "Develop reduced physics-based models for *AE-induced fast ion transport,"
- "Validate classical TRANSP predictions for 2nd NB line,"
- "F_{nb} inversion code for interpretation of fast ion data"

References

[1] M. Podesta *et al.,* Rev. Sci. Instrum. **79** (2008) 10E521.

[2] A. Bortolon *et al.,* Rev. Sci. Instrum. **81** (2010) 10D728.
[3] D. Liu *et al.,* Rev. Sci. Instrum. **77** (2006) 10F113.
[4] W.W. Heidbrink *et al.,* Commun. Comput. Phys. **10** (2011) 716.

[5] W.W. Heidbrink *et al.,* Plasma Phys. Cont. Fusion **53** (2011) 085007.
[6] M. Salewski *et al.,* Nucl. Fusion **52** (2012) 103008.

[7] W.W. Heidbrink *et al.,* Nucl. Fusion **52** (2012) 094005.
[8] D. Liu *et al.,* Plasma Phys. Cont. Fusion **52** (2010) 025006.

11.2.21 University of California – Los Angeles

Research Topic: Cross-Cutting Research Studies on NSTX-U

Principal, Co-Principal Investigators: P.I. - Dr. Tony Peebles, Co-P.I.s - Prof. T Carter
Participating Scientists: Dr. Neal A. Crocker and Dr. Shige Kubota
Participating Graduate Students: Mr. Jie Zhang
Funded under DOE Grant: DE-FG02-99ER54527

Introduction

UCLA, as an active NSTX-U team member, is contributing to the research priorities of NSTX-U with innovative, cross-cutting measurement techniques applied across a broad range of research topics. In particular, UCLA has developed two diagnostic systems, a 16 channel array of reflectometers and a 288 GHz polarimeter that will be used to significant effect in NSTX-U. These diagnostics will enable advances in areas such the study of fast-ion modes, turbulence and transport, and edge pedestal control. Working with Culham Research Fellow and recent UCLA graduate Dr. Jon Hillesheim, UCLA is also collaborating with MAST to adapt the reflectometer array for use as a Doppler Backscattering diagnostic (DBS). This would provide MAST with a unique measurement capability for spherical tokamaks (ST), the capability to probe intermediate-scale ($k_\perp \rho_s \sim 1-5$) density fluctuations, bridging the gap between BES ($k_\perp \rho_s \leq 1$) and high-k collective scattering. This innovative development of DBS opens up the possibility of bringing a similar capability to NSTX-U.

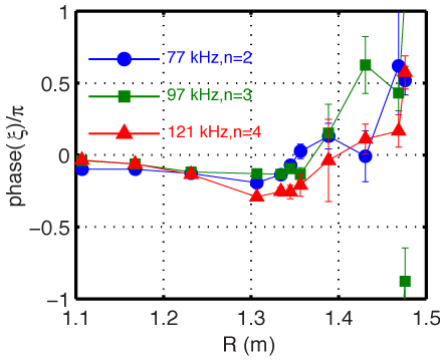

Figure 1: Phase of effective displacement of TAEs measured via reflectometer array [1].

Current research contributions to NSTX Upgrade

Fast-ion modes UCLA is contributing to the study of fast-ion modes in NSTX-U several ways. The reflectometer array consists of 16 fixed frequency reflectometers operating in the frequency range of 30 to 75 GHz. The system was operational in the 2010, permitting measurements of fast-ion mode structure in NSTX that contributed to several research priorities and guide the course of future research in NSTX-U. In particular, radial structure measurements were obtained for toroidicity-induced (TAE) [1], global (GAE) and compressional (CAE) Alfvén eigenmodes [1,2]. TAEs play a significant role in fast-ion transport and development of a predictive

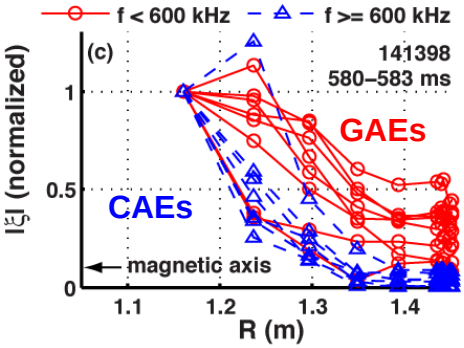

Figure 2: displacement ($|\xi|$) vs. R (normalized by $|\xi|$ at R=1.16 m) for CAEs (blue) and GAEs (red). (Adapted from [2].)

capability is a high research priority for NSTX-U. GAEs and CAEs are of particular interest because they have also been implicated as possible cause of enhanced core electron thermal transport.

The measurements of TAE radial structure, which included both amplitude and phase contribute significantly to the ongoing development of a predictive capability for transport. The measurements show a radial phase variation (Fig. 1) that is not consistent with expectation from ideal MHD, a theory that has been notably successful in predicting TAE structure in other cases [3,4]. This brings into question the limits of ideal MHD theory in predicting TAE structure. These measurements are currently being compared with calculations using M3D-K, a code that models a kinetic fast-ion population coupled to an MHD plasma [4]. The initial results are promising.

The measurement of CAE and GAE structure has had a significant impact in the investigation of the enhanced core thermal electron transport that has been observed to correlate with high frequency Alfvén eigenmode activity [5]. The amplitude and structure of CAEs and GAEs were measured in a high power, beam heated H-mode plasma similar to those in which the correlation was observed (Fig. 2) [1,2]. The measurements facilitated identification of the modes, allowing the CAEs to be distinguished from the GAEs. The two types of modes affect electron orbits differently, which must taken into account when making a theoretical prediction of transport for comparison with the experiment. Such modeling, which has previously considered only GAEs [6], is currently being adapted to consider CAEs as well.

Plasma Turbulence and Transport UCLA is contributing to the study of plasma turbulence in NSTX-U in several ways. The reflectometer array has been used to investigate edge turbulence in NSTX, where it has helped to advance understanding of H-mode edge stability and pedestal structure. In particular, it was used to measure the evolution of turbulence correlation length in the plasma edge during the ELM cycle [7]. With these results in conjunction with other measurements, it was possible to show that spatial scales at the pedestal top are found consistent with ion-scale microturbulence propagating in the ion diamagnetic direction and to make comparisons with gyrokinetic simulations.

Pedestal control UCLA is also contributing in the area of pedestal control. The reflectometer array has provided measurements of edge harmonic oscillation (EHO) mode structure [8] that help to motivate a possible technique for ELM suppression. The EHO is thought to be capable of suppressing ELMs, but only at larger amplitude than the internally driven (i.e. unstable) EHO that is experimentally observed. Modeling shows that the HHFW antenna can be used at low frequency (~ 5 kHz) to externally drive a large amplitude perturbation with a structure similar to that measured with the reflectometers.

Polarimeter Development UCLA has made significant progress preparing a 288 GHz polarimeter for operation on NSTX-U [9]. The polarimeter can monitor magnetic fluctuations inside the plasma, with applications to wide ranging research priorities including the study of fast-ion driven modes and neoclassical tearing modes. Another promising area of application for the polarimeter is the investigation of microtearing modes, which potentially play a significant role in electron thermal transport. UCLA graduate student Jie Zhang recently submitted a manuscript to Plasma Physics and Controlled Fusion showing synthetic diagnostic modeling using gyrokinetic simulations performed by Dr. Walter Guttenfelder of PPPL that demonstrate the polarimeter is sufficiently sensitive to detect microtearing modes in NSTX-U [10]. Another possible application for the polarimeter is to provide feedback in plasma control scenarios involving 3D fields by gauging the plasma response to the externally applied fields. Mr. Zhang has begun initial efforts working with Dr. Michael Van Zeeland of DIII-D to assess the polarimeter response to externally applied fields using M3D simulations.

Originally constructed for installation in NSTX in 2011, early commencement of the upgrade to NSTX-U prevented operation of the polarimeter. In preparation for NSTX-U, the polarimeter was installed on DIII-D for testing over a wide range of conditions similar those planned for NSTX-U. The polarimeter phase was measured for a large range of toroidal magnetic field (0.5 – 2 T), plasma current (0.3 & 1.0 MA) and line average density (0.95 & 1.7 x 10^{19} cm^{-3}). Plasma height was also varied substantially (± 20 cm, or ~ 25 % of the plasma vertical extent) to test the polarimeter under conditions where the polarimeter chord is far from the plasma midplane. The polarimeter measurements were compared with predictions from a synthetic diagnostic that models millimeter-wave propagation in the plasma, using EFIT equilibrium reconstructions and density profiles determined via Thomson scattering and the CO_2 interferometer. Good agreement was found over this broad range of conditions, including conditions where Faraday Rotation (polarization rotation due to B parallel to propagation) was the dominant effect and conditions where polarization was strongly influenced by the Cotton-Mouton effect (elliptization due to B transverse to propagation).

Collaboration with MAST – DBS development UCLA is collaborating with MAST, working with Culham Fusion Research Fellow and recent UCLA graduate Dr. Jon Hillesheim to adapt the UCLA reflectometer array for use as a DBS diagnostic, as well as utilize it for conventional reflectometry. (The array will be returned to NSTX-U for installation in 2014.) Doppler backscattering uses millimeter waves launched oblique to the cutoff surfaces to probe intermediate-scale ($k_\perp \rho_s \sim 1 - 5$) density fluctuations and plasma flows. These scales include trapped electron modes (TEM) and possibly extend into the electron temperature gradient (ETG) mode regime. The launched radiation backscatters from intermediate-scale turbulence with a Doppler shifted imparted by the propagation of the turbulence. The velocity of the turbulence is typically dominated by ExB flow of the background plasma, allowing E to be inferred, while the

backscattered power provides information about density fluctuation amplitude, both with good spatial (Δr < 1 cm) and temporal (Δt < 1μs) resolution. DBS has been deployed on numerous standard tokamaks, but, to date, has seen limited use in a spherical tokamak, and only in the extreme edge. The proposed collaboration would therefore provide MAST with a unique measurement capability for STs. There are currently no diagnostics for core turbulence at intermediate scales in MAST, or planned for NSTX-U. UCLA is currently exploring options to develop a DBS system for NSTX-U, so the lessons learned on MAST will be beneficial to future research efforts. The DBS measurements of plasma flows would also add powerful measurement capabilities to MAST, as well as NSTX-U if implemented there. Similar multichannel DBS systems have provided data for studies of geodesic acoustic modes [11] and zonal flows during the L-H transition [12]. The system will also be configured to operate as a conventional reflectometer while at MAST, enhancing MAST's capability to investigate fast-ion driven modes and fast-ion transport, allowing comparison with previous NSTX results in preparation for NSTX-U operation.

Summary of proposed research plan for 2014-18

The reflectometer array and polarimeter will be installed on NSTX-U for the start of plasma operations in late 2014. The polarimeter will be utilized in experimental investigation of microtearing modes and may also provide feedback for plasma control scenarios that involve the application 3D fields, such RWM control, ELM control, pedestal control through active EHO excitation. The reflectometer array will be exploited to further investigate edge fluctuations such as ELMs, EHOs and ion-scale turbulence in the pedestal with the goal of facilitating pedestal control. Both systems will be employed in the investigation of fast-ion driven modes. Integration of their measurements with density fluctuation and poloidal flow measurements obtained via BES will provide a powerful tool for validating the predictions of codes such as M3D-K.
The elements of our plan displayed in a timeline are:

Timeline

FY2014:

- Continue investigation of EHOs. Contribute reflectometry analysis to on-going investigation of ELMs and ion-scale pedestal turbulence.
- Continue integration (started FY2013) of CAE and GAE mode structure measurements with particle orbit code (ORBIT) to develop capability to predict electron thermal transport from mode structure measurements.
- Install polarimeter and reflectometers in anticipation of plasma operations in FY2015.

FY2015:

- Begin integrating mode structure diagnostics with fast-ion mode simulation (M3D-K, NOVA-K) and fast-ion orbit codes (ORBIT, SPIRAL) to predict transport based on measured mode structure. Begin comparisons with fast-ion population diagnostics (FIDA).
- Investigate fast-ion mode spectrum with new neutral beams.
- Exploit polarimeter to investigate coherent magnetic fluctuations (e.g. fast-ion modes) and microtearing modes. Assess potential for feedback in plasma control scenarios with 3D fields.
- Develop analysis techniques to integrate mode structure diagnostics (BES, reflectometers and polarimeter). Compare results with M3D-K and NOVA-K. Assess limits of ideal MHD theory.
- Investigate edge fluctuations (ELMs, pedestal turbulence, EHO) in new parameter regime. Contribute to development of pedestal and plasma control scenarios.
- Based on DBS development at MAST, aggressively pursue options to implement at NSTX-U

FY2016:

- Investigate changes in fast-ion mode spectrum at increasing I_P and B_T and in 3D fields.
- Investigate of CAEs and GAEs and their role in electron thermal transport at increasing I_P and B_T.
- Investigate edge fluctuations in new parameter regime.

FY2017-FY2018:

- Continue developing capability to predict of fast-ion transport from measured mode structure. Integration mode structure measurement and resulting fast-ion transport predictions with model of plasma and fast-ion population (TRANSP). Compare with fast-ion population diagnostics.
- Continue investigation of CAEs and GAEs and development of predictive capability for electron thermal transport from mode structure measurements.
- Continue investigate edge fluctuations and contribute to development of control scenarios.

Contributions to the NSTX-U 2014-18 Five Year Plan:

The cross-cutting research plan above contributes to multiple Topical Science Groups (TSG), including Waves and Energetic Particles (WEP), Turbulence and Transport (T&T), Boundary

Physics and Macroscopic Stability, whose contributions to the Five Year Plan are discussed in chapters 6, 3, 4 and 2, respectively. The plan above was defined in a process performed over CY2011-12 in coordination with the NSTX-U Research Team. The research defined above contributes heavily to the plan, with the perhaps most significant focus in the areas of Waves and Energetic Particles and Turbulence and Transport. A central goal of the WEP is the development of a predictive capability is the construction of reduced models for prediction of fast-ion-mode-induced fast-ion transport. Several aspects of the plan presented here related to fast-ion mode structure and magnetic fluctuation measurements directly address this goal. Several aspects of the plan related to investigation of microtearing modes and the role of CAEs & GAEs in electron thermal transport also advance the mission of the T&T to investigate the cause of electron thermal transport.

References

[1] N. A. Crocker, W. A. Peebles, S. Kubota, et al., "High spatial sampling global mode structure measurements via multichannel reflectometry in NSTX," Plasma Phys. Control. Fusion 53 (2011) 105001.
[2] N. A. Crocker, E. D. Fredrickson, N. N. Gorelenkov, et al., "Internal Amplitude, Structure and Identification of CAEs and GAEs in NSTX," To be published in Proceedings of the 24th IAEA Fusion Energy Conference, San Diego, USA, 8-13 October 2012, Sep. 2012, EX–P6–02. Also: updated version submitted to Nuclear Fusion.
[3] M. A. Van Zeeland, et al., "Radial structure of Alfven eigenmodes in the DIII-D tokamak through electron-cyclotron-emission measurements," Phys. Rev. Lett. 97, (2006) 135001
[4] G. Y. Fu, M. Podesta, N. Crocker, and E. Fredrickson, "M3D-K simulations of beam-driven Alfvén modes in NSTX," Joint US-EU Transport Taskforce Workshop TTF 2011: San Diego, California April 6-9, 2011. http://ttf2011.pppl.gov/
[5] D. Stutman, L. Delgado-Aparicio, N. Gorelenkov, et al., "Correlation between Electron Transport and Shear Alfvén Activity in the National Spherical Torus Experiment," Phys. Rev. Lett. 102, (2009) 115002.
[6] N. N. Gorelenkov, D. Stutman, K. Tritz, et al., "Anomalous electron transport due to multiple highfrequency beam ion driven Alfvén eigenmodes," Nucl. Fusion 50, (2010) 084012.
[7] A. Diallo, J. Canik, G.J. Kramer, et al., "Progress in characterization of the pedestal structure, stability and fluctuations during ELM cycle on NSTX," To be published in Proc. of the 24th IAEA FEC, San Diego, USA, 8-13 Oct. 2012, pp. EX-P4-04
[8] J.-K. Park, R. J. Goldston, E. D. Fredrickson, et al., "Observation of Edge Harmonic Oscillation in NSTX and Theoretical Study of its Active Control Using HHFW Antenna at Audio Frequencies," To be published in Proc. of the 24th IAEA FEC, San Diego, USA, 8-13 Oct. 2012, pp. EX/P4-33.

[9] J. Zhang, W. A. Peebles, T. A. Carter, N. A. Crocker, et al., "Design of a millimeter-wave polarimeter for NSTX-Upgrade and initial test on DIII-D," Rev. Sci. Ins. 83 (2012), pp. 10E321-1–3.
[10] J. Zhang, N. A. Crocker, W. A. Peebles, T. A. Carter and W Guttenfelder, "A sensitivity assessment of millimeter-wave polarimetry for measurement of magnetic fluctuations associated with microtearing modes in NSTX-U," Submitted to Plasma Phys. Control. Fusion.
[11] J. C. Hillesheim, W. A. Peebles, T. A. Carter, et al., "Experimental investigation of geodesic acoustic mode spatial structure, intermittency, and interaction with turbulence in the DIII-D tokamak," Phys. Plasmas 19, (2012) 022301
[12] L. Schmitz, L. Zeng, T. Rhodes, J. Hillesheim, et al., "Role of Zonal Flow Predator-Prey Oscillations in Triggering the Transition to H-Mode Confinement," Phys. Rev. Lett. 108, (2012) 155002

11.2.22 University of Illinois

Research Topic: Enhanced Lithium Pumping in the RLLD via LiMIT

Principal, Co-Principal Investigators: David Ruzic (PI/PD), Daniel Andruczyk (Co-I.)
Participating Scientists:
Participating Post-docs: 1
Participating Graduate Students: Wenyu Xu, Soonwook Jung, Peter Fiflis, Mike Christiansen
Participating Undergraduates: 10
Funded under DOE Grant: DE-SC0008587, DE-SC0008658, DE-ER54515

Introduction

There are many concerns that exist about the ability of divertor components to scale from the current limits of tungsten divertors (~5 MWm^{-2}) to much higher heat loads as may be expected in devices beyond ITER (>20 MWm^{-2}). Even current flowing liquid lithium divertor concepts, while alleviating many of the issues associated with solid divertors, may not be able to "take the heat" under conventional thinking. This thinking limits the operating temperature of the lithium to below 400 ^{o}C to avoid lithium evaporation. Once this restriction is relaxed, however, operation at much higher heat fluxes may be accessible. By taking advantage of liquid lithium in a radiative liquid lithium divertor (RLLD), large heat fluxes to the divertor may be distributed over a much wider area of the device [1]. As currently envisioned, the RLLD would utilize external pumps to move a small volume of liquid lithium through the device. In order to decrease the amount of power required for these pumps, it is proposed to propel the lithium through the RLLD via a LiMIT device [2], developed at the University of Illinois at Urbana-Champaign (UIUC), which would utilize TEMHD to pump lithium through the RLLD without the need for a mechanical pump. We have had direct experience working on NSTX in the past. The Langmuir probe array embedded in the LLD was an Illinois project staffed by an Illinois research engineer on site at PPPL.

Current research contributions to NSTX Upgrade

The Center for Plasma Material Interactions (CPMI) at UIUC are currently contributing to NSTX-U campaign in several ways:

1. Characterization of liquid lithium as a plasma facing component material. CPMI have provided data on both the material properties of liquid lithium and its compatibility with various materials.
    a. Thermoelectric properties of fusion relevant materials (stainless steel, tungsten, molybdenum, tantalum) have been performed as well as lithium and other potential liquid metal candidates such as tin [3].
    b. Wetting properties of lithium and tin with fusion relevant materials such as stainless steel, tungsten, molybdenum and tantalum have been characterized [4].

   c. With NSTX-U being mainly a carbon machine, understanding the plasma interactions with graphite and lithium covered graphite is of great importance. UIUC has been conducting studies in the IIAX device to better understand these interactions for NSTX-U [5].
2. Illinois is also providing support of the lithium dripper and granular injector systems. A theory for the formation of liquid metal droplets has been developed and initial experiments with a simple injector at UIUC and PPPL have been performed [6].
3. CPMI is embarking on the development of a new innovative liquid divertor PFC that can withstand high heat fluxes. This is based on the LiMIT concept. Thermoelectric-Driven Liquid-Metal Plasma-Facing Structures (TELS) [7] will extend the work that has been done at CPMI in four ways:
   a. Develop, refine and test new geometries for thermoelectrically driven structures that would be more relevant for fusion devices such as NSTX-U.
   b. Expansion of the Illinois pulsed and continuous systems so that pulsed plasma heat loads impinge on a surface that already has a continuous heat load.
   c. Increase the magnetic field to make it more relevant to fusion type environments that will be seen in NSTX-U.
   d. Study alternate PFC materials such as tin-lithium eutectics that may be relevant for fusion in the future.

   TELS will be built and tested at UIUC and is based on LiMIT, SLiDE and DEVeX and will investigate prototype designs for the RLLD that will be developed for NSTX-U.

Summary of proposed research plan for 2014-18

We propose to enhance the flow of liquid lithium through a RLLD for NSTX-U by utilizing TEMHD to actively pump the lithium. By combining experimental and modeling efforts, we propose to design and test a LiMIT style device to utilize TEMHD to achieve the aforementioned effect. Previous modeling efforts have made gains in determining the heat transfer within the device as well as the flow of the liquid lithium [8], and experiments both at the University of Illinois, and on HT-7 have demonstrated the viability of such a device [9]. Therefore, we propose to collaborate with the NSTX-U team on designing and implementing a LiMIT device for use in an RLLD system for NSTX-U.

The elements of our plan displayed in a timeline are:

Timeline

FY2014:

- Continue modeling efforts into the heat transfer and fluid flow of the LiMIT device.

- Continue experimental characterization of the LiMIT device under a variety of operating conditions.

FY2015:
- Using experimental and model data, design ideal LiMIT device for incorporation into the RLLD system
- Test viability of design with experimental capabilities at UIUC

FY2016:
- Continue testing of design viability, particularly under extreme (accident) conditions
- Begin construction of practical device for inclusion into the RLLD

FY2017:
- Installation and testing of the LIMIT-like RLLD and other flowing lithium test structures for NSTX-U
- Station a Research Engineer at PPPL to aid in operations and data analysis
- Work at Illinois on technological needs that arise.

FY2018:
- Station a Research Engineer at PPPL to aid in operations and data analysis
- Work at Illinois on technological needs that arise. Start design of next upgrade.

Contributions to the NSTX-U 2014-18 Five Year Plan:

The plan listed above is to install a LIMIT-like lithium delivery system to the RLLD. It has the advantages of being self-pumping and always presenting a clean fresh lithium surface to the heat flux. This is superior to other designs and much simpler. Illinois stands by to help with the design, engineering, assembly, testing and analysis of such a device.

References

[1] M. Ono *et al.*, IAEA Paper (2012). *Preprint*.
[2] D. N. Ruzic *et al.*, Nucl. Fusion **51** (2011) 102002.
[3] P. Fiflis *et al.*, submitted to J. Nuc. Mater. Feb 2013.
[4] P.Fiflis *et al.*, APS DPP, Providence RI, USA 29 Oct. – 02 Nov. 2012 B06-02.
[5] Raman *et al.*, J. Nuc. Mater (2013) 10.1016/j.jnucmat.2013.01.138.
[6] P. Fiflis *et al.*, submitted to Rev. Sci. Instrum. Feb 2013.
[7] D. Andruczyk *et al.*, APS DPP, Providence RI, USA 29 Oct. – 02 Nov. 2012 TP8-39.
[8] D. Curreli *et al.*, APS DPP, Providence RI, USA 29 Oct. – 02 Nov. 2012 CO7-04.
[9] D. N. Ruzic *et al.*, IAEA Paper (2012).

11.2.23 University of Tennessee, Knoxville (UTK)

Research Topic: Study of poloidal asymmetries of lithium coatings
Principal, Co-Principal Investigators: B. D. Wirth (PI/PD), R. Maingi (Co-I.)
Participating Scientists:
Participating Post-docs: A. Bortolon
Participating Graduate Students: 1
Participating Undergraduates: 0

Introduction

The development of stationary, high performance, long-pulse plasmas is stated as a high programmatic objective of the NSTX upgrade [1]. Previous experiments on NSTX demonstrated the beneficial effect of lithium coating in terms of energy confinement, profile peaking and ELM frequency. The use of lithium coating will remain a key element of the NSTX-U operation.

However, open questions remain as to which mechanisms govern the effectiveness of lithium coating and in particular the incremental improvements with amount of evaporated lithium [2]. The main objective of the UT-K program on NSTX-U is to evaluate the how the effectiveness of lithium evaporation is affected by poloidal and toroidal asymmetries of lithium coatings. To achieve this, the proposal entails installation of new diagnostics and leadership/participation in relevant experiments, as well as key modeling of the obtained data. The UT-K program grant was initiated in July 2012, with an annually renewable program through June 2016. Note that there is a strong synergy between the UT-K program and the ORNL boundary collaborative program on NSTX-U, with sharing of hardware and expertise.

To enable this study a new set of diagnostics are being be deployed, that will provide NSTX-U with spatially and spectroscopically resolved measurements of the previously un-sampled regions of the upper divertor and central stack wall. In addition, new infrared camera views of the same regions will ensure the heat flux measurements required as constraints for interpretative modeling. The improved diagnosis of the upper divertor will become increasingly important during the five-year plan as NSTX heating and pulse lengths are increased to full capability.

The novel measurements will permit to track the evolution of emission by different impurities (C, Li) from various regions of the wall. This will allow to study phenomena as lithium distribution, lithium migration and re-deposition, surface carbon-lithium chemistry and, ultimately, to assess the impact of each of these mechanisms on the effectiveness of lithium evaporation.

The added diagnostic capabilities will also support a range of other critical plasma boundary interface issues, including particle and heat sharing between the upper and lower divertors, as NSTX-U will employ more routinely the standard double null and "snowflake" configurations for power handling. The diagnostic will also be useful to study impurity migration when high-Z tiles will introduced as part of plasma facing components.

To accomplish the collaboration mission, interpretative 2-D modeling of the plasma boundary is envisioned, in particular using the SOLPS code as used in previous interpretive edge studies [3]. This will be coupled to an effort to model the dynamical evolution of the plasma facing material with first principle simulations.

Current research contributions to NSTX Upgrade

The near-term effort is predominantly devoted to the design and construction of the new diagnostics.

The spectroscopic emission from plasma facing surfaces away from the lower divertor will be collected into fiber optics by two different optic assemblies, providing 16 view-lines focused on the upper divertor region and 16 on central stack tiles. The spectral analysis is performed the acquisition room far from the experimental hall, by a multichannel, high-throughput, high dispersion spectrometer, equipped with a CCD detector. The use of broad band transmission components ensures the possibility to observe and track the evolution multiple impurity lines in the visible-UV range of wavelengths.

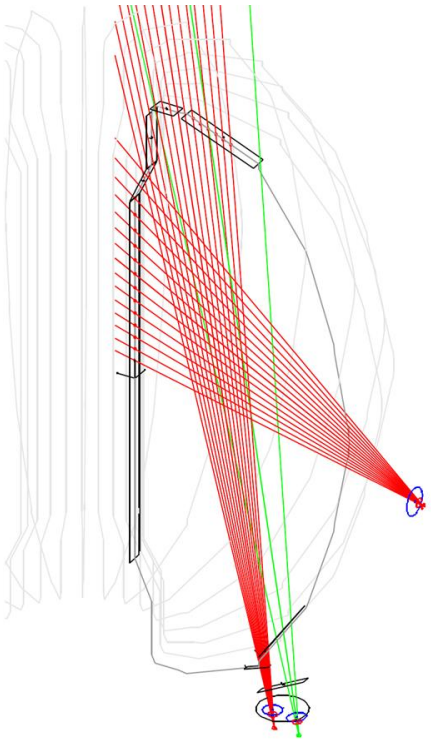

Figure 1 Schematic of view lines for the spectroscopic observation of upper divertor and central stack of NSTX-U (red). Field of view the fast IR camera (green).

Two new infrared cameras will monitor the tile temperature and heat deposition in the upper divertor and central stack. The use of lithium in NSTX-Upgrade requires that dual-band adapters be implemented, as presently used on the lower divertor, fast IR camera [4]. The center stack camera will likely be a standard 30 Hz or 60 Hz camera. The upper divertor camera is intended to be a similar camera, but may be superseded by a fast, dual-band IR camera planned by ORNL. In this case, UT-K staff will share responsibility for operation and data analysis with ORNL staff.

Presently, the conceptual design of the diagnostics described above is complete, and the main equipment elements are being acquired (spectrometer, fibers, lenses). Dedicated port access has been allocated, including two bottom windows (bay G) and two mid-plane windows at (bay J). A schematic of the observation geometry is shown in Figure 1.

Summary of proposed research plan for 2014-18

The research plan requires a first phase with high priority to the diagnostic installation (2014-2015), commissioning and operation. Along with the availability of validated data from the new diagnostics and with the establishment of the NSTX-U operation, the emphasis will shift on designing and performing plasma experiments dedicated to the scope of the collaboration, i.e. the study of the effectiveness lithium evaporation (2015-2016). At the same time, with the support of one graduate student, the plasma and material modeling effort will begin and to allow a proper the interpretation of the experiments (2016-2018).

Timeline

2014-2015:

- Finalize construction installation of spectroscopy diagnostic (collection optics, fiber bundles, spectrometer) and IR cameras (1 fast, 1 slow).
- Diagnostic calibration and alignment.
- Diagnostic commissioning and integration into NSTX-U acquisition system.
- Document first data from upper divertor and central stack.

2015-2016:

- Support NSTX-U activity with installed diagnostics.
- Perform dedicated plasma experiments to study poloidal distribution of Li coating in different divertor magnetic configurations.
- Apply plasma boundary modeling (SOLPS) to newly acquired data.

2016-2018:

- Upgrade the slow IR camera (25 Hz frame rate) to a fast IR camera (1 kHz frame rate).
- Model dynamic response of materials, using SOLPS plasma solutions.
- Assess the effect of poloidal variation in lithium deposition on plasma performance.

Contributions to the NSTX-U 2014-18 Five Year Plan:

Vlad Soukhanovskii, Ahmed Diallo, and Rajesh Maingi are the present leaders of the Boundary Physics topical science group and are responsible for overseeing the Boundary Physics chapter of the NSTX-U Five Year Plan. The plan above was defined in a process carried out over CY2011-12 in coordination with the NSTX-U Boundary Physics topical science group and contributes heavily to the 5 year plan.

References

[1] *2011 NSTX Program Letter for Research Collaboration Employing Innovative Diagnostics for FY 2012-2015* http://nstx.pppl.gov/DragNDrop/Program_PAC/Program_Letters/NSTX_Record_of_Discussion_FY2012.doc.

[2] Maingi R. et al. *Phys. Rev. Lett*. 107, 145004 (2011).

[3] Canik J.M., et al. *Phys. Plasmas* 18, 056118 (2011).

[4] McLean A. G. *Rev. Sci. Instrum.* 83, 053706 (2012).

11.2.24 University of Washington, Seattle

Research Topic: Solenoid-free current start-up with CHI and current ramp-up using NBI and RF

Principal, Co-Principal Investigators: Thomas R. Jarboe, Roger Raman

Participating Scientists: B.A. Nelson, D. Mueller, S.C. Jardin, C. Kessel, F. Poli, E.B. Hooper, F. Ebrahimi from Univ. of Washington, PPPL, LLNL and Univ. of New Hampshire

Funded under DOE Grant: DE-FG02-99ER54519 [T.R. Jarboe, R. Raman]

Introduction

Our plans are to continue to develop solenoid-free plasma start-up and current ramp-up on the NSTX-U using Coaxial Helicity Injection (CHI), originally developed on the HIT-II device at the University of Washington, and then to ramp-up the current produced by CHI using neutral beams and HHFW.

Transient CHI first developed on the HIT-II ST at the University of Washington was, then tested and further improved on the much larger NSTX device at PPPL [1,2,3]. These results coupled with recent simulations with the TSC code [4] have revealed many important aspects of CHI physics and its application to future machines. The key results are briefly summarized below.

- NSTX and HIT-II, two machines of vastly different size (NSTX plasma volume is 30 times that of HIT-II), have both achieved significant levels of start-up current through CHI. 300 kA start-up current has been demonstrated on NSTX [5,6,7].
- On NSTX, the method is highly efficient, producing more than 10 Amps/Joule of initial stored capacitor bank energy.
- The scaling to larger machines with higher toroidal field is quite favorable: NSTX achieves 10 times the current multiplication factor of HIT-II. Current multiplication is defined as the ratio of the CHI produced plasma current to injected current, which is over 50 in NSTX.
- In addition, the CHI generated plasmas on NSTX have desirable properties including low normalized internal inductance of 0.35, low electron density and low impurity content, as needed for subsequent non-inductive current ramp-up using NBI and RF waves.
- Simulations with the TSC code show agreement with the theoretical prediction for CHI as it is scaled to larger machines.

Current research contributions to NSTX Upgrade

Enhanced system capabilities for CHI on NSTX-U and our plans are:

- NSTX-U is planned to have 1 MW ECH capability that would increase the electron temperature of the CHI target as needed for direct coupling to neutral beams.
- Factor of two increase in the toroidal field which further increases the current multiplication factor and allows more poloidal flux to be injected at a given injector current.
- The injected poloidal flux capability in NSTX-U is more than 2.5 times that in NSTX. Because the generated plasma current magnitude is proportional to the injected poloidal flux, this would allow NSTX-U to generate well in excess of 400 kA start-up current, enough so that, neutral beams can efficiently couple to the plasma discharges.
- The CHI system operating voltage on NSTX-U will be increased from 1.7 kV in NSTX to up to 3 kV on NSTX-U. This should greatly improve CHI start-up capability in NSTX-U, as this increased voltage will allow more poloidal flux to be injected.
- NSTX-U will have capability for a second (new) 6 MW tangential neutral beam system that is well suited for driving current in the plasma. TSC simulations show that current ramp-up to the steady-state sustainment levels should be possible starting from an initial current level of less than 400 kA. Thus CHI has an adequate margin for the initial seed current magnitude.
- NSTX-U will incorporate metallic divertor plates, which should further improve plasma start-up by CHI by reducing low-Z impurities.

Summary of proposed research plan for 2014-18

We will establish transient CHI discharges in NSTX-U. These discharges will then be coupled to induction to assess flux savings and to compare with results from NSTX. CHI-started discharges will be heated using 28 GHz ECH to increase its electron temperature. These discharges will be further heated using HHFW. The RF heated CHI discharges will be ramped up in current using neutral beams for a demonstration of full solenoid-free current start-up and non-inductive ramp-up. In other experiments we will drive edge current in pre-established lower single null discharges and assess current penetration to the interior with and without the presence of edge magnetic fluctuations imposed by the NSTX-U non axis-symmetric coils.

In support of these experiments we will continue to use the TSC/TRANSP codes for simulating plasma start-up and current ramp-up. Plasma start-up simulations conducted with TSC/TRANSP will be used for establishing the initial transient CHI start-up discharges in NSTX-U. We are also working with E.B. Hooper (LLNL) and F. Ebrahimi (Univ. of New Hampshire) in developing a NIMROD model of NSTX/NSTX-U CHI start-up discharges. Towards the later part of the 5YR plan, we plan to use simulations from these codes in a predictive mode initially to support

NSTX-U research and later for understanding the requirements for solenoid-free plasma start-up and current ramp-up using CHI in a FNSF.

The elements of our plan displayed in a timeline are:

Timeline

FY2014:

- Continue analysis of NSTX CHI data and conduct TSC/TRANSP simulations to develop CHI start-up and current ramp-up scenarios for NSTX-U.
- Design a CHI system for the Quest ST in Japan to obtain additional information of CHI scaling with machine size.

FY2015:

- *Plasma start-up:* Establish transient CHI discharges using graphite lower divertor tiles, up to 0.8 T capability of NSTX-U, and full Li coating of the lower divertor tiles. Using the 2 kV capability of the CHI capacitor bank, assess maximum toroidal currents that can be generated by increasing the amount of injector flux and the size of the capacitor bank. Use the upper divertor buffer coils to suppress arcs.
- *Coupling to induction:* Couple the CHI generated plasma to inductive drive to show compatibility with inductive operation. Use a solenoid with zero pre-charge.

FY2016:

- *Plasma start-up:* Improve the magnitude of the closed flux CHI produced current by using Li coating of the upper divertor to further reduce the influx of low-Z impurities. The objective is to improve on the results from YR1 and to obtain 400 kA of closed flux plasma current that is suitable for meeting the needs for satisfying Thrust 2 during YRs 3-5. Compare to and improve the NIMROD simulations.
- *Coupling to induction -1:* Extending on the work from YR1 establish the flux savings that can be realized using the above plasma start-up target and with zero pre-charge in the central solenoid.
- *Coupling to induction -2:* Conduct an initial test of coupling to induction using 10 – 20% solenoid pre-charge. The goal is to use some solenoid flux to increase the magnitude of the generated plasma current, but by ramping the current in the solenoid to zero, so that it can be maintained at zero during sustained non-inductive operation.
- *Assess coupling to NBI:* In CHI discharges that are weakly driven by induction, measure and increase the magnitude of the neutral beam driven toroidal current. Compare these results to simulations using the TSC code that uses TRANSP to calculate the neutral beam power deposition profile and neutral beam current drive.

- *Edge current drive:* To a pre-formed lower single null discharge, apply a current pulse using the CHI capacitor bank and measure the presence of any edge driven current and the resulting changes to the edge current profile.

FY2017:

- *ECH heating of CHI discharge:* Heat a CHI started plasma using ECH both to demonstrate heating and a longer current decay time to provide a better target for NBI.
- *Plasma start-up:* Maximize the levels of CHI produced plasma currents using the new capabilities that will be available during YR3. These are (1) metal divertor plates, (2) 1 MW ECH, and (3) 2.5-3 kV CHI capability. All these should allow more injector flux to be injected into the vessel at reduced levels of low-Z impurities. If results are available from Quest, compare with Quest results to understand any differences between the two machines.
- *Couple CHI to NBI:* Using the best available CHI targets, conduct an initial test of the effectiveness of NBI coupling to a CHI generated target.
- *Couple to induction:* Couple to induction using the maximum possible solenoid pre-charge CHI allows. Ramp the solenoid current to zero, maintain the solenoid at near zero current, and test establishment of a >600kA high temperature plasma target for use by other TSGs for sustained non-inductive operation.
- *Edge current drive:* Based on YR2 results, to a pre-formed lower single null target, apply a current pulse using the DC power supplies to extend the magnitude and duration of the edge current pulse, and measure changes to the edge current profile, edge current penetration to the interior and changes to the plasma MHD stability limits, with and without the presence of edge magnetic fluctuations imposed by the non axis-symmetric coils.

FY2018:

- *Plasma start-up:* Maximize the levels of CHI produced plasma currents now also using the new cryo pump and assess its effectiveness in suppressing absorber arcs. Validate NIMROD simulations on CHI plasma start-up using NSTX-U results and begin to develop a NIMROD model for FNSF.
- *Couple CHI to NBI:* Using the best available CHI targets, ramp a CHI started discharge to 1 MA using a combination of NBI and bootstrap current over drive. Use experimental results to improve the NBI current drive model in NIMROD simulations.
- *Plasma start-up:* Compare results obtained from NSTX with other recent results from Quest. Of the more than 300 mWb of injector flux that is available in NSTX-U determine the maximum levels that are usable and use these results for CHI design studies for a FNSF. Use these results to improve the TSC model for FNSF

Contributions to the NSTX-U 2014-18 Five Year Plan:

R. Raman is the present leader of the Solenoid-free Plasma Start-up and Current Ramp-up topical science group and is responsible for overseeing chapter 8 write-up of the NSTX-U Five Year Plan. The plan above was defined in a process carried out over CY2011-12 in coordination with the NSTX-U Research Team. The research defined above contributes heavily to the plan.

References

[1] R. Raman, T.R. Jarboe, B.A. Nelson, et al., Phys. Rev. Lett., **90**, 075005 (2003)

[2] R. Raman, B.A. Nelson, M.G. Bell, et al., Phys. Rev. Lett., **97**, 175002 (2006)

[3] R. Raman, S.C. Jardin, J. Menard, et al., Nuclear Fusion **51**, 113018 (2011)

[4] T.R. Jarboe, Fusion Tech. **15**, 7 (1989)

[5] B.A. Nelson, T.R. Jarboe, D. Mueller, R. Raman, et al., Nuclear Fusion **51**, 063008 (2011)

[6] R. Raman, D. Mueller, B.A. Nelson, Phys. Rev. Lett., **104**, 095003 (2010)

[7] R. Raman, D. Mueller, T.R. Jarboe, et al., Physics of Plasmas **18**, 092504 (2011)

11.2.25 University of Washington, Seattle

Research Topic: Disruption Mitigation Studies on NSTX-U
Principal, Co-Principal Investigators: Roger Raman, Thomas R. Jarboe
Participating Scientists: D. Stotler (PPPL)
Participating Graduate Students: T. Abrams (PPPL)
Funded under DOE Grant: DE- SC0006757 [R. Raman, T.R. Jarboe]

Introduction

At present, MGI (Massive Gas Injection) is the most promising method for safely terminating disruptions in ITER. On ITER, because of the large minor radius of the device, the long transit times for the slow moving neutral gas, and the large scrape-off-layer flows, it is not known if a simple MGI pulse would be adequate for securely terminating an ITER discharge. While MGI experiments are being conducted at a number of tokamak facilities, the impact of varying the poloidal injection location has not been adequately studied, and injection into the private flux region has not been studied.

Additional insight into ways for reducing the total amount of injected gas and appropriate injection locations would further help optimize the MGI system for ITER. NSTX-U can offer new data by injecting gas into the private flux region and into the lower X-point region to determine if this is a more desirable location for massive gas injection.

Current research contributions to NSTX Upgrade

Injection from the private flux location has two advantages. First, the gas does not need to penetrate the scrape-off-layer region. Second, because the injection location is located near the high-field side region, the injected gas should be more rapidly transported to the interior as known from high-field side pellet injection research and from high-field side gas injection on NSTX-U. By comparing gas injection from this new location to results obtained from injecting a similar amount of gas from the conventional outer mid-plane region and from other poloidal locations, NSTX-U results on massive gas injection can provide additional insight and a new set of database for improving computational simulations and add new knowledge to disruption mitigation physics using massive gas injection.

With the help of D. Stotler (PPPL) and T. Abrams (PPPL), we are also modeling the gas penetration physics using the DEGAS-2 code [1,2,3]. The present plans are the determine the optimum injection location for NSTX-U and eventually to have the system on stand-by so that it could be automatically triggered based on sensor information that predicts an impending disruption. Such capability is also needed for a future ST based FNSF.

We are also developing (for NSTX-U) a new system for safely terminating discharges in ITER. The system, referred to as an Electromagnetic Particle Injector (EPI) propels a coaxial projectile, containing particulate matter of various sizes and composition, in a coaxial electromagnetic rail gun, then shatters it prior to injecting a dust of particles into the tokamak.

At the recent US Disruption Mitigation Workshop (GA, March 12-13, 2012) it was concluded that although the Massive Gas Injection system is the best understood for safely terminating discharges in ITER, both the time response of this system and the controllability of the amount of gas and impurities injected by this system for variations in the initial plasma current at which a disruption initiates may be inadequate to fully rely on this system. It was decided that other faster acting systems should also be tested and developed. During this meeting, we presented the EPI concept. It was noted that this system was more complex as compared to a conventional gas gun, but no technical flaws were identified. It was also suggested that a proto-type should be built and tested before considering it for ITER. The system is described in more detail in Chapter 2 of the NSTX 5YR plan document.

Summary of proposed research plan for 2014-18

We will install Massive Gas injectors at four poloidal locations on NSTX-U and measure the gas penetration efficiency and the thermal and current quench time scales when the poloidal gas injection location is varied. Reduction to divertor heat loads during normal and MGI forced disruptions will be measured. Eventually, the plan is to trigger these valves using sensor provided data of an impending disruption. We will also build and test an Electromagnetic Particle injector on NSTX-U in support of ITER research.

The elements of our plan displayed in a timeline are:

Timeline

FY2014:

- Model gas penetration through the SOL using DEGAS-2
- Design, build, test and install new MGI valves for NSTX-U
- Design, build and test the EPI injector for NSTX-U

FY2015:

- Using a low triangularity discharge, we will compare massive gas injection (using a combination of deuterium and helium) of gas injected into the lower X-point and private flux region to that from the vessel mid-plane.
- The shape of the plasma will be varied to make it highly triangular so that the outer strike point rests on the inner divertor plate and at a radius less than the radius of the gas

injection port. Gas will then be injected into the scrape-off-layer region near the divertor, which is now located in a region of high toroidal field. This injection location will be compared to mid-plane injection to understand the effects of gas penetration through the scrape-off layer that is located in regions of high vs. low toroidal field. The same combination of deuterium and helium will be used for these experiments to compare these results to those for the low triangularity discharges.

- During the first year of NSTX-U operations, much of the MGI studies will use a combination of deuterium and helium primarily to gain experience in conducting these studies on NSTX-U for the first time and to commission the diagnostics that will support MGI studies. Towards the end of YR1 operations we will conduct some tests in which neon is introduced as an additional impurity gas in the deuterium/helium gas mix used above to gain experience with the use of high-Z gas and to develop experiments for YR2 that will begin to use high-Z gasses.

FY2016:

- Based on YR1 results, a desired fraction of neon (in a combination of deuterium/helium carrier gas) will be used for all subsequent comparison experiments to be conducted this year.
- We will compare: (1) the gas transit and system response times, (2) propagation time for the cold front to reach the q=2 surface, (3) the amount of gas required for initiating a rapid thermal quench and (4) symmetry of the radiated power profile.
- We will simultaneously inject gas from three locations (bottom, mid-plane and top) to see if a cold mantle could be continually maintained around the disrupting plasma, and assess the benefits of multiple injection location for reducing localized radiation thermal loading.
- Finally, towards the end of YR2 operation, for a chosen condition from the YR2 experiments, neon will be replaced with argon to assess the benefits of each of these gases and to select the gas combination for YR 3 experiments.
- The primary objective for the EPI system during Year 2 (but before the end of FY2016) is to assess the EPI injector system's capability to initiate a forced thermal quench in less than 10ms after the system is triggered. This is for assessing its potential to meet ITER needs.

FY2017:

- Quantify the gas assimilation fraction for variations in the gas injection location and compare to DEGAS-2 modeling results. Assess if a full DEGAS-2 model is required for future work.

- Assess reduction in divertor heat loads and reduction in divertor halo currents for variations in the gas injection location.
- Measure asymmetries in the radiated power profile for variations in the gas injection location and for simultaneous gas injection from multiple locations.
- Obtain additional measurements using the EPI system to assess its benefits over the MGI system.

FY2018:

- Inject MGI at different times into a discharge in which the q-profile is evolving to understand the importance of the location of the q=2 surface to the plasma edge.
- For a high-powered NSTX-U discharge compare the thermal quench rates and the current quench rates for forced disruptions using MGI and EPI.
- We will work with groups using NIMROD, KPRAD, and if possible the EIRENE-SOLPS codes to simulate NSTX-U experimental observations. This is work will have been initiated during Year 1 of NSTX-U operations.
- Continue to include the NSTX-U MGI and EPI data into the ITER database to contribute to the continued understanding of these systems for ITER, future tokamaks and STs.
- We will trigger the MGI system based on sensor provided data on an impending disruption. Additionally, we will determine if the DM control system is capable of triggering a specific MGI valve based on the plasma configuration (i.e., downward vs. upward moving disruption)

Contributions to the NSTX-U 2014-18 Five Year Plan:

J.K. Park is the present leader of the Macro Stability topical science group and is responsible for overseeing chapter 2 of the NSTX-U Five Year Plan. The plan above was defined in a process carried out over CY2011-12 in coordination with the NSTX-U Research Team. The research defined above contributes heavily to the plan.

References

[1] R. Raman, D.P. Stotler, T. Abrams, et al., Massive gas injection plans for disruption mitigation studies in NSTX-U, IEEJ Transactions on Fundamentals and Materials, Vol. **132**, No. 7 pp 468-471 (2012)

[2] D. P. Stotler and C. F. F. Karney, Contrib. Plasma Phys. **34**, 392 (1994).

[3] D.P. Stotler, et al., J. Nucl. Mater., **196-198** (1992) 89

11.2.26 University of Wisconsin-Madison

Research Topic: Investigations of Long-Wavelength Turbulence and Instabilities in the Spherical Torus

Principal, Co-Principal Investigators: G.R. McKee (PI), R.J. Fonck, (Co-PI)
Participating Scientists: D. Smith
Participating Graduate Students: D. Thompson
Funded under DOE Grant: DE-SC0001288

Introduction

The University of Wisconsin-Madison is collaborating with Princeton Plasma Physics Laboratory to develop an advanced, multi-channel Beam Emission Spectroscopy (BES) diagnostic system for measuring turbulence and other instabilities in NSTX plasmas [1]. The principle goals of this collaboration are continued expansion and operation of BES and future related diagnostics, performing focused transport experiments on NSTX-U, exploring the properties and dynamics of turbulence and related instabilities, and seeking to validate comprehensive simulations of core and edge spherical torus plasmas. Understanding the unique aspects of turbulence and other long-wavelength instabilities in high-pressure spherical torus plasmas is crucial to comparing with conventional tokamak plasmas, challenging models and simulations of the ST configuration, optimizing performance, and projecting to future experiment designs.

BES measures density fluctuations associated with long-wavelength turbulence, MHD modes, Alfvenic modes, and pedestal instabilities in the core, edge and scrape-off regions of NSTX plasmas. The NSTX BES system is an advanced, highly modernized diagnostic that employs customized viewing optics to match the steep pitch angles of spherical torus plasmas, high throughput fiber bundles, fast optics and custom interference filters, and a new generation of cooled low-noise preamplifiers and detectors that were developed at UW [2]. BES observes Doppler-shifted Balmer (D_α) emission (n=3-2, λ~658-660 nm) from collisionally-excited neutral beam fluorescence. Deuterium beams are injected into NSTX plasmas with an energy of E_b = 70-90 keV via three nearly collinear ~2MW tangentially-directed co-current neutral beam sources. The diagnostic is fully remotely operable and has demonstrated high reliability, functionality, and utility.

The scientific program is carried out primarily by a full-time UW scientist (Dr. D. Smith), who is located on-site at PPPL, and we anticipate that a graduate student will join the program in 2014 when NSTX-U begins operations. Other part time scientists and technicians at UW assist with diagnostic development and scientific analysis. This UW-PPPL collaboration aligns well with

several major research elements of the NSTX program, DOE-FES goals, and supports a number of NSTX and JRT milestones.

Current research contributions to NSTX Upgrade

BES fluctuation measurements were acquired with an initial 16-channel and later 24-channel system for a wide range of experiments during the 2010-2011 NSTX operational campaigns [3]. 32 channels are currently deployed on NSTX, and 16 more are currently being developed at UW. The new channels will be deployed before the 2014 operations commence and will enable more comprehensive measurements of core, edge/pedestal and SOL fluctuation measurements.

Analysis to date has focused on the general characteristics of core and pedestal turbulence. Numerous valuable observations have been obtained that include: relatively long poloidal correlation lengths (~10-15 cm); strong suppression of turbulence in both the core and edge regions after an L-mode to H-mode transition; core-localized GAE modes that may drive electron thermal transport; TAE-mode bursts; pedestal-localized high-frequency coherent modes associated with ELM events in some H-mode conditions, long-wavelength pedestal turbulence [4], and edge fast-ion signals [5].

A comprehensive data base has been assembled that related pedestal turbulence properties, such as poloidal correlation lengths and wavenumber, decorrelation times, to pedestal parameters, including density, ion and electron temperatures, toroidal velocity, gradients therein, and radial electric field [6,7]. A model aggregation technique was used to determine the parametric dependencies between these turbulence and plasma parameters. General dependencies are found to be most consistent with trapped-electron mode, kinetic ballooning mode and microtearing modes [8], but not to ion temperature gradient modes. These dependencies are also consistent with turbulence regulation by flow shear. These results have been presented in major conferences and are submitted for publication. We will further develop and refine advanced analysis capabilities, including time-delay-estimation, velocimetry, and nonlinear techniques to more fully exploit the wealth of information available in these multipoint fluctuation data.

These results are being published in relevant plasma physics journals and are being presented at meetings and workshops, including: APS-DPP, Transport Task Force, High Temperature Plasma Diagnostics, IAEA-FEC, H-mode workshop, etc.; the new NSTX BES system is described in three publications by our group in Reviews of Scientific Instruments [1-3]. Of particular note, Dr. D. Smith presented an Invited Talk at the 2012 APS-DPP meeting, as well as an IAEA-FEC-2012 conference paper [7].

Summary of proposed research plan for 2014-18

We propose to develop and implement new diagnostic capability to enhance fluctuation diagnostic measurements at NSTX-U and exploit new experimental capabilities that will become available when NSTX-Upgrade is complete. The primary diagnostic goals are to:

- Increase the number of BES detection channels from 32 to 48
- Develop wide-field 2D turbulence imaging capability

A major component of this proposal is the expansion and enhancement of the BES system to allow for more comprehensive examination of turbulence and other instability properties in NSTX. The BES system will be expanded from 32 to 48 channels to allow for simultaneous core-to-edge sampling; this detector development is being be performed at UW.

A major diagnostic upgrade for this research program is to deploy 2D measurement capability for the outer region of the plasma to study turbulence and flow evolution during L-H transition, pedestal dynamics, instabilities across the ELM and in-between ELMs, as well as during ELM-suppressed or ELM-mitigated scenarios. Measurements to date have obtained radially and poloidally resolved density fluctuation measurements during this initial phase of operations to survey fluctuation characteristics. To exploit the radially and poloidally resolved measurement capability, and to explore the inherent 2D behavior of turbulence, we will deploy radially and poloidally resolved 2D measurement capability with BES. This will allow for several new scientific measurement capabilities that the present 1D configurations don't provide. These include:

- Modest spatial resolution, high-speed imaging of turbulent eddy structures.
- Radially resolved measurement of turbulence poloidal velocity, and velocity shear.
- Fully 2D correlation function, $\rho(r, \theta)$ and wavenumber spectrum: $S(k_r, k_\theta)$.
- Zonal flow structure
- Velocimetry (inferring 2D turbulence flow field)
- Nonlinear dynamics of turbulence-flow system

The pedestal region is unique for its high-pressure gradient, relatively narrow width, and high E_r shear. We will thus initially deploy a 2D viewing array in this edge region to probe the outer minor radius, separatrix and SOL region. We will explore with PPPL the feasibility of deploying a toroidally-displaced BES viewport on the new neutral beam to allow for toroidal mode number measurements of zonal flows and other low to medium-n instabilities.

We propose to perform a series of experiments to investigate the dependence and scaling properties of turbulence and transport. Parametric dependencies will be examined as a function of rotational shear, ρ^*, T_e/T_i, β_N (normalized plasma pressure), and, in combination with DIII-D, aspect-ratio. We will also investigate the effects of 3D radial fields on turbulence and the relationship between turbulence and pedestal modifications that drive or suppress ELMs,

depending on stability properties of the pedestal. In addition to core turbulence and transport, we will investigate the eigenmode structure and behavior energetic-particle-driven instabilities such as Toroidal and Global Alfvén Eigenmodes, and examine edge instabilities that limit the height and width of the pedestal, and drive ELMs.

We will also run advanced simulations of core and edge plasmas (e.g., GYRO, GEM and BOUT++) to support testing and validation studies through comprehensive comparison of multiple measured turbulence properties with simulations. Performing BOUT++ simulations will bring new capabilities to the NSTX program at a time when there is significant focus on edge physics. This will advance the development of a validated predictive capability for transport in magnetically confined plasmas. In addition, we will seek to perform NSTX-relevant experiments on affiliated experiments, such as Pegasus, DIII-D and MAST that will support our future NSTX experiments.

The elements of our plan displayed in a timeline are:

Timeline

FY2014:
- Implement 16 additional BES spatial channels (total to 48 channels)
- Deploy 2D channel configuration for edge viewing array (R140)
- Continue analysis of pedestal and core fluctuation characteristics
- Propose experiments to study core turbulence properties and dependencies as well as L-H transition dynamics

FY2015:
- Evaluate feasibility and design for a toroidally-displaced BES system
- Execute experiments on NSTX-U
- Continue analysis of L-H, pedestal and core fluctuation characteristics
- Bring a new graduate student to UW/NSTX-U collaboration

FY2016:
- Expand from 48 to 64 channels if resources become available
- Implement 2D core viewing array (R130)
- Continue analysis of L-H, pedestal and core fluctuation characteristics

FY2017:
- Deploy a high-resolution spectrometer for comprehensive beam emission spectral characterization

- Implement toroidally-displaced BES viewing optics, as feasible
- Continue analysis of L-H, pedestal and core fluctuation characteristics

FY2018:

- Continue analysis of L-H, pedestal and core fluctuation characteristics
- Consider deployment of UF-CHERS diagnostic for measuring ion temperature and toroidal velocity fluctuations for multifield turbulence studies
- Consider design and deployment of a low-coherence microwave backscattering diagnostic [9] for non-beam-based, high-resolution turbulence investigations

References

[1] "Overview of the beam emission spectroscopy diagnostic system on the National Spherical Torus Experiment," D. R. Smith, et al., Rev. Sci. Instrum. **81**, 10D717 (2010).

[2] "Low-Noise, High-Speed Detector Development for Optical Turbulence Fluctuation Measurements for NSTX," N. Schoenbeck *et al.*, Rev. Sci. Instrum. **81**, 10D718 (2010).

[3] Diagnostic performance of the beam emission spectroscopy system on the National Spherical Torus Experiment, D. R. Smith, R. J. Fonck, G. R. McKee, and D. S. Thompson, Rev. Sci. Instrum. **83**, 10D502 (2012).

[4] "Observation of ion scale fluctuations in the pedestal region during the edge-localized-mode cycle on the National Spherical Torus Experiment," A. Diallo *et al.*, Phys. Plasmas **20**, 012505 (2013).

[5] "Beam emission spectoscopy" diagnostics also measure edge fast-ion light, W. W. Heidbrink, G. R. McKee, D. R. Smith, and A. Bortolon, Plasma Phys. Control. Fusion **53**, 085007 (2011).

[6] "Characterization and parametric dependencies of low wavenumber pedestal turbulence in the National Spherical Torus Experiment," D. R. Smith, R. J. Fonck, G. R. McKee, D. S. Thompson, R. E. Bell, A. Diallo, W. Guttenfelder, S. M. Kaye, B. P. LeBlanc, and M. Podesta, *submitted to Phys. Plasmas* (2012).

[7] "Parametric dependencies of low-k turbulence in NSTX H-mode pedestals," D. R. Smith, R. J. Fonck, G. R. McKee, R. Bell, Y. Chen, A. Diallo, B. Dudson, S. Kaye, B. LeBlanc, R. Maingi, S. Parker, B. Stratton, and W. Wan, Proceedings of the 24th IAEA Fusion Energy Conference (2012).

[8] "Identification of microtearing modes below the ion gyroscale in the National Spherical Torus Experiment," D. R. Smith, W. Guttenfelder, B. P. LeBlanc, and D. R. Mikkelsen, Plasma Phys. Control. Fusion **53**, 035013 (2011).

[9] "Measuring plasma turbulence using low coherence microwave radiation," D. R. Smith, Appl. Phys. Let. **100**, 084107 (2012).

11.2.27 University of Wisconsin - Madison

Research Topic: Test of Point-Source Helicity Injection for Non-Solenoidal Startup in NSTX

Principal, Co-Principal Investigators: R.J. Fonck (PI), A.J. Redd (Co-PI)
Participating Post-docs: M.W. Bongard
Participating Graduate Students: E.T. Hinson
Funded under DOE Grants: DE-FG02-96ER54375 and DE-SC0006928

Introduction

Local Helicity Injection (LHI) is a non-solenoidal plasma startup and current drive technique, similar in concept to Coaxial Helicity Injection (CHI), except that the injector is relatively compact, may be located anywhere at the plasma boundary, and can in principle be withdrawn after plasma startup. Current is driven on open field lines at the tokamak edge, injecting both power and magnetic helicity. Over relatively short timescales MHD activity incorporates this increased magnetic helicity as an increase in the toroidal plasma current. Experimental studies using the Pegasus Toroidal Experiment have demonstrated the formation and growth of more than 170 kA of plasma current, using only 4 kA of driven open-field-line current.

This technique appears to be scalable to a device of the scale of the NSTX Upgrade (NSTX-U) and beyond, and the conceptual design of a 1 MA startup system for NSTX-U is presently under development in an external collaboration with the Pegasus team. This collaborative activity encompasses the materials and technology in any deployed NSTX-U injector, a deeper understanding of the physical processes that guide the injector design, and development of realistic operating scenarios for LHI startup to the 1 MA level on NSTX-U. The goal of this collaboration is the conceptual design of a cost-effective MA-class LHI-based startup system for deployment on NSTX-U.

Magnetic helicity, as the name suggests, is a measure of the helicity of the magnetic field lines in a volume of interest, analogous to vorticity of flow in a standard fluid. In a toroidal magnetized plasma, the magnetic helicity measures the linkage between the toroidal and poloidal magnetic fluxes. In a tokamak, where the toroidal magnetic field is almost entirely generated by external coils, the magnetic helicity is approximately proportional to the toroidal plasma current I_p, and magnetic helicity injection is equivalent to toroidal current drive. Experimentally, magnetic helicity is “injected” by driving current along field lines, increasing the helicity of that magnetic field. The ultimate current that can be driven and sustained by this technique is governed by two physical limits: a magnetic helicity limit and a helicity injection balance.

The first is a magnetic geometry limit, as described in the theory by J.B. Taylor [1], which sets an upper limit on the allowed I_p in terms of externally driven currents, the geometry of the confinement region, and the width of the driven region in the plasma. For a tokamak with toroidal field coil current I_{TF}, injected current I_{inj}, and width *w* of the driven plasma edge, the maximum plasma current scales [2] as the square root of $I_{TF} I_{inj} / w$.

The helicity balance limit is simply a balance between the rate of magnetic helicity injection and the resistive helicity dissipation, very similar to the usual balance of applied power to the total power dissipation. The effective loop voltage due to helicity injection is proportional to the helicity injection rate, itself proportional to the product of the bias voltage with the active cross-sectional area of the compact injector. Just as with power balance, the exact helicity injection rate necessary to create and sustain a target plasma against resistive dissipation depends upon the target I_p and the nature of the dissipation (*i.e.*, stochastic confinement and/or standard closed-flux confinement). Technological limits may place an upper bound of 1 kV for the bias voltage of any injector at the edge of a tokamak discharge, implying that order-of-magnitude increases in the helicity injection rate must be achieved through increases in the injector cross-sectional area.

Taken together, these two current limits dictate that any high-capability injector system will involve an injector with cross-sectional area on the order of 100 cm^2, shaped so as to be narrow in the radial direction, with the exact injector size dictated by the nature of the dissipation.

For recent experiments, the injector assemblies in the Pegasus device are located near the outboard midplane. Pegasus discharges formed by LHI start out near the outboard injectors, are relatively small with an apparently near-circular cross-section, and grow inward as the plasma current increases. This outboard formation allows the I_p growth to be enhanced by a ramp in the outer Poloidal Field (PF) coil currents, by using this outer-PF induction drive to increase the effective loop voltage on the discharge [2]. The outer-PF induction is actually the dominant current drive during the late I_p rampup phase. Variations in the I_p ramp rate correspond to variations in the driven J_T distribution, with rapid I_p ramps producing very hollow current density distributions, and slower ramps allowing more uniform current distribution throughout the plasma cross-section. These current profiles are then “frozen into” the discharge after the LHI is shut off, as it is sustained by other current drive techniques (solenoidal induction in the case of Pegasus), enabling the formation of high-current MHD-stable tokamak equilibria [3].

LHI can be quite flexible with regards to the location of the injector, with any particular injector location offering its own advantages and disadvantages. Early Pegasus injection experiments used divertor-region plasma guns [4], which had a relatively high helicity injection rate (in the high-field divertor region) and simple plasma radial position control. Outboard injection offers easier maintenance, better diagnostic access, and scope for significant outer-PF induction, at the

cost of a relatively lower helicity injection rate and more complicated radial position control requirements. That is, current buildup in outboard injection scenarios is much less demanding for the helicity injection system, but more demanding for the plasma control system. Designing the optimum injection system and corresponding operating scenario for NSTX-U or any other device will require understanding of these trade-offs, potentially with the limitations of the coil current supplies and plasma control system driving the conceptual design of the injector location, the helicity injector size, and the injection bias supply parameters.

Current research contributions to NSTX Upgrade

The ongoing collaboration with the Pegasus group encompasses the materials and technology of LHI, understanding of the relevant physics, and the conceptual design of a LHI-based MA-class startup system for NSTX-U. There are significant physics- and technology-based issues which impact the design, some of which have been described in the previous section, and all these issues must be resolved before proceeding:

- The electron emitter technology that will be used as a helicity injector in NSTX-U
- The minimum active area of the injector, related to the plasma confinement/dissipation
- Injection bias power supply requirements, related to injector bias impedance
- The location of the injector, related to the relative "weight" of PF induction in operations
- The radial width of the injected current channel
- Tokamak-like plasma formation in conditions relevant to NSTX-U operations
- NSTX-U machine access for deploying the helicity injection system
- Plasma-Material Interactions (PMI) at the injector structures

Each of these issues is the focus of specific research efforts, and each will be addressed and brought to some conclusion in the context of the planned research, as described in the next section. The following paragraphs outline recent results that advance some of these issues.

As described in Refs [5] and [6], there has been considerable evolution in the construction and understanding of the injection sources since the beginning of the formal collaboration in 2010. Early Pegasus helicity injection studies used relatively large active plasma sources (called "guns") to create a local discharge, which was then the source of free electrons for the injector bias current. These sources have intrinsic limitations on their cross-sectional area and discharge duration, which confound easy extrapolation to higher-I_p plasmas in Pegasus and NSTX-U. Subsequent experiments showed that a bare electrode, though conceptually and technologically simple, was inappropriate as a source of significant helicity injection. Experimental attention in the Pegasus program has thus shifted to gas-fed electrodes, to use the "hollow cathode" effect to give an extended uniform current source with sufficient area.

A parallel effort on Pegasus has greatly reduced the interactions between driven plasma and the material surfaces of the injectors, typically boron nitride sheathing of metallic injector components. A long-standing problem with these injectors is inadvertent arcing back from the injector face to structural components supporting the injector assembly, typically along boron nitride sheathing. This arcback heating of the boron nitride would cause material eruptions, which would fuel the plasma in an uncontrolled manner, introduce significant impurities, cause significant damage to injector components, and (by supplying large amounts of gas in an unexpected location) reduce voltage standoffs on the injector structure and make additional arcing easier. This arcback was prevented by the addition of a thin floating molybdenum plate behind the injector face, to shield the boron nitride without being charged to the injector potential. Additionally, each Pegasus injector assembly now incorporates a local scraper limiter to reduce PMI between the main discharge and boron nitride sheathing of the injector assembly.

Finally, the detailed shape of any deployed metallic electrode is now optimized to control the motion of inadvertently-created cathode hot spots, with any such spots kept away from boron nitride near the injector face. Together, these changes have led to a dramatic reduction in the uncontrolled fueling of LHI-driven Pegasus discharges, and a corresponding reduction in the impurity content of those plasmas. Each of these features will be used to improve the PMI aspects of any NSTX-U injector.

As described in Refs [7] and [8], scientific understanding of the impedance of the injector on the external bias circuit has also improved. The observed impedance for an active plasma source is consistent with a double layer sheath, with a low-current low-voltage operating regime that has bias current bounded by space charge limits (for a bias current that scales as the bias voltage to the three-halves power), and a high-voltage high-current regime constrained by the Alfven-Lawson magnetic current limit [9] (for bias current scaling as bias voltage to the one-half power). These models are also broadly consistent with the observed dependence on electron density, with the bias current increasing with increasing electron density at fixed bias voltage. However, these first-order models do not explain the mechanism for the observed dependence of the impedance upon the external fueling rates, and both theoretical development and detailed experiments are needed.

Summary of proposed research plan for FY2014-2018

The collaboration between the Pegasus and NSTX-U teams has the deliverable goal of producing a conceptual design for a MA-class LHI-based NSTX-U startup system. From this conceptual design, the detailed design for this startup system will take shape, in direct collaboration with PPPL science and engineering staff. Part of this detailed design activity should culminate in the installation of ports or port covers on the NSTX-U device that will enable machine access for the

LHI system. This installation activity should be targeted for the planned outage/upgrade in FY2016-2017, and would enable the LHI system to be installed without requiring a major interruption to NSTX-U operations, whether at the end of this five-year period or at the beginning of the next.

In the FY2014-2018 period, results from the separate Pegasus research program will naturally address physics and technology issues for LHI startup in NSTX-U. For example, studies of electron source technology for LHI on Pegasus will yield insights for extrapolation to NSTX-U parameters, and ultimately for choosing the optimum source technology for NSTX-U startup. Active plasma sources, as presently deployed on Pegasus, have one to three PFN-driven arc discharges of ~2 kA each, for durations of 8-10 milliseconds, compatible with inertial cooling of the plasma source structures. The size and current scales of these sources are consistent with a Pegasus startup dominated by outer-PF induction, with compact high current-density sources yielding a high Taylor I_p limit but relatively little helicity injection drive. In contrast, the timescales of NSTX-U startup (~100 milliseconds), along with a demand for higher-performance current drive, extrapolates to an LHI startup system that deploys tens of sources with lower arc currents, in order to meet the Taylor current limit for 1 MA startup. The longer timescales of NSTX-U startup would require active cooling of these plasma sources, with each source also having its own arc PFN, gas feed, and bias current connection. This complexity may be undesirable, especially if a passive large-area electron emitter can fulfill the requirements.

The Pegasus team is presently evaluating large-area gas-fed electrodes, using the hollow cathode effect to source electron current at each gas feed. Even if the hollow cathode effect leads to a viable injector technology for Pegasus parameters, the physics of this effect may not allow a simple extrapolation to the relatively high-field environment of NSTX-U. Pegasus experiments will be directed at demonstrations of viable large-area injectors, especially those that will extrapolate to relatively simple injector systems in NSTX-U.

LHI startup has been developed in Pegasus device, which has no large conducting structures near the confinement region and a relatively low base pressure. For presently unexplained reasons, LHI startup is somewhat sensitive to the initial conditions, and computational and experimental confirmation is needed to demonstrate that LHI startup can work in the presence of the NSTX-U passive plates and its relatively high base pressure.

Experiments will address the fundamental issues of the impedance of the injection source and the dissipation in LHI-driven plasmas, using a more capable Pegasus diagnostic set (including multi-point Thomson scattering, improved interferometry, and SXR). Both of these issues significantly impact the extrapolation to NSTX-U startup, via the minimum size of the injector and the requirements for the bias power supply.

Computational activities will also evolve from the present 0D/1D modeling developed for Pegasus and initial TSC validation activity to detailed modeling of LHI operating scenarios in both the Pegasus and NSTX-U devices. The 0D/1D modeling efforts will yield initial parameters for the helicity injector and bias power supply, as well as giving insight for the helicity dissipation and the optimum amount of PF induction to use in an LHI startup scenario. These results will be replicated and extended using detailed scenario modeling with the TSC code. Additionally, the formation of a poloidal null, a necessary condition for LHI startup, must also be modeled in the context of the NSTX-U coil set and the presence of the passive plates. As the conceptual design of the LHI startup system takes shape, the detailed modeling will shift in emphasis, to development of realistic operating scenarios relevant to LHI startup experiments in NSTX-U, from null formation to the initial relaxation, through the current rampup phase, up to reaching the 1 MA target plasma current.

Research Timeline during the FY2014-2018 Period

Items prefaced with "(P)" are Pegasus program activities that will inform this collaboration.
Items prefaced with "(N)" are specific activities related to this collaboration.

FY2014-2015:

- (P) Refine injector impedance model
- (P) Pursue the science and technology of large-area electron emitters that can be used for helicity injection in high-field NSTX-U parameters, including demonstration of injector technology relevant for NSTX-U
- (P) Evaluate the confinement and electron energy dissipation in LHI-driven discharges, both in terms of overall confinement properties and the corresponding MHD activity
- (N) Examine (computationally and experimentally) the conditions for initial relaxation in LHI discharges, under conditions relevant to NSTX-U
- (N) Detailed modeling of NSTX-U LHI startup scenarios, focusing especially on confirming and extending 0D/1D results regarding LHI-dominated current drive scenarios versus PF-induction contributions
- (N) Deepen dialogues with PPPL personnel, especially with regards to NSTX-U access and the use of PPPL-compliant materials and design parameters for the LHI startup system.

FY2016-2017:

- (N) Composition of conceptual design for MA-class LHI startup system
- (N) Installation of LHI port(s) on NSTX-U device during the FY2016-2017 outage/upgrade

FY2017-2018:

- (N) Projected start of incremental funding for startup system at the beginning of FY2017
- (N) Detailed design and design review activities, transitioning to fabrication when possible
- (N) Projected installation of the LHI system after the FY2018 run period
- (N) Composition of LHI startup experimental plans, in collaboration with PPPL staff

This timeline is illustrated with a Gantt chart, appended to the end of this section.

Contributions to the NSTX-U 2014-18 Five Year Plan:

Roger Raman is the present leader of the solenoid-free startup and rampup topical science group and is responsible for overseeing the "Plasma Formation and Rampup" chapter of the NSTX-U Five Year Plan. The plan above was defined in a process carried out over CY2011-12 in coordination with the NSTX-U Research Team. The research defined above contributes to the long-term goals of NSTX-U and the spherical torus, by demonstrating a non-solenoidal startup technique capable of generating a tokamak discharge that can be subsequently sustained using only the steady-state current drive systems. As planned, this research will not impact the NSTX-U 2014-2018 Five Year Plan in terms of operations, as the helicity injection system may not be installed and tested until the end of FY2018. However, the machine access required for the LHI system will be determined long before any installation, and whether this will require simply installing gate valve(s) on existing port(s) or creating new port(s), arranging this access will impact the upgrade activities during the FY2016-2017 outage.

References

[1] Taylor, J.B. "Relaxation and magnetic reconnection in plasmas," Rev. Mod. Phys. **58** (1986) 741.

[2] Battaglia, D.J., *et al*., "Tokamak startup using point-source DC helicity injection," Phys. Rev. Lett. **102** (2009) 225003; Battaglia, D.J., *et al*., "Tokamak startup using outboard current injection on the Pegasus Toroidal Experiment," Nucl. Fusion **51** (2011) 073029.

[3] Fonck, R.J., *et al*., "Nonsolenoidal startup and plasma stability at near-unity aspect ratio in the Pegasus Toroidal Experiment," 23rd IAEA Fusion Energy Conference, Daejon, Korea, October 2010, no. EXS/P2-07.

[4] Eidietis, N.W., *et al*., "Non-inductive production of ST plasmas with washer gun sources on the Pegasus Toroidal Experiment," J. Fusion Energy **26** (2007) 43.

[5] Fonck, R.J., *et al*., "Local Current Injector System for Nonsolenoidal Startup in a Low Aspect Ratio Tokamak," 24th IAEA Fusion Energy Conference, San Diego, USA, October 2012, no. FTP/P1-19.

[6] Redd, A.J., *et al*., "Feasibility study for Local Helicity Injection startup in the NSTX Upgrade (NSTX-U) device," 54th APS Division of Plasma Physics annual meeting, Providence, USA, October-November 2012.

[7] Redd, A.J., *et al*., "Local helicity injection startup and edge stability studies in the Pegasus Toroidal Experiment," 24th IAEA Fusion Energy Conference, San Diego, USA, October 2012, no. EX/P4-36.

[8] Bongard, M.W., et al., "Non-solenoidal startup through Local Helicity Injection in the Pegasus Toroidal Experiment," 54th APS Division of Plasma Physics annual meeting, Providence, USA, October-November 2012.

[9] Alfven, H., "On the motion of cosmic rays in interstellar space," Phys. Rev. **55** (1939) 425.

11.2.28 X Science LLC

Research Topic: Absolutely Calibrated Tangential Imaging of Divertor
Principal Investigator: Ricardo Maqueda
Participating Scientists (not funded by this grant): Vlad Soukhanovskii (LLNL)
Funded under DOE Grant: DE-SC0007979

Introduction

Researchers from X Science LLC are working on an upgrade to an existing diagnostic that can provide extremely useful information in divertor physics research. The lower divertor tangential imaging system of NSTX will be absolutely (i.e., photometrically) calibrated and this calibration will be maintained throughout the experimental campaign by measuring the transmission through the vacuum interface window and other optical components. The data obtained in NSTX-U will be used together with edge models to guide their development and implementation in NSTX-U and to indirectly obtain measurements of physics relevant quantities such as the densities in the divertor region of neutral deuterium and impurities like carbon and lithium.

Current research contributions to NSTX Upgrade

Work is currently underway to upgrade the lower divertor tangential imaging system of NSTX [1], adapting it to the NSTX-U device and being able to perform absolutely calibrated measurements. Figure 1 shows the planned field of view on the lower half of an equilibrium calculated for NSTX-U. This diagnostic system is usually operated with interference filters for deuterium (D_α, D_γ) or impurity line emission (LiI, LiII, CII, CIII, etc) which are located on a remote controlled filter. Fast-framing digital cameras are used to obtain highly resolved (1 kHz or better) measurements.

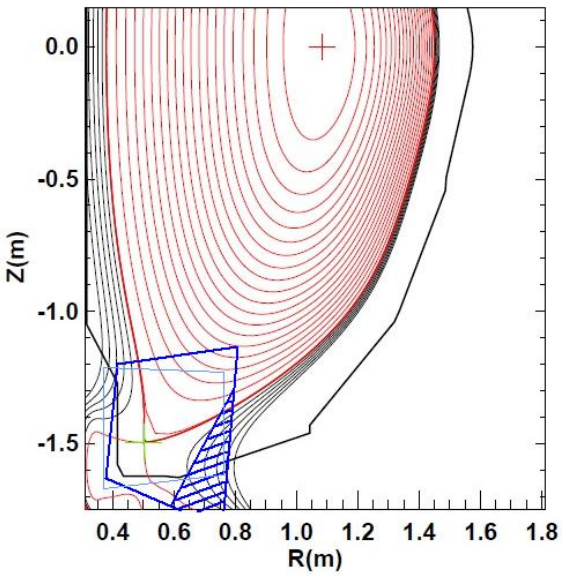

Figure 1: Planned view of lower divertor tangential camera system on NSTX-U (blue box). The dashed region is obstructed by near field tiles and other hardware.

The largest difficulty when performing the calibration for this imaging system resides not on the calibration itself but in maintaining this calibration throughout the several months-long experimental campaign. Coatings inevitably develop through the campaign on the vacuum

interface window and other invessel optics such as mirrors. One of the main aspects of the planned work, in addition to performing the calibration and making use of the data, resides in the implementation and use of invessel illumination hardware that will permit the measurement of the optics transmission as the campaign progresses.

Summary of proposed research plan for 2014-18

At this time several research tasks are planned for NSTX-U in the area of divertor physics. These include the further development of the snowflake divertor, development and assessment of divertor detachment and performance, generation and transport of impurities (and recycling) at the divertor, and study of 3-D field effects on divertor physics. NSTX-U is also planning the development and implementation of cryo-pumping in the lower divertor region. The use of the absolutely calibrated lower divertor tangential imaging system will assist in these research tasks as well as in the physics research of high-Z materials used as plasma facing components in the divertor region.

An important component of the research plan for 2014-2018 is the integration of the measurements obtained with this diagnostic with the modeling efforts within the NSTX-U team. The UEDGE fluid code [2] has been previously been used in NSTX [3] in a limited way but it is expected to be further developed for use in NSTX-U with the research efforts from team members from LLNL. The UEDGE code can then be used to generate background plasma conditions, with which neutral Monte Carlo codes like DEGAS2 [4] can be run to study neutral transport and, coupled to collision rate tables, obtain emission rates that can be compared to the measurements obtained with the calibrated divertor tangential camera

Conversely, once the codes have been benchmarked against the available diagnostics it is the results from these codes what would allow the indirect measurements of many physics parameters relevant to divertor research in NSTX-U. Perhaps the most immediate indirect measurements associated with the calibrated 2-D emission profiles obtained with the tangential divertor camera would be the deuterium neutral density and the impurity densities at the different ionization levels being observed. Another indirect measurement would be the diffusion and flow of deuterium and impurities (carbon, lithium and, possibly, high-Z materials). This measurement would be made easier if one can use transient and/or localized events in the field of view of the camera, like the localized injection of methane in DIII-D [5].

The elements of our plan displayed in a timeline are:

Timeline

FY2014:

- Complete design, fabrication and installation of hardware in NSTX-U.

FY2015:

- Obtain (first) absolutely calibrated tangential images of plasmas in lower divertor region.
- Invert images into emission profiles in the R, Z plane.
- Initiate comparisons with UEDGE runs.
- Obtain (first) measurements of deuterium density and impurity densities.

FY2016:

- Continue with measurements and analysis through the FY2016 experimental campaign.
- Perform transient/localized measurements to obtain diffusion coefficients and flow speeds of deuterium and impurities.

FY2017:

- TBD, current grant period ends in June 2016.

FY2018:

- TBD, current grant period ends in June 2016.

Contributions to the NSTX-U 2014-18 Five Year Plan:

The plan above contributes heavily to the research goals established in the 2014-2018 NSTX-U plan in the areas of divertor performance (Sections 4.2.4, 4.2.5 and 4.2.6): assessment and control of heat and particle fluxes by means of (further) development of advanced divertor configurations, physics of the impurity transport from the divertor PFCs (carbon, lithium, high-Z), and particle control via cryo-pumping.

References

[1] A. L. Roquemore, T. Biewer, D. Johnson, et al., Rev. Sci. Instrum. 75, 4190 (2004).
[2] T. D. Rognlien, G. D. Porter and D. D. Ryutov, J. Nucl. Mater. 266-269, 654 (1999).
[3] R. D. Smirnov, A. Yu. Pigarov, et al., Contrib. Plasma Phys. 50, 299 (2010).
[4] D. P. Stotler and C. F. F. Karney, Contrib. Plasma Phys. 34, 392 (1994).
[5] M. Groth, J. A. Boedo, N. H. Brooks, et al., Nucl. Fusion 49, 115002 (2009).